

NASA Technical Memorandum 89887

Bibliography of Lewis Research Center Technical Publications Announced in 1986

(NASA-TM-89887) BIBLIOGRAPHY OF LEWIS
RESEARCH CENTER TECHNICAL PUBLICATIONS
ANNOUNCED IN 1986 (NASA) 349 P CSCL 05B

N89-18259

G3/82 Unclass
0197301

May 1987

NASA

PREFACE

In 1986, Lewis Research Center's 1062 research authors published 440 technical publications that were announced to and reached the worldwide scientific community. The 440 papers included 223 symposium/seminar presentations and 82 articles sent directly to journals for publication. The number of seminar presentations was the second highest in Lewis history (226 in 1984), while the number of journal articles was the highest in Lewis history (74 in 1985). For many years, the number of articles submitted directly to journals for publication ranged between 40 and 50. In 1986, Lewis authors published approximately 69 percent of their research contributions in outside publications and the remainder as NASA research reports. Sixty-two percent of Lewis-authored society presentations and journal articles were addressed to members of the following technical societies: AIAA, 60 papers; ASME, 52 papers; SAE, 28 papers; ASM, 25 papers; IEEE, 21 papers; ASEE (American Society of Engineering Education), 17 papers; AIP (American Institute of Physics), 15 papers; ASLE, 13 papers; American Chemical Society, 12 papers; and ACS (American Ceramic Society), 12 papers.

In 1986, 293 contractor-authored research reports were produced. In addition, 11 patent applications were filed and 11 patents were issued.

Lewis hosted 12 research conferences in 1986. Seven of these resulted in NASA Conference Publications:

- NASA CP-2423, 20th Aerospace Mechanisms Symposium, May 7-9
- NASA CP-2427, Structural Ceramics, May 20-21, abstracts and figures
- NASA CP-2444, Turbine Engine Hot Section Technology 1986, October 21-22
- NASA CP-2465, Microgravity Fluid Management Symposium, September 9-10
- NASA CP-2473, Spacecraft 2000, July 29-31, figures and working group reports
- NASA CP-2475, Space Photovoltaic Research and Technology 1986, October 7-9
- NASA CP-2476, Spacecraft Fire Safety, August 20-21

In addition, three of these conference publications were published at Lewis and made available to the attendees when they registered at the conference: 20th Aerospace Mechanisms Symposium, Structural Ceramics, and Turbine Engine Hot Section Technology 1986. Other conferences hosted by Lewis in 1986 included

- First International Conference on Ion Nitriding, September 15-17
- Third Symposium on Nonlinear Constitutive Relations for High-Temperature Applications, June 11-13
- 1986 Advanced Turboprop Workshop, November 5-6
- Midwest Space Development Conference, October 17-19
- Technology Transfer Conference, September 25

Many Lewis authors have received awards for their contributions; among them are the following:

The 1986 Lewis Distinguished Paper Award was presented to Arthur N. Curren and Kenneth A. Jensen for their paper entitled "Textured Carbon on Copper: A Novel Surface With Extremely Low Secondary Electron Emission Characteristics." In addition, William F. Brown, Jr., a Distinguished Research Associate for the Aerospace Technology Directorate, received the Nadai Award from the American Society of Mechanical Engineers for outstanding contributions to the field of engineering materials.

A few Lewis-authored publications are not included in this compilation because of FEDD (For Early Domestic Dissemination) and ITAR (International Traffic in Arms Regulations) considerations which limit their announcement and distribution.

All the publications in this collection were announced in the 1986 issues of STAR (Scientific and Technical Aerospace Reports) and IAA (International Aerospace Abstracts).

The arrangement of the material is by NASA subject category, as noted in the Contents. The various indexes will help locate specific publications by subject, author, contractor organization, contract number, and report number.

George Mandel
Chief, Technical Information Services Division

TABLE OF CONTENTS

PREFACE

AERONAUTICS

Includes aeronautics (general); aerodynamics; air transportation and safety; aircraft communications and navigation; aircraft design, testing and performance; aircraft instrumentation; aircraft propulsion and power; aircraft stability and control; and research and support facilities (air).

For related information see also *Astronautics*.

1 AERONAUTICS (GENERAL) 1

2 AERODYNAMICS 1

Includes aerodynamics of bodies, combinations, wings, rotors, and control surfaces; and internal flow in ducts and turbomachinery.

For related information see also *34 Fluid Mechanics and Heat Transfer*

3 AIR TRANSPORTATION AND SAFETY 14

Includes passenger and cargo air transport operations; and aircraft accidents.

For related information see also *16 Space Transportation* and *85 Urban Technology and Transportation*.

4 AIRCRAFT COMMUNICATIONS AND NAVIGATION N.A.

Includes digital and voice communication with aircraft; navigation systems (satellite and ground based); and traffic control.

For related information see also *17 Space Communications, Spacecraft Communications, Command and Tracking* and *32 Communications and Radar*.

5 AIRCRAFT DESIGN, TESTING AND PERFORMANCE 16

Includes aircraft simulation technology.

For related information see also *18 Spacecraft Design, Testing and Performance* and *39 Structural Mechanics*. For land transportation vehicles see *85 Urban Technology and Transportation*.

6 AIRCRAFT INSTRUMENTATION 17

Includes cockpit and cabin display devices; and flight instruments.

For related information see also *19 Spacecraft Instrumentation* and *35 Instrumentation and Photography*.

7 AIRCRAFT PROPULSION AND POWER 17

Includes prime propulsion systems and systems components, e.g., gas turbine engines and compressors; and board auxiliary power plants for aircraft.

For related information see also *20 Spacecraft Propulsion and Power*, *28 Propellants and Fuels*, and *44 Energy Production and Conversion*.

8 AIRCRAFT STABILITY AND CONTROL 35

Includes aircraft handling qualities; piloting; flight controls; and autopilots.

For related information see also *05 Aircraft Design, Testing and Performance*.

09 RESEARCH AND SUPPORT FACILITIES (AIR) 36

Includes airports, hangars and runways; aircraft repair and overhaul facilities; wind tunnels; shock tubes; and aircraft engine test stands.

For related information see also *14 Ground Support Systems and Facilities (Space)*.

ASTRONAUTICS

Includes astronautics (general); astrodynamics; ground support systems and facilities (space); launch vehicles and space vehicles; space transportation; space communications, spacecraft communications, command and tracking; spacecraft design, testing and performance; spacecraft instrumentation; and spacecraft propulsion and power.

For related information see also *Aeronautics*

12 ASTRONAUTICS (GENERAL) 38

For extraterrestrial exploration see *91 Lunar and Planetary Exploration*.

13 ASTRODYNAMICS 43

Includes powered and free-flight trajectories; and orbital and launching dynamics.

14 GROUND SUPPORT SYSTEMS AND FACILITIES (SPACE) 43

Includes launch complexes, research and production facilities; ground support equipment, e.g., mobile transporters; and simulators.

For related information see also *09 Research and Support Facilities (Air)*.

15 LAUNCH VEHICLES AND SPACE VEHICLES 43

Includes boosters; operating problems of launch/space vehicle systems; and reusable vehicles.

For related information see also *20 Spacecraft Propulsion and Power*.

16 SPACE TRANSPORTATION 44

Includes passenger and cargo space transportation, e.g., shuttle operations; and space rescue techniques.

For related information see also *03 Air Transportation and Safety* and *18 Spacecraft Design, Testing and Performance*. For space suits see *54 Man/System Technology and Life Support*.

17 SPACE COMMUNICATIONS, SPACECRAFT COMMUNICATIONS, COMMAND AND TRACKING 44

Includes telemetry; space communications networks; astronavigation and guidance; and radio blackout.

For related information see also *04 Aircraft Communications and Navigation* and *32 Communications and Radar*.

18 SPACECRAFT DESIGN, TESTING AND PERFORMANCE

47

Includes satellites; space platforms; space stations; spacecraft systems and components such as thermal and environmental controls; and attitude controls.

For life support systems see *54 Man/System Technology and Life Support*. For related information see also *05 Aircraft Design, Testing and Performance*, *39 Structural Mechanics*, and *16 Space Transportation*.

19 SPACECRAFT INSTRUMENTATION

50

For related information see also *06 Aircraft Instrumentation* and *35 Instrumentation and Photography*.

20 SPACECRAFT PROPULSION AND POWER

50

Includes main propulsion systems and components, e.g. rocket engines; and spacecraft auxiliary power sources.

For related information see also *07 Aircraft Propulsion and Power*, *28 Propellants and Fuels*, *44 Energy Production and Conversion*, and *15 Launch Vehicles and Space Vehicles*.

CHEMISTRY AND MATERIALS

Includes chemistry and materials (general); composite materials; inorganic and physical chemistry; metallic materials; nonmetallic materials; propellants and fuels; and materials processing.

23 CHEMISTRY AND MATERIALS (GENERAL)

64

24 COMPOSITE MATERIALS

65

Includes physical, chemical, and mechanical properties of laminates and other composite materials.

For ceramic materials see *27 Nonmetallic Materials*.

25 INORGANIC AND PHYSICAL CHEMISTRY

71

Includes chemical analysis, e.g., chromatography; combustion theory; electrochemistry; and photochemistry.

For related information see also *77 Thermodynamics and Statistical Physics*.

26 METALLIC MATERIALS

79

Includes physical, chemical, and mechanical properties of metals, e.g., corrosion; and metallurgy.

27 NONMETALLIC MATERIALS

94

Includes physical, chemical, and mechanical properties of plastics, elastomers, lubricants, polymers, textiles, adhesives, and ceramic materials.

For composite materials see *24 Composite Materials*.

28 PROPELLANTS AND FUELS

106

Includes rocket propellants, igniters and oxidizers; their storage and handling procedures; and aircraft fuels.

For related information see also *07 Aircraft Propulsion and Power*, *20 Spacecraft Propulsion and Power*, and *44 Energy Production and Conversion*.

29 MATERIALS PROCESSING

N.A.

Includes space-based development of products and processes for commercial application.

For biological materials see *55 Space Biology*.

ENGINEERING

Includes engineering (general); communications and radar; electronics and electrical engineering; fluid mechanics and heat transfer; instrumentation and photography; lasers and masers; mechanical engineering; quality assurance and reliability; and structural mechanics.

For related information see also *Physics*.

31 ENGINEERING (GENERAL)

108

Includes vacuum technology; control engineering; display engineering; cryogenics; and fire prevention.

32 COMMUNICATIONS AND RADAR

108

Includes radar; land and global communications; communications theory; and optical communications.

For related information see also *04 Aircraft Communications and Navigation* and *17 Space Communications*. For search and rescue see *03 Air Transportation and Safety* and *16 Space Transportation*.

33 ELECTRONICS AND ELECTRICAL ENGINEERING

117

Includes test equipment and maintainability; components, e.g., tunnel diodes and transistors; microminiaturization; and integrated circuitry.

For related information see also *60 Computer Operations and Hardware* and *76 Solid-State Physics*.

34 FLUID MECHANICS AND HEAT TRANSFER

125

Includes boundary layers; hydrodynamics; fluidics; mass transfer and ablation cooling.

For related information see also *02 Aerodynamics* and *77 Thermodynamics and Statistical Physics*.

35 INSTRUMENTATION AND PHOTOGRAPHY

145

Includes remote sensors; measuring instruments and gages; detectors; cameras and photographic supplies; and holography.

For aerial photography see *43 Earth Resources and Remote Sensing*. For related information see also *06 Aircraft Instrumentation* and *19 Spacecraft Instrumentation*.

36 LASERS AND MASERS

150

Includes parametric amplifiers.

For related information see also *76 Solid-State Physics*.

37 MECHANICAL ENGINEERING

151

Includes auxiliary systems (nonpower); machine elements and processes; and mechanical equipment.

38 QUALITY ASSURANCE AND RELIABILITY

162

Includes product sampling procedures and techniques and quality control.

39 STRUCTURAL MECHANICS

161

Includes structural element design and weight analysis; fatigue; and thermal stress.

For applications see *05 Aircraft Design, Testing and Performance* and *18 Spacecraft Design, Testing and Performance*.

GEOSCIENCES

Includes geosciences (general); earth resources and remote sensing; energy production and conversion; environment pollution; geophysics; meteorology and climatology; and oceanography.

For related information see also *Space Sciences*.

42 GEOSCIENCES (GENERAL) N.A.

43 EARTH RESOURCES AND REMOTE SENSING N.A.

Includes remote sensing of earth resources by aircraft and spacecraft; photogrammetry; and aerial photography.

For instrumentation see 35 *Instrumentation and Photography*.

44 ENERGY PRODUCTION AND CONVERSION 179

Includes specific energy conversion systems, e.g., fuel cells; global sources of energy; geophysical conversion; and windpower.

For related information see also 07 *Aircraft Propulsion and Power*, 20 *Spacecraft Propulsion and Power*, and 28 *Propellants and Fuels*.

45 ENVIRONMENT POLLUTION 191

Includes atmospheric, noise, thermal, and water pollution.

46 GEOPHYSICS 191

Includes aeronomy; upper and lower atmosphere studies; ionospheric and magnetospheric physics; and geomagnetism.

For space radiation see 93 *Space Radiation*.

47 METEOROLOGY AND CLIMATOLOGY 191

Includes weather forecasting and modification.

48 OCEANOGRAPHY 192

Includes biological, dynamic, and physical oceanography; and marine resources.

For related information see also 43 *Earth Resources and Remote Sensing*.

LIFE SCIENCES

Includes life sciences (general); aerospace medicine; behavioral sciences; man/system technology and life support; and space biology.

1 LIFE SCIENCES (GENERAL) N.A.

2 AEROSPACE MEDICINE N.A.

Includes physiological factors; biological effects of radiation; and effects of weightlessness on man and animals.

3 BEHAVIORAL SCIENCES N.A.

Includes psychological factors; individual and group behavior; crew training and evaluation; and psychiatric research.

4 MAN/SYSTEM TECHNOLOGY AND LIFE SUPPORT 192

Includes human engineering; biotechnology; and space suits and protective clothing.

For related information see also 16 *Space Transportation*.

55 SPACE BIOLOGY N.A.

Includes exobiology; planetary biology; and extraterrestrial life.

MATHEMATICAL AND COMPUTER SCIENCES

Includes mathematical and computer sciences (general); computer operations and hardware; computer programming and software; computer systems; cybernetics; numerical analysis; statistics and probability; systems analysis; and theoretical mathematics.

59 MATHEMATICAL AND COMPUTER SCIENCES (GENERAL) 192

60 COMPUTER OPERATIONS AND HARDWARE 192

Includes hardware for computer graphics, firmware, and data processing.

For components see 33 *Electronics and Electrical Engineering*.

61 COMPUTER PROGRAMMING AND SOFTWARE 193

Includes computer programs, routines, algorithms, and specific applications, e.g., CAD/CAM.

62 COMPUTER SYSTEMS 194

Includes computer networks and special application computer systems.

63 CYBERNETICS 194

Includes feedback and control theory, artificial intelligence, robotics and expert systems.

For related information see also 54 *Man/System Technology and Life Support*.

64 NUMERICAL ANALYSIS 194

Includes iteration, difference equations, and numerical approximation.

65 STATISTICS AND PROBABILITY N.A.

Includes data sampling and smoothing; Monte Carlo method; and stochastic processes.

66 SYSTEMS ANALYSIS 196

Includes mathematical modeling; network analysis; and operations research.

67 THEORETICAL MATHEMATICS N.A.

Includes topology and number theory.

PHYSICS

Includes physics (general); acoustics; atomic and molecular physics; nuclear and high-energy physics; optics; plasma physics; solid-state physics; and thermodynamics and statistical physics.

For related information see also *Engineering*.

70 PHYSICS (GENERAL) 196

For precision time and time interval (PTTI) see 35 *Instrumentation and Photography*; for geophysics, astrophysics or solar physics see 46 *Geophysics*, 90 *Astrophysics*, or 92 *Solar Physics*.

- 71 ACOUSTICS** 196
Includes sound generation, transmission, and attenuation.
For noise pollution see 45 *Environment Pollution*.
- 72 ATOMIC AND MOLECULAR PHYSICS** 201
Includes atomic structure, electron properties, and molecular spectra.
- 73 NUCLEAR AND HIGH-ENERGY PHYSICS** 202
Includes elementary and nuclear particles; and reactor theory.
For space radiation see 93 *Space Radiation*.
- 74 OPTICS** 202
Includes light phenomena and optical devices.
For lasers see 36 *Lasers and Masers*.
- 75 PLASMA PHYSICS** 203
Includes magnetohydrodynamics and plasma fusion.
For ionospheric plasmas see 46 *Geophysics*. For space plasmas see 90 *Astrophysics*.
- 76 SOLID-STATE PHYSICS** 204
Includes superconductivity.
For related information see also 33 *Electronics and Electrical Engineering* and 36 *Lasers and Masers*.
- 77 THERMODYNAMICS AND STATISTICAL PHYSICS** 206
Includes quantum mechanics; theoretical physics; and Bose and Fermi statistics.
For related information see also 25 *Inorganic and Physical Chemistry* and 34 *Fluid Mechanics and Heat Transfer*.
- SOCIAL SCIENCES**
Includes social sciences (general); administration and management; documentation and information science; economics and cost analysis; law, political science, and space policy; and urban technology and transportation.
- 80 SOCIAL SCIENCES (GENERAL)** 207
Includes educational matters.
- 81 ADMINISTRATION AND MANAGEMENT** 207
Includes management planning and research.
- 82 DOCUMENTATION AND INFORMATION SCIENCE** 207
Includes information management; information storage and retrieval technology; technical writing; graphic arts; and micrography.
For computer documentation see 61 *Computer Programming and Software*.
- 83 ECONOMICS AND COST ANALYSIS** N.A.
Includes cost effectiveness studies.

- 84 LAW, POLITICAL SCIENCE AND SPACE POLICY** N.A.
Includes NASA appropriation hearings; aviation law space law and policy; international law; international cooperation; and patent policy.

- 85 URBAN TECHNOLOGY AND TRANSPORTATION** 21
Includes applications of space technology to urban problems; technology transfer; technology assessment and surface and mass transportation.
For related information see 03 *Air Transportation and Safety*, 16 *Space Transportation*, and 44 *Energy Production and Conversion*.

SPACE SCIENCES

- Includes space sciences (general); astronomy; astrophysics; lunar and planetary exploration; solar physics and space radiation.
For related information see also *Geosciences*.

- 88 SPACE SCIENCES (GENERAL)** 21

- 89 ASTRONOMY** N.A.
Includes radio, gamma-ray, and infrared astronomy and astrometry.

- 90 ASTROPHYSICS** 21
Includes cosmology; celestial mechanics; space plasmas; and interstellar and interplanetary gases and dust.
For related information see also 75 *Plasma Physics*.

- 91 LUNAR AND PLANETARY EXPLORATION** 21
Includes planetology; and manned and unmanned flights.
For spacecraft design or space stations see 18 *Spacecraft Design, Testing and Performance*.

- 92 SOLAR PHYSICS** N.A.
Includes solar activity, solar flares, solar radiation and sunspots.
For related information see 93 *Space Radiation*.

- 93 SPACE RADIATION** N.A.
Includes cosmic radiation; and inner and outer earth radiation belts.
For biological effects of radiation see 52 *Aerospace Medicine*. For theory see 73 *Nuclear and High-Energy Physics*.

GENERAL

- Includes aeronautical, astronautical, and space science related histories, biographies, and pertinent reports too broad for categorization; histories or broad overview of NASA programs.

- 99 GENERAL** 21

Note: N.A. means that no abstracts were assigned to this category for this issue.

SUBJECT INDEX	A-1
PERSONAL AUTHOR INDEX	B-1
CORPORATE SOURCE INDEX	C-1
CONTRACT NUMBER INDEX	D-1
REPORT/ACCESSION NUMBER INDEX	E-1

Bibliography of Lewis Research Center Technical Publications Announced in 1986

01

AERONAUTICS (GENERAL)

A86-11602*# National Aeronautics and Space Administration. Lewis Research Center, Cleveland, Ohio.

FUTURE DIRECTIONS IN AEROPROPULSION TECHNOLOGY
N. T. SAUNDERS and A. J. GLASSMAN (NASA, Lewis Research Center, Cleveland, OH) IN: International Symposium on Air Breathing Engines, 7th, Beijing, People's Republic of China, September 2-6, 1985, Proceedings. New York, AIAA, 1985, p. 3-22. Previously announced in STAR as N85-23685.

Future directions in aeropropulsion technology that have been identified in a series of studies recently sponsored by the U.S. Government are discussed. Advanced vehicle concepts that could become possible by the turn of the century are presented along with some of their projected capabilities. Key building-block propulsion technologies that will contribute to making these vehicle concepts a reality are discussed along with projections of their status by the year 2000. Some pertinent highlights of the NASA aeropropulsion program are included in the discussion. Author

N86-11146*# National Aeronautics and Space Administration. Lewis Research Center, Cleveland, Ohio.

DEVELOPMENT OF AN EXPLICIT MULTIGRID ALGORITHM FOR QUASI-THREE-DIMENSIONAL VISCOUS FLOWS IN TURBO-MACHINERY

R. V. CHIMA 1985 21 p refs Prepared for presentation at the 24th Aerospace Sci. Meeting, Reno, Nevada, 6-9 Jan. 1986; sponsored by AIAA

(NASA-TM-87128; E-2681; NAS 1.15:87128) Avail: NTIS HC A02/MF A01 CSCL 01B

A rapid quasi three-dimensional analysis was developed for blade-to-blade flows in turbomachinery. The analysis solves the unsteady Euler or thin layer Navier-Stokes equations in a body-fitted coordinate system. It accounts for the effects of rotation, radius change, and stream-surface thickness. The Baldwin-Lomax eddy-viscosity model is used for turbulent flows. The equations which are solved by a two-stage Runge-Kutta scheme made efficient by use of vectorization, a variable time-step, and a flux-based multigrid scheme, are described. A stability analysis is presented for the two-stage scheme. Results for a flat-plate model problem show the applicability of the method to axial, radial, and rotating geometries. Results for a centrifugal impeller and a radial diffuser show that the quasi three-dimensional viscous analysis can be a practical design tool. E.A.K.

02

AERODYNAMICS

Includes aerodynamics of bodies, combinations, wings, rotors, and control surfaces; and internal flow in ducts and turbomachinery.

A86-11065*# Scientific Research Associates, Inc., Glastonbury, Conn.

NUMERICAL STUDY OF THREE-DIMENSIONAL TURBULENT FLOW INTERACTIONS BETWEEN BLOCKAGE MODELS AND WIND TUNNELS INCLUDING LONGITUDINALLY SLOTTED TEST SECTIONS

S.-J. LIN and R. LEVY (Scientific Research Associates, Inc., Glastonbury, CT) AIAA, Applied Aerodynamics Conference, 3rd, Colorado Springs, CO, Oct. 14-16, 1985. 14 p. refs (Contract NAS3-24224)

(AIAA PAPER 85-5017)

A spatial forward-marching approach is applied to compute three-dimensional turbulent flows for several blockage models in free flight, in a solid wall wind tunnel, and in a wind tunnel with longitudinal slots in the test section. The effects of area blockage in the tunnel, model growth and tunnel wall boundary layers, and of the slots are included. The large blockage models are found to have significant wall interference effects which can be reduced by the slots. The effects of the latter are confined to the region near the tunnel wall. Model/wall interference effects are not limited to the effects of area blockage; in particular, boundary layer profile shapes for a wind tunnel model in a tunnel are different from shapes for a model in free flight even when slots are used. This indicates that the flow responds differently in these two cases with the same pressure gradient. C.D.

A86-14561*# Texas Technological Univ., Lubbock.

MULTISPARK FLOW VISUALIZATION OF LATERAL JET INJECTION INTO A SWIRLING CROSS FLOW

G. B. FERRELL (Texas Tech University, Lubbock), K. AOKI, and D. G. LILLEY (Oklahoma State University, Stillwater) Journal of Propulsion and Power (ISSN 0748-4658), vol. 1, Nov.-Dec. 1985, p. 485-487. Previously cited in issue 07, p. 836, Accession no. A85-19490. refs

(Contract NAG3-549)

A86-19644*# National Aeronautics and Space Administration. Lewis Research Center, Cleveland, Ohio.

DEVELOPMENT OF AN EXPLICIT MULTIGRID ALGORITHM FOR QUASI-THREE-DIMENSIONAL VISCOUS FLOWS IN TURBOMACHINERY

R. V. CHIMA (NASA, Lewis Research Center, Cleveland, OH) AIAA, Aerospace Sciences Meeting, 24th, Reno, NV, Jan. 6-9, 1986. 15 p. Previously announced in STAR as N86-11146. refs (AIAA PAPER 86-0032)

A rapid quasi three-dimensional analysis was developed for blade-to-blade flows in turbomachinery. The analysis solves the unsteady Euler or thin layer Navier-Stokes equations in a body-fitted coordinate system. It accounts for the effects of rotation, radius change, and stream-surface thickness. The Baldwin-Lomax eddy-viscosity model is used for turbulent flows. The equations

02 AERODYNAMICS

which are solved by a two-stage Runge-Kutta scheme made efficient by use of vectorization, a variable time-step, and a flux-based multigrid scheme, are described. A stability analysis is presented for the two-stage. Results for a flat-plate model problem show the applicability of the method to axial, radial, and rotating geometries. Results for a centrifugal impeller and a radial diffuser show that the quasi three-dimensional viscous analysis can be a practical design tool. E.A.K.

A86-20131*# Cornell Univ., Ithaca, N.Y.
AN IMPLICIT LU SCHEME FOR THE EULER EQUATIONS APPLIED TO ARBITRARY CASCADES

E. K. BURATYNSKI and D. A. CAUGHEY (Cornell University, Ithaca, NY) AIAA Journal (ISSN 0001-1452), vol. 24, Jan. 1986, p. 39-46. Previously cited in issue 06, p. 705, Accession no. A84-17925. refs
(Contract NAG3-19)

A86-20372*# National Aeronautics and Space Administration.
Lewis Research Center, Cleveland, Ohio.

CALCULATION OF THREE-DIMENSIONAL, VISCOUS FLOW THROUGH TURBOMACHINERY BLADE PASSAGE BY PARABOLIC MARCHING

T. KATSANIS (NASA, Lewis Research Center, Cleveland, OH) Journal of Propulsion and Power (ISSN 0748-4658), vol. 2, Jan.-Feb. 1986, p. 81-90. Previously cited in issue 18, p. 2611, Accession no. A85-39767. refs

A86-20942* National Aeronautics and Space Administration.
Lewis Research Center, Cleveland, Ohio.

ACCELERATED SOLUTION OF THE STEADY EULER EQUATIONS

G. M. JOHNSON (NASA, Lewis Research Center, Cleveland, OH) IN: Advances in computational transonics. Swansea, Wales, Pineridge Press, 1985, p. 473-501. refs

The present paper is concerned with two methods for the accelerated solution of the steady Euler equations. One method makes use of a second-order embedding to facilitate the derivation of the relaxation solution of the steady equations of motion, while the other method employs a multilevel-gridding concept to accelerate the convergence of a simple, explicit, time-marching scheme applied to the unsteady equations. It is pointed out that the surrogate equation technique provides a means for formulating problems involving the full steady Euler equations in such a way as to allow the use of relaxation solution procedures. It is, therefore, possible to solve either irrotational or rotational flow problems spanning the entire spectrum of subsonic, transonic, and supersonic conditions. The solutions can be obtained without an employment of either derived dependent variables, semidirect methods, or an unsteady formulation. G.R.

A86-22046*# Scientific Research Associates, Inc., Glastonbury, Conn.

CALCULATIONS OF TWO AND THREE-DIMENSIONAL TRANSONIC CASCADE FLOW FIELDS USING THE NAVIER-STOKES EQUATIONS

B. C. WEINBERG, R.-J. YANG, H. MCDONALD, and S. J. SHAMROTH (Scientific Research Associates, Inc., Glastonbury, CT) ASME, International Gas Turbine Conference and Exhibit, 30th, Houston, TX, Mar. 18-21, 1985. 10 p. refs
(Contract NAS3-23695)
(ASME PAPER 85-GT-66)

The multidimensional, ensemble-averaged, compressible, time-dependent Navier-Stokes equations have been used to study the turbulent flow field in two and three-dimensional turbine cascades. The viscous regions of the flow were resolved and non-slip boundary conditions were utilized on solid surfaces. The calculations were performed in a constructive 'O'-type grid which allows representation of the blade rounded trailing edge. Converged solutions were obtained in relatively few time steps (about 80-150) and comparisons for both surface pressure and heat transfer showed good agreement with data. The three-dimensional turbine

cascade calculation showed many of the expected flow-field features. Author

A86-22102*# Flow Application Research, Fremont, Calif.
MODELING THE 3-D FLOW EFFECTS ON DEVIATION ANGLE FOR AXIAL COMPRESSOR MIDDLE STAGES

W. B. ROBERTS (Flow Application Research, Fremont, CA), G. K. SEROVY (Iowa State University of Science and Technology, Ames), and D. M. SANDERCOCK (NASA, Lewis Research Center, Cleveland, OH) ASME, International Gas Turbine Conference and Exhibit, 30th, Houston, TX, Mar. 18-21, 1985. 7 p. refs
(Contract NAG3-521)
(ASME PAPER 85-GT-189)

A model of the spanwise variation of the three-dimensional flow effects on deviation is proposed for middle-stage rotors and stators. This variation is taken as the difference above or below that predicted by blade element theory at any spanwise location. It was found that the stator variation is strongly affected by the end-wall boundary-layer thickness as well as camber, solidity, and blade channel aspect ratio. Rotor variation was found to depend on end-wall boundary layer thickness and tip clearance normalized by blade span. If these parameters are known or can be calculated, the models provide a reasonable approximation to the spanwise variation of deviation for middle compressor stages operating at low to high subsonic inlet Mach numbers. Author

A86-22123*# National Aeronautics and Space Administration.
Lewis Research Center, Cleveland, Ohio.

MODEL EQUATION FOR SIMULATING FLOWS IN MULTISTAGE TURBOMACHINERY

J. J. ADAMCZYK (NASA, Lewis Research Center, Cleveland, OH) ASME, International Gas Turbine Conference and Exhibit, 30th, Houston, TX, Mar. 18-21, 1985. 13 p. Previously announced in STAR as N85-12036. refs
(ASME PAPER 85-GT-226)

A steady, three-dimensional average-passage equation system is derived for use in simulating multistage turbomachinery flows. These equations describe a steady, viscous flow that is periodic from blade passage to blade passage. From this system of equations, various reduced forms can be derived for use in simulating the three-dimensional flow field within multistage machinery. It is suggested that a properly scaled form of the averaged-passage equation system would provide an improved mathematical model for simulating the flow in multistage machines at design and, in particular, at off-design conditions. Author

A86-22693*# National Aeronautics and Space Administration.
Lewis Research Center, Cleveland, Ohio.

VELOCITY AND TEMPERATURE DECAY CHARACTERISTICS OF INVERTED-PROFILE JETS

U. VON GLAHN, J. GOODYKOONTZ, and C. WASSERBAUER (NASA, Lewis Research Center, Cleveland, OH) AIAA, Aerospace Sciences Meeting, 24th, Reno, NV, Jan. 6-9, 1986. 31 p. Previously announced in STAR as N86-14223. refs
(AIAA PAPER 86-0312)

In order to design efficient, lightweight flap systems for future engine under-the-wing STOL aircraft, the velocity and temperature decay rate of the jet plume must be increased relative to that for single-stream nozzles in order to provide local flap loads and structural temperatures within acceptable limits. The jet plume decay rate of dual flow engines can be increased by resorting to inverted-profile velocity and temperature nozzle concepts. The peak axial decay characteristics of model-scale, two-stream inverted-profile nozzle flows are empirically correlated. Also discussed are the radial and spreading characteristics of inverted-profile nozzle flows. Author

A86-22731*# National Aeronautics and Space Administration. Lewis Research Center, Cleveland, Ohio.

UNSTEADY PRESSURE MEASUREMENTS ON A BICONVEX AIRFOIL IN A TRANSONIC OSCILLATING CASCADE

L. M. SHAW, D. R. BOLDMAN, A. E. BUGGELE (NASA, Lewis Research Center, Cleveland, OH), and D. H. BUFFUM (Purdue University, West Lafayette, IN) ASME, Transactions, Journal of Engineering for Gas Turbines and Power (ISSN 0022-0825), vol. 108, Jan. 1986, p. 53-59. Previously announced in STAR as N85-15689. refs

(ASME PAPER 85-GT-212)

Flush-mounted dynamic pressure transducers were installed on the center airfoil of a transonic oscillating cascade to measure the unsteady aerodynamic response as nine airfoils were simultaneously driven to provide 1.2 deg of pitching motion about the midchord. Initial tests were performed at an incidence and angle of 0 deg and a Mach number of 0.65 in order to obtain results in a shock-free compressible flowfield. Subsequent tests were performed at an incidence angle of 7 deg and Mach number of 0.8 in order to observe the surface pressures with an oscillating shock near the leading edge of the airfoil. Results are presented for interblade phase angles of 90 and -90 deg and at blade oscillatory frequencies of 200 and 500 Hz (semi-chord reduced frequencies up to about 0.5 at a Mach number of 0.8). Results from the zero-incidence cascade are compared with a classical unsteady flat-plate analysis. Flow visualization results depicting the shock motion on the airfoils in the high-incidence cascade are discussed. The airfoil pressure data are tabulated. Author

A86-22732*# National Aeronautics and Space Administration. Lewis Research Center, Cleveland, Ohio.

AERODYNAMIC DETUNING ANALYSIS OF AN UNSTALLED SUPERSONIC TURBOFAN CASCADE

D. HOYNIK (NASA, Lewis Research Center, Cleveland, OH) and S. FLEETER (Purdue University, West Lafayette, IN) ASME, Transactions, Journal of Engineering for Gas Turbines and Power (ISSN 0022-0825), vol. 108, Jan. 1986, p. 60-67. Previously announced in STAR as N85-26670. refs

(ASME PAPER 85-GT-192)

An approach to passive flutter control is aerodynamic detuning, defined as designed passage-to-passage differences in the unsteady aerodynamic flow field of a rotor blade row. Thus, aerodynamic detuning directly affects the fundamental driving mechanism for flutter. A model to demonstrate the enhanced supersonic aeroelastic stability associated with aerodynamic detuning is developed. The stability of an aerodynamically detuned cascade operating in a supersonic inlet flow field with a subsonic leading edge locus analyzed, with the aerodynamic detuning accomplished by means of nonuniform circumferential spacing of adjacent rotor blades. The unsteady aerodynamic forces and moments on the blading are defined in terms of influence coefficients in a manner that permits the stability of both a conventional uniformly spaced rotor configuration as well as the detuned nonuniform circumferentially spaced rotor to be determined. With Verdon's uniformly spaced Cascade B as a baseline, this analysis is then utilized to demonstrate the potential enhanced aeroelastic stability associated with this particular type of aerodynamic detuning. Author

A86-22733*# National Aeronautics and Space Administration. Lewis Research Center, Cleveland, Ohio.

A THREE-DIMENSIONAL AXISYMMETRIC CALCULATION PROCEDURE FOR TURBULENT FLOWS IN A RADIAL VANELESS DIFFUSER

L. F. SCHUMANN (NASA, Lewis Research Center; U.S. Army, Propulsion Laboratory, Cleveland, OH) ASME, Transactions, Journal of Engineering for Gas Turbines and Power (ISSN 0022-0825), vol. 108, Jan. 1986, p. 118-124. Previously announced in STAR as N85-14798. refs

(ASME PAPER 85-GT-133)

An analytical model is proposed to calculate the three-dimensional axisymmetric turbulent flowfield in a radial vaneless diffuser. The model assumes that the radial and tangential

boundary layer profiles are approximated by power law profiles. Then, using the integrated radial and tangential momentum and continuity equations for the boundary layer and corresponding inviscid equations for the core flow, there results six ordinary differential equations in six unknowns which are easily solved using a Runge-Kutta technique. A model is also proposed for fully developed flow. The results using this technique were compared with the results from a three-dimensional viscous, axisymmetric duct code and with experimental data and good quantitative agreement was obtained. Author

A86-23141*# National Aeronautics and Space Administration. Lewis Research Center, Cleveland, Ohio.

UNSTEADY TRANSONIC FLOW OVER CASCADE BLADES

S. P. SURAMPUDI and J. J. ADAMCZYK (NASA, Lewis Research Center, Cleveland, OH) AIAA Journal (ISSN 0001-1452), vol. 24, Feb. 1986, p. 293-302. refs

An attempt is made to develop an efficient staggered cascade blade unsteady aerodynamics model for the neighborhood of March 1, representing the blade row by a rectilinear two-dimensional cascade of thin, flat plate airfoils. The equations of motion are derived on the basis of linearized transonic small perturbation theory, and an analytical solution is obtained by means of the Wiener-Hopf procedure. Making use of the transonic similarity law, the results obtained are compared with those of other linearized cascade analyses. A parametric study is conducted to find the effects of reduced frequency, stagger angle, solidity, and the location of the pitching axis on cascade stability. O.C.

A86-23854*# United Technologies Research Center, East Hartford, Conn.

THROUGH-FLOW MODELING OF AXIAL TURBOMACHINERY

R. P. DRING and H. D. JOSLYN (United Technologies Research Center, East Hartford, CT) ASME, Chinese Society of Aeronautics and Astronautics, and China National Aero-Technology Import and Export Corp., Beijing International Gas Turbine Symposium and Exposition, Beijing, People's Republic of China, Sept. 1-7, 1985. 12 p. refs

(Contract F33615-77-C-2083; NAS3-23157; N00014-84-C-0354)

(ASME PAPER 85-IGT-42)

Through-flow analysis practices are presently evaluated by comparing their results with the flow measured on a single-stage compressor rotor that had been tested at the nominal design flow coefficient of 0.85, using both thick and thin inlet endwall boundary layers. Sufficient experimental data was available for both the required aerodynamic input of the calculations and the detailed assessment of the computational results obtained. It is noted that, while through-flow theory reasonably characterizes many aspects of the flow, the features less well predicted suggest the need for a more precise formulation of the equation, and the inclusion of such often neglected effects as the radial component of blade force and/or the fluctuation terms due to the flow's nonaxisymmetry, as found in the phenomenon of blockage. O.C.

A86-23927*# Naval Postgraduate School, Monterey, Calif.

A NOVEL CENTRIFUGAL DIFFUSER TEST DEVICE

R. P. SHREEVE, H. D. SCHULZ, J. R. ERWIN (U.S. Naval Postgraduate School, Monterey, CA), and L. SCHUMANN (NASA, Lewis Research Center, Cleveland, OH) ASME, Chinese Society of Aeronautics and Astronautics, and China National Aero-Technology Import and Export Corp., Beijing International Gas Turbine Symposium and Exposition, Beijing, People's Republic of China, Sept. 1-7, 1985. 14 p. Army-supported research. refs

(ASME PAPER 85-IGT-135)

A large scale (2 in.-wide test vanes at 50-in. inlet diameter), low speed (100-200 ft/sec) steady flow radial cascade wind tunnel for diffuser studies was designed, built and tested. The apparatus was shown to provide flow angles (from radial) in the range of 58-72 deg with suitable spanwise profiles. The novel flow angle control mechanism was shown to work, but measured flow angles were somewhat smaller than expected. The mechanism for controlling case-wall boundary layer profile did not behave as predicted. Attempts to predict the generated flow both analytically

02 AERODYNAMICS

and with computational codes are compared with initial measurements. The low speed apparatus will be used to obtain detailed data for diffuser design and analysis code verification, and to provide experience toward the design of a high speed device. Author

A86-24693* Cleveland State Univ., Ohio.

UNSTEADY TRANSONIC FLOW IN CASCADES

S. P. SURAMPUDI (Cleveland State University, OH) and J. J. ADAMCZYK (NASA, Lewis Research Center, Cleveland, OH) IN: Unsteady aerodynamics of turbomachines and propellers; Proceedings of the Symposium, Cambridge, England, September 24-27, 1984. Cambridge, Cambridge University, 1984, p. 255-260. Previously announced in STAR as N84-32351. refs

There is a need for methods to predict the unsteady air loads associated with flutter of turbomachinery blading at transonic speeds. The results of such an analysis in which the steady relative flow approaching a cascade of thin airfoils is assumed to be transonic, irrotational, and isentropic is presented. The blades in the cascade are allowed to undergo a small amplitude harmonic oscillation which generates a small unsteady flow superimposed on the existing steady flow. The blades are assumed to oscillate with a prescribed motion of constant amplitude and interblade phase angle. The equations of motion are obtained by linearizing about a uniform flow the inviscid nonheat conducting continuity and momentum equations. The resulting equations are solved by employing the Weiner Hopf technique. The solution yields the unsteady aerodynamic forces acting on the cascade at Mach number equal to 1. Making use of an unsteady transonic similarity law, these results are compared with the results obtained from linear unsteady subsonic and supersonic cascade theories. A parametric study is conducted to find the effects of reduced frequency, solidity, stagger angle, and position of pitching axis on the flutter. Author

A86-24920* National Aeronautics and Space Administration, Lewis Research Center, Cleveland, Ohio.

VORTEX GENERATORS AS A MEANS FOR INCREASING ROTOR PERFORMANCE

R. D. CORRIGAN and J. M. SAVINO (NASA, Lewis Research Center, Cleveland, OH) IN: Intersociety Energy Conversion Engineering Conference, 20th, Miami Beach, FL, August 18-23, 1985, Proceedings. Volume 3. Warrendale, PA, Society of Automotive Engineers, Inc., 1985, p. 3.663-3.668. refs

Field tests on a horizontal axis wind turbine (HAWT) have shown that Vortex Generators (VGs) can increase the efficiency of large propeller type (horizontal axis) wind turbines. VGs are devices which are attached to the surfaces of an aerodynamic body to influence the boundary layer behavior. It is pointed out that VGs were originally developed for delaying stall on aircraft wings. An investigation was conducted regarding the possibility to employ VGs also for the improvement of the performance of an intermediate size HAWT with a diameter in the range from 24 to 46 meters. This investigation included wind tunnel tests involving a rotor blade tip section, and field tests. The wind tunnel tests showed that VGs can improve the peak lift capabilities of the section while only slightly increasing the drag. The field tests showed that VGs can increase the rotor power in winds above 6 m/s. G.R.

A86-26412* Clemson Univ., S.C.

INVERSE DESIGN OF AXISYMMETRIC FLOW PASSAGES USING COMPRESSIBLE VISCOUS FLOW THEORY

F. NTONE and T.-T. YANG (Clemson University, SC) (International Conference on Inverse Design Concepts in Engineering Sciences, Austin, TX, Oct. 17-19, 1984) Communications in Applied Numerical Methods (ISSN 0748-8025), vol. 2, Jan.-Feb. 1986, p. 83-89. Research supported by the South Carolina Energy Research and Development Center. refs (Contract NAG3-538)

A study reported by Yang and Hudson (1971) was extended by Nelson (1971), who presented a method of inverse design for axisymmetric diffusers. The diffusers obtained with the aid of this

method were found to function well under certain conditions, while, for other cases, a modification of the analytical design procedure was required. An outline is provided of the method of inverse solution in simple axisymmetric internal flow passages. Attention is given to governing equations, the method of solution, and examples which illustrate the feasibility of the design procedure. The discussed method, which is based on viscous compressible flow theory, has some limitations. However, it is expected to yield good designs in many practical cases in which the existing design must be modified. G.R.

A86-28538*# California Univ., Los Angeles.

AN ANALYTICAL MODEL FOR THE VORTICITY ASSOCIATED WITH A TRANSVERSE JET

A. R. KARAGOZIAN (California, University, Los Angeles) AIAA Journal (ISSN 0001-1452), vol. 24, March 1986, p. 429-436. Previously cited in issue 17, p. 2427, Accession no. A84-38042. refs (Contract NAG3-543)

A86-28682* Cincinnati Univ., Ohio.

THREE DIMENSIONAL FLOW PHENOMENA IN FLUID MACHINERY; PROCEEDINGS OF THE WINTER ANNUAL MEETING, MIAMI BEACH, FL, NOVEMBER 17-22, 1985

A. HAMED, ED. (Cincinnati, University, OH), J. HERRING, ED. (Dynamics of Princeton, NJ), and L. POVINELLI, ED. (NASA, Lewis Research Center, Cleveland, OH) Meeting sponsored by ASME. New York, American Society of Mechanical Engineers (Fluids Engineering Symposia Series. Volume FED-32), 1985, 235 p. For individual items see A86-28683 to A86-28707.

For papers presented in this volume provide an overview of the latest developments in experimental measurements and analytical and numerical predictions of three-dimensional flows in fluid machinery. Topics discussed include three-dimensional cascade testing of turbine nozzles at high exit Mach number; the use of a secondary flow computation in the compressor design process; an experimental investigation of static propeller flow field; and calculation of three-dimensional boundary layers on rotating turbine blades. Papers are also presented on a three-dimensional solution method for turbomachinery analysis; analysis of rotational inviscid flows in curved passages; and a mathematical model for the analysis of fluid flow in a scroll. V.L.

A86-28702*# National Aeronautics and Space Administration, Lewis Research Center, Cleveland, Ohio.

THREE-DIMENSIONAL INVISCID ANALYSIS OF RADIAL-TURBINE FLOW AND A LIMITED COMPARISON WITH EXPERIMENTAL DATA

Y. K. CHOO (NASA, Lewis Research Center, Cleveland, OH) and K. C. CIVINSKAS (U.S. Army, Propulsion Laboratory, Cleveland, OH) IN: Three dimensional flow phenomena in fluid machinery; Proceedings of the Winter Annual Meeting, Miami Beach, FL, November 17-22, 1985. New York, American Society of Mechanical Engineers, 1985, p. 181-190. Previously announced in STAR as N86-10017. refs

The three-dimensional inviscid DENTON code is used to analyze flow through a radial-inflow turbine rotor. Experimental data from the rotor are compared with analytical results obtained by using the code. The experimental data available for comparison are the radial distributions of circumferentially averaged values of absolute flow angle and total pressure downstream of the rotor exit. The computed rotor-exit flow angles are generally underturned relative to the experimental values, which reflect the boundary-layer separation at the trailing edge and the development of wakes downstream of the rotor. The experimental rotor is designed for a higher-than-optimum work factor of 1.126 resulting in a nonoptimum positive incidence and causing a region of rapid flow adjustment and large velocity gradients. For this experimental rotor, the computed radial distribution of rotor-exit to turbine-inlet total pressure ratios are underpredicted due to the errors in the finite-difference approximations in the regions of rapid flow adjustment, and due to using the relatively coarser grids in the middle of the blade region where the flow passage is highly

three-dimensional. Additional results obtained from the three-dimensional inviscid computation are also presented, but without comparison due to the lack of experimental data. These include quasi-secondary velocity vectors on cross-channel surfaces, velocity components on the meridional and blade-to-blade surfaces, and blade surface loading diagrams. Computed results show the evolution of a passage vortex and large streamline deviations from the computational streamwise grid lines. Experience gained from applying the code to a radial turbine geometry is also discussed.

Author

A86-35855* Ohio State Univ., Columbus.

THE AERODYNAMICS OF ROTOR BLADES WITH ICE SHAPES ACCRETED IN HOVER AND IN LEVEL FLIGHT

J. D. LEE (Ohio State University, Columbus) and R. J. SHAW (NASA, Lewis Research Center, Cleveland, OH) IN: American Helicopter Society, Annual Forum, 41st, Fort Worth, TX, May 15-17, 1985, Proceedings. Alexandria, VA, American Helicopter Society, 1985, p. 735-742. refs

Through a series of flights in artificial clouds, ice accretions on the main rotor of a UH-1H helicopter were documented in detail upon landing by silicone-rubber molds for both hover and level flights. Full scale reproductions of typical accretions in hover were fabricated by means of epoxy castings and used for a wind-tunnel test program. Surface static pressure distributions were recorded and used to evaluate lift and pitching moment increments while drag was determined by wake surveys. For comparison, accreted ice shapes are presented for two level flight cases as well as preliminary analytical predictions.

Author

A86-35855* National Aeronautics and Space Administration. Lewis Research Center, Cleveland, Ohio.

FLOW FIELD AND NEAR AND FAR SOUND FIELD OF A SUBSONIC JET

K. B. M. Q. ZAMAN (NASA, Lewis Research Center, Cleveland, OH) *Journal of Sound and Vibration* (ISSN 0022-460X), vol. 106, April 8, 1986, p. 1-16. refs

Flow and sound field data are presented for a 2.54 cm diameter air jet at a Mach number of 0.50 and a Reynolds number of 300,000. Distributions of mean velocity, turbulence intensities, Reynolds stress, spectral components of turbulence as well as of the near field pressure, together with essential characteristics of the far field sound are reported. This detailed set of data for one particular flow, erstwhile unavailable in the literature, is expected to help promote and calibrate subsonic jet noise theories. 'Source locations' in terms of the turbulence maxima, coupling between the entrainment dynamics and the near pressure field, the sound radiation paths, and the balance in mass, momentum and sound energy fluxes are discussed. The results suggest that the large scale coherent structures of the jet govern the 'source locations' by controlling the turbulence and also strongly influence the near field pressure fluctuations.

Author

A86-38480* National Aeronautics and Space Administration. Lewis Research Center, Cleveland, Ohio.

ANALYSIS OF FULLY STALLED COMPRESSOR

W. ROSTAFINSKI (NASA, Lewis Research Center, Cleveland, OH) AIAA and ASME, Fluid Mechanics, Plasma Dynamics and Lasers Conference, 4th, Atlanta, GA, May 12-14, 1986. 9 p. Previously announced in STAR as N86-20357. refs (AIAA PAPER 86-1123)

An analysis yields a model for energy transfer in compressor stages operating in the closed-throttle condition. The derivation indicates that three geometry parameters (hub/tip ratio, aspect ratio, and rotor blade setting angle) influence the values of pressure coefficient when the compressor flow is close to zero.

Author

A86-38896* California Univ., Los Angeles.

PACKET FLUTTER AND AERODYNAMIC MODES FOR NON-HOMOGENEOUS AIRFOIL CASCADES IN HIGHLY DISTORTED, PERIODIC, STATIONARY THROUGHFLOWS

V. G. MENGLE (California, University, Los Angeles) IN: Structures, Structural Dynamics and Materials Conference, 27th, San Antonio, TX, May 19-21, 1986, Technical Papers. Part 2. New York, American Institute of Aeronautics and Astronautics, 1986, p. 131-141. refs

(Contract NAG3-483)

(AIAA PAPER 86-0848)

An analytical investigation of the general flutter characteristics of periodically detuned airfoil cascades kept in periodically nonuniform basic flows is conducted under the assumption of linearized aerodynamics. The existence of certain packet flutter modes is studied, as are the specific aerodynamic modes to be used in the calculation of the aerodynamic coefficients such that the number of blade passages in the computational domain is minimized. The interpretation of the critical flutter condition for nonuniform flows is examined.

C.D.

A86-39064* Pennsylvania State Univ., University Park.

LASER DOPPLER VELOCIMETER MEASUREMENT IN THE TIP REGION OF A COMPRESSOR ROTOR

K. N. S. MURTHY and B. LAKSHMINARAYANA (Pennsylvania State University, University Park) *AIAA Journal* (ISSN 0001-1452), vol. 24, May 1986, p. 807-814. Previously cited in issue 18, p. 2569, Accession no. A84-39304. refs

(Contract NSG-3212)

A86-39089* Pennsylvania State Univ., University Park.

COMPUTATION OF VISCOUS FLOWS IN TURBOMACHINERY CASCADES WITH A SPACE-MARCHING METHOD

M. POUAGARE, B. LAKSHMINARAYANA, and T. R. GOVINDAN (Pennsylvania State University, University Park) (Computation of internal flows: Methods and applications; Proceedings of the Energy Sources Technology Conference, New Orleans, LA, February 12-16, 1984, p. 1-10) *Journal of Propulsion and Power* (ISSN 0748-4658), vol. 2, May-June 1986, p. 266-274. Previously cited in issue 02, p. 141, Accession no. A85-11631. refs

(Contract NSG-3266)

A86-39090* United Technologies Research Center, East Hartford, Conn.

THREE-DIMENSIONAL INVISCID FLOW IN MIXERS. I - MIXER ANALYSIS USING A CARTESIAN GRID

T. J. BARBER (United Technologies Research Center, East Hartford, CT), G. L. MULLER, S. M. RAMSAY (United Technologies Corp., Pratt and Whitney, East Hartford, CT), and E. M. MURMAN (MIT, Cambridge, MA) *Journal of Propulsion and Power* (ISSN 0748-4658), vol. 2, May-June 1986, p. 275-281. Previously cited in issue 07, p. 837, Accession no. A85-19510. refs

(Contract NAS3-23039)

A86-41723* Cornell Univ., Ithaca, N.Y.

TRANSONIC POTENTIAL FLOW IN HYPERBOLIC NOZZLES

M. PARK and D. A. CAUGHEY (Cornell University, Ithaca, NY) *AIAA Journal* (ISSN 0001-1452), vol. 24, June 1986, p. 1037-1039. refs

(Contract NAG3-19)

The full potential equation for the classical problem of transonic flow through a hyperbolic nozzle (with or without a shock wave) is solved in conservation form using the finite volume method of Jameson and Caughey (1977). Either a first or a second-order numerical viscosity is added in the direction of the flow, explicitly, in conservation form. A multigrid alternating direction implicit method is used to solve the difference equations, and the results obtained are compared with analytical and numerical results from previous researches.

O.C.

02 AERODYNAMICS

A86-42687*# National Aeronautics and Space Administration. Lewis Research Center, Cleveland, Ohio.

AN LU IMPLICIT SCHEME FOR HIGH SPEED INLET ANALYSIS

S. YOON (NASA, Lewis Research Center; Sverdrup Technology, Inc., Cleveland, OH) and A. JAMESON (Princeton University, NJ) AIAA, ASME, SAE, and ASEE, Joint Propulsion Conference, 22nd, Huntsville, AL, June 16-18, 1986. 7 p. refs (AIAA PAPER 86-1520)

A numerical method is developed to analyze the inviscid flowfield of a high speed inlet by the solution of the Euler equations. The LU implicit scheme in conjunction with adaptive dissipation proves to be an efficient and robust nonoscillatory shock capturing technique for high Mach number flows as well as for transonic flows. Author

A86-42688*# National Aeronautics and Space Administration. Lewis Research Center, Cleveland, Ohio.

IMPROVED EULER ANALYSIS OF ADVANCED TURBOPROP PROPELLER FLOWS

O. YAMAMOTO, J. M. BARTON (Sverdrup Technology, Inc., Middleburg Heights, OH), and L. J. BOBER (NASA, Lewis Research Center, Cleveland, OH) AIAA, ASME, SAE, and ASEE, Joint Propulsion Conference, 22nd, Huntsville, AL, June 16-18, 1986. 10 p. refs (Contract NAS3-24105)

(AIAA PAPER 86-1521)

An implicit approximate factorization scheme in conjunction with a new boundary treatment was used to compute the inviscid flow field about an advanced high-speed propeller. The method of characteristics was used to apply impermeable boundary conditions. The convergence history of numerical calculations shows substantial decrease in the residual error decay. Euler solutions were computed for SR-3 propeller geometry and the results were compared with the experimental data and previous numerical results. Author

A86-42709*# Lockheed-Georgia Co., Marietta.

EVALUATION OF PROPELLER/NACELLE INTERACTIONS IN THE PTA PROGRAM

A. S. ALJABRI, V. LYMAN, and R. J. PARKER (Lockheed-Georgia Co., Marietta) AIAA, ASME, SAE, and ASEE, Joint Propulsion Conference, 22nd, Huntsville, AL, June 16-18, 1986. 11 p. refs (Contract NAS3-24339)

(AIAA PAPER 86-1552)

Advanced highly-loaded propellers are proposed to power transport aircraft that cruise at high subsonic speeds giving significant fuel savings over the equivalent turbofan engine. In order to realize these savings, the propeller must be installed so that the aerodynamics of the propeller/nacelle combination do not lead to excessive cyclic blade stresses or installation losses. The on-going, NASA sponsored, Propfan Test Assessment Program (PTA) has provided the first high-speed wind-tunnel data on an installed propfan complete with an inlet. This paper presents computational techniques that allow: (1) optimization of inlet plane location, (2) contouring of lip and cowl, and (3) estimation of propeller cyclic loads due to a nonuniform flowfield. These computational methods, in spite of the complexity of the configuration and the slipstream effects, provide predictions of aerodynamic performance which are in excellent agreement with wind-tunnel data. Author

A86-42740*# Pennsylvania State Univ., University Park.

A COMPARISON OF COMPUTATIONAL METHODS FOR THREE-DIMENSIONAL, TURBULENT TURBOMACHINERY FLOW FIELDS

K. R. KIRTLEY, M. WARFIELD, and B. LAKSHMINARAYANA (Pennsylvania State University, University Park) AIAA, ASME, SAE, and ASEE, Joint Propulsion Conference, 22nd, Huntsville, AL, June 16-18, 1986. 11 p. refs

(Contract NSG-3266)

(AIAA PAPER 86-1599)

A space-marching method and a time-marching method have been used to compute the three-dimensional turbulent flow in an end wall cascade of airfoils. Using an identical grid and turbulence model, the two codes were used to predict a variety of flow quantities. Predictions by the two methods are compared to each other and to experimental data. In general both methods predict measured quantities well, with a small edge in prediction accuracy going to the space-marching method. Secondary flow comparisons show the time-marching solution more accurately predicting the underturning of the flow in the outer portion of the end wall boundary layer while the space-marching method more accurately predicted the overturning of the flow very near the end wall. The prediction comparisons are discussed along with computational details and other attributes of the two methods. Author

A86-42760*# National Aeronautics and Space Administration. Lewis Research Center, Cleveland, Ohio.

A NUMERICAL ANALYSIS APPLIED TO HIGH ANGLE OF ATTACK THREE-DIMENSIONAL INLETS

D. P. HWANG (NASA, Lewis Research Center, Cleveland, OH) AIAA, ASME, SAE, and ASEE, Joint Propulsion Conference, 22nd, Huntsville, AL, June 16-18, 1986. 9 p. Previously announced in STAR as N86-24658. refs

(AIAA PAPER 86-1527)

The three-dimensional analytical methods used to analyze subsonic high angle of attack inlets are described. The methods are shown to be in good agreement with experimental results for various three-dimensional high angle of attack inlets. The methods are used to predict aerodynamic characteristics of scarf and slotted-lip inlets. E.A.K.

A86-46316*# United Technologies Research Center, East Hartford, Conn.

THREE-DIMENSIONAL INVISCID FLOW IN MIXERS. II - ANALYSIS OF TURBOFAN FORCED MIXERS

T. J. BARBER (United Technologies Research Center, East Hartford, CT), G. L. MULLER, S. M. RAMSAY (Pratt and Whitney, East Hartford, CT), and E. M. MURMAN (MIT, Cambridge, MA) Journal of Propulsion and Power (ISSN 0748-4658), vol. 2, July-Aug. 1986, p. 339-344. refs

(Contract NAS3-23039)

A small disturbance formulation for the three-dimensional potential analysis of the inviscid flow over a turbofan forced mixer configuration in which the governing equations are reduced by means of a flux volume formulation along a Cartesian grid is presently extended to include the effects of power addition within the potential formulation. Calculations are presented for practical turbofan mixer designs, and comparison calculations are also given with measured surface pressure distributions and measured axial velocity profiles. O.C.

A86-46324*# Virginia Polytechnic Inst. and State Univ., Blacksburg.

REAL GAS EFFECTS ON THE NUMERICAL SIMULATION OF A HYPERSONIC INLET

W.-F. NG (Virginia Polytechnic Institute and State University, Blacksburg), T. J. BENSON, and W. G. KUNIK (NASA, Lewis Research Center, Cleveland, OH) Journal of Propulsion and Power (ISSN 0748-4658), vol. 2, July-Aug. 1986, p. 381, 382.

The present use of a parabolized Navier-Stokes solver to accurately simulate the flowfield in a supersonic inlet yields good agreement between numerical analysis and experiment for a Mach 7.4 inlet under cruise conditions, with an internal compression

ratio of 8. The significance of real gas effects on the performance calculation of a hypersonic inlet is demonstrated, with small changes in the ratio of specific heats resulting in a substantial change in the calculated pitot pressure ratio. O.C.

A86-48117*# Avco Corp., Stratford, Conn.
COMPUTATION OF THREE-DIMENSIONAL, ROTATIONAL FLOW THROUGH TURBOMACHINERY BLADE ROWS FOR IMPROVED AERODYNAMIC DESIGN STUDIES

S. V. SUBRAMANIAN, R. BOZZOLA (AVCO Corp., AVCO Lycoming Textron, Stratford, CT), and L. A. POVINELLI (NASA, Lewis Research Center, Cleveland, OH) ASME, International Gas Turbine Conference and Exhibit, 31st, Duesseldorf, West Germany, June 8-12, 1986. 7 p. refs
 (ASME PAPER 86-GT-26)

The performance of a three dimensional computer code developed for predicting the flowfield in stationary and rotating turbomachinery blade rows is described in this study. The four stage Runge-Kutta numerical integration scheme is used for solving the governing flow equations and yields solution to the full, three dimensional, unsteady Euler equations in cylindrical coordinates. This method is fully explicit and uses the finite volume, time marching procedure. In order to demonstrate the accuracy and efficiency of the code, steady solutions were obtained for several cascade geometries under widely varying flow conditions. Computed flowfield results are presented for a fully subsonic turbine stator and a low aspect ratio, transonic compressor rotor blade under maximum flow and peak efficiency design conditions. Comparisons with Laser Anemometer measurements and other numerical predictions are also provided to illustrate that the present method predicts important flow features with good accuracy and can be used for cost effective aerodynamic design studies.

Author

A86-48126*# National Aeronautics and Space Administration. Lewis Research Center, Cleveland, Ohio.

VALIDATION OF VISCOUS AND INVISCID COMPUTATIONAL METHODS FOR TURBOMACHINERY COMPONENTS

L. A. POVINELLI (NASA, Lewis Research Center, Cleveland, OH) ASME, International Gas Turbine Conference and Exhibit, 31st, Duesseldorf, West Germany, June 8-12, 1986. 11 p. Previously announced in STAR as N86-16194. refs
 (ASME PAPER 86-GT-42)

An assessment of several three-dimensional computer codes used at the NASA Lewis Research Center is presented. Four flow situations are examined, for which both experimental data and computational results are available. The four flows form a basis for the evaluation of the computational procedures. It is concluded that transonic rotor flow at peak efficiency conditions may be calculated with a reasonable degree of accuracy, whereas, off-design conditions are not accurately determined. Duct flows and turbine cascade flows may also be computed with reasonable accuracy whereas radial inflow turbine flow remains a challenging problem.

Author

A86-48153*# United Technologies Research Center, East Hartford, Conn.

ON THE APPLICATION OF A LINEARIZED UNSTEADY POTENTIAL-FLOW ANALYSIS TO FAN-TIP CASCADES

W. J. USAB, JR. and J. M. VERDON (United Technologies Research Center, East Hartford, CT) ASME, International Gas Turbine Conference and Exhibit, 31st, Duesseldorf, West Germany, June 8-12, 1986. 9 p. refs
 (Contract F33515-79-C-2087; NAS3-23696)
 (ASME PAPER 86-GT-87)

A linearized potential flow analysis, which accounts for the effects of nonuniform steady flow phenomena on the unsteady response to prescribed blade motions, has been applied to five two-dimensional cascade configurations. These include a flat-plate cascade and three cascades which are representative of the tip sections of current fan designs. Here the blades are closely spaced, highly staggered, and operate at low mean incidence. The fifth configuration is a NASA Lewis cascade of symmetric biconvex

airfoils for which experimental measurements are available. Numerical solutions are presented that clearly illustrate the effects and importance of blade geometry and mean blade loading on the linearized unsteady response at high subsonic inlet Mach number and high blade-vibrational frequency. In addition, a good qualitative agreement is shown between the analytical predictions and experimental measurements for the cascade of symmetric biconvex airfoils. Finally, recommendations on the research needed to extend the range of application of linearized unsteady aerodynamic analyses are provided. Author

A86-48181*# Cincinnati Univ., Ohio.

THREE-DIMENSIONAL FLOW FIELD MEASUREMENTS IN A RADIAL INFLOW TURBINE SCROLL USING LDV

M. F. MALAK, A. HAMED, and W. TABAKOFF (Cincinnati, University, OH) ASME, International Gas Turbine Conference and Exhibit, 31st, Duesseldorf, West Germany, June 8-12, 1986. 7 p. refs
 (Contract NAG3-26)
 (ASME PAPER 86-GT-122)

The results of an experimental study of the three-dimensional flow field in a radial inflow turbine scroll are presented. A two-color LDV system was used in the measurement of three orthogonal velocity components at 758 points located throughout the scroll and the unvaned portion of the nozzle. The cold flow experimental results are presented for through-flow velocity contours and the cross velocity vectors. Author

A86-48229*# City Coll. of the City Univ. of New York.

THREE-DIMENSIONAL FLUID FLOW PHENOMENA IN THE BLADE END WALL CORNER REGION

B. K. HAZARIKA, R. RAJ (City College, New York), and D. R. BOLDMAN (NASA, Lewis Research Center, Cleveland, OH) ASME, International Gas Turbine Conference and Exhibit, 31st, Duesseldorf, West Germany, June 8-12, 1986. 14 p. refs
 (Contract NAG3-122)
 (ASME PAPER 86-GT-179)

Flow visualization, static and total pressure measurements, and mean velocity profile measurements with a single-sensor inclined hot wire probe, are used in a study of three-dimensional flow at a turbine blade end wall corner region for six critical axial stations along the blade chord. Three vortices are identified: (1) a horseshoe vortex near the leading edge; (2) a corner eddy between the horseshoe vortex and the corner; and (3) a vortex at the rear portion of the corner due to the corner eddy's secondary flow. Attention is given to the relative size and rate-of-spread of the vortices in the streamwise direction. O.C.

A86-48236*# Pennsylvania State Univ., University Park.

THREE-DIMENSIONAL BOUNDARY LAYER ON A COMPRESSOR ROTOR BLADE AT PEAK PRESSURE RISE COEFFICIENT

B. LAKSHMINARAYANA and P. POPOVSKI (Pennsylvania State University, University Park) ASME, International Gas Turbine Conference and Exhibit, 31st, Duesseldorf, West Germany, June 8-12, 1986. 10 p. refs
 (Contract NSG-3212)
 (ASME PAPER 86-GT-186)

A comprehensive study of the three-dimensional turbulent boundary layer on a compressor rotor blade at peak pressure rise coefficient is reported in this paper. The measurements were carried out at various chordwise and radial locations on a compressor rotor blade using a rotating miniature 'V' configuration hot-wire probe. The data are compared with the measurement at the design condition. Substantial changes in the blade boundary layer characteristics are observed, especially in the outer sixteen percent of the blade span. The increased chordwise pressure gradient and the leakage flow at the peak pressure coefficient have a cumulative effect in increasing the boundary layer growth on the suction surface. The leakage flow has a beneficial effect on the pressure surface. The momentum and boundary layer thicknesses increase substantially from those at the design condition, especially near the outer radii of the suction surface. Author

02 AERODYNAMICS

A86-48261*# National Aeronautics and Space Administration. Lewis Research Center, Cleveland, Ohio.

A MODEL FOR CLOSING THE INVISCID FORM OF THE AVERAGE-PASSAGE EQUATION SYSTEM

J. J. ADAMCZYK (NASA, Lewis Research Center, Cleveland, OH), R. A. MULAC, and M. L. CELESTINA (Sverdrup Technology, Inc., Middleburg Heights, OH) ASME, International Gas Turbine Conference and Exhibit, 31st, Duesseldorf, West Germany, June 8-12, 1986. 9 p. Previously announced in STAR as N86-14224. refs

(ASME PAPER 86-GT-227)

A mathematical model is proposed for closing or mathematically completing the system of equations which describes the time average flow field through the blade passages of multistage turbomachinery. These equations referred to as the average passage equation system govern a conceptual model which has proven useful in turbomachinery aerodynamic design and analysis. The closure model is developed so as to insure a consistency between these equations and the axisymmetric through flow equations. The closure model was incorporated into a computer code for use in simulating the flow field about a high speed counter rotating propeller and a high speed fan stage. Results from these simulations are presented. Author

A86-48274*# United Technologies Corp., East Hartford, Conn. **HORSESHOE VORTEX FORMATION AROUND A CYLINDER**

W. A. ECKERLE (United Technologies Research Center, East Hartford, CT) and L. S. LANGSTON (Connecticut, University, Storrs) ASME, International Gas Turbine Conference and Exhibit, 31st, Duesseldorf, West Germany, June 8-12, 1986. 9 p. refs (Contract NSG-3238)

(ASME PAPER 86-GT-246)

An experimental investigation was conducted to characterize a symmetrical horseshoe vortex system in front of and around a single large-diameter right cylinder centered between the sidewalls of a wind tunnel. Surface flow visualization and surface static pressure measurements as well as extensive mean velocity and pressure measurements in and around the vortex system were acquired. The results lend new insight into the formation and development of the vortex system. Contrary to what has been assumed previously, a strong vortex was not identified in the streamwise plane of symmetry, but started a significant angular distance away from it. Rather than the multiple vortex systems reported by others, only a single primary vortex and saddle point were found. The scale of the separation process at the saddle point was much smaller than the scale of the approaching boundary layer thickness. Results of the present study not only shed light on such phenomena as the nonsymmetrical endwall flow in axial turbomachinery but can also be used as a test case for three-dimensional computational fluid mechanics computer codes. Author

A86-48315*# Army Propulsion Lab., Cleveland, Ohio. **EFFECT OF AREA RATIO ON THE PERFORMANCE OF A 5.5:1 PRESSURE RATIO CENTRIFUGAL IMPELLER**

L. F. SCHUMANN, D. A. CLARK (NASA, Lewis Research Center and U.S. Army Propulsion Directorate, Cleveland, OH), and J. R. WOOD (NASA, Lewis Research Center, Cleveland, OH) ASME, International Gas Turbine Conference and Exhibit, 31st, Duesseldorf, West Germany, June 8-12, 1986. 15 p. Previously announced in STAR as N86-19290. refs (ASME PAPER 86-GT-303)

A centrifugal impeller which was initially designed for a pressure ratio of approximately 5.5 and a mass flow rate of 0.959 kg/sec was tested with a vaneless diffuser for a range of design point impeller area ratios from 2.322 to 2.945. The impeller area ratio was changed by successively cutting back the impeller exit axial width from an initial value of 7.57 mm to a final value of 5.97 mm. In all, four separate area ratios were tested. For each area ratio a series of impeller exit axial clearances was also tested. Test results are based on impeller exit surveys of total pressure, total temperature, and flow angle at a radius 1.115 times the impeller exit radius. Results of the tests at design speed, peak

efficiency, and an exit tip clearance of 8 percent of exit blade height show that the impeller equivalent pressure recovery coefficient peaked at a design point area ratio of approximately 2.748 while the impeller aerodynamic efficiency peaked at a lower value of area ratio of approximately 2.55. The variation of impeller efficiency with clearance showed expected trends with a loss of approximately 0.4 points in impeller efficiency for each percent increase in exit axial tip clearance for all impellers tested.

Author

A86-49585*# National Aeronautics and Space Administration. Lewis Research Center, Cleveland, Ohio.

PLUME CHARACTERISTICS OF SINGLE-STREAM AND DUAL-FLOW CONVENTIONAL AND INVERTED-PROFILE NOZZLES AT EQUAL THRUST

U. H. VON GLAHN and J. H. GOODYKOONTZ (NASA, Lewis Research Center, Cleveland, OH) AIAA, Applied Aerodynamics Conference, 4th, San Diego, CA, June 9-11, 1986. 38 p. Previously announced in STAR as N86-26285. refs

(AIAA PAPER 86-1809)

The plume velocity and temperature decay rates of single-stream, conventional dual-flow and inverted-profile dual-flow nozzles are compared at equal values of ideal thrust over a wide range of flow conditions. The comparisons are made in terms of constant velocity and temperature contour maps. The results show that both dual-flow nozzle types have much greater plume velocity and temperature decay rates than those of equivalent thrust single-stream nozzles when the respective secondary flows were at ambient temperature. With hot secondary flows, the inverted-profile dual-flow plumes decayed significantly faster than those of single-stream nozzles; however, the decay rates for the conventional dual-flow streams were about the same as those for the single-stream nozzles. Consequently, with hot secondary flows, the inverted-profile dual-flow plumes decayed much faster than the conventional dual-flow plumes at equal thrust. Author

A86-49612*# National Aeronautics and Space Administration. Lewis Research Center, Cleveland, Ohio.

APPLICATION OF A COMPUTATIONAL MODEL FOR VORTEX GENERATORS IN SUBSONIC INTERNAL FLOWS

W. G. KUNIK (NASA, Lewis Research Center, Cleveland, OH) AIAA, ASME, SAE, and ASEE, Joint Propulsion Conference, 22nd, Huntsville, AL, June 16-18, 1986. 24 p. Previously announced in STAR as N86-26545. refs

(AIAA PAPER 86-1458)

A model for the analysis of vortex generators in a fully viscous subsonic internal flow is evaluated. A vorticity source term is used in a modified form of the Parabolized Navier-Stokes equations to model the shed vortex. Computed results are compared with idealized flow vortex paths, and with experimental data for vortex generators embedded in a thick turbulent boundary layer. The analysis is also compared with experimental data for a separated diffusing S-duct and for a diffusing S-duct with vortex generators. Quantitative comparisons are shown for the latter three cases. Emphasis is placed on verifying the ability of the model to predict global distortions in the flow field. Author

A86-49625*# National Aeronautics and Space Administration. Lewis Research Center, Cleveland, Ohio.

PRELIMINARY RESULTS OF UNSTEADY BLADE SURFACE PRESSURE MEASUREMENTS FOR THE SR-3 PROPELLER

L. J. HEIDELBERG and B. J. CLARK (NASA, Lewis Research Center, Cleveland, OH) AIAA, Aeroacoustics Conference, 10th, Seattle, WA, July 9-11, 1986. 25 p. Previously announced in STAR as N86-27213. refs

(AIAA PAPER 86-1893)

Unsteady blade surface pressures were measured on an advanced, highly swept propeller known as SR-3. These measurements were obtained because the unsteady aerodynamics of these highly loaded transonic blades is important to noise generation and aeroelastic response. Specifically, the response to periodic angle-of-attack change was measured for both two- and eight-bladed configurations over a range of flight Mach numbers

from 0.4 to 0.85. The periodic angle-of-attack change was obtained by placing the propeller axis at angles up to 4 deg to the flow. Most of the results are presented in terms of the unsteady pressure coefficient variation with Mach number. Both cascade and Mach number effects were largest on the suction surface near the leading edge. The results of a three-dimensional Euler code applied in a quasi-steady fashion were compared to measured data at the reduced frequency of 0.1 and showed relatively poor agreement. Pressure waveforms are shown that suggest shock phenomena may play an important part in the unsteady pressure response at some blade locations. Author

N86-10017*# National Aeronautics and Space Administration. Lewis Research Center, Cleveland, Ohio.

THREE-DIMENSIONAL INVISCID ANALYSIS OF RADIAL TURBINE FLOW AND A LIMITED COMPARISON WITH EXPERIMENTAL DATA

Y. K. CHOO and K. C. CIVINSKAS (Army Aviation Research and Technology Activity) 1985 28 p refs To be presented at the ASME Winter Ann. Meeting, 3-Dimensional Flow Phenomena in Fluid Machinery Symp., Miami, Fla., 17-22 Nov. 1985 (NASA-TM-87091; E-2679; NAS 1.15:87091; USAAVSCOM-TR-85-C-12) Avail: NTIS HC A03/MF A01 CSDL 01A

The three-dimensional inviscid DENTON code is used to analyze flow through a radial-inflow turbine rotor. Experimental data from the rotor are compared with analytical results obtained by using the code. The experimental data available for comparison are the radial distributions of circumferentially averaged values of absolute flow angle and total pressure downstream of the rotor exit. The computed rotor-exit flow angles are generally underpredicted relative to the experimental values, which reflect the boundary-layer separation at the trailing edge and the development of wakes downstream of the rotor. The experimental rotor is designed for a higher-than-optimum work factor of 1.126 resulting in a nonoptimum positive incidence and causing a region of rapid flow adjustment and large velocity gradients. For this experimental rotor, the computed radial distribution of rotor-exit to turbine-inlet total pressure ratios are underpredicted due to the errors in the finite-difference approximations in the regions of rapid flow adjustment, and due to using the relatively coarser grids in the middle of the blade region where the flow passage is highly three-dimensional. Additional results obtained from the three-dimensional inviscid computation are also presented, but without comparison due to the lack of experimental data. These include quasi-secondary velocity vectors on cross-channel surfaces, velocity components on the meridional and blade-to-blade surfaces, and blade surface loading diagrams. Computed results show the evolution of a passage vortex and large streamline deviations from the computational streamwise grid lines. Experience gained from applying the code to a radial turbine geometry is also discussed.

Author

N86-10019*# National Aeronautics and Space Administration. Lewis Research Center, Cleveland, Ohio.

FORCED RESPONSE ANALYSIS OF AN AERODYNAMICALLY DETUNED SUPERSONIC TURBOMACHINE ROTOR

D. HOYNIK and S. FLEETER (Purdue Univ., West Lafayette, Ind.) 1985 24 p refs Presented at 10th Bien. Design Eng. Div. Conf. and Exhibit on Mech. Vibration and Noise, Cincinnati, 10-13 Sep. 1985; sponsored by ASME (NASA-TM-87093; E-2685; NAS 1.15:87093) Avail: NTIS HC A02/MF A01 CSDL 01A

High performance aircraft-engine fan and compressor blades are vulnerable to aerodynamically forced vibrations generated by inlet flow distortions due to wakes from upstream blade and vane rows, atmospheric gusts, and maldistributions in inlet ducts. In this report, an analysis is developed to predict the flow-induced forced response of an aerodynamically detuned rotor operating in a supersonic flow with a subsonic axial component. The aerodynamic detuning is achieved by alternating the circumferential spacing of adjacent rotor blades. The total unsteady aerodynamic loading acting on the blading, as a result of the convection of the

transverse gust past the airfoil cascade and the resulting motion of the cascade, is developed in terms of influence coefficients. This analysis is used to investigate the effect of aerodynamic detuning on the forced response of a 12-blade rotor, with Verdon's Cascade B flow geometry as a uniformly spaced baseline configuration. The results of this study indicate that, for forward traveling wave gust excitations, aerodynamic detuning is very beneficial, resulting in significantly decreased maximum-amplitude blade responses for many interblade phase angles. Author

N86-13295*# National Aeronautics and Space Administration. Lewis Research Center, Cleveland, Ohio.

A FORTRAN COMPUTER CODE FOR CALCULATING FLOWS IN MULTIPLE-BLADE-ELEMENT CASCADES

E. R. MCFARLAND Nov. 1985 29 p refs (NASA-TM-87104; E-2701; NAS 1.15:87104) Avail: NTIS HC A03/MF A01 CSDL 01A

A solution technique has been developed for solving the multiple-blade-element, surface-of-revolution, blade-to-blade flow problem in turbomachinery. The calculation solves approximate flow equations which include the effects of compressibility, radius change, blade-row rotation, and variable stream sheet thickness. An integral equation solution (i.e., panel method) is used to solve the equations. A description of the computer code and computer code input is given in this report. Author

N86-14219*# National Aeronautics and Space Administration. Lewis Research Center, Cleveland, Ohio.

SEMIEMPIRICAL METHOD OF DETERMINING FLOW COEFFICIENTS FOR PITOT RAKE MASS FLOW RATE MEASUREMENTS

C. J. TREFNY Nov. 1985 17 p refs (NASA-TM-87144; E-2772; NAS 1.15:87144) Avail: NTIS HC A02/MF A01 CSDL 01A

Flow coefficients applicable to area-weighted pitot rake mass flow rate measurements are presented for fully developed, turbulent flow in an annulus. A turbulent velocity profile is generated semiempirically for a given annulus hub-to-tip radius ratio and integrated numerically to determine the ideal mass flow rate. The calculated velocities at each probe location are then summed, and the flow rate as indicated by the rake is obtained. The flow coefficient to be used with the particular rake geometry is subsequently obtained by dividing the ideal flow rate by the rake-indicated flow rate. Flow coefficients ranged from 0.903 for one probe placed at a radius dividing two equal areas to 0.984 for a 10-probe area-weighted rake. Flow coefficients were not a strong function of annulus hub-to-tip radius ratio for rakes with three or more probes. The semiempirical method used to generate the turbulent velocity profiles is described in detail. Author

N86-14223*# National Aeronautics and Space Administration. Lewis Research Center, Cleveland, Ohio.

VELOCITY AND TEMPERATURE DECAY CHARACTERISTICS OF INVERTED-PROFILE JETS

U. VONGLAHN, J. GODDYKOONTZ, and C. WASSERBAUER 1985 32 p refs To be presented at the 24th Aerospace Sciences Meeting, Reno, Nevada, 6-9 January 1986; sponsored by American Inst. of Aeronautics and Astronautics Previously announced in IAA as A86-22693 (NASA-TM-87159; E-2681; NAS 1.15:87159; AIAA-86-0312) Avail: NTIS HC A03/MF A01 CSDL 01A

In order to design efficient, lightweight flap systems for future engine under-the-wing STOL aircraft, the velocity and temperature decay rate of the jet plume must be increased relative to that for single-stream nozzles in order to provide local flap loads and structural temperatures within acceptable limits. The jet plume decay rate of dual flow engines can be increased by resorting to inverted-profile velocity and temperature nozzle concepts. The peak axial decay characteristics of model-scale, two-stream inverted-profile nozzle flows are empirically correlated. Also discussed are the radial and spreading characteristics of inverted-profile nozzle flows. Author

02 AERODYNAMICS

N86-14224*# National Aeronautics and Space Administration. Lewis Research Center, Cleveland, Ohio.

A MODEL FOR CLOSING THE INVISCID FORM OF THE AVERAGE-PASSAGE EQUATION SYSTEM

J. J. ADAMCZYK, R. A. MULAC (Sverdrup Technology, Inc., Middleburg Heights, Ohio), and M. L. CELESTINA (Sverdrup Technology, Inc., Middleburg Heights, Ohio) 1985 15 p refs To be presented at the 31st International Gas Turbine Conference, Dusseldorf, West Germany, 8-12 June 1986; sponsored by the American Society of Mechanical Engineers (NASA-TM-87199; E-2854; NAS 1.15:87199) Avail: NTIS HC A02/MF A01 CSCL 01A

A mathematical model is proposed for closing or mathematically completing the system of equations which describes the time average flow field through the blade passages of multistage turbomachinery. These equations referred to as the average passage equation system govern a conceptual model which has proven useful in turbomachinery aerodynamic design and analysis. The closure model is developed so as to insure a consistency between these equations and the axisymmetric through flow equations. The closure model was incorporated into a computer code for use in simulating the flow field about a high speed counter rotating propeller and a high speed fan stage. Results from these simulations are presented. Author

N86-16194*# National Aeronautics and Space Administration. Lewis Research Center, Cleveland, Ohio.

VALIDATION OF VISCOUS AND INVISCID COMPUTATIONAL METHODS FOR TURBOMACHINERY COMPONENTS

L. A. POVINELLI 1986 19 p refs Proposed for presentation at the 31st International Gas Turbine Conference, Dusseldorf, West Germany; sponsored by ASME (NASA-TM-87193; E-2765; NAS 1.15:87193) Avail: NTIS HC A02/MF A01 CSCL 01A

An assessment of several three-dimensional computer codes used at the NASA Lewis Research Center is presented. Four flow situations are examined, for which both experimental data and computational results are available. The four flows form a basis for the evaluation of the computational procedures. It is concluded that transonic rotor flow at peak efficiency conditions may be calculated with a reasonable degree of accuracy, whereas, off-design conditions are not accurately determined. Duct flows and turbine cascade flows may also be computed with reasonable accuracy whereas radial inflow turbine flow remains a challenging problem. Author

N86-16195*# National Aeronautics and Space Administration. Lewis Research Center, Cleveland, Ohio.

A NUMERICAL SIMULATION OF THE INVISCID FLOW THROUGH A COUNTER-ROTATING PROPELLER

M. L. CELESTINA (Sverdrup Technology, Inc., Cleveland, Ohio), R. A. MULAC (Sverdrup Technology, Inc., Cleveland, Ohio), and J. H. ADAMCZYK 1986 23 p refs Proposed for presentation at the 31st International Gas Turbine Conference, Dusseldorf, West Germany, 8-12 Jun. 1986; sponsored by ASME (NASA-TM-87200; E-2855; NAS 1.15:87200) Avail: NTIS HC A02/MF A01 CSCL 01A

The results of a numerical simulation of the time-averaged inviscid flow field through the blade rows of a multiblade row turboprop configuration are presented. The governing equations are outlined along with a discussion of the solution procedure and coding strategy. Numerical results obtained from a simulation of the flow field through a modern high-speed turboprop will be shown. Author

N86-19289*# National Aeronautics and Space Administration. Lewis Research Center, Cleveland, Ohio.

A TWO-DIMENSIONAL NUMERICAL STUDY OF THE FLOW INSIDE THE COMBUSTION CHAMBERS OF A MOTORED ROTARY ENGINE

T. I. P. SHIH (Florida Univ., Gainesville), S. L. YANG (Florida Univ., Gainesville), and H. J. SCHOCK 1986 16 p refs Presented at the SAE International Congress and Exposition, Detroit, Mich., 24-28 Feb. 1986 (Contract NAG3-363) (NASA-TM-87212; E-2871; NAS 1.15:87212; SAE-860615) Avail: NTIS HC A02/MF A01 CSCL 01A

A numerical study was performed to investigate the unsteady, multidimensional flow inside the combustion chambers of an idealized, two-dimensional, rotary engine under motored conditions. The numerical study was based on the time-dependent, two-dimensional, density-weighted, ensemble-averaged conservation equations of mass, species, momentum, and total energy valid for two-component ideal gas mixtures. The ensemble-averaged conservation equations were closed by a K-epsilon model of turbulence. This K-epsilon model of turbulence was modified to account for some of the effects of compressibility, streamline curvature, low-Reynolds number, and preferential stress dissipation. Numerical solutions to the conservation equations were obtained by the highly efficient implicit-factored method of Beam and Warming. The grid system needed to obtain solutions were generated by an algebraic grid generation technique based on transfinite interpolation. Results of the numerical study are presented in graphical form illustrating the flow patterns during intake, compression, gaseous fuel injection, expansion, and exhaust. Author

N86-19290*# National Aeronautics and Space Administration. Lewis Research Center, Cleveland, Ohio.

EFFECT OF AREA RATIO ON THE PERFORMANCE OF A 5.5:1 PRESSURE RATIO CENTRIFUGAL IMPELLER

L. F. SCHUMANN (Army Aviation Research and Technology Activity, Cleveland, Ohio), D. A. CLARK (Army Aviation Research and Technology Activity, Cleveland, Ohio), and J. R. WOOD 1986 40 p refs Proposed for presentation at the 31st International Gas Turbine Conference and Exhibition, Dusseldorf, West Germany, 8-12 Jun. 1986; sponsored by the American Society of Mechanical Engineers (NASA-TM-87237; E-2190; NAS 1.15:87237; USAVSCOM-TR-85-C-21; TR-85-C-21) Avail: NTIS HC A03/MF A01 CSCL 01A

A centrifugal impeller which was initially designed for a pressure ratio of approximately 5.5 and a mass flow rate of 0.959 kg/sec was tested with a vaneless diffuser for a range of design point impeller area ratios from 2.322 to 2.945. The impeller area ratio was changed by successively cutting back the impeller exit axial width from an initial value of 7.57 mm to a final value of 5.97 mm. In all, four separate area ratios were tested. For each area ratio a series of impeller exit axial clearances was also tested. Test results are based on impeller exit surveys of total pressure, total temperature, and flow angle at a radius 1.115 times the impeller exit radius. Results of the tests at design speed, peak efficiency, and an exit tip clearance of 8 percent of exit blade height show that the impeller equivalent pressure recovery coefficient peaked at a design point area ratio of approximately 2.748 while the impeller aerodynamic efficiency peaked at a lower value of area ratio of approximately 2.55. The variation of impeller efficiency with clearance showed expected trends with a loss of approximately 0.4 points in impeller efficiency for each percent increase in exit axial tip clearance for all impellers tested. Author

N86-20357*# National Aeronautics and Space Administration. Lewis Research Center, Cleveland, Ohio.

ANALYSIS OF FULLY STALLED COMPRESSOR

W. ROSTAFINSKI 1986 14 p refs Proposed for presentation at the 4th Joint Fluid Mechanics, Plasma Dynamics and Laser Conference, Atlanta, Ga., 12-14 May 1986; sponsored by AIAA and the American Society of Mechanical Engineers (NASA-TM-87254; E-2944; NAS 1.15:87254) Avail: NTIS HC A02/MF A01 CSCL 21E

An analysis yields a model for energy transfer in compressor stages operating in the closed-throttle condition. The derivation indicates that three geometry parameters (hub/tip ration, aspect ration, and rotor blade setting angle) influence the values of pressure coefficient when the compressor flow is close to zero.

Author

N86-21505*# National Aeronautics and Space Administration. Lewis Research Center, Cleveland, Ohio.

APPLICATION OF A LINEARIZED UNSTEADY AERODYNAMIC ANALYSIS TO STANDARD CASCADE CONFIGURATIONS Final Report

J. M. VERDON and W. J. USAB, JR. Washington NASA Jan. 1986 56 p refs (Contract NAS3-22257)

(NASA-CR-3940; R85-956896-4; E-2686; NAS 1.26:3940) Avail: NTIS HC A04/MF A01 CSCL 01A

A linearized potential flow analysis, which accounts for the effects of nonuniform steady flow phenomena on the linearized unsteady aerodynamic response to prescribed blade motions, has been applied to five cascade configurations. These include the first, fifth, eighth and ninth standard configurations proposed as a result of the Second International Symposium on Aeroelasticity in Turbomachines and a NASA Lewis flutter cascade. Selected results from this study, including comparisons between analytical predictions and the experimental measurements submitted for three of the foregoing configurations, are described. The correlation between theory and experiment for the first standard configuration (a compressor cascade operating at low Mach number and frequency) is quite good. Moreover, the predictions and measurements for the NASA Lewis cascade of symmetric biconvex airfoils show good qualitative agreement. However, wide discrepancies exist between the theoretical predictions and the experimental measurements for the fifth standard configuration (a subsonic transonic fan tip cascade). These can be partially attributed to conditions being imposed in the experiment which differ from those commonly used in unsteady aerodynamic analyses.

Author

N86-21513*# National Aeronautics and Space Administration. Lewis Research Center, Cleveland, Ohio.

THE PREDICTED EFFECT OF AERODYNAMIC DETUNING ON COUPLED BENDING-TORSION UNSTALLED SUPERSONIC FLUTTER

D. HOYNIK and S. FLEETER 1986 30 p refs Prepared for presentation at the 31st International Gas Turbine Conference, Dusseldorf, West Germany, 8-12 Jun. 1986; sponsored by ASME Prepared in cooperation with Purdue Univ., West Lafayette, Ind. (NASA-TM-87240; E-2915; NAS 1.15:87240) Avail: NTIS HC A03/MF A01 CSCL 01A

A mathematical model is developed to predict the enhanced coupled bending-torsion unstalled supersonic flutter stability due to alternate circumferential spacing aerodynamic detuning of a turbomachine rotor. The translational and torsional unsteady aerodynamic coefficients are developed in terms of influence coefficients, with the coupled bending-torsion stability analysis developed by considering the coupled equations of motion together with the unsteady aerodynamic loading. The effect of this aerodynamic detuning on coupled bending-torsion unstalled supersonic flutter as well as the verification of the modeling are then demonstrated by considering an unstable 12 bladed rotor, with Verdon's uniformly spaced Cascade B flow geometry as a baseline. However, with the elastic axis and center of gravity at 60 percent of the chord, this type of aerodynamic detuning has a

minimal effect on stability. For both uniform and nonuniform circumferentially space rotors, a single degree of freedom torsion mode analysis was shown to be appropriate for values of the bending-torsion natural frequency ratio lower than 0.6 and higher 1.2. When the elastic axis and center of gravity are not coincident, the effect of detuning on cascade stability was found to be very sensitive to the location of the center of gravity with respect to the elastic axis. In addition, it was determined that when the center of gravity was forward of an elastic axis located at midchord, a single degree of freedom torsion model did not accurately predict cascade stability.

Author

N86-21517*# National Aeronautics and Space Administration. Lewis Research Center, Cleveland, Ohio.

AN ANALYSIS FOR THE SOUND FIELD PRODUCED BY RIGID WIDE CORD DUAL ROTATION PROPELLERS OF HIGH SOLIDARITY IN COMPRESSIBLE FLOW

S. M. RAMACHANDRA and L. J. BOBER 1986 42 p refs Presented at the 24th Aerospace Sciences Meeting, Reno, Nev., 6-8 Jan. 1986; sponsored by AIAA

(NASA-TM-87178; E-2826; NAS 1.15:87178) Avail: NTIS HC A03/MF A01 CSCL 01A

An unsteady lifting service theory for the counter-rotating propeller is presented using the linearized governing equations for the acceleration potential and representing the blades by a surface distribution of pulsating acoustic dipoles distributed according to a modified Birnbaum series. The Birnbaum series coefficients are determined by satisfying the surface tangency boundary conditions on the front and rear propeller blades. Expressions for the combined acoustic resonance modes of the front prop, the rear prop and the combination are also given.

Author

N86-23563*# Sverdrup Technology, Inc., Cleveland, Ohio.

AN LU IMPLICIT SCHEME FOR HIGH SPEED INLET ANALYSIS Final Report

S. YOON and A. JAMESON (Princeton Univ., N.J.) Apr. 1986 17 p refs Prepared for presentation at the 22nd Joint Propulsion Conference, Huntsville, Ala., 16-18 Jun. 1986; cosponsored by AIAA, ASME, SAE, ASEE

(Contract NAS3-24105) (NASA-CR-175098; NAS 1.26:175098; AIAA-86-1520) Avail: NTIS HC A02/MF A01 CSCL 01A

A numerical method is developed to analyze the inviscid flowfield of a high speed inlet by the solution of the Euler equations. The lower-upper implicit scheme in conjunction with adaptive dissipation proves to be an efficient and robust nonoscillatory shock capturing technique for high Mach number flows as well as for transonic flows.

Author

N86-24658*# National Aeronautics and Space Administration. Lewis Research Center, Cleveland, Ohio.

A NUMERICAL ANALYSIS APPLIED TO HIGH ANGLE OF ATTACK THREE-DIMENSIONAL INLETS

D. P. HWANG 1986 16 p refs Presented at the 22nd Joint Propulsion Conference, Huntsville, Ala., 16-18 Jun. 1986; sponsored by AIAA, ASME, SAE, and ASEE

(NASA-TM-87298; E-3004; NAS 1.15:87298; AIAA-86-1627) Avail: NTIS HC A02/MF A01 CSCL 01A

The three-dimensional analytical methods used to analyze subsonic high angle of attack inlets are described. The methods are shown to be in good agreement with experimental results for various three-dimensional high angle of attack inlets. The methods are used to predict aerodynamic characteristics of scarf and slotted-lip inlets.

E.A.K.

02 AERODYNAMICS

N86-24667*# National Aeronautics and Space Administration. Lewis Research Center, Cleveland, Ohio.

IN-FLIGHT MEASUREMENTS OF WING ICE SHAPES AND WING SECTION DRAG INCREASES CAUSED BY NATURAL ICING CONDITIONS

K. MIKKELSEN, N. JUHASZ, R. RANAUDO, R. MCKNIGHT, R. FREEDMAN, and J. GREISSING May 1986 27 p refs (NASA-TM-87301; E-3013; NAS 1.15:87301) Avail: NTIS HC A03/MF A01 CSCL 01A

Aircraft icing flight research was performed in natural icing conditions with a twin engine computer type STOL aircraft. In-flight measurements were made of the icing cloud environment, the shape of the ice accretion on the wing, and the corresponding increase in the wing section drag. Results are presented for three icing encounters. On one flight, the wing section drag coefficient increased 35 percent over the uniced baseline for cruise conditions while a 43 percent increase was observed at an aircraft angle of attack of 6.2 degrees. Author

N86-26285*# National Aeronautics and Space Administration. Lewis Research Center, Cleveland, Ohio.

PLUME CHARACTERISTICS OF SINGLE-STREAM AND DUAL-FLOW CONVENTIONAL AND INVERTED-PROFILE NOZZLES AT EQUAL THRUST

U. H. VONGLAHN and J. H. GOODYKOONTZ 1986 39 p refs Presented at the 4th Applied Aerodynamics Conference, San Diego, Calif. 9-11 Jun. 1986; sponsored by AIAA (NASA-TM-87323; E-3060; NAS 1.15:87323; AIAA-86-1809) Avail: NTIS HC A03/MF A01 CSCL 01A

The plume velocity and temperature decay rates of single-stream, conventional dual-flow and inverted-profile dual-flow nozzles are compared at equal values of ideal thrust over a wide range of flow conditions. The comparisons are made in terms of constant velocity and temperature contour maps. The results show that both dual-flow nozzle types have much greater plume velocity and temperature decay rates than those of equivalent thrust single-stream nozzles when the respective secondary flows were at ambient temperature. With hot secondary flows, the inverted-profile dual-flow plumes decayed significantly faster than those of single-stream nozzles; however, the decay rates for the conventional dual-flow streams were about the same as those for the single-stream nozzles. Consequently, with hot secondary flows, the inverted-profile dual-flow plumes decayed much faster than the conventional dual-flow plumes at equal thrust. Author

N86-27186*# Kansas Univ., Lawrence. Dept. of Aerospace Engineering.

EXPERIMENTAL AND ANALYTICAL INVESTIGATION OF A FREEZING POINT DEPRESSANT FLUID ICE PROTECTION SYSTEM M.S. Thesis. Final Report

A. E. ALBRIGHT Sep. 1984 149 p (Contract NAG3-273) (NASA-CR-174758; NAS 1.26:174758) Avail: NTIS HC A07/MF A01 CSCL 01A

A glycol-exuding porous leading edge ice protection system was tested in the NASA Icing Research Tunnel. Stainless steel mesh, laser drilled titanium, and composite panels were tested on two general aviation wing sections. Two different glycol-water solutions were evaluated. Minimum glycol flow rates required for anti-icing were obtained as a function of angle of attack, liquid water content, volume median drop diameter, temperature, and velocity. Ice accretions formed after five minutes of icing were shed in three minutes or less using a glycol fluid flow equal to the anti-ice flow rate. Two methods of predicting anti-ice flow rates are presented and compared with a large experimental data base of anti-ice flow rates over a wide range of icing conditions. The first method presented in the ADS-4 document typically predicts flow rates lower than the experimental flow rates. The second method, originally published in 1983, typically predicts flow rates up to 25 percent higher than the experimental flow rates. This method proved to be more consistent between wing-panel configurations. Significant correlation coefficients between the

predicted flow rates and the experimental flow rates ranged from .867 to .947. Author

N86-27213*# National Aeronautics and Space Administration. Lewis Research Center, Cleveland, Ohio.

PRELIMINARY RESULTS OF UNSTEADY BLADE SURFACE PRESSURE MEASUREMENTS FOR THE SR-3 PROPELLER

L. J. HEIDELBERG and B. J. CLARK 1986 26 p Presented at the 10th Aeroacoustics Conference, Seattle, Wash., 9-11 Jul. 1986

(NASA-TM-87352; E-3106; NAS 1.15:87352; AIAA-86-1893) Avail: NTIS HC A03/MF A01 CSCL 01A

Unsteady blade surface pressures were measured on an advanced, highly swept propeller known as SR-3. These measurements were obtained because the unsteady aerodynamics of these highly loaded transonic blades is important to noise generation and aeroelastic response. Specifically, the response to periodic angle-of-attack change was measured for both two- and eight-bladed configurations over a range of flight Mach numbers from 0.4 to 0.85. The periodic angle-of-attack change was obtained by placing the propeller axis at angles up to 4 deg to the flow. Most of the results are presented in terms of the unsteady pressure coefficient variation with Mach number. Both cascade and Mach number effects were largest on the suction surface near the leading edge. The results of a three-dimensional Euler code applied in a quasi-steady fashion were compared to measured data at the reduced frequency of 0.1 and showed relatively poor agreement. Pressure waveforms are shown that suggest shock phenomena may play an important part in the unsteady pressure response at some blade locations. Author

N86-28053*# National Aeronautics and Space Administration. Lewis Research Center, Cleveland, Ohio.

LASER FRINGE ANEMOMETRY FOR AERO ENGINE COMPONENTS

A. J. STRAZISAR 1986 54 p Presented at the 67th Symposium of the AGARD Propulsion and Energetics Panel on Advanced Instrumentation for Aero Engine Components, Philadelphia, Pa., 19-23 May 1986

(NASA-TM-88798; E-3135; NAS 1.15:88798) Avail: NTIS HC A02/MF A01 CSCL 01A

Advances in flow measurement techniques in turbomachinery continue to be paced by the need to obtain detailed data for use in validating numerical predictions of the flowfield and for use in the development of empirical models for those flow features which cannot be readily modelled numerically. The use of laser anemometry in turbomachinery research has grown over the last 14 years in response to these needs. Based on past applications and current developments, this paper reviews the key issues which are involved when considering the application of laser anemometry to the measurement of turbomachinery flowfields. Aspects of laser fringe anemometer optical design which are applicable to turbomachinery research are briefly reviewed. Application problems which are common to both laser fringe anemometry (LFA) and laser transit anemometry (LTA) such as seed particle injection, optical access to the flowfield, and measurement of rotor rotational position are covered. The efficiency of various data acquisition schemes is analyzed and issues related to data integrity and error estimation are addressed. Real-time data analysis techniques aimed at capturing flow physics in real time are discussed. Finally, data reduction and analysis techniques are discussed and illustrated using examples taken from several LFA turbomachinery applications. Author

N86-28055*# National Aeronautics and Space Administration. Lewis Research Center, Cleveland, Ohio.

ROTOR WAKE CHARACTERISTICS OF A TRANSONIC AXIAL FLOW FAN

M. D. HATHAWAY (Army Aviation Research and Technology Activity, Cleveland, Ohio), J. GERTZ (Massachusetts Inst. of Tech., Cambridge), A. EPSTEIN, and A. J. STRAZISAR 1985 13 p Presented at the 21st Joint Propulsion Conference, Monterey, Calif., 8-10 Jul. 1985; sponsored by AIAA, SAE, ASME and ASEE Previously announced in IAA as A85-43974

(NASA-TM-87073; E-2644; USAAVSCOM-TR-85-C-8; AIAA-85-1133; NAS 1.15:87073) Avail: NTIS HC A02/MF A01 CSCL 01A

State of the art turbomachinery flow analysis codes are not capable of predicting the viscous flow features within turbomachinery blade wakes. Until efficient 3D viscous flow analysis codes become a reality there is therefore a need for models which can describe the generation and transport of blade wakes and the mixing process within the wake. To address the need for experimental data to support the development of such models, high response pressure measurements and laser anemometer velocity measurements were obtained in the wake of a transonic axial flow fan rotor.

Author

N86-28063*# United Technologies Research Center, East Hartford, Conn.

MEASUREMENTS OF A TURBULENT HORSESHOE VORTEX FORMED AROUND A CYLINDER Final Report

W. A. ECKERLE and L. S. LANGSTON (Connecticut Univ., Storrs) Washington NASA Jun. 1986 206 p

(Contract NSG-3238)

(NASA-CR-3986; E-3027; NAS 1.26:3986) Avail: NTIS HC A10/MF A01 CSCL 01A

An experimental investigation was conducted to characterize a symmetrical horseshoe vortex system in front of and around a single large-diameter right cylinder centered between the sidewalls of a wind tunnel. Surface flow visualization and surface static pressure measurements as well as extensive mean velocity and pressure measurements in and around the vortex system were acquired. The results lend new insight into the formation and development of the vortex system. Contrary to what has been assumed previously, a strong vortex was not identified in the streamwise plane of symmetry, but started a significant angular distance away from it. Rather than the multiple vortex systems reported by others, only a single primary vortex and saddle point were found. The scale of the separation process at the saddle point was much smaller than the scale of the approaching boundary layer thickness. Results of the present study not only shed light on such phenomena as the nonsymmetrical endwall flow in axial turbomachinery but can also be used as a test case for three-dimensional computational fluid mechanics computer codes.

Author

N86-29773*# Texas A&M Univ., College Station. Dept. of Aerospace Engineering.

EXPERIMENTAL AND THEORETICAL STUDY OF PROPELLER SPINNER/SHANK INTERFERENCE M.S. Thesis

C. C. CORNELL May 1986 143 p

(Contract NAS3-272)

(NASA-CR-176954; NAS 1.26:176954) Avail: NTIS HC A07/MF A01 CSCL 01A

A fundamental experimental and theoretical investigation into the aerodynamic interference associated with propeller spinner and shank regions was conducted. The research program involved a theoretical assessment of solutions previously proposed, followed by a systematic experimental study to supplement the existing data base. As a result, a refined computational procedure was established for prediction of interference effects in terms of interference drag and resolved into propeller thrust and torque components. These quantities were examined with attention to engineering parameters such as two spinner finess ratios, three blade shank forms, and two/three/four/six/eight blades. Consideration of the physics of the phenomena aided in the logical

deduction of two individual interference quantities (cascade effects and spinner/shank juncture interference). These interference effects were semi-empirically modeled using existing theories and placed into a compatible form with an existing propeller performance scheme which provided the basis for examples of application.

Author

N86-30693*# Texas A&M Univ., College Station. Dept. of Aerospace Engineering.

AERODYNAMIC DATA BANKS FOR CLARK-Y, NACA 4-DIGIT AND NACA 16-SERIES AIRFOIL FAMILIES Final Report

K. D. KORKAN, J. CAMBA, III, and P. M. MORRIS Jan. 1986 272 p

(Contract NAS3-272)

(NASA-CR-176883; NAS 1.26:176883) Avail: NTIS HC A12/MF A01 CSCL 01A

With the renewed interest in propellers as means of obtaining thrust and fuel efficiency in addition to the increased utilization of the computer, a significant amount of progress was made in the development of theoretical models to predict the performance of propeller systems. Inherent in the majority of the theoretical performance models to date is the need for airfoil data banks which provide lift, drag, and moment coefficient values as a function of Mach number, angle-of-attack, maximum thickness to chord ratio, and Reynolds number. Realizing the need for such data, a study was initiated to provide airfoil data banks for three commonly used airfoil families in propeller design and analysis. The families chosen consisted of the Clark-Y, NACA 16 series, and NACA 4 digit series airfoils. The various component of each computer code, the source of the data used to create the airfoil data bank, the limitations of each data bank, program listing, and a sample case with its associated input-output are described. Each airfoil data bank computer code was written to be used on the Amdahl Computer system, which is IBM compatible and uses Fortran.

Author

N86-31536*# Hamilton Standard, Windsor Locks, Conn.

SYSTEM DESIGN AND INTEGRATION OF THE LARGE-SCALE ADVANCED PROP-FAN

B. P. HUTH Aug. 1984 97 p

(Contract NAS3-23051)

(NASA-CR-174789; NAS 1.26:174789; HSER-9333) Avail: NTIS HC A05/MF A01 CSCL 01A

In recent years, considerable attention has been directed toward improving aircraft fuel consumption. Studies have shown that blades with thin airfoils and aerodynamic sweep extend the inherent efficiency advantage that turboprop propulsion systems have demonstrated to the higher speed to today's aircraft. Hamilton Standard has designed a 9-foot diameter single-rotation Prop-Fan. It will test the hardware on a static test stand, in low speed and high speed wind tunnels and on a research aircraft. The major objective of this testing is to establish the structural integrity of large scale Prop-Fans of advanced construction, in addition to the evaluation of aerodynamic performance and the aeroacoustic design. The coordination efforts performed to ensure smooth operation and assembly of the Prop-Fan are summarized. A summary of the loads used to size the system components, the methodology used to establish material allowables and a review of the key analytical results are given.

Author

N86-31537*# National Aeronautics and Space Administration. Lewis Research Center, Cleveland, Ohio.

COMPARISON OF ANALYTICAL AND EXPERIMENTAL PERFORMANCE OF A WIND-TUNNEL DIFFUSER SECTION

R. J. SHYNE, R. D. MOORE, and D. R. BOLDMAN 1986 13 p Presented at the 58th Annual Conference of the National Technical Association, Washington, D.C., 23-28 Jun. 1986

(NASA-TM-88795; E-3130; NAS 1.15:88795) Avail: NTIS HC A02/MF A01 CSCL 01A

Wind tunnel diffuser performance is evaluated by comparing experimental data with analytical results predicted by an one-dimensional integration procedure with skin friction coefficient, a two-dimensional interactive boundary layer procedure for

03 AIR TRANSPORTATION AND SAFETY

analyzing conical diffusers, and a two-dimensional, integral, compressible laminar and turbulent boundary layer code. Pressure, temperature, and velocity data for a 3.25 deg equivalent cone half-angle diffuser (37.3 in., 94.742 cm outlet diameter) was obtained from the one-tenth scale Altitude Wind Tunnel modeling program at the NASA Lewis Research Center. The comparison is performed at Mach numbers of 0.162 ($Re = 3.097 \times 10^6$), 0.326 ($Re = 6.2737 \times 10^6$), and 0.363 ($Re = 7.0129 \times 10^6$). The Reynolds numbers are all based on an inlet diffuser diameter of 32.4 in., 82.296 cm, and reasonable quantitative agreement was obtained between the experimental data and computational codes. Author

03

AIR TRANSPORTATION AND SAFETY

Includes passenger and cargo air transport operations; and aircraft accidents.

A86-14427* National Aeronautics and Space Administration. Lewis Research Center, Cleveland, Ohio.

ICE SHAPES AND THE RESULTING DRAG INCREASE FOR A NACA 0012 AIRFOIL

W. OLSEN, R. SHAW, and J. NEWTON (NASA, Lewis Research Center, Cleveland, OH) AIAA, Aerospace Sciences Meeting, 22nd, Reno, NV, Jan. 9-12, 1984. 30 p. Previously announced in STAR as N85-27839. refs (AIAA PAPER 84-0109)

Experimental measurements of the ice shapes and resulting drag increases were measured in the NASA-Lewis Icing Research Tunnel. The measurements were made over a large range of conditions (e.g., airspeed and temperature, drop size and liquid water content of the cloud, and the angle of attack of the airfoil). The measured drag increase did not agree with the existing correlation. Additional results were given which are helpful in understanding the ice structure and the way it forms, and in improving the ice accretion modeling theories. There are data on the ice surface roughness, on the effect of the ice shape on the local droplet catch, and on the relative importance of various parts of the ice shape on the drag increase. Experimental repeatability is also discussed. Author

A86-35656* Sikorsky Aircraft, Stratford, Conn.

THE PERFORMANCE CHARACTERISTICS OF SIMULATED ICE ON ROTORCRAFT AIRFOILS

R. J. FLEMMING (United Technologies Corp., Sikorsky Aircraft Div., Stratford, CT), R. J. SHAW (NASA, Lewis Research Center, Cleveland, OH), and J. D. LEE (Ohio State University, Columbus) IN: American Helicopter Society, Annual Forum, 41st, Fort Worth, TX, May 15-17, 1985, Proceedings. Alexandria, VA, American Helicopter Society, 1985, p. 743-757. refs

Attention is given to the results of NASA-sponsored rotorcraft icing research which was aimed at the formulation of a predictive method for the computation of performance penalties due to rotor and airfoil icing. Parametric simulated ice test results obtained in wind tunnels are compared with those of other investigations. These comparisons indicate that proper design of simulated ice shapes can adequately represent ice on airfoil sections, with incremental lift, drag, and pitching moments matching those generated in icing wind tunnels. O.C.

A86-49107* National Aeronautics and Space Administration. Lewis Research Center, Cleveland, Ohio.

NASA'S AIRCRAFT ICING ANALYSIS PROGRAM

R. J. SHAW (NASA, Lewis Research Center, Cleveland, OH) IN: ICAS, Congress, 15th, London, England, September 7-12, 1986, Proceedings. Volume 2. New York, American Institute of Aeronautics and Astronautics, Inc., 1986, p. 1254-1269. refs

An overview of the NASA ongoing efforts to develop an aircraft icing analysis capability is presented. Discussions are included of the overall and long term objectives of the program as well as current capabilities and limitations of the various computer codes being developed. Descriptions are given of codes being developed to analyze two- and three-dimensional trajectories of water droplets, airfoil ice accretion, aerodynamic performance degradation of components and complete aircraft configurations, electrothermal deicer, fluid freezing point depressant antideicer and electro-impulse deicer. The need for bench mark and verification data to support the code development is also discussed, and selected results of experimental programs are presented. Author

N86-20379* Wichita State Univ., Kans.

PARTICLE TRAJECTORY COMPUTATION ON A 3-DIMENSIONAL ENGINE INLET Final Report Ph.D. Thesis

J. J. KIM Jan. 1986 115 p refs

(Contract NAG3-566)

(NASA-CR-175023; NAS 1.26:175023; DOT-FAA-CT-86-1) Avail: NTIS HC A06/MF A01 CSCL 01C

A 3-dimensional particle trajectory computer code was developed to compute the distribution of water droplet impingement efficiency on a 3-dimensional engine inlet. The computed results provide the essential droplet impingement data required for the engine inlet anti-icing system design and analysis. The droplet trajectories are obtained by solving the trajectory equation using the fourth order Runge-Kutta and Adams predictor-corrector schemes. A compressible 3-D full potential flow code is employed to obtain a cylindrical grid definition of the flowfield on and about the engine inlet. The inlet surface is defined mathematically through a system of bi-cubic parametric patches in order to compute the droplet impingement points accurately. Analysis results of the 3-D trajectory code obtained for an axisymmetric droplet impingement problem are in good agreement with NACA experimental data. Experimental data are not yet available for the engine inlet impingement problem analyzed. Applicability of the method to solid particle impingement problems, such as engine sand ingestion, is also demonstrated. Author

N86-20380* Toledo Univ., Ohio. Coll. of Engineering.

A NUMERICAL AND EXPERIMENTAL INVESTIGATION OF ELECTROCHEMICAL AIRCRAFT DEICING M.S. Thesis Final Report

K. L. LEFFEL Jan. 1986 268 p refs

(Contract NAG3-72)

(NASA-CR-175024; NAS 1.26:175024) Avail: NTIS HC A12/MF A01 CSCL 01C

This study was composed of three parts. The first part involved the extension of an existing transient two dimensional numerical code for an electrothermal deicer so that it would simulate the situation where a variable thickness ice layer existed at the outer surface. The Enthalpy Method was used to simulate the phase change, and Gauss-Seidel iteration was used to solve the resulting system of finite difference equations. A set of criteria were developed for determining when a variable thickness ice layer had an effect on deicer performance. The second part was the acquisition and analysis of experimental data. The test model was a section of a Bell UH-1H helicopter blade equipped with an electrothermal deicer. A total of fifty-two thermocouples were utilized to document the thermal response of the blade and deicer assembly. In the deicing runs, the experimental temperature response data clearly showed when melting, shedding or refreezing occurred. The tests illustrated that the criterion for shedding in the three cases where it did occur was that the abrasion shield interface temperature was 32 to 34 F. The third part concerned the validation of a one dimensional transient thermal model of an

electrothermal deicer by comparison of the predictions with the experimental data. The Enthalpy Method was found to effectively model the phase change which occurred, and the ice shedding algorithm employed in the simulation was also evaluated. Author

N86-22558*# Ohio State Univ., Columbus. Aeronautical and Astronautical Research Lab.

WIND TUNNEL TESTS OF ROTOR BLADE SECTIONS WITH REPLICATIONS OF ICE FORMATIONS ACCRETED IN HOVER Final Report

J. D. LEE, J. H. BERGER (Fluidyne Engineering Corp., Columbus, Ohio), and T. J. MCDONALD (Fluidyne Engineering Corp., Columbus, Ohio) Mar. 1986 31 p refs

(Contract NAG3-374)

(NASA-CR-175089; NAS 1.26:175089) Avail: NTIS HC A03/MF A01 CSCL 01C

Full scale reproductions of ice accretions molded during the documentation of a hover test program were fabricated by means of epoxy castings and used for a wind tunnel test program. Surface static pressure distributions were recorded and used to evaluate lift and pitching moment increments while drag was determined by wake surveys. Through the range of the tests, corresponding to those conditions encountered in hover and in flat pitch, integration of the pressure distributions showed negligible changes in lift and in pitching moment, but the drag was significantly increased. Author

N86-22559*# Fluidyne Engineering Corp., Columbus, Ohio.

DOCUMENTATION OF ICE SHAPES ACCRETED ON THE MAIN ROTOR OF A UH-1H HELICOPTER IN LEVEL FLIGHT Final Report

M. K. HANSON and J. D. LEE (Ohio State Univ., Columbus) Mar. 1986 14 p refs

(Contract NAG3-374)

(NASA-CR-175088; NAS 1.26:175088) Avail: NTIS HC A02/MF A01 CSCL 01C

Icing tests were conducted on a UH-1H helicopter in level flight behind a spray tanker near Duluth, Minnesota, during the winter of 1983-84 as part of the joint NASA/Army HIFT program. On landing, the ice formations on the main rotor were documented by casting a set of ten-inch molds on the blade using a Dow-Corning silicone rubber compound which was initially liquid at sub-freezing temperatures. Such documentation was accomplished for eight flights in which the temperature ranged from -11 C to -22 C and the in-cloud flight times ranged from 5 to 9 minutes. Author

N86-23577*# Sverdrup Technology, Inc., Cleveland, Ohio.

ANALYTICAL DETERMINATION OF PROPELLER PERFORMANCE DEGRADATION DUE TO ICE ACCRETION Final Report

T. L. MILLER Apr. 1986 138 p refs

(Contract NAS3-24105)

(NASA-CR-175092; NAS 1.26:175092) Avail: NTIS HC A07/MF A01 CSCL 01C

A computer code has been developed which is capable of computing propeller performance for clean, glaze, or rime iced propeller configurations, thereby providing a mechanism for determining the degree of performance degradation which results from a given icing encounter. The inviscid, incompressible flow field at each specified propeller radial location is first computed using the Theodorsen transformation method of conformal mapping. A droplet trajectory computation then calculates droplet impingement points and airfoil collection efficiency for each radial location, at which point several user-selectable empirical correlations are available for determining the aerodynamic penalties which arise due to the ice accretion. Propeller performance is finally computed using strip analysis for either the clean or iced propeller. In the iced mode, the differential thrust and torque coefficient equations are modified by the drag and lift coefficient increments due to ice to obtain the appropriate iced values. Comparison with available experimental propeller icing data shows good agreement in several cases. The code's capability to properly predict iced thrust coefficient, power coefficient, and

propeller efficiency is shown to be dependent on the choice of empirical correlation employed as well as proper specification of radial icing extent. Author

N86-27268*# Wichita State Univ., Kans. Coll. of Engineering.

ANALYSES AND TESTS FOR DESIGN OF AN ELECTRO-IMPULSE DE-ICING SYSTEM Interim Report

G. W. ZUMWALT, R. L. SCHRAG, W. D. BERNHART, and R. A. FRIEDBERG May 1985 198 p

(Contract NAG3-284)

(NASA-CR-174919; AR-85-1; NAS 1.26:174919) Avail: NTIS HC A09/MF A01 CSCL 01C

De-icing of aircraft by using the electro-magnetic impulse phenomenon was proposed and demonstrated in several European countries. However, it is not available as a developed system due to lack of research on the basic physical mechanisms and necessary design parameters. The de-icing is accomplished by rapidly discharging high voltage capacitors into a wire coil rigidly supported just inside the aircraft skin. Induced eddy currents in the skin create a repulsive force resulting in a hammer-like force which cracks, de-bonds, and expels ice on the skin surface. The promised advantages are very low energy, high reliability of de-icing, and low maintenance. Three years of Electro-Impulse De-icing (EIDI) research is summarized and the analytical studies and results of testing done in the laboratory, in the NASA Icing Research Tunnel, and in flight are presented. If properly designed, EIDI was demonstrated to be an effective and practical ice protection system for small aircraft, turbojet engine inlets, elements of transport aircraft, and shows promise for use on helicopter rotor blades. Included are practical techniques of fabrication of impulse coils and their mountings. The use of EIDI with nonmetallic surface materials is also described. Author

N86-30022# Akron Univ., Ohio.

JET FUEL VISCOSITY AT LOW TEMPERATURES WITH NOTES ON N-ALKALINE CRYSTALS Final Report

D. SCHRUBEN In FAA Proceedings of Fuel Safety Workshop p 317-356 31 Dec. 1985

(Contract NAG3-488)

(NASA-CR-174911; NAS 1.26:174911) Avail: NTIS HC A17/MF A01 CSCL 21D

Apparatus and procedures were developed to collect jet fuel viscosity versus temperature data for temperatures down to about -60 deg C in a manner compatible with prior jet fuel data bases generated with the Brookfield viscometer. Viscosity data showed good reproducibility even at temperatures a few degrees into the two-phase region. The viscosity-temperature relationship could be correlated by two linear segments when plotted as a standard log-log type representation. The breakpoint between the high and low temperature line segments is the filter flow temperature, a fuel characteristic approximated by the freezing point. A generalized correlation appears sufficiently accurate for many design or performance calculations. In the low temperature two-phase region, wax precipitation is significant. Qualitative literature was quantitatively analyzed along with data in this study to plot crystal size versus composition for the fuel model C sub 20-C sub 24 n-alkane system in solvent. This suggested that wax mixtures tend towards smaller crystal sizes than pure wax species. Complex mixtures in jet fuels lead to two-phase states, at least in some instances, that have small enough crystals to be treated as a continuum. Author

N86-31548*# National Aeronautics and Space Administration. Lewis Research Center, Cleveland, Ohio.

NASA'S AIRCRAFT ICING ANALYSIS PROGRAM

R. J. SHAW 1986 26 p Presented at the International Conference of the Aeronautical Sciences (ICAS), London, England, 7-12 Sept. 1986

(NASA-TM-88791; E-3121; NAS 1.15:88791) Avail: NTIS HC A03/MF A01 CSCL 01C

An overview of the NASA ongoing efforts to develop an aircraft icing analysis capability is presented. Discussions are included of the overall and long term objectives of the program as well as

05 AIRCRAFT DESIGN, TESTING AND PERFORMANCE

current capabilities and limitations of the various computer codes being developed. Descriptions are given of codes being developed to analyze two and three dimensional trajectories of water droplets, airfoil ice accretion, aerodynamic performance degradation of components and complete aircraft configurations, electrothermal deicer, fluid freezing point depressant antideicer and electro-impulse deicer. The need for bench mark and verification data to support the code development is also discussed, and selected results of experimental programs are presented. Author

05

AIRCRAFT DESIGN, TESTING AND PERFORMANCE

Includes aircraft simulation technology.

A86-19940* # Wichita Univ., Kans.

DESIGNING AN ELECTRO-IMPULSE DE-ICING SYSTEM

G. W. ZUMWALT and R. A. FRIEDBERG (Wichita State University, KS) AIAA, Aerospace Sciences Meeting, 24th, Reno, NV, Jan. 6-9, 1986. 9 p. refs

(Contract NAG3-284)

(AIAA PAPER 86-0545)

Basic principles and parameters for a system to deice aircraft with electromagnetic impulses are described. The physical basis for deicing by such impulses is explained, and the requirements involved in the electrodynamic design, structural dynamic design, and system design are discussed. Some manufacturing and testing problems and techniques are described. C.D.

A86-19942* # Wichita Univ., Kans.

A STRUCTURAL DYNAMICS INVESTIGATION RELATED TO EIDI APPLICATIONS

W. D. BERNHART (Wichita State University, KS) and P. H. GIEN AIAA, Aerospace Sciences Meeting, 24th, Reno, NV, Jan. 6-9, 1986. 9 p. refs

(Contract NAG3-284)

(AIAA PAPER 86-0550)

A method for modeling the structural dynamics of electro-impulse deicing is presented. A guideline for building a representative finite element model is discussed together with the experimental determination of the force pulse parameters used in the computational model. The results from the computer solution are compared with experimental results for a semi-cylindrical shell. This preliminary comparison indicated that typical structural dynamic responses may be predicted in the near coil field for the duration of the forcing pulse. The sensitivity of the response to both geometric and electrical parameters is also discussed. Author

A86-35668* # Texas A&M Univ., College Station.

PERFORMANCE DEGRADATION OF HELICOPTERS DUE TO ICING - A REVIEW

K. D. KORKAN (Texas A & M University, College Station), L. DADONE (Boeing Vertol Co., Philadelphia, PA), and R. J. SHAW (NASA, Lewis Research Center, Cleveland, OH) AHS, Annual Forum and Technology Display, 41st, Fort Worth, TX, May 15-17, 1985, Paper. 22 p. refs

(Contract NAG3-242)

Methodology developed to predict the performance degradation of rotating systems in natural icing conditions is described and discussed. Theoretical studies of the increments performance degradation due to icing involving the propeller, helicopter in hover and forward flight, and XV-15 propulsion modes are summarized. Related experimental studies on the NACA 0012 airfoil and model helicopter with/without generic ice shapes are reviewed. The results of these experimental and theoretical studies are used to suggest refinements to current methodology. C.D.

A86-38336* National Aeronautics and Space Administration. Ames Research Center, Moffett Field, Calif.

THE STOL PERFORMANCE OF A TWO-ENGINE, USB POWERED-LIFT AIRCRAFT WITH CROSS-SHAFTED FANS

V. C. STEVENS, S. B. WILSON, III (NASA, Ames Research Center, Moffett Field, CA), and C. A. ZOLA (NASA, Lewis Research Center, Cleveland, OH) SAE, Aerospace Technology Conference and Exposition, Long Beach, CA, Oct. 14-17, 1985. 8 p. (SAE PAPER 851839)

The short takeoff and landing capabilities that characterize the performance of powered-lift aircraft are dependent on engine thrust and are, therefore, severely affected by loss of an engine. This paper shows that the effects of engine loss on the short takeoff and landing performance of powered-lift aircraft can be effectively mitigated by cross-shafting the engine fans in a twin-engine configuration. Engine-out takeoff and landing performances are compared for three powered-lift aircraft configurations: one with four engines, one with two engines, and one with two engines in which the fans are cross-shafted. The results show that the engine-out takeoff and landing performance of the cross-shafted two-engine configuration is significantly better than that of the two-engine configuration without cross-shafting. Author

A86-42704* # Garrett Turbine Engine Co., Phoenix, Ariz.

ADVANCED TECHNOLOGY PAYOFFS FOR FUTURE ROTORCRAFT, COMMUTER AIRCRAFT, CRUISE MISSILE, AND APU PROPULSION SYSTEMS

M. A. TURK and P. K. ZEINER (Garrett Turbine Engine Co., Phoenix, AZ) AIAA, ASME, SAE, and ASEE, Joint Propulsion Conference, 22nd, Huntsville, AL, June 16-18, 1986. 10 p. Army-supported research.

(Contract NAS3-24544)

(AIAA PAPER 86-1545)

In connection with the significant advances made regarding the performance of larger gas turbines, challenges arise concerning the improvement of small gas turbine engines in the 250 to 1000 horsepower range. In response to these challenges, the NASA/Army-sponsored Small Engine Component Technology (SECT) study was undertaken with the objective to identify the engine cycle, configuration, and component technology requirements for the substantial performance improvements desired in year-2000 small gas turbine engines. In the context of this objective, an American turbine engine company evaluated engines for four year-2000 applications, including a rotorcraft, a commuter aircraft, a supersonic cruise missile, and an auxiliary power unit (APU). Attention is given to reference missions, reference engines, reference aircraft, year-2000 technology projections, cycle studies, advanced engine selections, and a technology evaluation. G.R.

A86-45449* # National Aeronautics and Space Administration. Lewis Research Center, Cleveland, Ohio.

AN EXPERIMENTAL INVESTIGATION OF REDUCING ADVANCED TURBOPROP CABIN NOISE BY WING SHIELDING

J. H. DITTMAR (NASA, Lewis Research Center, Cleveland, OH) AIAA, Aerodynamics Conference, 10th, Seattle, WA, July 9-11, 1986. 18 p. Previously announced in STAR as N86-25218. refs (AIAA PAPER 86-1966)

An experimental investigation was undertaken to determine if wing shielding could reduce the noise impacting the fuselage of an advanced turboprop airplane. Four wings were tested behind two eight-bladed propeller models. Significant shielding of the propeller noise was observed and a particular wing-propeller geometry was identified to provide the most shielding. Specifically, an up-inboard rotation would be needed for a low-wing airplane and a down-inboard rotation for a high-wing airplane. As the axial Mach number was increased, the position where the shielding starts moved farther downstream. This shift in the start of shielding was roughly a straight line with respect to Mach number between $M = 0.7$ and $M = 0.8$. At $M = 0.85$ the start of shielding does not shift any farther downstream. A simple barrier noise-reduction model gave the same trends with transducer positions as did the data, and, if corrected for Mach number shift, the model might be used to provide estimates of the wing shielding. Besides providing

a barrier to the noise reaching the shielded area, the wing also reflects some of the noise back onto the unshielded area. This can make the noise difference between the unshielded and shielded areas of the fuselage larger than would be expected by simple wind shielding. Author

N86-26330* Wichita State Univ., Kans. Dept. of Aeronautical Engineering.

THEORETICAL ANALYSIS OF THE ELECTRICAL ASPECTS OF THE BASIC ELECTRO-IMPULSE PROBLEM IN AIRCRAFT DE-ICING APPLICATIONS

R. A. HENDERSON and R. L. SCHRAG Jun. 1986 108 p refs

(Contract NAG3-284)

(NASA-CR-176808; NAS 1.26:176808; AR-86-2) Avail: NTIS HC A06/MF A01 CSCL 01C

A summary of modeling the electrical system aspects of a coil and metal target configuration resembling a practical electro-impulse deicing (EIDI) installation, and a simple circuit for providing energy to the coil, was presented. The model was developed in sufficient theoretical detail to allow the generation of computer algorithms for the current in the coil, the magnetic induction on both surfaces of the target, the force between the coil and target, and the impulse delivered to the target. These algorithms were applied to a specific prototype EIDI test system for which the current, magnetic fields near the target surfaces, and impulse were previously measured. Author

N86-31562* National Aeronautics and Space Administration. Lewis Research Center, Cleveland, Ohio.

IN-FLIGHT PHOTOGRAMMETRIC MEASUREMENT OF WING ICE ACCRETIONS

R. C. MCKNIGHT, R. L. PALKO (Calspan Field Services, Inc., Arnold AFS, Tenn.), and R. L. HUMES 1986 14 p Presented at the 24th Aerospace Sciences Meeting, Reno, Nev., 6-8 Jan. 1986; sponsored by AIAA

(NASA-TM-87191; E-2847; NAS 1.15:87191) Avail: NTIS HC A02/MF A01 CSCL 01C

A photographic instrumentation system was developed for the Lewis icing research aircraft to measure wind ice accretions during flight. The system generates stereo photographs of the accretions which are then photogrammetrically measured by the Air Force Arnold Engineering and Development Center. The measurements yield a survey of spatial coordinates of an accretion's surface to an accuracy of at least + or - 0.08 cm. The accretions can then be matched to corresponding icing cloud and aerodynamic measurements. The system is being used to measure rime, mixed, and clear natural ice accretions. Author

06

AIRCRAFT INSTRUMENTATION

Includes cockpit and cabin display devices; and flight instruments.

N86-24691* John Carroll Univ., Cleveland, Ohio. Dept. of Physics.

TIME DOMAIN REFERENCING IN INTENSITY MODULATION FIBER OPTIC SENSING SYSTEMS Final Report

G. ADAMOVSKY Apr. 1986 9 p refs Presented at 1986 Quebec Symposium on Optical and Optoelectronics Applied Sciences and Engineering, Quebec, Ontario, 2-6 Jun. 1986; sponsored by Society of Photo-Optical Instrumentation Engineers (Contract NAG3-366)

(NASA-CR-175109; E-3049; NAS 1.26:175109) Avail: NTIS HC A02/MF A01 CSCL 01D

Intensity modulation sensors are classified depending on the way in which the reference and signal channels are separated: in space, wavelength (frequency), or time domains. To implement the time domain referencing different types of fiber optic (FO)

loops have been used. A pulse of short duration sent into the loop results in a series of pulses of different amplitudes. The information about the measured parameter is retrieved from the relative amplitudes of pulses in the same train. Author

07

AIRCRAFT PROPULSION AND POWER

Includes prime propulsion systems and systems components, e.g., gas turbine engines and compressors; and onboard auxiliary power plants for aircraft.

A86-11609* Army Propulsion Lab., Cleveland, Ohio.

COMBUSTION RESEARCH FOR GAS TURBINE ENGINES

E. J. MULARZ (U.S. Army, Propulsion Laboratory, Cleveland, OH) and R. W. CLAUS (NASA, Lewis Research Center, Cleveland, OH) IN: International Symposium on Air Breathing Engines, 7th, Beijing, People's Republic of China, September 2-6, 1985, Proceedings. New York, AIAA, 1985, p. 92-100. Army-supported research. Previously announced in STAR as N85-21164. refs

Research on combustion is being conducted at Lewis Research Center to provide improved analytical models of the complex flow and chemical reaction processes which occur in the combustor of gas turbine engines and other aeropropulsion systems. The objective of the research is to obtain a better understanding of the various physical processes that occur in the gas turbine combustor in order to develop models and numerical codes which can accurately describe these processes. Activities include in-house research projects, university grants, and industry contracts and are classified under the subject areas of advanced numerics, fuel sprays, fluid mixing, and radiation-chemistry. Results are high-lighted from several projects. Author

A86-11686* Stevens Inst. of Tech., Hoboken, N. J.

INFLUENCE OF ROTATION AND PRETWIST ON CANTILEVER FAN BLADE FLUTTER

F. SISTO and A. T. CHANG (Stevens Institute of Technology, Hoboken, NJ) IN: International Symposium on Air Breathing Engines, 7th, Beijing, People's Republic of China, September 2-6, 1985, Proceedings. New York, AIAA, 1985, p. 713-717. (Contract NAG3-47)

The fundamental and lowest frequency natural modes in a cantilever fan blade exhibit significant amounts of flexure and torsion coupled by pretwist and operation in a rotational force field. Consequently the flutter estimation of such blades requires an accurate structural description that incorporates these two effects, amongst others. A beam-type finite element model is used in this study with up to six spanwise elements, each element being pretwisted. Coalescence-type flutter is found with subsonic aerodynamics. Evidence of the aerodynamic resonance phenomenon is exhibited and the importance of including radially varying aerodynamic forces is brought out. Author

A86-13054* National Aeronautics and Space Administration. Lewis Research Center, Cleveland, Ohio.

FIBER OPTICS FOR PROPULSION CONTROL SYSTEMS

R. J. BAUMBICK (NASA, Lewis Research Center, Cleveland, OH) ASME, Transactions, Journal of Engineering for Gas Turbines and Power (ISSN 0022-0825), vol. 107, Oct. 1985, p. 851-855. Previously announced in STAR as N84-14111. (ASME PAPER 84-GT-97)

In aircraft systems with digital controls, fiberoptics has advantages over wire systems because of its inherent immunity to electromagnetic noise (EMI) and electromagnetic pulses (EMP). It also offers a weight benefit when metallic conductors are replaced by optical fibers. To take full advantage of the benefits of optical waveguides, passive optical sensors are also being developed to eliminate the need for electrical power to the sensor. Fiberoptics may also be used for controlling actuators on engine and airframe.

07 AIRCRAFT PROPULSION AND POWER

In this application, the optical fibers, connectors, etc. will be subjected to high temperature and vibrations. This paper discussed the use of fiber optics in aircraft propulsion systems together with the optical sensors and optically controlled actuators being developed to take full advantage of the benefits which fiber optics offers. The requirements for sensors and actuators in advanced propulsion systems are identified. The benefits of using fiber optics in place of conventional wire systems are discussed as well as the environmental conditions under which the optical components must operate. B.W.

A86-14226*# National Aeronautics and Space Administration. Lewis Research Center, Cleveland, Ohio.

SENSOR FAILURE DETECTION FOR JET ENGINES USING ANALYTICAL REDUNDANCY

W. C. MERRILL (NASA, Lewis Research Center, Cleveland, OH) Journal of Guidance, Control, and Dynamics (ISSN 0731-5090), vol. 8, Nov.-Dec. 1985, p. 673-682. Previously cited in issue 05, p. 553, Accession no. A85-16097. refs

A86-14338* National Aeronautics and Space Administration. Lewis Research Center, Cleveland, Ohio.

VIBRATION ANALYSIS OF ROTATING TURBOMACHINERY BLADES BY AN IMPROVED FINITE DIFFERENCE METHOD

K. B. SUBRAHMANYAM and K. R. V. KAZA (NASA, Lewis Research Center, Cleveland, OH) International Journal for Numerical Methods in Engineering (ISSN 0029-5981), vol. 21, Oct. 1985, p. 1871-1886. refs

The problem of calculating the natural frequencies and mode shapes of rotating blades is solved by an improved finite difference procedure based on second-order central differences. Lead-lag, flapping and coupled bending-torsional vibration cases of untwisted blades are considered. Results obtained by using the present improved theory have been observed to be close lower bound solutions. The convergence has been found to be rapid in comparison with the classical first-order finite difference method. While the computational space and time required by the present approach is observed to be almost the same as that required by the first-order theory for a given mesh size, accuracies of practical interest can be obtained by using the improved finite difference procedure with a relatively smaller matrix size, in contrast to the classical finite difference procedure which requires either a larger matrix or an extrapolation procedure for improvement in accuracy. Author

A86-14430*# Army Propulsion Lab., Cleveland, Ohio.

DEAN - A PROGRAM FOR DYNAMIC ENGINE ANALYSIS

G. G. SADLER (U.S. Army, Propulsion Laboratory, Cleveland, OH) and K. J. MELCHER (NASA, Lewis Research Center, Cleveland, OH) AIAA, SAE, and ASME, Joint Propulsion Conference, 21st, Monterey, CA, July 8-10, 1985. 17 p. Previously announced in STAR as N85-28945. refs (AIAA PAPER 85-1354)

The Dynamic Engine Analysis Program, DEAN, is a FORTRAN code implemented on the IBM/370 mainframe at NASA Lewis Research Center for digital simulation of turbofan engine dynamics. DEAN is an interactive program which allows the user to simulate engine subsystems as well as full engine systems with relative ease. The nonlinear first order ordinary differential equations which define the engine model may be solved by one of four integration schemes, a second order Runge-Kutta, a fourth order Runge-Kutta, an Adams Predictor-Corrector, or Gear's method for stiff systems. The numerical data generated by the model equations are displayed at specified intervals between which the user may choose to modify various parameters affecting the model equations and transient execution. Following the transient run, versatile graphics capabilities allow close examination of the data. DEAN's modeling procedure and capabilities are demonstrated by generating a model of simple compressor rig. Author

A86-14528*# General Electric Co., Cincinnati, Ohio.

SUBSCALE-MODEL AND FULL-SCALE ENGINE MIXED-FLOW EXHAUST SYSTEM PERFORMANCE COMPARISON

A. P. KUCHAR (General Electric Co., Advanced Engineering Technologies Dept., Cincinnati, OH) and R. CHAMBERLIN (NASA, Lewis Research Center, Cleveland, OH) Journal of Aircraft (ISSN 0021-8669), vol. 22, Nov. 1985, p. 950-955. Previously cited in issue 06, p. 723, Accession no. A84-17997. refs

A86-15225* Arnold Engineering Development Center, Arnold Air Force Station, Tenn.

RIBBON-BURNER SIMULATION OF T-700 TURBINE SHROUD FOR CERAMIC-LINED SEALS RESEARCH

J. K. LITTLE (USAF, Arnold Air Force Station, TN), G. P. ALLEN, G. McDONALD, and R. C. HENDRICKS (NASA, Lewis Research Center, Cleveland, OH) Ceramic Engineering and Science Proceedings (ISSN 0196-6219), vol. 6, July-Aug. 1985, p. 849-861. Previously announced in STAR as N85-19364. refs

Experimental and analytical studies were conducted to determine the acceptability of a ribbon-burner simulation of engine conditions for testing ceramic-lined turbine tip shrouds. The calculated values reveal that the ribbon burner establishes at least as harsh a thermal environment as is present at any time within the turbine shroud. Comparisons were made with ceramic components in a turboshaft engine. Author

A86-19196* Pennsylvania State Univ., University Park.

STABILITY OF LIMIT CYCLES IN FRICTIONALLY DAMPED AND AERODYNAMICALLY UNSTABLE ROTOR STAGES

A. SINHA (Pennsylvania State University, University Park) and J. H. GRIFFIN (Carnegie-Mellon University, Pittsburgh, PA) Journal of Sound and Vibration (ISSN 0022-460X), vol. 103, Dec. 8, 1985, p. 341-356. refs

(Contract NAG3-231)

This paper deals with the stability of limit cycles (Steady-State Oscillations) associated with the multi-degree-of-freedom model of a frictionally damped and aerodynamically unstable rotor stage. By using the first order averaging technique, a generalized criterion has been established to sort out those unstable limit cycles which govern the maximum transient amplitude beyond which the rotor stage becomes unstable. The stability of the remaining steady-state solutions is analyzed by linearizing the averaged system of differential equations. Numerical results are discussed for three-, four- and five-bladed disks. Author

A86-19677*# Purdue Univ., West Lafayette, Ind.

AN EXPERIMENTAL INVESTIGATION OF PROPELLER WAKES USING A LASER DOPPLER VELOCIMETER

R. M. SUNDAR (Embry-Riddle Aeronautical University, Prescott, AZ) and J. P. SULLIVAN (Purdue University, West Lafayette, IN) AIAA, Aerospace Sciences Meeting, 24th, Reno, NV, Jan. 6-9, 1986. 7 p.

(Contract NSG-3135)

(AIAA PAPER 86-0080)

The results of experimental investigations on three single rotation propellers are summarized in this paper. Force measurements showed a definite improvement in efficiency at low advance ratios and in static operation due to use of proplets. Extensive velocity measurements were made using a LDV system. The large amounts of data gathered are presented to reveal clearly the tip vortex streaming back from the propeller. The velocities were also processed using momentum theorem to obtain the thrust and power radial distributions as well as the integrated thrust and power coefficients. The thrust coefficient compared well with force measurements and theoretical prediction from vortex lattice and Goldstein analysis. However, the power coefficient calculated from the momentum analysis was consistently lower than the theoretical or measured values. The measured velocities were also used to compute the vorticity and the trajectory of the tip vortex in the wake behind the propeller. Author

A86-19678*# Flow Research, Inc., Kent, Wash.

PROPELLER DESIGN BY OPTIMIZATION

M. H. RIZK and W.-H. JOU (Flow Industries, Inc., Kent, WA) AIAA, Aerospace Sciences Meeting, 24th, Reno, NV, Jan. 6-9, 1986. 10 p. refs

(Contract NAS3-24533)

(AIAA PAPER 86-0081)

The feasibility of designing propellers by an optimization procedure is investigated. A scheme, which solves the full potential flow equation about a propeller by line relaxation, is modified so that the iterative solutions of the flow equation and the design parameters are updated simultaneously. Some technical problems in using optimization for designing propellers with maximum efficiency are identified. Approaches for overcoming these problems are presented. Author

A86-20369*# Texas A&M Univ., College Station.

A NUMERICAL METHOD FOR THE DESIGN AND ANALYSIS OF COUNTER-ROTATING PROPELLERS

S. C. PLAYLE, K. D. KORKAN, and E. VON LAVANTE (Texas A & M University, College Station) Journal of Propulsion and Power (ISSN 0748-4658), vol. 2, Jan.-Feb. 1986, p. 57-63. refs

(Contract NAG3-354)

(AIAA PAPER 84-1205)

A numerical method has been developed using the techniques of Lock and Theodorsen as described by Davidson to design and analyze counter-rotating propellers. The design method develops the optimum propeller geometry by calculating the planform and twist distribution for each propeller disk through the use of specific inputs of engine shaft horsepower, diameter, and disk spacing. The analysis method calculates the performance of a given counter-rotating propeller system at any flight condition. Using the NACA four-digit airfoil family, the performance of a counter-rotating propeller design for a given flight condition was investigated in the design and analysis mode. Author

A86-22068*# Princeton Univ., N. J.

VIBRATION CHARACTERISTICS OF MISTUNED SHROUDED BLADE ASSEMBLIES

O. O. BENDIKSEN (Princeton University, NJ) and N. A. VALERO ASME, International Gas Turbine Conference and Exhibit, 30th, Houston, TX, Mar. 18-21, 1985. 7 p. refs

(Contract NAG3-308)

(ASME PAPER 85-GT-115)

An investigation of the mode localization phenomenon associated with mistuning is presented for shrouded blade assemblies. The calculations are based on a generic finite element model, which permits modeling of arbitrary mistuning and both slipping and nonslipping shroud interfaces. The results presented indicate that interactions occur between mistuning and slip effects, with maximum mode localization occurring when the shrouds slip freely. Certain modes are found to be very sensitive to shroud slip, and in some cases completely change character when slip occurs. Mode localization is most pronounced in the predominantly bending modes, and varies considerably from mode to mode. As the ratio of interblade coupling strength to mistuning strength is increased, the effect of mistuning is observed to decrease significantly. This result has important implications for the flutter problem, since it suggests that the stabilization effect available from mistuning is significantly less for a shrouded rotor as compared to an unshrouded rotor. Author

A86-22081*# General Electric Co., Cincinnati, Ohio.

EVALUATION OF FUEL PREPARATION SYSTEMS FOR LEAN PREMIXING-PREVAPORIZING COMBUSTORS

W. J. DODDS and E. E. EKSTEDT (General Electric Co., Aircraft Engine Business Group, Cincinnati, OH) ASME, International Gas Turbine Conference and Exhibit, 30th, Houston, TX, Mar. 18-21, 1985. 5 p. refs

(Contract NAS3-22006)

(ASME PAPER 85-GT-137)

A series of experiments was carried out in order to produce design data for a premixing prevaporizing fuel-air mixture

preparation system for aircraft gas turbine engine combustors. The fuel-air mixture uniformity of four different system design concepts was evaluated over a range of conditions representing the cruise operation of a modern commercial turbofan engine. Operating conditions including pressure, temperature, fuel-to-air ratio, and velocity, exhibited no clear effect on mixture uniformity of systems using pressure-atomizing fuel nozzles and large-scale mixing devices. However, the performance of systems using atomizing fuel nozzles and large-scale mixing devices was found to be sensitive to operating conditions. Variations in system design variables were also evaluated and correlated. Mixing uniformity was found to improve with system length, pressure drop, and the number of fuel injection points per unit area. A premixing system capable of providing mixing uniformity to within 15 percent over a typical range of cruise operating conditions is demonstrated. I.H.

A86-22088*# Cornell Univ., Ithaca, N.Y.

A THEORY OF POST-STALL TRANSIENTS IN AXIAL COMPRESSION SYSTEMS. I - DEVELOPMENT OF EQUATIONS

F. K. MOORE (Cornell University, Ithaca, NY) and E. M. GREITZER (MIT, Cambridge, MA) ASME, International Gas Turbine Conference and Exhibit, 30th, Houston, TX, Mar. 16-21, 1985. 9 p. refs

(Contract NAG3-34; NSG-3208)

(ASME PAPER 85-GT-171)

An approximate theory is presented for post-stall transients in multistage axial compression systems. The theory leads to a set of three simultaneous nonlinear third-order partial differential equations for pressure rise, and average and disturbed values of flow coefficient, as functions of time and angle around the compressor. By a Galerkin procedure, angular dependence is averaged, and the equations become first order in time. These final equations are capable of describing the growth and possible decay of a rotating-stall cell during a compressor mass-flow transient. It is shown how rotating-stall-like and surge-like motions are coupled through these equations, and also how the instantaneous compressor pumping characteristic changes during the transient stall process. Author

A86-22089*# Massachusetts Inst. of Tech., Cambridge.

A THEORY OF POST-STALL TRANSIENTS IN AXIAL COMPRESSION SYSTEMS. II - APPLICATION

E. M. GREITZER (MIT, Cambridge, MA) and F. K. MOORE (Cornell University, Ithaca, NY) ASME, International Gas Turbine Conference and Exhibit, 30th, Houston, TX, Mar. 18-21, 1985. 9 p. refs

(Contract NSG-3208)

(ASME PAPER 85-GT-172)

Using the theory developed in Part I, calculations have been carried out to show the evolution of the mass flow, pressure rise, and rotating-stall cell amplitude during compression system post-stall transients. In particular, it is shown that the unsteady growth or decay of the stall cell can have a significant effect on the instantaneous compressor pumping characteristic and hence on the overall system behavior. A limited parametric study is carried out to illustrate the impact of different system features on transient behavior. It is shown, for example, that the ultimate mode of system response, surge or stable rotating stall, depends not only on the B parameter, but also on the compressor length-to-radius ratio. Small values of this latter quantity tend to favor the occurrence of surge, as do large values of B. Based on the analytical and numerical results, several specific topics are suggested for future research on post-stall transients. Author

07 AIRCRAFT PROPULSION AND POWER

A86-22090*# Pennsylvania State Univ., University Park.
END-WALL AND PROFILE LOSSES IN A LOW-SPEED AXIAL FLOW COMPRESSOR ROTOR

B. LAKSHMINARAYANA, N. SITARAM, and J. ZHANG (Pennsylvania State University, University Park, PA) ASME, International Gas Turbine Conference and Exhibit, 30th, Houston, TX, Mar. 18-21, 1985. 10 p. refs
(Contract NSG-3032)
(ASME PAPER 85-GT-174)

The blade-to-blade variation of relative stagnation pressure losses in the tip region inside the rotor of a single-stage, axial-flow compressor, is presented and interpreted in this paper. The losses are measured at two flow coefficients (one at the design point and the other at the near peak pressure rise point) to discern the effect of blade loading on the end-wall losses. The tip clearance losses are found to increase with an increase in the pressure rise coefficient. The losses away from the tip region and near the hub regions are measured downstream. The losses are integrated and interpreted in this paper. Author

A86-24677*# Massachusetts Inst. of Tech., Cambridge.
AEROELASTIC FORMULATIONS FOR TURBOMACHINES AND PROPELLERS

E. F. CRAWLEY (MIT, Cambridge, MA) IN: Unsteady aerodynamics of turbomachines and propellers; Proceedings of the Symposium, Cambridge, England, September 24-27, 1984. Cambridge, Cambridge University, 1984, p. 13-28. Navy-supported research. refs
(Contract NSG-3079)

The task of the aeroelastic analysis is to combine the formulations of the structural dynamic and unsteady aerodynamic models in a consistent manner, to solve the resulting aeroelastic model to determine the dynamic behavior (e.g., stability, forced vibration), and to interpret those results for both qualitative trends, and quantitative detail. A review of the various formulations of the aeroelastic problem and a comparison of their relative advantages will be the subject of this paper. Specifically, the topics to be addressed are: the formulation of the aeroelastic problem, including a summary of the relations necessary to transform various diverse structural and aerodynamic models to a consistent notation for oscillatory motion; an approximate transformation for arbitrary temporal behavior; and a brief review of the applicable solution techniques. Author

A86-25743*# General Electric Co., Cincinnati, Ohio.
THE DYNAMICS OF A FLEXIBLE BLADED DISC ON A FLEXIBLE ROTOR IN A TWO-ROTOR SYSTEM

V. C. GALLARDO and M. J. STALLONE (General Electric Co., Aircraft Engine Business Group, Cincinnati, OH) IN: International Conference on Vibrations in Rotating Machinery, 3rd, Heslington, England, September 11-13, 1984, Proceedings. London, Mechanical Engineering Publications, Ltd., 1984, p. 383-390. refs
(Contract NAS3-23281)

This paper describes the development of the analysis of the transient dynamic response of a bladed disk on a flexible rotor. The rotating flexible bladed disk is considered as a module in a complete turbine engine structure. The analysis of the flexible bladed disk (FBD) module is developed for the non-equilibrated one-diameter axial mode. The FBD motion is considered as a sum of two standing axial waves constrained to the rotor. The FBD is coupled inertially and gyroscopically to its rotor support, and indirectly through connecting elements, to the adjacent rotor and/or other supporting structures. Incorporated in the basic Turbine Engine Transient Response Analysis program (TETRA), the FBD module is demonstrated with a two-rotor model where the FBD can be excited into resonance by an unbalance in the adjacent rotor and at a frequency equal to the differential rotor speed. The FBD module also allows the analysis of two flexible bladed disks in the same rotor. Author

A86-26636*# National Aeronautics and Space Administration.
Lewis Research Center, Cleveland, Ohio.

PREDICTION OF THE STRUCTURE OF FUEL SPRAYS IN GAS TURBINE COMBUSTORS

J.-S. SHUEN (NASA, Lewis Research Center; Sverdrup Technology, Inc., Cleveland, OH) AIAA, Aerospace Sciences Meeting, 24th, Reno, NV, Jan. 6-9, 1986. 16 p. Previously announced in STAR as N86-16218. refs
(Contract NAS3-24105)
(AIAA PAPER 86-0450)

The structure of fuel sprays in a combustion chamber is theoretically investigated using computer models of current interest. Three representative spray models are considered: (1) a locally homogeneous flow (LHF) model, which assumes infinitely fast interphase transport rates; (2) a deterministic separated flow (DSF) model, which considers finite rates of interphase transport but ignores effects of droplet/turbulence interactions; and (3) a stochastic separated flow (SSF) model, which considers droplet/turbulence interactions using random sampling for turbulence properties in conjunction with random-walk computations for droplet motion and transport. Two flow conditions are studied to investigate the influence of swirl on droplet life histories and the effects of droplet/turbulence interactions on flow properties. Comparison of computed results with the experimental data show that general features of the flow structure can be predicted with reasonable accuracy using the two separated flow models. In contrast, the LHF model overpredicts the rate of development of the flow. While the SSF model provides better agreement with measurements than the DSF model, definitive evaluation of the significance of droplet/turbulence interaction is not achieved due to uncertainties in the spray initial conditions. D.O.E.

A86-26893*# Toledo Univ., Ohio.

THE EFFECTS OF STRONG SHOCK LOADING ON COUPLED BENDING-TORSION FLUTTER OF TUNED AND MISTUNED CASCADES

B. C. BUSBEY (Toledo University; Teledyne CAE, OH), T. G. KEITH, JR. (NASA, Lewis Research Center, Cleveland, OH), and K. R. V. KAZA (Toledo, University, OH) IN: Fluid-structure interaction and aerodynamics damping; Proceedings of the Tenth Biennial Conference on Mechanical Vibration and Noise, Cincinnati, OH, September 10-13, 1985. New York, American Society of Mechanical Engineers, 1985, p. 93-108. refs
(Contract NSG-3139)

This paper presents an investigation of the effects of strong in-passage shock waves on coupled bending-torsion flutter of both tuned and mistuned cascades. The aerodynamic and inertial coupling between the bending and torsional motions of each blade are included in the analytical model. Analysis revealed (1) that the shock loading has a beneficial effect on torsional flutters of both tuned and mistuned cascades and (2) that alternating bending mistuning has a beneficial effect on shock load induced bending flutter. The latter finding becomes important when shock induced bending flutter is a problem. Author

A86-26901*# National Aeronautics and Space Administration.
Lewis Research Center, Cleveland, Ohio.

VIBRATIONS OF BLADES AND BLADED DISK ASSEMBLIES; PROCEEDINGS OF THE TENTH BIENNIAL CONFERENCE ON MECHANICAL VIBRATION AND NOISE, CINCINNATI, OH, SEPTEMBER 10-13, 1985

R. E. KIELB, ED. (NASA, Lewis Research Center, Cleveland, OH) and N. F. RIEGER, ED. Conference sponsored by ASME. New York, American Society of Mechanical Engineers, 1985, 123 p. For individual items see A86-26902 to A86-26914.

The papers presented in this volume provide an overview of recent theoretical and analytical research in bladed disk assemblies, with particular attention given to forced response, mistuning, and damping. Specific topics discussed include the response of mistuned bladed disk assemblies; forced response analysis of an aerodynamically detuned supersonic turbomachine rotor; dynamic analysis of blade groups using component mode synthesis; and

pendulum dynamic vibration absorbers for reducing blade vibration in industrial fans. V.L.

A86-26902*# National Aeronautics and Space Administration. Lewis Research Center, Cleveland, Ohio.

FORCED RESPONSE ANALYSIS OF AN AERODYNAMICALLY DETUNED SUPERSONIC TURBOMACHINE ROTOR

D. HOYNIK (NASA, Lewis Research Center, Cleveland, OH) and S. FLEETER (Purdue University, West Lafayette, IN) IN: Vibrations of blades and bladed disk assemblies; *Proceedings of the Tenth Biennial Conference on Mechanical Vibration and Noise*, Cincinnati, OH, September 10-13, 1985. New York, American Society of Mechanical Engineers, 1985, p. 1-13. NASA-supported research. refs

The effect of aerodynamic detuning on the supersonic flow induced forced response behavior of a turbomachine blade row is analyzed using an aeroelastic model. The rotor is modeled as a flat plate airfoil cascade representing an unwrapped rotor annulus; the aerodynamic detuning is achieved by alternating the circumferential spacing of adjacent rotor blades. The total unsteady aerodynamic loading on the blading, due to the convection of the transverse gust past the airfoil cascade as well as that resulting from the motion of the cascade, is developed in terms of influence coefficients. The model developed here is then used to analyze the effect of aerodynamic detuning on the flow induced forced response behavior of a twelve-bladed rotor with Verdon's Cascade B flow geometry. V.L.

A86-26905*# Carnegie-Mellon Univ., Pittsburgh, Pa.

THE EFFECT OF LIMITING AERODYNAMIC AND STRUCTURAL COUPLING IN MODELS OF MISTUNED BLADED DISK VIBRATION

P. BASU and J. H. GRIFFIN (Carnegie-Mellon University, Pittsburgh, PA) IN: Vibrations of blades and bladed disk assemblies; *Proceedings of the Tenth Biennial Conference on Mechanical Vibration and Noise*, Cincinnati, OH, September 10-13, 1985. New York, American Society of Mechanical Engineers, 1985, p. 31-40. refs

(Contract NAG3-367)

A model has been developed for studying the effect of mistuning on bladed disk vibration which has the unique feature that the extent of aerodynamic and structural interaction which it simulates can be readily varied from full coupling of all blades on the disk to coupling of each blade with only its nearest neighbors. Simulations utilizing the resulting algorithm show that limited coupling models may be used to predict the statistical distribution of blade amplitudes that characterizes the mistuning effect, which in turn determines stage durability. This approach is used to study the effect of changing various system parameters on amplitude scatter. Gas density, the number of blades on the disk, disk stiffness, and the engine order of the excitation are considered. The results are used to draw some conclusions about how to improve laboratory tests and component design. Author

A86-31595*# National Aeronautics and Space Administration. Lewis Research Center, Cleveland, Ohio.

AERODYNAMIC AND STRUCTURAL DETUNING OF SUPERSONIC TURBOMACHINE ROTORS

D. HOYNIK (NASA, Lewis Research Center, Cleveland, OH) and S. FLEETER (Purdue University, West Lafayette, IN) (Structures, Structural Dynamics, and Materials Conference, 26th, Orlando, FL, April 15-17, 1985, Technical Papers, Part 2, p. 500-514) *Journal of Propulsion and Power* (ISSN 0748-4658), vol. 2, Mar.-Apr. 1986, p. 161-167. Previously cited in issue 13, p. 1850, Accession no. A85-30378. refs

A86-32956*# United Technologies Research Center, East Hartford, Conn.

DYNAMIC CHARACTERISTICS OF AN ASSEMBLY OF PROP-FAN BLADES

A. V. SRINIVASAN (United Technologies Research Center, East Hartford, CT), R. E. KIELB, and C. LAWRENCE (NASA, Lewis Research Center, Cleveland, OH) ASME, Transactions, Journal of Engineering for Gas Turbines and Power (ISSN 0022-0825), vol. 108, April 1986, p. 306-312. refs (ASME PAPER 85-GT-134)

In contrast to conventional propellers, propfan blades are thin and highly swept-back, thereby giving rise to large bending and twisting deformations and complex vibratory characteristics. Aerodynamic performance depends on the extent of steady state deformation, and the aeroelastic response depends on the vibratory frequency and mode shape. Attention is presently given to the principal results of structural analyses for a five-bladed propfan assembly; these results are compared with test data. The results encompass both steady deformations and vibratory frequencies and mode shapes in a vacuum centrifugal environment. O.C.

A86-32957*# Pennsylvania State Univ., University Park.

INFLUENCE OF FRICTION DAMPERS ON TORSIONAL BLADE FLUTTER

A. SINHA (Pennsylvania State University, University Park), J. H. GRIFFIN (Carnegie-Mellon University, Pittsburgh, PA), and R. E. KIELB (NASA, Lewis Research Center, Cleveland, OH) ASME, Transactions, Journal of Engineering for Gas Turbines and Power (ISSN 0022-0825), vol. 108, April 1986, p. 313-318. refs (ASME PAPER 85-GT-170)

This paper deals with the stabilizing effects of dry friction on torsional blade flutter. A lumped parameter model with single degree of freedom per blade has been used to represent the rotor stage. The well-known cascade theories for incompressible and supersonic flows have been used to determine the allowable increase in fluid velocity relative to the blade. It has been found that the effectiveness of friction dampers in controlling flutter can be substantial. Author

A86-35400* Alphatech, Inc., Burlington, Mass.

APPLICATION OF FDI METRICS TO DETECTION AND ISOLATION OF SENSOR FAILURES IN TURBINE ENGINES

J. L. WEISS, A. S. WILLSKY, K. R. PATTIPATI, and J. S. ETERNO (Alphatech, Inc., Burlington, MA) IN: 1985 American Control Conference, 4th, Boston, MA, June 19-21, 1985, *Proceedings*. Volume 2. New York, Institute of Electrical and Electronics Engineers, 1985, p. 1114-1120. refs (Contract NAS3-24078)

This paper develops a framework for the design of failure detection and isolation (FDI) algorithms. Rather than trying to apply 'optimal' techniques in a top-down manner, the system redundancies are evaluated with respect to their ability to provide reliable FDI information. Previous work of Pattipati et al. (1984) and Weiss et al. (1984) defined a useful context and several useful analytical results, which provide a basis for the FDI design methodology developed here. A general decision structure which can take advantage of redundancy evaluation is presented, and examples of typical design considerations are discussed. The operation of the decision structure is then demonstrated for a sensor FDI application involving the F-100 jet engine. Author

A86-35402* Systems Control Technology, Inc., Palo Alto, Calif. **ROBUST DETECTION, ISOLATION, AND ACCOMMODATION FOR SENSOR FAILURES**

A. EMAMI-NAEINI, M. M. AKHTER, and S. M. ROCK (Systems Control Technology, Inc., Palo Alto, CA) IN: 1985 American Control Conference, 4th, Boston, MA, June 19-21, 1985, *Proceedings*. Volume 2. New York, Institute of Electrical and Electronics Engineers, 1985, p. 1129-1134. refs (Contract NAS3-24079)

Recent advances in multivariable robust control system design are extended to sensor failure, detection, isolation, and accommodation (FDIA) and estimator design. A new concept called

07 AIRCRAFT PROPULSION AND POWER

threshold selector is introduced. It represents a significant and innovative tool for the analysis and synthesis of FDIA algorithms. Analytical results are obtained for the SISO case to compute optimal thresholds and size of minimum detectable failures, and a computer-aided technique is developed for the multivariable case. The techniques have been applied to sensor FDIA for an aircraft turbine engine control system. Author

A86-35403* Scientific Systems, Inc., Cambridge, Mass.
BIFURCATION TECHNIQUES FOR NONLINEAR DYNAMIC ANALYSIS OF COMPRESSOR STALL PHENOMENA

H. C. RAZAVI and R. K. MEHRA (Scientific Systems, Inc., Cambridge, MA) IN: 1985 American Control Conference, 4th, Boston, MA, June 19-21, 1985, Proceedings. Volume 2. New York, Institute of Electrical and Electronics Engineers, 1985, p. 1135-1142. refs

(Contract NAS3-24089; NSF CEE-81-00491)

Compressor stall phenomena is analyzed from nonlinear control theory viewpoint, based on bifurcation-catastrophe techniques. This new approach appears promising and offers insight into such well known compressor instability problems as surge and rotating stall; furthermore it suggests strategies for recovery from stall. Three interlocking dynamic nonlinear state space models are developed. It is shown that the problem of rotating stall can be viewed as an (induced) bifurcation of solution of the unstalled model. Hysteresis effect is shown to exist in the stall/recovery process. Surge cycles are observed to develop for some critical parameter values. It is shown that the oscillatory behavior is due to development of limit cycles, generated by Hopf bifurcation of solutions. Both stable and unstable limit cycles are observed. To further illustrate the usefulness of the methodology some partial computation of domains of attraction of equilibria is carried out, and parameter sensitivity analysis is performed. Author

A86-35614* General Electric Co., Lynn, Mass.

THE APPLICATION OF LQR SYNTHESIS TECHNIQUES TO THE TURBOSHAFT ENGINE CONTROL PROBLEM

W. H. PFEIL, G. DE LOS REYES (General Electric Co., Aircraft Engine Business Group, Lynn, MA), and G. A. BOBULA (NASA, Lewis Research Center; U.S. Army, Propulsion Laboratory, Cleveland, OH) IN: American Helicopter Society, Annual Forum, 41st, Fort Worth, TX, May 15-17, 1985, Proceedings. Alexandria, VA, American Helicopter Society, 1985, p. 189-196. refs (Contract NAS3-22763)

A power turbine governor was designed for a recent-technology turboshaft engine coupled to a modern, articulated rotor system using Linear Quadratic Regulator (LQR) and Kalman Filter (KF) techniques. A linear, state-space model of the engine and rotor system was derived for six engine power settings from flight idle to maximum continuous. An integrator was appended to the fuel flow input to reduce the steady-state governor error to zero. Feedback gains were calculated for the system states at each power setting using the LQR technique. The main rotor tip speed state is not measurable, so a Kalman Filter of the rotor was used to estimate this state. The crossover of the system was increased to 10 rad/s compared to 2 rad/sec for a current governor. Initial computer simulations with a nonlinear engine model indicate a significant decrease in power turbine speed variation with the LQR governor compared to a conventional governor. Author

A86-37827*# Nielsen Engineering and Research, Inc., Mountain View, Calif.

UNSTEADY FORCES ON COUNTER-ROTATING PROPELLER BLADES

D. J. LESIEUTRE (Nielsen Engineering and Research, Inc., Mountain View, CA) and J. P. SULLIVAN (Purdue University, West Lafayette, IN) IN: Applied Aerodynamics Conference, 4th, San Diego, CA, June 9-11, 1986, Technical Papers. New York, American Institute of Aeronautics and Astronautics, 1986, p. 229-236. refs

(Contract NSG-3135)

(AIAA PAPER 86-1804)

Unsteady forces experienced by counter-rotating propeller blades are examined in this paper. A fully coupled vortex lattice model of counter-rotation is used to obtain a quasi-steady solution to the propeller loadings, and an unsteady Sears (1941) analysis provides an estimate of the unsteady loads from the quasi-steady results. The vortex lattice method predicts the overall performance of counter-rotation well, based on comparisons of measured and predicted results. The effects of propeller spacing and blade number on the unsteady loadings are investigated. The peak-to-peak variation about the mean of the unsteady loads on the rear propeller varied from 9 percent for a 2 x 2 counter-rotation system to 2 percent for an 8 x 8 system. Author

A86-38892*# Purdue Univ., West Lafayette, Ind.

PASSIVE CONTROL OF AERODYNAMICALLY FORCED VIBRATIONS OF SUPERSONIC TURBOMACHINE ROTORS BY SPLITTER BLADES

S. FLEETER, D. A. TOPP (Purdue University, West Lafayette, IN), and D. HOYNIK (NASA, Lewis Research Center, Cleveland, OH) IN: Structures, Structural Dynamics and Materials Conference, 27th, San Antonio, TX, May 19-21, 1986, Technical Papers. Part 2. New York, American Institute of Aeronautics and Astronautics, 1986, p. 77-88. NASA-supported research. refs (AIAA PAPER 86-0844)

An aeroelastic model is developed to examine the use of splitter blades as a passive detuning mechanism for flow induced forced response of unstalled supersonic turbomachine rotors. The splitters introduce aerodynamic and structural detuning to the rotor design. The relationship between aerodynamic and structural detuning and the location and chord lengths of splitters is analyzed. The model is applied to the flow induced response of four 12-blade rotors with Verdon's (1973) Cascade B flow geometry. The data reveal that for gusts characterized by forward and backward traveling waves the splitters generally decrease the maximum amplitudes of response; however, for some gust load interblade phase angles, such as -180 deg and 120 deg the splitters did not reduce the amplitudes of response. I.F.

A86-38894*# Purdue Univ., West Lafayette, Ind.

THREE DIMENSIONAL UNSTEADY AERODYNAMICS AND AEROELASTIC RESPONSE OF ADVANCED TURBOPROPS

M. H. WILLIAMS and C.-C. HWANG (Purdue University, West Lafayette, IN) IN: Structures, Structural Dynamics and Materials Conference, 27th, San Antonio, TX, May 19-21, 1986, Technical Papers. Part 2. New York, American Institute of Aeronautics and Astronautics, 1986, p. 116-124. refs

(Contract NAG3-499)

(AIAA PAPER 86-0846)

A method for the prediction of steady and unsteady aerodynamic loads and aeroelastic response of advanced turboprops is presented. The aerodynamic analysis uses three dimensional unsteady linearized compressible flow theory to compute the blade pressure distribution. The aeroelastic analysis is based on a normal mode representation of the structure. The method is applicable to both conventional and advanced turbo-prop configurations, provided that blade stall and transonic shock waves are not important factors. Aerodynamic results are presented which validate the model in various limits by comparisons to alternative theories and experimental data. Finally, results of a stability analysis of an advanced turboprop are given, with comparisons to measurements made at NASA Lewis Research Center. Author

A86-41726*# Texas A&M Univ., College Station.
NUMERICAL EVALUATION OF PROPELLER NOISE INCLUDING NONLINEAR EFFECTS

K. D. KORKAN, E. VON LAVANTE (Texas A&M University, College Station), and L. J. BOBER (NASA, Lewis Research Center, Cleveland, OH) AIAA Journal (ISSN 0001-1452), vol. 24, June 1986, p. 1043-1045. refs
 (Contract NAG3-354)

Propeller noise in the acoustic near field is presently determined through the integration of the pressure-time history in the tangential direction of a numerically generated flowfield around a propfan of SR-3 type, including the shock wave system in the vicinity of the propeller tip. This acoustic analysis yields overall sound pressure levels, and the associated frequency spectra, as a function of observer location. O.C.

A86-42702*# General Motors Corp., Indianapolis, Ind.
ROTORCRAFT PROPULSION FOR YEAR 2000 PLUS
 T. R. LARKIN, D. V. STATON, and H. C. MONGIA (General Motors Corp., Allison Gas Turbine Div., Indianapolis, IN) AIAA, ASME, SAE, and ASEE, Joint Propulsion Conference, 22nd, Huntsville, AL, June 16-18, 1986. 6 p. Army-supported research.
 (Contract NAS3-24542)
 (AIAA PAPER 86-1543)

The objective of this study was to identify high-payoff technologies for year 2000 small gas turbine engines for rotorcraft application. A current state-of-the-art technology Allison gas turbine engine was used as a baseline and three advanced concepts were studied: the simple cycle engine, a waste heat recovery cycle, and a wave rotor engine cycle. For the simple cycle engine, two general arrangements were considered: the traditional concentric spool arrangement and a nonconcentric spool arrangement. Both a regenerative and a recuperative cycle were studied for the waste heat recovery cycle. An extensive cycle optimization procedure was performed for each configuration under study using relative direct operating cost (DOC) as the figure of merit. A high pressure ratio nonconcentric engine provided the greatest reduction in DOC with a 16.5 percent improvement.

Author

A86-42703*# Avco Lycoming Div., Stratford, Conn.
SMALL ENGINE TECHNOLOGY PAYOFFS FOR FUTURE COMMUTER AIRCRAFT

H. KAEHLER and W. SCHNEIDER (Avco Lycoming Textron, Stratford, CT) AIAA, ASME, SAE, and ASEE, Joint Propulsion Conference, 22nd, Huntsville, AL, June 16-18, 1986. 12 p. Army-supported research.
 (Contract NAS3-24545)
 (AIAA PAPER 86-1544)

High payoff technologies for a year 2000 regenerative cycle turboprop engine were identified for a 19 passenger commuter aircraft application. A series of engines incorporating eight levels of advanced technologies were studied and their impact on aircraft performance was evaluated. Four advanced technologies are recommended to achieve a potential reduction in fuel burn of 38.3 percent. At \$1.00 per gallon fuel price, a potential direct operating cost (DOC) benefit of 12.5 percent is obtained. At \$2.00 per gallon, the potential DOC benefit increases to 17.0 percent.

Author

A86-42705*# Teledyne CAE, Toledo, Ohio.
YEAR 2000 SMALL ENGINE TECHNOLOGY PAYOFFS IN CRUISE MISSILES

B. SINGH and E. H. BENSTEIN (Teledyne, Inc., Teledyne CAE, Toledo, OH) AIAA, ASME, SAE, and ASEE, Joint Propulsion Conference, 22nd, Huntsville, AL, June 16-18, 1986. 9 p. Army-supported research.
 (Contract NAS3-24541)
 (AIAA PAPER 86-1546)

A study has been conducted for advanced small (450-850 pounds thrust) gas turbine engines for a subsonic strategic cruise missile application, using projected year-2000 technology. Engine performance and configuration analyses were performed for two

and three spool turbofan and propfan engine concepts. Mission and Life Cycle Cost (LCC) analyses were performed in which the candidate engines were compared to the baseline engine over a prescribed mission. The advanced technology engines reduced system LCC up to 41 percent relative to the baseline engine. The critical aerodynamic materials and mechanical systems necessary for turbine engine technology were identified. Author

A86-42755*# Purdue Univ., West Lafayette, Ind.
TRANSIENT ENGINE PERFORMANCE WITH WATER INGESTION

T. HAYKIN and S. N. B. MURTHY (Purdue University, West Lafayette, IN) AIAA, ASME, SAE, and ASEE, Joint Propulsion Conference, 22nd, Huntsville, AL, June 16-18, 1986. 21 p. refs
 (Contract NAG3-481)
 (AIAA PAPER 86-1621)

The immediate effects on the transient performance of a generic, high bypass ratio jet engine on account of water ingestion are discussed. The air compression subsystem has been analyzed with respect to four aerothermodynamic and mechanical processes associated with two-phase fluid flow and the engine simulation has been carried out under three limiting cases of interest in practice, one pertaining to draining of water at the end of compression and the other two, to partial evaporation at two different locations in the burner. General observations are made on engine operability as a function of engine and control design under various engine and (control input) sensor operating conditions, with various mass fractions of water in the air-water mixture entering the engine, during various pilot-initiated power demand changes.

Author

A86-45504*# United Technologies Corp., Windsor Locks, Conn.
PROPELLER NOISE CAUSED BY BLADE TIP RADIAL FORCES

D. B. HANSON (United Technologies Corp., Hamilton Standard Div., Windsor Locks, CT) AIAA, Aeroacoustics Conference, 10th, Seattle, WA, July 9-11, 1986. 11 p. Research supported by United Technologies Corp. refs
 (Contract NAS3-23720; NAS3-23051)
 (AIAA PAPER 86-1892)

New experimental evidence which indicates the presence of leading edge and tip edge vortex flow on Prop-Fans is examined, and performance and noise consequences are addressed. It was shown that the tip edge vortex is a significant noise source, particularly for unswept Prop-Fan blades. Preliminary calculations revealed that the addition of the tip side edge source to single rotation Prop-Fans during take off conditions improved the agreement between experiment and theory at blade passing frequency. At high-speed conditions such as the Prop-Fan cruise point, the tip loading effect tends to cancel thickness noise. K.k.

A86-48141*# National Aeronautics and Space Administration.
LEWIS RESEARCH CENTER, CLEVELAND, OHIO.

COMPUTATIONAL ENGINE STRUCTURAL ANALYSIS
 C. C. CHAMIS and R. H. JOHNS (NASA, Lewis Research Center, Cleveland, OH) ASME, International Gas Turbine Conference and Exhibit, 31st, Duesseldorf, West Germany, June 8-12, 1986. 12 p. Previously announced in STAR as N86-19663. refs
 (ASME PAPER 86-GT-70)

A significant research activity at the NASA Lewis Research Center is the computational simulation of complex multidisciplinary engine structural problems. This simulation is performed using computational engine structural analysis (CESA) which consists of integrated multidisciplinary computer codes in conjunction with computer post-processing for problem-specific application. A variety of the computational simulations of specific cases are described in some detail in this paper. These case studies include: (1) aeroelastic behavior of bladed rotors, (2) high velocity impact of fan blades, (3) blades-loss transient response, (4) rotor/stator/squeeze-film/bearing interaction, (5) blade-fragment/rotor-burst containment, and (6) structural behavior of advanced swept turboprops. These representative case studies are selected to demonstrate the breath of the problems analyzed and the role

07 AIRCRAFT PROPULSION AND POWER

of the computer including post-processing and graphical display of voluminous output data. Author

A86-48145*# Calspan Corp., Buffalo, N. Y.
HEAT-FLUX MEASUREMENTS FOR THE ROTOR OF A FULL-STAGE TURBINE. I - TIME-AVERAGED RESULTS
M. G. DUNN (Calspan Research Center, Buffalo, NY) ASME, International Gas Turbine Conference and Exhibit, 31st, Duesseldorf, West Germany, June 8-12, 1986. 8 p. refs (Contract NAG3-469; NAG3-581) (ASME PAPER 86-GT-77)

Blade measurements of time-averaged flux distribution are obtained with and without gas injection for a full-stage rotating turbine. Results are presented along the blade in the flow direction at 10, 50, and 90 percent span locations for both the pressure and suction surfaces; enough measurements were obtained to present spanwise distributions as well. The results suggest that the suction surface laminar flat plate prediction is in reasonable agreement with the data from the stagnation point up to about 10 percent of the wetted distance. The influence of upstream nozzle guide vane injection is to significantly increase the local blade heat flux in the immediate vicinity of the leading edge. O.C.

A86-48146*# Calspan Corp., Buffalo, N. Y.
HEAT-FLUX MEASUREMENTS FOR THE ROTOR OF A FULL-STAGE TURBINE. II - DESCRIPTION OF ANALYSIS TECHNIQUE AND TYPICAL TIME-RESOLVED MEASUREMENTS
M. G. DUNN, W. K. GEORGE, W. J. RAE, S. H. WOODWARD, J. C. MOLLER (Calspan Research Center, Buffalo, NY) et al. ASME, International Gas Turbine Conference and Exhibit, 31st, Duesseldorf, West Germany, June 8-12, 1986. 10 p. refs (Contract NAG3-469; NAG3-581) (ASME PAPER 86-GT-78)

An analytical technique for obtaining the time-resolved heat flux of a turbine blade is applied to the case of a TFE 731-2 hp full-stage rotating turbine. In order to obtain the heat flux values from the thin film gage temperature histories, a finite difference procedure is used to solve the heat equation with variable thermal properties. After setting out the data acquisition and analysis procedures, their application is illustrated for three midspan locations on the blade and operation at the design flow function. Results demonstrate that the magnitude of the heat flux fluctuation due to vane-blade interaction is large by comparison to the time-averaged heat flux at all investigated locations; FFT of a portion of the heat flux record illustrates that the dominant frequencies occur at the wake-cutting frequency and its harmonics. O.C.

A86-48163*# Massachusetts Inst. of Tech., Cambridge.
ANALYTICAL AND EXPERIMENTAL INVESTIGATION OF THE COUPLED BLADED DISK/SHAFT WHIRL OF A CANTILEVERED TURBOFAN
E. F. CRAWLEY, E. H. DUCHARME, and D. R. MOKADAM (MIT, Cambridge, MA) ASME, International Gas Turbine Conference and Exhibit, 31st, Duesseldorf, West Germany, June 8-12, 1986. 9 p. refs (Contract NAG3-200) (ASME PAPER 86-GT-98)

A simple analytical model for the structural dynamics of a rotating blade/rigid disk/flexible cantilevered shaft system yields the equations of motion expressed in the rotating frame, showing that the blade's one-nodal diameter modes dynamically couple to the rigid body whirling motion of the shaft-disk system. This analytical model is correlated with the results of a structural dynamic experiment performed on an aeroelastic rotor fan that is similar to a high bypass ratio shroudless turbofan. The agreement between the predicted and experimental natural frequencies is good, and suggests significant interaction of the one-nodal diameter blade modes with the shaft-disk modes. O.C.

A86-48224*# National Aeronautics and Space Administration, Lewis Research Center, Cleveland, Ohio.

TOWARD IMPROVED DURABILITY IN ADVANCED COMBUSTORS AND TURBINES - PROGRESS IN PREDICTION OF THERMOMECHANICAL LOADS

D. E. SOKOLOWSKI and C. R. ENSIGN (NASA, Lewis Research Center, Cleveland, OH) ASME, International Gas Turbine Conference and Exhibit, 31st, Duesseldorf, West Germany, June 8-12, 1986. 13 p. refs (ASME PAPER 86-GT-172)

NASA is sponsoring the Turbine Engine Hot Section Technology (HOST) Project to address the need for improved durability in advanced combustors and turbines. Analytical and experimental activities aimed at more accurate prediction of the aerothermal environment, the thermomechanical loads, the material behavior and structural responses to such loading, and life predictions for high temperature cyclic operation have been underway for several years and are showing promising results. Progress is reported in the development of advanced instrumentation and in the improvement of combustor aerothermal and turbine heat transfer models that will lead to more accurate prediction of thermomechanical loads. Author

A86-48231*# John Deere Technologies International, Inc., Wood-Ridge, N.J.
STRATIFIED CHARGE ROTARY ENGINE FOR GENERAL AVIATION

R. E. MOUNT (John Deere Technologies International Inc., Rotary Engine Div., Wood-Ridge, NJ), A. M. PARENTE (Avco Corp., Avco Lycoming Div., Williamsport, PA), and W. F. HADY (NASA, Lewis Research Center, Cleveland, OH) ASME, International Gas Turbine Conference and Exhibit, 31st, Duesseldorf, West Germany, June 8-12, 1986. 10 p. refs (ASME PAPER 86-GT-181)

A development history, a current development status assessment, and a design feature and performance capabilities account are given for stratified-charge rotary engines applicable to aircraft propulsion. Such engines are capable of operating on Jet-A fuel with substantial cost savings, improved altitude capability, and lower fuel consumption by comparison with gas turbine powerplants. Attention is given to the current development program of a 400-hp engine scheduled for initial operations in early 1990. Stratified charge rotary engines are also applicable to ground power units, airborne APUs, shipboard generators, and vehicular engines. O.C.

A86-48257*# United Technologies Corp., East Hartford, Conn.
ATOMIZATION AND COMBUSTION CHARACTERISTICS OF ANTIMISTING FUELS USING JT8D AND AIR-BOOST INJECTORS

J. B. KENNEDY and A. J. FLORENTINO (United Technologies Corp., East Hartford, CT) ASME, International Gas Turbine Conference and Exhibit, 31st, Duesseldorf, West Germany, June 8-12, 1986. 9 p. refs (Contract NAS3-22045) (ASME PAPER 86-GT-223)

The atomization levels of antimisting fuels are presently determined for a JT8D fuel injector, a low emission airblast JT8D injector, and an air-boost injector, at operating conditions simulating engine operating conditions. The effects of the use of antimisting kerosene (AMK) on component performance are also studied in the case of an in-service JT8D engine. The use of the AMK fuel causes a decline in the quality of the spray, most notably as a large increase in the Sauter mean diameter for all three injector types. In addition, the idle patterning data obtained indicate that the low emission injector fuel distribution changed from a hollow cone Jet A spray having no fuel at its center to a semihollow spray cone in the case of AMK; this change could disrupt the combustor primary zone recirculation pattern. O.C.

A86-49611*# National Aeronautics and Space Administration. Lewis Research Center, Cleveland, Ohio.

SMALL GAS TURBINE COMBUSTOR EXPERIMENTAL STUDY - COMPLIANT METAL/CERAMIC LINER AND PERFORMANCE EVALUATION

W. A. ACOSTA (NASA, Lewis Research Center; U.S. Army, Propulsion Directorate, Cleveland, OH) and C. T. NORGREN (NASA, Lewis Research Center, Cleveland, OH) AIAA, ASME, SAE, and ASEE, Joint Propulsion Conference, 22nd, Huntsville, AL, June 16-18, 1986. 11 p. refs
(AIAA PAPER 86-1452)

Combustor research relating to the development of fuel efficient small gas turbine engines capable of meeting future commercial and military aviation needs is currently underway at NASA Lewis. As part of this combustor research, a basic reverse-flow combustor has been used to investigate advanced liner wall cooling techniques. Liner temperature, performance, and exhaust emissions of the experimental combustor utilizing compliant metal/ceramic liners were determined and compared with three previously reported combustors that featured: (1) splash film-cooled liner walls; (2) transpiration cooled liner walls; and (3) counter-flow film cooled panels. Author

A86-49614*# National Aeronautics and Space Administration. Lewis Research Center, Cleveland, Ohio.

PERSPECTIVES ON DILUTION JET MIXING

J. D. HOLDEMAN (NASA, Lewis Research Center, Cleveland, OH) and R. SRINIVASAN (Garrett Turbine Engine Co., Phoenix, AZ) AIAA, ASME, SAE, and ASEE, Joint Propulsion Conference, 22nd, Huntsville, AL, June 16-18, 1986. 31 p. refs
(AIAA PAPER 86-1611)

A microcomputer code which displays 3-D oblique and 2-D plots of the temperature distribution downstream of jets mixing with a confined crossflow has been used to investigate the effects of varying the several independent flow and geometric parameters on the mixing. Temperature profiles calculated with this empirical model are presented to show the effects of orifice size and spacing, momentum flux ratio, density ratio, variable temperature mainstream, flow area convergence, orifice aspect ratio, and opposed and axially staged rows of jets. Author

N86-11158*# National Aeronautics and Space Administration. Lewis Research Center, Cleveland, Ohio.

SUMMARY OF RECENT NASA PROPELLER RESEARCH

D. C. MIKKELSON, G. A. MITCHELL, and L. J. BOBER *In* AGARD Aerodyn. and Acoustics of Propellers 24 p Feb. 1985 refs Previously announced as N84-32344
Avail: NTIS HC A20/MF A01 CSCL 01A

Advanced high speed propellers offer large performance improvements for aircraft that cruise in the Mach 0.7 to 0.8 speed regime. At these speeds, studies indicate that there is a 15 to near 40 percent block fuel savings and associated operating cost benefits for advanced turboprops compared to equivalent technology turbofan powered aircraft. Recent wind tunnel results for five eight to ten blade advanced models are compared with analytical predictions. Test results show that blade sweep was important in achieving net efficiencies near 80 percent at Mach 0.8 and reducing nearfield cruise noise about 6 dB. Lifting line and lifting surface aerodynamic analysis codes are under development and some results are compared with propeller force and probe data. Also, analytical predictions are compared with some initial laser velocimeter measurements of the flow field velocities of an eight bladed 45 swept propeller. Experimental aeroelastic results indicate that cascade effects and blade sweep strongly affect propeller aeroelastic characteristics. Comparisons of propeller nearfield noise data with linear acoustic theory indicate that the theory adequately predicts nearfield noise for subsonic tip speeds, but overpredicts the noise for supersonic tip speeds. B.W.

N86-11512*# National Aeronautics and Space Administration. Lewis Research Center, Cleveland, Ohio.

COMBUSTION HOT SECTION TECHNOLOGY

D. B. ERCEGOVIC *In its* Turbine Eng. Hot Sect. Technol. (HOST) p 129-133 Oct. 1983 refs

Avail: NTIS HC A11/MF A01 CSCL 21E

The overall objective of the Turbine Engine Hot Section Technology Combustion Project is to develop and verify improved and more accurate analysis methods for increasing the ability to design with confidence the combustion system for advanced aircraft turbine engines. The analysis methods developed will be generically applicable to combustion systems and not restricted to one specific engine or manufacturer. This project's approach was to first assess and evaluate existing combustor aerothermal analysis models by means of a contracted effort initiated during FY 1982. This evaluation effort has assessed and quantified known models' strengths and deficiencies. During FY 1984 the Aerothermal Modeling Program, Phase 2 will be initiated, which is expected to have contracted model development efforts in the areas of improved numerical methods for turbulent viscous flows, flow interactions, and fuel spray flow foekd interactions. A Phase 3 effort is planned to address remaining model deficiencies. The primary inhouse effort in this area will be the determination of high pressure flame radiation characteristics in a full annular combustor. This experiment will be conducted in the NASA LeRC High Pressure Facility with the results compiled into a comprehensive flame radiation and liner heat flux model. Author

N86-11513*# National Aeronautics and Space Administration. Lewis Research Center, Cleveland, Ohio.

HOT STRUCTURAL ANALYSIS PROGRAM OVERVIEW

R. H. JOHNS *In its* Turbine Eng. Hot Sect. Technol. (HOST) p 153-158 Oct. 1983

Avail: NTIS HC A11/MF A01 CSCL 21E

Hot section components of aircraft gas turbine engines are subjected to severe thermal structural loading conditions, especially during the start up and take off portions of the engine cycle. The most severe and damaging stresses and strains are those induced by the steep thermal gradients induced during the start up transient. These transient stresses and strains are also the most difficult to predict, in part because of the temperature gradients and distributions are not well known or readily predictable, and also because the cyclic elastic viscoplastic behavior of the materials at these extremes of temperature and strain are not well known or readily predictable. A broad spectrum of structures related technology programs is underway to address these deficiencies. One element of the structures program is developing improved time varying thermal mechanical load models for the entire engine mission cycle from start up to shutdown. Another major part of the program is the development of new and improved nonlinear 3-D finite elements and associated structural analysis programs, including the development of temporal elements with time dependent properties to account for creep effects in the materials and components. Author

N86-11515*# General Electric Co., Cincinnati, Ohio.

COMPONENT-SPECIFIC MODELING

M. L. ROBERTS *In* NASA. Lewis Research Center Turbine Eng. Hot Sect. Technol. (HOST) p 165-173 Oct. 1983 (Contract NAS3-23687)

Avail: NTIS HC A11/MF A01 CSCL 21E

The overall objective of this program is to develop and verify a series of interdisciplinary modeling and analysis techniques which have been specialized to address three specific hot section components. These techniques will incorporate data as well as theoretical methods from many diverse areas, including cycle and performance analysis, heat transfer analysis, linear and nonlinear stress analysis, and mission analysis. Building on the proven techniques already available in these fields, the new methods developed through this contract will be integrated to provide an accurate, efficient, and unified approach to analyzing combustor burner liners, hollow air cooled turbine blades, and air cooled turbine vanes. For these components, the methods developed will

07 AIRCRAFT PROPULSION AND POWER

predict temperature, deformation, stress, and strain histories throughout a complete flight mission. Author

N86-12226*# Pratt and Whitney Aircraft Group, East Hartford, Conn. Engineering Div.

TURBINE BLADE AND VANE HEAT FLUX SENSOR DEVELOPMENT, PHASE 2 Final Report, Sep. 1982 - Jul. 1985
W. H. ATKINSON, M. A. CYR, and R. R. STRANGE Oct. 1985
85 p refs

(Contract NAS3-23629)

(NASA-CR-174995; NAS 1.26:174995; PWS-5914-39) Avail:

NTIS HC A05/MF A01 CSCL 21E

The development of heat flux sensors for gas turbine blades and vanes and the demonstration of heat transfer measurement methods are reported. The performance of the heat flux sensors was evaluated in a cylinder in cross flow experiment and compared with two other heat flux measurement methods, the slug calorimeter and a dynamic method based on fluctuating gas and surface temperature. Two cylinders, each instrumented with an embedded thermocouple sensor, a Gardon gauge, and a slug calorimeter, were fabricated. Each sensor type was calibrated using a quartz lamp bank facility. The instrumented cylinders were then tested in an atmospheric pressure combustor rig at conditions up to gas stream temperatures of 1700K and velocities to Mach 0.74. The test data are compared to other measurements and analytical prediction. E.A.K.

N86-12227*# National Aeronautics and Space Administration. Lewis Research Center, Cleveland, Ohio.

FLUID MACHINES: EXPANDING THE LIMITS, PAST AND FUTURE

M. J. HARTMANN and D. M. SANDERCOCK 1985 46 p refs
Presented at the Winter Ann. Meeting of the Am. Soc. of Mech. Eng., Miami Beach, Fla., 17-22 Nov. 1985

(NASA-TM-87161; E-2793; NAS 1.15:87161) Avail: NTIS HC

A03/MF A01 CSCL 21E

During the 40 yr period from 1940 to 1980, the capabilities and operating limits of fluid machines were greatly extended. This was due to a research program, carried out to meet the needs of aerospace programs. Some of the events are reviewed. Overall advancements of all machinery components are discussed followed by a detailed examination of technology advancements in axial compressors and pumps. Future technology needs are suggested. E.A.K.

N86-13328*# Teledyne Continental Motors, Muskegon, Mich.
LIGHTWEIGHT TWO-STROKE CYCLE AIRCRAFT DIESEL ENGINE TECHNOLOGY ENABLEMENT PROGRAM, VOLUME 1 Final Report, Dec. 1979 - Aug. 1985

P. D. FREEN, S. G. BERENYI, A. P. BROUWERS, and M. E. MOYNIHAN Aug. 1985 116 p

(Contract NAS3-22218)

(NASA-CR-174923-VOL-1; NAS 1.26:174923-VOL-1) Avail:

NTIS HC A06/MF A01 CSCL 21G

An experimental Single Cylinder Test Engine Program is conducted to confirm the analytically projected performance of a two-stroke cycle diesel engine for aircraft applications. The test engine delivered 78kW indicated power from 1007cc displacement, operating at 3500 RPM on Schnuerle loop scavenged two-stroke cycle. Testing confirms the ability of a proposed 4-cylinder version of such an engine to reach the target power at altitude, in a highly turbocharged configuration. The experimental program defines all necessary parameters to permit design of a multicylinder engine for eventual flight applications; including injection system requirement, turbocharging, heat rejection, breathing, scavenging, and structural requirements. The multicylinder engine concept is configured to operate with an augmented turbocharger, but with no primary scavenge blower. The test program is oriented to provide a balanced turbocharger compressor to turbine power balance without an auxiliary scavenging system. Engine cylinder heat rejection to the ambient air has been significantly reduced and the minimum overall turbocharger efficiency required is within the range of commercially available turbochargers. Analytical studies

and finite element modeling is made of insulated configurations of the engines - including both ceramic and metallic versions. A second generation test engine is designed based on current test results. Author

N86-13329*# Teledyne Continental Motors, Muskegon, Mich.
LIGHTWEIGHT TWO-STROKE CYCLE AIRCRAFT DIESEL ENGINE TECHNOLOGY ENABLEMENT PROGRAM, VOLUME 2 Final Report, Dec. 1979 - Aug. 1985

P. D. FREEN, S. G. BERENYI, A. P. BROUWERS, and M. E. MOYNIHAN Aug. 1985 150 p refs

(Contract NAS3-22218)

(NASA-CR-174923-VOL-2; NAS 1.26:174923-VOL-2) Avail:

NTIS HC A07/MF A01 CSCL 21G

An experimental Single Cylinder Test Engine Program is conducted to confirm the analytically projected performance of a two-stroke cycle diesel engine for aircraft applications. Testing confirms the ability of a proposed 4-cylinder version of such an engine to reach the target power at altitude in a highly turbocharged configuration. The experimental program defines all necessary parameters to permit a design of a multicylinder engine for eventual flight applications. Author

N86-13330*# Teledyne Continental Motors, Muskegon, Mich.
LIGHTWEIGHT TWO-STROKE CYCLE AIRCRAFT DIESEL ENGINE TECHNOLOGY ENABLEMENT PROGRAM, VOLUME 3 Final Report, Dec. 1979 - Aug. 1985

P. D. FREEN, S. G. BERENYI, A. P. BROUWERS, and M. E. MOYNIHAN Aug. 1985 282 p

(Contract NAS3-22218)

(NASA-CR-174923-VOL-3; NAS 1.26:174923-VOL-3) Avail:

NTIS HC A13/MF A01 CSCL 21G

An experimental Single Cylinder Test Engine Program is conducted to confirm the analytically projected performance of a two-stroke cycle diesel engine for aircraft applications. Testing confirms the ability of a proposed 4-cylinder version of such an engine to reach the target power at altitude in a highly turbocharged configuration. The experimental program defines all necessary parameters to permit design of a multicylinder engine for eventual flight applications. Author

N86-14272*# Pratt and Whitney Aircraft, East Hartford, Conn. Engineering Div.

PRELIMINARY DESIGN OF A SUPERSONIC CRUISE AIRCRAFT HIGH-PRESSURE TURBINE Final Report

L. D. ACETO and J. C. CALDERBANK 2 Nov. 1983 128 p refs

(Contract NAS3-20357)

(NASA-CR-174878; NAS 1.26:174878; PWA-5923-14) Avail:

NTIS HC A07/MF A01 CSCL 21E

Development of the supersonic cruise aircraft engine continued in this National Aeronautics and Space Administration (NASA) sponsored Pratt and Whitney program for the Preliminary Design of an Advanced High-Pressure Turbine. Airfoil cooling concepts and the technology required to implement these concepts received particular emphasis. Previous supersonic cruise aircraft mission studies were reviewed and the Variable Stream Control Engine (VSCE) was chosen as the candidate or the preliminary turbine design. The design was evaluated for the supersonic cruise mission. The advanced technology to be generated from these designs showed benefits in the supersonic cruise application and subsonic cruise application. The preliminary design incorporates advanced single crystal materials, thermal barrier coatings, and oxidation resistant coatings for both the vane and blade. The 1990 technology vane and blade designs have cooled turbine efficiency of 92.3 percent, 8.05 percent Wae cooling and a 10,000 hour life. An alternate design with 1986 technology has 91.9 percent efficiency and 12.43 percent Wae cooling at the same life. To achieve these performance and life results, technology programs must be pursued to provide the 1990's technology assumed for this study. Author

N86-15313*# National Aeronautics and Space Administration. Lewis Research Center, Cleveland, Ohio.

DYNAMIC RESPONSE OF FILM THICKNESS IN SPIRAL-GROOVE FACE SEALS

E. DIRUSSO Dec. 1985 22 p refs
(NASA-TP-2544; E-2683; NAS 1.60:2544) Avail: NTIS HC A02/MF A01 CSCL 21E

Tests were performed on an inward- and an outward-pumping spiral-groove face seal to experimentally determine the film thickness response to seal seat motions and to gain insight into the effect of secondary seal friction on film thickness behavior. Film thickness, seal seat axial motion, seal frictional torque, and film axial load were recorded as functions of time. The experiments revealed that for sinusoidal axial oscillations of the seal seat, the primary ring followed the seal seat motion very well. For a skewed seal seat, however, the primary ring did not follow the seal seat motion, and load-carrying capacity was degraded. Secondary seal friction was varied over a wide range to determine its effect on film thickness dynamics. The seals were tested with ambient air at room temperature and atmospheric pressure as the fluid medium. The test speed ranged from 7000 to 20,000 rpm. Seal tangential velocity ranged from 34 to 98 m/sec (113 to 323 ft/sec). Author

N86-16218*# Sverdrup Technology, Inc., Cleveland, Ohio.
PREDICTION OF THE STRUCTURE OF FUEL SPRAYS IN GAS TURBINE COMBUSTORS Final Report

J. S. SHUEN Dec. 1985 17 p refs Presented at the 24th Aerospace Sciences Meeting, Reno, Nev., 6-9 Jan. 1986; sponsored by AIAA

(Contract NAS3-24105)
(NASA-CR-175028; E-2837; NAS 1.26:175028; AIAA-86-0450)
Avail: NTIS HC A02/MF A01 CSCL 21E

The structure of fuel sprays in a combustion chamber is theoretically investigated using computer models of current interest. Three representative spray models are considered: (1) a locally homogeneous flow (LHF) model, which assumes infinitely fast interphase transport rates; (2) a deterministic separated flow (DSF) model, which considers finite rates of interphase transport but ignores effects of droplet/turbulence interactions; and (3) a stochastic separated flow (SSF) model, which considers droplet/turbulence interactions using random sampling for turbulence properties in conjunction with random-walk computations for droplet motion and transport. Two flow conditions are studied to investigate the influence of swirl on droplet life histories and the effects of droplet/turbulence interactions on flow properties. Comparison of computed results with the experimental data show that general features of the flow structure can be predicted with reasonable accuracy using the two separated flow models. In contrast, the LHF model overpredicts the rate of development of the flow. While the SSF model provides better agreement with measurements than the DSF model, definitive evaluation of the significance of droplet/turbulence interaction is not achieved due to uncertainties in the spray initial conditions. DOE

N86-16219*# National Aeronautics and Space Administration. Lewis Research Center, Cleveland, Ohio.

COMPARISON OF CALCULATED AND EXPERIMENTAL CASCADE PERFORMANCE FOR CONTROLLED-DIFFUSION COMPRESSOR STATOR BLADING

N. L. SANGER and R. P. SHREEVE (Naval Postgraduate School, Monterey, Calif.) 1986 22 p refs Presented at International Gas Turbine Conference and Exhibit, Dusseldorf, West Germany, 8-12 Jun. 1986; sponsored by ASME

(NASA-TM-87167; E-2805; NAS 1.15:87167) Avail: NTIS HC A04/MF A01 CSCL 21E

The mid-span section of a previously reported controlled-diffusion compressor stator has been experimentally evaluated in cascade. Measurements are taken over a range of incidence angles for blade chord Reynolds numbers from 470,000 to 690,000. Blade chord length is 12.7 cm, aspect ratio is 2.0, and solidity is 1.67. Measurements include conventional cascade performance parameters as well as blade surface pressures. Computations are made for the inviscid flow field, surface boundary

layers, and loss for several of the blade inlet angle conditions, are compared against corresponding data. Author

N86-16220*# Virginia Polytechnic Inst. and State Univ., Blacksburg. Dept. of Mechanical Engineering.

THERMODYNAMIC EVALUATION OF TRANSONIC COMPRESSOR ROTORS USING THE FINITE VOLUME APPROACH Annual Report, 20 Dec. 1984 - 19 Dec. 1985

J. MOORE, S. NICHOLSON, and J. G. MOORE Dec. 1985 118 p refs

(Contract NAG3-593)
(NASA-CR-176428; NAS 1.26:176428; JM/85-11) Avail: NTIS HC A06/MF A01 CSCL 21E

Research at NASA Lewis Research Center gave the opportunity to incorporate new control volumes in the Denton 3-D finite-volume time marching code. For duct flows, the new control volumes require no transverse smoothing and this allows calculations with large transverse gradients in properties without significant numerical total pressure losses. Possibilities for improving the Denton code to obtain better distributions of properties through shocks were demonstrated. Much better total pressure distributions through shocks are obtained when the interpolated effective pressure, needed to stabilize the solution procedure, is used to calculate the total pressure. This simple change largely eliminates the undershoot in total pressure down-stream of a shock. Overshoots and undershoots in total pressure can then be further reduced by a factor of 10 by adopting the effective density method, rather than the effective pressure method. Use of a Mach number dependent interpolation scheme for pressure then removes the overshoot in static pressure downstream of a shock. The stability of interpolation schemes used for the calculation of effective density is analyzed and a Mach number dependent scheme is developed, combining the advantages of the correct perfect gas equation for subsonic flow with the stability of 2-point and 3-point interpolation schemes for supersonic flow. Author

N86-16221*# National Aeronautics and Space Administration. Lewis Research Center, Cleveland, Ohio.

SIMULATING A SMALL TURBOSHAFT ENGINE IN REAL-TIME MULTIPROCESSOR SIMULATOR (RTMPS) ENVIRONMENT

E. J. MILNER and D. J. ARPASI Jan. 1986 25 p refs Presented at the SCS Multiconference, San Diego, Calif., 23-25 Jan. 1986; sponsored by the Society for Computer Simulation

(NASA-TM-87216; E-2876; NAS 1.15:87216) Avail: NTIS HC A02/MF A01 CSCL 21E

A Real-Time Multiprocessor Simulator (RTMPS) has been developed at NASA Lewis Research Center. The RTMPS uses parallel microprocessors to achieve computing speeds needed for real-time engine simulation. This report describes the use of the RTMPS system to simulate a small turboshaft engine. The process of programming the engine equations and distributing them over one, two, and four processors is discussed. Steady-state and transient results from the RTMPS simulation are compared with results from a main-frame-based simulation. Processor execution times and the associated execution time savings for the two and four processor cases are presented using actual data obtained from the RTMPS system. Included is a discussion of why the minimum achievable calculation time for the turboshaft engine model was attained using four processors. Finally, future enhancements to the RTMPS system are discussed including the development of a generalized partitioning algorithm to automatically distribute the system equations among the processors in optimum fashion. Author

07 AIRCRAFT PROPULSION AND POWER

N86-20389* National Aeronautics and Space Administration. Lewis Research Center, Cleveland, Ohio.

METHOD FOR IMPROVING THE FUEL EFFICIENCY OF A GAS TURBINE ENGINE Patent

G. A. COFFINBERRY, inventor (to NASA) (General Electric Co., Cincinnati, Ohio) 5 Nov. 1985 8 p 30 Aug. 1982 (NASA-CASE-LEW-13142-2; US-PATENT-4,550,561; US-PATENT-APPL-SN-413101; US-PATENT-CLASS-60-39.02; US-CLASS-60-39.07; US-PATENT-CLASS-60-736) Avail: US Patent and Trademark Office CSCL 21E

An energy recovery system is provided for an aircraft gas turbine engine of the type in which some of the pneumatic energy developed by the engine is made available to support systems such as an environmental control system. In one such energy recovery system, some of the pneumatic energy made available to but not utilized by the support system is utilized to heat the engine fuel immediately prior to the consumption of the fuel by the engine. Some of the recovered energy may also be utilized to heat the fuel in the fuel tanks. Provision is made for multiengine applications wherein energy recovered from one engine may be utilized by another one of the engines or systems associated therewith.

Official Gazette of the U.S. Patent and Trademark Office

N86-20390*# Scientific Research Associates, Inc., Glastonbury, Conn.

INFLUENCE OF LARGE-SCALE MOTION ON TURBULENT TRANSPORT FOR CONFINED COAXIAL JETS. VOLUME 2: NAVIER-STOKES CALCULATIONS OF SWIRLING AND NONSWIRLING CONFINED COAXIAL JETS Final Report

B. C. WEINBERG and H. McDONALD Jan. 1986 57 p refs (Contract NAG3-350)

(NASA-CR-175036; NAS 1.26:175036) Avail: NTIS HC A04/MF A01 CSCL 21E

The existence of large scale coherent structures in turbulent shear flows has been well documented. Discrepancies between experimental and computational data suggest a necessity to understand the roles they play in mass and momentum transport. Using conditional sampling and averaging on coincident two-component velocity and concentration velocity experimental data for swirling and nonswirling coaxial jets, triggers for identifying the structures were examined. Concentration fluctuation was found to be an adequate trigger or indicator for the concentration-velocity data, but no suitable detector was located for the two-component velocity data. The large scale structures are found in the region where the largest discrepancies exist between model and experiment. The traditional gradient transport model does not fit in this region as a result of these structures. The large scale motion was found to be responsible for a large percentage of the axial mass transport. The large scale structures were found to convect downstream at approximately the mean velocity of the overall flow in the axial direction. The radial mean velocity of the structures was found to be substantially greater than that of the overall flow.

Author

N86-20391*# Clemson Univ., S.C. Dept. of Mechanical Engineering.

VISCOUS COMPRESSIBLE FLOW DIRECT AND INVERSE COMPUTATION AND ILLUSTRATIONS Final Report

T. T. YANG and F. NTONE Jan. 1986 102 p refs (Contract NAG3-538)

(NASA-CR-175037; NAS 1.26:175037) Avail: NTIS HC A06/MF A01 CSCL 21E

An algorithm for laminar and turbulent viscous compressible two dimensional flows is presented. For the application of precise boundary conditions over an arbitrary body surface, a body-fitted coordinate system is used in the physical plane. A thin-layer approximation of the Navier-Stokes equations is introduced to keep the viscous terms relatively simple. The flow field computation is performed in the transformed plane. A factorized, implicit scheme is used to facilitate the computation. Sample calculations, for Couette flow, developing pipe flow, an isolated airflow, two dimensional compressor cascade flow, and segmental compressor

blade design are presented. To a certain extent, the effective use of the direct solver depends on the user's skill in setting up the gridwork, the time step size and the choice of the artificial viscosity. The design feature of the algorithm, an iterative scheme to correct geometry for a specified surface pressure distribution, works well for subsonic flows. A more elaborate correction scheme is required in treating transonic flows where local shock waves may be involved.

Author

N86-20392*# Oklahoma State Univ., Stillwater.

MEASUREMENTS OF A SINGLE LATERAL JET INJECTED INTO SWIRLING CROSSFLOW M.S. Thesis Final Report

L. H. ONG and D. G. LILLEY Jan. 1986 92 p refs (Contract NAG3-549)

(NASA-CR-175040; NAS 1.26:175040) Avail: NTIS HC A05/MF A01 CSCL 21E

Experiments have been conducted to document the time-mean and turbulent flowfield of a deflected turbulent jet in a confined swirling crossflow. The jet-to-crossflow velocity ratio of 4 was investigated with swirler vane angles of 45 and 70 degrees. A six-orientation single hot-wire technique was used to measure the velocities and turbulence properties of the flow. In addition, a five-hole pitot probe technique was used to measure the time-mean velocities or verification purposes. The results are presented in the form of r-x plots to aid visualization of the fully three-dimensional flowfield. The swirl in the crossflow intensified the local velocity at the location of the injected jet, which effectively reduced the jet-to-crossflow velocity ratio. This caused the trajectory of the injected jet to follow the path of the local flow direction of the crossflow, and reduce its penetration into the crossflow. The time-mean velocity measurements using the hot-wire corresponded to pitot-probe data obtained in identical flow conditions. Turbulence stress data show the same trends as previous swirl flow data without lateral injection. The lateral jet was found to deflect the axis of the precessing vortex core.

Author

N86-20393*# California Univ., Berkeley.

AERODYNAMIC PROPERTIES OF TURBULENT COMBUSTION FIELDS Final Report

C. K. HSIAO and A. K. OPPENHEIM Nov. 1985 136 p (Contract NAG3-131)

(NASA-CR-175005; NAS 1.26:175005) Avail: NTIS HC A07/MF A01 CSCL 21E

Flow fields involving turbulent flames in premixed gases under a variety of conditions are modeled by the use of a numerical technique based on the random vortex method to solve the Navier-Stokes equations and a flame propagation algorithm to trace the motion of the front and implement the Huygens principle, both due to Chorin. A successive over-relaxation hybrid method is applied to solve the Euler equation for flows in an arbitrarily shaped domain. The method of images, conformal transformation, and the integral-equation technique are also used to treat flows in special cases, according to their particular requirements. Salient features of turbulent flame propagation in premixed gases are interpreted by relating them to the aerodynamic properties of the flow field. Included among them is the well-known cellular structure of flames stabilized by bluff bodies, as well as the formation of the characteristic tulip shape of flames propagating in ducts. In its rudimentary form, the mechanism of propagation of a turbulent flame is shown to consist of: (1) rotary motion of eddies at the flame front, (2) self-advancement of the front at an appropriate normal burning speed, and (3) dynamic effects of expansion due to exothermicity of the combustion reaction. An idealized model is used to illustrate these fundamental mechanisms and to investigate basic aerodynamic features of flames in premixed gases. The case of a confined flame stabilized behind a rearward-facing step is given particular care and attention. Solutions are shown to be in satisfactory agreement with experimental results, especially with respect to global properties such as the average velocity profiles and reattachment length.

Author

N86-20394*# Oklahoma Univ., Norman. School of Mechanical and Aerospace Engineering.

EXPERIMENTS ON OPPOSED LATERAL JETS INJECTED INTO SWIRLING CROSSFLOW M.S. Thesis Final Report

C. B. MCMURRY and D. G. LILLEY Jan. 1986 116 p refs (Contract NAG3-549)

(NASA-CR-175041; NAS 1.26:175041) Avail: NTIS HC A06/MF A01 CSCL 21E

Experiments have been conducted to obtain the time-mean and turbulent quantities of opposed lateral jets in a low speed, nonreacting flowfield. A jet-to-crossflow velocity ratio of $R = v_{\text{jet}}/v_{\text{crossflow}} = 4$ was used throughout the experiments, with swirl vane angles of $d = 0$ (swirler removed), 45 and 70 deg used with the crossflow. Flow visualization techniques used were neutrally-buoyant helium-filled soap bubbles and multispark photography in order to obtain the gross flowfield characteristics. Measurements of time-mean and turbulent quantities were obtained utilizing a six-orientation single hot-wire technique. For the nonswirling case, the jets were found not to penetrate past the test-section centerline, in contrast to the single lateral jet with the same jet-to-crossflow velocity ratio. In the swirling cases, the crossflow remains in a narrow region near the wall of the test section. The opposed jets are swept from their vertical courses into spiral trajectories close to the confining walls. Extensive results are presented in r-x plane plots. Author

N86-20395*# Connecticut Univ., Storrs.

INFLUENCE OF LARGE-SCALE MOTION ON TURBULENT TRANSPORT FOR CONFINED COAXIAL JETS. VOLUME 1: ANALYTICAL ANALYSIS OF THE EXPERIMENTAL DATA USING CONDITIONAL SAMPLING Final Report

D. C. BRONDUM and J. C. BENNETT Jan. 1986 136 p refs (Contract NAG3-350)

(NASA-CR-175035; NAS 1.26:175035) Avail: NTIS HC A07/MF A01 CSCL 21E

The existence of large scale coherent structures in turbulent shear flows has been well documented. Discrepancies between experimental and computational data suggest a necessity to understand the roles they play in mass and momentum transport. Using conditional sampling and averaging on coincident two component velocity and concentration velocity experimental data for swirling and nonswirling coaxial jets, triggers for identifying the structures were examined. Concentration fluctuation was found to be an adequate trigger or indicator for the concentration-velocity data, but no suitable detector was located for the two component velocity data. The large scale structures are found in the region where the largest discrepancies exist between model and experiment. The traditional gradient transport model does not fit in this region as a result of these structures. The large scale motion was found to be responsible for a large percentage downstream at approximately the mean velocity of the overall flow in the axial direction. The radial mean velocity of the structures was found to be substantially greater than that of the overall flow. Author

N86-21545*# Purdue Univ., West Lafayette, Ind. School of Mechanical Engineering.

SPONTANEOUS IGNITION DELAY CHARACTERISTICS OF HYDROCARBON FUEL-AIR MIXTURES Final Report

A. H. LEFEBVRE, W. G. FREEMAN, and L. H. COWELL Feb. 1986 102 p refs

(Contract NAG3-226)

(NASA-CR-175064; NAS 1.26:175064) Avail: NTIS HC A06/MF A01 CSCL 21E

The influence of pressure on the autoignition characteristics of homogeneous mixtures of hydrocarbon fuels in air is examined. Autoignition delay times are measured for propane, ethylene, methane, and acetylene in a continuous flow apparatus featuring a multi-point fuel injector. Results are presented for mixture temperatures from 670K to 1020K, pressures from 1 to 10 atmospheres, equivalence ratios from 0.2 to 0.7, and velocities from 5 to 30 m/s. Delay time is related to pressure, temperature, and fuel concentration by global reaction theory. The results show

variations in global activation energy from 25 to 38 kcal/kg-mol, pressure exponents from 0.66 to 1.21, and fuel concentration exponents from 0.19 to 0.75 for the fuels studied. These results are generally in good agreement with previous studies carried out under similar conditions. Author

N86-21546*# General Motors Corp., Indianapolis, Ind. Gas Turbines Div.

TURBINE VANE EXTERNAL HEAT TRANSFER. VOLUME 1: ANALYTICAL AND EXPERIMENTAL EVALUATION OF SURFACE HEAT TRANSFER DISTRIBUTIONS WITH LEADING EDGE SHOWERHEAD FILM COOLING

E. R. TURNER, M. D. WILSON, L. D. HYLTON, and R. M. KAUFMAN Jul. 1985 246 p refs

(Contract NAS3-23695)

(NASA-CR-174827; NAS 1.26:174827; EDR-11984-VOL-1) Avail: NTIS HC A11/MF A01 CSCL 21E

Progress in predictive design capabilities for external heat transfer to turbine vanes was summarized. A two dimensional linear cascade (previously used to obtain vane surface heat transfer distributions on nonfilm cooled airfoils) was used to examine the effect of leading edge shower head film cooling on downstream heat transfer. The data were used to develop and evaluate analytical models. Modifications to the two dimensional boundary layer model are described. The results were used to formulate and test an effective viscosity model capable of predicting heat transfer phenomena downstream of the leading edge film cooling array on both the suction and pressure surfaces, with and without mass injection. B.G.

N86-23597*# California Univ., Irvine. Dept. of Mechanical Engineering.

EFFECT OF LIQUID DROPLETS ON TURBULENCE IN A ROUND GASEOUS JET Final Report

A. A. MOSTAFA and S. E. ELGHOBASHI Feb. 1986 209 p refs

(Contract NAG3-176)

(NASA-CR-175063; NAS 1.26:175063) Avail: NTIS HC A10/MF A01 CSCL 21E

The main objective of this investigation is to develop a two-equation turbulence model for dilute vaporizing sprays or in general for dispersed two-phase flows including the effects of phase changes. The model that accounts for the interaction between the two phases is based on rigorously derived equations for turbulence kinetic energy (K) and its dissipation rate epsilon of the carrier phase using the momentum equation of that phase. Closure is achieved by modeling the turbulent correlations, up to third order, in the equations of the mean motion, concentration of the vapor in the carrier phase, and the kinetic energy of turbulence and its dissipation rate for the carrier phase. The governing equations are presented in both the exact and the modeled forms. The governing equations are solved numerically using a finite-difference procedure to test the presented model for the flow of a turbulent axisymmetric gaseous jet laden with either evaporating liquid droplets or solid particles. The predictions include the distribution of the mean velocity, volume fractions of the different phases, concentration of the evaporated material in the carrier phase, turbulence intensity and shear stress of the carrier phase, droplet diameter distribution, and the jet spreading rate. The predictions are in good agreement with the experimental data. Author

N86-23598*# Garrett Turbine Engine Co., Phoenix, Ariz.

LOW-COST SINGLE-CRYSTAL TURBINE BLADES, VOLUME 2

T. E. STRANGMAN, R. E. DENNIS, and B. R. HEATH Apr. 1984 42 p refs

(Contract NAS3-20073)

(NASA-CR-174652; NAS 1.26:174652; G-21-4314-2) Avail: NTIS HC A03/MF A01 CSCL 21E

The overall objectives of Project 3 were to develop the exothermic casting process to produce uncooled single-crystal (SC) HP turbine blades in MAR-M 247 and higher strength derivative alloys and to validate the materials process and components

07 AIRCRAFT PROPULSION AND POWER

through extensive mechanical property testing, rig testing, and 200 hours of endurance engine testing. These Program objectives were achieved. The exothermic casting process was successfully developed into a low-cost nonproprietary method for producing single-crystal castings. Single-crystal MAR-M 247 and two derivatives DS alloys developed during this project, NASAIR 100 and SC Alloy 3, were fully characterized through mechanical property testing. SC MAR-M 247 shows no significant improvement in strength over directionally solidified (DS) MAR-M 247, but the derivative alloys, NASAIR 100 and Alloy 3, show significant tensile and fatigue improvements. Firtree testing, holography, and strain-gauge rig testing were used to determine the effects of the anisotropic characteristics of single-crystal materials. No undesirable characteristics were found. In general, the single-crystal material behaved similarly to DS MAR-M 247. Two complete engine sets of SC HP turbine blades were cast using the exothermic casting process and fully machined. These blades were successfully engine-tested. Author

N86-24693*# United Technologies Research Center, East Hartford, Conn.

ADVANCED TURBOPROP VIBRATORY CHARACTERISTICS Final Report

A. V. SRINIVASAN and G. B. FULTON Apr. 1984 104 p refs (Contract NAS3-23533)
(NASA-CR-174708; NAS 1.26:174708; R84-956627-1) Avail: NTIS HC A06/MF A01 CSCL 21E

The assembly of SR5 advanced turboprop blades to develop a structural dynamic data base for swept props is reported. Steady state blade deformation under centrifugal loading and vibratory characteristics of the rotor assembly were measured. Vibration was induced through a system of piezoelectric crystals attached to the blades. Data reduction procedures are used to provide deformation, mode shape, and frequencies of the assembly at predetermined speeds. Author

N86-24694*# National Aeronautics and Space Administration, Lewis Research Center, Cleveland, Ohio.

LOW-SPEED PERFORMANCE OF AN AXISYMMETRIC, MIXED-COMPRESSION, SUPERSONIC INLET WITH AUXILIARY INLETS

C. J. TREFNY and J. W. WASSERBAUER Feb. 1986 63 p refs
(NASA-TP-2557; E-2771; NAS 1.60:2557) Avail: NTIS HC A04/MF A01 CSCL 21E

A test program was conducted to determine the aerodynamic performance and acoustic characteristics associated with the low-speed operation of a supersonic, axisymmetric, mixed-compression inlet with auxiliary inlets. Blow-in-auxiliary doors were installed on the NASA Ames P inlet. One door per quadrant was located on the cowl in the subsonic diffuser section of the inlet. Auxiliary inlets with areas of 20 and 40 percent of the inlet capture area were tested statically and at free-stream Mach numbers of 0.1 and 0.2. The effects of boundary layer bleed inflow were investigated. A JT8D fan simulator driven by compressed air was used to pump inlet flow and to provide a characteristic noise signature. Baseline data were obtained at static free-stream conditions with the sharp P-inlet cowl lip replaced by a blunt lip. Auxiliary inlets increased overall total pressure recovery of the order of 10 percent. Author

N86-24695*# Beech Aircraft Corp., Wichita, Kans.

EVALUATION OF PROPFAN PROPULSION APPLIED TO GENERAL AVIATION

R. W. AWKER Mar. 1986 146 p refs
(Contract NAS3-24349)
(NASA-CR-175020; NAS 1.26:175020) Avail: NTIS HC A07/MF A01 CSCL 21E

Propfan propulsion on business aircraft was evaluated. Comparisons, in terms of cost and performance, were made between propfan propulsion systems and conventional turbofan propulsion systems on a typical business aircraft. In addition,

configuration and cost sensitivity studies were conducted to further assess the potential of propfan propulsion. Author

N86-24697*# National Aeronautics and Space Administration, Lewis Research Center, Cleveland, Ohio.

A REAL-TIME SIMULATION EVALUATION OF AN ADVANCED DETECTION, ISOLATION AND ACCOMMODATION ALGORITHM FOR SENSOR FAILURES IN TURBINE ENGINES

W. C. MERRILL and J. C. DELAAT 1986 17 p refs Presented at the American Control Conference, Seattle, Wash., 18-20 Jun. 1986; sponsored by IEEE
(NASA-TM-87289; E-2995; NAS 1.15:87289) Avail: NTIS HC A02/MF A01 CSCL 21E

An advanced sensor failure detection, isolation, and accommodation (ADIA) algorithm has been developed for use with an aircraft turbofan engine control system. In a previous paper the authors described the ADIA algorithm and its real-time implementation. Subsequent improvements made to the algorithm and implementation are discussed, and the results of an evaluation presented. The evaluation used a real-time, hybrid computer simulation of an F100 turbofan engine. Author

N86-25357*# Douglas Aircraft Co., Inc., Long Beach, Calif.

TURBOFAN AFT DUCT SUPPRESSOR STUDY PROGRAM LISTING AND USER'S GUIDE Final Report

M. C. JOSHI and R. E. KRAFT May 1983 104 p
(Contract NAS3-22766)
(NASA-CR-175067; NAS 1.26:175067) Avail: NTIS HC A06/MF A01 CSCL 21E

A description of the structure of the Annular Flow Duct Program (AFDP) for the calculation of acoustic suppression due to treatment in a finite length annular duct carrying sheared flow is presented. Although most appropriate for engine exhaust ducts, this program can be used to study sound propagation in any duct that maintains annular geometry over a considerable length of the duct. The program is based on the modal analysis of sound propagation in ducts with axial segments of different wall impedances. For specified duct geometry, wall impedance, flow and acoustic conditions in the duct (including mode amplitude distribution of the source) and duct termination reflection characteristics, the program calculates the suppression due to the treatment in the duct. The presence of forward and backward traveling modes in the duct due to the reflection and redistribution of modes at segment interfaces and duct end terminations are taken into account in the calculations. The effects of thin wall boundary layers (with a linear or mean flow velocity profile) on the acoustic propagation are also included in the program. A functional description of the major subroutines is included and a sample run is provided with an explanation of the output. M.G.

N86-26336*# National Aeronautics and Space Administration, Lewis Research Center, Cleveland, Ohio.

SUMMARY OF INVESTIGATIONS OF ENGINE RESPONSE TO DISTORTED INLET CONDITIONS

T. J. BIESADNY, W. M. BRAITHWAITE, R. H. SOEDER, and M. ABDELWAHAB 1986 34 p refs Proposed for presentation at the 68th Meeting of the Propulsion and Energetics Panel, Munich, West Germany, 8-9 Sep. 1986; sponsored by AGARD
(NASA-TM-87317; E-3048; NAS 1.15:87317) Avail: NTIS HC A03/MF A01 CSCL 21E

A survey is presented of experimental and analytical experience of the NASA Lewis Research Center in engine response to inlet temperature and pressure distortions. This includes a description of the hardware and techniques employed, and a summary of the highlights of experimental investigations and analytical modeling. Distortion devices successfully simulated inlet distortion, and knowledge was gained about compression system response to different types of distortion. A list of NASA research references is included. Author

N86-27282*# Hamilton Standard, Windsor Locks, Conn.
LARGE-SCALE ADVANCED PROP-FAN (LAP) PITCH CHANGE ACTUATOR AND CONTROL DESIGN REPORT

R. A. SCHWARTZ, P. CARVALHO, and M. J. CUTLER 31 Jan. 1986 187 p Original document contains color illustrations (Contract NAS3-23051)
 (NASA-CR-174788; NAS 1.26:174788) Avail: NTIS HC A09/MF A01 CSCL 01A

In recent years, considerable attention has been directed toward improving aircraft fuel consumption. Studies have shown that the high inherent efficiency previously demonstrated by low speed turboprop propulsion systems may now be extended to today's higher speed aircraft if advanced high-speed propeller blades having thin airfoils and aerodynamic sweep are utilized. Hamilton Standard has designed a 9-foot diameter single-rotation Large-Scale Advanced Prop-Fan (LAP) which will be tested on a static test stand, in a high speed wind tunnel and on a research aircraft. The major objective of this testing is to establish the structural integrity of large-scale Prop-Fans of advanced construction in addition to the evaluation of aerodynamic performance and aeroacoustic design. This report describes the operation, design features and actual hardware of the (LAP) Prop-Fan pitch control system. The pitch control system which controls blade angle and propeller speed consists of two separate assemblies. The first is the control unit which provides the hydraulic supply, speed governing and feather function for the system. The second unit is the hydro-mechanical pitch change actuator which directly changes blade angle (pitch) as scheduled by the control.

Author

N86-27283*# Pratt and Whitney Aircraft, East Hartford, Conn. Commercial Products Div.

STRUCTURAL TAILORING OF ENGINE BLADES (STAEBL) THEORETICAL MANUAL

K. W. BROWN Mar. 1985 51 p
 (Contract NAS3-22525)
 (NASA-CR-175112; NAS 1.26:175112; PWA-5774-40) Avail: NTIS HC A04/MF A01 CSCL 21E

This Theoretical Manual includes the theories included in the Structural Tailoring of Engine Blades (STAEBL) computer program which was developed to perform engine fan and compressor blade numerical optimizations. These blade optimizations seek a minimum weight or cost design that satisfies practical blade design constraints, by controlling one to twenty design variables. The STAEBL constraint analyses include blade stresses, vibratory response, flutter, and foreign object damage. Blade design variables include airfoil thickness at several locations, blade chord, and construction variables: hole size for hollow blades, and composite material layout for composite blades.

Author

N86-27284*# Pratt and Whitney Aircraft, East Hartford, Conn. Commercial Products Div.

STRUCTURAL TAILORING OF ENGINE BLADES (STAEBL) USER'S MANUAL

K. W. BROWN Mar. 1985 106 p
 (Contract NAS3-22525)
 (NASA-CR-175113; NAS 1.26:175113; PWA-5774-39) Avail: NTIS HC A06/MF A01 CSCL 21E

This User's Manual contains instructions and demonstration case to prepare input data, run, and modify the Structural Tailoring of Engine Blades (STAEBL) computer code. STAEBL was developed to perform engine fan and compressor blade numerical optimizations. This blade optimization seeks a minimum weight or cost design that satisfies realistic blade design constraints, by tuning one to twenty design variables. The STAEBL constraint analyses include blade stresses, vibratory response, flutter, and foreign object damage. Blade design variables include airfoil thickness at several locations, blade chord, and construction variables: hole size for hollow blades, and composite material layout for composite blades.

Author

N86-27285*# Massachusetts Inst. of Tech., Cambridge. Gas Turbine and Plasma Dynamics Lab.

CHANNEL FLOW MODELING OF IMPINGEMENT COOLING OF A ROTATING TURBINE BLADE

J. J. KOO Dec. 1984 94 p
 (Contract NAG3-335)
 (NASA-CR-177206; NAS 1.26:177206; GTPDL-181) Avail: NTIS HC A05/MF A01 CSCL 21E

Local heat transfer distributions in impingement cooling have been measured by Kreatsoulas and Prieser for a range of conditions which model those in actual turbine blades, including the effects of rotation. These data were reported as local Nusselt numbers, but referred to coolant supply conditions. By means of a channel flow modeling of the flow in the supply and impingement passages, the same data are here presented in terms of local Nusselt number distributions such as are used in design. The results in this form are compared to the nonrotating impingement results of Chupp and to the rotating but nonimpingement results of Morris. Rotation reduces the mean Nusselt numbers from these found by Chupp by about 30 percent, and introduces important radial variations which are sensitive to rotation and to leading edge stagger angle.

Author

N86-28085*# National Aeronautics and Space Administration. Lewis Research Center, Cleveland, Ohio.

UNIFORM ENGINE TESTING PROGRAM PHASE 7: NASA LEWIS RESEARCH CENTER SECOND ENTRY

T. J. BIESIADNY, L. A. BURKARDT, M. ABDELWAHAB, W. M. BRAITHWAITE, T. A. KIRCHGESSNER, and D. SILVER Jul. 1986 69 p
 (NASA-TM-87272; E-2971; NAS 1.15:87272) Avail: NTIS HC A04/MF A01 CSCL 21E

The propulsion and Energetics Panel, Working Group 15, of the Advisory Group for Aerospace Research and Development (AGARD) is sponsoring a Uniform Engine Testing Program (UETP). In this program, two jet engines were tested under identical conditions in certain NATO altitude and ground-level facilities as a means of correlating these facilities. With this second entry, NASA documented engine deterioration that may have occurred since inception of the UETP. Additionally, NASA investigated anomalies discovered during review of data from the five facilities which had participated in the program between the two NASA entries.

Author

N86-28086*# Oklahoma State Univ., Stillwater. School of Mechanical and Aerospace Engineering.

LATERAL JET INJECTION INTO TYPICAL COMBUSTOR FLOWFIELDS

D. G. LILLEY Washington NASA Jul. 1986 97 p
 (Contract NAG3-549)
 (NASA-CR-3997; NAS 1.26:3997) Avail: NTIS HC A05/MF A01 CSCL 21E

The experimental problem of lateral jet injection into typical flow fields in the absence of combustion was studied. All flow fields being investigated have no expansion of the crossflow (the test section to swirler diameter ratio $D/d = 1$), after its passage through an optional swirler (with swirl vane angle $\phi = 0$ (swirler removed), 45, and 70 degree). The lateral jet(s) is(are) located one test-section diameter downstream of the test-section inlet ($x/D = 1$). The lateral jets have round-sectioned nozzles, each of which has an area of 1/100th of the cross sectional area of the crossflow ($A_{sub j}/A_{sub c} = 1/100$). Jet-to-crossflow velocity ratios of $R = v_{sub j}/u_{sub o} = 2, 4, \text{ and } 6$ were investigated. Helium-bubble low visualization, five-hole pitot probe time-mean velocity measurements, and single-wire time-mean velocity and normal and shear stress turbulence data were obtained in the research program.

Author

07 AIRCRAFT PROPULSION AND POWER

N86-28087*# General Electric Co., Cincinnati, Ohio. Aircraft Engine Business Group.

EFFECTS OF SURFACE CHEMISTRY ON HOT CORROSION LIFE Final Report

R. E. FRYXELL and G. E. LEESE (TRW, Inc., Cleveland, Ohio.) Jun. 1986 113 p

(Contract NAS3-23926)

(NASA-CR-179471; NAS 1.26:179471; R86AEB361) Avail: NTIS HC A06/MF A01 CSCL 21E

Burner rig tests were conducted under the following conditions: 900 C, hourly thermal cycling, 0.5 ppm sodium as NaCl in the gas stream, and Mach 0.3 velocity. The alloys tested were Udimet 700 (U700) and Rene 80, uncoated and with RT21, Codep, or NiCoCrAlY coatings. The tests, up to 1000 hours, included specimens in the as-processed condition and after aging at 1100 C in oxidizing or inert environments for up to 600 hours. Coil-inductance changes were measured for periodic nondestructive inspection of specimens and found useful in the following course of corrosion. Typical sulfidation observed in all cases was similar to that observed in service-run turbine components. Aging at 1100 C caused severe decrease in the hot corrosion life of RT21 and Codep coatings and a significant but lesser decrease in the life of NiCoCrAlY coatings. The extent of these decreases was much greater for all three coatings on U700 than on Rene substrates. A coating hot corrosion life-prediction model was proposed. The model requires time/temperature information for a turbine component at takeoff conditions as well as environmental contaminant information. Author

N86-28089*# Arizona State Univ., Tempe. Dept. of Mechanical and Aerospace Engineering.

ON THE MODELING OF LOW-REYNOLDS-NUMBER TURBULENCE Final Report

R. M. C. SO and G. J. YOO Washington NASA Jul. 1986 143 p

(Contract NAG3-167; NG0530-85-C-0191)

(NASA-CR-3994; E-3059; NAS 1.26:3994; CR-R85033) Avail:

NTIS HC A07/MF A01 CSCL 21E

A full Reynolds-stress closure that is capable of describing the flow all the way to the wall was formulated for turbulent flow through circular pipe. Since viscosity does not appear explicitly in the pressure redistribution terms, conventional high-number models for these terms are found to be applicable. However, the models for turbulent diffusion and viscous dissipation have to be modified to account for viscous diffusion near a wall. Two redistribution and two diffusion models are investigated for their effects on the model calculations. Wall correction to pressure redistribution modeling is also examined. Diffusion effects on calculated turbulent properties are further investigated by simplifying the transport equations to algebraic equations for Reynolds stress. Two approximations are explored. These are the equilibrium and nonequilibrium turbulence assumptions. Finally, the two-equation closure is also used to calculate the flow in question and the results compared with all the other model calculations. Fully developed pipe flows at two moderate Reynolds numbers are used to validate these model calculations. Author

N86-28946*# Massachusetts Inst. of Tech., Cambridge. Dept. of Aeronautics and Astronautics.

A SUPERSONIC FAN EQUIPPED VARIABLE CYCLE ENGINE FOR A MACH 2.7 SUPERSONIC TRANSPORT Final Report

T. S. TAVARES 22 Aug. 1985 107 p

(Contract NAG3-697)

(NASA-CR-177141; NAS 1.26:177141) Avail: NTIS HC A06/MF A01 CSCL 21E

The concept of a variable cycle turbofan engine with an axially supersonic fan stage as powerplant for a Mach 2.7 supersonic transport was evaluated. Quantitative cycle analysis was used to assess the effects of the fan inlet and blading efficiencies on engine performance. Thrust levels predicted by cycle analysis are shown to match the thrust requirements of a representative aircraft. Fan inlet geometry is discussed and it is shown that a fixed geometry conical spike will provide sufficient airflow throughout

the operating regime. The supersonic fan considered consists of a single stage comprising a rotor and stator. The concept is similar in principle to a supersonic compressor, but differs by having a stator which removes swirl from the flow without producing a net rise in static pressure. Operating conditions peculiar to the axially supersonic fan are discussed. Geometry of rotor and stator cascades are presented which utilize a supersonic vortex flow distribution. Results of a 2-D CFD flow analysis of these cascades are presented. A simple estimate of passage losses was made using empirical methods. Author

N86-28947*# Teledyne CAE, Toledo, Ohio.

VARIABLE AREA RADIAL TURBINE FABRICATION AND TEST PROGRAM

C. ROGO Aug. 1986 91 p

(Contract NAS3-23173; DA PROJ. 1L1-61101-AH-45)

(NASA-CR-175091; NAS 1.26:175091; AVSCOM-TR-86-C-13)

Avail: NTIS HC A05/MF A01 CSCL 21E

A variable area radial turbine with a moveable nozzle sidewall was experimentally evaluated. The turbine was designed for an advanced variable capacity gas turbine rotorcraft engine. The turbine has a mass flow rate of 2.27 kg/sec (5.0 lbs/sec), and a rotor inlet temperature of 1477K (2200 F). Testing was conducted at a reduced inlet temperature, but the aerodynamic parameters and Reynolds numbers were duplicated. Overall performance was obtained for a range of nozzle areas from 50% to 100% of the maximum area. The test program determined the effect on performance of: (1) Moving the hub or shroud sidewall; (2) Sidewall-vane clearance leakage; (3) Vaneless space geometry change; and (4) Nozzle cooling flows. Data were obtained for a range of pressure ratios and speeds and are presented in a number of performance maps. Author

N86-29818*# Oklahoma Univ., Norman.

TRANSMISSION LINE DESIGN FOR A POWER DISTRIBUTION SYSTEM AT 20 KHZ FOR AIRCRAFT

L. W. ZELBY, J. B. MATHES, and J. W. SHAWVER Washington NASA Jul. 1986 38 p

(Contract NAG3-508)

(NASA-CR-3987; NAS 1.26:2987) Avail: NTIS HC A03/MF A01 CSCL 21E

A low inductance, low characteristic impedance transmission line was designed for a 20 kHz power distribution system. Several different conductor configurations were considered: strip lines, interdigitated metal ribbons, and standard insulated wires in multiwire configurations (circular and rectangular cylindrical arrangements). The final design was a rectangular arrangement of multiple wires of the same gauge with alternating polarities from wire to wire. This offered the lowest inductance per unit length (on the order of several nanohenries/meter) and the lowest characteristic impedance (on the order of one Ohm). Standard multipin connectors with gold-plated elements were recommended with this transmission line, the junction boxes to be internally connected with flat metal ribbons for low inductance, and the line to be constructed in sections of suitable length. Computer programs for the calculation of inductance of multiwire lines and of capacitances of strip lines were developed. Author

N86-30731*# Virginia Polytechnic Inst. and State Univ., Blacksburg. Dept. of Mechanical Engineering.

THERMODYNAMIC EVALUATION OF TRANSONIC COMPRESSOR ROTORS USING THE FINITE VOLUME APPROACH Status Report

S. NICHOLSON and J. MOORE Aug. 1986 292 p

(Contract NAG3-593)

(NASA-CR-176947; NAS 1.26:176947; JM/86-6) Avail: NTIS HC A13/MF A01 CSCL 21E

A method was developed which calculates two-dimensional, transonic, viscous flow in ducts. The finite volume, time marching formulation is used to obtain steady flow solutions of the Reynolds-averaged form of the Navier Stokes equations. The entire calculation is performed in the physical domain. The method is currently limited to the calculation of attached flows. The features

of the current method can be summarized as follows. Control volumes are chosen so that smoothing of flow properties, typically required for stability, is now needed. Different time steps are used in the different governing equations to improve the convergence speed of the viscous calculations. A new pressure interpolation scheme is introduced which improves the shock capturing ability of the method. A multi-volume method for pressure changes in the boundary layer allows calculations which use very long and thin control volumes. A special discretization technique is also used to stabilize these calculations. A special formulation of the energy equation is used to provide improved transient behavior of solutions which use the full energy equation. The method is then compared with a wide variety of test cases. The freestream Mach numbers range from 0.075 to 2.8 in the calculations. Transonic viscous flow in a converging diverging nozzle is calculated with the method; the Mach number upstream of the shock is approximately 1.25. The agreement between the calculated and measured shock strength and total pressure losses is good. Essentially incompressible turbulent boundary layer flow in an adverse pressure gradient is calculated and the computed distribution of mean velocity and shear stress are in good agreement with the measurements. At the other end of the Mach number range, a flat plate turbulent boundary layer with a freestream Mach number of 2.8 is calculated using the full energy equation; the computed total temperature distribution and recovery factor agree well with the measurements when a variable Prandtl number is used through the boundary layer. Author

N86-30732*# Systems Control Technology, Inc., Palo Alto, Calif.

ROBUST DETECTION, ISOLATION AND ACCOMMODATION FOR SENSOR FAILURES Final Report

A. EMAMI-NAEINI, M. M. AKHTER, and S. M. ROCK Jul. 1986 164 p

(Contract NAS3-24079)

(NASA-CR-174825; NAS 1.26:174825; SCT-85-5449) Avail: NTIS HC A08/MF A01 CSCL 21E

The objective is to extend the recent advances in robust control system design of multivariable systems to sensor failure detection, isolation, and accommodation (DIA), and estimator design. This effort provides analysis tools to quantify the trade-off between performance robustness and DIA sensitivity, which are to be used to achieve higher levels of performance robustness for given levels of DIA sensitivity. An innovations-based DIA scheme is used. Estimators, which depend upon a model of the process and process inputs and outputs, are used to generate these innovations. Thresholds used to determine failure detection are computed based on bounds on modeling errors, noise properties, and the class of failures. The applicability of the newly developed tools are demonstrated on a multivariable aircraft turbojet engine example. A new concept call the threshold selector was developed. It represents a significant and innovative tool for the analysis and synthesis of DIA algorithms. The estimators were made robust by introduction of an internal model and by frequency shaping. The internal mode provides asymptotically unbiased filter estimates. The incorporation of frequency shaping of the Linear Quadratic Gaussian cost functional modifies the estimator design to make it suitable for sensor failure DIA. The results are compared with previous studies which used thresholds that were selected empirically. Comparison of these two techniques on a nonlinear dynamic engine simulation shows improved performance of the new method compared to previous techniques Author

N86-30733*# Detroit Diesel Allison, Indianapolis, Ind.

FEASIBILITY STUDY FOR CONVERTIBLE ENGINE TORQUE CONVERTER

Oct. 1985 72 p

(Contract NAS3-24092)

(NASA-CR-175082; NAS 1.26:175082; EDR-12118) Avail: NTIS HC A04/MF A01 CSCL 21E

The feasibility study has shown that a dump/fill type torque converter has excellent potential for the convertible fan/shaft engine. The torque converter space requirement permits internal

housing within the normal flow path of a turboprop engine at acceptable engine weight. The unit permits operating the engine in the turboprop mode by decoupling the fan. To convert to turboprop mode, the torque converter overdrive capability bring the fan speed up to the power turbine speed to permit engagement of a mechanical lockup device when the shaft speed are synchronized. The conversion to turboprop mode can be made without drop of power turbine speed in less than 10 sec. Total thrust delivered to the aircraft by the propeller, fan, and engine during transient can be controlled to prevent loss of air speed or altitude. Heat rejection to the oil is low, and additional oil cooling capacity is not required. The turboprop engine aerodynamic design is basically uncompromised by convertibility and allows proper fan design for quiet and efficient cruise operation. Although the results of the feasibility study are exceedingly encouraging, it must be noted that they are based on extrapolation of limited existing data on torque converters. A component test program with three trial torque converter designs and concurrent computer modeling for fluid flow, stress, and dynamics, updated with test results from each unit, is recommended. Author

N86-31582*# National Aeronautics and Space Administration. Lewis Research Center, Cleveland, Ohio.

SMALL GAS TURBINE COMBUSTOR EXPERIMENTAL STUDY: COMPLIANT METAL/CERAMIC LINER AND PERFORMANCE EVALUATION

W. A. ACOSTA (Army Aviation Research and Development Command, Cleveland, Ohio) and C. T. NORGREN 1986 16 p Presented at the 22nd Joint Propulsion Conference, Huntsville, Ala., 16-18 Jun. 1986; sponsored by AIAA, ASME, SAE, and ASEE

(NASA-TM-87304; E-3016; NAS 1.15:87304) Avail: NTIS HC A02/MF A01 CSCL 21E

Combustor research relating to the development of fuel efficient small gas turbine engines capable of meeting future commercial and military aviation needs is currently underway at NASA Lewis. As part of this combustor research, a basic reverse-flow combustor has been used to investigate advanced liner wall cooling techniques. Liner temperature, performance, and exhaust emissions of the experimental combustor utilizing compliant metal/ceramic liners were determined and compared with three previously reported combustors that featured: (1) splash film-cooled liner walls; (2) transpiration cooled liner walls; and (3) counter-flow film cooled panels. Author

N86-31583*# National Aeronautics and Space Administration. Lewis Research Center, Cleveland, Ohio.

VISUALIZATION OF FLOWS IN A MOTORED ROTARY COMBUSTION ENGINE USING HOLOGRAPHIC INTERFEROMETRY

Y. R. HICKS, H. J. SCHOCK, J. E. CRAIG (Spectron Development Labs., Inc., Costa Mesa, Calif.), H. L. UMSTATTER, and D. Y. LEE 1986 15 p Presented at the 22nd Joint Propulsion Conference, Huntsville, Ala., 16-18 Jun. 1986; sponsored by AIAA, ASME, SAE and ASEE

(NASA-TM-88804; E-3148; NAS 1.15:88804; AIAA-86-1557) Avail: NTIS HC A02/MF A01 CSCL 21E

The use of holographic interferometry to view the small- and large-scale flow field structures in the combustion chamber of a motored Wankel engine assembly is described. In order that the flow patterns of interest could be observed, small quantities of helium were injected with the intake air. Variation of the air flow patterns with engine speed, helium flow rate, and rotor position are described. The air flow at two locations within the combustion chamber was examined using this technique. Author

07 AIRCRAFT PROPULSION AND POWER

N86-31584*# National Aeronautics and Space Administration. Lewis Research Center, Cleveland, Ohio.

DESCRIPTION OF A 20 KILOHERTZ POWER DISTRIBUTION SYSTEM

I. G. HANSEN Aug. 1986 7 p Presented at the 21st Intersociety Energy Conversion Engineering Conference, San Diego, Calif., 25-29 Aug. 1986; cosponsored by ACS, SAE, ANS, ASME, IEEE, AIAA, and AIChE

(NASA-TM-87346; NAS 1.15:87346) Avail: NTIS HC A02/MF A01 CSCL 21E

A single phase, 440 VRMS, 20 kHz power distribution system with a regulated sinusoidal wave form is discussed. A single phase power system minimizes the wiring, sensing, and control complexities required in a multi-sourced redundantly distributed power system. The single phase addresses only the distribution link; multiphase lower frequency inputs and outputs accommodation techniques are described. While the 440 V operating potential was initially selected for aircraft operating below 50,000 ft, this potential also appears suitable for space power systems. This voltage choice recognizes a reasonable upper limit for semiconductor ratings, yet will direct synthesis of 220 V, 3 power. A 20 kHz operating frequency was selected to be above the range of audibility, minimize the weight of reactive components, yet allow the construction of single power stages of 25 to 30 kW. The regulated sinusoidal distribution system has several advantages. With a regulated voltage, most ac/dc conversions involve rather simple transformer rectifier applications. A sinusoidal distribution system, when used in conjunction with zero crossing switching, represents a minimal source of EMI. The present state of 20 kHz power technology includes computer controls of voltage and/or frequency, low inductance cable, current limiting circuit protection, bi-directional power flow, and motor/generator operating using standard induction machines. A status update and description of each of these items and their significance is presented. M.G.

N86-31585*# National Aeronautics and Space Administration. Lewis Research Center, Cleveland, Ohio.

AEROPROPULSION OPPORTUNITIES FOR THE 21ST CENTURY

W. C. STRACK 1986 32 p Presented at the Scenario for 21st Century Aero Engine Design Seminar, Bristol, England, 16-17 May 1986; sponsored by the Institute of Mechanical Engineers (NASA-TM-88817; E-3177; NAS 1.15:88817) Avail: NTIS HC A03/MF A01 CSCL 21E

A large number of novel aeropropulsion system concepts are presented for subsonic through hypersonic applications offering large potential improvements. Collectively, these examples illustrate the revolutionary opportunities and challenges that could enable truly revolutionary aircraft capabilities in the future. Certainly not all of these concepts will ultimately prove fruitful. Nevertheless, the sheer number of existing concepts, including many unmentioned herein, is so large and the applications so vast, that the prognosis for the future of aeropropulsion is very encouraging indeed.

Author

N86-31586*# National Aeronautics and Space Administration. Lewis Research Center, Cleveland, Ohio.

A PARAMETRIC STUDY OF A GAS-GENERATOR AIRTURBO RAMJET (ATR)

C. A. SNYDER 1986 19 p Presented at the 22nd Joint Propulsion Conference, Huntsville, Ala., 16-18 Jun. 1986; sponsored by AIAA, ASME, SAE and ASEE (NASA-TM-88808; E-3156; NAS 1.15:88808) Avail: NTIS HC A02/MF A01 CSCL 21E

Parametric engine performance calculations were carried out for an airturbo ramjet (ATR). A LOX-LH2 rocket powered turbine powered the compressor. The engine was flown over a typical flight path up to Mach 5 to show the effect of engine off design operation. The compressor design efficiency, compressor pressure ratio, rocket turbine efficiency, rocket turbine inlet temperature, and rocket chamber pressure were varied to show their effect on engine net thrust and specific impulse at Mach 5 cruise. Estimates of engine weights as a function of the ratio of compressor air to

rocket propellant flow and rocket chamber pressure are also included. In general, the Mach 5 results indicate that increasing the amount of rocket gas produced increased thrust but decreased the specific impulse. The engine performance was fairly sensitive to rocket chamber pressure, especially at higher compressor pressure ratios. At higher compressor pressure ratios, the engine thrust was sensitive to turbine inlet temperature. At all compressor pressure ratios, the engine performance was not sensitive to compressor or turbine efficiency. Author

N86-31587*# National Aeronautics and Space Administration. Lewis Research Center, Cleveland, Ohio.

AN OVERVIEW OF THE SMALL ENGINE COMPONENT TECHNOLOGY (SECT) STUDIES

M. R. VANCO, W. T. WINTUCKY, and R. W. NIEDZWIECKI Jun. 1986 20 p Presented at the 22nd Joint Propulsion Conference, Huntsville, Ala., 16-18 Jun. 1986; cosponsored by AIAA, ASME, SAE, and ASEE

(NASA-TM-88796; E-3131; NAS 1.15:88796; USAAVSCOM-TR-86-C-23; AIAA-86-1542) Avail: NTIS HC A02/MF A01 CSCL 21E

The objectives of the joint NASA/Army SECT Studies were to identify high payoff technologies for year 2000 small gas turbine engine applications and to provide a technology plan for guiding future research and technology efforts applicable to rotorcraft, commuter and general aviation aircraft and cruise missiles. Competitive contracts were awarded to Allison, AVCO Lycoming, Garrett, Teledyne CAE and Williams International. This paper presents an overview of the contractors' study efforts for the commuter, rotorcraft, cruise missile, and auxiliary power (APU) applications with engines in the 250 to 1,000 horsepower size range. Reference aircraft, missions and engines were selected. Advanced engine configurations and cycles with projected year 2000 component technologies were evaluated and compared with a reference engine selected by the contractor. For typical commuter and rotorcraft applications, fuel savings of 22 percent to 42 percent can be attained. For \$1/gallon and \$2/gallon fuel, reductions in direct operating cost range from 6 percent to 16 percent and from 11 percent to 17 percent respectively. For subsonic strategic cruise missile applications, fuel savings of 38 percent to 54 percent can be achieved which allows 35 percent to 60 percent increase in mission range and life cycle cost reductions of 40 percent to 56 percent. High payoff technologies have been identified for all applications. Author

N86-31588*# National Aeronautics and Space Administration. Lewis Research Center, Cleveland, Ohio.

TURBULENT DISPERSION OF THE ICING CLOUD FROM SPRAY NOZZLES USED IN ICING TUNNELS

C. J. MAREK and W. A. OLSEN, JR. May 1986 17 p Presented at the 3rd International Workshop on Atmospheric Icing of Structures, Vancouver, British Columbia, 6-8 May 1986 (NASA-TM-87316; E-3047; NAS 1.15:87316) Avail: NTIS HC A02/MF A01 CSCL 21E

To correctly simulate flight in natural icing conditions, the turbulence in an icing simulator must be as low as possible. But some turbulence is required to mix the droplets from the spray nozzles and achieve an icing cloud of uniform liquid water content. The goal for any spray system is to obtain the widest possible spray cloud with the lowest possible turbulence in the test section of a icing tunnel. This investigation reports the measurement of turbulence and the three-dimensional spread of the cloud from a single spray nozzle. The task was to determine how the air turbulence and cloud width are affected by spray bars of quite different drag coefficients, by changes in the turbulence upstream of the spray, the droplet size, and the atomizing air. An ice accretion grid, located 6.3 m downstream of the single spray nozzle, was used to measure cloud spread. Both the spray bar and the grid

AIRCRAFT STABILITY AND CONTROL

Includes aircraft handling qualities; piloting; flight controls; and autopilots.

were located in the constant velocity test section. Three spray bar shapes were tested: the short blunt spray bar used in the NASA Lewis Icing Research Tunnel, a thin 14.6 cm chord airfoil, and a 53 cm chord NACA 0012 airfoil. At the low airspeed (56 km/hr) the ice accretion pattern was axisymmetric and was not affected by the shape of the spray bar. At the high airspeed (169 km/hr) the spread was 30 percent smaller than at the low airspeed. For the widest cloud the spray bars should be located as far upstream in the low velocity plenum of the icing tunnel. Good comparison is obtained between the cloud spread data and predictions from a two-dimensional cloud mixing computer code using the two equation turbulence (k epsilon g) model. Author

N86-32432* # National Aeronautics and Space Administration. Lewis Research Center, Cleveland, Ohio.

PERSPECTIVES ON DILUTION JET MIXING

J. D. HOLDEMAN and R. SRINIVASAN (Garrett Turbine Engine Co., Phoenix, Ariz.) Mar. 1986 32 p Presented at the Spring Meeting of the Central States Section of the Combustion Inst., Cleveland, Ohio, 5-6 May 1986 and the 22nd Joint Propulsion Conference, Huntsville, Ala., 16-18 Jun. 1986; sponsored by AIAA, ASME, SAE, and ASEE

(NASA-TM-87294; E-2975; NAS 1.15:87294; AIAA-86-1611)

Avail: NTIS HC A03/MF A01 CSCL 21E

A microcomputer code which displays 3-D oblique and 2-D plots of the temperature distribution downstream of jets mixing with a confined crossflow has been used to investigate the effects of varying the several independent flow and geometric parameters on the mixing. Temperature profiles calculated with this empirical model are presented to show the effects of orifice size and spacing, momentum flux ratio, density ratio, variable temperature mainstream, flow area convergence, orifice aspect ratio, and opposed and axially staged rows of jets. Author

N86-32433* # National Aeronautics and Space Administration. Lewis Research Center, Cleveland, Ohio.

STRUCTURAL DYNAMIC MEASUREMENT PRACTICES FOR TURBOMACHINERY AT THE NASA LEWIS RESEARCH CENTER

L. J. KIRALY 1986 30 p Presented at the Symposium on Propulsion Instrumentation, Jiangyou, China, 6-10 Oct. 1986; sponsored by NASA and Chinese Aeronautical Establishment (NASA-TM-88857; E-3245; NAS 1.15:88857) Avail: NTIS HC A03/MF A01 CSCL 51C

Methods developed for measuring blade and rotor-shaft system response include optical systems, transient instruments, and special digital data processing equipment. Optical methods offer some distinct benefits for blade vibration measurement. Transient and steady state measurements of the response of rotor-shaft systems strongly affect analytical methods development. Digital computing systems allow processing of large volumes of high speed data from rotating blade sets. Also, digital systems develop useful vibration response signatures from randomly excited systems. Research facilities include the spin rig facility and the transient rotor response lab. Author

A86-40681* # National Aeronautics and Space Administration. Lewis Research Center, Cleveland, Ohio.

THE MEASUREMENT OF AIRCRAFT PERFORMANCE AND STABILITY AND CONTROL AFTER FLIGHT THROUGH NATURAL ICING CONDITIONS

R. J. RANAUDO, K. L. MIKKELSEN, R. C. MCKNIGHT, R. F. IDE, A. L. REEHORST (NASA, Lewis Research Center, Cleveland, OH) et al. AIAA, AHS, CASI, DGLR, IES, ISA, ITEA, SETP, and SFTE, Flight Testing Conference, 3rd, Las Vegas, NV, Apr. 2-4, 1986. 46 p. Previously announced in STAR as N86-22582. refs (AIAA PAPER 86-9758)

The effects of airframe icing on the performance and stability and control of a twin-engine commuter-class aircraft were measured by the NASA Lewis Research Center. This work consisted of clear air tests with artificial ice shapes attached to the horizontal tail, and natural icing flight tests in measured icing clouds. The clear air tests employed static longitudinal flight test methods to determine degradation in stability margins for four simulated ice shapes. The natural icing flight tests employed a data acquisition system, which was provided under contract to NASA by Kohlman Systems Research Incorporated. This system used a performance modeling method and modified maximum likelihood estimation (MMLE) technique to determine aircraft performance degradation and stability and control. Flight test results with artificial ice shapes showed that longitudinal, stick-fixed, static margins are reduced on the order of 5 percent with flaps up. Natural icing tests with the KSR system corroborated these results and showed degradation in the elevator control derivatives on the order of 8 to 16 percent depending on wing flap configuration. Performance analyses showed the individual contributions of major airframe components to the overall degradation in lift and drag. Author

N86-22582* # National Aeronautics and Space Administration. Lewis Research Center, Cleveland, Ohio.

THE MEASUREMENT OF AIRCRAFT PERFORMANCE AND STABILITY AND CONTROL AFTER FLIGHT THROUGH NATURAL ICING CONDITIONS

R. J. RANAUDO, K. L. MIKKELSEN, R. C. MCKNIGHT, R. F. IDE, A. L. REEHORST, J. L. JORDAN, W. C. SCHINSTOCK, and S. J. PLATZ 1986 46 p refs Presented at the 3rd Flight Testing Conference, Las Vegas, Nev., 2-4 Apr. 1986; cosponsored by AIAA, CASI, DGLR, IES, ISA, ITEA, SETP, and SFTE Prepared in cooperation with Kohlman Systems Research, Inc., Lawrence, Kansas

(NASA-TM-87265; E-2982; NAS 1.15:87265; AIAA-86-9758)

Avail: NTIS HC A03/MF A01 CSCL 01C

The effects of airframe icing on the performance and stability and control of a twin-engine commuter-class aircraft were measured by the NASA Lewis Research Center. This work consisted of clear air tests with artificial ice shapes attached to the horizontal tail, and natural icing flight tests in measured icing clouds. The clear air tests employed static longitudinal flight test methods to determine degradation in stability margins for four simulated ice shapes. The natural icing flight tests employed a data acquisition system, which was provided under contract to NASA by Kohlman Systems Research Incorporated. This system used a performance modeling method and modified maximum likelihood estimation (MMLE) technique to determine aircraft performance degradation and stability and control. Flight test results with artificial ice shapes showed that longitudinal, stick-fixed, static margins are reduced on the order of 5 percent with flaps up. Natural icing tests with the KSR system corroborated these results and showed degradation in the elevator control derivatives on the order of 8 to 16 percent depending on wing flap configuration. Performance

09 RESEARCH AND SUPPORT FACILITIES (AIR)

analyses showed the individual contributions of major airframe components to the overall degradation in lift and drag. Author

09

RESEARCH AND SUPPORT FACILITIES (AIR)

Includes airports, hangars and runways; aircraft repair and overhaul facilities; wind tunnels; shock tubes; and aircraft engine test stands.

A86-19654*# National Aeronautics and Space Administration. Lewis Research Center, Cleveland, Ohio.

WIND TUNNEL TURNING VANES OF MODERN DESIGN

T. F. GELDER, R. D. MOORE, J. M. SANZ, and E. R. MCFARLAND (NASA, Lewis Research Center, Cleveland, OH) AIAA, Aerospace Sciences Meeting, 24th, Reno, NV, Jan. 6-9, 1986. 15 p. Previously announced in STAR as N86-12239. refs (AIAA PAPER 86-0044)

Rehabilitation of the Altitude Wind Tunnel includes the need for new corner turning vanes to match its upgraded performance. The design and experimental performance results from a 0.1-full scale model of the highest speed corner ($M = 0.35$) are presented and discussed along with some two dimensional inviscid analyses of two vane corners. With a vane designed by an inverse two dimensional technique, the overall corner loss was about 12 percent of the inlet dynamic pressure of which about 4 percent was caused by vane skin friction. Comparable values with a conventionally designed circular arc vane were about 14 percent overall with about 7 percent due to skin friction. E.A.K.

A86-24727*# National Aeronautics and Space Administration. Lewis Research Center, Cleveland, Ohio.

CURRENT WIND TUNNEL CAPABILITY AND PLANNED IMPROVEMENTS AT LEWIS RESEARCH CENTER

D. N. BOWDITCH (NASA, Lewis Research Center, Cleveland, OH) IN: Aerodynamic Testing Conference, 14th, West Palm Beach, FL, March 5-7, 1986, Technical Papers. New York, American Institute of Aeronautics and Astronautics, 1986, p. 1-11. refs (AIAA PAPER 86-0728)

The NASA Lewis 8 x 6-ft and 10 x 10-ft supersonic wind tunnels furnish the capability for propulsion system tests in the Mach 0.4-3.5 range; the 9 x 15-ft wind tunnel at the facility addresses propulsion installation problems at the lower, takeoff and landing speeds, further providing an excellent anechoic environment in which to measure propeller and fan noise. The NASA Lewis Icing Research Tunnel is the largest of its kind in the free world. The currently mothballed Hypersonic Tunnel Facility could furnish the best available simulations of nonvitiated Mach 5-7 test conditions. Studies are underway to identify prospective performance-enhancing modifications for these facilities in the 1990s and beyond. O.C.

A86-24744*# National Aeronautics and Space Administration. Lewis Research Center, Cleveland, Ohio.

PROGRESS IN THE LEWIS RESEARCH CENTER ALTITUDE WIND TUNNEL (AWT) MODELING PROGRAM

C. C. CIEPLUCH, R. R. BURLEY, D. E. GROESBECK, and J. A. MAREK (NASA, Lewis Research Center, Cleveland, OH) IN: Aerodynamic Testing Conference, 14th, West Palm Beach, FL, March 5-7, 1986, Technical Papers. New York, American Institute of Aeronautics and Astronautics, 1986, p. 183-192. refs (AIAA PAPER 86-0757)

The rehabilitation of the AWT at the NASA Lewis Research Center is under study with the goal of providing a modern subsonic wind tunnel for conducting propulsion system/airframe integration, isolated propulsion system, propulsion acoustics and adverse weather tests. Because of the increased Mach number capability (from Mach 0.6 to 0.9 plus) and the incorporation of acoustic and adverse weather capabilities into an existing tunnel, the AWT

rehabilitation represents a significant technical challenge. In order to reduce the risk associated with such an undertaking, an extensive AWT modeling program is being conducted to guide and verify the tunnel design. Significant findings and progress in this modeling program are the subject of this paper. Author

A86-24745*# National Aeronautics and Space Administration. Lewis Research Center, Cleveland, Ohio.

DEVELOPMENT AND APPLICATION OF DYNAMIC SIMULATIONS OF A SUBSONIC WIND TUNNEL

J. R. SZUCH, G. L. COLE, R. C. SEIDEL, and D. J. ARPASI (NASA, Lewis Research Center, Cleveland, OH) IN: Aerodynamic Testing Conference, 14th, West Palm Beach, FL, March 5-7, 1986, Technical Papers. New York, American Institute of Aeronautics and Astronautics, 1986, p. 193-202. refs (AIAA PAPER 86-0758)

Efforts are currently underway at NASA Lewis to improve and expand ground test facilities and to develop supporting technologies to meet anticipated aeropropulsion research needs. Many of these efforts have been focused on a proposed rehabilitation of the Altitude Wind Tunnel (AWT). In order to insure a technically sound design, an AWT modeling program (both analytical and physical) was initiated to provide input to the AWT final design process. This paper describes the approach taken to develop analytical, dynamic computer simulations of the AWT, and the use of these simulations as test-beds for (1) predicting the dynamic response characteristics of the AWT and (2) evaluating proposed AWT control concepts. Plans for developing a portable, real-time simulator for the AWT facility are also described. Author

A86-26620*# National Aeronautics and Space Administration. Lewis Research Center, Cleveland, Ohio.

STUDY OF ICE ACCRETION ON ICING WIND TUNNEL COMPONENTS

J. E. NEWTON and W. OLSEN (NASA, Lewis Research Center, Cleveland, OH) AIAA, Aerospace Sciences Meeting, 24th, Reno, NV, Jan. 6-9, 1986. 23 p. Previously announced in STAR as N86-16232.

(AIAA PAPER 86-0290)

In a closed loop icing wind tunnel the icing cloud is simulated by introducing tiny water droplets through an array of nozzles upstream of the test section. This cloud will form ice on all tunnel components (e.g., turning vanes, inlet guide vanes, fan blades, and the heat exchanger) as the cloud flows around the tunnel. These components must have the capacity to handle their icing loads without causing significant tunnel performance degradation during the course of an evening's run. To aid in the design of these components for the proposed Altitude Wind Tunnel (AWT) at NASA Lewis Research Center the existing Icing Research Tunnel (IRT) is used to measure icing characteristics of the IRT's components. The results from the IRT are scaled to the AWT to account for the AWT's larger components and higher velocities. The results show that from 90 to 45 percent of the total spray cloud froze out on the heat exchanger. Furthermore, the first set of turning vanes downstream of the test section, the FOD screen and the fan blades show significant ice formation. The scaling shows that the same results would occur in the AWT. Author

A86-39948*# Massachusetts Inst. of Tech., Cambridge.

EXPERIMENTAL MEASUREMENTS OF HEAT TRANSFER FROM AN ICED SURFACE DURING ARTIFICIAL AND NATURAL CLOUD ICING CONDITIONS

M. S. KIRBY and R. J. HANSMAN, JR. (MIT, Cambridge, MA) AIAA and ASME, Joint Thermophysics and Heat Transfer Conference, 4th, Boston, MA, June 2-4, 1986. 11 p. FAA-supported research. refs

(Contract NGL-22-009-640; NAG3-666)

(AIAA PAPER 86-1352)

The heat transfer behavior of accreting ice surfaces in natural (flight test) and simulated (wind tunnel) cloud icing conditions have been studied. Observations of wet and dry ice growth regimes as measured by ultrasonic pulse-echo techniques were made. Observed wet and dry ice growth regimes at the stagnation point

of a cylinder were compared with those predicted using a quasi steady-state heat balance model. A series of heat transfer coefficients were employed by the model to infer the local heat transfer behavior of the actual ice surfaces. The heat transfer in the stagnation region was generally inferred to be higher in wind tunnel icing tests than in natural, flight, icing conditions. Author

N86-12239*# National Aeronautics and Space Administration. Lewis Research Center, Cleveland, Ohio.

WIND TUNNEL TURNING VANES OF MODERN DESIGN

T. F. GELDER, R. D. MOORE, J. M. SANZ, and E. R. MCFARLAND 1985 23 p refs Proposed for presentation at the 24th Aerospace Sci. Meeting, Reno, Nev., 6-8 Jan. 1986; sponsored by AIAA

(NASA-TM-87146; E-2775; NAS 1.15:87146; AIAA-86-0044)

Avail: NTIS HC A02/MF A01 CSCL 14B

Rehabilitation of the Altitude Wind Tunnel includes the need for new corner turning vanes to match its upgraded performance. The design and experimental performance results from a 0.1-full scale model of the highest speed corner ($M = 0.35$) are presented and discussed along with some two dimensional inviscid analyses of two vane corners. With a vane designed by an inverse two dimensional technique, the overall corner loss was about 12% of the inlet dynamic pressure of which about 4% was caused by vane skin friction. Comparable values with a conventionally designed circular arc vane were about 14% overall with about 7% due to skin friction. E.A.K.

N86-15323*# Kansas Univ. Center for Research, Inc., Lawrence.

AN ANALYSIS OF CROSS-COUPLING OF A MULTICOMPONENT JET ENGINE TEST STAND USING FINITE ELEMENT MODELING TECHNIQUES Final Report

W. G. SCHWEIKHARD and W. N. SINGNOI 1985 55 p refs (Contract NAG3-85)

(NASA-CR-176424; NAS 1.26:176424) Avail: NTIS HC A04/MF A01 CSCL 14B

A two axis thrust measuring system was analyzed by using a finite element computer program to determine the sensitivities of the thrust vectoring nozzle system to misalignment of the load cells and applied loads, and the stiffness of the structural members. Three models were evaluated: (1) the basic measuring element and its internal calibration load cells; (2) the basic measuring element and its external load calibration equipment; and (3) the basic measuring element, external calibration load frame and the altitude facility support structure. Alignment of calibration loads was the greatest source of error for multiaxis thrust measuring systems. Uniform increases or decreases in stiffness of the members, which might be caused by the selection of the materials, have little effect on the accuracy of the measurements. It is found that the POLO-FINITE program is a viable tool for designing and analyzing multiaxis thrust measurement systems. The response of the test stand to step inputs that might be encountered with thrust vectoring tests was determined. The dynamic analysis show a potential problem for measuring the dynamic response characteristics of thrust vectoring systems because of the inherently light damping of the test stand. E.A.K.

N86-16232*# National Aeronautics and Space Administration. Lewis Research Center, Cleveland, Ohio.

STUDY OF ICE ACCRETION ON ICING WIND TUNNEL COMPONENTS

J. E. NEWTON and W. OLSEN 1986 24 p refs Presented at the 24th Aerospace Sciences Meeting, Reno, Nev., 6-8 Jan. 1986; sponsored by AIAA

(NASA-TM-87095; E-3828; NAS 1.15:87095) Avail: NTIS HC A02/MF A01 CSCL 01E

In a closed loop icing wind tunnel the icing cloud is simulated by introducing tiny water droplets through an array of nozzles upstream of the test section. This cloud will form ice on all tunnel components (e.g., turning vanes, inlet guide vanes, fan blades, and the heat exchanger) as the cloud flows around the tunnel. These components must have the capacity to handle their icing

loads without causing significant tunnel performance degradation during the course of an evening's run. To aid in the design of these components for the proposed Altitude Wind Tunnel (AWT) at NASA Lewis Research Center the existing Icing Research Tunnel (IRT) is used to measure icing characteristics of the IRT's components. The results from the IRT are scaled to the AWT to account for the AWT's larger components and higher velocities. The results show that from 90 to 45 percent of the total spray cloud froze out on the heat exchanger. Furthermore, the first set of turning vanes downstream of the test section, the FOD screen and the fan blades show significant ice formation. The scaling shows that the same results would occur in the AWT. Author

N86-16233*# National Aeronautics and Space Administration. Lewis Research Center, Cleveland, Ohio.

PROGRESS IN THE LEWIS RESEARCH CENTER ALTITUDE WIND TUNNEL (AWT) MODELING PROGRAM

C. C. CIEPLUCH, R. R. BURLEY, D. E. GROESBECK, and J. C. MAREK 1986 19 p refs Proposed for presentation at the 14th Aerodynamic Testing Conference, West Palm Beach, Fla., 5-7 Mar. 1986; sponsored by AIAA

(NASA-TM-87194; E-2850; NAS 1.15:87194) Avail: NTIS HC A02/MF A01 CSCL 14B

The rehabilitation of the Altitude Wind Tunnel (AWT) at the NASA Lewis Research Center is under study with the goal of providing a modern subsonic wind tunnel for conducting propulsion system/airframe integration, isolated propulsion system, propulsion acoustics and adverse weather tests. Because of the increased Mach number capability (from Mach 0.6 to 0.9 plus) and the incorporation of acoustic and adverse weather capabilities into an existing tunnel, the AWT rehabilitation represents a significant technical challenge. In order to reduce the risk associated with such an undertaking, and extensive AWT modeling program is being conducted to guide and verify the tunnel design. Significant findings and progress in this modeling program are the subject of this paper. Author

N86-18329*# National Aeronautics and Space Administration. Lewis Research Center, Cleveland, Ohio.

CURRENT WIND TUNNEL CAPABILITY AND PLANNED IMPROVEMENTS AT LEWIS RESEARCH CENTER

D. N. BOWDITCH 1986 24 p refs Prepared for presentation at the 14th Aerodynamic Testing Conference, West Palm Beach, Fla., 5-7 Mar. 1986; sponsored by AIAA

(NASA-TM-87190; E-2844; NAS 1.15:87190) Avail: NTIS HC A02/MF A01 CSCL 14B

As the propulsion and power generation center of NASA, Lewis has designed its wind tunnels for propulsion research. Therefore, the 8 by 6 Foot Supersonic Wind Tunnel and the 10 by 10 Foot Supersonic Wind Tunnel provide the capability to test operating propulsion systems from Mach 0.4 to 3.5. The 9 by 15 Foot Wind Tunnel can investigate propulsion installation problems at the lower takeoff and landing speeds and provides an excellent anechoic environment to measure propeller and fan noise. The Lewis Central Air System provides steady air supplies to 450 psi, and exhaust to 3 in. of mercury absolute, which are available to the wind tunnels for simulation of jets and engine induced flows. The Lewis Icing Research Tunnel is the largest in the free world that can produce icing conditions throughout the year. Rehabilitation of the Altitude Wind Tunnel at Lewis would allow testing of propulsion systems in the upper left hand corner which would be a unique capability. Also, in a mothballed state at Lewis, the Hypersonic Tunnel Facility could provide the best simulation of nonvitiated Mach 5-7 test conditions available. Studies are currently being made of the Lewis facilities to identify enhancements of their research potential for the 1990's and beyond. Author

N86-27291*# Wichita State Univ., Kans. Dept. of Aeronautical Engineering.

DE-ICING OF THE ALTITUDE WIND TUNNEL TURNING VANES BY ELECTRO-MAGNETIC IMPULSE Final Report

G. W. ZUMWALT and R. ROSS Mar. 1986 79 p

(Contract NAG3-607)

(NASA-CR-177260; NAS 1.26:177260) Avail: NTIS HC A05/MF A01 CSCL 14B

The Altitude Wind Tunnel at the NASA-Lewis facility is being proposed for a refurbishment and modernization. Two major changes are: (1) the increasing of the test section Mach number to 0.90, and (2) the addition of spray nozzles to provide simulation of flight in icing clouds. Features to be retained are the simulation of atmospheric temperature and pressure to 50,000 foot altitude and provision for full-scale aircraft engine operation by the exhausting of the aircraft combustion gases and ingestion of air to replace that used in combustion. The first change required a re-design of the turning vanes in the two corners downstream of the test section due to the higher Mach number at the corners. The second change threatens the operation of the turning vanes by the expected ice build-up, particularly on the first-corner vanes. De-icing by heat has two drawbacks: (1) an extremely large amount of heat is required, and (2) the melted ice would tend to collect as ice on some other surfaces in the tunnel, namely, the tunnel propellers and the cooling coils. An alternate de-icing method had been under development for three years under NASA-Lewis grants to the Wichita State University. This report describes the electro-impulse de-icing (EIDI) method and the testing work done to assess its applicability to wind tunnel turning vane de-icing. Tests were conducted in the structural dynamics laboratory and in the NASA Icing Research Tunnel. Good ice protection was achieved at lower power consumption and at a wide range of tunnel operations conditions. Recommendations for design and construction of the system for this application of the EIDI method are given.

Author

N86-28101*# National Aeronautics and Space Administration. Lewis Research Center, Cleveland, Ohio.

EXPERIMENTAL EVALUATION OF TWO TURNING VANE DESIGNS FOR HIGH-SPEED CORNER OF 0.1-SCALE MODEL OF NASA LEWIS RESEARCH CENTER'S PROPOSED ALTITUDE WIND TUNNEL

R. D. MOORE, D. R. BOLDMAN, and R. J. SHYNE Apr. 1986 130 p

(NASA-TP-2570; E-2831; NAS 1.60:2570) Avail: NTIS HC A07/MF A01 CSCL 14B

Two turning vane designs were experimentally evaluated for corner 1 (downstream of the test section) of a 0.1-scale model of the NASA Lewis Research Center's proposed Altitude Wind Tunnel (AWT). Vane A was a controlled-diffusion airfoil shape; vane B was a circular-arc airfoil shape. The vane designs were tested over corner inlet Mach numbers from 0.16 to 0.465. Several modifications in vane setting angle and vane spacing were also evaluated for vane A. The overall performance obtained from total pressure rakes indicated that vane B had a slightly lower loss coefficient than vane A. At Mach 0.35 (the design Mach number without the engine exhaust removal scoop), the loss coefficients were 0.150 and 0.178 for vanes B and A, respectively. Resetting the vane A angle by -5 deg. (vane A10) to turn the flow toward the outside corner reduced the loss coefficient to 0.119. The best configuration (vane A10) was also tested with a simulated engine exhaust removal scoop. The loss coefficient for that configuration was 0.164 at Mach 0.41 (the approximate design Mach number with the scoop).

Author

ASTRONAUTICS (GENERAL)

A86-29586*# National Aeronautics and Space Administration. Lewis Research Center, Cleveland, Ohio.

SPACECRAFT 2000

K. A. FAYMON (NASA, Lewis Research Center, Cleveland, OH) IN: Communication Satellite Systems Conference, 11th, San Diego, CA, March 17-20, 1986, Technical Papers. New York, American Institute of Aeronautics and Astronautics, 1986, p. 88-91. refs (AIAA PAPER 86-0616)

The Spacecraft 2000 program has been conceived by NASA with the objective to maintain the U.S. in a strong technical position in the space arena. The program is to involve a cooperative NASA/industry effort with long-range technology development aims. The technology areas addressed are related to spacecraft power, spacecraft energy storage, power management and distribution, autonomous operation-control, onboard systems integration, secondary propulsion, communications technologies, and systems/subsystems technology verification. Aspects of Spacecraft 2000 interactions with industry are discussed, taking into account visitations of NASA personnel to selected industrial concerns, most critical concerns (general), major technical concern, technology drivers for future spacecraft power systems, technology considerations for secondary propulsion, and questions of commercialization. Plans related to a Spacecraft 2000 program formulation are also considered.

G.R.

N86-10083*# Rensselaer Polytechnic Inst., Troy, N.Y.

INFLUENCE OF MELT CONVECTION ON SOLID-LIQUID INTERFACE UNDER TERRESTRIAL AND REDUCED GRAVITY ENVIRONMENTS

M. E. GLICKSMAN IN NASA, Washington Microgravity Sci. and Appl. Program Tasks p 60-62 May 1985 refs (Contract NAG3-333)

Avail: NTIS HC A10/MF A01 CSCL 22A

Solidification and crystal growth processes involve thermal and solutal gradients within a molten phase. In the presence of gravity, such gradients result in convective flows which interact with diffusion fields at the solid-liquid interface. Dendritic growth kinetics was studied in transparent model systems which freeze similarly to most metals. Succinonitrile shows a strong influence of convection at supercoolings below about 1K. Fluid flows adjacent to solid-liquid interfaces and the behavior of shear flows in vertical annular geometries are studied. Novel low-frequency eigenstates were discovered and classified as coupled modes, for their involvement with interfacial deformation coupled to the fluid flow, and are unknown in systems without deformable interfaces. The dependence of coupled convection modes on interfacial geometry, gravity, fluid properties, and transformation characteristics studied for several annual flow arrangements with nominally pure solid-liquid systems.

E.A.K.

N86-10086*# Michigan Technological Univ., Houghton. Dept. of Metallurgical Engineering.

THE DEVELOPMENT AND PREVENTION OF CHANNEL SEGREGATION DURING ALLOY SOLIDIFICATION

A. HELLAWELL IN NASA, Washington Microgravity Sci. and Appl. Program Tasks p 65-66 May 1985 refs (Contract NAG3-560)

Avail: NTIS HC A10/MF A01 CSCL 22A

During alloy solidification, interdendritic microsegregation causes density differences between entrapped liquid and bulk liquid which provides a driving force for convection. One of the consequences of this effect is the formation of long, nearly vertical liquid channels, rich in solute, flowing through the solid-liquid mushy zone somewhat as a river and tributary system. In ingot castings where the heat flow is vertically downwards and the solute less dense than the

solute the convective flow is antiparallel with the flow caused by contraction on freezing. Identification of the mechanisms involved in these two problems is discussed. It is known that certain types of bulk liquid movements can inhibit channel development and the mechanism by which they do so are examined. E.A.K.

N86-10090*# Case Western Reserve Univ., Cleveland, Ohio. Dept. of Metallurgy and Materials Science.

SOLIDIFICATION FUNDAMENTALS

V. LAXMANAN and J. F. WALLACE /in NASA, Washington Microgravity Sci. and Appl. Program Tasks p 72-73 May 1985 refs

(Contract NAG3-417)

Avail: NTIS HC A10/MF A01 CSCL 22A

The fundamental aspects of a variety of solidification phenomena were studied, taking advantage of the unique opportunities offered by the microgravity environment of space. Containerless processing and an understanding of the role of fluids induced by gravitational effects are the two major objectives justifying an experimental program in reduced gravity. The solidification phenomena which are likely to benefit are: macro and microsegregation, columnar-equiaxed transition, pore formation, and undercooling. E.A.K.

N86-10093*# Wisconsin Univ., Madison. Dept. of Metallurgical and Mineral Engineering.

CONTAINERLESS PROCESSING OF UNDERCOOLED MELTS

J. H. PEREPEZKO /in NASA, Washington Microgravity Sci. and Appl. Program Tasks p 76 May 1985 (Contract NAG3-436)

Avail: NTIS HC A10/MF A01 CSCL 22A

The physical mechanisms controlling liquid undercooling were studied for application to solidification processing methods. The undercooling potential of containerless processing was assessed on droplet samples of high melting temperature metals drop tube and drop tower facilities and in a laboratory-scale apparatus. New insight into nucleation and crystal growth will be obtained in undercooled liquids of high melting temperature iron and nickel-base systems. The processing parameters include melt superheat, droplet size and particle statistics and droplet surface coating. The solidification behavior is determined by thermal analysis and by structural and metallographic characterization. E.A.K.

N86-10107*# National Aeronautics and Space Administration. Lewis Research Center, Cleveland, Ohio.

TRANSPORT PROCESSES IN SOLUTION CRYSTAL GROWTH

A. T. CHAI /in NASA, Washington Microgravity Sci. and Appl. Program Tasks p 96 May 1985

Avail: NTIS HC A10/MF A01 CSCL 22A

The objective of this effort is to conduct fundamental research in reduced gravity on transport processes occurring during solution crystal growth. Experimental techniques will be developed to monitor and control key parameters at the interface between a growing crystal and the solution from which it grows. Techniques developed will lead to an in-space experiment in the Shuttle. The focus will be on non-incurive ground-based laboratory measurements of model systems and the definition of requirements for space experimentation. Initially, aqueous solutions will be used for easier control and instrumentation. Model systems with imposed steady flows and simplified boundary conditions will be studied for characterization. Various nonincurive measurement techniques are being investigated for proper applications in a newly built laboratory capable of flow visualization, laser Doppler velocimetry, Schlieren photography, specklegram, holographic interferometry, and Raman spectroscopy. Author

N86-10108*# California Univ., Berkeley.

FREE SURFACE PHENOMENA UNDER LOW- AND ZERO-GRAVITY CONDITIONS

P. CONCUS, D. COLES (California Inst. of Tech.), R. FINN (Stanford Univ.), and L. HESSELINK (Stanford Univ.) /in NASA, Washington Microgravity Sci. and Appl. Program Tasks p 97 May 1985 (Contract NAG3-147)

Avail: NTIS HC A10/MF A01 CSCL 22A

In a low- or zero-gravity environment the free surface of a liquid can behave in striking, unexpected ways. For example, in a partially filled container, a free surface that is well behaved under terrestrial conditions can rise to an arbitrarily large height or even fail to exist when gravity is absent. An answer is sought to the central mathematical questions: Under what conditions can free surfaces exist and what are their properties? -- and experimental questions of what means can be devised to observe and to measure the surfaces quantitatively. Current activity focuses on material selection and the design of optical diagnostic methods for in-space experiments. These experiments will test mathematical predictions of discontinuous transition from existence to nonexistence of capillary free surfaces in certain geometric configurations under zero gravity conditions. Liquids and container materials suitable for achieving the required contact-angle range and optical properties are being investigated, as well as the effects of contaminants and fluid motion on contact angle. The optical diagnostic technique investigation concerns laser-induced fluorescence, including emphasis on data on acquisition, sources and detectors, reliability, data management, and computer control. Author

N86-10110*# Toledo Univ., Ohio.

MASS TRANSPORT PHENOMENA BETWEEN BUBBLES AND DISSOLVED GASES IN LIQUIDS UNDER REDUCED GRAVITY CONDITIONS

K. J. DEWITT and J. L. BROCKWELL (Union Carbide Technical Center) /in NASA, Washington Microgravity Sci. and Appl. Program Tasks p 100-101 May 1985 (Contract NAG3-34)

Avail: NTIS HC A10/MF A01 CSCL 22A

The long term objective of the experiment is to observe the dissolution of isolated, immobile gas bubbles of specified size and composition in a solvent liquid of known concentration in the reduced gravity environment of earth orbit. Preliminary bubble dissolution experiment conducted both in the NASA Lewis 2.2 sec drop tower and in normal gravity using SO₂ - Toluene system were not completely successful in their objective. The method of gas injection and lack of bubble interface stability experienced due to the extreme solubility of SO in Toluene has the effects of changing the problem from that of bubble dissolution to one of bubble formation stability and subsequent dissolution in a liquid of unknown initial solute concentration. Current work involves further experimentation in order to refine the bubble injection system and to investigate the concept of having a bubble with a critical radius in a state of unstable equilibrium. R.J.F.

N86-10113*# Maryland Univ., College Park.

LIGHT SCATTERING TESTS OF FUNDAMENTAL THEORIES OF TRANSPORT PROPERTIES IN THE CRITICAL REGION

R. W. GAMMON and M. R. MOLDOVER (NBS, Washington, D.C.) /in NASA, Washington Microgravity Sci. and Appl. Program Tasks p 106 May 1985 (Contract NAG3-470)

Avail: NTIS HC A10/MF A01 CSCL 22A

The objective of this program is to measure the decay rates of critical density fluctuations in a simple fluid (xenon) very near its liquid-vapor critical point using laser light scattering and photon correlation spectroscopy. Such experiments have been severely limited on Earth by the presence of gravity which causes large density gradients in the sample when the compressibility diverges approaching the critical point. The goal is to measure decay rates deep in the critical region where the scaled wavevector is the order of 1000. This will require loading the sample to 0.01% of the critical density and taking data as close as 3 microKelvin to

12 ASTRONAUTICS (GENERAL)

the critical temperature ($T_c = 289.72$ K). Other technical problems have to be addressed such as multiple scattering and the effect of wetting layers. The ability to avoid multiple scattering by using a thin sample (100 microns) was demonstrated, as well as a temperature history which can avoid wetting layers satisfactory temperature control and measurement, and accurate sample loading. Thus the questions of experimental art are solved leaving the important engineering tasks of mounting the experiment to maintain alignment during flight and automating the state-of-the-art temperature bridges for microcomputer control of the experiment.

R.J.F.

N86-10117*# National Aeronautics and Space Administration. Lewis Research Center, Cleveland, Ohio.

SURFACE TENSION INDUCED INSTABILITIES IN REDUCED GRAVITY: THE BENARD PROBLEM

E. KOSCHMIEDER (Texas Univ., Austin) and A. T. CHAI /in NASA, Washington Microgravity Sci. and Appl. Program Tasks p 110 May 1985

(Contract NAG3-303)

Avail: NTIS HC A10/MF A01 CSCL 22A

A Benard convection experiment has been set up, and the onset of convection in shallow layers of silicone oil two millimeters or less deep has been studied. The onset has been observed visually or has been determined by the break in the heat transfer curve which accompanies the onset of convection. The outcome of these experiments has been very surprising, from the point of view of theoretical expectations. The onset of convection at temperature differences far below the critical value for fluid depths smaller than 2mm was observed. The discrepancy between experiments and theory increases with decreasing fluid depth. According to theoretical considerations, the effects of surface tension become more important as the fluid depth is decreased. Actually, one observes that the onset of convection takes place in two stages. There is first an apparently surface tension driven instability, occurring at subcritical temperature differences according to conventional theory. If then the temperature difference is increased, a second instability occurs which transform the first pattern into conventional strong hexagonal Benard cells. The second instability is in agreement with the critical temperature gradients predicted by Nield.

R.J.F.

N86-10123*# Arizona State Univ., Tempe. Dept. of Mechanical and Aerospace Engineering.

ENERGY STABILITY OF THERMOCAPILLARY CONVECTION IN MODELS OF THE FLOAT ZONE PROCESS Abstract Only

G. P. NEITZEL and D. F. JANKOWSKI /in NASA, Washington Microgravity Sci. and Appl. Program Tasks p 118 May 1985

(Contract NAG3-568)

Avail: NTIS HC A10/MF A01 CSCL 22A

The energy-stability of thermocapillary convection in models of the float-zone, crystal-growing process was studied. Stability limits, as functions of pertinent parameters, that will identify conditions which will not allow the existence of an undesirable oscillatory flow instability were determined. Such instabilities may occur in the space processing of semiconductor materials. The determination of the stability limits will involve two sets of numerical computations: (1) solution of the nonlinear governing equations together with the appropriate boundary conditions to determine the basic state (in general, velocity, pressure and temperature fields and the displacement of free surfaces and interfaces); and (2) solution of a nonlinear Euler-Lagrange systems for the energy-stability limit. Both computations, while difficult, should be within the scope of available computer capability and available concepts in numerical analysis. Finite-element methods are attractive candidates for the numerical work.

G.L.C.

N86-10124*# Case Western Reserve Univ., Cleveland, Ohio. Dept. of Mechanical and Aerospace Engineering.

SURFACE-TENSION DRIVEN CONVECTION

S. OSTRACH and Y. KAMOTANI /in NASA, Washington Microgravity Sci. and Appl. Program Tasks p 119-120 May 1985

(Contract NAG3-570)

Avail: NTIS HC A10/MF A01 CSCL 22A

The present experiments are directed to examine surface-tension gradients. The surface-tension induced convection under reduced gravity it's comparison with normal gravity convection with all other identical conditions are studied. The intensities of such flows and their penetration depth below the free surface are also determined. In this way, the dominant role of a free surface in a reduced-gravity environment is indicated. The interface between two fluid phases can influence the motion of fluids when either the interface has finite curvature or when the interfacial tension varies from point to point. In both cases, forces appear in the interfacial region that can affect or generate fluid motions.

G.L.C.

N86-10125*# National Aeronautics and Space Administration. Lewis Research Center, Cleveland, Ohio.

THERMOCAPILLARY MOTION RESEARCH

T. T. PETERSON and A. T. CHAI /in NASA, Washington Microgravity Sci. and Appl. Program Tasks p 121 May 1985

Avail: NTIS HC A10/MF A01 CSCL 22A

Fundamental microgravity research on interfacial surface tension driven motion by a linear temperature gradient was conducted. A vertical linear temperature gradient will be established within a test container filled with a host fluid. The thermal gradient will be positive in the upward vertical direction to avoid any free convective currents. With minimal disturbance, a single immiscible fluid droplet will be introduced into the host fluid. As predicted by existing theory, the droplet will move in the direction of higher temperature due to tangential shear stresses created by surface tension variations along the periphery of the droplet.

G.L.C.

N86-10128*# Colorado Univ., Boulder. Dept. of Chemical Engineering.

THERMOCAPILLARY AND DIFFUSOCAPILLARY MIGRATION OF A FLUID DROP

R. L. SANI /in NASA, Washington Microgravity Sci. and Appl. Program Tasks p 126 May 1985

(Contract NAG3-493)

Avail: NTIS HC A10/MF A01 CSCL 22A

The migration of bubbles, or drops, plays an important role in many engineering science and space manufacturing problems. In material science processes as in the manufacturing of glasses, etc., gas bubbles can be formed from the by-products of chemical reactions or gas trapped in the interstices of the raw material. In the low-g environment of space, forces other than gravitational must be utilized as a bubble separation technique. It is well-known that gradients in interfacial tension on the bubbles' surface can promote droplet motion in the direction of decreasing interfacial tension and hence provide such a separation mechanism. Thus, the role of thermocapillary and diffusocapillary migration of a bubble, or drop, can be of paramount interest in materials processing in space.

G.L.C.

N86-10129*# Princeton Univ., N. J. Dept. of Chemical Engineering.

TRANSPORT PROCESSES RESEARCH

D. A. SAVILLE and W. B. RUSSEL /in NASA, Washington Microgravity Sci. and Appl. Program Tasks p 127 May 1985

(Contract NAG3-447)

Avail: NTIS HC A10/MF A01 CSCL 22A

Fundamental research in reduced gravity on transport processes occurring during crystallization and/or during solidification processes was studied. The details of the transport processes in various materials processing modes will be systematically studied. A Shuttle experiment will be planned to provide a better understanding of the role of fluid motion on the formation of

morphological patterns and roles of these patterns in solid composition. The approach to the research will involve theoretical modeling of transport processes, non-incursive ground-based laboratory measurements of model systems, and the definition of requirements for space experimentation. Author

N86-10130*# Princeton Univ., N. J. Dept. of Chemical Engineering.

ELECTROHYDRODYNAMICS

D. A. SAVILLE /in NASA, Washington Microgravity Sci. and Appl. Program Tasks p 128 May 1985

(Contract NAG3-259)

Avail: NTIS HC A10/MF A01 CSCL 22A

Models of electrohydrodynamic processes involving liquids with poorly ionized solutes at high (applied) field strengths were developed and tested. Extant theories which account for the details of physico-chemical processes associated with charged interfaces deal mainly with low field strengths and fully ionized solutes. The model used to describe processes at high field strengths--the leaky dielectric--omits consideration of electric double-layers, adsorption at interfaces, and chemical processes involved in the dissociation and recombination of solute species. Thus, even though the model depicts some features associated with bulk fluid motion, it fails to give a comprehensive picture. One example of the shortcomings of both the classical model of electrokinetics at low field strengths and the leaky-dielectric model for high field strengths is found in the field strength dependence of the mobility of small particles in apolar liquids. The research will provide a more general model of electrohydrodynamic phenomena capable of application in diverse circumstances. G.L.C.

N86-10132*# Aerodyne Research, Inc., Billerica, Mass.

EXPERIMENTAL AND THEORETICAL ANALYSIS OF CHEMICAL VAPOR DEPOSITION WITH PREDICTION OF GRAVITY EFFECTS

C. D. STINESPRING and K. E. SPEAR (Pennsylvania State Univ.) /in NASA, Washington Microgravity Sci. and Appl. Program Tasks p 130 May 1985

(Contract NAS3-23934)

Avail: NTIS HC A10/MF A01 CSCL 22A

A combined experimental and theoretical study to characterize the effects of gravitationally-induced transport on atmospheric pressure silicon epitaxy by SiH₄ pyrolysis is planned. Experimentally, flow regimes in which free convective transport contributes to the Chemical Vapor Deposition (CVD) process will be identified, and, for these conditions, the flow and deposition process will be characterized. Specifically, this will include measurements of three dimensional temperature variations using in situ Rayleigh scattering, gas phase composition profiles using laser absorption and fluorescence techniques, and deposition rates and defect densities. Subsequently, the free convective transport contribution to the CVD process will be minimized and/or altered while leaving deposition chemistry unaltered, and the characterization will be repeated. Based on these analyses, the effects of gravitationally-induced transport on atmospheric pressure CVD will be assessed. G.L.C.

N86-10160*# California Univ., San Diego, La Jolla. Energy Center.

PARTICLE CLOUD COMBUSTION EXPERIMENT

A. L. BERLAD /in NASA, Washington Microgravity Sci. and Appl. Program Tasks p 182 May 1985 refs

(Contract NAG3-381)

Avail: NTIS HC A10/MF A01 CSCL 22A

Preparation of flight experiment designs is supported by experimental studies of acoustically induced mixing process, optical transmissivities of particle cloud distributions, wall saturation effects and their control through the use of electrically neutral flame tube materials and surfaces, and the pyrolysis-vaporization kinetics of selected organic particulates. Drop tower tests of stabilized particle cloud flames have allowed valuable comparison of $g = 0$ and $g = 1$ (upwards and downwards) stabilized flame propagation. These stabilized flame data will be valuable assists in dealing with the

freely propagating particle cloud flame data anticipated through Space Shuttle experimentation. Supporting theoretical studies emphasize comprehensive flame propagation and extinction relations among premixed single phase (gaseous) flames and premixed particle cloud flames, for both stabilized and freely propagating flames. Author

N86-10161*# Science Applications, Inc., Chatsworth, Calif. Combustion Science and Advanced Technology Dept.

BUOYANCY EFFECTS UPON VAPOR FLAME AND EXPLOSION PROCESSES

R. B. EDELMAN and P. T. HARSHA /in NASA, Washington Microgravity Sci. and Appl. Program Tasks p 183 May 1985 refs

(Contract NAS3-22822)

Avail: NTIS HC A10/MF A01 CSCL 22A

The objective of this microgravity project is to develop an experimental and theoretical analyses critical to the understanding of the coupling of buoyancy and turbulence generation and its effect on fuel-air mixing, flame intensity and flame propagation in jet diffusion flames. The experiment is designed to examine certain effects of buoyancy acting on a diffusion flame in which the flame is directed either upward or downward. This change from negative to positive g is observed to significantly alter the flame shape although all other operating conditions are the same for both configurations. However, to perform this experiment a significant coaxial secondary air flow is needed in order to prevent flow reversal when the flame is inverted. The theoretical analysis that has been developed handles the secondary air flow and the extreme change in gravity vector direction. Thus the data will provide a measure of credibility of the analysis which will then be used to assist in the design of the actual zero- g experiment. F.M.R.

N86-10162*# California Univ., Berkeley.

A FUNDAMENTAL STUDY OF SMOLDERING WITH EMPHASIS ON EXPERIMENTAL DESIGN FOR ZERO-G

P. J. PAGNI and A. C. FERNANDEZ-PELLO /in NASA, Washington Microgravity Sci. and Appl. Program Tasks p 184 May 1985

(Contract NAG3-443)

Avail: NTIS HC A10/MF A01 CSCL 22A

The objective of this section of the microgravity project is to identify key sets of low-gravity experiments which would critically compliment a larger set of more easily performed normal-gravity experiments to explain the phenomena found in smoldering combustion. It is planned to follow through on the conceptual design of these experiments by participating in the future in the fabrication of the refined apparatus and in the data collection and interpretation. Low-gravity experiments are appropriate for smoldering combustion because of the complexity of smoldering which requires every means possible to discriminate among the many chemical and physical mechanisms active in most smoldering combustion scenarios. Efforts will be primarily analytical, attempting to identify appropriate approximations and dominant dimensionless groups based on existing data and state-of-the-art combustion modelling. Transient stability questions such as ignition, extinction and the choices among charring, tarring, or flaming modes will be included. F.M.R.

N86-10163*# Carnegie-Mellon Univ., Pittsburgh, Pa.

IGNITION AND FLAME SPREAD ABOVE LIQUID FUEL POOLS

W. A. SIRIGNANO /in NASA, Washington Microgravity Sci. and Appl. Program Tasks p 185 May 1985

(Contract NAG3-404)

Avail: NTIS HC A10/MF A01 CSCL 22A

Phenomena of ignition and flame spread above liquid fuel pools are studied and factors that can improve fire safety are determined. Dominant mechanisms for convective heat transfer and impact on ignition and flame spread above liquid fuel pools will be determined from these efforts. The approach is: (1) analytical and computational studies to evaluate scaling factors; (2) experimental design, development, and operation in laboratory at Earth's gravity; (3) experimental design for drop towers at NASA Lewis Research

12 ASTRONAUTICS (GENERAL)

Center; (4) development and operation of drop tower experiments together with NASA Lewis Research personnel and; (5) develop recommendations for Lear Jet and/or Space Shuttle experiments. Through this research, a mathematical model of two-phase systems is formulated and is being coded for the computer. F.M.R.

N86-10164*# Illinois Univ., Urbana.

FLAMMABILITY LIMITS OF GASES UNDER LOW GRAVITY CONDITIONS

R. A. STREHLOW *In* NASA, Washington Microgravity Sci. and Appl. Program Tasks p 186-187 May 1985 refs (Contract NAS3-23770)

Avail: NTIS HC A10/MF A01 CSCL 22A

The purpose of this combustion science investigation is to determine the effect of zero, fractional, and super gravity on the flammability limits of a premixed methane air flame in a standard 51 mm diameter flammability tube and to determine, if possible, the fluid flow associated with flame passage under zero-g conditions and the density (and hence, temperature) profiles associated with the flame under conditions of incipient extinction. This is accomplished by constructing an appropriate apparatus for placement in NASA's Lewis Research Center Lear Jet facility and flying the prescribed g-trajectories while the experiment is being performed. Data is recorded photographically using the visible light of the flame. The data acquired is: (1) the shape and propagation velocity of the flame under various g-conditions for methane compositions that are inside the flammable limits, and (2) the effect of gravity on the limits. Real time accelerometer readings for the three orthogonal directions are displayed in full view of the cameras and the framing rate of the cameras is used to measure velocities. F.M.R.

N86-10165*# Princeton Univ., N. J.

FUNDAMENTAL STUDIES OF DROPLET COMBUSTION AT REDUCED GRAVITY

F. A. WILLIAMS *In* NASA, Washington Microgravity Sci. and Appl. Program Tasks p 188 May 1985 (Contract NAG3-380)

Avail: NTIS HC A10/MF A01 CSCL 22A

Reduced gravity is used to carry out scientific investigations of droplet combustion. In earlier work a preliminary conceptual design had been developed for droplet burning experiments for Spacelab. Refinements of the earlier work with special consideration given to possible experiments for Mid-Deck Modules of the Space Shuttle is discussed. A re-evaluation of suitable experiments on droplet combustion is done to ascertain whether influences of reduced buoyancy on time-dependent processes of heat and mass transfer in the gas or in the liquid on extinction processes or on disruptive burning phenomena are best suited for further investigation. Components of the experimental apparatus, which include a droplet dispensing system, a droplet positioning system, a droplet ignition system and provision for recording, primarily photographically, the combustion of the individual droplet in a chamber having a controlled gas atmosphere, are studied to determine optimal approaches to the experimental design. Methods for data reduction and interpretation are being made more specific, particularly in the context of an objective to calculate overall gas-phase chemical-kinetic parameters for the combustion from observations of extinction conditions in different atmospheres. F.M.R.

N86-10173*# National Aeronautics and Space Administration. Lewis Research Center, Cleveland, Ohio.

MICROGRAVITY MATERIALS SCIENCE LABORATORY

S. J. GRISAFFE *In* NASA, Washington Microgravity Sci. and Appl. Program Tasks p 199 May 1985
Avail: NTIS HC A10/MF A01 CSCL 22A

A Microgravity Materials Science Laboratory (MMSL) has been planned, designed, and is being developed. This laboratory will support related efforts to define the requirements for the Microgravity and Materials Processing Laboratory (MMPF) and the MMPF Test Bed for the Space Station. The MMSL will serve as a check out and training facility for science mission specialists for STS, Spacelab and Space Station prior to the full operation of

the MMPF Test Bed. The focus of the MMSL will be on experiments related to the understanding of metal/ceramic/glass solidification, high perfection crystal growth and fluid physics. This ground-based laboratory will be used by university/industry/government researchers to examine and become familiar with the potential of new microgravity materials science concepts and to conduct longer term studies aimed at fully developing a 1-g understanding of materials and processing phenomena. Such research will help create new high quality concepts for space experiments and will provide the basis for modeling, theories, and hypotheses upon which key space experiments can be defined and developed.

Author

N86-10261*# National Aeronautics and Space Administration. Lewis Research Center, Cleveland, Ohio.

DENDRITIC SOLIDIFICATION IN A BINARY ALLOY MELT: STEADY-STATE VERSUS MORPHOLOGICAL STABILITY THEORIES

V. LAYMANAN *In* ESA Fifth European Symp. on Mater. Sci. under Microgravity. Results of Spacelab 1 p 403-407 Dec. 1984 refs Sponsored in part by NASA

Avail: NTIS HC A21/MF A01

A model for dendritic growth in a binary alloy melt, in the presence of a positive temperature gradient in the liquid, is presented. The model describes satisfactorily the transition from a dendritic interface to a planar interface at very low and very large growth rates. A dendrite tip stability parameter is derived, strictly from steady state considerations, without resorting to a perturbation analysis. The estimates of the parameter agree with those obtained by models based on perturbation analyses.

Author (ESA)

N86-18334*# Wyle Labs., Inc., Huntsville, Ala.

ACCOMMODATION REQUIREMENTS FOR MICROGRAVITY SCIENCE AND APPLICATIONS RESEARCH ON SPACE STATION Interim Report, 24 May - 24 Dec. 1985

M. L. UHRAN, L. R. HOLLAND, and W. O. WEAR Dec. 1985 225 p

(Contract NAS3-24654)

(NASA-CR-175038; NAS 1.26:175038; JN67801) Avail: NTIS HC A10/MF A01 CSCL 22A

Scientific research conducted in the microgravity environment of space represents a unique opportunity to explore and exploit the benefits of materials processing in the virtual absence of gravity induced forces. NASA has initiated the preliminary design of a permanently manned space station that will support technological advances in process science and stimulate the development of new and improved materials having applications across the commercial spectrum. A study is performed to define from the researchers' perspective, the requirements for laboratory equipment to accommodate microgravity experiments on the space station. The accommodation requirements focus on the microgravity science disciplines including combustion science, electronic materials, metals and alloys, fluids and transport phenomena, glasses and ceramics, and polymer science. User requirements have been identified in eleven research classes, each of which contain an envelope of functional requirements for related experiments having similar characteristics, objectives, and equipment needs. Based on these functional requirements seventeen items of experiment apparatus and twenty items of core supporting equipment have been defined which represent currently identified equipment requirements for a pressurized laboratory module at the initial operating capability of the NASA space station.

Author

ASTRODYNAMICS

Includes powered and free-flight trajectories; and orbital and launching dynamics.

N86-11212*# Ohio State Univ., Columbus. ElectroScience Lab.
CALCULATION OF ALLOWABLE ORBITAL SPACINGS FOR THE FIXED-SATELLITE SERVICE

Y. YAMAMURA and C. A. LEVIS Jul. 1985 78 p refs
 (Contract NAG3-159)
 (NASA-CR-176273; NAS 1.26:176273; TR-716548-1) Avail:
 NTIS HC A05/MF A01 CSCL 22A

Minimum satellite separations are calculated which satisfy a given carrier-to-interference protection ratio for the Fixed-Satellite Service (FSS) on a single-entry basis, assuming circular antenna beams. The results are presented in the form of universal contour curves, in which antenna-centered angles are the coordinates, and also in terms of the more conventional longitude and latitude separations. It is shown that orbit capacity increases with decreasing service-area size and that, for practical service areas, capacity is increased if the longitude of a satellite does not differ too greatly from that of the service area it serves. Author

N86-17417*# National Aeronautics and Space Administration.
 Lewis Research Center, Cleveland, Ohio.

RADIATION EXPOSURE AND PERFORMANCE OF MULTIPLE BURN LEO-GEO ORBIT TRANSFER TRAJECTORIES

S. H. GORLAND /in Johns Hopkins Univ. The 1985 JANNAF Propulsion Meeting, Volume 1 p 383-389 Apr. 1985 refs
 Previously announced as N85-21228 Sponsored in part by NASA

Avail: Chemical Propulsion Information Agency, Johns Hopkins Rd., Laurel, Md. 20707 HC \$78.98 CSCL 21H

Many potential strategies exist for the transfer of spacecraft from low Earth orbit (LEO) to geosynchronous (GEO) orbit. One strategy has generally been utilized, that being a single impulsive burn at perigee and a GEO insertion burn at apogee. Multiple burn strategies were discussed for orbit transfer vehicles (OTVs) but the transfer times and radiation exposure, particularly for potentially manned missions, were used as arguments against those options. Quantitative results concerning the trip time and radiation encountered by multiple burn orbit transfer missions in order to establish the feasibility of manned missions, the vulnerability of electronics, and the shielding requirements are presented. The performance of these multiple burn missions is quantified in terms of the payload and propellant variances from the minimum energy mission transfer. The missions analyzed varied from one to eight perigee burns and ranged from a high thrust, 1 g, acceleration, cryogenic hydrogen-oxygen chemical propulsion system for a continuous burn, 0.001 g acceleration, hydrogen, fueled resistojet propulsion system with a trip time of 60 days. Author

GROUND SUPPORT SYSTEMS AND FACILITIES (SPACE)

Includes launch complexes, research and production facilities; ground support equipment, e.g., mobile transporters; and simulators.

N86-18338*# National Aeronautics and Space Administration.
 Lewis Research Center, Cleveland, Ohio.

15 LAUNCH VEHICLES AND SPACE VEHICLES

DEVELOPMENT AND APPLICATION OF DYNAMIC SIMULATIONS OF A SUBSONIC WIND TUNNEL

J. R. SZUCH, G. L. COLE, R. C. SEIDEL, and D. J. ARPASI 1986 16 p refs Prepared for presentation at the 14th Aerodynamic Testing Conference, West Palm Beach, Fla., 5-7 Mar. 1986; sponsored by AIAA
 (NASA-TM-87211; E-2870; NAS 1.15:87211) Avail: NTIS HC A02/MF A01 CSCL 14B

Efforts are currently underway at NASA Lewis to improve and expand ground test facilities and to develop supporting technologies to meet anticipated aeropropulsion research needs. Many of these efforts have been focused on a proposed rehabilitation of the Altitude Wind Tunnel (AWT). In order to insure a technically sound design, an AWT modeling program (both analytical and physical) was initiated to provide input to the AWT final design process. This paper describes the approach taken to develop analytical, dynamic computer simulations of the AWT, and the use of these simulations as test-beds for: (1) predicting the dynamic response characteristics of the AWT, and (2) evaluating proposed AWT control concepts. Plans for developing a portable, real-time simulator for the AWT facility are also described. Author

LAUNCH VEHICLES AND SPACE VEHICLES

Includes boosters; operating problems of launch/space vehicle systems; and reusable vehicles.

A86-38943*# Jet Propulsion Lab., California Inst. of Tech., Pasadena.

MODAL TEST/ANALYSIS CORRELATION FOR CENTAUR G PRIME LAUNCH VEHICLE

J. CHEN, T. ROSE, M. TRUBERT, B. WADA (California Institute of Technology, Jet Propulsion Laboratory, Pasadena), and F. SHAKER (NASA, Lewis Research Center, Cleveland, OH) IN: Structures, Structural Dynamics and Materials Conference, 27th, San Antonio, TX, May 19-21, 1986, Technical Papers. Part 2. New York, American Institute of Aeronautics and Astronautics, 1986, p. 621-633. refs

(Contract NAS7-918)

(AIAA PAPER 86-1002)

A modal test was performed on the Centaur G Prime launch vehicle for the purpose of verifying the loads analysis model. This paper describes the procedure by which modal parameters obtained in this test were correlated with the corresponding analytical predictions. Based on this correlation the stiffness model of the shuttle trunnion system has been modified. The evolution of the model updating and the final results are described. Author

N86-23616*# National Aeronautics and Space Administration.
 Lewis Research Center, Cleveland, Ohio.

SSME FUELSIDE PREBURNER TWO-DIMENSIONAL ANALYSIS

T. J. VANOVERBEKE and R. W. CLAUS 1986 19 p refs
 Prepared for presentation at the Central States Meeting of the Combustion Inst., Cleveland, Ohio, 5-6 May 1986

(NASA-TM-87299; E-3010; NAS 1.15:87299) Avail: NTIS HC A02/MF A01 CSCL 20H

The flow field within the fuelside preburner of the Space Shuttle

15 LAUNCH VEHICLES AND SPACE VEHICLES

Main Engine is calculated using a reacting flow code (REACT2D). Inlet and modeling parameters involved in the numerical calculation are systematically varied to establish the sensitivity of the calculated exit temperature profile. It is found that differences in the inlet equivalence ratio have a large effect on the turbine inlet temperature profile. A variety of preburner inlet modeling changes such as inlet turbulence level, modeling the gases as burned, unburned, premixed, or unmixed, are shown to have a smaller effect on the calculated turbine inlet temperature profile. Also, the form of finite differencing used is shown to have an effect on the temperature profile. Author

N86-24722*# National Aeronautics and Space Administration. Lewis Research Center, Cleveland, Ohio.

PASSIVE EDDY-CURRENT DAMPING AS A MEANS OF VIBRATION CONTROL IN CRYOGENIC TURBOMACHINERY

R. E. CUNNINGHAM Feb. 1986 14 p refs
(NASA-TP-2562; E-2762; NAS 1.60:2562) Avail: NTIS HC A02/MF A01 CSCL 13I

Lateral shaft vibrations produced by a rotating unbalance weight were damped by means of eddy currents generated in copper conductors that were precessing cyclicly in the gap formed by the pole faces of C-shaped, permanent magnets. The damper assembly, which was located at the lower bearing support of a vertically oriented rotor was completely immersed in liquid nitrogen during the test run. The test rotor was operated over a speed range from 800 to 10,000 rpm. Three magnet/conductor designs were evaluated. Experimental damping coefficients varied from 180 to 530 N sec/m. Reasonable agreement was noted for theoretical values of damping for these same assemblies. Values of damping coefficients varied from 150 to 780 N sec/m. The results demonstrate that passive eddy-current damping is a viable candidate for vibration control in cryogenic turbomachinery.

Author

N86-31621*# National Aeronautics and Space Administration. Lewis Research Center, Cleveland, Ohio.

CENTAUR ENGINE GIMBAL FRICTION CHARACTERISTICS UNDER SIMULATED THRUST LOAD

J. W. ASKEW Sep. 1986 21 p
(NASA-TM-87335; E-3080; NAS 1.15:87335) Avail: NTIS HC A02/MF A01 CSCL 20H

An investigation was performed to determine the friction characteristics of the engine gimbal system of the Centaur upper stage rocket. Because the Centaur requires low-gain autopilots in order to meet all stability requirements for some configurations, control performance (response to transients and limit-cycle amplitudes) depends highly on these friction characteristics. Forces required to rotate the Centaur engine gimbal system were measured under a simulated thrust load of 66,723 N (15,000 lb) and in an altitude/thermal environment. A series of tests was performed at three test conditions; ambient temperature and pressure, ambient temperature and vacuum, and cryogenic temperature and vacuum. Gimbal rotation was controlled, and tests were performed in which rotation amplitude and frequency were varied by using triangular and sinusoidal waveforms. Test data revealed an elastic characteristic of the gimbal, independent of the input signal, which was evident prior to true gimbal sliding. The torque required to initiate gimbal sliding was found to decrease when both pressure and temperature decreased. Results from the low amplitude and low frequency data are currently being used in mathematically modeling the gimbal friction characteristics for Centaur autopilot performance studies. M.G.

16

SPACE TRANSPORTATION

Includes passenger and cargo space transportation, e.g., shuttle operations; and space rescue techniques.

A86-32906*# National Aeronautics and Space Administration. Lewis Research Center, Cleveland, Ohio.

NASA LEWIS RESEARCH CENTER LOW-GRAVITY FLUID MANAGEMENT TECHNOLOGY PROGRAM

J. C. AYDELOTT, M. J. CARNEY (NASA, Lewis Research Center, Cleveland, OH), and J. I. HOCHSTEIN (Washington, University, St. Louis, MO) IN: Man's permanent presence in space; Proceedings of the Third Annual Aerospace Technology Symposium, New Orleans, LA, November 7, 8, 1985. New Orleans, LA, American Institute of Aeronautics and Astronautics, 1985, 56 p. Previously announced in STAR as N86-11218. refs

A history of the Lewis Research Center in space fluid management technology program is presented. Current programs which include numerical modeling of fluid systems, heat exchanger/radiator concept studies, and the design of the Cryogenic Fluid Management Facility are discussed. Recent analytical and experimental activities performed to support the Shuttle/Centaur development activity are highlighted. Author

N86-11218*# National Aeronautics and Space Administration. Lewis Research Center, Cleveland, Ohio.

NASA LEWIS RESEARCH CENTER LOW-GRAVITY FLUID MANAGEMENT TECHNOLOGY PROGRAM

J. C. AYDELOTT, M. J. CARNEY, and J. I. HOCHSTEIN (Washington Univ., St. Louis) Nov. 1985 56 p refs Presented at the JANNAF Safety and Environ. Protection Subcomm. Meeting, Monterey, Calif., 4-7 Nov. 1985 and at the AIAA/GNOS 3rd Ann. Aerospace Technol. Symp., New Orleans, 7-8 Nov. 1985 (NASA-TM-87145; E-2774; NAS 1.15:87145; AIAA/GNOS-85-002) Avail: NTIS HC A04/MF A01 CSCL 22B

A history of the Lewis Research Center in space fluid management technology program is presented. Current programs which include numerical modeling of fluid systems, heat exchanger/radiator concept studies, and the design of the Cryogenic Fluid Management Facility are discussed. Recent analytical and experimental activities performed to support the Shuttle/Centaur development activity are highlighted. Author

17

SPACE COMM., SPACECRAFT COMM., COMMAND & TRACKING

Includes telemetry; space communications networks; astronavigation and guidance; and radio blackout.

A86-29580*# National Aeronautics and Space Administration. Lewis Research Center, Cleveland, Ohio.

APPLICATION OF INTERSATELLITE LINKS TO DOMESTIC SATELLITE SYSTEMS

D. S. PONCHAK and R. L. SPENCE (NASA, Lewis Research Center, Cleveland, OH) IN: Communication Satellite Systems Conference, 11th, San Diego, CA, March 17-20, 1986, Technical Papers. New York, American Institute of Aeronautics and Astronautics, 1986, p. 29-38. Previously announced in STAR as N86-16249. refs
(AIAA PAPER 86-0604)

The results of a study on intersatellite link (ISL) applications for domestic satellite communications are presented. It was determined if any technical, economic, or performance benefits could be gained by introducing intersatellite links into a domestic

satellite communication network. Several key systems issues of domestic ISL's are addressed. These include the effect of a skewed traffic distribution on the selection of ISL satellite orbit locations, tolerable satellite spacing, and crosslink traffic-handling requirements. An ISL technology assessment is made by performing a parametric link analysis for several microwave and optical implementations. The impact of the crosslink on the end-to-end link performance is investigated for both regenerative and nonregenerative ISL architectures. A comparison is made between single satellite systems operating at C-, and Ku-bands and the corresponding ISL systems in terms of ground segment cost, space segment cost, and net link performance. Results indicate that ISL's can effectively expand the CONUS orbital arc, with a 60 GHz ISL implementation being the most attractive. Author

A86-29599* Ohio State Univ., Columbus.

THE ROLE OF SERVICE AREAS IN THE OPTIMIZATION OF FSS ORBITAL AND FREQUENCY ASSIGNMENTS

C. A. LEVIS, C.-W. WANG, Y. YAMAMURA, C. H. REILLY (Ohio State University, Columbus), and D. J. GONSALVEZ IN: Communication Satellite Systems Conference, 11th, San Diego, CA, March 17-20, 1986, Technical Papers. New York, American Institute of Aeronautics and Astronautics, 1986, p. 190-198. refs (Contract NAG3-159) (AIAA PAPER 86-0636)

An implicit relationship is derived which relates the topocentric separation of two satellites required for a given level of single-entry protection to the separation and orientation of their service areas. The results are presented explicitly for circular beams and topocentric angles. A computational approach is given for elliptical beams and for use with longitude and latitude variables. It is found that the geocentric separation depends primarily on the service area separation, secondarily on a parameter which characterizes the electrical design, and only slightly on the mean orbital position of the satellites. Both linear programming and mixed integer programming algorithms are implemented. Possible objective function choices are discussed, and explicit formulations are presented for the choice of the sum of the absolute deviations of the orbital locations from some prescribed 'ideal' location set. A test problem involving six service areas is examined with results that are encouraging with respect to applying the linear programming procedure to larger scenarios. C.D.

A86-29616* National Aeronautics and Space Administration. Lewis Research Center, Cleveland, Ohio.

TESTING OF 30-GHZ LOW NOISE RECEIVERS

M. J. CONROY (NASA, Lewis Research Center, Cleveland, OH) and R. J. KERCZEWSKI (NASA, Lewis Research Center; Analex Corp., Cleveland, OH) IN: Communication Satellite Systems Conference, 11th, San Diego, CA, March 17-20, 1986, Technical Papers. New York, American Institute of Aeronautics and Astronautics, 1986, p. 326-340. Previously announced in STAR as N86-13627. refs (AIAA PAPER 86-0654)

NASA-sponsored studies of the growth in communications traffic have indicated that the frequency spectrum allocated to fix-service satellites at the C and Ku bands will reach saturation by the early 1990's. The next higher frequency bands allocated for communications satellites are 27.5 to 30 GHz for the uplink and 17.7 to 20.2 GHz for the downlink. Current plans for developing satellite systems that use these bands include a NASA demonstration satellite (ACTS). One of the components identified as critical to the success of that mission is a 27.5 to 30 GHz satellite receiver. In response to that identification, NASA has sponsored the development of such a receiver to the proof-of-concept (POC) level. Design and fabrication of such POC model receivers was carried out under parallel contracts awarded to LNR Communications, Inc. of Hauppauge, New York and to ITT Defense Communications Division of Nutley, New Jersey. The most significant of the performance goals were a 5 dB maximum noise figure, a 2.5 GHz passband, and 20 dB RF to IF gain. Following delivery of hardware from each of the contractors, an in-house test program was undertaken at NASA's Lewis Research

Center in order to verify the contractor-reported performance and to provide a comparison of the two receivers under identical test conditions. The present paper reports the results of those tests.

Author

A86-29628* National Aeronautics and Space Administration. Lewis Research Center, Cleveland, Ohio.

MMIC ANTENNA TECHNOLOGY DEVELOPMENT IN THE 30/20 GIGAHERTZ BAND

J. SMETANA, T. J. KASCAK, and R. E. ALEXOVICH (NASA, Lewis Research Center, Cleveland, OH) IN: Communication Satellite Systems Conference, 11th, San Diego, CA, March 17-20, 1986, Technical Papers. New York, American Institute of Aeronautics and Astronautics, 1986, p. 430-443. Previously announced in STAR as N86-17368. refs (AIAA PAPER 86-0666)

This paper presents a progress summary of NASA's efforts in developing 20 and 30 GHz GaAs MMIC devices and an advanced satellite communications antenna system using these devices. In the interest of preserving resources such as frequency spectrum and orbital space the antenna system is being developed with multiple fixed spot beams and multiple scanning spot beams. NASA set high goals for the MMIC development to push GaAs technology. These goals and the main features of the MMIC devices are discussed. Some packaging and characterization considerations are also discussed. The 20 GHz transmit antenna and 30 GHz receive antenna are being developed separately. The approach selected is to perform contractual configuration studies, purchase a 20-GHz experimental antenna system (EAS) and perform in-house evaluation. The features and key specifications of the EAS are discussed. Additional supporting technologies such as effects of coupling on modest sized arrays, MMIC matching techniques, in-house analytical capability, wideband and dual frequency microstrip patch array development, and MMIC packaging techniques are described. Some plans for future work are also discussed. Author

A86-29659* Motorola, Inc., Scottsdale, Ariz.

ON THE EFFECTIVENESS OF ONBOARD PROCESSING

L. L. MOY, D. R. CARROLL (Motorola, Inc., Government Electronics Group, Scottsdale, AZ), and R. J. JIRBERG (NASA, Lewis Research Center, Cleveland, OH) IN: Communication Satellite Systems Conference, 11th, San Diego, CA, March 17-20, 1986, Technical Papers. New York, American Institute of Aeronautics and Astronautics, 1986, p. 672-675. NASA-supported research. refs (AIAA PAPER 86-0721)

The effectiveness of onboard processing in communications satellites is discussed, and the interrelationships between the various elements of onboard processing are described. An overview is given of NASA's Advanced Communications Technology Satellite (ACTS), emphasizing its baseboard processor. The onboard processing features of ACTS are described, including frequency reuse, signal regeneration, TDMA/FDMA demand assigned multiple access, forward error correction, routing, and dynamic reconfiguration. The terminals of the ACTS ground segment are described, and comparisons are made between satellite onboard processing and other technologies. C.D.

A86-34591* Ohio State Univ., Columbus.

ADAPTIVE ANTENNA ARRAYS FOR WEAK INTERFERING SIGNALS

I. J. GUPTA and A. A. KSIENSKI (Ohio State University, Columbus) IEEE Transactions on Antennas and Propagation (ISSN 0018-926X), vol. AP-34, March 1986, p. 420-426. refs (Contract NAG3-536)

It is shown that conventional adaptive arrays are unable to suppress weak interfering signals. To overcome this problem, the feedback loops controlling the array weights were modified, reducing the noise level by reducing the correlation between the noise components of the two inputs to the loop correlator. Various techniques to decorrelate these noise components are discussed. An expression is derived for the amount of noise decorrelation required to achieve a specified interference suppression. The

results are of interest in connection with satellite communications.
Author

A86-35318* Motorola, Inc., Scottsdale, Ariz.

HARD ACTS TO FOLLOW

L. MOY (Motorola, Inc., Government Electronics Group, Scottsdale, AZ) Space (ISSN 0267-954X), vol. 2, Mar.-May 1986, p. 4-6, 8, 10, 12.

(Contract NAS3-23790)

The Advanced Communications Technology Satellite (ACTS), the third phase of NASA's 30/20 GHz satellite communications program, is praised for its frugal usage of both the geosynchronous orbital arch and the frequency spectrum resources necessary for communications satellites. Its objective is to verify Ka-band satellite communications concepts and to develop a flight and ground system for validation of the multibeam communications proof-of-concept technologies. The ACTS ground segment (comprised of four types of terminals) is designed to compliment the spacecraft for the SS launch in 1989. Precise coordination between the ground and spacecraft segments is performed by the baseband processor (BBP), which is an in-orbit switchboard, and the tracking error word, which enables the ground terminals to remain synchronized with onboard timing. Fixed spot beams and scan beams, comprising the two types of spot beams used, both operate at the same frequency and hence, conserve frequency resources. In addition, the time division multiple access serves to enhance system efficiency. It is concluded that Ka-band satellites are a practical approach to the better usage of those resources potentially threatened by communications satellites. Comprehensive graphs and block diagrams of the system are included. K.K.

N86-16249* National Aeronautics and Space Administration. Lewis Research Center, Cleveland, Ohio.

APPLICATION OF INTERSATELLITE LINKS TO DOMESTIC SATELLITE SYSTEMS

D. S. PONCHAK and R. L. SPENCE 1986 17 p refs Proposed for presentation at the 11th Communications Satellite Systems Conference, San Diego, Calif., 16-20 Mar. 1986; sponsored by AIAA

(NASA-TM-87215; E-2829; NAS 1.15:87215) Avail: NTIS HC A02/MF A01 CSCL 09F

The results of a study on intersatellite link (ISL) applications for domestic satellite communications are presented. It was determined if any technical, economic, or performance benefits could be gained by introducing intersatellite links into a domestic satellite communication network. Several key systems issues of domestic ISL's are addressed. These include the effect of a skewed traffic distribution on the selection of ISL satellite orbit locations, tolerable satellite spacing, and crosslink traffic-handling requirements. An ISL technology assessment is made by performing a parametric link analysis for several microwave and optical implementations. The impact of the crosslink on the end-to-end link performance is investigated for both regenerative and nonregenerative ISL architectures. A comparison is made between single satellite systems operating at C-, and Ku-bands and the corresponding ISL systems in terms of ground segment cost, space segment cost, and net link performance. Results indicate that ISL's can effectively expand the CONUS orbital arc, with a 60 GHz ISL implementation being the most attractive. Author

N86-17368* National Aeronautics and Space Administration. Lewis Research Center, Cleveland, Ohio.

MMIC ANTENNA TECHNOLOGY DEVELOPMENT IN THE 30/20 GIGAHERTZ BAND

J. SMETANA, T. J. KASCAK, and R. E. ALEXOVICH 1986 22 p refs Proposed for presentation at 11th Annual Communications Satellite Systems Conference, San Diego, Calif., 16-20 Mar. 1986; sponsored by AIAA

(NASA-TM-87192; E-2848; NAS 1.15:87192) Avail: NTIS HC A02/MF A01 CSCL 09F

This paper presents a progress summary of NASA's efforts in developing 20 and 30 GHz GaAs MMIC devices and an advanced

satellite communications antenna system using these devices. In the interest of preserving resources such as frequency spectrum and orbital space the antenna system is being developed with multiple fixed spot beams and multiple scanning spot beams. NASA set high goals for the MMIC development to push GaAs technology. These goals and the main features of the MMIC devices are discussed. Some packaging and characterization considerations are also discussed. The 20 GHz transmit antenna and 30 GHz receive antenna are being developed separately. The approach selected is to perform contractual configuration studies, purchase a 20-GHz experimental antenna system (EAS) and perform in-house evaluation. The features and key specifications of the EAS are discussed. Additional supporting technologies such as effects of coupling on modest sized arrays, MMIC matching techniques, in-house analytical capability, wideband and dual frequency microstrip patch array development, and MMIC packaging techniques are described. Some plans for future are also discussed. Author

N86-18341*# Ohio State Univ., Columbus. ElectroScience Lab. THE ROLE OF SERVICE AREAS IN THE OPTIMIZATION OF FSS ORBITAL AND FREQUENCY ASSIGNMENTS

C. A. LEVIS, C. W. WANG, Y. YAMAMURA, C. H. REILLY, and D. J. GONSALVEZ Dec. 1985 31 p refs

(Contract NAG3-159)

(NASA-CR-176488; NAS 1.26:176488; TR-716548-3) Avail: NTIS HC A03/MF A01 CSCL 17B

A relationship is derived, on a single-entry interference basis, for the minimum allowable spacing between two satellites as a function of electrical parameters and service-area geometries. For circular beams, universal curves relate the topocentric satellite spacing angle to the service-area separation angle measured at the satellite. The corresponding geocentric spacing depends only weakly on the mean longitude of the two satellites, and this is true also for elliptical antenna beams. As a consequence, if frequency channels are preassigned, the orbital assignment synthesis of a satellite system can be formulated as a mixed-integer programming (MIP) problem or approximated by a linear programming (LP) problem, with the interference protection requirements enforced by constraints while some linear function is optimized. Possible objective-function choices are discussed and explicit formulations are presented for the choice of the sum of the absolute deviations of the orbital locations from some prescribed ideal location set. A test problem is posed consisting of six service areas, each served by one satellite, all using elliptical antenna beams and the same frequency channels. Numerical results are given for the three ideal location prescriptions for both the MIP and LP formulations. The resulting scenarios also satisfy reasonable aggregate interference protection requirements. Author

N86-18343* National Aeronautics and Space Administration. Lewis Research Center, Cleveland, Ohio.

BIT ERROR RATE TESTING OF A PROOF-OF-CONCEPT MODEL BASEBAND PROCESSOR

J. B. STOVER and G. FUJIKAWA Jan. 1986 41 p refs

(NASA-TM-87206; E-2861; NAS 1.15:87206) Avail: NTIS HC A03/MF A01 CSCL 09F

Bit-error-rate tests were performed on a proof-of-concept baseband processor. The BBP, which operates at an intermediate frequency in the C-Band, demodulates, demultiplexes, routes, remultiplexes, and remodulates digital message segments received from one ground station for retransmission to another. Test methods are discussed and test results are compared with the Contractor's test results. Author

N86-31625*# National Aeronautics and Space Administration. Lewis Research Center, Cleveland, Ohio.

ACTS EXPERIMENTS PROGRAM

R. J. SCHERTLER 1986 12 p. Proposed for presentation at Globecom '86, Houston, Tex., 1-4 Dec. 1986; sponsored by the Institute of Electrical and Electronics Engineers (NASA-TM-88820; E-3182; NAS 1.15:88820) Avail: NTIS HC A02/MF A01 CSCL 17B

An overview of the ACTS Experiments Program is presented. ACTS is being developed and will flight test the advanced technologies associated with: a Ka-band multibeam antenna, onboard signal processing and switching as well as laser communications. A nominal 3 yr experiments program is planned. Through the experiments program, the capabilities of the ACTS system will be made available to U.S. industry, university and government experimenters to test, prove the feasibility and evaluate the key ACTS system technologies. Communication modes of operation using the baseband processor and microwave switch matrix are presented, along with the antenna coverage pattern. Potential experiment categories are also presented and briefly discussed. An overall schedule of activities associated with the experiments program is outlined. Results of the ACTS Experiments Program will provide information vital to successful industry implementation of ACTS technology in a future operational system. Author

18

SPACECRAFT DESIGN, TESTING AND PERFORMANCE

Includes satellites; space platforms; space stations; spacecraft systems and components such as thermal and environmental controls; and attitude controls.

A86-35338* National Aeronautics and Space Administration. Lewis Research Center, Cleveland, Ohio.

LINEARIZATION OF DIGITAL DERIVED RATE ALGORITHM FOR USE IN LINEAR STABILITY ANALYSIS

R. E. GRAHAM and T. W. PORADA (NASA, Lewis Research Center, Cleveland, OH) IN: 1985 American Control Conference, 4th, Boston, MA, June 19-21, 1985, Proceedings. Volume 1. New York, Institute of Electrical and Electronics Engineers, 1985, p. 139-143. Previously announced in STAR as N85-23904. refs

The digital derived rate (DDR) algorithm is used to calculate the rate of rotation of the Centaur upper-stage rocket. The DDR is highly nonlinear algorithm, and classical linear stability analysis of the spacecraft cannot be performed without linearization. The performance of this rate algorithm is characterized by a gain and phase curve that drop off at the same frequency. This characteristic is desirable for many applications. A linearization technique for the DDR algorithm is investigated. The linearization method is described. Examples of the results of the linearization technique are illustrated, and the effects of linearization are described. A linear digital filter may be used as a substitute for performing classical linear stability analyses, while the DDR itself may be used in time response analysis. Author

A86-38883*# Martin Marietta Aerospace, Denver, Colo.

HYBRID DEPLOYABLE/ERECTABLE SOLAR DYNAMIC BOX TRUSS SYSTEM

J. V. COYNER, JR. (Martin Marietta Corp., Denver, CO) and T. B. IRVINE (NASA, Lewis Research Center, Cleveland, OH) IN: Structures, Structural Dynamics and Materials Conference, 27th, San Antonio, TX, May 19-21, 1986, Technical Papers. Part 1. New York, American Institute of Aeronautics and Astronautics, 1986, p. 764-768.

(AIAA PAPER 86-0955)

The design of a hybrid deployable/erectable solar dynamic box truss power generation system for the initial operation capability

(IOC) of the Space Shuttle is examined. An organic Rankine cycle heat engine for IOC solar power generation is studied. The design configuration is a simple parabolic concentration where the receiver is located in the focal plane with its aperture at the focal point. The relationship between concentrator size and collection efficiency is analyzed. The geometry of the deployable graphite/epoxy box truss ring and the reflective panels of the system are described. Mass properties and dynamic analyses are performed to evaluate the center of gravity location and moments of inertia characteristics of the energy conversion subsystem (ECS). The deployable/erectable truss is applicable for large IR space telescopes and center and offset fed ECSs. I.F.

A86-39907*# Grumman Aerospace Corp., Bethpage, N.Y.

HEAT PIPE RADIATOR TECHNOLOGY FOR SPACE POWER SYSTEMS

A. W. CARLSON, E. GUSTAFSON (Grumman Aerospace Corp., Space Systems Div., Bethpage, NY), and B. A. ERCEGOVIC (NASA, Lewis Research Center, Cleveland, OH) AIAA and ASME, Joint Thermophysics and Heat Transfer Conference, 4th, Boston, MA, June 2-4, 1986. 11 p. refs

(Contract NAS3-24665)

(AIAA PAPER 86-1300)

High-reliability high-performance deployable monogroove and dual-slot heat pipe radiator systems to meet the requirements for electric power in future space missions, such as the 300-kW(e) electric power demand projected for NASA's Space Station, are discussed. Analytical model trade studies of various configurations show the advantages of the dual-slot heat pipe radiator for high temperature applications as well as its weight reduction potential over the 50-350 F temperature range. The ammonia-aluminum monogroove heat pipe, limited to below-180 F operating temperatures, is under development, and can employ methanol-stainless steel heat pipes to achieve operating temperatures in excess of 300 F. Dual-slot heat pipe configuration proof-of-concept testing was begun in 1985. R.R.

A86-42619*# Boeing Aerospace Co., Huntsville, Ala.

SPACE STATION BENEFITS FROM ECLS - PROPULSION SYSTEM SYNERGISM

S. M. BRENNAN (Boeing Aerospace Co., Huntsville, AL) and R. M. DONOVAN (NASA, Lewis Research Center, Cleveland, OH) AIAA, ASME, SAE, and ASEE, Joint Propulsion Conference, 22nd, Huntsville, AL, June 16-18, 1986. 14 p. refs

(Contract NAS3-23353)

(AIAA PAPER 86-1407)

Benefits of integrating the Space Station Environmental Control and Life Support (ECLS) system with the propulsion system are addressed in this paper for various levels of ECLS closure. Effluents generated by the ECLS system are used to augment or even supplement the propulsion system. Potential benefits include reductions in logistic weights and volumes, fixed weights and volumes, power requirements, and in total station systems cost. Author

A86-49553*# National Aeronautics and Space Administration. Lewis Research Center, Cleveland, Ohio.

FLUID MANAGEMENT AND ITS ROLE IN THE FUTURE OF SPACE STATION

J. SALZMAN, R. VERNON, M. HILL, and T. PETERSON (NASA, Lewis Research Center, Cleveland, OH) AIAA, Space Station in the Twenty-first Century, Meeting, Reno, NV, Sept. 3-5, 1986. 14 p. refs

(AIAA PAPER 86-2301)

Technological challenges and suggested plans for meeting them pertaining to fluid management in the Space Station are discussed. A short overview is given of the major Space Station systems and operations which employ or rely on fluid management, followed by a description of the general system issues and challenges encountered in managing fluids in space. Examples of some current and near term activities directed toward providing the understanding and technologies necessary to overcome relevant problems are presented. Finally, suggested plans for similar but longer range

18 SPACECRAFT DESIGN, TESTING AND PERFORMANCE

research and development activities are offered. These plans emphasize the requirements and benefits of expanded in-space experiments, with the ultimate aim of using the Space Station as a facility for fluid management research and technology development efforts. C.D.

A86-49621*# National Aeronautics and Space Administration. Lewis Research Center, Cleveland, Ohio.

LIQUID DROPLET RADIATOR PROGRAM AT THE NASA LEWIS RESEARCH CENTER

A. F. PRESLER, C. E. COLES, P. S. DIEM-KIRSOP, and K. A. WHITE, III (NASA, Lewis Research Center, Cleveland, OH) AIAA and ASME, Joint Thermophysics and Heat Transfer Conference, 4th, Boston, MA, June 2-4, 1986. 9 p. Previously announced in STAR as N86-12246. refs (ASME PAPER 86-HT-15)

The NASA Lewis Research Center and the Air Force Rocket Propulsion Laboratory (AFRPL) are jointly engaged in a program for technical assessment of the Liquid Droplet Radiator (LDR) concept as an advanced high performance heat ejection component for future space missions. NASA Lewis has responsibility for the technology needed for the droplet generator, for working fluid qualification, and for investigating the physics of droplets in space; NASA Lewis is also conducting systems/mission analyses for potential LDR applications with candidate space power systems. For the droplet generator technology task, both micro-orifice fabrication techniques and droplet stream formation processes have been experimentally investigated. High quality micro-orifices (to 50 micron diameter) are routinely fabricated with automated equipment. Droplet formation studies have established operating boundaries for the generation of controlled and uniform droplet streams. A test rig is currently being installed for the experimental verification, under simulated space conditions, of droplet radiation heat transfer performance analyses and the determination of the effect radiative emissivity of multiple droplet streams. Initial testing has begun in the NASA Lewis Zero-Gravity Facility for investigating droplet stream behavior in microgravity conditions. This includes the effect of orifice wetting on jet dynamics and droplet formation. Results for both Brayton and Stirling power cycles have identified favorable mass and size comparisons of the LDR with conventional radiator concepts. B.W.

N86-12246*# National Aeronautics and Space Administration. Lewis Research Center, Cleveland, Ohio.

LIQUID DROPLET RADIATOR PROGRAM AT THE NASA LEWIS RESEARCH CENTER

A. F. PRESLER, C. E. COLES, P. S. DIEM-KIRSOP, and K. A. WHITE, III 1985 23 p refs Prepared for presentation at the 4th Thermophys. and Heat Transfer Conf., Boston, 2-4 Jun. 1986; sponsored by AIAA and ASME (NASA-TM-87139; E-2745; NAS 1.15:87139) Avail: NTIS HC A02/MF A01 CSCL 20D

The NASA Lewis Research Center and the Air Force Rocket Propulsion Laboratory (AFRPL) are jointly engaged in a program for technical assessment of the Liquid Droplet Radiator (LDR) concept as an advanced high performance heat ejection component for future space missions. NASA Lewis has responsibility for the technology needed for the droplet generator, for working fluid qualification, and for investigating the physics of droplets in space; NASA Lewis is also conducting systems/mission analyses for potential LDR applications with candidate space power systems. For the droplet generator technology task, both micro-orifice fabrication techniques and droplet stream formation processes have been experimentally investigated. High quality micro-orifices (to 50 micron diameter) are routinely fabricated with automated equipment. Droplet formation studies have established operating boundaries for the generation of controlled and uniform droplet streams. A test rig is currently being installed for the experimental verification, under simulated space conditions, of droplet radiation heat transfer performance analyses and the determination of the effect radiative emissivity of multiple droplet streams. Initial testing has begun in the NASA Lewis Zero-Gravity Facility for investigating droplet stream behavior in microgravity

conditions. This includes the effect of orifice wetting on jet dynamics and droplet formation. Results for both Brayton and Stirling power cycles have identified favorable mass and size comparisons of the LDR with conventional radiator concepts. B.W.

N86-17418*# Martin Marietta Aerospace, Denver, Colo.

DESIGN OPTIMIZATION FOR A SPACE BASED, REUSABLE ORBIT TRANSFER VEHICLE

L. REDD /in Johns Hopkins Univ. The 1985 JANNAF Propulsion Meeting, Volume 1 p 391-401 Apr. 1985 (Contract NAS3-23858)

Avail: Chemical Propulsion Information Agency, Johns Hopkins Rd., Laurel, Md. 20707 HC \$78.98 CSCL 22B

Future NASA and DOD missions will benefit from high performance, reusable orbit transfer vehicles. With the advent of a space station, advanced engine technology, and various new vehicle concepts, reusable orbit transfer vehicles that provide significant economic benefits and mission capability improvements will be realized. Engine and vehicle design criteria previously have lacked definition with regard to issues such as space basing and servicing, man-rating and reliability, performance, mission flexibility, and life cycle cost for a reusable vehicle. The design study described here has resulted in the definition of a reusable orbit transfer vehicle concept and subsequent recommendations for the design criteria of an advanced LO2/LH2 engine. These design criteria include number of engines per vehicle, nozzle design, etc. The major characteristics of the vehicle preliminary design include low lift to drag aerocapture capability, a main propulsion system failure criteria of fail operational/fail safe, and either two main engines with a high performance attitude control system for back-up or three main engines with which to meet this failure criteria. In addition, a maintenance approach has been established for the advanced vehicle concept. Author

N86-26358*# Evansville Univ., Ind. Dept. of Physics.

THEORETICAL STUDY ON THE EFFECT OF THE DESIGN OF SMALL (MILLI-NEWTON) THRUSTER JETS ON MOLECULAR CONTAMINATION FOR THE SPACE STATION Final Report, 15 Nov. 1985 - 30 Jun. 1986

B. R. RILEY 1986 44 p refs

(Contract NAG3-674)

(NASA-CR-177263; NAS 1.26:177263) Avail: NTIS HC A03/MF A01 CSCL 22B

The self-induced molecular contamination around the space station could have adverse effects on space station components (for example solar panels) as well as scientific experiments that might be done on or near the space station. Aerospace engineers need to design a space station (SS) propulsion system that keeps the SS in a stable orbit and at the same time does not allow the propellant gases to interfere with the experiments of the user. One scenario that might accomplish the above requirements is to use an electrothermal propulsion system, resistojet, that will thrust continuously in the hundreds of milli-Newton range which will provide a constant altitude for the SS with a low g environment. As a first attempt to understand the contamination from such a propulsion system, a point source model was developed. The numerical results of the point source model are given. Number column densities for CO2 are presented as a function of direction of observation (line of sight), temperature of the exit gas, and mean exit velocity. All the results are for a constant exhaust rate of 5,000 kg/year. In addition, a mathematical model to study the effect of nozzle design on the induced molecular environment around the space station produced by simple gas propellants is described. The mathematical model would allow one to follow the expansion of the gas from the throat of a nozzle to the nozzle exit plane and then into the space external to the nozzle. M.G.

N86-27402*# RCA Astro-Electronics Div., Princeton, N. J.
COMMUNICATIONS PLATFORM PAYLOAD DEFINITION STUDY

H. W. CLOPP, T. A. HAWKES, C. R. BERTLES, B. A. PONTANO (Communications Satellite Corp., Clarksburg, Md.), and T. KAO (Washington, D.C. NASA Jul. 1986 245 p (Contract NAS3-24236) (NASA-CR-174986; NAS 1.26:174986) Avail: NTIS HC A11/MF A01 CSCL 22B

Large geostationary communications platforms were investigated in a number of studies since 1974 as a possible means to more effectively utilize the geostationary arc and electromagnetic spectrum and to reduce overall satellite communications system costs. The commercial feasibility of various communications platform payload concepts circa 1998 was addressed. Promising payload concepts were defined, recurring costs were estimated, and critical technologies needed to enable eventual commercialization were identified. Ten communications service aggregation scenarios describing potential groupings of service were developed for a range of conditions. Payload concepts were defined for four of these scenarios: (1) Land Mobile Satellite Service (LMSS) meets 100% of Contiguous United States (CONUS) plus Canada demand with a single platform; (2) Fixed Satellite Service (FSS) (trunking + Customer Premises Service (CPS)), meet 20% of CONUS demand; (3) FSS (trunking + CPS + video distribution), 10 to 13% of CONUS demand; and (4) FSS (20% of demand) + Inter Satellite Links (ISL) + Tracking and Data Relay Satellite System (TDRSS)/Tracking and Data Acquisition System (TDAS) Data Distribution. Author

N86-27403*# Ford Aerospace and Communications Corp., Palo Alto, Calif.

COMMUNICATION PLATFORM PAYLOAD DEFINITION (CPPD) STUDY. VOLUME 1: EXECUTIVE SUMMARY Final Report, Jun. 1984 - Jul. 1985

E. M. HUNTER Mar. 1986 40 p (Contract NAS3-24235) (NASA-CR-174928; NAS 1.26:174928; WDL-TR-10631-VOL-1) Avail: NTIS HC A03/MF A01 CSCL 22B

This is Volume 1 (Executive Summary) of the Ford Aerospace & Communications Corporation Final Report for the Communication Platform Payload Definition (CPPD) Study program conducted for NASA Lewis Research Center under contract No. NAS3-24235. This report presents the results of the study effort leading to five potential platform payloads to service CONUS and WARC Region 2 traffic demand as projected to the year 2008. The report addresses establishing the data bases, developing service aggregation scenarios, selecting and developing 5 payload concepts, performing detailed definition of the 5 payloads, costing them, identifying critical technology, and finally comparing the payloads with each other and also with non-aggregated equivalent services. Author

N86-27404*# Ford Aerospace and Communications Corp., Palo Alto, Calif.

COMMUNICATION PLATFORM PAYLOAD DEFINITION (CPPD) STUDY. VOLUME 2: TECHNICAL REPORT Final Report, Jun. 1984 - Jul. 1985

E. M. HUNTER, T. DRIGGERS, and R. JORASCH Mar. 1986 598 p (Contract NAS3-24235) (NASA-CR-174929; NAS 1.26:174929; WDL-TR-10632-VOL-2) Avail: NTIS HC A25/MF A01 CSCL 22B

This is Volume 2 (Technical Report) of the Ford Aerospace & Communications Corporation Final Report for the Communication Platform Payload Definition (CPPD) Study program conducted for NASA Lewis Research Center under contract No. NAS3-24235. This report presents the results of the study effort leading to five potential platform payloads to service CONUS and WARC Region 2 traffic demand as projected to the year 2008. The report addresses establishing the data bases, developing service aggregation scenarios, selecting and developing 5 payload concepts, performing detailed definition of the 5 payloads, costing

them, identifying critical technology, and finally comparing the payloads with each other and also with non-aggregated equivalent services. Author

N86-27405*# Ford Aerospace and Communications Corp., Palo Alto, Calif.

COMMUNICATION PLATFORM PAYLOAD DEFINITION (CPPD) STUDY. VOLUME 3: ADDENDUM Final Report, Jun. 1984 - Jul. 1985

E. M. HUNTER, T. DRIGGERS, and R. JORASCH Mar. 1986 424 p (Contract NAS3-24235) (NASA-CR-174930; NAS 1.26:174930; WDL-TR-10633-VOL-3) Avail: NTIS HC A18/MF A01 CSCL 22B

This is Volume 3 (Addendum) of the Ford Aerospace & Communications Corporation Final Report for the Communication Platform Payload Definition (CPPD) Study Program conducted for NASA Lewis Research Center under contract No. NAS3-24235. This report presents the results of the study effort leading to five potential platform payloads to service CONUS and WARC Region 2 traffic demand as projected to the year 2008. The report addresses establishing the data bases, developing service aggregation scenarios, selecting and developing 5 payload concepts, performing detailed definition of the 5 payloads, costing them, identifying critical technology, and finally comparing the payloads with each other and also with non-aggregated equivalent services. Author

N86-27407*# RCA Astro-Electronics Div., Princeton, N. J.
COMMUNICATIONS PLATFORM PAYLOAD DEFINITION STUDY, EXECUTIVE SUMMARY

H. W. CLOPP, T. A. HAWKES, C. R. BERTLES, B. A. PONTANO (Communications Satellite Corp., Washington, D.C.), and T. KAO (Jul. 1986 34 p (Contract NAS3-24236) (NASA-CR-174985; NAS 1.26:174985) Avail: NTIS HC A03/MF A01 CSCL 22B

Large geostationary communications platforms have been investigated in a number of studies since 1974 as a possible means to more effectively utilize the geostationary orbital arc and electromagnetic spectrum and to reduce overall satellite communications system costs. This NASA Lewis sponsored study addresses the commercial feasibility of various communications platform payload concepts circa 1998. It defines promising payload concepts, estimates recurring costs and identifies critical technologies needed to permit eventual commercialization. Ten communications service aggregation scenarios describing potential groupings of services were developed for a range of conditions. Payload concepts were defined for four of these scenarios: (1) Land Mobile Satellite Service (LMSS), meet 100% of CONUS plus Canada demand with a single platform; (2) Fixed Satellite Service (FSS) (Trunking + Customer Premises Service (CPS), meet 20% of CONUS demands; (3) FSS (Trunking + video distribution), 10 to 13% of CONUS demand; and (4) FSS (20% of demand) + Inter Satellite Links (ISL) + TDRSS/TDAS Data Distribution. Author

N86-31634*# National Aeronautics and Space Administration. Lewis Research Center, Cleveland, Ohio.

EFFECT OF AN OXYGEN PLASMA ON THE PHYSICAL AND CHEMICAL PROPERTIES OF SEVERAL FLUIDS FOR THE LIQUID DROPLET RADIATOR

D. A. GULINO and C. E. COLES 1986 12 p Proposed for presentation at the 25th Aerospace Sciences Meeting, Reno, Nev., 12-15 Jan. 1987; sponsored by the American Institute of Aeronautics and Astronautics (NASA-TM-88839; E-3222; NAS 1.15:88839) Avail: NTIS HC A02/MF A01 CSCL 07D

The Liquid Droplet Radiator is one of several radiator systems currently under investigation by NASA Lewis Research Center. It involves the direct exposure of the radiator working fluid to the space environment. An area of concern is the potential harmful effects of the low-Earth-orbit atomic oxygen environment on the

19 SPACECRAFT INSTRUMENTATION

radiator working fluid. To address this issue, seven candidate fluids were exposed to an oxygen plasma environment in a laboratory plasma asher. The fluids studied included Dow Corning 705 Diffusion Pump Fluid, polymethylphenylsiloxane and polydimethylsiloxane, both of which are experimental fluids made by Dow Corning, Fomblin Z25, made by Montedison, and three fluids from the Krytox family of fluids, Krytox 143AB, 1502, and 16256, which are made by DuPont. The fluids were characterized by noting changes in visual appearance, physical state, mass, and infrared spectra. Of the fluids tested, the Fomblin and the three Krytox were the least affected by the oxygen plasma. The only effect noted was a change in mass, which was most likely due to an oxygen-catalyzed depolymerization of the fluid molecule. Author

19

SPACECRAFT INSTRUMENTATION

N86-21575*# National Aeronautics and Space Administration. Lewis Research Center, Cleveland, Ohio.

ANALYSIS OF A SPACECRAFT INSTRUMENT BALL BEARING ASSEMBLY LUBRICATED BY A PERFLUOROALKYLETHER

W. MORALES, W. R. JONES, JR., and D. H. BUCKLEY Mar. 1986 9 p refs
(NASA-TM-87260; E-2885; NAS 1.15:87260) Avail: NTIS HC A02/MF A01 CSCL 22B

An analysis of a spacecraft instrument ball bearing assembly, subjected to a scanning life test, was performed to determine the possible cause of rotational problems involving these units aboard several satellites. The analysis indicated an ineffective transfer of a fluorinated liquid lubricant from a phenolic retainer to the bearing balls. Part of the analysis led to a novel HPLC separation method employing a fluorinated mobile phase in conjunction with silica based size exclusion columns. Author

20

SPACECRAFT PROPULSION AND POWER

Includes main propulsion systems and components, e.g., rocket engines; and spacecraft auxiliary power sources.

A86-12676*# National Aeronautics and Space Administration. Lewis Research Center, Cleveland, Ohio.

SPACE STATION POWER SYSTEM

A. F. FORESTIERI and C. R. BARAONA (NASA, Lewis Research Center, Cleveland, OH) IEEE Transactions on Aerospace and Electronic Systems (ISSN 0018-9251), vol. AES-20, Nov. 1984, p. 666-671.

It is pointed out that space station planning at NASA began when NASA was created in 1958. However, the initiation of the program for a lunar landing delayed the implementation of plans for a space station. The utility of a space station was finally demonstrated with Skylab, which was launched in 1972. In May 1982, the Space Station Task Force was established to provide focus and direction for space station planning activities. The present paper provides a description of the planning activities, giving particular attention to the power system. The initial space station will be required to supply 75 kW of continuous electrical power, 60 kW for the customer and 15 kW for space station needs. Possible alternative energy sources for the space station include solar planar or concentrator arrays of either silicon or gallium arsenide. G.R.

A86-14429*# National Aeronautics and Space Administration. Lewis Research Center, Cleveland, Ohio.

MANRATING ORBITAL TRANSFER VEHICLE PROPULSION

L. P. COOPER (NASA, Lewis Research Center, Cleveland, OH) AIAA, SAE, and ASME, Joint Propulsion Conference, 21st, Monterey, CA, July 8-10, 1985. 13 p. Previously announced in STAR as N85-25385. refs
(AIAA PAPER 85-1226)

The expended capabilities for Orbital Transfer Vehicles (OTV) which will be needed to meet increased payload requirements for transporting materials and men to geosynchronous orbit are discussed. The requirement to provide manrating offers challenges and opportunities to the propulsion system designers. The propulsion approaches utilized in previous manned space vehicles of the United States are reviewed. The principals of reliability analysis are applied to the Orbit Transfer Vehicle. Propulsion system options are characterized in terms of the test requirements to demonstrate reliability goals and are compared to earlier vehicle approaches. E.A.K.

A86-14431*# National Aeronautics and Space Administration. Lewis Research Center, Cleveland, Ohio.

PRIMARY PROPULSION OF ELECTROTHERMAL, ION, AND CHEMICAL SYSTEMS FOR SPACE-BASED RADAR ORBIT TRANSFER

S.-Y. WANG and P. J. STAIGER (NASA, Lewis Research Center, Cleveland, OH) AIAA, SAE, and ASME, Joint Propulsion Conference, 21st, Monterey, CA, July 8-10, 1985. 16 p. Previously announced in STAR as N85-27972. refs
(AIAA PAPER 85-1477)

An orbit transfer mission concept has been studied for a Space-Based Radar (SBR) where 40 kW required for radar operation is assumed available for orbit transfer propulsion. Arcjet, pulsed electrothermal (PET), ion, and storable chemical systems are considered for the primary propulsion. Transferring two SBR per shuttle flight to 1112 km/60 deg using electrical propulsion systems offers an increased payload at the expense of increased trip time, up to 2000 kg each, which may be critical for survivability. Trade offs between payload mass, transfer time, launch site, inclination, and height of parking orbits are presented. Author

A86-14445*# National Aeronautics and Space Administration. Lewis Research Center, Cleveland, Ohio.

ELECTRODE EROSION IN ARC DISCHARGES AT ATMOSPHERIC PRESSURE

T. L. HARDY (NASA, Lewis Research Center, Cleveland, OH) AIAA, DGLR, and JSASS, International Electric Propulsion Conference, 18th, Alexandria, VA, Sept. 30-Oct. 2, 1985. 15 p. Previously announced in STAR as N85-34178. refs
(AIAA PAPER 85-2018)

An experimental investigation was performed in an effort to measure and increase lifetime of electrodes in an arcjet thruster. The electrode erosion of various anode and cathode materials was measured after tests in an atmospheric pressure nitrogen arc discharge at powers less than 1 kW. A free-burning arc configuration and a constricted arc configuration were used to test the materials. Lanthanum hexaboride and thoriated tungsten had low cathode erosion rates while thoriated tungsten and pure tungsten had the lowest anode erosion rates of the materials tested. Anode cooling, reverse gas flow, an external magnetic fields were all found to reduce electrode mass loss. Author

A86-14446*# National Aeronautics and Space Administration. Lewis Research Center, Cleveland, Ohio.

HOLLOW CATHODES IN HIGH PRESSURE ARC DISCHARGES

T. L. HARDY and F. M. CURRAN (NASA, Lewis Research Center, Cleveland, OH) AIAA, DGLR, and JSASS, International Electric Propulsion Conference, 18th, Alexandria, VA, Sept. 30-Oct. 2, 1985. 8 p. Previously announced in STAR as N85-34179. refs
(AIAA PAPER 85-2035)

An orified hollow cathode was tested at high pressure to improve lifetime and efficiency in arcjet thrusters. It is indicated that the arc would not operate with emission from the insert above 200

torr in nitrogen regardless of insert material, orifice diameter, or gas flow direction. Emission occurred from the insert in argon and xenon although it could not be ascertained whether diffuse or spot emission existed within the cathode. Over the extended range of configurations and operating parameters explored the desired diffuse emission mode could not be obtained at high enough pressures for orified hollow cathodes to operate in the range which is considered for arcjet applications. E.A.K.

A86-14447* National Aeronautics and Space Administration. Lewis Research Center, Cleveland, Ohio.

AN ANALYSIS OF LOW-THRUST, RESISTOJET REBOOST FOR THE SPACE STATION

P. F. PENKO, P. J. STAIGER, and M. J. BUR (NASA, Lewis Research Center, Cleveland, OH) AIAA, DGLR, and JSASS, International Electric Propulsion Conference, 18th, Alexandria, VA, Sept. 30-Oct. 2, 1985. 7 p. refs (AIAA PAPER 85-2042)

This paper presents results of an analysis of low-thrust orbit maintenance of the Space Station. Propellant requirements and transfer times are given for reboost of the station through various altitude increments. The reboost can readily be accomplished with thrust levels that subject the station to an acceleration of less than the desired upper limit of 10 to the -5th g's. The variation in time and the probabilistic aspect of the predicted upper-atmospheric density as well as the variation in time of sun-pointing drag areas were taken into account. Estimates of the propellant requirements at different times during an 11-year solar cycle are given. It is shown that the amount of CO₂ available from the station life-support system is sufficient, over most of the solar cycle, to provide the propellant for a resistojet orbit-maintenance system.

Author

A86-17831* National Aeronautics and Space Administration. Lewis Research Center, Cleveland, Ohio.

NASA ELECTRIC PROPULSION TECHNOLOGY

F. D. BERKOPEC, J. R. STONE (NASA, Lewis Research Center, Cleveland, OH), and G. ASTON (California Institute of Technology, Jet Propulsion Laboratory, Pasadena) AIAA, JSASS, and DGLR, International Electric Propulsion Conference, 18th, Alexandria, VA, Sept. 30-Oct. 2, 1985. 17 p. refs (AIAA PAPER 85-1999)

It is pointed out that the requirements for future electric propulsion cover an extremely large range of technical and programmatic characteristics. A NASA program is to provide options for the many potential mission applications, taking into account work on electrostatic, electromagnetic, and electrothermal propulsion systems. The present paper is concerned with developments regarding the three classes of electric propulsion. Studies concerning electrostatic propulsion are concerned with ion propulsion for primary propulsion for planetary and earth-orbit transfer vehicles, stationkeeping for geosynchronous spacecraft, and ion thruster systems. In connection with investigations related to electromagnetic propulsion, attention is given to electromagnetic launchers, the Hall current thruster, and magnetoplasmadynamic thrusters. In a discussion of electrothermal developments, space station resistojets are considered along with high performance resistojets, arcjets, and a laser thruster. G.R.

A86-17833* National Aeronautics and Space Administration. Lewis Research Center, Cleveland, Ohio.

HEATERLESS IGNITION OF INERT GAS ION THRUSTER HOLLOW CATHODES

M. F. SCHATZ (NASA, Lewis Research Center, Cleveland, OH) AIAA, JSASS, and DGLR, International Electric Propulsion Conference, 18th, Alexandria, VA, Sept. 30-Oct. 2, 1985. 13 p. Previously announced in STAR as N85-34177. refs (AIAA PAPER 85-2008)

Heaterless inert gas ion thruster hollow cathodes were investigated with the aim of reducing ion thruster complexity and increasing ion thruster reliability. Cathodes heated by glow discharges are evaluated for power requirements, flowrate

requirements, and life limiting mechanisms. An accelerated cyclic life test is presented. E.A.K.

A86-17835* National Aeronautics and Space Administration. Lewis Research Center, Cleveland, Ohio.

COMPATIBILITY OF GRAIN-STABILIZED PLATINUM WITH CANDIDATE PROPELLANTS FOR RESISTOJETS

M. V. WHALEN and S. P. GRISNIK (NASA, Lewis Research Center, Cleveland, OH) AIAA, JSASS, and DGLR, International Electric Propulsion Conference, 18th, Alexandria, VA, Sept. 30-Oct. 2, 1985. 21 p. Previously announced in STAR as N86-10279. refs (AIAA PAPER 85-2014)

An examination is conducted into the suitability of grain-stabilized Pt as a resistojet thruster material for Space Station auxiliary propulsion. A series of 1000-hour tests was conducted in CO₂, H₂, and NH₃ at 1400 C; another series was conducted at 500 C in CH₄ for the same duration. SEM, Auger electron microscopy, and depth profiling analysis were used to determine the effects of propellants on the material surface as well as to evaluate possible material contamination and possible grain growth. Carbon deposition is noted on the surface of Pt/Y₂O₃ and Pt/ZrO₂ in both the CO₂ and CH₄ environments. O.C.

A86-17850* National Aeronautics and Space Administration. Lewis Research Center, Cleveland, Ohio.

STATUS OF ADVANCED ORBITAL TRANSFER PROPULSION

L. P. COOPER (NASA, Lewis Research Center, Cleveland, OH) IAF, International Astronautical Congress, 36th, Stockholm, Sweden, Oct. 7-12, 1985. 25 p. Previously announced in STAR as N85-35225. refs (IAF PAPER 85-164)

A new Orbital Transfer Vehicle (OTV) propulsion system that will be used in conjunction with the Space Shuttle, Space Station and Orbit Maneuvering Vehicle is discussed. The OTV will transfer men, large space structures and conventional payloads between low earth and higher energy orbits. Space probes carried by the OTV will continue the exploration of the solar system. When lunar bases are established, the OTV will be their transportation link to earth. Critical engine design considerations based upon the need for low cost payload delivery, space basing, reusability, aeroassist maneuvering, low g transfers of large space structures and man rating are described. The importance of each of these to propulsion design is addressed. Specific propulsion requirements discussed are: (1) high performance H₂/O₂ engine; (2) multiple engine configurations totalling no more than 15,000 lbf thrust 15 to 20 hr life; (3) space maintainable modular design; (4) health monitoring capability; and (5) safety and mission success with backup auxiliary propulsion. E.A.K.

A86-17851* Arizona State Univ., Tempe. **RAPID EVALUATION OF ION THRUSTER LIFETIME USING OPTICAL EMISSION SPECTROSCOPY**

B. A. ROCK, M. L. PARSONS (Arizona State University, Tempe), and M. A. MANTENIEKS (NASA, Lewis Research Center, Cleveland, OH) AIAA, JSASS, and DGLR, International Electric Propulsion Conference, 18th, Alexandria, VA, Sept. 30-Oct. 2, 1985. 46 p. Previously announced in STAR as N86-10280. refs (AIAA PAPER 85-2011)

A major life-limiting phenomenon of electric thrusters is the sputter erosion of discharge chamber components. Thrusters for space propulsion are required to operate for extended periods of time, usually in excess of 10,000 hr. Lengthy and very costly life-tests in high-vacuum facilities have been required in the past to determine the erosion rates of thruster components. Alternative methods for determining erosion rates which can be performed in relatively short periods of time at considerably lower costs are studied. An attempt to relate optical emission intensity from an ion bombarded surface (screen grid) to the sputtering rate of that surface is made. The model used a kinetic steady-state (KSS) approach, balancing the rates of population and depopulation of ten low-lying excited states of the sputtered molybdenum atom (Mo) with those of the ground state to relate the spectral intensities of the various transitions of the Mo to the population densities.

20 SPACECRAFT PROPULSION AND POWER

Once this is accomplished, the population density can be related to the sputtering rate of the target. Radiative and collisional modes of excitation and decay are considered. Since actual data has not been published for Mol excitation rate and decay constants, semiempirical equations are used. The calculated sputtering rate and intensity is compared to the measured intensity and sputtering rates of the 8 and 30 cm ion thrusters. Author

A86-18041*# Michigan State Univ., East Lansing.
MEASUREMENT OF ENERGY DISTRIBUTION IN FLOWING HYDROGEN MICROWAVE PLASMAS

R. CHAPMAN, T. MORIN, M. FINZEL, and M. C. HAWLEY (Michigan State University, East Lansing) Journal of Spacecraft and Rockets (ISSN 0022-4650), vol. 22, Nov.-Dec. 1985, p. 626-630. refs
(Contract NSG-3299)

An electrothermal propulsion concept utilizing a microwave plasma system as the mechanism to convert electromagnetic energy into kinetic energy of a flowing gas is investigated. A calorimetry system enclosing a microwave plasma system has been developed to accurately measure the energy inputs and outputs of the microwave plasma system. The rate of energy transferred to the gas can be determined to within + or - 1.8 W from an energy balance around the microwave plasma system. The percentage of the power absorbed by the microwave plasma system transferred to the hydrogen gas as it flows through the system is found to increase with the increasing flow rate, to decrease with the increasing pressure, and to be independent of the absorbed power. An upper bound for the hydrogen gas temperature is estimated from the energy content, heat capacity, and flow rate of the gas stream. A lower bound for an overall heat-transfer coefficient is then calculated, characterizing the energy loss from the hydrogen gas stream to the air cooling of the plasma discharge tube wall. The heat-transfer coefficient is found to increase with the increasing flow rate and pressure and to be independent of the absorbed power. This result indicates that a convective-type mechanism is responsible for the energy transfer. Author

A86-18042*# Colorado State Univ., Fort Collins.
CURRENT COLLECTION FROM THE SPACE PLASMA THROUGH DEFECTS IN SOLAR ARRAY INSULATION

R. S. ROBINSON (Colorado State University, Fort Collins), R. P. STILLWELL, and H. R. KAUFMAN Journal of Spacecraft and Rockets (ISSN 0022-4650), vol. 22, Nov.-Dec. 1985, p. 631-641. refs
(Contract NSG-3196)

Operating high-voltage solar arrays in the space environment can result in anomalously large currents being collected through small insulation defects. Tests simulating the electron collection have shown that there are two major collection modes. The first involves current enhancement by means of a surface phenomenon involving secondary electron emission from the surrounding insulator. In the second mode, the current collection is enhanced by vaporization and ionization of the insulator material, in addition to the surface enhancement of the first mode. The electron collection due to surface enhancement (first mode) has been modeled. Using this model, simple calculations yield realistic predictions. Author

A86-18043*# McGill Univ., Montreal (Quebec).
RADIATION ENERGY RECEIVER FOR SOLAR PROPULSION SYSTEMS

D. F. G. RAULT (McGill University, Montreal, Canada) Journal of Spacecraft and Rockets (ISSN 0022-4650), vol. 22, Nov.-Dec. 1985, p. 642-648. Previously cited in issue 16, p. 2319, Accession no. A83-36281. refs
(Contract NAG3-16)

A86-19834*# Systems Science and Software, La Jolla, Calif.
THRESHOLD DETERMINING MECHANISMS FOR DISCHARGES IN HIGH VOLTAGE SOLAR ARRAYS

D. E. PARKS, G. A. JONGEWARD, I. KATZ, and V. A. DAVIS (Systems Science and Software, La Jolla, CA) AIAA, Aerospace Sciences Meeting, 24th, Reno, NV, Jan. 6-9, 1986. 7 p. refs
(Contract NAS3-23881)
(AIAA PAPER 86-0364)

A theory is developed to account for the observed properties of discharges of solar arrays immersed in plasma. The theory is based on the assumption that a thin layer of insulating contaminant covers any metallic surface exposed to the plasma. Quantities derivable from the theory include a voltage threshold for arcing. The existence of the threshold and its predicted weak dependence on plasma density appear consistent with experimental results. Author

A86-19835*# Colby Coll., Waterville, Maine.
CIRCUIT TRANSIENTS DUE TO NEGATIVE BIAS ARCS-II

R. N. METZ (Colby College, Waterville, ME) AIAA, Aerospace Sciences Meeting, 24th, Reno, NV, Jan. 6-9, 1986. 6 p. refs
(Contract NAG3-576)
(AIAA PAPER 86-0366)

Two new models of negative-bias arcing on a solar cell power system in Low Earth Orbit are presented. One is an extended, analytical model and the other is a non-linear, numerical model. The models are based on an earlier analytical model in which the interactions between solar cell interconnects and the space plasma as well as the parameters of the power circuit are approximated linearly. Transient voltages due to arcs struck at the negative thermal of the solar panel are calculated in the time domain. The new models treat, respectively, further linear effects within the solar panel load circuit and non-linear effects associated with the plasma interactions. Results of computer calculations with the models show common-mode voltage transients of the electrically floating solar panel struck by an arc comparable to the early model but load transients that differ substantially from the early model. In particular, load transients of the non-linear model can be more than twice as great as those of the early model and more than twenty times as great as the extended, linear model. Author

A86-24778* National Aeronautics and Space Administration.
Lewis Research Center, Cleveland, Ohio.

SPACE STATION POWER SYSTEM ADVANCED DEVELOPMENT

A. F. FORESTIERI, C. R. BARAONA, and M. E. VALGORA (NASA, Lewis Research Center, Cleveland, OH) IN: Intersociety Energy Conversion Engineering Conference, 20th, Miami Beach, FL, August 18-23, 1985, Proceedings. Volume 1. Warrendale, PA, Society of Automotive Engineers, Inc., 1985, p. 1.9-1.16.

The objectives of the Space Station Advanced Development Program are related to the development of a set of design options and/or new capabilities to support Space Station development and operation, taking into account also a quantification of the performance and risk of key state-of-the-art technologies, and a reduction of the cost and schedule risk in Space Station development. Attention is given to the photovoltaic power system, a solar dynamic system, and aspects of power management and distribution. A major issue will be the selection of the power generation system. In view of the advantages of the solar dynamic system, it is attempted to resolve issues associated with this system. G.R.

A86-24790* National Aeronautics and Space Administration. Lewis Research Center, Cleveland, Ohio.

DESIGN TRADEOFFS FOR A SPACE STATION SOLAR-BRAYTON POWER SYSTEM

J. L. KLANN and P. J. STAIGER (NASA, Lewis Research Center, Cleveland, OH) IN: Intersociety Energy Conversion Engineering Conference, 20th, Miami Beach, FL, August 18-23, 1985, Proceedings, Volume 1. Warrendale, PA, Society of Automotive Engineers, Inc., 1985, p. 1.84-1.97. refs

Mass, area, and station-keeping propellant needs have been estimated for a typical system. And, although important criteria such as cost, Shuttle packaging, and erection/deployment schemes were not considered, the documented trends should aid in many of the design choices to be made. Effects on system characteristics were examined for: three heat storage salts with melting temperatures from 743 to 1121 K; parabolic and Cassegrainian mirrors; module power levels of 20 and 40 kW; and, alternate pumped-loop, tube-and-fin radiator configurations, with and without micrometeoroid armoring. Author

A86-24808* National Aeronautics and Space Administration. Lewis Research Center, Cleveland, Ohio.

TETHERED NUCLEAR POWER FOR THE SPACE STATION

D. J. BENTS (NASA, Lewis Research Center, Cleveland, OH) IN: Intersociety Energy Conversion Engineering Conference, 20th, Miami Beach, FL, August 18-23, 1985, Proceedings, Volume 1. Warrendale, PA, Society of Automotive Engineers, Inc., 1985, p. 1.210-1.227. Previously announced in STAR as N85-26912. refs

A nuclear space power system the SP-100 is being developed for future missions where large amounts of electrical power will be required. Although it is primarily intended for unmanned spacecraft, it can be adapted to a manned space platform by tethering it above the station through an electrical transmission line which isolates the reactor far away from the inhabited platform and conveys its power back to where it is needed. The transmission line, used in conjunction with an instrument rate shield, attenuates reactor radiation in the vicinity of the space station to less than one-one hundredth of the natural background which is already there. This combination of shielding and distance attenuation is less than one-tenth the mass of boom-mounted or onboard man-rated shields that are required when the reactor is mounted nearby. This paper describes how connection is made to the platform (configuration, operational requirements) and introduces a new element the coaxial transmission tube which enables efficient transmission of electrical power through long tethers in space. Design methodology for transmission tubes and tube arrays is discussed. An example conceptual design is presented that shows SP-100 at three power levels 100 kWe, 300 kWe, and 1000 kWe connected to space station via a 2 km HVDC transmission line/tether. Power system performance, mass, and radiation hazard are estimated with impacts on space station architecture and operation. B.W.

A86-24836* National Aeronautics and Space Administration. Lewis Research Center, Cleveland, Ohio.

SPACE POWER SYSTEMS - 'SPACECRAFT 2000'

K. A. FAYMON (NASA, Lewis Research Center, Cleveland, OH) IN: Intersociety Energy Conversion Engineering Conference, 20th, Miami Beach, FL, August 18-23, 1985, Proceedings, Volume 1. Warrendale, PA, Society of Automotive Engineers, Inc., 1985, p. 1.422-1.424.

The program 'Spacecraft 2000' has the objective to identify critical, high-payoff, potential spacecraft technologies, taking into account the formulation, advocacy, and the management of the requisite technology development programs. This program represents a joint NASA-industry program. The technology areas addressed by 'Spacecraft 2000' are related to spacecraft power/energy storage, thermal control/thermal management, power management and distribution, autonomous operation-control, on-board system integration, spacecraft environmental interactions, secondary propulsion, communications technologies, a total system response approach, and system-subsystem technology verification. The expected benefits of a development of advanced technologies

include decreased spacecraft bus system weights, decreased mission costs, increased reliability/lifetimes, and increased operational flexibility. G.R.

A86-24857* National Aeronautics and Space Administration. Lewis Research Center, Cleveland, Ohio.

DESIGN OF A REGENERATIVE FUEL CELL SYSTEM FOR SPACE STATION

M. A. HOBERECHT and L. L. RIEKER (NASA, Lewis Research Center, Cleveland, OH) IN: Intersociety Energy Conversion Engineering Conference, 20th, Miami Beach, FL, August 18-23, 1985, Proceedings, Volume 2. Warrendale, PA, Society of Automotive Engineers, Inc., 1985, p. 2.202-2.207.

The NASA Space Station will employ alkaline regenerative fuel cells (RFCs) as its sole electrochemical energy storage system, in virtue of demonstrated technology readiness and a high degree of system-level design flexibility. NASA Johnson and NASA Lewis are currently engaged in the development of a 10-kW alkaline engineering model system, for 1987 delivery, which will encompass a fully autonomous 120-V system with 55 percent overall electrical efficiency and a 20,000-hr service life. O.C.

A86-26492*# National Aeronautics and Space Administration. Lewis Research Center, Cleveland, Ohio.

HEAT TRANSFER IN SPACE POWER AND PROPULSION SYSTEMS

R. C. HENDRICKS, R. J. SIMONEAU, and J. W. DUNNING, JR. (NASA, Lewis Research Center, Cleveland, OH) Mechanical Engineering (ISSN 0025-6501), vol. 108, Feb. 1986, p. 40-52.

NASA's planned Space Station has projected power requirements in the 75-300 kW range; attention is presently given to the range of power system configurations thus far proposed. These are a silicon solar cell system incorporating regenerative fuel cell or battery storage, with a 10-year lifetime, a solar-dynamic power system with phase-change or regenerative fuel cell energy storage, and a combination of these two alternatives. A development status evaluation is also given for the propulsion systems that may be used by next-generation boosters. These include such novel airbreathing systems as turboramjets, air liquefaction cycle rockets, airturboramjet/rockets, and supersonic combustion ramjets. O.C.

A86-37054*# Martin Marietta Corp., Denver, Colo.

LH2 ON-ORBIT STORAGE TANK SUPPORT TRUNNION DESIGN AND VERIFICATION

W. J. BAILEY, D. A. FESTER, and J. M. TOTH, JR. (Martin Marietta Corp., Denver, CO) Cryogenic Engineering Conference, Boston, MA, Aug. 12-16, 1985, Paper. 14 p. (Contract NAS3-23355; NAS3-23245)

A detailed fatigue analysis was conducted to provide verification of the trunnion design in the reusable Cryogenic Fluid Management Facility for Shuttle flights and to assess the performance capability of the trunnion E-glass/S-glass epoxy composite material. Basic material property data at ambient and liquid hydrogen temperatures support the adequacy of the epoxy composite for seven-mission requirement. Testing of trunnions fabricated to the flight design has verified adequate strength and fatigue properties of the design to meet the requirements of seven Shuttle flights. I.S.

A86-37062*# National Aeronautics and Space Administration. Lewis Research Center, Cleveland, Ohio.

AN EXPERIMENTAL STUDY OF ENERGY LOSS MECHANISMS AND EFFICIENCY CONSIDERATIONS IN THE LOW POWER DC ARCJET

F. M. CURRAN (NASA, Lewis Research Center, Cleveland, OH) AIAA, JSASS, and DGLR, International Electric Propulsion Conference, 18th, Alexandria, VA, Sept. 30-Oct. 2, 1985. 24 p. Previously announced in STAR as N86-11224. refs (AIAA PAPER 85-2017)

The potential utility of the low power dc arcjet in auxiliary propulsion was investigated. It was indicated that improvements in the areas of stability, energy efficiency, reliability, and electrode erosion are necessary to obtain a useful device. A water-cooled

20 SPACECRAFT PROPULSION AND POWER

arcjet simulator was tested to investigate both the energy loss mechanisms at the electrodes and the stability of different conventional arcjet configurations in the presence of a vortex flow field. It is shown that in certain configurations only 25 to 30 percent of the input energy is lost to the electrodes. It is also shown that vortex stabilization is not difficult to obtain in many cases at the flow rates used and that a careful starting procedure is effective in minimizing electrode damage. E.A.K.

A86-37063*# National Aeronautics and Space Administration. Lewis Research Center, Cleveland, Ohio.

EXPERIMENTAL PERFORMANCE OF A 1-KILOWATT ARCJET THRUSTER

S. NAKANISHI (NASA, Lewis Research Center, Cleveland, OH) AIAA, JSASS, and DGLR, International Electric Propulsion Conference, 18th, Alexandria, VA, Sept. 30-Oct. 2, 1985. 30 p. Previously announced in STAR as N86-10281. refs (AIAA PAPER 85-2033)

A formerly unused cathode and anode/nozzle assembly from a flight model arcjet was tested with nitrogen, hydrogen, and nitrogen-hydrogen mixture simulating ammonia decomposition products at arc power levels from about 300 to 950 W. Two different power sources and two nozzle configurations were tested at low background pressures to exclude facility effects. Increased nozzle expansion ratio improved cold flow nozzle efficiency from 0.8 to 0.9. Hydrogen thrust efficiency of 0.26 at 872 sec specific impulse matched some 1964 performance on a similar device. Simulated ammonia thrust efficiency was 0.31 at 422 sec. Spontaneously occurring voltage mode changes at constant arc current could be partially stabilized with appropriate power source characteristics. In the higher voltage mode specific impulse was higher, but thrust efficiency changed only slightly from that of the lower voltage mode. Sustained tests of up to 2 hr duration exhibited no apparent performance degradation with time. Author

A86-38895*# National Aeronautics and Space Administration. Lewis Research Center, Cleveland, Ohio.

STRUCTURAL TAILORING OF SSME TURBOPUMP BLADES (SSME/STAEBL)

R. RUBINSTEIN (Sverdrup Technology, Inc., Middleburg Heights, OH) and C. C. CHAMIS (NASA, Lewis Research Center, Cleveland, OH) IN: Structures, Structural Dynamics and Materials Conference, 27th, San Antonio, TX, May 19-21, 1986, Technical Papers. Part 2. New York, American Institute of Aeronautics and Astronautics, 1986, p. 125-130.

(AIAA PAPER 86-0847)

Computer structural optimization is applied to the design of Space Shuttle main engine turbopump blades. The optimization is implemented by the program SSME/STAEBL. A general description of this program is given. Design optimization studies for typical blade designs are presented. Author

A86-39877*# Washington Univ., St. Louis, Mo.

EFFECT OF SUBCOOLING ON THE ON-ORBIT PRESSURIZATION RATE OF CRYOGENIC PROPELLANT TANKAGE

J. I. HOCHSTEIN, H.-C. JI (Washington University, St. Louis, MO), and J. C. AYDELOTT (NASA, Lewis Research Center, Cleveland, OH) AIAA and ASME, Joint Thermophysics and Heat Transfer Conference, 4th, Boston, MA, June 2-4, 1986. 10 p. refs (Contract NAG3-578)

(AIAA PAPER 86-1253)

The SOLA-ECLIPSE code is being developed to enable prediction of the behavior of cryogenic propellants in spacecraft tankage. A brief description of the formulations used for modeling heat transfer and for determining thermodynamic state is presented. Code performance is verified through comparison to experimental data for the self-pressurization of scale model liquid hydrogen tanks. SOLA-ECLIPSE is used to examine the effect of initial subcooling of the liquid phase on the self-pressurization rate of an on-orbit full scale liquid hydrogen tank typical for a chemical propulsion Orbital Transfer Vehicle. The computational predictions show that even small amounts of subcooling will significantly

decrease the self-pressurization rate. Further, if the cooling is provided by a Thermodynamic Vent System, it is concluded that small levels of subcooling will maximize propellant conservation.

Author

A86-39906*# TRW, Inc., Redondo Beach, Calif.

SOLAR DYNAMIC POWER FOR THE SPACE STATION

J. S. ARCHER and E. S. DIAMANT (TRW, Inc., Redondo Beach, CA) AIAA and ASME, Joint Thermophysics and Heat Transfer Conference, 4th, Boston, MA, June 2-4, 1986. 8 p. (Contract NAS3-24655)

(AIAA PAPER 86-1299)

This paper describes a computer code which provides a significant advance in the systems analysis capabilities of solar dynamic power modules. While the code can be used to advantage in the preliminary analysis of terrestrial solar dynamic modules its real value lies in the adaptations which make it particularly useful for the conceptualization of optimized power modules for space applications. In particular, as illustrated in the paper, the code can be used to establish optimum values of concentrator diameter, concentrator surface roughness, concentrator rim angle and receiver aperture corresponding to the main heat cycle options - Organic Rankine and Brayton - and for certain receiver design options. The code can also be used to establish system sizing margins to account for the loss of reflectivity in orbit or the seasonal variation of insolation. By the simulation of the interactions among the major components of a solar dynamic module and through simplified formulations of the major thermal-optic-thermodynamic interactions the code adds a powerful, efficient and economic analytical tool to the repertory of techniques available for the design of advanced space power systems. Author

A86-40595*# National Aeronautics and Space Administration. Lewis Research Center, Cleveland, Ohio.

PROBABILISTIC STRUCTURAL ANALYSIS METHODS FOR CRITICAL SSME PROPULSION COMPONENTS

C. C. CHAMIS (NASA, Lewis Research Center, Cleveland, OH) IN: Space Systems Technology Conference, San Diego, CA, June 9-12, 1986, Technical Papers. New York, American Institute of Aeronautics and Astronautics, 1986, p. 133-144. refs (AIAA PAPER 86-1188)

The development of a three-dimensional inelastic analysis methodology for the Space Shuttle main engine (SSME) structural components is described. The methodology is composed of: (1) composite load spectra, (2) probabilistic structural analysis methods, (3) the probabilistic finite element theory, and (4) probabilistic structural analysis. The progress in the development of generic probabilistic models for various individual loads which consist of a steady state load, a periodic load, a random load, and a spike, is discussed. The capabilities of the Numerical Evaluation of Stochastic Structures Under Stress finite element code designed for probabilistic structural analysis of the SSME are examined. Variation principles for formulation probabilistic finite elements and a structural analysis for evaluating the geometric and material properties tolerances on the structural response of turbopump blades are being designed. I.F.

A86-42616*# Technion, Inc., Irvine, Calif.

A 10,000 HOUR LIFE MULTIPROPELLANT ENGINE FOR SPACE STATION APPLICATIONS

T. K. PUGMIRE, G. L. CANN (Technion, Inc., Irvine, CA), B. HECKERT (Rockwell International Corp., Canoga Park, CA), and J. S. SOVEY (NASA, Lewis Research Center, Cleveland, OH) AIAA, ASME, SAE, and ASCE, Joint Propulsion Conference, 22nd, Huntsville, AL, June 16-18, 1986. 9 p. Research supported by Johnson Matthey, Inc. and Engelhard Corp. refs (AIAA PAPER 86-1403)

A review of the design background and operating objectives of a multipropellant resistojet is presented. An engine has been designed to operate with carbon dioxide, methane, water, hydrazine decomposition products and hydrogen. Design performance has been constrained to ensure a 10,000-hour life. The engine, constructed primarily of grain stabilized platinum, is to operate at

temperatures up to 1400 C. General performance guidelines, design and fabrication methods are reported. Author

A86-42617*# Textron Bell Aerospace Co., Buffalo, N. Y.
A LONG-LIFE 50 LBF H₂/O₂ THRUSTER FOR SPACE STATION AUXILIARY PROPULSION

J. M. SENNEFF (Bell Aerospace Textron, Buffalo, NY) and G. P. RICHTER (NASA, Lewis Research Center, Cleveland, OH) AIAA, ASME, SAE, and ASEE, Joint Propulsion Conference, 22nd, Huntsville, AL, June 16-18, 1986. 9 p. refs (AIAA PAPER 86-1404)

In preparation for the development of a manned Space Station, the National Aeronautics and Space Administration (NASA) is conducting a program to develop technology related to on-board Auxiliary Propulsion Systems. To develop the required thruster technology to support the Space Station project, the NASA Lewis Research Center has sponsored a development program based on a unique 'reverse flow' concept where the fuel is injected 'backwards' in the chamber to cool the spherical combustor wall. This combustor was based on previous developments at the 50-lbf, 1000-lbf, and 1500-lbf thrust levels. This paper describes the design and test program carried out to demonstrate a new 50-lbf thruster, the design which was based on this previous technology. Included are the test results for the initial mixture ratio 4 thruster which can operate with uncooled Cres (stainless steel) combustor walls. In addition, the effort to operate a thruster redesigned for operation at a mixture ratio of eight for potential integration with the life support system is described. Author

A86-42633*# CHAM of North America, Inc., Huntsville, Ala.
COMPUTATIONAL SIMULATION OF LIQUID ROCKET INJECTOR ANOMALIES

A. J. PRZEKAS, A. K. SINGHAL, L. T. TAM (CHAM of North America, Inc., Huntsville, AL), and K. DAVIDIAN (NASA, Lewis Research Center, Cleveland, OH) AIAA, ASME, SAE, and ASEE, Joint Propulsion Conference, 22nd, Huntsville, AL, June 16-18, 1986. 10 p. refs (AIAA PAPER 86-1424)

A computer model has been developed to analyze the three-dimensional two-phase reactive flows in liquid fueled rocket combustors. The model is designed to study the influence of liquid propellant injection nonuniformities on the flow pattern, combustion and heat transfer within the combustor. The Eulerian-Lagrangian approach for simulating polydisperse spray flow, evaporation and combustion has been used. Full coupling between the phases is accounted for. A nonorthogonal, body fitted coordinate system along with a conservative control volume formulation is employed. The physical models built into the model include a kappa-epsilon turbulence model, a two-step chemical reaction, and the six-flux radiation model. Semiempirical models are used to describe all interphase coupling terms as well as chemical reaction rates. The purpose of this study was to demonstrate an analytical capability to predict the effects of reactant injection nonuniformities (injection anomalies) on combustion and heat transfer within the rocket combustion chamber. The results show promising application of the model to comprehensive modeling of liquid propellant rocket engines. Author

A86-42640*# National Aeronautics and Space Administration. Lewis Research Center, Cleveland, Ohio.

PERFORMANCE AND ENDURANCE TESTS OF A MULTIPROPELLANT RESISTOJET FOR SPACE STATION AUXILIARY PROPULSION

W. E. MORREN, M. V. WHALEN (NASA, Lewis Research Center, Cleveland, OH), and J. S. SOVEY AIAA, ASME, SAE, and ASEE, Joint Propulsion Conference, 22nd, Huntsville, AL, June 16-18, 1986. 12 p. Previously announced in STAR as N86-24748. refs (AIAA PAPER 86-1435)

This paper presents the results of an effort to demonstrate the technology readiness of a long-life multipropellant resistojet for space station auxiliary propulsion. Experiments were performed to evaluate the compatibility of grain-stabilized platinum tubes at temperatures up to 1400 deg C in environments of CO₂, CH₄,

NH₃, H₂O, and H₂. All samples tested showed extrapolated lifetimes in excess of 10,000 hr based on 10 percent mass loss as end-of-life. However, samples tested in an ammonia atmosphere at 1400 deg C showed severe pitting, which raised concerns about the compatibility of grain-stabilized platinum with ammonia-containing atmospheres. Additional tests showed that reducing the metal temperature to about 900 deg C (+ or - 100 deg C) significantly reduced this adverse effect. Author

A86-42676*# National Aeronautics and Space Administration. Lewis Research Center, Cleveland, Ohio.

LOW POWER DC ARCJET OPERATION WITH HYDROGEN/NITROGEN PROPELLANT MIXTURES

F. M. CURRAN (NASA, Lewis Research Center, Cleveland, OH) and S. NAKANISHI (NASA, Lewis Research Center; Analox Corp., Cleveland, OH) AIAA, ASME, SAE, and ASEE, Joint Propulsion Conference, 22nd, Huntsville, AL, June 16-18, 1986. 15 p. Previously announced in STAR as N86-25407. refs (AIAA PAPER 86-1505)

The arcjet assembly from a flight model system was modified with a new thoriated tungsten nozzle insert and has been tested with hydrogen-nitrogen mixtures simulating the decomposition products of ammonia and hydrazine. Arcjet power consumption ranged from 0.7 to 1.15 kW depending on low rate, input current, and mixture composition. At a nominal 1 kW power level the ammonia mixtures thrust efficiency was about 0.31 at specific impulse values ranging between 460 and 500 sec. Hydrazine mixtures gave similar thrust efficiencies at the same power level with specific impulse values between 395 and 430 sec. Large, spontaneous voltage mode changes were not observed once the thruster had passed a period of instability immediately following start up. This period of instability, and the startup at low pressure, were seen as major causes of constrictor damage during the tests. Author

A86-42682*# National Aeronautics and Space Administration. Lewis Research Center, Cleveland, Ohio.

STRUCTURAL INTEGRITY AND DURABILITY FOR SPACE SHUTTLE MAIN ENGINE AND FUTURE REUSABLE SPACE PROPULSION SYSTEMS

S. J. MARSIK (NASA, Lewis Research Office, Cleveland, OH) and H. T. GAWRYLOWICZ (NASA, Washington, DC) AIAA, ASME, SAE, and ASEE, Joint Propulsion Conference, 22nd, Huntsville, AL, June 16-18, 1986. 9 p. Previously announced in STAR as N86-25408. refs (AIAA PAPER 86-1513)

NASA is conducting a program which will establish a technology base for the orderly evolution of reusable space propulsion systems. As part of that program, NASA initiated a Structural Integrity and Durability effort for advanced high-pressure oxygen-hydrogen rocket engine technology. That effort focuses on the development of: (1) accurate analytical models to describe flow fields; aerothermodynamic loads; structural responses; and fatigue/fracture, from which life prediction codes can be evolved; and (2) advanced instrumentation with capabilities to verify the codes in an SSME-like environment as well as the potential for future use as diagnostic sensors for real-time condition monitoring of critical engine components. Author

A86-42799*# National Aeronautics and Space Administration. Lewis Research Center, Cleveland, Ohio.

NASA ELECTROTHERMAL AUXILIARY PROPULSION TECHNOLOGY

J. R. STONE (NASA, Lewis Research Center, Cleveland, OH) AIAA, ASME, SAE, and ASEE, Joint Propulsion Conference, 22nd, Huntsville, AL, June 16-18, 1986. 19 p. Previously announced in STAR as N86-24749. refs (AIAA PAPER 86-1703)

Electrothermal auxiliary propulsion systems provide high performance options which can have major mission benefits. There are several electrothermal concepts which offer a range of characteristics and benefits. Resistojets are the highest thrust to power option and are currently operational at mission average

20 SPACECRAFT PROPULSION AND POWER

values of specific impulse, 1 sub sp approximately 295 sec. Long life, multipropellant resistojets are being developed for the Space Station, and resistojet technology advancements are being pursued to improve the 1 sub sp by more than 20 percent for resistojets used in satellite applications. Direct current arcjets have the potential of 1 sub sp over 400 sec with storable propellants and should provide over 1000 sec with hydrogen. Advanced concepts are being investigated to provide high power density options and possible growth to primary propulsion applications. Broad based experimental and analytical research and technology programs of NASA are summarized and recent significant advances are reviewed. Author

A86-49613*# National Aeronautics and Space Administration. Lewis Research Center, Cleveland, Ohio.

POWER ELECTRONICS FOR A 1-KILOWATT ARCJET THRUSTER

R. P. GRUBER (NASA, Lewis Research Center, Cleveland, OH) AIAA, ASME, SAE, and ASEE, Joint Propulsion Conference, 22nd, Huntsville, AL, June 16-18, 1986. 21 p. Previously announced in STAR as N86-25409. refs (AIAA PAPER 86-1507)

After more than two decades, new space mission requirements have revived interest in arcjet systems. The preliminary development and demonstration of new, high efficiency, power electronic concepts for start up and steady state control of dc arcjets is reported. The design comprises a pulse width modulated power converter which is closed loop configured to give fast current control. An inductor, in series with the arcjet, serves the dual role of providing instantaneous current control, as well as a high voltage arc ignition pulse. Benchmark efficiency, transient response, regulation, and ripple data are presented. Tests with arcjets demonstrate that the power electronics breadboard can start thrusters consistently with no apparent damage and transfer reliably to the nondestructive high voltage arc mode in less than a second. Author

A86-49615*# National Aeronautics and Space Administration. Lewis Research Center, Cleveland, Ohio.

CURRENT EVALUATION OF THE TRIPROPELLANT CONCEPT

R. L. ZURAWSKI (NASA, Lewis Research Center, Cleveland, OH) AIAA, ASME, SAE, and ASEE, Joint Propulsion Conference, 22nd, Huntsville, AL, June 16-18, 1986. 28 p. Previously announced in STAR as N86-28124. refs (AIAA PAPER 86-1698)

An analytical study was conducted to determine the specific-impulse advantages of adding metals to conventional liquid-bipropellant systems. These tripropellant systems theoretically offer higher specific impulse and increased propellant density compared with bipropellant systems. Metals considered were Be, Li, and Al. Bipropellant systems were H₂/O₂, N₂H₄/N₂O₄, RP-1/O₂, and H₂/F₂. Thermochemical calculations were performed for sea-level expansion from 6.895-MN/sq. m. (1000-Psia) chamber pressure over a wide range of mixture ratios and propellant compositions. Three-dimensional plots characterize the specific impulse of each tripropellant system. Technology issues pertinent to metallized propellant systems are discussed. Author

A86-49640*# Aerojet Technical Systems Co., Sacramento, Calif.

LONGITUDINAL MODE COMBUSTION INSTABILITIES OF A HIGH-PRESSURE FUEL-RICH LOX/RP-1 PREBURNER

J. J. FANG (Aerojet TechSystems Co., Sacramento, CA) Joint-Army-Navy-NASA-Air Force Interagency Propulsion Committee, Combustion Meeting, 22nd, California Institute of Technology, Pasadena, CA, Oct. 7-11, 1985, Paper. 14 p. refs (Contract NAS3-22647)

During the hot-fire testing of a high-pressure fuel-rich LOX/RP-1 preburner, longitudinal mode combustion instabilities were observed. This paper presents the experimental data showing how the instability varied with the chamber pressure, mixture ratio, chamber length and turbulence ring. Technical rationales are given

for the test-to-test hardware configuration changes that eventually led to the stable result. Author

N86-10279*# National Aeronautics and Space Administration. Lewis Research Center, Cleveland, Ohio.

COMPATIBILITY OF GRAIN-STABILIZED PLATINUM WITH CANDIDATE PROPELLANTS FOR RESISTOJETS

M. V. WHALEN and S. P. GRISNIK 1985 21 p refs Presented at the 18th Intern. Elec. Propulsion Conf., Alexandria, Va., 30 Sep. - 2 Oct. 1985; cosponsored by AIAA, DGLR and JSASS (NASA-TM-87118; E-2725; NAS 1.15:87118; AIAA-85-2014) Avail: NTIS HC A02/MF A01 CSCL 211

Resistojets are candidates for space station auxiliary propulsion, and should be characterized by both long life and multipropellant operations, requirements limited by available materials. Grain stabilized platinum is examined for use as a resistojet thruster material. Use of platinum in other applications indicates it can be used at moderately high temperatures for extended periods of time. Past results indicate that grain-stabilized platinum should be sufficiently inert in candidate propellant environments. Therefore, compatibility of platinum-yttria (P/Y₂O₃) and platinum-zirconia (Pt/ZrO₂) with carbon dioxide, methane, hydrogen and ammonia is examined. A series of 1000 hr tests in CO₂, H₂, and NH₃ is conducted at 1400 C and a series of 1000 hr tests in CH₄ is conducted at about 500 C. Scanning electron microscopy, Auger electron spectroscopy and depth profiling analysis are then used to determine the effects of propellants on the material surface, to evaluate possible material contamination and to evaluate grain growth. The results indicate that there is carbon deposition on the surface of the Pt/Y₂O₃ and Pt/ZrO₂ in both the CO₂ and CH₄ environments. In the H₂ environment, the Pt/Y₂O₃ and Pt/ZrO₂ specimen surfaces are roughened. After exposure to the NH₃ environment, the Pt/Y₂O₃ and Pt/ZrO₂ are roughened and pitted over the entire heated area with some pitted areas along the grain boundaries. SEM photos show grain growth in cross-sectional views of all the Pt/Y₂O₃ samples and the Pt/ZrO₂ samples, except that tested in methane. Mass loss measurements indicate that Pt/Y₂O₃ and Pt/ZrO₂ would last in excess of 200,000 hr in each propellant environment. However, in NH₃ both Pt/Y₂O₃ and Pt/ZrO₂ are severely pitted, with voids up to 50 percent into the material. Pt/Y₂O₃ and Pt/ZrO₂ are not recommended for high temperature service in NH₃. Author

N86-10280*# National Aeronautics and Space Administration. Lewis Research Center, Cleveland, Ohio.

RAPID EVALUATION OF ION THRUSTER LIFETIME USING OPTICAL EMISSION SPECTROSCOPY

B. A. ROCK (Arizona State Univ.), M. A. MANTENIEKS (Arizona State Univ.), and M. L. PARSONS 1985 47 p refs Presented at the 18th Intern. Elec. Propulsion Conf., Alexandria, Va., 30 Sep. - 2 Oct. 1985; cosponsored by AIAA, JSASS, and DGLR (NASA-TM-87103; E-2700; NAS 1.15:87103; AIAA-85-2011) Avail: NTIS HC A03/MF A01 CSCL 21H

A major life-limiting phenomenon of electric thrusters is the sputter erosion of discharge chamber components. Thrusters for space propulsion are required to operate for extended periods of time, usually in excess of 10,000 hr. Lengthy and very costly life-tests in high-vacuum facilities have been required in the past to determine the erosion rates of thruster components. Alternative methods for determining erosion rates which can be performed in relatively short periods of time at considerably lower costs are studied. An attempt to relate optical emission intensity from an ion bombarded surface (screen grid) to the sputtering rate of that surface is made. The model used a kinetic steady-state (KSS) approach, balancing the rates of population and depopulation of ten low-lying excited states of the sputtered molybdenum atom (Mo) with those of the ground state to relate the spectral intensities of the various transitions of the MoI to the population densities. Once this is accomplished, the population density can be related to the sputtering rate of the target. Radiative and collisional modes of excitation and decay are considered. Since actual data has not been published for MoI excitation rate and decay constants, semiempirical equations are used. The calculated sputtering rate

and intensity is compared to the measured intensity and sputtering rates of the 8 and 30 cm ion thrusters. Author

N86-10281*# National Aeronautics and Space Administration. Lewis Research Center, Cleveland, Ohio.

EXPERIMENTAL PERFORMANCE OF A 1-KILOWATT ARCJET THRUSTER

S. NAKANISHI 1985 30 p refs
(NASA-TM-87131; E-2744; NAS 1.15:87131) Avail: NTIS HC A03/MF A01 CSCL 21C

A formerly unused cathode and anode/nozzle assembly from a flight model arcjet was tested with nitrogen, hydrogen, and nitrogen-hydrogen mixture simulating ammonia decomposition products at arc power levels from about 300 to 950 W. Two different power sources and two nozzle configurations were tested at low back-ground pressures to exclude facility effects. Increased nozzle expansion ratio improved cold flow nozzle efficiency from 0.8 to 0.9. Hydrogen thrust efficiency of 0.26 at 872 sec specific impulse matched some 1964 performance on a similar device. Simulated ammonia thrust efficiency was 0.31 at 422 sec. Spontaneously occurring voltage mode changes at constant arc current could be partially stabilized with appropriate power source characteristics. In the higher voltage mode specific impulse was higher, but thrust efficiency changed only slightly from that of the lower voltage mode. Sustained tests of up to 2 hr duration exhibited no apparent performance degradation with time. Author

N86-11224*# National Aeronautics and Space Administration. Lewis Research Center, Cleveland, Ohio.

AN EXPERIMENTAL STUDY OF ENERGY LOSS MECHANISMS AND EFFICIENCY CONSIDERATION IN THE LOW POWER DC ARCJET

F. M. CURRAN 1985 24 p refs Presented at the 18th Intern. Elec. Propulsion Conf., Alexandria, Va., 30 Sep. - 2 Oct. 1985; sponsored by AIAA, JSASS, and DGLR
(NASA-TM-87123; E-2733; NAS 1.15:87123; AIAA-85-2017)
Avail: NTIS HC A02/MF A01 CSCL 21C

The potential utility of the low power dc arcjet in auxiliary propulsion was investigated. It was indicated that improvements in the areas of stability, energy efficiency, reliability, and electrode erosion are necessary to obtain a useful device. A water-cooled arcjet simulator was tested to investigate both the energy loss mechanisms at the electrodes and the stability of different conventional arcjet configurations in the presence of a vortex flow field. It is shown that in certain configurations only 25 to 30% of the input energy is lost to the electrodes. It is also shown that vortex stabilization is not difficult to obtain in many cases at the flow rates used and that a careful starting procedure is effective in minimizing electrode damage. E.A.K.

N86-15339*# Boeing Aerospace Co., Seattle, Wash.
SPACE STATION PROPULSION REQUIREMENTS STUDY Final Report

C. L. WILKINSON and S. M. BRENNAN Aug. 1985 484 p
(Contract NAS3-23353)
(NASA-CR-174934; NAS 1.26:174934; D180-28264-1) Avail: NTIS HC A21/MF A01 CSCL 21H

Propulsion system requirements to support Low Earth Orbit (LEO) manned space station development and evolution over a wide range of potential capabilities and for a variety of STS servicing and space station operating strategies are described. The term space station and the overall space station configuration refers, for the purpose of this report, to a group of potential LEO spacecraft that support the overall space station mission. The group consisted of the central space station at 28.5 deg or 90 deg inclinations, unmanned free-flying spacecraft that are both tethered and untethered, a short-range servicing vehicle, and a longer range servicing vehicle capable of GEO payload transfer. The time phasing for preferred propulsion technology approaches is also investigated, as well as the high-leverage, state-of-the-art advancements needed, and the qualitative and quantitative benefits of these advancements on STS/space station operations. The

time frame of propulsion technologies applicable to this study is the early 1990's to approximately the year 2000. Author

N86-16258*# National Aeronautics and Space Administration. Lewis Research Center, Cleveland, Ohio.

RELIABILITY AND MASS ANALYSIS OF DYNAMIC POWER CONVERSION SYSTEMS WITH PARALLEL OF STANDBY REDUNDANCY

A. J. JUHASZ and H. S. BLOOMFIELD 1985 16 p refs
Presented at the 2nd Symposium on Space Nuclear Power Systems, Albuquerque, N. Mex., 14-16 Jan. 1985; sponsored by New Mexico Univ.
(NASA-TM-87189; E-2668; NAS 1.15:87189) Avail: NTIS HC A02/MF A01 CSCL 21F

A combinatorial reliability approach is used to identify potential dynamic power conversion systems for space mission applications. A reliability and mass analysis is also performed, specifically for a 100 kWe nuclear Brayton power conversion system with parallel redundancy. Although this study is done for a reactor outlet temperature of 1100K, preliminary system mass estimates are also included for reactor outlet temperatures ranging up to 1500 K.

Author

N86-16259*# Little (Arthur D.), Inc., Cambridge, Mass.

LIQUID BELT RADIATOR DESIGN STUDY Final Report

W. P. TEAGAN and K. F. FITZGERALD Jan. 1986 53 p refs
(Contract NAS3-23889)
(NASA-CR-174901; NAS 1.26:174901) Avail: NTIS HC A04/MF A01 CSCL 22B

The Liquid Belt Radiator (LBR) is an advanced concept developed to meet the needs of anticipated future space missions. A previous study documented the advantages of this concept as a lightweight, easily deployable alternative to present day space heat rejection systems. The technical efforts associated with this study concentrate on refining the concept of the LBR as well as examining the issues of belt dynamics and potential application of the LBR to intermediate and high temperature heat rejection applications. A low temperature point design developed in previous work is updated assuming the use of diffusion pump oil, Santovac-6, as the heat transfer media. Additional analytical and design effort is directed toward determining the impact of interface heat exchanger, fluid bath sealing, and belt drive mechanism designs on system performance and mass. The updated design supports the earlier result by indicating a significant reduction in system specific system mass as compared to heat pipe or pumped fluid radiator concepts currently under consideration (1.3 kg/sq m versus 5 kg/sq m).

Author

N86-17386*# National Aeronautics and Space Administration. Lewis Research Center, Cleveland, Ohio.

SMALL, TWO-STAGE, PARTIAL-ADMISSION TURBINE

R. F. SUTTON (Rockwell International Corp., Canoga Park, Calif.), J. L. BOYNTON (Rockwell International Corp., Canoga Park, Calif.), and D. SCHEER /in Johns Hopkins Univ. The 1985 JANNAF Propulsion Meeting, Volume 1 p 55-62 Apr. 1985 Sponsored in part by NASA

Avail: Chemical Propulsion Information Agency, Johns Hopkins Rd., Laurel, Md. 20707 HC \$78.98 CSCL 21H

The Rocketdyne Orbital Transfer Vehicle (OTV) cryogenic, rocket engine system, high pressure, liquid hydrogen turbopump was designed with a two-stage, partial-admission axial turbine. The turbine is basically two single-stage, partial-admission, subsonic impulse stages designed so the kinetic energy leaving the first-stage rotor is discharged directly into the second-stage nozzle at nominal operation to minimize staging losses. Very little data were available in the literature for this type of turbine design. Therefore, it was decided to test a full-size model of the turbine design using ambient-temperature gaseous nitrogen as the working fluid. The tester design features a variable orientation second-stage nozzle to determine the optimum circumferential location for highest performance. The tester also features the capability to vary the nozzle arcs of admission and incorporates quartz windows to study the flowfield upstream of the second-stage nozzle using a laser

20 SPACECRAFT PROPULSION AND POWER

velocimeter. The test operations will probe the efficiency and flow characteristics for three arcs of admission and the effects of second-stage nozzle circumferential orientations over wide ranges of speed and pressure ratios as well as the interstage pressure distributions. Author

N86-17387*# National Aeronautics and Space Administration. White Sands Test Facility, N. Mex.

AN EXPERIMENTAL DATA BASE FOR MATERIAL SELECTION AND DESIGN OF HIGH-SPEED, HIGH-PRESSURE, OXYGEN TURBOMACHINERY

L. SCHOENMAN (Aerojet TechSystems Co., Sacramento, Calif.) and J. M. STOLTZFUS /in Johns Hopkins Univ. The 1985 JANNAP Propulsion Meeting, Volume 1 p 63-77 Apr. 1985 refs

(Contract NAS3-23772)

Avail: Chemical Propulsion Information Agency, Johns Hopkins Rd., Laurel, Md. 20707 HC \$78.98 CSCL 21H

New technologies for space-based, reusable, throttleable, cryogenic, orbit transfer propulsion are being evaluated. A variable-thrust (200 to 3000 lbf), 2000 psi chamber pressure, LO₂/LH₂ engine has been selected to demonstrate the 20-hour, 500-restart life goal, and a specific impulse of 480 lbf-sec/lbM. The advanced design uses warm oxygen to power a fully integrated turbopump that delivers 4500 psi LO₂. The selected engine cycle provides the following advantages over conventional expander cycle designs which use H₂ to drive the LH₂ and LO₂ pumps; higher engine operating pressures and performance in a smaller envelope, lower turbine operating temperatures, elimination of interpropellant seals and purges, and an extended throttling range. The design approach and results of testing to characterize materials for use in high-pressure gaseous oxygen are discussed. Test methods include particle impact testing in a sonic-flow, hot GO₂ streams and forced, high-speed friction rubbing testing. Materials are exposed to oxygen and nitrogen atmospheres at pressures of 100, 1000, and 3000 psi to identify separately the gas cooling effects from the metal oxidation effects at the rubbing surface. The selection of candidate design materials is based on an analytical parameter defined as the burn factor. Typical materials tested include carbon steel, stainless steel, nickel, copper, and monel alloys. Author

N86-17397*# National Aeronautics and Space Administration. Lewis Research Center, Cleveland, Ohio.

LOX/LH₂ VANE PUMP FOR AUXILIARY PROPULSION SYSTEMS

J. A. HEMMINGER and T. E. ULBRICHT /in Johns Hopkins Univ. The 1985 JANNAP Propulsion Meeting, Volume 1 p 161-170 Apr. 1985 refs Sponsored in part by NASA

Avail: Chemical Propulsion Information Agency, Johns Hopkins Rd., Laurel, Md. 20707 HC \$78.98 CSCL 21H

Positive displacement pumps offer potential efficiency advantages over centrifugal pumps for future low thrust space missions. Low flow rate applications, such as space station auxiliary propulsion or dedicated low thrust orbiter transfer vehicles, are typical of missions where low flow and high head rise challenge centrifugal pumps. The positive displacement vane pump for pumping of LOX and LH₂ is investigated. This effort has included: (1) a testing program in which pump performance was investigated for differing pump clearances and for differing pump materials while pumping LN₂, LOX, and LH₂; and (2) an analysis effort, in which a comprehensive pump performance analysis computer code was developed and exercised. An overview of the theoretical framework of the performance analysis computer code is presented, along with a summary of analysis results. Experimental results are presented for pump operating in liquid nitrogen. Included are data on the effects on pump performance of pump clearance, speed, and pressure rise. Pump suction performance is also presented. Author

N86-17404*# National Aeronautics and Space Administration. Lewis Research Center, Cleveland, Ohio.

CYCLIC STRUCTURAL ANALYSES OF ANISOTROPIC TURBINE BLADES FOR REUSABLE SPACE PROPULSION SYSTEMS

J. M. MANDERSCHIED and A. KAUFMAN /in Johns Hopkins Univ. The 1985 JANNAP Propulsion Meeting, Volume 1 p 237-245 Apr. 1985 Sponsored in part by NASA

Avail: Chemical Propulsion Information Agency, Johns Hopkins Rd., Laurel, Md. 20707 HC \$78.98 CSCL 21H

Turbine blades for reusable space propulsion systems are subjects to severe thermomechanical loading cycles that result in large inelastic strains and very short lives. These components require the use of anisotropic high temperature alloys to meet the safety and durability requirements of such systems. To assess the effects on blade life of material anisotropy, cyclic structural analyses are being performed for the first stage high pressure fuel turbopump blade (HPFTB) of the space shuttle main engine (SSME). The blade alloy is directionally solidified MAR-M 246 alloy. The analyses are based on a typical test stand engine cycle. Stress-strain histories at the airfoil critical location are computed using the MARC nonlinear finite element computer code. Author

N86-17405*# National Aeronautics and Space Administration. Lewis Research Center, Cleveland, Ohio.

ADVANCED RESEARCH AND TECHNOLOGY PROGRAM FOR ADVANCED HIGH PRESSURE OXYGEN-HYDROGEN ROCKET PROPULSION

S. J. MARSIK and S. F. MOREA (NASA. Marshall Space Flight Center, Huntsville, Ala.) /in Johns Hopkins Univ. The 1985 JANNAP Propulsion Meeting, Volume 1 p 247-256 Apr. 1985 refs Previously announced as N85-21231 Sponsored in part by NASA

Avail: Chemical Propulsion Information Agency, Johns Hopkins Rd., Laurel, Md. 20707 HC \$78.98 CSCL 21H

A research and technology program for advanced high pressure, oxygen-hydrogen rocket propulsion technology is presently being pursued by the National Aeronautics and Space Administration (NASA) to establish the basic discipline technologies, develop the analytical tools, and establish the data base necessary for an orderly evolution of the staged combustion reusable rocket engine. The need for the program is based on the premise that the USA will depend on the Shuttle and its derivative versions as its principal Earth-to-orbit transportation system for the next 20 to 30 yr. The program is focused in three principal areas of enhancement: (1) life extension, (2) performance, and (3) operations and diagnosis. Within the technological disciplines the efforts include: rotordynamics, structural dynamics, fluid and gas dynamics, materials fatigue/fracture/life, turbomachinery fluid mechanics, ignition/combustion processes, manufacturing/productibility/non-destructive evaluation methods and materials development/evaluation. An overview of the Advanced High Pressure Oxygen-Hydrogen Rocket Propulsion Technology Program Structure and Working Groups objectives are presented with highlights of several significant achievements. Author

N86-17416*# General Dynamics/Convair, San Diego, Calif.

ORBITAL TRANSFER VEHICLE ENGINE INTEGRATION STUDY

W. J. KETCHUM /in Johns Hopkins Univ. The 1985 JANNAP Propulsion Meeting, Volume 1 p 375-382 Apr. 1985 Prepared in cooperation with Aerojet Techsystems Co., Sacramento, Calif. (Contract NAS3-23772)

Avail: Chemical Propulsion Information Agency, Johns Hopkins Rd., Laurel, Md. 20707 HC \$78.98 CSCL 21H

Industry studies were undertaken to establish the technology base for an advanced engine for Orbital Transfer Vehicles for mid-1990s IOC. This paper presents the results of a study conducted by General Dynamics Convair Division, under contract to Aerojet TechSystems Company for NASA-LeRC, to define requirements, interface conditions, and operational design criteria for new LO₂/LH₂ propulsion systems applicable to future Orbit Transfer Vehicles, and to assess the impacts of space basing, man rating, and low-g transfer on propulsion system design

requirements. The primary study emphasis was to determine what the OTV engine thrust level should be, how many engines are required on the OTV, and how the OTV engine should be designed. This was accomplished by evaluating planned OTV missions and concepts to determine the requirements for the OTV propulsion system, conducting tradeoffs and comparisons to optimize OTV capability, and evaluating reliability and maintenance to determine the recommended OTV engine design for future development.

Author

N86-17425*# National Aeronautics and Space Administration. Lewis Research Center, Cleveland, Ohio.

VACUUM CHAMBER PRESSURE EFFECTS ON THRUST MEASUREMENTS

J. S. SOVEY, P. F. PENKO, S. P. GRISNIK, and M. V. WHALEN *In* Johns Hopkins Univ. The 1985 JANNAF Propulsion Meeting, Volume 1 p 469-474 Apr. 1985 refs Previously announced as N85-21259 Sponsored in part by NASA
 Avail: Chemical Propulsion Information Agency, Johns Hopkins Rd., Laurel, Md. 20707 HC \$78.98 CSCL 21H

Tests were conducted to investigate the effect of vacuum facility pressure on the performance of small thruster nozzles. Thrust measurements of two converging-diverging nozzles with an area ratio of 140 and an orifice plate flowing unheated nitrogen and hydrogen were taken over a wide range of vacuum facility pressures and nozzle throat Reynolds numbers. In the Reynolds number range of 2200 to 12,000 there was no discernable viscous effect on thrust below an ambient to total pressure ratio of 1000. In nearly all cases, flow separation occurred at a pressure ratio of about 1000. This was the upper limit for obtaining an accurate thrust measurement for a conical nozzle with an area ratio of 140.

Author

N86-17426*# National Aeronautics and Space Administration. Lewis Research Center, Cleveland, Ohio.

COMPATIBILITY EXPERIMENTS OF FACILITIES, MATERIALS, AND PROPELLANTS FOR ELECTROTHERMAL THRUSTERS

M. V. WHALEN, S. P. GRISNIK, and J. S. SOVEY *In* Johns Hopkins Univ. The 1985 JANNAF Propulsion Meeting, Volume 1 p 475-484 Apr. 1985 refs Previously announced as N85-21260 Sponsored in part by NASA
 Avail: Chemical Propulsion Information Agency, Johns Hopkins Rd., Laurel, Md. 20707 HC \$78.98 CSCL 21H

Experiments were performed to determine the compatibility of materials and propellants for electro-thermal thrusters. Candidate propellants for resistojets propulsion include carbon dioxide, methane, hydrogen, ammonia, and hydrazine. The materials being examined are grain stabilized platinum for resistojets for space station and rhenium for high performance resistojets for satellites. Heater mass loss and deterioration of materials were evaluated. A coiled tube of platinum, with yttria dispersed throughout the base material to inhibit grain growth, was tested in carbon dioxide at 1300 C for 2000 hr. Post-test examination indicated the platinum-yttria heater would last over 100,000 hr with less than 10 percent mass loss. Short-term compatibility tests were conducted to test the integrity of the platinum-yttria in hydrogen, methane, carbon dioxide/methane mixtures and ammonia environments. In each of these 100 hr tests, the platinum-yttria mass change indicated a minimum coil life of 100,000 hr. Facility related effects were investigated in materials tests using rhenium heated to high temperatures. Vacuum facility water reduction was monitored using a mass spectrometer. In vacuum environments obtained using only diffusion pumping and those obtained with the assistance of cryogenic equipment there were mass gains in the rhenium heaters. These mass gains were the result of the high amount of oxygen and water contained in the gas. Propellant purity and preferred test facility environments are discussed.

G.L.C.

N86-17869*# National Aeronautics and Space Administration. Lewis Research Center, Cleveland, Ohio.

SPACE STATION POWER MANAGEMENT AND DISTRIBUTION
 F. TEREN *In* its Space Photovoltaic Research and Technology 1985 p 279-285 1985

Avail: NTIS HC A13/MF A01 CSCL 10B

The power system architecture is presented by a series of schematics which illustrate the power management and distribution (PMAD) system at the component level, including converters, controllers, switchgear, rotary power transfer devices, power and data cables, remote power controllers, and load converters. Power distribution options, reference power management, and control strategy are also outlined. A summary of advanced development status and plans and an overview of system test plans are presented.

E.A.K.

N86-20493*# General Dynamics/Convair, San Diego, Calif. Advanced Space Programs.

ORBITAL TRANSFER VEHICLE ENGINE INTEGRATION STUDY Final Report

W. J. KETCHUM 30 Nov. 1984 51 p refs
 (Contract NAS3-23772; NASA ORDER L-814740)
 (NASA-CR-174842; NAS 1.26:174842; GDC-SP-84-050) Avail:
 NTIS HC A04/MF A01 CSCL 21H

NASA-LeRC is sponsoring industry studies to establish the technology base for an advanced engine for orbital transfer vehicles for mid-1990s IOC. Engine contractors are being assisted by vehicle contractors to define the requirements, interface conditions, and operational design criteria for new LO2-LH2 propulsion systems applicable to future orbit transfer vehicles and to assess the impacts on space basing, man rating, and low-G transfer missions on propulsion system design requirements. The results of a study is presented. The primary study emphasis was to determine what the OTV engine thrust level should be, how many engines are required on the OTV, and how the OTV engine should be designed. This was accomplished by evaluating planned OTV missions and concepts to determine the requirements for the OTV propulsion system, conducting tradeoffs and comparisons to optimize OTV capability, and evaluating reliability and maintenance to determine the recommended OTV engine design for future development.

Author

N86-20497*# Solar Turbines International, San Diego, Calif.
ROCKET THRUST CHAMBER THERMAL BARRIER COATINGS Final Report, Dec. 1981 - Oct. 1984

A. P. BATAKIS and J. W. VOGAN Jul. 1985 169 p refs
 (Contract NAS3-23262)
 (NASA-CR-175022; NAS 1.26:175022; SR85-R-5052-16) Avail:
 NTIS HC A08/MF A01 CSCL 21H

A research program was conducted to generate data and develop analytical techniques to predict the performance and reliability of ceramic thermal barrier coatings in high heat flux environments. A finite element model was used to analyze the thermomechanical behavior of coating systems in rocket thrust chambers. Candidate coating systems (using a copper substrate, NiCrAlY bond coat and ZrO₂.8Y₂O₃ ceramic overcoat) were selected for detailed study based on photomicrographic evaluations of experimental test specimens. The effects of plasma spray application parameters on the material properties of these coatings were measured and the effects on coating performance evaluated using the finite element model. Coating design curves which define acceptable operating envelopes for selected coating systems were constructed based on temperature and strain limitations. Spray gun power levels was found to have the most significant effect on coating structure. Three coating systems were selected for study using different power levels. Thermal conductivity, strain tolerance, density, and residual stress were measured for these coatings. Analyses indicated that extremely thin coatings (0.02 mm) are required to accommodate the high heat flux of a rocket thrust chamber and ensure structural integrity.

Author

20 SPACECRAFT PROPULSION AND POWER

N86-21577*# National Aeronautics and Space Administration. Lewis Research Center, Cleveland, Ohio.

TECHNOLOGY FOR BRAYTON-CYCLE POWERPLANTS USING SOLAR AND NUCLEAR ENERGY

R. E. ENGLISH Feb. 1986 15 p refs
(NASA-TP-2558; E-2761; NAS 1.60:2558) Avail: NTIS HC A02/MF A01 CSCL 10B

Brayton cycle gas turbines have the potential to use either solar heat or nuclear reactors for generating from tens of kilowatts to tens of megawatts of power in space, all this from a single technology for the power generating system. Their development could be the first step in an evolution of such powerplants for a very wide range of applications. At the low power level of only 10 kW, a power generating system has already demonstrated overall efficiency of 0.29 and operated 38 000 hr. Tests of improved components show that these components would raise that efficiency to 0.32, a value twice that demonstrated by any alternate concept. Because of this high efficiency, solar Brayton cycle power generators offer the potential to increase power per unit of solar collector area to levels exceeding four times that from photovoltaic powerplants using present technology for silicon solar cells. The technologies for solar mirrors and heat receivers are reviewed and assessed. This Brayton technology for solar powerplants is equally suitable for use with the nuclear reactors. The available long time creep data on the tantalum alloy ASTAR-811C show that such Brayton cycles can evolve to cycle peak temperatures of 1500 K (2240 F). And this same technology can be extended to generate 10 to 100 MW in space by exploiting existing technology for terrestrial gas turbines in the fields of both aircraft propulsion and stationary power generation.

Author

N86-21578*# National Aeronautics and Space Administration. Lewis Research Center, Cleveland, Ohio.

A BIBLIOGRAPHY OF ELECTROTHERMAL THRUSTER TECHNOLOGY, 1984

J. S. SOVEY, T. L. HARDY, and M. ENGLEHART (Paper Basics, Brookpark, Ohio) Mar. 1986 49 p
(NASA-TM-86998; E-2536; NAS 1.15:86998) Avail: NTIS HC A03/MF A01 CSCL 21C

Electrothermal propulsion concepts are briefly discussed as an introduction to a bibliography and author index. Nearly 700 citations are given for resistojets, thermal arcjets, pulsed electrothermal thrusters, microwave heated devices, solar thermal thrusters, and laser thermal thrusters.

Author

N86-24746*# Martin Marietta Aerospace, Denver, Colo. **ADVANCED ORBIT TRANSFER VEHICLE PROPULSION SYSTEM STUDY Final Report**

J. A. CATHCART, T. W. COOPER, R. M. CORRINGTON, S. T. CRONAU, S. C. FORGIE, M. J. HARDER, J. G. MCALLISTER, T. J. RUDMAN, V. W. STONEBACK et al. Feb. 1985 174 p refs
(Contract NAS3-23858)
(NASA-CR-174843; NAS 1.26:174843) Avail: NTIS HC A08/MF A01 CSCL 21H

A reusable orbit transfer vehicle concept was defined and subsequent recommendations for the design criteria of an advanced LO₂/LH₂ engine were presented. The major characteristics of the vehicle preliminary design include a low lift to drag aerocapture capability, main propulsion system failure criteria of fail operational/fail safe, and either two main engines with an attitude control system for backup or three main engines to meet the failure criteria. A maintenance and servicing approach was also established for the advanced vehicle and engine concepts. Design tradeoff study conclusions were based on the consideration of reliability, performance, life cycle costs, and mission flexibility.

B.G.

N86-24747*# National Aeronautics and Space Administration. Lewis Research Center, Cleveland, Ohio.

SPACE STATION 20-KHZ POWER MANAGEMENT AND DISTRIBUTION SYSTEM

I. G. HANSEN and G. R. SUNDBERG 1986 11 p refs
Presented at the Power Electronics Specialists Conference, Vancouver, British Columbia, 23-27 Jun. 1986; sponsored by Inst. of Electrical and Electronics Engineers
(NASA-TM-87314; E-3045; NAS 1.15:87314) Avail: NTIS HC A02/MF A01 CSCL 22B

During the conceptual design phase a 20-kHz power distribution system was selected as the reference for the space station. The system is single-phase 400 VRMS, with a sinusoidal wave form. The initial user power level will be 75 kW with growth to 300 kW. The high-frequency system selection was based upon considerations of efficiency, weight, safety, ease of control, interface with computers, and ease of paralleling for growth. Each of these aspects will be discussed as well as the associated trade-offs involved. An advanced development program has been instituted to accelerate the maturation of the high-frequency system. Some technical aspects of the advanced development will be discussed.

Author

N86-24748*# National Aeronautics and Space Administration. Lewis Research Center, Cleveland, Ohio.

PERFORMANCE AND ENDURANCE TESTS OF A MULTIPROPELLANT RESISTOJET FOR SPACE STATION AUXILIARY PROPULSION

W. E. MORREN, M. V. WHALEN, and J. S. SOVEY 1986 19 p refs
Presented at the 22nd Joint Propulsion Conference, Huntsville, Ala., 16-18 Jun. 1986; sponsored by AIAA, ASME, SAE, and ASEE
(NASA-TM-87278; E-2981; NAS 1.15:87278) Avail: NTIS HC A02/MF A01 CSCL 21H

This paper presents the results of an effort to demonstrate the technology readiness of a long-life multipropellant resistojet for space station auxiliary propulsion. Experiments were performed to evaluate the compatibility of grain-stabilized platinum tubes at temperatures up to 1400 deg C in environments of CO₂, CH₄, NH₃, H₂O, and H₂. All samples tested showed extrapolated lifetimes in excess of 10,000 hr based on 10 percent mass loss as end-of-life. However, samples tested in an ammonia atmosphere at 1400 deg C showed severe pitting, which raised concerns about the compatibility of grain-stabilized platinum with ammonia-containing atmospheres. Additional tests showed that reducing the metal temperature to about 900 deg C (+ or - 100 deg C) significantly reduced this adverse effect.

Author

N86-24749*# National Aeronautics and Space Administration. Lewis Research Center, Cleveland, Ohio.

NASA ELECTROTHERMAL AUXILIARY PROPULSION TECHNOLOGY

J. R. STONE 1986 26 p refs
Presented at the 22nd Joint Propulsion Conference, Huntsville, Ala., 16-18 Jun. 1986; sponsored by AIAA, ASME, SAE and ASEE
(NASA-TM-87281; E-2986; NAS 1.15:87281; AIAA-86-1703)
Avail: NTIS HC A02/MF A01 CSCL 21H

Electrothermal auxiliary propulsion systems provide high performance options which can have major mission benefits. There are several electrothermal concepts which offer a range of characteristics and benefits. Resistojets are the highest thrust to power option and are currently operational at mission average values of specific impulse, I_{sp} approximately 295 sec. Long life, multipropellant resistojets are being developed for the space station, and resistojets technology advancements are being pursued to improve the I_{sp} by more than 20 percent for resistojets used in satellite applications. Direct current arcjets have the potential of I_{sp} over 400 sec with storable propellants and should provide over 1000 sec with hydrogen. Advanced concepts are being investigated to provide high power density options and possible growth to primary propulsion applications. Broad based experimental and analytical research and technology programs of

NASA are summarized and recent significant advances are reviewed. Author

N86-25407*# National Aeronautics and Space Administration. Lewis Research Center, Cleveland, Ohio.

LOWER POWER DC ARCJET OPERATIONS WITH HYDROGEN HYDROGEN/NITROGEN PROPELLANT MIXTURES

F. M. CURRAN and S. NAKANISHI (Analex Corp., Cleveland, Ohio) 1986 23 p refs Presented at 22nd Joint Propulsion Conference, Huntsville, Ala., 16-18 Jun. 1986; sponsored by AIAA, ASME, SAE and American Society for Ecological Education (NASA-TM-87279; E-2982; NAS 1.15:87279) Avail: NTIS HC A02/MF A01 CSCL 21H

The arcjet assembly from a flight model system was modified with a new thoriated tungsten nozzle insert and has been tested with hydrogen-nitrogen mixtures simulating the decomposition products of ammonia and hydrazine. Arcjet power consumption ranged from 0.7 to 1.15 kW depending on low rate, input current, and mixture composition. At a nominal 1 kW power level the ammonia mixtures thrust efficiency was about 0.31 at specific impulse values ranging between 460 and 500 sec. Hydrazine mixtures gave similar thrust efficiencies at the same power level with specific impulse values between 395 and 430 sec. Large, spontaneous voltage mode changes were not observed once the thruster had passed a period of instability immediately following start up. This period of instability, and the startup at low pressure, were seen as major causes of constrictor damage during the tests. Author

N86-25408*# National Aeronautics and Space Administration. Lewis Research Center, Cleveland, Ohio.

STRUCTURAL INTEGRITY AND DURABILITY FOR SPACE SHUTTLE MAIN ENGINE AND FUTURE REUSABLE SPACE PROPULSION SYSTEMS

S. J. MARSIK and H. T. GAWRYLOWICZ 1986 18 p refs Presented at the 22nd Joint Propulsion Conference, Huntsville, Alabama, 16-18 Jun. 1986; sponsored by AIAA, ASME, SAE, and ASEE (NASA-TM-87280; E-2983; NAS 1.15:87280) Avail: NTIS HC A02/MF A01 CSCL 21H

NASA is conducting a program which will establish a technology base for the orderly evolution of reusable space propulsion systems. As part of that program, NASA initiated a Structural Integrity and Durability effort for advanced high-pressure oxygen-hydrogen rocket engine technology. That effort focuses on the development of: (1) accurate analytical models to describe flow fields; aerothermodynamic loads; structural responses; and fatigue/fracture, from which life prediction codes can be evolved; and (2) advanced instrumentation with capabilities to verify the codes in an SSME-like environment as well as the potential for future use as diagnostic sensors for real-time condition monitoring of critical engine components. Author

N86-25409*# National Aeronautics and Space Administration. Lewis Research Center, Cleveland, Ohio.

POWER ELECTRONICS FOR A 1-KILOWATT ARC JET THRUSTER

R. P. GRUBER 1986 23 p refs Presented at the 22nd Joint Propulsion Conference, Huntsville, Ala., 16-18 Jun. 1986; sponsored by AIAA, ASME, SAE and ASEE (NASA-TM-87340; E-3089; NAS 1.15:87340) Avail: NTIS HC A02/MF A01 CSCL 21H

After more than two decades, new space mission requirements have revived interest in arcjet systems. The preliminary development and demonstration of new, high efficiency, power electronic concepts for start up and steady state control of dc arcjets is reported. The design comprises a pulse width modulated power converter which is closed loop configured to give fast current control. An inductor, in series with the arcjet, serves the dual role of providing instantaneous current control, as well as a high voltage arc ignition pulse. Benchmark efficiency, transient response, regulation, and ripple data are presented. Tests with arcjets demonstrate that the power electronics breadboard can start

thrusters consistently with no apparent damage and transfer reliably to the nondestructive high voltage arc mode in less than a second. Author

N86-26369*# Rockwell International Corp., Canoga Park, Calif. Rocketdyne Div.

ORBIT TRANSFER ROCKET ENGINE TECHNOLOGY PROGRAM: ADVANCED ENGINE STUDY, TASK D.1/D.3 Interim Report

A. MARTINEZ, C. ERICKSON, and B. HINES Jan. 1986 237 p (Contract NAS3-23773) (NASA-CR-175084; NAS 1.26:175084; RI/RD86-116) Avail: NTIS HC A11/MF A01 CSCL 21H

Concepts for space maintainability of OTV engines were examined. An engine design was developed which was driven by space maintenance requirements and by a failure mode and effects (FME) analysis. Modularity within the engine was shown to offer cost benefits and improved space maintenance capabilities. Space operable disconnects were conceptualized for both engine change-out and for module replacement. Through FME mitigation the modules were conceptualized to contain the least reliable and most often replaced engine components. A preliminary space maintenance plan was developed around a controls and condition monitoring system using advanced sensors, controls, and condition monitoring concepts. A complete engine layout was prepared satisfying current vehicle requirements and utilizing projected component advanced technologies. A technology plan for developing the required technology was assembled. Author

N86-27418*# Sverdrup Technology, Inc., Cleveland, Ohio.

CHARACTERIZATION OF REAL GAS PROPERTIES FOR SPACE SHUTTLE MAIN ENGINE FUEL TURBINE AND PERFORMANCE CALCULATIONS Final Report

G. J. HARLOFF Jun. 1986 97 p (Contract NAS3-24105) (NASA-CR-175066; E-2938; NAS 1.26:175066) Avail: NTIS HC A05/MF A01 CSCL 21H

Real thermodynamic and transport properties of hydrogen, steam, the SSME mixture, and air are developed. The SSME mixture properties are needed for the analysis of the space shuttle main engine fuel turbine. The mixture conditions for the gases, except air, are presented graphically over a temperature range from 800 to 1200 K, and a pressure range from 1 to 500 atm. Air properties are given over a temperature range of 320 to 500 K, which are within the bounds of the thermodynamics programs used, in order to provide mixture data which is more easily checked (than H₂/H₂O). The real gas property variation of the SSME mixture is quantified. Polynomial expressions, needed for future computer analysis, for viscosity, Prandtl number, and thermal conductivity are given for the H₂/H₂O SSME fuel turbine mixture at a pressure of 305 atm over a range of temperatures from 950 to 1140 K. These conditions are representative of the SSME turbine operation. Performance calculations are presented for the space shuttle main engine (SSME) fuel turbine. The calculations use the air equivalent concept. Progress towards obtaining the capability to evaluate the performance of the SSME fuel turbine, with the H₂/H₂O mixture, is described. Author

N86-27419*# Iowa Univ., Iowa City. Dept. of Physics and Astronomy.

IMPROVEMENT OF ION THRUSTER DESIGN Final Report

R. T. CARPENTER 1986 139 p (Contract NAG3-206) (NASA-CR-177223; NAS 1.26:177223) Avail: NTIS HC A07/MF A01 CSCL 21C

Two types of measurements were performed on ion thrusters equipped with SmCo magnets in either ring cusp or line cusp arrangements. Langmuir probes were used to measure plasma potential, electron density, and electron temperature in all regions inside the thruster. Loss fluxes to various surfaces were determined by measuring the currents to foils attached to or imbedded in the surface. Data were obtained for several sets of discharge voltages and currents. The loss currents were determined from current vs

20 SPACECRAFT PROPULSION AND POWER

voltage characteristics observed on a transistor curve tracer oscilloscope. Both ion and electron currents were measured to all parts of the walls and to all parts of the cathode assembly using collecting plates. These measurements were also made for various parameter sets. In line cusp configuration the plasma density is essentially as predicted by existing calculations. In the ring cusp arrangement the interior of the plasma contains an inhomogeneous and relatively large magnetic field so the geometry is decidedly two-dimensional and the models of Self (1967) and of Kino and Sham (1966) do not agree. B.G.

N86-28122*# National Aeronautics and Space Administration. Lewis Research Center, Cleveland, Ohio.

A 20 KILOHERTZ SPACE STATION POWER SYSTEM

I. G. HANSEN and F. J. WOLFF 1986 10 p Proposed for presentation at the 19th Annual Electronics and Aerospace Conference, Washington, D.C., 9 Sep. 1986; sponsored by IEEE (NASA-TM-88801; E-3140; NAS 1.15:88801) Avail: NTIS HC A02/MF A01 CSCL 10B

The space station represents the next major U.S. commitment in space. The efficient delivery of power to multiple user loads is key to that success. In 1969, NASA Lewis Research Center began a series of studies with component and circuit developments that led to the high frequency, bi-directional, four quadrant resonant driven converter. Additional studies and subsequent developments into the early 1980's have shown how the high frequency ac power system could provide overall advantages to many aerospace power systems. Because of its wide versatility, it also has outstanding advantages for the Space Station Program and its wide range of users. High frequency ac power provides higher efficiency, lower cost, and improved safety. The 20 kHz power system has exceptional flexibility, is inherently user friendly, and is compatible with all types of energy sources - photovoltaic, solar dynamic, rotating machines or nuclear. Lewis has recently completed development under contract a 25 kW, 20 kHz ac power distribution system testbed. The testbed demonstrates flexibility, versatility, and transparency to user technology as well as high efficiency, low mass, and reduced volume. Author

N86-28123*# National Aeronautics and Space Administration. Lewis Research Center, Cleveland, Ohio.

RAIL ACCELERATORS FOR SPACE TRANSPORTATION: AN EXPERIMENTAL INVESTIGATION

L. M. ZANA, W. R. KERSLAKE, and J. L. STURMAN May 1986 37 p (NASA-TP-2571; E-2754; NAS 1.60:2571) Avail: NTIS HC A03/MF A01 CSCL 09C

An experimental program was conducted at the Lewis Research Center with the objective of investigating the technical feasibility of rail accelerators for propulsion applications. Single-stage, plasma driven rail accelerators of small (4 by 6 mm) and medium (12.5 by 12.5 mm) bores were tested at peak accelerating currents of 50 to 450 kA. Streak-camera photography was used to provide a qualitative description of plasma armature acceleration. The effects of plasma blowby and varying bore pressure on the behavior of plasma armatures were studied. Author

N86-28124*# National Aeronautics and Space Administration. Lewis Research Center, Cleveland, Ohio.

CURRENT EVALUATION OF THE TRIPROPELLANT CONCEPT

R. L. ZURAWSKI Jun. 1986 30 p Presented at the AIAA/SAI/ASME/ASEE 22nd Joint Propulsion Conference, Huntsville, Ala., 16-18 Jun. 1986 (NASA-TP-2602; E-2863; NAS 1.60:2602) Avail: NTIS HC A03/MF A01 CSCL 21I

An analytical study was conducted to determine the specific-impulse advantages of adding metals to conventional liquid-bipropellant systems. These tripropellant systems theoretically offer higher specific impulse and increased propellant density compared with bipropellant systems. Metals considered were Be, Li, and Al. Bipropellant systems were H₂/O₂, N₂H₄/N₂O₄, RP-1/O₂, and H₂/F₂. Thermochemical calculations were performed for sea-level expansion from 6.895-MN/sq. m.

(1000-psia) chamber pressure over a wide range of mixture ratios and propellant compositions. Three-dimensional plots characterize the specific impulse of each tripropellant system. Technology issues pertinent to metallized propellant systems are discussed. Author

N86-28125*# National Aeronautics and Space Administration. Lewis Research Center, Cleveland, Ohio.

THE VOLTAGE THRESHOLD FOR ARCING FOR SOLAR CELLS IN LEO: FLIGHT AND GROUND TEST RESULTS

D. C. FERGUSON Mar. 1986 22 p Presented at the 24th AIAA Aerospace Sciences Meeting, Reno, Nev., 6-9 Jan. 1986 (NASA-TM-87259; E-2951; NAS 1.15:87259; AIAA-PAPER-86-0362) Avail: NTIS HC A02/MF A01 CSCL 10B

Ground and flight results of solar cell arcing in low Earth orbit (LEO) conditions are compared and interpreted. It is shown that an apparent voltage threshold for arcing may be produced by a strong power law dependence of arc rate on voltage, combined with a limited observation time. The change in this apparent threshold with plasma density is a reflection of the density dependence of the arc rate. A nearly linear dependence of arc rate on density is inferred from the data. A real voltage threshold for arcing for 2 by 2 cm solar cells may exist however, independent of plasma density, near -230 V relative to the plasma. Here, arc rates may change by more than an order of magnitude for a change of only 30 V in array potential. For 5.9 by 5.9 solar cells, the voltage dependence of the arc rate is steeper, and the data are insufficient to indicate the existence of an arcing increased by an atomic oxygen plasma, as is found in LEO, and by arcing from the backs of welded-through substrates. Author

N86-29901*# Pratt and Whitney Aircraft, West Palm Beach, Fla. Government Products Div.

OXIDIZER HEAT EXCHANGER COMPONENT TESTING Final Report

T. KMEC and P. KANIC Aug. 1986 60 p (Contract NAS3-24238) (NASA-CR-179487; NAS 1.26:179487; P/W/GPD-FR-19134-3) Avail: NTIS HC A04/MF A01 CSCL 21H

As part of the RL10 Rocket Engine Product Improvement Program, Oxidizer Heat Exchanger (OHE) stages 1, 2, and 3 were designed and fabricated during late 1983 and early 1984. The purpose of the OHE is to provide gaseous oxygen to the propellant injector for stable engine operation at tank head idle and pumped idle operating modes. This report summarizes the OHE stages 1 and 3 rig testing, and includes the separation of the stage 1-and-2 assembly and the remanifolding of stage 1. The OHE performance analysis and analytical model modifications for both stages are also presented. The flow tests were accomplished during the time period from 9 October 1984 to 12 November 1984. Author

N86-31646*# National Aeronautics and Space Administration. Lewis Research Center, Cleveland, Ohio.

TEST PROGRAM TO PROVIDE CONFIDENCE IN LIQUID OXYGEN COOLING OF HYDROCARBON FUELED ROCKET THRUST CHAMBERS

E. S. ARMSTRONG 1986 11 p Presented at the JANNAF Propulsion Meeting, New Orleans, La., 25-28 Aug. 1986 (NASA-TM-88816; E-3174; NAS 1.15:88816) Avail: NTIS HC A02/MF A01 CSCL 21H

An experimental program has been planned at the NASA Lewis Research Center to build confidence in the feasibility of liquid oxygen cooling for hydrocarbon fueled rocket engines. Although liquid oxygen cooling has previously been incorporated in test hardware, more runtime is necessary to gain confidence in this concept. In the previous tests, small oxygen leaks developed at the throat of the thrust chamber and film cooled the hot-gas side of the chamber wall without resulting in catastrophic failure. However, more testing is necessary to demonstrate that a catastrophic failure would not occur if cracks developed further upstream between the injector and the throat, where the boundary layer has not been established. Since under normal conditions cracks are expected to form in the throat region of the thrust

chamber, cracks must be initiated artificially in order to control their location. Several methods of crack initiation are discussed in this report. Four thrust chambers, three with cracks and one without, should be tested. The axial location of the cracks should be varied parametrically. Each chamber should be instrumented to determine the effects of the cracks, as well as the overall performance and durability of the chambers. Author

N86-31648*# Page (R. J.) Co., Santa Ana, Calif.
SLIP CASTING AND EXTRUDING SHAPES OF RHENIUM WITH METAL OXIDE ADDITIVES. 1: FEASIBILITY DEMONSTRATION
 F. A. BARR and R. J. PAGE Apr. 1986 17 p
 (Contract NAS3-23884)
 (NASA-CR-174970; NAS 1.26:174970) Avail: NTIS HC A02/MF A01 CSCL 11F

The feasibility of fabricating small rhenium parts with metal oxide additives by means of slip casting and extrusion techniques is described. The metal oxides, ZrO_2 and HfO_2 were stabilized into the cubic phase with Y_2O_3 . Additions of metal oxide to the rhenium of up to 15 weight percent were used. Tubes of 17 mm diameter with 0.5 mm walls were slip cast by adapting current ceramic oxide techniques. A complete cast double conical nozzle demonstrated the ability to meet shapes and tolerances. Extrusion of meter long tubing lengths of 3.9 mm o.d. x 2.3 mm i.d. final dimension is documented. Sintering schedules are presented to produce better than 95% of theoretical density parts. Finished machining was found possible were required by electric discharge machining and diamond grinding. Author

N86-31649*# National Aeronautics and Space Administration. Lewis Research Center, Cleveland, Ohio.
EVALUATION OF A HYBRID HYDROSTATIC BEARING FOR CRYOGENIC TURBOPUMP APPLICATION
 P. W. SPICA, N. P. HANNUM, and S. D. MEYER 1986 19 p
 (NASA-TM-87255; E-2945; NAS 1.15:87255) Avail: NTIS HC A02/MF A01 CSCL 13K

A hybrid hydrostatic bearing was designed to operate in liquid hydrogen at speeds to 80,000 rpm and radial loads to 440 n (100 lbf). The bearing assembly consisted of a pair of 20-mm angular-contact ball bearings encased in a journal, which was in turn supported by a fluid film of liquid hydrogen. The size and operating conditions of the bearing were selected to be compatible with the operating requirements of an advanced technology turbopump. Several test parameters were varied to characterize the bearing's steady-state operation. The rotation of the tester shaft was varied between 0 and 80,000 rpm. Bearing inlet fluid pressure was varied between 2.07 and 4.48 MPa (300 and 650 psia), while the fluid sump pressure was independently varied between 0.34 and 2.07 MPa (50 and 300 psia). The maximum radial load applied to the bearing was 440 N (110 lbf). Measured hybrid-hydrostatic-bearing stiffness was 1.5 times greater than predicted, while the fluid flow rate through the bearing was 35 to 65 percent less than predicted. Under two-phase fluid conditions, the stiffness was even greater and the flow rate was less. The optimal pressure ratio for the bearing should be between 0.2 and 0.55 depending on the balance desired between bearing efficiency and stiffness. Startup and shutdown cyclic tests were conducted to demonstrate the ability of the hybrid-hydrostatic-bearing assembly to survive at least a 300-firing-duty cycle. For a typical cycle, the shaft was accelerated to 50,000 rpm in 1.8 sec. The bearing operated for 337 start-stop cycles without failure. Author

N86-31650*# National Aeronautics and Space Administration. Lewis Research Center, Cleveland, Ohio.
PERFORMANCE CHARACTERISTICS OF RING-CUSP THRUSTERS WITH XENON PROPELLANT
 M. J. PATTERSON 1986 35 p Presented at the 22nd Joint Propulsion Conference, Huntsville, Ala., 16-18 Jun. 1986; sponsored by AIAA, ASME, SAE and ASEE
 (NASA-TM-87338; E-3085; NAS 1.15:87338; AIAA-86-1392)
 Avail: NTIS HC A03/MF A01 CSCL 21H

The performance characteristics and operating envelope of several 30-cm ring-cusp ion thrusters with xenon propellant were

investigated. Results indicate a strong performance dependence on the discharge chamber boundary magnetic fields and resultant distribution of electron currents. Significant improvements in discharge performance over J-series divergent-field thrusters were achieved for large throttling ranges, which translate into reduced cathode emission currents and reduced power dissipation which should be of significant benefit for operation at thruster power levels in excess of 10 kW. Mass spectrometry of the ion beam was documented for both the ring-cusp and J-series thrusters with xenon propellant for determination of overall thruster efficiency, and lifetime. Based on the lower centerline values of doubly charged ions in the ion beam and the lower operating discharge voltage, the screen grid erosion rate of the ring-cusp thruster is expected to be lower than the divergent-field J-series thruster by a factor of 2. Author

N86-31651*# National Aeronautics and Space Administration. Lewis Research Center, Cleveland, Ohio.
THE NONCAVITATING PERFORMANCE AND LIFE OF A SMALL VANE-TYPE POSITIVE DISPLACEMENT PUMP IN LIQUID HYDROGEN

T. E. ULBRICHT and J. A. HEMMINGER 1986 28 p Presented at the 22nd Joint Propulsion Conference, Huntsville, Ala., 16-18 Jun. 1986; sponsored by AIAA, ASME, SAE and ASEE
 (NASA-TM-87347; E-3100; NAS 1.15:87347; AIAA-86-1438)
 Avail: NTIS HC A03/MF A01 CSCL 21H

The low flow rate and high head rise requirements of hydrogen/oxygen auxiliary propulsion systems make the application of centrifugal pumps difficult. Positive displacement pumps are well-suited for these flow conditions, but little is known about their performance and life characteristics in liquid hydrogen. An experimental and analytical investigation was conducted to determine the performance and life characteristics of a vane-type, positive displacement pump. In the experimental part of this effort, mass flow rate and shaft torque were determined as functions of shaft speed and pump pressure rise. Since liquid hydrogen offers little lubrication in a rubbing situation, pump life is an issue. During the life test, the pump was operated intermittently for 10 hr at the steady-state point of 0.074 lbfm/sec (0.03 kg/sec) flow rate, 3000 psid (2.07 MPa) pressure rise, and 8000 rpm (838 rad/sec) shaft speed. Pump performance was monitored during the life test series and the results indicated no loss in performance. Material loss from the vanes was recorded and wear of the other components was documented. In the analytical part of this effort, a comprehensive pump performance analysis computer code, developed in-house, was used to predict pump performance. The results of the experimental investigation are presented and compared with the results of the analysis. Results of the life test are also presented. M.G.

N86-31652*# National Aeronautics and Space Administration. Lewis Research Center, Cleveland, Ohio.
ANALYSIS OF THE GAS PARTICLE RADIATOR (GPR)
 D. L. CHUBB Jul. 1986 35 p
 (NASA-TM-88786; E-2639-1; NAS 1.15:88786) Avail: NTIS HC A03/MF A01 CSCL 20D

The theoretical performance of a new space radiator concept, the gas particle radiator (GPR), is calculated. The GPR uses a gas containing emitting, submicron particles as the radiating media. A transparent window contains the gas particle mixture around the solid radiator emitting surface. A major advantage of the GPR is that large emissivity ($\epsilon_{sub T}$ is greater than or = 0.8) is achieved without the use of emissive coatings. A radiation heat transfer analysis shows that for a modest volume fraction (approx. 10⁻⁴) of submicron particles and gas thickness (approx. 1 cm) the emissivity, $\epsilon_{sub T}$, is limited by the window transmittance. Besides determining the emissivity, the window is the critical element for making it possible for the GPR to have lower mass than a tube type radiator. The window acts as a bumper to provide meteoroid protection for the radiator wall. The GPR was compared to a proposed titanium wall, potassium heat pipe radiator. For both radiators operating at a power level of 1.01 MW at 775 K it

20 SPACECRAFT PROPULSION AND POWER

was calculated that the GPR mass was 31 percent lower than the heat pipe radiator. Author

N86-32520*# National Aeronautics and Space Administration. Lewis Research Center, Cleveland, Ohio.

ELECTRICAL POWER SYSTEM FOR THE U.S. SPACE STATION

D. L. NORED and G. J. HALLINAN (Rockwell International Corp., Canoga Park, Calif.) 1986 12 p Presented at the 37th Congress of the International Astronautical Federation, Innsbruck, Austria, 4-11 Oct. 1986

(NASA-TM-88856; E-3249; NAS 1.15:88856; IAF-86-37) Avail:

NTIS HC A02/MF A01 CSCL 840

The Space Station Electrical Power System presents many interesting challenges. It will be much larger than previous space power systems, and it must be designed for on-orbit maintenance and replacement, along with having a growth capability. The power generation, energy storage, and power management and distribution (PMAD) subsystems comprise the primary elements of the overall system. Each was analyzed by NASA Lewis Research Center and its two contractors -- Rocketdyne and TRW -- in the definition studies of the program to determine the optimum approach to minimize initial costs and life cycle costs. For the PMAD subsystem, a ring bus architecture operating at 440 V, 20 kHz, single phase, was selected. Photovoltaic and solar dynamic power generation subsystems were both studied. Major tradeoffs were made for each subsystem and for the overall system, and a hybrid system (both photovoltaic and solar dynamic) was selected. Author

N86-32521*# National Aeronautics and Space Administration. Lewis Research Center, Cleveland, Ohio.

THE SPACE STATION POWER SYSTEM

C. R. BARAONA 1986 12 p Presented at the Fifth Conference on Photovoltaic Generators in Space, Noordwijk, Netherlands, 30 Sep. - 4 Oct. 1986; sponsored by ESA

(NASA-TM-88847; E-3237; NAS 1.15:88847) Avail: NTIS HC A02/MF A01 CSCL 22B

The manned space station is the next major NASA program. It presents many challenges to the power system designers. The power system in turn is a major driver on the overall configuration. In this paper, the major requirements and guidelines that affect the station configuration and the power system are explained. The evolution of the space station power system from the NASA program development-feasibility phase through the current preliminary design phase is described. Several early station concepts, both fanciful and feasible, are described and linked to the present concept. The recently completed Phase B trade study selections of photovoltaic system technologies are described in detail. A summary of the present solar dynamic and power management and distribution systems is also given for completeness. Author

N86-32522*# National Aeronautics and Space Administration. Lewis Research Center, Cleveland, Ohio.

PROVEN, LONG-LIFE HYDROGEN/OXYGEN THRUST CHAMBERS FOR SPACE STATION PROPULSION

G. P. RICHTER and H. G. PRICE 1986 20 p Presented at the 1986 JANNAF Propulsion Meeting, New Orleans, La., 26-28 Aug. 1986; sponsored by JANNAF Interagency Propulsion Committee

(NASA-TM-88822; E-3171; NAS 1.15:88822) Avail: NTIS HC A02/MF A01 CSCL 21H

The development of the manned space station has necessitated the development of technology related to an onboard auxiliary propulsion system (APS) required to provide for various space station attitude control, orbit positioning, and docking maneuvers. A key component of this onboard APS is the thrust chamber design. To develop the required thrust chamber technology to support the Space Station Program, the NASA Lewis Research Center has sponsored development programs under contracts with Aerojet TechSystems Company and with Bell Aerospace Textron Division of Textron, Inc. During the NASA Lewis sponsored program

with Aerojet TechSystems, a 25 lb sub f hydrogen/oxygen thruster has been developed and proven as a viable candidate to meet the needs of the Space Station Program. Likewise, during the development program with Bell Aerospace, a 50 lb sub f hydrogen/oxygen Thrust Chamber has been developed and has demonstrated reliable, long-life expectancy at anticipated space station operating conditions. Both these thrust chambers were based on design criteria developed in previous thruster programs and successfully verified in experimental test programs. Extensive thermal analyses and models were used to design the thrusters to achieve total impulse goals of 2 x 10 to the 6th power lb sub f-sec. Test data for each thruster will be compared to the analytical predictions for the performance and heat transfer characteristics. Also, the results of thrust chamber life verification tests will be presented. Author

23

CHEMISTRY AND MATERIALS (GENERAL)

A86-17483* National Aeronautics and Space Administration. Lewis Research Center, Cleveland, Ohio.

FABRICATION OF CERAMIC SUBSTRATE-REINFORCED AND FREE FORMS BY MANDREL PLASMA SPRAYING METAL-CERAMIC COMPOSITES

R. J. QUENTMEYER, G. MCDONALD, and R. C. HENDRICKS (NASA, Lewis Research Center, Cleveland, OH) Journal of Vacuum Science and Technology A (ISSN 0734-2101), vol. 3, Nov.-Dec. 1985, p. 2450-2455. Previously announced in STAR as N85-23926. refs

Components fabricated of, or coated with, ceramics have lower parasitic cooling requirements. Techniques are discussed for fabricating thin-shell ceramic components and ceramic coatings for applications in rocket or jet engine environments. Thin ceramic shells with complex geometric forms involving convolutions and reentrant surfaces were fabricated by mandrel removal. Mandrel removal was combined with electroplating or plasma spraying and isostatic pressing to form a metal support for the ceramic. Rocket engine thrust chambers coated with 0.08 mm (3 mil) of ZrO₂-8Y₂O₃ had no failures and a tenfold increase in engine life. Some measured mechanical properties of the plasma-sprayed ceramic are presented. B.G.

A86-30051* National Aeronautics and Space Administration. Lewis Research Center, Cleveland, Ohio.

FRACTURE TOUGHNESS TESTS ON PLASMA-SPRAYED COATINGS

C. C. BERNDT (NASA, Lewis Research Center, Cleveland, OH) IN: Advances in fracture research (Fracture 84). Volume 4. Oxford and New York, Pergamon Press, 1986, p. 2545-2552. Research supported by the Australian Welding Research Association. refs (Contract NCC3-27)

Fracture toughness measurements have been performed on plasma-sprayed coatings. The intrinsic fracture toughness of plasma-sprayed coatings may be ascertained by means of a double cantilever beam (DCB) test. Emphasis is placed on calibration of the specimen geometry. Representative values for alumina coatings are presented. Author

A86-49855* National Aeronautics and Space Administration. Lewis Research Center, Cleveland, Ohio.

DUAL-ION-BEAM DEPOSITION OF CARBON FILMS WITH DIAMOND-LIKE PROPERTIES

M. J. MIRTICH, D. M. SWEC (NASA, Lewis Research Center, Cleveland, OH), and J. C. ANGUS (Case Western Reserve University, Cleveland, OH) Thin Solid Films (ISSN 0040-6090), vol. 131, 1985, p. 245-254. Previously announced in STAR as N84-31512. refs

A single and dual ion beam system was used to generate amorphous carbon films with diamond like properties. A methane/argon mixture at a molar ratio of 0.28 was ionized in the low pressure discharge chamber of a 30-cm-diameter ion source. A second ion source, 8 cm in diameter was used to direct a beam of 600 eV Argon ions on the substrates (fused silica or silicon) while the deposition from the 30-cm ion source was taking place. Nuclear reaction and combustion analysis indicate H/C ratios for the films to be 1.00. This high value of H/C, it is felt, allowed the films to have good transmittance. The films were impervious to reagents which dissolve graphitic and polymeric carbon structures. Although the measured density of the films was approximately 1.8 gm/cu cm, a value lower than diamond, the films exhibited other properties that were relatively close to diamond. These films were compared with diamond like films generated by sputtering a graphite target. Author

N86-11272*# Boeing Aerospace Co., Seattle, Wash.

CHARACTERIZATION METHODOLOGY FOR PMR-15

A. B. HUNTER /in NASA. Lewis Research Center High Temp. Polymer Matrix Composites p 151-156 Sep. 1985 (Contract NAS3-22523)

Avail: NTIS HC A18/MF A01 CSCL 07A

Characterization of model compounds, monomers, resin solutions and cure cycles of PMR-15 polyimide are performed. Successful separation of various reaction products is also accomplished by liquid chromatography. The PMR-15 cure analysis is performed by fourier transform spectroscopy and gas chromatograph - mass spectrometry. Characterization receiving inspection tests for Quality Control are recommended. Author

N86-13370*# National Aeronautics and Space Administration. Lewis Research Center, Cleveland, Ohio.

MODIFICATIONS OF SYSTEM FOR ELEVATED TEMPERATURE TENSILE TESTING AND STRESS-STRAIN MEASUREMENT OF METAL MATRIX COMPOSITES

J. O. DIAZ 1985 21 p refs Presented at the 1st Symposium on Testing Technology of Metal Matrix Composites, Nashville, 18-20 Nov. 1985; sponsored by the American Society for Testing and Materials

(NASA-TM-87172; E-2813; NAS 1.15:87172) Avail: NTIS HC A02/MF A01 CSCL 11D

Composites consisting of tungsten alloy wires in superalloy matrices are being studied because they offer the potential for increased strength compared to current materials used at temperatures up to at least 1093 C (2000F). Previous research at the NASA Lewis Research Center and at other laboratories in the U.S., Europe, and Japan has demonstrated laboratory feasibility for fiber reinforced superalloys (FRS). The data for the mechanical and physical properties used to evaluate candidate materials is limited and a need exists for a more detailed and complete data base. The focus of this work is to develop a test procedure to provide a more complete FRS data base to quantitatively evaluate the composite's potential for component applications. This paper will describe and discuss the equipment and procedures under development to obtain elevated temperature tensile stress-strain, strength and modulus data for the first generation of tungsten fiber reinforced superalloy composite (TFRS) materials. Tensile stress-strain tests are conducted using a constant crosshead speed tensile testing machine and a modified load-strain measuring apparatus. Elevated temperature tensile tests are performed using a resistance wound commercial furnace capable of heating test specimens up to 1093 C (2000 F). Tensile stress-strain data are

obtained for hollow tubular stainless steel specimens serving as a prototype for future composite specimens. Author

N86-17472*# National Aeronautics and Space Administration. Lewis Research Center, Cleveland, Ohio.

EFFECT OF ARGON AND HYDROGEN ON DEPOSITION OF SILICON FROM TETROCHLOROSILANE IN COLD PLASMAS

R. R. MANORY, R. AVNI (Ben Gurion Univ. of the Negev, Beer Sheva, Israel), and A. GRILL (Ben Gurion Univ. of the Negev, Beer Sheva, Israel) 1985 16 p refs Presented at Fall Meeting of the Materials Research Society, Boston, Mass., 2-7 Dec. 1985

(NASA-TM-87219; E-2820; NAS 1.15:87219) Avail: NTIS HC A02/MF A01 CSCL 07D

The roles of Ar and H₂ on the decomposition of SiCl₄ in cold plasma were investigated by Langmuir probes and mass spectrometry. Decomposition of the reactant by Ar only has been found to be very slow. In presence of H₂ in the plasma SiCl₄ is decomposed by fast radical-molecule reactions which are further enhanced by Ar due to additional ion-molecule reactions in which more H radicals are produced. A model for the plasma-surface interactions during deposition of mu-Si in the Ar + H₂ + SiCl₄ system is presented. Author

N86-18442*# National Aeronautics and Space Administration. Lewis Research Center, Cleveland, Ohio.

GRAPHITE FIBER INTERCALATION: BASIC PROPERTIES OF COPPER CHLORIDE INTERCALATED FIBERS

D. A. JAWORSKE and J. D. MILLER (Kenyon Coll., Gambier, Ohio) 1986 16 p refs Presented at the Spring Meeting of the American Physical Society, Las Vegas, Nev., 31 Mar. - 4 Apr. 1986

(NASA-TM-87217; E-2877; NAS 1.15:87217) Avail: NTIS HC A02/MF A01 CSCL 07D

In situ resistance measurements were used to follow the intercalation of copper chloride in pitch-based fibers. Subsequent single fiber resistivity measurements reveal a large range of resistivities, from 13 to 160 micro-ohms cm. Additional density measurements reveal a bimodal distribution of mass densities. The dense fibers have lower resistivities and correspond to the stage III compound identified by X-ray diffraction. Neither resistivity nor density correlate with diameter. Both energy dispersive spectroscopy and mass density data suggest that excess chlorine resides in the intercalated fiber, resulting in a stoichiometry of C_{4.9n} CuCl_{2.5} (where n is the stage number) for the denser fibers. Finally, thermogravimetric analysis shows a 33 percent loss in mass upon heating to 700C. This loss in mass is attributed to loss of both chlorine and carbon. Author

24

COMPOSITE MATERIALS

Includes physical, chemical, and mechanical properties of laminates and other composite materials.

A86-13169* National Aeronautics and Space Administration. Lewis Research Center, Cleveland, Ohio.

A CERAMIC MATRIX COMPOSITE BASED ON POLYMERIZATION AND PYROLYSIS OF ETHYNYLATED AROMATICS

F. I. HURWITZ (NASA, Lewis Research Center, Cleveland, OH) IN: National SAMPE Symposium and Exhibition, 30th, Anaheim, CA, March 19-21, 1985, Proceedings. Covina, CA, Society for the Advancement of Material and Process Engineering, 1985, p. 1375-1386. refs

A number of ethynylated aromatic monomers recently have been synthesized which thermally homopolymerize and copolymerize to produce rigid, highly cross-linked polymers with high thermal stability (T_g of about 450 C). On pyrolysis, these

24 COMPOSITE MATERIALS

polymers lose few volatiles (more than 85 percent char yield) to yield carbon bodies of relatively low porosity. These properties render the ethynylated aromatics of significant interest as matrices for high temperature composites. Incorporation of a SiC particle filler in the matrix improves the rheology of the system and minimizes shrinkage during pyrolysis. Several unidirectional composites have been fabricated combining a graphite or boria-alumina-silica continuous reinforcement with an ethynylated aromatic polymer matrix and SiC filler. Thermogravimetric analysis of composite pyrolysis behavior was used to determine reaction kinetics and to establish a composite fabrication cycle. Composites retained 95 percent of their green weight on pyrolysis. Microstructure of the green and pyrolyzed composites is characterized for materials pyrolyzed at 600 C in vacuum and argon as well as for laminates heated at 1200 C in argon following cvrolysis. Author

A86-14718* Columbia Univ., New York.
INTERDIFFUSIONAL EFFECTS BETWEEN TUNGSTEN FIBERS AND AN IRON-NICKEL-BASE ALLOY

T. CAULFIELD, R. S. BELLOW, and J. K. TIEN (Columbia University, New York) Metallurgical Transactions A - Physical Metallurgy and Materials Science (ISSN 0360-2133), vol. 16A, Nov. 1985, p. 1961-1968. refs
(Contract NAG3-410)

Tungsten fibers in the INCOLOY 903 alloy were annealed for over 100 hours at 1038 C and 1200 C. It was found that interdiffusion results in the formation of a reaction zone. SEM-EDS probe analysis showed that the chemistries across this zone were constant, suggesting the zone was a compound phase. The composition of the compound was estimated to be that of a mu-type phase. The local chemistry (in atomic percent) at the reaction zone/alloy matrix interface was found to be approximately 8 pct W, 1.2 pct Nb, 40 pct Fe, 14 pct Co, and 36 pct Ni. In addition, recrystallization was observed in both the remaining tungsten fiber and the nearby INCOLOY 903 matrix after annealing at 1200 C, but not at 1038 C. The results of this study suggest that reaction zone growth kinetics can be minimized by the reduction of Co and Fe and the increase of W in the matrix alloy. Author

A86-19999* National Aeronautics and Space Administration. Lewis Research Center, Cleveland, Ohio.
LONGITUDINAL COMPRESSIVE FAILURE MODES IN FIBER COMPOSITES END ATTACHMENT EFFECTS ON IITRI TYPE TEST SPECIMENS

C. C. CHAMIS (NASA, Lewis Research Center, Cleveland, OH) and J. H. SINCLAIR Journal of Composites Technology and Research, vol. 7, Winter 1985, p. 129-135.

The end-attachment effects on longitudinal compressive strength of IITRI type specimen unidirectional fiber composites are formally assessed using finite-element analysis (FEA) in conjunction with composite mechanics. Sixteen different cases were analyzed to evaluate end-attachment effects (such as degree of misalignment, type of misalignment, progressive end-tab debonding, and specimen thickness) on stress distribution, peak stresses, buckling loads, and buckling mode shapes. The results obtained from the FEA and comparisons with fractured specimens show that eccentricities induce bending-type stresses which peak near the end-tabs and cause flexural type fracture. Also, guidelines are included for placing back-to-back strain gages to measure the presence/absence of possible end-attachment and eccentricity effects. Author

A86-20629* National Aeronautics and Space Administration. Lewis Research Center, Cleveland, Ohio.

A NEW PLY MODEL FOR INTERLAMINAR STRESS ANALYSIS
R. RAO VALISETTY (NASA, Lewis Research Center, Cleveland, OH) and L. W. REHFELD (Georgia Institute of Technology, Atlanta) IN: Delamination and debonding of materials. Philadelphia, PA, American Society for Testing and Materials, 1985, p. 52-68. refs

(Contract AF-AFOSR-82-0080; AF-AFOSR-83-0056)

An accurate estimate of interlaminar stresses is crucial to understanding, as well as predicting, many delamination-related failures in composite materials. A new model for ply-level sublaminate analysis is presented and applied. The homogeneous plate theory developed earlier by the authors (Valisetty and Rehfield, 1983) is further refined, and the equations are reduced appropriately for the classical finite-width free-edge laminate elasticity problem and a related delamination crack growth problem. It is applied to the laminate on a ply-by-ply basis. This theory incorporates all the essential physical effects and appears to be an adequate model for predicting the behavior of individual layers in equilibrium. On the basis of the number of equations and boundary conditions required for the implementation of layer equilibrium, this theory also appears to be the simplest of its kind presented so far. The stress induced in the free-edge region of a (0,90,90) laminate in uniform extension and the energy release rates for the delamination between the -30 deg and 90 deg plies of a (+, -30, +, -30, 90,90)s laminate are computed using the new analysis. The results are in excellent agreement with the existing numerical solutions. The new ply behavioral model appears to be very promising; it yields stresses and displacements that are statically and kinematically compatible at interlaminar surfaces. Author

A86-21486* National Aeronautics and Space Administration. Lewis Research Center, Cleveland, Ohio.

CREEP OF CHEMICALLY VAPOUR DEPOSITED SIC FIBRES
J. A. DICARLO (NASA, Lewis Research Center, Cleveland, OH) Journal of Materials Science (ISSN 0022-2461), vol. 21, Jan. 1986, p. 217-224. Previously announced in STAR as N85-14878. refs

The creep, thermal expansion, and elastic modulus properties for chemically vapor deposited SiC fibers were measured between 1000 and 1500 C. Creep strain was observed to increase logarithmically with time, monotonically with temperature, and linearly with tensile stress up to 600 MPa. The controlling activation energy was 480 + or - 20 kJ/mole. Thermal pretreatments near 1200 and 1450 C were found to significantly reduce fiber creep. These results coupled with creep recovery observations indicate that below 1400 C fiber creep is anelastic with negligible plastic component. This allowed a simple predictive method to be developed for describing fiber total deformation as a function of time, temperature, and stress. Mechanistic analysis of the property data suggests that fiber creep is the result of beta-SiC grain boundary sliding controlled by a small percent of free silicon in the grain boundaries. Author

A86-21731* National Aeronautics and Space Administration. Lewis Research Center, Cleveland, Ohio.

GRAPHITE/PMR POLYIMIDE COMPOSITES WITH IMPROVED TOUGHNESS

R. D. VANNUCCI and K. J. BOWLES (NASA, Lewis Research Center, Cleveland, OH) IN: National SAMPE Technical Conference, 17th, Kiamesha Lake, NY, October 22-24, 1985, Proceedings. Covina, CA, Society for the Advancement of Material and Process Engineering, 1985, p. 352A-363. Previously announced in STAR as N85-32148.

The toughness of composites made with modified PMR (Polymerization of monomer reactants) polyimides and Celion 6000 graphite fibers was studied. Various types/levels of monomer reactants containing flexible links were incorporated into PMR resin compositions used to prepare composites. The composites were evaluated for toughness using instrumented drop weight and 10 deg off axis tensile tests at room temperature, and for strength using flexure and short beam shear tests at room temperature

and at elevated temperature. The effect of resin composition on composite processability, thermo-oxidative stability, toughness and mechanical properties are discussed. Author

A86-27730* National Aeronautics and Space Administration. Lewis Research Center, Cleveland, Ohio.

AEROSPACE APPLICATIONS OF PMR POLYIMIDE COMPOSITES

T. T. SERAFINI (NASA, Lewis Research Center, Cleveland, OH) IN: ICCM - V; Proceedings of the Fifth International Conference on Composite Materials, San Diego, CA, July 29-August 1, 1985. Warrendale, PA, Metallurgical Society, Inc., 1985, p. 1007-1023. refs

The current status of the novel class of processable, addition-type polyimides known as PMR (for in situ polymerization of monomer reactants) polyimides, developed by NASA at the Lewis Research Center, is reviewed. Highlights of PMR technology studies conducted at NASA Lewis are presented. Several examples of industrial applications of PMR-15 polyimide composites to aerospace structural components are examined. C.D.

A86-27734* National Aeronautics and Space Administration. Lewis Research Center, Cleveland, Ohio.

DESIGNING FOR FIBER COMPOSITE STRUCTURAL DURABILITY IN HYGROTHERMOMECHANICAL ENVIRONMENTS

C. C. CHAMIS (NASA, Lewis Research Center, Cleveland, OH) IN: ICCM - V; Proceedings of the Fifth International Conference on Composite Materials, San Diego, CA, July 29-August 1, 1985. Warrendale, PA, Metallurgical Society, Inc., 1985, p. 1101-1113. Previously announced in STAR as N85-27978. refs

A methodology is described which can be used to design/analyze fiber composite structures subjected to complex hygrothermomechanical environments. This methodology includes composite mechanics and advanced structural analysis methods (finite element). Select examples are described to illustrate the application of the available methodology. The examples include: (1) composite progressive fracture; (2) composite design for high cycle fatigue combined with hot-wet conditions; and (3) general laminate design. Author

A86-35809* National Aeronautics and Space Administration. Lewis Research Center, Cleveland, Ohio.

PROGRESSIVE FRACTURE OF FIBER COMPOSITES

T. B. IRVINE and C. A. GINTY (NASA, Lewis Research Center, Cleveland, OH) Journal of Composite Materials (ISSN 0021-9983), vol. 20, March 1986, p. 166-184. refs

Refined models and procedures are described for determining progressive composite fracture in graphite/epoxy angleplied laminates. Unique Lewis Research Center capabilities are utilized including the Real-Time Ultrasonic C-San (RUSCAN) experimental facility and the Composite Durability Structural Analysis (CODSTRAN) computer code. CODSTRAN is used to predict the fracture progression based on composite mechanics, finite element stress analysis, and fracture criteria modules. The RUSCAN facility, CODSTRAN computer code, and scanning electron microscope are used to determine durability and identify failure mechanisms in graphite/epoxy composites. Results indicate that RUSCAN/CODSTRAN is an effective method of studying progressive fracture of composites. Author

A86-36999* National Aeronautics and Space Administration. Lewis Research Center, Cleveland, Ohio.

TETRAGLYCIDYL EPOXY RESINS AND GRAPHITE FIBER COMPOSITES CURED WITH FLEXIBILIZED AROMATIC DIAMINES

P. DELVIGS (NASA, Lewis Research Center, Cleveland, OH) Polymer Composites (ISSN 0272-8397), vol. 7, April 1986, p. 101-105. refs

Studies were performed to synthesize new ether modified, flexibilized aromatic diamine hardeners for curing epoxy resins. The effect of moisture absorption on the glass transition temperatures of a tetraglycidyl epoxy, MY 720, cured with

flexibilized hardeners and a conventional aromatic diamine was studied. Unidirectional composites, using epoxy-sized Celion 6000 graphite fiber as the reinforcement, were fabricated. The room temperature and 300 F mechanical properties of the composites, before and after moisture exposure, were determined. The Mode I interlaminar fracture toughness of the composites was characterized using a double cantilever beam technique to calculate the critical strain energy release rate. Author

A86-40596* National Aeronautics and Space Administration. Lewis Research Center, Cleveland, Ohio.

COMPUTATIONAL COMPOSITE MECHANICS FOR AEROSPACE PROPULSION STRUCTURES

C. C. CHAMIS (NASA, Lewis Research Center, Cleveland, OH) IN: Space Systems Technology Conference, San Diego, CA, June 9-12, 1986, Technical Papers. New York, American Institute of Aeronautics and Astronautics, 1986, p. 145-155. refs (AIAA PAPER 86-1190)

Specialty methods are presented for the computational simulation of specific composite behavior. These methods encompass all aspects of composite mechanics, impact, progressive fracture and component specific simulation. Some of these methods are structured to computationally simulate, in parallel, the composite behavior and history from the initial fabrication through several missions and even to fracture. Select methods and typical results obtained from such simulations are described in detail in order to demonstrate the effectiveness of computationally simulating (1) complex composite structural behavior in general and (2) specific aerospace propulsion structural components in particular. Author

A86-41070* National Aeronautics and Space Administration. Lewis Research Center, Cleveland, Ohio.

DYNAMIC STRESS ANALYSIS OF SMOOTH AND NOTCHED FIBER COMPOSITE FLEXURAL SPECIMENS

P. L. N. MURTHY and C. C. CHAMIS (NASA, Lewis Research Center, Cleveland, OH) IN: Composite materials: Testing and design; Proceedings of the Seventh Conference, Philadelphia, PA, April 2-4, 1984. Philadelphia, PA, American Society for Testing and Materials, 1986, p. 368-391. Previously announced in STAR as N84-25770.

A detailed analysis of the dynamic stress field in smooth and notched fiber composite (Charpy-type) specimens is reported in this paper. The analysis is performed with the aid of the direct transient response analysis solution sequence of MSC/NASTRAN. Three unidirectional composites were chosen for the study. They are S-Glass/Epoxy, Kevlar/Epoxy and T-300/Epoxy composite systems. The specimens are subjected to an impact load which is modeled as a triangular impulse with a maximum of 2000 lb and a duration of 1 ms. The results are compared with those of static analysis of the specimens subjected to a peak load of 2000 lb. For the geometry and type of materials studied, the static analysis results gave close conservative estimates for the dynamic stresses. Another interesting inference from the study is that the impact induced effects are felt by S-Glass/Epoxy specimens sooner than Kevlar/Epoxy or T-300/Epoxy specimens. Author

A86-42712* Material Concepts, Inc., Columbus, Ohio.

ADVANCED ROTARY ENGINE COMPONENTS UTILIZING FIBER REINFORCED MG CASTINGS

D. GODDARD, W. WHITMAN, R. PUMPHREY (Material Concepts, Inc., Columbus, OH), and C.-M. LEE AIAA, ASME, SAE, and ASCE, Joint Propulsion Conference, 22nd, Huntsville, AL, June 16-18, 1986, 7 p. (AIAA PAPER 86-1559)

Under a two-phase program sponsored by NASA, the technology for producing advanced rotary engine components utilizing graphite fiber-reinforced magnesium alloy casting is being developed. In Phase I, the successful casting of a simulated intermediate housing was demonstrated. In Phase II, the goal is to produce an operating rotor housing. The effort involves generation of a material property data base, optimization of parameters, and development of wear- and corrosion-resistant cast

24 COMPOSITE MATERIALS

surfaces and surface coatings. Results to date are described.

Author

A86-43010* Purdue Univ., West Lafayette, Ind.

DYNAMIC DELAMINATION CRACK PROPAGATION IN A GRAPHITE/EPOXY LAMINATE

C. T. SUN (Purdue University, West Lafayette, IN) and J. E. GRADY IN: Composite materials: Fatigue and fracture; Proceedings of the Symposium, Dallas, TX, October 24, 25, 1984. Philadelphia, PA, American Society for Testing and Materials, 1986, p. 5-31. refs (Contract NAG3-211)

The dynamic delamination crack propagation behavior during ballistic tests of (90/0)5s T-300/934 graphite/epoxy laminates with embedded interfacial cracks was investigated using high speed photography. The impact on the beam-like specimen was produced with a silicon rubber ball, and the crack propagation speeds and the threshold impact velocities required to initiate dynamic crack propagation were determined for several crack positions. The results suggest that the mode of crack propagation depends on the specimen geometry as well as the loading condition. A simplified finite element analysis of the experimental data obtained from one of the midplane-cracked specimens was used to estimate the critical strain energy release rate, which may determine the onset of unstable crack propagation. I.S.

N86-10290*# National Aeronautics and Space Administration. Lewis Research Center, Cleveland, Ohio.

PROGRESSIVE DAMAGE, FRACTURE PREDICTIONS AND POST MORTEM CORRELATIONS FOR FIBER COMPOSITES

1985 21 p refs Presented at Intern. Conf.: Post Failure Anal. Tech. Fiber Reinforced Composites, Dayton, Ohio, 1-3 Jul. 1985; sponsored by Air Force (NASA-TM-87101; E-2695; NAS 1.15:87101) Avail: NTIS HC A02/MF A01 CSCL 11D

Lewis Research Center is involved in the development of computational mechanics methods for predicting the structural behavior and response of composite structures. In conjunction with the analytical methods development, experimental programs including post failure examination are conducted to study various factors affecting composite fracture such as laminate thickness effects, ply configuration, and notch sensitivity. Results indicate that the analytical capabilities incorporated in the CODSTRAN computer code are effective in predicting the progressive damage and fracture of composite structures. In addition, the results being generated are establishing a data base which will aid in the characterization of composite fracture. Author

N86-11260*# National Aeronautics and Space Administration. Lewis Research Center, Cleveland, Ohio.

HIGH TEMPERATURE POLYMER MATRIX COMPOSITES

Washington Sep. 1985 409 p refs Conf. held in Cleveland, Ohio, 16-18 Mar. 1983 (NASA-CP-2385; E-2425; NAS 1.55:2385) Avail: NTIS HC A18/MF A01 CSCL 11D

These are the proceedings of the High Temperature Polymer Matrix Composites Conference held at the NASA Lewis Research Center on March 16 to 18, 1983. The purpose of the conference is to provide scientists and engineers working in the field of high temperature polymer matrix composites an opportunity to review, exchange, and assess the latest developments in this rapidly expanding area of materials technology. Technical papers are presented in the following areas: (1) matrix development; (2) adhesive development; (3) characterization; (4) environmental effects; and (5) applications.

N86-11276*# National Aeronautics and Space Administration. Lewis Research Center, Cleveland, Ohio.

PROPERTIES OF AUTOCLAVED GR/PI COMPOSITES MADE FROM IMPROVED TACK PMR-15 PREPREG

R. D. VANNUCCI In its High Temp. Polymer Matrix Composites p 207-215 Sep. 1985 refs Avail: NTIS HC A18/MF A01 CSCL 11D

Autoclave processing studies were conducted, using improved tack PMR-15 prepreg, to determine the effect of tack enhancing PMR resin modifications on composite processability and mechanical properties. Improved tack graphite fiber reinforced PMR-15 prepregs were prepared and exposed to ambient conditions for various times and then autoclave molded into composites. Composite specimens were prepared and tested for flexural and interlaminar shear strengths at room temperature and 316 C. The retention of flexural and interlaminar shear strength as a function of exposure in air at 316 C was also determined. The results show that the modified PMR resin solutions provide prepreg with improved tack and drape retention characteristics without adversely affecting processability or mechanical properties of autoclave molded graphite fiber reinforced PMR-15 composites. Author

N86-11278*# National Aeronautics and Space Administration. Lewis Research Center, Cleveland, Ohio.

RHEOLOGICAL, PROCESSING, AND 371 DEG C MECHANICAL PROPERTIES OF CELION 6000/N-PHENYLNADIMIDE MODIFIED PMR COMPOSITES

R. H. PATER In its High Temp. Polymer Matrix Composites p 243-256 Sep. 1985 refs Avail: NTIS HC A18/MF A01 CSCL 11D

The rheology, processing, and chemistry of newly developed N-phenylnadimide modified PMR (PMR-PN) polyimide resins are reviewed. The 371 C performance of their composites reinforced with Celion 6000 graphite fibers is also reviewed, along with the state of the art Celion 6000/PMR-15 composite. The effects of the 371 C exposure in air for up to 300 hr on the composite glass transition temperature, weight loss characteristics, and dimensional stability are presented. The changes in the composite 371 C interlaminar shear and flexural properties are also presented. In addition, composite interfacial degradation at a function of exposure time at 371 C was followed by scanning electron microscopy. The results suggest that the composite materials can be used at 371 C for at least 100 hr. Author

N86-11281*# National Aeronautics and Space Administration. Lewis Research Center, Cleveland, Ohio.

SURFACE PROTECTION OF GRAPHITE FABRIC/PMR-15 COMPOSITES SUBJECTED TO THERMAL OXIDATION

M. P. HANSON and T. T. SERAFINI In its High Temp. Polymer Matrix Composites p 287-297 Sep. 1985 refs Avail: NTIS HC A18/MF A01 CSCL 11D

Graphite fabric/PMR-15 laminates develop matrix cracks during long-term exposure in air at temperatures in the range of 500 to 600 F. This study was performed to demonstrate the effectiveness of incorporating graphite mat surface plies as a means of reducing the developing of matrix cracks. Celion 3000 graphite fabric/PMR-15 laminates were fabricated with graphite or graphite mat/325-mesh boron powder surface plies. Laminates without mat surface plies were also fabricated for control purposes. Composite flexural strength, flexural modulus, and interlaminar shear strength were determined at 288 C before and after long-term exposure (up to 1500 hr) in air at 316 C. The results of this study showed that the incorporation of graphite mat surface plies reduces matrix cracking and improves the elevated temperature mechanical property retention characteristics of the composites. Author

N86-12256*# National Aeronautics and Space Administration. Lewis Research Center, Cleveland, Ohio.

THE 371 DEG C MECHANICAL PROPERTIES OF GRAPHITE/POLYIMIDE COMPOSITES

P. DELVIGS 1985 14 p refs Presented at the 2nd Intern. Conf. on Polyimides, Ellenville, N.Y., 30 Oct. - 1 Nov. 1985; sponsored by the Society of Plastics Engineers, Inc. (NASA-TM-87122; E-2730; NAS 1.15:87122) Avail: NTIS HC A02/MF A01 CSCL 11D

A series of condensation polyimides based on pyromellitic dianhydride is synthesized and evaluated for potential application at 371 C. Several three- and four-ring benzenoid diamine systems containing oxygen bridging groups are investigated. Thermomechanical analysis of neat resin specimens indicate that the polyimide prepared from the dimethyl ester of pyromellitic acid (PMDE) and 2,2-bis[4-(4'-aminophenoxy) phenyl]-1,1,3,3,3-hexafluoropropane (BDAF) is the only resin system which has a glass transition temperature (T_g) above 371 C. The T_g of the PMDE/BDAF polyimide is found to be 390 C after a postcure air at 371 C for 24 hr. Unidirectional composites are fabricated from the PMDE/BDAF system and unsized Celion 6000 graphite fibers. Final cure temperatures in the range of 371 to 427 C with an applied pressure of 10.34 to 13.78 MPa are investigated. The void content of the composites ranges from 4.6 to 8.6 percent. Composites cured at 399 C under a pressure of 10.34 MPa and postcured in air at 371 C for 24 hr exhibit the highest 371 C interlaminar shear strength (ILSS, 40.7 MPa) and flexural strength (758 MPa). The thermo-oxidative stability of the composites is determined by subjecting specimens to isothermal exposure at 371 C in air at atmospheric pressure, as well as a pressure of 0.52 MPa. Specimens exposed at atmospheric pressure exhibit a weight loss of 12 percent after 200 hr of exposure and 88 percent retention of its original 371 C ILSS. In contrast, the specimens exposed at 0.52 MPa pressure exhibit a comparable weight loss after only 72 hr, and a 71 percent retention of its original 371 C ILSS. Author

N86-14316*# National Aeronautics and Space Administration. Lewis Research Center, Cleveland, Ohio.

INTERLAMINAR FRACTURE TOUGHNESS: THREE-DIMENSIONAL FINITE ELEMENT MODELING FOR END-NOTCH AND MIXED-MODE FLEXURE

P. L. N. MURTHY and C. C. CHAMIS 1985 28 p refs Presented at the Symposium on Toughened Composites, Houston, Texas, 13-15 March 1985; sponsored by the American Society for Testing and Materials (NASA-TM-87138; E-2626; NAS 1.15:87138) Avail: NTIS HC A03/MF A01 CSCL 11D

A computational procedure is described for evaluating End-Notch-Flexure (ENF) and Mixed-Mode-Flexure (MMF) interlaminar fracture toughness in unidirectional fiber composites. The procedure consists of a three-dimensional finite element analysis in conjunction with the strain energy release rate concept and with composite micromechanics. The procedure is used to analyze select cases of ENF and MMF. The strain energy release rate predicted by this procedure is in good agreement with limited experimental data. The procedure is used to identify significant parameters associated with interlaminar fracture toughness. It is also used to determine the critical strain energy release rate and its attendant crack length in ENF and/or MMF. This computational procedure has considerable versatility/generality and provides extensive information about interlaminar fracture toughness in fiber composites. Author

N86-17477*# National Aeronautics and Space Administration. Lewis Research Center, Cleveland, Ohio.

SPECIMEN GEOMETRY EFFECTS ON GRAPHITE/PMR-15

COMPOSITES DURING THERMO-OXIDATIVE AGING

K. J. BOWLES and A. MEYERS (Medical Coll. of Ohio, Toledo) 1986 19 p refs Proposed for presentation at the 31st National SAMPE Symposium and Exhibition, Las Vegas, Nev., 7-10 Apr. 1986

(NASA-TM-87204; E-2860; NAS 1.15:87204) Avail: NTIS HC A02/MF A01 CSCL 11D

Studies were conducted to establish the effects of specimen geometry on the thermo-oxidative stability and the mechanical properties retention of unidirectional Celion 12000 graphite fiber reinforced PMR-15 polyimide composites. Weight loss, flexural strength and interlaminar shear strength are measured at isothermal aging times as long as 1639 hr at a temperature of 316 C for three different specimen geometries. It is found that the three different types of specimen surfaces exhibit different values of weight loss/unit area. The mechanical properties retention is also found to be dependent on geometry for these composites. The interlaminar shear strength decreases significantly over the complete range of aging times. The flexural strength retention starts showing geometric dependency after about 1000 hr of aging at 316C. Weight loss fluxes, associated with the three different types of exposed surfaces, are calculated and used to develop an empirical mathematical model for predicting the weight loss behavior of unidirectional composites of arbitrary geometries. Data are presented comparing experimentally determined weight loss with weight loss values predicted using the empirical model. Author

N86-21614*# National Aeronautics and Space Administration. Lewis Research Center, Cleveland, Ohio.

INTEGRATED COMPOSITE ANALYZER (ICAN): USERS AND PROGRAMMERS MANUAL

P. L. N. MURTHY and C. C. CHAMIS Mar. 1986 77 p refs (NASA-TP-2515; E-2035; NAS 1.60:2515) Avail: NTIS HC A05/MF A01 CSCL 11D

The use of and relevant equations programmed in a computer code designed to carry out a comprehensive linear analysis of multilayered fiber composites is described. The analysis contains the essential features required to effectively design structural components made from fiber composites. The inputs to the code are constituent material properties, factors reflecting the fabrication process, and composite geometry. The code performs micromechanics, macromechanics, and laminate analysis, including the hygrothermal response of fiber composites. The code outputs are the various ply and composite properties, composite structural response, and composite stress analysis results with details on failure. The code is in Fortran IV and can be used efficiently as a package in complex structural analysis programs. The input-output format is described extensively through the use of a sample problem. The program listing is also included. The code manual consists of two parts. Author

N86-23661*# National Aeronautics and Space Administration. Lewis Research Center, Cleveland, Ohio.

FUNDAMENTAL STUDIES OF LOW VELOCITY IMPACT RESISTANCE OF GRAPHITE FIBER REINFORCED POLYMER MATRIX COMPOSITES Ph.D. Thesis

K. J. BOWLES Nov. 1985 241 p refs Previously announced as N86-10288

(NASA-TM-86886; E-2188; NAS 1.15:86886) Avail: NTIS HC A11/MF A01 CSCL 11D

A study was conducted to relate the impact resistance of graphite fiber reinforced composites with matrix properties through gaining an understanding of the basic mechanics involved in the deformation and fracture process, and the effect of the polymer matrix structure on these mechanisms. It was found that the resin matrix structure influences the composite impact resistance in at least two ways. The integration of flexibilizers into the polymer chain structure tends to reduce the $T_{sub g}$ and the mechanical properties of the polymer. The reduction in the mechanical

24 COMPOSITE MATERIALS

properties of the matrix does not enhance the composite impact resistance because it allows matrix controlled failure to initiate impact damage. It was found that when the instrumented dropweight impact tester is used as a means for assessing resin toughness, the resin toughness is enhanced by the ability of the clamped specimen to deflect enough to produce sufficient membrane action to support a significant amount of the load. The results of this study indicate that crossplied composite impact resistance is very much dependent on the matrix mechanical properties. Dissert. Abstr.

N86-24756*# National Aeronautics and Space Administration. Lewis Research Center, Cleveland, Ohio.

THERMOVISCOPLASTIC NONLINEAR CONSTITUTIVE RELATIONSHIPS FOR STRUCTURAL ANALYSIS OF HIGH TEMPERATURE METAL MATRIX COMPOSITES

C. C. CHAMIS and D. A. HOPKINS 1985 25 p refs Presented at First Symposium on Testing Technology of Metal Matrix Composites, Nashville, Tenn., 18-20, 1985; sponsored by American Society for Testing Materials (NASA-TM-87291; E-2998; NAS 1.15:87291) Avail: NTIS HC A02/MF A01 CSCL 11D

A set of thermoviscoplastic nonlinear constitutive relationships (1VP-NCR) is presented. The set was developed for application to high temperature metal matrix composites (HT-MMC) and is applicable to thermal and mechanical properties. Formulation of the TVP-NCR is based at the micromechanics level. The TVP-NCR are of simple form and readily integrated into nonlinear composite structural analysis. It is shown that the set of TVP-NCR is computationally effective. The set directly predicts complex materials behavior at all levels of the composite simulation, from the constituent materials, through the several levels of composite mechanics, and up to the global response of complex HT-MMC structural components. E.A.K.

N86-24757*# National Aeronautics and Space Administration. Lewis Research Center, Cleveland, Ohio.

A UNIQUE SET OF MICROMECHANICS EQUATIONS FOR HIGH TEMPERATURE METAL MATRIX COMPOSITES

D. A. HOPKINS and C. C. CHAMIS 1985 27 p refs Presented at the 1st Symposium on Testing Technology of Metal Matrix Composites, Nashville, Tenn., 18-20 Nov. 1985; sponsored by American Society for Testing and Materials (NASA-TM-87154; E-2780; NAS 1.15:87154) Avail: NTIS HC A03/MF A01 CSCL 11D

A unique set of micromechanics equations is presented for high temperature metal matrix composites. The set includes expressions to predict mechanical properties, thermal properties and constituent microstresses for the unidirectional fiber reinforced ply. The equations are derived based on a mechanics of materials formulation assuming a square array unit cell model of a single fiber, surrounding matrix and an interphase to account for the chemical reaction which commonly occurs between fiber and matrix. A three-dimensional finite element analysis was used to perform a preliminary validation of the equations. Excellent agreement between properties predicted using the micromechanics equations and properties simulated by the finite element analyses are demonstrated. Implementation of the micromechanics equations as part of an integrated computational capability for nonlinear structural analysis of high temperature multilayered fiber composites is illustrated. E.A.K.

N86-24759*# National Aeronautics and Space Administration. Lewis Research Center, Cleveland, Ohio.

SIMPLIFIED COMPOSITE MICROMECHANICS FOR PREDICTING MICROSTRESSES

C. C. CHAMIS 1986 27 p refs Presented at 41st Annual Conference of the Society of the Plastics Industry (SPI) Reinforced Plastics/Composites Inst., Atlanta, Ga., 27-31 Jan. 1986 (NASA-TM-87295; E-2782; NAS 1.15:87295) Avail: NTIS HC A03/MF A01 CSCL 11D

A unified set of composite micromechanics equations is summarized and described. This unified set is for predicting the

ply microstresses when the ply stresses are known. The set consists of equations of simple form for predicting three-dimensional stresses (six each) in the matrix, fiber, and interface. Several numerical examples are included to illustrate use and computational effectiveness of the equations in this unified set. Numerical results from these examples are discussed with respect to their significance on microcrack formation and, therefore, damage initiation in fiber composites. Author

N86-24760*# General Electric Co., Cincinnati, Ohio. Aircraft Engine Business Group.

EVALUATION OF CAPILLARY REINFORCED COMPOSITES Contractor Report, Sep. 1984 - Sep. 1985

J. E. CAHILL, J. F. HALASE, W. K. SOUTH, and L. J. STOFFER Sep. 1985 141 p Original contains color illustrations (Contract NAS3-24386) (NASA-CR-175061; NAS 1.26:175061) Avail: NTIS HC A07/MF A01 CSCL 11D

Anti-icing of the inlet of jet engines is generally performed with high pressure heated air that is directed forward from the compressor through a series of pipes to various manifolds located near the structures to be anti-iced. From these manifolds, the air is directed to all flowpath surfaces that may be susceptible to ice formation. There the anti-icing function may be performed by either heat conduction or film heating. Unfortunately, the prospect of utilizing lightweight, high strength composites for inlet structures of jet engines has been frustrated by the low transverse thermal conductivity of such materials. It was the objective of this program to develop an advanced materials and design concept for anti-icing composite structures. The concept that was evaluated used capillary glass tubes embedded on the surface of a composite structure with heated air ducted through the tubes. An analytical computer program was developed to predict the anti-icing performance of such tubes and a test program was conducted to demonstrate actual performance of this system. Test data and analytical code results were in excellent agreement. Both indicate feasibility of using capillary tubes for surface heating as a means for composite engine structures to combat ice accumulation. Author

N86-25417*# National Aeronautics and Space Administration. Lewis Research Center, Cleveland, Ohio.

FRACTURE CHARACTERISTICS OF ANGLEPLY LAMINATES FABRICATED FROM OVERAGED GRAPHITE/EPOXY PREPREG

C. A. GINTY and C. C. CHAMIS 1985 22 p refs Presented at Symposium on Fractography of Modern Engineering Materials, Nashville, Tenn., 18-19 Nov. 1985; Sponsored by American Society for Testing and Materials (NASA-TM-87266; E-2968; NAS 1.15:87266) Avail: NTIS HC A02/MF A01 CSCL 11D

A series of angleplyed graphite/epoxy laminates was fabricated from overaged prepreg and tested in tension to investigate the effects of overaged or advanced cure material on the degradation of laminate strength. Results, which include fracture stresses, indicate a severe degradation in strength. In addition, the fracture surfaces and microstructural characteristics are distinctly unlike any features observed in previous tests of this prepreg and laminate configuration. Photographs of the surfaces and microstructures reveal flat morphologies consisting of alternate rows of fibers and hackles. These fracture surface characteristics are independent of the laminate configurations. The photomicrographs are presented and compared with data from similar studies to show the unique characteristics produced by the overage prepreg. Analytical studies produced results which agreed with those from the experimental investigations. Author

N86-26376*# National Aeronautics and Space Administration. Lewis Research Center, Cleveland, Ohio.

COMPUTATIONAL SIMULATION OF PROGRESSIVE FRACTURE IN FIBER COMPOSITES

C. C. CHAMIS 1986 12 p refs Presented at the International Conference on Computational Mechanics, Tokyo, Japan, 25-28 May 1986

(NASA-TM-87341; E-3090; NAS 1.15:87341) Avail: NTIS HC A02/MF A01 CSCL 11D

Computational methods for simulating and predicting progressive fracture in fiber composite structures are presented. These methods are integrated into a computer code of modular form. The modules include composite mechanics, finite element analysis, and fracture criteria. The code is used to computationally simulate progressive fracture in composite laminates with and without defects. The simulation tracks the fracture progression in terms of modes initiating fracture, damage growth, and imminent global (catastrophic) laminate fracture. Author

N86-27426*# National Aeronautics and Space Administration. Lewis Research Center, Cleveland, Ohio.

THE CORRELATION OF LOW-VELOCITY IMPACT RESISTANCE OF GRAPHITE-FIBER-REINFORCED COMPOSITES WITH MATRIX PROPERTIES

K. J. BOWLES 1986 24 p Presented at the 8th Symposium on Composite Materials Testing and Design, Charleston, S. Car., 29 Apr. - 1 May 1986; sponsored by the American Society for Testing and Materials

(NASA-TM-87337; E-3084; NAS 1.15:87337) Avail: NTIS HC A02/MF A01 CSCL 11D

Summarized are basic studies that were conducted to correlate the impact resistance of graphite-fiber-reinforced composites with polymer matrix properties. Three crosslinked epoxy resins and a linear polysulfone were selected as composite matrices. As a group, these resins possess a significantly large range of mechanical properties. The mechanical properties of the resins and their respective composites were measured. Neat resin specimens and unidirectional and crossply composite specimens were impact tested with an instrumented dropweight tester. Impact resistances of the specimens were assessed on the basis of loading capability, energy absorption, and extent of damage. Author

N86-31663*# National Aeronautics and Space Administration. Lewis Research Center, Cleveland, Ohio.

FIBER COMPOSITE SANDWICH THERMOSTRUCTURAL BEHAVIOR: COMPUTATIONAL SIMULATION

C. C. CHAMIS, R. A. AIELLO, and P. L. N. MURTHY (Cleveland State Univ., Ohio) 1986 18 p Presented at the 27th Structures, Structural Dynamics and Materials Conference (SDM), San Antonio, Tex., 19-21 May 1986; sponsored by AIAA, ASME, ASCE and AHS

(NASA-TM-88787; E-3112; NAS 1.15:88787) Avail: NTIS HC A02/MF A01 CSCL 11D

Several computational levels of progressive sophistication/simplification are described to computationally simulate composite sandwich hygral, thermal, and structural behavior. The computational levels of sophistication include: (1) three-dimensional detailed finite element modeling of the honeycomb, the adhesive and the composite faces; (2) three-dimensional finite element modeling of the honeycomb assumed to be an equivalent continuous, homogeneous medium, the adhesive and the composite faces; (3) laminate theory simulation where the honeycomb (metal or composite) is assumed to consist of plies with equivalent properties; and (4) derivations of approximate, simplified equations for thermal and mechanical properties by simulating the honeycomb as an equivalent homogeneous medium. The approximate equations are combined with composite hygrothermomechanical and laminate theories to provide a simple and effective computational procedure for simulating the thermomechanical/thermostructural behavior of fiber composite sandwich structures. Author

N86-31664*# National Aeronautics and Space Administration. Lewis Research Center, Cleveland, Ohio.

ICAN: A VERSATILE CODE FOR PREDICTING COMPOSITE PROPERTIES

C. A. GINTY and C. C. CHAMIS 1986 20 p Presented at the 31st National SAMPE Symposium and Exhibition, Las Vegas, Nev., 7-10 Apr. 1986

(NASA-TM-87334; E-2017; NAS 1.15:87334) Avail: NTIS HC A02/MF A01 CSCL 11D

The Integrated Composites ANalyzer (ICAN), a stand-alone computer code, incorporates micromechanics equations and laminate theory to analyze/design multilayered fiber composite structures. Procedures for both the implementation of new data in ICAN and the selection of appropriate measured data are summarized for: (1) composite systems subject to severe thermal environments; (2) woven fabric/cloth composites; and (3) the selection of new composite systems including those made from high strain-to-fracture fibers. The comparisons demonstrate the versatility of ICAN as a reliable method for determining composite properties suitable for preliminary design. M.G.

25

INORGANIC AND PHYSICAL CHEMISTRY

Includes chemical analysis, e.g., chromatography; combustion theory; electrochemistry; and photochemistry.

A86-10201* Science Applications International Corp., Princeton, N.J.

TWO DIMENSIONAL, TRANSIENT CATALYTIC COMBUSTION OF CO-AIR ON PLATINUM

N. SINHA (SAI, Inc., Princeton, NJ), C. BRUNO (CNR, CNPM, Milan, Italy), and F. V. BRACCO (Princeton University, NJ) PCH/PhysicoChemical Hydrodynamics (ISSN 0191-9059), vol. 6, no. 4, 1985, p. 373-391. refs

(Contract AF-AFOSR-76-3052; NAG3-8)

The light off transient of catalytic combustion of lean CO-air mixtures in a platinum coated channel of a honeycomb monolith is studied with a model that resolves transient radial and axial

N86-29908*# National Aeronautics and Space Administration. Lewis Research Center, Cleveland, Ohio.

CARBON-RICH CERAMIC COMPOSITES FROM ETHYNYL AROMATIC PRECURSORS

F. I. HURWITZ 1986 13 p Presented at the Tenth Annual Conference on Composites and Advanced Ceramic Materials, Cocoa, Beach, Fla., 19-24 Jan. 1986; sponsored by the American Ceramic Society

(NASA-TM-88812; E-3167; NAS 1.15:88812) Avail: NTIS HC A02/MF A01 CSCL 11D

A number of polyfunctional aromatic acetylenes thermally polymerize at low temperatures (180 C) and pyrolyze with greater than 90 char yield. In nonoxidizing environments, they are thermally stable to 1450 C. These monomers were chosen as the basis of a model system to study the fabrication and mechanical properties of continuous filament ceramic matrix composite. Composites were fabricated from aryl poly(acetylenes), SiC particulate filler and graphite, Avco SiC, Nicalon and Nextel fibers. Microstructure, physical and mechanical properties are reported. Author

gradients in both the gas and the solid. For the conditions studied it is concluded that: the initial heat release occurs near the entrance at the gas-solid interface and is controlled by heterogeneous reactions; large spatial and temporal temperature gradients occur in the solid near the entrance controlled mostly by the availability of fuel; the temperature of the solid near the entrance achieves almost its steady state value before significant heating of the back; heterogeneous reactions and the gas heated up front and flowing downstream heat the back of the solid; the overall transient time is controlled by the thermal inertia of the solid and by forced convection; radiation significantly influences both transient and steady state particularly near the entrance; the oxidation of CO occurs mostly on the catalyst and becomes diffusion controlled soon into the transient. Author

A86-12413* National Aeronautics and Space Administration. Lewis Research Center, Cleveland, Ohio.

EFFECT OF GRAVITY ON LAMINAR PREMIXED GAS COMBUSTION. I - FLAMMABILITY LIMITS AND BURNING VELOCITIES

P. D. RONNEY (NASA, Lewis Research Center, Cleveland, OH; MIT, Cambridge, MA) and H. Y. WACHMAN (MIT, Cambridge, MA) Combustion and Flame (ISSN 0010-2180), vol. 62, Nov. 1985, p. 107-119. refs

A comparison of fuel-lean flammability limits and burning velocities in closed vessels for methane-air mixtures between zero-g and one-g at initial pressure of 50-1500 torr, made possible by the elimination of natural convection, is presented. Some of the findings are: the one-g upward flammability limit occurs at a mixture which has a burning velocity which is so low that flame propagation is impractical, that the one-g downward flammability limit is related to the inability of the flame front to propagate downward against buoyant forces, and that near-limit flame propagation at zero-g is mostly independent of the experimental apparatus. F.J.

A86-12414* National Aeronautics and Space Administration. Lewis Research Center, Cleveland, Ohio.

EFFECT OF GRAVITY ON LAMINAR PREMIXED GAS COMBUSTION. II - IGNITION AND EXTINCTION PHENOMENA

P. D. RONNEY (NASA, Lewis Research Center, Cleveland, OH; MIT, Cambridge, MA) Combustion and Flame (ISSN 0010-2180), vol. 62, Nov. 1985, p. 121-133. refs (Contract NAG3-173)

At the initial pressure of 50-1500 torr, the minimum ignition energies and flame radii for near-limit, limit, and sublimit fuel-lean methane-air mixtures burning at one-g and zero-g measured as a function of time, are examined. The same minimum ignition energy values are obtained at one-g and zero-g except for mixtures near zero-g flammability limit and leaner, where the zero-g values are much higher than the one-g values. The unstable flame propagation of sublimit mixtures at zero-g is observed to have a flame radius increasing in proportion to the square root of the time lapse from ignition and sudden extinction. This type of behavior is more pronounced at higher pressures. It is found that a flame-front instability is responsible for the flame extinguishment at zero-g. It is also found that gravitational forces stabilize upward flame propagation. V.L.

A86-12925* California Univ., Berkeley.

DYNAMIC FEATURES OF COMBUSTION

A. K. OPPENHEIM (California, University; California, University, Lawrence Berkeley Laboratory, Berkeley) Royal Society (London) Philosophical Transactions, Series A (ISSN 0080-4614), vol. 315, no. 1534, Sept. 26, 1985, p. 471-508. refs (Contract DE-AC03-76SF-00098; NSF CPE-83-02232; NAG3-131; NAG3-137)

The dynamic features of combustion are discussed for four important cases: ignition, inflammation, explosion, and detonation. Ignition, the initiation of a self-sustained exothermic process, is considered in the simplest case of a closed thermodynamic system and its stochastic distribution. Inflammation, the initiation and propagation of self-sustained flames, is presented for turbulent

flow. Explosion, the dynamic effects caused by the deposition of exothermic energy in a compressible medium, is illustrated by self-similar blast waves with energy deposition at the front and the adiabatic non-self-similar wave. Detonation, the most comprehensive illustration of all the dynamic effects of combustion, is discussed with a phenomenological account of the development and structure of the wave. C.D.

A86-15804*# Science Applications International Corp., Chatsworth, Calif.

EFFECTS OF BUOYANCY ON GAS JET DIFFUSION FLAMES - EXPERIMENT AND THEORY

R. B. EDELMAN and M. Y. BAHADORI (Science Applications International Corp., Chatsworth, CA) IAF, International Astronautical Congress, 36th, Stockholm, Sweden, Oct. 7-12, 1985. 8 p. refs

(Contract NAS3-22822)

(IAF PAPER 85-288)

Theoretical and experimental research on the effects of buoyancy on gas-jet diffusion flames is described. Part of this research involves an assessment of existing data obtained under reduced-gravity conditions. The results show that uncertainties in the current understanding of flame structure exist and further research is required before reliable predictions of ignition, stabilization, and propagation of flames under microgravity conditions can be made. Steady-state and transient theories have been developed and used in the analysis of existing drop-tower data and new data obtained from a stationary experiment involving inverted flames. The result of this research has led to the definition of a microgravity experiment to be performed in space. Author

A86-15805*# California Univ., Berkeley.

BUOYANCY EFFECTS ON SMOLDERING COMBUSTION

S. DOSANJH, J. PETERSON, A. C. FERNANDEZ-PELLO, and P. J. PAGNI (California, University, Berkeley) IAF, International Astronautical Congress, 36th, Stockholm, Sweden, Oct. 7-12, 1985. 31 p. refs

(Contract NAG3-443)

(IAF PAPER 85-289)

The effect of buoyancy on the rate of spread of a concurrent smolder reaction through a porous combustible material is investigated theoretically and experimentally. In the experiments, buoyant forces are controlled by varying the density difference, and the smolder rate spread through porous alpha cellulose (0.83 void fraction) is measured as a function of the ambient air pressure. The smolder velocity is found to increase with the ambient pressure; extinction occurs when the buoyancy forces cannot overcome the drag forces, indicating that diffusion by itself cannot support the spread of a smolder reaction. Theoretical predictions are found to be in good qualitative agreement with the experimental results. V.L.

A86-19389* State Univ. of New York, Stony Brook.

THEORY OF HOMOGENEOUS NUCLEATION - A CHEMICAL KINETIC VIEW

C. H. YANG and H. QIU (New York, State University, Stony Brook) Journal of Chemical Physics (ISSN 0021-9606), vol. 84, Jan. 1, 1986, p. 416-423. refs

(Contract NCC3-2)

A simple function with two undetermined parameters has been used in place of the Thomson-Gibbs relation to relate the activation energy of the vaporization reaction to cluster size. The parameters are iterated to assume optimum values in numerical computation so experimental data may be correlated. Calculations show this approach closely predicts and correlates available data for water, benzene, and ethanol. The nucleation formalism is redeveloped with an emphasis on the chemical kinetic view. Surface tension of the liquid and free energy of droplet formation are not used in its derivation. Author

A86-19962* California Univ., Berkeley.

TEMPERATURE AND VELOCITY PROFILES IN SOOTING FREE BOUNDARY LAYER FLAMES

J. A. ANG, P. J. PAGNI, T. G. MATAGA (California, University, Berkeley), J. M. MARGLE, and V. J. LYONS (NASA, Lewis Research Center, Cleveland, OH) AIAA, Aerospace Sciences Meeting, 24th, Reno, NV, Jan. 6-9, 1986. 10 p. NBS-supported research. refs

(AIAA PAPER 86-0575)

Temperature and velocity profiles are presented for cyclohexane, n-heptane, and iso-octane free, laminar, boundary layer, sooting, diffusion flames. Temperatures are measured with 3 mil Pt/Pt-13 percent Rh thermocouples. Corrected gas temperatures are derived by performing an energy balance of convection to and radiation from the thermocouple bead incorporating the variation of air conductivity and platinum emissivity with temperature. Velocities are measured using laser doppler velocimetry techniques. Profiles are compared with previously reported analytic temperature and velocity fields. Comparison of theoretical and experimental temperature profiles suggests improvement in the analytical treatment is needed, which accounts more accurately for the local soot radiation. The velocity profiles are in good agreement with the departure of the theory from observation partially due to the small fluctuations inherent in these free flows. Author

A86-20139* Pennsylvania State Univ., University Park.

DROP-TURBULENCE INTERACTIONS IN A DIFFUSION FLAME

J.-S. SHUEN, A. S. P. SOLOMON, and G. M. FAETH (Pennsylvania State University, University Park) AIAA Journal (ISSN 0001-1452), vol. 24, Jan. 1986, p. 101-108. Previously cited in issue 07, p. 874, Accession no. A85-19665. refs

(Contract NAG3-190)

A86-22751*

SYMPOSIUM (INTERNATIONAL) ON COMBUSTION, 20TH, UNIVERSITY OF MICHIGAN, ANN ARBOR, MI, AUGUST 12-17, 1984, PROCEEDINGS

Symposium sponsored by the Combustion Institute, Army, DOE, NASA, et al. Pittsburgh, PA, Combustion Institute, 1985, 2235 p. For individual items see A86-22752 to A86-22824.

(Contract DAAG29-84-M-0049; DAAG07-84-M-R031; DE-FG05-84ER-13166; NAS3-24261)

The present conference on combustion phenomena considers topics in automotive engine combustion, turbulent reacting flows, the modeling of practical combustion systems, reaction kinetics, combustion-generated particulates, combustion diagnostics, coal combustion process characteristics, fire-related phenomena, explosion/detonation phenomena, spray combustion, ignition/extinction, laminar flames, pollutant formation processes, practical combustor devices, and rocket propellant combustion. Attention is given to the contributions of combustion science to piston engine design, modeling and measurement techniques for turbulent combustion, the specific effects of energy, collisions, and transport processes in combustion chemistry kinetics, the formation of large molecules, particulates and ions in premixed hydrocarbon flames, the application of laser diagnostics to combustion systems, spark ignition energies for dust-air mixtures, the controlling mechanisms of flow-assisted flame spread, the ignition and combustion of coal-water slurries, spontaneous ignition of methane, turbulent and accelerating dust flames, and the temperature sensitivity of double base propellants. O.C.

A86-22755* Cornell Univ., Ithaca, N.Y.

PERIODIC OSCILLATIONS OBSERVED IN SWIRLING FLOWS WITH AND WITHOUT COMBUSTION

F. C. GOULDIN, R. N. HALTHORE, and B. T. VU (Cornell University, Ithaca, NY) IN: Symposium (International) on Combustion, 20th, Ann Arbor, MI, August 12-17, 1984, Proceedings. Pittsburgh, PA, Combustion Institute, 1985, p. 269-276. refs

(Contract DE-AC04-77CS-04508; NSG-3019)

Data obtained by laser induced Rayleigh scattering and hot-wire anemometry are used to study periodic oscillations in swirling flows

with and without combustion present. Power spectral density functions reveal the presence of energetic, periodic oscillations in the flow. A band of low frequency oscillations (25-100 Hz) is observed on and near the centerline in the presence of a recirculation zone and is attributed to axial oscillations of the recirculation zone which are amplified with combustion by an interaction between the mechanism for flow recirculation and flow changes induced by combustion. High frequency oscillations between 300-500 Hz are observed in an annular region located in the vortex core. A stability analysis is performed, and it is concluded that these oscillations are most likely helical waves resulting from hydrodynamic instability in the vortex core upstream of the test section. Author

A86-22774* California Univ., Berkeley.

NUMERICAL SIMULATION OF A TURBULENT FLAME STABILIZED BEHIND A REARWARD-FACING STEP

C. C. HSIAO, A. K. OPPENHEIM, A. J. CHORIN (California, University, Berkeley), and A. F. GHONIEM (MIT, Cambridge, MA) IN: Symposium (International) on Combustion, 20th, Ann Arbor, MI, August 12-17, 1984, Proceedings. Pittsburgh, PA, Combustion Institute, 1985, p. 495-504. refs

(Contract DE-AC03-76SF-0098; NSF CPE-81-15163; NAG3-131)

Flow of combustible mixtures in a plane channel past a smooth contraction followed by an abrupt expansion, in a typical dump combustor configuration, is modeled by a two-dimensional numerical technique based on the random vortex method. Both the inert and the reacting case are considered. In the latter, the flame is treated as an interface, self-advancing at a prescribed normal burning speed, while the dynamic effects of expansion due to the exothermicity of combustion are expressed by volumetric source lines delineated by its front. Solutions are shown to be in satisfactory agreement with experimental results, especially with respect to global properties such as the average velocity profiles and the reattachment length. The stochastic turbulent velocity components manifest interesting differences, especially near the walls where three-dimensional effects of turbulence are expected to be of importance. Author

A86-22793* Kentucky Univ., Lexington.

BACKWARD BOUNDARY LAYERS IN DOWNWARD FLAME SPREAD

M. VEDHA-NAYAGAM and R. A. ALTENKIRCH (Kentucky, University, Lexington) IN: Symposium (International) on Combustion, 20th, Ann Arbor, MI, August 12-17, 1984, Proceedings. Pittsburgh, PA, Combustion Institute, 1985, p. 1583-1589; Discussion, p. 1589, 1590. refs

(Contract NSG-3114; NAG3-258)

The gas-phase combustion of a vertical fuel slab pyrolyzing at a finite rate under downward flame spread conditions is investigated theoretically. The backward boundary layer character of the flow is exploited, and a transformation that shifts the singularity associated with boundary-layer equations to a location, upstream of flame lift-off, where the surface temperature is nearly ambient, is employed. The boundary-layer flow is matched asymptotically for large Grashof number to a potential flow that allows the flow induced by the flame and along the upstream surface of the fuel bed to be calculated. Gas-phase temperature and velocity predictions are compared to experiment, and although analysis of the gas phase is emphasized, an approximate spread rate, based on a solid-phase energy balance, is calculated. Author

A86-22813* Keio Univ., Yokohama (Japan).

EFFECTS OF PREFERENTIAL DIFFUSION ON THE BURNING INTENSITY OF CURVED FLAMES

M. MIZOMOTO, Y. ASAKA, S. IKAI (Keio University, Yokohama, Japan), and C. K. LAW (Northwestern University, Evanston, IL) IN: Symposium (International) on Combustion, 20th, Ann Arbor, MI, August 12-17, 1984, Proceedings. Pittsburgh, PA, Combustion Institute, 1985, p. 1933-1939. refs

(Contract NAG3-361)

Using the Bunsen flame as a model curved flame, the coupled influence of preferential diffusion and flame stretch on the burning

intensity of lean and rich mixtures of methane, propane, butane, ethylene, and hydrogen with air has been experimentally studied. The results substantiate theoretical predictions and quantify previous experimental observations that, for mixtures whose effective Lewis numbers (Le) are less than unity, the flame temperature is less than the adiabatic flame temperature. This temperature also decreases towards the flame tip, which has the largest curvature and therefore may locally extinguish. The dominance of diffusional transport in influencing the intensity of curved flames is demonstrated by showing that the tip opening of the highly diffusive hydrogen/air flames occurs at constant hydrogen equivalence ratios of about 1.15 to 1.20, being almost independent of the flow intensity and uniformity. Author

A86-22814* Chinese Academy of Sciences, Peking.
ON THE DETERMINATION OF LAMINAR FLAME SPEEDS FROM STRETCHED FLAMES

C. K. WU (Chinese Academy of Sciences, Institute of Mechanics, Beijing, People's Republic of China) and C. K. LAW (Northwestern University, Evanston, IL) IN: Symposium (International) on Combustion, 20th, Ann Arbor, MI, August 12-17, 1984, Proceedings . Pittsburgh, PA, Combustion Institute, 1985, p. 1941-1948; Discussion, p. 1949. refs
(Contract NAG3-361; DE-AC02-84ER-13173)

The effects of stretch on the determination of the laminar flame speed are experimentally studied by using the positively-stretched stagnation flame and negatively-stretched bunsen flame, and by using lean and rich mixtures of methane, propane, butane, and hydrogen with air whose effective Lewis numbers are either greater or less than unity. Results demonstrate that flame speed determination can be influenced by stretch through two factors: (1) Preferential diffusion which tends to increase or decrease the flame temperature and burning rate depending on the effective Lewis number, and (2) Flow divergence which causes the flame speed to assume higher values when evaluated at the upstream boundary of the preheat zone instead of the reaction zone. Recent data on flame speed including the present ones are then examined from the unified viewpoint of flame stretch, leading to satisfactory resolution of the discrepancies between them. The present study also proposes a methodology of determining the laminar flame speeds by using the stagnation flame and linearly extrapolating the data to zero stretch rate. Author

A86-22816* Northwestern Univ., Evanston, Ill.
AN EXPERIMENTAL INVESTIGATION ON FLAME INTERACTION AND THE EXISTENCE OF NEGATIVE FLAME SPEEDS

S. H. SOHRAB, Z. Y. YE, and C. K. LAW (Northwestern University, Evanston, IL) IN: Symposium (International) on Combustion, 20th, Ann Arbor, MI, August 12-17, 1984, Proceedings . Pittsburgh, PA, Combustion Institute, 1985, p. 1957-1964; Discussion, p. 1964, 1965. refs
(Contract NAG3-361)

Downstream interaction between two counterflow premixed flames of different stoichiometries are investigated. Various flame configurations are observed and quantified; these include the binary system of two lean or rich flames, the triplet system of a lean and a rich flame separated by a diffusion flame, and single diffusion flames with some degree of premixedness. Extinction limits are determined for methane/air and butane/air mixtures over the entire range of mixture concentrations. Results show that these extinction limits can be significantly modified in the presence of interaction such that a mixture much beyond the flammability limit can still burn if it is supported by a stronger flame. The experiment also demonstrates the existence of negative flames whose propagation velocity is in the same general direction as that of the bulk convective flow. Implications of the present results on the flammability of stratified mixtures and on the modeling of turbulent flames are discussed. Author

A86-23352* Westinghouse Research and Development Center, Pittsburgh, Pa.

TRANSMISSION ELECTRON MICROSCOPIC EXAMINATION OF PHOSPHORIC ACID FUEL CELL COMPONENTS

A. PEBLER (Westinghouse Research and Development Center, Pittsburgh, PA) (Electrochemical Society, Meeting, New Orleans, LA, Oct. 7-12, 1985) Electrochemical Society, Journal (ISSN 0013-4651), vol. 133, Jan. 1986, p. 9-17. DOE-supported research. refs
(Contract DEN3-290)

Transmission electron microscopy (TEM) was used to physically characterize tested and untested phosphoric acid fuel cell (PAFC) components. Those examined included carbon-supported platinum catalysts, carbon backing paper, and Teflon-bonded catalyst layers at various stages of fabrication and after testing in pressurized PAFC's. Applicability of electron diffraction and electron energy loss spectroscopy for identifying the various phases was explored. The discussion focuses on the morphology and size distribution of platinum, the morphology and structural aspects of Teflon in catalyst layers, and the structural evidence of carbon corrosion. Reference is made to other physical characterization techniques where appropriate. A qualitative model of the catalyst layer that emerged from the TEM studies is presented. Author

A86-29070* Purdue Univ., West Lafayette, Ind.
INFLUENCE OF TEMPERATURE AND HYDROXYL CONCENTRATION ON INCIPIENT SOOT FORMATION IN PREMIXED FLAMES

M. M. HARRIS, G. B. KING, and N. M. LAURENDEAU (Purdue University, West Lafayette, IN) Combustion and Flame (ISSN 0010-2180), vol. 64, April 1986, p. 99-112. refs
(Contract NAG3-360)

Critical equivalence ratios $\phi(c)$ have been measured as a function of temperature (1600-1880 K) for premixed flames at atmospheric pressure. The five fuels studied are methane, ethane, propane, ethylene, and acetylene. The flames were stabilized on a flat flame burner and the temperatures were measured using sodium D-line reversal. A linear relationship is found between $\ln \phi(c)$ and $1/T$ for each fuel. Based on a global kinetic model in which soot precursors are formed by fuel pyrolysis and oxidized by OH, a predictive correlation has been developed which shows the influence of temperature, OH concentration, and C/H ratio on sooting tendency. This correlation describes all of the measured $\phi(c)$ versus temperature data, suggesting that the overall mechanism of soot formation is similar among aliphatic fuels. Author

A86-32752* Northwestern Univ., Evanston, Ill.
THEORY OF INTERACTIVE COMBUSTION OF COUNTERFLOW PREMIXED FLAMES

S. H. SOHRAB, Z. Y. YE, and C. K. LAW (Northwestern University, Evanston, IL) Combustion Science and Technology (ISSN 0010-2202), vol. 45, no. 1-2, 1986, p. 27-45. refs
(Contract NAG3-361; DE-FG03-84ER-13274)

The framework of large activation energy asymptotics is used in an investigation of the extinction characteristics of two interacting premixed flames in counterflow configuration, analyzing the interactive combustion modes of two lean premixed flames, two rich premixed flames, and one of each type of flame separated by a diffusion flame. Regions corresponding to symbiotic combustion of two lean or two rich premixed flames exist in which either flame will be extinguished in the absence of the other. Conditions for the existence of superadiabatic flames within mixtures outside of the conventional flammability limit compositions are established, and practical implications of flame interaction for combustion in inhomogeneous mixtures are discussed. O.C.

A86-32958* National Aeronautics and Space Administration. Lewis Research Center, Cleveland, Ohio.

NEW INTEGRATION TECHNIQUES FOR CHEMICAL KINETIC RATE EQUATIONS. II - ACCURACY COMPARISON

K. RADHAKRISHNAN (NASA, Lewis Research Center, Cleveland, OH) ASME, Transactions, Journal of Engineering for Gas Turbines and Power (ISSN 0022-0825), vol. 108, April 1986, p. 348-353. Previously announced in STAR as N85-13798. refs (ASME PAPER 85-GT-30)

A comparison of the accuracy of several techniques recently developed for solving stiff differential equations is presented. The techniques examined include two general purpose codes EEPISODE and LSOE developed for an arbitrary system of ordinary differential equations, and three specialized codes CHEMEQ, CREKID, and GCKP84 developed specifically to solve chemical kinetic rate equations. The accuracy comparisons are made by applying these solution procedures to two practical combustion kinetics problems. Both problems describe adiabatic, homogeneous, gas phase chemical reactions at constant pressure, and include all three combustion regimes: induction heat release, and equilibration. The comparisons show that LSOE is the most efficient code - in the sense that it requires the least computational work to attain a specified accuracy level. An important finding is that an iterative solution of the algebraic enthalpy conservation equation for the temperature can be more accurate and efficient than computing the temperature by integrating its time derivative.

M.G.

A86-34238* Case Western Reserve Univ., Cleveland, Ohio.

ADSORPTION OF O₂, SO₂, AND SO₃ ON NICKEL OXIDE - MECHANISM FOR SULFATE FORMATION

S. P. MEHANDRU and A. B. ANDERSON (Case Western Reserve University, Cleveland, OH) Electrochemical Society, Journal (ISSN 0013-4651), vol. 133, April 1986, p. 828-832. refs (Contract NAG3-341)

Calculations based on the atom superposition and electron delocalization molecular orbital technique suggest that O₂ will adsorb preferentially end-on at an angle 45 deg from normal on a nickel cation site on the (100) surface of NiO. SO₂ adsorption is also stronger on the nickel site; SO₂ bonds through the sulfur atom in a plane perpendicular to the surface. Adsorption energies for SO₃ on the nickel and oxygen sites are comparable in the preferred orientation in which the SO₃ plane is parallel to the surface. The calculations suggest that the strength of adsorption varies as O₂ greater than SO₂ greater than SO₃. On activation, SO₃ adsorbed to an O(2-) site forms a trigonal pyramidal SO₄ species which yields, with a low barrier, a tetrahedral sulfate anion. Subsequently the anion reorients on the surface. Alternative mechanisms which require the formation of Ni(3+) or O(-) are discussed. NiSO₄ thus formed may play a passivating role for the corrosion of Ni at low temperatures in the SO₂ + O₂ + SO₃ atmospheres and an active role at high temperatures, as discussed in the experimental literature.

Author

A86-35126* Louisiana State Univ., Baton Rouge.

SHOCK-TUBE PYROLYSIS OF CHLORINATED HYDROCARBONS - FORMATION OF SOOT

M. FRENKLACH, J. P. HSU, D. L. MILLER, and R. A. MATULA (Louisiana State University, Baton Rouge) Combustion and Flame (ISSN 0010-2180), vol. 64, May 1986, p. 141-155. refs (Contract EPA-CR-809140-10; NAG3-477)

Soot formation in pyrolysis of chlorinated methanes, their mixtures with methane, and chlorinated ethylenes were studied behind reflected shock waves by monitoring the attenuation of an He-Ne laser beam. An additional single-pulse shock-tube study was conducted for the pyrolysis of methane, methyl chloride, and dichloromethane. The experiments were performed at temperatures 1300-3000 K, pressures of 0.4-3.6 bar, and total carbon atom concentrations of 1-5 x 10 to the 17th atoms cu cm. The amounts of soot produced in the pyrolysis of chlorinated hydrocarbons are larger than that of their nonchlorinated counterparts. The sooting behavior and product distribution can be generally explained in terms of chlorine-catalyzed chemical reaction mechanisms. The

pathway to soot from chlorinated methanes and ethylenes with high H:Cl ratio proceeds via the formation of C₂H, C₂H₂, and C₂H₃ species. For chlorinated hydrocarbons with low H:Cl ratio, the formation of C₂ and its contribution to soot formation at high temperatures becomes significant. There is evidence for the importance of HCl radical and its reactions in the pyrolysis of dichloromethane.

Author

A86-38090* National Aeronautics and Space Administration. Lewis Research Center, Cleveland, Ohio.

NEW INTEGRATION TECHNIQUES FOR CHEMICAL KINETIC RATE EQUATIONS. I - EFFICIENCY COMPARISON

K. RADHAKRISHNAN (NASA, Lewis Research Center, Cleveland, OH) Combustion Science and Technology (ISSN 0010-2202), vol. 46, no. 1-2, 1986, p. 59-81. refs (Contract NAG3-294)

A comparison of the efficiency of several recently developed numerical techniques for solving chemical kinetic rate equations is presented. The solution procedures examined include two general-purpose codes, EEPISODE and LSOE, developed as multipurpose differential equation solvers, and three specialized codes, CHEMEQ, CREKID, and GCKP84, developed specifically for chemical kinetics. The efficiency comparison is made by applying these codes to two practical combustion kinetics problems. Both problems describe adiabatic, constant-pressure, gas-phase chemical reactions and include all three combustion regimes: induction, heat release, and equilibration. The comparison shows that LSOE is the fastest routine currently available for solving chemical kinetic rate equations. An important finding is that an iterative solution of the algebraic enthalpy conservation equation for temperature can be significantly faster than evaluation of the temperature by integration of its time derivative. Significant increases in computational speed are realized by updating the reaction rate constants only when the temperature change exceeds an amount Delta-T that is problem dependent. An approximate expression for the automatic evaluation of Delta-T is presented and is shown to result in increased computational speed.

Author

A86-40677* National Aeronautics and Space Administration. Lewis Research Center, Cleveland, Ohio.

THE REACTIONS OF COBALT, IRON AND NICKEL IN SO₂ ATMOSPHERES SIMILARITIES AND DIFFERENCES

N. S. JACOBSON (NASA, Lewis Research Center, Cleveland, OH) and W. L. WORRELL (Pennsylvania, University, Philadelphia) IN: Transport in nonstoichiometric compounds. New York, Plenum Publishing Corp., 1985, p. 451-461. Previously announced in STAR as N85-11217. refs (Contract NSF DMR-79-23647)

The reactions of cobalt, iron and nickel in SO₂ atmospheres are reviewed and compared. A mixed oxide-sulfide product layer is observed in all cases. Cobalt and nickel exhibit similar behavior. The observed rates are near the sulfidation rates, and the reaction rate is strongly influenced by the outward diffusion of metal through an interconnected sulfide network. A continuous interconnected sulfide is not observed in the oxide-sulfide scales formed on iron, and the reaction rates are more difficult to summarize. The differences and similarities among the three metals are explained in terms of the absence of scale-gas equilibrium and the ratio of the metal diffusivity in the corresponding oxide and sulfide.

Author

A86-40834* Princeton Univ., N. J.

THE HIGH-TEMPERATURE OXIDATION OF AROMATIC HYDROCARBONS

K. BREZINSKY (Princeton University, NJ) Progress in Energy and Combustion Science (ISSN 0360-1285), vol. 12, no. 1, 1986, p. 1-24. Research supported by the Mobil Oil Corp. refs (Contract F49620-82-K-0011; NAG3-310)

Chemical mechanisms of the atmospheric pressure, high-temperature (875-1500 K) gas-phase oxidation of benzene, toluene, ethylbenzene, and propylbenzene are described and discussed. Oxidation trends evident from turbulent flow reactor experiments serve as the basis for the mechanisms of the oxidation

of benzene and alkylated aromatics. The potential effects of very high temperatures and pressures on the chemistry of oxidation of aromatics are described. The oxidation of benzene and phenyl radical has been found to proceed in a stepwise C6-C5-C4 sequence. Species profiles obtained from flow-reactor experiments suggest that the oxidation of benzene and phenyl radical follows the generalized route via phenoxy, cyclopentadienyl and butadienyl radical. The oxidation of the C4 species branches into multiple pathways that yield copious amounts of ethylene and acetylene. Certain major trends are evident: the alkylated aromatics on initial attack either form styrene, benzyl radical or benzene. The styrene reacts further to produce a benzyl radical or benzene. The oxidation of an alkylated aromatic hydrocarbon appears eventually to reduce to the oxidation of either phenyl radical or benzene. Author

A86-41711* Flow Research, Inc., Kent, Wash.
DIRECT NUMERICAL SIMULATIONS OF A REACTING MIXING LAYER WITH CHEMICAL HEAT RELEASE
 P. A. MCMURTRY, W.-H. JOU, J. J. RILEY, and R. W. METCALFE (Flow Research Co., Kent, WA) AIAA Journal (ISSN 0001-1452), vol. 24, June 1986, p. 962-970. Previously cited in issue 07, p. 874, Accession no. A85-19548. refs
 (Contract NAS3-24229)

A86-43456* National Aeronautics and Space Administration. Lewis Research Center, Cleveland, Ohio.
ANGLE-RESOLVED AUGER ELECTRON SPECTRA INDUCED BY NEON ION IMPACT ON ALUMINUM
 S. V. PEPPER and P. R. ARON (NASA, Lewis Research Center, Cleveland, OH) Surface Science (ISSN 0039-6028), vol. 169, 1986, p. 14-38. refs

Auger electron emission from aluminum bombarded with 1 to 5 keV neon ions was studied by angle-resolved electron spectroscopy. The position and shape of the spectral features depended on the incident ion energy, angle of ion incidence, and electron take-off angle with respect to the aluminum surface. These spectral dependencies were interpreted in terms of the Doppler shift given to the Auger electron velocity by the excited atom ejected into the vacuum. For oblique ion incidence it is concluded that a flux of high energy atoms are ejected in a direction close to the projection of the ion beam on the target surface. In addition, a new spectral feature was found and identified as due to Auger emission from excited neon in the aluminum matrix. Author

A86-43457* National Aeronautics and Space Administration. Lewis Research Center, Cleveland, Ohio.
BINARY COLLISION MODEL FOR NEON AUGER SPECTRA FROM NEON ION BOMBARDMENT OF THE ALUMINUM SURFACE
 S. V. PEPPER (NASA, Lewis Research Center, Cleveland, OH) Surface Science (ISSN 0039-6028), vol. 169, 1986, p. 39-56. refs

A model is developed to account for the angle-resolved Auger spectra from neon ion bombardment of the aluminum surface recently obtained by Pepper and Aron. The neon is assumed to be excited in a single asymmetric neon-aluminum-collision and scattered back into the vacuum where it emits an Auger electron. The velocity of the Auger electron acquires a Doppler shift by virtue of the emission from a moving source. The dependence of the Auger peak shape and energy on the incident ion energy, angle of incidence and on the angle of Auger electron emission with respect to the surface is presented. Satisfactory agreement with the angle resolved experimental observations is obtained. The dependence of the angle-integrated Auger yield on the incident ion energy and angle of incidence is also obtained and shown to be in satisfactory agreement with available experimental evidence. Author

A86-47069* North Carolina State Univ., Raleigh.
DRY ETCHING OF BETA-SiC IN CF₄ AND CF₄ + O₂ MIXTURES

J. W. PALMOUR, R. F. DAVIS (North Carolina State University, Raleigh), T. M. WALLETT, and K. B. BHASIN (NASA, Lewis Research Center, Cleveland, OH) Journal of Vacuum Science and Technology A (ISSN 0734-2101), vol. 4, May-June 1986, pt. I, p. 590-593. refs
 (Contract N00014-82-K-0182)

Dry etching of cubic (100) beta-SiC single-crystal thin films produced via chemical-vapor deposition (CVD) has been performed in CF₄ and CF₄ + O₂ mixtures, in both the reactive-ion-etching (RIE) and plasma-etching modes. The latter process yielded measurable etch rates, but produced a dark surface layer which appears, from the results of secondary-ion mass spectrometry, to be residual SiC. The RIE samples had no residual layer, but Auger electron spectroscopy did reveal a C-rich surface. The optimal RIE conditions were obtained with 10 sccm of pure CF₄ at 40 mtorr and a power density of 0.548 W/sq cm, giving an etch rate of 23.3 nm/min. Neither the increase of temperature between 293 and 573 K, nor the incremental addition of O₂ to CF₄ to 50 percent, produced any strong effect on the etch rates of SiC during RIE. Pictorial evidence of fine line structures produced by RIE of beta-SiC films are also presented. Author

A86-47078* Case Western Reserve Univ., Cleveland, Ohio.
CARBON MONOXIDE PRODUCTION IN LOW ENERGY OXYGEN ION BOMBARDMENT OF PYROLYTIC GRAPHITE AND KAPTON SURFACES

C. C. HORTON, T. G. ECK, and R. W. HOFFMAN (Case Western Reserve University, Cleveland, OH) Journal of Vacuum Science and Technology A (ISSN 0734-2101), vol. 4, May-June 1986, pt. II, p. 1236-1239. refs
 (Contract NAG3-426)

The results of an investigation of the interaction of low energy oxygen ions with pyrolytic graphite and Kapton surface are reported. CO molecules emitted from the surface as a result of the ion bombardment were detected by a mass spectrometer. Because the ion-induced signals were small compared to that arising from the CO background pressure in the vacuum system, the ion beam was modulated and the modulated component of the CO signal measured with a lock-in amplifier. The quantum yield (CO molecules emitted per incident oxygen ion) for graphite rose from 1.9 at 4.5 eV ion energy to 6.6 at 465 eV. Comparable yields were obtained for Kapton. The large size of the yields suggests contributions to the reaction process from the background O₂ molecules in the vacuum system. Author

A86-47083* National Aeronautics and Space Administration. Lewis Research Center, Cleveland, Ohio.

SURFACE MODIFICATION STRATEGIES FOR (100)3C-SiC
 J. J. BELLINA, JR. (Saint Mary's College, Notre Dame, IN), J. FERRANTE (NASA, Lewis Research Center, Cleveland, OH), and M. V. ZELLER (Notre Dame, University, IN) Journal of Vacuum Science and Technology A (ISSN 0734-2101), vol. 4, May-June 1986, pt. II, p. 1692-1695. refs
 (Contract NAG3-426)

Several surface modification techniques were performed in situ in an ultrahigh vacuum as part of a program to develop electrical contacts on the (100) face of cubic SiC. The Auger electron spectroscopy line shapes and peak-to-peak heights of the Si LVV and CKLL transitions indicated changes in surface stoichiometry, bonding, and short range order. Changes in the low-energy electron diffraction pattern identified changes in the symmetry of long range ordering on the surface. Heating above 1050 C depleted the surface of Si with an activation energy of 120 kcal/mol, resulting eventually in a disordered graphitic layer which was several atomic layers thick. Bombardment by Ar ions of energies greater than 1000 eV enhanced the Si to C ratio on the surface and destroyed the LEED pattern. Long range order was recovered by simultaneous heating and ion bombardment. Finally, adsorption of Cr on the Ar ion damaged surface and subsequent desorption left a

reconstructed, $p(2 \times 1)\text{Si}$ enriched surface. Similar treatments with Al did not produce a surface reconstruction. Author

A86-49864* National Aeronautics and Space Administration. Lewis Research Center, Cleveland, Ohio.

THE BETA-SiC(100) SURFACE STUDIED BY LOW ENERGY ELECTRON DIFFRACTION, AUGER ELECTRON SPECTROSCOPY, AND ELECTRON ENERGY LOSS SPECTRA
M. DAYAN (NASA, Lewis Research Center, Cleveland, OH)
Journal of Vacuum Science and Technology A (ISSN 0734-2101), vol. 4, Jan.-Feb. 1986, p. 38-45. refs

The beta-SiC(100) surface has been studied by low energy electron diffraction, Auger electron spectroscopy, high resolution electron energy loss spectra (HREELS), and core level excitation EELS. Two new Si-terminated phases have been discovered, one with (3×2) symmetry, and the other with (2×1) symmetry. Models are presented to describe these phases. New results, for the C-rich surface, are presented and discussed. In addition, core level excitation EELS results are given and compared with theory. Author

N86-12268* National Aeronautics and Space Administration. Lewis Research Center, Cleveland, Ohio.

EVALUATION PARAMETERS FOR THE ALKALINE FUEL CELL OXYGEN ELECTRODE

J. SINGER and V. SRINIVASAN (Bowling Green State Univ., Ohio) Nov. 1985 13 p refs
(NASA-TM-87155; E-2669; NAS 1.15:87155) Avail: NTIS HC A02/MF A01 CSCL 07D

Studies were made of Pt- and Au-catalyzed porous electrodes, designed for the cathode of the alkaline H_2/O_2 fuel cell, employing cyclic voltammetry and the floating half-cell method. The purpose was to obtain parameters from the cyclic voltammograms which could predict performance in the fuel cell. It was found that a satisfactory relationship between these two types of measurement could not be established; however, useful observations were made of relative performance of several types of carbon used as supports for noble metal catalysts and of some Au catalysts. The best half-cell performance with H_2/O_2 in a 35 percent KOH electrolyte at 80 C was given by unsupported fine particle Au on Teflon; this electrode is used in the Orbiter fuel cell. Author

N86-14331* Drexel Univ., Philadelphia, Pa. Dept. of Mechanical Engineering and Mechanics.

TRANSITION REGION IGNITION CHARACTERISTICS OF N-HEPTANE FUEL SPRAYS

A. M. DANIS, N. P. CERNANSKY, and I. NAMER Apr. 1985 24 p refs Presented at the Joint Western and Central States Section Combustion Institute Meeting, San Antonio, Texas, 22-23 Apr. 1985

(Contract NAG3-382)
(NASA-CR-176364; NAS 1.26:176364; WS/CSCI-85-1-6B) Avail: NTIS HC A02/MF A01 CSCL 21B

Ignition studies were performed on monodisperse n-heptane sprays at atmospheric pressure over a range of equivalence ratios and droplet diameters. A capacitive discharge spark ignition system was used as the ignition source, providing independent control of spark energy and duration. Preliminary measurements were made to optimize spark duration and spark gap, optimum conditions being those at which the maximum frequency or probability of ignition was observed. The effect of spark duration on ignition frequency for several spark energies was determined for equivalence ratios of 0.5 and 1.0 and initial droplet diameters of 28 and 68 microns. Spark duration had little effect on ignition frequency over the entire 15 to 170 μs range examined. Spark durations of 70 to 80 μs were used for all subsequent work. The spark gap was optimized at equivalence ratios of 0.6, 0.8 and 1.0 and initial droplet diameters of 30, 40, 50, 60 and 70 microns by varying the electrode spacing from 0.5 to 5.0 mm while maintaining a constant spark energy. The optimum gap was determined to be 3.0 mm for nearly all conditions. Author

N86-19417* National Aeronautics and Space Administration. Lewis Research Center, Cleveland, Ohio.

A THIN FILM DEGRADATION STUDY OF A FLUORINATED POLYETHER LIQUID LUBRICANT USING AN HPLC METHOD

W. MORALES 1986 27 p refs Proposed for presentation at the 1986 Annual Meeting of the American Society of Lubrication Engineers, Toronto, Ontario, 12-15 May 1986
(NASA-TM-87221; E-2886; NAS 1.15:87221) Avail: NTIS HC A03/MF A01 CSCL 07D

A High Pressure Liquid Chromatography (HPLC) separation method was developed to study and analyze a fluorinated polyether fluid which is promising liquid lubricant for future applications. This HPLC separation method was used in a preliminary study investigating the catalytic effect of various metal, metal alloy, and ceramic engineering materials on the degradation of this fluid in a dry air atmosphere at 345 C. Using a 440 C stainless steel as a reference catalytic material it was found that a titanium alloy and a chromium plated material degraded the fluorinated polyether fluid substantially more than the reference material. Author

N86-20517* Drexel Univ., Philadelphia, Pa. Dept. of Mechanical Engineering and Mechanics.

COMBUSTION CHARACTERISTICS IN THE TRANSITION REGION OF LIQUID FUEL SPRAYS Final Report, Jan. 1983 - Sep. 1985

N. P. CERNANSKY, I. NAMER, and R. J. TIDONA Jan. 1986 56 p refs

(Contract NAG3-382; DREXEL PROJ. 1098)
(NASA-CR-176564; NAS 1.26:176564) Avail: NTIS HC A04/MF A01 CSCL 21B

A number of important effects have been observed in the droplet size transition region in spray combustion systems. In this region, where the mechanism of flame propagation is transformed from diffusive to premixed dominated combustion, the following effects have been observed: (1) maxima in burning velocity; (2) extension of flammability limits; (3) minima in ignition energy; and (4) minima in NO_x formation. A monodisperse aerosol generator has been used to form and deliver a well controlled liquid fuel spray to the combustion test section where measurements of ignition energy have been made. The ignition studies were performed on monodisperse n-heptane sprays at atmospheric pressure over a range of equivalence ratios and droplet diameters. A capacitive discharge spark ignition system was used as the ignition source, providing independent control of spark energy and duration. Preliminary measurements were made to optimize spark duration and spark gap, optimum conditions being those at which the maximum frequency or probability of ignition was observed. Using the optimum electrode spacing and spark duration, the frequency of ignition was determined as a function of spark energy for three overall equivalence ratios (0.6, 0.8, and 1.0) and for initial droplet diameters of 25, 40, 50, 60, and 70 μm . B.W.

N86-21635* National Aeronautics and Space Administration. Lewis Research Center, Cleveland, Ohio.

METHANE OXIDATION BEHIND REFLECTED SHOCK WAVES: IGNITION DELAY TIMES MEASURED BY PRESSURE AND FLAME BAND EMISSION

T. A. BRABBS and T. F. ROBERTSON (Case Western Reserve Univ., Cleveland, Ohio) 1986 23 p refs Presented at the Central States Meeting of the Combustion Inst., Cleveland, Ohio, 5-6 May 1986

(NASA-TM-87268; E-2956; NAS 1.15:87268) Avail: NTIS HC A02/MF A01 CSCL 21B

Ignition delay data were recorded for three methane-oxygen-argon mixtures ($\phi = 0.5, 1.0, 2.0$) for the temperature range 1500 to 1920 K. Quiet pressure traces enabled us to obtain delay times for the start of the experimental pressure rise. These times were in good agreement with those obtained from the flame band emission at 3700 Å. The data correlated well with the oxygen and methane dependence of Lifshitz, but showed a much stronger temperature dependence ($\phi = 0.5$ $\Delta E = 51.9$, $\phi = 1.0$ $\Delta E = 58.8$, $\phi = 2.0$ $\Delta E = 58.7$ Kcal). The effect of probe location on the delay time

25 INORGANIC AND PHYSICAL CHEMISTRY

measurement was studied. It appears that the probe located 83 mm from the reflecting surface measured delay times which may not be related to the initial temperature and pressure. It was estimated that for a probe located 7 mm from the reflecting surface, the measured delay time would be about 10 microseconds too short, and it was suggested that delay times less than 100 microsecond should not be used. The ignition period was defined as the time interval between start of the experimental pressure rise and 50 percent of the ignition pressure. This time interval was measured for three gas mixtures and found to be similar (40 to 60 micro sec) for $\phi = 1.0$ and 0.5 but much longer (100 to 120) microsecond for $\phi = 2.0$. It was suggested that the ignition period would be very useful to the kinetic modeler in judging the agreement between experimental and calculated delay times.

Author

N86-25431*# National Aeronautics and Space Administration. Lewis Research Center, Cleveland, Ohio.

IGNITION DELAY TIMES OF BENZENE AND TOLUENE WITH OXYGEN IN ARGON MIXTURES

A. BURCAT (Israel Inst. of Tech., Haifa.), C. SNYDER, and T. BRABBS May 1985 15 p refs

(NASA-TM-87312; E-3041; NAS 1.15:87312) Avail: NTIS HC A02/MF A01 CSCL 20B

The ignition delay times of benzene and toluene with oxygen diluted in argon were investigated over a wide range of conditions. For benzene the concentration ranges were 0.42 to 1.69 percent fuel and 3.78 to 20.3 percent oxygen. The temperature range was 1212 to 1748 K and the reflected shock pressures were 1.7 to 7.89 atm. Statistical evaluation of the benzene experiments provided an overall equation which is given. For toluene the concentration ranges were 0.5 to 1.5 percent fuel and 4.48 to 13.45 percent oxygen. The temperature range was 1339 to 1797 K and the reflected shock pressures were 1.95 to 8.85 atm. The overall ignition delay equation for toluene after a statistical evaluation is also given. Detailed experimental information is provided.

Author

N86-27434*# California Univ., San Diego.

FLAME PROPAGATION AND EXTINCTION IN PARTICLE CLOUDS Final Technical Report, 2 Jan 1984 - 31 Aug. 1985

A. L. BERLAD and N. D. JOSHI Jan. 1986 7 p

(Contract NAG3-473)

(NASA-CR-177304; NAS 1.26:177304) Avail: NTIS HC A02/MF A01 CSCL 21B

Two phase flame propagation and extinction theory required to support the corresponding experiments planned for the space shuttle is being developed. Also being planned are specialized collaborative, experimental and theoretical NASA UCSD studies needed to support the ongoing definition of needed experimental hardware, experimental procedures, data acquisition philosophy, and other ground based support activities required to assure the success of space shuttle based experiments concerned with combustion of clouds of particulates at reduced gravitational conditions. The further development of relations delineating premixed particle cloud and premixed gaseous systems as well as burner stabilized and freely propagating flame systems is considered.

E.R.

N86-28136*# Case Western Reserve Univ., Cleveland, Ohio. Dept. of Physics.

A STUDY OF KAPTON DEGRADATION UNDER SIMULATED SHUTTLE ENVIRONMENT Final Report, 1 May 1983 - 30 Apr. 1986

T. G. ECK and R. W. HOFFMAN Jul. 1986 9 p

(Contract NAG3-426)

(NASA-CR-176850; NAS 1.26:176850) Avail: NTIS HC A02/MF A01 CSCL 07D

A system was developed which employs a source of low energy oxygen ion to simulate the shuttle low Earth orbit environment. This source, together with diagnostic tools including surface analysis and mass spectroscopic capability, was used to measure the dependence of ion energy of the oxygen induced CO signals

from pyrolytic graphite and Kapton. For graphite the CO signal was examined at energies ranging from 4.5 to 465 eV and for Kapton from 4.5 to 188 eV. While the relative quantum yields inferred from the data are reasonably precise, there are large uncertainties in the absolute yields because of the assumptions necessary to convert the measured signal strengths to quantum yields. These assumptions are discussed in detail.

B.G.

N86-28139*# Illinois Univ., Urbana. Dept. of Aeronautical and Astronautical Engrg.

THE BEHAVIOR OF FUEL-LEAN PREMIXED FLAMES IN A STANDARD FLAMMABILITY LIMIT TUBE UNDER CONTROLLED GRAVITY CONDITIONS Final Report, Jan. - Dec. 1985

B. L. WHERLEY and R. A. STREHLOW Jul. 1986 143 p (Contract NCC3-35)

(NASA-CR-177132; NAS 1.26:177132; AAE-86-3; UILU-ENG-86-0503) Avail: NTIS HC A07/MF A01 CSCL 21B

Fuel-lean flames in methane-air mixtures from 4.90 to 6.20 volume percent fuel and propane-air mixtures from 1.90 to 3.00 volume percent fuel were studied in the vicinity of the limit for a variety of gravity conditions. The limits were determined and the behavior of the flames studied for one g upward, one g downward, and zero g propagation. Photographic records of all flammability tube firings were obtained. The structure and behavior of these flames were detailed including the variations of the curvature of the flame front, the skirt length, and the occurrence of cellular instabilities with varying gravity conditions. The effect of ignition was also discussed. A survey of flame speeds as a function of mixture strength was made over a range of lean mixture compositions for each of the fuels studied. The results were presented graphically with those obtained by other researchers. The flame speed for constant fractional gravity loadings were plotted as a function of gravity loadings from 0.0 up to 2.0 g's against flame speeds extracted from the transient gravity flame histories for corresponding gravity loadings. The effects of varying gravity conditions on the extinguishment process for upward and downward propagating flames were investigated.

Author

N86-31680*# National Aeronautics and Space Administration. Lewis Research Center, Cleveland, Ohio.

A MATHEMATICAL APPROACH FOR EVALUATING NICKEL-HYDROGEN CELLS

H. F. LEIBECKI 1986 18 p Proposed for presentation at the 1986 Fall Annual Meeting of the AIChE, Miami, Fla., 2-7 Nov. 1986

(NASA-TM-88803; E-3114; NAS 1.15:88803) Avail: NTIS HC A02/MF A01 CSCL 10C

A mathematical equation is presented which gives a quantitative relationship between time-voltage discharge curves, when a cell's ampere-hour capacity is determined at a constant discharge current. In particular the equation quantifies the initial exponential voltage decay; the rate of voltage decay; the overall voltage shift of the curve and the total capacity of the cell at the given discharge current. The results of 12 nickel-hydrogen boiler plate cells cycled to 80 percent depth-of-discharge (DOD) are discussed in association with these equations.

Author

METALLIC MATERIALS

Includes physical, chemical, and mechanical properties of metals, e.g., corrosion; and metallurgy.

A86-11478* National Aeronautics and Space Administration. Lewis Research Center, Cleveland, Ohio.

SLOW PLASTIC STRAIN RATE COMPRESSIVE FLOW IN BINARY COAL INTERMETALLICS

J. D. WHITTENBERGER (NASA, Lewis Research Center, Cleveland, OH) *Materials Science and Engineering* (ISSN 0025-5416), vol. 73, Aug. 1985, p. 87-96. refs

Constant-velocity elevated temperature compression tests have been conducted on a series of binary CoAl intermetallics produced by hot extrusion of blended prealloyed powders. The as-extruded materials were polycrystalline, and they retained their nominal 10-micron grain size after being tested between 1100 and 1400 K at strain rates ranging from 2×10 to the -4 th to 2×10 to the -7 th per sec. Significant plastic flow was obtained in all cases; while cracking was observed, much of this could be due to failure at matrix-oxide interfaces along extrusion stringers rather than to solely intergranular fracture. A maximum in flow strength occurs at an aluminum-to-cobalt ratio of 0.975, and the stress exponent appears to be constant for aluminum-to-cobalt ratios of 0.85 or more. It is likely that very aluminum-deficient materials deform by a different mechanism than do other compositions. Author

A86-12995*# National Aeronautics and Space Administration. Lewis Research Center, Cleveland, Ohio.

THE INFLUENCE OF COBALT, TANTALUM, AND TUNGSTEN ON THE MICROSTRUCTURE OF SINGLE CRYSTAL NICKEL-BASE SUPERALLOYS

M. V. NATHAL (NASA, Lewis Research Center, Cleveland, OH) and L. J. EBERT (Case Western Reserve University, Cleveland, OH) *Metallurgical Transactions A - Physical Metallurgy and Materials Science* (ISSN 0360-2133), vol. 16A, Oct. 1985, p. 1849-1862. refs

(Contract NSG-330)

The influence of composition on the microstructure of single crystal nickel-base superalloys was investigated. Co was replaced by Ni, and Ta was replaced by either Ni or W, according to a matrix of compositions based on MAR-M247. Substitution of Ni for Co caused an increase in gamma-prime solvus temperature, an increase in gamma-gamma-prime lattice mismatch, and the precipitation of W-rich phases in the alloys with high refractory metal levels. Substitution of Ni for Ta caused large decreases in gamma-prime solvus temperature, gamma-prime volume fraction, and gamma-gamma-prime lattice mismatch, whereas substitution of W for Ta resulted in smaller decreases in these features. For the alloys with gamma-prime particles that remained coherent, substitution of Ni for Co caused an increase in gamma-prime coarsening rate. The two alloys with the largest magnitude of lattice mismatch possessed gamma-prime particles which lost coherency during unstressed aging and exhibited anomalously low coarsening rates. Creep exposure at 1000 C resulted in the formation of gamma-prime lamellae oriented perpendicular to the applied stress axis in all alloys. Author

A86-12996*# National Aeronautics and Space Administration. Lewis Research Center, Cleveland, Ohio.

THE INFLUENCE OF COBALT, TANTALUM, AND TUNGSTEN ON THE ELEVATED TEMPERATURE MECHANICAL PROPERTIES OF SINGLE CRYSTAL NICKEL-BASE SUPERALLOYS

M. V. NATHAL (NASA, Lewis Research Center, Cleveland, OH) and L. J. EBERT (Case Western Reserve University, Cleveland, OH) *Metallurgical Transactions A - Physical Metallurgy and Materials Science* (ISSN 0360-2133), vol. 16A, Oct. 1985, p. 1863-1870. refs

The influence of composition on the tensile and creep strength of 001-line oriented nickel-base superalloy single crystals at temperatures near 1000 C was investigated. Cobalt, tantalum, and tungsten concentrations were varied according to a matrix of compositions based on the single crystal version of MAR-M247. For alloys with the baseline refractory metal level of 3 wt pct Ta and 10 wt pct W, decreases in Co level from 10 to 0 wt pct resulted in increased tensile and creep strength. Substitution of 2 wt pct W for 3 wt pct Ta resulted in decreased creep life at high stresses, but improved life at low stresses. Substitution of Ni for Ta caused large reductions in tensile strength and creep resistance, and corresponding increases in ductility. For these alloys with low Ta-plus-W totals, strength was independent of Co level. The effects of composition on properties were related to the microstructural features of the alloys. In general, high creep strength was associated with high levels of gamma-prime volume fraction, gamma-gamma-prime lattice mismatch, and solid solution hardening. Author

A86-13801* National Aeronautics and Space Administration. Lewis Research Center, Cleveland, Ohio.

EROSION OF ALUMINUM 6061-T6 UNDER CAVITATION ATTACK IN MINERAL OIL AND WATER

B. C. S. RAO and D. H. BUCKLEY (NASA, Lewis Research Center, Cleveland, OH) *Wear* (ISSN 0043-1648), vol. 105, Sept. 16, 1985, p. 171-182. refs

Studies of the erosion of aluminum 6061-T6 under cavitation attack in distilled water, ordinary tap water and a viscous mineral oil are presented. The mean depth of penetration for the mineral oil was about 40 percent of that for water at the end of a 40 min test. The mean depth of penetration and its rate did not differ significantly for distilled and tap water. The mean depth of penetration rate for both distilled and tap water increased to a maximum and then decreased with test duration, while that for mineral oil had a maximum during the initial period. The ratio $h/2a$ of the pit depth h to the pit diameter $2a$ varied from 0.04 to 0.13 in water and from 0.06 to 0.20 in mineral oil. Scanning electron microscopy indicates that the pits are initially formed over the grain boundaries and precipitates while the surface grains are deformed under cavitation attack. Author

A86-14719* National Aeronautics and Space Administration. Lewis Research Center, Cleveland, Ohio.

THE DEVELOPMENT OF GAMMA-GAMMA-PRIME LAMELLAR STRUCTURES IN A NICKEL-BASE SUPERALLOY DURING ELEVATED TEMPERATURE MECHANICAL TESTING

R. A. MACKAY (NASA, Lewis Research Center, Cleveland, OH) and L. J. EBERT (Case Western Reserve University, Cleveland, OH) *Metallurgical Transactions A - Physical Metallurgy and Materials Science* (ISSN 0360-2133), vol. 16A, Nov. 1985, p. 1969-1982. refs

(Contract NSG-3246)

The kinetics of the formation and subsequent development of the directional coarsening of the gamma-prime precipitate in model Ni-Al-Mo-Ta superalloy single crystals are examined during tensile creep under various stress levels at 982 and 1038 C. Special attention is given to the gamma and gamma-prime relation to creep time and strain in order to trace the changing gamma-gamma-prime morphology. Directional coarsening of gamma-prime is found to begin during primary creep and its rate is shown to increase with an increase in temperature or stress level. The length of gamma-prime thickness increased linearly with

time up to a plateau reached after the onset of steady state creep. The raft thickness, equal to the gamma-prime size, remained constant at this initial value up through the onset of the tertiary creep. The interlaminar spacing indicates the stability of directionally coarsened structure. F.J.

A86-16257* National Aeronautics and Space Administration. Lewis Research Center, Cleveland, Ohio.

MECHANICAL-CONTACT-INDUCED TRANSFORMATION FROM THE AMORPHOUS TO THE PARTIALLY CRYSTALLINE STATE IN METALLIC GLASS

K. MIYOSHI and D. H. BUCKLEY (NASA, Lewis Research Center, Cleveland, OH) IN: Metallurgical coatings 1984; Proceedings of the Eleventh International Conference, San Diego, CA, April 9-13, 1984. Volume 1. Lausanne, Switzerland, Elsevier Sequoia, S.A., 1984, p. 363-373. Previously announced in STAR as N84-20673. refs

Friction and wear tests were conducted with 3.2- and 6.4-millimeter-diameter aluminum oxide spheres sliding, in reciprocating motion, on a Fe67Co18B14Si1 metallic foil. Crystallites with a size range of 10 to 150 nanometers were produced on the wear surface of the amorphous alloy. A strong interaction between transition metals and metalloids such as silicon and boron results in strong segregation during repeated sliding, provides preferential transition metal-metalloid clustering in the amorphous alloy, and subsequently produces the diffused honeycomb structure formed by dark grey bands and primary crystals, that is, alpha-Fe in the matrix. Large plastic flow occurs on an amorphous alloy surface with sliding and the flow film of the alloy transfers to the aluminum oxide pin surface. Multiple slip bands due to shear deformation are observed on the side of the wear track. Two distinct types of wear debris were observed as a result of sliding: an alloy wear debris, and/or powdery-whiskery oxide debris. A.R.H.

A86-16270* National Aeronautics and Space Administration. Lewis Research Center, Cleveland, Ohio.

FAILURE ANALYSIS OF PLASMA-SPRAYED THERMAL BARRIER COATINGS

C. C. BERNDT and R. A. MILLER (NASA, Lewis Research Center, Cleveland, OH) IN: Metallurgical coatings 1984; Proceedings of the Eleventh International Conference, San Diego, CA, April 9-13, 1984. Volume 2. Lausanne, Switzerland, Elsevier Sequoia, S.A., 1984, p. 173-184. Previously announced in STAR as N84-31347. refs

(Contract NCC3-27)

Thermally induced failure processes of plasma-sprayed thermal barrier coatings are examined. Cracking processes give rise to noise which was monitored by acoustic emission (AE) techniques. The sequential failure of coatings was examined from samples which were thermally cycled. Coatings of yttria-stabilized zirconia with and without a NiCrAlZr bond coat were plasma-sprayed onto U700 alloy rod. In some cases the substrate was intentionally overheated during deposition of the thermal protection system to check how this process variable influenced the AE response of the specimen. In this way a qualitative appraisal of how process variables affect coating integrity could be discerned in terms of cracking behavior. Results from up to seven consecutive thermal cycles are reported here. Coating failure was observed in all cases. Failure of the thermal protection system is progressive, since cracking and crack growth were observed prior to ultimate failure. Thus catastrophic failure occurs at some stage when there is a transformation from the microcrack to a macrocrack network.

Author

A86-16272* National Aeronautics and Space Administration. Lewis Research Center, Cleveland, Ohio.

PERFORMANCE OF THERMAL BARRIER COATINGS IN HIGH HEAT FLUX ENVIRONMENTS

R. A. MILLER and C. C. BERNDT (NASA, Lewis Research Center, Cleveland, OH) IN: Metallurgical coatings 1984; Proceedings of the Eleventh International Conference, San Diego, CA, April 9-13, 1984. Volume 2. Lausanne, Switzerland, Elsevier Sequoia, S.A., 1984, p. 195-202. Previously announced in STAR as N84-24772. refs

Thermal barrier coatings were exposed to the high temperature and high heat flux produced by a 30 kW plasma torch. Analysis of the specimen heating rates indicates that the temperature drop across the thickness of the 0.038 cm ceramic layer was about 1100 C after 0.5 sec in the flame. An as-sprayed ZrO2-8 percent Y2O3 specimens survived 3000 of the 0.5 sec cycles with failing. Surface spalling was observed when 2.5 sec cycles were employed but this was attributed to uneven heating caused by surface roughness. This surface spalling was prevented by smoothing the surface with silicon carbide paper or by laser glazing. A coated specimen with no surface modification but which was heat treated in argon also did not surface spall. Heat treatment in air led to spalling in as early as 2 cycle from heating stresses. Failures at edges were investigated and shown to be a minor source of concern. Ceramic coatings formed from ZrO2-12 percent Y2O3 or ZrO2-20 percent Y2O3 were shown to be unsuited for use under the high heat flux conditions of this study. Author

A86-16276* Michigan Technological Univ., Houghton.

MODELING DEGRADATION AND FAILURE OF NI-CR-AL OVERLAY COATINGS

J. A. NESBITT and R. W. HECKEL (Michigan Technological University, Houghton, MI) IN: Metallurgical coatings 1984; Proceedings of the Eleventh International Conference, San Diego, CA, April 9-13, 1984. Volume 2. Lausanne, Switzerland, Elsevier Sequoia, S.A., 1984, p. 281-290. Previously announced in STAR as N84-27858. refs

(Contract NAS3-244)

Degradation of a Ni-16Cr-25Al-0.06Zr overlay coating on a Ni-22Cr substrate was examined after oxidation accompanied by thermal cycling. Concentration/distance profiles were measured in the coating and substrate after various one-hour cycles at 1150 C. A numerical model was developed to simulate coating degradation by simultaneous oxidation and coating/substrate interdiffusion. The validity of the model was confirmed by comparison of predicted and measured concentration/distance profiles. The ability of the model to identify critical system parameters was demonstrated for the case of initial Al and Cr content of the coating and substrate. M.G.

A86-16906* National Aeronautics and Space Administration. Lewis Research Center, Cleveland, Ohio.

METALLIC GLASS AS A TEMPERATURE SENSOR DURING ION PLATING

K. MIYOSHI, T. SPALVINS, and D. H. BUCKLEY (NASA, Lewis Research Center, Cleveland, OH) (International Conference on Metallurgical Coatings, San Diego, CA, Apr. 9-13, 1984) Thin Solid Films (ISSN 0040-6090), vol. 127, 1985, p. 115-122. Previously announced in STAR as N84-17351. refs

The temperature of the interface and/or a superficial layer of a substrate during ion plating was investigated using a metallic glass of the composition Fe67Co18B14Si1 as the substrate and as the temperature sensor. Transmission electron microscopy and diffraction studies determined the microstructure of the ion-plated gold film and the substrate. Results indicate that crystallization occurs not only in the film, but also in the substrate. The grain size of crystals formed during ion plating was 6 to 60 nm in the gold film and 8 to 100 nm in the substrate at a depth of 10 to 15 micrometers from the ion-plated interface. The temperature rise of the substrate during ion plating was approximately 500 C. Discontinuous changes in metallurgical microstructure, and physical, chemical, and mechanical properties during the amorphous to crystalline transition in metallic glasses make metallic

glasses extremely useful materials for temperature sensor applications in coating processes. A.R.H.

A86-17477* National Aeronautics and Space Administration. Lewis Research Center, Cleveland, Ohio.

FRICTIONAL AND STRUCTURAL CHARACTERIZATION OF ION-NITRIDED LOW AND HIGH CHROMIUM STEELS

T. SPALVINS (NASA, Lewis Research Center, Cleveland, OH) *Journal of Vacuum Science and Technology A* (ISSN 0734-2101), vol. 3, Nov.-Dec. 1985, p. 2329-2333. Previously announced in STAR as N85-23085. refs

Low Cr steels AISI 41410, AISI 4340, and high Cr austenitic stainless steels AISI 304, AISI 316 were ion nitrided in a dc glow discharge plasma consisting of a 75 percent H₂ - 25 percent N₂ mixture. Surface compound layer phases were identified, and compound layer microhardness and diffusion zone microhardness profiles were established. Distinct differences in surface compound layer hardness and diffusion zone profiles were determined between the low and high Cr alloy steels. The high Cr stainless steels after ion nitriding displayed a hard compound layer and an abrupt diffusion zone. The compound layers of the high Cr stainless steels had a columnar structure which accounts for brittleness when layers are exposed to contact stresses. The ion nitrided surfaces of high and low Cr steels displayed a low coefficient of friction with respect to the untreated surfaces when examined in a pin and disk tribotester. Author

A86-20436* Toledo Univ., Ohio.

INTERACTION OF SULFURIC ACID CORROSION AND MECHANICAL WEAR OF IRON

G. W. P. RENGSTORFF (Toledo, University, OH), K. MIYOSHI, and D. H. BUCKLEY (NASA, Lewis Research Center, Cleveland, OH) *ASLE Transactions*, vol. 29, Jan. 1986, p. 43-49; Discussion, p. 49, 50; Author's Reply, p. 50, 51. Previously announced in STAR as N84-27857. refs

Friction and wear experiment were conducted with elemental iron sliding on aluminum oxide in aerated sulfuric acid at concentrations ranging from very dilute (0.00007 N; i.e., 4 ppm) to very concentrated (96 percent acid). Load and reciprocating sliding speed were kept constant. With the most dilute acid concentration of 0.00007 to 0.0002 N, a complex corrosion product formed that was friable and often increased friction and wear. At slightly higher concentrations of 0.001 N, metal losses were essentially by wear alone. Because no buildup of corrosion products occurred, this acid concentration became the standard from which to separate metal loss from direct corrosion and mechanical wear losses. When the acid concentration was increased to 5 percent (1 N), the well-established high corrosion rate of iron in sulfuric acid strongly dominated the total wear loss. This strong corrosion increased to 30 percent acid and decreased somewhat to 50 percent acid in accordance with expectations. However, the low corrosion of iron expected at acid concentrations of 65 to 96 percent was not observed in the wear area. It was apparent that the normal passivating film was being worn away and a galvanic cell established that rapidly attacked the wear area. Under the conditions where direct corrosion losses were highest, the coefficient of friction was the lowest. Author

A86-20982* Massachusetts Inst. of Tech., Cambridge.

THERMAL-MECHANICAL FATIGUE CRACK GROWTH IN INCONEL X-750

N. MARCHAND and R. M. PELLOUX (MIT, Cambridge, MA) IN: Time-dependent fracture; Proceedings of the Eleventh Canadian Fracture Conference, Ottawa, Canada, June 14, 15, 1984. Dordrecht, Martinus Nijhoff Publishers, 1985, p. 167-178. Previously announced in STAR as N85-15877. refs (Contract NAG3-280)

Thermal-mechanical fatigue crack growth (TMFCG) was studied in a 'gamma-gamma' nickel base superalloy Inconel X-750 under controlled load amplitude in the temperature range from 300 to 650 C. In-phase (T sub max at sigma sub max), out-of-phase (T sub min at sigma sub max), and isothermal tests at 650 C were performed on single-edge notch bars under fully reversed cyclic

conditions. A dc electrical potential method was used to measure crack length. The electrical potential response obtained for each cycle of a given wave form and R value yields information on crack closure and crack extension per cycle. The macroscopic crack growth rates are reported as a function of delta K and the relative magnitude of the TMFCG are discussed in the light of the potential drop information and of the fractographic observations. R.S.F.

A86-21849* National Aeronautics and Space Administration. Lewis Research Center, Cleveland, Ohio.

TEMPERATURE DEPENDENCE OF GAMMA-GAMMA PRIME LATTICE MISMATCH IN NICKEL-BASE SUPERALLOYS

M. V. NATHAL, R. A. MACKAY, and R. G. GARLICK (NASA, Lewis Research Center, Cleveland, OH) *Materials Science and Engineering* (ISSN 0025-5416), vol. 75, Nov. 1985, p. 195-205. refs

High temperature X-ray diffraction techniques were used to determine the gamma-gamma prime lattice mismatch of three different nickel-base superalloys at temperatures between 18 and 1000 C. The measurements were performed on oriented single-crystal disks which had been aged to produce a semicoherent gamma-gamma prime structure. The thermal expansion of the lattice parameters of the gamma and gamma-prime phases was described by a second-order polynomial expression. The expansion of the gamma-prime phase was consistently smaller than that of the gamma phase, which caused the lattice mismatch to become more negative at higher temperatures. It was also shown that high values of lattice mismatch resulted in increased rates of directional gamma-prime coarsening during elevated temperature creep exposure. Author

A86-23324* National Aeronautics and Space Administration. Lewis Research Center, Cleveland, Ohio.

EROSION OF PHOSPHOR BRONZE UNDER CAVITATION ATTACK IN A MINERAL OIL

B. C. S. RAO and D. H. BUCKLEY (NASA, Lewis Research Center, Cleveland, OH) *Journal of Testing and Evaluation* (ISSN 0090-3973), vol. 14, Jan. 1986, p. 13-18. refs

Experimental investigations on erosion of a copper alloy, phosphor bronze, under cavitation attack in a viscous mineral oil are presented. The details of pit formation and erosion were studied using scanning electron microscopy. The mean depth of penetration, the variations in surface roughness, and the changes in erosion pit size were studied. Cavitation pits formed initially over the grain boundaries while the surface grains were plastically deformed. Erosion of surface grains occurred largely by ductile fracture involving microcracking and removal in layers. The ratio h/a of the depth h to half width a of cavitation pits increased with test duration from 0.047 to 0.55. Author

A86-28951* Connecticut Univ., Storrs.

FRACTURE MECHANICS APPLIED TO NONISOTHERMAL FATIGUE CRACK GROWTH

E. H. JORDAN (Connecticut, University, Storrs) and G. J. MEYERS (McGraw-Edison Co., Worthington Compressors Div., Buffalo, NY) *Engineering Fracture Mechanics* (ISSN 0013-7944), vol. 23, no. 2, 1986, p. 345-358. refs (Contract NAS3-22550)

Twelve nonisothermal fatigue crack growth tests were performed on Hastelloy-X tubular specimens in which strain and temperature varied simultaneously. Conditions were selected to include nominally elastic and nominally plastic conditions and temperatures up to 982 C. A number of parameters, including the stress intensity factor, strain intensity factor, and J-integral, were examined for their ability to correlate the data. There was no decisive difference between the success of the three parameters. Each parameter correlated data from different strain ranges to within no worse than a factor of 2.1 on da/dN. The effect of strain temperature cycle shape was investigated and found to be moderate, while a strain hold of 1 min had very little effect. An attempt was made to predict nonisothermal test results from isothermal data. These predictions were better than those made

by using peak test temperature isothermal data but still not within scatter. Author

A86-29722* National Aeronautics and Space Administration. Lewis Research Center, Cleveland, Ohio.
STUDIES ON THE HOT CORROSION OF A NICKEL-BASE SUPERALLOY, UDIMET 700

A. K. MISRA (NASA, Lewis Research Center, Cleveland, OH) Oxidation of Metals (ISSN 0030-770X), vol. 25, April 1986, p. 129-161. Previously announced in STAR as N85-11224. refs (Contract NCC3-43)

The hot corrosion of a nickel-base superalloy, Udimet 700, was studied in the temperature range of 884 to 965 C and with different amounts of Na₂SO₄. Two different modes of degradation were identified: (1) formation of Na₂MoO₄-MoO₃ melt and fluxing by this melt, and (2) formation of large interconnected sulfides. The dissolution of Cr₂O₃, TiO₂ in the Na₂SO₄ melt does not play a significant role in the overall corrosion process. The conditions for the formation of massive interconnected sulfides were identified and a mechanism of degradation due to sulfide formation is described. The formation of Na₂MoO₄-MoO₃ melt requires an induction period and various physiochemical processes during the induction period were identified. The factors affecting the length of the induction period were also examined. The melt penetration through the oxide appears to be the prime mode of degradation whether the degradation is due to the formation of sulfides or the formation of the Na₂MoO₄-MoO₃ melt. Author

A86-30010* Case Western Reserve Univ., Cleveland, Ohio.
THE CRACK LAYER APPROACH TO TOUGHNESS CHARACTERIZATION IN STEEL

M. BESSENDORFF and A. CHUDNOVSKY (Case Western Reserve University, Cleveland, OH) IN: Advances in fracture research (Fracture 84). Volume 3. Oxford and New York, Pergamon Press, 1986, p. 1663-1670. refs (Contract NAG3-223)

In a study of the laws of crack propagation and toughness characterization, it is feasible to employ two alternative approaches, including the fracture mechanics approach and the material science approach. The crack layer (CL) theory discussed by Khandogin and Chudnovsky (1978) and Chudnovsky (1980) considers the crack together with the surrounding defects as one system which has several degrees of freedom. It is pointed out that the CL theory defines the relationship between the parameters of fracture mechanics and the characteristics of microstructural changes which are the subject of material science. Experiments are described, taking into account a toughness characterization test and microscopic studies. Attention is given to a phenomenological study of toughness characterization, the morphology of crack layer, and the evaluation of energy stored in the dislocation network. G.R.

A86-30041* IIT Research Inst., Chicago, Ill.
CREEP-RUPTURE AND FRACTOGRAPHIC ANALYSIS OF STIRLING ENGINE SUPERALLOYS TESTED IN AIR AND 15 MPa HYDROGEN

S. BHATTACHARYYA (IIT Research Institute, Chicago, IL) and R. H. TITRAN (NASA, Lewis Research Center, Cleveland, OH) IN: Advances in fracture research (Fracture 84). Volume 3. Oxford and New York, Pergamon Press, 1986, p. 2221-2229. DOE-supported research. refs (Contract DEN3-217)

A brief comparative analytical and microstructural evaluation of creep-rupture performance of two iron-base superalloys in air and 15 MPa of hydrogen, is presented. Creep rupture data are presented for the sheet alloy 19-9DL and the cast alloy XF-818, including temperature, initial stress, rupture life, minimum creep rate, time to reach one percent creep strain, and total elongation. In 19-9DL, both rupture life and minimum creep rate are more sharply dependent on small stress changes than in XF-818 in the given environment, and 19-9DL appears to become a more creep-resistant material with increasing Q (apparent activation energy) while the opposite is noted for XF-818. There appears to be no environmental effect on minimum creep rate for 19-9DL,

whereas Q becomes less negative for XF-818 for 15 MPa of H₂. Multiple cracks leading to rupture are observed on the fracture surfaces, with sheet specimens showing many more cracks close to the fracture surface than cast specimens. C.D.

A86-30610* National Aeronautics and Space Administration. Lewis Research Center, Cleveland, Ohio.

EFFECT OF MULTIPLE STRAIN-ANNEAL CYCLES ON THE 1000 C CREEP BEHAVIOUR OF GAMMA/GAMMA PRIME-ALPHA

J. D. WHITTENBERGER, B. C. BUZEK (NASA, Lewis Research Center, Cleveland, OH), and G. WIRTH (DFVLR, Cologne, West Germany) Journal of Materials Science (ISSN 0022-2461), vol. 21, March 1986, p. 923-930. refs

Various multiple strain-anneal cycles (1000 C) were imposed on specimens of the directionally solidified eutectic (DSE) alloy gamma/gamma prime-alpha to identify thermomechanical processing methods (TMP) which would improve the creep behavior. Specimens of the Ni-32.3Mo-6.3Al wt pct alloy were grown with a modified Bridgman technique. Some of the cylindrical specimens were alternately heat-treated at 900 C, then strained, or heat-treated only, while other specimens were annealed at 900 C after swaging and then worked at ambient temperature. The specimens were all examined microstructurally using transmission electron microscopy, some before and after being exposed to constant-load compression tests at 1000 C. The creep strain increased for all TMP specimens for strain rates of at least 2 millionths per sec. Strain rates of about 2 ten millionths per sec were only improved with strain annealing with 13 percent work at ambient temperature. A slight improvement, compared to as-grown materials, was observed in the 1000 C creep behavior of materials annealed at 900 C. Strain-annealing was found to introduce three-dimensional dislocation networks into the gamma-prime matrix. M.S.K.

A86-31746* National Aeronautics and Space Administration. Lewis Research Center, Cleveland, Ohio.

OPTIMIZATION OF THE NI-CR-AL-Y/ZR02-Y2O3 THERMAL BARRIER SYSTEM

S. STECURA (NASA, Lewis Research Center, Cleveland, OH) Advanced Ceramic Materials (ISSN 0883-5551), vol. 1, Jan. 1986, p. 68-76. Previously announced in STAR as N85-15878. refs

The effects of bond and thermal barrier coating compositions, thicknesses, and densities on air plasma spray deposited Ni-Cr-Al-Y/ZrO₂-Y₂O₃ life were evaluated in cyclic furnace oxidation tests at temperatures from 1110 to 1220 C. An empirical relation was developed to give life as a function of the above parameters. The thermal barrier system tested which had the longest life consisted of Ni-35.0 wt pct Cr-5.9 wt pct Al-0.95 wt pct Y bond coating and ZrO₂-6.1 wt pct Y₂O₃ thermal barrier coating. Author

A86-34687*# Connecticut Univ., Storrs.
IMPACT WEAR OF IRON RICH SUPERALLOYS

S. F. WAYNE, H. NOWOTNY (Connecticut, University, Storrs), and S. L. RICE (Central Florida, University, Orlando) IN: Wear of materials 1985; Proceedings of the International Conference, Vancouver, Canada, April 14-18, 1985. New York, American Society of Mechanical Engineers, 1985, p. 567-571. refs (Contract NAG3-271)

The impact-sliding wear resistance of chill cast and aligned eutectic Fe-base superalloys against M42 and 17-4 PH steel counterface materials is examined. The aligned material tests were run with carbide fibers perpendicular to the counterface contact surface and the characterization focused on fracture processes as observed in the subsurface microstructure of the worn materials. Metallographic analyses were performed on specimens exposed to various numbers of repetitive impact load cycles, and for comparison, two other aligned composites were tested with the same fiber orientation under identical test conditions against hardened M42 tool steel. A strong improvement was found in wear resistance of an aligned eutectic structure as compared to the corresponding randomized chill cast structure. Experiments with the softer 17-4 counterface were characterized by transfer

onto the Fe-base superalloy, and the cracks formed were oriented transverse to the relative sliding direction and occurred in a periodic fashion. Observations in subsurface regions of the worn materials indicated crack intergranularity with an occasional transgranular fracture of the M7C3 carbide phase. K.K.

A86-35697* National Aeronautics and Space Administration. Lewis Research Center, Cleveland, Ohio.

THE TENSILE AND FATIGUE DEFORMATION STRUCTURES IN A SINGLE CRYSTAL NI-BASE SUPERALLOY

T. P. GABB, R. V. MINER, and J. GAYDA (NASA, Lewis Research Center, Cleveland, OH) Scripta Metallurgica (ISSN 0036-9748), vol. 20, April 1986, p. 513-518. refs

Dislocation structures produced in Rene N4 crystals of various orientations deformed in tension and low cycle fatigue (LCF) at 760 and 980 degrees C were examined in order to elucidate the observed differences in stress-strain behavior. Specimens tensile tested at 760 degrees C displayed significant crystallographic orientation dependences in mechanical response but comparable inhomogeneous dislocation structures. LCF specimens of various orientations had comparable cyclic stress-strain curves and generally similar somewhat more homogeneous dislocation structures. Tensile specimens at the higher temperature had comparable mechanical response and corresponding similar quite homogeneous dislocation structures with gamma' faulting; and LCF specimens had orientation-dependent mechanical response but comparable homogeneous loose dislocation networks. D.H.

A86-37073* National Aeronautics and Space Administration. Lewis Research Center, Cleveland, Ohio.

NA2SO4 INDUCED CORROSION OF NICKEL AT HIGH TEMPERATURE

A. K. MISRA (NASA, Lewis Research Center, Cleveland, OH) ASM, International Conference on Surface Modifications and Coatings, Toronto, Canada, Oct. 14-16, 1985, Paper. 18 p. refs

Sodium sulfate-induced corrosion of nickel was studied at 900 C as a function of oxygen partial pressure. For high O2 partial pressures, accelerated corrosion during the first few minutes occurred by rapid penetration of the melt along the metal grain boundaries. A mechanism is proposed to explain this phenomenon. Repetitive scale metal detachment was observed for corrosion in lower O2 partial pressures and during the later period of corrosion in higher O2 partial pressures. The effect of preoxidation on the hot corrosion has also been studied. An induction period is observed before the onset of rapid corrosion for the preoxidized samples; the onset of rapid corrosion is associated with sudden cracking of the scale. The length of the induction period for the preoxidized samples is a function of the length of preoxidation, and appears to be related to the structure of the oxide scale after the preoxidation treatment. Author

A86-37238* National Aeronautics and Space Administration. Lewis Research Center, Cleveland, Ohio.

MECHANISM OF NA2SO4-INDUCED CORROSION OF MOLYBDENUM CONTAINING NICKEL-BASE SUPERALLOYS AT HIGH TEMPERATURES. I - CORROSION IN ATMOSPHERES CONTAINING O2 ONLY. II - CORROSION IN O2 + SO2 ATMOSPHERES

A. K. MISRA (NASA, Lewis Research Center, Cleveland, OH) Electrochemical Society, Journal (ISSN 0013-4651), vol. 133, May 1986, p. 1029-1042. refs

Kinetics of the Na2SO4-induced corrosion of the molybdenum-containing nickel-base superalloys, B-1900 and Udimet 700, coated with Na2MoO4, has been studied in oxygen atmosphere at temperatures ranging from 750 to 950 C. Because the gas turbine atmosphere always contains some SO2 and SO3, the effect of atmospheric SO2 content on corrosion of Udimet-700 has also been studied. It was found that in the O2 atmosphere the melt in the catastrophic corrosion phase consists of Na2MoO4 plus MoO3, with the onset of the catastrophic corrosion coinciding with the appearance of MoO3. In the presence of low levels of atmospheric SO2 (below 0.24 percent), the melt during catastrophic corrosion contains, in addition to Na2MoO4 and MoO3, some

quantities of Na2SO4. At the levels of SO2 above 1 percent, no catastrophic corrosion was observed. At these SO2 levels, internal sulfidation appears to be the primary mode of degradation. I.S.

A86-44038* Connecticut Univ., Storrs.

CONSTRUCTING MULTICOMPONENT PHASE DIAGRAMS BY OVERLAPPING ZPF LINES

H. GUPTA, J. E. MORRIS, and H. NOWOTNY (Connecticut, University, Storrs) Scripta Metallurgica (ISSN 0036-9748), vol. 20, June 1986, p. 889-894. refs (Contract NAG3-271)

A procedure is introduced which can be used to draw isothermal sections from a multicomponent phase diagram in a matter of minutes, regardless of the diagram complexity. In the proposed method, the zero phase fraction (ZPF) lines are drawn separately for all phases existing in the system; by overlapping these ZPF lines, the desired section is obtained. Two examples - with five components and eight components - are given to illustrate the method. Regarding the second example, it is noted that although the final diagram may be altered to create discontinuities in slope at intersection points, the diagram remains unchanged from a topological standpoint. Thus, the overlapping ZPF lines supply all the information needed to construct complex diagrams. Even if many more phases and components are involved, the final diagram can be drawn with equal facility. D.H.

A86-45091* Stanford Univ., Calif.

DISLOCATIONS IN EXTRUDED CO-49.3 AT. PCT AL

D. L. YANEY, W. D. NIX (Stanford University, CA), and A. R. PELTON (USDA, Ames Laboratory, IA) Journal of Materials Science (ISSN 0022-2461), vol. 21, June 1986, p. 2083-2087. refs (Contract NAG3-248)

Polycrystalline Co-49.3 at. pct Al, which had been extruded at 1505 K, was examined using transmission electron microscopy. Diffraction contrast analysis showed that $b = 100$ as well as $b = 111$ line dislocations contribute to elevated temperature deformation in CoAl. Therefore, it was concluded that sufficient slip systems exist in CoAl to allow for general plasticity in the absence of diffusional mechanisms. Line dislocations of the type $b = 001$ were observed on both 110 and 100 planes while $b = 111$ line dislocations were observed on 1-10 planes. Author

A86-45715* National Aeronautics and Space Administration. Lewis Research Center, Cleveland, Ohio.

THE CYCLIC STRESS-STRAIN BEHAVIOR OF A NICKEL-BASE SUPERALLOY AT 650 C

T. P. GABB (NASA, Lewis Research Center, Cleveland, OH) and G. E. WELSCH (Case Western Reserve University, Cleveland, OH) Scripta Metallurgica (ISSN 0036-9748), vol. 20, July 1986, p. 1049-1054. refs

It is pointed out that examinations of the monotonic tensile and fatigue behaviors of single crystal nickel-base superalloys have disclosed orientation-dependent tension-compression anisotropies and significant differences in the mechanical response of octahedral and cube slip at intermediate temperatures. An examination is conducted of the cyclic hardening response of the single crystal superalloy PWA 1480 at 650 C. In the considered case, tension-compression anisotropy is present, taking into account primarily conditions under which a single slip system is operative. Aspects of a deformation by single slip are considered along with cyclic hardening anisotropy in tension and compression. It is found that specimens deforming by octahedral slip on a single slip system have similar hardening responses in tensile and low cycle fatigue loading. Cyclic strain hardening is very low for specimens displaying single slip. G.R.

A86-46564* IIT Research Inst., Chicago, Ill.

HIGH-PRESSURE CREEP TESTS

S. BHATTACHARYA, J. LAMOUREUX (IIT Research Institute, Chicago, IL), and C. HALES (Cambridge University, England) *Journal of Metals* (ISSN 0148-6608), vol. 38, July 1986, p. 35-38. DOE-sponsored research. refs (Contract DEN3-217; DEN3-303)

The automotive Stirling engine, presently being developed by the U.S. Department of Energy and NASA, uses high-pressure hydrogen as a working fluid; its long-term effects on the properties of alloys are relatively unknown. Hence, creep-rupture testing of wrought and cast high-temperature alloys in high-pressure hydrogen is an essential part of the research supporting the development of the Stirling cycle engine. Attention is given to the design, development, and operation of a 20 MPa hydrogen high-temperature multispecimen creep-rupture possessing high sensitivity. This pressure vessel allows for the simultaneous yet independent testing of six specimens. The results from one alloy, XF-818, are presented to illustrate how reported results are derived from the raw test data. K.K.

A86-47243* Dartmouth Coll., Hanover, N.H.

THE EFFECTS OF GRAIN SIZE ON THE FLOW AND FRACTURE OF LONG-RANGE ORDERED ALLOYS

E. M. SCHULSON (Dartmouth College, Hanover, NH) IN: High-temperature ordered intermetallic alloys; Proceedings of the Symposium, Boston, MA, November 26-28, 1984. Pittsburgh, PA, Materials Research Society, 1985, p. 193-204. refs (Contract DE-AC02-81ER-10907; DE-FG02-84ER-45148; NAG3-13)

The effects of grain size on the mechanical properties of long-range ordered alloys are examined with reference to the short-term behavior of aluminide intermetallics. It is shown that in those L1(2) alloys which exhibit anomalous thermal strengthening, the grain size affects the magnitude of the strengthening. In some cases it also affects ductility, whereby the tensile elongation and the tensile strength increase as the grain size decreases below a critical point. It is also believed that grain size may affect the partitioning of microalloying elements, such as boron, in Ni3Al. V.L.

A86-47252* National Aeronautics and Space Administration. Lewis Research Center, Cleveland, Ohio.

HIGH TEMPERATURE PROPERTIES OF EQUIATOMIC FeAl WITH TERNARY ADDITIONS

R. H. TITRAN (NASA, Lewis Research Center, Cleveland, OH), K. M. VEDULA, and G. G. ANDERSON (Case Western Reserve University, Cleveland, OH) IN: High-temperature ordered intermetallic alloys; Proceedings of the Symposium, Boston, MA, November 26-28, 1984. Pittsburgh, PA, Materials Research Society, 1985, p. 309-317. refs

The aluminide intermetallic compounds are considered potential structural materials for aerospace applications. The B2 binary aluminide FeAl has a melting point in excess of 1500 K, is of simple cubic structure, exists over a wide range of composition with solubility for third elements and is potentially self-protecting in extreme environments. The B2 FeAl compound has been alloyed with 1 to 5 at. pct ternary additions of Si, Ti, Zr, Hf, Cr, Ni, Co, Nb, Ta, Mo, W, and Re. The alloys were prepared by blending a third elemental powder with pre-alloyed binary FeAl powder. Consolidation was by hot extrusion at 1250 K. Annealing studies on the extruded rods showed that the third element addition can be classified into three categories based upon the amount of homogenization and the extent of solid solutioning. Constant strain rate compression tests were performed to determine the flow stress as a function of temperature and composition. The mechanical strength behavior was dependent upon the third element homogenization classification. Author

A86-47259* National Aeronautics and Space Administration. Lewis Research Center, Cleveland, Ohio.

THE B2 ALUMINIDES AS ALTERNATIVE MATERIALS

J. R. STEPHENS (NASA, Lewis Research Center, Cleveland, OH) IN: High-temperature ordered intermetallic alloys; Proceedings of the Symposium, Boston, MA, November 26-28, 1984. Pittsburgh, PA, Materials Research Society, 1985, p. 381-395. Previously announced in STAR as N85-19076. refs

The potential of the B2 aluminides as structural material alternatives for the strategic element containing superalloys currently used in gas turbine engines is being explored with emphasis on the equiatomic Fe and Ni aluminides. Although Co is a strategic material, the equiatomic Co aluminide is also being studied to gain a more complete understanding of these fourth period intermetallics. Research focuses on initial processing techniques such as ingot melting, power metallurgy, and rapid solidification with and without additional thermomechanical processing; high temperature deformation primarily compressive creep; compositional effects within the binary B2 aluminides; third-element alloying addition effects on high temperature strength and oxidation resistance, and near room temperature ductility as influenced by processing, alloying, and grain size. Various programs now underway are reviewed and some highlights of research results are presented. A.R.H.

A86-47261* Case Western Reserve Univ., Cleveland, Ohio.

ALLOYS BASED ON NiAl FOR HIGH TEMPERATURE APPLICATIONS

K. VEDULA, V. PATHARE, I. ASLANIDIS (Case Western Reserve University, Cleveland, OH), and R. H. TITRAN (NASA, Lewis Research Center, Cleveland, OH) IN: High-temperature ordered intermetallic alloys; Proceedings of the Symposium, Boston, MA, November 26-28, 1984. Pittsburgh, PA, Materials Research Society, 1985, p. 411-421. NASA-supported research. Previously announced in STAR as N85-21322. refs

The NiAl alloys for potential high temperature applications were studied. Alloys were prepared by powder metallurgy techniques. Flow stress values at slow strain rates and high temperatures were measured. Some ternary alloying additions (Hf, Ta and Nb) were identified. The mechanism of strengthening in alloys containing these additions appears to be a form of particle dislocation interaction. The effects of grain size and stoichiometry in binary alloys are also presented. E.A.K.

A86-47263* National Aeronautics and Space Administration. Lewis Research Center, Cleveland, Ohio.

RAPIDLY SOLIDIFIED NiAl AND FeAl

D. J. GAYDOSH (NASA, Lewis Research Center, Cleveland, OH) and M. A. CRIMP (Case Western Reserve University, Cleveland, OH) IN: High-temperature ordered intermetallic alloys; Proceedings of the Symposium, Boston, MA, November 26-28, 1984. Pittsburgh, PA, Materials Research Society, 1985, p. 429-436. Previously announced in STAR as N85-20042. refs

Melt spinning was used to produce rapidly solidified ribbons of the B2 intermetallics NiAl and FeAl. Both Fe-40Al and Fe-45Al possessed some bend ductility in the as spun condition. The bend ductility of Fe-40Al, Fe-45Al, and equiatomic NiAl increased with subsequent heat treatment. Heat treatment at approximately 0.85 T (sub m) resulted in significant grain growth in equiatomic FeAl and in all the NiAl compositions. Low bend ductility in both FeAl and NiAl generally coincided with intergranular failure, while increased bend ductility was characterized by increasing amounts of transgranular cleavage fracture. Author

A86-47266* Case Western Reserve Univ., Cleveland, Ohio.

HIGH TEMPERATURE OXIDATION OF BETA-NIAL

J. K. KOYCHAK, T. E. MITCHELL (Case Western Reserve University, Cleveland, OH), and J. L. SMIALEK (NASA, Lewis Research Center, Cleveland, OH) IN: High-temperature ordered intermetallic alloys; Proceedings of the Symposium, Boston, MA, November 26-28, 1984. Pittsburgh, PA, Materials Research Society, 1985, p. 475-484. refs

(Contract NAG3-498)

The oxidation of single crystal beta-NiAl has been studied primarily using electron microscopy. Oriented metastable Al₂O₃ phases form during transient oxidation at 800 C. Specific orientation relationships exist on all metal orientations studied and are a result of the small mismatch along aligned close-packed directions in the cation sublattices of the metal and oxide. Transformation of the metastable Al₂O₃ phases at 1100 C results in an oxide morphology described as the 'lacey' structure of alpha-Al₂O₃ scales. This structure results from impingement of oriented patches of alpha-Al₂O₃ as the transformation initiates and moves radially parallel to the surface. Scale growth occurs by diffusion along high angle grain boundaries. A drastic reduction in oxidation rate accompanies the change in oxide morphology. Author

A86-48037* National Aeronautics and Space Administration. Lewis Research Center, Cleveland, Ohio.

THE RESPONSE OF COBALT-FREE UDIMET 700 TYPE ALLOY TO MODIFIED HEAT TREATMENTS

F. H. HARF (NASA, Lewis Research Center, Cleveland, OH) Journal of Materials Science (ISSN 0022-2461), vol. 21, July 1986, p. 2497-2508. Previously announced in STAR as N85-20043. refs

A superalloy based on Udimet 700, in which all of the cobalt was replaced by nickel, was prepared from hot isostatically pressed prealloyed powders. This material was given various heat treatments consisting of partial solutioning and aging in a sequence of four different temperatures. Comparisons were made of microstructures and mechanical properties. Best results were obtained by partially solutioning at 1145 deg C and aging through a sequence of 870, 1030, 650 and 760 deg C. This heat treatment also provided significantly improved properties for wrought material of the same composition. The results suggest that cobalt free Udimet 700 should be considered as a substitute for Udimet 700 with the standard 17 percent cobalt content. R.J.F.

A86-48973* National Aeronautics and Space Administration. Lewis Research Center, Cleveland, Ohio.

A STUDY OF SPECTRUM FATIGUE CRACK PROPAGATION IN TWO ALUMINUM ALLOYS. I - SPECTRUM SIMPLIFICATION. II - INFLUENCE OF MICROSTRUCTURES

J. TELESMA (NASA, Lewis Research Center, Cleveland, OH) and S. D. ANTOLOVICH (Georgia Institute of Technology, Atlanta) Engineering Fracture Mechanics (ISSN 0013-7944), vol. 24, no. 3, 1986, p. 453-459, 461-473, 475-477. Research supported by Northrop Corp. refs

An investigation of the fatigue crack propagation FCP behavior of two aluminum alloys is performed to simulate spectrum loading conditions found at critical locations in high performance fighter aircraft. Negative loads are shown to be eliminated for the tension-compression spectrum for low to intermediate maximum stress intensities, and load interactions are found to be more significant at higher stress intensities and with more plasticity at the crack tip. In the second part, the influence of microstructural features including grain size, inclusions, and dispersoids on constant amplitude and spectrum crack growth behavior in aluminum alloys is studied. At low stress intensities the I/M alloy demonstrated better FCP resistance than the P/M 7091 alloy for both constant amplitude and spectrum testing, and the inhomogeneous planar slip and large grain size of 7050 limit dislocation interactions, thereby improving FCP performance. R.R.

A86-49600* National Aeronautics and Space Administration. Lewis Research Center, Cleveland, Ohio.

TRIBOLOGICAL CHARACTERISTICS OF GOLD FILMS DEPOSITED ON METALS BY ION PLATING AND VAPOR DEPOSITION

K. MIYOSHI, T. SPALVINS, and D. H. BUCKLEY (NASA, Lewis Research Center, Cleveland, OH) (International Conference on Solid Lubrication, 3rd, Denver, CO, Aug. 5-9, 1984) Wear (ISSN 0043-1648), vol. 108, 1986, p. 169-184. Previously announced in STAR as N84-17352. refs

The graded interface between an ion-plated film and a substrate is discussed as well as the friction and wear properties of ion-plated gold. X-ray photoelectron spectroscopy (XPS) depth profiling and microhardness depth profiling were used to investigate the interface. The friction and wear properties of ion-plated and vapor-deposited gold films were studied both in an ultra high vacuum system to maximize adhesion and in oil to minimize adhesion. The results indicate that the solubility of gold on the substrate material controls the depth of the graded interface. Thermal diffusion and chemical diffusion mechanisms are thought to be involved in the formation of the gold-nickel interface. In iron-gold graded interfaces the gold was primarily dispersed in the iron and thus formed a physically bonded interface. The hardness of the gold film was influenced by its depth and was also related to the composition gradient between the gold and the substrate. The graded nickel-gold interface exhibited the highest hardness because of an alloy hardening effect. The effects of film thickness on adhesion and friction were established. S.L.

A86-49690* National Aeronautics and Space Administration. Lewis Research Center, Cleveland, Ohio.

THE PLASTIC COMPRESSIBILITY OF 7075-T651 ALUMINUM-ALLOY PLATE

A. D. FREED (NASA, Lewis Research Center, Cleveland, OH) and B. I. SANDOR (Wisconsin, University, Madison) Experimental Mechanics (ISSN 0014-4851), vol. 26, June 1986, p. 119-121. Research supported by the Lockheed-Georgia Co. refs

The change in volume, and therefore the change in mass density, of an aluminum alloy was measured in uniaxial tension using clip-on extensometers. The experimental data do not agree with the assumption of plastic incompressibility found in the classical theories of plasticity. In fact, the elastic and plastic volume changes are of the same order of magnitude. Plastic anisotropy is thought to be the prime cause of this plastic compressibility. Author

A86-49856* National Aeronautics and Space Administration. Lewis Research Center, Cleveland, Ohio.

ADVANCED THERMAL BARRIER SYSTEM BOND COATINGS FOR USE ON NICKEL-, COBALT- AND IRON-BASE ALLOY SUBSTRATES

S. STECURA (NASA, Lewis Research Center, Cleveland, OH) Thin Solid Films (ISSN 0040-6090), vol. 136, 1986, p. 241-256. Previously announced in STAR as N85-31283. refs

New and improved Ni-, Co-, and Fe-base bond coatings have been identified for the ZrO₂-Y₂O₃ thermal barrier coatings to be used on Ni-, Co-, and Fe-base alloy substrates. These bond coatings were evaluated in a cyclic furnace between 1120 and 1175 C. It was found that MCrAlYb (where M = Ni, Co, or Fe) bond coating thermal barrier systems have significantly longer lives than MCrAlY bond coating thermal barrier systems. The longest life was obtained with the FeCrAlYb thermal barrier system followed by NiCrAlYb and CoCrAlYb thermal barrier systems in that order. Author

A86-50279* National Aeronautics and Space Administration. Lewis Research Center, Cleveland, Ohio.

THE INFLUENCE OF GRAIN SIZE AND COMPOSITION ON SLOW PLASTIC FLOW IN FEAL BETWEEN 1100 AND 1400 K

J. D. WHITTENBERGER (NASA, Lewis Research Center, Cleveland, OH) Materials Science and Engineering (ISSN 0025-5416), vol. 77, 1986, p. 103-113. refs

The slow plastic flow properties of a series of binary B2 FeAl intermetallics at elevated temperatures, and ranging in aluminum content from 39.8 to 48.7 at. pct, were investigated using constant-velocity compression tests at strain rates from 2×10 to the $-3rd$ to 2×10 to the $-7th$. Two deformation mechanisms with the same activation energy are found. For the mode with a stress component of 6, the strength increases with decreasing grain size, probably as a result of Hall-Petch behavior, while for the mode with stress component of 3, the strength increases with increasing grain size, probably due to the action of diffusional creep. Creep in the high stress exponent mode can be described in terms of the initial grain size because the large-angle grain structure is replaced by a small-angle grain microstructure of similar grain diameter during deformation. R.R.

A86-50321* National Aeronautics and Space Administration. Lewis Research Center, Cleveland, Ohio.

ORIENTATION AND TEMPERATURE DEPENDENCE OF SOME MECHANICAL PROPERTIES OF THE SINGLE-CRYSTAL NICKEL-BASE SUPERALLOY RENE N4. I - TENSILE BEHAVIOR

R. V. MINER, J. GAYDA, T. P. GABB (NASA, Lewis Research Center, Cleveland, OH), and R. C. VOIGT (Kansas, University, Lawrence) Metallurgical Transactions A - Physical Metallurgy and Materials Science (ISSN 0360-2133), vol. 17A, March 1986, p. 491-496. refs

Single crystal specimens of a nickel-base superalloy with axes near 001, 011, and -112 were tested in tension at room temperature, 760, and 980 C. The alloy Rene N-4, was developed for gas turbine engine blades and has the nominal composition 3.7 Al, 4.2 Ti, 4 Ta, 0.5 Nb, 6 W, 1.5 Mo, 9 Cr, 7.5 Co, balance Ni, (all in weight percent). Analysis of slip band traces, specimen axis rotation, and dislocation Burgers vectors showed that at 760 and 980 C primary cube slip supplanted normal octahedral slip for the -112 line-oriented specimens. The other two orientations, which have lower resolved shear stresses on the cube system, exhibited octahedral slip at all three temperatures. The critical resolved shear stress is considerably greater on the cube system than on the octahedral system at room temperature. However, at 760 and 980 C the critical resolved shear stresses on the two systems are about the same. While the room temperature and 980 C yield strengths for the two orientations exhibiting octahedral slip could be rationalized on the basis of resolved shear stress, those at 760 C could not. Such violations of Schmid's law have previously been observed in other superalloys and single phase gamma-prime. Author

A86-50322* National Aeronautics and Space Administration. Lewis Research Center, Cleveland, Ohio.

ORIENTATION AND TEMPERATURE DEPENDENCE OF SOME MECHANICAL PROPERTIES OF THE SINGLE-CRYSTAL NICKEL-BASE SUPERALLOY RENE N4. II - LOW CYCLE FATIGUE BEHAVIOR

T. P. GABB, J. GAYDA, and R. V. MINER (NASA, Lewis Research Center, Cleveland, OH) Metallurgical Transactions A - Physical Metallurgy and Materials Science (ISSN 0360-2133), vol. 17A, March 1986, p. 497-505. refs

The low cycle fatigue (LCF) properties of a single-crystal nickel-base superalloy Rene N4, have been examined at 760 and 980 C in air. Specimens having crystallographic orientations near the 001, 011, -111, 023, -236, and -145 lines were tested in fully reversed, total-strain-controlled LCF tests at a frequency of 0.1 Hz. At 760 C, this alloy exhibited orientation dependent tension-compression anisotropies of yielding which continued to failure. Also at 760 C, orientations exhibiting predominately single slip exhibited serrated yielding for many cycles. At 980 C, orientation

dependencies of yielding behavior were smaller. In spite of the tension-compression anisotropies, cyclic stress range-strain range behavior was not strongly orientation dependent for either test temperature. Fatigue life on a total strain range basis was highly orientation dependent at 760 and 980 C and was related chiefly to elastic modulus, low modulus orientations having longer lives. Stage I crack growth on 111 planes was dominant at 760 C, while Stage II crack growth occurred at 980 C. Crack initiation generally occurred at near-surface micropores, but occasionally at oxidation spikes in the 980 C tests. Author

A86-50323* National Aeronautics and Space Administration. Lewis Research Center, Cleveland, Ohio.

ORIENTATION AND TEMPERATURE DEPENDENCE OF SOME MECHANICAL PROPERTIES OF THE SINGLE-CRYSTAL NICKEL-BASE SUPERALLOY RENE N4. III - TENSION-COMPRESSION ANISOTROPY

R. V. MINER, T. P. GABB, J. GAYDA (NASA, Lewis Research Center, Cleveland, OH), and K. J. HEMKER Metallurgical Transactions A - Physical Metallurgy and Materials Science (ISSN 0360-2133), vol. 17A, March 1986, p. 507-512. Previously announced in STAR as N85-22660. refs

Single crystal superalloy specimens with various crystallographic directions along their axes were tested in compression at room temperature, 650, 760, 870, and 980 deg C. These results are compared with the tensile behavior studied previously. The alloy, Rene N4, was developed. R.J.F.

N86-10311* National Aeronautics and Space Administration. Lewis Research Center, Cleveland, Ohio.

CREEP-FATIGUE BEHAVIOR OF NICOALY COATED PWA 1480 SUPERALLOY SINGLE CRYSTALS

R. V. MINER, J. GAYDA, and M. G. HEBSUR 1985 20 p refs Presented at the Symp. on Low-Cycle Fatigue Directions for the Future, Bolton Landing, N.Y., 30 Sep. - 4 Oct. 1985; sponsored by American Society for Testing Materials (NASA-TM-87110; E-2710; NAS 1.15:87110) Avail: NTIS HC A02/MF A01 CSCL 11F

Single crystal specimens of a Ni base superalloy, PWA 1480, with a low pressure plasma sprayed NiCoCrAlY coating were tested in various 0.1 Hz fatigue and creep fatigue cycles both at 1015 and 1050 C. Creep fatigue tests of the cp, pc, and cc types were conducted with various constant total strain ranges employing creep dwells at various constant stresses. Considerable cyclic softening occurred as was evidenced particularly by rapidly increasing creep rates in the creep fatigue tests. The cycle time in the creep fatigue tests typically decreased by more than 80 percent at 0.5 N sub f. Though cyclic life did correlate with delta epsilon sub in a better correlation existed with sub f for both the fatigue and creep fatigue tests, and poor correlations were observed with either sigma sub max or the average cycle time. A model containing both delta sigma and delta sigma (sub in), N sub f = alpha delta sigma (sub in) beta delta sigma gamma, with best fit values of sigma for each cycle type, but the same values of beta and gamma, was found to provide good correlations. Life lines were not greatly different among the cycle types, differing only by a factor of about three. The cp cycle life line was lowest for both test temperatures, however among the other three cycle types there was no consistent ranking. For all test types failure occurred predominately by multiple internal cracking originating at pores. The strong correlation of life with delta sigma may reflect a significant crack growth period in the life of the specimens. B.W.

N86-12292* National Aeronautics and Space Administration. Lewis Research Center, Cleveland, Ohio.

INFLUENCE OF LOAD INTERACTIONS ON CRACK GROWTH AS RELATED TO STATE OF STRESS AND CRACK CLOSURE

J. TELESMA Sep. 1985 22 p refs (NASA-TM-87117; E-2724; NAS 1.15:87117) Avail: NTIS HC A02/MF A01 CSCL 11F

Fatigue crack propagation (FCP) after an application of a low-high loading sequence was investigated as a function of specimen thickness and crack closure. No load interaction effects

were detected for specimens in a predominant plane strain state. However, for the plane stress specimens, initially high FCP rates after transition to a higher stress intensity range were observed. The difference in observed behavior was explained by examining the effect of the resulting closure stress intensity values on the effective stress intensity range. Author

N86-12293*# National Aeronautics and Space Administration. Lewis Research Center, Cleveland, Ohio.

ELLIPSOMETRIC SURFACE ANALYSIS OF WEAR TRACKS PRODUCED BY DIFFERENT LUBRICANTS

J. L. LAUER, N. MARXER, and W. R. JONES, JR. Oct. 1985 20 p refs Presented at the Tribology Conf., Atlanta, 8-10 Oct. 1985; sponsored by ASLE and ASME (Contract NAG3-22; DAAG24-83-K-0058) (NASA-TM-87142; E-2769; NAS 1.15:87142) Avail: NTIS HC A02/MF A01 CSCL 11H

A scanning ellipsometer with high spatial resolution was used to analyze wear tracks generated on M-50 surfaces operated in several lubricant formulations. These formulations included a pure ester base stock of trimethylol propane triheptanoate with additives of either benzotriazole (BTZ), dioctyldiphenylamine (DODPA), or tricresylphosphate (TCP). Results indicated that BTZ and TCP produced patchy oxide surface films consisting mainly of Fe₃O₄. DODPA produced a much more uniform oxide film. These findings may explain the tendency of lubricant formulations containing TCP to scuff more readily than those containing only antioxidants. Author

N86-12294*# National Aeronautics and Space Administration. Lewis Research Center, Cleveland, Ohio.

FATIGUE CRACK PROPAGATION OF NICKEL-BASE SUPERALLOYS AT 650 DEG C

J. GAYDA, T. P. GABB, and R. V. MINER Oct. 1985 22 p refs Presented at the Symp. on Low-Cycle Fatigue Directions for the Future, Bolton Landing, N.Y., 30 Sep. - 4 Oct. 1985; sponsored by American Society for Testing and Materials (NASA-TM-87150; E-2778; NAS 1.15:87150) Avail: NTIS HC A02/MF A01 CSCL 11F

The 650 C fatigue crack propagation behavior of two nickel-base superalloys, Rene 95 and Waspaloy, is studied with particular emphasis placed on understanding the roles of creep, environment, and two key grain boundary alloying additions, boron and zirconium. Comparison of air and vacuum data shows the air environment to be detrimental over a wide range of frequencies for both alloys. More in-depth analysis on Rene 95 shows at lower frequencies, such as 0.02 Hz, failure in air occurs by intergranular, environmentally-assisted creep crack growth, while at higher frequencies, up to 5.0 Hz, environmental interactions are still evident but creep effects are minimized. The effect of B and Zr in Waspaloy is found to be important where environmental and/or creep interactions are presented. In those instances, removal of B and Zr dramatically increases crack growth and it is therefore plausible that effective dilution of these elements may explain a previously observed trend in which crack growth rates increase with decreasing grain size. Author

N86-12295*# National Aeronautics and Space Administration. Lewis Research Center, Cleveland, Ohio.

AN UPDATE OF THE TOTAL-STRAIN VERSION OF SRP

J. F. SALTSMAN and G. R. HALFORD Oct. 1985 27 p refs Presented at the Symp. on Low Cycle Fatigue: Direc. for the Future, Lake George, N.Y., 30 Sep. - 4 Oct. 1985; sponsored by American Society for Testing and Materials, American Inst. of Mining, Metallurgical and Petroleum Engineers, and American Society for Metals (NASA-TP-2499; E-2575; NAS 1.60:2499) Avail: NTIS HC A03/MF A01 CSCL 11F

An updated procedure for characterizing an alloy and predicting cyclic life by using the total strain range version of strainrange partitioning (TS-SRP) has been developed. The principal feature of this update is a new procedure for determining the intercept of time dependent elastic strain range versus cyclic life lines. The

procedure is based on an established relation between failure and the cyclic stress-strain response of an alloy. The stress-strain response is characterized by empirical equations presented in this report. These equations were determined with the aid of a cyclic constitutive model. The procedures presented herein reduce the testing required to characterize an alloy. Failure testing is done only in the high strain, low life regime; cyclic stress-strain response is determined from tests conducted in both the high and low strain regimes. These tests are carried out to stability of the stress-strain hysteresis loop but not to failure. Thus both the time and costs required to characterize an alloy are greatly reduced. This approach was evaluated and verified for two nickel base superalloys, AF2-1DA and Inconel 718. Author

N86-13407*# National Aeronautics and Space Administration. Lewis Research Center, Cleveland, Ohio.

POLYMER, METAL AND CERAMIC MATRIX COMPOSITES FOR ADVANCED AIRCRAFT ENGINE APPLICATIONS

D. L. MCDANELS, T. T. SERAFINI, and J. A. DICARLO 1985 26 p refs Presented at the Advanced Composites Conference, Detroit, 3-4 Dec. 1985; sponsored by ASME (NASA-TM-87132; E-2746; NAS 1.15:87132) Avail: NTIS HC A03/MF A01 CSCL 11F

Advanced aircraft engine research within NASA Lewis is being focused on propulsion systems for subsonic, supersonic, and hypersonic aircraft. Each of these flight regimes requires different types of engines, but all require advanced materials to meet their goals of performance, thrust-to-weight ratio, and fuel efficiency. The high strength/weight and stiffness/weight properties of resin, metal, and ceramic matrix composites will play an increasingly key role in meeting these performance requirements. At NASA Lewis, research is ongoing to apply graphite/polyimide composites to engine components and to develop polymer matrices with higher operating temperature capabilities. Metal matrix composites, using magnesium, aluminum, titanium, and superalloy matrices, are being developed for application to static and rotating engine components, as well as for space applications, over a broad temperature range. Ceramic matrix composites are also being examined to increase the toughness and reliability of ceramics for application to high-temperature engine structures and components. Author

N86-13408*# National Aeronautics and Space Administration. Lewis Research Center, Cleveland, Ohio.

THE EFFECT OF COBALT CONTENT IN U-700 TYPE ALLOYS ON DEGRADATION OF ALUMINIDE COATINGS

I. ZAPLATYNSKY Nov. 1985 15 p refs (NASA-TM-87173; E-2798; NAS 1.15:87173) Avail: NTIS HC A02/MF A01 CSCL 11F

The influence of cobalt content in U-700 type alloys on the behavior of aluminide coatings is studied in burner rig cyclic oxidation tests at 1100C. It is determined that aluminide coatings on alloys with higher cobalt offer better oxidation protection than the same coatings on alloys containing less cobalt. Author

N86-13409*# National Aeronautics and Space Administration. Lewis Research Center, Cleveland, Ohio.

CURRENT VIEWPOINTS ON OXIDE ADHERENCE MECHANISMS

J. L. SMIALEK and R. BROWNING 1985 17 p refs Presented at the 168th Meeting of the Electrochemical Society, Las Vegas, Nev., 15-18 Oct. 1985 (NASA-TM-87168; E-2806; NAS 1.15:87168) Avail: NTIS HC A02/MF A01 CSCL 11F

Additional hot stage Auger experiments have provided surface segregation data for NiCrAl + or - Y or Zr alloys in agreement with other investigations. This data, combined with experimental and theoretical evidence of the Al₂O₃-metal bond strength, is presented in support of a chemical mechanism of Al₂O₃ scale adhesion. Both the detrimental effects of sulfur segregation and the beneficial effects of dopant segregation may be important. Chemical features of the dopants are compared in light of these proposed mechanisms, namely delta H sub f (sulfide), delta H

sub f (oxide), electron orbital configuration, and insolubility in Ni.
Author

N86-14354*# Drexel Univ., Philadelphia, Pa.
STRUCTURE-PROPERTY CHARACTERIZATION OF RHEOCAST AND VADER PROCESSED IN-100 SUPERALLOY Ph.D. Thesis. Final Report
J. J. A. CHENG and D. APELIAN Jun. 1985 234 p refs
(Contract NAG3-14)
(NASA-CR-175014; NAS 1.26:175014) Avail: NTIS HC A11/MF A01 CSCL 11F

Two recent solidification processes have been applied in the production of IN-100 nickel-base superalloy: rheocasting and vacuum arc double electrode remelting (VADER). A detailed microstructural examination has been made of the products of these two processes; associated tensile strength and fatigue crack propagation (FCP) rate at an elevated temperature were evaluated. In rheocasting, processing variables that have been evaluated include stirring speed, isothermal stirring time and volume fraction solid during isothermal stirring. VADER processed IN-100 was purchased from Special Metals Corp., New Hartford, NY. As-cast ingots were subjected to hot isostatic pressing (HIP) and heat treatment. Both rheocasting and VADER processed materials yield fine and equiaxed spherical structures, with reduced macrosegregation in comparison to ingot materials. The rheocast structures are discussed on the basis of the Vogel-Doherty-Cantor model of dendrite arm fragmentation. The rheocast ingots evaluated were superior in yield strength to both VADER and commercially cast IN-100 alloy. Rheocast and VADER ingots may have higher crack propagation resistance than P/M processed material.

Author

N86-14355*# Wisconsin Univ., Madison.
UNDERCOOLING AND SOLIDIFICATION BEHAVIOR IN THE INSB-SB SYSTEM M.S. Thesis. Final Report
J. A. GRAVES Sep. 1985 217 p refs
(Contract NAS3-14)
(NASA-CR-175013; NAS 1.26:175013) Avail: NTIS HC A10/MF A01 CSCL 11F

Use of the droplet emulsion technique has been successful in studying the undercooling and crystallization behavior of Sb, InSb, and an InSb-Sb eutectic alloy. Both droplet size and imposed cooling rate were influential in controlling the extent of liquid undercooling. The droplet surface coating was of significant importance in determining the resultant solidification product structure through its effect on nucleation kinetics. The maximum undercooling for pure Sb was extended from 0.08 to 0.23 T sub m. While simple crushing techniques provided a dramatic increase in droplet undercooling over the bulk material, emulsification treatments both enhanced this undercooling and allowed successful formation of a metastable simple cubic Sb phase. This phase was stable to temperatures approaching the melting point. The simple cubic phase was detected in droplet samples processed using DTA, air and water quenching, and drop tube processing under a helium gas atmosphere. A deviation in the InSb parent ingot composition limited interpretation of the line compound results, however, emulsification techniques extended the undercooling of this material to 0.17 T sub L and provided a stable, protective surface coating for the droplets. Emulsification of the eutectic alloy was effective at producing various levels of undercooling from 0.1 to 0.2 T sub E. Microstructural examination revealed a normal-type eutectic structure in the undercooled droplets indicating that solidification occurred within the coupled zone and that this zone is somewhat symmetric about the eutectic composition.

B.W.

N86-14356*# Texas A&M Univ., College Station. Dept. of Aerospace Engineering.
DEVELOPMENT OF CONSTITUTIVE MODELS FOR CYCLIC PLASTICITY AND CREEP BEHAVIOR OF SUPER ALLOYS AT HIGH TEMPERATURE Final Report
W. E. HAISLER 30 Sep. 1983 161 p refs
(Contract NAG3-31; RESEARCH FOUNDATION PROJ. 4246)
(NASA-CR-176418; NAS 1.26:176418) Avail: NTIS HC A08/MF A01 CSCL 11F

An uncoupled constitutive model for predicting the transient response of thermal and rate dependent, inelastic material behavior was developed. The uncoupled model assumes that there is a temperature below which the total strain consists essentially of elastic and rate insensitive inelastic strains only. Above this temperature, the rate dependent inelastic strain (creep) dominates. The rate insensitive inelastic strain component is modeled in an incremental form with a yield function, blow rule and hardening law. Revisions to the hardening rule permit the model to predict temperature-dependent kinematic-isotropic hardening behavior, cyclic saturation, asymmetric stress-strain response upon stress reversal, and variable Bauschinger effect. The rate dependent inelastic strain component is modeled using a rate equation in terms of back stress, drag stress and exponent n as functions of temperature and strain. A sequence of hysteresis loops and relaxation tests are utilized to define the rate dependent inelastic strain rate. Evaluation of the model has been performed by comparison with experiments involving various thermal and mechanical load histories on 5086 aluminum alloy, 304 stainless steel and Hastelloy X.

Author

N86-15378*# National Aeronautics and Space Administration. Lewis Research Center, Cleveland, Ohio.
THERMAL-MECHANICAL FATIGUE TEST APPARATUS FOR METAL MATRIX COMPOSITES AND JOINT ATTACHMENTS
L. J. WESTFALL and D. W. PETRASEK 1985 21 p refs
Presented at 1st Symposium on Testing Technology of Metal Matrix Composites, Nashville, Tenn., 18-20 Nov. 1985; sponsored by American Society for Testing and Materials
(NASA-TM-87187; E-2773; NAS 1.15:87187) Avail: NTIS HC A02/MF A01 CSCL 11F

Two thermal-mechanical fatigue (TMF) test facilities were designed and developed, one to test tungsten fiber reinforced metal matrix composite specimens at temperature up to 1430C (2600F) and another to test composite/metal attachment bond joints at temperatures up to 760C (1400 F). The TMF facility designed for testing tungsten fiber reinforced metal matrix composites permits test specimen temperature excursions from room temperature to 1430C (2600F) with controlled heating and loading rates. A strain-measuring device measures the strain in the test section of the specimen during each heating and cooling cycle with superimposed loads. Data is collected and recorded by a computer. The second facility is designed to test composite/metal attachment bond joints and to permit heating to a maximum temperature of 760C (1400F) within 10 min and cooling to 150C (300F) within 3 min. A computer controls specimen temperature and load cycling.

Author

N86-15380*# National Aeronautics and Space Administration. Lewis Research Center, Cleveland, Ohio.
CREEP RUPTURE BEHAVIOR OF STIRLING ENGINE MATERIALS
R. H. TITRAN, C. M. SCHEUERMAN, and J. R. STEPHENS Oct. 1985 10 p refs
Presented at the Advanced Technology Development Contractors Coordination Meeting, Dearborn, Mich., 21-24 Oct. 1985; sponsored by DCJE
(Contract DE-A101-77CS-51044)
(NASA-TM-87209; E-2846; DOE/NASA/51044-37; NAS 1.15:87209) Avail: NTIS HC A012/MF A01 CSCL 11F

The automotive Stirling engine, being investigated jointly by the Department of Energy and NASA Lewis as an alternate to the internal combustion engine, uses high-pressure hydrogen as the working fluid. The long-term effects of hydrogen on the high temperature strength properties of materials is relatively unknown.

This is especially true for the newly developed low-cost iron base alloy NASAUT 4G-A1. This iron-base alloy when tested in air has creep-rupture strengths in the directionally solidified condition comparable to the cobalt base alloy HS-31. The equiaxed (investment cast) NASAUT 4G-A1 has superior creep-rupture to the equiaxed iron-base alloy XF-818 both in air and 15 MPa hydrogen. Author

N86-16334*# National Aeronautics and Space Administration. Lewis Research Center, Cleveland, Ohio.

THERMAL AGING EFFECTS IN REFRACTORY METAL ALLOYS

J. R. STEPHENS 1986 28 p refs Presented at the 3rd Symposium on Space Nuclear Power Systems, Albuquerque, N. Mex., 13-15 Jan. 1986; sponsored by the American Nuclear Society

(NASA-TM-87210; E-2869; NAS 1.15:87210) Avail: NTIS HC A03/MF A01 CSCL 11F

The alloys of niobium and tantalum are attractive from a strength and compatibility viewpoint for high operating temperatures required in materials for fuel cladding, liquid metal transfer, and heat pipe applications in space power systems that will supply from 100 kWe to multi-megawatts for advanced space systems. To meet the system requirements, operating temperatures ranging from 1100 to 1600 K have been proposed. Expected lives of these space power systems are from 7 to 10 yr. A program is conducted at NASA Lewis to determine the effects of long-term, high-temperature exposure on the microstructural stability of several commercial tantalum and niobium alloys. Variables studied in the investigation include alloy composition, pre-age annealing temperature, aging time, temperature, and environment (lithium or vacuum), welding, and hydrogen doping. Alloys are investigated by means of cryogenic bend tests and tensile tests. Results show that the combination of tungsten and hafnium or zirconium found in commercial alloys such as T-111 and Cb-752 can lead to aging embrittlement and increased susceptibility to hydrogen embrittlement of ternary and more complex alloys. Modification of alloy composition helps to eliminate the embrittlement problem. Author

N86-17531*# IIT Research Inst., Chicago, Ill.
CREEP-RUPTURE BEHAVIOR OF IRON SUPERALLOYS IN HIGH-PRESSURE HYDROGEN Final Report

S. BHATTACHARYYA and W. PETERMAN Dec. 1985 52 p refs

(Contract DEN3-363; DE-AI01-77CS-51040)
(NASA-CR-175027; DOE/NASA/0363-1; NAS 1.26:175027; IITRI-M06136-9) Avail: NTIS HC A04/MF A01 CSCL 11F

The creep-rupture behavior of a newly developed cast alloy NASAUT 4G-A1 with 15% Cr, 15% Mn, and 1.5% C was evaluated in 15 MPa H₂ at 775 C and 825 C. The alloy is intended for automotive Stirling heater head application. Rupture life, minimum creep rate, and time to 1% strain data were analyzed using the Orowan-Sherby-Dorn temperature compensated technique, and the 3500-h rupture life stress and stress to obtain 1% strain in 3500 h were estimated. The analyses indicated that 3500-h mean rupture stress at 775 C is 140 MPa, exceeding the design stress of 119 MPa. The predicted mean stress to 1% creep in 3500 h was 57.8 MPa and had a very wide scatter indicating a lack of reproducibility in the alloy structure. For a case alloy, NASAUT 4G-A1 indicated significant ductility with maximum elongation in the range of 6.0 to 13.6% at 775 C. Hydrogen did not seem to affect the stable carbides though some methane was noted in the chamber gas, presumably arising from chamber structural members of lesser stability. The microstructure contained some voids, pores, inclusions, and intermetallic separations, which caused the observed scatter in data. Author

N86-20541*# National Aeronautics and Space Administration. Lewis Research Center, Cleveland, Ohio.

ALLOY CHEMISTRY AND MICROSTRUCTURAL CONTROL TO MEET THE DEMANDS OF THE AUTOMOTIVE STIRLING ENGINE Final Report

J. R. STEPHENS 1986 38 p refs Proposed for presentation at MiCon 1986, Philadelphia, Pa., 15-16 May 1986; sponsored by the American Society for Testing Materials

(Contract DE-AI01-85CE-50112)
(NASA-TM-87250; E-2892; DOE/NASA/50112-63; NAS 1.15:87250) Avail: NTIS HC A03/MF A01 CSCL 11F

The automotive Stirling engine now under development by DOE/NASA as an alternative to the internal combustion engine, imposes severe materials requirements for the hot portion of the engine. Materials selected must be low cost and contain a minimum of strategic elements so that availability is not a problem. Heater head tubes contain high pressure hydrogen on the inside and are exposed to hot combustion gases on the outside surface. The cylinders and regenerator housings must be readily castable into complex shapes having varying wall thicknesses and be amenable to brazing and welding operations. Also, high strength, oxidation resistance, resistance to hydrogen permeation, cyclic operation, and long-life are required. A research program conducted by NASA Lewis focused on alloy chemistry and microstructural control to achieve the desired properties over the life of the engine. Results of alloy selection, characterization, evaluation, and actual engine testing of selected materials are presented. Author

N86-20542*# Syracuse Univ., N. Y. Dept. of Mechanical and Aerospace Engineering.

GRAIN BOUNDARY OXIDATION AND OXIDATION ACCELERATED FATIGUE CRACK NUCLEATION AND PROPAGATION

H. W. LIU and Y. OSHIDA Jan. 1986 19 p refs Presented at the Minnowbrook Conference on Life Prediction for High Temperature Gas Turbine Materials, Blue Mountain Lake, N.Y., 27-30 Aug. 1985 Sponsored in part by the HOST Program (Contract NAG3-348)

(NASA-CR-175050; NAS 1.26:175050) Avail: NTIS HC A02/MF A01 CSCL 11F

Fatigue life at elevated temperatures is often shortened by oxidation. Grain boundary oxidation penetrates deeper than the surface oxidation. Therefore, grain boundary oxide penetration could be the primary cause of accelerated fatigue crack nucleation and propagation, and the shortened fatigue life at elevated temperatures. Grain boundary oxidation kinetics was studied and its statistical scatter was analyzed by the Weibull's distribution function. The effects of grain boundary oxidation on shortened fatigue life was analyzed and discussed. A model of intermittent microcracks of the grain boundary oxide was proposed for the fatigue crack growth in the low frequency region. The proposed model is consistent with the observations that fatigue crack growth rate in the low frequency region with hold time at K_{sub max} is inversely proportional to cyclic frequency and that crack growth is intergranular. Author

N86-21656*# Case Western Reserve Univ., Cleveland, Ohio. Dept. of Metallurgy and Materials Science.

EFFECT OF BORON ON TENSILE PROPERTIES OF B2 BEAL Final Report

M. CRIMP and K. VEDULA Feb. 1986 17 p refs

(Contract NAG3-563; DE-AI-01-77CS-51040)
(NASA-CR-175074; DOE/NASA/0563-1; NAS 1.26:175074)
Avail: NTIS HC A02/MF A01 CSCL 11F

Small additions of boron were shown to improve the room temperature ductility of the intermetallic compound Ni₃Al. Boron is believed to segregate to the grain boundaries and strengthen them, allowing the inherent ductility of the grains to be achieved. The present study was undertaken to see if boron has a similar effect on the low temperature tensile properties of the equiatomic intermetallic compound FeAl. A binary alloy without boron is compared with an alloy containing 0.78 at % B (0.2 wt %) B, by tensile testing over the temperature range of 300 K to 640 K.

Both alloys were processed by powder metallurgy. Results showed that 0.78 at % B addition to FeAl does indeed change the room temperature fracture mode from intergranular to transgranular, suggesting a strengthening of grain boundaries. The alloy containing boron is, however, still brittle at room temperature. A slight decrease in the ductile to brittle transition temperature is, nevertheless, observed. In addition a significant increase in strength of the alloy is observed with boron addition. Author

N86-21658*# National Aeronautics and Space Administration. Lewis Research Center, Cleveland, Ohio.

ROLE OF MOLYBDENUM IN THE NA SUB 250 SUB 4 INDUCED CORROSION OF SUPERALLOYS AT HIGH TEMPERATURES

A. K. MISRA (Case Western Research Univ., Cleveland, Ohio) 1986 29 p refs Presented at the TMS-AIME Annual Meeting, New Orleans, La., 2-6 Mar. 1986

(NASA-TM-87235; E-2905; NAS 1.15:87235) Avail: NTIS HC A03/MF A01 CSCL 11F

Sodium sulfate induced corrosion of a molybdenum containing nickel-base superalloy, Udimet 700, was studied in laboratory furnace tests and in a high velocity (Mach 0.3) burner rig. The effect of SO₂ content in the atmosphere on the corrosion behavior in the laboratory furnace tests was determined. Catastrophic corrosion occurs only when the melt contains MoO₃ in addition to Na₂SO₄ and Na₂MoO₄. The conditions under which catastrophic corrosion occurs are identified and a mechanism is described to explain the catastrophic corrosion. Author

N86-21659*# National Aeronautics and Space Administration. Lewis Research Center, Cleveland, Ohio.

UNDERCOOLED AND RAPIDLY QUENCHED NI-MO ALLOYS

S. N. TEWARI and T. K. GLASGOW (Defence Metallurgical Research Lab., Hyderabad, India) 1986 19 p refs Presented at the Hume Rothery Memorial Symposium on Undercooled Alloy Phases at the AIME Annual Meeting, New Orleans, La., 2-6 Mar. 1986 Sponsored in part by National Research Council

(NASA-TM-87257; E-2947; NAS 1.15:87257) Avail: NTIS HC A02/MF A01 CSCL 11F

Hypoeutectic, eutectic, and hypereutectic nickel-molybdenum alloys were rapidly solidified by both bulk undercooling and melt spinning techniques. Alloys were undercooled in both electromagnetic levitation and differential thermal analysis equipment. The rate of recalescence depended upon the degree of initial undercooling and the nature (faceted or nonfaceted) of the primary nucleating phase. Alloy melts were observed to undercool more in the presence of primary Beta (NiMo intermetallic) phase than in gamma (fcc solid solution) phase. Melt spinning resulted in an extension of molybdenum solid solubility in gamma nickel, from 28 to 37.5 at % Mo. Although the microstructures observed by undercooling and melt spinning were similar the microsegregation pattern across the gamma dendries was different. The range of microstructures evolved was analyzed in terms of the nature of the primary phase to nucleate, its subsequent dendritic growth, coarsening and fragmentation, and final solidification of interfendritic liquid. Author

N86-21661*# National Aeronautics and Space Administration. Lewis Research Center, Cleveland, Ohio.

VARIABLES CONTROLLING FATIGUE CRACK GROWTH OF SHORT CRACKS

J. TELESMA, D. M. FISHER, and D. HOLKA (Michigan Technological Univ., Houghton) Dec. 1985 20 p refs Presented at the International Conference on Fatigue, Corrosion Cracking, Fracture Mechanics, and Failure Analysis, Salt Lake City, Utah, 2-6 Dec. 1985; sponsored by American Society for Metals

(NASA-TM-87208; E-2865; NAS 1.15:87208) Avail: NTIS HC A02/MF A01 CSCL 11F

A study was conducted to evaluate the roles of crack closure and microstructure in the fatigue growth of short cracks. Testing was performed at R ratios of 0.1, 0.5, and 0.7. At all R ratios short cracks exhibited accelerated growth rates in comparison to long cracks. It was concluded that crack closure could not entirely account for the accelerated growth rates of short cracks. The

accelerated growth rates occurred over crack lengths on the order of grain size, suggesting a strong influence of microstructure. A significant effect of grain boundaries and inclusions on short crack FCG behavior was observed. For very short crack lengths, fatigue growth rates do not appear to be a function of either delta K or R ratio. Author

N86-22686*# National Aeronautics and Space Administration. Lewis Research Center, Cleveland, Ohio.

INFLUENCE OF FATIGUE CRACK WAKE LENGTH AND STATE OF STRESS ON CRACK CLOSURE

J. TELESMA and D. M. FISHER 1986 27 p refs Presented at the International Symposium on Fatigue Crack Closure, 1-2 May 1986; sponsored by the American Society for Testing and Materials

(NASA-TM-87292; E-2999; NAS 1.15:87292) Avail: NTIS HC A03/MF A01 CSCL 11F

The location of crack closure with respect to crack wake and specimen thickness under different loading conditions was determined. The rate of increase of K sub CL in the crack wake was found to be significantly higher for plasticity induced closure in comparison to roughness induced closure. Roughness induced closure was uniform throughout the thickness of the specimen while plasticity induced closure levels were 50 percent higher in the near surface region than in the midthickness. The influence of state of stress on low-high load interaction effects was also examined. Load interaction effects differed depending upon the state of stress and were explained in terms of delta K sub eff. Author

N86-22687*# National Aeronautics and Space Administration. Lewis Research Center, Cleveland, Ohio.

CERAMIC THERMAL BARRIER COATINGS FOR ELECTRIC UTILITY GAS TURBINE ENGINES

R. A. MILLER 1986 15 p refs Presented at the 3rd Berkeley Conference on Corrosion, Erosion, and Wear of Materials, Berkeley, Calif., 29-31 Jan. 1986; sponsored by the National Association of Corrosion Engineers

(NASA-TM-87288; E-2994; NAS 1.15:87288) Avail: NTIS HC A02/MF A01 CSCL 11F

Research and development into thermal barrier coatings for electric utility gas turbine engines is reviewed critically. The type of coating systems developed for aircraft applications are found to be preferred for clear fuel electric utility applications. These coating systems consists of a layer of plasma sprayed zirconia-yttria ceramic over a layer of MCrAlY bond coat. They are not recommended for use when molten salts are presented. Efforts to understand coating degradation in dirty environments and to develop corrosion resistant thermal barrier coatings are discussed. Author

N86-22688*# Case Western Reserve Univ., Cleveland, Ohio. Dept. of Metallurgy and Materials Science.

HIGH TEMPERATURE DISPERSION STRENGTHENING OF NIAL Final Report

M. SHERMAN and K. VEDULA Mar. 1986 15 p refs (Contract NAG3-387)

(NASA-CR-175073; NAS 1.26:175073) Avail: NTIS HC A02/MF A01 CSCL 11F

A potential high temperature strengthening mechanism for alloys based on the intermetallic compound NiAl was investigated. This study forms part of an overall program at NASA Lewis Research Center for exploring the potential of alloys based on NiAl for high temperature applications. An alloy containing 2.26 at% Nb and produced by hot extrusion of blended powders was examined in detail using optical and electron microscopy. Interdiffusion between the blended Nb and NiAl powders results in the formation of intermediate phases. A fine dispersion of precipitates of a hexagonal, ordered NiAlNb phases in a matrix of NiAl can be produced and this results in strengthening of the alloy by interfering with dislocation motion at high temperature. These precipitates are, however, found to coarsen during the high temperature (1300

K) deformation at slow strain rates and this may impose some limitations on the use of this strengthening mechanism. Author

N86-24813* National Aeronautics and Space Administration. Lewis Research Center, Cleveland, Ohio.

APPLICATION OF AN ATMOSPHERIC PRESSURE SAMPLING MASS SPECTROMETER TO CHLORINATION REACTIONS

N. S. JACOBSON 1986 20 p refs Presented at the 115th TMS-AIME Annual Meeting, New Orleans, La., 2-6 Mar. 1986; sponsored by Metallurgical Society (NASA-TM-87270; E-2888; NAS 1.15:87270) Avail: NTIS HC A02/MF A01 CSCL 11F

An atmospheric pressure mass spectrometric sampling system, based on a free jet expansion was used to study certain M-Cl-O reactions at high temperatures. The apparatus enables the volatile species from a 1-atm chemical process to be directly identified with a mass spectrometer which operates at approx. 10 to the minus 8th power torr. Studies for both pure metals and alloys are discussed. It is shown that this mass spectrometer system aids in identifying the volatile species, and provides fundamental information on the reaction mechanism. E.A.K.

N86-24817* Case Western Reserve Univ., Cleveland, Ohio. Dept. of Metallurgy and Materials Science.

CORROSION OF NICKEL AND COBALT BASE ALLOYS IN SULFATE MELTS AT 750 DEG C Final Report

A. K. MISRA Apr. 1986 31 p refs Presented at the 169th Meeting of the Electrochemical Society, Boston, Mass., 4-9 May 1986

(Contract NCC3-43)

(NASA-CR-175111; E-3035; NAS 1.26:175111) Avail: NTIS HC A03/MF A01 CSCL 11F

The corrosion of Ni, Co, plus several nickel and cobalt-base alloys was studied at 750 C in the presence of molten sulfate mixtures and in an atmosphere consisting of O₂ + 0.12% SO₂+SO₃. The melt system selected were Na₂SO₄-Li₂SO₄ and Na₂SO₄-CoSO₄. The corrosion of pure metals took place by the formation of a mixed oxide plus sulfide scale. A mixed oxide plus sulfide of the base metal is also formed during the initial stage of corrosion of the alloys; however, subsequently a Cr rich sulfide is formed underneath the outer base metal rich scale. With time, the outer part of the inner scale oxidizes to an oxide and more sulfides are formed beneath the oxide. The inner scale is formed as a continuous layer for the low Cr containing alloys and the inner scale is formed in localized sites in the form of pits for the higher Cr containing alloys. Author

N86-24818* Massachusetts Inst. of Tech., Cambridge. Dept. of Materials Science and Engineering.

THERMAL-MECHANICAL FATIGUE BEHAVIOR OF NICKEL-BASE SUPERALLOYS Final Report

R. M. PELLOUX and N. MARCHAND Mar. 1986 186 p refs (Contract NAG3-280)

(NASA-CR-175048; NAS 1.26:175048; USAAVSCOM-TR-86-C-4) Avail: NTIS HC A09/MF A01 CSCL 11F

The main achievements of a 36-month research program are presented. The main objective was to gain more insight into the problem of crack growth under thermal mechanical fatigue (TMF) conditions. This program was conducted at M.I.T. for the period of September 1982 to September 1985. The program was arranged into five technical tasks. Under Task I, the literature of TMF data was reviewed. The goal was to identify the crack propagation conditions in aircraft engines (hot section) and to assess the validity of conventional fracture mechanics parameters to address TMF crack growth. The second task defined the test facilities, test specimen and the testing conditions needed to establish the effectiveness of data correlation parameters identified in Task I. Three materials (Inconel X-750, Hastelloy-X, and B-1900) were chosen for the program. Task II was accomplished in collaboration with Pratt & Whitney Aircraft engineers. Under Task III, a computerized testing system to measure the TMF behavior (LCF and CG behaviors) of various alloys systems was built. The software used to run isothermal and TMF tests was also developed. Built

around a conventional servohydraulic machine, the system is capable of push-pull tests under stress or strain and temperature controlled conditions in the temperature range of 25C to 1050C. A crack propagation test program was defined and conducted under Task IV. The test variables included strain range, strain rate (frequency) and temperature. Task V correlated and generalized the Task IV data for isothermal and variable temperature conditions so that several crack propagation parameters could be compared and evaluated. The structural damage (mode of cracking and dislocation substructure) under TMF cycling was identified and contrasted with the isothermal damage to achieve a sound fundamental mechanistic understanding of TMF. Author

N86-25453* National Aeronautics and Space Administration. Lewis Research Center, Cleveland, Ohio.

TENSILE BEHAVIOR OF FE-40AL ALLOYS WITH B AND ZR ADDITIONS

D. J. GAYDOSH and M. V. NATHAL 1986 27 p refs Presented at the 1986 TMS-AIME Annual Meeting, New Orleans, La., 2-6 Mar. 1986

(NASA-TM-87290; E-2997; NAS 1.15:87290) Avail: NTIS HC A03/MF A01 CSCL 11F

Both Fe-40Al and Fe-40Al-0.1Zr with and without B were produced by the hot extrusion of powdered metal. Tensile properties were determined from room temperature to 1100 K in air. All of the materials possessed some ductility at room temperature, and addition of B caused an increase in ductility and a change in fracture mode from intergranular to transgranular cleavage. At high temperatures, failure was caused primarily by the formation of grain boundary cavities in all of the alloys. The effect of Zr addition was unclear because of the complexity of the various microstructures. Comparison of air and vacuum testing at high temperatures revealed that an apparent oxidation assisted mechanism reduced high temperature ductility in these alloys, especially at 900 K. Author

N86-25454* Pennsylvania State Univ., University Park. Dept. of Engineering Science and Mechanics.

AXIAL AND TORSIONAL FATIGUE BEHAVIOR OF WASPALOY Final Report

S. ZAMRIK, M. MIRDAMADI, and F. ZAHIRI Apr. 1986 27 p (Contract NAG3-264)

(NASA-CR-175052; NAS 1.26:175052; USAAVSCOM-TR-86-C-14) Avail: NTIS HC A02/MF A01 CSCL 11F

The cyclic flow response and crack growth behavior of Waspaloy at room temperature and 650 C under tensile loading and torsional loading was studied, for two conditions of Waspaloy: fine grain, large gamma prime size; coarse grain, small gamma prime size. The fine grain material showed 5 to 10 percent hardening after about 10 percent of life, with sequent softening to failure at both temperature levels. The coarse grain material showed either stable response or monotonic softening to failure. Early crack initiation was observed on planes of maximum shear, with eventual branching to principle planes under torsional loading; cracks were always normal to load axis under tensile loading. Also, crack paths were intergranular at 650 C, mostly transgranular at room temperature. Author

N86-25455* Georgia Inst. of Tech., Atlanta. School of Materials Engineering.

YIELDING AND DEFORMATION BEHAVIOR OF THE SINGLE CRYSTAL NICKEL-BASE SUPERALLOY PWA 1480

W. W. MILLIGAN, JR. May 1986 96 p refs (Contract NAG3-503)

(NASA-CR-175100; NAS 1.26:175100; USAAVSCOM-TR-86-C-18) Avail: NTIS HC A05/MF A01 CSCL 11F

Interrupted tensile tests were conducted to fixed plastic strain levels in 100 ordered single crystals of the nickel based superalloy PWA 1480. Testing was done in the range of 20 to 1093 C, at strain rate of 0.5 and 50%/min. The yield strength was constant from 20 to 760 C, above which the strength dropped rapidly and became a strong function of strain rate. The high temperature

data were represented very well by an Arrhenius type equation, which resulted in three distinct temperature regimes. The deformation substructures were grouped in the same three regimes, indicating that there was a fundamental relationship between the deformation mechanisms and activation energies. Models of the yielding process were considered, and it was found that no currently available model was fully applicable to this alloy. It was also demonstrated that the initial deformation mechanism (during yielding) was frequently different from that which would be inferred by examining specimens which were tested to failure. Author

N86-26414*# National Aeronautics and Space Administration. Lewis Research Center, Cleveland, Ohio.

HEAT TREATMENT FOR SUPERALLOY Patent Application

F. H. HARF, inventor (to NASA) 24 Feb. 1986 11 p
(NASA-CASE-LEW-14262-1; NAS 1.71:LEW-14261-1;
US-PATENT-APPL-SN-832296) Avail: NTIS HC A02/MF A01
CSCL 11F

A cobalt-free nickel-base superalloy composed of in weight % 15 Cr - 5 Mo - 3.5 Ti - 4 Al - 0.07 (max) C - remainder Ni is given a modified heat treatment. With this heat treatment the cobalt-free alloy achieves certain of the mechanical properties of the corresponding cobalt-containing nickel-base superalloy at 1220 F (650 C). Thus, strategic cobalt can be replaced with nickel in the superalloy. NASA

N86-27444*# Case Western Reserve Univ., Cleveland, Ohio. Dept. of Metallurgy and Materials Science.

THE EVOLUTION AND GROWTH OF AL₂O₃ SCALES ON BETA-NIAL Ph.D. Thesis. Final Report

J. K. DOYCHAK May 1986 242 p
(Contract NAG3-498)
(NASA-CR-175097; NAS 1.26:175097) Avail: NTIS HC A11/MF
A01 CSCL 11F

The formation and growth of Al₂O₃ scales on (beta)-NiAl were studied using electron microscopy and other analytical techniques to gain an understanding of the oxidation properties of (beta)-NiAl and of alumina-forming alloys, in general. The transient and mature stages of oxidation were studied as well as the transformation stage during which the oxide scale transforms from metastable Al₂O₃ phases to the thermodynamically stable alpha-Al₂O₃ phase. The transient oxidation stages were studied at 800 deg C and for short times at 1100C. At 800C, the scales consist predominantly of delta-Al₂O₃ which forms by cation vacancy ordering in the defective spinel lattice of gamma-Al₂O₃. At 1100C, a fast-growth morphology of theta-Al₂O₃ forms as a surface layer over delta-Al₂O₃. For both oxidation temperatures, the scales are often epitaxially oriented with respect to the metal. The transient scales grow by outward cation diffusion as evidenced by surface growth morphologies. The transformation to alpha-Al₂O₃ occurs within 1 hour at 1100C by a nucleation and radial growth process. The large volume decrease associated with the transformation results in a highly strained alpha-Al₂O₃ microstructure. A change in scale growth mechanism from outward cation to inward anion diffusion allows transient surface morphologies to be smoothed by surface diffusion. The mature stage of oxidation involves the growth of an alpha-Al₂O₃ scale having the lacey morphology formed as a result of the gamma yields alpha transformation. Growth of the scale occurs by counterdiffusion along grain boundaries resulting in ridges formed by impingement of alpha-Al₂O₃ nuclei during the transformation stage. Also scale growth occurs by inward oxygen diffusion through healed cracks; the cracks result from transformation stresses. The measured growth rates of scales having the lacey morphology are an order of magnitude less than fine-grained alpha-Al₂O₃ scales. Metal orientations were found to have a large effect on oxide morphologies during all stages of oxidation. Author

N86-28164*# National Aeronautics and Space Administration. Lewis Research Center, Cleveland, Ohio.

MICROMECHANISMS OF THERMOMECHANICAL FATIGUE: A COMPARISON WITH ISOTHERMAL FATIGUE

R. C. BILL 1986 21 p Presented at the International Spring Conference Fatigue at High Temperatures, Paris, France, 9-11 Jun. 1986; sponsored by the Societe Francaise de Metallurgie Prepared in cooperation with Army Aviation Research and Technology Activity, Cleveland, Ohio
(NASA-TM-87331; E-3075; NAS 1.15:87331;
USAAVSCOM-TR-86-C-7) Avail: NTIS HC A02/MF A01 CSCL 11F

Thermomechanical Fatigue (TMF) experiments were conducted on Mar-M 200, B-1900, and PWA-1480 (single crystals) over temperature ranges representative of gas turbine airfoil environments. The results were examined from both a phenomenological basis and a micromechanical basis. Depending on constituents present in the superalloy system, certain micromechanisms dominated the crack initiation process and significantly influenced the TMF lives as well as sensitivity of the material to the type TMF cycle imposed. For instance, high temperature cracking around grain boundary carbides in Mar-M 200 resulted in short in-phase TMF lives compared to either out-of-phase or isothermal lives. In single crystal PWA-1480, the type of coating applied was seen to be the controlling factor in determining sensitivity to the type of TMF cycle imposed. Micromechanisms of deformation were observed over the temperature range of interest to the TMF cycles, and provided some insight as to the differences between TMF damage mechanisms and isothermal damage mechanisms. Finally, the applicability of various life prediction models to TMF results was reviewed. Current life prediction models based on isothermal data must be modified before being generally applied to TMF. Author

N86-28165*# National Aeronautics and Space Administration. Lewis Research Center, Cleveland, Ohio.

COMPRESSIVE CREEP BEHAVIOR OF ALLOYS BASED ON B2 FEAL

N. MANTRAVADI (Case Western Reserve Univ., Cleveland, Ohio), K. VEDULA, D. GAYDOSH, and R. H. TITRAN 1986 16 p Presented at the IMS-AIME Annual Meeting, New Orleans, La., 2-6 Mar. 1986
(Contract NSG3-387)
(NASA-TM-87293; E-3000; NAS 1.15:87293) Avail: NTIS HC A02/MF A01 CSCL 11F

Alloys based on FeAl are attractive alternate materials for environmental resistance at intermediate temperatures. Addition of small amounts of Nb, Hf, Ta, Mo, Zr, and B were shown to improve the compressive creep of this alloy at 1100 K. Boron, in particular, was found to have a synergistic effect along with Zr in providing properties substantially better than the binary alloy. This improvement seems to be related to the higher activation energy found for this alloy, suggesting a modification in the diffusion behavior due to the alloying additions. Author

N86-31699*# National Aeronautics and Space Administration. Lewis Research Center, Cleveland, Ohio.

THE LOW CYCLE FATIGUE BEHAVIOR OF A PLASMA-SPRAYED COATING MATERIAL

J. GAYDA, T. P. GABB, and R. V. MINER, JR. 1986 17 p Presented at the 1986 TMS-AIME Annual Meeting, New Orleans, La., 2-6 Mar. 1986
(NASA-TM-87318; E-3050; NAS 1.15:87318) Avail: NTIS HC A02/MF A01 CSCL 11F

Single crystal nickel-base superalloys employed in turbine blade applications are often used with a plasma spray coating for oxidation and hot corrosion resistance. These coatings may also affect fatigue life of the superalloy substrate. As part of a large program to understand the fatigue behavior of coated single crystals, fully reversed, total strain controlled fatigue tests were run on a free standing NiCoCrAlY coating alloy, PWA 276, at 0.1 Hz. Fatigue tests were conducted at 650 C, where the NiCoCrAlY alloy has modest ductility, and at 1050 C, where it is extremely

ductile, showing tensile elongation in excess of 100 percent. At the lower test temperature, deformation induced disordering softened the NiCoCrAlY alloy, while at the higher test temperature cyclic hardening was observed which was linked to gradual coarsening of the two phase microstructure. Fatigue life of the NiCoCrAlY alloy was significantly longer at the higher temperature. Further, the life of the NiCoCrAlY alloy exceeds that of coated, /001/-oriented PWA 1480 single crystals at 1050 C, but at 650 C the life of the coated crystal is greater than that of the NiCoCrAlY alloy on a total strain basis. Author

N86-31700*# National Aeronautics and Space Administration. Lewis Research Center, Cleveland, Ohio.

MICROSTRUCTURE-PROPERTY RELATIONSHIPS IN DIRECTIONALLY SOLIDIFIED SINGLE CRYSTAL NICKEL-BASE SUPERALLOYS

R. A. MACKAY and M. V. NATHAL 1986 37 p Presented at MiCon 1986: Optimization of Processing, Properties and Service Performance through Microstructural Control, Philadelphia, Pa., 15-16 May 1986; sponsored by ASTM (NASA-TM-88788; E-3122; NAS 1.15:88788) Avail: NTIS HC A03/MF A01 CSCL 11F

Some of the microstructural features which influence the creep properties of directionally solidified and single crystal nickel-base superalloys are discussed. Gamma precipitate size and morphology, gamma-gamma lattice mismatch, phase instability, alloy composition, and processing variations are among the factors considered. Recent experimental results are reviewed and related to the operative deformation mechanisms and to the corresponding mechanical properties. Special emphasis is placed on the creep behavior of single crystal superalloys at high temperatures, where directional gamma gamma coarsening is prominent, and at lower temperatures, where gamma coarsening rates are significantly reduced. It can be seen that very subtle changes in microstructural features can have profound effects on the subsequent properties of these materials. M.G.

N86-31701*# National Aeronautics and Space Administration. Lewis Research Center, Cleveland, Ohio.

THE CONTINUING BATTLE AGAINST DEFECTS IN NICKEL-BASE SUPERALLOYS

R. L. DRESHFIELD 1986 27 p Presented at the 115th TMS Annual Meeting, New Orleans, La., 2-6 Mar. 1986; sponsored by AIME (NASA-TM-87343; E-3092; NAS 1.15:87343) Avail: NTIS HC A03/MF A01 CSCL 11F

In the six decades since the identification of age hardenable nickel-base superalloys their compositions and microstructures have changed markedly. Current alloys are tailored for specific applications. Thus their microstructures are defined for that application. This paper briefly reviews the evolution of superalloy microstructures and comments on the appearance and implications of microstructural defects in high performance superalloys. It is seen that new alloys and processes have generated new types of defects. Thus as the industry continues to develop new alloys and processes it must remain vigilant toward the identification and control of new types of defects. Author

N86-31702*# National Aeronautics and Space Administration. Lewis Research Center, Cleveland, Ohio.

THE EFFECT OF VARIATIONS OF COBALT CONTENT ON THE CYCLIC OXIDATION RESISTANCE OF SELECTED NI-BASE SUPERALLOYS

C. A. BARRETT Mar. 1986 24 p Presented at the Annual Meeting of the Metallurgical Society of the American Inst. of Mining, Metallurgical, and Petroleum Engineers, New Orleans, La., 2-6 Mar. 1986 (NASA-TM-87297; E-2952; NAS 1.15:87297) Avail: NTIS HC A02/MF A01 CSCL 11F

Cobalt levels were systematically varied in the Ni-base turbine alloys U-700 (cast), U-700m(PM/HIP), Waspaloy, Mar-M-247, In-738, Nimonic-115, U-720, and SX-R-150. The cobalt levels ranged from 0 wt % to the nominal commercial content in each

alloy. The alloys were tested in cyclic oxidation in static air at 1000, 1100 and 1150 C for 500, 200 and 100 hr respectively. An oxidation attack parameter, Ka derived from the specific weight change versus time data was used to evaluate the oxidation behavior of the alloys along with X-ray diffraction analysis of the surface oxides. The alloys tend to form either Cr₂O₃/chromite spinel or Al₂O₃/aluminate spinel depending on the Cr/Al ratio in the alloys. Alloys with a ratio of 3.5 or higher tend to favor the Cr oxides while those under 3.0 form mostly Al oxides. In general the Al₂O₃/aluminate spinel forming alloys have the better oxidation resistance. Increased cobalt content lowers the scaling resistance of the higher Cr alloys while a 5.0 wt % Co content is optimum for the Al controlling alloys. The refractory metals, particularly Ta, appear beneficial to both types of oxides perhaps due to the formation of the omni-present trirutile Ni(Ta,Cb,Mo,W)2O₆. Both scales break down as increasing amounts of NiO is formed.

Author

N86-32556*# National Aeronautics and Space Administration. Lewis Research Center, Cleveland, Ohio.

ION-BEAM NITRIDING OF STEELS Patent Application

J. SALIK, inventor (to NASA) and T. E. HUBBELL, JR., inventor (to NASA) 29 Jan. 1986 11 p (NASA-CASE-LEW-14104-2; US-PATENT-APPL-SN-823713; NAS 1.71:LEW-14104-2) Avail: NTIS HC A02/MF A01 CSCL 11F

A surface of a steel substrate is nitrided without external heating by exposing it to a beam of nitrogen ions under a low pressure. The pressure is much lower than that employed for ion-nitriding, and an ion source is used instead of a glow discharge. Both of these features reduce the introduction of impurities into the substrate surface. NASA

N86-32557*# National Aeronautics and Space Administration. Lewis Research Center, Cleveland, Ohio.

CREEP PROPERTIES OF PWC-11 BASE METAL AND WELDMENTS AS AFFECTED BY HEAT TREATMENT

R. H. TITRAN, T. J. MOORE, and T. L. GROBSTEIN 1986 19 p Presented at the 115th TMS Annual Meeting, New Orleans, La., 2-6 Mar. 1986; sponsored by AIME (NASA-TM-88842; E-3227; NAS 1.15:88842) Avail: NTIS HC A02/MF A01 CSCL 11F

In a preliminary study using single specimens for each condition, PWC-11 (a niobium-base alloy with a nominal composition of Nb-1%Zr-0.1%C) was creep tested at 1350 K and 40 MPa. Base metal specimens and specimens with transverse electron beam welds were tested with and without a 1000 hr, 1350 K aging treatment prior to testing. In the annealed condition (1 hr at 1755 K + 2 hr at 1475 K), the base metal exhibited superior creep strength compared to the nonaged condition, reaching 1 percent strain in 3480 hr. A 1000 hr, 1350 K aging treatment prior to creep testing had a severe detrimental effect on creep strength of the base metal and transverse electron beam weldments, reducing the time to attain 1 percent strain by an order of magnitude. Extrapolated temperature compensated creep rates indicate that the present heat of PWC-11 may be four times as creep resistant as similarly tested Nb-1%Zr. The extrapolated stress to achieve 1 percent creep strain in 7 yr at 1350 K is 2.7 MPa for annealed Nb-1%Zr and 12 MPa for annealed and aged PWC-11 base metal with and without a transverse electron beam weld.

Author

NONMETALLIC MATERIALS

Includes physical, chemical, and mechanical properties of plastics, elastomers, lubricants, polymers, textiles, adhesives, and ceramic materials.

A86-10825* National Aeronautics and Space Administration. Lewis Research Center, Cleveland, Ohio.

SURFACE EFFECTS OF CORROSIVE MEDIA ON HARDNESS, FRICTION, AND WEAR OF MATERIALS

K. MIYOSHI, D. H. BUCKLEY, H. ISHIGAKI (NASA, Lewis Research Center, Cleveland, OH), and G. W. P. RENGSTORFF IN: Wear of materials 1985. New York, ASME, 1985, p. 302-312. Previously announced in STAR as N85-15896. refs

Hardness, friction, and wear experiments were conducted with magnesium oxide exposed to various corrosive media and also with elemental iron and nickel exposed to water and NaOH. Chlorides such as MgCl₂ and sodium containing films were formed on cleaved magnesium oxide surfaces. The MgCl₂ films softened the magnesium oxide surfaces and caused high friction and great deformation. Hardness was strongly influenced by the pH value of the HCl-containing solution. The lower the pH, the lower the microhardness. Neither the pH value of nor the immersion time in NaOH containing, NaCl containing, and HNO₃ containing solutions influenced the microhardness of magnesium oxide. NaOH formed a protective and low friction film on iron surfaces. The coefficient of friction and the wear for iron were low at concentrations of NaOH higher than 0.01 N. An increase in NaOH concentration resulted in a decrease in the concentration of ferric oxide on the iron surface. It took less NaOH to form a protective, low friction film on nickel than on iron. R.S.F.

A86-11076* National Aeronautics and Space Administration. Lewis Research Center, Cleveland, Ohio.

ANGULAR PARTICLE IMPINGEMENT STUDIES OF THERMOPLASTIC MATERIALS AT NORMAL INCIDENCE

P. V. RAO and D. H. BUCKLEY (NASA, Lewis Research Center, Cleveland, OH) ASLE, Annual Meeting, 40th, Las Vegas, NV, May 6-9, 1985. 16 p. refs (ASLE PREPRINT 85-AM-3A-1)

Scanning electron microscope studies were conducted to characterize the erosion resistance of polymethyl methacrylate (PMMA), polycarbonate (PC), polytetrafluoroethylene (PTFE), and ultra-high-molecular-weight polyethylene (UHMWPE). Erosion was caused by a jet of angular microparticles of crushed glass at normal incidence. Material built up above the original surface on all of the materials. As erosion progressed, this buildup disappeared. UHMWPE was the most resistant material and PMMA the least. The most favorable properties for high erosion resistance were high values of ultimate elongation, maximum service temperature, and strain energy and a low value of the modulus of elasticity. Erosion-rate-versus-time curves of PC and PTFE exhibited incubation, acceleration, and steady-state periods. PMMA also exhibited a deceleration period, and an incubation period with deposition was observed for UHMWPE. Author

A86-11175* National Aeronautics and Space Administration. Lewis Research Center, Cleveland, Ohio.

LOW-WEAR PARTIALLY FLUORINATED POLYIMIDES

R. L. FUSARO and W. F. HADY (NASA, Lewis Research Center, Cleveland, OH) ASLE Transactions (ISSN 0569-8197), vol. 28, Oct. 1985, p. 542-550. Previously announced in STAR as N84-24808. refs

Tribological studies were conducted on five different polyimide solid bodies formulated from the diamine 2,2-bis 4-(4-aminophenoxy)phenyl hexafluoropropane (4-BDAF) and the dianhydrides pyromellitic acid (PMDS) and bensophenonetetracarboxylic acid (BTDA). The following polyimides were evaluated: 4-BDAF/PMDA, 4-BDAF/BTDA, 4-BDAF/80 mole percent PMDA,

20 mole percent BTDA, 4-BDAF/60 mole percent BTDA. Friction coefficients, polyimide wear rates, polyimide surface morphology and transfer films were evaluated at sliding speeds of 0.31 to 11.6 m/s and at temperatures of 25 C to 300 C. The results indicate that the tribological properties are highly dependent on the composition of the polyimide and on the experimental conditions. Two polyimides were found which produced very low wear rates but very high friction coefficients (greater than 0.85) under ambient conditions. They offer considerable potential for high traction types of application such as brakes. Author

A86-12416* National Aeronautics and Space Administration. Lewis Research Center, Cleveland, Ohio.

DENSIFICATION AND PROPERTIES OF ALPHA-SILICON CARBIDE

S. DUTTA (NASA, Lewis Research Center, Cleveland, OH) American Ceramic Society, Communications (ISSN 0002-7820), vol. 68, Oct. 1985, p. C-269, C-270. refs

The sintering behavior of alpha-SiC with B and C sintering aids and without sintering aids was investigated experimentally. The sintering was performed for 30-60 min in argon flow at 2150 and 2200 C. The density of the sintered bars was determined by weighing and measuring the bars, four-point flexure tests were conducted on machined bars, and the Weibull modulus was determined by regression analysis. It is found that type 1 alpha-SiC powder, which does not densify, can be sintered to a high final density (in excess of 96 percent of the theoretical value) using B and C sintering aids. Flexure test results and Weibull modulus data suggest that the strength of the alpha-SiC ceramic is greatly affected by processing flaws and also by inclusions and machining flaws. V.L.

A86-13179* Army Research and Technology Labs., Cleveland, Ohio.

EFFECT OF SUBSTITUTED PHENYLNADIMIDES ON PROCESSING AND PROPERTIES OF PMR POLYIMIDE COMPOSITES

W. B. ALSTON (U.S. Army, Propulsion Laboratory, Cleveland, OH) and R. W. LAUVER (NASA, Lewis Research Center, Cleveland, OH) IN: National SAMPE Symposium and Exhibition, 30th, Anaheim, CA, March 19-21, 1985, Proceedings. Covina, CA, Society for the Advancement of Material and Process Engineering, 1985, p. 1622-1638. Previously announced in STAR as N85-14929. refs

Three nitrophenylnadimide cure initiators and two phenylnadimides (without nitros) were evaluated as additives to PMR-15 resins and Celion 6000 graphite fiber composites. The results of a resin screening study eliminated all of the additives except 3-nitrophenylnadimide (NO2PN) for use as a low temperature curing additive for PMR-15. Thus, NO2PN and the two control additives were investigated in PMR-15 formulations from which Celion 6000 graphite fiber/PMR-15 composites were processed both with low temperature (274 C) and normal (316 C) cure cycles. Comparisons of the two processing cycles, the resultant glass transition temperatures (T_g), the ambient, 274 and 316 C composite mechanical properties determined before and after 316 C postcure, the 316 C thermo-oxidative weight losses and the retention of 316 C composite mechanical properties are presented. Empirical correlations of the type and amount of nadimide additives with processing parameters, T_g, composite mechanical properties, composite thermo-oxidative stability and long term retention of 316 C composite mechanical properties are also presented. Author

A86-14428* National Aeronautics and Space Administration. Lewis Research Center, Cleveland, Ohio.

ION BEAM SPUTTER-DEPOSITED THIN FILM COATINGS FOR PROTECTION OF SPACECRAFT POLYMERS IN LOW EARTH ORBIT

B. A. BANKS, M. J. MIRTICH, S. K. RUTLEDGE, D. M. SWEC (NASA, Lewis Research Center, Cleveland, OH), and H. K. NAHRA (Cleveland State University, OH) AIAA, Aerospace Sciences Meeting, 23rd, Reno, NV, Jan. 14-17, 1985. 17 p. Previously announced in STAR as N85-30137. refs (AIAA PAPER 85-0420)

Ion beam sputter-deposited thin films at Al_2O_3 , SiO_2 , and a codeposited mixture of predominantly SiO_2 with small amounts of fluoropolymer were evaluated both in laboratory plasma ashing tests and in space on board Shuttle flight STS-8 for effectiveness in preventing oxidation of polyimide Kapton. Measurements of mass loss and optical performance of coated and uncoated polyimide samples exposed to the low earth orbital environment are presented. Optical techniques were used to measure loss rates of protective films exposed to atomic oxygen. Results of the analysis of the space flight exposed samples indicate that thin film metal oxide coatings are very effective in protecting the polyimide. Metal oxide coatings with a small amount of fluoropolymer codeposited have the additional benefit of great flexibility. Author

A86-15226* Case Western Reserve Univ., Cleveland, Ohio. **FINITE ELEMENT ANALYSIS OF RESIDUAL STRESS IN PLASMA-SPRAYED CERAMIC**

R. L. MULLEN (Case Western Reserve University, Cleveland, OH), R. C. HENDRICKS, and G. MCDONALD (NASA, Lewis Research Center, Cleveland, OH) Ceramic Engineering and Science Proceedings (ISSN 0196-6219), vol. 6, July-Aug. 1985, p. 871-879. refs

Residual stress in a ZrO_2 - Y_2O_3 ceramic coating resulting from the plasma spraying operation is calculated. The calculations were done using the finite element method. Both thermal and mechanical analysis were performed. The resulting residual stress field was compared to the measurements obtained by Hendricks and McDonald. Reasonable agreement between the predicted and measured moment occurred. However, the resulting stress field is not in pure bending. Author

A86-15229* Illinois Univ., Urbana. **CHARACTER OF LASER-GLAZED, PLASMA-SPRAYED ZIRCONIA COATINGS ON STAINLESS STEEL SUBSTRATA**

G. S. FISCHMAN, C. H. CHEN, J. M. RIGSBEE, and S. D. BROWN (Illinois, University, Urbana) Ceramic Engineering and Science Proceedings (ISSN 0196-6219), vol. 6, July-Aug. 1985, p. 908-918. refs (Contract DE-AC02-76ER-01198; NAG3-495)

Partially stabilized zirconia was applied as coatings to 316L stainless steel substrata using an 80-kw arc-plasma unit. Some of these coating-substrate systems were subsequently glazed using a 10 kw CO_2 continuous-wavelength laser. SEM was used to characterize the microstructures of the coatings and coating-substrate interfaces. Results are reported and discussed. Author

A86-15230* National Aeronautics and Space Administration. Lewis Research Center, Cleveland, Ohio.

FUNDAMENTAL TRIBOLOGICAL PROPERTIES OF CERAMICS D. H. BUCKLEY and K. MIYOSHI (NASA, Lewis Research Center, Cleveland, OH) Ceramic Engineering and Science Proceedings (ISSN 0196-6219), vol. 6, July-Aug. 1985, p. 919-939. Previously announced in STAR as N85-15893. refs

When a ceramic is brought into contact with itself, another ceramic, or a metal, strong bond forces can develop between the materials. Adhesion between a ceramic and itself or another solid are discussed from a theoretical consideration of the nature of the surfaces and experimentally by relating bond forces to the interface resulting from solid state contact. Elastic, plastic, and fracture behavior of ceramics in solid-state contact are discussed as they relate to friction and wear. The contact load necessary to

initiate fracture in ceramics is shown to be appreciably reduced with tangential motion. Both friction and wear of ceramics are anisotropic and relate to crystal structure as with metals. Both free energy of oxide formation and the d valence bond character of metals are related to the friction and wear characteristics for metals in contact with ceramics. Lubrication is found to increase the critical load necessary to initiate fracture of ceramics with sliding or rubbing contact. R.S.F.

A86-15237* Garrett Turbine Engine Co., Phoenix, Ariz. **COMPARISON OF THE CONTACT STRESS AND FRICTION BEHAVIOR OF SiC AND ZrO_2 MATERIALS**

L. J. LINDBERG and D. W. RICHESON (Garrett Turbine Engine Co., Phoenix, AZ) Ceramic Engineering and Science Proceedings (ISSN 0196-6219), vol. 6, July-Aug. 1985, p. 1059-1066. refs (Contract N00014-80-C-0870; DEN3-167; DEN3-324)

Studies were performed to further elucidate the friction and contact-stress characteristics of structural ceramic materials. New data for fully stabilized and partially stabilized zirconia ceramics are compared with prior test results for sintered SiC. The comparison provides further evidence that the high temperature friction characteristics of sintered SiC are strongly influenced by the presence of a viscous surface layer. The results also show that a ceramic material with lower coefficient of friction and higher fracture toughness has increased resistance to strength-reducing surface damage due to contact stress. Author

A86-15238* Florida Univ., Gainesville. **PROPERTIES OF SILICON SUSPENSIONS AND SLIP-CAST BODIES**

M. D. SACKS and G. W. SCHEIFFELE (Florida, University, Gainesville) Ceramic Engineering and Science Proceedings (ISSN 0196-6219), vol. 6, July-Aug. 1985, p. 1109-1123. refs (Contract DEN3-167)

The effect of varying pH, sonication times, and solid loading of silicon powder suspensions on the properties of powder/water suspensions and on the resulting pore characteristics of slip-cast bodies was studied. Aqueous suspensions of ground an aged silicon powder (of 0.3 micron median Stokes diameter and containing 1.3 vol pct Fe_2O_3 powder) were prepared, with solids loading in the range of 30-56 vol pct, and were adjusted to varying pH values by addition of either HCl or NH_4OH or NaOH. Suspension aliquots were sonicated for 0, 15, 30, or 60 min. Suspensions were characterized by zeta potentials, ionic strength, and viscosity. Pore characteristics of cast bodies were determined by mercury porosimetry. It was found that intermediate pH values (pH 7-9), long sonication (60 min), and high solid loadings (56 vol pct) produced samples with highest green densities and smallest median pore radius. I.S.

A86-15239* National Aeronautics and Space Administration. Lewis Research Center, Cleveland, Ohio.

FACTORS INFLUENCING THE BALL MILLING OF Si_3N_4 IN WATER

M. R. FREEDMAN, J. D. KISER, and T. P. HERBELL (NASA, Lewis Research Center, Cleveland, OH) Ceramic Engineering and Science Proceedings (ISSN 0196-6219), vol. 6, July-Aug. 1985, p. 1124-1134. Previously announced in STAR as N85-19136. refs

A statistical study of the ball milling of Si_3N_4 powder in Si_3N_4 hardware was undertaken to understand how the resulting increase in specific surface area is related to solids loading and mill speed. An attempt was made to optimize milling conditions. The degree of communication was more dependent upon solids loading than mill speed. A practical grinding limit between 0.5 and 0.75 microns was achieved in 144 hr independent of solids loading. Ball mill wear and media wear were independent of both solids loading and mill speed. E.A.K.

A86-15240* National Aeronautics and Space Administration. Lewis Research Center, Cleveland, Ohio.

PARAMETRIC EVALUATION OF BALL MILLING OF SIC IN WATER

J. D. KISER, T. P. HERBELL, and M. R. FREEDMAN (NASA, Lewis Research Center, Cleveland, OH) Ceramic Engineering and Science Proceedings (ISSN 0196-6219), vol. 6, July-Aug. 1985, p. 1135-1145. Previously announced in STAR as N85-21356. refs

A statistically designed experiment was conducted to determine optimum conditions for ball milling alpha-SiC in water. The influence of pH adjustment, volume percent solids loading, and mill rotational speed on grinding effectiveness was examined. An equation defining the effect of those milling variables on specific surface area was obtained. The volume percent solids loading of the slurry had the greatest influence on the grinding effectiveness in terms of increase in specific surface area. As grinding effectiveness improved, mill and media wear also increased. Contamination was minimized by use of sintered alpha-SiC milling hardware. Author

A86-16255* Case Western Reserve Univ., Cleveland, Ohio.

COMPOSITION AND PROPERTIES OF THE SO-CALLED 'DIAMOND-LIKE' AMORPHOUS CARBON FILMS

J. C. ANGUS, J. E. STULTZ, P. J. SHILLER (Case Western Reserve University, Cleveland, OH), J. R. MACDONALD (Guelph, University, Canada), M. J. MIRTICH (NASA, Lewis Research Center, Cleveland, OH) et al. IN: Metallurgical coatings 1984; Proceedings of the Eleventh International Conference, San Diego, CA, April 9-13, 1984. Volume 1. Lausanne, Switzerland, Elsevier Sequoia, S.A., 1984, p. 311-320. NASA-supported research. refs

The composition of amorphous 'diamond-like' films made by direct low energy ion beam deposition, R.F. discharge and sputtering was determined by nuclear reaction analysis, IR spectroscopy and microcombustion chemical analysis. The nuclear reaction analysis showed very similar hydrogen depth profiles for all three types of samples. The atomic ratio of hydrogen to carbon was approximately 0.2 at the film surface and rose to approximately 1.0 at a depth of 500 Å. The integrated intensity of the C-H stretching band at about 2900 per cm indicates that the amount of chemically bonded hydrogen is less than the total hydrogen content. Combustion analysis confirmed the overall atomic ratio of hydrogen to carbon determined by nuclear reaction analysis. The chemical state of the non-bonded hydrogen was not determined; however, the effective diffusion coefficient computed from the hydrogen depth profile was extremely low. This indicates either that the films are exceedingly impermeable or that the non-bonded hydrogen requires an additional activated step to leave the films, e.g., desorption or chemical reaction. Author

A86-16269* State Univ. of New York, Stony Brook.

NEUTRON AND X-RAY DIFFRACTION OF PLASMA-SPRAYED ZIRCONIA-YTTRIA THERMAL BARRIER COATINGS

N. R. SHANKAR, H. HERMAN (New York, State University, Stony Brook), S. P. SINGHAL (NBS, Washington, DC), and C. C. BERNDT (NASA, Lewis Research Center, Cleveland, OH) IN: Metallurgical coatings 1984; Proceedings of the Eleventh International Conference, San Diego, CA, April 9-13, 1984. Volume 2. Lausanne, Switzerland, Elsevier Sequoia, S.A., 1984, p. 159-171. refs (Contract NAG3-164)

ZrO₂-7.8mol. pct. YO_{1.5}, a fused powder, and ZrO₂-8.7mol. pct. YO_{1.5}, a pre-reacted powder, were plasma-sprayed onto steel substrates. Neutron diffraction and X-ray diffraction of the as-received powder, the powder plasma sprayed into water, as-sprayed coatings, and coatings heat-treated for 10 and 100 h were carried out to study phase transformations and ordering of the oxygen ions on the oxygen sublattice. The as-received fused powder has a much lower monoclinic percentage than does the pre-reacted powder, this resulting in a much lower monoclinic percentage in the coating. Heat treatment increases the percentages of the cubic and monoclinic phases, while decreasing the tetragonal content. An ordered tetragonal phase is detected by the presence of extra neutron diffraction peaks. These phase transformations and ordering will result in volume changes. The

implications of these transformations on the performance of partially stabilized zirconia thermal barrier coatings is discussed. Author

A86-16271* National Aeronautics and Space Administration. Lewis Research Center, Cleveland, Ohio.

DEPOSITION STRESS EFFECTS ON THE LIFE OF THERMAL BARRIER COATINGS ON BURNER RIGS

J. W. WATSON and S. R. LEVINE (NASA, Lewis Research Center, Cleveland, OH) IN: Metallurgical coatings 1984; Proceedings of the Eleventh International Conference, San Diego, CA, April 9-13, 1984. Volume 2. Lausanne, Switzerland, Elsevier Sequoia, S.A., 1984, p. 185-193. Previously announced in STAR as N84-25830. refs

A study of the effect of plasma spray processing parameters on the life of a two layer thermal barrier coating was conducted. The ceramic layer was plasma sprayed at plasma arc currents of 900 and 600 amps onto uncooled tubes, cooled tubes, and solid bars of Waspalloy in a lathe with 1 or 8 passes of the plasma gun. These processing changes affected the residual stress state of the coating. When the specimens were tested in a Mach 0.3 cyclic burner rig at 1130 deg C, a wide range of coating lives resulted. Processing factors which reduced the residual stress state in the coating, such as reduced plasma temperature and increased heat dissipation, significantly increased coating life. Author

A86-17479* National Aeronautics and Space Administration. Lewis Research Center, Cleveland, Ohio.

TRIBOLOGICAL PROPERTIES OF BORON NITRIDE SYNTHESIZED BY ION BEAM DEPOSITION

K. MIYOSHI, D. H. BUCKLEY, and T. SPALVINS (NASA, Lewis Research Center, Cleveland, OH) Journal of Vacuum Science and Technology A (ISSN 0734-2101), vol. 3, Nov.-Dec. 1985, p. 2340-2344. Previously announced in STAR as N85-21355. refs

The adhesion and friction behavior of boron nitride films on 440 C bearing stainless steel substrates was examined. The thin films containing the boron nitride were synthesized using an ion beam extracted from a borazine plasma. Sliding friction experiments were conducted with BN in sliding contact with itself and various transition metals. It is indicated that the surfaces of atomically cleaned BN coating film contain a small amount of oxides and carbides, in addition to boron nitride. The coefficients of friction for the BN in contact with metals are related to the relative chemical activity of the metals. The more active the metal, the higher is the coefficient of friction. The adsorption of oxygen on clean metal and BN increases the shear strength of the metal - BN contact and increases the friction. The friction for BN-BN contact is a function of the shear strength of the elastic contacts. Clean BN surfaces exhibit relatively strong interfacial adhesion and high friction. The presence of adsorbates such as adventitious carbon contaminants on the BN surfaces reduces the shear strength of the contact area. In contrast, chemically adsorbed oxygen enhances the shear strength of the BN-BN contact and increases the friction. E.A.K.

A86-17484* National Aeronautics and Space Administration. Lewis Research Center, Cleveland, Ohio.

FILM AND INTERSTITIAL FORMATION OF METALS IN PLASMA-SPRAYED CERAMICS

R. C. HENDRICKS, G. MCDONALD (NASA, Lewis Research Center, Cleveland, OH), and R. L. MULLEN (Case Western Reserve University, Cleveland, OH) Journal of Vacuum Science and Technology A (ISSN 0734-2101), vol. 3, Nov.-Dec. 1985, p. 2456-2458. Previously announced in STAR as N85-22756. refs

A method is described to electrodeposit noble metals such as platinum and ordinary metals such as copper on and within plasma-sprayed ceramic materials and ceramic fiber materials. Low-density ceramic fiber bodies were vacuum impregnated with plating solution and attached to an electrode. Light micrographs illustrating the density and location of deposited materials are presented and discussed. Voids in the plasma-sprayed ceramic were filled with deposits that vary from spherical to lens-shaped circular and have particle size corresponding to the full range of

void size. Multiple coatings of ceramic and metal can be sequenced. Author

A86-17495* California Univ., Los Angeles.

PRETREATMENT EFFECTS ON THE MORPHOLOGY AND PROPERTIES OF ALUMINUM OXIDE THERMALLY GROWN ON NICOCHALY

S. PRAKASH, R. BUDHANI, H. J. DOERR, C. V. DESHPANDEY, and R. F. BUNSHAH (California, University, Los Angeles) Journal of Vacuum Science and Technology A (ISSN 0734-2101), vol. 3, Nov.-Dec. 1985, p. 2551-2556. refs (Contract NAG3-451)

The effect of pretreatments on the morphology and properties of aluminum oxide thermally grown from NiCoCrAlY was investigated. The goal was to optimize process steps to produce a highly adherent, continuous, and insulating aluminum oxide. Two pretreatments were carried out, one in vacuum (about 0.0001 Torr) at 1350 K for 5 h, and the other consisting of deposition of a 1-micron thick Al₂O₃ film by activated reactive evaporation. Samples were subsequently oxidized thermally at 1000 C for 50 h at 0.5 Torr oxygen pressure. The two pretreatments were carried out on electron-beam evaporation NiCoCrAlY, about 120 microns thick, deposited on a superalloy turbine blade substrate. The results showed that the thermally grown oxide was significantly different in microstructure, surface topography and in its adherence to the NiCoCrAlY for the two pretreatments. Optimum results were obtained by combining the two pretreatments to produce an adherent, continuous, and insulating oxide film on the NiCoCrAlY-coated superalloy substrate. Author

A86-20435* Rensselaer Polytechnic Inst., Troy, N.Y.

OPTICAL AND OTHER PROPERTIES CHANGES OF M-50 BEARING STEEL SURFACES FOR DIFFERENT LUBRICANTS AND ADDITIVES PRIOR TO SCUFFING

J. L. LAUER, N. MARXER (Rensselaer Polytechnic Institute, Troy, NY), and W. R. JONES, JR. (NASA, Lewis Research Center, Cleveland, OH) ASLE Transactions, vol. 29, Jan. 1986, p. 13-24. Previously announced in STAR as N84-34620. refs (Contract NAG3-222; AF-AFOSR-81-0005; DAAG24-83-K-0058)

An ester lubricant base oil containing one or more standard additives to protect against wear, corrosion, and oxidation was used in an experimental ball/plate elastohydrodynamic contact under load and speed conditions such as to induce scuffing failure in short times. Both the ball and the plate were of identically treated M-50 steel. After various periods of operating time the wear track on the plate was examined with an interference microscope of plus or minus 30 Å depth resolution and sometimes also with a scanning ellipsometer and an Auger spectrometer. The optically deduced surface profiles varied with wavelength, indicating the presence of surface coatings, which were confirmed by the other instruments. As scuffing was approached, a thin (approximately Å) oxide layer and a carbide layer formed in the wear track in particular when tricresylphosphate antiwear additive was present in the lubricant. The rates of the formation of these layers and their reactivity toward dilute alcoholic HCl depended strongly on the lubricant and additives. Based on these results suggestions for improved formulations and a test method for bearing reliability could be proposed. R.J.F.

A86-20437* National Aeronautics and Space Administration. Lewis Research Center, Cleveland, Ohio.

SIMULATION OF LUBRICATING BEHAVIOR OF A THIOETHER LIQUID LUBRICANT BY AN ELECTROCHEMICAL METHOD

W. MORALES (NASA, Lewis Research Center, Cleveland, OH) ASLE Transactions, vol. 29, Jan. 1986, p. 67-73; Discussion, p. 73, 74; Author's Reply, p. 74. Previously announced in STAR as N84-23764. refs

An electrochemical cell was constructed to explore the possible radical anion forming behavior of a thioether liquid lubricant. The electrochemical behavior of the thioether was compared with the electrochemical behavior of biphenyl, which is known to form radical anions. Under controlled conditions biphenyl undergoes a reversible reaction to a radical anion, whereas the thioether undergoes an

irreversible reduction yielding several products. These results are discussed in relation to boundary lubrication. Author

A86-20992* National Aeronautics and Space Administration. Lewis Research Center, Cleveland, Ohio.

KINETICS AND MECHANISM OF CORROSION OF SiC BY MOLTEN SALTS

N. S. JACOBSON (NASA, Lewis Research Center, Cleveland, OH) American Ceramic Society, Journal (ISSN 0002-7820), vol. 69, Jan. 1986, p. 74-82. refs

Corrosion of sintered alpha-SiC under thin films of Na₂CO₃/CO₂, Na₂SO₄/O₂, and Na₂SO₄/SO₃ was investigated at 1000 C. Chemical analysis was used to follow silicate and silica evolution as a function of time. This information coupled with morphology observations leads to a detailed corrosion mechanism. In all cases the corrosion reactions occur primarily in the first few hours. In the Na₂CO₃/CO₂ case, rapid oxidation and dissolution lead to a thick layer of silicate melt in about 0.25 h. After this, silica forms a protective layer on the carbide. In the Na₂SO₄/O₂ case, a similar mechanism occurs. In the Na₂SO₄/SO₃ case, a porous nonprotective layer of SiO₂ grows directly on the carbide, and a silicate melt forms above this. In addition, SiO₂ and regenerated Na₂SO₄ form at the melt/gas interface due to reaction of silicate with SO₃ and SO₂ + O₂. The reaction slows when the lower silica layer becomes nonporous. Author

A86-23921*# SOHIO Engineered Materials Co., Niagara Falls, N.Y.

SINTERED ALPHA SILICON CARBIDE CERAMICS FOR HIGH TEMPERATURE STRUCTURAL APPLICATION - STATUS REVIEW AND RECENT DEVELOPMENTS

R. S. STORM, W. D. G. BOECKER, C. H. MCMURTRY, and M. SRINIVASAN (Sohio Engineered Materials Co., Niagara Falls, NY) ASME, Chinese Society of Aeronautics and Astronautics, and China National Aero-Technology Import and Export Corp., Beijing International Gas Turbine Symposium and Exposition, Beijing, People's Republic of China, Sept. 1-7, 1985. 9 p. DOE-supported research. refs

(Contract DEN3-17; DEN3-168; DEN3-167) (ASME PAPER 85-IGT-127)

The physical properties of sintered alpha silicon carbide are reviewed, including the effect of oxidation at high temperatures. Net shape fabricated components are described which have undergone extensive testing in heat engine applications. Properties of an SiC/TiB₂ composite material, which has significantly improved fracture toughness, are presented. Author

A86-24956* National Aeronautics and Space Administration. Lewis Research Center, Cleveland, Ohio.

SELECTED FRETTING-WEAR-RESISTANT COATINGS FOR Ti-6 PCT AL-4 PCT V ALLOY

R. C. BILL (NASA, Lewis Research Center, Cleveland, OH) (Institution of Mechanical Engineers, Fretting Wear Seminar, Nottingham, England, Apr. 2, 3, 1985) Wear (ISSN 0043-1648), vol. 106, Nov. 1985, p. 283-301. refs

The ability of several wear-resistant coatings to reduce fretting in the Ti-6Al-4V alloy is investigated. The experimental apparatus and procedures for evaluating fretting in uncoated Ti-6Al-4V alloy and in the alloy with plasma-sprayed coatings, polymer-bonded coating, and surface treatments are described. The wear volume and wear rate for the alloys are measured and compared. It is concluded that Al₂O₃ with 13 percent TiO₂, preoxidation and nitride surface treatments, and MoS₂ sputtering result in wear-resistant surfaces; however, the polyimide coating is the most wear resistant coating in both dry and moist air, and it causes the least wear to the uncoated alloy surface. I.F.

A86-26341* National Aeronautics and Space Administration. Lewis Research Center, Cleveland, Ohio.

STRUCTURE AND GRAIN COARSENING DURING THE SINTERING OF ALUMINA

N. J. SHAW (NASA, Lewis Research Center, Cleveland, OH; Leeds, University, England) and R. J. BROOK (Leeds, University, England) American Ceramic Society, Journal (ISSN 0002-7820), vol. 69, Feb. 1986, p. 107-110. refs

The pore surface area (S_p) and grain-boundary area (S_{gb}) were measured during the sintering of undoped and doped (100 ppm MgO) alumina compacts. Since the presence of the additive affects only S_{gb} (raising it at a given value of the density), pinning of the boundaries by solid-solution drag is the only additive function evidenced by the results. The importance of such pinning even at densities as low as 75 percent of theoretical is linked to the existence of microstructural inhomogeneities. Author

A86-30052* National Aeronautics and Space Administration. Lewis Research Center, Cleveland, Ohio.

TENSILE ADHESION TEST MEASUREMENTS ON PLASMA-SPRAYED COATINGS

C. C. BERNDT (NASA, Lewis Research Center, Cleveland, OH) IN: Advances in fracture research (Fracture 84). Volume 4. Oxford and New York, Pergamon Press, 1986, p. 2553-2559. refs (Contract NCC3-27)

Adhesion measurements on plasma-sprayed coatings are briefly studied, including a critical analysis of the experimental scatter for duplicate tests. The application of a simple method which presents adhesion strength data in a fracture mechanics perspective is demonstrated. Available data are analyzed in a way which suggests an approach to finding the overall defect contribution to reducing the apparent strength of coatings. C.D.

A86-31825* National Aeronautics and Space Administration. Lewis Research Center, Cleveland, Ohio.

ENVIRONMENTAL STABILITY OF INTERCALATED GRAPHITE FIBERS

J. R. GAIER and D. A. JAWORSKIE (NASA, Lewis Research Center, Cleveland, OH) Synthetic Metals (ISSN 0379-6779), vol. 12, 1985, p. 525-532. Previously announced in STAR as N85-26992. refs

Graphite fibers intercalated with bromine, iodine monochloride, ferric chloride, and cupric chloride were subjected to stability tests under four environments which are encountered by engineering materials in the aerospace industry: ambient laboratory conditions, as would be experienced during handling operations and terrestrial applications; high vacuum, as would be experienced in space applications; high humidity, as would be experienced in marine applications; and high temperature, as would be experienced in some processing steps and applications. Monitoring the resistance of the fibers at ambient laboratory conditions revealed that only the ferric chloride intercalated fibers were unstable, due to absorption of water from the air. All four types of intercalated fibers were unstable, due to absorption of water from the air. All four types of intercalated fibers were stable for long periods under high vacuum. Ferric chloride, cupric chloride, and iodine monochloride intercalated fibers were sensitive to high humidity conditions. All intercalated fibers began to degrade above 250 C. The order of their thermal stability, from lowest to highest, was cupric chloride, iodine monochloride, bromine, and ferric chloride. Of the four types of intercalated fibers tested, the bromine intercalated fibers appear to have the most potential for application, based on environmental stability. Author

A86-33113* National Aeronautics and Space Administration. Lewis Research Center, Cleveland, Ohio.

EFFECT OF SOLUTION CONCENTRATION AND AGING CONDITIONS ON PMR-15 RESIN

G. D. ROBERTS and R. D. VANNUCCI (NASA, Lewis Research Center, Cleveland, OH) SAMPE Journal (ISSN 0091-1062), vol. 22, Mar.-Apr. 1986, p. 24-28, 213.

High performance liquid chromatography is utilized to evaluate the effect of temperature, solution concentration, and aging time

on PMR-15 resin solutions. Fifty- and 70-wt percent PMR-15 resin solutions were prepared from the mixture of 5-norbornene-2,3-dicarboxylic ester (NE) acid, 4,4'-methylenedianiline (MDA), methanol, and 3,3',4,4'-benzophenonetetracarboxylic dimethyl ester (BTDE) acid solution. It is observed that in PMR-15 resin solution aged for 35 days at room temperature NE and MDA react to form amide and imide intermediates. The precipitation data reveal that in the 70-wt percent solution precipitation occurs after 12 days and in the 50-wt percent solution after 20 days; however, at lower temperatures (-11 C, and 2 C) no precipitation is detected. It is concluded that storage of resin solutions and powders at reduced temperatures extends shelf life by reducing the rate of imide formation. I.F.

A86-33495* National Aeronautics and Space Administration. Lewis Research Center, Cleveland, Ohio.

EFFECT OF GRAIN-BOUNDARY CRYSTALLIZATION ON THE HIGH-TEMPERATURE STRENGTH OF SILICON NITRIDE

L. A. PIERCE, D. M. MIESKOWSKI, and W. A. SANDERS (NASA, Lewis Research Center, Cleveland, OH) Journal of Materials Science (ISSN 0022-2461), vol. 21, April 1986, p. 1345-1348. refs

Si₃N₄ specimens having the composition 88.7 wt pct Si₃N₄-4.9 wt pct SiO₂-6.4 wt pct Y₂O₃ were sintered at 2140 C under 25 atm N₂ for 1 h and then subjected to a 5 h anneal at 1500 C. Crystallization of an amorphous grain-boundary phase resulted in the formation of Y₂Si₂O₇. The short-time 1370 C strength of this material was compared with that of material of the same composition having no annealing treatment. No change in strength was noted. This is attributed to the refractory nature of the yttrium-rich grain-boundary phase (apparently identical in both glassy and crystalline phases) and the subsequent domination of the failure process by common processing flaws. Author

A86-34177* National Aeronautics and Space Administration. Lewis Research Center, Cleveland, Ohio.

TRIBOLOGICAL PROPERTIES OF GRAPHITE-FIBER-REINFORCED, PARTIALLY FLUORINATED POLYIMIDE COMPOSITES

R. L. FUSARO and W. F. HADY (NASA, Lewis Research Center, Cleveland, OH) ASLE Transactions (ISSN 0569-8197), vol. 29, April 1986, p. 214-222. Previously announced in STAR as N85-18153. refs

Graphite-fiber-reinforced polyimide (GFRPI) composites were formulated from three new partially fluorinated polyimides and three types of graphite fiber. Nine composites were molded into pins and evaluated in a pin-on-disk tribometer. Friction coefficients, wear rates, pin wear surface morphology, and transfer film formation were assessed at 25 and 300 C. Also assessed was the effect of sliding speed on friction. Wear was up to two orders of magnitude lower at 25 C and up to one order of magnitude lower at 300 C than with previously formulated NASA GFRPI composites. Author

A86-34179* National Aeronautics and Space Administration. Lewis Research Center, Cleveland, Ohio.

CONTACT ANGLE AND SURFACE TENSION MEASUREMENTS OF A FIVE-RING POLYPHENYL ETHER

W. R. JONES, JR. (NASA, Lewis Research Center, Cleveland, OH) ASLE transactions (ISSN 0569-8197), vol. 29, April 1986, p. 276-282. Previously announced in STAR as N85-15897. refs

Contact angle measurements were performed for a five-ring polyphenyl ether isomeric mixture on M-50 steel in a dry nitrogen atmosphere. Two different techniques were used: (1) a tilting plate apparatus, and (2) a sessile drop apparatus. Measurements were made for the temperature range 25 to 190 C. Surface tension was measured by a differential maximum bubble pressure technique over the range 23 to 220 C in room air. The critical surface energy of spreading (γ_{sp} /sub c/) was determined for the polyphenyl ether by plotting the cosine of the contact angle (θ) versus the surface tension (γ_{LV}). The straight line intercept at cosine $\theta = 1$ is defined as γ_{sp} (sub c). γ_{sp} (sub c) was found to be 30.1 dyn/cm for the tilting plate technique

and 31.3 dyn/cm for the sessile drop technique. These results indicate that the polyphenyl ether is inherently autophobic (i.e., it will not spread on its own surface film until its surface tension is less than $\gamma \cos \theta$). This phenomenon is discussed in light of the wettability and wear problems encountered with this fluid.

Author

A86-35702* Cleveland State Univ., Ohio.

NEGATIVE MAGNETORESISTANCE OF PITCH-BASED CARBON FIBERS TEMPERATURE AND PRESSURE DEPENDENCE

P. D. HAMBOURGER (Cleveland State University, OH) *Applied Physics Communications* (ISSN 0277-9374), vol. 5, no. 4, 1985-86, p. 223-230. refs
(Contract NCCC-19)

The negative transverse magnetoresistance of high-modulus pitch-based carbon fibers has been measured over the temperature range 1.3-4.2 K at ambient pressure and at 4.2 K under hydrostatic pressure up to 16 kbar. At low fields (less than 0.5 torr) the magnitude of the magnetoresistance increases markedly as the temperature is lowered from 4.2 K to 1.3 K, in disagreement with Bright's theoretical model, and decreases with pressure at the rate -0.6 percent/kbar.

Author

A86-36328* National Aeronautics and Space Administration. Lewis Research Center, Cleveland, Ohio.

BURNER RIG CORROSION OF SiC AT 1000 C

N. S. JACOBSON, C. A. STEARNS, and J. L. SMIALEK (NASA, Lewis Research Center, Cleveland, OH) *Advanced Ceramic Materials* (ISSN 0883-5551), vol. 1, April 1986, p. 154-161. refs

Sintered alpha-SiC was examined in both oxidation and hot corrosion with a burner rig at 400 kPa (4 atm) and 1000 C with a flow velocity of 94 m/s. Oxidation tests for times to 46 h produced virtually no attack, whereas tests with 4 ppm Na produced extensive corrosion in 13.5 h. Thick glassy layers composed primarily of sodium silicate formed in the salt corrosion tests. This corrosion attack caused severe pitting on the silicon carbide substrate and led to a 32 percent decrease in strength, compared to the as-received material. Parallel furnace tests of Na₂SO₄/air-induced attack yielded basically similar results, with slight product composition differences. The differences are explained in terms of the continuous sulfate deposition which occurs in a burner rig.

Author

A86-36330* National Aeronautics and Space Administration. Lewis Research Center, Cleveland, Ohio.

STRENGTH AND MICROSTRUCTURE OF Si₃N₄ SINTERED WITH ZrO₂ ADDITIONS

W. A. SANDERS and D. M. MIESKOWSKI (NASA, Lewis Research Center, Cleveland, OH) *Advanced Ceramic Materials* (ISSN 0883-5551), vol. 1, April 1986, p. 166-173. refs

Densities greater than 99 percent of theoretical were obtained with stabilized ZrO₂ additions to Si₃N₄. Material sintered at 2140 C under 2.5 MPa nitrogen overpressure with 3.8, 9.9, and 13.4 wt pct ZrO₂ had a predominantly equiaxed grain size ranging from 0.2 to 7.0 microns. At 1370 C, the latter composition exhibited a flexural strength of about 487 MPa, equal to that of a finer-grain-size, hot-pressed Si₃N₄ + ZrO₂ material having excellent high-temperature static fatigue properties. Transmission electron microscopy of the sintered Si₃N₄ revealed a glassy grain-boundary phase at all three ZrO₂ levels and partially crystalline triple points for the 9.9 and 13.4 wt pct ZrO₂-containing materials. Slow crack growth was observed for 1370 C flexure tests and correlated with nonlinear load deflection traces for stresses greater than 503 MPa. The crystallization of the grain-boundary glass is interpreted as beneficial to the attainment of high (1370 C) flexural strength.

Author

A86-37141* National Aeronautics and Space Administration. Lewis Research Center, Cleveland, Ohio.

NONDESTRUCTIVE CHARACTERIZATION OF STRUCTURAL CERAMICS

S. J. KLIMA and G. Y. BASKLINI (NASA, Lewis Research Center, Cleveland, OH) *SAMPE Quarterly* (ISSN 0036-0821), vol. 17, April 1986, p. 13-19. Previously announced in STAR as N86-22970. refs

Ultrasonic velocity and attenuation measurements were used to characterize density and microstructure in monolithic silicon nitride and silicon carbide. Research samples of these structural ceramics exhibited a wide range of density and microstructural variations. It was shown that bulk density variations correlate with and can be estimated by velocity measurements. Variations in microstructural features such as grain size or shape and pore morphology had a minor effect on velocity. However, these features had a pronounced effect on ultrasonic attenuation. The ultrasonic results are supplemented by low-energy radiography and scanning laser acoustic microscopy.

Author

A86-40682* National Aeronautics and Space Administration. Lewis Research Center, Cleveland, Ohio.

THE EFFECTS OF METALS AND INHIBITORS ON THERMAL OXIDATIVE DEGRADATION REACTIONS OF UNBRANCHED PERFLUOROALKYL ETHERS

W. R. JONES, JR., K. J. L. PACIOREK, D. H. HARRIS, M. E. SMYTHE, J. H. NAKAHARA, and R. H. KRATZER (NASA, Lewis Research Center, Cleveland, OH) *I & EC - Industrial and Engineering Chemistry, Product Research and Development* (ISSN 0196-4321), vol. 24, Sept. 1985, p. 417-420. Previously announced in STAR as N83-34049. refs

Thermal oxidative degradation studies were performed on unbranched perfluoroalkylethers at 288 C in oxygen. Metals and alloys studied included Ti, Al, and Ti (4 Al, 4 Mn). The mechanism of degradation was by chain scission. Ti and Al promoted less degradation than Ti (4 Al, 4 Mn). The two inhibitors investigated (a perfluorophenyl phosphine and a phosphotriazine) reduced degradation rates by several orders of magnitude. Both inhibitors were effective for the same duration (75 to 100 hours). The phosphotriazine appeared to provide more surface protection.

Author

A86-44425* National Aeronautics and Space Administration. Lewis Research Center, Cleveland, Ohio.

THE USE OF SILVER IN SELF-LUBRICATING COATINGS FOR EXTREME TEMPERATURES

H. E. SLINNEY (NASA, Lewis Research Center, Cleveland, OH) *ASLE Transactions* (ISSN 0569-8197), vol. 29, July 1986, p. 370-376. Previously announced in STAR as N85-20127. refs

The advantages and disadvantages of elemental silver as a tribological material are discussed. It is demonstrated that the relatively high melting point of 961 deg C, softness, marked plasticity, and thermochemical stability of silver combine to make this metal useful in thin film solid lubricant coatings over a wide temperature range. Disadvantages of silver during sliding, except when used as a thin film, are shown to be gross ploughing due to plastic deformation under load with associated high friction and excessive transfer to counterface surfaces. This transfer generates an irregular surface topography with consequent undesirable changes in bearing clearance distribution. Research to overcome these disadvantages of element silver is described. A comparison is made of the tribological behavior of pure silver with that of silver formulated with other metals and high-temperature solid lubricants. The composite materials are prepared by co-depositing the powdered components with an airbrush followed by furnace heat treatment or by plasma-spraying. Composite coatings were formulated which are shown to be self-lubricating over repeated, temperature cycles from low temperature to about 900 deg C.

Author

A86-47068* National Aeronautics and Space Administration. Lewis Research Center, Cleveland, Ohio.

THIN FILM GROWTH RATE EFFECTS FOR PRIMARY ION BEAM DEPOSITED DIAMONDLIKE CARBON FILMS

D. NIR and M. MIRTICH (NASA, Lewis Research Center, Cleveland, OH) *Journal of Vacuum Science and Technology A* (ISSN 0734-2101), vol. 4, May-June 1986, pt. 1, p. 560-563. refs

Diamonlike carbon (DLC) films were grown by primary ion beam deposition and the growth rates were measured for various beam energies, types of hydrocarbon gases and their ratio to Ar, and substrate materials. The growth rate had a linear dependence upon hydrocarbon content in the discharge chamber, and only small dependence on other parameters. For given deposition conditions a threshold in the atomic ratio of carbon to argon gas was identified below which films did not grow on fused silica substrate, but grew on Si substrate and on existing DLC films. Ion source deposition parameters and substrate material were found to affect the deposition threshold and film growth rates. Author

A86-47070* Pennsylvania State Univ., University Park.

MASS SPECTROMETRIC STUDIES OF THE ELECTRICAL BREAKDOWN OF THIN POLYMER FILMS

B. R. F. KENDALL, V. S. ROHRER, and V. J. BOJAN (Pennsylvania State University, University Park) *Journal of Vacuum Science and Technology A* (ISSN 0734-2101), vol. 4, May-June 1986, pt. 1, p. 598-601. refs

(Contract NSG-3301)

The composition of the neutral particles released during the electrical breakdown of 50-micron and 75-micron insulating films of the type used on spacecraft exteriors investigated experimentally using a time-of-flight mass spectrometer triggered by the breakdown event. The experimental apparatus is described in detail, and the results are presented in photographs. It is found that the particle flux from Teflon FEP and PFA films comprise mainly fluorocarbon fragments, some with mass 350 amu or greater, but the flux from Kapton oxygen-ion-beam treated Kapton, Tefzel, and Mylar comprises mainly molecules of mass 44 amu or less. T.K.

A86-48405* National Aeronautics and Space Administration. Lewis Research Center, Cleveland, Ohio.

CHARACTERIZATION AND MEASUREMENT OF POLYMER WEAR

D. H. BUCKLEY and P. R. ARON (NASA, Lewis Research Center, Cleveland, OH) *IN: Polymer wear and its control*. Washington, DC, American Chemical Society, 1985, p. 287-302. Previously announced in STAR as N84-21739. refs

Analytical tools which characterize the polymer wear process are discussed. The devices discussed include: visual observation of polymer wear with SEM, the quantification with surface profilometry and ellipsometry, to study the chemistry with AES, XPS and SIMS, to establish interfacial polymer orientation and accordingly bonding with QUARTIR, polymer state with Raman spectroscopy and stresses that develop in polymer films using a X-ray double crystal camera technique. Author

N86-10341* National Aeronautics and Space Administration. Lewis Research Center, Cleveland, Ohio.

TRIBOLOGICAL PROPERTIES OF STRUCTURAL CERAMICS

D. H. BUCKLEY and K. MIYOSHI Sep. 1985 103 p refs Submitted for publication (NASA-TM-87105; E-2649; NAS 1.15:87105) Avail: NTIS HC A06/MF A01 CSCL 11B

The tribological and lubricated behavior of both oxide and nonoxide ceramics are reviewed in this chapter. Ceramics are examined in contact with themselves, other harder materials and metals. Elastic, plastic and fracture behavior of ceramics in solid state contact is discussed. The contact load necessary to initiate fracture in ceramics is shown to be appreciably reduced with tangential motion. Both friction and wear of ceramics are anisotropic and relate to crystal structure as has been observed with metals. Grit size effects in two and three body abrasive wear are observed for ceramics. Both free energy of oxide formation and the d valence bond character of metals are related to the friction and wear

characteristics for metals in contact with ceramics. Surface contaminants affect friction and adhesive wear. For example, carbon on silicon carbide and chlorine on aluminum oxide reduce friction while oxygen on metal surfaces in contact with ceramics increases friction. Lubrication increases the critical load necessary to initiate fracture of ceramics both in indentation and with sliding or rubbing. Ceramics compositions both as coatings and in composites are described for the high temperature lubrication of both alloys and ceramics. Author

N86-11263*# National Aeronautics and Space Administration. Lewis Research Center, Cleveland, Ohio.

PMR POLYIMIDES FROM SOLUTIONS CONTAINING MIXED ENDCAPS

P. DELVIGS *In its High Temp. Polymer Matrix Composites* p 23-34 Sep. 1985 refs

Avail: NTIS HC A18/MF A01 CSCL 11B

Previous studies have shown that partial substitution of p-aminostyrene (PAS) for the monomethylester of endo-5-norbornene-2, 3-dicarboxylic acid (NE) lowered the cure temperature of PMR polyimides from 316 to 260 C, but the modified PMR polyimides required higher compression-molding pressures than state-of-the-art PMR-15. In this study PMR polyimides are prepared employing three encaps: NE, PAS, and endo-N-phenyl-5-norbornene-2,3-dicarboximide (PN). The effect of PN addition on the processing characteristics and glass transition temperatures of graphite fiber-reinforced PMR composites is studied. The room temperature and short-time 316 C mechanical properties of the composites are determined. The weight loss and mechanical property retention characteristics of the composites after exposure in air at 316 C are also determined. Author

N86-11266*# Case Western Reserve Univ., Cleveland, Ohio. Dept. of Chemistry.

THE SYNTHESIS, CHARACTERIZATION AND THERMAL CHEMISTRY OF MODIFIED NORBORNENYL PMR ENDCAPS

C. N. SUKENIK, W. M. RITCHEY, V. MALHOTRA, and U. VARDE *In NASA. Lewis Research Center High Temp. Polymer Matrix Composites* p 79-90 Sep. 1985 refs (Contract NAG3-163)

Avail: NTIS HC A18/MF A01 CSCL 11B

As part of a program to further the understanding of the polymerization of Nadic-Endcapped PMR systems, a series of model Norbornenyl-imides has been synthesized and their thermal behavior explored. Their syntheses and characterizations as well as their rearrangement and polymerization chemistry are described. Monomer isomerization at temperatures as low as 125 C and oligomer formation at somewhat higher temperatures are observed. Approximate relative rates for competing isomerization pathways are established and some information is obtained about the details of oligomer formation. The relationship of this data to current PMR systems is briefly discussed. Author

N86-11267*# National Aeronautics and Space Administration. Lewis Research Center, Cleveland, Ohio.

ALL-AROMATIC BIPHENYLENE END-CAPPED POLYQUINOLINE AND POLYIMIDE MATRIX RESINS

J. P. DROSKE (Colorado State Univ.), J. K. STILLE (Colorado State Univ.), and W. B. ALSTON *In its High Temp. Polymer Matrix Composites* p 91-95 Sep. 1985 refs

Avail: NTIS HC A18/MF A01 CSCL 11B

Biphenylene end-capped polyquinoline and polyimide resins afford low void content graphite-reinforced composites with good initial properties. However, with both resins, rapid degradation occurs during oxidative isothermal aging at elevated temperatures. The degradation is not observed during isothermal aging under a nitrogen atmosphere which suggests that the biphenylene end-cap (or the resulting crosslink/chain extension structures) is not particularly thermooxidatively stable. The nature of the thermooxidative instability is currently under investigation. Author

N86-11271*# National Aeronautics and Space Administration. Lewis Research Center, Cleveland, Ohio.

CHEMICAL CONTROL OF RATE AND ONSET TEMPERATURE OF NADIMIDE POLYMERIZATION

R. W. LAUVER *In its* High Temp. Polymer Matrix Composites p 137-149 Sep. 1985 refs

Avail: NTIS HC A18/MF A01 CSCL 11B

The chemistry of norbornenyl capped imide compounds (nadimides) is briefly reviewed with emphasis on the contribution of Diels-Alder reversion in controlling the rate and onset of the thermal polymerization reaction. Control of onset temperature of the cure exotherm by adjusting the concentration of maleimide is demonstrated using selected model compounds. The effects of nitrophenyl compounds as free radical retarders on nadimide reactivity are discussed. A simple copolymerization model is proposed for the overall nadimide cure reaction. An approximate numerical analysis is carried out to demonstrate the ability of the model to simulate the trends observed for both maleimide and nitrophenyl additions. Author

N86-11275*# National Aeronautics and Space Administration. Lewis Research Center, Cleveland, Ohio.

REPLACEMENT OF MDA WITH MORE OXIDATIVELY STABLE DIAMINES IN PMR-POLYIMIDES

W. B. ALSTON *In its* High Temp. Polymer Matrix Composites p 187-205 Sep. 1985 refs

Avail: NTIS HC A18/MF A01 CSCL 11B

Studies are performed to investigate the effect of substituting 4,4'-oxydianiline and 1,1-bis(4-aminophenyl)-1-phenyl-2,2,2-trifluoroethane for the 4,4'-methylenedianiline in PMR polyimide matrix resin. Graphite fiber reinforced composites are fabricated from unsized Celion 6000 and PMR-polyimide matrix resins having formulated molecular weights in the range of 1500 to 2400. The composite processing characteristics are investigated and the initial room temperature and 316 C (600 F) composite mechanical properties are determined. Comparative 316 C composite weight losses and 316 C mechanical properties retention after prolonged 316 C air exposure are also determined. Author

N86-12310*# National Aeronautics and Space Administration. Lewis Research Center, Cleveland, Ohio.

MOLTEN SALT CORROSION OF SiC: PITTING MECHANISM

N. S. JACOBSON and J. L. SMIALEK Oct. 1985 12 p refs Presented at the 168th Meeting of the Electrochem. Soc., Las Vegas, Nev., 13-18 Oct. 1985

(NASA-TM-87143; E-2770; NAS 1.15:87143) Avail: NTIS HC A02/MF A01 CSCL 11G

Thin films of Na₂SO₄ and Na₂CO₃ at 1000 C lead to severe pitting of sintered alpha-SiC. These pits are important as they cause a strength reduction in this material. The growth of product layers is related to pit formation for the Na₂CO₃ case. The early reaction stages involve repeated oxidation and dissolution to form sodium silicate. This results in severe grain boundary attack. After this a porous silica layer forms between the sodium silicate melt and the SiC. The pores in this layer appear to act as paths for the melt to reach the SiC and create larger pits. Author

N86-12311*# National Aeronautics and Space Administration. Lewis Research Center, Cleveland, Ohio.

STRUCTURE-TO-GLASS TRANSITION TEMPERATURE RELATIONSHIPS IN HIGH TEMPERATURE STABLE CONDENSATION POLYIMIDES

W. B. ALSTON and R. F. GRATZ (Mary Washington Coll., Fredericksburg, Va.) 1985 19 p refs Presented at the 2nd Intern. Conf. on Polyimides, Ellenville, N.Y., 30 Oct. - 1 Nov. 1985; sponsored by the Society of Plastics Engineers, Inc.

(Contract DA PROJ. 1L1-61101-AH-45) (NASA-TM-87113; E-2714; NAS 1.15:87113; USAAVSCOM-TR-85-C-18) Avail: NTIS HC A02/MF A01 CSCL 11B

The presence of a hexafluoroisopropylidene (6F) connecting group in aryl dianhydrides used to prepare aromatic condensation

polyimides provides high glass transition temperature ($T_{sub g}$) polyimides with excellent thermo-oxidative stability. The purpose of this study was to determine if a trifluorophenyl-ethylidene (3F) connecting group would have a similar effect on the $T_{sub g}$ of aromatic condensation polyimides. A new dianhydride containing the 3F connecting group was synthesized. This dianhydride and an aromatic diamine also containing the 3F connecting group were used together and in various combinations with known diamines or known dianhydrides, respectively, to prepare new 3F containing condensation polyimides. Known polyimides, including some with the 6F connecting linkage, were also prepared for comparison purposes. The new 3F containing polymers and the comparison polymers were prepared by condensation polymerization via the traditional amic-acid polymerization method in N,N-dimethylacetamide solvent. The solutions were characterized by determining their inherent viscosities and then were thermally converted into polyimide films under nitrogen atmosphere at 300 to 500 C. The $T_{sub g}$'s of the films and resin discs were then determined by thermomechanical analysis and were correlated as a function of the final processing temperatures of the films and resin discs. The results showed that similarities existed in the $T_{sub g}$'s depending on the nature of the connecting linkage in the monomers used to prepare the condensation polyimides. B.W.

N86-13495*# National Aeronautics and Space Administration. Lewis Research Center, Cleveland, Ohio.

FRACTURE TOUGHNESS OF Si3N4 MEASURED WITH SHORT BAR CHEVRON-NOTCHED SPECIMENS

J. A. SALEM and J. L. SHANNON, JR. 1985 19 p refs Presented at Basic Sci. Meeting of the Am. Ceram. Soc., Baltimore, 17-19 Nov. 1985

(NASA-TM-87153; E-2749; NAS 1.15:87153) Avail: NTIS HC A02/MF A01 CSCL 11G

The short bar chevron-notched specimen is used to measure the plane strain fracture toughness of hot pressed Si₃N₄. Specimen proportions and chevron-notch angle are varied, thereby varying the amount of crack extension to maximum load (upon which $K_{sub IC}$ is based). The measured toughness (4.68 ± 0.19 MNm to the 3/2 power) is independent of these variations, inferring that the material has a flat crack growth resistance curve. Author

N86-15394*# National Aeronautics and Space Administration. Lewis Research Center, Cleveland, Ohio.

TEXTURED CARBON ON COPPER: A NOVEL SURFACE WITH EXTREMELY LOW SECONDARY ELECTRON EMISSION CHARACTERISTICS

A. N. CURREN and K. A. JENSEN Dec. 1985 16 p refs (NASA-TP-2543; E-2674; NAS 1.60:2543) Avail: NTIS HC A02/MF A01 CSCL 11G

Experimentally determined values of true secondary electron emission and relative values of reflected primary electron yield for a range of primary electron beam energies and beam impingement angles are presented for a series of novel textured carbon surfaces on copper substrates. (All copper surfaces used in this study were oxygen-free, high-conductivity grade). The purpose of this investigation is to provide information necessary to develop high-efficiency multistage depressed collectors (MDC's) for microwave amplifier traveling-wave tubes (TWT's) for communications and aircraft applications. To attain the highest TWT signal quality and overall efficiency, the MDC electrode surface must have low secondary electron emission characteristics. While copper is the material most commonly used for MDC electrodes, it exhibits relatively high levels of secondary electron emission unless its surface is treated for emission control. The textured carbon surface on copper substrate described in this report is a particularly promising candidate for the MDC electrode application. Samples of textured carbon surfaces on copper substrates typical of three different levels of treatment are prepared and tested for this study. The materials are tested at primary electron beam energies of 200 to 2000 eV and at direct (0 deg) to near-grazing (85 deg) beam impingement angles. True secondary

27 NONMETALLIC MATERIALS

electron emission and relative reflected primary electron yield characteristics of the textured surfaces are compared with each other and with those of untreated copper. All the textured carbon surfaces on copper substrate tested exhibited sharply lower secondary electron emission characteristics than those of an untreated copper surface. Author

N86-16379*# National Aeronautics and Space Administration. Lewis Research Center, Cleveland, Ohio.

ANALYSIS OF A THIOETHER LUBRICANT BY INFRARED FOURIER MICROEMISSION SPECTROPHOTOMETRY

W. R. JONES, JR., W. MORALES, and J. L. LAUER (Rensselaer Polytechnic Inst., Troy, N.Y.) Jan. 1986 16 p refs (NASA-TM-87195; E-2691; NAS 1.15:87195) Avail: NTIS HC A02/MF A01 CSCL 11H

An infrared Fourier microemission spectrophotometer is used to obtain spectra (wavenumber range, 630 to 1230 0.1 cm) from microgram quantities of thioether lubricant samples deposited on aluminum foil. Infrared bands in the spectra are reproducible and could be identified as originating from aromatic species (1,3-disubstituted benzenes). Spectra from all samples (neat and formulated, used and unused) are very similar. Additives (an acid and a phosphinate) present in low concentration (0.10 percent) in the formulated fluid are not detected. This instrument appears to be a viable tool in helping to identify lubricant components separated by liquid chromatography. Author

N86-16381*# Dow Corning Corp., Midland, Mich. **ORGANOSILOXANE WORKING FLUIDS FOR THE LIQUID DROPLET RADIATOR Final Report**

R. R. BUCH and A. R. HUNTRESS Dec. 1985 174 p refs (Contract NAS3-24400) (NASA-CR-175033; NAS 1.26:175033) Avail: NTIS HC A08/MF A01 CSCL 11G

Siloxane-based working fluids for advanced space radiators requiring direct fluid exposure to the space environment are evaluated. Isolation of five candidate fluids by vacuum distillation from existing siloxane polymers is discussed. The five fluids recovered include a polydimethylsiloxane, three phenyl-containing siloxanes, and a methylhexylsiloxane. Vapor pressures and viscosities for the five fluids are reported over the temperature range of 250 to 400 K. Use of thermal-gravimetric analysis to reliably estimate vapor pressures of 10 to the -8 power Pascals is described. Polydimethylsiloxane (PDMS) and polymethylphenylsiloxane (PMPS) are selected from the five candidate fluids based on favorable vapor pressure and viscosity, as well as perceived stability in low-Earth orbit environments. Characterization of these fluids by infrared spectroscopy, Si-29 NMR, gel-permeation chromatography, and liquid chromatography is presented. Both fluids consist of narrow molecular weight distributions, with average molecular weights of about 2500 for PDMS and 1300 for PMPS. Author

N86-19457* National Aeronautics and Space Administration. Lewis Research Center, Cleveland, Ohio.

HIGH TEMPERATURE RESISTANT POLYIMIDE FROM TETRA ESTER, DIAMINE, DIESTER AND N-ARYLNADIMIDE Patent

R. H. PATER, inventor (to NASA) 24 Dec. 1985 8 p Filed 13 Oct. 1982 (NASA-CASE-LEW-13864-1; US-PATENT-4,560,742; US-PATENT-APPL-SN-434087; US-PATENT-CLASS-528-342; US-PATENT-CLASS-528-229; US-PATENT-CLASS-528-322; US-PATENT-CLASS-528345) Avail: US Patent and Trademark Office CSCL 11B

The invention described relates to improved polyimide resins which are noted for their high thermal and oxidative stability, high strength at elevated temperatures and which exhibit many other outstanding physical and chemical properties, especially useful in high temperature applications. The polyimides are prepared by the reaction, with application of heat of a mixture of monomers comprising: (1) a dialkyl or tetraalkyl ester of an aromatic tetracarboxylic acid, (2) and aromatic diamine, (3) a monoalkyl or dialkyl ester of a dicarboxylic acid, and (4) a N-arylnadimide such

as N-phenylnadimide. Polyimides of monomers (1), (2) and (3) are known. Official Gazette of the U.S. Patent and Trademark Office

N86-19458* National Aeronautics and Space Administration. Lewis Research Center, Cleveland, Ohio.

OXIDATION PROTECTION COATINGS FOR POLYMERS Patent

M. J. MIRTICH, J. S. SOVEY, and B. A. BANKS, inventors (to NASA) 24 Dec. 1985 6 p Filed 11 Sep. 1984 (NASA-CASE-LEW-14072-1; US-PATENT-4,560,577; US-PATENT-APPL-SN-649330; US-PATENT-CLASS-427-38; US-PATENT-CLASS-427-248.1; US-PATENT-CLASS-204/298; US-PATENT-CLASS-204-192-R; US-PATENT-CLASS-204-192-C; US-PATENT-CLASS-204-192-D; US-PATENT-CLASS-428-702; US-PATENT-CLASS-428-473.5; US-PATENT-CLASS-428-446) Avail: US Patent and Trademark Office CSCL 11B

A polymeric substrate is coated with a metal oxide film to provide oxidation protection in low Earth orbital environments. The film contains about 4 volume percent polymer to provide flexibility. A coil of polymer material moves through an ion beam as it is fed between reels. The ion beam first cleans the polymer material surface and then sputters the film material from a target onto this surface.

Official Gazette of the U.S. Patent and Trademark Office

N86-19464*# Case Western Reserve Univ., Cleveland, Ohio. Dept. of Civil Engineering.

ANALYSIS OF THE TRANSIENT BEHAVIOR OF RUBBING COMPONENTS Final Report

M. B. QUEZDOU and R. L. MULLEN 19 Feb. 1986 51 p refs (Contract NAG3-369) (NASA-CR-176546; NAS 1.26:176546) Avail: NTIS HC A04/MF A01 CSCL 11G

Finite element equations are developed for studying deformations and temperatures resulting from frictional heating in sliding system. The formulation is done for linear steady state motion in two dimensions. The equations include the effect of the velocity on the moving components. This gives spurious oscillations in their solutions by Galerkin finite element methods. A method called streamline upwind scheme is used to try to deal with this deficiency. The finite element program is then used to investigate the friction of heating in gas path seal. Author

N86-19465*# National Aeronautics and Space Administration. Lewis Research Center, Cleveland, Ohio.

HOW TO EVALUATE SOLID LUBRICANT FILMS USING A PIN-ON-DISK TRIBOMETER

R. L. FUSARO 1986 22 p refs Proposed for presentation at the 1986 Annual Meeting of the American Society of Lubrication Engineers, Toronto, Ontario, 12-15 May 1986 (NASA-TM-87236; E-2909; NAS 1.15:87236) Avail: NTIS HC A02/MF A01 CSCL 11D

Over the years, the author has evaluated and compared hundreds of solid lubricant films using a pin-on-disk tribometer. The intent of this paper is to describe to the reader experimental techniques and some of parameters that have been observed to be important for the evaluation and development of new solid lubricant films. Pin-on-disk tribometers will be described and discussed as will experimental methods for evaluating solid lubricant materials. Methods of preparing surfaces for the coating of the thin films and different methods for applying the films will be reviewed. Factors that affect solid lubricant performance will also be discussed. Two different macroscopic mechanisms of solid lubricant film wear exist. These will be characterized schematically, and methods of measuring wear will be examined. Author

N86-20568*# National Aeronautics and Space Administration. Lewis Research Center, Cleveland, Ohio.

COMPOSITION OPTIMIZATION OF SELF-LUBRICATING CHROMIUM CARBIDE-BASED COMPOSITE COATINGS FOR USE TO 760 DEG C Final Report

C. DELLACORTE and H. E. SLINEY 1986 27 p refs Proposed for presentation at the American Society of Lubrication Engineers Annual Meeting, Toronto, Ontario, 12-15 May 1986

(Contract DE-AI01-85CE-50112)

(NASA-TM-87261; E-2953; DOE/NASA/50112-64; NAS

1.15:87261) Avail: NTIS HC A03/MF A01 CSCL 11H

This paper describes new compositions of self-lubricating coatings that contain chromium carbide. A bonded chromium carbide was used as the base stock because of the known excellent wear resistance and the chemical stability of chromium carbide. Additives were silver and barium fluoride/calcium fluoride eutectic. The coating constituents were treated as a ternary system consisting of: (1) the bonded carbide base material, (2) silver, and (3) the eutectic. A study to determine the optimum amounts of each constituent was performed. The various compositions were prepared by powder blending. The blended powders were then plasma sprayed onto superalloy substrates and diamond ground to the desired coating thickness. Friction and wear studies were performed at temperatures from 25 to 760 C in helium and hydrogen. A variety of counterface materials were evaluated with the objective of discovering a satisfactory metal/coating sliding combination for potential applications such as piston ring/cylinder liner couples for Stirling engines. Author

N86-21682*# National Aeronautics and Space Administration. Lewis Research Center, Cleveland, Ohio.

A NEW CHROMIUM CARBIDE-BASED TRIBOLOGICAL COATING FOR USE TO 900 DEG C WITH PARTICULAR REFERENCE TO THE STIRLING ENGINE Final Report

H. E. SLINEY 1986 17 p refs Presented at the International Conference on Metallurgical Coatings, San Diego, Calif., 7-11 Apr. 1986; sponsored by the American Vacuum Society and the American Society for Metals

(Contract DE-AI01-85CE-50112)

(NASA-TM-87274; E-2977; DOE/NASA/50112-65; NAS

1.15:87274) Avail: NTIS HC A02/MF A01 CSCL 11G

A new chromium carbide-based coating (PS 200) is described. This coating is shown to have good friction and wear properties over a wide temperature range. A nickel alloy-bonded chromium carbide coating was used as a baseline material for comparison with experimental formulated coatings. Coatings were plasma sprayed onto metal disks, then diamond ground to a thickness of 0.025 cm. Friction and wear were determined using a pin on disk tribometer at temperatures from 25 to 900 C in hydrogen, helium, and air. Pin materials included several metallic alloys and silicon carbide. It was found that appropriate additions of metallic silver and of barium fluoride/calcium fluoride eutectic to the baseline carbide composition significantly reduced friction coefficients while preserving, and in some cases, even enhancing wear resistance. The results of this study demonstrate that PS 200 is a promising coating composition to consider for high temperature aerospace and advanced heat engine applications. The excellent results in hydrogen make this coating of particular interest for use in the Stirling engine. Author

N86-21683*# National Aeronautics and Space Administration. Lewis Research Center, Cleveland, Ohio.

A COMPARISON OF THE BROMINATION DYNAMICS OF PITCH-BASED AND VAPOR-GROWN GRAPHITE FIBERS

J. R. GAIER 1986 16 p refs Presented at the March Meeting of the American Physical Society, Las Vegas, Nev., 31 Mar. - 4 Apr. 1986

(NASA-TM-87275; E-2978; NAS 1.15:87275) Avail: NTIS HC A02/MF A01 CSCL 11G

The electrical resistance of pitch based P-100 fibers and experimental organic vapor grown fibers was recorded in-situ during bromination and subsequent exposure to ambient laboratory air. The results indicate that the bromination and debromination

reactions proceed much slower for vapor grown fibers than for pitch based. While this may be due in part to the larger diameter of the vapor grown fibers, the majority of the effect can probably be attributed to the differences in graphene plane orientation between the fiber types. Although the reactions are slower in the vapor grown than in the pitch based fibers, the extent of reaction as measured by the change in electrical resistance is essentially the same, with comparable (or larger) decreases in resistivity. The bromination reaction proceeds with one or more plateaus in the resistance versus time curves, which suggests staging and strengthens the argument that these fibers produce true intercalation compounds. Author

N86-22713*# Pratt and Whitney Aircraft, East Hartford, Conn. Engineering Div.

THERMAL BARRIER COATING LIFE PREDICTION MODEL DEVELOPMENT Annual Report

K. D. SHEFFLER and J. T. DEMASI Nov. 1985 92 p refs

(Contract NAS3-23944)

(NASA-CR-175087; NAS 1.26:175087; AR-1) Avail: NTIS HC A05/MF A01 CSCL 11G

A methodology was established to predict thermal barrier coating life in an environment simulative of that experienced by gas turbine airfoils. Specifically, work is being conducted to determine failure modes of thermal barrier coatings in the aircraft engine environment. Analytical studies coupled with appropriate physical and mechanical property determinations are being employed to derive coating life prediction model(s) on the important failure mode(s). An initial review of experimental and flight service components indicates that the predominant mode of TBC failure involves thermomechanical spallation of the ceramic coating layer. This ceramic spallation involves the formation of a dominant crack in the ceramic coating parallel to and closely adjacent to the metal-ceramic interface. Initial results from a laboratory test program designed to study the influence of various driving forces such as temperature, thermal cycle frequency, environment, and coating thickness, on ceramic coating spalling life suggest that bond coat oxidation damage at the metal-ceramic interface contributes significantly to thermomechanical cracking in the ceramic layer. Low cycle rate furnace testing in air and in argon clearly shows a dramatic increase of spalling life in the non-oxidizing environments. Author

N86-24835*# National Aeronautics and Space Administration. Lewis Research Center, Cleveland, Ohio.

A PRELIMINARY STUDY OF ESTER OXIDATION ON AN ALUMINUM SURFACE USING CHEMILUMINESCENCE

W. R. JONES, JR., M. A. MEADOR, and W. MORALES 1986 32 p refs Presented at the Annual Meeting of the American Society of Lubrication Engineers, Toronto, Ontario, 12-15 May 1986

(NASA-TM-87242; E-2647; NAS 1.15:87242) Avail: NTIS HC A03/MF A01 CSCL 11C

The oxidation characteristics of a pure ester (trimethylolpropane triheptanoate) were studied by using a chemiluminescence technique. Tests were run in a thin-film micro-oxidation apparatus with an aluminum alloy catalyst. Conditions included a pure oxygen atmosphere and a temperature range of 176 to 206 C. Results indicated that oxidation of the ester (containing 10 to the minus 3 power M diphenylanthracene as an intensifier) was accompanied by emission of light. The maximum intensity of light emission ($I_{\text{sub max}}$) was a function of the amount of ester, the concentration of intensifier, and the test temperature. The induction period or the time to reach one-half of maximum intensity ($t_{\text{sub 1/2}}$) was an inverse function of test temperature. Decreases in light emission at the later stages of a test were caused by depletion of the intensifier. Author

27 NONMETALLIC MATERIALS

N86-24836*# National Aeronautics and Space Administration. Lewis Research Center, Cleveland, Ohio.

IMPROVED CONSOLIDATION OF SILICON CARBIDE

M. R. FREEDMAN and M. L. MILLARD (General electric co., Evendale, Ohio) 1986 14 p refs Presented at the 10th Annual Conference on Composites and Advanced Ceramic Materials, Cocoa Beach, Fla., 19-22 Jan. 1986; sponsored by American Ceramic Society (NASA-TM-87243; E-2921; NAS 1.15:87243) Avail: NTIS HC A02/MF A01 CSCL 11C

Alpha silicon carbide powder was consolidated by both dry and wet methods. Dry pressing in a double acting steel die yielded sintered test bars with an average flexural strength of 235.6 MPa with a critical flaw size of approximately 100 micro m. An aqueous slurry pressing technique produced sintered test bars with an average flexural strength of 440.8 MPa with a critical flaw size of approximately 25 micro m. Image analysis revealed a reduction in both pore area and pore size distribution in the slurry pressed sintered test bars. The improvements in the slurry pressed material properties are discussed in terms of reduced agglomeration and improved particle packing during consolidation. Author

N86-24837*# National Aeronautics and Space Administration. Lewis Research Center, Cleveland, Ohio.

ADEQUACY OF SURFACE ANALYTICAL TOOLS FOR STUDYING THE TRIBOLOGY OF CERAMICS

H. E. SLINNEY Apr. 1986 21 p refs (NASA-TM-87308; E-2756; NAS 1.15:87308) Avail: NTIS HC A02/MF A01 CSCL 11C

Surface analytical tools are very beneficial in tribological studies of ceramics. Traditional methods of optical microscopy, XRD, XRF, and SEM should be combined with newer surface sensitive techniques especially AES and XPS. ISS and SIMS can also be useful in providing additional composition details. Tunneling microscopy and electron energy loss spectroscopy are less known techniques that may also prove useful. Author

N86-24838*# National Aeronautics and Space Administration. Lewis Research Center, Cleveland, Ohio.

ABRASION AND DEFORMED LAYER FORMATION OF MANGANESE-ZINC FERRITE IN SLIDING CONTACT WITH LAPPING TAPES

K. MIYOSHI, D. H. BUCKLEY, and K. TANAKA (Kanazawa Univ. Japan) 1986 27 p refs Presented at the ASME/ASLE Tribology Conference, Pittsburgh, Pa., 19-22 Oct. 1986 (NASA-TM-87249; E-2891; NAS 1.15:87249) Avail: NTIS HC A03/MF A01 CSCL 11C

Wear experiments were conducted using replication electron microscopy and reflection electron diffraction to study abrasion and the deformed layers produced in single-crystal Mn-Zn ferrite simulated heads during contact with lapping tapes. The crystalline state of the head is changed drastically during the abrasion process. Crystalline states ranging from nearly amorphous to highly textured polycrystalline can be produced on the wear surface of a single-crystal Mn-Zn ferrite head. The total thickness of the deformed layer was approximately 0.8 microns. This thickness increased as the load and abrasive grit size increased. The anisotropic wear of the ferrite was found to be inversely proportional to the hardness of the wear surface. The wear was lower in the order 211 111 10 0110. The wear of the ferrite increased markedly with an increase in sliding velocity and abrasive grit size. Author

N86-24839*# National Aeronautics and Space Administration. Lewis Research Center, Cleveland, Ohio.

PARTICLE SIZE REDUCTION OF Si₃N₄ WITH Si₃N₄ MILLING HARDWARE

T. P. HERBELL, M. R. FREEDMAN, and J. D. KISER 1986 19 p refs Presented at the 10th Annual Conference on Composites and Advanced Ceramic Materials, Cocoa Beach, Fla., 19-24 Jan. 1986; sponsored by the American Ceramic Society (NASA-TM-86864-REV; E-2328-1; NAS 1.15:86864-REV) Avail: NTIS HC A02/MF A01 CSCL 11C

The grinding of Si₃N₄ powder using reaction bonded Si₃N₄ attrition, vibratory, and ball mills with Si₃N₄ media was examined. The rate of particle size reduction and the change in the chemical composition of the powder were determined in order to compare the grinding efficiency and the increase in impurity content resulting from mill and media wear for each technique. Attrition and vibratory milling exhibited rates of specific surface area increase that were approximately eight times that observed in ball milling. Vibratory milling introduced the greatest impurity pickup. Author

N86-25473*# National Aeronautics and Space Administration. Lewis Research Center, Cleveland, Ohio.

SPUTTERED CADMIUM OXIDE AS A SURFACE PRETREATMENT FOR GRAPHITE SOLID LUBRICANT FILMS

R. L. FUSARO 1986 32 p refs To be presented at the ASME/ASLE Tribology Conf., Pittsburgh, Pa., 19-22 Oct. 1986 (NASA-TM-87300; E-3011; NAS 1.15:87300) Avail: NTIS HC A03/MF A01 CSCL 11H

Sputtered films of cadmium oxide were applied to sand blasted AISI 440C HT stainless steel disks as a surface pretreatment for the application of rubbed graphite films. Mixtures of cadmium oxide and graphite were applied to the nonpretreated sandblasted metal and evaluated. The results were compared to graphite films applied to other commercially available surface pretreatments. It is found that sputtered CdO pretreated surfaces increase the endurance lives of the graphite films and decrease the counterface steady state wear rate of the pins almost an order of magnitude compared to commercially available pretreatments. The CdO additions in general improved the tribological properties of graphite. The greatest benefit occurred when it was applied to the substrate rather than mixing it with the graphite and that sputtered films of CdO perform much better than rubbed CdO films. Author

N86-25474*# National Aeronautics and Space Administration. Lewis Research Center, Cleveland, Ohio.

IMPROVED PERFLUOROALKYLETHYER FLUID DEVELOPMENT

W. R. JONES, JR., K. PACIOREK (Ultrasystems, Inc., Irvine, Calif.), J. NAKAHARA, M. SMYTHE, and R. KRATZER 1986 18 p refs Presented at the International Symposium on Chemical Aspects of Wear, Friction, and Lubrication, New York, N.Y., 14-18 April 1986; sponsored by American Chemical Society (NASA-TM-87276; E-2928; NAS 1.15:87276) Avail: NTIS HC A02/MF A01 CSCL 11C

The feasibility of transforming a commercial linear perfluoroalkylether fluid into a material stable in the presence of metals and metal alloys in oxidizing atmospheres at 300 C without the loss of the desirable viscosity temperature characteristics was determined. The approach consisted of thermal oxidative treatment in the presence of catalyst to remove weak links, followed by transformation of the created functional groups into phospho-s-triazine linkages. It found that the experimental material obtained in 66% yield from the commercial fluid exhibits, over an 8 hr period at 300 C in the presence of Ti(4Al, 4Mn) alloy, thermal oxidative stability better by a factor of 2.6x1000 based on volatiles evolved than the commercial product. The viscosity and molecular weight of the developed fluid are unchanged and are essentially identical with the commercial material. No metal corrosion occurs with the experimental fluid at 300 C. E.A.K.

N86-25475*# National Aeronautics and Space Administration. Lewis Research Center, Cleveland, Ohio.

THE PREPARATION OF NEW PERFLUOROETHER FLUIDS EXHIBITING EXCELLENT THERMAL-OXIDATIVE STABILITIES

W. R. JONES, JR., T. R. BIERSCHEK (Exfluor Research Corp., Austin, Tex.), T. J. JUHLKE, H. KAWA (Exfluor Research Corp.), and R. J. LAGOW (Exfluor Research Corp., Austin, Tex.) 1986 19 p refs Presented at the International Symposium on Chemical Aspects of Friction, Wear and Lubrication, New York, N.Y., 13-18 Apr. 1986; sponsored by the American Chemical Society (NASA-TM-87284; E-2919; NAS 1.15:87284) Avail: NTIS HC A02/MF A01 CSCL 11C

A series of low molecular weight perfluoroalkylethers (PFAE) were synthesized by direct fluorination. Viscosity-temperature properties and oxidation stabilities were determined. Viscosity-temperature correlations indicated that increases in branching and increases in the size of the branching substituent caused a deterioration in viscometric properties (i.e., an increase in ASTM slope). In addition, increasing the ratio of carbon to oxygen in these compounds also increased the ASTM slope. Preliminary oxidation stability tests indicated that highly branched PFAE fluids (i.e., those containing quaternary carbons) may be less stable than either those containing a single trifluoromethyl pendant group or those containing no branching at all. Author

N86-25476*# National Aeronautics and Space Administration. Lewis Research Center, Cleveland, Ohio.

TRIBOLGY OF SELECTED CERAMICS AT TEMPERATURES TO 900 DEG C

H. E. SLINNEY, T. P. JACOBSON, D. DEADMORE, and K. MIYOSHI 1986 23 p refs Presented at 10th Annual Conference on Composites and Advanced Ceramic Materials, Cocoa Beach, Fla., 19-24 Jan. 1986; sponsored by American Ceramic Society (NASA-TM-87267; E-2969; NAS 1.15:87267) Avail: NTIS HC A02/MF A01 CSCL 11B

Results of fundamental and focused research on the tribological properties of ceramics are discussed. The basic friction and wear characteristics are given for ceramics of interest for use in gas turbine, adiabatic diesel, and Stirling engine applications. The importance of metal oxides in ceramic/metal sliding combinations is illustrated. The formulation and tribological additives are described. Friction and wear data are given for carbide and oxide-based composite coatings for temperatures to at least 900 C. Author

N86-26434*# National Aeronautics and Space Administration. Lewis Research Center, Cleveland, Ohio.

OXIDATION PROTECTING COATINGS FOR POLYMERS Patent Application

J. S. SOVEY, inventor (to NASA), B. A. BANKS, inventor (to NASA), and M. J. MIRTICH, inventor (to NASA) 27 Feb. 1986 12 p Sponsored by NASA (NASA-CASE-LEW-14072-3; NAS 1.71:LEW-14072-3; US-PATENT-APPL-SN-834977) Avail: NTIS HC A02/MF A01 CSCL 11B

A polymeric substrate is coated with a metal oxide film to provide oxidation protection in low Earth orbital environments. The film contains about four volume percent polymer to provide flexibility. NASA

N86-27452*# National Aeronautics and Space Administration. Lewis Research Center, Cleveland, Ohio.

CHARACTERIZATION OF THE TRIBOLOGICAL COATING COMPOSITION 77 WT % CaF_2 - 23 WT % LiF FUSED TO IN-750 ALLOY

D. L. DEADMORE and H. E. SLINNEY Jun. 1986 13 p (NASA-TM-87342; E-3091; NAS 1.15:87342) Avail: NTIS HC A02/MF A01 CSCL 11B

A coating composed of 77 wt % CaF_2 - 23 wt % LiF fused on IN-750 nickel-based alloy was studied using SEM, XRD, EDX, and optical microscopic methods. The surfaces examined were the as-fused coating with no subsequent treatment, the coating

after ultrasonic cleaning in water, and the uncoated polished and etched metal. It was found that the coating reacts during fusion with Ti and Nb rich inclusions in the alloy. Numerous small rectangular crystallites of $\text{Ca}(\text{Ti},\text{Nb})$ oxide are formed beneath an overlay of fused fluoride composition. These crystallites are stubby and appear to be embedded in the metal substrate surface. It is known from previous studies that this coating-alloy system has good tribological properties in extreme conditions, such as liquid fluorine. It has been concluded from the present study that the short firmly embedded crystalline protuberances contribute to the coating adherence and thereby to enhanced coating wear life.

Author

N86-28194*# National Aeronautics and Space Administration. Lewis Research Center, Cleveland, Ohio.

MICROGRAVITY POLYMERS

Jun. 1986 22 p Proceedings of a Workshop held in Cleveland, Ohio, 9 May 1985

(NASA-CP-2392; E-2707; NAS 1.55:2392) Avail: NTIS HC A02/MF A01 CSCL 11B

A one-day, interactive workshop considering the effects of gravity on polymer materials science was held in Cleveland, Ohio, on May 9, 1985. Selected programmatic and technical issues were reviewed to introduce the field to workshop participants. Parallel discussions were conducted in three disciplinary working groups: polymer chemistry, polymer physics, and polymer engineering. This proceedings presents summaries of the workshop discussions and conclusions. Author

N86-29041*# National Aeronautics and Space Administration. Lewis Research Center, Cleveland, Ohio.

STRUCTURE-TO-PROPERTY RELATIONSHIPS IN ADDITION CURED POLYMERS 2: RESIN TG COMPOSITE INITIAL MECHANICAL PROPERTIES OF NORBORNENYL CURED POLYIMIDE RESINS

W. B. ALSTON 1986 13 p To be presented at the 18th National SAMPE Technical Conference, Seattle, Washington, 7-9 Oct. 1986

(NASA-TM-88794; E-2979; NAS 1.15:88794; USAVSCOM-TR-86-C-22) Avail: NTIS HC A02/MF A01 CSCL 11C

PRM (polymerization of monomeric reactants) methodology was used to prepare thirty different polyimide oligomeric resins. Monomeric composition as well as chain length between sites of crosslinks were varied to examine their effects on glass transition temperature (T_g) of the cured/postcured resins. An almost linear correlation of T_g versus molecular distance between the crosslinks was observed. An attempt was made to correlate T_g with initial mechanical properties (flexural strength and interlaminar shear strength) of unidirectional graphite fiber composites prepared with these resins. However, the scatter in mechanical strength data prevented obtaining as clear a correlation as was observed for the structural modification/crosslink distance versus T_g . Instead, only a range of composite mechanical properties was obtained at the test temperatures studied (room temperature, 288 and 316 C). Perhaps more importantly, what did become apparent during the attempted correlation study was: (1) that PMR methodology could be used to prepare composites from resins that contain a wide variety of monomer modifications, and (2) that these composites almost invariably provided satisfactory initial mechanical properties as long as the resins selected were melt processable. Author

N86-29042*# Southwest Research Inst., San Antonio, Tex. **SLIDING SEAL MATERIALS FOR ADIABATIC ENGINES, PHASE 2 Interim Report, Feb. 1985 - Feb. 1986**

J. LANKFORD and W. WEI Apr. 1986 54 p (Contract DEN3-352; DE-AI01-86CE-50162)

(NASA-CR-179475; DOE/NASA/0352-2; NAS 1.26:179475; REPT-06-7963) Avail: NTIS HC A04/MF A01 CSCL 11B

An essential task in the development of the heavy-duty adiabatic diesel engine is identification and improvements of reliable, low-friction piston seal materials. In the present study, the sliding

27 NONMETALLIC MATERIALS

friction coefficients and wear rates of promising carbide, oxide, and nitride materials were measured under temperature, environmental, velocity, and loading conditions that are representative of the adiabatic engine environment. In addition, silicon nitride and partially stabilized zirconia disks were ion implanted with TiNi, Ni, Co, and Cr, and subsequently run against carbide pins, with the objective of producing reduced friction via solid lubrication at elevated temperature. In order to provide guidance needed to improve materials for this application, the program stressed fundamental understanding of the mechanisms involved in friction and wear. Electron microscopy was used to elucidate the micromechanisms of wear following wear testing, and Auger electron spectroscopy was used to evaluate interface/environment interactions which seemed to be important in the friction and wear process. Unmodified ceramic sliding couples were characterized at all temperatures by friction coefficients of 0.24 and above. The coefficient at 800 C in an oxidizing environment was reduced to below 0.1, for certain material combinations, by the ion implantation of TiNi or Co. This beneficial effect was found to derive from lubricious Ti, Ni, and Co oxides.

Author

N86-31728*# National Aeronautics and Space Administration. Lewis Research Center, Cleveland, Ohio.

EFFECT OF CRYSTALLOGRAPHICAL AND GEOMETRICAL CHANGES OF A FERRITE HEAD ON MAGNETIC SIGNALS DURING THE SLIDING PROCESS WITH MAGNETIC TAPE

K. MIYOSHI, D. H. BUCKLEY, and K. TANAKA (Kanazawa Univ., Japan) 1986 26 p Presented at the Joint Tribology Conference, Pittsburgh, Pa., 19-22 Oct. 1986; sponsored by ASLE and ASME (NASA-TM-87277; E-2955; NAS 1.15:87277) Avail: NTIS HC A03/MF A01 CSCL 14E

This paper reviews changes in the crystalline structure and geometry of lapped Mn-Zn ferrite heads in sliding contact with magnetic tape and the effects of these changes on magnetic signals. A highly textured, polycrystalline structure was produced on the surface of a single-crystal Mn-Zn ferrite head when it was finished with an aluminum oxide lapping tape. Sliding this lapped surface against a magnetic tape produced a nearly amorphous structure. The sliding process led to a degradation in readback signal of 1 to 2 dB (short-wavelength recording). Furthermore, wear of the magnetic head caused geometrical changes in the head surface. The signal read back with the worn magnetic head was sensitive to operating parameters such as head displacement and tape tension. A change in operating parameters created head-to-tape spacings and, consequently, excessive gains or losses in the readback signal.

Author

N86-31729*# National Aeronautics and Space Administration. Lewis Research Center, Cleveland, Ohio.

CORRELATION OF PROCESSING AND SINTERING VARIABLES WITH THE STRENGTH AND RADIOGRAPHY OF SILICON NITRIDE

W. A. SANDERS and G. Y. BAKLINI (Cleveland State Univ., Ohio) 1986 37 p Presented at the Tenth Annual Conference on Composites and Advanced Ceramic Materials, Cocoa Beach, Fla., 19-24 Jan. 1986; sponsored by the American Ceramic Society

(NASA-TM-87251; E-2934; NAS 1.15:87251) Avail: NTIS HC A03/MF A01 CSCL 11G

A sintered Si₃N₄-SiO₂-Y₂O₃ composition, NASA 6Y, was developed that reached four-point flexural average strength/standard deviation values of 857/36, 544/33, and 462/59 MPa at room temperature, 1200 and 1370 C respectively. These strengths represented improvements of 56, 38, and 21 percent over baseline properties at the three test temperatures. At room temperature the standard deviation was reduced by over a factor of three. These accomplishments were realized by the iterative utilization of conventional x-radiography to characterize structural (density) uniformity as affected by systematic changes in powder processing and sintering parameters. Accompanying the improvement in mechanical properties was a change in the type of flaw causing failure from a pore to a large columnar beta-

Si₃N₄ grain typically 40 to 80 microns long, 10 to 30 microns wide, and with an aspect ratio of 5:1.

Author

N86-32569* National Aeronautics and Space Administration. Lewis Research Center, Cleveland, Ohio.

APPARATUS FOR PRODUCING OXIDATION PROTECTION COATINGS FOR POLYMERS Patent

M. J. MIRTICH, inventor (to NASA), J. S. SOVEY, inventor (to NASA), and A. BANKS, inventor (to NASA) 5 Aug. 1986 7 p Division of US-Patent-Appl-SN-649330, 14 Sep. 1984, US-Patent-4,560,577 Filed 31 Jul. 1985 Supersedes N86-19463 (24 - 10, p 1560)

(NASA-CASE-LEW-14072-2; US-PATENT-4,604,181;

US-PATENT-APPL-SN-761235; US-PATENT-CLASS-204-298;

US-PATENT-CLASS-204-192C; US-PATENT-CLASS-204-192D)

Avail: US Patent and Trademark Office CSCL 11B

A polymeric substrate is coated with a metal oxide film to provide oxidation protection in low Earth orbital environments. The film contains about 4 volume percent polymer to provide flexibility. A coil of polymer materials moves through an ion beam as it is fed between reels. The ion beam first cleans the polymer material surface and then sputters the film material from a target onto this surface.

Official Gazette of the U.S. Patent and Trademark Office

N86-32573*# National Aeronautics and Space Administration. Lewis Research Center, Cleveland, Ohio.

THE MILLING OF PRISTINE AND BROMINATED P-100 GRAPHITE FIBERS

M. E. DILLEHAY (Cleveland State Univ., Ohio) and J. R. GAIER Sep. 1986 12 p

(NASA-TM-88828; E-3203; NAS 1.15:88828) Avail: NTIS HC

A02/MF A01 CSCL 11G

Techniques were developed for the ball milling of pristine and brominated P-100 graphite fibers. Because of the lubrication properties of graphite, large ball loads (50 percent by volume) were required. Use of 2-propanol as a milling medium enhanced the efficiency of the process. Milled brominated P-100 fibers had resistivities which were indistinguishable from milled pristine P-100 fibers. Apparent loss of bromine from the brominated fibers suggests that bromine would not be the intercalate of choice in applications where milled fibers of this type are required. Other intercalates which do not degas may be more appropriate for a milled fiber application. These same results, however, do provide evidence that bromine molecules leave the fiber surface when removed from overpressure of bromine. While exploring possible solvent media for milling purposes, it was found that brominated fibers are stable in a wide variety of organic solvents.

Author

28

PROPELLANTS AND FUELS

Includes rocket propellants, igniters, and oxidizers; their storage and handling procedures; and aircraft fuels.

A86-10028*# United Technologies Research Center, East Hartford, Conn.

DEPOSIT FORMATION AND HEAT-TRANSFER CHARACTERISTICS OF HYDROCARBON ROCKET FUELS

A. J. GIOVANETTI, L. J. SPADACCINI, and E. J. SZETELA (United Technologies Research Center, East Hartford, CT) Journal of Spacecraft and Rockets (ISSN 0022-4650), vol. 22, Sept.-Oct. 1985, p. 574-580. Research supported by the United Technologies Corp. Previously cited in issue 06, p. 749, Accession no. A84-18142. refs

(Contract NAS3-23344)

A86-19929*# United Technologies Research Center, East Hartford, Conn.

LONG TERM DEPOSIT FORMATION IN AVIATION TURBINE FUEL AT ELEVATED TEMPERATURE

A. J. GIOVANETTI and E. J. SZETELA (United Technologies Research Center, East Hartford, CT) AIAA, Aerospace Sciences Meeting, 24th, Reno, NV, Jan. 6-9, 1986. 10 p.

(Contract NAS3-24091)

(AIAA PAPER 86-0525)

An experimental characterization is conducted for the relationships between deposit mass, operating time, and temperature, in coking associated with aviation fuels under conditions simulating those typical of turbine engine fuel systems. Jet A and Suntech A fuels were tested in stainless steel tubing heated to 420-750 K, over test durations of between 3 and 730 hr and at fuel velocities of 0.07-1.3 m/sec. Deposit rates are noted to be a strong function of tube temperature; for a given set of test conditions, deposition rates for Suntech A exceed those of Jet A by a factor of 10. Deposition rates increased markedly with test duration for both fuels. The heated tube data obtained are used to develop a global chemical kinetic model for fuel oxidation and carbon deposition. O.C.

A86-23922*# United Technologies Research Center, East Hartford, Conn.

FUEL DEPOSIT CHARACTERISTICS AT LOW VELOCITY

E. J. SZETELA, A. J. GIOVANETTI (United Technologies Research Center, East Hartford, CT), and S. COHEN (NASA, Lewis Research Center, Cleveland, OH) ASME, Chinese Society of Aeronautics and Astronautics, and China National Aero-Technology Import and Export Corp., Beijing International Gas Turbine Symposium and Exposition, Beijing, People's Republic of China, Sept. 1-7, 1985. 7 p. refs

(Contract NAS3-24091)

(ASME PAPER 85-IGT-130)

An experimental characterization has been made of the relationship between deposit mass, operating time, and temperature in studies of aviation gas turbine fuel thermal stability, in order to support fuel system designs that are more efficient through deposit buildup prevention. A novel thermal stability test apparatus has been developed for the determination of deposition rates over a range of temperatures, in tests of up to several hundred hours duration. In the case of heated stainless steel tubes at low velocity with Jet A fuel, the deposits obtained were thick, porous, and nonuniform. O.C.

A86-37074*# TRW, Inc., Redondo Beach, Calif.

RESISTOJET OPERATION WITH VARIOUS PROPELLANTS

S. ZAFRAN (TRW, Inc., TRW Space and Technology Group, Redondo Beach, CA) AIAA, SAE, ASME, and ASEE, Joint Propulsion Conference, 21st, Monterey, CA, July 8-10, 1985. 6 p. refs

(Contract NAS3-23265)

(AIAA PAPER 85-1158)

A flight-qualified electrothermal thruster demonstrated its adaptability to a variety of propellants. Originally qualified for operation with hydrazine propellant, it was operated with nitrogen, hydrogen, and ammonia propellants, demonstrating 73, 61, and 52 percent overall efficiency with these propellants, respectively, when tested over a wide range of operating conditions. By introducing a preheater to admit hot, rather than cold, propellant inlet gases to the thruster's augmentation heat exchanger, delivered specific impulse closer to theoretical performance limits should be achieved. Author

A86-38393*# Drexel Univ., Philadelphia, Pa.

IGNITION CHARACTERISTICS OF RICH N-HEPTANE FUEL SPRAYS IN THE TRANSITION REGION

A. M. DANIS, N. P. CERNANSKY, and I. NAMER (Drexel University, Philadelphia, PA) ASME, Winter Annual Meeting, Miami Beach, FL, Nov. 17-21, 1985. 7 p. refs

(Contract NAG3-382)

(ASME PAPER 85-WA/HT-46)

Ignition studies were performed on monodisperse n-heptane sprays at atmospheric pressure over a range of equivalence ratios and droplet diameters. A capacitive discharge spark ignition system was used as the ignition source, providing independent control of spark energy and duration. Preliminary measurements were made to optimize spark duration and spark gap, optimum conditions being those at which the maximum frequency or probability of ignition was observed. Using the optimum electrode spacing and spark duration, the frequency of ignition was determined as a function of spark energy for three overall equivalence ratios (0.6, 0.8, and 1.0) and for initial droplet diameters of 25, 40, 50, 60, and 70 microns. An LDA system was used to determine the actual equivalence ratio at the spark gap, which varied from 1.5 to 4.7. The spark energy at which the frequency of ignition was 90 percent was defined as the minimum ignition energy. These data indicated that the ignitability of the sprays was enhanced as the equivalence ratio was increased, but was diminished as the droplet size was increased. The increase in minimum ignition energy with increasing droplet size and fixed equivalence ratio was nearly linear over the range of parameters studied. However, the effect became smaller with increasing equivalence ratio. Author

A86-38394*# Drexel Univ., Philadelphia, Pa.

ANALYSIS OF THE EFFECTS OF FUEL SPRAY CHARACTERISTICS ON NO(X) FORMATION

H. SARV and N. P. CERNANSKY (Drexel University, Philadelphia, PA) ASME, Winter Annual Meeting, Miami Beach, FL, Nov. 17-21, 1985. 9 p. refs

(Contract NAG3-1)

(ASME PAPER 85-WA/HT-47)

Results from experimental and analytical studies on NO(x) formation in a one-dimensional monodisperse spray combustion system are reported. In a previous investigation, an optimum droplet diameter was reported for minimizing NO(x) emissions. In this paper, the effects of enhanced prevaporization and droplet interactions in addition to droplet size effects on NO(x) formation are investigated by air preheating experiments. These phenomena have been incorporated into an analytical model which predicts NO(x) formed from the combustion of monodisperse fuel sprays. Both, experimental and computed results indicate the importance of the extent of prevaporization and droplet interactions on NO(x) production. Preflame vaporization controls the gas phase stoichiometry which has a significant effect on the volume of the hot gases surrounding a fuel droplet where NO(x) is formed. On the other hand, the release of fuel vapor from the droplet to the reaction zone is influenced by droplet interactions which reduce the volume of the hot gases and NO(x) production by bringing the flame closer to the droplet surface. Author

N86-21704*# Virginia Polytechnic Inst. and State Univ., Blacksburg, Dept. of Chemistry.

DEVELOPMENT OF LC-13C NMR Final Annual Report, 10 Jan. 1984 - 9 Jan. 1985

H. C. DORN, J. S. WANG, and T. E. GLASS 17 Mar. 1986 20 p. refs

(Contract NAG3-517)

(NASA-CR-176656; NAS 1.26:176656) Avail: NTIS HC A02/MF A01 CSCL 21D

This study involves the development of C-13 nuclear resonance as an on-line detector for liquid chromatography (LC-C-13 NMR) for the chemical characterization of aviation fuels. The initial focus of this study was the development of a high sensitivity flow C-13 NMR probe. Since C-13 NMR sensitivity is of paramount concern, considerable effort during the first year was directed at new NMR probe designs. In particular, various toroid coil designs were

28 PROPELLANTS AND FUELS

examined. In addition, corresponding shim coils for correcting the main magnetic field (B sub 0) homogeneity were examined. Based on these initial probe design studies, an LC-C-13 NMR probe was built and flow C-13 NMR data was obtained for a limited number of samples. Author

N86-25502*# Rensselaer Polytechnic Inst., Troy, N.Y. Dept. of Mechanical Engineering.

EMISSION FTIR ANALYSES OF THIN MICROSCOPIC PATCHES OF JET FUEL RESIDUES DEPOSITED ON HEATED METAL SURFACES Final Report

J. L. LAUER and P. VOGEL 30 May 1986 95 p refs

(Contract NAG3-205)

(NASA-CR-176786; NAS 1.26:176786) Avail: NTIS HC A05/MF A01 CSCL 21D

The relationship of fuel stability to fuel composition and the development of mechanisms for deposit formation were investigated. Fuel deposits reduce heat transfer efficiency and increase resistance to fuel flow and are highly detrimental to aircraft performance. Infrared emission Fourier transform spectroscopy was chosen as the primary method of analysis because it was sensitive enough to be used in-situ on tiny patches of monolayers or of only a few molecular layers of deposits which generally proved completely insoluble in any nondestructive solvents. Deposits of four base fuels were compared; dodecane, a dodecane/tetralin blend, commercial Jet A fuel, and a broadened-properties jet fuel particularly rich in polynuclear aromatics. Every fuel in turn was provided with and without small additions of such additives as thiophene, furan, pyrrole, and copper and iron naphthenates.

B.G.

N86-27460*# Santa Clara Univ., Calif. Dept. of Mechanical Engineering Research.

RESEARCH AND DEVELOPMENT OF NEAT ALCOHOL FUEL USAGE IN AUTOMOBILES

R. K. PEFLEY, L. BROWNING, S. ESPANOLA, B. PULLMAN, R. GURURANGAN, and N. SAITO Jun. 1984 147 p

(Contract NAG3-143)

(NASA-CR-174813; DOE/NASA/0143-1; NAS 1.26:174813; DOE/NBB-0067; ME84-1) Avail: NTIS HC A07/MF A01 CSCL 21D

The study is an extension of previous work. Its topical coverage ranges from research in the forms of experimental operation of engines in cold chambers and a photochemical smog chamber with allied computer modeling of the thermofluid mechanics of cold engine starting and photochemical smog through engine corrosion and wear studies, to vehicle operation, which includes a description of the engineering development of after-market conversion kits to change Ford Pinto vehicles from gasoline to alcohol. Although further research is recommended, evidence presented contributes positively to the view that it is feasible to operate neat alcohol fleets in the range of 1000-10,000 vehicles, without major operational difficulties and without exacerbating the environmental, health and safety risks associated with petroleum fuels. Author

N86-28261*# Rensselaer Polytechnic Inst., Troy, N.Y. Dept. of Materials Engineering.

DETERMINATION OF SOLID MASS FRACTION IN PARTIALLY FROZEN HYDROCARBON FUELS Final Report

E. M. COTTERELL, R. MOSSADEGH, A. J. BRUCE, and C. T. MOYNIHAN Jul. 1986 90 p

(Contract NAG3-213)

(NASA-CR-179472; NAS 1.26:179472) Avail: NTIS HC A05/MF A01 CSCL 07D

Filtration procedures alone are insufficient to determine the amounts of crystalline solid in a partially frozen hydrocarbon distillate fraction. This is due to the nature of the solidification process by which a large amount of liquid becomes entrapped within an interconnected crystalline structure. A technique has been developed to supplement filtration methods with an independent determination of the amount of liquid in the precipitate thereby revealing the actual value of mass percent crystalline solid, %S.

A non-crystallizing dye is injected into the fuel and used as a tracer during the filtration. The relative concentrations of the dye in the filtrate and precipitate fractions is subsequently detected by a spectrophotometric comparison. The filtration apparatus was assembled so that the temperature of the sample is recorded immediately above the filter. Also, a second method of calculation has been established which allows significant reduction in test time while retaining acceptable accuracy of results. Data have been obtained for eight different kerosene range hydrocarbon fuels. Author

N86-30023*# United Technologies Research Center, East Hartford, Conn.

ROLE OF FUEL CHEMICAL PROPERTIES ON COMBUSTOR RADIATIVE HEAT LOAD

T. J. ROSFJORD 19 Apr. 1984 36 p

(Contract NAS3-23167)

(NASA-CR-177096; NAS 1.26:177096) Avail: NTIS HC A03/MF A01 CSCL 21I

In an attempt to rigorously study the fuel chemical property influence on combustor radiative heat load, United Technologies Research Center (UTRC) has conducted an experimental program using 25 test fuels. The burner was a 12.7-cm dia cylindrical device fueled by a single pressure-atomizing injector. Fuel physical properties were de-emphasized by selecting injectors which produced high-atomized, and hence rapidly-vaporizing sprays. The fuels were specified to cover the following wide ranges of chemical properties; hydrogen, 9.1 to 15- (wt) pct; total aromatics, 0 to 100 (vol) pct; and naphthalene, 0 to 30 (vol) pct. They included standard fuels, specialty products and fuel blends. Fuel naphthalene content exhibited the strongest influence on radiation of the chemical properties investigated. Smoke point was a good global indicator of radiation severity. Author

31

ENGINEERING (GENERAL)

Includes vacuum technology; control engineering; display engineering; cryogenics; and fire prevention.

A86-37053*# Martin Marietta Corp., Denver, Colo.

CRYOGENIC FLUID MANAGEMENT FACILITY

R. N. EBERHARDT and W. J. BAILEY (Martin Marietta Corp., Denver, CO) Cryogenic Engineering Conference, Boston, MA, Aug. 12-16, 1985, Paper. 11 p.

(Contract NAS3-23355)

The Cryogenic Fluid Management Facility is a reusable test bed which is designed to be carried within the Shuttle cargo bay to investigate the systems and technologies associated with the efficient management of cryogenics in space. Cryogenic fluid management consists of the systems and technologies for: (1) liquid storage and supply, including capillary acquisition/expulsion systems which provide single-phase liquid to the user system, (2) both passive and active thermal control systems, and (3) fluid transfer/resupply systems, including transfer lines and receiver tanks. The facility contains a storage and supply tank, a transfer line and a receiver tank, configured to provide low-g verification of fluid and thermal models of cryogenic storage and transfer processes. The facility will provide design data and criteria for future subcritical cryogenic storage and transfer system applications, such as Space Station life support, attitude control, power and fuel depot supply, resupply tankers, external tank (ET) propellant scavenging, and ground-based and space-based orbit transfer vehicles (OTV). Author

COMMUNICATIONS AND RADAR

Includes radar; land and global communications; communications theory; and optical communications.

N86-20587*# National Aeronautics and Space Administration. Lewis Research Center, Cleveland, Ohio.

ION BEAM SPUTTER ETCHING Patent Application

B. A. BANKS and S. K. RUTLEDGE, inventors (to NASA) 13 Sep. 1985 12 p

(NASA-CASE-LEW-13899-1; NAS 1.71:LEW-13899-1; US-PATENT-APPL-SN-775968) Avail: NTIS HC A02/MF A01 CSCL 13H

An ion beam etching process which forms extremely high aspect ratio surface microstructures using thin sputter masks is utilized in the fabrication of integrated circuits. A carbon rich sputter mask together with unmasked portions of a substrate is bombarded with inert gas ions while simultaneous carbon deposition occurs. The arrival of the carbon deposit is adjusted to enable the sputter mask to have a near zero or even slightly positive increase in thickness with time while the unmasked portions have a high net sputter etch rate. NASA

N86-24869*# National Aeronautics and Space Administration. Lewis Research Center, Cleveland, Ohio.

CRITERIA FOR SIGNIFICANCE OF SIMULTANEOUS PRESENCE OF BOTH CONDENSIBLE VAPORS AND AEROSOL PARTICLES ON MASS TRANSFER (DEPOSITION) RATES

S. A. GOEKOGLU (Case Western Res. Univ., Cleveland Ohio) Feb. 1986 17 p refs

(NASA-TM-87247; E-2929; NAS 1.15:87247) Avail: NTIS HC A02/MF A01

The simultaneous presence of aerosol particles and condensible vapors in a saturated boundary layer which may affect deposition rates to subcooled surfaces because of vapor-particle interactions is discussed. Scavenging of condensible vapors by aerosol particles may lead to increased particle size and decreased vapor mass fraction, which alters both vapor and particle deposition rates. Particles, if sufficiently concentrated, may also coagulate. Criteria are provided to assess the significance of such phenomena when particles are already present in the mainstream and are not created inside the boundary layer via homogeneous nucleation. It is determined that there is direct proportionality with: (1) the mass concentration of both condensible vapors and aerosol particles; and (2) the square of the boundary layer thickness to particle diameter ratio (δd sub p) square. Inverse proportionality was found for mainstream to surface temperature difference if thermophoresis dominates particle transport. It is concluded that the square of the boundary layer thickness to particle diameter ratio is the most critical factor to consider in deciding when to neglect vapor-particle interactions. Author

N86-32587* National Aeronautics and Space Administration. Lewis Research Center, Cleveland, Ohio.

TEXTURED CARBON SURFACES ON COPPER BY SPUTTERING Patent

A. N. CURREN, inventor (to NASA), K. A. JENSEN, inventor (to NASA), and R. F. ROMAN, inventor (to NASA) 19 Aug. 1986 8 p Filed 10 Oct. 1984 Supersedes N85-20151 (23 - 11, p 1615)

(NASA-CASE-LEW-14130-1; US-PATENT-4,607,193; US-PATENT-APPL-SN-659475; US-PATENT-CLASS-315-538; US-PATENT-CLASS-204-192C; US-PATENT-CLASS-204-192D; US-PATENT-CLASS-204-298; US-PATENT-CLASS-313-106; US-PATENT-CLASS-313-107; US-PATENT-CLASS-427-39) Avail: US Patent and Trademark Office CSCL 13H

A very thin layer of highly textured carbon is applied to a copper surface by a triode sputtering process. A carbon target and a copper substrate are simultaneously exposed to an argon plasma in a vacuum chamber. The resulting carbon surface is characterized by a dense, random array of needle like spires or peaks which extend perpendicularly from the copper surface. The coated copper is especially useful for electrode plates in multistage depressed collectors.

Official Gazette of the U.S. Patent and Trademark Office

A86-19184* Massachusetts Inst. of Tech., Cambridge.

OPTIMIZED THREE-DIMENSIONAL LENSES FOR WIDE-ANGLE SCANNING

C. M. RAPPAPORT (MIT, Cambridge, MA) and A. I. ZAGHLOUL (COMSAT Laboratories, Clarksburg, MD) IEEE Transactions on Antennas and Propagation (ISSN 0018-926X), vol. AP-33, Nov. 1985, p. 1227-1236. Research supported by the Communications Satellite Corp. refs (Contract NAS3-23250)

Three-dimensional bootlace lens antennas with two and four focal points can be optimized to produce high-quality scanned beams over a wide field of view. For two-dimensional scanning, the planar feed locus is replaced by a curved feed locus designed to minimize path length errors. Comparisons with previous bootlace lens designs demonstrate the advantages of this focal distribution. The bifocal lens shows good scanning performance in both principal and orthogonal planes. The quadrifocal lens performs better in its principal plane than in its orthogonal plane. It is also shown that the quadrifocal lens can be realized with a planar outer surface and a circular focal arc, and improved scanning performance is still achievable. Further optimization of the focal arc and/or relaxation of the planar outer surface condition results in quadrifocal lenses with negligible phase errors in the principal plane. Author

A86-21882* Motorola, Inc., Scottsdale, Ariz.

THE BASEBAND PROCESSOR IN FUTURE SATELLITE COMMUNICATION SYSTEMS

R. E. THOMAS and D. R. CARROLL (Motorola, Inc., Communication Div., Scottsdale, AZ) IN: EASCON '84; Proceedings of the Seventeenth Annual Electronics and Aerospace Conference, Washington, DC, September 10-12, 1984. New York, Institute of Electrical and Electronics Engineers, 1984, p. 151-155. refs (Contract NAS3-22502)

This paper provides a description of a baseband processor planned for satellite communication systems operating in Ka band. The satellite based interconnection of individual earth terminals is described in terms of uplink and downlink message formats, and the on-board processing signal flow. Advanced technology requirements and developments are reviewed including current activity in custom large scale integrated circuit development. Author

A86-29611*# National Aeronautics and Space Administration. Lewis Research Center, Cleveland, Ohio.

TECHNOLOGY ACHIEVEMENTS AND PROJECTIONS FOR COMMUNICATION SATELLITES OF THE FUTURE

J. W. BAGWELL (NASA, Lewis Research Center, Cleveland, OH) IN: Communication Satellite Systems Conference, 11th, San Diego, CA, March 17-19, 1986, Technical Papers. New York, American Institute of Aeronautics and Astronautics, 1986, p. 289-297. Previously announced in STAR as N86-17595. refs (AIAA PAPER 86-0649)

Multibeam systems of the future using monolithic microwave integrated circuits to provide phase control and power gain are contrasted with discrete microwave power amplifiers from 10 to 75 W and their associated waveguide feeds, phase shifters and power splitters. Challenging new enabling technology areas include advanced electrooptical control and signal feeds. Large scale MMIC's will be used incorporating on chip control interfaces, latching, and phase and amplitude control with power levels of a few watts each. Beam forming algorithms for 80 to 90 deg wide angle scanning and precise beam forming under wide ranging environments will be required. Satellite systems using these

dynamically reconfigured multibeam antenna systems will demand greater degrees of beam interconnectivity. Multiband and multiservice users will be interconnected through the same space platform. Monolithic switching arrays operating over a wide range of RF and IF frequencies are contrasted with current IF switch technology implemented discretely. Size, weight, and performance improvements by an order of magnitude are projected. Author

A86-29638*# National Aeronautics and Space Administration. Lewis Research Center, Cleveland, Ohio.

OPTICAL TECHNIQUES TO FEED AND CONTROL GAAS MMIC MODULES FOR PHASED ARRAY ANTENNA APPLICATIONS

K. B. BHASIN, G. ANZIC, R. R. KUNATH, and D. J. CONNOLLY (NASA, Lewis Research Center, Cleveland, OH) IN: Communication Satellite Systems Conference, 11th, San Diego, CA, March 17-20, 1986, Technical Papers. New York, American Institute of Aeronautics and Astronautics, 1986, p. 506-513. Previously announced in STAR as N86-16458. refs (AIAA PAPER 86-0687)

A complex signal distribution system is required to feed and control GaAs monolithic microwave integrated circuits (MMICs) for phased array antenna applications above 20 GHz. Each MMIC module will require one or more RF lines, one or more bias voltage lines, and digital lines to provide a minimum of 10 bits of combined phase and gain control information. In a closely spaced array, the routing of these multiple lines presents difficult topology problems as well as a high probability of signal interference. To overcome GaAs MMIC phased array signal distribution problems optical fibers interconnected to monolithically integrated optical components with GaAs MMIC array elements are proposed as a solution. System architecture considerations using optical fibers are described. The analog and digital optical links to respectively feed and control MMIC elements are analyzed. It is concluded that a fiber optic network will reduce weight and complexity, and increase reliability and performance, but higher power will be required. Author

A86-29656*# Toledo Univ., Ohio.

SIMULATED PERFORMANCE OF THE NASA 30/20 GHZ TEST TRANSPONDER USING MULTI-H PHASE CODED MODULATION

C. B. MEADER (M/A-COM, Inc., Government Systems Group, Vienna, VA), S. C. KWATRA (Toledo, University, OH), and G. H. STEVENS (NASA, Lewis Research Center, Cleveland, OH) IN: Communication Satellite Systems Conference, 11th, San Diego, CA, March 17-20, 1986, Technical Papers. New York, American Institute of Aeronautics and Astronautics, 1986, p. 644-650. refs (Contract NCC3-22; NAG3-157) (AIAA PAPER 86-0717)

The performance of a proposed NASA 30/20 GHz satellite communications system is studied for multi-h phase coded modulation (MHPM) schemes. The techniques used to model and simulate a satellite communications channel including transmitter, receiver, filters, nonlinearities, and interferers are presented. The performance of various MHPM schemes is compared for several different channel configurations. As a measure of performance, the probability of bit error vs E_b/N_0 is computed using a Monte Carlo simulation technique. It is found that, regardless of the channel configuration, MHPM schemes can provide power efficiency over serial minimum shift keying modulation. Author

A86-29664*# National Aeronautics and Space Administration. Lewis Research Center, Cleveland, Ohio.

AN ANALYSIS OF BIDIRECTIONAL USE OF FREQUENCIES FOR SATELLITE COMMUNICATIONS

W. A. WHYTE, JR., E. F. MILLER (NASA, Lewis Research Center, Cleveland, OH), T. SULLIVAN, and J. E. MILLER (ORI, Inc., Landover, MA) IN: Communication Satellite Systems Conference, 11th, San Diego, CA, March 17-20, 1986, Technical Papers. New York, American Institute of Aeronautics and Astronautics, 1986, p. 705-715. Previously announced in STAR as N86-18585. refs (AIAA PAPER 86-0635)

The bi-directional use of frequencies allocated for space communications has the potential to double the orbit/spectrum

capacity available. The technical feasibility of reverse band use (RBU) at C-band (4 GHz uplinks and 6 GHz downlinks) is studied. The analysis identifies the constraints under which both forward and reverse band use satellite systems can share the same frequencies with terrestrial, line of sight transmission systems. The results of the analysis show that RBU satellite systems can be similarly sized to forward band use (FBU) satellite systems. In addition, the orbital separation requirements between RBU and FBU satellite systems are examined. The analysis shows that a carrier to interference ratio of 45 dB can be maintained between RBU and FBU satellites separated by less than 0.5 deg., and that a carrier to interference ratio of 42 dB can be maintained in the antipodal case. Rain scatter propagation analysis shows that RBU and FBU earth stations require separation distances of less than 10 km at a rain rate of 13.5 mm/hr escalating to less than 100 km at a rain rate of 178 mm/hr for earth station antennas in the 3 to 10 m range. Author

A86-39542* Lockheed Missiles and Space Co., Sunnyvale, Calif.

STRATEGY FOR REFLECTOR PATTERN CALCULATION - LET THE COMPUTER DO THE WORK

P. T. LAM (Lockheed Missiles and Space Co., Inc., Sunnyvale, CA), S.-W. LEE (Illinois, University, Urbana), C. C. HUNG (DRG, San Jose, CA), and R. ACOSTA (NASA, Lewis Research Center, Cleveland, OH) IEEE Transactions on Antennas and Propagation (ISSN 0018-926X), vol. AP-34, April 1986, p. 592-595. Previously announced in STAR as N86-12485. refs

Using high frequency approximations, the secondary pattern of a reflector antenna can be calculated by numerically evaluating a radiation integral $I(u,v)$. In recent years, tremendous effort has been expended to reducing $I(u,v)$ to Fourier integrals. These reduction schemes are invariably reflector geometry dependent. Hence, different analyses/computer software development must be carried out for different reflector shapes/boundaries. It is pointed out, that, as the computer power improves, these reduction schemes are no longer necessary. Comparable accuracy and computation time can be achieved by evaluating $I(u,v)$ by a brute force FFT described in this note. Furthermore, there is virtually no restriction on the reflector geometry by using the brute force FFT. Author

A86-49567*# National Aeronautics and Space Administration. Lewis Research Center, Cleveland, Ohio.

IMPACT OF THE 1985 SPACE WORLD ADMINISTRATIVE RADIO CONFERENCE ON FREQUENCY/ORBIT PLANNING AND USE

E. F. MILLER (NASA, Lewis Research Center, Cleveland, OH) AIAA, Annual Communications Satellite Systems Conference, 11th, San Diego, CA, Mar. 16-20, 1986. 7 p. Previously announced in STAR as N86-24881.

(AIAA PAPER 86-0634)

The 1985 World Administrative Radio Conference (WARC-ORB-85) was held to determine which space radio services should be planned and which planning methods should be used. The second session of this Conference (WARC-ORB-88) will meet to develop the required plans. This paper presents the results of WARC-ORB-85, assesses the impact of those decisions, and identifies the intersessional work to be conducted by administrations and the CCIR (consultative Committee on International Radio). The major decisions of WARC-ORB-85 were: (1) the restriction of additional planning to the fixed satellite service at identified frequencies; and (2) the selection of a planning method consisting of two parts: (a) an allotment plan, and (b) improved procedures. The paper also discusses WARC-ORB-85 decisions relative to the Region 2 broadcast satellite service plans at 12 GHz, feederlink planning for Regions 1 and 3 broadcast satellites at 12 GHz, and sound broadcast satellite service. Author

N86-49568*# National Aeronautics and Space Administration. Lewis Research Center, Cleveland, Ohio.

AN ANALYSIS OF BI-DIRECTIONAL USE OF FREQUENCIES FOR SATELLITE COMMUNICATIONS

W. A. WHYTE, JR., E. F. MILLER (NASA, Lewis Research Center, Cleveland, OH), T. SULLIVAN, and J. E. MILLER (ORI, Inc., Landover, MD) AIAA, Annual Communications Satellite Systems Conference, 11th, San Diego, CA, Mar. 16-20, 1986. 18 p. Previously announced in STAR as N86-18585. refs (AIAA PAPER 86-0635)

The bi-directional use of frequencies allocated for space communications has the potential to double the orbit/spectrum capacity available. The technical feasibility of reverse band use (RBU) at C-band (4 GHz uplinks and 6 GHz downlinks) is studied. The analysis identifies the constraints under which both forward and reverse band use satellite systems can share the same frequencies with terrestrial, line of sight transmission systems. The results of the analysis show that RBU satellite systems can be similarly sized to forward band use (FBU) satellite systems. In addition, the orbital separation requirements between RBU and FBU satellite systems are examined. The analysis shows that a carrier to interference ratio of 45 dB can be maintained between RBU and FBU satellites separated by less than 0.5 deg, and that a carrier to interference ratio of 42 dB can be maintained in the antipodal case. Rain scatter propagation analysis shows that RBU and FBU earth stations require separation distances of less than 10 km at a rain rate of 13.5 mm/hr escalating to less than 100 km at a rain rate of 178 mm/hr for earth station antennas in the 3 to 10 m range. Author

N86-10377*# Illinois Univ., Urbana. Electromagnetics Lab. **NUMERICAL METHODS FOR ANALYZING ELECTROMAGNETIC SCATTERING** *Selmannual Report*, 25 Mar. - 24 Sep. 1985

S. W. LEE, Y. T. LO, S. L. CHUANG, and C. S. LEE 24 Sep. 1985 176 p refs (Contract NAG3-475) (NASA-CR-176141; NAS 1.26:176141) Avail: NTIS HC A09/MF A01 CSCL 20N

Attenuation properties of the normal modes in an overmoded waveguide coated with a lossy material were analyzed. It is found that the low-order modes, can be significantly attenuated even with a thin layer of coating if the coating material is not too lossy. A thinner layer of coating is required for large attenuation of the low-order modes if the coating material is magnetic rather than dielectric. The Radar Cross Section (RCS) from an uncoated circular guide terminated by a perfect electric conductor was calculated and compared with available experimental data. It is confirmed that the interior irradiation contributes to the RCS. The equivalent-current method based on the geometrical theory of diffraction (GTD) was chosen for the calculation of the contribution from the rim diffraction. The RCS reduction from a coated circular guide terminated by a PEC are planned schemes for the experiments are included. The waveguide coated with a lossy magnetic material is suggested as a substitute for the corrugated waveguide.

N86-10379*# National Aeronautics and Space Administration. Lewis Research Center, Cleveland, Ohio.

TEST RESULTS FOR 20-GHZ GAAS FET SPACECRAFT POWER AMPLIFIER

K. A. SHALKHAUSER Aug. 1985 22 p refs (NASA-TM-87072; E-2573; NAS 1.15:87072) Avail: NTIS HC A02/MF A01 CSCL 09C

Test were conducted to measure the performance of the 20-GHz solid state, proof-of-concept amplifier. The amplifier operates over the 17.7 to 20.2-GHz frequency range and uses high power gallium arsenide field effect transistors. The amplifier design and test methods are briefly described. NASA and contractor performance data are compared. Author

N86-10380*# National Aeronautics and Space Administration. Lewis Research Center, Cleveland, Ohio.

A DUAL FREQUENCY MICROSTRIP ANTENNA FOR KA BAND

R. Q. LEE and M. F. BADDOUR 1985 12 p refs Presented at 1985 Antenna Appl. Symp., 18-20 Sep. 1985; sponsored by Illinois Univ. and RADC, Monticello, Ill. (NASA-TM-87124; E-2737; NAS 1.15:87124) Avail: NTIS HC A02/MF A01 CSCL 20N

For fixed satellite communication systems at Ka band with downlink at 17.7 to 20.2 GHz and uplink at 27.5 to 30.0 GHz, the focused optics and the unfocused optics configurations with monolithic phased array feeds have often been used to provide multiple fixed and multiple scanning spot beam coverages. It appears that a dual frequency microstrip antenna capable of transmitting and receiving simultaneously is highly desirable as an array feed element. This paper describes some early efforts on the development and experimental testing of a dual frequency annular microstrip antenna. The antenna has potential application for use in conjunction with a monolithic microwave integrated circuit device as an active radiating element in a phased array of phased array feeds. The antenna is designed to resonate at TM sub 12 and TM sub 13 modes and tuned with a circumferential microstrip ring to vary the frequency ratio. Radiation characteristics at both the high and low frequencies are examined. Experimental results including radiating patterns and swept frequency measurements are presented. Author

N86-10381*# National Aeronautics and Space Administration. Lewis Research Center, Cleveland, Ohio.

A NUMERICAL METHOD FOR APPROXIMATING ANTENNA SURFACES DEFINED BY DISCRETE SURFACE POINTS

R. Q. LEE and R. ACOSTA 1985 10 p refs Presented at 1985 Antenna Appl. Symp., 18-20 Sep. 1985; sponsored by Illinois Univ. and RADC, Monticello, Ill. (NASA-TM-87125; E-2738; NAS 1.15:87125) Avail: NTIS HC A02/MF A01 CSCL 20N

A simple numerical method for the quadratic approximation of a discretely defined reflector surface is described. The numerical method was applied to interpolate the surface normal of a parabolic reflector surface from a grid of nine closest surface points to the point of incidence. After computing the surface normals, the geometrical optics and the aperture integration method using the discrete Fast Fourier Transform (FFT) were applied to compute the radiation patterns for a symmetric and an offset antenna configurations. The computed patterns are compared to that of the analytic case and to the patterns generated from another numerical technique using the spline function approximation. In the paper, examples of computations are given. The accuracy of the numerical method is discussed. Author

N86-11401*# National Aeronautics and Space Administration. Lewis Research Center, Cleveland, Ohio.

CHARACTERIZATION OF MMIC DEVICES FOR ACTIVE ARRAY ANTENNAS

J. SMETANA, E. FARR (Illinois Univ., Urbana), and R. MITTRA (Illinois Univ., Urbana) In RADC Proc. of the 1984 Antenna Appl. Symp. p 57-82 Jan. 1985 refs Previously announced as N85-15779 Avail: NTIS HC A13/MF A01 CSCL 09C

Certain aspects of monolithic microwave integrated circuit (MMIC) interconnectivity were investigated. Considerations that lead to preserving the inherently reproducible characteristics of the MMIC are proposed. It is shown that at radio frequencies (RF) greater than 20 GHz, the transition from the MMIC device to other transmission media must be an accurate RF match. It is proposed that the RF match is sufficiently critical to include the transition as part of the delivered MMIC package. The model to analyze several transitions is presented. This model consists of a succession of abrupt discontinuities in printed circuit transmission lines. The analysis of these discontinuities is achieved by the Spectral Galerkin technique, to establish the modes and mode that special effects should be coordinated by the active array

antenna industry toward standardization of MMIC packaging and characterization. Author

N86-11407*# National Aeronautics and Space Administration. Lewis Research Center, Cleveland, Ohio.

CIRCULARLY POLARIZED MICROSTRIP ANTENNAS

Y. T. LO (Illinois Univ., Urbana), B. ENGST (Illinois Univ., Urbana), and R. Q. H. LEE /in RADC Proc. of the 1984 Antenna Appl. Symp. p 197-218 Jan. 1985 refs

Avail: NTIS HC A13/MF A01 CSCL 20N

A simple microstrip antenna can be made to radiate EM waves of any polarization, in particular, the circular polarization (CP) without any phasing network and power divider. A simple and accurate theory for this family of antennas was developed. However, the CP bandwidth, (CPBW) the bandwidth in which the axial ratio (AR) is less than a certain specified value, is very small. Most of the experimental designs were made for a feed placed along the diagonal of the patch. It is shown that there are practically infinitely many possible designs with different feed location. The speculation that other designs might give a wider bandwidth is clarified and an effective method for broadening the bandwidth is shown. E.A.K.

N86-12485*# National Aeronautics and Space Administration. Lewis Research Center, Cleveland, Ohio.

STRATEGY FOR REFLECTOR PATTERN CALCULATION: LET THE COMPUTER DO THE WORK

P. T. LAM (Illinois Univ., Urbana), S. W. LEE (Illinois Univ., Urbana), C. C. HUNG (Lockheed Missiles and Space Co., Sunnyvale, Calif.), and R. ACOUSTA Oct. 1985 9 p refs

(Contract NAG3-149)

(NASA-TM-87137; E-2755; NAS 1.15:87137) Avail: NTIS HC

A02/MF A01 CSCL 20N

Using high frequency approximations, the secondary pattern of a reflector antenna can be calculated by numerically evaluating a radiation integral $I(u,v)$. In recent years, tremendous effort has been expended to reducing $I(u,v)$ to Fourier integrals. These reduction schemes are invariably reflector geometry dependent. Hence, different analyses/computer software development must be carried out for different reflector shapes/boundaries. It is pointed out, that, as the computer power improves, these reduction schemes are no longer necessary. Comparable accuracy and computation time can be achieved by evaluating $I(u,v)$ by a brute force FFT described in this note. Furthermore, there is virtually no restriction on the reflector geometry by using the brute force FFT. Author

N86-13627*# National Aeronautics and Space Administration. Lewis Research Center, Cleveland, Ohio.

TESTING OF 30-GHZ LOW NOISE RECEIVERS

M. J. CONROY and R. J. KERCZEWSKI (Analex Corp.) 1985 24 p refs Proposed for presentation at the 11th Annual Communication Satellite Systems Conference, San Diego, Calif., 16-20 Mar. 1986; sponsored by AIAA

(NASA-TM-87171; E-2809; NAS 1.15:87171) Avail: NTIS HC

A02/MF A01 CSCL 20N

NASA-sponsored studies of the growth in communications traffic have indicated that the frequency spectrum allocated to fix-service satellites at the C and Ku bands will reach saturation by the early 1990's. The next higher frequency bands allocated for communications satellites are 27.5 to 30 GHz for the uplink and 17.7 to 20.2 GHz for the downlink. Current plans for developing satellite systems that use these bands include a NASA demonstration satellite (ACTS). One of the components identified as critical to the success of that mission is a 27.5 to 30 GHz satellite receiver. In response to that identification, NASA has sponsored the development of such a receiver to the proof-of-concept (POC) level. Design and fabrication of such POC model receivers was carried out under parallel contracts awarded to LNR Communications, Inc. of Hauppauge, New York and to ITT Defense Communications Division of Nutley, New Jersey. The most significant of the performance goals were a 5 db maximum noise figure, a 2.5 GHz passband, and ≤ 0 dB Rf to If gain. Following

delivery of hardware from each of the contractors, an in-house test program was undertaken at NASA's Lewis Research Center in order to verify the contractor-reported performance and to provide a comparison of the two receivers under identical test conditions. The present paper reports the results of those tests. Author

N86-14477*# National Aeronautics and Space Administration. Lewis Research Center, Cleveland, Ohio.

SECONDARY PATTERN COMPUTATION OF AN ARBITRARILY SHAPED MAIN REFLECTOR Final Report

P. T. C. LAM (Illinois Univ., Urbana), S. W. LEE (Illinois Univ., Urbana), and R. J. ACOSTA Nov. 1985 120 p refs Previously announced as N84-25909

(NASA-TM-87162; E-2796; NAS 1.15:87162) Avail: NTIS HC A06/MF A01 CSCL 20N

The secondary pattern of a perfectly conducting offset main reflector being illuminated by a point feed at an arbitrary location is studied. The method of analysis is based upon the application of the Fast Fourier Transform (FFT) to the aperture fields obtained using geometrical optics (GO) and geometrical theory of diffraction (GTD). Key features of the present work are (1) the reflector surface is completely arbitrary, (2) the incident field from the feed is most general with arbitrary polarization and location, and (3) the edge diffraction is calculated by either UAT or by UTD. Comparison of this technique for an offset parabolic reflector with the Jacobi-Bessel and Fourier-Bessel techniques shows good agreement. Near field, far field, and scan data of a large reflector are presented. Author

N86-14479*# National Aeronautics and Space Administration. Lewis Research Center, Cleveland, Ohio.

SECONDARY PATTERN COMPUTATION OF AN OFFSET REFLECTOR ANTENNA

R. J. ACOSTA Nov. 1985 20 p refs

(NASA-TM-87160; E-2791; NAS 1.15:87160) Avail: NTIS HC

A02/MF A01 CSCL 20N

Reflector antennas are widely used in communications satellite systems because they provide high gain at low cost. In analyzing reflector antennas the computation of the secondary pattern is the main concern. A computer program for calculating the secondary pattern of an offset reflector has been developed and implemented at the NASA Lewis Research Center. The theoretical foundation for this program is based on the use of geometrical optics to describe the fields from the feed to the reflector surface and to the aperture plane. The resulting aperture field distribution is then transformed to the far-field zone by the fast Fourier transform algorithm. Comparing this technique with other well-known techniques (the geometrical theory of diffraction, physical optics (Jacobi-Bessel), etc.) shows good agreement for large (diameter of 100 lambda or greater) reflector antennas. Author

N86-16451*# Princeton Synergetics, Inc., N.J.

EVALUATION OF SPACECRAFT TECHNOLOGY PROGRAMS (EFFECTS ON COMMUNICATION SATELLITE BUSINESS VENTURES), VOLUME 1 Final Report

J. S. GREENBURG, C. GAELICK, M. KAPLAN (Spacotech, Inc.), J. FISHMAN, and C. HOPKINS (Econ, Inc., San Jose, Calif.) Sep. 1985 186 p refs 2 Vol.

(Contract NAS3-23886)

(NASA-CR-174978; NAS 1.26:174978) Avail: NTIS HC A09/MF A01 CSCL 17B

Commercial organizations as well as government agencies invest in spacecraft (S/C) technology programs that are aimed at increasing the performance of communications satellites. The value of these programs must be measured in terms of their impacts on the financial performance of the business ventures that may ultimately utilize the communications satellites. An economic evaluation and planning capability was developed and used to assess the impact of NASA on-orbit propulsion and space power programs on typical fixed satellite service (FSS) and direct broadcast service (DBS) communications satellite business

ventures. Typical FSS and DBS spin and three-axis stabilized spacecraft were configured in the absence of NASA technology programs. These spacecraft were reconfigured taking into account the anticipated results of NASA specified on-orbit propulsion and space power programs. In general, the NASA technology programs resulted in spacecraft with increased capability. The developed methodology for assessing the value of spacecraft technology programs in terms of their impact on the financial performance of communication satellite business ventures is described. Results of the assessment of NASA specified on-orbit propulsion and space power technology programs are presented for typical FSS and DBS business ventures. R.J.F.

N86-16452*# Princeton Synergetics, Inc., N.J.
EVALUATION OF SPACECRAFT TECHNOLOGY PROGRAMS (EFFECTS ON COMMUNICATION SATELLITE BUSINESS VENTURES), VOLUME 2 Final Report

J. S. GREENBURG, M. KAPLAN (Spacotech, Inc.), J. FISHMAN, and C. HOPKINS (Econ, Inc., San Jose, Calif.) Sep. 1985 155 p 2 Vol.

(Contract NAS3-23886)

(NASA-CR-174979; NAS 1.26:174979) Avail: NTIS HC A08/MF A01 CSCL 17B

The computational procedures used in the evaluation of spacecraft technology programs that impact upon commercial communication satellite operations are discussed. Computer programs and data bases are described. R.J.F.

N86-16457*# National Aeronautics and Space Administration. Lewis Research Center, Cleveland, Ohio.
MONOLITHIC OPTICAL INTEGRATED CONTROL CIRCUITRY FOR GAAS MMIC-BASED PHASED ARRAYS

K. B. BHASIN, G. E. PONCHAK, and T. J. KASCAK 1985 17 p refs Presented at the Symposium on Optical and Electro-Optical Engineering, Cambridge, Mass., 15-20 Sep. 1985; sponsored by the Society for Photo-Instrumentation Engineering (NASA-TM-87183; E-2835; NAS 1.15:87183) Avail: NTIS HC A02/MF A01 CSCL 09C

Gallium arsenide (GaAs) monolithic microwave integrated circuits (MMIC's) show promise in phased-array antenna applications for future space communications systems. Their efficient usage will depend on the control of amplitude and phase signals for each MMIC element in the phased array and in the low-loss radiofrequency feed. For a phased array containing several MMIC elements a complex system is required to control and feed each element. The characteristics of GaAs MMIC's for 20/30-GHz phased-array systems are discussed. The optical/MMIC interface and the desired characteristics of optical integrated circuits (OIC's) for such an interface are described. Anticipated fabrication considerations for eventual full monolithic integration of optical integrated circuits with MMIC's on a GaAs substrate are presented. E.A.K.

N86-16458*# National Aeronautics and Space Administration. Lewis Research Center, Cleveland, Ohio.

OPTICAL TECHNIQUES TO FEED AND CONTROL GAAS MMIC MODULES FOR PHASED ARRAY ANTENNA APPLICATIONS

K. B. BHASIN, G. ANZIC, R. R. KUNATH, and D. J. CONNOLLY 1986 13 p refs Proposed for presentation at the 11th Communications Satellite Systems Conference, San Diego, Calif., 16-20 Mar. 1986; sponsored by AIAA

(NASA-TM-87218; E-2880; NAS 1.15:87218) Avail: NTIS HC A02/MF A01 CSCL 20N

A complex signal distribution system is required to feed and control GaAs monolithic microwave integrated circuits (MMICs) for phased array antenna applications above 20 GHz. Each MMIC module will require one or more RF lines, one or more bias voltage lines, and digital lines to provide a minimum of 10 bits of combined phase and gain control information. In a closely spaced array, the routing of these multiple lines presents difficult topology problems as well as a high probability of signal interference. To overcome GaAs MMIC phased array signal distribution problems optical fibers interconnected to monolithically integrated optical components with

GaAs MMIC array elements are proposed as a solution. System architecture considerations using optical fibers are described. The analog and digital optical links to respectively feed and control MMIC elements are analyzed. It is concluded that a fiber optic network will reduce weight and complexity, and increase reliability and performance, but higher power will be required. Author

N86-16461*# National Aeronautics and Space Administration. Lewis Research Center, Cleveland, Ohio.

COMPENSATION OF REFLECTOR SURFACE DISTORTIONS USING CONJUGATE FIELD MATCHING

R. J. ACOSTA 1986 9 p refs Proposed for presentation at the International IEEE A/P-S Symposium and National Radio Science Meeting, Philadelphia, Pa., 9-13 Jun. 1986

(NASA-TM-87198; E-2852; NAS 1.15:87198) Avail: NTIS HC A02/MF A01 CSCL 20N

The feasibility of compensating for reflector surface distortions has been investigated. The performance characteristics (gain, sidelobe level, null location, beamwidth, etc.) of space communication reflector antenna systems degrade as the reflector surface distorts due to thermal effects from a varying solar flux. The technique reported here will maintain the design radiation performance independently of thermal effects on the reflector surface. With the advent of monolithic microwave integrated circuits (MMIC), a greater flexibility in array-fed reflector system design can be achieved. MMIC arrays provides independent control of amplitude and phase for each of many radiating elements of the feed array. The conjugate field matching technique provide a basis for obtaining the required element excitations under surface distortion for maintaining the design radiation performance. It is assumed that the surface characteristics (x, y, z, first derivatives, and second derivatives) under distortion are known. Author

N86-17595*# National Aeronautics and Space Administration. Lewis Research Center, Cleveland, Ohio.

TECHNOLOGY ACHIEVEMENTS AND PROJECTIONS FOR COMMUNICATION SATELLITES OF THE FUTURE

J. W. BAGWELL 1986 13 p refs Proposed for presentation at the 11th Communications Satellite Systems Conference, San Diego, Calif., 16-20 Mar. 1986; sponsored by AIAA

(NASA-TM-87201; E-2856; NAS 1.15:87201) Avail: NTIS HC A02/MF A01 CSCL 17B

Multibeam systems of the future using monolithic microwave integrated circuits to provide phase control and power gain are contrasted with discrete microwave power amplifiers from 10 to 75 W and their associated waveguide feeds, phase shifters and power splitters. Challenging new enabling technology areas include advanced electrooptical control and signal feeds. Large scale MMIC's will be used incorporating on chip control interfaces, latching, and phase and amplitude control with power levels of a few watts each. Beam forming algorithms for 80 to 90 deg. wide angle scanning and precise beam forming under wide ranging environments will be required. Satellite systems using these dynamically reconfigured multibeam antenna systems will demand greater degrees of beam interconnectivity. Multiband and multiservice users will be interconnected through the same space platform. Monolithic switching arrays operating over a wide range of RF and IF frequencies are contrasted with current IF switch technology implemented discretely. Size, weight, and performance improvements by an order of magnitude are projected. Author

N86-18585*# National Aeronautics and Space Administration. Lewis Research Center, Cleveland, Ohio.

AN ANALYSIS OF BI-DIRECTIONAL USE OF FREQUENCIES FOR SATELLITE COMMUNICATIONS

W. A. WHYTE, JR., E. F. MILLER, T. SULLIVAN (ORI, Inc., Landover, Md.), and J. E. MILLER (ORI, Inc., Landover, Md.) 1986 19 p refs Prepared for presentation at the 11th Annual Communications Satellite Systems Conference, San Diego, Calif., 16-20 Mar. 1986; sponsored by AIAA (NASA-TM-87226; E-2894; NAS 1.15:87226) Avail: NTIS HC A02/MF A01 CSCL 17B

The bi-directional use of frequencies allocated for space communications has the potential to double the orbit/spectrum capacity available. The technical feasibility of reverse band use (RBU) at C-band (4 GHz uplinks and 6 GHz downlinks) is studied. The analysis identifies the constraints under which both forward and reverse band use satellite systems can share the same frequencies with terrestrial, line of sight transmission systems. The results of the analysis show that RBU satellite systems can be similarly sized to forward band use (FBU) satellite systems. In addition, the orbital separation requirements between RBU and FBU satellite systems are examined. The analysis shows that a carrier to interference ratio of 45 dB can be maintained between RBU and FBU satellites separated by less than 0.5 deg., and that a carrier to interference ratio of 42 dB can be maintained in the antipodal case. Rain scatter propagation analysis shows that RBU and FBU Earth stations require separation distances to less than 10 km at a rain rate of 13.5 mm/hr escalating to less than 100 km at a rain rate of 178 mm/hr for Earth station antennas in the 3 to 10 m range. Author

N86-18586*# National Aeronautics and Space Administration. Lewis Research Center, Cleveland, Ohio.

COMPUTATION OF THE RADIATION CHARACTERISTICS OF A GENERALIZED PHASED ARRAY

R. J. ACOSTA Jan. 1986 29 p refs (NASA-TM-87185; E-2836; NAS 1.15:87185) Avail: NTIS HC A03/MF A01 CSCL 20N

With the advent of monolithic microwave integrated circuit (MMIC) technology, the phased array has become a key component in the design of advanced antenna systems. Array-fed antennas are used extensively in today's multiple beam satellite antennas. A computer program based on a very efficient numerical technique for calculating the radiated power (Romberg integration), directivity, and radiation pattern of a phased array is described. The formulation developed is very general, and takes into account arbitrary element polarization, E- and H-plane element pattern, element location, and complex element excitation. For comparison purposes sample cases have been presented. Excellent agreement has been obtained for all cases. Also included are a user guide and a copy of the computer program. Author

N86-19493*# Ohio State Univ., Columbus. Dept. of Electrical Engineering.

ENGINEERING CALCULATIONS FOR COMMUNICATIONS SATELLITE SYSTEMS PLANNING Interim Report, 16 Jul. 1984 - 15 Jul. 1985

C. H. REILLY, C. A. LEVIS, C. MOUNT-CAMPBELL, D. J. GONSALVEZ, C. W. WANG, and Y. YAMAMURA 1985 46 p refs

(Contract NAG3-159) (NASA-CR-176555; NAS 1.26:176555; REPT-716548-2) Avail: NTIS HC A03/MF A01 CSCL 17B

Computer-based techniques for optimizing communications-satellite orbit and frequency assignments are discussed. A gradient-search code was tested against a BSS scenario derived from the RARC-83 data. Improvement was obtained, but each iteration requires about 50 minutes of IBM-3081 CPU time. Gradient-search experiments on a small FSS test problem, consisting of a single service area served by 8 satellites, showed quickest convergence when the satellites were all initially placed near the center of the available orbital arc with moderate spacing. A transformation technique is proposed for investigating

the surface topography of the objective function used in the gradient-search method. A new synthesis approach is based on transforming single-entry interference constraints into corresponding constraints on satellite spacings. These constraints are used with linear objective functions to formulate the co-channel orbital assignment task as a linear-programming (LP) problem or mixed integer programming (MIP) problem. Globally optimal solutions are always found with the MIP problems, but not necessarily with the LP problems. The MIP solutions can be used to evaluate the quality of the LP solutions. The initial results are very encouraging. Author

N86-19494*# National Aeronautics and Space Administration. Lewis Research Center, Cleveland, Ohio.

RADIOFREQUENCY TESTING OF SATELLITE SEGMENT OF SIMULATED 30/20 GHZ SATELLITE COMMUNICATIONS SYSTEM

R. F. LEONARD and R. KERCZEWSKI (Analex Corp., Cleveland, Ohio) Nov. 1985 26 p refs (NASA-TM-87163; E-2797; NAS 1.15:87163) Avail: NTIS HC A03/MF A01 CSCL 17B

A laboratory communications system has been developed that can serve as a test bed for the evaluation of advanced microwave (30/20 GHz) components produced under NASA technology programs. The system will ultimately permit the transmission of a stream of high-rate (220 Mbps) digital data from the originating user, through a ground terminal, through a hardware-simulated satellite, to a receiving ground station, to the receiving user. This report contains the results of radiofrequency testing of the satellite portion of that system. Data presented include output spurious responses, attainable signal-to-noise ratios, a baseline power budget, usable frequency bands, phase and amplitude response data for each of the frequency bands, and the effects of power level variation. Author

N86-22782*# Case Western Reserve Univ., Cleveland, Ohio. Dept. of Electrical Engineering and Applied Physics.

MUTUAL COUPLING EFFECTS IN ANTENNA ARRAYS, VOLUME 1

Final Technical Report, 15 May 1982 - 31 Mar. 1986

R. E. COLLIN Mar. 1986 178 p refs

(Contract NAG3-291)

(NASA-CR-176699; NAS 1.26:176699; WGR-86-4-VOL-1) Avail: NTIS HC A09/MF A01 CSCL 20N

Mutual coupling between rectangular apertures in a finite antenna array, in an infinite ground plane, is analyzed using the vector potential approach. The method of moments is used to solve the equations that result from setting the tangential magnetic fields across each aperture equal. The approximation uses a set of vector potential model functions to solve for equivalent magnetic currents. A computer program was written to carry out this analysis and the resulting currents were used to determine the co- and cross-polarized far zone radiation patterns. Numerical results for various arrays using several modes in the approximation are presented. Results for one and two aperture arrays are compared against published data to check on the agreement of this model with previous work. Computer derived results are also compared against experimental results to test the accuracy of the model. These tests of the accuracy of the program showed that it yields valid data. Author

N86-23781*# Ohio State Univ., Columbus. ElectroScience Lab. BROADCASTING SATELLITE SERVICE SYNTHESIS USING GRADIENT AND CYCLIC COORDINATE SEARCH PROCEDURES

C. H. REILLY, C. A. MOUNT-CAMPBELL, D. J. GONSALVEZ, C. H. MARTIN, C. A. LEVIS, and C. W. WANG Feb. 1986 39 p refs

(Contract NAG3-159)

(NASA-CR-176708; NAS 1.26:176708; TR-716548-4) Avail: NTIS HC A03/MF A01 CSCL 17B

Two search techniques are considered for solving satellite synthesis problems. Neither is likely to find a globally optimal solution. In order to determine which method performs better and

what factors affect their performance, we design an experiment and solve the same problem under a variety of starting solution configuration-algorithm combinations. Since there is no randomization in the experiment, we present results of practical, rather than statistical, significance. Our implementation of a cyclic coordinate search procedure clearly finds better synthesis solutions than our implementation of a gradient search procedure does with our objective of maximizing the minimum C/I ratio computed at test points on the perimeters of the intended service areas. The length of the available orbital arc and the configuration of the starting solution are shown to affect the quality of the solutions found.

Author

N86-24875* Martin Marietta Aerospace, Denver, Colo.
SATELLITE VOICE BROADCAST. VOLUME 1: EXECUTIVE SUMMARY Final Report, Apr. 1984 - Jun. 1985
 E. E. BACHTELL, S. S. BETTADAPUR, J. V. COYNER, and C. E. FARRELL Nov. 1985 17 p refs
 (Contract NAS3-24233)
 (NASA-CR-175016; NAS 1.26:175016) Avail: NTIS HC A02/MF A01 CSCL 17B

An Executive Summary of the Satellite Voice Broadcast System Study designs are synthesized for direct sound broadcast satellite systems for HF-, VHF-, and Ku-bands. Methods are developed and used to predict satellite weight, volume, and RF performance for the various concepts considered. Cost and schedule risk assessments are performed to predict time and cost required to implement selected concepts. Technology assessments and tradeoffs are made to identify critical enabling technologies that require development to bring technical risk to acceptable levels for full scale development.

Author

N86-24876* Martin Marietta Aerospace, Denver, Colo.
SATELLITE VOICE BROADCAST. VOLUME 2: SYSTEM STUDY Final Report, Apr. 1984 - Jun. 1985
 E. E. BACHTELL, S. S. BETTADAPUR, J. V. COYNER, and C. E. FARRELL Nov. 1985 261 p refs 2 Vol.
 (Contract NAS3-24233)
 (NASA-CR-175017; NAS 1.26:175017; MTR-85-556-VOL-2)
 Avail: NTIS HC A12/MF A01 CSCL 17B

The Technical Volume of the Satellite Broadcast System Study is presented. Designs are synthesized for direct sound broadcast satellite systems for HF-, VHF-, L-, and Ku-bands. Methods are developed and used to predict satellite weight, volume, and RF performance for the various concepts considered. Cost and schedule risk assessments are performed to predict time and cost required to implement selected concepts. Technology assessments and tradeoffs are made to identify critical enabling technologies that require development to bring technical risk to acceptable levels for full scale development.

Author

N86-24877* TRW Space Technology Labs., Redondo Beach, Calif. Federal Systems Div.
SATELLITE VOICE BROADCAST SYSTEM STUDY, VOLUME 2 Technical Report, 11 Apr. 1984 - 11 Jul. 1985
 M. HORSTEIN Jul. 1985 335 p refs 3 Vol.
 (Contract NAS3-24232)
 (NASA-CR-174905; NAS 1.26:174905) Avail: NTIS HC A15/MF A01 CSCL 17B

This study investigates the feasibility of providing Voice of America (VOA) broadcasts by satellite relay, rather than via terrestrial relay stations. Satellite voice broadcast systems are described for three different frequency bands: HF (26 MHz), VHF (68 MHz), and L-band (1.5 GHz). The geographical areas of interest at HF and L-band include all major land masses worldwide with the exception of the U.S., Canada, and Australia. Geostationary satellite configurations are considered for both frequency bands. In addition, a system of subsynchronous, circular satellites with an orbit period of 8 hours is developed for the HF band. VHF broadcasts, which are confined to the Soviet Union, are provided by a system of Molniya satellites. Satellites intended for HF or VHF broadcasting are extremely large and heavy. Satellite designs presented here are limited in size and weight to the capability of

the STS/Centaur launch vehicle combination. Even so, at HF it would take 47 geostationary satellites or 20 satellites in 8-hour orbits to fully satisfy the voice-channel requirements of the broadcast schedule provided by VOA. On the other hand, three Molniya satellites suffice for the geographically restricted schedule at VHF. At L-band, only four geostationary satellites are needed to meet the requirements of the complete broadcast schedule. Moreover, these satellites are comparable in size and weight to current satellites designed for direct broadcast of video program material.

Author

N86-24878* TRW, Inc., Redondo Beach, Calif.
SATELLITE VOICE BROADCAST SYSTEM STUDY. VOLUME 1: EXECUTIVE SUMMARY Contractor Report, 11 Apr. 1984 - 11 Jul. 1985
 M. HORSTEIN Jul. 1985 46 p , 1-45 NOV.
 (Contract NAS3-24232)
 (NASA-CR-174904; NAS 1.26:174904) Avail: NTIS HC A03/MF A01 CSCL 17B

The feasibility of providing Voice of America (VOA) broadcasts by satellite relay was investigated. Satellite voice broadcast systems are described for three different frequency bands: HF, FHV, and L-band. Geostationary satellite configurations are considered for both frequency bands. A system of subsynchronous, circular satellites with an orbit period of 8 hours was developed for the HF band. The VHF broadcasts are provided by a system of Molniya satellites. The satellite designs are limited in size and weight to the capability of the STS/Centaur launch vehicle combination. At L-band, only four geostationary satellites are needed to meet the requirements of the complete broadcast schedule. These satellites are comparable in size and weight to current satellites designed for the direct broadcast of video program material.

Author

N86-24881* National Aeronautics and Space Administration. Lewis Research Center, Cleveland, Ohio.
IMPACT OF THE 1985 SPACE WORLD ADMINISTRATIVE RADIO CONFERENCE ON FREQUENCY/ORBIT PLANNING AND USE
 E. F. MILLER 1986 8 p refs Presented at the 11th Annual Communications Satellite Systems Conference, San Diego, Calif., 16-20 Mar. 1986; sponsored by the American Inst. of Aeronautics and Astronautics
 (NASA-TM-87285; E-2976; NAS 1.15:87285) Avail: NTIS HC A02/MF A01 CSCL 17B

The 1985 World Administrative Radio Conference (WARC-ORB-85) was held to determine which space radio services should be planned and which planning methods should be used. The second session of this Conference (WARC-ORB-88) will meet to develop the required plans. This paper presents the results of WARC-ORB-85, assesses the impact of those decisions, and identifies the intersessional work to be conducted by administrations and the CCIR (Consultative Committee on International Radio). The major decisions of WARC-ORB-85 were: (1) the restriction of additional planning to the fixed satellite service at identified frequencies; and (2) the selection of a planning method consisting of two parts (a) an allotment plan, and (b) improved procedures. The paper also discusses WARC-ORB-85 decisions relative to the Region 2 broadcast satellite service plans at 12 GHz, feederlink planning for Regions 1 and 3 broadcast satellites at 12 GHz, and sound broadcast satellite service.

Author

N86-25650* National Aeronautics and Space Administration. Lewis Research Center, Cleveland, Ohio.
NEAR-FIELD SPILLOVER FROM A SUBREFLECTOR: THEORY AND EXPERIMENT
 S. W. LEE (Illinois Univ., Urbana-Champaign), R. ACOSTA, A. R. CHERRETTE, and P. T. LAM (Lockheed Missiles and Space Co., Sunnyvale, Calif.) May 1986 32 p refs
 (Contract NAG3-419)
 (NASA-TM-88763; NAS 1.15:88763; ELR-86-5;
 UILU-ENG-86-2547) Avail: NTIS HC A03/MF A01 CSCL 20N

In a dual reflector antenna, the spillover from the subreflector is important in determining the accuracy of near-field

32 COMMUNICATIONS AND RADAR

measurements. This is especially so when some of the feed elements are placed far away from the focus. A high-frequency GTD analysis of the spillover field over a plane just behind the subreflector is presented. Special attention is given to the field near the incident shadow boundary and the role played by the slope diffraction term. Computations are in excellent agreement with experimental results. Author

N86-26489*# Operations Research, Inc., Silver Spring, Md.
SPECTRUM ORBIT UTILIZATION PROGRAM TECHNICAL MANUAL SOUP5 VERSION 3.8

J. DAVIDSON, H. R. OTTEY, P. SAWITZ, and F. S. ZUSMAN
13 Dec. 1984 77 p refs
(Contract NAS3-22885)
(NASA-CR-174944; NAS 1.26:174944; TR-2390) Avail: NTIS
HC A05/MF A01 CSCL 17B

The underlying engineering and mathematical models as well as the computational methods used by the SOUP5 analysis programs, which are part of the R2BCSAT-83 Broadcast Satellite Computational System, are described. Included are the algorithms used to calculate the technical parameters and references to the relevant technical literature. The system provides the following capabilities: requirements file maintenance, data base maintenance, elliptical satellite beam fitting to service areas, plan synthesis from specified requirements, plan analysis, and report generation/query. Each of these functions are briefly described. B.G.

N86-30037*# Illinois Univ., Urbana. Electromagnetic Communication Lab.

MMIC DEVICES FOR ACTIVE PHASED ARRAY ANTENNAS Final Report

R. MITTRA 31 Jul. 1986 61 p
(Contract NCC3-8)
(NASA-CR-176990; NAS 1.26:176990) Avail: NTIS HC A04/MF A01 CSCL 20N

The use of finlines for microwave monolithic integrated circuit application in the 20 to 40 GHz frequency range. Other wave guiding structures, are also examined from a comparative point of view and some conclusions are drawn on the basis of the results.

N86-30039*# Illinois Univ., Urbana-Champaign. Electromagnetics Lab.

A SIMPLE CIRCULAR-POLARIZED ANTENNA: CIRCULAR WAVEGUIDE HORN COATED WITH LOSSY MAGNETIC MATERIAL

C. S. LEE, S. W. LEE, and D. W. JUSTICE Aug. 1986 32 p
(Contract NAG3-475)
(NASA-CR-177092; NAS 1.26:177092; UILU-ENG-86-2554; ELSR-86-8) Avail: NTIS HC A03/MF A01 CSCL 20N

A circular waveguide horn coated with a lossy material in its interior wall can be used as an alternative to a corrugated waveguide for radiating a circularly polarized (CP) field. To achieve good CP radiation, the diameter of the structure must be larger than the free-space wavelength, and the coating material must be sufficiently lossy and magnetic. This device is cheaper and lighter in weight than the corrugated one. Author

N86-31760*# Ford Aerospace and Communications Corp., Palo Alto, Calif. Western Development Labs. Div.

SPACECRAFT MULTIBEAM ANTENNA SYSTEM FOR 30/20 GHZ Final Report

T. E. ROBERTS and W. F. SCOTT 10 Jan. 1984 70 p
(Contract NAS3-22498)
(NASA-CR-174654; NASA4-1-5-Z-F; NAS 1.26:174654; WDL-TR-10138) Avail: NTIS HC A04/MF A01 CSCL 17B

The major technical tasks that led to the definitions of operational and demonstration multiple beam antenna (MBA) flight systems and a proof of concept model (POC) are described. Features of the POC Model and its measured performance are presented in detail. Similar MBA's are proposed for transmitting and receiving with the POC Model representing the 20 GHz transmitting antenna. This POC MBA is a dual shaped-surface reflector system utilizing a movable free array to simulate complete

CONUS coverage. The beam forming network utilizes ferrite components for switching from one beam to another. Measured results for components, subsystems and the complete MBA confirm the feasibility of the approach and also show excellent correlation with calculated values. Author

N86-32598*# National Aeronautics and Space Administration. Lewis Research Center, Cleveland, Ohio.

NEAR-FIELD SPILLOVER FROM A SUBREFLECTOR: THEORY AND EXPERIMENT

S. W. LEE (Illinois Univ., Urbana), R. ACOSTA, A. R. CHERRETTE, and P. T. LAM (Lockheed Missiles and Space Co., Sunnyvale, Calif.) Sep. 1986 20 p
(Contract NAG-419)
(NASA-TM-88818; E-3178; NAS 1.15:88818) Avail: NTIS HC A02/MF A01 CSCL 20N

In a dual reflector antenna, the spillover from the subreflector is important in determining the accuracy of near-field measurements. This is especially so when some of the feed elements are placed far away from the focus. In this paper, we present a high-frequency GTD analysis of the spillover field over a plane just behind the subreflector. Special attention is given to the field near the incident shadow boundary and the role played by the slope diffraction term. Our computations are in excellent agreement with experimental results. Author

N86-32600*# Ohio State Univ., Columbus. ElectroScience Lab.
A HIGH FREQUENCY ANALYSIS OF ELECTROMAGNETIC PLANE WAVE SCATTERING BY PERFECTLY-CONDUCTING SEMI-INFINITE PARALLEL PLATE AND RECTANGULAR WAVEGUIDES WITH ABSORBER COATED INNER WALLS

H. M. NOH and P. H. PATHAK Sep. 1986 218 p
(Contract NAG3-476)
(NASA-CR-179759; NAS 1.26:179759; TR-715723-1) Avail: NTIS HC A10/MF A01 CSCL 20N

An approximate but sufficiently accurate high frequency solution which combines the uniform geometrical theory of diffraction (UTD) and the aperture integration (AI) method is developed for analyzing the problem of electromagnetic (EM) plane wave scattering by an open-ended, perfectly-conducting, semi-infinite hollow rectangular waveguide (or duct) with a thin, uniform layer of lossy or absorbing material on its inner wall, and with a planar termination inside. In addition, a high frequency solution for the EM scattering by a two dimensional (2-D), semi-infinite parallel plate waveguide with a absorber coating on the inner walls is also developed as a first step before analyzing the open-ended semi-infinite three dimensional (3-D) rectangular waveguide geometry. The total field scattered by the semi-infinite waveguide consists firstly of the fields scattered from the edges of the aperture at the open-end, and secondly of the fields which are coupled into the waveguide from the open-end and then reflected back from the interior termination to radiate out of the open-end. The first contribution to the scattered field can be found directly via the UTD ray method. The second contribution is found via the AI method which employs rays to describe the fields in the aperture that arrive there after reflecting from the interior termination. It is assumed that the direction of the incident plane wave and the direction of observation lie well inside the forward half space that exists outside the half space containing the semi-infinite waveguide geometry. Also, the medium exterior to the waveguide is assumed to be free space. Author

ELECTRONICS AND ELECTRICAL ENGINEERING

Includes test equipment and maintainability; components, e.g., tunnel diodes and transistors; microminiaturization; and integrated circuitry.

A86-11998* Illinois Univ., Urbana.

CRYOGENIC OPERATION OF PSEUDOMORPHIC ALGAAS/IN-GAAS SINGLE-QUANTUM-WELL MODFETS
W. T. MASSELINK, A. KETTERSON, J. KLEM, W. KOPP, and H. MORKOC (Illinois, University, Urbana) Electronics Letters (ISSN 0013-5194), vol. 21, Sept. 26, 1985, p. 937-939. USAF-supported research. refs
(Contract NAG3-613)

The 77 K operation of AlGaAs/InGaAs MODFETs has been investigated. The structures, grown by MBE, make use of a 200 Å undoped In(0.15)Ga(0.85)As quantum well for electron confinement and an Si-doped Al(0.15)Ga(0.85)As top barrier. The MODFETs with 1 micron gate lengths exhibit extrinsic transconductances of 360 mS/mm and maximum currents of 310 mA/mm at 77 K. The use of a low Al mole fraction AlGaAs/InGaAs heterojunction makes it possible to avoid the persistent trapping effects encountered in AlGaAs/GaAs MODFETs without sacrificing device performance.

Author

A86-14481*# Virginia Polytechnic Inst. and State Univ., Blacksburg.

RESONANT POWER PROCESSORS. I - STATE PLANE ANALYSIS
R. ORUGANTI and F. C. LEE (Virginia Polytechnic Institute and State University, Blacksburg) IEEE and Industrial Applications Society, Meeting, 19th, Chicago, IL, Sept. 30-Oct. 4, 1984, Paper. 8 p. refs
(Contract NAG3-405)

State-plane techniques in conjunction with piecewise-linear analysis is employed to study the steady-state and transient characteristics of a series resonant converter. With the direct viewing of the resonant tank energy and the device switching instants, the state portrayal provides unique insights into the complex behavior of the converter. Operation of the converter under both continuous and discontinuous current modes and at frequencies both below and above resonant frequency are discussed.

Author

A86-14482*# Virginia Polytechnic Inst. and State Univ., Blacksburg.

RESONANT POWER PROCESSORS. II - METHODS OF CONTROL
R. ORUGANTI and F. C. LEE (Virginia Polytechnic Institute and State University, Blacksburg) IEEE and Industrial Applications Society, Meeting, 19th, Chicago, IL, Sept. 30-Oct. 4, 1984, Paper. 11 p. refs
(Contract NAG3-405)

The nature of resonant converter control is discussed. Employing the state-portrait, different control methods for series resonant converter are identified and their performance evaluated based on their stability, response to control and load changes and range of operation. A new control method, optimal-trajectory control, is proposed which, by utilizing the state trajectories as control laws, continuously monitors the energy level of the resonant tank. The method is shown to have superior control properties especially under transient operation.

Author

A86-18814* Illinois Univ., Urbana.

HIGH TRANSCONDUCTANCE INGAAS/ALGAAS PSEUDOMORPHIC MODULATION-DOPED FIELD-EFFECT TRANSISTORS
A. KETTERSON, M. MOLONEY, W. T. MASSELINK, J. KLEM, R. FISCHER (Illinois, University, Urbana) et al. IEEE Electron Device Letters (ISSN 0741-3106), vol. EDL-6, Dec. 1985, p. 628-630. USAF-supported research. refs
(Contract NAG3-613)

Pseudomorphic In_{0.15}Ga_{0.85}As/Al_{0.15}Ga_{0.85}As modulation-doped field effect transistors (MODFET's) exhibiting extremely good dc characteristics have been successfully fabricated. The dc transconductance in these strained-layer structures of 270 mS/mm was measured for 1-micron gate, normally-on devices at 300 K. Maximum drain current levels are 290 mA/mm, with excellent pinch-off and saturation characteristics. The transconductance increased to 360 mS/mm at 77 K while no persistent photoconductivity or drain collapse was observed. Preliminary microwave results indicate a 300-K current gain cutoff frequency of about 20 GHz. These results are equivalent to the best GaAs/AlGaAs MODFET results and are due in part to the improved transport properties and carrier confinement in the InGaAs quantum well.

Author

A86-24811* National Aeronautics and Space Administration, Lewis Research Center, Cleveland, Ohio.

PERFORMANCE ANALYSIS OF RADIATION COOLED DC TRANSMISSION LINES FOR HIGH POWER SPACE SYSTEMS
G. E. SCHWARZE (NASA, Lewis Research Center, Cleveland, OH) IN: Intersociety Energy Conversion Engineering Conference, 20th, Miami Beach, FL, August 18-23, 1985, Proceedings. Volume 1. Warrendale, PA, Society of Automotive Engineers, Inc., 1985, p. 1.252-1.269. Previously announced in STAR as N85-28222.

As space power levels increase to meet mission objectives and also as the transmission distance between power source and load increases, the mass, volume, power loss, and operating voltage and temperature become important system design considerations. This analysis develops the dependence of the specific mass and percent power loss on the power and voltage levels, transmission distance, operating temperature and conductor material properties. Only radiation cooling is considered since the transmission line is assumed to operate in a space environment. The results show that the limiting conditions for achieving low specific mass, percent power loss, and volume for a space-type dc transmission line are the permissible transmission voltage and operating temperature. Other means to achieve low specific mass include the judicious choice of conductor materials. The results of this analysis should be immediately applicable to power system trade-off studies including comparisons with ac transmission systems.

Author

A86-24831* Toledo Univ., Ohio.

INVERTER DESIGN FOR HIGH FREQUENCY POWER DISTRIBUTION
R. J. KING (Toledo, University, Ohio) IN: Intersociety Energy Conversion Engineering Conference, 20th, Miami Beach, FL, August 18-23, 1985, Proceedings. Volume 1. Warrendale, PA, Society of Automotive Engineers, Inc., 1985, p. 1.394-1.399. refs
(Contract NAG3-418)

A class of simple resonantly commutated inverters are investigated for use in a high power (100 KW - 1000 KW) high frequency (10 KHz - 20 KHz) AC power distribution system. The Mapham inverter is found to provide a unique combination of large thyristor turn-off angle and good utilization factor, much better than an alternate 'current-fed' inverter. The effects of loading the Mapham inverter entirely with rectifier loads are investigated by simulation and with an experimental 3 KW 20 KHz inverter. This inverter is found to be well suited to a power system with heavy rectifier loading.

Author

A86-24844* TRW Space Technology Labs., Redondo Beach, Calif.

10 KW SOLAR ARRAY SWITCHING UNIT PERFORMANCE TEST RESULTS

G. W. FLECK, J. W. LEPISTO (TRW, Inc., Space and Technology Group, Redondo Beach, CA), and M. FORKOSH (NASA, Lewis Research Center, Cleveland, OH) IN: Intersociety Energy Conversion Engineering Conference, 20th, Miami Beach, FL, August 18-23, 1985, Proceedings. Volume 1. Warrendale, PA, Society of Automotive Engineers, Inc., 1985, p. 1.486-1.491.

Solar array switching unit (SASU) technology is an attractive candidate for output power regulation of solar arrays. It offers greater efficiency, lower parts count, modularity and expandability. Since the SASU has switching frequencies upwards of 15 kHz, it was necessary to determine the performance characteristics of the SASU with a real solar array and to assess the impact of long lead lengths on the switching characteristics. To accommodate these requirements, TRW developed a 10 kW, 120 volt SASU which was tested for steady state and transient resistive and converter type loadings. The results of these tests are presented and discussed in this paper. Author

A86-25525* Systems Science and Software, La Jolla, Calif. **THE ROLE OF UNNEUTRALIZED SURFACE IONS IN NEGATIVE POTENTIAL ARCING**

G. A. JONGEWARD, I. KATZ, M. J. MANDELL, and D. E. PARKS (Systems Science and Software, La Jolla, CA) (IEEE, DNA, Sandia National Laboratories, and NASA, 1985 Annual Conference on Nuclear and Space Radiation Effects, 22nd, Monterey, CA, July 22-24, 1985) IEEE Transactions on Nuclear Science (ISSN 0018-9499), vol. NS-32, Dec. 1985, p. 4087-4091. refs (Contract NAS3-23881)

The observed arcing on negatively biased solar arrays exposed to plasma environments is shown to be due to an effective charge layer on the interconnect formed by ion collection from the plasma. Time scales to form this layer are shown to be in agreement with experimental observations. A quantitative theory is presented which predicts arcing threshold dependence on plasma density and external potentials. After breakdown, the discharge process is modeled as space charge limited transport to nearby coverslips. Peak currents and decay times predicted by this model are compared with experimental observations. Author

A86-26051* Tuskegee Inst., Ala. **CHARACTERISATION OF PLASMA IN A RAIL GUN**

P. K. RAY (Tuskegee Institute, AL) IEE Proceedings, Part A - Physical Science, Measurement and Instrumentation, Management and Education, Reviews (ISSN 0143-702X), vol. 133, pt. A, no. 1, Jan. 1986, p. 38-44. refs (Contract NAG3-76)

The mechanism of plasma and projectile acceleration in a DC rail gun is described from a microscopic point of view through the establishment of the Hall field. The plasma conductivity is shown to be a tensor, indicating that there is a small component of current parallel to the direction of acceleration. The plasma characteristics are evaluated in the experiment of Bauer et. al., as a function of plasma mass through a simple fluid mechanical analysis of the plasma. By equating the energy dissipated in the plasma with the radiation heat loss, the properties of the plasma are determined. Author

A86-34882* Texas Instruments, Inc., Dallas. **10-30 GHZ MONOLITHIC GAAS TRAVELLING-WAVE DIVIDER/COMBINER**

H. Q. TSERNG and P. SAUNIER (Texas Instruments Control Research Laboratories, Dallas) Electronics Letters (ISSN 0013-5194), vol. 21, Oct. 10, 1985, p. 950, 951. (Contract NAS3-23781)

A four-way monolithic GaAs traveling-wave power divider/combiner has been designed, fabricated and evaluated. With a design center frequency of 20 GHz, a bandwidth of from 10 GHz to 30 GHz has been measured. The insertion loss per dividing or combining action is less than 0.5 dB, with isolation

between ports no worse than 20 dB. The input/output VSWRs are better than 2:1 across the same band. This divider/combiner can readily be used with monolithic GaAs power FET amplifiers to produce a several-fold increase in output powers over the 10 to 30 GHz frequency range. Author

A86-35718* Virginia Polytechnic Inst. and State Univ., Blacksburg.

NONDESTRUCTIVE CHARACTERIZATION OF RBSOA OF HIGH-POWER BIPOLAR TRANSISTORS

M. M. JOVANOVIĆ, F. C. LEE, and D. Y. CHEN (Virginia Polytechnic Institute and State University, Blacksburg) (IEEE, Annual Power Electronics Specialists Conference, 16th, Toulouse, France, June 24-28, 1985) IEEE Transactions on Aerospace and Electronic Systems (ISSN 0018-9251), vol. AES-22, March 1986, p. 138-145. refs

(Contract NAG3-99; JPL-956684)

Reverse-bias safe operating area (RBSOA) of high-power Darlington transistors is characterized using a 120 A/1000 V nondestructive reverse-bias second breakdown tester designed and fabricated at Virginia Polytechnic Institute and State University. Elaborate RBSOA characteristics are generated with different forward/reverse base drives and collector current levels. The effects of elevated case temperature and second-base drive on RBSOA of four-terminal Darlington devices are also discussed. Author

A86-36009* Illinois Univ., Urbana-Champaign. **DC AND MICROWAVE CHARACTERISTICS OF A HIGH CURRENT DOUBLE INTERFACE GAAS/INGAAS/ALGAAS PSEUDOMORPHIC MODULATION-DOPED FIELD-EFFECT TRANSISTOR**

T. HENDERSON, J. KLEM, C. K. PENG, J. S. GEDYMIN, W. KOPP (Illinois, University, Urbana) et al. Applied Physics Letters (ISSN 0003-6951), vol. 48, April 21, 1986, p. 1080-1082. USAF-supported research. refs (Contract NAG3-613)

Extremely large current double interface GaAs/In(0.15)-Ga(0.85)As/Al(0.15)Ga(0.85)As pseudomorphic modulation-doped field-effect transistors (MODFET's) grown by molecular beam epitaxy were achieved. The 1-micron gate devices studied have peak current levels (430 mA/mm at 300 K and 483 mA/mm at 77 K) roughly one and a half to two times that found in single interface pseudomorphic MODFET's. These devices also retain high transconductances over a broad range of gate voltage, peaking at 312 mS/mm at 300 K and 362 mS/mm at 77 K. Excellent microwave performance is also obtained with a maximum frequency of oscillation (f-max) of 37 GHz and a current gain cut-off frequency of as high as 23 GHz at 300 K. An output power level of 14 dBm (1 dB gain compression) was obtained at 6 GHz for a 290-micron gate width. This double interface single quantum well MODFET may be of great importance in millimeter wave power amplifiers. Author

A86-37295* Illinois Univ., Urbana. **DETERMINATION OF CARRIER SATURATION VELOCITY IN HIGH-PERFORMANCE IN(Y)GA(1-Y)AS/AL(X)GA(1-X)AS MODULATION-DOPED FIELD-EFFECT TRANSISTORS (WITH Y BETWEEN 0 AND 0.2)**

T. S. HENDERSON, W. T. MASSELINK, W. KOPP, and H. MORKOC (Illinois, University, Urbana) IEEE Electron Device Letters (ISSN 0741-3106), vol. EDL-7, May 1986, p. 288-290. USAF-supported research. refs (Contract NAG3-613)

The relation between the intrinsic transconductance per unit gate width and the carrier saturation velocity, v_{sat} , is used to determine v_{sat} for several high-performance pseudomorphic MODFET's with different InAs mole fractions (y). Measurements of $\ln(y)Ga(1-y)As/AlGaAs$ MODFET's grown by MBE were found to give accurate v_{sat} values at 77 K. Devices with y between 0 and 0.20 were shown to have higher v_{sat} than conventional GaAs/AlGaAs MODFET's. An optimum y value for peak v_{sat} ,

which may optimize overall device performance, is expected.

R.R.

A86-39472*# National Aeronautics and Space Administration. Lewis Research Center, Cleveland, Ohio.

A MATHEMATICAL MODEL FOR THE DOUBLY-FED WOUND ROTOR GENERATOR. II

F. J. BRADY (NASA, Lewis Research Center, Cleveland, OH) IEEE Transactions on Energy Conversion (ISSN 0885-8969), vol. EC-1, June 1986, p. 180-183. Previously announced in STAR as N84-17479. refs

A mathematical analysis of a doubly-fed wound rotor generator is presented. The constraints of constant stator voltage and frequency to the circuit equations were applied and expressions for the currents and voltages in the machine obtained. The derived variables are redefined as direct and quadrature components. In addition, the apparent (complex) power for both the rotor and the stator are derived in terms of these redefined components.

Author

A86-40431* Virginia Polytechnic Inst. and State Univ., Blacksburg.

STATE-PLANE ANALYSIS OF PARALLEL RESONANT CONVERTER

R. ORUGANTI and F. C. LEE (Virginia Polytechnic Institute and State University, Blacksburg) IN: PESC '85; Annual Power Electronics Specialists Conference, 16th, Toulouse, France, June 24-28, 1985, Record. New York, Institute of Electrical and Electronics Engineers, Inc., 1985, p. 56-73. refs (Contract NAG3-551)

A method for analyzing the complex operation of a parallel resonant converter is developed, utilizing graphical state-plane techniques. The comprehensive mode analysis uncovers, for the first time, the presence of other complex modes besides the continuous conduction mode and the discontinuous conduction mode and determines their theoretical boundaries. Based on the insight gained from the analysis, a novel, high-frequency resonant buck converter is proposed. The voltage conversion ratio of the new converter is almost independent of load.

Author

A86-40449*# National Aeronautics and Space Administration. Lewis Research Center, Cleveland, Ohio.

A NEW VERY HIGH VOLTAGE SEMICONDUCTOR SWITCH

G. R. SUNDBERG (NASA, Lewis Research Center, Cleveland, OH) IN: PESC '85; Annual Power Electronics Specialists Conference, 16th, Toulouse, France, June 24-28, 1985, Record. New York, Institute of Electrical and Electronics Engineers, Inc., 1985, p. 273-279. Previously announced in STAR as N85-20246. refs

A new family of semiconductor switches using double injection techniques and compensated deep impurities is described. They have the potential to raise switching voltages a factor of 10 higher (up to 100 kV) than p-n junction devices while exhibiting extremely low (or zero) forward voltage. Several potential power switching applications are indicated.

E.A.K.

A86-40462* Toledo Univ., Ohio.

ROTARY TRANSFORMER DESIGN WITH FIXED MAGNETIZING AND/OR LEAKAGE INDUCTANCES

T. A. STUART, R. J. KING, and H. SHAMSEDDIN (Toledo, University, OH) IN: PESC '85; Annual Power Electronics Specialists Conference, 16th, Toulouse, France, June 24-28, 1985, Record. New York, Institute of Electrical and Electronics Engineers, Inc., 1985, p. 480-487. refs (Contract NAG3-478)

A design algorithm is considered for transformers that must transfer electric power across a rotating interface. Among other features, this procedure allows the designer to minimize either weight or losses for either a fixed magnetizing inductance or a fixed leakage inductance. Numerical results are included to indicate the design trade-offs between various parameters.

Author

A86-41343* Honeywell, Inc., Bloomington, Minn.

KA-BAND MONOLITHIC GAIN CONTROL AMPLIFIER

J. GEDDES, V. SOKOLOV, and T. CONTOLATIS (Honeywell, Inc., Bloomington, MN) Electronics Letters (ISSN 0013-5194), vol. 22, April 24, 1986, p. 503, 504. (Contract NAS3-23356)

A monolithic gain control amplifier for Ka-band has been developed based on 0.25 micron-gate-length dual-gate FETs fabricated on ion-implanted material. A single-stage monolithic amplifier gives a gain of 6 dB at 31 GHz including fixture losses with a gain control range of over 20 dB. The device and IC design and fabrication are described.

Author

A86-43914* Illinois Univ., Urbana.

HIGH-FREQUENCY NOISE OF $\text{In}(y)\text{Ga}(1-y)\text{As}/\text{Al}(x)\text{Ga}(1-x)\text{As}$ MODFETS AND COMPARISON TO $\text{GaAs}/\text{Al}(x)\text{Ga}(1-x)\text{As}$ MODFETS

H. MORKOC, T. HENDERSON, W. KOPP, and C. K. PENG (Illinois, University, Urbana) Electronics Letters (ISSN 0013-5194), vol. 22, May 22, 1986, p. 578-580. USAF-supported research. refs (Contract NAG3-613)

Noise parameter measurements for recently developed 1 micron gate $\text{In}(y)\text{Ga}(1-y)\text{As}/\text{Al}(0.15)\text{Ga}(0.85)\text{As}$ MODFETs have been performed at 8 GHz at room and cryogenic temperatures. Owing to the relatively small $C(\text{gs/sq rt})/g(\text{m})$ ratio in these devices compared to identical conventional $\text{GaAs}/\text{AlGaAs}$ MODFETs, both room- and cryogenic temperature noise figures have been reduced. In addition, the light sensitivity and drift in noise figure at cryogenic temperatures observed in conventional $\text{GaAs}/\text{AlGaAs}$ MODFETs have been substantially reduced.

Author

A86-44078* Illinois Univ., Urbana.

NORMAL MODES IN AN OVERMODED CIRCULAR WAVEGUIDE COATED WITH LOSSY MATERIAL

C. S. LEE, S.-W. LEE, and S.-L. CHUANG (Illinois, University, Urbana) IEEE Transactions on Microwave Theory and Techniques (ISSN 0018-9480), vol. MTT-34, July 1986, p. 773-785. refs (Contract NAG3-475)

The normal modes in an overmoded waveguide coated with a lossy material are analyzed, particularly for their attenuation properties as a function of coating material, layer thickness, and frequency. When the coating material is not too lossy, the low-order modes are highly attenuated even with a thin layer of coating. This coated guide serves as a mode suppressor of the low-order modes, which can be particularly useful for reducing the radar cross section of a cavity structure such as a jet engine inlet. When the coating material is very lossy, low-order modes fall into two distinct groups: highly and lowly attenuated modes. However, as a/λ (a = radius of the cylinder; λ = the free-space wavelength) increases, the separation between these two groups becomes less distinctive. The attenuation constants of most of the low-order modes become small and decrease as a function of λ^2/a^2 .

Author

A86-45194*# National Aeronautics and Space Administration. Lewis Research Center, Cleveland, Ohio.

VERIFICATION OF AN IMPROVED COMPUTATIONAL DESIGN PROCEDURE FOR TWT-DYNAMIC REFOCUSER-MDC SYSTEMS WITH SECONDARY ELECTRON EMISSION LOSSES

P. RAMINS, D. A. FORCE, R. W. PALMER, J. A. DAYTON, JR. (NASA, Lewis Research Center, Cleveland, OH), and H. G. KOSMAHL (Analex Corp., Cleveland, OH) IEEE Transactions on Electron Devices (ISSN 0018-9383), vol. ED-33, Jan. 1986, p. 85-90.

A computational procedure for the design of TWT-refocuser-MDC systems was used to design a short 'dynamic' refocusing system and highly efficient four-stage depressed collector for a 200-W 8-18-GHz TWT. The computations were carried out with advanced multidimensional computer programs which model the electron beam as a series of disks of charge and follow their trajectories from the RF input of the TWT, through the slow-wave structure and refocusing section, to their points of impact in the depressed collector. Secondary emission losses in

the MDC were treated semiquantitatively by injecting a representative beam of secondary electrons into the MDC analysis at the point of impact of each primary beam. A comparison of computed and measured TWT and MDC performance showed very good agreement. The electrodes of the MDC were fabricated from a particular form of isotropic graphite that was selected for its low secondary electron yield, thermal expansion characteristics, ease of machinability and vacuum properties. This MDC was tested at CW for more than 1000 h with negligible degradation in TWT and MDC performances. Author

A86-45195* National Aeronautics and Space Administration. Lewis Research Center, Cleveland, Ohio.

VOLTAGE-CONTROLLING MECHANISMS IN LOW-RESISTIVITY SILICON SOLAR CELLS - A UNIFIED APPROACH

V. G. WEIZER, C. K. SWARTZ, R. E. HART, and M. P. GODLEWSKI (NASA, Lewis Research Center, Cleveland, OH) IEEE Transactions on Electron Devices (ISSN 0018-9383), vol. ED-33, Jan. 1986, p. 156-158. refs

An experimental technique is used to determine the relative values of the base and emitter components of the dark saturation current of six types of high-voltage low-resistivity silicon solar cells. One of the surprising findings is the suggestion that the magnitude of the minority-carrier mobility may be process-dependent. Author

A86-46638* Illinois Univ., Urbana.

INPUT IMPEDANCE OF A PROBE-FED CIRCULAR MICROSTRIP ANTENNA WITH THICK SUBSTRATE

M. DAVIDOVITZ and Y. T. LO (Illinois, University, Urbana) IEEE Transactions on Antennas and Propagation (ISSN 0018-926X), vol. AP-34, July 1986, p. 905-911. refs (Contract NAG3-418)

A method of computing the input impedance for the probe fed circular microstrip antenna with thick dielectric substrate is presented. Utilizing the framework of the cavity model, the fields under the microstrip patch are expanded in a set of modes satisfying the boundary conditions on the eccentrically located probe, as well as on the cavity magnetic wall. A mode-matching technique is used to solve for the electric field at the junction between the cavity and the coaxial feed cable. The reflection coefficient of the transverse electromagnetic (TEM) mode incident in the coaxial cable is determined, from which the input impedance of the antenna is computed. Measured data are presented to verify the theoretical calculations. Results of the computation of various losses for the circular printed antenna as a function of substrate thickness are also included. Author

A86-46649* National Aeronautics and Space Administration. Lewis Research Center, Cleveland, Ohio.

CONVENIENT MOUNTING METHOD FOR ELECTRICAL MEASUREMENTS OF THIN SAMPLES

L. G. MATUS and R. L. SUMMERS (NASA, Lewis Research Center, Cleveland, OH) Review of Scientific Instruments (ISSN 0034-6748), vol. 57, July 1986, p. 1437, 1438.

A method for mounting thin samples for electrical measurements is described. The technique is based on a vacuum chuck concept in which the vacuum chuck simultaneously holds the sample and established electrical contact. The mounting plate is composed of a glass-ceramic insulating material and the surfaces of the plate and vacuum chuck are polished. The operation of the vacuum chuck is examined. The contacts on the sample and mounting plate, which are sputter-deposited through metal masks, are analyzed. The mounting method was utilized for van der Pauw measurements. I.F.

A86-47077* Cincinnati Univ., Ohio.

DIAMONDLIKE CARBON FILMS ON SEMICONDUCTORS FOR INSULATED-GATE TECHNOLOGY

V. J. KAPOOR (Cincinnati, University, OH), M. J. MIRTICH, and B. A. BANKS (NASA, Lewis Research Center, Cleveland, OH) Journal of Vacuum Science and Technology A (ISSN 0734-2101), vol. 4, May-June 1986, pt. 1, p. 1013-1017. NASA-supported research. refs

MIS structures are fabricated on p-type InP, GaAs, and Si substrated by direct ionization of 25-percent CH₄ in Ar and ion-beam deposition of 70-nm-thick diamondlike films, followed by application of Al gate electrodes and ohmic contacts. The films are found to have bandgap 0.9-1.1 eV, resistivity 8.1 Mohm cm, breakdown field strength 1 MV/cm, and density 1.8 g/cu cm, to be thermally stable up to 400 C, and to undergo rapid decomposition above 450 C. The electrical properties of the MIS structures are significantly improved by sputter cleaning the substrates with a 1-keV 2-mA/sq cm Ar beam for 2 min at 300 microtorr prior to C-film deposition. The resulting structures have fixed insulator charge number densities 4 x 10 to the 12th/sq cm (InP), 7.5 x 10 to the 12th/sq cm (GaAs), and 9 x 10 to the 11th/sq cm (Si) and interface state densities (5, 200, and 0.5) x 10 to the 12th/sq cm eV, respectively. It is suggested that the low optical bandgap and resistivity of the C films and the high insulator-charge and interface-state densities make them unstable as gate dielectrics for microelectronics. T.K.

A86-49617*# National Aeronautics and Space Administration. Lewis Research Center, Cleveland, Ohio.

TWT EFFICIENCY ENHANCEMENT WITH TEXTURED CARBON SURFACES ON COPPER MDC ELECTRODES

A. N. CURREN and P. RAMINS (NASA, Lewis Research Center, Cleveland, OH) International Electron Devices Meeting, Washington, DC, Dec. 1-4, 1985, Paper. 3 p. refs

A method of improving the efficiency of multistage depressed collectors (MDC's) for traveling-wave tubes (TWT's) has been demonstrated at the NASA Lewis Research Center. A significant increase in MDC efficiency was brought about by the application of a thin layer of highly-textured carbon to the surfaces of oxygen-free, high-conductivity (OFHC) copper collector electrodes in an experimental TWT. The textured carbon layer was applied by means of a NASA developed sputtering procedure. In an experimental investigation recently completed, this electrode surface modification resulted in an increase in MDC efficiency by as much as 8.6 percentage points relative to that of the same MDC with untreated copper electrode surfaces. This increase in MDC efficiency was reflected by an increase in overall TWT efficiency by as much as 5.4 percentage points. Author

N86-12509*# National Aeronautics and Space Administration. Lewis Research Center, Cleveland, Ohio.

PERFORMANCE AND TEMPERATURE DEPENDENCIES OF PROTON IRRADIATED N/P GAAS AND N/P SILICON CELLS

I. WEINBERG, C. K. SWARTZ, and R. E. HART, JR. 1985 10 p refs Presented at the 18th Photovoltaic Specialists Conf., Las Vegas, Nev., 21-25 Oct. 1985; sponsored by IEEE (NASA-TM-87136; E-2753; NAS 1.15:87136) Avail: NTIS HC A02/MF A01 CSCL 09C

The n/p homojunction GaAs cell is found to be more radiation resistant than p/nheteroface GaAs under 10 MeV proton irradiation. Both GaAs cell types outperform conventional silicon n/p cells under the same conditions. An increase temperature dependency of maximum power for the GaAs n/p cells is attributed largely to differences in Voc between the two GaAs cell types. These results and diffusion length considerations are consistent with the conclusion that p-type GaAs is more radiation resistant than n-type and therefore that the n/p configuration is possibly favored for use in the space radiation environment. However, it is concluded that additional work is required in order to choose between the two GaAs cell configurations. Author

N86-13643*# National Aeronautics and Space Administration. Lewis Research Center, Cleveland, Ohio.

VERIFICATION OF COMPUTER-AIDED DESIGNS OF TRAVELING-WAVE TUBES UTILIZING NOVEL DYNAMIC REFOCUSERS AND GRAPHITE ELECTRODES FOR THE MULTISTAGE DEPRESSED COLLECTOR

P. RAMINS, H. G. KOSMAHL, D. A. FORCE, R. W. PALMER, and J. A. DAYTON, JR. Oct. 1985 26 p refs (NASA-TP-2524; E-2566; NAS 1.60:2524) Avail: NTIS HC A03/MF A01 CSCL 09A

A computational procedure for the design of TWT-refocuser-MDC systems was used to design a short dynamic refocusing system and highly efficient four-stage depressed collector for a 200-W, 8- to 18-GHz, TWT. The computations were carried out with advanced, multidimensional computer programs which model the electron beam as a series of disks of charge and follow their trajectories from the RF input of the TWT, through the slow-wave structure and refocusing section, to their points of impact in the depressed collector. Secondary emission losses in the MDC were treated semi-quantitatively by injecting a representative beam of secondary electrons into the MDC analysis at the point of impact of each primary beam. A comparison of computed and measured TWT and MDC performance showed very good agreement. The electrodes of the MDC were fabricated from a particular form of isotropic graphite that was selected for its low secondary electron yield, ease of machinability, and vacuum properties. This MDC was tested (at CW) for more than 1000 hr with negligible degradation in TWT and MDC performances.

Author

N86-13645*# National Aeronautics and Space Administration. Lewis Research Center, Cleveland, Ohio.

POTENTIAL FOR USE OF INDIUM PHOSPHIDE SOLAR CELLS IN THE SPACE RADIATION ENVIRONMENT

I. WEINBERG, C. K. SWARTZ, and R. E. HART, JR. 1985 9 p refs Presented at the 18th Photovoltaic Specialists Conference, Las Vegas, Nev., 21-25 Oct. 1985; sponsored by IEEE (NASA-TM-87157; E-2785; NAS 1.15:87157) Avail: NTIS HC A02/MF A01 CSCL 09C

Indium phosphide solar cells were observed to have significantly higher radiation resistance than either GaAs or Si after exposure to 10 MeV proton irradiation data and previous 1 MeV electron data together with projected efficiencies for InP, it was found that these latter cells produced more output power than either GaAs or Si after specified fluences of 10 MeV protons and 1 MeV electrons. Estimates of expected performance in a proton dominated space orbit yielded much less degradation for InP when compared to the remaining two cell types. It was concluded that, with additional development to increase efficiency, InP solar cells would perform significantly better than either GaAs or Si in the space radiation environment.

Author

N86-14499*# SRI International Corp., Menlo Park, Calif.

DEVELOPMENT PROGRAM ON A COLD CATHODE ELECTRON GUN Annual Report

C. A. SPINDT and C. E. HOLLAND Jan. 1985 70 p refs (Contract NAS3-23776; SRI PROJ. 5723) (NASA-CR-174792; NAS 1.26:174792) Avail: NTIS HC A04/MF A01 CSCL 09A

During this phase of the cathode development program, SRI improved the multiple electron beam exposure system used to print hole patterns for the cathode arrays, studied anisotropic etch processes, conducted cathode investigations using an emission microscope, reviewed possible alternate materials for cathode fabrication, studied cathode storage techniques, conducted high power operation experiments, and demonstrated high-current-density operation with small arrays of tips.

Author

N86-15544*# California Inst. of Tech., Pasadena. Power Electronics Group.

INPUT CURRENT SHAPED AC-TO-DC CONVERTERS Semiannual Status Report

Dec. 1985 38 p refs (Contract NAG3-615) (NASA-CR-176438; NAS 1.26:176438) Avail: NTIS HC A03/MF A01 CSCL 09C

Input current shaping techniques for ac-to-dc converters were investigated. Input frequencies much higher than normal, up to 20 kHz were emphasized. Several methods of shaping the input current waveform in ac-to-dc converters were reviewed. The simplest method is the LC filter following the rectifier. The next simplest method is the resistor emulation approach in which the inductor size is determined by the converter switching frequency and not by the line input frequency. Other methods require complicated switch drive algorithms to construct the input current waveshape. For a high-frequency line input, on the order of 20 kHz, the simple LC cannot be discarded so peremptorily, since the inductor size can be compared with that for the resistor emulation method. In fact, since a dc regulator will normally be required after the filter anyway, the total component count is almost the same as for the resistor emulation method, in which the filter is effectively incorporated into the regulator.

E.A.K.

N86-16486*# Alphatech, Inc., Burlington, Mass.

ROBUST DETECTION-ISOLATION-ACCOMMODATION FOR SENSOR FAILURES Final Report

J. L. WEISS, K. R. PATTIPATI, A. S. WILLSKY, J. S. ETERNO, and J. T. CRAWFORD Sep. 1985 220 p refs (Contract NAS3-24078) (NASA-CR-174797; NAS 1.26:174797; TR-213-1) Avail: NTIS HC A10/MF A01 CSCL 09C

The results of a one year study to: (1) develop a theory for Robust Failure Detection and Identification (FDI) in the presence of model uncertainty, (2) develop a design methodology which utilizes the robust FDI theory, (3) apply the methodology to a sensor FDI problem for the F-100 jet engine, and (4) demonstrate the application of the theory to the evaluation of alternative FDI schemes are presented. Theoretical results in statistical discrimination are used to evaluate the robustness of residual signals (or parity relations) in terms of their usefulness for FDI. Furthermore, optimally robust parity relations are derived through the optimization of robustness metrics. The result is viewed as decentralization of the FDI process. A general structure for decentralized FDI is proposed and robustness metrics are used for determining various parameters of the algorithm.

Author

N86-16487*# National Aeronautics and Space Administration. Lewis Research Center, Cleveland, Ohio.

DESCRIPTION AND TEST RESULTS OF A VARIABLE SPEED, CONSTANT FREQUENCY GENERATING SYSTEM Final Report

F. J. BRADY Dec. 1985 18 p refs (Contract DE-AI01-76ET-20320) (NASA-TM-87181; DOE/NASA/20320-67; E-2830; NAS 1.15:87181) Avail: NTIS HC A02/MF A01 CSCL 09C

The variable-speed, constant frequency generating system developed for the Mod-0 wind turbine is presented. This report describes the system as it existed at the conclusion of the project. The cycloconverter control circuit is described including the addition of field-oriented control. The laboratory test and actual wind turbine test results are included.

Author

33 ELECTRONICS AND ELECTRICAL ENGINEERING

N86-17456* National Aeronautics and Space Administration. Lewis Research Center, Cleveland, Ohio.

DESIGN OF HIGH-VOLTAGE, HIGH-POWER, SOLID STATE REMOTE POWER CONTROLLERS FOR AEROSPACE APPLICATIONS

J. C. STURMAN / In ESA Proceedings of ESA Sessions at the 16th IEEE Annual Power Electronics Specialists Conference p 207-216 May 1985 refs
Avail: NTIS HC A15/MF A01

Two general types of remote power controllers (RPC's), which combine the functions of a circuit breaker and a switch, were developed for use in dc aerospace systems. Power-switching devices used in the designs are the gate-turnoff thyristor (GTO) and MOSFET. The RPC's can switch dc voltages to 1200 V and currents to 1000 A. Seven different units were constructed and subjected to laboratory and thermal vacuum testing. Two of these were dual units that switch both positive and negative voltages simultaneously. The RPC's using MOSFET's have slow turnon and turnoff times which limit surge currents and voltage spiking from high di/dt. The GTO's have much faster transition times. All RPC's have programmable overload tripout proportional to $I_{sq} T$ and microsecond tripout for large overloads. Author (ESA)

N86-20671* National Aeronautics and Space Administration. Lewis Research Center, Cleveland, Ohio.

PIEZOELECTRIC DEICING DEVICE Patent

R. C. FINKE and B. A. BANKS, inventors (to NASA) 8 Oct. 1985 5 p Filed 7 Aug. 1984 Continuation of abandoned US-Patent-Appl-SN-469867, filed 25 Feb. 1983
(NASA-CASE-LEW-13773-2; US-PATENT-4,545,553;
US-PATENT-APPL-SN-638541; US-PATENT-CLASS-244-134-D;
US-PATENT-CLASS-39-25.35; US-PATENT-CLASS-310-324)
Avail: US Patent and Trademark Office CSCL 09A

A fast voltage pulse is applied to a transducer which comprises a composite of multiple layers of alternately polarized piezoelectric material. These layers are bonded together and positioned over the curved leading edge of an aircraft wing structure. Each layer is relatively thin and metallized on both sides. The strain produced in the transducer causes the composite to push forward resulting in detachment and breakup of ice on the leading edge of the aircraft wing.

Official Gazette of the U.S. Patent and Trademark Office

N86-20672* National Aeronautics and Space Administration. Lewis Research Center, Cleveland, Ohio.

HYBRID POWER SEMICONDUCTOR Patent

D. Y. CHEN 15 Oct. 1985 5 p Filed 30 Sep. 1983
(NASA-CASE-LEW-13922-1; US-PATENT-4,547,686;
US-PATENT-APPL-SN-537614; US-PATENT-CLASS-307-570;
US-PATENT-CLASS-307-264; US-PATENT-CLASS-307-270;
US-PATENT-CLASS-307-566; US-PATENT-CLASS-307-572)
Avail: US Patent and Trademark Office CSCL 09A

The voltage rating of a bipolar transistor may be greatly extended while at the same time reducing its switching time by operating it in conjunction with FETs in a hybrid circuit. One FET is used to drive the bipolar transistor while the other FET is connected in series with the transistor and an inductive load. Both FETs are turned on or off by a single drive signal of load power, the second FET upon ceasing conduction, rendering one power electrode of the bipolar transistor open. Means are provided to dissipate currents which flow after the bipolar transistor is rendered nonconducting.

Official Gazette of the U.S. Patent and Trademark Office

N86-20680* National Aeronautics and Space Administration. Lewis Research Center, Cleveland, Ohio.

METHOD AND APPARATUS FOR REBALANCING A REDOX FLOW CELL SYSTEM Patent Application

R. F. GAHN, inventor (to NASA) 25 Jun. 1985 11 p
(NASA-CASE-LEW-14127-1; NAS 1.71:LEW-14127-1;
US-PATENT-APPL-SN-748536) Avail: NTIS HC A02/MF A01
CSCL 09A

A rebalance cell is provided for a REDOX electrochemical system of the type with anode and cathode fluids which are aqueous HCl solutions with two metal species in each. The rebalance cell has a cathode compartment and a chlorine compartment separated by an ion permeable membrane. By applying an electrical potential to the rebalance cell while circulating cathode fluid through the cathode compartment and while circulating an identical fluid through the chlorine compartment, any significant imbalance of the REDOX system is prevented. NASA

N86-20700# Massachusetts Inst. of Tech., Cambridge. Lab. for Electromagnetic and Electronic Systems.

VARIABLE-RELUCTANCE MOTOR DRIVES FOR ELECTRIC VEHICLE PROPULSION Ph.D. Thesis Final Report

J. H. LANG and F. J. VALLESE 1 May 1985 217 p Sponsored in part by DOE/JPL, Pasadena, Calif.
(Contract NAG3-257; DE-A101-78CS-54209)
(NASA-CR-176566; JPL-9950-1037; NAS 1.26:176566;
DE85-017585; DOE/CS-54209) Avail: NTIS HC A10/MF A01
CSCL 09A

A methodology is presented for the design of a variable reluctance motor drive having high specific torque, power output and efficiency. Models are developed that describe the magnetic terminal relations of the VRM. These models are based on a flux-tube analysis that is motivated by numerically obtained finite-difference magnetic simulations. The result is a model for the flux-linkage/phase-current characteristic of the VRM. Intrinsic to this model is the estimation of maximum and minimum inductance as well the incremental inductance during bulk saturation. Also fundamental is the behavior of the flux linkage during local pole-tip saturation and due to bulk core saturation. The drive-oriented treatment of modelling and design uncovered important design interactions between the VRM, its inverter, and its excitation. The experimental 3.8-kW drive operated as expected, verifying the models and the design optimizations developed for VRM drives. These experimental results were projected to the 60-kW level, indicating that a 60-kW drive could be constructed with a VRM having a mass of approximately 65 kg, and an efficiency in excess of 95% at and below peak power output. DOE

N86-21742* National Aeronautics and Space Administration. Lewis Research Center, Cleveland, Ohio.

LINEARIZED TRAVELING WAVE AMPLIFIER WITH HARD LIMITER CHARACTERISTICS Patent

H. G. KOSMAHL, inventor (to NASA) 14 Jan. 1986 7 p Filed 20 Mar. 1985 Continuation-in-part of US-Patent-Appl-SN-492522, filed 9 May 1983, abandoned
(NASA-CASE-LEW-13981-2; US-PATENT-4,564,787;
US-PATENT-APPL-SN-714051; US-PATENT-CLASS-315-3.6;
US-PATENT-CLASS-315-3.5; US-PATENT-CLASS-315-39.3;
US-PATENT-CLASS-330-43) Avail: US Patent and Trademark Office CSCL 09A

A dynamic velocity taper is provided for a traveling wave tube with increased linearity to avoid intermodulation of signals being amplified. In a traveling wave tube, the slow wave structure is a helix including a sever. A dynamic velocity taper is provided by gradually reducing the spacing between the repeating elements of the slow wave structure which are the windings of the helix. The reduction which takes place coincides with the output point of helix. The spacing between the repeating elements of the slow wave structure is ideally at an exponential rate because the curve increases the point of maximum efficiency and power, at an exponential rate. A coupled cavity traveling wave tube having cavities is shown. The space between apertured discs is gradually reduced from 0.1% to 5% at an exponential rate. Output power

(or efficiency) versus input power for a commercial tube is shown.
Official Gazette of the U.S. Patent and Trademark Office

N86-21755*# National Aeronautics and Space Administration. Lewis Research Center, Cleveland, Ohio.

PROGRAMMABLE, AUTOMATED TRANSISTOR TEST SYSTEM
L. V. TRUONG and G. R. SUNDBURG 1986 25 p refs
Presented at the 3rd Symposium on Space Nuclear Power Systems, Albuquerque, N. Mex., 13-16 Jan. 1986
(NASA-TP-2554; E-2768; NAS 1.60:2554) Avail: NTIS HC A02/MF A01 CSCL 09A

A programmable, automated transistor test system was built to supply experimental data on new and advanced power semiconductors. The data will be used for analytical models and by engineers in designing space and aircraft electric power systems. A pulsed power technique was used at low duty cycles in a nondestructive test to examine the dynamic switching characteristic curves of power transistors in the 500 to 1000 V, 10 to 100 A range. Data collection, manipulation, storage, and output are operator interactive but are guided and controlled by the system software. Author

N86-21757*# National Aeronautics and Space Administration. Lewis Research Center, Cleveland, Ohio.

OPTICALLY CONTROLLED PHASED ARRAY ANTENNA CONCEPTS USING GaAs MONOLITHIC MICROWAVE INTEGRATED CIRCUITS

R. R. KUNATH and K. B. BHASIN 1986 9 p refs To be presented at the Optical Control Techniques Applied to Antennas and Propagation Session of the International IEEE AP-S/URSI Symposium, Philadelphia, Pa., 9-13 Jun. 1986
(NASA-TM-87229; E-2887; NAS 1.15:87229) Avail: NTIS HC A02/MF A01 CSCL 09A

The desire for rapid beam reconfigurability and steering has led to the exploration of new techniques. Optical techniques have been suggested as potential candidates for implementing these needs. Candidates generally fall into one of two areas: those using fiber optic Beam Forming Networks (BFNs) and those using optically processed BFNs. Both techniques utilize GaAs Monolithic Microwave Integrated Circuits (MMICs) in the BFN, but the role of the MMIC for providing phase and amplitude variations is largely eliminated by some new optical processing techniques. This paper discusses these two types of optical BFN designs and provides conceptual designs of both systems. Author

N86-24906*# Hughes Research Labs., Torrance, Calif.
DESIGNING A 25-KILOWATT HIGH FREQUENCY SERIES RESONANT

R. R. ROBSON Apr. 1984 16 p refs Presented at POWERCON 11, 11th Annual International Power Electronics Conference and Exhibit, Dallas, Tex., 9-13 Apr. 1984
(Contract NAS3-23159)
(NASA-CR-176774; NAS 1.26:176774) Avail: NTIS HC A02/MF A01 CSCL 09C

The feasibility of processing 25 kW of power with a single, transistorized, 20 kHz, series resonant converter stage has been demonstrated by the successful design, development, fabrication, and testing of such a device. It employs four Westinghouse D7ST transistors in a full-bridge configuration and operates from a 250-to-350-Vdc input bus. The unit has an overall worst-case efficiency of 93.5% at its full rated output of 1000 V and 25 A dc. A solid-state dc input circuit breaker and output-transient-current limiters are included in and integrated into the design. Circuit details of the converter are presented along with test data. Author

N86-24907*# National Aeronautics and Space Administration. Lewis Research Center, Cleveland, Ohio.

ANALYSIS OF OPTICALLY CONTROLLED MICROWAVE/MILLI-METER WAVE DEVICE STRUCTURES

R. N. SIMONS and K. B. BHASIN 1986 17 p refs Presented at International Microwave Symposium, Baltimore, Md., 2-4 Jun. 1986; sponsored by IEEE
(NASA-TM-87246; E-2926; NAS 1.15:87246) Avail: NTIS HC A02/MF A01 CSCL 09C

The light-induced voltage and the change in the source-to-drain channel current under optical illumination higher than the semiconductor bandgap for GaAs MESFET, InP MESFET, Al_{0.3}Ga_{0.7}As/GaAs high electron mobility transistor (HEMT) and GaAs permeable base transistor (PBT) were analytically obtained. The GaAs PBT and GaAs MESFET have much higher sensitivity than InP MESFET. The Al_{0.3}Ga_{0.7}As/GaAs HEMT is observed to have the highest sensitivity. Variation in device parasitics due to optical illumination and its effect on the cutoff frequencies $f_{sub T}$ and $f_{sub max}$ are also investigated. Author

N86-25693*# California Inst. of Tech., Pasadena. Power Electronics Group.

INPUT-CURRENT SHAPED AC TO DC CONVERTERS Final Report

May 1986 49 p refs
(Contract NAG3-615)
(NASA-CR-176787; NAS 1.26:176787; EE116-81) Avail: NTIS HC A03/MF A01 CSCL 09A

The problem of achieving near unity power factor while supplying power to a dc load from a single phase ac source of power is examined. Power processors for this application must perform three functions: input current shaping, energy storage, and output voltage regulation. The methods available for performing each of these three functions are reviewed. Input current shaping methods are either active or passive, with the active methods divided into buck-like and boost-like techniques. In addition to large reactances, energy storage methods include resonant filters, active filters, and active storage schemes. Fast voltage regulation can be achieved by post regulation or by supplementing the current shaping topology with an extra switch. Some indications of which methods are best suited for particular applications concludes the discussion. Author

N86-25694*# Wisconsin Univ., Madison. Dept. of Electrical and Computer Engineering.

POWER CONVERSION DISTRIBUTION SYSTEM USING A RESONANT HIGH-FREQUENCY AC LINK

P. K. SOOD and T. A. LIPO 1986 6 p
(Contract NAG3-492)
(NASA-CR-176804; NAS 1.26:176804) Avail: NTIS HC A02/MF A01 CSCL 10B

Static power conversion systems based on a resonant high frequency (HF) link offers a significant reduction in the size and weight of the equipment over that achieved with conventional approaches, especially when multiple sources and loads are to be integrated. A faster system response and absence of audible noise are the other principal characteristics of such systems. A conversion configuration based on a HF link which is suitable for applications requiring distributed power is proposed. Author

N86-26520*# National Aeronautics and Space Administration. Lewis Research Center, Cleveland, Ohio.

INDIUM PHOSPHIDE SOLAR CELLS: STATUS AND PROSPECTS FOR USE IN SPACE

I. WEINBERG and D. J. BRINKER 1986 11 p Presented at 21st Intersociety Energy Conversion Engineering Conference (IECEC), San Diego, Calif. 25-29 Aug. 1986; sponsored by American Ceramic Society, SAE, American Nuclear Society, IEEE, AIAA and American Institute of Chemical Engineers
(NASA-TM-87315; E-3046; NAS 1.15:87315) Avail: NTIS HC A02/MF A01 CSCL 10A

The current status of indium phosphide cell research is reviewed and state of the art efficiencies compared to those of GaAs and

Si. It is shown that the radiation resistance of InP cells is superior to that of either GaAs or Si under 1 MeV electron and 10 MeV proton irradiation. Using lightweight blanket technology, a SEP array structure and projected cell efficiencies, array specific powers are obtained for all three cell types. Array performance is calculated as a function of time in orbit. The results indicate that arrays using InP cells can outperform those using GaAs or Si in orbits where radiation is a significant cell degradation factor. It is concluded that InP solar cells are excellent prospects for future use in the space radiation environment. Author

N86-27578*# National Aeronautics and Space Administration. Lewis Research Center, Cleveland, Ohio.

NEAR-FIELD TESTING OF THE 30 GHZ TRW PROOF-OF-CONCEPT MULTIBEAM ANTENNA

R. R. KUNATH, JR. and R. J. ZAKRAJSEK 1986 11 p. Proposed for presentation at the Antenna Measurements Techniques Association 8th Annual Meeting and Symposium, Ottawa, Ontario, 23-25 Sep. 1986; sponsored by the National Research Council of Canada and the AMTA

(NASA-TM-87357; E-3115; NAS 1.15:87357) Avail: NTIS HC A02/MF A01 CSCL 09C

Near-field testing was conducted on the 30 GHz TRW proof-of-concept (POC) Multibeam Antenna (MBA). The TRW POC MBA is a dual offset Cassegrain reflector system using a 2.7 m main reflector. This configuration was selected to assess the ability to create both multiple fixed and scanned spot beams. The POC configuration investigated frequency reuse via spatial separation of beams, polarization selectivity and time division multiple access scanning at 30 GHz. Measurements of directivity, sidelobe level, and pattern were made at NASA Lewis Research Center's Near-Field Antenna Test Facility. Presented in this paper are complete results of these measurements. Included is a detailed discussion of all testing procedures and parameters. Results of additional testing used to evaluate diffraction effects of the subreflector and distortions of the main reflector are also presented. Author

N86-28323*# SRI International Corp., Menlo Park, Calif.
THERMIONIC NOISE MEASUREMENTS FOR ON-LINE DISPENSER CATHODE DIAGNOSTICS FOR LINEAR BEAM MICROWAVE TUBES Final Report, Feb. 1984 - Aug. 1985

C. HOLLAND and I. BRODIE Aug. 1985 48 p

(Contract NAS3-23777; SRI PROJ-6923)

(NASA-CR-175105; NAS 1.26:175105) Avail: NTIS HC A03/MF A01 CSCL 09C

A test stand has been set up to measure the current fluctuation noise properties of B- and M-type dispenser cathodes in a typical TWT gun structure. Noise techniques were used to determine the work function distribution on the cathode surfaces. Significant differences between the B and M types and significant changes in the work function distribution during activation and life are found. In turn, knowledge of the expected work function can be used to accurately determine the cathode-operating temperatures in a TWT structure. Noise measurements also demonstrate more sensitivity to space charge effects than the Miram method. Full automation of the measurements and computations is now required to speed up data acquisition and reduction. The complete set of equations for the space charge limited diode were programmed so that given four of the five measurable variables (J, J sub O, T, D, and V) the fifth could be computed. Using this program, we estimated that an rms fluctuation in the diode spacing d in the frequency range of 145 Hz about 20 kHz of only about 10 to the -5 power A would account for the observed noise in a space charge limited diode with 1 mm spacing. Author

N86-30068*# National Aeronautics and Space Administration. Lewis Research Center, Cleveland, Ohio.

HYTESS 2: A HYPOTHETICAL TURBOFAN ENGINE SIMPLIFIED SIMULATION WITH MULTIVARIABLE CONTROL AND SENSOR ANALYTICAL REDUNDANCY

W. C. MERRILL Jun. 1986 39 p

(NASA-TM-87344; E-3014; NAS 1.15:87344) Avail: NTIS HC A03/MF A01 CSCL 21E

A hypothetical turbofan engine simplified simulation with a multivariable control and sensor failure detection, isolation, and accommodation logic (HYTESS II) is presented. The digital program, written in FORTRAN, is self-contained, efficient, realistic and easily used. Simulated engine dynamics were developed from linearized operating point models. However, essential nonlinear effects are retained. The simulation is representative of the hypothetical, low bypass ratio turbofan engine with an advanced control and failure detection logic. Included is a description of the engine dynamics, the control algorithm, and the sensor failure detection logic. Details of the simulation including block diagrams, variable descriptions, common block definitions, subroutine descriptions, and input requirements are given. Example simulation results are also presented. Author

N86-30073*# Westinghouse Research and Development Center, Pittsburgh, Pa.

DOUBLE-INJECTION, DEEP-IMPURITY SWITCH DEVELOPMENT Final Report, 27 Feb. 1984 - 28 Feb. 1985

D. W. WHITSON 28 Mar. 1985 120 p

(Contract NAS3-23882)

(NASA-CR-174936; NAS 1.26:174936; WRDC-85-9F4-DIDIS-R1)

Avail: NTIS HC A06/MF A01 CSCL 09A

The overall objective of this program was the development of device design and process techniques for the fabrication of a double-injection, deep-impurity (DI) sup 2 silicon switch that operates in the 2-10 kV range with conduction current values of 5 A at 2 kV and 1 A at 10 kV. Other major specifications include a holding voltage of 10 V with no gate current, 10 microsec switching time, and power dissipation of 50 W at 75 C. It was decided to concentrate on the lateral circular devices in order to optimize the gold diffusion. This resulted in devices that are much better switches (approx. 1 micro sec switching time), and in a gold diffusion process that is much more controllable than those previously developed. Some results with injection-gated devices were also obtained. The current conduction for V less than VT was analyzed and seen to agree, for the most part, with Lampert's theory. Various sections of this report describe the device designs, wafer-processing techniques, and various measurements which include ac and dc characteristics and four-point probe. Author

N86-31792*# National Aeronautics and Space Administration. Lewis Research Center, Cleveland, Ohio.

A SENSOR FAILURE SIMULATOR FOR CONTROL SYSTEM RELIABILITY STUDIES

K. J. MELCHER, J. C. DELAAT, W. C. MERRILL, L. G. OBERLE, G. G. SADLER, and J. H. SCHAEFER 1986 43 p

(NASA-TM-87271; E-3137; NAS 1.15:87271) Avail: NTIS HC A03/MF A01 CSCL 09A

A real-time Sensor Failure Simulator (SFS) was designed and assembled for the Advanced Detection, Isolation, and Accommodation (ADIA) program. Various designs were considered. The design chosen features an IBM-PC/XT. The PC is used to drive analog circuitry for simulating sensor failures in real-time. A user defined scenario describes the failure simulation for each of the five incoming sensor signals. Capabilities exist for editing, saving, and retrieving the failure scenarios. The SFS has been tested closed-loop with the Controls Interface and Monitoring (CIM) unit, the ADIA control, and a real-time F100 hybrid simulation. From a productivity viewpoint, the menu driven user interface has proven to be efficient and easy to use. From a real-time viewpoint, the software controlling the simulation loop executes at greater than 100 cycles/sec. Author

N86-31793*# National Aeronautics and Space Administration. Lewis Research Center, Cleveland, Ohio.

SPACE SOLAR CELL RESEARCH: PROBLEMS AND POTENTIAL

D. J. FLOOD 1986 13 p Presented at the Conference on Photovoltaics for Commercial Solar Power, Cambridge, Mass., 15-19 Sep. 1986; sponsored by the Society of Photo-Optical Instrumentation Engineers (NASA-TM-88833; E-3212; NAS 1.15:88833) Avail: NTIS HC A02/MF A01 CSCL 10A

The value of a passive, maintenance-free, renewable energy source was apparent in the early days of the space program, and the silicon solar cell was pressed into service. Efficiencies of those early space solar arrays were low, and lifetimes shorter than hoped for, but within a decade significant advances had been made in both areas. Better performance was achieved through improvements in silicon single crystal material, better device designs, and a better understanding of the factors that affect the performance of a solar cell in space. Chief among the latter, particularly for the mid-to-high altitude (HEO) and geosynchronous (GEO) orbits, are the effects of the naturally occurring particulate radiation environment. Although not as broadly important to the photovoltaic community at large as increased efficiency, the topic of radiation damage is critically important to use of solar cells in space, and is a major component of the NASA research program in space photovoltaics. A brief overview of some of the opportunities and challenges for space photovoltaic applications is given, and some of the current research directed at achieving high efficiency and controlling radiation damage in space solar cells is discussed. Author

N86-32627*# National Aeronautics and Space Administration. Lewis Research Center, Cleveland, Ohio.

POTENTIAL HIGH EFFICIENCY SOLAR CELLS: APPLICATIONS FROM SPACE PHOTOVOLTAIC RESEARCH

D. J. FLOOD 1986 15 p Presented at the Winter Annual Meeting of the American Inst. of Chemical Engineers, Miami Beach, Fla., 2-7 Nov. 1986

(NASA-TM-88832; E-3194; NAS 1.15:88832) Avail: NTIS HC A02/MF A01 CSCL 09C

NASA involvement in photovoltaic energy conversion research development and applications spans over two decades of continuous progress. Solar cell research and development programs conducted by the Lewis Research Center's Photovoltaic Branch have produced a sound technology base not only for the space program, but for terrestrial applications as well. The fundamental goals which have guided the NASA photovoltaic program are to improve the efficiency and lifetime, and to reduce the mass and cost of photovoltaic energy conversion devices and arrays for use in space. The major efforts in the current Lewis program are on high efficiency, single crystal GaAs planar and concentrator cells, radiation hard InP cells, and superlattice solar cells. A brief historical perspective of accomplishments in high efficiency space solar cells will be given, and current work in all of the above categories will be described. The applicability of space cell research and technology to terrestrial photovoltaics will be discussed. Author

N86-32629*# National Aeronautics and Space Administration. Lewis Research Center, Cleveland, Ohio.

SECONDARY-ELECTRON-EMISSION LOSSES IN MULTISTAGE DEPRESSED COLLECTORS AND TRAVELING-WAVE-TUBE EFFICIENCY IMPROVEMENTS WITH CARBON COLLECTOR ELECTRODE SURFACES

P. RAMINS and B. T. EBIHARA Sep. 1986 23 p (NASA-TP-2622; E-3062; NAS 1.60:2622) Avail: NTIS HC A02/MF A01 CSCL 09C

Secondary-electron-emission losses in multistage depressed collectors (MDC's) and their effects on overall traveling-wave-tube (TWT) efficiency were investigated. Two representative TWT's and several computer-modeled MDC's were used. The experimental techniques provide the measurement of both the TWT overall and the collector efficiencies. The TWT-MDC performance was

optimized and measured over a wide range of operating conditions, with geometrically identical collectors, which utilized different electrode surface materials. Comparisons of the performance of copper electrodes to that of various forms of carbon, including pyrolytic and isotropic graphites, were stressed. The results indicate that: (1) a significant improvement in the TWT overall efficiency was obtained in all cases by the use of carbon, rather than copper electrodes, and (2) that the extent of this efficiency enhancement depended on the characteristics of the TWT, the TWT operating point, the MDC design, and collector voltages. Ion textured graphite was found to be particularly effective in minimizing the secondary-electron-emission losses. Experimental and analytical results, however, indicate that it is at least as important to provide a maximum amount of electrostatic suppression of secondary electrons by proper MDC design. Such suppression, which is obtained by ensuring that a substantial suppressing electric field exists over the regions of the electrodes where most of the current is incident, was found to be very effective. Experimental results indicate that, with proper MDC design and the use of electrode surfaces with low secondary-electron yield, degradation of the collector efficiency can be limited to a few percent. Author

34

FLUID MECHANICS AND HEAT TRANSFER

Includes boundary layers; hydrodynamics; fluidics; mass transfer; and ablation cooling.

A86-11237*# Pennsylvania State Univ., University Park.

STRUCTURE OF NONEVAPORATING SPRAYS. II - DROP AND TURBULENCE PROPERTIES

A. S. P. SOLOMON, J.-S. SHUEN, Q.-Z. ZHANG, and G. M. FAETH (Pennsylvania State University, University Park) AIAA Journal (ISSN 0001-1452), vol. 23, Nov. 1985, p. 1724-1730. refs (Contract NAG3-190)

This is the second part of a study reporting structure measurements in the dilute portion of axisymmetric nonevaporating sprays. Measurements are compared with predictions of three typical methods for analyzing sprays: (1) locally homogeneous flow (LHF) analysis, where slip between the phases is neglected; (2) deterministic separated flow (DSF) analysis, where slip is considered but effects of drop interactions with turbulence are ignored; and (3) stochastic separated flow (SSF) analysis, where both slip and effects of drop interactions with turbulence are considered. This part of the study reports measurements of mean and fluctuating drop velocities, the variation of Sauter mean diameter, and gas-phase turbulence properties in the dilute portion of the sprays. Best agreement between predictions and measurements was obtained with the SSF analysis. For present measurements in the dilute region (void fraction greater than 99.1 percent), effects of drops on gas-phase turbulence properties (turbulence modulation) were small. However, as the dense spray regions near the injector were approached, the measurements indicated modification of turbulence properties by drop motion. Author

A86-11676*# Cleveland State Univ., Ohio.

EFFECT OF FREE STREAM TURBULENCE ON FLOW SEPARATION

R. S. R. GORLA (Cleveland State University, OH) IN: International Symposium on Air Breathing Engines, 7th, Beijing, People's Republic of China, September 2-6, 1985, Proceedings. New York, AIAA, 1985, p. 640-643. refs (Contract NAG3-548)

An analysis is presented to study the influence of free stream turbulence on separation in the case of crossflow over a circular cylinder. An eddy diffusivity model has been formulated and the governing momentum equation has been solved numerically. A correlation parameter has been suggested to correlate the angle

34 FLUID MECHANICS AND HEAT TRANSFER

of separation. It has been found that the angle of separation increases with increasing free stream turbulence intensity.

Author

A86-11937* Arizona State Univ., Tempe.

CONCENTRATION DISTRIBUTIONS IN CYLINDRICAL COMBUSTORS

S. A. AHMED and R. M. C. SO (Arizona State University, Tempe) IN: Experimental measurements and techniques in turbulent reactive and non-reactive flows; Proceedings of the Winter Annual Meeting, New Orleans, LA, December 9-14, 1984. New York, ASME, 1984, p. 91-106. refs
(Contract NAG3-260)

Experimental studies have been conducted with the aim to obtain a better understanding of the fluid dynamics of mixing in gas turbine combustors, and solid fuel ramjet combustors subject to spin. The present investigation represents a continuation of studies conducted by So et al. (1984). It is also concerned with the verification of some conclusions reported by Ahmed et al. (1984). Attention is given to the experimental facility and instrumentation, centerline concentration measurements, mean concentration profiles, and a comparison of concentration and axial velocity results in the case of swirling flow. G.R.

A86-11938* United Technologies Research Center, East Hartford, Conn.

SCALAR AND MOMENTUM TURBULENT TRANSPORT EXPERIMENTS WITH SWIRLING AND NONSWIRLING FLOWS

B. V. JOHNSON, R. ROBACK (United Technologies Research Center, East Hartford, CT), and J. C. BENNETT (Connecticut, University, Storrs) IN: Experimental measurements and techniques in turbulent reactive and non-reactive flows; Proceedings of the Winter Annual Meeting, New Orleans, LA, December 9-14, 1984. New York, ASME, 1984, p. 107-119. refs
(Contract NAS3-22771)

Combustor models for the aircraft gas turbine industry have been obtained because of the need to reduce the costs of developing improved performance and more durable engines. A few years ago, it became apparent that the mass concentration and velocity predictions provided by the computer codes were not representing the data measured in some confined recirculating flows. It is pointed out that errors in the mass concentration distribution are an especially serious problem because of their influence on the heat release, temperature, and reactant distributions. Combined mass and momentum turbulent transport experiments with swirling and nonswirling flow have been conducted with the objective to obtain an experimental data base which can be used to evaluate and improve the turbulent transport submodels employed in the aerothermal models. The present paper is mainly concerned with the overall characteristics of the mass turbulent transport processes in complex flows with recirculation and the deficiencies of the conventional models. G.R.

A86-13061* National Aeronautics and Space Administration, Lewis Research Center, Cleveland, Ohio.

LOCAL HEAT-TRANSFER MEASUREMENTS ON A LARGE SCALE-MODEL TURBINE BLADE AIRFOIL USING A COMPOSITE OF A HEATER ELEMENT AND LIQUID CRYSTALS

S. A. HIPPENSTEELE, L. M. RUSSELL, and F. J. TORRES (NASA, Lewis Research Center, Cleveland, OH) ASME, Transactions, Journal of Engineering for Gas Turbines and Power (ISSN 0022-0825), vol. 107, Oct. 1985, p. 953-960. Previously announced in STAR as N85-33435. refs
(ASME PAPER 85-GT-59)

Local heat transfer coefficients were experimentally mapped along the midchord of a five-time-size turbine blade airfoil in a static cascade operated at room temperature over a range of Reynolds numbers. The test surface consisted of a composite of commercially available materials: a mylar sheet with a layer of cholesteric liquid crystals, that change color with temperature, and a heater sheet made of a carbon-impregnated paper, that produces uniform heat flux. After the initial selection and calibration of the

composite sheet, accurate, quantitative, and continuous heat transfer coefficients were mapped over the airfoil surface. The local heat transfer coefficients are presented for Reynolds numbers from 2.8×10^5 to the 5th power to 7.6×10^5 to the 5th power. Comparisons are made with analytical values of heat transfer coefficients obtained from the STANS boundary layer code. Also, a leading edge separation bubble was revealed by thermal and flow visualization. Author

A86-13068* Clemson Univ., S.C.

HEAT TRANSFER AND FLUID MECHANICS MEASUREMENTS IN TRANSITIONAL BOUNDARY LAYER FLOWS

T. WANG (Clemson University, SC), T. W. SIMON (Minnesota, University, Minneapolis), and J. BUDDHAVARAPU (TSI, Inc., St. Paul, MN) ASME, Transactions, Journal of Engineering for Gas Turbines and Power (ISSN 0022-0825), vol. 107, Oct. 1985, p. 1007-1015. Research supported by the University of Minnesota. Previously announced in STAR as N85-31439. refs
(Contract NAG3-286)
(ASME PAPER 85-GT-113)

Experimental results are presented to document hydrodynamic and thermal development of flat-plate boundary layers undergoing natural transition. Local heat transfer coefficients, skin friction coefficients and profiles of velocity, temperature and Reynolds normal and shear stresses are presented. A case with no transition and transitional cases with 0.68 percent and 2.0 percent free-stream disturbance intensities were investigated. The locations of transition are consistent with earlier data. A late-laminar state with significant levels of turbulence is documented. In late-transitional and early-turbulent flows, turbulent Prandtl number and conduction layer thickness values exceed, and the Reynolds analogy factor is less than, values previously measured in fully turbulent flows. Author

A86-15800* National Aeronautics and Space Administration, Lewis Research Center, Cleveland, Ohio.

SURFACE TEMPERATURE DISTRIBUTION ALONG A THIN LIQUID LAYER DUE TO THERMOCAPILLARY CONVECTION

C.-L. LAI and A.-T. CHAI (NASA, Lewis Research Center, Cleveland, OH) IAF, International Astronautical Congress, 36th, Stockholm, Sweden, Oct. 7-12, 1985. 13 p. Previously announced in STAR as N85-34357. refs
(IAF PAPER 85-282)

The surface temperature distributions due to thermocapillary convections in a thin liquid layer with heat fluxes imposed on the free surface were investigated. The nondimensional analysis predicts that, when convection is important, the characteristics length scale in the flow direction L , and the characteristic temperature difference $\Delta T_{\text{sub } 0}$ can be represented by L and $\Delta T_{\text{sub } 0}$ approx. $(A_2 Ma)^{1/4} \Delta T_{\text{sub } R}$, respectively, where $L_{\text{sub } R}$ and $\Delta T_{\text{sub } R}$ are the reference scales used in the conduction dominant situations with A denoting the aspect ratio and Ma the Marangoni number. Having L and $\Delta T_{\text{sub } 0}$ defined, the global surface temperature gradient $\Delta T_{\text{sub } 0}/L$, the global thermocapillary driving force, and other interesting features can be determined. Numerical calculations involving a Gaussian heat flux distribution are presented to justify these two relations. E.A.K.

A86-16311* United Technologies Research Center, East Hartford, Conn.

LOW REYNOLDS NUMBER SEPARATION BUBBLE RESEARCH AT UTRC

W. P. PATRICK and D. E. EDWARDS (United Technologies Research Center, East Hartford, CT) IN: Conference on Low Reynolds Number Airfoil Aerodynamics, Notre Dame, IN, June 16-18, 1985, Proceedings. Notre Dame, IN, University of Notre Dame, 1985, p. 153-167. refs
(Contract NAS3-23693)

The facilities and techniques being applied in investigations of laminar separation bubbles on low Re airfoils at the United Technologies Research Center are described. The research is focused on developing a database and predictive models for use in designing compressor, fan and turbine blades. Flow data are

gathered primarily by laser Doppler velocimetry. Experimental procedures are being devised which will permit formation of a short bubble for characterizations of the velocity profiles in and around the bubble and boundary layer. Further tests are directed at defining the size and location of the bubble and the transition in the separated shear layer. The sensitivity of the bubble to alterations in the Re, pressure gradient, turbulence intensity and the turbulence scales will be examined. The effects of surface curvature and roughness on the bubble will also be studied. Details of the wind tunnel facility and the steps being taken to define conditions for reliably producing the short bubble are outlined.

M.S.K.

A86-16468* Lockheed-Georgia Co., Marietta.

TONE EXCITED JETS. III - FLOW MEASUREMENTS

J. LEPICOVSKY, K. K. AHUJA, and R. H. BURRIN (Lockheed-Georgia Co., Marietta, GA) *Journal of Sound and Vibration* (ISSN 0022-460X), vol. 102, Sept. 8, 1985, p. 71-91. Research supported by Lockheed-Georgia Co. refs (Contract NAS3-21987)

This paper describes the effects of upstream excitation on the flow characteristics of tone-excited jet under static as well as simulated forward velocity conditions. The data presented include axial and radial distributions of mean velocities and turbulence intensities as functions of excitation conditions. Results for both unheated and heated jets are presented. The measured distributions of pressures associated with the large-scale turbulence are also presented for some test conditions.

Author

A86-17041* National Aeronautics and Space Administration. Lewis Research Center, Cleveland, Ohio.

SCATTERING OF ACOUSTIC WAVES INTO TOLLMIE-SCHLICHTING WAVES BY SMALL STREAMWISE VARIATIONS IN SURFACE GEOMETRY

M. E. GOLDSTEIN (NASA, Lewis Research Center, Cleveland, OH) *Journal of Fluid Mechanics* (ISSN 0022-1120), vol. 154, May 1985, p. 509-529. refs

By using the triple-deck scaling of Stewartson (1969) and Messiter (1970) it is shown that small but relatively sudden surface geometry variations that produce only very weak static pressure variations can nevertheless produce strong, i.e. $O(1)$, coupling between an externally imposed acoustic disturbance and a spatially growing Tollmien-Schlichting wave. The analysis provides a qualitative explanation of the Leehey and Shapiro (1979) boundary-layer receptivity measurements and is in good quantitative agreement with the Aizin and Poliakov (1979) experiment. It may also explain why small 'trip wires' can promote early transition.

Author

A86-19419* California Inst. of Tech., Pasadena.

FINITE-AMPLITUDE STEADY WAVES IN PLANE VISCOUS SHEAR FLOWS

F. A. MILINAZZO and P. G. SAFFMAN (California Institute of Technology, Pasadena) *Journal of Fluid Mechanics* (ISSN 0022-1120), vol. 160, Nov. 1985, p. 281-295. refs (Contract NAG3-179; DE-AT03-76ER-72012; N00014-85-K-0205) (AD-A165461)

Computations of two-dimensional solutions of the Navier-Stokes equations are carried out for finite-amplitude waves on steady unidirectional flow. Several cases are considered. The numerical method employs pseudospectral techniques in the streamwise direction and finite differences on a stretched grid in the transverse direction, with matching to asymptotic solutions when unbounded. Earlier results for Poiseuille flow in a channel are re-obtained, except that attention is drawn to the dependence of the minimum Reynolds number on the physical constraint of constant flux or constant pressure gradient. Attempts to calculate waves in Couette flow by continuation in the velocity of a channel wall fail. The asymptotic suction boundary layer is shown to possess finite-amplitude waves at Reynolds numbers orders of magnitude less than the critical Reynolds number for linear instability. Waves in the Blasius boundary layer and unsteady Rayleigh profile are calculated by employing the artifice of adding a body force to

cancel the spatial or temporal growth. The results are verified by comparison with perturbation analysis in the vicinity of the linear-instability critical Reynolds numbers.

Author

A86-19651* Connecticut Univ., Storrs.

NUMERICAL AND EXPERIMENTAL INVESTIGATION OF NONSWIRLING AND SWIRLING CONFINED JETS

D. C. BRONDUM, J. C. BENNETT (Connecticut, University, Storrs), B. C. WEINBERG, and H. MCDONALD (Scientific Research Associates, Inc., Glastonbury, CT) AIAA, Aerospace Sciences Meeting, 24th, Reno, NV, Jan. 6-9, 1986. 15 p. refs (Contract NAG3-350) (AIAA PAPER 86-0040)

An investigation of the influence of large scale structures on the flow development for coaxial jets with sudden expansion (with and without swirl) is presented. Both an experimental study and numerical predictions were performed for a configuration corresponding to that considered by Johnson and Bennett and Roback and Johnson. The effects of large scale structures on the swirling and nonswirling flows are documented, in particular their influence on turbulence modeling and the numerical simulation. The ensemble-averaged, time-dependent Navier-Stokes equations are solved by an LBI procedure to predict the turbulent flow field. Effects of artificial dissipation and placement of the upstream boundary in the numerical computation are also discussed.

Author

A86-19661* Oklahoma State Univ., Stillwater.

HOT-WIRE MEASUREMENTS OF A SINGLE LATERAL JET INJECTED INTO SWIRLING CROSSFLOW

D. G. LILLEY (Oklahoma State University, Stillwater), L. H. ONG, and C. B. MCMURRY AIAA, Aerospace Sciences Meeting, 24th, Reno, NV, Jan. 6-9, 1986. 11 p. refs (Contract NAG3-549) (AIAA PAPER 86-0055)

In the present experiments documenting the time-mean and turbulent flowfield of a deflected turbulent jet in a combined, swirling crossflow, attention is given to a jet-to-crossflow velocity ratio of 4 at swirler vane angles of 45 and 70 deg. The results obtained are presented in the form of r - x plots in order to aid in three-dimensional flowfield visualization. The time-mean velocity measurements were found to closely correspond to pitot-probe data obtained in identical flow conditions. The lateral jet was found to deflect the axis of the precessing vortex core.

O.C.

A86-19746* Dayton Univ., Ohio.

NUMERICAL SIMULATION OF UNSTEADY FLOW IN AN AXISYMMETRIC SHEAR LAYER

J. N. SCOTT (Dayton, University, OH) and W. L. HANKEY (Wright State University, Dayton, OH) AIAA, Aerospace Sciences Meeting, 24th, Reno, NV, Jan. 6-9, 1986. 12 p. refs (Contract NAG3-526) (AIAA PAPER 86-0202)

Numerical simulation of unsteady flow in an axisymmetric subsonic shear layer is accomplished by solving the time-dependent compressible Navier-Stokes equations. The objective of the effort is to investigate by numerical means the influence of various flow parameters on the shear layer behavior. The parameters investigated include the velocity ratio of two streams, total temperature, and nozzle lip thickness. The computations are performed on a CRAY-IS computer using McCormack's explicit finite difference scheme. The computed results generally show qualitative agreement with experimental data.

Author

A86-20150*# National Aeronautics and Space Administration. Lewis Research Center, Cleveland, Ohio.

THERMOPHORETICALLY AUGMENTED MASS TRANSFER RATES TO SOLID WALLS ACROSS LAMINAR BOUNDARY LAYERS

S. A. GOKOGLU (NASA, Lewis Research Center, Cleveland, OH; Yale University, New Haven, CT) and D. E. ROSNER (Yale University, New Haven, CT) AIAA Journal (ISSN 0001-1452), vol. 24, Jan. 1986, p. 172-179. refs

(Contract F49620-82-K-0020; NAG3-201)

Predictions of mass transfer (heavy vapor and small particle deposition) rates to solid walls, including the effects of thermal (Soret) diffusion ('thermophoresis' for small particles), are made by numerically solving the two-dimensional self-similar forced convection laminar boundary-layer equations with variable properties, covering the particle size range from vapor molecules up to the size threshold for inertial (dynamical nonequilibrium) effects. The effect of thermophoresis is predicted to be particularly important for submicron particle deposition on highly cooled solid surfaces, with corresponding enhancement factors at atmospheric conditions being over a thousand-fold at $T(w)/T(e)$ equal to about 0.6. As a consequence of this mass transfer mechanism, the particle size dependence of the mass transfer coefficient to a cooled wall will be much weaker than for the corresponding case of isothermal capture by Brownian-convective diffusion. Author

A86-20362*# National Aeronautics and Space Administration. Lewis Research Center, Cleveland, Ohio.

MODELING DILUTION OF JET FLOWFIELDS

J. D. HOLDEMAN (NASA, Lewis Research Center, Cleveland, OH) and R. SRINIVASAN (Garrett Turbine Engine Co., Phoenix, AZ) Journal of Propulsion and Power (ISSN 0748-4658), vol. 2, Jan.-Feb. 1986, p. 4-10. Previously cited in issue 21, p. 3046, Accession no. A84-44183. refs

A86-20370*# Oklahoma State Univ., Stillwater.

SWIRLING FLOWS IN TYPICAL COMBUSTOR GEOMETRIES

D. G. LILLEY (Oklahoma State University, Stillwater) Journal of Propulsion and Power (ISSN 0748-4658), vol. 2, Jan.-Feb. 1986, p. 64-72. Previously cited in issue 07, p. 897, Accession no. A85-19574. refs

(Contract NAG3-74)

A86-20951* Purdue Univ., Indianapolis, Ind.

APPLICATIONS OF VARIATIONAL PRINCIPLES IN COMPUTING ROTATIONAL FLOWS

A. ECER and H. U. AKAY (Purdue University, Indianapolis, IN) IN: Advances in computational transonics. Swansea, Wales, Pineridge Press, 1985, p. 777-810. refs

(Contract NSG-3294)

Ecer and Akay (1983) have developed a variational formulation of rotational flow for Euler equations. The present paper provides a summary of these developments. The considered variational formulation provides a transformation of a type considered by Clebsch (1859). In this transformation, a new set of variables replaces the more commonly used primitive variables $u(i)$, ρ and p . Here, $u(i)$ denotes the velocity components, while ρ is the density, and p the pressure. The employed transformation produces a natural uncoupling of the equations when written in a quasi-linear form. After obtaining the governing equations in terms of the 'Clebsch variables', a solution scheme developed for calculating steady flows is discussed. Attention is given to numerical solutions of Euler equations based on the derived variational principles, and a study of inviscid, separated flows is conducted. G.R.

A86-20952* National Aeronautics and Space Administration. Lewis Research Center, Cleveland, Ohio.

STEADY INVISCID THREE-DIMENSIONAL FLOWS

J. J. ADAMCZYK and S.-C. CHANG (NASA, Lewis Research Center, Cleveland, OH) IN: Advances in computational transonics. Swansea, Wales, Pineridge Press, 1985, p. 813-834. refs

The present analysis combines some of the theoretical concepts suggested by Hawthorne (1955) with a numerical integration

procedure suggested by Martin (1978). The resulting algorithm is for inviscid subsonic flows. Thus, it is restricted to high Reynolds number flows. Chang and Adamczyk (1983) have provided a detailed derivation of the present algorithm along with a discussion of its stability bounds. The present paper represents a summary of this work. The integration of the continuity equation is considered along with an evaluation of the entropy, total temperature, and vorticity field. Attention is given to the shear-flow algorithm construction, and an application to a shear flow in a turning channel. A description of numerical results is also provided. The discussed algorithm represents a new procedure for solving inviscid subsonic three-dimensional rotational flows. G.R.

A86-21029* Cincinnati Univ., Ohio.

MULTI-GRID TECHNIQUE FOR THE SOLUTION OF INCOMPRESSIBLE NAVIER-STOKES EQUATIONS

K. N. GHIA and U. GHIA (Cincinnati University, OH) IN: Computational methods in viscous flows. Swansea, Wales, Pineridge Press, 1984, p. 101-135. refs

(Contract AF-AFOSR-80-0160; NSG-3267; NAG3-194; N00167-79-M-4413)

A computationally efficient method is proposed for obtaining fine-mesh solutions of the Navier-Stokes equations for high-Re flow, including separation. The method involves implementing a multi-grid solution procedure with suitably chosen elements, such that the resulting overall solution technique is efficient as well as robust. The robustness and efficiency of the solution technique are demonstrated by applying it to three model problems: flow in a driven cavity, downstream asymptotic flow in curved ducts of square and polar sections, and Newmann boundary-value problem in clustered curvilinear orthogonal coordinates. V.L.

A86-22026*# United Technologies Research Center, East Hartford, Conn.

HIGH WEBER NUMBER SMD CORRELATIONS FOR PRESSURE ATOMIZERS

J. B. KENNEDY (United Technologies Research Center, East Hartford, CT) ASME, International Gas Turbine Conference and Exhibit, 30th, Houston, TX, Mar. 18-21, 1985. 5 p. refs

(Contract NAS3-23167) (ASME PAPER 85-GT-37)

Recently acquired experimental data are presented which reveal that, for Weber number (We) greater than 10.0, the atomization from simplex pressure atomizers is significantly greater than would be predicted from previously derived Sauter mean diameter (SMD) correlations. A different SMD correlation is required to accurately predict the experimental data. Below We of about 10.0, the atomization is dominated by inertial forces and bag-type breakup results. Above We of about 10.0, shear-type breakup occurs and results in a very fine spray which can accurately be predicted using a quadratic expression in ΔP . The correlation is extended to include fuel property effects, and SMD is found to vary linearly with fuel surface tension, while the influence of the fuel viscosity is not apparent. C.D.

A86-22053*# National Aeronautics and Space Administration. Lewis Research Center, Cleveland, Ohio.

HEAT TRANSFER RESULTS AND OPERATIONAL CHARACTERISTICS OF THE NASA LEWIS RESEARCH CENTER HOT SECTION CASCADE TEST FACILITY

H. J. GLADDEN, F. C. YEH, and D. L. FRONEK (NASA, Lewis Research Center, Cleveland, OH) ASME, International Gas Turbine Conference and Exhibit, 30th, Houston, TX, Mar. 18-21, 1985. 11 p. Previously announced in STAR as N85-15133. refs (ASME PAPER 85-GT-82)

The NASA Lewis Research Center gas turbine hot section test facility has been developed to provide a real-engine environment with well known boundary conditions for the aerothermal performance evaluation/verification of computer design codes. The initial aerothermal research data obtained are presented and the operational characteristics of the facility are discussed. This facility is capable of testing at temperatures and pressures up to 1600 K and 18 atm which corresponds to a vane

exit Reynolds number range of 0.5×1 million to 2.5×1 million based on vane chord. The component cooling air temperature can be independently modulated between 330 and 700 K providing gas-to-coolant temperature ratios similar to current engine application. Research instrumentation of the test components provide conventional pressure and temperature measurements as well as metal temperatures measured by IR-photography. The primary data acquisition mode is steady state through a 704 channel multiplexer/digitizer. The test facility was configured as an annular cascade of full coverage film cooled vanes for the initial series of research tests. Author

A86-22054*# National Aeronautics and Space Administration. Lewis Research Center, Cleveland, Ohio.

A REVIEW AND ANALYSIS OF BOUNDARY LAYER TRANSITION DATA FOR TURBINE APPLICATION

R. E. GAUGLER (NASA, Lewis Research Center, Cleveland, OH) ASME, International Gas Turbine Conference and Exhibit, 30th, Houston, TX, Mar. 18-21, 1985. 8 p. Previously announced in STAR as N85-10306. refs (ASME PAPER 85-GT-83)

A symposium on transition in turbines was held at the NASA Lewis Research Center. One recommendation of the working groups was the collection of existing transition data to provide standard cases against which models could be tested. A number of data sets from the open literature that include heat transfer data in apparently transitional boundary layers, with particular application to the turbine environment, were reviewed and analyzed to extract transition information from the heat transfer data. The data sets reviewed cover a wide range of flow conditions, from low speed, flat plate tests to full scale turbine airfoils operating at simulated turbine engine conditions. The results indicate that free stream turbulence and pressure gradient have strong, and opposite, effects on the location of the start of transition and on the length of the transition zone. R.S.F.

A86-22055*# National Aeronautics and Space Administration. Lewis Research Center, Cleveland, Ohio.

PRELIMINARY RESULTS OF A STUDY OF THE RELATIONSHIP BETWEEN FREE STREAM TURBULENCE AND STAGNATION REGION HEAT TRANSFER

G. J. VANFOSSEN, JR. and R. J. SIMONEAU (NASA, Lewis Research Center, Cleveland, OH) ASME, International Gas Turbine Conference and Exhibit, 30th, Houston, TX, Mar. 18-21, 1985. 12 p. Previously announced in STAR as N85-11317. refs (ASME PAPER 85-GT-84)

The mechanism that causes free stream turbulence to increase heat transfer in the stagnation region of turbine vanes and blades was studied. The work is being conducted in a wind tunnel at atmospheric conditions to facilitate measurements of turbulence and heat transfer. The model size is scaled up to simulate Reynolds numbers (based on leading edge diameter) that are to be expected on a turbine blade leading edge. Reynolds numbers from 13,000 to 177,000 were run in the present tests. Spanwise averaged heat transfer measurement with high and low turbulence were made with rough and smooth surface stagnation regions. Results of these measurements show that the boundary layer remains laminar in character even in the presence of free stream turbulence at the Reynolds numbers tested. If roughness is added the boundary layer becomes transitional as evidenced by the heat transfer increase with increasing distance from the stagnation line. Hot wire measurements near the stagnation region downstream of an array of parallel wires have shown that vorticity in the form of mean velocity gradients is amplified as flow approaches the stagnation region. Author

A86-22125*# National Aeronautics and Space Administration. Lewis Research Center, Cleveland, Ohio.

EXPERIMENTAL STUDY OF THE SPRAY CHARACTERISTICS OF A RESEARCH AIRBLAST ATOMIZER

W. A. ACOSTA (NASA, Lewis Research Center; U.S. Army, Propulsion Laboratory, Cleveland, OH) ASME, International Gas Turbine Conference and Exhibit, 30th, Houston, TX, Mar. 18-21, 1985. 8 p. Previously announced in STAR as N85-15727. refs (ASME PAPER 85-GT-229)

Airblast atomization was studied using an especially designed atomizer in which the liquid first impinges on a splash plate, then is directed radially outward and is atomized by the air passing through two concentric, vaned swirlers that swirl the air in opposite directions. The effect of flow conditions, air mass velocity (mass flow rate per unit area) and liquid to air ratio on the mean drop size was studied. Seven different ethanol solutions were used to simulate changes in fuel physical properties. The range of atomizing air velocities was from 30 to 80 m/s. The mean drop diameter was measured at ambient temperature (295 K) and atmospheric pressure. Author

A86-22413* Case Western Reserve Univ., Cleveland, Ohio.

OSCILLATORY THERMOCAPILLARY FLOWS

S. OSTRACH, Y. KAMOTANI, and C. L. LAI (Case Western Reserve University, Cleveland, OH) (International Conference on Physicochemical Hydrodynamics, 5th, Tel Aviv, Israel, Dec. 16-21, 1984) PCH/PhysicoChemical Hydrodynamics (ISSN 0191-9059), vol. 6, no. 5-6, 1985, p. 585-599. refs (Contract NAG3-411)

Experimental and theoretical research conducted to understand the physical mechanism of oscillatory thermocapillary convection is discussed. A physical model that plausibly describes the cause of thermocapillary flow oscillations and to yield the proper parameters for identifying their onset is considered. Strong convection indicated by a large Marangoni number, as well as free surface deformation, appear to be important factors for the onset of the convection. C.D.

A86-22615* Virginia Univ., Charlottesville.

SIMPLEX FINITE ELEMENT ANALYSIS OF VISCOUS INCOMPRESSIBLE FLOW WITH PENALTY FUNCTION FORMULATION

P. E. ALLAIRE, M. C. ROSEN, and J. G. RICE (Virginia, University, Charlottesville) Finite Elements in Analysis and Design (ISSN 0168-874X), vol. 1, April 1985, p. 71-88. refs (Contract NAG3-180)

Viscous flow calculations are important for the determination of separated flows, recirculating flows, secondary flows and so on. This paper presents a penalty function approach for the finite element analysis of steady incompressible viscous flow. A simplex element is used with linear velocity and constant pressure in contrast to other works which usually employ higher order elements. Simplex elements yield analytical expressions for the element matrices which in turn lead to efficient solutions. Earlier works have partially indicated how constraint and lock-up problems might be avoided for simplex elements. This paper extends the earlier works by indicating the approach in detail and verifying that it is successful for several applications not discussed in the literature so far. Solution times and accuracy considerations are discussed for Couette flow, plane Poiseuille flow, a driven cavity problem, and laminar and turbulent flow over a step. Author

A86-22676*# National Aeronautics and Space Administration. Lewis Research Center, Cleveland, Ohio.

PREDICTION OF HEAT RELEASE EFFECTS ON A MIXING LAYER

M. FARSHCHI (NASA, Lewis Research Center; Sverdrup Technology, Inc., Cleveland, OH) AIAA, Aerospace Sciences Meeting, 24th, Reno, NV, Jan. 6-9, 1986. 14 p. refs (Contract NAS3-24105) (AIAA PAPER 86-0058)

A fully second-order closure model for turbulent reacting flows is suggested based on Favre statistics. For diffusion flames the

34 FLUID MECHANICS AND HEAT TRANSFER

local thermodynamic state is related to a single conserved scalar. The properties of pressure fluctuations are analyzed for turbulent flows with fluctuating density. Closure models for pressure correlations are discussed and modelled transport equations for Reynolds stresses, turbulent kinetic energy dissipation, density-velocity correlations, scalar moments and dissipation are presented and solved, together with the mean equations for momentum and mixture fraction. Solutions of these equations are compared with the experimental data for high heat release free mixing layers of fluorine and hydrogen in a nitrogen diluent.

Author

A86-22682*# Pennsylvania State Univ., University Park.
COMPUTATION OF TURBULENT ROTATING CHANNEL FLOW WITH AN ALGEBRAIC REYNOLDS STRESS MODEL

M. J. WARFIELD and B. LAKSHMINARAYANA (Pennsylvania State University, University Park) AIAA, Aerospace Sciences Meeting, 24th, Reno, NV, Jan. 6-9, 1986. 10 p. refs
(Contract NGT-39-009-802; NSG-3266)
(AIAA PAPER 86-0214)

An Algebraic Reynolds Stress Model has been implemented to modify the Kolmogorov-Prandtl eddy viscosity relation to produce an anisotropic turbulence model. The eddy viscosity relation becomes a function of the local turbulent production to dissipation ratio and local turbulence/rotation parameters. The model is used to predict fully-developed rotating channel flow over a diverse range of rotation numbers. In addition, predictions are obtained for a developing channel flow with high rotation. The predictions are compared with the experimental data available. Good predictions are achieved for mean velocity and wall shear stress over most of the rotation speeds tested. There is some prediction breakdown at high rotation (rotation number greater than .10) where the effects of the rotation on turbulence become quite complex. At high rotation and low Reynolds number, the laminarization on the trailing side represents a complex effect of rotation which is difficult to predict with the described models.

Author

A86-22735*# Southwest Research Inst., Houston, Tex.
EFFECT OF ELEVATED TEMPERATURE AND PRESSURE ON SPRAYS FROM SIMPLEX SWIRL ATOMIZERS

L. G. DODGE (Southwest Research Institute, San Antonio, TX) and J. A. BIAGLOW (NASA, Lewis Research Center, Cleveland, OH) ASME, Transactions, Journal of Engineering for Gas Turbines and Power (ISSN 0022-0825), vol. 108, Jan. 1986, p. 209-215. refs

(Contract NAS3-24090)
(ASME PAPER 85-GT-58)

An examination is made of the effects of air temperature and pressure on the spray quality of a moderately high capacity pressure swirl atomizer spraying jet-A and No. 2 diesel fuel. Drop size distributions, in terms of both Sauter mean diameter (SMD) and the width of the distribution given by the Rosin-Rammler N parameter, are determined over a variety of air conditions. Close to the nozzle, limited data suggest that the SMDs were a strong function of air density, but independent of air temperature. Trends of SMD and N are shown as a function of distance from the nozzle at all conditions, indicating some of the evaporation characteristics of fuel sprays.

O.C.

A86-23131*# Massachusetts Inst. of Tech., Cambridge.
FORMATION AND INFLAMMATION OF A TURBULENT JET

A. F. GHONIEM (MIT, Cambridge, MA), D. Y. CHEN (General Motors Corp., Allison Gas Turbine Div., Indianapolis, IN), and A. K. OPPENHEIM (California, University, Berkeley) AIAA Journal (ISSN 0001-1452), vol. 24, Feb. 1986, p. 224-229. Previously cited in issue 06, p. 769, Accession no. A84-18171. refs
(Contract W-7405-ENG-48; NAG3-131; NSF CPE-81-15163)

A86-24463* Akron Univ., Ohio.

AN EXPERIMENTAL INVESTIGATION AND SOME ANALYTICAL CONSIDERATIONS CONCERNING THE VAPOROUS/GASEOUS CAVITY CHARACTERISTICS OF AN ECCENTRIC SHAFT SEAL OR BEARING

M. J. BRAUN (Akron, University, OH) and R. C. HENDRICKS (NASA, Lewis Research Center, Cleveland, OH) IN: Heat and mass transfer in rotating machinery. Washington, DC, Hemisphere Publishing Corp., 1984, p. 201-213. refs

A86-24468* Stanford Univ., Calif.

ANALYSIS OF THE UNCERTAINTIES IN VELOCITY MEASUREMENTS WITH TRIPLE HOT-WIRE PROBES

M. N. FROTA and R. J. MOFFAT (Stanford University, CA) IN: Heat and mass transfer in rotating machinery. Washington, DC, Hemisphere Publishing Corp., 1984, p. 293-306. USAF-supported research. refs
(Contract NAG3-3)

A detailed computerized sensitivity analysis of the triple hot-wire equations has been performed in order to delineate the uncertainties associated with measurements of the velocity components. Absolute and relative uncertainties for the instantaneous hot-wire outputs are calculated as functions of roll and pitch angles, based on a constant probability combination of the uncertainties in the inputs. From the results, it is concluded that the small inherent difficulties associated with the triple hot-wire data do not reflect artifacts introduced by the data processing. Fixed errors present in the V and W channels of the output are due to the nonzero measuring volume of the triple wire probe, and are entirely predictable.

C.D.

A86-24496*# National Aeronautics and Space Administration, Lewis Research Center, Cleveland, Ohio.

THEORETICAL MODELING OF THE VAPOR CAVITATION IN DYNAMICALLY LOADED JOURNAL BEARINGS

D. E. BREWE (NASA, Lewis Research Center; U.S. Army, Propulsion Directorate, Cleveland, OH) ASME and ASLE, Joint Lubrication Conference, Atlanta, GA, Oct. 8-10, 1985. 10 p. Previously announced in STAR as N86-10463. refs
(ASME PAPER 85-TRIB-51)

A theoretical investigation is made of the evolution of a vapor-bubble for a submerged journal bearing under dynamically loaded conditions using the Elrod algorithm. This method conserves mass throughout the computational domain. A comparison study is performed to determine some of the consequences of applying a nonconservative theory (pseudo-Gumbel BC) to a dynamic problem. A complete dynamic cycle of a journal whirling in a circular path is chosen for the basis of comparison. Significant differences are observed in the load components near the end of the cycle. Further, good agreement with experiment is found for stationary and nonstationary cavitation.

Author

A86-25567* Flow Research, Inc., Kent, Wash.

DIRECT NUMERICAL SIMULATIONS OF CHEMICALLY REACTING TURBULENT MIXING LAYERS

J. J. RILEY, R. W. METCALFE, and S. A. ORSZAG (Flow Research Co., Kent, WA) Physics of Fluids (ISSN 0031-9171), vol. 29, Feb. 1986, p. 406-422. refs
(Contract NAS3-23531)

The results of direct numerical simulations of chemically reacting, turbulent mixing layers are presented. The reaction considered is a binary, irreversible reaction with no heat release, so that only the effect of the turbulence on the chemical reaction is investigated. The simulation results are shown to be consistent with similarity theory, and are found to be in approximate agreement with laboratory data, even though there are no adjustable parameters in the method.

Author

A86-26606*# Michigan Univ., Ann Arbor.

SPRAY ATOMIZATION AND COMBUSTION

G. M. FAETH (Michigan, University, Ann Arbor) AIAA, Aerospace Sciences Meeting, 24th, Reno, NV, Jan. 6-9, 1986. 17 p. refs (Contract NAG3-190; AF-AFOSR-85-0244; N00014-80-C-0517; N00014-85-C-0148) (AIAA PAPER 86-0136)

New theoretical and experimental methods for studying sprays are reviewed. Common methods to analyze dilute sprays are described and used to interpret recent measurements of the structure of dilute sprays and related dispersed turbulent jets. Particle-laden jets, nonevaporating, evaporating, and combusting sprays, and noncondensing and condensing bubbly jets are examined and used to initially evaluate current analytical methods for a wide range of conditions. Dense sprays are briefly discussed. C.D.

A86-26614*# Houston Univ., Tex.

FREE SHEAR FLOWS - ORGANIZED STRUCTURES AND EFFECTS OF EXCITATION

A. K. F. HUSSAIN, H. S. HUSAIN, J. TSO, M. HAYAKAWA (Houston, University, TX), K. B. M. Q. ZAMAN (NASA, Lewis Research Center, Cleveland, OH; Houston, University, TX) et al. AIAA, Aerospace Sciences Meeting, 24th, Reno, NV, Jan. 6-9, 1986. 13 p. NSF-supported research. refs (Contract N00014-85-K-0126; NAG3-408) (AIAA PAPER 86-0235)

Recent studies of free shear flows are reviewed. Included are experimental studies of: excited and unexcited circular and elliptic jets, plane wake and mixing layers, and effects of excitation on augmentation and reduction of jet turbulence and jet noise. It is shown that proper excitation can produce both large increases and large decreases in turbulence and Reynolds stress level, mixing and noise generation, suggesting promising technological applications of self-excited jets such as whistler jets. It is also argued that 'ribs' or longitudinal vortices play an important role in production and mixing in free, and perhaps all, turbulent shear flows. The 'cut-and-connect' interaction of vortical structures is proposed as a key mechanism for coherent structure breakdown, mixing, turbulence production, and aerodynamic noise generation. A simple analysis of the viscous vorticity equation using symmetry of configurations of vortical structures before and after the interaction gives realistic predictions. Author

A86-26630*# Wichita State Univ., Kans.

AN EXPERIMENTAL METHOD FOR MEASURING DROPLET IMPINGEMENT EFFICIENCY ON TWO- AND THREE-DIMENSIONAL BODIES

M. PAPADAKIS, G. W. ZUMWALT (Wichita State University, KS), J. J. KIM, R. ELANGOVA, G. A. FREUND, JR. (Boeing Military Airplane Co., Wichita, KS) et al. AIAA, Aerospace Sciences Meeting, 24th, Reno, NV, Jan. 6-9, 1986. 9 p. FAA-supported research. refs (Contract NAG3-566) (AIAA PAPER 86-0406)

An efficient and accurate method is described for extracting water droplet impingement efficiency data from dye impregnated blotter paper samples obtained by employing a dye-tracer technique in wind tunnel spray tests. The method is based on laser reflectance spectroscopy. A brief description of the test method, instrumentation, and data reduction system is also presented. Preliminary test results and analyses are included for a cylinder and a 65(2)015 airfoil. Author

A86-28649*# National Aeronautics and Space Administration. Lewis Research Center, Cleveland, Ohio.

BOUNDARY PERTURBATION METHOD FOR FREE BOUNDARY PROBLEM IN CONVECTIVELY COOLED CONTINUOUS CASTING

R. SIEGEL (NASA, Lewis Research Center, Cleveland, OH) ASME, Transactions, Journal of Heat Transfer (ISSN 0022-1481), vol. 108, Feb. 1986, p. 230-234. refs

Novel mathematical techniques are here used to treat general boundary conditions in convectively cooled continuous ingot casting problems, applying a constant convective heat transfer coefficient at the ingot sides (so that the temperature distribution along the sides is unknown). The problem is first inverted to treat the physical coordinates as dependent variables of temperature and heat flow, mapping the ingot into a region that is nearly rectangular. A boundary perturbation method is then used to obtain an analytical solution in this near-rectangular region. Solidification interface shapes depend on two dimensionless parameters: one is a function of the casting velocity, while the other is dependent on the convective heat transfer coefficient at the cooled wall. O.C.

A86-28696*# United Technologies Research Center, East Hartford, Conn.

CALCULATION OF THREE-DIMENSIONAL BOUNDARY LAYERS ON ROTATING TURBINE BLADES

O. L. ANDERSON (United Technologies Research Center, East Hartford, CT) IN: Three dimensional flow phenomena in fluid machinery; Proceedings of the Winter Annual Meeting, Miami Beach, FL, November 17-22, 1985. New York, American Society of Mechanical Engineers, 1985, p. 121-132. refs (Contract NAS3-23716)

An assessment has been made of the applicability of a three dimensional boundary layer analysis to the calculation of heat transfer and streamline flow patterns on the surfaces of both stationary and rotating turbine passages. In support of this effort, an analysis has been developed to calculate a general nonorthogonal surface coordinate system for arbitrary three dimensional surfaces and also to calculate the boundary layer edge conditions for compressible flow using the surface Euler equations and experimental pressure distributions. Using available experimental data to calibrate the method, calculations are presented for the endwall, and suction surfaces of a stationary cascade and for the pressure surface of a rotating turbine blade. The results strongly indicate that the three dimensional boundary layer analysis can give good predictions of the flow field and heat transfer on the pressure, suction, and endwall surfaces in a gas turbine passage. Author

A86-29029* National Aeronautics and Space Administration. Lewis Research Center, Cleveland, Ohio.

FREE BOUNDARY SHAPE OF A CONVECTIVELY COOLED SOLIDIFIED REGION

R. SIEGEL (NASA, Lewis Research Center, Cleveland, OH) International Journal of Heat and Mass Transfer (ISSN 0017-9310), vol. 29, Feb. 1986, p. 309-315. refs

The two-dimensional steady-state shape of a solidified region, such as a frost layer, was determined analytically for formation on a plate that is convectively cooled. The nonuniform shape of the layer is produced by exposure to a spatially nonuniform distribution of radiant energy. For high convective cooling the cooled wall approaches a uniform temperature, and an exact solution is obtained for the free boundary shape. For a lesser amount of convective cooling, the variation in temperature along the cooled boundary is treated by a boundary perturbation method. Some illustrative examples are given that show the effects of nonuniform heating and the magnitude of convective heat transfer at the cooled wall. Only one boundary condition is approximated by the perturbation solution; all of the other boundary conditions are satisfied exactly. The calculated results given here were found to satisfy the approximate boundary condition within a very small error. Author

A86-29419* Rensselaer Polytechnic Inst., Troy, N.Y. **INTERACTION OF FLOWS WITH THE CRYSTAL-MELT INTERFACE**

M. E. GLICKSMAN (Rensselaer Polytechnic Institute, Troy, NY), S. R. CORIELL, and G. B. MCFADDEN (NBS, Gaithersburg, MD) IN: Annual review of fluid mechanics. Volume 18. Palo Alto, CA, Annual Reviews, Inc., 1986, p. 307-335. refs
(Contract NAG3-33; NASA ORDER H-27954-B)

The coupling between a crystal-melt interface and fluid flow is investigated. The solidification boundary conditions at the crystal-melt interface are described. The influences of morphological and double-diffusive instabilities during directional solidification on the interface are studied. The experiments by Glicksman and Mickaloni (1982) and Fang et al. (1985) which examine the relationship between the hydrodynamic state of the phase melt and phase-change interface are analyzed. The Rayleigh-Benard problem, and the effect of crystal-melt interaction on the Rayleigh number are examined. Various applications for melt-flow interactions with solid-liquid interface to engineering and welding are discussed. I.F.

A86-30211* Michigan State Univ., East Lansing. **ENTRAINMENT REGION PHENOMENA FOR A LARGE PLANE SHEAR LAYER**

S. K. ALI, C. L. KLEWICKI, P. J. DISIMILE, I. LAWSON, and J. F. FOSS (Michigan State University, East Lansing) IN: Symposium on Turbulent Shear Flows, 5th, Ithaca, NY, August 7-9, 1985, Proceedings. University Park, PA, Pennsylvania State University, 1985, p. 3.7-3.12. refs
(Contract NAG2-86; NAG1-287; NAG3-574)

The subatmospheric test section of the present free shear layer facility allows the entrainment air to be introduced with a negligible disturbance level. The very low frequency oscillations, which are prominently observed in the entrainment stream and which are present throughout the shear layer, are attributed to an inherent instability in the transition from a boundary layer to a free shear layer state. The basic features of the disturbance field are documented herein. Author

A86-30218* Flow Research, Inc., Kent, Wash. **COHERENT STRUCTURES IN A TURBULENT MIXING LAYER - A COMPARISON BETWEEN DIRECT NUMERICAL SIMULATIONS AND EXPERIMENTS**

R. W. METCALFE, S. MENON (Flow Research Co., Kent, WA), and A. K. M. F. HUSSAIN (Houston, University, TX) IN: Symposium on Turbulent Shear Flows, 5th, Ithaca, NY, August 7-9, 1985, Proceedings. University Park, PA, Pennsylvania State University, 1985, p. 4.13-4.19. refs
(Contract N00014-82-C-0600; N00014-85-K-0126; NAS3-23531)

An education scheme has been developed in an attempt to determine the characteristics of large-scale vortical structures in a turbulent mixing layer. This analysis scheme has been applied to a set of experimental data taken in a new, larger mixing layer facility designed to minimize boundary and resonance effects. A similar scheme has been developed to apply to the results of a direct numerical simulation of a temporally growing mixing layer. A comparison of the two approaches shows important similarities in the coherent structures. The numerical simulations indicate that low levels of coherent forcing can dramatically change the evolution of the mixing layer. In the absence of such forcing, the numerical simulations and experiments show a lack of regularity in the transverse position, spacing, amplitude, shape and spanwise coherence of the large-scale vortical structures. Author

A86-34377* National Aeronautics and Space Administration. Lewis Research Center, Cleveland, Ohio. **CONVECTIVE AND ABSOLUTE INSTABILITY OF A VISCOUS LIQUID JET**

S. J. LEIB and M. E. GOLDSTEIN (NASA, Lewis Research Center, Cleveland, OH) Physics of Fluids (ISSN 0031-9171), vol. 29, April 1986, p. 952-954. refs

The effect of viscosity on the capillary instability of a liquid jet is examined. The critical Weber number for convective instability

is determined as a function of Reynolds number and comparison is made with the inviscid limit. It is shown that certain waves that are neutral in the inviscid case exhibit growth for finite Reynolds numbers. Author

A86-38388* Arizona State Univ., Tempe. **A COMPARISON OF THREE ALGEBRAIC STRESS CLOSURES FOR COMBUSTOR FLOW CALCULATIONS**

M. NIKJOOY, R. M. C. SO (Arizona State University, Tempe), and B. C. HWANG (David W. Taylor Naval Ship Research and Development Center, Annapolis, MD) ASME, Winter Annual Meeting, Miami Beach, FL, Nov. 17-21, 1985. 10 p. refs
(Contract NAG3-260)
(ASME PAPER 85-WA/FE-3)

A comparison is made of the performance of two locally nonequilibrium and one equilibrium algebraic stress closures in calculating combustor flows. Effects of four different pressure-strain models on these closure models are also analyzed. The results show that the pressure-strain models have a much greater influence on the calculated mean velocity and turbulence field than the algebraic stress closures, and that the best mean strain model for the pressure-strain terms is that proposed by Launder, Reece and Rodi (1975). However, the equilibrium algebraic stress closure with the Rotta return-to-isotropy model (1951) for the pressure-strain terms gives as good a correlation with measurements as when the Launder et al. mean strain model is included in the pressure-strain model. Finally, comparison of the calculations with the standard k-epsilon closure results show that the algebraic stress closures are better suited for simple turbulent flow calculations. Author

A86-38427* Sverdrup Technology, Inc., Cleveland, Ohio. **PARAMETRIC EFFECTS OF CFL NUMBER AND ARTIFICIAL SMOOTHING ON NUMERICAL SOLUTIONS USING IMPLICIT APPROXIMATE FACTORIZATION ALGORITHM**

E. O. DASO (Sverdrup Technology, Inc., Middleburg Heights, OH) AIAA and ASME, Fluid Mechanics, Plasma Dynamics and Lasers Conference, 4th, Atlanta, GA, May 12-14, 1986. 11 p. refs
(Contract NAS3-24105)
(AIAA PAPER 86-1059)

An implicit approximate factorization algorithm is employed to quantify the parametric effects of Courant number and artificial smoothing on numerical solutions of the unsteady 3-D Euler equations for a windmilling propeller (low speed) flow field. The results show that propeller global or performance characteristics vary strongly with Courant number and artificial dissipation parameters, though the variation is such less severe at high Courant numbers. Candidate sets of Courant number and dissipation parameters could result in parameter-dependent solutions. Parameter-independent numerical solutions can be obtained if low values of the dissipation parameter-time step ratio are used in the computations. Furthermore, it is realized that too much artificial damping can degrade numerical stability. Finally, it is demonstrated that highly resolved meshes may, in some cases, delay convergence, thereby suggesting some optimum cell size for a given flow solution. It is suspected that improper boundary treatment may account for the cell size constraint. Author

A86-38442* National Aeronautics and Space Administration. Lewis Research Center, Cleveland, Ohio. **AN EFFICIENT METHOD FOR SOLVING THE STEADY EULER EQUATIONS**

M.-S. LIOU (NASA, Lewis Research Center, Cleveland, OH) AIAA and ASME, Fluid Mechanics, Plasma Dynamics and Lasers Conference, 4th, Atlanta, GA, May 12-14, 1986. 14 p. refs
(Contract AF-AFOSR-84-0327)
(AIAA PAPER 86-1079)

An efficient numerical procedure for solving a set of nonlinear partial differential equations, the steady Euler equations, using Newton's linearization procedure is presented. A theorem indicating quadratic convergence for the case of differential equations is demonstrated. A condition for the domain of quadratic convergence $\Omega(2)$ is obtained which indicates that whether an

approximation lies in $\Omega(2)$ depends on the rate of change and the smoothness of the flow vectors, and hence is problem-dependent. The choice of spatial differencing, of particular importance for the present method, is discussed. The treatment of boundary conditions is addressed, and the system of equations resulting from the foregoing analysis is summarized and solution strategies are discussed. The convergence of calculated solutions is demonstrated by comparing them with exact solutions to one and two-dimensional problems. C.D.

A86-38575* Arizona State Univ., Tempe.
CONCENTRATION DISTRIBUTIONS IN A MODEL COMBUSTOR

S. A. AHMED and R. M. C. SO (Arizona State University, Tempe) Experiments in Fluids (ISSN 0723-4864), vol. 4, no. 2, 1986, p. 107-113. refs
(Contract NAG3-260)

A hot-wire concentration probe with a spatial resolution of 0.13 mm is used to measure concentration in a model cylindrical combustor. The flow inside the combustor is simulated by injecting a helium jet into a cylindrical confinement with or without swirling air flow present. Mean concentrations are essentially zero outside of the jet region, indicating complete confinement of the scalar field by the swirling flow. Consequently, concentration fluctuations are found to be relatively weak compared to velocity fluctuations, and are maximum off-axis at a point which corresponds to the interface between helium and air flows. However, in the absence of a swirling air flow, the helium diffuses quickly to fill the combustor. The resulting helium concentrations are constant and do not resemble the jet-like behavior of the velocity field. Author

A86-39077* Purdue Univ., West Lafayette, Ind.
A STAGNATION PRESSURE PROBE FOR DROPLET-LADEN AIR FLOW

S. N. B. MURTHY, C. M. EHRESMAN (Purdue University, West Lafayette, IN), and M. LEONARDO Journal of Propulsion and Power (ISSN 0748-4658), vol. 2, May-June 1986, p. 195, 196. Previously cited in issue 07, p. 898, Accession no. A85-19672. refs
(Contract F33615-78-C-2401; NAG3-62)

A86-39865* Centro Tecnico Aeroespacial, San Jose dos Campos (Brazil).

RELAMINARIZATION OF THE BOUNDARY LAYER OVER A FLAT PLATE IN SHOCK TUBE EXPERIMENTS

J. N. HINCKEL (Centro Tecnico Aeroespacial, Sao Jose dos Campos, Brazil) and H. T. NAGAMATSU (Rensselaer Polytechnic Institute, Troy, NY) AIAA and ASME, Joint Thermophysics and Heat Transfer Conference, 4th, Boston, MA, June 2-4, 1986. 7 p. refs
(Contract NAG3-292; NSF MED-80-06806)
(AIAA PAPER 86-1238)

The relaminarization of the boundary layer over a flat plate in the shock tube was investigated by using the partially reflected shock wave technique. The flow Mach number was approximately 0.14, which corresponds to the inlet flow Mach number for the first row of vanes in a gas turbine. The thin film platinum heat gauges were used to measure the heat transfer rate and the Stanton number was calculated from the oscilloscope voltage traces. The Reynolds number was varied by changing the operation pressure of the shock tube and the values varied from 2.3×10 to the 4th to 5.3×10 to the 5th. For a Reynolds number range of 7×10 to the 4th to 3.5×10 to the 5th, the relaminarization of the boundary layer was observed. This phenomenon is due to the decay of the turbulence level in the flow as the reflected shock wave moves upstream from the flat plate. As the Reynolds number increased, the relaminarization was delayed and the delay was related to the turbulence generated by the reflected shock wave. Author

A86-40578* Oakland Univ., Rochester, Mich.

LIQUID DROPLET RADIATOR THERMAL CHARACTERISTICS
R. H. EDGERTON (Oakland University, Rochester, MI) and P. S. DIEM-KIRSOP (NASA, Lewis Research Center, Cleveland, OH) IN: Space Systems Technology Conference, San Diego, CA, June 9-12, 1986, Technical Papers. New York, American Institute of Aeronautics and Astronautics, 1986, p. 4-14. refs
(AIAA PAPER 86-1162)

The effects of droplet size, emissivity, and spacing on the liquid droplet radiator (LDR) performance space heat rejection system are investigated. The procedures for predicting surface emissivity of semitransparent droplets as a function of absorptivity and radius are examined. The relation between absorptivity, reflectivity, transmissivity, and emissivity is studied. It is observed that for droplets in the 25-200 micron range the radius affects emissivity. The thermal performance of an array of droplet streams is described using a thermal radiation model. Droplet temperatures are calculated; it is shown that outside droplet streams are more effective than interior droplets for arrays in the range of radius to spacing ratio from 0.05-0.2. Temperature distributions as a function of droplet size, emissivity, and velocity are presented. The heat transfer performance of a LDR is evaluated in terms of fin effectiveness. The equivalent sheet emissivities of droplet streams are examined. I.F.

A86-41242* National Aeronautics and Space Administration. Lewis Research Center, Cleveland, Ohio.

A NEW APPROACH FOR SOLVING THE THREE-DIMENSIONAL STEADY EULER EQUATIONS. I - GENERAL THEORY

S.-C. CHANG and J. J. ADAMCZYK (NASA, Lewis Research Center, Cleveland, OH) Journal of Computational Physics (ISSN 0021-9991), vol. 60, Aug. 1986, p. 23-61. refs

The present iterative procedure combines the Clebsch potentials and the Munk-Prim (1947) substitution principle with an extension of a semidirect Cauchy-Riemann solver to three dimensions, in order to solve steady, inviscid three-dimensional rotational flow problems in either subsonic or incompressible flow regimes. This solution procedure can be used, upon discretization, to obtain inviscid subsonic flow solutions in a 180-deg turning channel. In addition to accurately predicting the behavior of weak secondary flows, the algorithm can generate solutions for strong secondary flows and will yield acceptable flow solutions after only 10-20 outer loop iterations. O.C.

A86-41721* National Aeronautics and Space Administration. Lewis Research Center, Cleveland, Ohio.

COUPLING CONDITIONS FOR INTEGRATING BOUNDARY LAYER AND ROTATIONAL INVISCID FLOW

P. M. SOCKOL (NASA, Lewis Research Center, Cleveland, OH) and W. A. JOHNSTON (Aerospace Corp., El Segundo, CA) AIAA Journal (ISSN 0001-1452), vol. 24, June 1986, p. 1033-1035.

The matching of a boundary layer and a rotational inviscid flow is reexamined by extending the Johnson and Sockol (1979) coupling conditions to include the case where the boundary layer solution includes the second-order effects of the freestream vorticity and the total temperature gradient. It is pointed out that two of the three conditions are not independent. If the boundary layer solution satisfies the appropriate momentum and energy integral equations, it follows that the imposition of the normal mass flux condition insures that the conditions on a normal flux of streamwise momentum and total enthalpy will also be satisfied. O.C.

A86-41725* Wisconsin Univ., Milwaukee.

TRIPLE-VELOCITY PRODUCTS IN A CHANNEL WITH A BACKWARD-FACING STEP

R. S. AMANO and P. GOEL (Wisconsin, University, Milwaukee) AIAA Journal (ISSN 0001-1452), vol. 24, June 1986, p. 1040-1043. refs
(Contract NAG3-546)

Attention is given to the evaluation of tripple velocity products in the reattaching and developing region behind a backward facing step. The change in tripple velocity products is significant in the wake region, yielding substantial variation in the diffusion rate of

the Reynolds stresses. Four models of the third-order closure are examined, and the results are compared with the experimental data for Chandrsuda and Bradshaw (1980). O.C.

A86-42656*# Calspan Corp., Buffalo, N. Y.
TURBINE-STAGE HEAT TRANSFER - COMPARISON OF SHORT-DURATION MEASUREMENTS WITH STATE-OF-THE-ART PREDICTIONS

W. J. RAE, D. B. TAULBEE, K. C. CIVINKAS (Calspan-UB Research Center, Buffalo, NY), and M. G. DUNN (NASA, Lewis Research Center, Cleveland, OH; Calspan-UB Research Center, Buffalo, NY) AIAA, ASME, SAE, and ASEE, Joint Propulsion Conference, 22nd, Huntsville, AL, June 16-18, 1986. 24 p. refs (Contract NAG3-469; NAG3-581) (AIAA PAPER 86-1465)

Comparisons are made between calculated and measured heat-transfer distributions on the midspan locations of the stators and rotors of two turbine stages. The agreement is generally good, except in regions near the leading edge, and is better for blading of higher aspect ratio. It is suggested that the discrepancies near the leading edge are caused by free-stream turbulence, and attempts to improve the modeling of this factor show improved agreement. Author

A86-42711*# Florida Univ., Gainesville.
FLUID FLOW AND FUEL-AIR MIXING IN A MOTORED TWO-DIMENSIONAL WANKEL ROTARY ENGINE

T. I.-P. SHIH (Florida, University, Gainesville), H. L. NGUYEN (NASA, Lewis Research Center, Cleveland, OH), and J. STEGEMAN (NASA, Lewis Research Center, Cleveland; Toledo, University, OH) AIAA, ASME, SAE, and ASEE, Joint Propulsion Conference, 22nd, Huntsville, AL, June 16-18, 1986. 11 p. refs (Contract NAG3-363) (AIAA PAPER 86-1556)

The implicit-factored method of Beam and Warming was employed to obtain numerical solutions to the conservation equations of mass, species, momentum, and energy to study the unsteady, multidimensional flow and mixing of fuel and air inside the combustion chambers of a two-dimensional Wankel rotary engine under motored conditions. The effects of the following engine design and operating parameters on fluid flow and fuel-air mixing during the intake and compression cycles were studied: engine speed, angle of gaseous fuel injection during compression cycle, and speed of the fuel leaving fuel injector. Author

A86-42738*# Scientific Research Associates, Inc., Glastonbury, Conn.

NUMERICAL ANALYSIS OF SOME SUPERSONIC VISCOUS FLOWS RELATED TO INLET AND NOZZLE SYSTEMS

Y.-N. KIM, R. C. BUGGELN, and H. MCDONALD (Scientific Research Associates, Inc., Glastonbury, CT) AIAA, ASME, SAE, and ASEE, Joint Propulsion Conference, 22nd, Huntsville, AL, June 16-18, 1986. 13 p. refs (Contract NAS3-22759; NAS3-23053; NAS3-24224) (AIAA PAPER 86-1597)

A numerical method originally developed for three-dimensional supersonic inlet flow calculations is extended and applied to the study of two-dimensional and three-dimensional flows associated with arbitrary propulsion systems. The method is based on the forward spatial marching solution of a reduced form of the three-dimensional steady Navier-Stokes equations in which streamwise pressure gradients are retained in both the subsonic and supersonic regions. The present paper briefly describes the analysis and then shows three applications. In the first application, a wall transpiration study has been performed for the two-dimensional shock wave/turbulent boundary layer interaction flow field with application to an inlet configuration. The second application treats a rectangular high speed inlet with a swept sideplate including the effects of sideplate spillage. Finally, the method is utilized to analyze the interaction of an under-expanded supersonic jet with an ambient flow. Computed results are examined and compared with available experimental measurements. It is demonstrated that the present numerical method is capable of

numerically simulating complex two- and three-dimensional flows relevant to hypersonic propulsion systems in a manner which both shows good agreement with data when such data is available, and which shows the complex flow features in the absence of data. Author

A86-42739*# United Technologies Research Center, East Hartford, Conn.

ASSESSMENT OF A PARABOLIC ANALYSIS FOR AXISYMMETRIC INTERNAL FLOWS IN ROCKET AND TURBOMACHINERY DUCTS

G. D. POWER and O. L. ANDERSON (United Technologies Research Center, East Hartford, CT) AIAA, ASME, SAE, and ASEE, Joint Propulsion Conference, 22nd, Huntsville, AL, June 16-18, 1986. 14 p. refs (Contract NAS3-24338) (AIAA PAPER 86-1598)

The flow paths in gas turbine passages encompass a wide range of flow properties such as Reynolds number and Mach number as well as many other variable flow conditions such as swirl, free-stream turbulence, and laminar/turbulent transition. An existing computer program, the Axisymmetric Diffuser Duct (ADD) code, which calculates compressible, turbulent, swirling flow through axisymmetric ducts has been modified to include the effects of free-stream turbulence and laminar/turbulent transition. The program has been evaluated on a matrix of test cases to determine its accuracy, robustness, and limits of applicability. This improved version of the ADD code calculates solutions which compare well with available data and can now be applied to a wider range of problems than previously possible. In addition a concept called local enhancement was developed and tested on a simple two-dimensional geometry in order to demonstrate a method to reduce computer time. In this concept the pressure distribution is calculated on a coarse grid using the ADD code and the viscous layer is locally enhanced using a boundary layer analysis. By applying this concept, an order of magnitude reduction in computer time was possible without any loss in accuracy. Author

A86-42752*# United Technologies Research Center, East Hartford, Conn.

FORCED MIXER LOBES IN EJECTOR DESIGNS

W. M. PRESZ, JR. (Western New England College, Springfield, MA), B. L. MORIN (United Technologies Research Center, East Hartford, CT), and R. G. GOUSY AIAA, ASME, SAE, and ASEE, Joint Propulsion Conference, 22nd, Huntsville, AL, June 16-18, 1986. 11 p. refs (Contract NAG3-610) (AIAA PAPER 86-1614)

Forced mixer lobes in augmentor primary ejectors obtain a 100-percent increase in pumping over conventional design, together with nearly complete mixing in very short mixing ducts, through the generation of large scale axial vorticity in the mixing duct. The vorticity causes rapid mixing of the primary and secondary flows with low losses; since mixing length is minimized, wall friction losses are reduced, allowing more secondary flow to be pumped for a given total pressure in the primary flow. Analytical results are presented that are judged to have significant implications for future ejector test work. O.C.

A86-42780*# United Technologies Research Center, East Hartford, Conn.

MASS AND MOMENTUM TURBULENT TRANSPORT EXPERIMENTS WITH SWIRLING CONFINED COAXIAL JETS. II

R. ROBACK and B. V. JOHNSON (United Technologies Research Center, East Hartford, CT) AIAA, ASME, SAE, and ASEE, Joint Propulsion Conference, 22nd, Huntsville, AL, June 16-18, 1986. 11 p. (Contract NAS3-22771) (AIAA PAPER 86-1665)

An experimental study of mixing downstream of swirling coaxial jets discharging into an expanded duct was conducted to obtain data for the evaluation and improvement of turbulent transport

models currently used in a variety of computational procedures throughout the combustion community. A combination of laser velocimeter and laser induced fluorescence techniques was employed to obtain mean and fluctuating velocity and concentration distributions at selected axial and radial locations throughout the flow field. Flow visualization techniques were also employed to determine qualitatively the time dependent characteristics of the flow and the scale of turbulence. Simultaneous two component velocity and concentration/velocity measurements provided data which were used to determine the average momentum and mass transport rates for each of three measurement planes. Mixing for swirling flows occurred in several steps of axial and radial mean convective flow and was completed in one-third the length required for nonswirling flow. Comparison of the mass and momentum transport processes for swirling and nonswirling flows indicated that large differences existed in these processes between the two flows. Author

A86-42812*# Wisconsin Univ., Milwaukee.
TURBULENCE ENERGY AND DIFFUSION TRANSPORT IN A SEPARATING AND REATTACHING FLOW
 R. S. AMANO (Wisconsin, University, Milwaukee) and P. GOEL AIAA, ASME, SAE, and ASEE, Joint Propulsion Conference, 22nd, Huntsville, AL, June 16-18, 1986. 10 p. refs
 (Contract NAG3-546)
 (AIAA PAPER 86-1724)

For accurate prediction of the turbulent flow in separated and reattaching regions, it is necessary to incorporate the second- and third-moments of turbulent fluctuations. The turbulence energy and the energy dissipation rate equations are modified by incorporating the second-order closure. Moreover, the third-order closure with near-wall correction is developed for the evaluation of the diffusive action of the second-moments. After comparison of the results with experimental data, it is shown that the models developed here improve the prediction of triple-velocity correlations in both recirculating and developing flow regions. Author

A86-42813*# National Aeronautics and Space Administration, Lewis Research Center, Cleveland, Ohio.
CHARACTERIZATION OF SIMULATED SMALL-DROPLET FUEL SPRAYS
 R. D. INGEBO (NASA, Lewis Research Center, Cleveland, OH) AIAA, ASME, SAE, and ASEE, Joint Propulsion Conference, 22nd, Huntsville, AL, June 16-18, 1986. 7 p. Previously announced in STAR as N86-24961. refs
 (AIAA PAPER 86-1725)

A two-fluid pneumatic atomizer operating at relatively high liquid and gas pressures produced water sprays that simulated small-droplet clouds of liquid fuel for use in studying vaporization and fuel-air mixing effects on combustor performance and emissions. To characterize the sprays, a scattered-light scanning instrument was developed and measurements of volume median or volume mean diameter, $D_{sub\ 0.5}$, were correlated with $D_{sub\ 0}$, $W_{sub\ w}$, and $W_{sub\ n}$, i.e., orifice diameter, water, and nitrogen gas flow rates, respectively, to give the general expression: $D_{sub\ 0.5} \approx (D_{sub\ 0}^{0.2} (W_{sub\ w})^m (W_{sub\ n})^n)$, which yields $D_{sub\ 0.5} = 45 (D_{sub\ 0}^{0.2} (W_{sub\ w})^m (W_{sub\ n})^n)$ (W sub w sup -1.2). Values of $D_{sub\ 0}$, $W_{sub\ w}$, and $W_{sub\ n}$ are in centimeters and grams/second, respectively. Farther downstream at an axial distance of 6.7 cm, exponent m increased from 0.2 to 0.4 and exponent n decreased from -1.2 to -1.0 and at a distance of 25 cm downstream of the atomizer, n decreased to -0.8. The increase in exponent m and decrease in exponent n was attributed to a loss of very small droplets from the spray due primarily to vaporization and diffusion effects on clouds of small droplets traveling a distance of 25 cm. Author

A86-43037* Pennsylvania State Univ., University Park.
A SPACE-MARCHING METHOD FOR VISCOUS INCOMPRESSIBLE INTERNAL FLOWS
 M. POUAGARE and B. LAKSHMINARAYANA (Pennsylvania State University, University Park) Journal of Computational Physics (ISSN 0021-9991), vol. 64, June 1986, p. 389-415. refs
 (Contract NSG-3266)

A numerical algorithm for calculating steady subsonic two-dimensional incompressible channel flows in ducts is developed and extended to three-dimensional flows. A space-marching method similar to that developed by Schiff and Steger (1980) for supersonic flows is applied, and numerical results for developing laminar flows in a two-dimensional channel, in a straight square duct, and in a mildly curved square duct are presented graphically. Good agreement with experimental data and analytical results is found. T.K.

A86-45441*# Lockheed-Georgia Co., Marietta.
SOME UNRESOLVED QUESTIONS ON HOT-JET MIXING CONTROL THROUGH ARTIFICIAL EXCITATION
 K. K. AHUJA, J. LEPICOVSKY, and W. H. BROWN (Lockheed-Georgia Co., Marietta) AIAA, Aeroacoustics Conference, 10th, Seattle, WA, July 9-11, 1986. 10 p. refs
 (Contract NAS3-23708)
 (AIAA PAPER 86-1956)

The problem of the mixing enhancement of heated jets through acoustic excitation is addressed using a 5.08 cm diameter jet operating at Mach numbers as high as 1.12 and at temperatures reaching 670 K. An experimental investigation is carried out to determine why high-speed heated jets are not as responsive to internal excitation as low-speed heated jets. Results are also presented which are related to the flow structure in the presence of screech and under the influence of external excitation. It is shown that, if sufficiently high excitation levels are used, the heated jets, even at high levels, can be modified by artificial excitation. Nonetheless, it is concluded that, for the test facility and test conditions used in the present study, the high-Mach-number heated jets are considerably less excitable than the similarly heated low-Mach-number jets. K.K.

A86-46307*# Pennsylvania State Univ., University Park.
COMPUTATION OF TURBULENT FLOWS ON ROTATING BODIES AND DUCTS
 M. POUAGARE and B. LAKSHMINARAYANA (Pennsylvania State University, University Park) Journal of Propulsion and Power (ISSN 0748-4658), vol. 2, July-Aug. 1986, p. 289, 290. refs
 (Contract NSG-3266)

A K-epsilon model for three-dimensional boundary layers modified to include anisotropy and one modified for rotating flows are described. Based on these models, the predictions of a space-marching code show good agreement with the flow data for a rotating cylinder and a rotating channel. Author

A86-46314*# Lockheed-Georgia Co., Marietta.
ACOUSTIC CONTROL OF FREE JET MIXING
 J. LEPICOVSKY, K. K. AHUJA, W. H. BROWN (Lockheed-Georgia Co., Marietta), and P. J. MORRIS (Pennsylvania State University, University Park) Journal of Propulsion and Power (ISSN 0748-4658), vol. 2, July-Aug. 1986, p. 323-330. Previously cited in issue 10, p. 1392, Accession no. A85-25951. refs
 (Contract NAS3-23708)

A86-46318*# California Univ., Los Angeles.
VORTEX MODELING OF SINGLE AND MULTIPLE DILUTION JET MIXING IN A CROSS FLOW
 A. R. KARAGOZIAN (California, University, Los Angeles), T. T. NGUYEN, and C. N. KIM Journal of Propulsion and Power (ISSN 0748-4658), vol. 2, July-Aug. 1986, p. 354-360. Previously cited in issue 19, p. 2797, Accession no. A85-40701. refs
 (Contract NAG3-543)

A86-47012* Illinois Inst. of Tech., Chicago.

FINITE ELEMENT SIMULATION OF TEMPERATURE DEPENDENT FREE SURFACE FLOWS

M. S. ENGELMAN (Illinois Institute of Technology, Chicago) and R. L. SANI (Cooperative Institute for Research in Environmental Sciences; Colorado, University, Boulder) IN: Numerical methods in laminar and turbulent flow; Proceedings of the Fourth International Conference, Swansea, Wales, July 9-12, 1985. Part 2. Swansea, Wales, Pineridge Press, 1985, p. 1325-1335. refs (Contract DAAG29-82-C-0010; NAG3-493)

The method of Engelman and Sani (1984) for a finite-element simulation of incompressible surface flows with a free and/or moving fluid interface, such as encountered in crystal growth and coating and polymer technology, is extended to temperature-dependent flows, including the effect of temperature-dependent surface tension. The basic algorithm of Saito and Scriven (1981) and Ruschak (1980) has been generalized and implemented in a robust and versatile finite-element code that can be employed with relative ease for the simulation of free-surface problems in complex geometries. As a result, the costly dependence on the Newton-Raphson algorithm has been eliminated by replacing it with a quasi-Newton iterative method, which nearly retains the superior convergence properties of the Newton-Raphson method. I.S.

A86-48140* National Aeronautics and Space Administration. Lewis Research Center, Cleveland, Ohio.

DETERMINATION OF CONVECTIVE DIFFUSION HEAT/MASS TRANSFER RATES TO BURNER RIG TEST TARGETS COMPARABLE IN SIZE TO CROSS-STREAM JET DIAMETER

S. A. GOKOGLU and G. J. SANTORO (NASA, Lewis Research Center, Cleveland, OH) ASME, International Gas Turbine Conference and Exhibit, 31st, Duesseldorf, West Germany, June 8-12, 1986. 11 p. Previously announced in STAR as N86-13678. refs

(ASME PAPER 86-GT-68)

Two sets of experiments have been performed to be able to predict the convective diffusion heat/mass transfer rates to a cylindrical target whose height and diameter are comparable to, but less than, the diameter of the circular cross-stream jet, thereby simulating the same geometric configuration as a typical burner rig test specimen located in the cross-stream of the combustor exit nozzle. The first set exploits the naphthalene sublimation technique to determine the heat/mass transfer coefficient under isothermal conditions for various flow rates (Reynolds numbers). The second set, conducted at various combustion temperatures and Reynolds numbers, utilized the temperature variation along the surface of the above-mentioned target under steady-state conditions to estimate the effect of cooling (dilution) due to the entrainment of stagnant room temperature air. The experimental information obtained is used to predict high temperature, high velocity corrosive salt vapor deposition rates in burner rigs on collectors that are geometrically the same. The agreement with preliminary data obtained from Na2SO4 vapor deposition experiments is found to be excellent. Author

A86-48187* Klein, Schanzlin und Becker A.G., Frankenthal (West Germany).

LASER VELOCIMETER MEASUREMENTS IN SHROUDED AND UNSHROUDED RADIAL FLOW PUMP IMPELLERS

C. P. HAMKINS (Klein, Schanzlin und Becker AG, Frankenthal, West Germany) and R. D. FLACK (Virginia, University, Charlottesville) ASME, International Gas Turbine Conference and Exhibit, 31st, Duesseldorf, West Germany, June 8-12, 1986. 7 p. Research supported by the ROMAC Industrial Research Program and Goulds Pumps, Inc. refs

(Contract NAG3-180)

(ASME PAPER 86-GT-129)

Shrouded and unshrouded versions of a four-vaned radial flow impeller with a design flow coefficient of 0.063 were tested in a volute pump using a two-component frequency-shifted laser velocimeter. Velocity profiles were measured at six flow rates and at four radial and six circumferential positions in the volute. The

variations of the velocity from blade to blade and in the axial direction were measured and are presented. A passage vortex caused by tip leakage and relative casing wall velocity was found in the unshrouded impeller. The tip leakage did not accumulate in the suction wake region; the suction wake region was only 30 to 50 percent as large in the unshrouded impeller as compared to the shrouded impeller. The slip was 30 percent higher in the unshrouded impeller and the variation of slip with flow rate is presented. At no measured position in the impellers did the slip factor reach unity; the closest approach was 0.90. Reverse loadings of the vanes at outer radii were found for flow rates below the impeller/volute matching point for both impellers. Author

A86-48218* Virginia Univ., Charlottesville.

FLOW VISUALIZATION OF SECONDARY FLOWS IN THREE CURVE DUCTS

G. M. SANZ and R. D. FLACK (Virginia, University, Charlottesville) ASME, International Gas Turbine Conference and Exhibit, 31st, Duesseldorf, West Germany, June 8-12, 1986. 8 p. Research supported by the University of Virginia. refs

(Contract NAG3-180)

(ASME PAPER 86-GT-166)

Streak photography flow measurements are made for secondary flows in three 90-deg curved ducts of square cross section and different radii of curvature, at Dean numbers of 15,000-36,000 and radius ratios of 0.5, 2.3, and 3.0. Attention is given to secondary flow patterns for three cross sections in each bend: the inlet zero-deg plane, the midpoint 45-deg plane, and the outlet 90-deg plane. After a rapid transition region, the pressure-driven secondary flow patterns were characterized by flow moving toward the outer curved wall at the axial midplane and returning to the inner wall along the duct walls. The 0.5-radius ratio elbow was found to have the greatest influence on upstream inlet conditions. O.C.

A86-49442* Pennsylvania State Univ., University Park.

FLOW AND ATOMIZATION IN FLASHING INJECTORS

A. S. P. SOLOMON, S. D. RUPPRECHT, L.-D. CHEN, and G. M. FAETH (Pennsylvania State University, University Park) Atomisation and Spray Technology (ISSN 0266-3481), vol. 1, 1985, p. 53-76. refs

(Contract NSG-3306)

Flashing injection involves expanding a fluid through an injector until a supersaturated state is reached, causing a portion of the fluid to flash to a vapor. This investigation considered the flow, atomization and spreading properties of flashing injectors with flowing liquids containing dissolved gases (Jet A/air) as well as superheated liquids (Freon-11). The use of a two-stage expansion process, separated by an expansion chamber, was found to be beneficial for good atomization properties of flashing injection - particularly for dissolved gas systems. Both locally homogeneous and separated flow models provided good predictions of injector flow properties. Conventional correlations for drop sizes from pressure and airblast injectors were successfully modified, using the separated flow model to prescribe injector exit conditions, and to correlate drop size measurements. Additional experimental results are provided for spray angles of sprays from flashing injectors. Author

A86-49829* Arizona State Univ., Tempe.

LOCAL EQUILIBRIUM ASSUMPTION FOR ROUND JET CALCULATIONS

R. M. C. SO (Arizona State University, Tempe) and B. C. HWANG (David W. Taylor Naval Ship Research and Development Center, Annapolis, MD) AIAA Journal (ISSN 0001-1452), vol. 24, Aug. 1986, p. 1388-1390. refs

(Contract NAG3-167; NAG3-260)

The similarity solutions of So and Hwang (1986) for self-preserving incompressible turbulent round jets are used to derive closed-form similarity solutions to the k and epsilon equations, and the effect of the local-equilibrium assumption (LEA) on round-jet computations is evaluated. Numerical results are presented graphically and compared with the experimental data of Wagnanski and Fiedler (1969) and the computational results of

Lauder et al. (1972) and Vollmers and Rotta (1977). It is found that when the LEA is accounted for, the jet-centerline turbulent kinetic energy k_0 decays as $1/x$ (where x is the axial coordinate), whereas without accounting for LEA it decays as $1/(x \text{ squared})$; $1/x$ decay is shown to be in better agreement with observations.

T.K.

A86-50275* National Aeronautics and Space Administration. Lewis Research Center, Cleveland, Ohio.

IS NAVIER-STOKES TURBULENCE CHAOTIC?

R. G. DEISSLER (NASA, Lewis Research Center, Cleveland, OH) Physics of Fluids (ISSN 0031-9171), vol. 29, May 1986, p. 1453-1457. refs

Whether turbulent solutions of the Navier-Stokes equations are chaotic is considered. Initially neighboring solutions for a low-Reynolds-number fully developed turbulence are compared. The turbulence is sustained by a nonrandom time-independent external force. The solutions separate exponentially with time, having a positive Liapunov characteristic exponent. Thus the turbulence is characterized as chaotic.

Author

N86-10461*# Stanford Univ., Calif. Thermosciences Div. **FILM COOLING ON A CONVEX WALL: HEAT TRANSFER AND HYDRODYNAMIC MEASUREMENTS FOR FULL AND PARTIAL COVERAGE Final Report**

K. FURUHAMA, R. J. MOFFAT, J. P. JOHNSTON, and W. M. KAYS Aug. 1985 170 p refs (Contract NAG3-3)

(NASA-CR-174964; NAS 1.26:174964) Avail: NTIS HC A08/MF A01 CSCL 20D

Turbine-blade cooling is an important issue for high-efficiency turbine engines, and discrete-hole injection is widely used as a cooling method. In the present study, detailed measurements were made of the heat transfer and hydrodynamics of a film-cooled flow on a convex wall, both for full and partial coverage. Two important parameters were altered: the blowing ratio, m , and the number of rows of injection holes. Three values of m were tested: $m = 0.2, 0.4$, and 0.6 . In the blown region, $m = 0.4$ results in the lowest Stanton numbers of the three blowing ratios tested. This indicates that the value of $m = 0.4$ is near optimum on the convex wall from the point of view of cooling effect by injection. In the recovery region, Stanton numbers gradually approach the no injection values. Although the heat-transfer behavior during recovery from injection looks relatively complicated, the behavior of Stanton number can be explained in terms of two mechanisms: recovery from the thermal effect of injection and recovery from the turbulence augmentation. This interpretation of the data is supported by the hydrodynamic and temperature-profile measurements. For partial blowing cases, the data follow the full-coverage values inside the blown region. In the unblown region, both in the curved and in the flat plate, the effect of the number of blown rows is clearly seen. Hydrodynamic boundary-layer profiles were measured with the aid of a triple hot-water probe. Three mean-velocity components and six turbulence quantities were simultaneously measured, and inside the blown region strong three-dimensionality was observed.

Author

N86-10463*# National Aeronautics and Space Administration. Lewis Research Center, Cleveland, Ohio.

THEORETICAL MODELING OF THE VAPOR CAVITATION IN DYNAMICALLY LOADED JOURNAL BEARINGS

D. E. BREWE 1985 35 p refs Presented at the Tribology Conf., Atlanta, 8-10 Oct. 1985; cosponsored by Am. Soc. of Lubrication Engr., and ASME Sponsored in part by Army (NASA-TM-87076; E-2651; USAAVSCOM-TR-85-C-15; NAS 1.15:87076) Avail: NTIS HC A03/MF A01 CSCL 13I

A theoretical investigation is made of the evolution of a vapor-bubble for a submerged journal bearing under dynamically loaded conditions using the Elrod algorithm. This method conserves mass throughout the computational domain. A comparison study is performed to determine some of the consequences of applying a nonconservative theory (pseudo-Gumbel BC) to a dynamic problem. A complete dynamic cycle of a journal whirling in a circular

path is chosen for the basis of comparison. Significant differences are observed in the load components near the end of the cycle. Further, good agreement with experiment is found for stationary and nonstationary cavitation.

Author

N86-11425*# National Aeronautics and Space Administration. Lewis Research Center, Cleveland, Ohio.

THEORETICAL AND EXPERIMENTAL COMPARISON OF VAPOR CAVITATION IN DYNAMICALLY LOADED JOURNAL BEARINGS

D. E. BREWE, B. J. HAMROCK (Ohio State Univ., Columbus), and B. A. JACOBSON (Lulea Univ.) 1985 16 p refs Proposed for presentation at the Intern. Symp. on Cavitation, Sendai, Japan, 16-19 Apr. 1986 Prepared in cooperation with Army Aviation Research and Development Command, Cleveland, Ohio

(NASA-TM-87121; E-2729; NAS 1.15:87121; USAAVSCOM-TR-85-C-19) Avail: NTIS HC A02/MF A01 CSCL 20D

Vapor cavitation for a submerged journal bearing under dynamically loaded conditions was investigated. The observation of vapor cavitation in the laboratory was done by high-speed photography. It was found that vapor cavitation occurs when the tensile stress applied to the oil exceeded the tensile strength of the oil or the binding of the oil to the surface. The theoretical solution to the Reynolds equation is determined numerically using a moving boundary algorithm. This algorithm conserves mass throughout the computational domain including the region of cavitation and its boundaries. An alternating direction implicit (ADI) method is used to effect the time march. A rotor undergoing circular whirl was studied. Predicted cavitation behavior was analyzed by three-dimensional computer graphic movies. The formation, growth, and collapse of the bubble in response to the dynamic conditions is shown. For the same conditions of dynamic loading, the cavitation bubble was studied in the laboratory using high-speed photography.

E.A.K.

N86-11505*# National Aeronautics and Space Administration. Lewis Research Center, Cleveland, Ohio.

TURBINE HEAT TRANSFER

J. E. ROHDE In *its* Turbine Eng. Hot Sect. Technol. (HOST) p 73-77 Oct. 1983

Avail: NTIS HC A11/MF A01 CSCL 20D

Improved turbine durability and performance and reduced development cost will all result from improved methods of predicting turbine metal temperatures. Better metal temperature prediction methods require improvements in the methods of predicting the hot gas flow over the turbine airfoils and the cooling air flow inside the airfoil and in the methods of predicting the heat transfer rates on both the hot gas side and coolant side of the airfoil. The overall HOST Turbine Heat Transfer effort is directed at improving all four of these areas of concern.

G.L.C.

N86-11506*# Tennessee Univ. Space Inst., Tullahoma.

GAS FLOW ENVIRONMENTAL AND HEAT TRANSFER NONROTATING 3D PROGRAM

T. GEIL and J. STEINHOFF In NASA. Lewis Research Center Turbine Eng. Hot Sect. Technol. (HOST) p 79-86 Oct. 1983 (Contract NAS3-23278)

Avail: NTIS HC A11/MF A01 CSCL 20D

A complete set of benchmark quality data for the flow and heat transfer within a large rectangular turning duct is being compiled. These data will be used to evaluate and verify three dimensional internal viscous flow models and computational codes. The analytical objective is to select such a computational code and define the capabilities of this code to predict the experimental results. Details of the proper code operation will be defined and improvements to the code modeling capabilities will be formulated.

G.L.C.

34 FLUID MECHANICS AND HEAT TRANSFER

N86-11507*# Detroit Diesel Allison, Mich.

GAS SIDE HEAT TRANSFER

L. D. HYLTON /in NASA. Lewis Research Center Turbine Eng. Hot Sect. Technol. (HOST) p 87-99 Oct. 1983 refs (Contract NAS3-22761; NAS3-23695)

Avail: NTIS HC A11/MF A01 CSCL 20D

Improvements in methods for predicting heat transfer rates on the hot gas side of turbine airfoils are necessary for improved turbine durability and performance. The development and verification of improved analytical models requires a systematic, closely coupled experimental and analytical program. G.L.C.

N86-11508*# United Technologies Research Center, East Hartford, Conn.

ASSESSMENT OF A 3-D BOUNDARY LAYER CODE TO PREDICT HEAT TRANSFER AND FLOW LOSSES IN A TURBINE

V. N. VATSA /in NASA. Lewis Research Center Turbine Eng. Hot Sect. Technol. (HOST) p 101-106 Oct. 1983 refs (Contract NAS3-23716)

Avail: NTIS HC A11/MF A01 CSCL 20D

The prediction of the complete flow field in a turbine passage is an extremely difficult task due to the complex three dimensional pattern which contains separation and attachment lines, a saddle point and horseshoe vortex. Whereas, in principle such a problem can be solved using full Navier-Stokes equations, in reality methods based on a Navier-Stokes solution procedure encounter difficulty in accurately predicting surface quantities (e.g., heat transfer) due to grid limitations imposed by the speed and size of the existing computers. On the other hand the overall problem is strongly three dimensional and too complex to be analyzed by the current design methods based on inviscid and/or viscous strip theories. Thus there is a strong need for enhancing the current prediction techniques through inclusion of 3-D viscous effects. A potentially simple and cost effective way to achieve this is to use a prediction method based on three dimensional boundary layer (3-DBL) theory. The major objective of this program is to assess the applicability of such a 3-DBL approach for the prediction of heat loads, boundary layer growth, pressure losses and streamline skewing in critical areas of a turbine passage. A brief discussion of the physical problem addressed here along with the overall approach is presented.

Author

N86-13677*# National Aeronautics and Space Administration. Lewis Research Center, Cleveland, Ohio.

HEAT TRANSFER AND PRESSURE DROP PERFORMANCE OF A FINNED-TUBE HEAT EXCHANGER PROPOSED FOR USE IN THE NASA LEWIS ALTITUDE WIND TUNNEL

G. J. VANFOSSEN Nov. 1985 27 p refs

(NASA-TM-87151; E-2623; NAS 1.15:87151) Avail: NTIS HC A03/MF A01 CSCL 20D

A segment of the heat exchanger proposed for use in the NASA Lewis Altitude Wind Tunnel (AWT) facility has been tested under dry and icing conditions. The heat exchanger has the largest pressure drop of any component in the AWT loop. It is therefore critical that its performance be known at all conditions before the final design of the AWT is complete. The heat exchanger segment is tested in the NASA Lewis Icing Research Tunnel (IRT) in order to provide an icing cloud environment similar to what will be encountered in the AWT. Dry heat transfer and pressure drop data are obtained and compared to correlations available in the literature. The effects of icing sprays on heat transfer and pressure drop are also investigated.

Author

N86-13678*# National Aeronautics and Space Administration. Lewis Research Center, Cleveland, Ohio.

DETERMINATION OF CONVECTIVE DIFFUSION HEAT/MASS TRANSFER RATES TO BURNER RIG TEST TARGETS COMPARABLE IN SIZE TO CROSS-STREAM JET DIAMETER

S. A. GOEKOGLU (Case Western Reserve Univ.) and G. J. SANTORO 1985 15 p refs Proposed for presentation at the 31st International Gas Turbine Conference, Dusseldorf, 8-12 Jun. 1986; sponsored by ASME

(NASA-TM-87176; E-2722; NAS 1.15:87176) Avail: NTIS HC A02/MF A01 CSCL 20D

Two sets of experiments have been performed to be able to predict the convective diffusion heat/mass transfer rates to a cylindrical target whose height and diameter are comparable to, but less than, the diameter of the circular cross-stream jet, thereby simulating the same geometric configuration as a typical burner rig test specimen located in the cross-stream of the combustor exit nozzle. The first set exploits the naphthalene sublimation technique to determine the heat/mass transfer coefficient under isothermal conditions for various flow rates (Reynolds numbers). The second set, conducted at various combustion temperatures and Reynolds numbers, utilized the temperature variation along the surface of the above-mentioned target under steady-state conditions to estimate the effect of cooling (dilution) due to the entrainment of stagnant room temperature air. The experimental information obtained is used to predict high temperature, high velocity corrosive salt vapor deposition rates in burner rigs on collectors that are geometrically the same. The agreement with preliminary data obtained from Na₂SO₄ vapor deposition experiments is found to be excellent.

Author

N86-13679*# National Aeronautics and Space Administration. Lewis Research Center, Cleveland, Ohio.

LUBRICATION OF NONCONFORMAL CONTACTS Ph.D. Thesis

Y. R. JENG Sep. 1985 154 p refs

(Contract NCC3-30)

(NASA-TM-87120; E-2728; NAS 1.15:87120) Avail: NTIS HC

A08/MF A01 CSCL 20D

Minimum film thickness results for piezoviscous-rigid regime of lubrication are developed for a compressible Newtonian fluid with Roelands viscosity. The results provide a basis for the analysis and design of a wide range of machine elements operating in the piezoviscous-rigid regime of lubrication. A new numerical method of calculating elastic deformation in contact stresses is developed using a biquadratic polynomial to approximate the pressure distribution on the whole domain analyzed. The deformation of every node is expressed as a linear combination of the nodal pressures whose coefficients can be combined into an influence coefficient matrix. This approach has the advantages of improved numerical accuracy, less computing time and smaller storage size required for influence matrix. The ideal elastohydrodynamic lubrication is extended to real bearing systems in order to gain an understanding of failure mechanisms in machine elements. The improved elastic deformation calculation is successfully incorporated into the EHL numerical scheme. Using this revised numerical technique and the flow factor model developed by Patir and Cheng (1978) the surface roughness effects on the elastohydrodynamic lubrication of point contact is considered. Conditions typical of an EHL contact in the piezoviscous-elastic regime entrained in pure rolling are investigated. Results are compared with the smooth surface solutions. Experiments are conducted to study the transient EHL effects in instrument ball bearings.

Author

N86-15625*# Arizona State Univ., Tempe.
HEAT TRANSFER CHARACTERISTICS WITHIN AN ARRAY OF IMPINGING JETS. EFFECTS OF CROSSFLOW TEMPERATURE RELATIVE TO JET TEMPERATURE Final Report
 L. W. FLORSCHUETZ and C. C. SU Washington NASA Oct. 1985 175 p refs
 (Contract NSG-3075)
 (NASA-CR-3936; E-2696; NAS 1.26:3936; CR-R-85020) Avail: NTIS HC A08/MF A01 CSCL 20D

Spanwise average heat fluxes, resolved in the streamwise direction to one stream-wise hole spacing were measured for two-dimensional arrays of circular air jets impinging on a heat transfer surface parallel to the jet orifice plate. The jet flow, after impingement, was constrained to exit in a single direction along the channel formed by the jet orifice plate and heat transfer surface. The crossflow originated from the jets following impingement and an initial crossflow was present that approached the array through an upstream extension of the channel. The regional average heat fluxes are considered as a function of parameters associated with corresponding individual spanwise rows within the array. A linear superposition model was employed to formulate appropriate governing parameters for the individual row domain. The effects of flow history upstream of an individual row domain are also considered. The results are formulated in terms of individual spanwise row parameters. A corresponding set of streamwise resolved heat transfer characteristics formulated in terms of flow and geometric parameters characterizing the overall arrays is described. E.A.K.

N86-16518*# Tennessee Univ. Space Inst., Tullahoma.
MEAN VELOCITY AND TURBULENCE MEASUREMENTS IN A 90 DEG CURVED DUCT WITH THIN INLET BOUNDARY LAYER Final Report, Apr. 1982 - Sep. 1984
 R. A. CRAWFORD, C. E. PETERS, J. STEINHOFF, J. O. HORNKOHL, J. NOURINEJAD, and K. RAMACHANDRAN Dec. 1985 188 p refs
 (Contract NAS3-23278)
 (NASA-CR-174811; NAS 1.26:174811; UTSI/85-08) Avail: NTIS HC A09/MF A01 CSCL 02D

The experimental database established by this investigation of the flow in a large rectangular turning duct is of benchmark quality. The experimental Reynolds numbers, Deans numbers and boundary layer characteristics are significantly different from previous benchmark curved-duct experimental parameters. This investigation extends the experimental database to higher Reynolds number and thinner entrance boundary layers. The 5% to 10% thick boundary layers, based on duct half-width, results in a large region of near-potential flow in the duct core surrounded by developing boundary layers with large crossflows. The turbulent entrance boundary layer case at $Re_{sub} = 328,000$ provides an incompressible flowfield which approaches real turbine blade cascade characteristics. The results of this investigation provide a challenging benchmark database for computational fluid dynamics code development. Author

N86-16519*# Wisconsin Univ., Milwaukee. Dept. of Mechanical Engineering.
IMPROVEMENT OF THE SECOND- AND THIRD-MOMENT MODELING OF TURBULENCE: A STUDY OF REYNOLDS-STRESS CLOSURE MODEL Semiannual Progress Report, 15 Jul. 1985 - 15 Jan. 1986
 R. S. AMANO and P. GOEL Jan. 1986 96 p refs
 (Contract NAG3-546)
 (NASA-CR-176478; NAS 1.26:176478; REPT-94E/2623E; TF/86/1) Avail: NTIS HC A05/MF A01 CSCL 20D

Four parts of the Reynolds-stress closure modeling are reported: (1) improvement of the k and ϵ equations; (2) development of the third-moment transport equation; (3) formulation of the diffusion coefficient of the momentum equation by using the algebraic-stress model of turbulence; and (4) the application of the Reynolds-stress model to a heat exchanger problem. It was demonstrated that the third-moment transport model improved the prediction of the triple-velocity products in the recirculating and

reattaching flow regions in comparison with the existing algebraic models for the triple-velocity products. Optimum values for empirical coefficients are obtained for the prediction of the backward-facing step flows. A functional expression is derived for the coefficient of the momentum diffusion by employing the algebraic-stress model. The second-moment closure is applied to a heat transfer problem. The computations for the flow in a corrugated-wall channel show that the second-moment closure improves the prediction of the heat transfer rates by 30% over the $k - \epsilon$ model. E.A.K.

N86-17665*# Case Western Reserve Univ., Cleveland, Ohio. Dept. of Mechanical and Aerospace Engineering.
LOW REYNOLD'S NUMBER BOUNDARY LAYERS IN A DISTURBED ENVIRONMENT Ph.D. Thesis - August, 1985 - Final Report
 D. K. PAIK and E. RESHOTKO Jan. 1986 98 p
 (Contract NAG3-230)
 (NASA-CR-175031; NAS 1.26:175031) Avail: NTIS HC A05/MF A01 CSCL 20D

Studies of flat plate boundary layer development were made in a low speed wind tunnel at turbulence levels from 2% to 7%. Only transitional and turbulent flows were observed in the range $280 < Re_{sub} < 700$. The mean turbulent velocity profiles display law-of-the-wall behavior but have negligible wake component. The u' disturbance profiles compare well with those of other experiments, the peak value of u'/u_{sub} being about 2.5. The effect of free-stream turbulence level on turbulent skin friction can be nicely correlated with those of other investigations on a plot of $u_{sub} \epsilon / u_{sub} \tau$ versus $Re_{sub} \theta$. A discussion on the u' spectra for the transitional boundary-layers is presented. Author

N86-18646*# National Aeronautics and Space Administration. Lewis Research Center, Cleveland, Ohio.
EXPERIMENTS FOR THE DETERMINATION OF CONVECTIVE DIFFUSION HEAT/MASS TRANSFER TO BURNER RIG TEST TARGETS COMPARABLE IN SIZE TO JET STREAM DIAMETER
 G. J. SANTORO and S. A. GOEKOGLU (Case Western Reserve Univ., Cleveland, Ohio) 1986 30 p refs Proposed for presentation at the 1986 Winter Annual Meeting of the American Society of Mechanical Engineers, Anaheim, Calif., 30 Nov. - 5 Dec. 1986
 (NASA-TM-87196; E-2794; NAS 1.15:87196) Avail: NTIS HC A03/MF A01 CSCL 20D

The application of a recently formulated vapor transport theory to predict deposition rates of corrosive salts from alkali-seeded combustion gases of a small-capacity, high-velocity, atmospheric-pressure burner rig was hampered by the relatively large dimensions of the cylindrical deposit collector compared to the diameter of the combustion gas stream. The relative dimensions lead to a highly nonadiabatic combustion gas flow around the collector and necessitate two series of experiments. In the first series, mass transfer coefficients are determined by utilizing the naphthalene sublimation technique. The second series of experiments determines the dilution effect on the sodium species concentrations due to the entrainment of ambient air. This second series involves the measurement of the temperature variation along the surface of the collector under steady state conditions. Vapor deposition rates are determined exploiting this information and the results are found to compare favorably with experimentally obtained rates. Author

34 FLUID MECHANICS AND HEAT TRANSFER

N86-18647*# National Aeronautics and Space Administration. Lewis Research Center, Cleveland, Ohio.

STUDY OF JOURNAL BEARING DYNAMICS USING 3-DIMENSIONAL MOTION PICTURE GRAPHICS

D. E. BREWE and D. J. SOSOKA Nov. 1985 8 p Presented at the ASEE Engineering Design Graphics Division Midyear Meeting, West Lafayette, Ind., 24-26 Nov. 1985 (NASA-TM-87205; E-2862; NAS 1.15:87205; USAAVSCOM-TR-86-C-3) Avail: NTIS HC A02/MF A01 CSCL 20D

Computer generated motion pictures of three dimensional graphics are being used to analyze journal bearings under dynamically loaded conditions. The motion pictures simultaneously present the motion of the journal and the pressures predicted within the fluid film of the bearing as they evolve in time. The correct prediction of these fluid film pressures can be complicated by the development of cavitation within the fluid. The numerical model that is used predicts the formation of the cavitation bubble and its growth, downstream movement, and subsequent collapse. A complete physical picture is created in the motion picture as the journal traverses through the entire dynamic cycle. Author

N86-19555*# National Aeronautics and Space Administration. Lewis Research Center, Cleveland, Ohio.

A MODEL FOR THE INFLUENCE OF PRESSURE ON THE BULK MODULUS AND THE INFLUENCE OF TEMPERATURE ON THE SOLIDIFICATION PRESSURE FOR LIQUID LUBRICANTS

B. O. JACOBSON and P. VINET 1986 21 p refs Proposed for presentation at the 1986 AMSE/ASLE Tribology Conference, Pittsburgh, Pa., 19-22 Oct. 1986 (NASA-TM-87230; E-2833; NAS 1.15:87230) Avail: NTIS HC A02/MF A01 CSCL 20D

Two pressure chambers, for compression experiments with liquids from zero to 2.2 GPa pressure, are described. The experimentally measured compressions are then compared to theoretical values given by an isothermal model of equation of state recently introduced for solids. The model describes the pressure and bulk modulus as a function of compression for different types of lubricants with a very high accuracy up to the pressure limit of the high pressure chamber used (2.2 GPa). In addition the influence of temperature on static solidification pressure was found to be a simple function of the thermal expansion of the fluid. Author

N86-19556*# National Aeronautics and Space Administration. Lewis Research Center, Cleveland, Ohio.

STARVATION EFFECTS ON THE HYDRODYNAMIC LUBRICATION OF RIGID NONCONFORMAL CONTACTS IN COMBINED ROLLING AND NORMAL MOTION

M. K. GHOSH, B. J. HAMROCK (Ohio State Univ., Columbus), and D. E. BREWE (Army Aviation Research and Technology Activity, Cleveland, Ohio) 1986 28 p refs (NASA-TM-87174; E-2817; NAS 1.15:87174; USAAVSCOM-TR-85-C-20) Avail: NTIS HC A03/MF A01 CSCL 20D

The effect of inlet starvation on the hydrodynamic lubrication of lightly loaded rigid nonconformal contacts in combined rolling and normal motion is determined through a numerical solution of the Reynolds' equation for an isoviscous, incompressible lubricant. Starvation is effected by systematically reducing the fluid inlet level. The pressures are taken to be ambient at the inlet meniscus boundary and Reynolds' boundary condition is applied for film rupture in the exit region. Results are presented for the dynamic performance of the starved contacts in combined rolling and normal motion for both normal approach and separation. During normal approach the dynamic load ratio (i.e. ratio of dynamic to steady state load capacity) increases considerably with increase in the inlet starvation. The effect of starvation on the dynamic peak pressure ratio is relatively small. Further, it has been observed that with increasing starvation, film thickness effects become significant in the dynamic behavior of the nonconformal contacts. For significantly starved contacts the dynamic load ratio increases with increase in film thickness during normal approach and a similar

reduction is observed during separation. A similar effect is noted for the dynamic peak pressure ratio. Author

N86-19558*# National Aeronautics and Space Administration. Lewis Research Center, Cleveland, Ohio.

TWO-PHASE FLOWS AND HEAT TRANSFER WITHIN SYSTEMS WITH AMBIENT PRESSURE ABOVE THE THERMODYNAMIC CRITICAL PRESSURE

R. C. HENDRICKS, M. J. BRAUN (Akron Univ., Ohio), and R. L. MULLEN (Case Western Reserve Univ., Cleveland, Ohio) 1986 8 p refs Proposed for presentation at the 8th International Heat Transfer Conference, San Francisco, Calif., 17-22 Aug. 1986 (NASA-TM-87228; E-2897; NAS 1.15:87228) Avail: NTIS HC A02/MF A01 CSCL 20D

In systems where the design inlet and outlet pressures $P_{sub\ amb}$ are maintained above the thermodynamic critical pressure $P_{sub\ c}$, it is often assumed that heat and mass transfer are governed by single-phase relations and that two-phase flows cannot occur. This simple rule of thumb is adequate in many low-power designs but is inadequate for high-performance turbomachines, boilers, and other systems where two-phase regions can exist even though $P_{sub\ amb} > P_{sub\ c}$. Heat and mass transfer and rotordynamic-fluid-mechanic restoring forces depend on momentum differences, and those for a two-phase zone can differ significantly from those for a single-phase zone. By using a laminar, variable-property bearing code and a rotating boiler code, pressure and temperature surfaces were determined that illustrate nesting of a two-phase region within a supercritical pressure region. The method of corresponding states is applied to bearings with reasonable rapport. E.A.K.

N86-20722*# Deutsche Forschungs- und Versuchsanstalt fuer Luft- und Raumfahrt, Goettingen (West Germany). Abteilung Turbulenzforschung.

SHEAR LAYER EXCITATION, EXPERIMENT VERSUS THEORY

D. W. BECHERT and B. STAHL 1984 86 p refs (Contract NAG3-198) (NASA-CR-176604; NAS 1.26:176604; DFVLR-FB-84-26) Avail: NTIS HC A05/MF A01

The acoustical excitation of shear layers is investigated. Acoustical excitation causes the so-called orderly structures in shear layers and jets. Also, the deviations in the spreading rate between different shear layer experiments are due to the same excitation mechanism. Measurements in the linear interaction region close to the edge from which the shear layer is shed are examined. Two sets of experiments (Houston 1981 and Berlin 1983/84) are discussed. The measurements were carried out with shear layers in air using hot wire anemometers and microphones. The agreement between these measurements and the theory is good. Even details of the fluctuating flow field correspond to theoretical predictions, such as the local occurrence of negative phase speeds. Author

N86-21794*# National Aeronautics and Space Administration. Lewis Research Center, Cleveland, Ohio.

EFFECT OF A ROTOR WAKE ON THE LOCAL HEAT TRANSFER ON THE FORWARD HALF OF A CIRCULAR CYLINDER

K. A. MOREHOUSE and R. J. SIMONEU Mar. 1986 22 p refs Presented at the 8th International Heat Transfer Conference, San Francisco, Calif., 17-22 Aug. 1986 (NASA-TM-87234; E-2751; NAS 1.15:87234) Avail: NTIS HC A02/MF A01 CSCL 20D

Turbine rotor-stator wake dynamics was simulated by a spoked wheel rotating in annular flow, generating rotor wakes. Spanwise averaged circumferentially local heat transfer in the circular cylindrical leading edge region of a turbine airfoil was obtained. Reynolds numbers ranged from 35,000 to 175,000. Strouhal numbers ranged from 0.63 to 2.50. Wakes were generated by 2 sets of circular cylindrical bars, 1.59 and 3.18 mm in diameter. The rotor could be rotated either clockwise or counterclockwise. Grid turbulence was introduced upstream yielding freestream turbulence of 1.0 to 2.5% at the stator. Data represented an extensive body of local heat transfer coefficients, which can be used to model the leading edge region of a turbine airfoil. In the

presence of rotor wakes, an asymmetry from the leeward to windward side was noted. Windward side levels were 30 to 40% higher than the corresponding leeward side. Author

N86-21797*# National Aeronautics and Space Administration. Lewis Research Center, Cleveland, Ohio.

PIEZOVISCIOUS EFFECTS IN NONCONFORMAL CONTACTS LUBRICATED HYDRODYNAMICALLY

Y. R. JENG, B. J. HAMROCK, and D. E. BREWE (Army Aviation Research and Technology Activity-AVSCOM, Lewis Research Center, Cleveland, Ohio) May 1985 36 p refs Presented at the Annual Meeting of the American Society of Lubrication Engineers, Las Vegas, Nev., 5-9 May 1985 (NASA-TM-87141; E-2767; NAS 1.15:87141; USAAVSCOM-TR-86-C-1) Avail: NTIS HC A03/MF A01 CSCL 20D

The analysis is concerned with the piezoviscous-rigid regime of lubrication for the general case of elliptical contacts. In this regime several formulas of the lubricant film thickness have been proposed by Hamrock and Dowson, by Dowson et al., and more recently by Houpert. However, either they do not include the load parameter W , which has a strong effect on film thickness, or they overestimate the film thickness by using the Barus formula for pressure-viscosity characteristics. The Roelands formula was used for the pressure-viscosity relationship. The effects of the dimensionless load, speed, and materials parameters, the radius ratio, and the lubricant entrainment direction were investigated. The dimensionless load parameter was varied over a range of one order of magnitude. The dimensionless speed parameter was varied by 5.6 times the lowest value. Conditions corresponding to the use of solid materials of steel, bronze, and silicon nitride and lubricants of paraffinic and naphthenic mineral oil were considered in obtaining the exponent in the dimensionless materials parameter. The radius ratio was varied from 0.2 to 64 (a configuration approaching a line contact). Forty-one cases were used in obtaining a minimum film thickness formula. Contour plots indicate in detail the pressure developed between the contacting solids. Author

N86-22890*# National Aeronautics and Space Administration. Lewis Research Center, Cleveland, Ohio.

EXPERIMENTAL VERIFICATION OF CORROSIVE VAPOR DEPOSITION RATE THEORY IN HIGH VELOCITY BURNER RIGS

S. A. GOKOGLU (Case Western Reserve Univ., Cleveland, Ohio) and G. J. SANTORO 1986 12 p refs Presented at 3rd Conference on High Temperature Alloys for Gas Turbines and Other Applications, Liege, Belgium, 6-9 October 1986; sponsored by Commission of the European Communities (NASA-TM-87287; E-2993; NAS 1.15:87287) Avail: NTIS HC A02/MF A01 CSCL 20D

The ability to predict deposition rates is required to facilitate modelling of high temperature corrosion by fused salt condensates in turbine engines. A corrosive salt vapor deposition theory based on multicomponent chemically frozen boundary layers (CFBL) has been successfully verified by high velocity burner rig experiments. The experiments involved internally air-impingement cooled, both rotating full and stationary segmented cylindrical collectors located in the crossflow of sodium-seeded combustion gases. Excellent agreement is found between the CFBL theory and the experimental measurements for both the absolute amounts of Na_2SO_4 deposition rates and the behavior of deposition rate with respect to collector temperature, mass flowrate (velocity) and Na concentration. Author

N86-22892*# Arizona State Univ., Tempe. Dept. of Mechanical and Aerospace Engineering.

HEAT TRANSFER TO TWO-PHASE AIR/WATER MIXTURES FLOWING IN SMALL TUBES WITH INLET DISEQUILIBRIUM Final Report

J. M. JANSSEN, L. W. FLORSCHUETZ, and J. P. FISZDON Mar. 1986 100 p refs (Contract NSG-3075) (NASA-CR-175076; NAS 1.26:175076) Avail: NTIS HC A05/MF A01 CSCL 20D

The cooling of gas turbine components was the subject of considerable research. The problem is difficult because the available coolant, compressor bleed air, is itself quite hot and has relatively poor thermophysical properties for a coolant. Injecting liquid water to evaporatively cool the air prior to its contact with the hot components was proposed and studied, particularly as a method of cooling for contingency power applications. Injection of a small quantity of cold liquid water into a relatively hot coolant air stream such that evaporation of the liquid is still in process when the coolant contacts the hot component was studied. No approach was found whereby heat transfer characteristics could be confidently predicted for such a case based solely on prior studies. It was not clear whether disequilibrium between phases at the inlet to the hot component section would improve cooling relative to that obtained where equilibrium was established prior to contact with the hot surface. Author

N86-23854*# National Aeronautics and Space Administration. Lewis Research Center, Cleveland, Ohio.

LIQUID-VAPOR INTERFACE LOCATIONS IN A SPHEROIDAL CONTAINER UNDER LOW GRAVITY

M. J. CARNEY Apr. 1986 27 p refs (NASA-TM-87147; E-2936; NAS 1.15:87147) Avail: NTIS HC A03/MF A01 CSCL 20D

As a part of the general study of liquid behavior in low gravity environments, an experimental investigation was conducted to determine if there are equilibrium liquid-vapor interface configurations that can exist at more than one location in oblate spheroidal containers under reduced gravity conditions. Static contact angles of the test liquids on the spheroid surface were restricted to near 0 deg. The experiments were conducted in a low gravity environment. An oblate spheroidal tank was tested with an eccentricity of 0.68 and a semimajor axis of 2.0 cm. Both quantitative and qualitative data were obtained on the liquid-vapor interface configuration and position inside the container. The results of these data, and their impact on previous work in this area, are discussed. Of particular interest are those equilibrium interface configurations that can exist at multiple locations in the container. Author

N86-23856*# Garrett Turbine Engine Co., Phoenix, Ariz.

DILUTION JET MIXING PROGRAM, SUPPLEMENTARY REPORT

R. SRINIVASAN and C. WHITE Mar. 1986 397 p refs (Contract NAS3-22110) (NASA-CR-175043; NAS 1.26:175043; REPT-21-4705) Avail: NTIS HC A17/MF A01 CSCL 20D

The velocity and temperature distributions predicted by a 3-D numerical model and experimental measurements are compared. Empirical correlations for the jet velocity trajectory developed are presented. The measured velocity distributions for all test cases of phase through phase 3 are presented in the form of contour and oblique plots. Quantification of the effects of the following on the jet mixing characteristics with a confined crossflow are: (1) orifice geometry momentum flux ratio and density ratio; (2) nonuniform mainstream temperature and velocity profiles upstream of dilution orifices; (3) cold versus hot jet injection; (4) cross-stream flow are a convergence as encountered in practical dilution zone geometries; (5) 2-D slot versus circular orifices; (6) discrete noncircular orifices; (7) single-sided versus opposed jets; (8) single row of jets. E.A.K.

34 FLUID MECHANICS AND HEAT TRANSFER

N86-23857*# Sverdrup Technology, Inc., Cleveland, Ohio.
PREDICTION OF HEAT RELEASE EFFECTS ON A MIXING LAYER Final Report

M. FARSHCHI Feb. 1986 26 p refs Presented at the 24th Aerospace Science Meeting, Reno, Nev., 6-9 Jan. 1986; sponsored by American Inst. of Aeronautics and Astronautics Previously announced in IAA as A86-22676

(Contract NAS3-24105)

(NASA-CR-175044; E-2845; NAS 1.26:175044) Avail: NTIS HC A03/MF A01 CSCL 20D

A fully second-order closure model for turbulent reacting flows is suggested based on Favre statistics. For diffusion flames the local thermodynamic state is related to single conserved scalar. The properties of pressure fluctuations are analyzed for turbulent flows with fluctuating density. Closure models for pressure correlations are discussed and modeled transport equations for Reynolds stresses, turbulent kinetic energy dissipation, density-velocity correlations, scalar moments and dissipation are presented and solved, together with the mean equations for momentum and mixture fraction. Solutions of these equations are compared with the experimental data for high heat release free mixing layers of fluorine and hydrogen in a nitrogen diluent.

Author

N86-24931*# General Electric Co., Cincinnati, Ohio. Aircraft Engine Business Group.

BURNER LINER THERMAL/STRUCTURAL LOAD MODELING: TRANCITS PROGRAM USER'S MANUAL

R. MAFFEO Aug. 1985 45 p refs

(Contract NAS3-23272)

(NASA-CR-174891; NAS 1.26:174891; R85AEB452) Avail: NTIS HC A03/MF A01 CSCL 20D

Transfer Analysis Code to Interface Thermal/Structural Problems (TRANCITS) is discussed. The TRANCITS code satisfies all the objectives for transferring thermal data between heat transfer and structural models of combustor liners and it can be used as a generic thermal translator between heat transfer and stress models of any component, regardless of the geometry. The TRANCITS can accurately and efficiently convert the temperature distributions predicted by the heat transfer programs to those required by the stress codes. It can be used for both linear and nonlinear structural codes and can produce nodal temperatures, elemental centroid temperatures, or elemental Gauss point temperatures. The thermal output of both the MARC and SINDA heat transfer codes can be interfaced directly with TRANCITS, and it will automatically produce stress model codes formatted for NASTRAN and MARC. Any thermal program and structural program can be interfaced by using the neutral input and output forms supported by TRANCITS.

E.A.K.

N86-24932*# Brown Univ., Providence, R. I. Div. of Engineering.

CONTRIBUTIONS TO THE UNDERSTANDING OF LARGE-SCALE COHERENT STRUCTURES IN DEVELOPING FREE TURBULENT SHEAR FLOWS

J. T. C. LIU Apr. 1986 219 p refs

(Contract NAG1-379; NAG3-673; NSF MSM-83-20307; NSF

INT-85-14196; NATO-343/85)

(NASA-CR-176772; NAS 1.26:176772) Avail: NTIS HC A10/MF A01 CSCL 20D

Advances in the mechanics of boundary layer flow are reported. The physical problems of large scale coherent structures in real, developing free turbulent shear flows, from the nonlinear aspects of hydrodynamic stability are addressed. The presence of fine grained turbulence in the problem, and its absence, lacks a small parameter. The problem is presented on the basis of conservation principles, which are the dynamics of the problem directed towards extracting the most physical information, however, it is emphasized that it must also involve approximations.

E.A.K.

N86-24933*# Kansas Univ. Center for Research, Inc., Lawrence.

STATISTICAL PREDICTION OF DYNAMIC DISTORTION OF INLET FLOW USING MINIMUM DYNAMIC MEASUREMENT. AN APPLICATION TO THE MELICK STATISTICAL METHOD AND INLET FLOW DYNAMIC DISTORTION PREDICTION WITHOUT RMS MEASUREMENTS Final Report

W. G. SCHWEIKHARD and Y. S. CHEN Apr. 1986 216 p refs 2 Vol.

(Contract NAG3-11)

(NASA-CR-176764; NAS 1.26:176764) Avail: NTIS HC A10/MF A01 CSCL 20D

The Melick method of inlet flow dynamic distortion prediction by statistical means is outlined. A hypothetical vortex model is used as the basis for the mathematical formulations. The main variables are identified by matching the theoretical total pressure rms ratio with the measured total pressure rms ratio. Data comparisons, using the HIMAT inlet test data set, indicate satisfactory prediction of the dynamic peak distortion for cases with boundary layer control device vortex generators. A method for the dynamic probe selection was developed. Validity of the probe selection criteria is demonstrated by comparing the reduced-probe predictions with the 40-probe predictions. It is indicated that the the number of dynamic probes can be reduced to as few as two and still retain good accuracy.

E.A.K.

N86-24934*# National Aeronautics and Space Administration. Lewis Research Center, Cleveland, Ohio.

UNSTEADY HEAT TRANSFER AND DIRECT COMPARISON TO STEADY-STATE MEASUREMENTS IN A ROTOR-WAKE EXPERIMENT

J. E. OBRIEN, R. J. SIMONEAU, J. E. LAGRAFF (Syracuse Univ.), and K. A. MOREHOUSE Jan. 1986 21 p refs Presented at the 8th International Heat Transfer Conference, San Francisco, Calif., 17-22 Aug. 1986

(NASA-TM-87220; E-2757; NAS 1.15:87220) Avail: NTIS HC A02/MF A01 CSCL 20D

Circumferentially local and time-resolved heat transfer measurements were obtained for a circular cylinder in crossflow located downstream of a rotating spoked wheel wake generator in a steady flow tunnel. The unsteady heat transfer effects were obtained by developing an extension of a thin film gauge technique employed to date exclusively in short-duration facilities. The time-average thin film results and conventional steady-state heat transfer measurements were compared. Time-averaged wake-induced stagnation heat transfer enhancement levels above the nowake case were about 10% for the four cylinder Reynolds numbers. This enhancement level was nearly independent of bar passing frequency and was related directly to the time integral of the heat transfer spikes observed at the bar passing frequency. It is observed that the wake-induced heat transfer spikes have peak magnitudes averaging 30 to 40% above the interwake heat transfer level.

E.A.K.

N86-24938*# Garrett Turbine Engine Co., Phoenix, Ariz.

DILUTION JET MIXING PROGRAM, PHASE 3 Final Report

R. SRINIVASAN, E. COLEMAN, G. MYERS, and C. WHITE Sep. 1985 186 p refs

(Contract NAS3-22110)

(NASA-CR-174884; NAS 1.26:174884; GARRETT-21-5418)

Avail: NTIS HC A09/MF A01 CSCL 20D

The main objectives for the NASA Jet Mixing Phase 3 program were: extension of the data base on the mixing of single sided rows of jets in a confined cross flow to discrete slots, including streamlined, bluff, and angled injections; quantification of the effects of geometrical and flow parameters on penetration and mixing of multiple rows of jets into a confined flow; investigation of in-line, staggered, and dissimilar hole configurations; and development of empirical correlations for predicting temperature distributions for discrete slots and multiple rows of dilution holes.

Author

N86-24955*# Kansas Univ. Center for Research, Inc., Lawrence.

REVIEW AND EVALUATION OF RECENT DEVELOPMENTS IN MELICK INLET DYNAMIC FLOW DISTORTION PREDICTION AND COMPUTER PROGRAM DOCUMENTATION AND USER'S MANUAL ESTIMATING MAXIMUM INSTANTANEOUS INLET FLOW DISTORTION FROM STEADY-STATE TOTAL PRESSURE MEASUREMENTS WITH FULL, LIMITED, OR NO DYNAMIC DATA Final Report

W. G. SCHWEIKHARD and S. R. DENNON Apr. 1986 257 p refs

(Contract NAG3-11)

(NASA-CR-176765; NAS 1.26:176765) Avail: NTIS HC A12/MF A01 CSCL 20D

A review of the Melick method of inlet flow dynamic distortion prediction by statistical means is provided. These developments include the general Melick approach with full dynamic measurements, a limited dynamic measurement approach, and a turbulence modelling approach which requires no dynamic rms pressure fluctuation measurements. These modifications are evaluated by comparing predicted and measured peak instantaneous distortion levels from provisional inlet data sets. A nonlinear mean-line following vortex model is proposed and evaluated as a potential criterion for improving the peak instantaneous distortion map generated from the conventional linear vortex of the Melick method. The model is simplified to a series of linear vortex segments which lay along the mean line. Maps generated with this new approach are compared with conventionally generated maps, as well as measured peak instantaneous maps. Inlet data sets include subsonic, transonic, and supersonic inlets under various flight conditions. Author

N86-25726*# National Aeronautics and Space Administration. Lewis Research Center, Cleveland, Ohio.

THERMOMECHANICAL DESIGN CRITERIA FOR CERAMIC-COATED SURFACES

R. L. MULLEN (Case Western Reserve Univ., Cleveland, Ohio.), J. PADOVAN (Akron Univ., Ohio.), M. J. BRAUN, B. T. F. CHUNG, G. McDONALD, and R. C. HENDRICKS 1986 27 p refs

Proposed for presentation at the 6th CIMTEC World Congress on High Tech Ceramics, Milan, Italy, 23-28 June 1986; sponsored by the Italian Ministry for Science and Technology, ENEA and American Ceramic Society

(NASA-TM-87328; E-3002; NAS 1.15:87328) Avail: NTIS HC A03/MF A01 CSCL 20D

Some early history of ceramic applications is presented. Finite element modeling of components to determine service and fabrication loads found inelastic behavior and residual stresses to be significant to component life. Inelastic behavior mitigates peak strains but enhances residual strains. Results of furnace, Mach 0.3 burner, and engine tests are discussed and categorized into design criteria (loading, geometry, fabrication, materials, analysis, and testing). These design rules and finite element analyses are brought to bear on two test cases: turboshaft engine seals, and rocket thrust chambers. Author

N86-26545*# National Aeronautics and Space Administration. Lewis Research Center, Cleveland, Ohio.

APPLICATION OF A COMPUTATIONAL MODEL FOR VORTEX GENERATORS IN SUBSONIC INTERNAL FLOWS

W. G. KUNIK 1986 24 p refs Presented at the 22nd Joint Propulsion Conference, Huntsville, Ala., 16-18 Jun. 1986; sponsored by AIAA, ASME, SAE and ASCE

(NASA-TM-87327; E-3072; NAS 1.15:87327; AIAA-86-1458) Avail: NTIS HC A02/MF A01 CSCL 20D

A model for the analysis of vortex generators in a fully viscous subsonic internal flow is evaluated. A vorticity source term is used in a modified form of the Parabolized Navier-Stokes equations to model the shed vortex. Computed results are compared with idealized flow vortex paths, and with experimental data for vortex generators embedded in a thick turbulent boundary layer. The analysis is also compared with experimental data for a separated diffusing S-duct and for a diffusing S-duct with vortex generators.

Quantitative comparisons are shown for the latter three cases. Emphasis is placed on verifying the ability of the model to predict global distortions in the flow field. Author

N86-26546*# Virginia Polytechnic Inst. and State Univ., Blacksburg. Dept. of Mechanical Engineering.

THERMODYNAMIC EVALUATION OF TRANSONIC COMPRESSOR ROTORS USING THE FINITE VOLUME APPROACH Semiannual Status Report, 20 Dec. 1985 - 31 May 1986

S. NICHOLSON and J. MOORE 1986 81 p

(Contract NAG3-593)

(NASA-CR-176840; NAS 1.26:176840; JM/86-2) Avail: NTIS HC A05/MF A01 CSCL 20D

The finite volume explicit time marching method was refined and improved. Previously, extension had been made to the finite volume method to improve the accuracy of the calculation of total pressure in inviscid flow, extend the method to allow the calculation of laminar and turbulent boundary layers in internal flows, and improve the shock capturing properties of the method by introducing a Mach number dependent interpolation scheme for the pressure used in the calculating the density. The current work extends these developments by using the new pressure interpolation scheme in two dimensional viscous calculations, including a more complete description of the viscous stresses, introducing a criteria for the transverse upwind differencing which is a function of the ratio of transverse and streamwise mass fluxes, and allowing the calculation of internal flow where boundary layers are present on both walls of the duct. The manner in which the viscous stresses are evaluated in the nonorthogonal, nonuniform grid is detailed. The convergence is investigated and results for calculations of laminar flow in a converging duct are presented. Results for calculations of transonic flow in a converging-diverging nozzle are presented and the results are compared with Sajben's measurements and calculations by others. Author

N86-27607*# Pennsylvania State Univ., State College. Applied Research Lab.

THE BOUNDARY LAYER ON COMPRESSOR CASCADE BLADES Semiannual Progress Report, 1 Dec. 1985 - 1 Jun. 1986

S. DEUTSCH and W. C. ZIERKE 1986 20 p

(Contract NSG-3264)

(NASA-CR-177279; NAS 1.26:177279) Avail: NTIS HC A02/MF A01 CSCL 20D

The purpose of NASA Research Grant NSG-3264 is to characterize the flowfield about an airfoil in a cascade at chord Reynolds number ($R_{sub C}$) near 5×10 to the 5th power. The program is experimental and combines laser Doppler velocimeter (LDV) measurements with flow visualization techniques in order to obtain detailed flow data, e.g., boundary layer profiles, points of separation and the transition zone, on a cascade of highly-loaded compressor blades. The information provided by this study is to serve as benchmark data for the evaluation of current and future compressor cascade predictive models, in this way aiding in the compressor design process. Summarized is the research activity for the period 1 December 1985 through 1 June 1986. Progress made from 1 June 1979 through 1 December 1985 is presented. Detailed measurements have been completed at the initial cascade angle of 53 deg. (incidence angle 5 degrees). A three part study, based on that data, has been accepted as part of the 1986 Gas Turbine Conference and will be submitted for subsequent journal publication. Also presented are data for a second cascade angle of 45 deg (an incidence angle of 3 degrees). Author

34 FLUID MECHANICS AND HEAT TRANSFER

N86-28378*# National Aeronautics and Space Administration. Lewis Research Center, Cleveland, Ohio.

DIFFUSION FLAME EXTINCTION IN SLOW CONVECTIVE FLOW UNDER MICROGRAVITY ENVIRONMENT

C. H. CHEN 1986 16 p Proposed for presentation at the Microgravity Fluid Mechanics Symposium, Anaheim, Calif., 10-11 Dec. 1986; sponsored by ASME (NASA-TM-88799; E-3137; NAS 1.15:88799) Avail: NTIS HC A02/MF A01 CSCL 20D

A theoretical analysis is presented to study the extinction characteristics of a diffusion flame near the leading edge of a thin fuel plate in slow, forced convective flows in a microgravity environment. The mathematical model includes two-dimensional Navier-Stokes momentum, energy and species equations with one-step overall chemical reaction using second-order finite rate Arrhenius kinetics. Radiant heat loss on the fuel plate is applied in the model as it is the dominant mechanism for flame extinguishment in the small convective flow regime. A parametric study based on the variation of convective flow velocity, which varies the Damkohler number (Da), and the surface radiant heat loss parameter (S) simultaneously, is given. An extinction limit is found in the regime of slow convective flow when the rate of radiant heat loss from fuel surface outweighs the rate of heat generation due to combustion. The transition from existent envelope flame to extinguishment consists of gradual flame contraction in the opposed flow direction together with flame temperature reduction as the convective flow velocity decreases continuously until the extinction limit is reached. A case of flame structure subjected to surface radiant heat loss is also presented and discussed. Author

N86-30093*# Dayton Univ., Ohio.

NUMERICAL SIMULATION OF THE FLOWFIELD OVER ICE ACCRETION SHAPES Semiannual Progress Report, 30 Apr. 1985 - 30 Apr. 1986

J. N. SCOTT Apr. 1986 19 p Submitted for publication (Contract NAG3-665) (NASA-CR-176960; NAS 1.26:176960) Avail: NTIS HC A02/MF A01 CSCL 20D

The primary goals are directed toward the development of a numerical method for computing flow about ice accretion shapes and determining the influence of these shapes on flow degradation. It is expedient to investigate various aspects of icing independently in order to assess their contribution to the overall icing phenomena. The specific aspects to be examined include the water droplet trajectories with collection efficiencies and phase change on the surface, the flowfield about specified shapes including lift, drag, and heat transfer distribution, and surface roughness effects. The configurations computed were models of ice accretion shapes formed on a circular cylinder in the NASA Lewis Icing Research Tunnel. An existing Navier-Stokes program was modified to compute the flowfield over four shapes (2, 5, and 15 minute models of glaze ice, and a 15 minute accumulation of rime ice). B.G.

N86-30960*# Carnegie-Mellon Univ., Pittsburgh, Pa. Dept. of Mechanical Engineering.

MEASUREMENTS IN LIQUID FUEL SPRAYS Final Report, 15 Dec. 1983 - 14 Dec. 1985

N. CHIGIER and C. P. MAO 1985 51 p (Contract NCC3-37) (NASA-CR-177088; NAS 1.26:177088) Avail: NTIS HC A04/MF A01 CSCL 20D

A ground test facility is being established at NASA Lewis Research Center to simulate the environmental and flight conditions needed to study adverse weather effects. One of the most important components is the water spray system which consists of many nozzles fitted on spray bars. Water is injected through air-assisted atomizers to generate uniform size drops to simulate icing in clouds. The primary objective is to provide experimental data on drop size distribution over a wide range of operating conditions. Correlation equations for mean drop size and initial injection parameters are being determined to assist in the design and modification of the Altitude Wind Tunnel. Special emphasis is

being placed on the study of the aerodynamic structure of the air-assisted atomizer sprays. Detailed measurements of the variation of drop size distribution and velocity as a function of time and space are being made. Accurate initial and boundary conditions are being provided for computer model evaluation.

B.G.

N86-31000*# Mechanical Technology, Inc., Latham, N. Y. PERFORMANCE OF OIL PUMPING RINGS: AN ANALYTICAL AND EXPERIMENTAL STUDY Final Report

M. W. EUSEPI, J. A. WALOWIT, O. PINKUS, and P. HOLMES Jan. 1986 233 p (Contract DEN3-256; DE-AI01-85CE-50112) (NASA-CR-175083; DOE/NASA-0256/1; NAS 1.26:175083; MTI-86TR17) Avail: NTIS HC A11/MF A01 CSCL 20D

A steady-state design computer program was developed to predict the performance of pumping rings as functions of geometry, applied loading, speed, ring modulus, and fluid viscosity. Additional analyses were developed to predict transient behavior of the ring and the effects of temperature rises occurring in the hydrodynamic film between the ring and shaft. The analysis was initially compared with previous experimental data and then used to design additional rings for further testing. Tests were performed with Rulon, carbon-graphite, and babbit rings. The design analysis was used to size all of the rings and to select the ranges of clearances, thickness, and loading. Although full quantitative agreement was lacking, relative agreement existed in that rings that were predicted to perform well theoretically, generally performed well experimentally. Some causes for discrepancies between theory and experiment are believed to be due to starvation, leakage past the secondary seal at high pressures, and uncertainties in the small clearances and local inlet temperatures to the pumping ring. A separate preliminary analysis was performed for a pumping Leningrader seal. This analysis can be used to predict the film thickness and flow rate through the seal as a function of pressure, speed, loading, and geometry. M.G.

N86-31826*# Michigan Univ., Ann Arbor. Heat Transfer Lab. MODELING OF ZERO GRAVITY VENTING: STUDIES OF TWO-PHASE HEAT TRANSFER UNDER REDUCED GRAVITY Final Report

H. MERTE, JR. Aug. 1986 66 p (Contract NAG3-403) (NASA-CR-179662; NAS 1.26:179662) Avail: NTIS HC A04/MF A01 CSCL 20D

The objective is to predict the pressure response of a saturated liquid-vapor system when undergoing a venting or depressurization process in zero gravity at low vent rates. An experimental investigation of the venting of cylindrical containers partially filled with initially saturated liquids was previously conducted under zero-gravity conditions and compared with an analytical model which incorporated the effect of interfacial mass transfer on the ullage pressure response during venting. A new model is presented to improve the estimation of the interfacial mass transfer. Duhammel's superposition integral is incorporated to approximate the transient temperature response of the interface, treating the liquid as a semi-infinite solid with conduction heat transfer. Account is also taken of the condensation taking place within the bulk of a saturated vapor as isentropic expansion takes place. Computational results are presented for the venting of R-11 from a given vessel and initial state for five different venting rates over a period of three seconds, and compared to prior NASA experiments. An improvement in the prediction of the final pressure takes place, but is still considerably below the measurements.

Author

INSTRUMENTATION AND PHOTOGRAPHY

Includes remote sensors; measuring instruments and gages; detectors; cameras and photographic supplies; and holography.

A86-13059*# National Aeronautics and Space Administration. Lewis Research Center, Cleveland, Ohio.

HIGH-TEMPERATURE THERMOCOUPLE AND HEAT FLUX GAUGE USING A UNIQUE THIN FILM-HARDWARE HOT JUNCTION

C. H. LIEBERT, R. HOLANDA, S. A. HIPPENSTEELE, and C. A. ANDRACCHIO (NASA, Lewis Research Center, Cleveland, OH) ASME, Transactions, Journal of Engineering for Gas Turbines and Power (ISSN 0022-0825), vol. 107, Oct. 1985, p. 938-944. Previously announced in STAR as N85-16096. refs (ASME PAPER 85-GT-18)

A special thin film-hardware material thermocouple (TC) and heat flux gauge concept for a reasonably high temperature and high flux flat plate heat transfer experiment was fabricated and tested to gauge temperatures of 911 K. This concept was developed for minimal disturbance of boundary layer temperature and flow over the plates and minimal disturbance of heat flux through the plates. Comparison of special heat flux gauge Stanton number output at steady-state conditions with benchmark literature data was good and agreement was within a calculated uncertainty of the measurement system. Also, good agreement of special TC and standard TC outputs was obtained and the results are encouraging. Oxidation of thin film thermoelements was a primary failure mode after about 5 of operation. Author

A86-16378*# National Aeronautics and Space Administration. Lewis Research Center, Cleveland, Ohio.

THREE COMPONENT VELOCITY MEASUREMENTS USING FABRY-PEROT INTERFEROMETER

R. G. SEASHOLTZ and L. J. GOLDMAN (NASA, Lewis Research Center, Cleveland, OH) IN: International Symposium on Applications of Laser Anemometry to Fluid Mechanics, 2nd, Lisbon, Portugal, July 2-5, 1984, Proceedings. Lisbon, Instituto Superior Tecnico, 1985, p. 8.6 (6 p.). Previously announced in STAR as N84-26010. refs

A method for measuring the three components of mean flow velocity using a backscatter optical system based on a confocal Fabry-Perot interferometer is described. An analysis of the expected uncertainties in the velocity component measurements is presented along with experimental data taken in a free jet at two flow velocities (100 and 300 m/s). Author

A86-19670*#

BOUNDARY LAYER MEASUREMENTS ON AN AIRFOIL IN CASCADE USING LASER DOPPLER ANEMOMETRY

F. W. WILLIAMS AIAA, Aerospace Sciences Meeting, 24th, Reno, NV, Jan. 6-9, 1986. 14 p. refs (Contract NSG-3265) (AIAA PAPER 86-0072)

Laser Doppler anemometry (LDA) was used to obtain detailed boundary layer data at 89.3 percent chord on the pressure surface of a double circular arc compressor blade in cascade. The measurements were taken at a chord Reynolds number of 5.0×10^5 to the 5th and a cascade angle of 53 degrees. The mean velocity, local turbulence intensity, skewness, and kurtosis were determined from the measured velocity probability distributions. The mean velocity profile and the local turbulence intensity profile had classical shapes. Also, the skewness and kurtosis had commonly observed shapes through out the boundary layer, reaching maximum values for Y/δ between 0.5 and 1.1 and Gaussian values for Y/δ greater than 1.1. A comparison was made between data taken with and without the Bragg cell and no significant differences were found. Author

A86-19726*# Stanford Univ., Calif.

SIMULTANEOUS MEASUREMENTS OF VELOCITY AND PRESSURE FIELDS IN SUBSONIC AND SUPERSONIC FLOWS THROUGH IMAGE-INTENSIFIED DETECTION OF LASER-INDUCED FLUORESCENCE

B. HILLER, L. M. COHEN, and R. K. HANSON (Stanford University, CA) AIAA, Aerospace Sciences Meeting, 24th, Reno, NV, Jan. 6-9, 1986. 11 p. refs (Contract F49620-83-K-0004; NAG3-285) (AIAA PAPER 86-0161)

An optical technique is presented for combined, spatially resolved measurements of two-dimensional velocity and pressure fields in compressible flows. The single-mode frequency of an argon laser is fixed in the wing of an absorption line of iodine molecules, seeded in an underexpanded round jet of nitrogen gas. The emitted fluorescence, being proportional to the amount of absorbed radiation and hence the absorption line-shape function, is detected with an intensified 100×100 photodiode array camera. A single-microchannel-plate image intensifier is fiber-optically coupled to the array in order to improve time resolution and SNR. Three components of the velocity vector in a cross-sectional plane are sequentially probed with four laser sheets from three different directions. By shifting the laser frequency in one of the sheets with a piezo-tuned intra-cavity etalon, the slope of the absorption line can be measured in situ in order to provide the required scaling factor for the velocity measurement. With its short measurement times of less than 250 ms, this method is well suited for blow-down wind tunnel experiments. Author

A86-20798* John Carroll Univ., Cleveland, Ohio.

WAVELENGTH-DIVISION MULTIPLEXED DIGITAL OPTICAL POSITION TRANSDUCER

K. FRITSCH (John Carroll University, Cleveland, OH) and G. BEHEIM (NASA, Lewis Research Center, Cleveland, OH) Optics Letters (ISSN 0146-9592), vol. 11, Jan. 1986, p. 1-3.

A novel concept for a digital optical position transducer is presented. This compact and rugged device is electrically passive and requires only a dual-fiber optical link. Wavelength division of a broad-spectrum semiconductor light source is employed to multiplex the channels of a 10-bit digital position encoder. A preliminary design was evaluated and found to have a 10-dB on-off contrast ratio and a 12-dB insertion loss. Author

A86-22700*# National Aeronautics and Space Administration. Lewis Research Center, Cleveland, Ohio.

FORMATION AND CHARACTERIZATION OF SIMULATED SMALL DROPLET ICING CLOUDS

R. D. INGEBO (NASA, Lewis Research Center, Cleveland, OH) AIAA, Aerospace Sciences Meeting, 24th, Reno, NV, Jan. 6-9, 1986. 12 p. Previously announced in STAR as N86-14554. (AIAA PAPER 86-0409)

Two pneumatic two-fluid atomizers operating at high liquid and gas pressures produced water sprays that simulated small droplet clouds for use in studying icing effects on aircraft performance. To measure median volume diameter, MVD or $D_{sub 50}$, of small droplet water sprays, a scattered-light scanning instrument was developed. Drop size data agreed fairly well with calculated values at water and nitrogen pressures of 60 and 20 psig, respectively, and at water and nitrogen pressures of 250 and 100 psig, respectively, but not very well at intermediate values of water and nitrogen pressure. MVD data were correlated with $D_{sub O}$, $W_{sub N}$, and $W_{sub w}$, i.e., orifice diameter, nitrogen, and water flowrate, respectively, to give the expression for MVD in microns. Author

35 INSTRUMENTATION AND PHOTOGRAPHY

A86-26909*# National Aeronautics and Space Administration. Lewis Research Center, Cleveland, Ohio.

THE USE OF AN OPTICAL DATA ACQUISITION SYSTEM FOR BLADED DISK VIBRATION ANALYSIS

C. LAWRENCE and E. H. MEYN (NASA, Lewis Research Center, Cleveland, OH) IN: Vibrations of blades and bladed disk assemblies; Proceedings of the Tenth Biennial Conference on Mechanical Vibration and Noise, Cincinnati, OH, September 10-13, 1985. New York, American Society of Mechanical Engineers, 1985, p. 65-73. Previously announced in STAR as N85-15184. refs

A new concept in instrumentation was developed by engineers at NASA Lewis Research Center to collect vibration data from multi-bladed rotors. This new concept, known as the optical data acquisition system, uses optical transducers to measure bladed tip deflections by reflection of light beams off the tips of the blades as they pass in front of the optical transducer. By using an array of transducers around the perimeter of the rotor, detailed vibration signals can be obtained. In this study, resonant frequencies and mode shapes were determined for a 56 bladed rotor using the optical system. Frequency data from the optical system was also compared to data obtained from strain gauge measurements and finite element analysis and was found to be in good agreement. Author

A86-28541*# Maryland Univ., College Park.

ACCURACY AND DIRECTIONAL SENSITIVITY OF THE SINGLE-WIRE TECHNIQUE

T. W. JACKSON (Maryland, University, College Park) and D. G. LILLEY (Oklahoma State University, Stillwater) AIAA Journal (ISSN 0001-1452), vol. 24, March 1986, p. 451-458. USAF-supported research. Previously cited in issue 06, p. 774. Accession no. A84-18047. refs (Contract NAG3-74)

A86-29280*# National Aeronautics and Space Administration. Lewis Research Center, Cleveland, Ohio.

LENS COLLIMATION AND TESTING USING A TWYMAN-GREEN INTERFEROMETER WITH A SELF-PUMPED PHASE-CONJUGATING MIRROR

W. L. HOWES (NASA, Lewis Research Center, Cleveland, OH) Applied Optics (ISSN 0003-6935), vol. 25, Feb. 15, 1986, p. 473, 474. refs

Ordinarily Twyman-Green interferometers are employed testing optical elements. In a modification of the basic configuration, the ordinary mirror in the test arm is replaced with a self-pumped phase-conjugating mirror using a barium titanate crystal. It is shown that, with a redefinition of components, the new configuration permits retention and improvement of the optical element testing function while simultaneously serving as a sensitive test for collimation. The optical path difference resulting from the double pass in the original Twyman-Green interferometer approximately equals that of the single pass and phase conjugation in the modification. G.R.

A86-29755*# National Aeronautics and Space Administration. Lewis Research Center, Cleveland, Ohio.

IMPLEMENTATION OF A NEW TYPE OF TIME-OF-FLIGHT LASER ANEMOMETER

M. P. WERNET (NASA, Lewis Research Center, Cleveland, OH) and R. V. EDWARDS (Case Western Reserve University, Cleveland, OH) Applied Optics (ISSN 0003-6935), vol. 25, March 1, 1986, p. 644-648. refs (Contract NAG3-2)

A new time-of-flight (TOF) laser anemometer system utilizing a spatial lead-lag filter for bipolar pulse generation has been constructed and tested. This new TOF has been modified to enable measurements in turbulent flows near walls. Good results have been obtained as close as 100 microns from a surface, with a 140-mm focal length final lens. Lading's theory for the behavior of the measurement variance has been confirmed for this configuration. Author

A86-32046* National Aeronautics and Space Administration. Lewis Research Center, Cleveland, Ohio.

FIBRE-OPTIC THERMOMETER USING SEMICONDUCTOR-ETALON SENSOR

G. BEHEIM (NASA, Lewis Research Center, Cleveland, OH) Electronics Letters (ISSN 0013-5194), vol. 22, Feb. 27, 1986, p. 238, 239. refs

A fiber-optic thermometer is described which uses a thick-film SiC sensing etalon. The etalon's temperature-dependent phase shift is determined by analyzing its spectral reflectance, using an LED and a tunable Michelson interferometer. Temperatures from 20 to 1000 C are measured with better than 0.5 deg C resolution. Author

A86-34431*# National Aeronautics and Space Administration. Lewis Research Center, Cleveland, Ohio.

FILTER INDUCED ERRORS IN LASER ANEMOMETRY USING COUNTER-PROCESSOR

L. A. OBERLE and R. G. SEASHOLTZ (NASA, Lewis Research Center, Cleveland, OH) IN: International Symposium on Laser Anemometry, 2nd, Miami Beach, FL, November 17-22, 1985, Proceedings. New York, American Society of Mechanical Engineers, 1985, p. 221-230. Previously announced in STAR as N85-30288. refs

Simulations of laser Doppler anemometer (LDA) systems have focused primarily on noise studies or biasing errors. Another possible source of error is the choice of filter types and filter cutoff frequencies. Before it is applied to the counter portion of the signal processor, a Doppler burst is filtered to remove the pedestal and to reduce noise in the frequency bands outside the region in which the signal occurs. Filtering, however, introduces errors into the measurement of the frequency of the input signal which leads to inaccurate results. Errors caused by signal filtering in an LDA counter-processor data acquisition system are evaluated and filters for a specific application will reduce these errors are chosen. E.A.K.

A86-38359* National Aeronautics and Space Administration. Lewis Research Center, Cleveland, Ohio.

A COMPARISON OF ELECTRONIC HETERODYNE MOIRE DEFLECTOMETRY AND ELECTRONIC HETERODYNE HOLOGRAPHIC INTERFEROMETRY FOR FLOW MEASUREMENTS

A. J. DECKER (NASA, Lewis Research Center, Cleveland, OH) and J. STRICKER (NASA, Lewis Research Center, Cleveland, OH, Technion - Israel Institute of Technology, Haifa, Israel) SAE, Aerospace Technology Conference and Exposition, Long Beach, CA, Oct. 14-17, 1985. 16 p. Previously announced in STAR as N85-32302. refs (SAE PAPER 851896)

Electronic heterodyne moire deflectometry and electronic heterodyne holographic interferometry are compared as methods for the accurate measurement of refractive index and density change distributions of phase objects. Experimental results are presented to show that the two methods have comparable accuracy for measuring the first derivative of the interferometric fringe shift. The phase object for the measurements is a large crystal of KD P, whose refractive index distribution can be changed accurately and repeatably for the comparison. Although the refractive index change causes only about one interferometric fringe shift over the entire crystal, the derivative shows considerable detail for the comparison. As electronic phase measurement methods, both methods are very accurate and are intrinsically compatible with computer controlled readout and data processing. Heterodyne moire is relatively inexpensive and has high variable sensitivity. Heterodyne holographic interferometry is better developed, and can be used with poor quality optical access to the experiment. Author

A86-38460*# Pennsylvania State Univ., University Park.
RECENT SKIN FRICTION TECHNIQUES FOR COMPRESSIBLE FLOWS

G. S. SETTLES (Pennsylvania State University, University Park)
 AIAA and ASME, Fluid Mechanics, Plasma Dynamics and Lasers
 Conference, 4th, Atlanta, GA, May 12-14, 1986. 11 p. refs
 (Contract NAG3-527)
 (AIAA PAPER 86-1099)

A brief review is given of developments over the last decade in techniques for the measurement of skin friction in compressible airflows. Emphasis is placed on mean measurements beneath turbulent boundary layers in the supersonic and hypersonic flow regimes. Recent improvements in existing techniques such as the skin friction balance, Preston tube, sublayer fence, and heat transfer analogy are discussed. New or potential techniques including optical and acoustic measurements are also treated. Finally, new results are presented on the adaptation of the recently-developed laser interferometer skin friction meter for use in high-speed wind tunnels. Author

A86-39521*# National Aeronautics and Space Administration.
 Lewis Research Center, Cleveland, Ohio.

RANGE FINDING USING FREQUENCY-MODULATED LASER DIODE

G. BEHEIM (NASA, Lewis Research Center, Cleveland, OH) and
 K. FRITSCH (John Carroll University, Cleveland, OH) Applied
 Optics (ISSN 0003-6935), vol. 25, May 1, 1986, p. 1439-1442.
 refs

(Contract NAG3-571)

A coherent-optical time-of-flight range-finding technique is proposed which uses a simple inexpensive device. Target range is determined by modulating a laser diode's optical frequency and measuring the change in the phase of the light reflected back into the laser. Target velocity as well as range can be measured using this approach. The device is described, and experimental evidence is presented to show the feasibility of measuring distance with subcentimeter resolution over a 1.5-m range. Author

A86-42770*# Pratt and Whitney Aircraft, West Palm Beach, Fla.

FURTHER DEVELOPMENT OF THE DYNAMIC GAS TEMPERATURE MEASUREMENT SYSTEM

D. L. ELMORE, W. W. ROBINSON, and W. B. WATKINS (United Technologies Corp., Pratt and Whitney, West Palm Beach, FL)
 AIAA, ASME, SAE, and ASEE, Joint Propulsion Conference, 22nd,
 Huntsville, AL, June 16-18, 1986. 8 p.

(Contract NAS3-24228)

(AIAA PAPER 86-1648)

A compensated thermocouple measurement method was experimentally verified. Dynamic signal content from an atmospheric pressure laboratory burner was measured by the dynamic temperature sensor and a relatively delicate fine-wire resistance thermometer. Compensated data from the two dynamic temperature sensor thermoelements were compared with the compensated fine-wire data in the frequency domain. Absolute differences between spectral line amplitudes measured with different sensors are small relative to the mean temperature and verify the compensation method. Increases in precision of the measurement method require optimization of several factors, and directions for further work are identified. Author

A86-46353*# National Aeronautics and Space Administration.
 Lewis Research Center, Cleveland, Ohio.

RELIABILITY OF SCANNING LASER ACOUSTIC MICROSCOPY FOR DETECTING INTERNAL VOIDS IN STRUCTURAL CERAMICS

D. J. ROTH and G. Y. BAAKLINI (NASA, Lewis Research Center, Cleveland, OH) Advanced Ceramic Materials (ISSN 0883-5551), vol. 1, July 1986, p. 252-258. Previously announced in STAR as N86-16599. refs

The reliability of 100 MHz scanning laser acoustic microscopy (SLAM) for detecting internal voids in sintered specimens of silicon nitride and silicon carbide was evaluated. The specimens contained

artificially implanted voids and were positioned at depths ranging up to 2 mm below the specimen surface. Detection probability of 0.90 at a 0.95 confidence level was determined as a function of material, void diameter, and void depth. The statistical results presented for void detectability indicate some of the strengths and limitations of SLAM as a nondestructive evaluation technique for structural ceramics. Author

N86-11452*# National Aeronautics and Space Administration.
 Lewis Research Center, Cleveland, Ohio.

DEVELOPMENT OF SEEDING TECHNIQUES FOR SMALL SUPERSONIC WIND TUNNEL

W. R. HINGST and R. M. CHRISS (Toledo Univ.) In NASA.
 Langley Research Center Wind Tunnel Seeding Systems for Laser
 Velocimeters p 189-202 Oct. 1985 refs

Avail: NTIS HC A12/MF A01 CSCL 14B

The NASA Lewis 1x1 foot supersonic wind tunnel is used to experimentally verify computational methods. This tunnel, which is continuous running, operates from laboratory-wide high pressure air and vacuum systems. As such, the air does not recirculate but makes a single pass through the tunnel. The Mach number is varied with interchangeable nozzle blocks and has a range from Mach 1.6 to 4.0. Dry and filtered air is available up to pressures of 3 atmospheres. The air enters the tunnel system through a plenum having flow straighteners and 6 fine mesh screens. The exit of the plenum provides smooth contraction with an area ratio of approximately 20 that, along with the screens, provides a uniform flow for the nozzle. Author

N86-11497*# National Aeronautics and Space Administration.
 Lewis Research Center, Cleveland, Ohio.

HOST INSTRUMENTATION R AND D PROGRAM OVERVIEW

D. R. ENGLUND In its Turbine Eng. Hot Sect. Technol. (HOST)
 p 7-9 Oct. 1983

Avail: NTIS HC A11/MF A01 CSCL 14B

The HOST Instrumentation R&D program is focused on two categories of instrumentation. One category is that required to characterize the environment imposed on the hot section components of turbine engines. This category includes instruments for measuring gas flow, gas temperature, and heat flux. The second category is that for measuring the effect of the environment on the hot section components. This category includes strain measuring instruments and an optical system for viewing the interior of an operating combustor to detect cracks, buckling, carbon buildup, etc. G.L.C.

N86-11499*# Pratt and Whitney Aircraft, East Hartford, Conn.
 Engineering Div.

DYNAMIC GAS TEMPERATURE MEASUREMENT SYSTEM

D. L. ELMORE, W. W. ROBINSON, and W. B. WATKINS In
 NASA. Lewis Research Center Turbine Eng. Hot Sect. Technol.
 (HOST) p 17-35 Oct. 1983 refs

(Contract NAS3-23154)

Avail: NTIS HC A11/MF A01 CSCL 14B

A gas temperature measurement system with compensated frequency response of 1 KHz and capability to operate in the exhaust of a gas turbine combustor was developed. Environmental guidelines for this measurement are presented, followed by a preliminary design of the selected measurement method. Transient thermal conduction effects were identified as important; a preliminary finite-element conduction model quantified the errors expected by neglecting conduction. A compensation method was developed to account for effects of conduction and convection. This method was verified in analog electrical simulations, and used to compensate dynamic temperature data from a laboratory combustor and a gas turbine engine. Detailed data compensations are presented. Analysis of error sources in the method were done to derive confidence levels for the compensated data. G.L.C.

35 INSTRUMENTATION AND PHOTOGRAPHY

N86-11500*# United Technologies Research Center, East Hartford, Conn.

HIGH TEMPERATURE STATIC STRAIN SENSOR DEVELOPMENT PROGRAM

C. HULSE, R. BAILEY, and H. GRANT (Pratt and Whitney Aircraft Group, East Hartford, Conn.) / In NASA. Lewis Research Center Turbine Eng. Hot Sect. Technol. (HOST) p 37-40 Oct. 1983 (Contract NAS3-23722)

Avail: NTIS HC A11/MF A01 CSCL 14B

Electrical resistance strain gages useful for static strain measurements on nickel or cobalt superalloy parts inside a gas turbine engine on a test stand are being developed. Measurements of this type are of great importance in meeting the goals of the HOST program because, without reliable knowledge of the stresses and strains which exist in specific components, it will be difficult to fully appreciate where improvements in design and materials can be implemented. The first part of the effort consisted of a strain gage alloy development program which will be followed by an investigation of complete strain gage systems which will use the best of the alloys developed together with other system improvements. G.L.C.

N86-14554*# National Aeronautics and Space Administration. Lewis Research Center, Cleveland, Ohio.

FORMATION AND CHARACTERIZATION OF SIMULATED SMALL DROPLET ICING CLOUDS

R. D. INGEBO Jan. 1986 13 p refs Proposed for presentation at the 24th Aerospace Sciences Meeting, Reno, Nev., 6-8 Jan. 1986; sponsored by AIAA (NASA-TM-87180; E-2828; NAS 1.15:87180) Avail: NTIS HC A02/MF A01 CSCL 14B

Two pneumatic two-fluid atomizers operating at high liquid and gas pressures produced water sprays that simulated small droplet clouds for use in studying icing effects on aircraft performance. To measure median volume diameter, MVD or $D_{sub\ 0.5}$, of small droplet water sprays, a scattered-light scanning instrument was developed. Drop size data agreed fairly well with calculated values at water and nitrogen pressures of 60 and 20 psig, respectively, and at water and nitrogen pressures of 250 and 100 psig, respectively, but not very well at intermediate values of water and nitrogen pressure. MVD data were correlated with $D_{sub\ 0}$, $W_{sub\ N}$, and $W_{sub\ w}$, i.e., orifice diameter, nitrogen, and water flowrate, respectively, to give the expression for MVD in microns. Author

N86-21817*# United Technologies Research Center, East Hartford, Conn.

DEMONSTRATION TEST OF BURNER LINER STRAIN MEASURING SYSTEM Final Report

K. A. STETSON Jun. 1984 96 p refs

(Contract NAS3-23690)

(NASA-CR-174743; NAS 1.26:174743; R84-926376-15) Avail:

NTIS HC A05/MF A01 CSCL 14B

A demonstration test was conducted for two systems of static strain measurement that had been shown to have potential for application jet engine combustors. A modified JT12D combustor was operated in a jet burner test stand while subjected simultaneously to both systems of instrumentation, i.e., Kanthal A-1 wire strain gages and laser speckle photography. A section of the burner was removed for installation and calibration of the wire gages, and welded back into the burner. The burner test rig was modified to provide a viewing port for the laser speckle photography such that the instrumented section could be observed during operation. Six out of ten wire gages survived testing and showed excellent repeatability. The extensive precalibration procedures were shown to be effective in compensating for the large apparent strains associated with these gages. Although all portions of the speckle photography system operated satisfactorily, a problem was encountered in the form of optical inhomogeneities in the hot, high-pressure gas flowing by the combustor case which generate large and random apparent strain distributions. Author

N86-22915*# National Aeronautics and Space Administration. Lewis Research Center, Cleveland, Ohio.

THE DETERMINATION OF THE DIRECTION OF THE OPTIC AXIS OF UNIAXIAL CRYSTALLINE MATERIALS

J. A. LOCK (Cleveland State Univ., Ohio), H. J. SCHOCK, and C. A. REGAN Apr. 1986 21 p refs

(NASA-TM-86892; E-2364; NAS 1.15:86892) Avail: NTIS HC A02/MF A01 CSCL 20F

The birefringence of crystalline substances in general, and of sapphire in particular, is described. A test is described whose purpose is to determine the direction of the optic axis of a cylindrically machined single crystal of sapphire. This test was performed on the NASA Lewis sapphire cylinder and it was found that the optic axis made an angle of 18 deg with the axis of symmetry of the cylinder. Author

N86-24958*# National Aeronautics and Space Administration. Lewis Research Center, Cleveland, Ohio.

BEAM-MODULATION METHODS IN QUANTITATIVE AND FLOW VISUALIZATION HOLOGRAPHIC INTERFEROMETRY

A. DECKER 1986 21 p refs Presented at Advanced Instrumentation for Engine Components, Philadelphia, Pa., 19-23 May 1986; sponsored by AGARD

(NASA-TM-87306; E-3029; NAS 1.15:87306) Avail: NTIS HC A02/MF A01 CSCL 14E

This report discusses heterodyne holographic interferometry and time-average holography with a frequency shifted reference beam. Both methods will be used for the measurement and visualization of internal transonic flows, where the target facility is a flutter cascade. The background and experimental requirements for both methods are reviewed. Measurements using heterodyne holographic interferometry are presented. The performance of the laser required for time-average holography of time-varying transonic flows is discussed. Author

N86-24959*# National Aeronautics and Space Administration. Lewis Research Center, Cleveland, Ohio.

APPARATUS FOR ELECTRICAL MEASUREMENTS OF THIN FILMS FROM 77 TO 1000 K

L. G. MATUS and R. L. SUMMERS Mar. 1986 7 p refs

(NASA-TM-87256; E-2839-1; NAS 1.15:87256) Avail: NTIS HC A02/MF A01 CSCL 14B

A novel method of mounting thin samples for electrical measurements is described. A vacuum chuck holds a mounting plate, which, in turn, holds the sample. Contacts on the mounting plate establish electrical connection to the sample. The attachment of wires directly to the samples is unnecessary. Measurements can be made at temperatures from 77 to 1000 K. As an application of the apparatus, resistivity and Hall measurements of a thin silicon carbide sample are presented. Author

N86-24961*# National Aeronautics and Space Administration. Lewis Research Center, Cleveland, Ohio.

CHARACTERIZATION OF SIMULATED SMALL-DROPLET FUEL SPRAYS

R. D. INGEBO 1986 10 p refs Proposed for presentation at the 22nd Joint Propulsion Conference, Huntsville, Ala., 16-19 Jun. 1986; sponsored by the AIAA, ASME, SAE and ASEE

(NASA-TM-87286; E-2987; NAS 1.15:87286) Avail: NTIS HC A02/MF A01 CSCL 14B

A two-fluid pneumatic atomizer operating at relatively high liquid and gas pressures produced water sprays that simulated small-droplet clouds of liquid fuel for use in studying vaporization and fuel-air mixing effects on combustor performance and emissions. To characterize the sprays, a scattered-light scanning instrument was developed and measurements of volume median or volume mean diameter, $D_{sub\ 0.5}$, were correlated with $D_{sub\ 0}$, $W_{sub\ w}$, and $W_{sub\ n}$, i.e., orifice diameter, water, and nitrogen gas flow rates, respectively, to give the general expression: $D_{sub\ 0.5} \approx (D_{sub\ 0} \sup 0.2) (W_{sub\ w} \sup m) (W_{sub\ n} \sup n)$, which yields $D_{sub\ 0.5} = 45 (D_{sub\ 0} \sup 0.2) (W_{sub\ w} \sup 0.2) (W_{sub\ n} \sup 0.2) (W_{sub\ w} \sup -1.2)$. Values of $D_{sub\ 0}$, $W_{sub\ w}$, and $W_{sub\ n}$ are in centimeters and grams/second, respectively. Farther

downstream at an axial distance of 6.7 cm, exponent m increased from 0.2 to 0.4 and exponent n decreased from -1.2 to -1.0 and at a distance of 25 cm downstream of the atomizer, n decreased to -0.8. The increase in exponent m and decrease in exponent n was attributed to a loss of very small droplets from the spray due primarily to vaporization and diffusion effects on clouds of small droplets traveling a distance of 25 cm. Author

N86-24964* National Aeronautics and Space Administration. Lewis Research Center, Cleveland, Ohio.

RAMP-INTEGRATION TECHNIQUE FOR CAPACITANCE-TYPE BLADE-TIP CLEARANCE MEASUREMENT

G. R. SARMA and J. P. BARRANGER 1986 13 p refs Presented at the Aerospace Industries/Test Measurement Symposium, Seattle, Wash., 5-8 May 1986; sponsored by Instrument Society of America (NASA-TM-87241; E-2916; NAS 1.15:87241) Avail: NTIS HC A02/MF A01 CSCL 14B

The analysis of a proposed new technique for capacitance type blade tip clearance measurement is presented. The capacitance between the blade tip and a mounted capacitance electrode within a guard ring forms one of the feedback elements of a high speed operational amplifier. The differential equation governing the operational amplifier circuit is formulated and solved for two types of inputs to the amplifier - a constant voltage and a ramp. The resultant solutions shows an output that contains a term that is proportional to the derivative of the product of the input voltage and the time constant of the feedback network. The blade tip clearance capacitance is obtained by subtracting the output of a balancing reference channel followed by integration. The proposed sampled data algorithm corrects the environmental effects and varying rotor speeds on-line, making the system suitable for turbine instrumentation. System requirements, block diagrams, and typical application are included. Author

N86-24967* National Aeronautics and Space Administration. Lewis Research Center, Cleveland, Ohio.

COMBINED FRINGE AND FABRY-PEROT LASER ANEMOMETER FOR THREE COMPONENT VELOCITY MEASUREMENTS IN TURBINE STATOR CASCADE FACILITY

R. G. SEASHOLTZ and L. J. GOLDMAN 1986 23 p refs Presented at the 67th Symposium of the AGARD Propulsion and Energetics Panel on Advanced Instrumentation for Aero Engine Components, 19-23 May 1986, Philadelphia, Pa. (NASA-TM-87322; E-3058; NAS 1.15:87322) Avail: NTIS HC A02/MF A01 CSCL 14B

A laser anemometer is described that was developed for use in a 508 mm diameter annular turbine stator cascade facility. All three velocity components are measured through a single restricted optical port, both within the stator vane row and downstream of the vanes. The measurements are made through a cylindrical window in the casing that matches the tip radius of the cascade. The stator tested has a contoured hub endwall that results in a large radial flow near the hub. The anemometer uses a standard fringe configuration (LFA) with a fluorescent aerosol seed to measure the axial and circumferential velocity components. The radial component is measured with a confocal Fabry-Perot interferometer. The two configurations are combined in a single optical system and can operate simultaneously. Data are presented to illustrate the capabilities of the system. Author

N86-26596* Sverdrup Technology, Inc., Cleveland, Ohio. **CALIBRATION OF DROPLET SIZING AND LIQUID WATER CONTENT INSTRUMENTS: SURVEY AND ANALYSIS Interim Report**

E. C. HOVENAC May 1986 30 p refs Sponsored in part by FAA, Atlantic City, N.J. (Contract NAS3-24105) (NASA-CR-175099; E-3025; NAS 1.26:175099; FAA-CT-86-19) Avail: NTIS HC A03/MF A01 CSCL 14B

Results are presented for phase 1 of an effort to establish a unified calibration capability for instruments used for aircraft icing certification and aircraft icing research. Various calibration, data

correction, and verification procedures are reviewed and some new techniques are developed for droplet sizing instruments and liquid water content meters. These instruments include a forward scattering spectrometer probe, an optical array probe, and hot-wire type liquid water content meters. Work planned for phase 2 of the effort is described. Author

N86-26599* Rensselaer Polytechnic Inst., Troy, N.Y. Dept. of Mechanical Engineering, Aeronautical Eng.

POLARIZATION MODULATED ELLIPSOMETRY Final Report

J. L. LAUER and N. MARXER 10 Jul. 1986 114 p (Contract NAG3-222) (NASA-CR-177264; NAS 1.26:177264) Avail: NTIS HC A06/MF A01 CSCL 14B

For the investigation of the composition and thickness of thin nonuniform films on bearing and other tribological surfaces an automated ellipsometer was built, which is extremely sensitive to relative changes in thickness and composition of surface films. These changes can be seen by scanning across the surface with 20 micrometer lateral resolution. By measuring at different angles of incidence one can determine the film thickness and identify the material of the film by its complex index of refraction. For the analysis of organic layers on top of several metallic layers it was necessary to develop mathematical procedures to increase the absolute precision of the instrument. The ellipsometer is described in detail, and the precision is discussed. The actual performance of the ellipsometer was tested on three experiments. In the first one the composition and thickness of patches of an oxide film inside a wear track were determined. In the second the thickness of a carbon overcoat sputtered on a computer disk was measured: the carbon was identified as graphitic and of random orientation. In the third thickness of silicon oxide on top of a silicon substrate was found. Important features of this apparatus are: (1) accurate settings of the polarization stages and the angle of incidence (both automated); (2) high precision in the determination of the ellipsometric parameters without calibration prior to an experiment; and (3) very accurate scanning modes with high spatial resolution. Author

N86-27617* National Aeronautics and Space Administration. Lewis Research Center, Cleveland, Ohio.

IDENTIFICATION OF DIFFERENCES BETWEEN FINITE ELEMENT ANALYSIS AND EXPERIMENTAL VIBRATION DATA

C. LAWRENCE Jun. 1986 33 p (NASA-TM-87336; E-3082; NAS 1.15:87336) Avail: NTIS HC A03/MF A01 CSCL 14B

An important problem that has emerged from combined analytical/experimental investigations is the task of identifying and quantifying the differences between results predicted by F.E. analysis and results obtained from experiment. The objective of this study is to extend and evaluate the procedure developed by Sidhu for correlation of linear F.E. and modal test data to include structures with viscous damping. The desirability of developing this procedure is that the differences are identified in terms of physical mass, damping, and stiffness parameters instead of in terms of frequencies and modes shapes. Since the differences are computed in terms of physical parameters, locations of modeling problems can be directly identified in the F.E. model. From simulated data it was determined that the accuracy of the computed differences increases as the number of experimentally measured modes included in the calculations is increased. When the number of experimental modes is at least equal to the number of translational degrees of freedom in the F.E. model both the location and magnitude of the differences can be computed very accurately. When the number of modes is less than this amount the location of the differences may be determined even though their magnitudes will be under estimated. Author

35 INSTRUMENTATION AND PHOTOGRAPHY

N86-31030*# General Electric Co., Wilmington, Mass. Aircraft Instruments Dept.

HIGH ACCURACY FUEL FLOWMETER Final Report

1986 346 p

(Contract NAS3-22139)

(NASA-CR-174869; NAS 1.26:174869) Avail: NTIS HC A15/MF A01 CSCL 14B

All three flowmeter concepts (vortex, dual turbine, and angular momentum) were subjected to experimental and analytical investigation to determine the potential prototype performance. The three concepts were subjected to a comprehensive rating. Eight parameters of performance were evaluated on a zero-to-ten scale, weighted, and summed. The relative ratings of the vortex, dual turbine, and angular momentum flowmeters are 0.71, 1.00, and 0.95, respectively. The dual turbine flowmeter concept was selected as the primary candidate and the angular momentum flowmeter as the secondary candidate for prototype development and evaluation.

B.G.

N86-31857*# National Aeronautics and Space Administration. Lewis Research Center, Cleveland, Ohio.

PARAMETRIC STUDY OF BEAM REFRACTION PROBLEMS ACROSS LASER ANEMOMETER WINDOWS

A. K. OWEN Jun. 1986 33 p Presented at the Third International Symposium on Applications of Laser Anemometry to Fluid Mechanics, Lisbon, Portugal, 7-9 Jul. 1986; sponsored by the Instituto Superior Tecnico

(NASA-TM-87350; E-3064; NAS 1.15:87350;

USAAVSCOM-TR-86-C-16) Avail: NTIS HC A03/MF A01 CSCL 14B

The experimenter is often required to view flows through a window with a different index of refraction than either the medium being observed or the medium that the laser anemometer is immersed in. The refraction that occurs at the window surfaces may lead to undesirable changes in probe volume position or beam crossing angle and can lead to partial or complete beam uncrossing. This report describes the results of a parametric study of this problem using a ray tracing technique to predict these changes. The windows studied were a flat plate and a simple cylinder. For the flat-plate study: (1) surface thickness, (2) beam crossing angle, (3) bisecting line - surface normal angle, and (4) incoming beam plane surface orientation were varied. For the cylindrical window additional parameters were also varied: (1) probe volume immersion, (2) probe volume off-radial position, and (3) probe volume position out of the R-theta plane of the lens. A number of empirical correlations were deduced to aid the interested reader in determining the movement, uncrossing, and change in crossing angle for a particular situation.

Author

N86-31859*# National Aeronautics and Space Administration. Lewis Research Center, Cleveland, Ohio.

ADVANCED OPTICAL MEASURING SYSTEMS FOR MEASURING THE PROPERTIES OF FLUIDS AND STRUCTURES

A. J. DECKER 1986 37 p Presented at the Symposium on Propulsion Instrumentation, Jiangyou, China, 6-10 Oct. 1986; sponsored by NASA and the Chinese Aeronautical Establishment (NASA-TM-88829; E-3204; NAS 1.15:88829) Avail: NTIS HC A03/MF A01 CSCL 20F

Four advanced optical models are reviewed for the measurement of visualization of flow and structural properties. Double-exposure, diffuse-illumination, holographic interferometry can be used for three-dimensional flow visualization. When this method is combined with optical heterodyning, precise measurements of structural displacements or fluid density are possible. Time-average holography is well known as a method for displaying vibrational mode shapes, but it also can be used for flow visualization and flow measurements. Deflectometry is used to measure or visualize the deflection of light rays from collimation. Said deflection occurs because of refraction in a fluid or because of reflection from a tilted surface. The moire technique for deflectometry, when combined with optical heterodyning, permits very precise measurements of these quantities. The rainbow

schlieren method of deflectometry allows varying deflection angles to be encoded with colors for visualization.

Author

N86-32702*# National Aeronautics and Space Administration. Lewis Research Center, Cleveland, Ohio.

RESEARCH INSTRUMENTATION FOR HOT SECTION COMPONENTS OF TURBINE ENGINES

D. R. ENGLUND 1986 22 p Presented at the Symposium on Propulsion Instrumentation, Jiangyou, China, 6-10 Oct. 1986; sponsored by NASA and Chinese Aeronautical Establishment (NASA-TM-88851; E-3241; NAS 1.15:88851) Avail: NTIS HC A02/MF A01 CSCL 82B

Programs to develop research instrumentation for use on hot section components of turbine engines are discussed. These programs can be separated into two categories: one category includes instruments which can measure the environment within the combustor and turbine components, the other includes instruments which measure the response of engine components to the imposed environment. Included in the first category are instruments to measure total heat flux and fluctuating gas temperature. High temperature strain measuring systems, thin film sensors (e.g., turbine blade thermocouples) and a system to view the interior of a combustor during engine operation are programs which comprise the second category. The paper will describe the state of development of these sensors and measuring systems and, in some cases, show examples of measurements made with this instrumentation. The discussion will cover work done at NASA Lewis and at various contractor facilities.

Author

N86-32703*# National Aeronautics and Space Administration. Lewis Research Center, Cleveland, Ohio.

ADVANCED INSTRUMENTATION FOR AERONAUTICAL PROPULSION RESEARCH

M. J. HARTMANN 1986 23 p Presented at the Symposium on Propulsion Instrumentation, Jiangyou, China, 6-10 Oct. 1986; sponsored by NASA and Chinese Aeronautical Establishment (NASA-TM-88853; E-3244; NAS 1.15:88853) Avail: NTIS HC A02/MF A01 CSCL 14B

The development and use of advanced instrumentation and measurement systems are key to extending the understanding of the physical phenomena that limit the advancement of aer propulsion systems. The data collected by using these systems are necessary to verify numerical models and to increase the technologists' intuition into the physical phenomena. The systems must be versatile enough to allow their use with older technology measurement systems, with computer-based data reduction systems, and with existing test facilities. Researchers in all aer propulsion fields contribute to the development of these systems.

Author

36

LASERS AND MASERS

Includes parametric amplifiers.

A86-40662* National Aeronautics and Space Administration. Lewis Research Center, Cleveland, Ohio.

REASSESSMENT OF THE THEORY OF STIMULATED RAMAN SCATTERING

G. C. FRALICK (NASA, Lewis Research Center, Cleveland, OH) and R. T. DECK (Toledo, University, OH) Physical Review B, 3rd Series (ISSN 0163-1829), vol. 32, Nov. 15, 1985, p. 6207-6213. refs

A modification of the standard theory of stimulated Raman scattering (SRS) first proposed by Sparks (1974, 1975) is analyzed and shown to incorporate a possibly important physical effect; however, its original formulation is incorrect. The analysis is based on an exact numerical integration of the coupled equations of the modified theory, the results of which are compared with both the

conventional theory of SRS and with one set of experimental data. A reformulation of the modified theory is suggested that leads to a gain which is in somewhat better agreement with the data than is the conventional theory. Author

N86-11465*# Purdue Univ., West Lafayette, Ind. School of Mechanical Engineering.

CHARACTERISTICS OF AN AXISYMMETRIC SUDDEN EXPANSION FLOW Progress Report, 1 Jul. 1984 - 1 Jul. 1985 W. H. STEVENSON and H. D. THOMPSON 1 Jul. 1985 17 p refs

(Contract NAG3-502)

(NASA-CR-176278; NAS 1.26:176278) Avail: NTIS HC A02/MF A01 CSCL 20E

A two-color, two component Laser Doppler Velocimeter (LDV) system operating in forward scatter has been developed in order to make simultaneous measurements of the axial and radial velocity components in an axisymmetric sudden expansion flow with and without combustion. The LDV system includes Bragg cell modulators in the four beam paths to allow a net frequency shift of 5MHz in both the green and blue beams. This permits an unambiguous measurement of negative velocities and also eliminates incomplete signal bias. The green beam probe volume has a waist diameter of 0.200 mm and is approximately 2mm long. The blue beam has a probe volume waist of 0.250 mm and is approximately 1 mm long. The scattered light from the probe volume is separated so that approximately 80% of each color passes to its respective photomultiplier tube by using a dichroic filter. Narrow bandpass filters are used to further filter unwanted signals before they are detected. A schematic diagram of the LDV system is shown. Author

N86-11503*# National Aeronautics and Space Administration. Lewis Research Center, Cleveland, Ohio.

LASER ANEMOMETRY FOR HOT SECTION APPLICATIONS

R. G. SEASHOLTZ, L. G. OBERLE, and D. H. WEIKLE *In its* Turbine Eng. Hot Sect. Technol (HOST) p57-67 Oct. 1983 refs

Avail: NTIS HC A11/MF A01 CSCL 20E

Laser anemometers (LA's) for use in the study of the hot section components of turbomachinery are being developed. Specifically, laser anemometers are being developed for use in the 50.8-cm (20-in.) diameter warm turbine and high-pressure turbine (HPT) facilities at Lewis. A brief review of the status of the program along with some preliminary data taken in an open-jet burner are presented. G.L.C.

37

MECHANICAL ENGINEERING

Includes auxiliary systems (nonpower); machine elements and processes; and mechanical equipment.

A86-11016* Rensselaer Polytechnic Inst., Troy, N.Y.

ELLIPSOIDAL SURFACE ANALYSIS OF WEAR TRACKS PRODUCED BY DIFFERENT LUBRICANTS

J. L. LAUER, N. MARXER (Rensselaer Polytechnic Institute, Troy, NY), and W. R. JONES, JR. (NASA, Lewis Research Center, Cleveland, OH) ASLE and ASME, Tribology Conference, Atlanta, GA, Oct. 8-10, 1985. 8 p. refs

(Contract NAG3-22; DAAG24-83-K-0058)

(ASLE PREPRINT 85-TC-5A-2)

Ellipsometric analyses of wear tracks in bearings of M-50 steel were carried out after operation under severe conditions with different lubricant additives. The base lubricant was a synthetic ester. It was found that the surface and wear additives benzotriazole and tricresylphosphate produced very patchy oxide layers. Dioctyldiphenylamine, a common antioxidant, on the other hand produced smoother films. The analyses were performed with a

specially designed and constructed ellipsometer of very high (20 micron) spatial resolution. The results are consistent with data obtained by Auger electron spectroscopy. Author

A86-11091* SKF Industries, Inc., King of Prussia, Pa.

TRACTION FORCES AT SOLID-LUBRICATED ROLLING-SLIDING CONTACTS

B. B. AGGARWAL and R. L. BOVENKERK (SKF Industries, Inc., King of Prussia, PA) ASLE, Annual Meeting, 40th, Las Vegas, NV, May 6-9, 1985. 7 p. refs

(Contract DEN3-323)

(ASLE PREPRINT 85-AM-4E-2)

A single-element traction rig was used to measure the traction forces at a solid-lubricated contact of a ball against a flat disk at room temperature under combine rolling and sliding. The load and speed conditions were selected to match those anticipated for bearing applications in adiabatic diesel engines. Traction vs slide/roll ratio curves were similar to those for liquid lubricants but the traction forces were an order of magnitude higher. The test data were used to derive equations to predict traction force as a function of contact stress and rolling speed. The data showed that the magnitude of traction forces were almost the same for all the lubricants tested. The lubricants, should, therefore, be selected on the basis of their ability to limit the wear of contact surfaces. Author

A86-14466*# Akron Univ., Ohio.

LIFE AND RELIABILITY MODELING OF BEVEL GEAR REDUCTIONS

M. SAVAGE, C. K. BRIKMANIS (Akron, University, OH), D. G. LEWICKI, and J. J. COY (NASA, Lewis Research Center; U.S. Army, Propulsion Laboratory, Cleveland, OH) ASME, National Design Engineering Conference, Chicago, IL, Mar. 11-13, 1985. 9 p. Previously announced in STAR as N85-27227. refs

(ASME PAPER 85-DE-7)

A reliability model is presented for bevel gear reductions with either a single input pinion or dual input pinions of equal size. The dual pinions may or may not have the same power applied for the analysis. The gears may be straddle mounted or supported in a bearing quill. The reliability model is based on the Weibull distribution. The reduction's basic dynamic capacity is defined as the output torque which may be applied for one million output rotations of the bevel gear with a 90 percent probability of reduction survival. Author

A86-14467*# Mechanical Technology, Inc., Latham, N. Y.

OPERATIONAL MAINTENANCE DATA BASE DEVELOPMENT FOR KINEMATIC STIRLING ENGINES

A. RICHEY and G. SMITH (Mechanical Technology, Inc., Latham, NY) ASME, Energy-Sources and Technology Conference and Exhibition, Dallas, TX, Feb. 17-21, 1985. 6 p. DOE-supported research. refs

(Contract DEN3-32)

(ASME PAPER 85-DGP-20)

In the initial stages of developing the automotive Stirling engine (ASE), data has been accumulated under the program's Quality Assurance Report (QAR) program to identify problem areas encountered during engine operation. This data has been used as the basis for developing design modifications to existing hardware, identifying diagnostic techniques and instrumentation, and providing guidance towards component and system development requirements for future engine designs, such as the Mod II engine currently in the initial design stage. The QAR has proven itself to be an essential part of the ASE Program, and has successfully guided the development of the automotive application of this emerging engine technology. Author

A86-15227* National Aeronautics and Space Administration. Lewis Research Center, Cleveland, Ohio.

EXPERIMENTAL STUDY OF CERAMIC-COATED TIP SEALS FOR TURBOJET ENGINES

T. J. BIESIADNY, G. McDONALD, R. C. HENDRICKS (NASA, Lewis Research Center, Cleveland, OH), G. A. KLANN (U.S. Army, Propulsion Laboratory, Cleveland, OH), E. S. LASSOW (Howmet Turbine Components Corp., Whitehall, MI) et al. Ceramic Engineering and Science Proceedings (ISSN 0196-6219), vol. 6, July-Aug. 1985, p. 880-895. Previously announced in STAR as N85-19363. refs

Ceramic gas-path seals were fabricated and successfully operated over 1000 cycles from flight idle to maximum power in a small turboshaft engine. The seals were fabricated by plasma spraying zirconia over a NiCoCrAlX bond coat on the Haynes 25 substrate. Coolant-side substrate temperatures and related engine parameters were recorded. Post-test inspection revealed mudflat surface cracking with penetration to the ceramic bond-coat interface. Author

A86-16258* National Aeronautics and Space Administration. Lewis Research Center, Cleveland, Ohio.

FRICTIONAL AND MORPHOLOGICAL PROPERTIES OF AU-MOS₂ FILMS SPUTTERED FROM A COMPACT TARGET

T. SPALVINS (NASA, Lewis Research Center, Cleveland, OH) IN: Metallurgical coatings 1984; Proceedings of the Eleventh International Conference, San Diego, CA, April 9-13, 1984. Volume 1. Lausanne, Switzerland, Elsevier Sequoia, S.A., 1984, p. 375-384. Previously announced in STAR as N84-20858. refs

AuMoS₂ films 0.02 to 1.2 microns thick were sputtered from target compacted from 5 wt pct. Au + 95 wt pct. MoS₂, to investigate the frictional and morphological film growth characteristics. The gold dispersion effects in MoS₂ films are of interest to increase the densification and strengthening of the film structure. Three microstructural growth stages were identified on the nano-micro-macrostructural level. During sliding both sputtered Au-MoS₂ and MoS₂ films have a tendency to break within the columnar region. The remaining or effective film, about 0.2 microns thick, performs the lubrication. The Au-MoS₂ films displayed a lower friction coefficient with a high degree of frictional stability and less wear debris generation as compared to pure MoS₂ films. The more favorable frictional characteristics of the Au-MoS₂ films are attributed to the effective film thickness and the high density packed columnar zone which has a reduced effect on the fragmentation of the tapered crystallites during fracture. M.G.

A86-18700* National Aeronautics and Space Administration. Lewis Research Center, Cleveland, Ohio.

NEW DIRECTIONS IN LUBRICATION, MATERIALS, WEAR, AND SURFACE INTERACTIONS - TRIBOLOGY IN THE 80'S

W. R. LOOMIS, ED. (NASA, Lewis Research Center, Cleveland, OH) Park Ridge, NJ, Noyes Publications, 1985, 867 p. No individual items are abstracted in this volume; Previously announced in STAR as N84-23891, N84-25047.

New directions in tribology are described. A range of topics is addressed, extending from fundamental research on tribological materials of all kinds and their surface effects, to final technological applications in mechanical components such as bearings, gears, and seals. The general topics addressed include: importance and definition of materials in tribology; future directions of research in adhesion and friction, wear and wear-resistant materials, and liquid lubricants and additives; status and new directions in elastohydrodynamic lubrication and solid lubricants; and tribological materials for mechanical components of the future. C.D.

A86-19375* National Aeronautics and Space Administration. Lewis Research Center, Cleveland, Ohio.

LUBRICATION AND PERFORMANCE OF HIGH-SPEED ROLLING-ELEMENT BEARINGS

E. V. ZARETSKY, F. T. SCHULLER, and H. H. COE (NASA, Lewis Research Center, Cleveland, OH) Lubrication Engineering (ISSN 0024-7154), vol. 41, Oct. 1985, p. 725-732. Previously announced in STAR as N85-21658. refs

Trends in aircraft engine operating speeds have dictated the need for rolling-element bearings capable of speeds to 3 million DN. A review of high-speed rolling-element bearing state-of-the-art performance and lubrication is presented. Through the use of under-race lubrication and bearing thermal management bearing operation can be obtained to speeds of 3 million DN. Jet lubricated ball bearings are limited to 2.5 million DN for large bore sizes and to 3 million DN for small bore sizes. Current computer programs are able to predict bearing thermal performance. Author

A86-22748*# National Aeronautics and Space Administration. Lewis Research Center, Cleveland, Ohio.

EXPERIMENTAL STIFFNESS OF TAPERED BORE SEALS

D. P. FLEMING (NASA, Lewis Research Center, Cleveland, OH) ASME, Transactions, Journal of Vibration, Acoustics, Stress, and Reliability in Design (ISSN 0739-3717), vol. 108, Jan. 1986, p. 91-94. Previously announced in STAR as N85-25847. refs (ASME PAPER 85-DET-12)

The stiffness of tapered-bore ring seals was measured with air as the sealed fluid. Static stiffness agreed fairly well with results of a previous analysis. Cross-coupled stiffness due to shaft rotation was much less than predicted. It is suggested that part of the disparity may be due to simplifying assumptions in the analysis; however, these do not appear to account for the entire difference observed. E.A.K.

A86-24481*# Texas A&M Univ., College Station.

THEORY VERSUS EXPERIMENT FOR THE ROTORDYNAMIC COEFFICIENTS OF ANNULAR GAS SEALS. I - TEST FACILITY AND APPARATUS

D. W. CHILDS, C. E. NELSON, C. NICKS, J. SCHARRER, D. ELROD (Texas A & M University, College Station) et al. ASME and ASLE, Joint Lubrication Conference, Atlanta, GA, Oct. 8-10, 1985, 6 p. Previously announced in STAR as N85-19417. refs (Contract NAG3-181; F49620-82-K-0033) (ASME PAPER 85-TRIB-1)

A facility and apparatus are described for determining the rotordynamic coefficients and leakage characteristics of annular gas seals. The coefficients and leakage characteristics of annular gas seals. The apparatus has a current top speed of 8000 cpm with a nominal seal diameter of 15.24 cm (6 in.). The air supply unit yields a seal pressure ratio of approximately 7. An external shaker is used to excite the test rotor. The capability to independently calculate all rotordynamic coefficients at a given operating condition with one excitation frequency are discussed. Author

A86-24864* National Aeronautics and Space Administration. Lewis Research Center, Cleveland, Ohio.

OPERATING CHARACTERISTICS OF A 0.87 KW-HR FLYWHEEL ENERGY STORAGE MODULE

S. H. LOEWENTHAL, R. J. PARKER, E. V. ZARETSKY (NASA, Lewis Research Center, Cleveland, OH), and H. W. SCIBBE (Goodyear Aerospace Corp., Akron, OH) IN: Intersociety Energy Conversion Engineering Conference, 20th, Miami Beach, FL, August 18-23, 1985, Proceedings. Volume 2. Warrendale, PA, Society of Automotive Engineers, Inc., 1985, p. 2.361-2.371. Previously announced in STAR as N85-28371. refs

Discussion is given of the design and loss characteristics of 0.87 kW-hr (peak) flywheel energy storage module suitable for aerospace and automotive applications. The maraging steel flywheel rotor, a 46-cm-(18-in-) diameter, 58-kg (128-lb) tapered disk, delivers 0.65 kW-hr of usable energy between operating speeds of 10,000 and 20,000 rpm. The rotor is supported by 20- and 25-mm bore diameter, deep-groove ball bearings, lubricated

by a self-replenishing wick type lubrication system. To reduce aerodynamic losses, the rotor housing was evacuated to vacuum levels from 40 to 200 millitorr. Dynamic rotor instabilities uncovered during testing necessitated the use of an elastometric-bearing damper to limit shaft excursions. Spindown losses from bearing, seal, and aerodynamic drag at 50 millitorr typically ranged from 64 to 193 W at 10,000 and 20,000 rpm, respectively. Discharge efficiency of the flywheel system exceeded 96 percent at torque levels greater than 21 percent of rated torque. Author

A86-24884* National Aeronautics and Space Administration. Lewis Research Center, Cleveland, Ohio.

OVERVIEW OF THE 1985 NASA LEWIS RESEARCH CENTER SP-100 FREE-PISTON STIRLING ENGINE ACTIVITIES

J. G. SLABY (NASA, Lewis Research Center, Cleveland, OH) IN: Intersociety Energy Conversion Engineering Conference, 20th, Miami Beach, FL, August 18-23, 1985, Proceedings. Volume 3. Warrendale, PA, Society of Automotive Engineers, Inc., 1985, p. 3.180-3.188. Previously announced in STAR as N85-27769. refs

This effort is keyed on the design, fabrication, assembly, and testing of a 25 kWe Stirling space-power technology-feasibility demonstrator engine. Another facet of the SP-100 project covers the status of a 9000-hr endurance test conducted on a 2 kWe free-piston Stirling/linear alternator system employing hydrostatic gas bearings. Dynamic balancing of the RE-1000 engine (a 1 kWe free-piston Stirling engine) using a passive dynamic absorber will be discussed along with the results of a parametric study showing the relationships of Stirling power converter specific weight and efficiency as functions of Stirling engine heater to cooler temperature ratio. Planned tests will be described covering a hydrodynamic gas bearing concept for potential SP-100 application. Author

A86-24890* National Aeronautics and Space Administration. Lewis Research Center, Cleveland, Ohio.

RE-1000 FREE-PISTON STIRLING ENGINE UPDATE

J. SCHREIBER (NASA, Lewis Research Center, Cleveland, OH) IN: Intersociety Energy Conversion Engineering Conference, 20th, Miami Beach, FL, August 18-23, 1985, Proceedings. Volume 3. Warrendale, PA, Society of Automotive Engineers, Inc., 1985, p. 3.248-3.253. Previously announced in STAR as N86-11668.

A free piston Stirling engine was tested. The tests performed over the past several years on the single cylinder engine were designed to investigate the dynamics of a free piston Stirling engine. The data are intended to be used primarily for computer code validation. The tests designed to investigate the sensitivity of the engine performance to variations in working space pressure, heater and cooler temperatures, regenerator porosity, power piston mass and displacer dynamics were completed. In addition, some data were recorded with alternate working fluids. A novel resonant balance system for the engine was also tested. Some preliminary test results of the tests performed are presented along with an outline of future tests to be run with the engine coupled to a hydraulic output unit. A description of the hydraulic output unit is given. Author

A86-30599* Akron Univ., Ohio.

ANALYSIS OF A TWO ROW HYDROSTATIC JOURNAL BEARING WITH VARIABLE PROPERTIES, INERTIA EFFECTS AND SURFACE ROUGHNESS

M. J. BRAUN (Akron, University, OH), M. L. ADAMS, and R. L. MULLEN (Case Western Reserve University, Cleveland, OH) (Tel Aviv University, Technion - Israel Institute of Technology, University of the Negev, et al., Israel Conference on Mechanical Engineering, 18th, Technion - Israel Institute of Technology, Haifa, Israel, June 27, 28, 1984) Israel Journal of Technology (ISSN 0021-2202), vol. 22, no. 2-3, 1984-1985, p. 155-164. refs (Contract NAG3-304)

A computer algorithm for simulation of hydrostatic journal bearing pressure-flow behavior has been generated. The effects taken into account are inertia, cavitation, variable properties (isothermal bearing) and roughness. The program has been specifically tailored for simulation of the hybrid bearing of the

cryogenic turbopumps of the main shuttle engine. Due to the high pressure (515 psia) of the supply line no cavitation has been found. The influence of the roughness effects have been found to become important only when the surface-roughness order of magnitude is comparable with that of the bearing clearance itself. Pocket edge inertia and variable properties have been found to have quite an important influence upon the pocket pressure, field pressure distribution and lubricant mass flow. Author

A86-34010*# National Aeronautics and Space Administration. Lewis Research Center, Cleveland, Ohio.

OPERATING ASPECTS OF AN OIL PUMPING RING SEAL

P. J. SMITH (NASA, Lewis Research Center, Cleveland, OH) and T. G. KEITH, JR. (Toledo, University, OH) ASME, Transactions, Journal of Tribology (ISSN 0742-4787), vol. 108, April 1986, p. 275-281. refs

(Contract NSG-3156)

(ASME PAPER 85-TRIB-29)

Past analyses have left several unanswered questions regarding the operation of a pumping ring seal. This paper addresses some of these unresolved problems. In particular, treatment of the film-ring interfacial boundary condition and the return portion of the pumping cycle are numerically investigated. Further a simple model is proposed to determine whether or not the seal operates fully flooded. Author

A86-36298* Michigan Univ., Ann Arbor.

A MESH RE-ZONING TECHNIQUE FOR FINITE ELEMENT SIMULATIONS OF METAL FORMING PROCESSES

J.-C. CHENG and N. KIKUCHI (Michigan, University, Ann Arbor) International Journal for Numerical Methods in Engineering (ISSN 0029-5981), vol. 23, Feb. 1986, p. 219-228. refs

(Contract NSF MSM-84-10876; NAG3-388)

Based on some fundamental properties of finite element approximations, a mesh re-zoning scheme is proposed for finite element simulations of metal forming problems. It is demonstrated that this technique is indispensable in analyzing many difficult forming processes, especially when there exist corners or very irregular shapes on the boundaries. The algorithm is tested by a backward extrusion process and direct extrusion through a square die. Author

A86-37048* Detroit Diesel Allison, Indianapolis, Ind.

LIFE CYCLE COST ASSESSMENT OF FUTURE LOW HEAT REJECTION ENGINES

D. R. PETERSEN (General Motors Corp., Detroit Diesel Allison Div., Indianapolis, IN) SAE, International Congress and Exposition, Detroit, MI, Feb. 24-28, 1986. 14 p.

(Contract DEN3-329)

(SAE PAPER 860444)

The Adiabatic Diesel Engine Component Development (ADECD) represents a project which has the objective to accelerate the development of highway truck engines with advanced technology aimed at reduced fuel consumption. The project comprises three steps, including the synthesis of a number of engine candidate designs, the coupling of each with a number of systems for utilizing exhaust gas energy, and the evaluation of each combination in terms of desirability. Particular attention is given to the employed evaluation method and the development of this method. The objective of Life Cycle Cost (LCC) evaluation in the ADECD program was to select the best from among 42 different low heat rejection engine (LHRE)/exhaust energy recovery system configurations. The LCC model is discussed along with a maintenance cost model, the evaluation strategy, the selection of parameter ranges, and a full factorial analysis. G.R.

A86-38310* AiResearch Casting Co., Torrance, Calif. **FABRICATION OF CERAMIC COMPONENTS FOR ADVANCED GAS TURBINE ENGINES**

F. LIU and E. SOLIDUM (AiResearch Casting Co., Torrance, CA) SAE, Aerospace Technology Conference and Exposition, Long Beach, CA, Oct. 14-17, 1985. 12 p. DOE-sponsored research. refs

(Contract DEN3-167)

(SAE PAPER 851786)

The AGT101 ceramic gas turbine engine feasibility study has made use of the slip casting of silicon or silicon nitride powders to produce either reaction-bonded or sintered components such as turbine rotors, turbine shrouds, and inner and outer diffusers. Attention is given to the effects of processing parameters on the microstructure and properties of the finished components; the parameters encompass powder particle size distribution, casting slip viscosity, pH, and solid content fraction. The green slip cast components were consolidated by nitriding, sintering, or sinter/HIPping. O.C.

A86-38311* AiResearch Casting Co., Torrance, Calif. **PROCESSING STUDY OF INJECTION MOLDING OF SILICON NITRIDE FOR ENGINE APPLICATIONS**

M. E. RORABAUGH and H. C. YEH (AiResearch Casting Co., Torrance, CA) SAE, Aerospace Technology Conference and Exposition, Long Beach, CA, Oct. 14-17, 1985. 7 p.

(Contract NAS3-24385)

(SAE PAPER 851787)

The high hardness of silicon nitride, which is currently under consideration as a structural material for such hot engine components as turbine blades, renders machining of the material prohibitively costly; the near net shape forming technique of injection molding is accordingly favored as a means for component fabrication. Attention is presently given to the relationships between injection molding processing parameters and the resulting microstructural and mechanical properties of the resulting engine parts. An experimental program has been conducted under NASA sponsorship which tests the quality of injection molded bars of silicon nitride at various stages of processing. O.C.

A86-38312* General Motors Corp., Indianapolis, Ind. **METHODS FOR IMPROVING RELIABILITY IN CERAMIC TURBINE ROTORS**

D. A. TURNER and L. E. GROSECLOSE (General Motors Corp., Allison Gas Turbine Div., Indianapolis, IN) SAE, Aerospace Technology Conference and Exposition, Long Beach, CA, Oct. 14-17, 1985. 8 p. DOE-supported research.

(Contract DEN3-168)

(SAE PAPER 851788)

Evaluation of Carborundum (CBO) injection-molded sintered alpha silicon carbide (SiC) AGT 100 gasifier turbine rotors by spin testing established a baseline for material strength characteristics. Spin test results of a subsequent group of rotors demonstrated a reduction in average failure speed. Post-test fracture analysis identified surface and near-surface flaws in the back face region to be the typical failure origins. Corrective actions were initiated to address the elimination of the strength controlling flaws. Initial evaluation of rotors fabricated to these process modifications indicates improvements in overall surface quality and average burst speed. Author

A86-38617* North Carolina State Univ., Raleigh. **LINEAR DYNAMIC COUPLING IN GEARED ROTOR SYSTEMS**

J. W. DAVID (North Carolina State University, Raleigh) and L. D. MITCHELL (Virginia Polytechnic Institute and State University, Blacksburg) ASME, Transactions, Journal of Vibration, Acoustics, Stress, and Reliability in Design (ISSN 0739-3717), vol. 108, April 1986, p. 171-176. refs

(Contract NSG-3239)

(ASME PAPER 85-DET-11)

The effects of high frequency oscillations caused by the gear mesh, on components of a geared system that can be modeled as rigid discs are analyzed using linear dynamic coupling terms.

The coupled, nonlinear equations of motion for a disc attached to a rotating shaft are presented. The results of a trial problem analysis show that the inclusion of the linear dynamic coupling terms can produce significant changes in the predicted response of geared rotor systems, and that the produced sideband responses are greater than the unbalanced response. The method is useful in designing gear drives for heavy-lift helicopters, industrial speed reducers, naval propulsion systems, and heavy off-road equipment. I.S.

A86-38620* Arizona State Univ., Tempe. **PARAMETER SENSITIVITY IN THE DYNAMICS OF ROTOR-BEARING SYSTEMS**

M. RAJAN, H. D. NELSON (Arizona State University, Tempe), and W. J. CHEN ASME, Transactions, Journal of Vibration, Acoustics, Stress, and Reliability in Design (ISSN 0739-3717), vol. 108, April 1986, p. 197-206. refs

(Contract NAG3-580)

(ASME PAPER 85-DET-35)

When designing a rotor system it is frequently desirable to have at hand a set of design sensitivity coefficients which quantitatively predict a change in specific system characteristics to changes in design parameters. This paper presents eigenvalue sensitivity coefficients for the damped natural frequencies of whirl of general linear rotor system modeled by finite element discretization. In addition, a simple and direct method for calculation of the damped critical speeds is presented, which utilizes the eigenvalue sensitivity with respect to the spin speed. It is shown that the combination of design parameter and spin speed whirl frequency sensitivity coefficients may be used to also evaluate the damped critical speed sensitivity coefficients. Author

A86-40656* Illinois Univ., Chicago. **GENERATION OF SPIRAL BEVEL GEARS WITH ZERO KINEMATICAL ERRORS AND COMPUTER AIDED SIMULATION OF THEIR MESHING AND CONTACT**

F. L. LITVIN, W.-J. TSUNG (Illinois, University, Chicago), and J. J. COY (NASA, Lewis Research Center; U.S. Army, Propulsion Laboratory, Cleveland, OH) IN: Computers in engineering 1985. Volume 1. New York, American Society of Mechanical Engineers, 1985, p. 335-339. refs

There is proposed a method for generation of Gleason's spiral bevel gears which provides the following properties of meshing and contact: (1) the contact normal keeps its original direction within the neighborhood of the main contact point; (2) the contact ellipse moves along the gear tooth surface; and (3) the kinematical errors caused by Gleason's method of cutting are almost zero. Computer programs for the simulation of meshing and bearing contact are developed. Author

A86-40678* Illinois Univ., Chicago. **GENERATED SPIRAL BEVEL GEARS - OPTIMAL MACHINE-TOOL SETTINGS AND TOOTH CONTACT ANALYSIS**

F. L. LITVIN, W.-J. TSUNG (Illinois, University, Chicago), J. J. COY (NASA, Lewis Research Center; U.S. Army, Propulsion Laboratory, Cleveland, OH), and C. HEINE (Dana Corp., Fort Wayne, IN) SAE, 1985 International Off-Highway and Powerplant Congress and Exposition, Milwaukee, WI, Sept. 9-12, 1985. 9 p. Previously announced in STAR as N85-34405. refs

(SAE PAPER 851573)

Geometry and kinematic errors were studied for Gleason generated spiral bevel gears. A new method was devised for choosing optimal machine settings. These settings provide zero kinematic errors and an improved bearing contact. The kinematic errors are a major source of noise and vibration in spiral bevel gears. The improved bearing contact gives improved conditions for lubrication. A computer program for tooth contact analysis was developed, and thereby the new generation process was confirmed. The new process is governed by the requirement that during the generation process there is directional constancy of the common normal of the contacting surfaces for generator and generated surfaces of pinion and gear. E.A.K.

A86-40683*# California State Univ., Long Beach.
AN INVESTIGATION OF THE TRANSIENT THERMAL ANALYSIS OF SPUR GEARS

L. E. EL-BAYOUMY, L. S. AKIN (California State University, Long Beach), and D. P. TOWNSEND (NASA, Lewis Research Center, Cleveland, OH) ASME, Transactions, Journal of Mechanisms, Transmission, and Automation in Design, vol. 107, Dec. 1985, p. 541-548. Previously announced in STAR as N84-28088. refs (ASME PAPER 84-DET-92)

A finite element computer program is developed for evaluating the transient behavior of surface temperature in high performance spur gears. The time dimension is implemented using two and three point finite difference schemes. The different schemes are provided for the purpose of numerical stability and convergence studies. A detailed explanation of the gear cooling process leading to the establishment of a modified Blok model is also included. Other conventional models for approximating the heat transfer coefficients are available for comparison. Preliminary results are given showing snap shots of gear temperature contours at the initial stages of tooth engagement. M.A.C.

A86-45255*# National Aeronautics and Space Administration. Lewis Research Center, Cleveland, Ohio.

EFFICIENCY OF NONSTANDARD AND HIGH CONTACT RATIO INVOLUTE SPUR GEARS

N. E. ANDERSON (NASA, Lewis Research Center; U.S. Army, Propulsion Laboratory, Cleveland, OH) and S. H. LOEWENTHAL (NASA, Lewis Research Center, Cleveland, OH) ASME, Transactions, Journal of Mechanisms, Transmission, and Automation in Design, vol. 108, March 1986, p. 119-126. Previously announced in STAR as N84-29223. refs (ASME PAPER 84-DET-172)

A power loss prediction was extended to include involute spur gears of nonstandard proportions. The method is used to analyze the effects of modified addendum, tooth thickness, and gear center distance in addition to the parameters previously considered which included gear diameter, pitch, pressure angle, face width, oil viscosity, speed, and torque. Particular emphasis was placed on high contact ratio gearing (contact ratios greater than two). Despite their higher sliding velocities, high contact ratio gears are designed to levels of efficiency comparable to those of conventional gears while retaining their advantages through proper selection of gear geometry. Author

A86-43541*# National Aeronautics and Space Administration. Lewis Research Center, Cleveland, Ohio.

FAST APPROACH FOR CALCULATING FILM THICKNESSES AND PRESSURES IN ELASTOHYDRODYNAMICALLY LUBRICATED CONTACTS AT HIGH LOADS

L. G. HOUPERT and B. J. HAMROCK (NASA, Lewis Research Center, Cleveland, OH) ASME, Transactions, Journal of Tribology (ISSN 0742-4787), vol. 108, July 1986, p. 411-419; Discussion, p. 419, 420; Authors' Closure, p. 420. Previously announced in STAR as N85-30242. refs (ASME PAPER 85-TRIB-42)

The film thicknesses and pressures in elasto-hydrodynamically lubricated contacts have been calculated for a line contact by using an improved version of Okamura's approach. The new approach allows for lubricant compressibility, the use of Roelands' viscosity, a general mesh (nonconstant step), and accurate calculations of the elastic deformation. The new approach is described, and the effects on film thickness, pressure, and pressure spike of each of the improvements are discussed. Successful runs have been obtained at high pressure (to 4.8 GPa) with low CPU times. Author

A86-45256*# National Aeronautics and Space Administration. Lewis Research Center, Cleveland, Ohio.

FATIGUE LIFE ANALYSIS OF A TURBOPROP REDUCTION GEARBOX

D. G. LEWICKI, J. J. COY (NASA, Lewis Research Center; U.S. Army, Propulsion Laboratory, Cleveland, OH), J. D. BLACK (General Motors Corp., Allison Gas Turbine Div., Indianapolis, IN), and M. SAVAGE (Akron, University, OH) ASME, Transactions, Journal of Mechanisms, Transmission, and Automation in Design, vol. 108, June 1986, p. 255-262. Previously announced in STAR as N85-27228. refs (ASME PAPER 85-DET-10)

A fatigue life analysis of the Allison T56/501 turboprop reduction gearbox was developed. The life and reliability of the gearbox was based on the lives and reliabilities of the main power train bearings and gears. The bearing and gear lives were determined using the Lundberg-Palmgren theory and a mission profile. The five planet bearing set had the shortest calculated life among the various gearbox components, which agreed with field experience where the planet bearing had the greatest incidences of failure. The analytical predictions of relative lives among the various bearings were in reasonable agreement with field experience. The predicted gearbox life was in excellent agreement with field data when the material life adjustment factors alone were used. The gearbox had a lower predicted life in comparison with field data when no life adjustment factors were used or when lubrication life adjustment factors were used either alone or in combination with the material factors. Author

A86-43542*# National Aeronautics and Space Administration. Lewis Research Center, Cleveland, Ohio.

LUBRICANT AND ADDITIVE EFFECTS ON SPUR GEAR FATIGUE LIFE

D. P. TOWNSEND, E. V. ZARETSKY, and H. W. SCIBBE (NASA, Lewis Research Center, Cleveland, OH) ASME, Transactions, Journal of Tribology (ISSN 0742-4787), vol. 108, July 1986, p. 468-475; Discussion, p. 476; Authors' Closure, p. 476, 477. Previously announced in STAR as N85-28373. refs (ASME PAPER 85-TRIB-14)

Spur gear endurance tests were conducted with six lubricants using a single lot of consumable-electrode vacuum melted (CEVM) AISI 9310 spur gears. The six lubricants was divided into four batches each of which had a different additive content. Lubricant tested with a phosphorus-type load carrying additive showed a statistically significant improvement in life over lubricants without this type of additive. The presence of sulfur type antiwear additives in the lubricant did not appear to affect the surface fatigue life of the gears. No statistical difference in life was produced with those lubricants of different base stocks but with similar viscosity, pressure-viscosity coefficients and antiwear additives. Gears tested with a 0.1 wt pct sulfur and 0.1 wt pct phosphorus EP additives in the lubricant had reactive films that were 200 to 400 (0.8 to 1.6 microns) thick. Author

A86-45257*# National Aeronautics and Space Administration. Lewis Research Center, Cleveland, Ohio.

SPIN ANALYSIS OF CONCENTRATED TRACTION CONTACTS

S. H. LOEWENTHAL (NASA, Lewis Research Center, Cleveland, OH) ASME, Transactions, Journal of Mechanisms, Transmission, and Automation in Design, vol. 108, March 1986, p. 77-84. Previously announced in STAR as N84-27042. refs (ASME PAPER 84-DET-99)

Spin, the result of a mismatch in contact radii on either side of the point of rolling, has a detrimental effect on traction contact performance. It occurs in concentrated contacts having conical or contoured rolling elements, such as those in traction drives or angular contact bearings, and is responsible for an increase in contact heating and power loss. The kinematics of spin producing contact geometries and the subsequent effect on traction and power loss are investigated. The influence of lubricant traction characteristics and contact geometries that minimize spin are also addressed. Author

A86-45391* Carnegie-Mellon Univ., Pittsburgh, Pa.

TURBULENT TWO-PHASE FLOW IN ANNULAR SEALS

P. A. BEATTY and W. F. HUGHES (Carnegie-Mellon University, Pittsburgh, PA) ASLE, Annual Meeting, 41st, Toronto, Canada, May 12-15, 1986. 8 p. refs

(Contract NAG3-166)

(ASLE PREPRINT 86-AM-4G-3)

Steady, turbulent two-phase fluid flow in a rotating annular seal with no eccentricity is analyzed. The fluid is assumed to be a homogeneous mixture of liquid and vapor in thermodynamic equilibrium. Further, the flow is assumed to be adiabatic, but the effects due to heat generation by viscous dissipation are accounted for fully. Solution of the model governing differential equations is accomplished by use of a fourth-order Runge-Kutta numerical integration scheme. The calculation of mass leakage rates under choked and unchoked conditions are discussed and the phenomenon of all-liquid choked flow is explained. Several numerical examples are presented supposing cryogenic oxygen as the sealed fluid.

Author

A86-47354*# Sverdrup Technology, Inc., Cleveland, Ohio.

TORSIONAL VIBRATIONS AND DYNAMIC LOADS IN A BASIC PLANETARY GEAR SYSTEM

R. AUGUST (Sverdrup Technology, Inc., Cleveland, OH) and R. KASUBA (Cleveland State University, OH) ASME, Transactions, Journal of Vibration, Acoustics, Stress, and Reliability in Design (ISSN 0739-3717), vol. 108, July 1986, p. 348-353. Research supported by Cleveland State University. refs

(Contract NAG3-186)

An iterative method has been developed for analyzing dynamic loads in a light weight basic planetary gear system. The effects of fixed, semi-floating, and fully-floating sun gear conditions have been emphasized. The load dependent variable gear mesh stiffness were incorporated into a practical torsional dynamic model of a planetary gear system. The dynamic model consists of input and output units, shafts, and a planetary train. In this model, the sun gear has three degrees of freedom; two transverse and one rotational. The planets, ring gear, and the input and output units have one degree of freedom, (rotation) thus giving a total of nine degrees of freedoms for the basic system. The ring gear has a continuous radial support. The results indicate that the fixed sun gear arrangement with accurate or errorless gearing offers in general better performance than the floating sun gear system.

Author

A86-48109*# Texas A&M Univ., College Station.

EXPERIMENTAL ROTORDYNAMIC COEFFICIENT RESULTS FOR TEETH-ON-ROTOR AND TEETH-ON-STATOR LABYRINTH GAS SEALS

D. W. CHILDS and J. K. SCHARRER (Texas A & M University, College Station) ASME, International Gas Turbine Conference and Exhibit, 31st, Duesseldorf, West Germany, June 8-12, 1986. 6 p. refs

(Contract NAS3-181; F49620-82-K-0033)

(ASME PAPER 86-GT-12)

An experimental test facility is used to measure the rotordynamic coefficients of teeth-on-rotor and teeth-on-stator labyrinth gas seals. Direct damping coefficients are presented for these seals for the first time. The results are presented for the two seal configurations at identical operating conditions, and show that, in a rotordynamic sense, the teeth-on-stator seal is more stable than the teeth-on-rotor seal, for inlet tangential velocity in the direction of rotation.

Author

A86-49624* Michigan Technological Univ., Houghton.

STRESS AND DEFORMATION MODELING OF MULTIPLE ROTARY COMBUSTION ENGINE TROCHOID HOUSINGS

W. M. LYCHUK, S. A. BRADLEY, C. R. VILMANN, C. E. PASSERELLO (Michigan Technological University, Houghton), and C.-M. LEE (NASA, Lewis Research Center, Cleveland, OH) SAE, International Congress and Exposition, Detroit, MI, Feb. 24-28, 1986. 10 p. refs

(SAE PAPER 860614)

This paper documents the development of the capability to produce finite element models of alternate trochoid housing configurations. The effort needed to produce these models is greatly reduced by the use of a newly developed specialized finite element preprocessor which is described. The results of static stress comparisons conducted on a Mazda trochoid housing are presented. Planned future development of this modeling capability to operational situations is also presented.

Author

N86-10551*# National Aeronautics and Space Administration, Lewis Research Center, Cleveland, Ohio.

MEASUREMENT OF THE DENSITY OF BASE FLUIDS AT PRESSURES 0.422 TO 2.20 GPa

B. J. HAMROCK, B. O. JACOBSON (Lulea Univ.), and S. I. BERGSTROEM (Lulea Univ.) 1985 22 p refs Presented at the Ann. Meeting of the Am. Soc. of Lubrication Engrs., Toronto, 12-15 May 1986

(NASA-TM-87114; E-2650; NAS 1.15:87114) Avail: NTIS HC

A02/MF A01 CSCL 20D

The influence of pressure on the density of six base fluids is experimentally studied for a range of pressures from 0.422 to 2.20 GPa. An important parameter used to describe the results is the change in relative volume with change in pressure $dv \text{ sub } r/dp$. For pressures less than the solidification pressure ($p \text{ ps}$) a small change in pressure results in a large change in $dv \text{ sub } r/ps$. For pressures greater than the solidification pressure ($p \text{ ps}$) there is no change in $dv \text{ sub } r/dp$ with changing pressure. The solidification pressures of the base fluids varies considerably, as do the slopes that the experimental data assumes for $p \text{ ps}$. A new formula is developed that describes the effect of pressure on density in terms of four constants. These constants vary for the different base fluids tested.

Author

N86-10552*# National Aeronautics and Space Administration, Lewis Research Center, Cleveland, Ohio.

THE MECHANISM OF EROSION OF METALLIC MATERIALS UNDER CAVITATION ATTACK

B. C. S. RAO (Case Western Reserve Univ.) and D. H. BUCKLEY 1985 18 p refs Proposed for presentation at the Intern. Symp. on Cavitation, Sendai, 16-19 Apr. 1986; sponsored by Japan Society of Mechanical Engineers, ASME, Institution of Mechanical Engineers (British), JSCE and International Association for Hydraulic Research

(NASA-TM-87133; E-2684; NAS 1.15:87133) Avail: NTIS HC

A02/MF A01 CSCL 11F

The mean depth of penetration rates (MDPRs) of eight polycrystalline metallic materials, Al 6061-T6, Cu, brass, phosphor bronze, Ni, Fe, Mo, and Ti-5Al-2.5Sn exposed to cavitation attack in a viscous mineral oil with a 20 kHz ultrasonic oscillator vibrating at 50 micron amplitude are reported. The titanium alloy followed by molybdenum have large incubation periods and small MDPRs. The incubation periods correlate linearly with the inverse of hardness and the average MDPRs correlate linearly with the inverse of tensile strength of materials. The linear relationships yield better statistical parameters than geometric and exponential relationships. The surface roughness and the ratio of pit depth to pit width (h/a) increase with the duration of cavitation attack. The ratio h/a varies from 0.1 to 0.8 for different materials. Recent investigations (20) using scanning electron microscopy to study deformation and pit formation features are briefly reviewed. Investigations with single crystals indicate that the geometry of pits and erosion are dependent on their orientation.

Author

N86-11474*# Pratt and Whitney Aircraft, East Hartford, Conn. Engineering Div.

LATERAL DAMPERS FOR THRUST BEARINGS Final Report

D. H. HIBNER and D. R. SZAFIR Aug. 1985 79 p refs

(Contract NAS3-23932)

(NASA-CR-174924; NAS 1.26:174924; PWA-5966-17) Avail:

NTIS HC A05/MF A01 CSCL 13I

The development of lateral damping schemes for thrust bearings was examined, ranking their applicability to various engine classes, selecting the best concept for each engine class and performing an in-depth evaluation. Five major engine classes were considered: large transport, military, small general aviation, turboshaft, and non-manrated. Damper concepts developed for evaluation were: curved beam, constrained and unconstrained elastomer, hybrid boost bearing, hydraulic thrust piston, conical squeeze film, and rolling element thrust face. Author

N86-11475*# National Aeronautics and Space Administration. Lewis Research Center, Cleveland, Ohio.

PROTECTIVE COATINGS OF METAL SURFACES BY COLD PLASMA TREATMENT

R. MANORY and A. GRILL (Ben Gurion Univ. of the Negev, Beer Sheva) Oct. 1985 15 p refs

(NASA-TM-87152; E-2747-1; NAS 1.15:87152) Avail: NTIS HC

A02/MF A01 CSCL 11F

The cold plasma techniques for deposition of various types of protective coatings are reviewed. The main advantage of these techniques for deposition of ceramic films is the lower process temperature, which enables heat treating of the metal prior to deposition. In the field of surface hardening of steel, significant reduction of treatment time and energy consumption were obtained. A simple model for the plasma - surface reactions in a cold plasma system is presented, and the plasma deposition techniques are discussed in view of this model. Author

N86-12609*# National Aeronautics and Space Administration. Lewis Research Center, Cleveland, Ohio.

SURFACE FATIGUE LIFE AND FAILURE CHARACTERISTICS OF EX-53, CBS 1000M, AND AISI 9310 GEAR MATERIALS

D. P. TOWNSEND Oct. 1985 14 p refs

(NASA-TP-2513; E-2578; NAS 1.60:2513) Avail: NTIS HC

A02/MF A01 CSCL 13I

Spur gear endurance tests and rolling-element surface fatigue tests are conducted to investigate EX-53 and CBS 1000M steels for use as advanced application gear materials, to determine their endurance characteristics, and to compare the results with the standard AISI 9310 gear material. The gear pitch diameter is 8.89 cm (3.50 in). Gear test conditions are an oil inlet temperature of 320 K (116 F), an oil outlet temperature of 350 K (170 F), a maximum Hertz stress of 1.71 GPa (248 ksi), and a speed of 10,000 rpm. Bench-type rolling-element fatigue tests are conducted at ambient temperature with a bar specimen speed of 12,500 rpm and a maximum Hertz stress of 4.83 GPa (700 ksi). The EX-53 test gears have a surface fatigue life of twice that of the AISI 9310 spur gears. The CBS 1000M test gears have a surface fatigue life of more than twice that of the AISI 9310 spur gears. However, the CBS 1000M gears experience a 30-percent tooth fracture failure which limits its use as a gear material. The rolling-contact fatigue lines of RC bar specimens of EX-53 and AISI 9310 are approximately equal. However, the CBS 1000M RC specimens have a surface fatigue life of about 50 percent that of the AISI 9310. Author

N86-13734*# National Aeronautics and Space Administration. Lewis Research Center, Cleveland, Ohio.

DESIGN OF TRACTION DRIVES

S. H. LOEWENTHAL and E. V. ZARETSKY Oct. 1985 49 p refs Submitted for publication

(NASA-RP-1154; E-2143; NAS 1.61:1154) Avail: NTIS HC

A03/MF A01 CSCL 13I

Traction drives are among the simplest of all speed-changing mechanisms. Because of their simplicity and their ability to smoothly and continuously adjust speed, they are excellent choices for many

drive system applications. They have been used in industrial service for more than 100 years. Today's traction drives have power capacities which rival the best gear and belt drives due to modern traction fluids and highly fatigue-resistant bearing steels. This report summarizes methods to analyze and size traction drives. Lubrication principles, contact kinematics, stress, fatigue life, and performance prediction methods are presented. The effects of the lubricant's traction characteristics on life and power loss are discussed. An example problem is given which illustrates the effects of spin on power loss. Loading mechanism design and the design of nonlubricated friction wheels and rings are also treated. Author

N86-14612*# National Aeronautics and Space Administration. Lewis Research Center, Cleveland, Ohio.

GEARING

J. J. COY (Army Aviation Research and Technology Activity, Cleveland, Ohio), D. P. TOWNSEND, and E. V. ZARETSKY Dec. 1985 70 p refs

(NASA-RP-1152; E-2003; NAS 1.61:1152; AVSCOM-TR-84-C-15)

Avail: NTIS HC A04/MF A01 CSCL 13I

Gearing technology in its modern form has a history of only 100 years. However, the earliest form of gearing can probably be traced back to fourth century B.C. Greece. Current gear practice and recent advances in the technology are drawn together. The history of gearing is reviewed briefly in the Introduction. Subsequent sections describe types of gearing and their geometry, processing, and manufacture. Both conventional and more recent methods of determining gear stress and deflections are considered. The subjects of life prediction and lubrication are additions to the literature. New and more complete methods of power loss predictions as well as an optimum design of spur gear meshes are described. Conventional and new types of power transmission systems are presented. Author

N86-14613*# National Aeronautics and Space Administration. Lewis Research Center, Cleveland, Ohio.

PHENOMENOLOGICAL STUDY OF THE BEHAVIOR OF SOME SILICA FORMERS IN A HIGH VELOCITY JET FUEL BURNER

J. D. CAWLEY and R. F. HANDSCHUH Oct. 1985 26 p refs

(NASA-TM-87127; E-2711; NAS 1.15:87127;

USAAVSCOM-TR-85-C-17) Avail: NTIS HC A03/MF A01

CSCL 13I

Samples of four silica formers: single crystal SiC, sintered alpha-SiC, reaction sintered Si₃N₄ and polycrystalline MoSi₂, were subjected to a Mach 1 jet fuel burner for 1 hr, at a sample temperature of 1375 deg C (2500 deg F). Two phenomena were identified which may be deleterious to a gas turbine application of these materials. The glass layer formed on the MoSi₂ deformed appreciably under the aerodynamic load. A scale developed on the samples of the other materials which consisted of particular matter from the gas stream entrapped in a SiO₂ matrix. Author

N86-17408*# National Aeronautics and Space Administration. Lewis Research Center, Cleveland, Ohio.

ADVANCED SEALS FOR LIQUID OXYGEN (LOX) TURBOPUMPS

W. SHAPIRO, R. HAMM, and J. A. HEMMINGER (NASA. Lewis Research Center, Cleveland, Ohio) /in Johns Hopkins Univ. The 1985 JANNAF Propulsion Meeting, Volume 1 p 281-290 Apr. 1985 refs

(Contract NAS3-23260)

Avail: Chemical Propulsion Information Agency, Johns Hopkins Rd., Laurel, Md. 20707 HC \$78.98 CSCL 11A

Reliability, life and vehicle pay load can be enhanced by improved seals on space vehicle propulsion systems. Development of two types of fluid-film seals for application to advanced LOX turbomachines are summarized. The first is a floating ring, helium buffered seal whose function is to exclude intrusion of liquid oxygen (LOX) into the turbine drive. The other is a spiral groove, LOX, face-type configuration designed to break down pressure and minimize leakage of LOX. The Rayleigh-step, floating ring gas seals require low clearances to minimize leakage and stiff films to assure tracking excursions of the rotor and to overcome Coulomb

friction between the rings and housings. The design and test results of these buffer seals are described. Results indicate significant performance improvement over seals used on contemporary engines. The possibilities of reducing helium storage requirements and thus increasing payload appear promising. A unique configuration of spiral groove LOX seal was required to avoid detrimental vaporization in the flow path. It was found that fluid turbulence and inertia influence groove geometry and in particular groove depth must be much greater than spiral groove seals using conventional fluids. Author

N86-17748*# Transmission Research, Inc., Cleveland, Ohio.
CONSTITUTIVE MODELLING OF LUBRICANTS IN CONCENTRATED CONTACTS AT HIGH SLIDE TO ROLL RATIOS Interim Report

J. L. TEVAARWERK Dec. 1985 85 p refs

(Contract DEN3-35)

(NASA-CR-175029; NAS 1.26:175029; IR-4) Avail: NTIS HC A05/MF A01 CSCL 11H

A constitutive lubricant friction model for rolling/sliding concentrated contacts such as gears and cams was developed, based upon the Johnson and Tevaarwerk fluid rheology model developed earlier. The friction model reported herein differs from the earlier rheological models in that very large slide to roll ratios can now be accommodated by modifying the thermal response of the model. Also the elastic response of the fluid has been omitted from the model, thereby making it much simpler for use in the high slide to roll contacts. The effects of this simplification are very minimal on the outcome of the predicted friction losses (less than 1%). In essence then the lubricant friction model developed for the high slide to roll ratios treats the fluid in the concentrated contact as consisting of a nonlinear viscous element that is pressure, temperature, and strain rate dependent in its shear response. The fluid rheological constants required for the prediction of the friction losses at different contact conditions are obtained by traction measurements on several of the currently used gear lubricants. An example calculation, using this model and the fluid parameters obtained from the experiments, shows that it correctly predicts trends and magnitude of gear mesh losses measured elsewhere for the same fluids tested here. Author

N86-19606* National Aeronautics and Space Administration. Lewis Research Center, Cleveland, Ohio.

COMPLIANT HYDRODYNAMIC FLUID JOURNAL BEARING Patent

E. L. WARREN, inventor (to NASA) 12 Nov. 1985 6 p Filed 24 Apr. 1984

(NASA-CASE-LEW-13670-1; US-PATENT-4,552,466;

US-PATENT-APPL-SN-603374; US-PATENT-CLASS-384-103;

US-PATENT-CLASS-384-106) Avail: US Patent and Trademark Office

An air bearing structure is described that prevents destructive bending moments within the top foil. Welds are eliminated by mounting the top bearing foil in the bearing cartridge sleeve without using a space block. Tabs or pins at the end of the top bearing foil are restrained by slots or stops formed in the cartridge sleeve. These structural members are free to move in a direction normal to the shaft while being restrained from movement in the direction of shaft rotation.

Official Gazette of the U.S. Patent and Trademark Office

N86-19616*# National Aeronautics and Space Administration. Lewis Research Center, Cleveland, Ohio.

EFFECT ON INTERFERENCE FITS ON ROLLER BEARING FATIGUE LIFE

H. L. COE and E. V. ZARETSKY Jan. 1986 24 p refs

(NASA-TM-87165; E-2516; NAS 1.15:87165) Avail: NTIS HC

A02/MF A01 CSCL 13I

An analysis was performed to determine the effects of inner-ring speed and press fits on roller bearing fatigue life. The effects of the resultant hoop and radial stresses on the principal stresses were considered. The maximum shear stresses below the Hertzian contact were determined for different conditions of inner-ring speed

and load, and were applied to a conventional roller bearing life analysis. The effect of mean stress was determined using Goodman diagram approach. Hoop stresses caused by press fits and centrifugal force can reduce bearing life by as much as 90 percent. Use of a Goodman diagram predicts life reductions of 20 to 30 percent. The depth of the maximum shear stress remains virtually unchanged. Author

N86-20808*# General Motors Corp., Indianapolis, Ind. Allison Gas Turbine Div.

ADVANCED GAS TURBINE (AGT) TECHNOLOGY REPORT Annual Report, Jan. - Dec. 1984

Jun. 1985 139 p

(Contract DEN3-168; DE-AI01-77CS-51040)

(NASA-CR-175018; DOE/NASA/0168-9; NAS 1.26:175018;

EDR-12070) Avail: NTIS HC A07/MF A01 CSCL 21A

Engine testing, ceramic component fabrication and evaluation, component performance rig testing, and producibility experiments at Pontiac comprised AGT 100 activities of this period, January to December 1984. Two experimental engines were available and allowed the evaluation of eight experimental assemblies. Operating time accumulated was 115 hr of burning and 156 hr total. Total cumulative engine operating time is now 225 hr. Build number 11 and 12 of engine S/N 1 totaled 28 burning hours and constituted a single assembly of the engine core--the compressor, both turbines, and the gearbox. Build number 11 of engine S/N 1 included a 1:07 hr continuous test at 100% gasifier speed (86,000 rpm). Build number 8 of engine S/N 2 was the first engine test with a ceramic turbine rotor. A mechanical loss test of an engine assembly revealed the actual losses to be near the original design allowance. Component development activity included rig testing of the compressor, combustor, and regenerator. Compressor testing was initiated on a rig modified to control the transfer of heat between flow path, lubricating oil, and structure. Results show successful thermal decoupling of the rig and lubricating/cooling oil. Rig evaluation of a reduced-friction compressor was initiated. Combustor testing covered qualification of ceramic parts for engine use, mapping of operating range limits, and evaluation of a relocated igniter plug. Several seal refinements were tested on the hot regenerator rig. An alternate regenerator disk, extruded MAS, was examined and found to be currently inadequate for the AGT 100 application. Also, a new technique for measuring leakage was explored on the regenerator rig. Ceramic component activity has focused on the development of state-of-the-art material strength characteristics in full-scale hardware. Injection-molded sintered alpha-SiC rotors were produced at Carborundum in an extensive process and tool optimization study. Author

N86-20809*# National Aeronautics and Space Administration. Lewis Research Center, Cleveland, Ohio.

ADHESION AND WEAR RESISTANCE OF MATERIALS

D. H. BUCKLEY 1986 30 p refs Proposed for presentation at the Hartstoffsichten zur Verschleissminderung, Bad Honnef, West Germany, 5-7 May 1986; sponsored by max-Planck-Inst. fuer Metallforschung

(NASA-TM-87239; E-2914; NAS 1.15:87239) Avail: NTIS HC A03/MF A01 CSCL 11H

Recent studies into the nature of bonding at the interface between two solids in contact or a solid and deposited film have provided a better understanding of those properties important to the adhesive wear resistance of materials. Analytical and experimental progress are reviewed. For simple metal systems the adhesive bond forces are related to electronic wave function overlap. With metals in contact with nonmetals, molecular-orbital energy, and density of states, respectively can provide insight into adhesion and wear. Experimental results are presented which correlate adhesive forces measured between solids and the electronic surface structures. Orientation, surface reconstruction, surface segregation, adsorption are all shown to influence adhesive interfacial strength. The interrelationship between adhesion and the wear of the various materials as well as the life of coatings applied to substrates are discussed. Metallic systems addressed include simple metals and alloys and these materials in contact

with themselves, both oxide and nonoxide ceramics, diamond, polymers, and inorganic coating compounds, has diamondlike carbon. Author

N86-21856*# National Aeronautics and Space Administration. Lewis Research Center, Cleveland, Ohio.

QUASI-MODAL VIBRATION CONTROL BY MEANS OF ACTIVE CONTROL BEARINGS

K. NONAMI and D. P. FLEMING 1986 12 p refs To be presented at the International Conference on Rotordynamics, Tokyo, Japan, 14-17 Sep. 1986; sponsored in part by IFTOMM, and the Japan Society of Mechanical Engineers (NASA-TM-87232; E-2899; NAS 1.15:87232) Avail: NTIS HC A02/MF A01 CSCL 13I

This paper investigates a design method of an active control bearing system with only velocity feedback. The study provides a new quasi-modal control method for a control system design of an active control bearing system in which feedback coefficients are determined on the basis of a modal analysis. Although the number of sensors and actuators is small, this quasi-modal control method produces a control effect close to an ideal modal control. Author

N86-23936*# General Electric Co., Cincinnati, Ohio. Aircraft Engine Business Group.

EXTENDED PARAMETRIC REPRESENTATION OF COMPRESSOR FANS AND TURBINES. VOLUME 1: CMGEN USER'S MANUAL Final Report, Aug. 1982 - Oct. 1983

G. L. CONVERSE and R. G. GIFFIN Mar. 1984 60 p refs 3 Vol.

(Contract NAS3-23055)
(NASA-CR-174645; NAS 1.26:174645; R84AEB378-VOL-1)
Avail: NTIS HC A04/MF A01 CSCL 13I

A modeling technique for fans, boosters, and compressors has been developed which will enable the user to obtain consistent and rapid off-design performance from design point input. The fans and compressors are assumed to be multi-stage machines incorporating front variable stators. The boosters are assumed to be fixed geometry machines. The modeling technique has been incorporated into time sharing program to facilitate its use. Because this report contains a description of the input output data, values of typical inputs, and examples cases, it is suitable as a user's manual. This report is the first of a three volume set describing the parametric representation of compressors, fans, and turbines. The titles of the three volumes are as follows: (1) Volume 1 CMGEN USER's Manual (Parametric Compressor Generator); (2) Volume 2 PART USER's Manual (parametric Turbine); (3) Volume 3 MODFAN USER's Manual (Parametric Modulating Flow Fan). Author

N86-23937*# General Electric Co., Cincinnati, Ohio. Aircraft Engine Business Group.

EXTENDED PARAMETRIC REPRESENTATION OF COMPRESSOR FANS AND TURBINES. VOLUME 2: PART USER'S MANUAL (PARAMETRIC TURBINE) Final Report, Aug. 1982 - Oct. 1983

G. L. COVERSE Mar. 1984 61 p refs 3 Vol.
(Contract NAS3-23055)
(NASA-CR-174646; NAS 1.26:174646; R84AEB379-VOL-2)
Avail: NTIS HC A04/MF A01 CSCL 13I

A turbine modeling technique has been developed which will enable the user to obtain consistent and rapid off-design performance from design point input. This technique is applicable to both axial and radial flow turbine with flow sizes ranging from about one pound per second to several hundred pounds per second. The axial flow turbines may or may not include variable geometry in the first stage nozzle. A user-specified option will also permit the calculation of design point cooling flow levels and corresponding changes in efficiency for the axial flow turbines. The modeling technique has been incorporated into a time-sharing program in order to facilitate its use. Because this report contains a description of the input output data, values of typical inputs, and example cases, it is suitable as a user's manual. This report

is the second of a three volume set. The titles of the three volumes are as follows: (1) Volume 1 CMGEN USER's Manual (Parametric Compressor Generator); (2) Volume 2 PART USER's Manual (Parametric Turbine); (3) Volume 3 MODFAN USER's Manual (Parametric Modulation Flow Fan). Author

N86-23938*# General Electric Co., Cincinnati, Ohio. Aircraft Engine Business Group.

EXTENDED PARAMETRIC REPRESENTATION OF COMPRESSOR FANS AND TURBINES. VOLUME 3: MODFAN USER'S MANUAL (PARAMETRIC MODULATING FLOW FAN) Final Report, Aug. 1982 - Oct. 1983

G. L. CONVERSE Mar. 1984 50 p refs 3 Vol.
(Contract NAS3-23055)
(NASA-CR-174647; NAS 1.26:174647; R84AEB380-VOL-3)
Avail: NTIS HC A03/MF A01 CSCL 13I

A modeling technique for single stage flow modulating fans or centrifugal compressors has been developed which will enable the user to obtain consistent and rapid off-design performance from design point input. The fan flow modulation may be obtained by either a VIGV (variable inlet guide vane) or a VPF (variable pitch rotor) option. Only the VIGV option is available for the centrifugal compressor. The modeling technique has been incorporated into a time-sharing program to facilitate its use. Because this report contains a description of the input output data, values of typical inputs, and examples cases, it is suitable as a user's manual. This report is the last of a three volume set describing the parametric representation of compressor fans, and turbines. The titles of the three volumes are as follows: (1) Volume 1 CMGEN USER's Manual (Parametric Compressor Generator); (2) Volume 2 PART USER's Manual (Parametric Turbine); (3) Volume 3 MODFAN USER's Manual (Parametric Modulating Flow Fan). Author

N86-24990*# Akron Univ., Ohio. Dept. of Mechanical Engineering.

SYSTEM LIFE AND RELIABILITY MODELING FOR HELICOPTER TRANSMISSIONS Final Report

M. SAVAGE and C. K. BRIKMANIS Washington Apr. 1986 202 p refs
(Contract NAG3-55)

(NASA-CR-3967; E-2889; NAS 1.26:3967) Avail: NTIS HC A10/MF A01 CSCL 05C

A computer program which simulates life and reliability of helicopter transmissions is presented. The helicopter transmissions may be composed of spiral bevel gear units and planetary gear units - alone, in series or in parallel. The spiral bevel gear units may have either single or dual input pinions, which are identical. The planetary gear units may be stepped or unstepped and the number of planet gears carried by the planet arm may be varied. The reliability analysis used in the program is based on the Weibull distribution lives of the transmission components. The computer calculates the system lives and dynamic capacities of the transmission components and the transmission. The system life is defined as the life of the component or transmission at an output torque at which the probability of survival is 90 percent. The dynamic capacity of a component or transmission is defined as the output torque which can be applied for one million output shaft cycles for a probability of survival of 90 percent. A complete summary of the life and dynamic capacity results is produced by the program. Author

N86-24991*# Irwin (Arthur S.) Co., Inc., Bemus Point, N.Y. **REVIEW AND CRITICAL ANALYSIS: ROLLING-ELEMENT BEARINGS FOR SYSTEM LIFE AND RELIABILITY Final Report**

A. S. IRWIN, W. J. ANDERSON, and W. J. DERNER Mar. 1985 234 p
(Contract NAS3-23520)

(NASA-CR-174710; NAS 1.26:174710; USAAVSCOM-TR-85-F-1)
Avail: NTIS HC A11/MF A01 CSCL 13I

A ball and cylindrical roller bearing technical specification which incorporates the latest state-of-the-art advancements was prepared

37 MECHANICAL ENGINEERING

for the purpose of improving bearing reliability in U.S. Army aircraft. The current U.S. Army aviation bearing designs and applications, including life analyses, were analyzed. A bearing restoration and refurbishment specification was prepared to improve bearing availability. Author

N86-24992*# National Aeronautics and Space Administration. Lewis Research Center, Cleveland, Ohio.
TESTING OF YUH-61A HELICOPTER TRANSMISSION IN NASA LEWIS 2240-KW (3000-HP FACILITY
A. M. MITCHELL, F. B. OSWALD, and F. T. SCHULLER Mar. 1986 28 p refs
(NASA-TP-2538; E-2801; NAS 1.60:2538) Avail: NTIS HC A03/MF A01 CSCL 01C

A helicopter transmission that was being considered for the Army's Utility Tactical Transport Attack System (UTTAS) was tested in the NASA Lewis 2240-kW (3000-hp) test facility to obtain the transmission's operational data. The results will form a vibration and efficiency data base for evaluation similar-class helicopter transmissions. The transmission's mechanical efficiency was determined to be 98.7 percent at its rated power level of 2080 kW (2792 hp). At power levels up to 113 percent of rated the transmission displayed 56 percent higher vibration acceleration levels on the right input than on the left input. Both vibration signature analysis and final visual inspection indicated that the right input spiral-bevel gear had poor contact patterns. The highest vibration meter level was 52 g's rms at the accessory gear, which had free-wheeling gearsets. At 113 percent power and 100 percent rated speed the vibration meter levels generally ranged from 3 to 25 g's rms. Author

N86-25790* National Aeronautics and Space Administration. Lewis Research Center, Cleveland, Ohio.
VARIABLE FRICTION SECONDARY SEAL FOR FACE SEALS Patent
E. DIRUSSO, inventor (to NASA) 8 Apr. 1986 5 p Filed 16 Nov. 1984 Supersedes N85-20377 Sponsored by NASA
(NASA-CASE-LEW-14170-1; US-PATENT-4,580-791; US-PATENT-APPL-SN-672224; US-PATENT-CLASS-227-27; US-PATENT-CLASS-227-28) Avail: US Patent and Trademark Office CSCL 11A

Vibration and stability of a primary seal ring is controlled by a secondary seal system. An inflatable bladder which forms a portion of the secondary seal varies the damping applied to this seal ring. The amplitude of vibration of the primary seal ring is sensed with a proximity probe that is connected to a microprocessor in a control system. The bladder pressure is changed by the control system to mitigate any sensed instability or vibration.

Official Gazette of the U.S. Patent and Trademark Office

N86-25793*# National Aeronautics and Space Administration. Lewis Research Center, Cleveland, Ohio.
GENERATION OF SPIRAL BEVEL GEARS WITH ZERO KINEMATICAL ERRORS AND COMPUTER AIDED TOOTH CONTACT ANALYSIS
F. L. LITVIN (Illinois Univ., Chicago.), W. J. TSUNG, J. J. COY, and C. HEINE (Dana Corp., Fort Wayne, Ind.) Mar. 1986 21 p refs Presented at the 2nd World Congress on Gearing, Paris, France, 2-5 Mar. 1986
(Contract NAG3-48)
(NASA-TM-87273; E-2932; NAS 1.15:87273; USAAVSCOM-TR-86-C-2) Avail: NTIS HC A02/MF A01 CSCL 131

Kinematic errors in spiral bevel gears are a major source of noise and vibrations in transmissions. A method for the generation of Gleason's spiral bevel gears which provides conjugated gear tooth surfaces and an improved bearing contact was developed. A computer program for the simulation of meshing, misalignment, and bearing contact was written. Author

N86-26629*# Garrett Turbine Engine Co., Phoenix, Ariz.
PRELIMINARY EVALUATION OF A COMPOUND CYCLE ENGINE FOR SHIPBOARD GENSETS

J. G. CASTOR and W. T. WINTUCKY (National Aeronautics and Space Administration. Lewis Research Center, Cleveland, Ohio.) Jun. 1986 29 p Sponsored by NASA. Prepared in cooperation with Naval Ship Research and Development Center, Annapolis, Md. Development Center, Annapolis, Md.
(Contract NAS3-24346)
(NASA-CR-179451; NAS 1.26:179451; DTNSRDC-PASD-CR-1886; GARRETT-21-5869; AVSCOM-TR-86-C-20) Avail: NTIS HC A03/MF A01 CSCL 131

The results of a thermodynamic cycle (SFC) and weight analysis performed to establish engine configuration, size, weight and performance are reported. Baseline design configuration was a 2,000 hour MTBO Compound Cycle Engine (CCE) for a helicopter application. The CCE configuration was extrapolated out to a 10,000 MTBO for a shipboard genset application. The study showed that an advanced diesel engine design (CCE) could be substantially lighter and smaller (79% and 82% respectively) than today's contemporary genset diesel engine. Although the CCE was not optimized, it had about a 7% reduction in mission fuel consumption over today's genset diesels. The CCE is a turbocharged, power-compounded, high power density, low-compression ratio diesel engine. Major technology development areas are presented. Author

N86-27640*# National Aeronautics and Space Administration. Lewis Research Center, Cleveland, Ohio.
APPLICATION OF LASER ANEMOMETRY TO TURBOMACHINERY FLOW FIELD MEASUREMENTS
A. J. STRAZISAR /n Von Karman Inst. for Fluid Dynamics Measurement Techniques in Turbomachines, Volume 1 122 p 1985
Avail: NTIS HC A18/MF A01

The application of laser anemometry to the measurement of turbomachinery flow fields is reviewed. Choices of optical configuration, seed particle generation, and seed injection techniques are discussed. The modification of experimental facilities to gain optical access is considered. The efficiency of data acquisition schemes is analyzed and issues related to data integrity and error estimation are addressed. Data reduction and analysis techniques for extracting and understanding the flow physics from laser anemometer measurements are presented. Author (ESA)

N86-27643*# Rockwell International Corp., Canoga Park, Calif. Rocketdyne Div.
SSME LONG-LIFE BEARINGS Final Report, Jan. 1982 - July 1986

M. F. BUTNER and B. T. MURPHY Jul. 1986 163 p
(Contract NAS3-23623)
(NASA-CR-179455; NAS 1.26:179455; RI/RD86-168) Avail: NTIS HC A08/MF A01 CSCL 131

Hybrid hydrostatic/ball bearings for LH2 and LO2 service in turbopumps were studied as a means of improving speed and life capabilities. Four hybrid bearing configurations were designed with emphasis on achieving maximum stiffness and damping. Parallel load bearings were tested at steady-state and transient conditions with LH2 (externally fed) and LN2 (internally fed). The hydrostatic elements were tested with Freon 113 for empirical determination of dynamic characteristics. Tests using an eccentric journal for loading showed the externally and internally fed hydrostatic bearings to have significant separated coefficients of direct stiffness and damping. For the internally fed bearing, the strongly speed-dependent cross-coupling stiffness arising from fluid swirl, along with significant cross-coupling damping, resulted in low net effective stiffness and damping. The test method used can produce separated coefficients with a sufficiently elliptic journal orbit; otherwise, only net effective coefficients combining direct and cross-coupling terms can be determined. Testing with nonsynchronous excitation is recommended to avoid this restriction. Investigation of hard materials, including ceramics, is recommended as a means of eliminating the need for the rolling bearing for

startup and shutdown support. The testing was performed in 1984 (LH2), 1985 (LN2) and 1985-86 (Freon). Author

N86-27657*# National Aeronautics and Space Administration. Lewis Research Center, Cleveland, Ohio.

ELECTRODYNAMIC TETHER TECHNOLOGY CONSIDERATIONS

J. C. KOLECKI *In* NASA, Washington Applications of Tethers in Space: Workshop Proceedings, Vol. 2 p 383-386 Jun. 1986

Avail: NTIS HC A23/MF A01 CSCL 131

The electrodynamic tether operation was studied. Plasma contactors, power management and conditioning, and exposure of materials were considered. Multikilowatt electrodynamic tether systems need a variety of supporting technologies in order to be viable. The area of interface between the high voltage end of the electrodynamic tether and the user was not addressed, however, it must be in order for the successful and safe operation of the system. E.R.

N86-27661*# National Aeronautics and Space Administration. Lewis Research Center, Cleveland, Ohio.

NEW METHODOLOGY FOR SHAFT DESIGN BASED ON LIFE EXPECTANCY

S. H. LOEWENTHAL 1986 20 p Presented at the International Original Equipment Manufacturers Design Conference, New York, N.Y., 9-11 Dec. 1986

(NASA-TM-87354; E-3109; NAS 1.15:87354) Avail: NTIS HC A02/MF A01 CSCL 131

The design of power transmission shafting for reliability has not historically received a great deal of attention. However, weight sensitive aerospace and vehicle applications and those where the penalties of shaft failure are great, require greater confidence in shaft design than earlier methods provided. This report summarizes a fatigue strength-based, design method for sizing shafts under variable amplitude loading histories for limited or unlimited service life. Moreover, applications factors such as press-fitted collars, shaft size, residual stresses from shot peening or plating, corrosive environments can be readily accommodated into the framework of the analysis. Examples are given which illustrate the use of the method, pointing out the large life penalties due to occasional cyclic overloads. Author

N86-28433*# Cincinnati Univ., Ohio. Dept. of Mechanical and Industrial Engineering.

DYNAMIC LOADING ON PARALLEL SHAFT GEARS Final Report

H. H. (EDWARD) LIN (Memphis State Univ., Tenn.) and R. L. HUSTON Jul. 1986 80 p

(Contract NSG-3188)

(NASA-CR-179473; NAS 1.26:179473; UC-MIE-051586-19)

Avail: NTIS HC A05/MF A01 CSCL 131

A computer-based analysis of the dynamic effects of spur gear systems is presented. The method of analysis with its associated computer code is capable of determining the dynamic response of spur gear systems having involute tooth profiles and standard contact ratios. Various parameters affecting the system dynamic behavior are examined. Numerical results of the analysis are compared with semi-empirical formulae, AGMA (American Gear Manufacturers Association) formulae, and experimental data. A close correlation with the experimental data is obtained. Author

N86-30160*# National Aeronautics and Space Administration. Lewis Research Center, Cleveland, Ohio.

INSTABILITY IN ROTATING MACHINERY

Dec. 1985 458 p Symposium held in Carson City, Nev., 10-14 Jun. 1985; sponsored by Bently Rotor Dynamics Research Corp.

(NASA-CP-2409; E-2652; NAS 1.55:2409) Avail: NTIS HC

A21/MF A01 CSCL 131

The proceedings contain 45 papers on a wide range of subjects including flow generated instabilities in fluid flow machines, cracked shaft detection, case histories of instability phenomena in compressors, turbines, and pumps, vibration control in turbomachinery (including antiswirl techniques), and the simulation

and estimation of destabilizing forces in rotating machines. The symposium was held to serve as an update on the understanding and control of rotating machinery instability problems.

N86-30167*# National Aeronautics and Space Administration. Lewis Research Center, Cleveland, Ohio.

TWO-PHASE FLOWS WITHIN SYSTEMS WITH AMBIENT PRESSURE

R. C. HENDRICKS, M. J. BRAUN (Akron Univ., Ohio.), R. L. WHEELER, III, and R. L. MULLEN (Case Western Reserve Univ., Cleveland, Ohio.) *In its* Instability in Rotating Machinery (date) p 83-96 Dec. 1985

Avail: NTIS HC A21/MF A01 CSCL 131

In systems where the design inlet and outlet pressures are maintained above the thermodynamic critical pressure, it is often assumed that two phase flows within the system cannot occur. Designers rely on this simple rule of thumb to circumvent problems associated with a highly compressible two phase flow occurring within the supercritical pressure system along with the uncertainties in rotordynamics, load capacity, heat transfer, fluid mechanics, and thermophysical property variations. The simple rule of thumb is adequate in many low power designs but is inadequate for high performance turbomachines and linear systems, where two phase regions can exist even though outlet pressure is greater than critical pressure. Rotordynamic-fluid-mechanic restoring forces depend on momentum differences, and those for a two phase zone can differ significantly from those for a single-phase zone. Using the Reynolds equation the angular velocity, eccentricity, geometry, and ambient conditions are varied to determine the point of two phase flow incipience. Author

N86-30206*# National Aeronautics and Space Administration. Lewis Research Center, Cleveland, Ohio.

FEASIBILITY STUDY OF A DISCRETE BEARING/ROLLER DRIVE ROTARY JOINT FOR THE SPACE STATION

S. H. LOEWENTHAL and F. T. SCHULLER Jul. 1986 43 p

(NASA-TM-88800; E-3138; NAS 1.15:88800) Avail: NTIS HC

A03/MF A01 CSCL 131

The most critical mechanism on board the proposed space station is the continuously rotating joint which must accurately align the solar power units with the sun during earth orbit. The feasibility of a multiple, discrete bearing supported joint driven by a self-loading, pinch drive actuator was investigated for this application. This concept appears to offer greater protection against catastrophic jamming, less sensitivity to adverse thermal gradients, greater accessibility to in-orbit servicing or replacement and greater adaptability to very large (5 m) truss members than to more conventional continuous support bearing/gear reducer joints. Analytical trade studies performed herein establish that a discrete cam roller bearing support system having eight hangers around a continuous ring would provide sufficient radial and bending stiffness to prevent any degradation in the fundamental frequencies of the solar wing structure. Furthermore, it appears that the pinch roller drive mechanism can be readily sized to meet or exceed system performance and service life requirements. Wear life estimates based on experimental data for a steel roller coated with an advanced polyimide film show a continuous service life more than two orders of magnitude greater than required for this application. Author

N86-31889*# National Aeronautics and Space Administration. Lewis Research Center, Cleveland, Ohio.

SURFACE FATIGUE AND FAILURE CHARACTERISTICS OF HOT FORGED POWDER METAL AISI 4620, AISI 4640, AND MACHINED AISI 4340 STEEL SPUR GEARS

D. P. TOWNSEND 1986 34 p Presented at the Annual Meeting of the American Society of Lubrication Engineers, Toronto, Ontario, 12-15 May 1986

(NASA-TM-87330; E-3024; NAS 1.15:87330) Avail: NTIS HC

A03/MF A01 CSCL 131

Spur gear surface fatigue endurance tests were conducted to investigate hot forged powder metal AISI 4620 and 4640 steel for use as a gear material, to determine endurance characteristics

37 MECHANICAL ENGINEERING

and to compare the results with machined AISI 4340 and 9310 steel gear materials. The as-forged and unground SISI 4620 gear exhibited a 10 percent fatigue life that was approximately one-fourth of that for AISI 9310 and less than one-half that for the AISI 4340 gears. The forged and finish ground AISI 4620 gears exhibited a 10 percent life, approximately 70 percent that of AISI 9310 and slightly better than that of AISI 4340. The AISI 4640 hot forged gears had less fracture toughness and slightly less fatigue life than the AISI 4620 test gears. Author

N86-32740*# National Aeronautics and Space Administration. Lewis Research Center, Cleveland, Ohio.

THERMAL STRESS MINIMIZED, TWO COMPONENT, TURBINE SHROUD SEAL Patent Application

R. F. HANDSCHUH, inventor (to NASA) 18 Jun. 1986 17 p (NASA-CASE-LEW-14212-1; US-PATENT-APPL-SN-875798; NAS 1.71:LEW-14212-1) Avail: NTIS HC A02/MF A01 CSCL 11A

In a turbine machine, a two component shroud seal which maximizes insulation and sealing around the rotating turbine blades and made by independently fabricating each of the two components then joining them together is disclosed. The two components may be joined together at room temperature. The resulting shroud seal provides greater engine efficiency and thrust. NASA

N86-32741*# Rockwell International Corp., Canoga Park, Calif. Rocketdyne Div.

SMALL CENTRIFUGAL PUMPS FOR LOW-THRUST ROCKET ENGINES Interim Report

R. B. FURST 21 Mar. 1986 114 p (Contract NAS3-23164)

(NASA-CR-174913; NAS 1.26:174913; RI/RD85-183) Avail: NTIS HC A06/MF A01 CSCL 13K

Six small, low specific speed centrifugal pump configurations were designed, fabricated, and tested. The configurations included shrouded, and 25 and 100% admission open face impellers with 2 inch tip diameters; 25, 50, and 100% emission vaned diffusers; and volutes with conical exits. Impeller tip widths varied from 0.030 inch to 0.052 inch. Design specific speeds ($N_{sub s} = \text{RPM} \cdot \text{GPM}^{0.5} \cdot \text{FT}^{0.75}$) were 430 (four configurations) and 215 (two configurations). The six configurations were tested with water as the pumped fluid. Noncavitating performance results are presented for the design speed of 24,500 rpm over a flowrate range from 1 to 6 gpm for the $N_{sub s} = 430$ configurations and test speeds up to 29,000 rpm over a flowrate range from 0.3 to 1.2 gpm for the $N_{sub s} = 215$ configurations. Cavitating performance results are presented over a flowrate range from 60 to 120% of design flow. Fabrication of the small pump components is also discussed. Author

N86-32742*# Texas A&M Univ., College Station.

A COMPARISON OF EXPERIMENTAL AND THEORETICAL RESULTS FOR LEAKAGE, PRESSURE GRADIENTS, AND ROTORDYNAMIC COEFFICIENTS FOR TAPERED ANNULAR GAS SEAL Progress Report

D. A. ELROD and D. W. CHILDS Sep. 1986 128 p (Contract NAG3-181)

(NASA-CR-179709; NAS 1.26:179709; TRC-SEAL-4-86) Avail: NTIS HC A07/MF A01 CSCL 11A

A brief review of current annular seal theory and a discussion of the predicted effect on stiffness of tapering the seal stator are presented. An outline of Nelson's analytical-computational method for determining rotordynamic coefficients for annular compressible-flow seals is included. Modifications to increase the maximum rotor speed of an existing air-seal test apparatus at Texas A&M University are described. Experimental results, including leakage, entrance-loss coefficients, pressure distributions, and normalized rotordynamic coefficients, are presented for four convergent-tapered, smooth-rotor, smooth-stator seals. A comparison of the test results shows that an inlet-to-exit clearance ratio of 1.5 to 2.0 provides the maximum direct stiffness, a clearance ratio of 2.5 provides the greatest stability, and a clearance ratio of 1.0 provides the least stability. The experimental results are compared to theoretical results from Nelson's analysis with good

agreement. Test results for cross-coupled stiffness show less sensitivity of fluid prerotation than predicted. Author

N86-32743*# General Electric Co., Cincinnati, Ohio. Aircraft Engine Business Group.

IMPROVED FRACTURE TOUGHNESS CORROSION-RESISTANT BEARING MATERIAL Final Report, 1981-1984

E. N. BAMBERGER and A. H. NAHM Jan. 1986 81 p (Contract NAS3-22508)

(NASA-CR-174990; NAS 1.26:174990; R86AEB104) Avail: NTIS HC A05/MF A01 CSCL 13I

A development program was performed to establish whether a corrosion-resistant bearing material, such as a 14Cr steel, could be modified to allow carburization, thereby providing the excellent fracture toughness characteristics feasible with this process. The alloy selected for investigation was AMS 5749. Several modifications were made including the addition of a small amount of nickel for austenite stabilization. While some promising results were achieved, the primary objective of an acceptable combination of case hardness and microstructure was not attained. Because the high chromium content presents a serious problem in achieving a viable carburizing cycle, a number of experimental steels having lower chromium contents (8 to 12%) were produced in laboratory quantities and evaluated. The results were basically the same as those initially obtained with the modified AMS 5749. Corrosion tests were performed on AMS 5749, AISI M50, and 52100 bearing steels as well as some of the lower chromium steels. These tests showed that a reduced chromium level (10 to 12%) provided essentially the same corrosion protection as the 14Cr steels. Author

38

QUALITY ASSURANCE AND RELIABILITY

Includes product sampling procedures and techniques; and quality control.

A86-13192*# National Aeronautics and Space Administration. Lewis Research Center, Cleveland, Ohio.

MEASUREMENT OF ULTRASONIC VELOCITY USING PHASE-SLOPE AND CROSS-CORRELATION METHODS

D. R. HULL, H. E. KAUTZ, and A. VARY (NASA, Lewis Research Center, Cleveland, OH) Materials Evaluation (ISSN 0025-5327), vol. 43, Oct. 1985, p. 1455-1460. Previously announced in STAR as N84-34769. refs

Computer implemented phase-slope and cross-correlation methods are introduced for measuring time delays between pairs of broadband ultrasonic pulse-echo signals for determining velocity in engineering materials. The phase-slope and cross-correlation methods are compared with the overlap method which is currently in wide use. Comparison of digital versions of the three methods shows similar results for most materials having low ultrasonic attenuation. However, the cross-correlation method is preferred for highly attenuating materials. An analytical basis for the cross-correlation method is presented. Examples are given for the three methods investigated to measure velocity in representative materials in the megahertz range. Author

A86-31745* National Aeronautics and Space Administration. Lewis Research Center, Cleveland, Ohio.

RADIOGRAPHIC DETECTABILITY LIMITS FOR SEEDED VOIDS IN SINTERED SILICON CARBIDE AND SILICON NITRIDE

G. Y. BAAKLINI, J. D. KISER, and D. J. ROTH (NASA, Lewis Research Center, Cleveland, OH) Advanced Ceramic Materials (ISSN 0883-5551), vol. 1, Jan. 1986, p. 43-49. Previously announced in STAR as N85-21674. refs

Conventional and microfocus X-radiographic techniques were compared to determine relative detectability limits for voids in green and sintered SiC and Si₃N₄. The relative sensitivity of the

techniques was evaluated by comparing their ability to detect voids that were artificially introduced by a seeding process. For projection microfocus radiography the sensitivity of void detection at a 90/95 probability of detection/confidence level is 1.5 percent of specimen thickness in sintered SiC and Si₃N₄. For conventional contact radiography the sensitivity is 2.5 percent of specimen thickness. It appears that microfocus projection radiography is preferable to conventional contact radiography in cases where increased sensitivity is required and where the additional complexity of the technique can be tolerated. E.A.K.

A86-35575* National Aeronautics and Space Administration. Lewis Research Center, Cleveland, Ohio.

NDE OF ADVANCED CERAMICS

S. J. KLIMA (NASA, Lewis Research Center, Cleveland, OH) Materials Evaluation (ISSN 0025-5327), vol. 44, April 1986, p. 571-576. refs

Radiographic, ultrasonic, and scanning laser acoustic microscopy (SLAM) techniques were used to characterize silicon nitride and silicon carbide modulus-of-rupture test specimens in various stages of fabrication. Conventional and microfocus X-ray techniques were found capable of detecting minute high-density inclusions in as-received powders, green compacts, and fully densified specimens. Significant density gradients in sintered bars were observed by radiography, ultrasonic velocity, and SLAM. Ultrasonic attenuation was found sensitive to microstructural variations due to grain and void morphology and distribution. SLAM was capable also of detecting voids, inclusions, and cracks in finished test bars. Consideration is given to the potential for applying thermoacoustic microscopy techniques to green and densified ceramics. Some limitations and the detection probability statistics of the aforementioned nondestructive evaluation (NDE) processes are also discussed. Author

A86-39027* National Aeronautics and Space Administration. Lewis Research Center, Cleveland, Ohio.

RELIABILITY OF VOID DETECTION IN STRUCTURAL CERAMICS BY USE OF SCANNING LASER ACOUSTIC MICROSCOPY

D. J. ROTH, S. J. KLIMA, J. D. KISER (NASA, Lewis Research Center, Cleveland, OH), and G. Y. BAAKLINI (Cleveland State University, OH) Materials Evaluation (ISSN 0025-5327), vol. 44, May 1986, p. 762-769, 761. Previously announced in STAR as N85-32337. refs

The reliability of scanning laser acoustic microscopy (SLAM) for detecting surface voids in structural ceramic test specimens was statistically evaluated. Specimens of sintered silicon nitride and sintered silicon carbide, seeded with surface voids, were examined by SLAM at an ultrasonic frequency of 100 MHz in the as fired condition and after surface polishing. It was observed that polishing substantially increased void detectability. Voids as small as 100 micrometers in diameter were detected in polished specimens with 0.90 probability at a 0.95 confidence level. In addition, inspection times were reduced up to a factor of 10 after polishing. The applicability of the SLAM technique for detection of naturally occurring flaws of similar dimensions to the seeded voids is discussed. A FORTRAN program listing is given for calculating and plotting flaw detection statistics. Author

A86-45150* National Aeronautics and Space Administration. Lewis Research Center, Cleveland, Ohio.

QUANTITATIVE FLAW CHARACTERIZATION WITH SCANNING LASER ACOUSTIC MICROSCOPY

E. R. GENERAZIO and D. J. ROTH (NASA, Lewis Research Center, Cleveland, OH) Materials Evaluation (ISSN 0025-5327), vol. 44, June 1986, p. 863-870. Previously announced in STAR as N86-22983. refs

Surface roughness and diffraction are two factors that have been observed to affect the accuracy of flaw characterization with scanning laser acoustic microscopy. Inaccuracies can arise when the surface of the test sample is acoustically rough. It is shown that, in this case, Snell's law is no longer valid for determining the direction of sound propagation within the sample. The

relationship between the direction of sound propagation within the sample, the apparent flaw depth, and the sample's surface roughness is investigated. Diffraction effects can mask the acoustic images of minute flaws and make it difficult to establish their size, depth, and other characteristics. It is shown that for Fraunhofer diffraction conditions the acoustic image of a subsurface defect corresponds to a two-dimensional Fourier transform. Transforms based on simulated flaws are used to infer the size and shape of the actual flaw. Author

A86-48143* National Aeronautics and Space Administration. Lewis Research Center, Cleveland, Ohio.

NONDESTRUCTIVE TECHNIQUES FOR CHARACTERIZING MECHANICAL PROPERTIES OF STRUCTURAL MATERIALS - AN OVERVIEW

A. VARY and S. J. KLIMA (NASA, Lewis Research Center, Cleveland, OH) ASME, International Gas Turbine Conference and Exhibit, 31st, Duesseldorf, West Germany, June 8-12, 1986. 10 p. Previously announced in STAR as N86-19636. refs (ASME PAPER 86-GT-75)

An overview of nondestructive evaluation (NDE) is presented to indicate the availability and application potentials of techniques for quantitative characterization of the mechanical properties of structural materials. The purpose is to review NDE techniques that go beyond the usual emphasis on flow detection and characterization. Discussed are current and emerging NDE techniques that can verify and monitor intrinsic properties (e.g., tensile, shear, and yield strengths; fracture toughness, hardness, ductility; elastic moduli) and underlying microstructural and morphological factors. Most of the techniques described are, at present, neither widely applied nor widely accepted in commerce and industry because they are still emerging from the laboratory. The limitations of the techniques may be overcome by advances in applications research and instrumentation technology and perhaps by accommodations for their use in the design of structural parts. Author

A86-48298* National Aeronautics and Space Administration. Lewis Research Center, Cleveland, Ohio.

NDE OF STRUCTURAL CERAMICS

S. J. KLIMA and A. VARY (NASA, Lewis Research Center, Cleveland, OH) ASME, International Gas Turbine Conference and Exhibit, 31st, Duesseldorf, West Germany, June 8-12, 1986. 8 p. Previously announced in STAR as N86-16598. refs (ASME PAPER 86-GT-279)

Radiographic, ultrasonic, scanning laser acoustic microscopy (SLAM), and thermo-acoustic microscopy techniques were used to characterize silicon nitride and silicon carbide modulus-of-rupture test specimens in various stages of fabrication. Conventional and microfocus X-ray techniques were found capable of detecting minute high density inclusions in as-received powders, green compacts, and fully densified specimens. Significant density gradients in sintered bars were observed by radiography, ultrasonic velocity, and SLAM. Ultrasonic attenuation was found sensitive to microstructural variations due to grain and void morphology and distribution. SLAM was also capable of detecting voids, inclusions and cracks in finished test bars. Consideration is given to the potential for applying thermo-acoustic microscopy techniques to green and densified ceramics. The detection probability statistics and some limitations of radiography and SLAM also are discussed. Author

N86-10561* National Aeronautics and Space Administration. Lewis Research Center, Cleveland, Ohio.

ULTRASONIC EVALUATION OF MECHANICAL PROPERTIES OF THICK, MULTILAYERED, FILAMENT WOUND COMPOSITES

H. E. KAUTZ Sep. 1985 36 p refs (NASA-TM-87088; E-2676; NAS 1.15:87088) Avail: NTIS HC A03/MF A01 CSCL 14D

A preliminary investigation is conducted to define capabilities and limitations of ultrasonic and acousto-ultrasonic measurements related to mechanical properties of filament wound graphite/epoxy composite structures. The structures studied are segments of

38 QUALITY ASSURANCE AND RELIABILITY

filament wound cylinders formed of multiple layers of hoop and helical windings. The segments consist of 24 to 35 layers and range from 3.02 to 3.34 cm in wall thickness. The resultant structures are anisotropic, heterogeneous, porous, and highly attenuating to ultrasonic frequencies greater than 1 MHz. The segments represent structures to be used for space shuttle booster cases. Ultrasonic velocity and acousto-ultrasonic stress wave factor measurement approaches are discussed. Correlations among velocity, density, and porosity, and between the acousto-ultrasonic stress wave factor and interlaminar shear strength are presented.

Author

N86-13749*# National Aeronautics and Space Administration. Lewis Research Center, Cleveland, Ohio.

PROBABILITY OF DETECTION OF INTERNAL VOIDS IN STRUCTURAL CERAMICS USING MICROFOCUS RADIOGRAPHY

G. Y. BAAKLINI and D. J. ROTH Nov. 1985 23 p refs (NASA-TM-87164; E-2800; NAS 1.15:87164) Avail: NTIS HC A02/MF A01 CSCL 14D

The reliability of microfocus x-radiography for detecting subsurface voids in structural ceramic test specimens was statistically evaluated. The microfocus system was operated in the projection mode using low X-ray photon energies (20 keV) and a 10 micro m focal spot. The statistics were developed for implanted subsurface voids in green and sintered silicon carbide and silicon nitride test specimens. These statistics were compared with previously-obtained statistics for implanted surface voids in similar specimens. Problems associated with void implantation are discussed. Statistical results are given as probability-of-detection curves at a 95 percent confidence level for voids ranging in size from 20 to 528 micro m in diameter.

Author

N86-16598*# National Aeronautics and Space Administration. Lewis Research Center, Cleveland, Ohio.

NDE OF STRUCTURAL CERAMICS

S. J. KLIMA and A. VARY 1986 14 p refs Proposed for presentation at the 31st International Gas Turbine Conference, Dusseldorf, West Germany, 8-12 Jun. 1986; sponsored by ASME (NASA-TM-87186; E-2840; NAS 1.15:87186) Avail: NTIS HC A02/MF A01 CSCL 14D

Radiographic, ultrasonic, scanning laser acoustic microscopy (SLAM), and thermo-acoustic microscopy techniques were used to characterize silicon nitride and silicon carbide modulus-of-rupture test specimens in various stages of fabrication. Conventional and microfocus X-ray techniques were found capable of detecting minute high density inclusions in as-received powders, green compacts, and fully densified specimens. Significant density gradients in sintered bars were observed by radiography, ultrasonic velocity, and SLAM. Ultrasonic attenuation was found sensitive to microstructural variations due to grain and void morphology and distribution. SLAM was also capable of detecting voids, inclusions and cracks in finished test bars. Consideration is given to the potential for applying thermo-acoustic microscopy techniques to green and densified ceramics. The detection probability statistics and some limitations of radiography and SLAM also are discussed.

Author

N86-16599*# National Aeronautics and Space Administration. Lewis Research Center, Cleveland, Ohio.

RELIABILITY OF SCANNING LASER ACOUSTIC MICROSCOPY FOR DETECTING INTERNAL VOIDS IN STRUCTURAL CERAMICS

D. J. ROTH and G. Y. BAAKLINI 1986 36 p refs Presented at the 10th Annual Conference on Composites and Advanced Ceramic Materials, Cocoa Beach, Fla., 19-22 Jan. 1986; sponsored by the American Ceramic Society (NASA-TM-87222; E-2864; NAS 1.15:87222) Avail: NTIS HC A03/MF A01 CSCL 14D

The reliability of 100 MHz scanning laser acoustic microscopy (SLAM) for detecting internal voids in sintered specimens of silicon nitride and silicon carbide was evaluated. The specimens contained artificially implanted voids and were positioned at depths ranging

up to 2 mm below the specimen surface. Detection probability of 0.90 at a 0.95 confidence level was determined as a function of material, void diameter, and void depth. The statistical results presented for void detectability indicate some of the strengths and limitations of SLAM as a nondestructive evaluation technique for structural ceramics.

Author

N86-19636*# National Aeronautics and Space Administration. Lewis Research Center, Cleveland, Ohio.

NONDESTRUCTIVE TECHNIQUES FOR CHARACTERIZING MECHANICAL PROPERTIES OF STRUCTURAL MATERIALS: AN OVERVIEW

A. VARY and S. J. KLIMA Dec. 1985 21 p refs Proposed for presentation at the 31st International Gas Turbine Conference, Dusseldorf, West Germany, 8-12 Jun. 1986; sponsored by ASME (NASA-TM-87203; E-2858; NAS 1.15:87203) Avail: NTIS HC A02/MF A01 CSCL 14D

An overview of nondestructive evaluation (NDE) is presented to indicate the availability and application potentials of techniques for quantitative characterization of the mechanical properties of structural materials. The purpose is to review NDE techniques that go beyond the usual emphasis on flaw detection and characterization. Discussed are current and emerging NDE techniques that can verify and monitor intrinsic properties (e.g., tensile, shear, and yield strengths; fracture toughness, hardness, ductility; elastic moduli) and underlying microstructural and morphological factors. Most of the techniques described are, at present, neither widely applied nor widely accepted in commerce and industry because they are still emerging from the laboratory. The limitations of the techniques may be overcome by advances in applications research and instrumentation technology and perhaps by accommodations for their use in the design of structural parts.

Author

N86-22962*# National Aeronautics and Space Administration. Lewis Research Center, Cleveland, Ohio.

ANALYTICAL ULTRASONICS IN MATERIALS RESEARCH AND TESTING

A. VARY Jan. 1986 357 p refs Conference held in Cleveland, Ohio, 13-14 Nov. 1984 (NASA-CP-2383; E-2486; NAS 1.55:2383) Avail: NTIS HC A16/MF A01 CSCL 20A

Research results in analytical ultrasonics for characterizing structural materials from metals and ceramics to composites are presented. General topics covered by the conference included: status and advances in analytical ultrasonics for characterizing material microstructures and mechanical properties; status and prospects for ultrasonic measurements of microdamage, degradation, and underlying morphological factors; status and problems in precision measurements of frequency-dependent velocity and attenuation for materials analysis; procedures and requirements for automated, digital signal acquisition, processing, analysis, and interpretation; incentives for analytical ultrasonics in materials research and materials processing, testing, and inspection; and examples of progress in ultrasonics for interrelating microstructure, mechanical properties, and dynamic response.

N86-25002*# Massachusetts Inst. of Tech., Cambridge. Dept. of Mechanical Engineering.

STRESS WAVES IN TRANSVERSELY ISOTROPIC MEDIA: THE HOMOGENEOUS PROBLEM Final Report

E. R. C. MARQUES and J. H. WILLIAMS, JR. Washington NASA May 1986 48 p refs (Contract NAG3-328) (NASA-CR-3977; E-2949; NAS 1.26:3977) Avail: NTIS HC A03/MF A01 CSCL 14D

The homogeneous problem of stress wave propagation in unbounded transversely isotropic media is analyzed. By adopting plane wave solutions, the conditions for the existence of the solution are established in terms of phase velocities and directions of particle displacements. Dispersion relations and group velocities are derived from the phase velocity expressions. The deviation angles (e.g., angles between the normals to the adopted plane

waves and the actual directions of their propagation) are numerically determined for a specific fiber-glass epoxy composite. A graphical method is introduced for the construction of the wave surfaces using magnitudes of phase velocities and deviation angles. The results for the case of isotropic media are shown to be contained in the solutions for the transversely isotropic media. Author

N86-25003*# Pratt and Whitney Aircraft, East Hartford, Conn. Engineering Div.

LIFE PREDICTION AND CONSTITUTIVE MODELS FOR ENGINE HOT SECTION ANISOTROPIC MATERIALS PROGRAM Annual Status Report

G. A. SWANSON, I. LINASK, D. M. NISSLEY, P. P. NORRIS, T. G. MEYER, and K. P. WALKER Feb. 1986 203 p refs (Contract NAS3-23939) (NASA-CR-174952; NAS 1.26:174952; PWA-5968-19) Avail: NTIS HC A09/MF A01 CSCL 14D

This report presents the results of the first year of a program designed to develop life prediction and constitutive models for two coated single crystal alloys used in gas turbine airfoils. The two alloys are PWA 1480 and Alloy 185. The two oxidation resistant coatings are PWA 273, an aluminide coating, and PWA 286, an overlay NiCoCrAlY coating. To obtain constitutive and/or fatigue data, tests were conducted on coated and uncoated PWA 1480 specimens tensile loaded in the 100, 110, 111, and 123 directions. A literature survey of constitutive models was completed for both single crystal alloys and metallic coating materials; candidate models were selected. One constitutive model under consideration for single crystal alloys applies Walker's micromechanical viscoplastic formulation to all slip systems participating in the single crystal deformation. The constitutive models for the overlay coating correlate the viscoplastic data well. For the aluminide coating, a unique test method is under development. LCF and TMF tests are underway. The two coatings caused a significant drop in fatigue life, and each produced a much different failure mechanism. Author

N86-25812*# National Aeronautics and Space Administration. Lewis Research Center, Cleveland, Ohio.

CONCEPTS FOR INTERRELATING ULTRASONIC ATTENUATION, MICROSTRUCTURE AND FRACTURE TOUGHNESS IN POLYCRYSTALLINE SOLIDS

A. VARY May 1986 30 p refs Presented at the Symposium on Solid Mechanics Research of Quantitative NDE, Evanston, Ill., 18-20 Sep. 1985 (NASA-TM-87339; E-3086; NAS 1.15:87339) Avail: NTIS HC A03/MF A01 CSCL 14D

Conceptual models are advanced for explaining and predicting empirical correlations found between ultrasonic measurements and fracture toughness of polycrystalline solids. The models lead to insights concerning microstructural factors governing fracture processes and associated stress wave interactions. Analysis of the empirical correlations suggested by the models indicate that, in addition to grain size and shape, grain boundary reflections, elastic anisotropy, and dislocation damping are factors that underly both fracture toughness and ultrasonic attenuation. One outcome is that ultrasonic attenuation can predict the size of crack blunting or process zones that develop in the vicinity active cracks in metals. This forms a basis for ultrasonic ranking according to variations in fracture toughness. Author

N86-27665*# Virginia Polytechnic Inst. and State Univ., Blacksburg. Dept. of Engineering Science and Mechanics.

ULTRASONIC STRESS WAVE CHARACTERIZATION OF COMPOSITE MATERIALS Final Report

J. C. DUKE, JR., E. G. HENNEKE, II, and W. W. STINCHCOMB Washington NASA May 1986 161 p (Contract NAG3-323) (NASA-CR-3976; E-2948; NAS 1.26:3976) Avail: NTIS HC A08/MF A01 CSCL 14D

The work reported covers three simultaneous projects. The first project was concerned with: (1) establishing the sensitivity of the acousto-ultrasonic method for evaluating subtle forms of

damage development in cyclically loaded composite materials, (2) establishing the ability of the acousto-ultrasonic method for detecting initial material imperfections that lead to localized damage growth and final specimen failure, and (3) characteristics of the NBS/Proctor sensor/receiver for acousto-ultrasonic evaluation of laminated composite materials. The second project was concerned with examining the nature of the wave propagation that occurs during acoustic-ultrasonic evaluation of composite laminates and demonstrating the role of Lamb or plate wave modes and their utilization for characterizing composite laminates. The third project was concerned with the replacement of contact-type receiving piezotransducers with noncontacting laser-optical sensors for acousto-ultrasonic signal acquisition. Author

N86-27666*# Massachusetts Inst. of Tech., Cambridge. Dept. of Mechanical Engineering.

WAVE PROPAGATION IN ANISOTROPIC MEDIUM DUE TO AN OSCILLATORY POINT SOURCE WITH APPLICATION TO UNIDIRECTIONAL COMPOSITES Final Report

J. H. WILLIAMS, JR., E. R. C. MARQUES, and S. S. LEE Washington NASA Jul. 1986 59 p (Contract NAG3-328)

(NASA-CR-4001; E-3093; NAS 1.26:4001) Avail: NTIS HC A04/MF A01 CSCL 14D

The far-field displacements in an infinite transversely isotropic elastic medium subjected to an oscillatory concentrated force are derived. The concepts of velocity surface, slowness surface and wave surface are used to describe the geometry of the wave propagation process. It is shown that the decay of the wave amplitudes depends not only on the distance from the source (as in isotropic media) but also depends on the direction of the point of interest from the source. As an example, the displacement field is computed for a laboratory fabricated unidirectional fiberglass epoxy composite. The solution for the displacements is expressed as an amplitude distribution and is presented in polar diagrams. This analysis has potential usefulness in the acoustic emission (AE) and ultrasonic nondestructive evaluation of composite materials. For example, the transient localized disturbances which are generally associated with AE sources can be modeled via this analysis. In which case, knowledge of the displacement field which arrives at a receiving transducer allows inferences regarding the strength and orientation of the source, and consequently perhaps the degree of damage within the composite. Author

N86-28250*# Aerojet Technical Systems Co., Sacramento, Calif.

LONGITUDINAL MODE COMBUSTION INSTABILITIES OF A HIGH-PRESSURE FUEL-RICH LOX/RP-1 PREBURNER

J. J. FANG In Johns Hopkins Univ. The 22nd JANNAF Combustion Meeting, Vol. 1 p 429-441 Oct. 1985 (Contract NAS3-22647)

Avail: CPIA, Laurel, Md. 20707 HC \$70.00 CSCL 21B

During the hot-fire testing of a high-pressure fuel-rich LOX/RP-1 preburner, longitudinal mode combustion instabilities were observed. The experimental data showing how the instability varied with the chamber pressure, mixture ratio, chamber length and turbulence ring are given. Technical rationales are given for the test-to-test hardware configuration changes that eventually led to the stable result. Author

N86-28445*# Virginia Polytechnic Inst. and State Univ., Blacksburg. Dept. of Engineering Science and Mechanics.

A STUDY OF THE STRESS WAVE FACTOR TECHNIQUE FOR NONDESTRUCTIVE EVALUATION OF COMPOSITE MATERIALS Final Report

A. SARRAFZADEH-KHOEE, M. T. KIERNAN, J. C. DUKE, JR., and E. G. HENNEKE, II Washington NASA Jul. 1986 33 p (Contract NAG3-172)

(NASA-CR-4002; E-3081; NAS 1.26:4002) Avail: NTIS HC A03/MF A01 CSCL 14D

The acousto-ultrasonic method of nondestructive evaluation is an extremely sensitive means of assessing material response. Efforts continue to complete the understanding of this method. In

38 QUALITY ASSURANCE AND RELIABILITY

order to achieve the full sensitivity of the technique, extreme care must be taken in its performance. This report provides an update of the efforts to advance the understanding of this method and to increase its application to the nondestructive evaluation of composite materials. Included are descriptions of a novel optical system that is capable of measuring in-plane and out-of-plane displacements, an IBM PC-based data acquisition system, an extensive data analysis software package, the azimuthal variation of acousto-ultrasonic behavior in graphite/epoxy laminates, and preliminary examination of processing variation in graphite-aluminum tubes. Author

N86-31065*# National Aeronautics and Space Administration. Lewis Research Center, Cleveland, Ohio.

DETERMINATION OF GRAIN SIZE DISTRIBUTION FUNCTION USING TWO-DIMENSIONAL FOURIER TRANSFORMS OF TONE PULSE ENCODED IMAGES

E. R. GENERAZIO Jun. 1986 24 p
(NASA-TM-88790; E-3125; NAS 1.15:88790) Avail: NTIS HC A02/MF A01 CSCL 11F

Microstructural images may be tone pulse encoded and subsequently Fourier transformed to determine the two-dimensional density of frequency components. A theory is developed relating the density of frequency components to the density of length components. The density of length components corresponds directly to the actual grain size distribution function from which the mean grain shape, size, and orientation can be obtained. Author

N86-31912*# National Aeronautics and Space Administration. Lewis Research Center, Cleveland, Ohio.

FACTORS THAT AFFECT RELIABILITY OF NONDESTRUCTIVE DETECTION OF FLAWS IN STRUCTURAL CERAMICS

S. J. KLIMA, G. Y. BAAKLINI (Cleveland State Univ., Ohio), and D. J. ROTH 1986 11 p Presented at the 2nd International Symposium on Ceramic Materials and Components for Engines, Luebeck-Travemuende, West Germany, 14-17 Apr. 1986; sponsored by the German Ceramic Society and the American Ceramic Society
(NASA-TM-87348; E-3096; NAS 1.15:87348) Avail: NTIS HC A02/MF A01 CSCL 14D

The factors that affect reliability of nondestructive detection of flaws in structural ceramics by microfocus radiography and scanning laser acoustic microscopy (SLAM) were investigated. Reliability of void detection in silicon nitride and silicon carbide by microfocus X-rays was affected by photon energy level, material chemistry in the immediate vicinity of the void, and the presence of loose powder aggregates inside the void cavity. The sensitivity of SLAM to voids was affected by material microstructure, the level of porosity, and the condition of the specimen surfaces. Statistical results are presented in the form of probability of detection as a function of void diameter for green compacts and sintered materials. Author

N86-31913*# National Aeronautics and Space Administration. Lewis Research Center, Cleveland, Ohio.

QUANTITATIVE VOID CHARACTERIZATION IN STRUCTURAL CERAMICS USING SCANNING LASER ACOUSTIC MICROSCOPY

D. J. ROTH, E. R. GENERAZIO, and G. Y. BAAKLINI (Cleveland State Univ., Ohio) 1986 23 p Proposed for presentation at the Basic Science, Electronics and Glass Divisions Joint Meeting, New Orleans, La., 2-5 Nov. 1986; sponsored by American Ceramic Society
(NASA-TM-88797; E-3166; NAS 1.15:88797) Avail: NTIS HC A02/MF A01 CSCL 14D

The ability of scanning laser acoustic microscopy (SLAM) to characterize artificially seeded voids in sintered silicon nitride structural ceramic specimens was investigated. Using trigonometric relationships and Airy's diffraction theory, predictions of internal void depth and size were obtained from acoustic diffraction patterns produced by the voids. Agreement was observed between actual and predicted void depths. However, predicted void diameters were

generally much greater than actual diameters. Precise diameter predictions are difficult to obtain due to measurement uncertainty and the limitations of 100 MHz SLAM applied to typical ceramic specimens. Author

N86-32764*# National Aeronautics and Space Administration. Lewis Research Center, Cleveland, Ohio.

ACOUSTO-ULTRASONIC VERIFICATION OF THE STRENGTH OF FILAMENT WOUND COMPOSITE MATERIAL

H. E. KAUTZ 1986 24 p Presented at the Pressure Vessel Conference, Chicago, Ill., 21-24 Jul. 1986; sponsored by the American Society of Mechanical Engineers
(NASA-TM-88827; E-3201; NAS 1.15:88827) Avail: NTIS HC A02/MF A01 CSCL 14D

The concept of acousto-ultrasonic (AU) waveform partitioning was applied to nondestructive evaluation of mechanical properties in filament wound composites (FWC). A series of FWC test specimens were subjected to AU analysis and the results were compared with destructively measured interlaminar shear strengths (ISS). AU stress-wave factor (SWF) measurements gave greater than 90 percent correlation coefficient upon regression against the ISS. This high correlation was achieved by employing the appropriate time and frequency domain partitioning as dictated by wave propagation path analysis. There is indication that different SWF frequency partitions are sensitive to ISS at different depths below the surface. Author

39

STRUCTURAL MECHANICS

Includes structural element design and weight analysis; fatigue; and thermal stress.

A86-18123* Massachusetts Inst. of Tech., Cambridge.

FINITE ELEMENTS BASED ON CONSISTENTLY ASSUMED STRESSES AND DISPLACEMENTS

T. H. H. PIAN (MIT, Cambridge, MA) Finite Elements in Analysis and Design (ISSN 0168-874X), vol. 1, Aug. 1985, p. 131-140. refs
(Contract NAG3-33; F33615-83-K-5016)

Finite element stiffness matrices are derived using an extended Hellinger-Reissner principle in which internal displacements are added to serve as Lagrange multipliers to introduce the equilibrium constraint in each element. In a consistent formulation the assumed stresses are initially unconstrained and complete polynomials and the total displacements are also complete such that the corresponding strains are complete in the same order as the stresses. Several examples indicate that resulting properties for elements constructed by this consistent formulation are ideal and are less sensitive to distortions of element geometries. The method has been used to find the optimal stress terms for plane elements, 3-D solids, axisymmetric solids, and plate bending elements. Author

A86-20706* Army Armament Research and Development Command, Watervliet, N. Y.

WIDE-RANGE DISPLACEMENT EXPRESSIONS FOR STANDARD FRACTURE MECHANICS SPECIMENS

J. A. KAPP (U.S. Army, Benet Weapons Laboratory, Watervliet, NY), B. GROSS (NASA, Lewis Research Center, Cleveland, OH), and G. S. LEGER IN: Fracture mechanics. Philadelphia, PA, American Society for Testing and Materials, 1985, p. 27-44.

Wide-range algebraic expressions for the displacement of cracked fracture mechanics specimens are developed. For each specimen two equations are given: one for the displacement as a function of crack length, the other for crack length as a function of displacement. All the specimens that appear in ASTM Test for Plane-Strain Fracture Toughness of Metallic Materials (E 399) are represented in addition to the crack mouth displacement for a

pure bending specimen. For the compact tension sample and the disk-shaped compact tension sample, the displacement at the crack mouth and at the load line are both considered. Only the crack mouth displacements for the arc-shaped tension samples are presented. The agreement between the displacements or crack lengths predicted by the various equations and the corresponding numerical data from which they were developed are nominally about 3 percent or better. These expressions should be useful in all types of fracture testing including fracture toughness, K-resistance, and fatigue crack growth. Author

A86-20709* National Aeronautics and Space Administration. Lewis Research Center, Cleveland, Ohio.

WIDE-RANGE WEIGHT FUNCTIONS FOR THE STRIP WITH A SINGLE EDGE CRACK

T. W. ORANGE (NASA, Lewis Research Center, Cleveland, OH) IN: Fracture mechanics. Philadelphia, PA, American Society for Testing and Materials, 1985, p. 95-105. Previously announced in STAR as N84-11512. refs

A closed form expression for the weight function for a strip with a single edge crack is presented. The expression is valid for relative crack lengths from zero to unity. It is based on the assumption that the shape of an opened edge crack can be approximated by a conic section. The results agree well with published values for weight functions, stress intensity factors, and crack mouth opening displacements. S.L.

A86-20710* National Aeronautics and Space Administration. Lewis Research Center, Cleveland, Ohio.

ANALYSIS OF AN EXTERNALLY RADIIALLY CRACK RING SEGMENT SUBJECT TO THREE-POINT RADIAL LOADING

B. GROSS, J. E. SRAWLEY, and J. L. SHANNON, JR. (NASA, Lewis Research Center, Cleveland, OH) IN: Fracture mechanics. Philadelphia, PA, American Society for Testing and Materials, 1985, p. 106-112. refs

The boundary collocation method was used to generate Mode I stress intensity and crack mouth opening displacement coefficients for externally radially (through-the-thickness) cracked ring segments subjected to three-point radial loading. Numerical results were obtained for ring segment outer-to-inner radius ratios (R_o/R_i) ranging from 1.10 to 2.50 and crack length to segment width ratios (a/W) ranging from 0.1 to 0.8. Stress intensity and crack mouth displacement coefficients were found to depend on the ratios R_o/R_i and a/W as well as the included angle between the directions of the reaction forces. Author

A86-22084*# National Aeronautics and Space Administration. Lewis Research Center, Cleveland, Ohio.

NASA LEWIS RESEARCH CENTER/UNIVERSITY GRADUATE RESEARCH PROGRAM ON ENGINE STRUCTURES

C. C. CHAMIS (NASA, Lewis Research Center, Cleveland, OH) ASME, International Gas Turbine Conference and Exhibit, 30th, Houston, TX, Mar. 18-21, 1985. 10 p. Previously announced in STAR as N85-18375.

(ASME PAPER 85-GT-159)

NASA Lewis Research Center established a graduate research program in support of the Engine Structures Research activities. This graduate research program focuses mainly on structural and dynamics analyses, computational mechanics, mechanics of composites and structural optimization. The broad objectives of the program, the specific program, the participating universities and the program status are briefly described. Author

A86-24219* Syracuse Univ., N. Y.

SHEAR FATIGUE CRACK GROWTH - A LITERATURE SURVEY

H. W. LIU (Syracuse University, NY) Fatigue and Fracture of Engineering Materials and Structures (ISSN 8756-758X), vol. 8, no. 4, 1985, p. 295-313. refs

(Contract NAG3-348)

Recent studies of shear crack growth are reviewed, emphasizing test methods and data analyses. The combined mode I and mode II elastic crack tip stress fields are considered. The development and design of the compact shear specimen are described, and

the results of fatigue crack growth tests using compact shear specimens are reviewed. The fatigue crack growth tests are discussed and the results of inclined cracks in tensile panels, center cracks in plates under biaxial loading, cracked beam specimens with combined bending and shear loading, center-cracked panels and double edge-cracked plates under cyclic shear loading are examined and analyzed in detail. C.D.

A86-26689* Akron Univ., Ohio.

HIERARCHIAL IMPLICIT DYNAMIC LEAST-SQUARE SOLUTION ALGORITHM

J. PADOVAN and J. LACKNEY (Akron, University, OH) Computers and Structures (ISSN 0045-7949), vol. 22, no. 3, 1986, p. 479-489. refs

(Contract NAG3-54)

This paper develops an implicit type transient solution strategy which possesses hierarchical levels of application. In particular, due to the manner of formulation, stiffness updating, assembly inversion, solution constraint, as well as iteration are all performed at a localized level. The level of iterative calculations depends on the type of hierarchical partitioning employed, namely degree of freedom, nodal, elemental, material/nonlinear group, substructural, and so on. Since the iterative solution process and application of constraints are applied at a local level, the resulting so-called hierarchical implicit solution algorithm possesses very stable and efficient numerical properties and is highly storage efficient. To demonstrate the scheme, the results of several benchmark examples are presented. These enable comparisons with the Newton-Raphson solved implicit transient solution method. Overall the comparisons illustrate the superior stability and efficiency of the hierarchical scheme. Author

A86-26896*# Illinois Univ., Urbana.

THREE-DIMENSIONAL HYBRID-STRESS FINITE ELEMENT ANALYSIS OF COMPOSITE LAMINATES WITH CRACKS AND CUTOUTS

S. S. WANG (Illinois, University, Urbana) IN: Pressure vessel components design and analysis; Proceedings of the Pressure Vessels and Piping Conference, New Orleans, LA, June 23-26, 1985. New York, American Society of Mechanical Engineers, 1985, p. 235-246. refs

(Contract NSG-3044)

A three-dimensional hybrid-stress finite element analysis of composite laminates containing cutouts and cracks is presented. Fully three-dimensional, hexahedral isoparametric elements of the hybrid-stress model are formulated on the basis of the Hellinger-Reissner variational principle. Traction-free edges, cutouts, and crack surfaces are modeled by imposition of exact traction boundary conditions along element surfaces. Special boundary and surface elements are constructed by introducing proper constraints on assumed stress functions. The Lagrangian multiplier technique is used to enforce ply-interface continuity conditions in hybrid bimaterial composite elements for modeling the interface region in a composite laminate. Two examples are given to illustrate the capability of the present method of approach: (1) the well-known delamination problem in an angle-ply laminate, and (2) the important problem of a composite laminate containing a circular hole. Results are presented in detail for each case. Implications of interlaminar and intralaminar crack initiation, growth and fracture in composites containing cracks and cutouts are discussed. Author

A86-26910* National Aeronautics and Space Administration. Lewis Research Center, Cleveland, Ohio.

VIBRATION AND BUCKLING OF ROTATING, PRETWISTED, PRECONED BEAMS INCLUDING CORIOLIS EFFECTS

K. B. SUBRAHMANYAM and K. R. V. KAZA (NASA, Lewis Research Center, Cleveland, OH) IN: Vibrations of blades and bladed disk assemblies; Proceedings of the Tenth Biennial Conference on Mechanical Vibration and Noise, Cincinnati, OH, September 10-13, 1985. New York, American Society of Mechanical Engineers, 1985, p. 75-87. Previously announced in STAR as N85-25893. refs

The effects of pretwist, precon, setting angle and Coriolis forces on the vibration and buckling behavior of rotating, torsionally rigid, cantilevered beams were studied. The beam is considered to be clamped on the axis of rotation in one case, and off the axis of rotation in the other. Two methods are employed for the solution of the vibration problem: (1) one based upon a finite-difference approach using second order central differences for solution of the equations of motion, and (2) based upon the minimum of the total potential energy functional with a Ritz type of solution procedure making use of complex forms of shape functions for the dependent variables. The individual and collective effects of pretwist, precon, setting angle, thickness ratio and Coriolis forces on the natural frequencies and the buckling boundaries are presented. It is shown that the inclusion of Coriolis effects is necessary for blades of moderate to large thickness ratios while these effects are not so important for small thickness ratio blades. The possibility of buckling due to centrifugal softening terms for large values of precon and rotation is shown. Author

A86-28653* Northwestern Univ., Evanston, Ill.

PROBABILISTIC FINITE ELEMENTS FOR TRANSIENT ANALYSIS IN NONLINEAR CONTINUA

W. K. LIU, T. BELYTSCHKO, and A. MANI (Northwestern University, Evanston, IL) IN: Advances in aerospace structural analysis; Proceedings of the Winter Annual Meeting, Miami Beach, FL, November 17-22, 1985. New York, American Society of Mechanical Engineers, 1985, p. 9-24. refs (Contract NAG3-535)

The probabilistic finite element method (PFEM), which is a combination of finite element methods and second-moment analysis, is formulated for linear and nonlinear continua with inhomogeneous random fields. Analogous to the discretization of the displacement field in finite element methods, the random field is also discretized. The formulation is simplified by transforming the correlated variables to a set of uncorrelated variables through an eigenvalue orthogonalization. Furthermore, it is shown that a reduced set of the uncorrelated variables is sufficient for the second-moment analysis. Based on the linear formulation of the PFEM, the method is then extended to transient analysis in nonlinear continua. The accuracy and efficiency of the method is demonstrated by application to a one-dimensional, elastic/plastic wave propagation problem. The moments calculated compare favorably with those obtained by Monte Carlo simulation. Also, the procedure is amenable to implementation in deterministic FEM based computer programs. Author

A86-28654* Rice Univ., Houston, Tex.

NUMERICAL SYNTHESIS OF TRI-VARIATE VELOCITY REALIZATIONS OF TURBULENCE

P.-T. D. SPANOS (Rice University, Houston, TX) and K. P. SCHULTZ (Lockheed Engineering and Management Services Co., Houston, TX) IN: Advances in aerospace structural analysis; Proceedings of the Winter Annual Meeting, Miami Beach, FL, November 17-22, 1985. New York, American Society of Mechanical Engineers, 1985, p. 25-35. refs (Contract NAG3-210)

An approach for synthesizing trivariate turbulence velocity field spatial realizations is presented. Some of the spatial frequency characteristics of the random velocity field are described by the von Karman spectrum. The simulation algorithm is based on an efficient autoregressive-moving average (ARMA) scheme involving coefficient square matrices of order three. The determination of

the efficient low order ARMA algorithm is preceded by the determination of a suitable high order autoregressive (AR) simulation algorithm. The numerical results are presented in a dimensionless form. Thus, they are applicable for any scale of turbulence. Author

A86-28655* MARC Analysis Research Corp., Palo Alto, Calif.

EFFICIENT ALGORITHMS FOR USE IN PROBABILISTIC FINITE ELEMENT ANALYSIS

J. B. DIAS and J. C. NAGTEGAAL (MARC Analysis Research Corp., Palo Alto, CA) IN: Advances in aerospace structural analysis; Proceedings of the Winter Annual Meeting, Miami Beach, FL, November 17-22, 1985. New York, American Society of Mechanical Engineers, 1985, p. 37-50. refs (Contract NAS3-24389)

This paper investigates the use of Fast Probability Integration (FPI) algorithms in a Finite Element environment. A method allowing the representation of correlated fields in terms of a vector of uncorrelated transformed variables, based on the spectral decomposition of the variance-covariance matrix is developed. The response of the deterministic model corresponding to selected perturbations of these uncorrelated variables is then obtained via a Newton-type iterative scheme. The results of the perturbed problems are used to construct a local representation of the model's behavior in the neighborhood of the deterministic state, which the FPI algorithm will use to estimate the reliability of the system. Although the proposed strategy has thus far only been applied to linear elastostatics, the extension of the method to a broader class of problems appears to be feasible. Author

A86-28659* Southwest Research Inst., San Antonio, Tex.

PROBABILISTIC STRUCTURAL ANALYSIS FOR SPACE PROPULSION SYSTEM COMPONENTS

O. H. BURNSIDE (Southwest Research Institute, San Antonio, TX) IN: Advances in aerospace structural analysis; Proceedings of the Winter Annual Meeting, Miami Beach, FL, November 17-22, 1985. New York, American Society of Mechanical Engineers, 1985, p. 87-102. refs (Contract NAS3-24389)

Probabilistic design and analysis methods for the achievement of greater reliability in structural systems are especially useful in those cases where the structure operates in such severe environments as that of the Space Shuttle. Attention is presently given to the development status of a NASA-sponsored program for probabilistic structural analysis methods applicable to current and future reusable space propulsion systems. Methodologies for the assessment of structural response by means of integrated finite element and probabilistic analysis techniques are discussed, with illustrative examples. O.C.

A86-34257* Virginia Polytechnic Inst. and State Univ., Blacksburg.

FACTORS INFLUENCING THE ULTRASONIC STRESS WAVE FACTOR EVALUATION OF COMPOSITE MATERIAL STRUCTURES

C. J. REBELLO (National Technical Systems, Hartwood, VA) and J. C. DUKE, JR. (Virginia Polytechnic Institute and State University, Blacksburg) Journal of Composites Technology and Research (ISSN 0885-6804), vol. 8, Spring 1986, p. 18-23. refs (Contract NAG3-323)

To demonstrate that the finite-element model can be used to investigate some of the factors influencing the ultrasonic stress wave evaluation of materials, a hypothetical case was studied in which classical vibration theory was used. Vibration analysis and experiments for the undamaged case were conducted on an isotropic aluminum plate and a unidirectional graphite-epoxy plate, using a point source to excite the plates. The finite-element solution correlated within eight percent with the exact method. The frequencies predicted by the finite-element model were observed in the experiments in both plates, although in the composite plate, additional frequencies were observed which could not be accounted for. Damaged isotropic plates were also considered. The effects of increasing damage severity with constant damage area, and

increasing damage area with constant severity on the resonant frequencies were analyzed. I.S.

A86-34444*# United Technologies Corp., East Hartford, Conn.
STRESS ANALYSIS OF GAS TURBINE ENGINE STRUCTURES USING THE BOUNDARY ELEMENT METHOD

R. B. WILSON, D. W. SNOW (United Technologies Corp., Engineering Div., Hartford, CT), and P. K. BANERJEE (New York, State University, Buffalo) IN: Advanced topics in boundary element analysis; Proceedings of the Winter Annual Meeting, Miami Beach, FL, November 17-22, 1985. New York, American Society of Mechanical Engineers, 1985, p. 45-63. refs
 (Contract NAS3-23697)

The theory of the boundary element method is briefly reviewed with particular reference to the feasibility of elastic and inelastic three-dimensional stress analysis of complex structures characteristic of gas turbine engine components. Particular requirements of gas turbine analysis are defined, and examples of the use of a boundary element code designed for the three-dimensional stress analysis of turbine components are presented. It is shown that the general-purpose boundary element code can accurately and efficiently analyze many of the gas turbine engine structures. V.L.

A86-34445*# State Univ. of New York, Buffalo.
ADVANCED THREE-DIMENSIONAL DYNAMIC ANALYSIS BY BOUNDARY ELEMENT METHODS

P. K. BANERJEE (New York, State University, Buffalo) and S. AHMA IN: Advanced topics in boundary element analysis; Proceedings of the Winter Annual Meeting, Miami Beach, FL, November 17-22, 1985. New York, American Society of Mechanical Engineers, 1985, p. 65-81. refs
 (Contract NAS3-23697)

Advanced formulations of boundary element method for periodic, transient transform domain and transient time domain solution of three-dimensional solids have been implemented using a family of isoparametric boundary elements. The necessary numerical integration techniques as well as the various solution algorithms are described. The developed analysis has been incorporated in a fully general purpose computer program BEST3D which can handle up to 10 subregions. A number of numerical examples are presented to demonstrate the accuracy of the dynamic analyses. Author

A86-34461*# MARC Analysis Research Corp., Palo Alto, Calif.
ITERATIVE METHODS FOR MIXED FINITE ELEMENT EQUATIONS

S. NAKAZAWA, J. C. NAGTEGAAL (MARC Analysis Research Corp., Palo Alto, CA), and O. C. ZIENKIEWICZ (Swansea, University College, Wales) IN: Hybrid and mixed finite element methods; Proceedings of the Winter Annual Meeting, Miami Beach, FL, November 17-22, 1985. New York, American Society of Mechanical Engineers, 1985, p. 57-67. refs
 (Contract NAS3-23697)

Iterative strategies for the solution of indefinite system of equations arising from the mixed finite element method are investigated in this paper with application to linear and nonlinear problems in solid and structural mechanics. The augmented Hu-Washizu form is derived, which is then utilized to construct a family of iterative algorithms using the displacement method as the preconditioner. Two types of iterative algorithms are implemented. Those are: constant metric iterations which does not involve the update of preconditioner; variable metric iterations, in which the inverse of the preconditioning matrix is updated. A series of numerical experiments is conducted to evaluate the numerical performance with application to linear and nonlinear model problems. Author

A86-34462*# Massachusetts Inst. of Tech., Cambridge.
HYBRID SOLID ELEMENT WITH A TRACTION-FREE CYLINDRICAL SURFACE

T. H. H. PIAN (MIT, Cambridge, MA) and Z. TIAN (Chinese Academy of Sciences, Graduate School, Beijing, People's Republic of China) IN: Hybrid and mixed finite element methods; Proceedings of the Winter Annual Meeting, Miami Beach, FL, November 17-22, 1985. New York, American Society of Mechanical Engineers, 1985, p. 69-75. refs
 (Contract NAG3-33)

An eight node solid element with two parallel faces and one traction-free cylindrical surface is derived using the assumed stress hybrid method. Cylindrical coordinates are used so that the assumed stresses satisfy the equilibrium equations as well as the traction-free condition over the cylindrical boundary. In the limiting case of plane stress conditions the assumed stresses also satisfy the compatibility conditions. Example solutions have demonstrated the advantage of using this special element for analyzing solids with circular holes. Author

A86-34464*# Georgia Inst. of Tech., Atlanta.
EXISTENCE AND STABILITY, AND DISCRETE BB AND RANK CONDITIONS, FOR GENERAL MIXED-HYBRID FINITE ELEMENTS IN ELASTICITY

W.-M. XUE and S. N. ATLURI (Georgia Institute of Technology, Atlanta) IN: Hybrid and mixed finite element methods; Proceedings of the Winter Annual Meeting, Miami Beach, FL, November 17-22, 1985. New York, American Society of Mechanical Engineers, 1985, p. 91-112. refs
 (Contract NAG3-346)

In this paper, all possible forms of mixed-hybrid finite element methods that are based on multi-field variational principles are examined as to the conditions for existence, stability, and uniqueness of their solutions. The reasons as to why certain 'simplified hybrid-mixed methods' in general, and the so-called 'simplified hybrid-displacement method' in particular (based on the so-called simplified variational principles), become unstable, are discussed. A comprehensive discussion of the 'discrete' BB-conditions, and the rank conditions, of the matrices arising in mixed-hybrid methods, is given. Some recent studies aimed at the assurance of such rank conditions, and the related problem of the avoidance of spurious kinematic modes, are presented. Author

A86-37799*# Akron Univ., Ohio.
INELASTIC HIGH-TEMPERATURE THERMOMECHANICAL RESPONSE OF CERAMIC COATED GAS TURBINE SEALS

J. PADOVAN (Akron, University, OH), D. DOUGHERTY (General Tire and Rubber Co., Akron, OH), and B. HENDRICKS (NASA, Lewis Research Center, Cleveland, OH) Journal of Thermal Stresses (ISSN 0149-5739), vol. 9, no. 1, 1986, p. 31-43. refs
 (Contract NAG3-265)

Through the use of a constrained Newton-Raphson time stepping finite element scheme, the inelastic thermomechanical response of ceramic coated gas turbine parts is considered. Due to the generality of the solution procedure developed, the combined thermoelastic-plastic-creep properties associated with ceramics is treated. This includes the handling of temperature-dependent elastic-plastic creep and thermal material properties. To illustrate the procedure, the thermomechanical response of ceramic coated outer gas path seals is considered. This includes the evaluation of time-dependent thermal ratcheting and its concomitant residual stress and strain fields. Author

A86-38838*# Georgia Inst. of Tech., Atlanta.

BOUNDING SOLUTIONS OF GEOMETRICALLY NONLINEAR VISCOELASTIC PROBLEMS

J. M. STUBSTAD and G. J. SIMITSES (Georgia Institute of Technology, Atlanta) IN: Structures, Structural Dynamics and Materials Conference, 27th, San Antonio, TX, May 19-21, 1986, Technical Papers. Part 1. New York, American Institute of Aeronautics and Astronautics, 1986, p. 343-352. Previously announced in STAR as N86-10860. refs

(Contract NAG3-534)

(AIAA PAPER 86-0943)

Integral transform techniques, such as the Laplace transform, provide simple and direct methods for solving viscoelastic problems formulated within a context of linear material response and using linear measures for deformation. Application of the transform operator reduces the governing linear integro-differential equations to a set of algebraic relations between the transforms of the unknown functions, the viscoelastic operators, and the initial and boundary conditions. Inversion either directly or through the use of the appropriate convolution theorem, provides the time domain response once the unknown functions have been expressed in terms of sums, products or ratios of known transforms. When exact inversion is not possible approximate techniques may provide accurate results. The overall problem becomes substantially more complex when nonlinear effects must be included. Situations where a linear material constitutive law can still be productively employed but where the magnitude of the resulting time dependent deformations warrants the use of a nonlinear kinematic analysis are considered. The governing equations will be nonlinear integro-differential equations for this class of problems. Thus traditional as well as approximate techniques, such as cited above, cannot be employed since the transform of a nonlinear function is not explicitly expressible.

Author

A86-38842*# National Aeronautics and Space Administration. Lewis Research Center, Cleveland, Ohio.

COMPOSITE SANDWICH THERMOSTRUCTURAL BEHAVIOR - COMPUTATIONAL SIMULATION

C. C. CHAMIS, R. A. AIELLO (NASA, Lewis Research Center, Cleveland, OH), and P. L. N. MURTHY (Cleveland State University, OH) IN: Structures, Structural Dynamics and Materials Conference, 27th, San Antonio, TX, May 19-21, 1986, Technical Papers. Part 1. New York, American Institute of Aeronautics and Astronautics, 1986, p. 370-381. refs

(AIAA PAPER 86-0948)

Computational methods have been developed for simulating the thermomechanical behavior of composite sandwiches, in which the analyses with several levels of progressive sophistication were used in conjunction with composite hygrothermomechanical theory. The sophistication levels include: (1) three-dimensional detailed finite element modeling of the honeycomb, the adhesive, and the composite faces; (2) three-dimensional finite element modeling assuming a homogeneous core; (3) laminate theory simulation; and (4) simple equations for predicting the equivalent properties of the honeycomb core. These levels have been packaged into a procedure embedded in a computer code streamlined for the simulation of the composite sandwich hygrothermal and structural behavior. It is shown that in order to properly simulate the thermomechanical response of the composite sandwich, all the honeycomb thermal and mechanical properties must be used.

I.S.

A86-38873*# Ohio State Univ., Columbus.

COMPUTER AIDED DERIVATION OF EQUATIONS FOR COMPOSITE MECHANICS PROBLEMS AND FINITE ELEMENT ANALYSES

N. SARIGUL (Ohio State University, Columbus) and C. C. CHAMIS (NASA, Lewis Research Center, Cleveland, OH) IN: Structures, Structural Dynamics and Materials Conference, 27th, San Antonio, TX, May 19-21, 1986, Technical Papers. Part 1. New York, American Institute of Aeronautics and Astronautics, 1986, p. 676-679. refs

(AIAA PAPER 86-1016)

Explicit equations are derived for analysis of multilayered fiber composites and for finite element analyses. The equations are obtained using a symbolic program and tested for various composite properties as well as for different fiber orientations. In order to analyze multilayered fiber composite structures, a variable thickness finite element is formulated. Examples of an airfoil geometry, simulated in a form of a cantilevered beam with various fiber orientations are studied.

Author

A86-39485*# Duke Univ., Durham, N. C.

FREQUENCY DOMAIN SOLUTIONS TO MULTI-DEGREE-OF-FREEDOM, DRY FRICTION DAMPED SYSTEMS UNDER PERIODIC EXCITATION

A. A. FERRI and E. H. DOWELL (Duke University, Durham, NC) IN: Dynamics and control of large structures; Proceedings of the Fifth Symposium, Blacksburg, VA, June 12-14, 1985. Blacksburg, VA, Virginia Polytechnic Institute and State University, 1985, p. 125-144. refs

(Contract AF-AFOSR-83-0346; NAG3-516)

The anticipated low damping level in large space structures (LSS) has been a major concern for the designers of these structures. Low damping degrades the free response and complicates the design of shape and attitude controllers for flexible spacecraft. Dry friction damping has been considered as a means of increasing the passive damping of LSS, by placing it in the joints and connecting junctures of structures. However, dry friction is highly nonlinear and, hence, analytical investigations are difficult to perform. Here, a multi-harmonic, frequency domain solution technique is developed and applied to a multi-DOF, dry friction damped system. It is seen that the multi-harmonic method is much more accurate than traditional, one harmonic solution methods. The method also compares well with time integration. Finally, comparisons are made with experimental results.

Author

A86-40695*# Georgia Inst. of Tech., Atlanta.

ON THE EQUIVALENCE OF THE INCREMENTAL HARMONIC BALANCE METHOD AND THE HARMONIC BALANCE-NEWTON RAPHSON METHOD

A. A. FERRI (Georgia Institute of Technology, Atlanta) ASME, Transactions, Journal of Applied Mechanics (ISSN 0021-8936), vol. 53, June 1986, p. 455-457. refs

(Contract NAG3-516)

A86-41673*# Georgia Inst. of Tech., Atlanta.

CONSTITUTIVE MODELING OF CYCLIC PLASTICITY AND CREEP, USING AN INTERNAL TIME CONCEPT

O. WATANABE and S. N. ATLURI (Georgia Institute of Technology, Atlanta) International Journal of Plasticity (ISSN 0749-6419), vol. 2, no. 2, 1986, p. 107-134. refs

(Contract NAG3-48)

Using the concept of an internal time as related to plastic strains, a differential stress-strain relation for elastoplasticity is rederived, such that (1) the concept of a yield-surface is retained; (2) the definitions of elastic and plastic processes are analogous to those in classical plasticity theory; and (3) its computational implementation, via a 'tangent-stiffness' finite element method and a 'generalized-midpoint-radial-return' stress-integration algorithm, is simple and efficient. Also, using the concept of an internal time, as related to both the inelastic strains as well as the Newtonian time, a constitutive model for creep-plasticity interaction, is discussed. The problem of modeling experimental data for plasticity and creep, by the present analytical relations, as accurately as

desired, is discussed. Numerical examples which illustrate the validity of the present relations are presented for the cases of cyclic plasticity and creep. Author

A86-43566* National Aeronautics and Space Administration. Lewis Research Center, Cleveland, Ohio.

MODE II FATIGUE CRACK GROWTH SPECIMEN DEVELOPMENT

R. J. BUZZARD, B. GROSS, and J. E. SRAWLEY (NASA, Lewis Research Center, Cleveland, OH) IN: Fracture mechanics; Proceedings of the Seventeenth National Symposium, Albany, NY, August 7-9, 1984. Philadelphia, PA, American Society for Testing and Materials, 1986, p. 329-345; Discussion, p. 345, 346. Previously announced in STAR as N84-29248. refs

A Mode II test specimen was developed which has potential application in understanding phenomena associated with mixed mode fatigue failures in high performance aircraft engine bearing races. The attributes of the specimen are: it contains one single ended notch, which simplifies data gathering and reduction; the fatigue crack grows in-line with the direction of load application; a single axis test machine is sufficient to perform testing; and the Mode I component is vanishingly small. Author

A86-43771* Akron Univ., Ohio.

LOCALLY BOUND CONSTRAINED NEWTON-RAPHSON SOLUTION ALGORITHMS

J. PADOVAN and R. MOSCARELLO (Akron, University, OH) Computers and Structures (ISSN 0045-7949), vol. 23, no. 2, 1986, p. 181-197. refs (Contract NAG3-54)

This paper develops strategies which enable the automatic adjustment of the constraint surfaces recently used to extend the range and numerical stability/efficiency of nonlinear finite-element equation solvers. In addition to handling kinematic and material induced nonlinearity, both pre- and postbuckling behavior can be treated. The scheme developed employs localized bounds on various hierarchical partitions of the field variables. These are used to resize, shape, and orient the global constraint surface, thereby enabling essentially automatic load/deflection incrementation. Due to the generality of the approach taken, it can be implemented in conjunction with constraints of arbitrary functional type. To benchmark the method, several numerical experiments are presented. These include problems involving kinematic and material nonlinearity, as well as, pre- and postbuckling characteristics. Author

A86-43774* Akron Univ., Ohio.

CONSTRAINED HIERARCHICAL LEAST SQUARE NONLINEAR EQUATION SOLVERS

J. PADOVAN and J. LACKNEY (Akron, University, OH) Computers and Structures (ISSN 0045-7949), vol. 23, no. 2, 1986, p. 251-263. refs (Contract NSG-3283)

The current paper develops a constrained hierarchical least square nonlinear equation solver. The procedure can handle the response behavior of systems which possess indefinite tangent stiffness characteristics. Due to the generality of the scheme, this can be achieved at various hierarchical application levels. For instance, in the case of finite element simulations, various combinations of either degree of freedom, nodal, elemental, substructural, and global level iterations are possible. Overall, this enables a solution methodology which is highly stable and storage efficient. To demonstrate the capability of the constrained hierarchical least square methodology, benchmarking examples are presented which treat structure exhibiting highly nonlinear pre- and postbuckling behavior wherein several indefinite stiffness transitions occur. Author

A86-44339* Syracuse Univ., N. Y.

FATIGUE CRACK GROWTH UNDER GENERAL-YIELDING CYCLIC-LOADING

Z. MINZHONG and H. W. LIU (Syracuse University, NY) ASME, Transactions, Journal of Engineering Materials and Technology (ISSN 0094-4289), vol. 108, July 1986, p. 201-205. refs (Contract NAG3-348)

In low cycle fatigue, cracks are initiated, and propagated under general-yielding cyclic loading. For general-yielding cyclic loading, Dowling and Begley (1976) have shown that fatigue crack growth rate correlates well with the measured Delta J. The correlation of da/dN with Delta J has also been studied by a number of other investigators. However, none of these studies has correlated da/dN with Delta J calculated specifically for the test specimens. Solomon measured fatigue crack growth in specimens in general-yielding cyclic loading. The crack tip fields for Solomon's specimens are calculated, using the finite element method, and the J-values of Solomon's tests are evaluated. The measured crack growth rate in Solomon's specimens correlates very well with the calculated Delta J. Author

A86-48245* National Aeronautics and Space Administration. Lewis Research Center, Cleveland, Ohio.

MASS BALANCING OF HOLLOW FAN BLADES

R. E. KIELB (NASA, Lewis Research Center, Cleveland, OH) ASME, International Gas Turbine Conference and Exhibit, 31st, Duesseldorf, West Germany, June 8-12, 1986. 7 p. Previously announced in STAR as N86-16611. refs (ASME PAPER 86-GT-195)

A typical section model is used to analytically investigate the effect of mass balancing as applied to hollow, supersonic fan blades. A procedure to determine the best configuration of an internal balancing mass to provide flutter alleviation is developed. This procedure is applied to a typical supersonic shroudless fan blade which is unstable in both the solid configuration and when it is hollow with no balancing mass. The addition of an optimized balancing mass is shown to stabilize the blade at the design condition. Author

A86-48271* Princeton Univ., N. J.

AEROELASTIC BEHAVIOR OF LOW ASPECT RATIO METAL AND COMPOSITE BLADES

J. F. WHITE, III and O. O. BENDIKSEN (Princeton University, NJ) ASME, International Gas Turbine Conference and Exhibit, 31st, Duesseldorf, West Germany, June 8-12, 1986. 10 p. refs (Contract NAG3-308) (ASME PAPER 86-GT-243)

The aeroelastic stability of titanium and composite blades of low aspect ratio is examined over a range of design parameters, using a Rayleigh-Ritz formulation. The blade modes include a plate-type mode to account for chordwise bending. Chordwise flexibility is found to have a significant effect on the unstalled supersonic flutter of low aspect ratio blades, and also on the stability of tip sections of shrouded fan blades. For blades with a thickness of less than approximately four percent of chord, the chordwise, second bending, and first torsion branches are all unstable at moderately high supersonic Mach numbers. For composite blades, the important structural coupling between bending and torsion cannot be modeled properly unless chordwise bending is accounted for. Typically, aft fiber sweep produces beneficial bending-torsion coupling that is stabilizing, whereas forward fiber sweep has the opposite effect. By using crossed-ply laminate configurations, critical aeroelastic modes can be stabilized. Author

A86-49133*# National Aeronautics and Space Administration. Lewis Research Center, Cleveland, Ohio.
UNIFIED CONSTITUTIVE MATERIALS MODEL DEVELOPMENT AND EVALUATION FOR HIGH-TEMPERATURE STRUCTURAL ANALYSIS APPLICATIONS

R. L. THOMPSON (NASA, Lewis Research Center, Cleveland, OH) and M. T. TONG (Sverdrup Technology, Inc., Cleveland, OH) IN: ICAS, Congress, 15th, London, England, September 7-12, 1986, Proceedings. Volume 2. New York, American Institute of Aeronautics and Astronautics, Inc., 1986, p. 1505a-1505s. refs

Unified constitutive material models were developed for structural analyses of aircraft gas turbine engine hot section components with particular application to an isotropic material used for combustor liners. Differential forms of models independently developed were considered in this study. These models combine the interactions of time-dependent (creep) and time-independent (plasticity) inelastic behavior of a material. Predicted stress-strain responses from these models were evaluated against cyclic isothermal and nonisothermal test results for uniaxial specimens of a nickel-base superalloy. The unified models were implemented in a nonlinear structural analysis code. Two unique NASA Lewis test facilities were used in the evaluation of the models for complex geometry specimens and evaluation of advanced temperature and high-temperature strain measurement instrumentation. Predicted nonlinear structural responses from one of the models for a flat plate and a segment of a conventional combustor liner are presented.

Author

N86-10579*# National Aeronautics and Space Administration. Lewis Research Center, Cleveland, Ohio.

JOINT RESEARCH EFFORT ON VIBRATIONS OF TWISTED PLATES, PHASE 1: FINAL RESULTS

R. E. KIELB, A. W. LEISSA, J. C. MACBAIN, and K. S. CARNEY Washington Sep. 1985 100 p refs
 (NASA-RP-1150; E-2576; NAS 1.61:1150) Avail: NTIS HC A05/MF A01 CSCL 20K

The complete theoretical and experimental results of the first phase of a joint government/industry/university research study on the vibration characteristics of twisted cantilever plates are given. The study is conducted to generate an experimental data base and to compare many different theoretical methods with each other and with the experimental results. Plates with aspect ratios, thickness ratios, and twist angles representative of current gas turbine engine blading are investigated. The theoretical results are generated by numerous finite element, shell, and beam analysis methods. The experimental results are obtained by precision matching a set of twisted plates and testing them at two laboratories. The second and final phase of the study will concern the effects of rotation.

Author

N86-10582*# National Aeronautics and Space Administration. Lewis Research Center, Cleveland, Ohio.

IMPROVED STUD CONFIGURATIONS FOR ATTACHING LAMINATED WOOD WIND TURBINE BLADES Final Report

J. R. FADOUL Sep. 1985 29 p refs
 (Contract DE-A101-76ET-20320)
 (NASA-TM-87109; DOE/NASA/20320-66; E-2709; NAS 1.15:87109) Avail: NTIS HC A03/MF A01

A series of bonded stud design configurations was screened on the basis of tension-tension cyclic tests to determine the structural capability of each configuration for joining a laminated wood structure (wind turbine blade) to a steel flange (wind turbine hub). Design parameters which affected the joint strength (ultimate and fatigue) were systematically varied and evaluated through appropriate testing. Two designs showing the most promise were used to fabricate additave testing. Two designs showing the most promise were used to fabricate additional test specimens to determine ultimate strength and fatigue curves. Test results for the bonded stud designs demonstrated that joint strengths approaching the 10,000 to 12,000 psi ultimate strength and 5000 psi high cycle fatigue strength of the wood epoxy composite could be achieved.

Author

N86-10588*# Georgia Inst. of Tech., Atlanta.

ANALYSIS OF LARGE, NON-ISOTHERMAL ELASTIC-VISCO-PLASTIC DEFORMATIONS

R. RIFF, R. L. CARLSON, and G. J. SIMITSES 1984 4 p refs

(Contract NAG3-534)

(NASA-CR-176220; NAS 1.26:176220) Avail: NTIS HC A02/MF A01 CSCL 20K

The development of a general mathematical model and solutions of test problems to analyze large nonisothermal elasto-visco-plastic deformations of structures is discussed. Geometric and material type nonlinearities of higher order are present in the development of the mathematical model and in the developed solution methodology.

DOE

N86-10589*# Southwest Research Inst., San Antonio, Tex.

CONSTITUTIVE MODELING FOR ISOTROPIC MATERIALS (HOST) Annual Status Report

U. S. LINDHOLM, K. S. CHAN, S. R. BODNER, R. M. WEBER, K. P. WALKER, and B. N. CASSENTI 20 Aug. 1985 185 p refs
 (Contract NAS3-23925)

(NASA-CR-174980; NAS 1.26:174980; SWRI-7576/30; ASR-2)

Avail: NTIS HC A09/MF A01 CSCL 20K

This report presents the results of the second year of work on a problem which is part of the NASA HOST Program. Its goals are: (1) to develop and validate unified constitutive models for isotropic materials, and (2) to demonstrate their usefulness for structural analyses of hot section components of gas turbine engines. The unified models selected for development and evaluation are that of Bodner-Partom and Walker. For model evaluation purposes, a large constitutive data base is generated for a B1900 + Hf alloy by performing uniaxial tensile, creep, cyclic, stress relation, and thermomechanical fatigue (TMF) tests as well as biaxial (tension/torsion) tests under proportional and nonproportional loading over a wide range of strain rates and temperatures. Systematic approaches for evaluating material constants from a small subset of the data base are developed. Correlations of the uniaxial and biaxial tests data with the theories of Bodner-Partom and Walker are performed to establish the accuracy, range of applicability, and integability of the models. Both models are implemented in the MARC finite element computer code and used for TMF analyses. Benchmark notch round experiments are conducted and the results compared with finite-element analyses using the MARC code and the Walker model.

Author

N86-11495*# National Aeronautics and Space Administration. Lewis Research Center, Cleveland, Ohio.

TURBINE ENGINE HOT SECTION TECHNOLOGY (HOST)

Oct. 1983 250 p refs Workshop held in Cleveland, Ohio, 25-26 Oct. 1983

(NASA-CP-2289; E-1816; NAS 1.55:2289) Avail: NTIS HC

A11/MF A01 CSCL 21E

A two-day workshop on the research and plans for turbine engine hot section durability problems was held on October 25 and 26, 1983, at the NASA Lewis Research Center. Presentations were made during six sessions, including structural analysis, fatigue and fracture, surface protective coatings, combustion, turbine heat transfer, and instrumentation, that dealt with the thermal and fluid environment around liners, blades, and vanes, and with material coatings, constitutive behavior, stress-strain response, and life prediction methods for the three components. The principal objective of each session was to disseminate the research results to date, along with future plans, in each of the six areas. Contract and government researchers presented results of their work.

N86-11496* National Aeronautics and Space Administration. Lewis Research Center, Cleveland, Ohio.

TURBINE ENGINE HOT SECTION TECHNOLOGY (HOST) PROJECT

D. E. SOKOLOWSKI and C. R. ENSIGN *In its Turbine Eng. Hot Sect. Technol. (HOST)* p 1-6 Oct. 1983

Avail: NTIS HC A11/MF A01 CSCL 21E

The Hot Section Technology (HOST) Project is a NASA-sponsored endeavor to improve the durability of advanced gas turbine engines for commercial and military aircraft. Through improvements in the analytical models and life prediction systems, designs for future hot section components, the combustor and turbine, will be more accurately analyzed and will incorporate features required for longer life in the more hostile operating environment of high performance engines. G.L.C.

N86-11501* United Technologies Research Center, East Hartford, Conn.

DEMONSTRATION TEST OF BURNER LINER STRAIN MEASUREMENT SYSTEMS: INTERIM RESULTS

K. A. STETSON and H. P. GRANT (Pratt and Whitney Aircraft, East Hartford, Conn.) *In NASA. Lewis Research Center Turbine Eng. Hot Sect. Technol. (HOST)* p 41-44 Oct. 1983

(Contract NAS3-23690)

Avail: NTIS HC A11/MF A01 CSCL 20K

Work is in progress to demonstrate two techniques for static strain measurements on a jet engine burner liner. Measurements are being made with a set of resistance strain gages made from Kanthal A-1 wire and via heterodyne speckle photogrammetry. The background of the program is presented along with current results. Author

N86-11514* General Electric Co., Cincinnati, Ohio. Aircraft Engine Business Group.

BURNER LINER THERMAL/STRUCTURAL LOAD MODELLING

R. J. MAFFEO *In NASA. Lewis Research Center Turbine Eng. Hot Sect. Technol. (HOST)* p 159-163 Oct. 1983

(Contract NAS3-23272)

Avail: NTIS HC A11/MF A01 CSCL 20K

The objective of this program is to develop a thermal data transfer computer program module for the burner liner thermal structural load modeling program. This will be accomplished by (1) reviewing existing methodologies for thermal data transfer and selecting three heat transfer codes for application in this program; (2) evaluating the selected codes to establish criteria for developing a computer program module to transfer thermal data from the heat transfer codes to selected stress analysis codes; (3) developing the automated thermal load transfer module; and (4) verifying and documenting the module. In aircraft turbine engine hot section components, cyclic thermal stresses are the most important damage mechanism. Consequently, accurate and reliable prediction of thermal loads is essential to improving durability. To achieve this goal, a considerable effort over the past 20 years has been devoted to the acquisition of engine temperature test data, as well as the development of accurate, reliable, and efficient computer codes for the prediction of steady state and transient temperatures and for the calculation of elastic and inelastic cyclic stresses and strains in hot section components. There is a need for continued development of these codes, because the availability of more accurate analysis techniques for complex configurations has enabled engine designers to use more sophisticated designs to achieve higher cycle efficiency and reduce weight. Author

N86-11518* National Aeronautics and Space Administration. Lewis Research Center, Cleveland, Ohio.

VALIDATION OF STRUCTURAL ANALYSIS METHODS USING BURNER LINER CYCLIC RIG TEST DATA

R. THOMPSON *In its Turbine Eng. Hot Sect. Technol. (HOST)* p 181-193 Oct. 1983

Avail: NTIS HC A11/MF A01 CSCL 20K

The objectives of the hot section technology (HOST) burner liner cyclic rig test program are basically threefold: (1) to assist in developing predictive tools needed to improve design analyses

and procedures for the efficient and accurate prediction of burner liner structural response; (2) to calibrate, evaluate and validate these predictive tools by comparing the predicted results with the experimental data generated in the tests; and (3) to evaluate existing as well as advanced temperature and strain measurement instrumentation, both contact and noncontact, in a simulated engine cycle environment. The data generated will include measurements of the thermal environment (metal surface temperatures) as well as structural (strain) and life (fatigue) responses of simulated burner liners and specimens under controlled boundary and operating conditions. These data will be used to calibrate, compare and validate analytical theories, methodologies and design procedures, as well as improvements in them, for predicting liner temperatures, stress-strain responses and cycles to failure. Comparison of predicted results with experimental data will be used to show where the predictive theories, etc. need improvements. In addition, as the predictive tools, as well as the tests, test methods, and data acquisition and reduction techniques, are developed and validated, a proven, integrated analysis/experiment method will be developed to determine the cyclic life of a simulated burner liner. Author

N86-11519* National Aeronautics and Space Administration. Lewis Research Center, Cleveland, Ohio.

HOST LINER CYCLIC FACILITIES

D. SCHULTZ *In its Turbine Eng. Hot Sect. Technol. (HOST)* p 195-204 Oct. 1983

Avail: NTIS HC A11/MF A01 CSCL 20K

The HOST Liner Cyclic Program is utilizing two types of test apparatus, rectangular box rigs and a full annular rig. To date two quartz lamp cyclic box rigs have been tested and a third is to begin testing in late October 1983. The box rigs are used to evaluate 5x8 inch rectangular linear samples. A 21 inch diameter outer liner simulator is also being built up for testing beginning in April 1984. All rigs are atmospheric rigs. The first box rig, a three 6-kVA lamp installation, was operated under adverse conditions to determine feasibility of using quartz lamps for cyclic testing. This work was done in December 1981 and looked promising. The second box rig, again using three 6-kVA lamps, was operated to obtain instrumentation durability information and initial data input to a Finite Element Model. This limited test program was conducted in August 1983. Five test plates were run. Instrumentation consisted of strain gages, thermocouples and thermal paint. The strain gages were found to fail at 1200 F as expected though plates were heated to 1700 F. The third box rig, containing four 6-kVA lamps, is in build up for testing to begin in late October 1983. In addition to 33 percent greater power input, this rig has provision for 400 F backside line cooling air and a viewing port suitable for IR camera viewing. The casing is also water cooled for extended durability. Author

N86-11520* National Aeronautics and Space Administration. Lewis Research Center, Cleveland, Ohio.

LIFE PREDICTION AND CONSTITUTIVE BEHAVIOR

G. R. HALFORD *In its Turbine Eng. Hot Sect. Technol. (HOST)* p 205-207 Oct. 1983

Avail: NTIS HC A11/MF A01 CSCL 20K

One of the primary drivers that prompted the initiation of the hot section technology (HOST) program was the recognized need for improved cyclic durability of costly hot section components. All too frequently, fatigue in one form or another was directly responsible for the less than desired durability, and prospects for the future weren't going to improve unless a significant effort was mounted to increase our knowledge and understanding of the elements governing cyclic crack initiation and propagation lifetime. Certainly one of the important factors is the ability to perform accurate structural stress-strain analyses on a routine basis to determine the magnitudes of the localized stresses and strains since it is these localized conditions that govern the initiation and crack growth processes. Developing the ability to more accurately predict crack initiation lifetimes and cyclic crack growth rates for the complex loading conditions found in turbine engine hot sections is of course the ultimate goal of the life prediction research efforts.

39 STRUCTURAL MECHANICS

It has been found convenient to divide the research efforts into those dealing with nominally isotropic and anisotropic alloys; the latter for application to directionally solidified and single crystal turbine blades. Author

N86-11521*# Pratt and Whitney Aircraft, East Hartford, Conn. CREEP FATIGUE LIFE PREDICTION FOR ENGINE HOT SECTION MATERIALS (ISOTROPIC)

V. MORENO /In NASA. Lewis Research Center Turbine Eng. Hot Sect. Technol. (HOST) p 209-210 Oct. 1983 (Contract NAS3-23288)

Avail: NTIS HC A11/MF A01 CSCL 20K

The activities performed during the first year of the NASA HOST Program, Creep Fatigue Life Prediction for Engine Hot Section Materials (Isotropic), being conducted by Pratt & Whitney Aircraft are summarized. The program is a 5 year, two part effort aimed at improving the high temperature crack initiation prediction technology for gas turbine hot section components. Significant results of the program produced thus far are discussed. Cast B1900 + Hf and wrought IN 718 were selected as the base and alternate materials, respectively. A single heat of B1900 + Hf was obtained and test specimens fabricated. The material was characterized with respect to grain size, gamma prime size, carbide distribution, and dislocation density. Monotonic tensile and creep testing has shown engineering properties within anticipated scatter for this material. Examination of the tensile tests has shown a transition from inhomogeneous planar slip within the grains at lower temperatures to more homogeneous matrix deformation. Examination of the creep tests has shown a transgranular failure mode at 1400 F and an intergranular failure mode at 1600 F and 1800 F. Author

N86-11526*# Connecticut Univ., Storrs. School of Engineering. ELEVATED TEMPERATURE BIAxIAL FATIGUE Final Report

E. H. JORDAN Oct. 1985 162 p refs

(Contract NAS3-160)

(NASA-CR-175009; NAS 1.26:175009) Avail: NTIS HC A08/MF A01 CSCL 20K

A 3 year experimental program for studying elevated temperature biaxial fatigue of a nickel based alloy Hastelloy-X has been completed. A new high temperature fatigue test facility with unique capabilities has been developed. Effort was directed toward understanding multiaxial fatigue and correlating the experimental data to the existing theories of fatigue failure. The difficult task of predicting fatigue lives for nonproportional loading was used as an ultimate test for various life prediction methods being considered. The primary means of reaching improved understanding were through several critical nonproportional loading experiments. The direction of cracking observed on failed specimens was also recorded and used to guide the development of the theory. Cyclic deformation responses were permanently recorded digitally during each test. It was discovered that the cracking mode switched from primarily cracking on the maximum shear planes at room temperature to cracking on the maximum normal strain planes at 649 C. In contrast to some other metals, loading path in nonproportional loading had little effect on fatigue lives. Strain rate had a small effect on fatigue lives at 649 C. Of the various correlating parameters the modified plastic work and octahedral shear stress were the most successful. Author

N86-13755*# Case Western Reserve Univ., Cleveland, Ohio. TIME DEPENDENCY OF STRAINRANGE PARTITIONING LIFE RELATIONSHIPS Final Report

S. KALLURI and S. S. MANSON Aug. 1984 64 p refs

(Contract NAG3-337)

(NASA-CR-174946; NAS 1.26:174946) Avail: NTIS HC A04/MF A01 CSCL 20K

The effect of exposure time (or creep rate) on the CP life relationship is established by conducting isothermal CP tests at varying exposure times on 316 Ss at 1300 and 1500 F. A reduction in the CP cycle life is observed with an increase in the exposure time of the CP test at a given inelastic strain-range. This phenomenon is characterized by modifying the Manson-Coffin type

of CP relationship. Two new life relationships: (1) the Steady State Creep Rate (SSRC) Modified CP life relationship, and (2) the Failure Time (FT) Modified CP life relationship, are developed in this report. They account for the effect of creep rate and exposure time within the CP type of waveform. The reduction in CP cyclic life in the long exposure time tests is attributed to oxidation and the precipitation of carbides along the grain boundaries. Author

N86-14688*# National Aeronautics and Space Administration. Lewis Research Center, Cleveland, Ohio.

SCARE: A POST-PROCESSOR PROGRAM TO MSC/NASTRAN FOR THE RELIABILITY ANALYSIS OF STRUCTURAL CERAMIC COMPONENTS

J. P. GYEKENYESI 1985 24 p refs To be presented at the 31st International Gas Turbine Conference and Exhibit, Dusseldorf, West Germany, 8-12 June 1986; sponsored by the American Society of Mechanical Engineers

(NASA-TM-87188; E-2654; NAS 1.15:87188) Avail: NTIS HC A02/MF A01 CSCL 20K

A computer program was developed for calculating the statistical fast fracture reliability and failure probability of ceramic components. The program includes the two-parameter Weibull material fracture strength distribution model, using the principle of independent action for polyaxial stress states and Batdorf's shear-sensitive as well as shear-insensitive crack theories, all for volume distributed flaws in macroscopically isotropic solids. Both penny-shaped cracks and Griffith cracks are included in the Batdorf shear-sensitive crack response calculations, using Griffith's maximum tensile stress or critical coplanar strain energy release rate criteria to predict mixed mode fracture. Weibull material parameters can also be calculated from modulus of rupture bar tests, using the least squares method with known specimen geometry and fracture data. The reliability prediction analysis uses MSC/NASTRAN stress, temperature and volume output, obtained from the use of three-dimensional, quadratic, isoparametric, or axisymmetric finite elements. The statistical fast fracture theories employed, along with selected input and output formats and options, are summarized. An example problem to demonstrate various features of the program is included. Author

N86-16610*# Akron Univ., Ohio. Dept. of Civil Engineering. THERMOMECHANICAL CYCLIC HARDENING BEHAVIOR OF HASTELLOY-X M.S. Thesis

P. A. BARTOLOTTA Nov. 1985 54 p refs

(Contract NAG3-379)

(NASA-CR-174999; NAS 1.26:174999) Avail: NTIS HC A04/MF A01 CSCL 20K

Experimental evidence of thermomechanical history dependence on the cyclic hardening behavior of a representative combustor liner material Hastelloy-X is presented, along with a discussion about the relevant concept of thermomechanical path dependence. Based on the experimental results, a discussion is given on the inadequacy of formulating nonisothermal constitutive equations solely on the basis of isothermal testing. Finally, the essence of a mathematical representation of thermoviscoplasticity is presented that qualitatively accounts for the observed hereditary behavior. This is achieved by formulating the scalar evolutionary equation in an established viscoplastic theory to reflect thermomechanical path dependence. Although the necessary nonisothermal tests for further quantifying the thermoviscoplastic model have been identified, such data are not yet available. Author

N86-16611*# National Aeronautics and Space Administration. Lewis Research Center, Cleveland, Ohio.

MASS BALANCING OF HOLLOW FAN BLADES

R. E. KIELB 1986 15 p refs Proposed for presentation at the 31st International Gas Turbine Conference and Exhibit, Dusseldorf, West Germany, 8-12 Jun. 1985; sponsored by ASME

(NASA-TM-87197; E-2851; NAS 1.15:87197) Avail: NTIS HC A02/MF A01 CSCL 20K

A typical section model is used to analytically investigate the effect of mass balancing as applied to hollow, supersonic fan

blades. A procedure to determine the best configuration of an internal balancing mass to provide flutter alleviation is developed. This procedure is applied to a typical supersonic shroudless fan blade which is unstable in both the solid configuration and when it is hollow with no balancing mass. The addition of an optimized balancing mass is shown to stabilize the blade at the design condition. Author

N86-16615*# National Aeronautics and Space Administration. Lewis Research Center, Cleveland, Ohio.

SIMPLIFIED CYCLIC STRUCTURAL ANALYSES OF SSME TURBINE BLADES

A. KAUFMAN and J. M. MANDERSCHIED 1986 17 p refs Proposed for presentation at the Conference on Advanced High Pressure Oxygen/Hydrogen Propulsion Technology, Huntsville, Ala., 14-16 May 1986; sponsored by NASA Marshall Space Flight Center (NASA-TM-87214; E-2873; NAS 1.15:87214) Avail: NTIS HC A02/MF A01 CSCL 20K

Anisotropic high-temperature alloys are used to meet the safety and durability requirements of turbine blades for high-pressure turbopumps in reusable space propulsion systems. The applicability to anisotropic components of a simplified inelastic structural analysis procedure developed at the NASA Lewis Research Center is assessed. The procedure uses as input the history of the total strain at the critical crack initiation location computed from elastic finite-element analyses. Cyclic heat transfer and structural analyses are performed for the first stage high-pressure fuel turbopump blade of the space shuttle main engine. The blade alloy is directionally solidified MAR-M 246 (nickel base). The analyses are based on a typical test stand engine cycle. Stress-strain histories for the airfoil critical location are computed using both the MARC nonlinear finite-element computer code and the simplified procedure. Additional cases are analyzed in which the material yield strength is arbitrarily reduced to increase the plastic strains and, therefore, the severity of the problem. Good agreement is shown between the predicted stress-strain solutions from the two methods. The simplified analysis uses about 0.02 percent (5 percent with the required elastic finite-element analyses) of the CPU time used by the nonlinear finite element analysis. Author

N86-17788*# Virginia Polytechnic Inst. and State Univ., Blacksburg. Dept. of Engineering Science and Mechanics. **CLOSURE OF FATIGUE CRACKS AT HIGH STRAINS Final Report**

N. S. IYER and N. E. DOWLING Dec. 1985 159 p refs (Contract NAG3-438) (NASA-CR-175021; NAS 1.26:175021) Avail: NTIS HC A08/MF A01 CSCL 20K

Experiments were conducted on smooth specimens to study the closure behavior of short cracks at high cyclic strains under completely reversed cycling. Testing procedures and methodology, and closure measurement techniques, are described in detail. The strain levels chosen for the study cover from predominantly elastic to grossly plastic strains. Crack closure measurements are made at different crack lengths. The study reveals that, at high strains, cracks close only as the lowest stress level in the cycle is approached. The crack opening is observed to occur in the compressive part of the loading cycle. The applied stress needed to open a short crack under high strain is found to be less than for cracks under small scale yielding. For increased plastic deformations, the value of $\sigma_{sub op}/\sigma_{sub max}$ is observed to decrease and approaches the value of R . Comparison of the experimental results with existing analysis is made and indicates the limitations of the small scale yielding approach where gross plastic deformation behavior occurs. Author

N86-17789*# National Aeronautics and Space Administration. Lewis Research Center, Cleveland, Ohio.

NONLINEAR BENDING-TORSIONAL VIBRATION AND STABILITY OF ROTATING, PRETWISTED, PRECONED BLADES INCLUDING CORIOLIS EFFECTS

K. B. SUBRAHMANYAM (Toledo Univ., Ohio), K. R. V. KAZA, G. V. BROWN, and C. LAWRENCE Jan. 1986 36 p refs Presented at Workshop on Dynamics and Aeroelastic Stability Modeling of Rotor Systems, Atlanta, Ga., 4-5 Dec. 1985; sponsored by Army and Georgia Inst. of Technology, Atlanta (NASA-TM-87207; NAS 1.15:87207) Avail: NTIS HC A03/MF A01 CSCL 20K

The coupled bending-bending-torsional equations of dynamic motion of rotating, linearly pretwisted blades are derived including large precone, second degree geometric nonlinearities and Coriolis effects. The equations are solved by the Galerkin method and a linear perturbation technique. Accuracy of the present method is verified by comparisons of predicted frequencies and steady state deflections with those from MSC/NASTRAN and from experiments. Parametric results are generated to establish where inclusion of only the second degree geometric nonlinearities is adequate. The nonlinear terms causing torsional divergence in thin blades are identified. The effects of Coriolis terms and several other structurally nonlinear terms are studied, and their relative importance is examined. Author

N86-18750*# National Aeronautics and Space Administration. Lewis Research Center, Cleveland, Ohio.

ESTIMATING THE R-CURVE FROM RESIDUAL STRENGTH DATA

T. W. ORANGE 1985 17 p refs Presented at the International Conference and Exhibition on Fatigue, Corrosion Cracking, Fracture Mechanics and Failure Analysis, Salt Lake City, Utah, 2-6 Dec. 1985; sponsored by the American Society for Metals (NASA-TM-87182; E-2832; NAS 1.15:87182) Avail: NTIS HC A02/MF A01 CSCL 20K

A method is presented for estimating the crack-extension resistance curve (R-curve) from residual-strength (maximum load against original crack length) data for precracked fracture specimens. The method allows additional information to be inferred from simple test results, and that information can be used to estimate the failure loads of more complicated structures of the same material and thickness. The fundamentals of the R-curve concept are reviewed first. Then the analytical basis for the estimation method is presented. The estimation method has been verified in two ways. Data from the literature (involving several materials and different types of specimens) are used to show that the estimated R-curve is in good agreement with the measured R-curve. A recent predictive blind round-robin program offers a more crucial test. When the actual failure loads are disclosed, the predictions are found to be in good agreement. Author

N86-19663*# National Aeronautics and Space Administration. Lewis Research Center, Cleveland, Ohio.

COMPUTATIONAL ENGINE STRUCTURAL ANALYSIS

C. C. CHAMIS and R. H. JOHNS 1986 20 p refs Proposed for presentation at the 31st International Gas Turbine Conference and Exhibit, Dusseldorf, West Germany, 8-12 Jun. 1986; sponsored by American Society of Mechanical Engineers (NASA-TM-87231; E-2898; NAS 1.15:87231) Avail: NTIS HC A02/MF A01 CSCL 20K

A significant research activity at the NASA Lewis Research Center is the computational simulation of complex multidisciplinary engine structural problems. This simulation is performed using computational engine structural analysis (CESA) which consists of integrated multidisciplinary computer codes in conjunction with computer post-processing for problem-specific application. A variety of the computational simulations of specific cases are described in some detail in this paper. These case studies include: (1) aeroelastic behavior of bladed rotors, (2) high velocity impact of fan blades, (3) blade-loss transient response, (4) rotor/stator/squeeze-film/bearing interaction, (5) blade-fragment/rotor-burst component, and (6) structural behavior of advanced swept turboprops.

39 STRUCTURAL MECHANICS

These representative case studies are selected to demonstrate the breath of the problems analyzed and the role of the computer including post-processing and graphical display of voluminous output data.

Author

N86-21909*# Ohio State Univ., Columbus. Dept. of Engineering Mechanics.

EXTENSIONS OF THE RITZ-GALERKIN METHOD FOR THE FORCED, DAMPED VIBRATIONS OF STRUCTURAL ELEMENTS

A. W. LEISSA and T. H. YOUNG /in AFWAL Vibration Damping 1984 Workshop Proceedings 21 p Nov. 1984

(Contract NAG3-424)

Avail: NTIS HC A99/MF A01 CSCL 20K

The Ritz-Galerkin methods were used to obtain approximate solutions for free undamped, vibration problems. It is demonstrated that these same methods may be used straightforwardly to analyze forced vibrations with damping without requiring the free vibration eigenfunctions. It was shown that the Galerkin method is an effective technique for these types of problems. The Ritz method has the advantage that it does not need to satisfy the force-type boundary conditions, which is particularly important for plates and shells. Proper functionals representing the forcing and damping terms were developed. Two types of damping--viscous and material (hysteretic) are discussed. Distributed and concentrated exciting forces are treated. Numerical results are obtained for cantilevered beams and rectangular plates. The rates of convergence of the solutions are shown. Approximate solutions from the present methods are compared with the exact solutions for the cantilever beam.

E.A.K.

N86-21932*# General Electric Co., Cincinnati, Ohio. Aircraft Engine Business Group.

BURNER LINER THERMAL-STRUCTURAL LOAD MODELING

R. MAFFEO 1986 205 p

(Contract NAS3-23272)

(NASA-CR-174892; NAS 1.26:174892) Avail: NTIS HC A10/MF

A01 CSCL 20K

The software package Transfer Analysis Code to Interface Thermal/Structural Problems (TRANCITS) was developed. The TRANCITS code is used to interface temperature data between thermal and structural analytical models. The use of this transfer module allows the heat transfer analyst to select the thermal mesh density and thermal analysis code best suited to solve the thermal problem and gives the same freedoms to the stress analyst, without the efficiency penalties associated with common meshes and the accuracy penalties associated with the manual transfer of thermal data.

E.A.K.

N86-21951*# Syracuse Univ., N. Y. Dept. of Mechanical and Aerospace Engineering.

FATIGUE CRACK GROWTH UNDER GENERAL-YIELDING CYCLIC-LOADING

Z. MINZHONG and H. W. LIU Feb. 1986 28 p refs

(Contract NAG3-348)

(NASA-CR-175049; NAS 1.26:175049) Avail: NTIS HC A03/MF

A01 CSCL 20K

In low cycle fatigue, cracks are initiated and propagated under general yielding cyclic loading. For general yielding cyclic loading, Dowling and Begley have shown that fatigue crack growth rate correlates well with the measured delta J. The correlation of da/dN with delta J was also studied by a number of other investigators. However, none of these studies have correlated da/dN with delta J calculated specifically for the test specimens. Solomon measured fatigue crack growth in specimens in general yielding cyclic loading. The crack tips fields for Solomon's specimens are calculated using the finite element method and the J values of Solomon's tests are evaluated. The measured crack growth rate in Solomon's specimens correlates very well with the calculated delta J.

Author

N86-21952*# Cincinnati Univ., Ohio. Dept. of Aerospace Engineering and Engineering Mechanics.

ANISOTROPIC CONSTITUTIVE MODEL FOR NICKEL BASE SINGLE CRYSTAL ALLOYS: DEVELOPMENT AND FINITE ELEMENT IMPLEMENTATION Final Report

L. T. DAME and D. C. STOFFER Mar. 1986 130 p refs

(Contract NAG3-511)

(NASA-CR-175015; NAS 1.26:175015) Avail: NTIS HC A07/MF A01 CSCL 20K

A tool for the mechanical analysis of nickel base single crystal superalloys, specifically Rene N4, used in gas turbine engine components is developed. This is achieved by a rate dependent anisotropic constitutive model implemented in a nonlinear three dimensional finite element code. The constitutive model is developed from metallurgical concepts utilizing a crystallographic approach. A non Schmid's law formulation is used to model the tension/compression asymmetry and orientation dependence in octahedral slip. Schmid's law is a good approximation to the inelastic response of the material in cube slip. The constitutive equations model the tensile behavior, creep response, and strain rate sensitivity of these alloys. Methods for deriving the material constants from standard tests are presented. The finite element implementation utilizes an initial strain method and twenty noded isoparametric solid elements. The ability to model piecewise linear load histories is included in the finite element code. The constitutive equations are accurately and economically integrated using a second order Adams-Moulton predictor-corrector method with a dynamic time incrementing procedure. Computed results from the finite element code are compared with experimental data for tensile, creep and cyclic tests at 760 deg C. The strain rate sensitivity and stress relaxation capabilities of the model are evaluated.

Author

N86-25822*# National Aeronautics and Space Administration. Lewis Research Center, Cleveland, Ohio.

CYCLIC CREEP ANALYSIS FROM ELASTIC FINITE-ELEMENT SOLUTIONS

A. KAUFMAN and S. Y. HWANG (South Carolina State Coll., Orangeburg) 1986 21 p refs Presented at the Southeastern Conference on Theoretical and Applied Mechanics, Columbia, S.C., 17-18 Apr. 1986

(NASA-TM-87213; E-2872; NAS 1.15:87213) Avail: NTIS HC A02/MFA01 CSCL 20K

A uniaxial approach was developed for calculating cyclic creep and stress relaxation at the critical location of a structure subjected to cyclic thermomechanical loading. This approach was incorporated into a simplified analytical procedure for predicting the stress-strain history at a crack initiation site for life prediction purposes. An elastic finite-element solution for the problem was used as input for the simplified procedure. The creep analysis includes a self-adaptive time incrementing scheme. Cumulative creep is the sum of the initial creep, the recovery from the stress relaxation and the incremental creep. The simplified analysis was exercised for four cases involving a benchmark notched plate problem. Comparisons were made with elastic-plastic-creep solutions for these cases using the MARC nonlinear finite-element computer code.

Author

N86-25850*# Michigan State Univ., East Lansing. Dept. of Metallurgy, Mechanics and Materials Science.

EXPERIMENTAL EVALUATION CRITERIA FOR CONSTITUTIVE MODELS OF TIME DEPENDENT CYCLIC PLASTICITY Final Report, 1 Jun. 1980 - 30 Sep. 1983

J. F. MARTIN 1986 13 p

(Contract NAG3-51)

(NASA-CR-176821; NAS 1.26:176821) Avail: NTIS HC A02/MF A01 CSCL 20K

Notched members were tested at temperatures far above those recorded till now. Simulation of the notch root stress response was accomplished to establish notch stress-strain behavior. Cyclic stress-strain profiles across the net-section were recorded and on-line direct notch strain control was accomplished. Data are compared to three analysis techniques with good results. The

objective of the study is to generate experimental data that can be used to evaluate the accuracy of constitutive models of time dependent cyclic plasticity. Author

N86-25851*# Case Western Reserve Univ., Cleveland, Ohio.
FATIGUE CRACK LAYER PROPAGATION IN SILICON-IRON Final Report

Y. BIROL, G. WELSCH, and A. CHUDNOVSKY May 1986 47 p refs
(Contract NAG3-223)
(NASA-CR-175115; NAS 1.26:175115) Avail: NTIS HC A03/MF A01 CSCL 20K

Fatigue crack propagation in metal is almost always accompanied by plastic deformation unless conditions strongly favor brittle fracture. The analysis of the plastic zone is crucial to the understanding of crack propagation behavior as it governs the crack growth kinetics. This research was undertaken to study the fatigue crack propagation in a silicon iron alloy. Kinetic and plasticity aspects of fatigue crack propagation in the alloy were obtained, including the characterization of damage evolution.

Author

N86-26651*# National Aeronautics and Space Administration.
Lewis Research Center, Cleveland, Ohio.

LOW-CYCLE THERMAL FATIGUE

G. R. HALFORD Feb. 1986 114 p refs
(NASA-TM-87225; E-2890; NAS 1.15:87225) Avail: NTIS HC A06/MF A01 CSCL 20K

A state-of-the-art review is presented of the field of thermal fatigue. Following a brief historical review, the concept is developed that thermal fatigue can be viewed as processes of unbalanced deformation and cracking. The unbalances refer to dissimilar mechanisms occurring in opposing halves of thermal fatigue loading and unloading cycles. Extensive data summaries are presented and results are interpreted in terms of the unbalanced processes involved. Both crack initiation and crack propagation results are summarized. Testing techniques are reviewed, and considerable discussion is given to a technique for thermal fatigue simulation, known as the bithermal fatigue test. Attention is given to the use of isothermal life prediction methods for the prediction of thermal fatigue lives. Shortcomings of isothermally-based life prediction methods are pointed out. Several examples of analyses and thermal fatigue life predictions of high technology structural components are presented. Finally, numerous dos and don'ts relative to design against thermal fatigue are presented.

Author

N86-26652*# Battelle Columbus Labs., Ohio.
NONLINEAR DAMAGE ANALYSIS: POSTULATE AND EVALUATION Final Report, 30 Sep. 1981 - 6 Apr. 1983

B. N. LEIS and T. P. FORTE 6 Apr. 1983 101 p refs
(Contract NAS3-22825)
(NASA-CR-168171; NAS 1.26:168171) Avail: NTIS HC A06/MF A01 CSCL 20K

The objective of this program is to assess the viability of a damage postulate which asserts that the fatigue resistance curve of a metal is history dependent due to inelastic action. The study focusses on OFE copper because this simple model material accentuates the inelastic action central to the damage postulate. Data relevant to damage evolution and crack initiation are developed via a study of surface topography. The effects of surface layer residual stresses are explored via comparative testing as were the effects in initial prestraining. The results of the study very clearly show the deformation history dependence of the fatigue resistance of OFE copper. Furthermore the concept of deformation history dependence is shown to qualitatively explain the fatigue resistance of all histories considered. Likewise quantitative predictions for block cycle histories are found to accurately track the observed results. In this respect the assertion that damage per cycle for a given level of the damage parameter is deformation history dependent appears to be physically justified.

Author

N86-27680*# National Aeronautics and Space Administration.
Lewis Research Center, Cleveland, Ohio.

RE-EXAMINATION OF CUMULATIVE FATIGUE DAMAGE ANALYSIS: AN ENGINEERING PERSPECTIVE

S. S. MANSON and G. R. HALFORD 1986 71 p Presented at the Symposium on Mechanics of Damage and Fatigue, Haifa-Tel Aviv, Israel, 1-5 Jul. 1985; sponsored by the International Union of Theoretical and Applied Mechanics
(NASA-TM-87325; E-3066; NAS 1.15:87325) Avail: NTIS HC A04/MF A01 CSCL 20K

A method which has evolved in our laboratories for the past 20 yr is re-examined with the intent of improving its accuracy and simplicity of application to engineering problems. Several modifications are introduced both to the analytical formulation of the Damage Curve Approach, and to the procedure for modifying this approach to achieve a Double Linear Damage Rule formulation which immensely simplifies the calculation. Improvements are also introduced in the treatment of mean stress for determining fatigue life of the individual events that enter into a complex loading history. While the procedure is completely consistent with the results of numerous two level tests that have been conducted on many materials, it is still necessary to verify applicability to complex loading histories. Caution is expressed that certain phenomena can also influence the applicability - for example, unusual deformation and fracture modes inherent in complex loading - especially if stresses are multiaxial. Residual stresses at crack tips, and metallurgical factors are also important in creating departures from the cumulative damage theories; examples of departures are provided.

Author

N86-27689*# Argonne National Lab., Ill.
EFFECTS OF A HIGH MEAN STRESS ON THE HIGH CYCLE FATIGUE LIFE OF PWA 1480 AND CORRELATION OF DATA BY LINEAR ELASTIC FRACTURE MECHANICS

S. MAJUMDAR and R. KWASNY Nov. 1985 28 p
(Contract NASA ORDER C-91113-D; W-31-109-ENG-38)
(NASA-CR-175057; NAS 1.26:175057; ANL-85-74) Avail: NTIS HC A03/MF A01 CSCL 20K

High-cycle fatigue tests using 5-mm-diameter smooth specimens were performed on the single crystal alloy PWA 1480 (001 axis) at 70F (room temperature) in air and at 100F (538C) in vacuum (10 to the -6 power torr). Tests were conducted at zero mean stress as well as at high tensile mean stress. The results indicate that, although a tensile mean stress, in general, reduces life, the reduction in fatigue strength, for a given mean stress at a life of one million cycles, is much less than what is predicted by the usual linear Goodman plot. Further, the material appears to be significantly more resistant to mean stress effects at 1000F than at 70F. Metallographic examinations of failed specimens indicate that failures in all cases are initiated from micropores of sizes of the order of 30 to 40 microns. Since the macroscopic stress-strain response in all cases was observed to be linear elastic, linear elastic fracture mechanics (LEFM) analyses were carried out to determine the crack growth curves of the material assuming that crack initiation from a micropore (a sub o = 40 microns) occurs very early in life. The results indicate that the calculated crack growth rates at an R (defined as the ratio between minimum stress to maximum stress) value of zero are approximately the same at 70F as at 1000F. However, the calculated crack growth rates at other R ratios, both positive and negative, tend to be higher at 70F than at 1000F. Calculated threshold effects at large R values tend to be independent of temperature in the temperature regime studied. They are relatively constant with increasing R ratio up to a value of about 0.6, beyond which the calculated threshold stress intensity factor range decreases rapidly with increasing R ratios.

Author

39 STRUCTURAL MECHANICS

N86-28455*# Texas A&M Univ., College Station. Dept. of Aerospace Engineering.

INTEGRATED RESEARCH IN CONSTITUTIVE MODELLING AT ELEVATED TEMPERATURES, PART 2 Final Report

W. E. HAISLER and D. H. ALLEN Jun. 1986 224 p

(Contract NAG3-491)

(NASA-CR-177233; NAS 1.26:177233; MM-4998-86-13-PT-2)

Avail: NTIS HC A10/MF A01 CSCL 20K

Four current viscoplastic models are compared experimentally with Inconel 718 at 1100 F. A series of tests were performed to create a sufficient data base from which to evaluate material constants. The models used include Bodner's anisotropic model; Krieg, Swearingen, and Rhode's model; Schmidt and Miller's model; and Walker's exponential model.

N86-28461*# National Aeronautics and Space Administration. Lewis Research Center, Cleveland, Ohio.

STRUCTURAL ANALYSIS OF TURBINE BLADES USING UNIFIED CONSTITUTIVE MODELS

A. KAUFMAN, M. TONG, J. F. SALTSMAN, and G. R. HALFORD

1986 12 p Proposed for presentation at the International Conference on Computers in Engine Technology, Cambridge, England, 24-27 Mar. 1987; sponsored by the Institution of Mechanical Engineers

(NASA-TM-88807; E-3155; NAS 1.15:88807) Avail: NTIS HC

A02/MF A01 CSCL 20K

The utility of advanced constitutive models and structural analysis methods in predicting the cyclic life of an air-cooled turbine blade is assessed. Five structural analysis methods were exercised in calculating the cyclic stress-strain response at the airfoil critical location. The methods studied were a cyclic elastic finite-element analysis, nonlinear finite-element analyses based on classical inelastic models and the unified models of Bodner and Walker, and a simplified inelastic procedure. These analyses were compared in terms of computing times and of predicted crack initiation lives using the Strainrange Partitioning method. Author

N86-28462*# Georgia Inst. of Tech., Atlanta. School of Engineering Science and Mechanics.

FORMULATION OF THE NONLINEAR ANALYSIS OF SHELL-LIKE STRUCTURES, SUBJECTED TO TIME-DEPENDENT MECHANICAL AND THERMAL LOADING Interim Technical Report, 15 Apr. 1984 - 14 Apr. 1986

G. J. SIMITSES, R. L. CARLSON, and R. RIFF 28 Jul. 1986 178 p

(Contract NAG3-534)

(NASA-CR-177194; NAS 1.26:177194) Avail: NTIS HC A09/MF

A01 CSCL 20K

A general mathematical model and solution methodologies for analyzing the structural response of thin, metallic shell structures under large transient, cyclic, or static thermomechanical loads was sought. Among the system responses associated with these loads and conditions are thermal buckling, creep buckling, and ratcheting. Thus geometric and material nonlinearities (of high order) can be anticipated and must be considered in developing the mathematical model. A complete, true ab-initio rate theory of kinematics and kinetics for continuum and curved thin structures, without any restriction on the magnitude of the strains or the deformations, was formulated. The time dependence and large strain behavior are incorporated through the introduction of the time rates of metric and curvature in two coordinate systems: fixed (spatial) and convected (material). The relations between the time derivative and the covariant derivative (gradient) was developed for curved space and motion, so the velocity components supply the connection between the equations of motion and the time rates of change of the metric and curvature tensors. A time and temperature dependent viscoplasticity model was formulated to account for finite strains and rotations. Author

N86-28464*# National Aeronautics and Space Administration. Lewis Research Center, Cleveland, Ohio.

THERMAL-FATIGUE AND OXIDATION RESISTANCE OF COBALT-MODIFIED UDIMET 700 ALLOY

P. T. BIZON and B. J. BARROW Apr. 1986 15 p

(NASA-TP-2591; E-2704; NAS 1.60:2591) Avail: NTIS HC

A02/MF A01 CSCL 20K

Comparative thermal-fatigue and oxidation resistances of cobalt-modified wrought Udimet 700 alloy (obtained by reducing the cobalt level by direct substitution of nickel) were determined from fluidized-bed tests. Bed temperatures were 1010 and 288 C (1850 and 550 C) for the first 5500 symmetrical 6-min cycles. From cycle 5501 to the 14000-cycle limit of testing, the heating bed temperature was increased to 1050 C (1922 F). Cobalt levels between 0 and 17 wt% were studied in both the bare and NiCrAlY overlay coated conditions. A cobalt level of about 8 wt% gave the best thermal-fatigue life. The conventional alloy specification is for 18.5% cobalt, and hence, a factor of 2 in savings of cobalt could be achieved by using the modified alloy. After 13500 cycles, all bare cobalt-modified alloys lost 10 to 13 percent of their initial weight. Application of the NiCrAlY overlay coating resulted in weight losses of 1/20 to 1/100 of that of the corresponding bare alloy. Author

N86-28467*# Virginia Polytechnic Inst. and State Univ., Blacksburg. Dept. of Engineering Science and Mechanics.

J-INTEGRAL ESTIMATES FOR CRACKS IN INFINITE BODIES Final Report

N. E. DOWLING Jul. 1986 42 p

(Contract NAG3-438)

(NASA-CR-179474; NAS 1.26:179474) Avail: NTIS HC A03/MF

A01 CSCL 20K

An analysis and discussion is presented of existing estimates of the J-integral for cracks in infinite bodies. Equations are presented which provide convenient estimates for Ramberg-Osgood type elastoplastic materials containing cracks and subjected to multiaxial loading. The relationship between J and the strain normal to the crack is noted to be only weakly dependent on state of stress. But the relationship between J and the stress normal to the crack is strongly dependent on state of stress. A plastic zone correction term often employed is found to be arbitrary, and its magnitude is seldom significant. Author

N86-29271*# National Aeronautics and Space Administration. Lewis Research Center, Cleveland, Ohio.

EXPERIMENTAL CLASSICAL FLUTTER REESULTS OF A COMPOSITE ADVANCED TURBOPROP MODEL

O. MEHMED and K. R. V. KAZA Jul. 1986 18 p Presented at the Biplinghoff Memorial Symposium on Recent Trends in Aeroelasticity, Structures and Structural Dynamics, Gainesville, Fla., 6-7 Feb., 1986; sponsored by Fla. Univ.

(NASA-TM-88792; E-3127; NAS 1.15:88792) Avail: NTIS HC

A02/MF A01 CSCL 20K

Experimental results are presented that show the effects of blade pitch angle and number of blades on classical flutter of a composite advanced turboprop (propfan) model. An increase in the number of blades on the rotor or the blade pitch angle is destabilizing which shows an aerodynamic coupling or cascade effect between blades. The flutter came in suddenly and all blades vibrated at the same frequency but at different amplitudes and with a common predominant phase angle between consecutive blades. This further indicates aerodynamic coupling between blades. The flutter frequency was between the first two blade normal modes, signifying an aerodynamic coupling between the normal modes. Flutter was observed at all blade pitch angles from small to large angles-of-attack of the blades. A strong blade response occurred, for four blades at the two-per-revolution (2P) frequency, when the rotor speed was near the crossing of the flutter mode frequency and the 2P order line. This is because the damping is low near the flutter condition and the interblade phase angle of the flutter mode and the 2P response are the same. Author

N86-30227*# Texas A&M Univ., College Station. Dept. of Aerospace Engineering.

INTEGRATED RESEARCH IN CONSTITUTIVE MODELLING AT ELEVATED TEMPERATURES, PART 1 Final Report

W. E. HAISLER and D. H. ALLEN Jun. 1986 332 p

(Contract NAG3-491)

(NASA-CR-177237; NAS 1.26:177237; MM-4998-86-13-PT-1)

Avail: NTIS HC A15/MF A01 CSCL 20K

Topics covered include: numerical integration techniques; thermodynamics and internal state variables; experimental lab development; comparison of models at room temperature; comparison of models at elevated temperature; and integrated software development.

N86-30236*# Cleveland State Univ., Ohio. Dept. of Civil Engineering.

COMPLIANCE MATRICES FOR CRACKED BODIES Final Report

R. BALLARINI Jul. 1986 8 p

(Contract NCC3-46)

(NASA-CR-179478; E-3158; NAS 1.26:179478) Avail: NTIS HC

A02/MF A01 CSCL 20K

An algorithm is presented which can be used to develop compliance matrices for cracked bodies. The method relies on the numerical solution of singular integral equations with Cauchy-type kernels and provides an efficient and accurate procedure for relating applied loadings to crack opening displacements. The algorithm should be of interest to those performing repetitive calculations in the analysis of experimental results obtained from fracture specimens. Author

N86-31920*# National Aeronautics and Space Administration. Lewis Research Center, Cleveland, Ohio.

INFLUENCE OF THIRD-DEGREE GEOMETRIC NONLINEARITIES ON THE VIBRATION AND STABILITY OF PRETWISTED, PRECONED, ROTATING BLADES

K. B. SUBRAHMANYAM and K. R. V. KAZA May 1986 43 p

(NASA-TM-87307; E-2988; NAS 1.15:87307) Avail: NTIS HC

A03/MF A01 CSCL 20K

The governing coupled flapwise bending, edgewise bending, and torsional equations are derived including third-degree geometric nonlinear elastic terms by making use of the geometric nonlinear theory of elasticity in which the elongations and shears are negligible compared to unity. These equations are specialized for blades of doubly symmetric cross section with linear variation of pretwist over the blade length. The nonlinear steady state equations and the linearized perturbation equations are solved by using the Galerkin method, and by utilizing the nonrotating normal modes for the shape functions. Parametric results obtained for various cases of rotating blades from the present theoretical formulation are compared to those produced from the finite element code MSC/NASTRAN, and also to those produced from an in-house experimental test rig. It is shown that the spurious instabilities, observed for thin, rotating blades when second degree geometric nonlinearities are used, can be eliminated by including the third-degree elastic nonlinear terms. Furthermore, inclusion of third degree terms improves the correlation between the theory and experiment. M.G.

ENERGY PRODUCTION AND CONVERSION

Includes specific energy conversion systems, e.g., fuel cells; global sources of energy; geophysical conversion; and windpower.

A86-12673* National Aeronautics and Space Administration. Lewis Research Center, Cleveland, Ohio.

THE EFFECT OF A DEFECTIVE BSF LAYER ON SOLAR CELL OPEN CIRCUIT VOLTAGE

V. G. WEIZER (NASA, Lewis Research Center, Cleveland, OH) Solar Cells (ISSN 0379-6787), vol. 14, July 1985, p. 241-248.

A straightforward analysis of special limiting cases has permitted the determination of the range of possible open circuit voltage losses due to a defective BSF (back surface field) layer. An important result of the analysis is the finding that it is possible to have a fully effective BSF region, regardless of the spatial distribution of the defective areas, as long as the total defective area is reduced below certain limits. Distributed defects were found to be much more harmful than lumped defects. Author

A86-24799* National Aeronautics and Space Administration. Lewis Research Center, Cleveland, Ohio.

DESIGN PRINCIPLES FOR NICKEL-HYDROGEN CELLS AND BATTERIES

L. H. THALLER, M. A. MANZO, and O. D. GONZALEZ-SANABRIA (NASA, Lewis Research Center, Cleveland, OH) IN: Intersociety Energy Conversion Engineering Conference, 20th, Miami Beach, FL, August 18-23, 1985, Proceedings. Volume 1. Warrendale, PA, Society of Automotive Engineers, Inc., 1985, p. 1.145-1.150. Previously announced in STAR as N85-31646.

Nickel-hydrogen cells and, more recently, bipolar batteries have been built by a variety of organizations. The design principles that have been used by the technology group at the NASA Lewis Research Center draw upon their extensive background in separator technology, alkaline fuel cell technology, and several alkaline cell technology areas. These design principles have been incorporated into both the more contemporary individual pressure vessel (IPV) designs that were pioneered by other groups, as well as the more recent bipolar battery designs using active cooling that are being developed at NASA Lewis Research Center and under contract. These principles are rather straightforward applications of capillary force formalisms, coupled with the slowly developing data base resulting from careful post test analyses. The objective of this overall effort is directed towards the low-earth-orbit (LEO) application where the cycle life requirements are much more severe than the geosynchronous-orbit (GEO) application. A summary of the design principles employed is presented along with a discussion of the recommendations for component pore sizes and pore size distributions, as well as suggested materials of construction. These will be made based on our experience in these areas to show how these design principles have been translated into operating hardware. Author

A86-24800* National Aeronautics and Space Administration. Lewis Research Center, Cleveland, Ohio.

INITIAL PERFORMANCE OF ADVANCED DESIGNS FOR IPV NICKEL-HYDROGEN CELLS

J. J. SMITHRICK (NASA, Lewis Research Center, Cleveland, OH) IN: Intersociety Energy Conversion Engineering Conference, 20th, Miami Beach, FL, August 18-23, 1985, Proceedings. Volume 1. Warrendale, PA, Society of Automotive Engineers, Inc., 1985, p. 1.151-1.157. Previously announced in STAR as N85-28444. refs

Advanced designs for individual pressure vessel nickel hydrogen cells were conceived which should improve the life cycle at deep depths of discharge and improve thermal management. Features of the designs which are new and not incorporated in either of the contemporary cells (Air Force/Hughes, Comsat) are: (1) the use of alternate methods of oxygen recombination, (2) use of serrated edge separators to facilitate movement of gas within the

44 ENERGY PRODUCTION AND CONVERSION

cell while still maintaining required physical contact with the wall wick, and (3) use of an expandable stack to accommodate some of the nickel electrode expansion. The designs also consider electrolyte volume requirements over the life of the cells, and are fully compatible with the Air Force/Hughes design. R.J.F.

A86-24802* Hughes Research Labs., Malibu, Calif. **KOH CONCENTRATION EFFECT ON THE CYCLE LIFE OF NICKEL-HYDROGEN CELLS**

H. S. LIM and S. A. VERZWYVELT (Hughes Research Laboratories, Malibu, CA) IN: Intersociety Energy Conversion Engineering Conference, 20th, Miami Beach, FL, August 18-23, 1985, Proceedings. Volume 1. Warrendale, PA, Society of Automotive Engineers, Inc., 1985, p. 1.165-1.170. refs (Contract NAS3-22238)

Effects of KOH concentration on the cycle life of a sintered-type nickel electrode were studied in a boiler plate nickel-hydrogen cell at 23 C using an accelerated 45-min cycle regime at 80 percent depth of discharge. The cycle life improved greatly as the KOH concentration decreased, although the initial capacity of the cell decreased slightly. The cycle life improved by a factor of two or more when the KOH concentration was reduced from 36 to 31 percent and by a similar factor from reductions of 31 to 26 percent. For many applications, this life improvement may outweigh the initial capacity decrease. Author

A86-24823* Ford Aerospace and Communications Corp., Palo Alto, Calif.

BIPOLAR NICKEL-HYDROGEN BATTERY DEVELOPMENT

C. W. KOEHLER, A. Z. APPLEWHITE (Ford Aerospace and Communications Corp., Palo Alto, CA), A. M. HALL, and P. G. RUSSELL (Yardney Corp., Battery Div., Pawcatuck, CT) IN: Intersociety Energy Conversion Engineering Conference, 20th, Miami Beach, FL, August 18-23, 1985, Proceedings. Volume 1. Warrendale, PA, Society of Automotive Engineers, Inc., 1985, p. 1.339-1.345.

(Contract NAS3-23879)

A comparison of the bipolar Ni-H₂ battery with other energy systems to be used in future high-power space systems is presented. The initial design for the battery under the NASA-sponsored program is described and the candidate stack components are evaluated, including electrodes, separator, electrolyte reservoir plate, and recombination sites. The compressibility of the cell elements, electrolyte activation, and thermal design are discussed. Manufacturing and prototype test results are summarized. C.D.

A86-24824* National Aeronautics and Space Administration. Lewis Research Center, Cleveland, Ohio.

LIFE CYCLE TEST RESULTS OF A BIPOLAR NICKEL HYDROGEN BATTERY

R. L. CATALDO (NASA, Lewis Research Center, Cleveland, OH) IN: Intersociety Energy Conversion Engineering Conference, 20th, Miami Beach, FL, August 18-23, 1985, Proceedings. Volume 1. Warrendale, PA, Society of Automotive Engineers, Inc., 1985, p. 1.346-1.351. Previously announced in STAR as N85-30480.

A history of low earth orbit laboratory test data on a 6.5 Ah bipolar nickel hydrogen battery designed and built at the NASA Lewis Research Center is presented. During the past several years the storage and Thermal Branch has been deeply involved in the design, development, and optimization of nickel hydrogen devices. The bipolar concept is a means of achieving the goal of producing an acceptable battery of higher energy density, able to withstand the demands of low earth orbiter regimes. Author

A86-24840* Massachusetts Inst. of Tech., Cambridge.

A PRELIMINARY STUDY OF THE MODIFIED ERICSSON FOR SPACE POWER

J. BERNER, J. F. LOUIS (MIT, Cambridge, MA), and A. JUHASZ (NASA, Lewis Research Center, Cleveland, OH) IN: Intersociety Energy Conversion Engineering Conference, 20th, Miami Beach, FL, August 18-23, 1985, Proceedings. Volume 1. Warrendale, PA, Society of Automotive Engineers, Inc., 1985, p. 1.452-1.458.

Simple modifications of the Ericsson cycle are analyzed for their application as high power, compact and reliable space power systems. They use the same components as the technologically advanced and reliable Brayton system. These modifications approximate the Ericsson cycle's isothermal expansion by several stages of expansion with reheat and the isothermal compression by several compression stages with intercooling. Preliminary cycle analysis including non-ideal components indicates potential advantages in both power per unit area and efficiency over the Brayton system. Evaluation of the system mass indicates a significant mass and radiator area advantage of a Modified Ericsson cycle using one reheat and one expansion stage when a high temperature titanium radiator is used. Whereas the configuration using one reheat and one intercooling with two stages of compression and expansion provided the lowest mass per unit power using a lower temperature aluminum radiator. Author

A86-24849* National Aeronautics and Space Administration. Lewis Research Center, Cleveland, Ohio.

CYCLING PERFORMANCE OF THE IRON-CHROMIUM REDOX ENERGY STORAGE SYSTEM

R. F. GAHN, N. H. HAGEDORN, and J. A. JOHNSON (NASA, Lewis Research Center, Cleveland, OH) IN: Intersociety Energy Conversion Engineering Conference, 20th, Miami Beach, FL, August 18-23, 1985, Proceedings. Volume 2. Warrendale, PA, Society of Automotive Engineers, Inc., 1985, p. 2.91-2.97. Previously announced in STAR as N85-27387. refs

Extended charge-discharge cycling of this electrochemical storage system at 65 C was performed on 14.5 sq cm single cells and a four cell, 867 sq cm bipolar stack. Both the anolyte and catholyte reactant fluids contained 1 molar concentrations of iron and chromium chlorides in hydrochloric acid and were separated by a low-selectivity, cation-exchange membrane. The effect of cycling on the chromium electrode and the cation-exchange membrane was determined. Bismuth and bismuth-lead catalyzed chromium electrodes and a radiation-grafted polyethylene membrane were evaluated by cycling between 5 and 85 percent state-of-charge at 80 mA/sq cm and by periodic charge-discharge polarization measurements to 140 mA/sq cm. Gradual performance losses were observed during cycling but were recoverable by completely discharging the system. Good scale-up to the 867 sq cm stack was achieved. The only difference appeared to be an unexplained resistive-type loss which resulted in a 75 percent W-hr efficiency (at 80 mA/sq cm versus 81 percent for the 14.5 sq cm cell). A new rebalance cell was developed to maintain reactant ionic balance. The cell successfully reduced ferric ions in the iron reactant stream to ferrous ions while chloride ions were oxidized to chlorine gas. Author

A86-24888* Stirling Thermal Motors, Inc., Ann Arbor, Mich. **LIQUID FUELED EXTERNAL HEATING SYSTEM FOR STM4-120 STIRLING ENGINE**

R. J. MEIJER, B. ZIPH, and T. M. GODETT (Stirling Thermal Motors, Inc., Ann Arbor, MI) IN: Intersociety Energy Conversion Engineering Conference, 20th, Miami Beach, FL, August 18-23, 1985, Proceedings. Volume 3. Warrendale, PA, Society of Automotive Engineers, Inc., 1985, p. 3.231-3.237. refs (Contract NAS3-23888)

The STM4-120 Stirling engine, currently under development at Stirling Thermal Motors, Inc., is a 40 kW variable stroke engine with indirect heating using a sodium heat pipe. The engine is functionally separated into an application independent Energy Conversion Unit (ECU) consisting of the Stirling cycle and drive heated by condensing sodium and the application dependent External Heating System (EHS), designed to supply the ECU with

sodium vapor heated by the particular energy source, connected by tubes with mechanical couplings. This paper describes an External Heating System for the STM4-120 ECU designed for the combustion of liquid fuel, comprised of a recuperative preheater, a combustion chamber, and a heat exchanger/evaporator where heat is transferred from the flue gas to the sodium causing it to evaporate. The design concept and projected performance are described and discussed. Author

A86-24889* National Aeronautics and Space Administration. Lewis Research Center, Cleveland, Ohio.

TEST RESULTS OF A 40 KW STIRLING ENGINE AND COMPARISON WITH THE NASA-LEWIS COMPUTER CODE PREDICTIONS

D. ALLEN (NASA, Lewis Research Center; Sverdrup Technology, Inc., Cleveland, OH) and J. CAIRELLI (NASA, Lewis Research Center, Cleveland, OH) IN: Intersociety Energy Conversion Engineering Conference, 20th, Miami Beach, FL, August 18-23, 1985, Proceedings. Volume 3. Warrendale, PA, Society of Automotive Engineers, Inc., 1985, p. 3.238-3.243.

A Stirling engine was tested without auxiliaries at NASA-Lewis. Three different regenerator configurations were tested with hydrogen. The test objectives were (1) to obtain steady-state and dynamic engine data, including indicated power, for validation of an existing computer model for this engine; and (2) to evaluate structurally the use of silicon carbide regenerators. This paper presents comparisons of the measured brake performance, indicated mean effective pressure, and cyclic pressure variations with those predicted by the code. The measured data tended to be lower than the computer code predictions. The silicon carbide foam regenerators appear to be structurally suitable, but the foam matrix tested severely reduced performance. Author

A86-40579* National Aeronautics and Space Administration. Lewis Research Center, Cleveland, Ohio.

DESIGN CONSIDERATIONS FOR ADVANCED BATTERY CONCEPTS

H. F. LEIBECKI and L. H. THALLER (NASA, Lewis Research Center, Cleveland, OH) IN: Space Systems Technology Conference, San Diego, CA, June 9-12, 1986, Technical Papers. New York, American Institute of Aeronautics and Astronautics, 1986, p. 15-21. refs (AIAA PAPER 86-1164)

A mathematical representation for the charge and discharge of a sodium-sulfur cell is developed. These equations are then used as the basis for a computerized model to examine the effects of cell arrangement in the design of a large multi-kilowatt battery from a group of hypothetical individual cells with known variations in their ampere hour capacity and internal resistance. The cycling characteristics of 216 individual cells arranged in six different configurations are evaluated with the view towards minimizing the adverse effects that are introduced due to the stochastic aspects of groupings of cells, as well as the possibility of cell failures in both the open and shorted mode. Although battery systems based on sodium-sulfur cells are described in this example, any of the newer electrochemical systems can be fitted into this framework by making appropriate modifications to the basic equations. Author

A86-49215* National Aeronautics and Space Administration. Lewis Research Center, Cleveland, Ohio.

MINORITY-CARRIER MOBILITY ANOMALIES IN LOW-RESISTIVITY SILICON SOLAR CELLS

V. G. WEIZER and R. DELOMBARD (NASA, Lewis Research Center, Cleveland, OH) Applied Physics Letters (ISSN 0003-6951), vol. 49, July 28, 1986, p. 201-203. refs

Measurement of the minority-carrier mobility in the base region of a high-voltage metal-insulator-N-P solar cell (Green et al., 1984), as well as in other 0.1-ohm cm cells, provides direct proof that the high voltages measured for that cell are due not only to improved emitter characteristics but to an improved base region as well. The base characteristics are shown to be quite sensitive to the effects of diffusion-induced lattice stress originating in the

emitter. The implications of these findings for the fabrication of high-efficiency cells are discussed. Author

N86-10643* National Aeronautics and Space Administration. Lewis Research Center, Cleveland, Ohio.

PHOTOVOLTAIC SYSTEMS IN REMOTE LOCATIONS: AN EXPERIENCE SUMMARY Final Report

A. F. RATAJCZAK 1985 19 p refs Presented at the Solar Appl. in Remote Locations Workshop, Las Cruces, N. Mex., 11-14 Mar. 1985

(Contract DE-AI01-79ET-20485)

(NASA-TM-87106; E-2703; DOE/NASA/20485-20; NAS 1.15:87106) Avail: NTIS HC A02/MF A01 CSCL 10A

Since 1979, the NASA Lewis Research Center has been responsible for the design, installation and operational support of 58 photovoltaic systems located in 27 countries. Together these systems contain 77.1 kW of photovoltaic modules and provide power for a variety of loads ranging from single low-power street light systems to a utility type power system for a village of over 150 people. Systems installation, reliability, operation, maintenance and repair experience is given and major problem areas are listed. Experience indicates that photovoltaic system technology is a proven technology, but that developing countries need to better posture themselves to acquire and utilize the technology. Recommendations are given. Author

N86-11666* National Aeronautics and Space Administration. Lewis Research Center, Cleveland, Ohio.

PHOTOVOLTAIC-POWERED VACCINE REFRIGERATOR: FREEZER SYSTEMS FIELD TEST RESULTS Final Report

A. F. RATAJCZAK Aug. 1985 99 p

(Contract DE-AI01-79ET-20485; PASA-NASA/DSB-5710-2-79)

(NASA-TM-86972-REV; E-2498; DOE/NASA/20485-18; NAS 1.15:86972-REV) Avail: NTIS HC A05/MF A01 CSCL 10B

A project to develop and field test photovoltaic-powered refrigerator/freezers suitable for vaccine storage was undertaken. Three refrigerator/freezers were qualified; one by Solar Power Corp. and two by Solvolt. Follow-on contracts were awarded for 19 field test systems and for 10 field test systems. A total of 29 systems were installed in 24 countries between October 1981 and October 1984. The project, systems descriptions, installation experiences, performance data for the 22 systems for which field test data was reported, an operational reliability summary, and recommendations relative to system designs and future use of such systems are explained. Performance data indicate that the systems are highly reliable and are capable of maintaining proper vaccine storage temperatures in a wide range of climatological and user environments. Author

N86-11667* Michigan State Univ., East Lansing. Div. of Engineering Research.

EFFECT OF ACCURACY OF WIND POWER PREDICTION ON POWER SYSTEM OPERATOR Final Report

R. A. SCHLUETER, G. SIGARI, and T. COSTI Jun. 1985 188 p refs

(Contract NAG3-399)

(NASA-CR-176300; NAS 1.26:176300; MSU-ENGR-85-026)

Avail: NTIS HC A09/MF A01 CSCL 10B

This research project proposed a modified unit commitment that schedules connection and disconnection of generating units in response to load. A modified generation control is also proposed that controls steam units under automatic generation control, fast responding diesels, gas turbines and hydro units under a feedforward control, and wind turbine array output under a closed loop array control. This modified generation control and unit commitment require prediction of trend wind power variation one hour ahead and the prediction of error in this trend wind power prediction one half hour ahead. An improved meter for predicting trend wind speed variation is developed. Methods for accurately simulating the wind array power from a limited number of wind speed prediction records was developed. Finally, two methods for predicting the error in the trend wind power prediction were developed. This research provides a foundation for testing and

44 ENERGY PRODUCTION AND CONVERSION

evaluating the modified unit commitment and generation control that was developed to maintain operating reliability at a greatly reduced overall production cost for utilities with wind generation capacity. Author

N86-11668*# National Aeronautics and Space Administration. Lewis Research Center, Cleveland, Ohio.

RE-1000 FREE-PISTON STIRLING ENGINE UPDATE

J. G. SCHREIBER 1985 20 p refs Presented at the 20th Intersoc. Energy Conversion Eng. Conf., Miami Beach, Fla., 18-23 Aug. 1985

(Contract DE-AI05-82OR-1005)

(NASA-TM-87126; E-2597; DOE/NASA/1005-6; NAS 1.15:87126)

Avail: NTIS HC A02/MF A01 CSCL 10B

A free piston Stirling engine was tested. The tests performed over the past several years on the single cylinder engine were designed to investigate the dynamics of a free piston Stirling engine. The data are intended to be used primarily for computer code validation. The tests designed to investigate the sensitivity of the engine performance to variations in working space pressure, heater and cooler temperatures, regenerator porosity, power piston mass and displacer dynamics were completed. In addition, some data were recorded with alternate working fluids. A novel resonant balance system for the engine was also tested. Some preliminary test results of the tests performed are presented along with an outline of future tests to be run with the engine coupled to a hydraulic output unit. A description of the hydraulic output unit is given. Author

N86-11670*# Michigan State Univ., East Lansing. Div. of Engineering Research.

AC MOTOR AND GENERATOR REQUIREMENTS FOR ISOLATED WECS

G. L. PARK, P. J. MCCLEER (Michigan Univ.), B. HANSON (SWX Corp.), B. WEINBERG, and O. KRAUSS Oct. 1985 82 p refs (Contract NAG3-530)

(NASA-CR-176315; DOE/NASA/0530-1; NAS 1.26:176315)

Avail: NTIS HC A05/MF A01 CSCL 10A

After surveying electrically driven loads used on productive farms, the investigators chose three pumps for testing at voltages and frequencies far outside the normal operating range. These loads extract and circulate water and move heat via air, and all are critical to farm productivity. The object was to determine the envelope of supply voltage and frequency over which these loads would operate stably for time intervals under 1 hour. This information is among that needed to determine the feasibility of supplying critical loads, in case of a utility outage, from a wind driven alternator whose output voltage and frequency will vary dramatically in most continental wind regimes. Other related work is surveyed. The salient features and limitations of the test configurations used and the data reduction are described. The development of simulation models suitable for a small computer are outlined. The results are primarily displayed on the voltage frequency plane with the general conclusion that the particular pump models considered will operate over the range of 50 to 90 Hz and a voltage band which starts below rated, decreases as frequency decreases, and is limited on the high side by excessive motor heating. For example, centrifugal pump operating voltage ranges as extensive .4 to 1.4 appear possible. Particular problems with starting, stalling due to lack of motor torque, high speed cavitation, and likely overheating are addressed in a listing of required properties for wind driven alternators and their controllers needed for use in the isolated or stand alone configuration considered. Author

N86-11671*# National Aeronautics and Space Administration. Lewis Research Center, Cleveland, Ohio.

A 25.5 PERCENT AMO GALLIUM ARSENIDE GRATING SOLAR CELL

V. G. WEIZER and M. P. GODLEWSKI 1985 10 p refs Presented at the 18th Photovoltaic Specialists Conf., Las Vegas, Nev., 21-25 Oct. 1985; sponsored by IEEE

(NASA-TM-87134; E-2748; NAS 1.15:87134) Avail: NTIS HC

A02/MF A01 CSCL 10A

Recent calculations have shown that significant open circuit voltage gains are possible with a dot grating junction geometry. The feasibility of applying the dot geometry to the GaAs cell was investigated. This geometry is shown to result in voltages approach 1.120 V and efficiencies well over 25 percent (AMO) if good collection efficiency can be maintained. The latter is shown to be possible if one chooses the proper base resistivity and cell thickness. The above advances in efficiency are shown to be possible in the P-base cell with only minor improvements in existing technology. Author

N86-12757*# Engelhard Corp., Edison, N.J. Specialty Chemicals Div.

DEVELOP AND TEST FUEL CELL POWERED ON-SITE INTEGRATED TOTAL ENERGY SYSTEMS: PHASE 3, FULL-SCALE POWER PLANT DEVELOPMENT Quarterly Technical Progress Report, Aug. - Oct. 1984

A. KAUFMAN, S. PUDICK, C. L. WANG, J. WERTH, and J. A. WHELAN 17 May 1985 15 p

(Contract DEN3-241; DE-AI01-80ET-17088)

(NASA-CR-174948; DOE/NASA-0241-15; NAS 1.26:174948;

QR-14) Avail: NTIS HC A02/MF A01 CSCL 10B

Two 25 cell stacks of the 13 inch x 23 inch cell size (about 4kW) remain on test after 4000 hours and 2900 hours, respectively, using simulated reformat fuel. These tests are focusing on the durability of fuel cell stack components developed through the end of 1983. Also, these stacks are serving as forerunners of a 25kW stack that will contain 175 cells of the same size and will employ the same technology base. The stack technology development program has focused on a new, low cost bipolar plate edge seal technique and evaluation of advanced cathode catalysts, an electrolyte replenishment system, and nonmetallic cooling plates in small stacks. Author

N86-12758*# Engelhard Corp., Edison, N.J. Specialty Chemicals Div.

DEVELOP AND TEST FUEL CELL POWERED ON-SITE INTEGRATED TOTAL ENERGY SYSTEMS: PHASE 3, FULL-SCALE POWER PLANT DEVELOPMENT Quarterly Technical Progress Report, Feb. - Apr. 1985

A. KAUFMAN, S. PUDICK, C. L. WANG, J. WERTH, and J. A. WHELAN 22 Jul. 1985 25 p

(Contract DEN3-241; DE-AI01-80ET-17088)

(NASA-CR-174998; DOE/NASA-0241-17; NAS 1.26:174998;

QR-16) Avail: NTIS HC A02/MF A01 CSCL 10B

A 25 cell stack of the 13 inch x 23 inch cell size (about 4kW) remains on test after 6000 hours, using simulated reformat fuel. A similar stack was previously shut down after 7000 hours on load. These tests were carried out for the purpose of assessing the durability of fuel cell stack components developed through the end of 1983. In light of the favorable results obtained, a 25kW stack that will contain 175 cells of the same size is being constructed using the same technology base. The components for the 25kW stack have been completed. A methanol steam reformer with a design output equivalent to 50kW has been constructed to serve as a hydrogen generator for the 25kW stack. This reformer and the balance of the fuel processing sub system are currently being tested and debugged. The stack technology development program focused on cost reduction in bipolar plates, nonmetallic cooling plates, and current collecting plates; more stable cathode catalyst support materials; more corrosion resistant metal hardware; and shutdown/start up tolerance. Author

N86-14727*# Case Western Reserve Univ., Cleveland, Ohio.
COMBUSTOR FLAME FLASHBACK Final Report
 M. P. PROCTOR and J. S. TIEN Jun. 1985 82 p refs
 (Contract NAG3-290; DE-AI01-77CS-51040)
 (NASA-CR-174961; DOE/NASA/0290-1; NAS 1.26:174961)
 Avail: NTIS HC A05/MF A01 CSCL 10B

A stainless steel, two-dimensional (rectangular), center-dump, premixed-prevaporized combustor with quartz window sidewalls for visual access was designed, built, and used to study flashback. A parametric study revealed that the flashback equivalence ratio decreased slightly as the inlet air temperature increased. It also indicated that the average premixer velocity and premixer wall temperature were not governing parameters of flashback. The steady-state velocity balance concept as the flashback mechanism was not supported. From visual observation several stages of burning were identified. High speed photography verified upstream flame propagation with the leading edge of the flame front near the premixer wall. Combustion instabilities (spontaneous pressure oscillations) were discovered during combustion at the dump plane and during flashback. The pressure oscillation frequency ranged from 40 to 80 Hz. The peak-to-peak amplitude (up to 1.4 psi) increased as the fuel/air equivalence ratio was increased attaining a maximum value just before flashback. The amplitude suddenly decreased when the flame stabilized in the premixer. The pressure oscillations were large enough to cause a local flow reversal. A simple test using ceramic fiber tufts indicated flow reversals existed at the premixer exit during flickering. It is suspected that flashback occurs through the premixer wall boundary layer flow reversal caused by combustion instability. A theoretical analysis of periodic flow in the premixing channel has been made. The theory supports the flow reversal mechanism. R.J.F.

N86-15722*# General Electric Co., Philadelphia, Pa. Advanced Energy Programs Dept.
MOD-5A WIND TURBINE GENERATOR PROGRAM DESIGN REPORT. VOLUME 2: CONCEPTUAL AND PRELIMINARY DESIGN, BOOK 1 Final Report, Jul. 1980 - Jun. 1984
 Aug. 1984 374 p 10 Vol.

(Contract DEN3-153; DE-AI01-79ET-20305)
 (NASA-CR-174735-VOL-2-BK-1; DOE/NASA/0153-VOL-2-BK-1;
 NAS 1.26:174735-VOL-2-BK-1; DOC-84AEPD004-VOL-2-BK-1)
 Avail: NTIS HC A16/MF A01 CSCL 10B

The design, development and analysis of the 7.3 MW MOD-5A wind turbine generator is documented. There are four volumes. In Volume 2, book 1 the requirements and criteria for the design are presented. The conceptual design studies, which defined a baseline configuration and determined the weights, costs and sizes of each subsystem, are described. The development and optimization of the wind turbine generator are presented through the description of the ten intermediate configurations between the conceptual and final designs. Analyses of the system's load and dynamics are presented. Author

N86-15723*# General Electric Co., Philadelphia, Pa. Advanced Energy Programs Dept.
MOD-5A WIND TURBINE GENERATOR PROGRAM DESIGN REPORT. VOLUME 2: CONCEPTUAL AND PRELIMINARY DESIGN, BOOK 2 Final Report, Jul. 1980 - Jun. 1984
 Aug. 1984 788 p refs 10 Vol.
 (Contract DEN3-153; DE-AI01-79ET-20305)
 (NASA-CR-174735-VOL-2-BK-2; DOE/NASA/0153-VOL-2-BK-2;
 NAS 1.26:174735-VOL-2-BK-2; DOC-84AEPD004-VOL-2-BK-2)
 Avail: NTIS HC A99/MF E03 CSCL 10B

The design, development and analysis of the 7.3 MW MOD-5A wind tunnel generator is documented. There are four volumes. In Volume 2, book 2 the requirements and criteria for the design are presented. The development tests, which determined or characterized many of the materials and components of the wind turbine generator, are described. Author

N86-15724*# General Electric Co., Philadelphia, Pa. Advanced Energy Programs Dept.
MOD-5A WIND TURBINE GENERATOR PROGRAM DESIGN REPORT. VOLUME 3: FINAL DESIGN AND SYSTEM DESCRIPTION, BOOK 1 Final Report, Jul. 1980 - Jun. 1984
 Aug. 1984 574 p 10 Vol.

(Contract DEN3-153; DE-AI01-79ET-20305)
 (NASA-CR-174735-VOL-3-BK-1; DOE/NASA/0153-VOL-3-BK-1;
 NAS 1.26:174735-VOL-3-BK-1; DOC-84AEPD004-VOL-3-BK-1)
 Avail: NTIS HC A24/MF A01 CSCL 10B

The design, development and analysis of the 7.3 MW MOD-5A wind turbine generator is documented. Volume 3, book 1 describes the performance and characteristics of the MOD-5A wind turbine generator in its final configuration. Each subsystem - the rotor, drivetrain, nacelle, tower and foundation is described in detail. Author

N86-15725*# General Electric Co., Philadelphia, Pa. Advanced Energy Programs Dept.
MOD-5A WIND TURBINE GENERATOR PROGRAM DESIGN REPORT. VOLUME 3: FINAL DESIGN AND SYSTEM DESCRIPTION, BOOK 2 Final Report, Jul. 1980 - Jun. 1984
 Aug. 1984 571 p 10 Vol.

(Contract DEN3-153; DE-AI01-79ET-20305)
 (NASA-CR-174735-VOL-3-BK-2; DOE/NASA/0153-VOL-3-BK-2;
 NAS 1.26:174735-VOL-3-BK-2; DOC-84AEPD004-VOL-3-BK-2)
 Avail: NTIS HC A24/MF A01 CSCL 10B

The design, development and analysis of the 7.3MW MOD-5A wind turbine generator is documented. The report is divided into four volumes: Volume 1 summarizes the entire MOD-5A program, Volume 2 discusses the conceptual and preliminary design phases, Volume 3 describes the final design of the MOD-5A, and Volume 4 contains the drawings and specifications developed for the final design. Volume 3, book 2 describes the performance and characteristics of the MOD-5A wind turbine generator in its final configuration. The subsystem for power generation, control, and instrumentation subsystems is described in detail. The manufacturing and construction plans, and the preparation of a potential site on Oahu, Hawaii, are documented. The quality assurance and safety plan, and analyses of failure modes and effects, and reliability, availability and maintainability are presented. Author

N86-15726*# General Electric Co., Philadelphia, Pa. Advanced Energy Programs Dept.
MOD-5A WIND TURBINE GENERATOR PROGRAM DESIGN REPORT. VOLUME 4: DRAWINGS AND SPECIFICATIONS, BOOK 1 Final Report, Jul. 1980 - Jun. 1984
 Aug. 1984 737 p refs 10 Vol.

(Contract DEN3-153; DE-AI01-79ET-20305)
 (NASA-CR-174735-VOL-4-BK-1; DOE/NASA/0153-VOL-4-BK-1;
 NAS 1.26:174735-VOL-4-BK-1; DOC-84AEPD004-VOL-4-BK-1)
 Avail: NTIS HC A99/MF E03 CSCL 10B

The design, development and analysis of the 7.3 MW MOD-5A wind turbine generator is documented. Volume 4 contains the drawings and specifications that were developed in preparation for building the MOD-5A wind turbine generator. This is the first of five books of volume four. It contains structural design criteria, generator step-up transformer specs, specs for design, fabrication and testing of the system, specs for the ground control enclosure, systems specs, slip ring specs, and control system specs. E.R.

44 ENERGY PRODUCTION AND CONVERSION

N86-15727*# General Electric Co., Philadelphia, Pa. Advanced Energy Programs Dept.

MOD-5A WIND TURBINE GENERATOR PROGRAM DESIGN REPORT. VOLUME 4: DRAWINGS AND SPECIFICATIONS, BOOK 2 Final Report, Jul. 1980 - Jun. 1984

Aug. 1984 450 p In NEPALI 10 Vol.
(Contract DEN3-153; DE-A101-79ET-20305)
(NASA-CR-174735-VOL-4-BK-2; DOE/NASA/0153-VOL-4-BK-2;
NAS 1.26:174735-VOL-4-BK-2; DOC-84AEPD004-VOL-4-BK-2)
Avail: NTIS HC A19/MF A01 CSCL 10B

The design, development and analysis of the 7.3 MW MOD-5A wind turbine generator is documented. There are four volumes. This volume contains the drawings and specifications that were developed in preparation for building the MOD-5A wind turbine generator. This is the second book of volume four. Some of the items it contains are specs for the emergency shutdown panel, specs for the simulator software, simulator hardware specs, site operator terminal requirements, control data system requirements, software project management plan, elastomeric teeter bearing requirement specs, specs for the controls electronic cabinet, and specs for bolt pretensioning. E.R.

N86-15728*# General Electric Co., Philadelphia, Pa. Advanced Energy Programs Dept.

MOD-5A WIND TURBINE GENERATOR PROGRAM DESIGN REPORT. VOLUME 4: DRAWINGS AND SPECIFICATIONS, BOOK 3 Final Report, Jul. 1980 - Jun. 1984

Aug. 1984 542 p 10 Vol.
(Contract DEN3-153; DE-A101-79ET-20305)
(NASA-CR-174735-VOL-4-BK-3; DOE/NASA/0153-VOL-4-BK-3;
NAS 1.26:174735-VOL-4-BK-3; DOC-84AEPD004-VOL-4-BK-3)
Avail: NTIS HC A23/MF A01 CSCL 10B

The design, development and analysis of the 7.3 MW MOD-5A wind turbine generator is documented. This volume contains the drawings and specifications developed for the final design. This volume is divided into 5 books of which this is the third, containing drawings 47A380074 through 47A380126. A full breakdown parts listing is provided as well as a where used list. E.R.

N86-15729*# General Electric Co., Philadelphia, Pa. Advanced Energy Programs Dept.

MOD-5A WIND TURBINE GENERATOR PROGRAM DESIGN REPORT. VOLUME 4: DRAWINGS AND SPECIFICATIONS, BOOK 4 Final Report, Jul. 1980 - Jun. 1984

Aug. 1984 622 p 10 Vol.
(Contract DEN3-153; DE-A101-79ET-20305)
(NASA-CR-174735-VOL-4-BK-4; DOE/NASA/0153-VOL-4-BK-4;
NAS 1.26:174735-VOL-4-BK-4; DOC-84AEPD004-VOL-4-BK-4)
Avail: NTIS HC A99/MF E03 CSCL 10B

The design, development and analysis of the 7.3 MW MOD-5A wind turbine generator are documented. There are four volumes. This volume contains the drawings and specifications that were developed in preparation for building the MOD-5A wind turbine generator. This volume contains 5 books of which this is the fourth, providing drawings 47A380128 through 47A387125. In addition to the parts listing and where-used list, the logic design of the controller software and the code listing of the controller software are provided. Also given are the aerodynamic profile coordinates. E.R.

N86-15730*# General Electric Co., Philadelphia, Pa. Advanced Energy Programs Dept.

MOD-5A WIND TURBINE GENERATOR PROGRAM DESIGN REPORT. VOLUME 4: DRAWINGS AND SPECIFICATIONS, BOOK 5 Final Report, Jul. 1980 - Jun. 1984

Aug. 1984 403 p 10 Vol.
(Contract DEN3-153; DE-A101-79ET-20305)
(NASA-CR-174735-VOL-4-BK-5; DOE/NASA/0153-VOL-4-BK-5;
NAS 1.26:174735-VOL-4-BK-5; DOC-84AEPD004-VOL-4-BK-5)
Avail: NTIS HC A18/MF A01 CSCL 10B

The design, development and analysis of the 7.3 MW MOD-5A wind turbine generator is documented. There are four volumes. This volume contains the drawings and specifications that were

developed in preparation for building the MOD-5A wind turbine generator. Detail drawings of several assemblies and subassemblies are given. This is the fifth book of volume 4.

Author

N86-17839*# National Aeronautics and Space Administration. Lewis Research Center, Cleveland, Ohio.

SPACE PHOTOVOLTAIC RESEARCH AND TECHNOLOGY 1985: HIGH EFFICIENCY, SPACE ENVIRONMENT, AND ARRAY TECHNOLOGY

1985 282 p refs Conference held in Cleveland, Ohio, 30 Apr. - 2 May 1985

(NASA-CP-2408; E-2706; NAS 1.55:2408) Avail: NTIS HC A13/MF A01 CSCL 10A

The seventh NASA Conference on Space Photovoltaic Research and Technology was held at NASA Lewis Research Center, Cleveland, Ohio, from 30 April until 2 May 1985. Its purpose was to assess the progress made, the problems remaining, and future strategy for space photovoltaic research. Particular emphasis was placed on high efficiency, space environment, and array technology.

N86-17843*# National Aeronautics and Space Administration. Lewis Research Center, Cleveland, Ohio.

GALLIUM ARSENIDE SOLAR CELL EFFICIENCY: PROBLEMS AND POTENTIAL

V. G. WEIZER and M. P. GODLEWSKI *In its* Space Photovoltaic Research and Technology 1985 p 41-50 1985 refs

Avail: NTIS HC A13/MF A01 CSCL 10A

Under ideal conditions the GaAs solar cell should be able to operate at an AMO efficiency exceeding 27 percent, whereas to date the best measured efficiencies barely exceed 19 percent. Of more concern is the fact that there has been no improvement in the past half decade, despite the expenditure of considerable effort. State-of-the-art GaAs efficiency is analyzed in an attempt to determine the feasibility of improving on the status quo. The possible gains to be had in the planar cell. An attempt is also made to predict the efficiency levels that could be achieved with a grating geometry. Both the N-base and the P-base BaAs cells in their planar configurations have the potential to operate at AMO efficiencies between 23 and 24 percent. For the former the enabling technology is essentially in hand, while for the latter the problem of passivating the emitter surface remains to be solved. In the dot grating configuration, P-base efficiencies approaching 26 percent are possible with minor improvements in existing technology. N-base grating cell efficiencies comparable to those predicted for the P-base cell are achievable if the N surface can be sufficiently passivated. Author

N86-17844*# Delaware Univ., Newark.

N/P GAAS CONCENTRATOR SOLAR CELLS WITH AN IMPROVED GRID AND BUSHBAR CONTACT DESIGN

G. C. DESALVO, E. H. MUELLER, and A. M. BARNETT *In* NASA. Lewis Research Center Space Photovoltaic Research and Technology 1985 p 51-59 1985 refs

(Contract NAG3-422)

Avail: NTIS HC A13/MF A01 CSCL 10A

The major requirements for a solar cell used in space applications are high efficiency at AMO irradiance and resistance to high energy radiation. Gallium arsenide, with a band gap of 1.43 eV, is one of the most efficient sunlight to electricity converters (25%) when the simple diode model is used to calculate efficiencies at AMO irradiance, GaAs solar cells are more radiation resistant than silicon solar cells and the N/P GaAs device has been reported to be more radiation resistant than similar P/N solar cells. This higher resistance is probably due to the fact that only 37% of the current is generated in the top N layer of the N/P cell compared to 69% in the top layer of a P/N solar cell. This top layer of the cell is most affected by radiation. It has also been theoretically calculated that the optimized N/P device will prove to have a higher efficiency than a similar P/N device. The use of a GaP window layer on a GaAs solar cell will avoid many of the inherent problems normally associated with a GaAlAs window

while still proving good passivation of the GaAs surface. An optimized circular grid design for solar cell concentrators has been shown which incorporates a multi-layer metallization scheme. This multi-layer design allows for a greater current carrying capacity for a unit area of shading, which results in a better output efficiency. Author

N86-17845*# Varian Associates, Palo Alto, Calif.
HIGH-EFFICIENCY ALGAAS-GAAS CASSEGRAINIAN CONCENTRATOR CELLS

J. G. WERTHEN, H. C. HAMAKER, G. F. VIRSHUP, C. R. LEWIS, and C. W. FORD /in NASA. Lewis Research Center Space Photovoltaic Research and Technology 1985 p 61-68 1985 refs

(Contract NAS3-23876)

Avail: NTIS HC A13/MF A01 CSCL 10A

AlGaAs-GaAs heteroface space concentrator solar cells have been fabricated by metalorganic chemical vapor deposition. AMO efficiencies as high as 21.1% have been observed both for p-n and np structures under concentration (90 to 100X) at 25 C. Both cell structures are characterized by high quantum efficiencies and their performances are close to those predicted by a realistic computer model. In agreement with the computer model, the n-p cell exhibits a higher short-circuit current density. Author

N86-17851*# National Aeronautics and Space Administration. Lewis Research Center, Cleveland, Ohio.

A POSSIBLE RADIATION-RESISTANT SOLAR CELL GEOMETRY USING SUPERLATTICES

C. GORADIA (Cleveland State Univ., Ohio), R. CLARK, and D. BRINKER (Cleveland State Univ., Ohio) /in its Space Photovoltaic Research and Technology 1985 p 111-118 1985 refs

Avail: NTIS HC A13/MF A01 CSCL 10A

A solar cell structure is proposed which uses a GaAs nipi doping superlattice. An important feature of this structure is that photogenerated minority carriers are very quickly collected in a time shorter than bulk lifetime in the fairly heavily doped n and p layers and these carriers are then transported parallel to the superlattice layers to selective ohmic contacts. Assuming that these already-separated carriers have very long recombination lifetimes, due to their across an indirect bandgap in real space, it is argued that the proposed structure may exhibit superior radiation tolerance along with reasonably high beginning-of-life efficiency. Author

N86-17856*# National Aeronautics and Space Administration. Lewis Research Center, Cleveland, Ohio.

RADIATION DAMAGE IN HIGH-RESISTIVITY SILICON SOLAR CELLS

I. WEINBERG, C. K. SWARTZ, and C. GORADIA (Cleveland State Univ., Ohio) /in its Space Photovoltaic Research and Technology 1985 p 159-163 1985 refs

Avail: NTIS HC A13/MF A01 CSCL 10A

High-resistivity silicon solar cells exhibit reduced radiation damage when light is incident on the gridded back surface. Under back illumination, radiation damage decreases as cell resistivity increases; under front illumination, radiation damage increases as cell resistivity increases. Thin back-illuminated cells outperform conventional 10 ohm cm 50 and 200 micron cells at low 1-MeV electron fluences. However, at higher fluences, the conventional cells exhibit superior radiation resistance. This is attributed to the low BOL diffusion lengths observed in the thin, back-illuminated cell. These results are discussed in terms of injected charge distributions, electric fields in the cell base, and the effects of a dominant boron-oxygen defect. E.A.K.

N86-17860*# National Aeronautics and Space Administration. Lewis Research Center, Cleveland, Ohio.

PERFORMANCE OF HUGHES GAAS CONCENTRATOR CELLS UNDER 1-MEV ELECTRON IRRADIATION

H. B. CURTIS and C. K. SWARTZ /in its Space Photovoltaic Research and Technology 1985 p 189-193 1985 refs

Avail: NTIS HC A13/MF A01 CSCL 10A

Several Hughes gallium arsenide (GaAs) concentrator cells were exposed to 1-MeV electrons at fluences up to 1×10^{15} to the 15th power electrons/sq cm. Performance data were taken after several fluences, at two temperatures, and at concentration levels from 1 to approx. 150x AMO. Data at 1 sun and 25 deg C were taken with an X-25 xenon-lamp solar simulator. Data at concentration were taken using a pulsed solar simulator with the assumption of a linear relationship between short-circuit current and irradiance. The cells are 5 by 5 mm with a 4-mm diameter illuminated area. E.A.K.

N86-17866*# National Aeronautics and Space Administration. Lewis Research Center, Cleveland, Ohio.

DEMONSTRATED RESULTS OF WELDED AND SOLDERED INTERCONNECTIONS

R. E. HART, JR. /in its Space Photovoltaic Research and Technology 1985 p 239-241 1985

Avail: NTIS HC A13/MF A01 CSCL 10A

Solar cell modules with welded and soldered interconnections were constructed using a flexible substrate material. These modules were thermally cycled between approx. 80 deg C at rates 100 cycles/day to demonstrate survivability under simulated low Earth orbit (LEO) temperature conditions. The modules, cycled in an inert atmosphere, show durability for 36,000 cycles. E.A.K.

N86-18773*# United Technologies Corp., South Windsor, Conn. Power Systems Div.

ONSITE 40-KILOWATT FUEL CELL POWER PLANT MANUFACTURING AND FIELD TEST PROGRAM Interim Report

Feb. 1985 162 p refs

(Contract DEN3-255; DE-AI31-80ET-17088)

(NASA-CR-174988; DOE/NASA/0255-1; NAS 1.26:174988;

FCR-6868) Avail: NTIS HC A08/MF A01 CSCL 10B

A joint Gas Research Institute and U.S. Department of Energy Program was initiated in 1982 to evaluate the use of fuel cell power systems for on-site energy service. Forty-six 40 kW fuel cell power plants were manufactured at the United Technologies Corporation facility in South Windsor, Connecticut, and are being delivered to host utilities and other program participants in the United States and Japan for field testing. The construction of the 46 fully-integrated power plants was completed in January 1985 within the constraints of the contract plan. The program has provided significant experience in the manufacture, acceptance testing, deployment, and support of on-site fuel cell systems. Initial field test results also show that these experimental power plants meet the performance and environmental requirements of a commercial specification. This Interim Report encompasses the design and manufacturing phases of the 40 kW Power Plant Manufacturing and Field Test program. The contract between UTC and NASA also provides UTC field engineering support to the host utilities, training programs and associated manuals for utility operating and maintenance personnel, spare parts support for a defined test period, and testing at UTC of a power plant made available from a preceding program phase. These activities are ongoing and will be reported subsequently. Author

N86-18774*# AeroVironment, Inc., Monrovia, Calif.

DEVELOPMENT AND TESTING OF TIP DEVICES FOR HORIZONTAL AXIS WIND TURBINES Final Report

G. W. GYATT and P. B. S. LISSAMAN May 1985 86 p refs

(Contract DEN3-341; DE-AI01-76ET-20320)

(NASA-CR-174991; DOE/NASA/0341-1; NAS 1.26:174991;

AV-FR-85/802) Avail: NTIS HC A05/MF A01 CSCL 10A

A theoretical and field experimental program has been carried out to investigate the use of tip devices on horizontal axis wind

turbine rotors. The objective was to improve performance by the reduction of tip losses. While power output can always be increased by a simple radial tip extension, such a modification also results in an increased gale load both because of the extra projected area and longer moment arm. Tip devices have the potential to increase power output without such a structural penalty. A vortex lattice computer model was used to optimize three basic tip configuration types for a 25 kW stall limited commercial wind turbine. The types were a change in tip planform, and a single-element and double-element nonplanar tip extension (winglets). A complete data acquisition system was developed which recorded three wind speed components, ambient pressure, temperature, and turbine output. The system operated unattended and could perform real-time processing of the data, displaying the measured power curve as data accumulated in either a bin sort mode or polynomial curve fit. Approximately 270 hr of performance data were collected over a three-month period. The sampling interval was 2.4 sec; thus over 400,000 raw data points were logged. Results for each of the three new tip devices, compared with the original tip, showed a small decrease (of the order of 1 kW) in power output over the measured range of wind speeds from cut-in at about 4 m/s to over 20 m/s, well into the stall limiting region. Changes in orientation and angle-of-attack of the winglets were not made. For aircraft wing tip devices, favorable tip shapes have been reported and it is likely that the tip devices tested in this program did not improve rotor performance because they were not optimally adjusted. Author

N86-18775*# National Aeronautics and Space Administration. Lewis Research Center, Cleveland, Ohio.

MOD-2 WIND TURBINE FIELD OPERATIONS EXPERIMENT Final Report

L. H. GORDON Dec. 1985 17 p refs

(Contract DE-AI01-76ET-20320)

(NASA-TM-87233; DOE/NASA/20320-69; E-2901; NAS 1.15:87233) Avail: NTIS HC A02/MF A01 CSCL 10A

The three-machine, 7.5 MW Goodnoe Hills located near Goldendale, Washington and is now in a research/experimental operations phase that offers a unique opportunity to study the effects of single and multiple wind turbines interacting with each other, the power grid; and the environment. Following a brief description of the turbine and project history, this paper addresses major problem areas and research and development test results. Field operations, both routine and nonroutine, are discussed. Routine operation to date has produced over 13,379,000 KWh of electrical energy during 11,064 hr of rotation. Nonroutine operation includes suspended activities caused by a crack in the low speed shaft that necessitated a redesign and reinstallation of this assembly on all three turbines. With the world's largest cluster back in full operation, two of the turbines will be operated over the next years to determine their value as energy producer. The third unit will be used primarily for conducting research tests requiring configuration changes to better understand the wind turbine technology. Technical areas summarized pertain to system performance and enhancements. Specific research tests relating to acoustics, TV interference, and wake effects conclude the paper. Author

N86-18776*# National Aeronautics and Space Administration. Lewis Research Center, Cleveland, Ohio.

SUMMARY OF TOWER DESIGNS FOR LARGE HORIZONTAL AXIS WIND TURBINES

G. R. FREDERICK (Toledo Univ., Ohio) and J. M. SAVINO 1986 21 p refs Presented at the Energy-Source Technology Conference and Exhibition, New Orleans, Louisiana, 23-27 Feb. 1986; sponsored by the American Society of Mechanical Engineers

(NASA-TM-87166; E-2803; DOE/NASA/20320-68; NAS 1.15:87166) Avail: NTIS HC A02/MF A01 CSCL 10A

Towers for large horizontal axis wind turbines, machines with a rotor axis height above 30 meters and rated at more than 500 kW, have varied in configuration, materials of construction, type of construction, height, and stiffness. For example, the U.S. large

HAWTs have utilized steel truss type towers and free-standing steel cylindrical towers. In Europe, the trend has been to use only free-standing and guyed cylindrical towers, but both steel and reinforced concrete have been used as materials of construction. These variations in materials of construction and type of construction reflect different engineering approaches to the design of cost effective towers for large HAWTs. Tower designs are the NASA/DOE Mod-5B presently being fabricated. Design goals and requirements that influence tower configuration, height and materials are discussed. In particular, experiences with United States large wind turbine towers are elucidated. Finally, current trends in tower designs for large HAWTs are highlighted. Author

N86-19721* National Aeronautics and Space Administration. Lewis Research Center, Cleveland, Ohio.

NEGATIVE ELECTRODE CATALYST FOR THE IRON CHROMIUM REDOX ENERGY STORAGE SYSTEM Patent

R. F. GAHN and N. H. HAGEDORN, inventors (to NASA) 24 Sep. 1985 7 p Filed 20 Aug. 1984

(NASA-CASE-LEW-14028-1; US-PATENT-4,543,302;

US-PATENT-APPL-SN-642310; US-PATENT-CLASS-429-15;

US-PATENT-CLASS-429-19; US-PATENT-CLASS-429-51;

US-PATENT-CLASS-429-109) Avail: US Patent and Trademark Office CSCL 10C

A redox cell which operates at elevated temperatures and which utilizes the same two metal couples in each of the two reactant fluids is disclosed. Each fluid includes a bismuth salt and may also include a lead salt. A low cost, cation permselective membrane separates the reactant fluids.

Official Gazette of the U.S. Patent and Trademark Office

N86-19742*# Georgia Inst. of Tech., Atlanta.

TECHNOLOGY FOR SATELLITE POWER CONVERSION Semiannual Technical Report, 27 May - 26 Oct. 1985

M. A. GOUKER, D. P. CAMPBELL, and J. J. GALLAGHER 29 Jan. 1986 35 p refs

(Contract NAG3-282; GTRI PROJ. 3244)

(NASA-CR-176554; NAS 1.26:176554) Avail: NTIS HC A03/MF A01 CSCL 10A

The dipole pattern of the antenna was confirmed and work on the MOM diode began. The antenna - detector structure was modified and the measurement apparatus reconfigured to permit precise antenna pattern measurements. Fabrication of the MOM diode was initiated after antenna action from the new structures was observed. A refined antenna structure was developed. The previous antenna design allowed currents induced by the incident radiation in the bonding wires to flow through the bolometer. The detector was thus responding to both the antenna and bonding wire currents. A low pass filter was added to the antenna structure to improve the detection scheme. The new design uses an interdigitated capacitor to prevent the induced current in the bonding wires from flowing through the detection element.

Author

N86-21978*# National Aeronautics and Space Administration. Lewis Research Center, Cleveland, Ohio.

LIGHTWEIGHT NICKEL ELECTRODE FOR NICKEL HYDROGEN CELLS AND BATTERIES

D. L. BRITTON 1986 10 p refs Presented at the 32nd International Power Sources Symposium, Cherry Hill, N.J., 9-12 Jun. 1986; sponsored by Army

(NASA-TM-87253; E-2942; NAS 1.15:87253) Avail: NTIS HC A02/MF A01 CSCL 10C

The nickel electrode was identified as the heaviest component of the nickel hydrogen (NiH₂) battery. The NASA Lewis Research Center is developing nickel electrodes for NiH₂ battery devices which will be lighter in weight and have higher energy densities when cycled under a low Earth orbit regime at deep depths of discharge. Lightweight plaques are first exposed to 31 percent potassium hydroxide for 3 months to determine their suitability for use as electrode substrates from a chemical corrosion standpoint. Pore size distribution and porosity of the plaques are then measured. The lightweight plaques examined are nickel foam, nickel

felt, nickel plastic and nickel plated graphite. Plaques are then electrochemically impregnated in an aqueous solution. Initial characterization tests of the impregnated plaques are performed at five discharge levels, C/2, 1.0 C, 1.37 C, 2.0C, and 2.74 C rates. Electrodes that passed the initial characterization screening test will be life cycle tested. Lightweight electrodes are approximately 30 to 50 percent lighter in weight than the sintered nickel electrode. Author

N86-21979*# TriSolar Corp., Bedford, Mass.
DEVELOPMENT OF A MICROPROCESSOR CONTROLLER FOR STAND-ALONE PHOTOVOLTAIC POWER SYSTEMS Final Report

A. R. MILLNER and D. L. KAUFMAN Jun. 1984 192 p
 (Contract DEN3-310; DE-AI01-79ET-20485)
 (NASA-CR-174723; DOE/NASA/0310-1; NAS 1.26:174723)
 Avail: NTIS HC A09/MF A01 CSCL 10B

A controller for stand-alone photovoltaic systems has been developed using a low power CMOS microprocessor. It performs battery state of charge estimation, array control, load management, instrumentation, automatic testing, and communications functions. Array control options are sequential subarray switching and maximum power control. A calculator keypad and LCD display provides manual control, fault diagnosis and digital multimeter functions. An RS-232 port provides data logging or remote control capability. A prototype 5 kW unit has been built and tested successfully. The controller is expected to be useful in village photovoltaic power systems, large solar water pumping installations, and other battery management applications. Author

N86-23035*# National Aeronautics and Space Administration.
 Lewis Research Center, Cleveland, Ohio.
ASSESSMENT OF COMMERCIALLY AVAILABLE AND EXPERIMENTAL HYDROGEN ELECTRODES

J. A. CHARLESTON 1986 9 p refs To be presented at the 32nd International Power Sources Symposium, Cherry Hill, N.J., 9-12 Jun. 1986; sponsored by Army
 (NASA-TM-87264; E-2958; NAS 1.15:87264) Avail: NTIS HC A02/MF A01 CSCL 10A

NASA Lewis Research Center is currently involved in advanced cell component development for nickel-hydrogen cells and batteries. Long life, high energy density, improved performance and reliability are required for energy storage systems in future space missions. Commercially available as well as experimental hydrogen electrodes were assessed and compared to the state-of-the-art hydrogen electrode that is currently being used in nickel-hydrogen batteries. These electrodes were evaluated by scanning electron microscopy and standard electrochemical polarization measurements. Production variables such as Teflon content and platinum catalyst loading were considered in order to assess various hydrogen electrodes with regard to the different electrode manufacturing processes. Author

N86-24007*# Illinois Univ., Urbana-Champaign. Dept. of Electrical and Computer Engineering.
SUPERLATTICES AND NIPi STRUCTURES IN NEW FORMS OF CASCADE SOLAR CELLS Semiannual Report, 23 Oct. 1985 - 22 Apr. 1986

J. P. LEBURTON and K. HESS 1986 11 p
 (Contract NAG3-507)
 (NASA-CR-176718; NAS 1.26:176718; SAR-4) Avail: NTIS HC A02/MF A01 CSCL 10A

The activity in the field of photovoltaic semiconductor superstructures is described. Progress was accomplished in the two principal directions previously defined in our initial proposal, i.e.: (1) Theoretical investigation of the optical properties of superlattices; and (2) New solar cell concepts and device modeling. Although important information concerning the optical constants of superlattices and multiple quantum well structures was obtained from our computer model, most of the theoretical efforts have progressively shifted from the former to the latter aspect of the project because of the discovery of a new kind of photovoltaic

device which may exhibit improved performances with respect to conventional solar cells. Author

N86-25039*# National Aeronautics and Space Administration.
 Lewis Research Center, Cleveland, Ohio.

PRINCIPLES FOR SYSTEM LEVEL ELECTROCHEMISTRY
 L. H. THALLER 1986 13 p refs Presented at the 15th International Power Sources Symposium, Brighton, England, 7-11 Sep. 1986
 (NASA-TM-87283; E-2908; NAS 1.15:87283) Avail: NTIS HC A02/MF A01 CSCL 10C

The higher power and higher voltage levels anticipated for future space missions have required a careful review of the techniques currently in use to preclude battery problems that are related to the dispersion characteristics of the individual cells. Not only are the out-of-balance problems accentuated in these larger systems, but the thermal management considerations also require a greater degree of accurate design. Newer concepts which employ active cooling techniques are being developed which permit higher rates of discharge and tighter packing densities for the electrochemical components. This paper will put forward six semi-independent principles relating to battery systems. These principles will progressively address cell, battery and finally system related aspects of large electrochemical storage systems. Author

N86-25040*# United Technologies Corp., South Windsor, Conn.
 Fuel Cell Operations.

ADVANCED ON-SITE POWER PLANT DEVELOPMENT TECHNOLOGY PROGRAM Annual Report, 1983

Jun. 1984 155 p refs
 (Contract DEN3-289; DE-AI21-80ET-17088)
 (NASA-CR-174709; DOE/NASA/0289-1; NAS 1.26:174709; PSD-FCR-5715) Avail: NTIS HC A08/MF A01 CSCL 10B

A 30-cell, full area short stack containing advanced cell features was tested for 2900 hours. A stack acid addition approach was selected and will be evaluated on the stack at 5000 hours test time. A brassboard inverter was designed and fabrication was initiated. Evaluation of this brassboard inverter will take place in 1984. A Teflon coated commercial heat exchanger was selected as the preferred approach for the acid condenser. A reformer catalyst with significantly less pressure drop and equivalent performance relative to the 40-K baseline catalyst was selected for the development reformer. The early 40-kW field power plant history was reviewed and adjustments were made to the On-Site Technology Development Program to address critical component issues. Author

N86-25042*# Georgia Inst. of Tech., Atlanta.
TECHNOLOGY FOR SATELLITE POWER CONVERSION Semiannual Technical Report

M. A. GOUKER, D. P. CAMPBELL, and J. J. GALLAGHER 16 May 1986 10 p refs
 (Contract NAG3-282)
 (NASA-CR-176777; NAS 1.26:176777) Avail: NTIS HC A02/MF A01 CSCL 10A

The work performed in this reporting period has concentrated on the metal-oxide-metal (MOM) diode. The fabrication procedure begins with the deposition of gold probing pads to provide a non-oxidizing contact to test the dc characteristics to the diode accurately. A thin patch capped with an insulating SiO₂ layer, is deposited next to form the first half of the diode. The other half of the diode, typically Ni, is deposited completing the conduction path from the oxidized edge of the Ni patch to the opposite gold probing pad. It is important in this step that the last metallization take place without exposing the newly oxidized surface to the atmosphere. Successful production of diodes has been achieved. Work on millimeter wave frequency rectennas incorporating known semiconductor diode technology has been initiated. Author

44 ENERGY PRODUCTION AND CONVERSION

N86-25046*# Hughes Research Labs., Malibu, Calif. LONG LIFE NICKEL ELECTRODES FOR A NICKEL-HYDROGEN CELL: CYCLE LIFE TESTS

H. S. LIM and S. A. VERZWYVELT 1985 14 p refs Previously announced as N84-33698
(Contract NAS3-22238)
(NASA-CR-174815; NAS 1.26:174815) Avail: NTIS HC A02/MF A01 CSCL 10C

In order to develop a long life nickel electrode for a Ni/H₂ cell, the cycle life of nickel electrodes was tested in Ni/H₂ boiler plate cells. A 19 test cell matrix was made of various nickel electrode designs including three levels each of plaque mechanical strength, median pore size of the plaque, and active material loading. Test cells were cycled to the end of their life (0.5v) in a 45 minute low Earth orbit cycle regime at 80% depth-of-discharge. It is shown that the active material loading level affects the cycle life the most with the optimum loading at 1.6 g/cc void. Mechanical strength does not affect the cycle life noticeably in the bend strength range of 400 to 700 psi. It is found that the best plaque is made of INCO nickel powder type 287 and has median pore size of 13 micron. R.J.F.

N86-25874* National Aeronautics and Space Administration. Lewis Research Center, Cleveland, Ohio.

OXYGEN RECOMBINATION IN INDIVIDUAL PRESSURE VESSEL NICKEL-HYDROGEN BATTERIES Patent

J. J. SMITHRICK, inventor (to NASA) 22 Apr. 1986 6 p Filed 27 Jun. 1984 Supersedes N84-29084 Sponsored by NASA
(NASA-CASE-LEW-13822-1; US-PATENT-4,584,249;
US-PATENT-APPL-SN-625077; US-PATENT-CLASS-429-57;
US-PATENT-CLASS-429-27; US-PATENT-CLASS-42-101) Avail:
US Patent and Trademark Office CSCL 10C

A metal-hydrogen cell is described which avoids damage and retards flooding of the hydrogen electrodes by providing for chemical recombination of oxygen and hydrogen in areas or sites remote from the hydrogen electrodes. In the metal-hydrogen cell, a plurality of electrical cell units are placed in a back to back relationship. The cells may be lined with a wick, having one or more catalyzed sites on the inner surface of the cell. Separators disposed between the respective metal and hydrogen electrodes of each cell unit are provided with gas directing notches around their peripheries to facilitate the desired movement of gasses within the metal-hydrogen cell. Any two metal electrodes separated by a gas screen are provided with gas tight sealing means between the electrodes at each aperture. The sealing means may be a ring of rubber or elastomeric material which is somewhat compressible but nonreactive with other materials in the cell.

Official Gazette of the U.S. Patent and Trademark Office

N86-25877*# Engelhard Corp., Edison, N.J. Specialty Chemicals Div.

DEVELOP AND TEST FUEL CELL POWERED ON-SITE INTEGRATED TOTAL ENERGY SYSTEMS Interim Report, Feb. 1981 - Jan. 1984

A. KAUFMAN and J. WERTH Oct. 1984 236 p
(Contract DEN3-241; DE-A101-80ET-17088)
(NASA-CR-174951; DOE/NASA-0241-12; NAS 1.26:174951)
Avail: NTIS HC A11/MF A01 CSCL 10B

Work has been performed leading toward the development of a 50kW on-site integrated energy system. A sub-scale 5kW system was constructed and tested in the steady-load (with shutdowns) and transient modes. A parallel effort has been conducted to develop the full-size sub-systems for the on-site system; these include the fuel cell stack, a methanol processor, and a d.c.-a.c. power conditioner. Stack technology development activities have been carried out to improve the performance, cost and reliability of stack components and hardware. In the fuel processing area, screening tests have been conducted for various methanol steam-reforming catalysts, and the preferred catalysts have been subjected to extended testing. Application-related work has been pursued largely under subcontracts. A study has been completed in which the applicability of on-site fuel cell cogeneration systems to various building types was analyzed and the potential economic

attractiveness ascertained. The overall system was analyzed in terms of its operating characteristics at part load and its response to transients. Preferred heating, ventilating, and air conditioning approaches for various building types using fuel cell cogeneration units are determined. Author

N86-26677*# National Aeronautics and Space Administration. Lewis Research Center, Cleveland, Ohio.

NICKEL-HYDROGEN SEPARATOR DEVELOPMENT

O. D. GONZALEZ-SANABRIA 1986 8 p refs Presented at the 21st Intersociety Energy Conversion Engineering Conference, San Diego, Calif., 25-29 Aug. 1986; sponsored by the ACS, SAE, ANS, ASME, IEEE, and AICHE
(NASA-TM-87332; E-3076; NAS 1.15:87332) Avail: NTIS HC A02/MF A01 CSCL 10C

The separator technology is a critical element in the nickel-hydrogen (Ni-H₂) systems. Previous research and development work carried out at NASA Lewis Research Center has determined that separators made from zirconium oxide (ZrO₂) and potassium titanate (PKT) fibers will function satisfactorily in Ni-H₂ cells without exhibiting the problems associated with the asbestos separators. These separators and their characteristics were previously discussed. A program was established to transfer the separator technology into a commercial production line. A detailed plan of this program will be presented and the preliminary results will be discussed. Author

N86-27708*# General Electric Co., Philadelphia, Pa. Advanced Energy Programs Dept.

MOD-5A WIND TURBINE GENERATOR PROGRAM DESIGN REPORT: VOLUME 1: EXECUTIVE SUMMARY Final Report

Aug. 1984 63 p
(Contract DEN3-153; DE0A101-79ET-20305)
(NASA-CR-174734; DOE/NASA-0153/1; NAS 1.26:174734)
Avail: NTIS HC A04/MF A01 CSCL 10A

The design, development and analysis of the 7.3 MW MOD-5A wind turbine generator covering work performed between July 1980 and June 1984 is discussed. The report is divided into four volumes: Volume 1 summarizes the entire MOD-5A program, Volume 2 discusses the conceptual and preliminary design phases, Volume 3 describes the final design of the MOD-5A, and Volume 4 contains the drawings and specifications developed for the final design. Volume 1, the Executive Summary, summarizes all phases of the MOD-5A program. The performance and cost of energy generated by the MOD-5A are presented. Each subsystem - the rotor, drivetrain, nacelle, tower and foundation, power generation, and control and instrumentation subsystems - is described briefly. The early phases of the MOD-5A program, during which the design was analyzed and optimized, and new technologies and materials were developed, are discussed. Manufacturing, quality assurance, and safety plans are presented. The volume concludes with an index of volumes 2 and 3. Author

N86-28511*# Toledo Univ., Ohio.

APPLICATION OF A PERSONAL COMPUTER FOR THE UNCOUPLED VIBRATION ANALYSIS OF WIND TURBINE BLADE AND COUNTERWEIGHT ASSEMBLIES Final Report

P. R. WHITE and R. R. LITTLE Dec. 1985 144 p
(Contract NCC3-5; DE-A101-76ET-20320)
(NASA-CR-175090; DOE/NASA/0005-3; NAS 1.26:175090)
Avail: NTIS HC A07/MF A01 CSCL 10A

A research effort was undertaken to develop personal computer based software for vibrational analysis. The software was developed to analytically determine the natural frequencies and mode shapes for the uncoupled lateral vibrations of the blade and counterweight assemblies used in a single bladed wind turbine. The uncoupled vibration analysis was performed in both the flapwise and chordwise directions for static rotor conditions. The effects of rotation on the uncoupled flapwise vibration of the blade and counterweight assemblies were evaluated for various rotor speeds up to 90 rpm. The theory, used in the vibration analysis codes, is based on a lumped mass formulation for the blade and counterweight assemblies. The codes are general so that other

designs can be readily analyzed. The input for the codes is generally interactive to facilitate usage. The output of the codes is both tabular and graphical. Listings of the codes are provided. Predicted natural frequencies of the first several modes show reasonable agreement with experimental results. The analysis codes were originally developed on a DEC PDP 11/34 minicomputer and then downloaded and modified to run on an ITT XTRA personal computer. Studies conducted to evaluate the efficiency of running the programs on a personal computer as compared with the minicomputer indicated that, with the proper combination of hardware and software options, the efficiency of using a personal computer exceeds that of a minicomputer. Author

N86-29409*# Akron Univ., Ohio. Dept. of Chemical Engineering.

THEORETICAL AND EXPERIMENTAL FLOW CELL STUDIES OF A HYDROGEN-BROMINE FUEL CELL, PART 1 M.S. Thesis. Final Report

R. F. SAVINELL and S. D. FRITTS 1 Mar. 1986 214 p

(Contract NAG3-500)

(NASA-CR-177165; NAS 1.26:177165) Avail: NTIS HC A10/MF A01 CSCL 10B

There is increasing interest in hydrogen-bromine fuel cells as both primary and regenerative energy storage systems. One promising design for a hydrogen-bromine fuel cell is a negative half cell having only a gas phase, which is separated by a cationic exchange membrane from a positive half cell having an aqueous electrolyte. The hydrogen gas and the aqueous bromide solution are stored external to the cell. In order to calculate the energy storage capacity and to predict and assess the performance of a single cell, the open circuit potential (OCV) must be estimated for different states of charge, under various conditions. Theoretical expressions were derived to estimate the OCV of a hydrogen-bromine fuel cell. In these expressions temperature, hydrogen pressure, and bromine and hydrobromic acid concentrations were taken into consideration. Also included are the effects of the Nafion membrane separator and the various bromide complex species. Activity coefficients were taken into account in one of the expressions. The sensitivity of these parameters on the calculated OCV was studied. Author

N86-29411*# United Technologies Corp., South Windsor, Conn. Power Systems Div.

ADVANCED ON-SITE POWER PLANT DEVELOPMENT TECHNOLOGY PROGRAM Annual Report, 1984

F. S. KEMP Feb. 1985 276 p

(Contract DEN3-289; DE-AI21-80ET-17088)

(NASA-CR-175007; NAS 1.26:175007; FCR-6848;

DOE/NASA/0389-3) Avail: NTIS HC A13/MF A01 CSCL 10B

A 30-cell stack was tested for 7200 hours. At 6000 hours the stack was successfully refilled with acid with no loss of performance. A second stack containing the advanced Configuration B cell package was fabricated and assembled for testing in 1985. A 200-kW brassboard inverter was successfully evaluated, verifying the design of the two-bridge ASCR circuit design. A fuel processing catalyst train was tested for 2000 hours verifying the catalyst for use in a 200-kW development reformer. The development reformer was fabricated for evaluation in 1985. The initial test plan was prepared for a 200-kW verification test article. Author

N86-30251*# National Aeronautics and Space Administration. Lewis Research Center, Cleveland, Ohio.

DESIGN AND INITIAL TESTING OF A ONE-BLADED 30-METER-DIAMETER ROTOR ON THE NASA/DOE MOD-O WIND TURBINE Final Report

R. D. CORRIGAN and C. B. F. ENSWORTH 1986 19 p

Presented at the Energy-Sources Technology Conference Exhibition, New Orleans, La., 23-28 Feb. 1986; sponsored by ASME

(Contract DE-AI01-76ET-20320)

(NASA-TM-88810; E-3162; DOE/NASA-20320/70; NAS

1.15:88810) Avail: NTIS HC A02/MF A01 CSCL 10A

The concept of a one-bladed horizontal-axis wind turbine has been of interest to wind turbine designers for many years. Many designs and economic analyses of one-bladed wind turbines have been undertaken by both United States and European wind energy groups. The analyses indicate significant economic advantages but at the same time, significant dynamic response concerns. In an effort to develop a broad data base on wind turbine design and operations, the NASA Wind Energy Project Office has tested a one-bladed rotor at the NASA/DOE Mod-O Wind Turbine Facility. This is the only known test on an intermediate-sized one-bladed rotor in the United States. The 15.2-meter-radius rotor consists of a tip-controlled blade and a counterweight assembly. A rigorous test series was conducted in the Fall of 1985 to collect data on rotor performance, drive train/generator dynamics, structural dynamics, and structural loads. This report includes background information on one-bladed rotor concepts, and Mod-O one-bladed rotor test configuration, supporting design analysis, the Mod-O one-blade rotor test plan, and preliminary test results. Author

N86-31979*# National Aeronautics and Space Administration. Lewis Research Center, Cleveland, Ohio.

PARAMETRIC AND CYCLE TESTS OF A 40-A-HR BIPOLAR NICKEL-HYDROGEN BATTERY

R. L. CATALDO 1986 12 p Presented at the 21st Intersociety Energy Conversion Engineering Conference (IECEC), San Diego, Calif., 25-29 Aug. 1986; sponsored by ACS, SAE, ANS, ASME, IEEE, AIAA and AIChE

(NASA-TM-88793; E-3102; NAS 1.15:88793) Avail: NTIS HC A02/MF A01 CSCL 10C

A series of tests was performed to characterize battery performance relating to certain operating parameters which included charge current, discharge current, temperature and pressure. The parameters were varied to confirm battery design concepts and to determine optimal operating conditions. Spacecraft power requirements are constantly increasing. Special spacecraft such as the Space Station and platforms will require energy storage systems of 130 and 25 kWh, respectively. The complexity of these high power systems will demand high reliability, and reduced mass and volume. A system that uses batteries for storage will require a cell count in excess of 400 units. These cell units must then be assembled into several batteries with over 100 cells in a series connected string. In an attempt to simplify the construction of conventional cells and batteries, the NASA Lewis Research Center battery systems group initiated work on a nickel-hydrogen battery in a bipolar configuration in early 1981. Features of the battery with this bipolar construction show promise in improving both volumetric and gravimetric energy densities as well as thermal management. Bipolar construction allows cooling in closer proximity to the cell components, thus heat removal can be accomplished at a higher rejection temperature than conventional cell designs. Also, higher current densities are achievable because of low cell impedance. Lower cell impedance is achieved via current flow perpendicular to the electrode face, thus reducing voltage drops in the electrode grid and electrode terminals tabs. Author

44 ENERGY PRODUCTION AND CONVERSION

N86-31980*# National Aeronautics and Space Administration. Lewis Research Center, Cleveland, Ohio.

EFFECT OF IMPREGNATION METHOD ON CYCLE LIFE OF THE NICKEL ELECTRODE

J. J. SMITHRICK 1986 9 p Presented at the 21st Intersociety Energy Conversion Engineering Conference (IECEC), San Diego, Calif., 25-29 Aug. 1986; sponsored by ACS, SAE, ANS, ASME, IEEE, AIAA and AIChE (NASA-TM-87326; E-3037; NAS 1.15:87326) Avail: NTIS HC A02/MF A01 CSCL 10C

The nickel electrode has been identified as the life limiting component for individual pressure vessel (IPV) nickel-hydrogen cells when cycled under a low earth orbit (LEO) cycle regime at deep depths of discharge. As a part of an overall program to develop a long life nickel electrode for nickel-hydrogen cells, the effect of two different methods of electrochemical impregnation on the cycle life of the nickel electrode was investigated. One method was the Pickett (aqueous/ethanolic) process. The other was the modified Bell (aqueous) process. The plaques for both impregnation methods were made by sintering dry carbonyl nickel powder in a reducing atmosphere. The plaques contain a nickel screen substrate. Electrodes made from both processes were cycle tested in Air Force design IPV nickel-hydrogen cells. The only factor different for this test was the method of plaque impregnation; all other factors were the same. The cells were cycled to failure under a 90 min LEO cycle regime at a deep depth of discharge (80 percent DOD). Failure for this test was defined to occur when the cell voltage degraded to 1.0 V prior to the completion of the 35 min discharge. Author

N86-31981*# National Aeronautics and Space Administration. Lewis Research Center, Cleveland, Ohio.

DESIGN CONSIDERATIONS FOR ADVANCED BATTERY CONCEPTS

H. F. LEIBECKI and L. H. THALLER 1986 16 p Presented at the 3rd Space Systems Technology Conference, San Diego, Calif., 9-12 Jun. 1986; sponsored by the American Institute of Aeronautics and Astronautics Previously announced in IAA as A86-40579 (NASA-TM-87319; E-3055; NAS 1.15:87319) Avail: NTIS HC A02/MF A01 CSCL 10C

A mathematical representation for the charge and discharge of a sodium-sulfur cell is developed. These equations are then used as the basis for a computerized model to examine the effects of cell arrangement in the design of a large multi-kilowatt battery from a group of hypothetical individual cells with known variations in their ampere hour capacity and internal resistance. The cycling characteristics of 216 individual cells arranged in six different configurations are evaluated with the view towards minimizing the adverse effects that are introduced due to the stochastic aspects of groupings of cells, as well as the possibility of cell failures in both the open and shorted mode. Although battery systems based on sodium-sulfur cells are described in this example, any of the newer electrochemical systems can be fitted into this framework by making appropriate modifications to the basic equations. Author

N86-31982*# National Aeronautics and Space Administration. Lewis Research Center, Cleveland, Ohio.

ESTIMATED HEATS OF FUSION OF FLUORIDE SALT MIXTURES SUITABLE FOR THERMAL ENERGY STORAGE APPLICATIONS

A. K. MISRA (Case Western Reserve Univ., Cleveland, Ohio.) and J. D. WHITTENBERGER May 1986 26 p (NASA-TM-87320; E-3057; NAS 1.15:87320) Avail: NTIS HC A03/MF A01 CSCL 10A

The heats of fusion of several fluoride salt mixtures with melting points greater than 973 K were estimated from a coupled analysis of the available thermodynamic data and phase diagrams. Simple binary eutectic systems with and without terminal solid solutions, binary eutectics with congruent melting intermediate phases, and ternary eutectic systems were considered. Several combinations of salts were identified, most notable the eutectics LiF-22CaF₂ and NaF-60MgF₂ which melt at 1039 and 1273 K respectively

which possess relatively high heats of fusion/gm (greater than 0.7 kJ/g). Such systems would seemingly be ideal candidates for the light weight, high energy storage media required by the thermal energy storage unit in advanced solar dynamic power systems envisioned for the future space missions. M.G.

N86-31983*# National Aeronautics and Space Administration. Lewis Research Center, Cleveland, Ohio.

SUMMARY OF NASA/DOE AILERON-CONTROL DEVELOPMENT PROGRAM FOR WIND TURBINES Final Report

D. R. MILLER 1986 26 p Presented at the Energy-Sources Technology Conference and Exhibition, New Orleans, La., 23-28 Feb. 1986; sponsored by American Society for Mechanical Engineers

(Contract DE-AI01-76ET-20320)

(NASA-TM-88811; DOE/NASA-20320/71; E-3163; NAS 1.15:88811) Avail: NTIS HC A03/MF A01 CSCL 10A

The development of aileron-control for wind turbines is discussed. Selected wind tunnel test results and full-scale rotor test results are presented for various types of ailerons. Finally, the current status of aileron-control development is discussed. Aileron-control was considered as a method of rotor control for use on wind turbines based on its potential to reduce rotor weight and cost. Following an initial feasibility study, a 20 percent chord aileron-control rotor was fabricated and tested on the NASA/DOE Mod-0 experimental wind turbine. Results from these tests indicated that the 20 percent chord ailerons regulated power and provided overspeed protection, but only over a very limited windspeed range. The next aileron-control rotor to be tested on the Mod-0 had 38 percent chord ailerons and test results showed these ailerons provided overspeed protection and power regulation over the Mod-0's entire operational windspeed range. Author

N86-31984*# Westinghouse Electric Corp., Pittsburgh, Pa. Advanced Energy Systems Div.

GAS COOLED FUEL CELL SYSTEMS TECHNOLOGY DEVELOPMENT Final Report, May 1983 - May 1984

J. M. FERET Aug. 1986 282 p

(Contract DEN3-290; DE-AI01-80ET-17088)

(NASA-CR-175047; DOE/NASA/0290-02; NAS 1.26:175047;

WAESD-TR-85-0030) Avail: NTIS HC A13/MF A01 CSCL 10A

The work performed during the Second Logical Unit of Work of a multi-year program designed to develop a phosphoric acid fuel cell (PAFC) for electric utility power plant application is discussed. The Second Logical Unit of Work, which covers the period May 14, 1983 through May 13, 1984, was funded by the U.S. Department of Energy, Office of Fossil Energy, Morgantown Energy Technology Center, and managed by the NASA Lewis Research Center. Author

N86-32875* National Aeronautics and Space Administration. Lewis Research Center, Cleveland, Ohio.

LITHIUM COUNTERDOPED SILICON SOLAR CELL Patent

I. WEINBERG, inventor (to NASA) and H. W. BRANDHORST, JR., inventor (to NASA) 26 Aug. 1986 7 p Filed 07 Nov. 1984 Supersedes N85-20535 (23 - 11, p 1672)

(NASA-CASE-LEW-14177-1; US-PATENT-4,608,452;

US-PATENT-APPL-SN-669140; US-PATENT-CLASS-136-261;

US-PATENT-CLASS-29-572; US-PATENT-CLASS-29-576B;

US-PATENT-CLASS-148-1.5; US-PATENT-CLASS-357-30;

US-PATENT-CLASS-357-91) Avail: US Patent and Trademark

Office CSCL 10A

The resistance to radiation damage of an n(+)-p boron doped silicon solar cell is improved by lithium counterdoping. Even though lithium is an n-dopant in silicon, the lithium is introduced in small enough quantities so that the cell base remains p-type. The lithium is introduced into the solar cell wafer by implantation of lithium ions whose energy is about 50 keV. After this lithium implantation, the wafer is annealed in a nitrogen atmosphere at 375 C for two hours. Official Gazette of the U.S. Patent and Trademark Office

ENVIRONMENT POLLUTION

Includes atmospheric, noise, thermal, and water pollution.

N86-14770* Drexel Univ., Philadelphia, Pa. Dept. of Mechanical Engineering and Mechanics.

OXIDES OF NITROGEN EMISSIONS FROM THE COMBUSTION OF MONODISPERSE LIQUID FUEL SPRAYS Ph.D. Thesis

H. SARV Jun. 1985 173 p refs

(Contract NAG3-1)

(NASA-CR-176373; NAS 1.26:176373) Avail: NTIS HC A08/MF A01 CSCL 13B

A study of NO sub x formation in a one dimensional monodisperse spray combustion system, which allowed independent droplet size variation, was conducted. Temperature, NO and NO sub x concentrations were measured in the transition region, encompassing a 26 to 74 micron droplet size range. Emission measurements of hydrocarbons, carbon monoxide, carbon dioxide and oxygen were also made. The equivalence ratio was varied between 0.8 and 1.2 for the fuels used, including methanol, isopropanol, n-heptane and n-octane. Pyridine and pyrrole were added to n-heptane as nitrogen-containing additives in order to simulate synthetic fuels. Results obtained from the postflame regions using the pure fuels indicate an optimum droplet size in the range of 43 to 58 microns for minimizing NO sub x production. For the fuels examined, the maximum NO sub x reductions relative to the small droplet size limit were about 10 to 20% for lean and 20 to 30% for stoichiometric and rich mixtures. This behavior is attributed to droplet interactions and the transition from diffusive to premixed type of burning. Preflame vaporization controls the gas phase stoichiometry which has a significant effect on the volume of the hot gases surrounding a fuel droplet, where NO sub x is formed.

R.J.F.

GEOPHYSICS

Includes aeronomy; upper and lower atmosphere studies; ionospheric and magnetospheric physics; and geomagnetism.

A86-48620* Massachusetts Inst. of Tech., Cambridge.

SIMULTANEOUS MEASUREMENTS OF CARBON MONOXIDE AND OZONE IN THE NASA GLOBAL ATMOSPHERIC SAMPLING PROGRAM (GASP)

R. E. NEWELL (MIT, Cambridge, MA) and M.-F. WU (NASA, Goddard Space Flight Center, Greenbelt, MD) IN: Atmospheric ozone; *Proceedings of the Quadrennial Ozone Symposium*, Halkidiki, Greece, September 3-7, 1984. Dordrecht, D. Reidel Publishing Co., 1985, p. 548-552. refs (Contract NAS3-22541; DE-AC02-76EV-12195)

It is noted that the Global Atmospheric Sampling Program (GASP) was intended to establish global baseline values of selected atmospheric constituents that could be used for studies of the dynamics of the sampled region as well as for modeling purposes. Instrument packages were carried on four Boeing 747 aircraft in routine commercial service. Carbon monoxide and ozone data were collected simultaneously from early 1977 to early 1979 when GASP terminated. CO was measured with an infrared absorption analyzer using dual isotope fluorescence. Ozone was measured via absorption of UV light. Correlations between the CO and the O3 are tabulated; they are clearly negative for both troposphere and stratosphere in middle latitudes, indicating that transport processes between the stratosphere and troposphere (discussed) dominate. But in the low latitude troposphere the correlations are positive, indicating the possible influence of photochemical effects. D.H.

METEOROLOGY AND CLIMATOLOGY

Includes weather forecasting and modification.

A86-17982* National Aeronautics and Space Administration. Lewis Research Center, Cleveland, Ohio.

MERIT - A NEW APPROACH TO UPPER AIR FORECASTING FOR AVIATION

R. STEINBERG (NASA, Lewis Research Center, Cleveland, OH) IN: Conference on Weather Forecasting and Analysis, 10th, Clearwater Beach, FL, June 25-29, 1984, Preprints. Boston, MA, American Meteorological Society, 1984, p. 249-254. refs

The development of a man/computer data enhancement and management system to provide very-short range upper air forecasts is examined. The forecast accuracy and precision problems encountered with the current numerical weather prediction models are discussed. The proposed system is to utilize both radiosonde data and automated pilot reports and provide a 2-12 hour analysis/forecast with a 3 hour forecast cycle. The minimum energy routes using interactive techniques (MERIT) system is described and a diagram is provided. The preliminary testing of a modified MERIT system reveals that the system is not as accurate as the Spectral 12 hour forecast, but is more accurate than the spectral 24 hour forecast. The complete testing and validation of the MERIT system is required before a comparison with present techniques is possible. I.F.

A86-28963* National Aeronautics and Space Administration. Lewis Research Center, Cleveland, Ohio.

A NOTE ON THE FINITE DIFFERENCING OF THE LINEARIZED PRIMITIVE EQUATIONS' LOWER BOUNDARY CONDITION

D. JACQMIN (NASA, Lewis Research Center, Cleveland, OH; Harvard University, Cambridge, MA) *Pure and Applied Geophysics* (ISSN 0033-4553), vol. 123, no. 3, 1985, p. 441-447. refs (Contract NSF ATM-82-05638; NGL-22-007-228)

This note examines the accuracy of finite difference solutions of the midlatitude primitive equations and the quasi-geostrophic equation. First order accurate forward differencing of the equations' lower boundary condition is shown to poorly simulate the radiating wave response to midlatitude heating. Forward differencing always exaggerates the magnitude of the radiating response. For a realistic heating height scale and for a reasonable mesh size this exaggeration is on the order of 50 percent. Central differencing of the lower boundary condition gives an error of only about 3 percent. Author

A86-37501* National Aeronautics and Space Administration. Lewis Research Center, Cleveland, Ohio.

UPPER AIR FORECASTING FOR AVIATION IN THE UNITED STATES

R. STEINBERG (NASA, Lewis Research Center, Cleveland, OH) IN: International Conference on the Aviation Weather System, 2nd, Montreal, Canada, June 19-21, 1985, Preprints. Boston, MA, American Meteorological Society, 1985, p. 289-294. refs

It is shown that the present forecast models used in the aviation digital forecast (ADF) product for automated flight planning in the U.S. did not improve in accuracy and precision over the past two decades. A new approach to the upper air forecasting is presented in the NASA/NOAA MERIT project. In MERIT, a concept of a tailored analysis is used, based on a high density automated aircraft report database (including radiosonde and satellite data), producing an accurate and precise description of the initial state of the atmosphere, and a relatively simple forecast model to move the forecast forward in time. The steadily updated 2-12 h forecasts provided every 3 h will be more efficient and accurate than the present 18 and 24 h forecasts provided every 12 hours. I.S.

48

OCEANOGRAPHY

Includes biological, dynamic, and physical oceanography; and marine resources.

N86-21092*# State Univ. of New York, Albany. Dept. of Geological Sciences.

WILSON STUDY CYCLES: RESEARCH RELATIVE TO OCEAN GEODYNAMIC CYCLES Final Report, 1 Jul. 1983 - 5 May 1985

W. S. F. KIDD 5 May 1985 23 p refs

(Contract NAG3-333)

(NASA-CR-176560; NAS 1.26:176560) Avail: NTIS HC A02/MF A01 CSCL 08C

The effects of conversion of Atlantic (rifted) margins to convergent plate boundaries; oceanic plateaus at subduction zones; continental collision and tectonic escape; southern Africa rifts; and global hot spot distribution on long term development of the continental lithosphere were studied. B.G.

54

MAN/SYSTEM TECHNOLOGY AND LIFE SUPPORT

Includes human engineering; biotechnology; and space suits and protective clothing.

A86-36172* Tufts Univ., Medford, Mass.

THE EFFECTS OF SYNTACTIC COMPLEXITY ON THE HUMAN-COMPUTER INTERACTION

R. A. CHECHILE, R. N. FLEISCHMAN, and D. M. SADOSKI (Tufts University, Medford, MA) Human Factors (ISSN 0018-7208), vol. 28, Feb. 1986, p. 11-22. refs

(Contract NAG3-51)

Three divided-attention experiments were performed to evaluate the effectiveness of a syntactic analysis of the primary task of editing flight route-way-point information. For all editing conditions, a formal syntactic expression was developed for the operator's interaction with the computer. In terms of the syntactic expression, four measures of syntactic were examined. Increased syntactic complexity did increase the time to train operators, but once the operators were trained, syntactic complexity did not influence the divided-attention performance. However, the number of memory retrievals required of the operator significantly accounted for the variation in the accuracy, workload, and task completion time found on the different editing tasks under attention-sharing conditions.

Author

N86-13899*# National Aeronautics and Space Administration. Lewis Research Center, Cleveland, Ohio.

MASS LOSS OF SHUTTLE SPACE SUIT ORTHOFABRIC UNDER SIMULATED IONOSPHERIC ATOMIC OXYGEN BOMBARDMENT

W. L. MILLER Nov. 1985 14 p refs

(NASA-TM-87149; E-2777; NAS 1.15:87149) Avail: NTIS HC A02/MF A01 CSCL 06K

Many polymeric materials used for thermal protection and insulation on spacecraft degrade significantly under prolonged bombardment by ionospheric atomic oxygen. The covering fabric of the multilayered shuttle space suit is composed of a loose weave of GORE-TEX fibers, Nomex and Kevlar-29, which are all polymeric materials. The complete evaluation of suit fabric degradation from ionospheric atomic oxygen is of importance in reevaluating suit lifetime and inspection procedures. The mass loss and visible physical changes of each test sample was determined. Kapton control samples and data from previous asher

and flight tests were used to scale the results to reflect ionospheric conditions at about 220 km altitude. It is predicted that the orthofabric loses mass in the ionosphere at a rate of about 66% of the original orthofabric mass/yr. The outer layer of the two-layer orthofabric test samples shows few easily visible signs of degradation, even when observed at 440X. It is concluded that the orthofabric could suffer significant loss of performance after much less than a year of total exposure time, while the degradation might be undetectable in post flight visual examinations of space suits. E.A.K.

59

MATHEMATICAL AND COMPUTER SCIENCES (GENERAL)

N86-26914*# National Aeronautics and Space Administration. Lewis Research Center, Cleveland, Ohio.

INCREASING PROCESSOR UTILIZATION DURING PARALLEL COMPUTATION RUNDOWN

W. H. JONES 1986 13 p refs Presented at the 1986 International Conference on Parallel Processing, St. Charles, Ill., 19-22 Aug. 1986; sponsored by IEEE

(NASA-TM-87349; E-3101; NAS 1.15:87349) Avail: NTIS HC A02/MF A01 CSCL 09B

Some parallel processing environments provide for asynchronous execution and completion of general purpose parallel computations from a single computational phase. When all the computations from such a phase are complete, a new parallel computational phase is begun. Depending upon the granularity of the parallel computations to be performed, there may be a shortage of available work as a particular computational phase draws to a close (computational rundown). This can result in the waste of computing resources and the delay of the overall problem. In many practical instances, strict sequential ordering of phases of parallel computation is not totally required. In such cases, the beginning of one phase can be correctly computed before the end of a previous phase is completed. This allows additional work to be generated somewhat earlier to keep computing resources busy during each computational rundown. The conditions under which this can occur are identified and the frequency of occurrence of such overlapping in an actual parallel Navier-Stokes code is reported. A language construct is suggested and possible control strategies for the management of such computational phase overlapping are discussed. Author

60

COMPUTER OPERATIONS AND HARDWARE

Includes hardware for computer graphics, firmware, and data processing.

A86-31571* Carnegie-Mellon Univ., Pittsburgh, Pa.

ERROR-SOURCE EFFECTS IN A HIGH-ACCURACY OPTICAL FINITE-ELEMENT PROCESSOR

B. K. TAYLOR and D. P. CASASSENT (Carnegie-Mellon University, Pittsburgh, PA) Applied Optics (ISSN 0003-6935), vol. 25, March 15, 1986, p. 966-975. NSF-supported research. refs

(Contract NAG1-575; NAG3-5)

High-accuracy optical linear algebra processors are addressed with attention to three new aspects. These include: their application to the solution of finite-element problems; the first error-source models for component errors in such processors; and the first analysis of error sources in such processors. Author

COMPUTER PROGRAMMING AND SOFTWARE

Includes computer programs, routines, and algorithms, and specific applications, e.g., CAD/CAM.

A86-36861*# National Aeronautics and Space Administration. Lewis Research Center, Cleveland, Ohio.

A COMPUTER ANALYSIS PROGRAM FOR INTERFACING THERMAL AND STRUCTURAL CODES

R. L. THOMPSON (NASA, Lewis Research Center, Cleveland, OH) and R. J. MAFFEO (General Electric Co., Cincinnati, OH) IN: Computers in engineering 1985; Proceedings of the International Computers in Engineering Conference and Exhibition, Boston, MA, August 4-8, 1985. Volume 2. New York, American Society of Mechanical Engineers, 1985, p. 289-295. Previously announced in STAR as N85-27264.

A software package has been developed to transfer three-dimensional transient thermal information accurately, efficiently, and automatically from a heat transfer analysis code to a structural analysis code. The code is called three-dimensional TRansfer ANalysis Code to Interface Thermal and Structural codes, or 3D TRANCITS. TRANCITS has the capability to couple finite difference and finite element heat transfer analysis codes to linear and nonlinear finite element structural analysis codes. TRANCITS currently supports the output of SINDA and MARC heat transfer codes directly. It will also format the thermal data output directly so that it is compatible with the input requirements of the NASTRAN and MARC structural analysis codes. Other thermal and structural codes can be interfaced using the transfer module with the neutral heat transfer input file and the neutral temperature output file. The transfer module can handle different elemental mesh densities for the heat transfer analysis and the structural analysis. Author

N86-19008*# National Aeronautics and Space Administration. Lewis Research Center, Cleveland, Ohio.

PARTITIONING AND PACKING MATHEMATICAL SIMULATION MODELS FOR CALCULATION ON PARALLEL COMPUTERS

D. J. ARPASI and E. J. MILNER 1986 38 p refs Prepared for Presentation at the 1986 International Conference on Parallel Processing, St. Charles, Ill., 19-22 Aug. 1986; sponsored by Pennsylvania State Univ. and IEEE Computer Society (NASA-TM-87170; E-2808; NAS 1.15:87170) Avail: NTIS HC A03/MF A01 CSCL 09B

The development of multiprocessor simulations from a serial set of ordinary differential equations describing a physical system is described. Degrees of parallelism (i.e., coupling between the equations) and their impact on parallel processing are discussed. The problem of identifying computational parallelism within sets of closely coupled equations that require the exchange of current values of variables is described. A technique is presented for identifying this parallelism and for partitioning the equations for parallel solution on a multiprocessor. An algorithm which packs the equations into a minimum number of processors is also described. The results of the packing algorithm when applied to a turbojet engine model are presented in terms of processor utilization. Author

N86-22150*# National Aeronautics and Space Administration. Lewis Research Center, Cleveland, Ohio.

A COMPUTER PROGRAM TO CALCULATE THE RESISTIVITY OF A THIN FILM DEPOSITED ON A CONDUCTIVE SUBSTRATE FROM FOUR-POINT PROBE MEASUREMENTS

L. G. OBERLE and G. C. FRALICK Mar. 1986 28 p refs (NASA-TM-87262; E-2954) Avail: NTIS HC A03/MF A01 CSCL 09B

A series of FORTRAN-77 programs is described which correct for the effect of a conducting substrate when a linear four-point probe is used to measure the resistivity of a thin film. The resistivity of the film is given in terms of the thicknesses of the film and

substrate, the known resistivity of the substrate, and the measured delta V/I. A full development is given as well as a complete description of the operation of the programs. The programs themselves can be obtained through COSMIC, and are identified as LEW No. 14381. Author

N86-27927*# Operations Research, Inc., Rockville, Md.

SPECTRUM ORBIT UTILIZATION PROGRAM DOCUMENTATION: SOUP5 VERSION 3.8 USER'S MANUAL, VOLUME 1, CHAPTERS 1 THROUGH 5 Final Report

J. DAVIDSON, H. R. OTTEY, P. SAWITZ, and F. S. ZUSMAN 10 Jun. 1985 194 p (Contract NAS3-22885) (NASA-CR-174889; NAS 1.26:174889; TR-2273-VOL-1) Avail: NTIS HC A09/MF A01 CSCL 09B

The underlying engineering and mathematical models as well as the computational methods used by the Spectrum Orbit Utilization Program 5 (SOUP5) analysis programs are described. Included are the algorithms used to calculate the technical parameters, and references to the technical literature. The organization, capabilities, processing sequences, and processing and data options of the SOUP5 system are described. The details of the geometric calculations are given. Also discussed are the various antenna gain algorithms; rain attenuation and depolarization calculations; calculations of transmitter power and received power flux density; channelization options, interference categories, and protection ratio calculation; generation of aggregate interference and margins; equivalent gain calculations; and how to enter a protection ratio template. B.G.

N86-27928*# Operations Research, Inc., Rockville, Md.

SPECTRUM ORBIT UTILIZATION PROGRAM DOCUMENTATION: SOUP5 VERSION 3.8 USER'S MANUAL, VOLUME 2, APPENDICES A THROUGH G Final Report

J. DAVIDSON, H. R. OTTEY, P. SAWITZ, and F. S. ZUSMAN 10 Jun. 1985 124 p (Contract NAS3-22885) (NASA-CR-174890; NAS 1.26:174890; TR-2273-VOL-2) Avail: NTIS HC A06/MF A01 CSCL 09B

The appendixes of the user manual are presented. Input forms which may be used to prepare data for the SOUP5V3.4 of the R2BCSAT-83 data base are given. The IBM job control language which can be used to run the SOUP5 system from a magnetic tape is described. Copies of a run using the delivered tape and IBM OS/MVS Job Control Language card deck are illustrated. Numerical limits on scenario data requests are listed. Error handling, error messages and editing procedures are also listed. Instructions as to how to enter a protection ratio template are given. And relation between PARC parameter, channelization, channel families, and interference categories are also listed. E.R.

N86-27930*# College of William and Mary, Williamsburg, Va. Dept. of Computer Science.

A HIGH-ORDER LANGUAGE FOR A SYSTEM OF CLOSELY COUPLED PROCESSING ELEMENTS Final Report

S. FEYOCK and W. R. COLLINS Jul. 1986 67 p (Contract NAG3-232) (NASA-CR-177280; NAS 1.26:177280) Avail: NTIS HC A04/MF A01 CSCL 09B

The research reported in this paper was occasioned by the requirements on part of the Real-Time Digital Simulator (RTDS) project under way at NASA Lewis Research Center. The RTDS simulation scheme employs a network of CPUs running lock-step cycles in the parallel computations of jet airplane simulations. Their need for a high order language (HOL) that would allow non-experts to write simulation applications and that could be implemented on a possibly varying network can best be fulfilled by using the programming language Ada. We describe how the simulation problems can be modeled in Ada, how to map a single, multi-processing Ada program into code for individual processors, regardless of network reconfiguration, and why some Ada language features are particularly well-suited to network simulations. Author

COMPUTER SYSTEMS

Includes computer networks and special application computer systems.

A86-32051* University of Southern California, Los Angeles.
PERFORMANCE EVALUATION OF A SIMULATED DATA-FLOW COMPUTER WITH LOW-RESOLUTION ACTORS

J. L. GAUDIOT (Southern California, University, Los Angeles) and M. D. ERCEGOVAC (California, University, Los Angeles) Journal of Parallel and Distributed Computing (ISSN 0743-7315), vol. 2, Nov. 1985, p. 321-351. refs
 (Contract NSF ECS-84-04345; NAG3-132)

Basic problems related to the exploitation of parallelism in a program include sequencing of the instructions and communication of the data. It is pointed out that the data-flow approach offers an elegant solution to the sequencing problem, since all data dependencies are automatically handled and only instructions with ready input sets are activated. It is shown that a change in the level of subcomputations (actors) affects communications costs. The concept of variable resolution is discussed, and the testbed environment is examined. Attention is given to the architecture of the processing elements, the communication network, and the simulators. A description of the analytical model is also provided. Simulation and results are discussed, taking into account test programs and allocation, the variation of the number of processing elements, the variation of the resolution in directed acyclic graphs, performance in processing loops, and array handling. G.R.

A86-28651*# National Aeronautics and Space Administration. Lewis Research Center, Cleveland, Ohio.

HARDWARE CONFIGURATION FOR A REAL-TIME MULTIPROCESSOR SIMULATOR

R. A. BLECH and A. D. WILLIAMS Jul. 1986 21 p
 (NASA-TM-88802; E-3141; NAS 1.15:88802) Avail: NTIS HC A02/MF A01 CSCL 09B

The Real-Time Multiprocessor Simulator (RTMPS) is a multiple microcomputer system used to investigate the application of parallel-processing concepts to real-time simulation. This users manual describes the set-up and installation considerations for the RTMPS hardware. Any modifications or further improvements to the RTMPS hardware will be documented in an addendum to this manual. Author

CYBERNETICS

Includes feedback and control theory, artificial intelligence, robotics and expert systems.

A86-35419* Notre Dame Univ., Ind.
NONLINEAR OPTIMAL CONTROL WITH TENSORS - SOME COMPUTATIONAL ISSUES

J. A. OSULLIVAN and M. K. SAIN (Notre Dame, University, IN) IN: 1985 American Control Conference, 4th, Boston, MA, June 19-21, 1985, Proceedings. Volume 3. New York, Institute of Electrical and Electronics Engineers, 1985, p. 1600-1605. refs
 (Contract NSG-3048)

Some computational issues associated with the calculation of optimal feedback controls for nonlinear systems in a tensor setting are described. The specific issues addressed pertain to the combinatorial nature of the loading of the elements into tensors used to represent the system, cost, and feedback, and the subsequent calculations involving these elements. Particular attention is given to: the symmetric tensor algebra which is a

natural setting for representing polynomials; the conversions between symmetric and nonsymmetric tensors; the general nature of the calculations required; and the solution equation for nonlinear optimal feedback control. It is concluded that nonlinear tensor feedback can improve performance both in terms of system responses and in terms of system stability region. B.J.

NUMERICAL ANALYSIS

Includes iteration, difference equations, and numerical approximation.

A86-20033* Massachusetts Inst. of Tech., Cambridge.
PROPAGATION AND STABILITY OF WAVELIKE SOLUTIONS OF FINITE DIFFERENCE EQUATIONS WITH VARIABLE COEFFICIENTS

M. B. GILES and W. T. THOMPCKINS, JR. (MIT, Cambridge, MA) Journal of Computational Physics (ISSN 0021-9991), vol. 58, May 15, 1985, p. 349-360. refs
 (Contract NAG3-9)

The propagation and dissipation of wavelike solutions to finite difference equations is analyzed on the basis of an asymptotic approach in which a wave solution is expressed as a product of a complex amplitude and an oscillatory phase function whose frequency and wavenumber may also be complex. An asymptotic expansion leads to a local dispersion relation for wavenumber and frequency; the first-order terms produce an equation for the amplitude in which the local group velocity appears as the convection velocity of the amplitude. Equations for the motion of wavepackets and their interaction at boundaries are derived, and a global stability analysis is carried out. B.J.

A86-30814* Cleveland State Univ., Ohio.
AN EMBEDDING METHOD FOR THE STEADY EULER EQUATIONS

S.-H. CHANG (Cleveland State University, OH) and G. M. JOHNSON (Institute for Computational Studies, Fort Collins, CO) Journal of Computational Physics (ISSN 0021-9991), vol. 63, March 1986, p. 191-200. refs
 (Contract NAG3-339)

Certain difficulties arise in connection with the numerical solution of a direct finite difference representation of the steady Euler equations. Johnson (1979, 1981, 1982) has, therefore, proposed a surrogate-equation technique, in which the first-order steady Euler equations are embedded in a certain second-order system of equations. The present paper is concerned with the theoretical justification for such an embedding approach. For the numerical solution of the two-dimensional steady Euler equations, it is shown that, under a continuity restriction, it is possible to solve a second-order embedded system together with appropriate additional boundary conditions. The result indicates that a more direct and potentially more efficient approach to the steady solutions exists than the alternative of solving the unsteady equations. G.R.

A86-35386* Ohio State Univ., Columbus.
POLYNOMIC NONLINEAR DYNAMICAL SYSTEMS - A RESIDUAL SENSITIVITY METHOD FOR MODEL REDUCTION

S. YURKOVICH (Ohio State University, Columbus), D. BUGAJSKI (Honeywell Systems and Research Center, Minneapolis, MN), and M. SAIN (Notre Dame, University, IN) IN: 1985 American Control Conference, 4th, Boston, MA, June 19-21, 1985, Proceedings. Volume 2. New York, Institute of Electrical and Electronics Engineers, 1985, p. 933-939. Research supported by the University of Notre Dame. refs
 (Contract NSG-3048)

The motivation for using polynomic combinations of system states and inputs to model nonlinear dynamics systems is founded

upon the classical theories of analysis and function representation. A feature of such representations is the need to make available all possible monomials in these variables, up to the degree specified, so as to provide for the description of widely varying functions within a broad class. For a particular application, however, certain monomials may be quite superfluous. This paper examines the possibility of removing monomials from the model in accordance with the level of sensitivity displayed by the residuals to their absence. Critical in these studies is the effect of system input excitation, and the effect of discarding monomial terms, upon the model parameter set. Therefore, model reduction is approached iteratively, with inputs redesigned at each iteration to ensure sufficient excitation of remaining monomials for parameter approximation. Examples are reported to illustrate the performance of such model reduction approaches. Author

A86-49850* Technion - Israel Inst. of Tech., Haifa.
ACCELERATION OF CONVERGENCE OF VECTOR SEQUENCES

A. SIDI (Technion - Israel Institute of Technology, Haifa, Israel), W. F. FORD (NASA, Lewis Research Center, Cleveland, OH), and D. A. SMITH (Duke University, Durham, NC) SIAM Journal of Numerical Analysis (ISSN 0036-1429), vol. 23, Feb. 1986, p. 178-196. Previously announced in STAR as N84-13885. refs (Contract NAS3-23606; NSG-3160)

A general approach to the construction of convergence acceleration methods for vector sequence is proposed. Using this approach, one can generate some known methods, such as the minimal polynomial extrapolation, the reduced rank extrapolation, and the topological epsilon algorithm, and also some new ones. Some of the new methods are easier to implement than the known methods and are observed to have similar numerical properties. The convergence analysis of these new methods is carried out, and it is shown that they are especially suitable for accelerating the convergence of vector sequences that are obtained when one solves linear systems of equations iterative. A stability analysis is also given, and numerical examples are provided. The convergence and stability properties of the topological epsilon algorithm are likewise given. Author

N86-10860* Georgia Inst. of Tech., Atlanta. School of Engineering Science and Mechanics.

BOUNDING SOLUTIONS OF GEOMETRICALLY NONLINEAR VISCOELASTIC PROBLEMS

J. M. STUBSTAD and G. J. SIMITSES 1985 3 p refs (Contract NAG3-534)
 (NASA-CR-176219; NAS 1.26:176219) Avail: NTIS HC A02/MF A01 CSCL 12A

Integral transform techniques, such as the Laplace transform, provide simple and direct methods for solving viscoelastic problems formulated within a context of linear material response and using linear measures for deformation. Application of the transform operator reduces the governing linear integro-differential equations to a set of algebraic relations between the transforms of the unknown functions, the viscoelastic operators, and the initial and boundary conditions. Inversion either directly or through the use of the appropriate convolution theorem, provides the time domain response once the unknown functions have been expressed in terms of sums, products or ratios of known transforms. When exact inversion is not possible approximate techniques may provide accurate results. The overall problem becomes substantially more complex when nonlinear effects must be included. Situations where a linear material constitutive law can still be productively employed but where the magnitude of the resulting time dependent deformations warrants the use of a nonlinear kinematic analysis are considered. The governing equations will be nonlinear integro-differential equations for this class of problems. Thus traditional as well as approximate techniques, such as cited above, cannot be employed since the transform of a nonlinear function is not explicitly expressible. Author

N86-26067* Kansas Univ. Center for Research, Inc., Lawrence. Structural Engineering and Engineering Materials.

THEORETICAL AND SOFTWARE CONSIDERATIONS FOR GENERAL DYNAMIC ANALYSIS USING MULTILEVEL SUBSTRUCTURED MODELS Final Report

R. J. SCHMIDT and R. H. DODDS, JR. Sep. 1985 189 p refs (Contract NAG3-32)
 (NASA-CR-176822; NAS 1.26:176822; KU-SM-15) Avail: NTIS HC A09/MF A01 CSCL 12A

The dynamic analysis of complex structural systems using the finite element method and multilevel substructured models is presented. The fixed-interface method is selected for substructure reduction because of its efficiency, accuracy, and adaptability to restart and reanalysis. This method is extended to reduction of substructures which are themselves composed of reduced substructures. The implementation and performance of the method in a general purpose software system is emphasized. Solution algorithms consistent with the chosen data structures are presented. It is demonstrated that successful finite element software requires the use of software executives to supplement the algorithmic language. The complexity of the implementation of restart and reanalysis procedures illustrates the need for executive systems to support the noncomputational aspects of the software. It is shown that significant computational efficiencies can be achieved through proper use of substructuring and reduction techniques without sacrificing solution accuracy. The restart and reanalysis capabilities and the flexible procedures for multilevel substructured modeling gives economical yet accurate analyses of complex structural systems. Author

N86-28661* National Aeronautics and Space Administration. Lewis Research Center, Cleveland, Ohio.

SOLUTION OF ELLIPTIC PARTIAL DIFFERENTIAL EQUATIONS BY FAST POISSON SOLVERS USING A LOCAL RELAXATION FACTOR. 1: ONE-STEP METHOD

S. C. CHANG May 1986 22 p Presented at the Ninth International Conference on Numerical Methods in Fluid Dynamics, Saclay, France, 25-29 Jun. 1984
 (NASA-TP-2529; E-2461-1; NAS 1.60:2529) Avail: NTIS HC A02/MF A01 CSCL 12A

An algorithm for solving a large class of two- and three-dimensional nonseparable elliptic partial differential equations (PDE's) is developed and tested. It uses a modified D'Yakanov-Gunn iterative procedure in which the relaxation factor is grid-point dependent. It is easy to implement and applicable to a variety of boundary conditions. It is also computationally efficient, as indicated by the results of numerical comparisons with other established methods. Furthermore, the current algorithm has the advantage of possessing two important properties which the traditional iterative methods lack; that is: (1) the convergence rate is relatively insensitive to grid-cell size and aspect ratio, and (2) the convergence rate can be easily estimated by using the coefficient of the PDE being solved. Author

N86-28662* National Aeronautics and Space Administration. Lewis Research Center, Cleveland, Ohio.

PHYSICAL AND NUMERICAL SOURCES OF COMPUTATIONAL INEFFICIENCY IN INTEGRATION OF CHEMICAL KINETIC RATE EQUATIONS: ETIOLOGY, TREATMENT AND PROGNOSIS

D. T. PRATT (Washington Univ., Seattle) and K. RADHAKRISHNAN May 1986 12 p (Contract NAG3-147)
 (NASA-TP-2590; E-2587; NAS 1.60:2590) Avail: NTIS HC A02/MF A01 CSCL 12A

The design of a very fast, automatic black-box code for homogeneous, gas-phase chemical kinetics problems requires an understanding of the physical and numerical sources of computational inefficiency. Some major sources reviewed in this report are stiffness of the governing ordinary differential equations (ODE's) and its detection, choice of appropriate method (i.e., integration algorithm plus step-size control strategy), nonphysical initial conditions, and too frequent evaluation of thermodynamic and kinetic properties. Specific techniques are recommended (and

66 SYSTEMS ANALYSIS

some advised against) for improving or overcoming the identified problem areas. It is argued that, because reactive species increase exponentially with time during induction, and all species exhibit asymptotic, exponential decay with time during equilibration, exponential-fitted integration algorithms are inherently more accurate for kinetics modeling than classical, polynomial-interpolant methods for the same computational work. But current codes using the exponential-fitted method lack the sophisticated stepsize-control logic of existing black-box ODE solver codes, such as EPISODE and LSODE. The ultimate chemical kinetics code does not exist yet, but the general characteristics of such a code are becoming apparent. Author

66

SYSTEMS ANALYSIS

Includes mathematical modeling; network analysis; and operations research.

A86-27036* National Aeronautics and Space Administration. Lewis Research Center, Cleveland, Ohio.

A LUMPED PARAMETER MATHEMATICAL MODEL FOR SIMULATION OF SUBSONIC WIND TUNNELS

S. M. KROSEL, G. L. COLE, W. M. BRUTON, and J. R. SZUCH May 1986 50 p refs

(NASA-TM-87324; E-3065; NAS 1.15:87324) Avail: NTIS HC A03/MF A01 CSDL 12B

Equations for a lumped parameter mathematical model of a subsonic wind tunnel circuit are presented. The equation state variables are internal energy, density, and mass flow rate. The circuit model is structured to allow for integration and analysis of tunnel subsystem models which provide functions such as control of altitude pressure and temperature. Thus the model provides a useful tool for investigating the transient behavior of the tunnel and control requirements. The model was applied to the proposed NASA Lewis Altitude Wind Tunnel (AWT) circuit and included transfer function representations of the tunnel supply/exhaust air and refrigeration subsystems. Both steady state and frequency response data are presented for the circuit model indicating the type of results and accuracy that can be expected from the model. Transient data for closed loop control of the tunnel and its subsystems are also presented, demonstrating the model's use as a control analysis tool. Author

70

PHYSICS (GENERAL)

A86-16521* Massachusetts Inst. of Tech., Cambridge.

GRID-FREE SIMULATION OF DIFFUSION USING RANDOM WALK METHODS

A. F. GHONIEM (MIT, Cambridge, MA) and F. S. SHERMAN (California, University, Berkeley) Journal of Computational Physics (ISSN 0021-9991), vol. 61, Oct. 1985, p. 1-37. refs

(Contract NAG3-131; NSF CPE-84-04811)

The simulation of the diffusion of a continuum field by the random walk (RW) displacement of a set of particles is considered. Elements of the gradients of the diffusive concentration are transported by computational particles. It is demonstrated that, by the use of concentration gradients in the RW process, statistical errors are reduced and each realization of the numerical solution is a representation of the exact solution. The algorithm is grid-free, and the computational elements move to follow the gradients;

hence, the algorithm is self-adaptive, and uniform resolution is achieved for all times. B.J.

71

ACOUSTICS

Includes sound generation, transmission, and attenuation.

A86-16466* Lockheed-Georgia Co., Marietta.

TONE EXCITED JETS. I - INTRODUCTION

H. K. TANNA and K. K. AHUJA (Lockheed-Georgia Co., Marietta, GA) Journal of Sound and Vibration (ISSN 0022-460X), vol. 102, Sept. 8, 1985, p. 57-61. Research supported by Lockheed Internal Research and Development Program. refs

(Contract NAS3-21987)

The major objective of the present study is an understanding of the mechanism of broadband jet noise augmentation due to upstream excitation, in terms of the relationship between excitation characteristics, changes in large scale and/or small scale turbulence structure of the jet, and sound radiated to the far field under both static and simulated forward velocity conditions. A systematic set of acoustic measurements was accordingly made for a range of flow conditions in the acoustic research facilities of a large transport aircraft manufacturer. After analyzing acoustic results, turbulence measurements were made with a laser velocimeter for those jet conditions at which jet noise amplification was important. A theory was developed to account for static and in-flight simulation results. O.C.

A86-16469* Lockheed-Georgia Co., Marietta.

TONE EXCITED JETS. IV - ACOUSTIC MEASUREMENTS

K. K. AHUJA and D. F. BLAKNEY (Lockheed-Georgia Co., Marietta, GA) Journal of Sound and Vibration (ISSN 0022-460X), vol. 102, Sept. 8, 1985, p. 93-117. Research supported by Lockheed Internal Research and Development Program. refs

(Contract NAS3-21987)

Attention is given to acoustic results from an experiment designed to deepen insight into the noise generated by a tone-excited jet, with emphasis on the mechanism of broadband jet noise amplification. Results are presented for both heated and unheated jets, with and without the effect of forward flight simulation over a range of excitation frequencies and levels, and for zero-order and first-order spinning modes. Broadband jet noise amplifications of up to 5 dB have been observed in this study. Relative velocity effects are the same for both excited and unexcited jets. It is concluded that small scale turbulence generates the additional broadband noise upon excitation of the jet by an upstream-injected discrete tone acoustic wave. O.C.

A86-16470* Florida State Univ., Tallahassee.

TONE EXCITED JETS. V - A THEORETICAL MODEL AND COMPARISON WITH EXPERIMENT

C. K. W. TAM (Florida State University, Tallahassee) and P. J. MORRIS (Pennsylvania State University, University Park) Journal of Sound and Vibration (ISSN 0022-460X), vol. 102, Sept. 8, 1985, p. 119-151. Research supported by Lockheed Internal Research and Development Program. refs

(Contract NAS3-21987)

A mathematical model of tone-excited jets is developed which consists of two major components: a mathematical description of the process by which the intrinsic instability waves of the jet are excited by the upstream tones; and the modeling of the nonlinear interaction between the mean flow of the jet, the excited large-scale instability waves or turbulence structure, and the fine scale turbulence. It is assumed that each of these jet flow components can be characterized by a few parameters, which are then related by conservation equations that are supplemented by closure models. This quasi-linear model's results are compared with experimental measurements, and good agreement is obtained over

a wide range of excitation frequencies and excitation levels.

O.C.

A86-20130*# National Aeronautics and Space Administration. Lewis Research Center, Cleveland, Ohio.

TIME-DEPENDENT WAVE ENVELOPE FINITE DIFFERENCE ANALYSIS OF SOUND PROPAGATION

K. J. BAUMEISTER (NASA, Lewis Research Center, Cleveland, OH) AIAA Journal (ISSN 0001-1452), vol. 24, Jan. 1986, p. 32-38. Previously cited in issue 05, p. 640, Accession no. A85-16102. refs

A86-20364*# National Aeronautics and Space Administration. Lewis Research Center, Cleveland, Ohio.

THE EFFECT OF ACOUSTIC REFLECTIONS ON COMBUSTOR NOISE MEASUREMENTS

R. G. HUFF (NASA, Lewis Research Center, Cleveland, OH) Journal of Propulsion and Power (ISSN 0748-4658), vol. 2, Jan.-Feb. 1986, p. 18-24. Previously cited in issue 05, p. 640, Accession no. A85-16103. refs

A86-20795* Missouri Univ., Rolla.

A NUMERICAL MODEL OF ACOUSTIC CHOKING. II - SHOCKED SOLUTIONS

N. J. WALKINGTON and W. EVERSMA (Missouri-Rolla, University, Rolla) Journal of Sound and Vibration (ISSN 0022-460X), vol. 104, Jan. 8, 1986, p. 81-107. refs (Contract NSG-3231)

The one dimensional equations of gas dynamics are used to model subsonic acoustic choking. This model can accommodate non-linear distortion of waves and the eventual formation of shock waves. Several finite differencing schemes are adapted to obtain solutions. The results obtained with the various schemes are compared with the asymptotic results available. The results suggest that no one finite differencing scheme gives solutions significantly better than the others and that most of the difference solutions are close to the asymptotic results. If the acoustic shock wave is sufficiently strong it almost annihilates the acoustic wave; in this situation numerical errors may dominate the results. Such solutions involve very large acoustic attenuations. Author

A86-22747*# National Aeronautics and Space Administration. Lewis Research Center, Cleveland, Ohio.

REVERBERATION EFFECTS ON DIRECTIONALITY AND RESPONSE OF STATIONARY MONOPOLE AND DIPOLE SOURCES IN A WIND TUNNEL

K. J. BAUMEISTER (NASA, Lewis Research Center, Cleveland, OH) ASME, Transactions, Journal of Vibration, Acoustics, Stress, and Reliability in Design (ISSN 0739-3717), vol. 108, Jan. 1986, p. 82-90. Previously announced in STAR as N85-31443. refs (ASME PAPER 85-WA/NCA-1)

Analytical solutions for the three dimensional inhomogeneous wave equation with flow in a hardwall rectangular wind tunnel and in the free field are presented for a stationary monopole noise source. Dipole noise sources are calculated by combining two monopoles 180 deg out of phase. Numerical calculations for the modal content, spectral response and directivity for both monopole and dipole sources are presented. In addition, the effect of tunnel alterations, such as the addition of a mounting plate, on the tunnels reverberant response are considered. In the frequency range of practical importance for the turboprop response, important features of the free field directivity can be approximated in a hardwall wind tunnel with flow if the major lobe of the noise source is not directed upstream. However, for an omnidirectional source, such as a monopole, the hardwall wind tunnel and free field response are not comparable. Author

A86-26542*# National Aeronautics and Space Administration. Lewis Research Center, Cleveland, Ohio.

SCALING ATTENUATION DATA CHARACTERIZES CHANGES IN MATERIAL MICROSTRUCTURE

E. R. GENERAZIO (NASA, Lewis Research Center, Cleveland, OH) (NASA and ASM, Analytical Ultrasonics in Materials Research and Testing Conference, Cleveland, OH, Nov. 13, 14, 1984) Materials Evaluation (ISSN 0025-5327), vol. 44, Feb. 1986, p. 198-202, 208. refs

Ultrasonic attenuation was measured for polycrystalline samples of nickel and copper with various grain-size distributions produced by heat treatment. Attenuation as a function of frequency was determined for a sample having a known mean grain diameter D . It was found that, once this function is determined, it can be scaled to determine the mean grain size of other samples of the same material with different mean grain diameters. These results were obtained using broadband pulse-echo ultrasound in the 25 to 100 MHz frequency range. The results suggest an ultrasonic, nondestructive approach for verifying heat treatment of metals.

Author

A86-31593*# Lockheed-Georgia Co., Marietta.

AN EXPERIMENTAL STUDY OF TONE-EXCITED HEATED JETS

J. LEPICOVSKY, K. K. AHUJA, and M. SALIKUDDIN (Lockheed-Georgia Co., Marietta) Journal of Propulsion and Power (ISSN 0748-4658), vol. 2, Mar.-Apr. 1986, p. 149-154. Previously cited in issue 01, p. 75, Accession no. A85-10882. refs

(Contract NAS3-23708)

A86-35857* Lockheed-Georgia Co., Marietta.

NON-LINEAR EFFECTS IN FINITE AMPLITUDE WAVE PROPAGATION THROUGH DUCTS AND NOZZLES

M. SALIKUDDIN and W. H. BROWN (Lockheed-Georgia Co., Marietta) Journal of Sound and Vibration (ISSN 0022-460X), vol. 106, April 8, 1986, p. 71-106. Research sponsored by the Lockheed Independent Research and Development Program. refs (Contract NAS3-20797)

In this paper an extensive study of non-linear effects in finite amplitude wave propagation through ducts and nozzles is summarized. Some results from earlier studies are included to illustrate the non-linear effects on the transmission characteristics of duct and nozzle terminations. Investigations, both experimental and analytical, were carried out to determine the magnitudes of the effects for high intensity pulse propagation. The results derived from these investigations are presented in this paper. They include the effect of the sound intensity on the acoustic characteristics of duct and nozzle terminations, the extent of the non-linearities in the propagation of high intensity impulsive sound inside the duct and out into free field, the acoustic energy dissipation mechanism at a termination as shown by flow visualizations, and quantitative evaluations by experimental and analytical means of the influence of the intensity of a sound pulse on the dissipation of its acoustic power. Author

A86-41689*# Missouri Univ., Rolla.

MODELING WIND TUNNEL EFFECTS ON THE RADIATION CHARACTERISTICS OF ACOUSTIC SOURCES

W. EVERSMA (Missouri-Rolla, University, Rolla) and K. J. BAUMEISTER (NASA, Lewis Research Center, Cleveland, OH) Journal of Aircraft (ISSN 0021-8669), vol. 23, June 1986, p. 455-463. Previously cited in issue 05, p. 641, Accession no. A85-16104. refs

A86-45492*# Arizona Univ., Tucson.

NOISE GENERATED BY CONVECTED GUSTS INTERACTING WITH SWEEP AIRFOIL CASCADES

E. ENVIA and E. J. KERSCHEN (Arizona, University, Tucson)
AIAA, Aeroacoustics Conference, 10th, Seattle, WA, July 9-11, 1986. 10 p. refs
(Contract NAG3-357)
(AIAA PAPER 86-1872)

An analysis is developed for the noise generated by the interaction of a rotor viscous wake with a cascade of swept stator vanes. The stator vanes span a channel formed by infinite parallel walls and containing a subsonic mean flow. High frequency interactions, for which the noise generation is concentrated at the vane leading edge, are considered. The analysis utilizes a superposition of the solution to the isolated stator vane problem, presented in an earlier paper, to develop an approximate solution to the cascade problem. The rotor wake model includes the features of wake circumferential lean and a linear spanwise variation of the magnitude of the wake deficit velocity. Calculations are presented which show that, for rotor wakes with moderate circumferential lean, stator sweep produces substantial reductions in noise level. The vane sweep must be oriented to enhance the phase lags along the vane leading edge produced by wake lean. The noise levels are found to be fairly insensitive to spanwise variations in the wake deficit. Author

A86-45493*# Arizona Univ., Tucson.

INFLUENCE OF AIRFOIL CAMBER ON CONVECTED GUST INTERACTION NOISE

M. R. MYERS and E. J. KERSCHEN (Arizona, University, Tucson)
AIAA, Aeroacoustics Conference, 10th, Seattle, WA, July 9-11, 1986. 11 p. refs
(Contract NAG3-357)
(AIAA PAPER 86-1873)

This paper investigates the effect of airfoil steady loading on the sound generated by the interaction of an airfoil with a convected disturbance. A previous theory, which included only the incidence angle contribution to the mean loading, is extended to include camber. The theory is based on a linearization of the Euler equations about a nonuniform, $O(1)$ Mach number subsonic mean flow. The discussion concentrates on the case of a slightly cambered airfoil at small incidence angle, interacting with a gust whose wavelength is short compared to the airfoil chord. The small parameter representing the amount of camber and incidence, and the large parameter representing the ratio of airfoil chord to disturbance wavelength, are utilized in a singular perturbation solution to the governing equations. Acoustic power calculations reveal that the amount of sound generated increases significantly with increased loading. More importantly, it is shown that the radiated acoustic power correlates very well with the strength of the mean flow around the leading edge. Author

A86-45500*# Lockheed-Georgia Co., Marietta.

DEVELOPMENT OF AN IMPULSIVE NOISE SOURCE TO STUDY THE ACOUSTIC REFLECTION CHARACTERISTICS OF HARD-WALLED WIND TUNNELS

M. SALIKUDDIN, R. H. BURRIN, K. K. AHUJA, and H. W. BARTEL (Lockheed-Georgia Co., Marietta) AIAA, Aeroacoustics Conference, 10th, Seattle, WA, July 9-11, 1986. 12 p.
(Contract NAS3-24339)
(AIAA PAPER 86-1887)

Two impulsive sound sources, one using multiple acoustic drivers and the other using a spark discharge were developed to study the acoustic reflection characteristics of hard-walled wind tunnels, and the results of laboratory tests are presented. The analysis indicates that though the intensity of the pulse generated by the spark source was higher than that obtained from the acoustic source, the number of averages needed for a particular test may require an unacceptably long tunnel-run time due to the low spark generation repeat rate because of capacitor charging time. The additional hardware problems associated with the longevity of electrodes and electrode holders in sustaining the impact of

repetitive spark discharges, show the multidriver acoustic source to be more suitable for this application. R.R.

A86-45501*# Lockheed-Georgia Co., Marietta.

ACOUSTIC REFLECTION CONTAMINATION MEASUREMENTS IN THE 16-FOOT NASA LANGLEY TRANSONIC WIND TUNNEL

R. H. BURRIN, M. SALIKUDDIN, K. K. AHUJA, and H. W. BARTEL (Lockheed-Georgia Co., Marietta) AIAA, Aeroacoustics Conference, 10th, Seattle, WA, July 9-11, 1986. 12 p. refs
(Contract NAS3-24339)
(AIAA PAPER 86-1888)

The Propfan Test Assessment (PTA) contract, awarded recently to Lockheed by the NASA-Lewis Research Center, required a comprehensive series of near field acoustic measurements. These were to use transducers mounted on the surfaces on a one-ninth scale model of the Gulfstream G-II aircraft, modified to the PTA single propfan testbed configuration. The 16-foot Transonic Wind Tunnel at the NASA Langley Research Center was chosen as the facility to be used for these model acoustic tests. Since the tunnel was hard-walled, it is not clear to what extent the propfan noise signals, reaching the various transducers, might be contaminated by reflections from the walls. A Multidriver Acoustic Source was built, and using an impulse and time domain averaging technique, the reflection contaminations in the wind tunnel were measured at selected microphone locations. Results of the investigations of near field measurements exists, due to reflections from the hard walls of the wind tunnel. Author

A86-49566*# National Aeronautics and Space Administration. Lewis Research Center, Cleveland, Ohio.

AN APPROACH TO THE CALCULATION OF THE PRESSURE FIELD PRODUCED BY RIGID WIDE CHORD DUAL ROTATION PROPELLERS OF HIGH SOLIDITY IN COMPRESSIBLE FLOW

S. M. RAMACHANDRA and L. J. BOBER (NASA, Lewis Research Center, Cleveland, OH) AIAA, Aerospace Sciences Meeting, 24th, Reno, NV, Jan. 6-8, 1986. 41 p. Previously announced in STAR as N86-21517. refs
(AIAA PAPER 86-0467)

An unsteady lifting service theory for the counter-rotating propeller is presented using the linearized governing equations for the acceleration potential and representing the blades by a surface distribution of pulsating acoustic dipoles distributed according to a modified Birnbaum series. The Birnbaum series coefficients are determined by satisfying the surface tangency boundary conditions on the front and rear propeller blades. Expressions for the combined acoustic resonance modes of the front prop, the rear prop and the combination are also given. Author

A86-49806*# Georgia Inst. of Tech., Atlanta.

AN ITERATIVE FINITE ELEMENT-INTEGRAL TECHNIQUE FOR PREDICTING SOUND RADIATION FROM TURBOFAN INLETS IN STEADY FLIGHT

S. J. HOROWITZ, R. K. SIGMAN, and B. T. ZINN (Georgia Institute of Technology, Atlanta) AIAA Journal (ISSN 0001-1452), vol. 24, Aug. 1986, p. 1256-1262. Previously cited in issue 06, p. 812, Accession no. A82-17796. refs
(Contract NSG-3036)

N86-12007*# National Aeronautics and Space Administration. Lewis Research Center, Cleveland, Ohio.

NUMERICAL TECHNIQUES IN ACOUSTICS

K. J. BAUMEISTER, comp. Oct. 1985 35 p refs Meeting held in Miami Beach, Fla., 17-21 Nov. 1985; sponsored by the ASME
(NASA-CP-2404; E-2758; NAS 1.55:2404) Avail: NTIS HC A03/MF A01 CSCL 20A

This is the compilation of abstracts of the Numerical Techniques in Acoustics Forum held at the ASME's Winter Annual Meeting. This forum was for informal presentation and information exchange of ongoing acoustic work in finite elements, finite difference, boundary elements and other numerical approaches. As part of this forum, it was intended to allow the participants time to raise

questions on unresolved problems and to generate discussions on possible approaches and methods of solution.

N86-12011*# Texas A&M Univ., College Station. Dept. of Aerospace Engineering.

A NUMERICAL METHOD OF CALCULATING PROPELLER NOISE INCLUDING ACOUSTIC NONLINEAR EFFECTS Abstract Only

K. D. KORKAN *In* NASA. Lewis Research Center Numerical Tech. in Acoustics p 9-10 Oct. 1985 refs (Contract NAG3-354)

Avail: NTIS HC A03/MF A01 CSCL 20A

Using the transonic flow fields(s) generated by the NASPROP-E computer code for an eight blade SR3-series propeller, a theoretical method is investigated to calculate the total noise values and frequency content in the acoustic near and far field without using the Flowcs Williams - Hawkings equation. The flow field is numerically generated using an implicit three dimensional Euler equation solver in weak conservation law form. Numerical damping is required by the differencing method for stability in three dimensions, and the influence of the damping on the calculated acoustic values is investigated. The acoustic near field is solved by integrating with respect to time the pressure oscillations induced at a stationary observer location. The acoustic far field is calculated from the near field primitive variables as generated by NASPROP-E computer code using a method involving a perturbation velocity potential as suggested by Hawkings in the calculation of the acoustic pressure time-history at a specified far field observed location. the methodologies described are valid for calculating total noise levels and are applicable to any propeller geometry for which a flow field solution is available. Author

N86-14006*# National Aeronautics and Space Administration. Lewis Research Center, Cleveland, Ohio.

PRELIMINARY MEASUREMENT OF THE NOISE FROM THE 2/9 SCALE MODEL OF THE LARGE-SCALE ADVANCED PROPPAN (LAP) PROPELLER, SR-7A

J. H. DITTMAR Sep. 1985 22 p refs (NASA-TM-87116; E-2718; NAS 1.15:87116) Avail: NTIS HC A02/MF A01 CSCL 02A

Noise data on the Large-scale Advanced Propfan (LAP) propeller model SR-7A were taken into the NASA Lewis 8- by 6-Foot Wind Tunnel. The maximum blade passing tone decreases from the peak level when going to higher helical tip Mach numbers. This noise reduction points to the use of higher propeller speeds as a possible method to reduce airplane cabin noise while maintaining high flight speed and efficiency. Comparison of the SR-7A blade passing noise with the noise of the similarly designed SR-3 propeller shows good agreement as expected. The SR-7A propeller is slightly noisier than the SR-3 model in the plane of rotation at the cruise condition. Projections of the tunnel model data are made to the full-scale LAP propeller mounted on the test bed aircraft and compared with design predictions. The prediction method is conservative in the sense that it overpredicts the projected model data. Author

N86-14007*# National Aeronautics and Space Administration. Lewis Research Center, Cleveland, Ohio.

SOME DESIGN PHILOSOPHY FOR REDUCING THE COMMUNITY NOISE OF ADVANCED COUNTER-ROTATION PROPELLERS

J. H. DITTMAR Aug. 1985 29 p refs (NASA-TM-87099; E-2692; NAS 1.15:87099) Avail: NTIS HC A03/MF A01 CSCL 20A

Advanced counter-rotation propellers have been indicated as possibly generating an unacceptable amount of noise for the people living near an airport. This report has explored ways to reduce this noise level, which is treated as being caused by the interaction of the upstream propeller wakes and vortices with the downstream propeller. The noise reduction techniques fall into two categories: (1) reducing the strength of the wakes and vortices, and (2) reducing the response of the downstream blades to them. The noise from the wake interaction was indicated as being reduced by increased

propeller spacing and decreased blade drag coefficient. The vortex-interaction noise could be eliminated by having the vortex pass over the tips of the downstream blade, and it could be reduced by increased spacing or decreased initial circulation. The downstream blade response could be lessened by increasing the reduced frequency parameter omega or by phasing of the response from different sections to have a mutual cancellation effect. Uneven blade to blade spacing for the downstream blading was indicated as having a possible effect on the annoyance of counter-rotation propeller noise. Although there are undoubtedly additional methods of noise reduction not covered in this report, the inclusion of the design methods discussed would potentially result in a counter-rotation propeller that is acceptably quiet. Author

N86-19125*# National Aeronautics and Space Administration. Lewis Research Center, Cleveland, Ohio.

LABORATORY EXPERIMENTS ON ACTIVE SUPPRESSION OF ADVANCED TURBOPROP NOISE

J. H. DITTMAR Dec. 1985 18 p refs (NASA-TM-87129; E-2740; NAS 1.15:87129) Avail: NTIS HC A02/MF A01 CSCL 20A

The noise generated by supersonic tip speed propellers may be a cabin environment problem for future propeller-driven airplanes. Active suppression from speakers inside the airplane cabin has been proposed for canceling out this noise. The potential of active suppression of advanced turboprop noise was tested by using speakers in a rectangular duct. Experiments were first performed with sine wave signals. The results compared well with the ideal cancellation curve of noise as a function of phase angle. Recorded noise signals from subsonic and supersonic tip speed propellers were then used in the duct to deterthe potential for canceling their noise. The subsonic propeller data showed significant cancellations but less than those obtained with the sine wave. The blade-passing-tone cancellation curve for the supersonic propeller was very similar to the subsonic curve, indicating that it is potentially just as easy to cancel supersonic as subsonic propeller blade-passing-tone noise. Propeller duct data from a recorded propeller source and spatial data taken on a propeller-drive airplane showed generally good agreement when compared versus phase angle. This agreement, combined with the similarity of the subsonic and supersonic duct propeller data, indicates that the area of cancellation for advanced supersonic propellers will be similar to that measured on the airplane. Since the area of cancellation on the airplane was small, a method for improving the active noise suppression by using outside speakers is discussed. Author

N86-22970*# National Aeronautics and Space Administration. Lewis Research Center, Cleveland, Ohio.

ULTRASONIC CHARACTERIZATION OF STRUCTURAL CERAMICS

S. J. KLIMA and G. Y. BAAKLINI *In* its Analytical Ultrasonics in Materials Research and Testing p 117-126 Jan. 1986 refs Avail: NTIS HC A16/MF A01 CSCL 20A

Ultrasonic velocity and attenuation measurements were used to characterize density and microstructure in monolithic silicon nitride and silicon carbide. Research samples of these structural ceramics exhibited a wide range of density and microstructural variations. It was shown that bulk density variations correlate with and can be estimated by velocity measurements. Variations in microstructural features such as grain size or shape and pore morphology had a minor effect on velocity. However, these features had a pronounced effect on ultrasonic attenuation. The ultrasonic results are supplemented by low-energy radiography and scanning laser acoustic microscopy. Author

N86-22973*# Virginia Polytechnic Inst. and State Univ., Blacksburg.

ANALYTICAL ULTRASONICS FOR EVALUATION OF COMPOSITE MATERIALS RESPONSE. PART 2: GENERATION AND DETECTION

J. C. DUKE, JR. and E. G. HENNEKE, II /In NASA. Lewis Research Center Analytical Ultrasonics in Materials Research and Testing p 153-168 Jan. 1986 refs

(Contract NSG3-172; NAG3-323)

Avail: NTIS HC A16/MF A01 CSCL 20A

To evaluate the response of composite materials, it is imperative that the input excitation as well as the observed output be well characterized. This characterization ideally should be in terms of displacements as a function of time with high spatial resolution. Additionally, the ability to prescribe these features for the excitation is highly desirable. Various methods for generating and detecting ultrasound in advanced composite materials are examined. Characterization and tailoring of input excitation is considered for contact and noncontact, mechanical, and electromechanical devices. Type of response as well as temporal and spatial resolution of detection methods are discussed as well. Results of investigations at Virginia Tech in application of these techniques to characterizing the response of advanced composites are presented.

Author

N86-22975*# National Aeronautics and Space Administration. Lewis Research Center, Cleveland, Ohio.

EFFECT OF STRESS ON ULTRASONIC PULSES IN FIBER REINFORCED COMPOSITES

J. H. HEMANN (Cleveland State Univ., Ohio) and G. Y. BAAKLINI /In its Analytical Ultrasonics in Materials Research and Testing p 181-191 Jan. 1986 refs Previously announced in IAA as N83-33180

(Contract NAG3-106)

Avail: NTIS HC A16/MF A01 CSCL 20A

An acoustical-ultrasonic technique was used to demonstrate relationships existing between changes in attenuation of stress waves and tensile stress on an eight ply 0 degree graphite-epoxy fiber reinforced composite. All tests were conducted in the linear range of the material for which no mechanical or macroscopic damage was evident. Changes in attenuation were measured as a function of tensile stress in the frequency domain and in the time domain. Stress wave propagation in these specimens was dispersive, i.e., the wave speed depends on frequency. Wave speeds varied from 267,400 cm/sec to 680,000 cm/sec as the frequency of the signal was varied from 150 kHz to 1.9 MHz which strongly suggests that flexural/lamb wave modes of propagation exist. The magnitude of the attenuation changes depended strongly on tensile stress. It was further observed that the wave speeds increased slightly for all tested frequencies as the stress was increased.

Author

N86-22977*# National Aeronautics and Space Administration. Lewis Research Center, Cleveland, Ohio.

ULTRASONIC VERIFICATION OF MICROSTRUCTURAL CHANGES DUE TO HEAT TREATMENT

E. R. GENERAZIO /In its Analytical Ultrasonics in Materials Research and Testing p 207-217 Jan. 1986 refs

Avail: NTIS HC A16/MF A01 CSCL 20A

Ultrasonic attenuation was measured for polycrystalline samples of nickel and copper with various grain-size distributions produced by heat treatment. Attenuation as a function of frequency was determined for a sample having a known mean grain diameter. Once this function was determined, it could be scaled to determine the mean grain size of other samples of the same material with different mean grain diameters. These results were obtained by using broadband pulse-echo ultrasound in the 25 to 100 MHz frequency range. The results suggest an ultrasonic, nondestructive approach for verifying heat treatment of metals.

R.J.F.

N86-22980*# National Aeronautics and Space Administration. Lewis Research Center, Cleveland, Ohio.

TRANSFER FUNCTION CONCEPT FOR ULTRASONIC CHARACTERIZATION OF MATERIAL MICROSTRUCTURES

A. VARY and H. E. KAUTZ /In its Analytical Ultrasonics in Materials Research and Testing p 251-297 Jan. 1986 refs

Avail: NTIS HC A16/MF A01 CSCL 20A

The approach given depends on treating material microstructures as elastomechanical filters that have analytically definable transfer functions. These transfer functions can be defined in terms of the frequency dependence of the ultrasonic attenuation coefficient. The transfer function concept provides a basis for synthesizing expressions that characterize polycrystalline materials relative to microstructural factors such as mean grain size, grain-size distribution functions, and grain boundary energy transmission. Although the approach is nonrigorous, it leads to a rational basis for combining the previously mentioned diverse and fragmented equations for ultrasonic attenuation coefficients.

Author

N86-22983*# National Aeronautics and Space Administration. Lewis Research Center, Cleveland, Ohio.

QUANTITATIVE FLAW CHARACTERIZATION WITH SCANNING LASER ACOUSTIC MICROSCOPY

E. R. GENERAZIO and D. J. ROTH /In its Analytical Ultrasonics in Materials Research and Testing p 341-358 Jan. 1986 refs

Avail: NTIS HC A16/MF A01 CSCL 20A

Surface roughness and diffraction are two factors that have been observed to affect the accuracy of flaw characterization with scanning laser acoustic microscopy. In accuracies can arise when the surface of the test sample is acoustically rough. It is shown that, in this case, Snell's law is no longer valid for determining the direction of sound propagation within the sample. The relationship between the direction of sound propagation within the sample, the apparent flaw depth, and the sample's surface roughness is investigated. Diffraction effects can mask the acoustic images of minute flaws and make it difficult to establish their size, depth, and other characteristics. It is shown that for Fraunhofer diffraction conditions the acoustic image of a subsurface defect corresponds to a two-dimensional Fourier transform. Transforms based on simulated flaws are used to infer the size and shape of the actual flaw.

Author

N86-23371*# General Electric Co., Cincinnati, Ohio. Aircraft Engine Business Group.

FREE JET FEASIBILITY STUDY OF A THERMAL ACOUSTIC SHIELD CONCEPT FOR AST/VCE APPLICATION-DUAL FLOW. COMPREHENSIVE DATA REPORT. VOLUME 1: TEST NOZZLES AND ACOUSTIC DATA

B. A. JANARDAN, J. F. BRAUSCH, and A. O. PRICE Oct. 1984 501 p refs 2 Vol.

(Contract NAS3-22137)

(NASA-CR-174817; NAS 1.26:174817; R84AEB570) Avail: NTIS HC A22/MF A01 CSCL 20A

Acoustic and diagnostic data that were obtained to determine the influence of selected geometric and aerodynamic flow variables of coannular nozzles with thermal acoustic shields are summarized in this comprehensive data report. A total of 136 static and simulated flight acoustic test points were conducted with 9 scale-model nozzles. The tested nozzles included baseline (unshielded), 180 deg shielded, and 360 deg shielded dual flow coannular plug configurations. The baseline configurations include a high radius ratio unsuppressed coannular plug nozzle and a coannular plug nozzle and a coannular plug nozzle with a 20-chute outer stream suppressor. The tests were conducted at nozzle temperatures and pressure typical of operating conditions of variable cycle engine.

Author

N86-23372*# General Electric Co., Cincinnati, Ohio. Aircraft Engine Business Group.

FREE-JET FEASIBILITY STUDY OF A THERMAL ACOUSTIC SHIELD CONCEPT FOR AST/VCE APPLICATION-DUAL STREAM NOZZLES. COMPREHENSIVE DATA REPORT. VOLUME 2: LASER VELOCIMETER AND SUPPRESSOR. BASE PRESSURE DATA

B. A. JANARDAN, J. F. BRAUSCH, and A. O. PRICE Oct. 1984 234 p 2 Vol.

(Contract NAS3-22137)

(NASA-CR-174818; NAS 1.26:174818; R84AEB570) Avail: NTIS HC A11/MF A01 CSCL 20A

Acoustic and diagnostic data that were obtained to determine the influence of selected geometric and aerodynamic flow variables of coannular nozzles with thermal acoustic shields are summarized in this comprehensive data report. A total of 136 static and simulated flight acoustic test points were conducted with 9 scale-model nozzles. Aerodynamic laser velocimeter measurements were made for four selected plumes. In addition, static pressure data in the chute base region of the suppressor configurations were obtained to assess the influence of the shield stream on the suppressor base drag. Author

N86-25217*# National Aeronautics and Space Administration. Lewis Research Center, Cleveland, Ohio.

AN ESTIMATE OF THE ENROUTE NOISE OF AN ADVANCED TURBOPROP AIRPLANE NASA-TM-87302 E-3020 NAS 1.15:87302 HC A02/MF A01

J. H. DITTMAR Apr. 1986 24 p refs

(NASA-TM-87302; E-3020; NAS 1.15:87302) Avail: NTIS HC A02/MF A01 CSCL 20A

The enroute noise of an Advanced Turboprop powered aircraft was estimated. The measured noise levels were roughly equivalent in annoyance to the noise 15.24 m from an automobile traveling at 80 km/h. It is felt that these levels would not illicit noise complaints from urban areas during the day but might be a slight annoyance in rural areas or in urban areas at night. Although it is not felt that the enroute noise is a major problem, it is indicated that a reduction in the enroute noise could improve the acceptability of advance turboprop airplanes. Author

N86-25218*# National Aeronautics and Space Administration. Lewis Research Center, Cleveland, Ohio.

AN EXPERIMENTAL INVESTIGATION OF REDUCING ADVANCED TURBOPROP CABIN NOISE BY WING SHIELDING

J. H. DITTMAR 1986 37 p refs Presented at the 10th Aeroacoustics Conference, Seattle, Wash., 9-11 Jul. 1986; sponsored by AIAA

(NASA-TM-87112; E-2713; NAS 1.15:87112) Avail: NTIS HC A03/MF A01 CSCL 20A

An experimental investigation was undertaken to determine if wing shielding could reduce the noise impacting the fuselage of an advanced turboprop airplane. Four wings were tested behind two eight-bladed propeller models. Significant shielding of the propeller noise was observed and a particular wing-propeller geometry was identified to provide the most shielding. Specifically, an up-inboard rotation would be needed for a low-wing airplane and a down-inboard rotation for a high-wing airplane. As the axial Mach number was increased, the position where the shielding starts moved farther downstream. This shift in the start of shielding was roughly a straight line with respect to Mach number between $M = 0.7$ and $M = 0.8$. At $M = 0.85$ the start of shielding does not shift any farther downstream. A simple barrier noise-reduction model gave the same trends with transducer positions as did the data, and, if corrected for Mach number shift, the model might be used to provide estimates of the wing shielding. Besides providing a barrier to the noise reaching the shielded area, the wing also reflects some of the noise back onto the unshielded area. This can make the noise difference between the unshielded and shielded areas of the fuselage larger than would be expected by simple wind shielding. Author

N86-29630*# National Aeronautics and Space Administration. Lewis Research Center, Cleveland, Ohio.

MODELING THE EFFECTS OF WIND TUNNEL WALL ABSORPTION ON THE ACOUSTIC RADIATION CHARACTERISTICS OF PROPELLERS

K. J. BAUMEISTER and W. EVERSMAN (Missouri Univ., Rolla.) Jul. 1986 21 p Presented at the 10th Aeroacoustics Conference, Seattle, Wash., 9-11 Jul. 1986; sponsored by AIAA

(NASA-TM-87333; E-2812; NAS 1.15:87333; AIAA-86-1876)

Avail: NTIS HC A02/MF A01 CSCL 20A

Finite element theory is used to calculate the acoustic field of a propeller in a soft walled circular wind tunnel and to compare the radiation patterns to the same propeller in free space. Parametric solutions are present for a 'Gutin' propeller for a variety of flow Mach numbers, admittance values at the wall, microphone position locations, and propeller to duct radius ratios. Wind tunnel boundary layer is not included in this analysis. For wall admittance nearly equal to the characteristic value of free space, the free field and ducted propeller models agree in pressure level and directionality. In addition, the need for experimentally mapping the acoustic field is discussed. Author

N86-32247*# National Aeronautics and Space Administration. Lewis Research Center, Cleveland, Ohio.

EFFECT OF TRIANGULAR ELEMENT ORIENTATION ON FINITE ELEMENT SOLUTIONS OF THE HELMHOLTZ EQUATION

K. J. BAUMEISTER 1986 23 p Proposed for presentation at the 1986 Winter Annual Meeting of the American Society of Mechanical Engineers, Anaheim, Calif., 7-12 Dec. 1986

(NASA-TM-87351; E-2734; NAS 1.15:87351) Avail: NTIS HC

A02/MF A01 CSCL 20A

The Galerkin finite element solutions for the scalar homogeneous Helmholtz equation are presented for no reflection, hard wall, and potential relief exit terminations with a variety of triangular element orientations. For this group of problems, the correlation between the accuracy of the solution and the orientation of the linear triangle is examined. Nonsymmetric element patterns are found to give generally poor results in the model problems investigated, particularly for cases where standing waves exist. For a fixed number of vertical elements, the results showed that symmetric element patterns give much better agreement with corresponding exact analytical results. In laminated wave guide application, the symmetric pyramid pattern is convenient to use and is shown to give excellent results. Author

72

ATOMIC AND MOLECULAR PHYSICS

Includes atomic structure, electron properties, and molecular spectra.

A86-11391* Case Western Reserve Univ., Cleveland, Ohio.

CALCULATION OF RECOIL IMPLANTATION PROFILES USING KNOWN RANGE STATISTICS

C. D. FUNG and R. E. AVILA (Case Western Reserve University, Cleveland, OH) Journal of Applied Physics (ISSN 0021-8979), vol. 58, Oct. 15, 1985, p. 3039-3043. refs

(Contract NAG3-490; NSF ECS-81-06693)

A method has been developed to calculate the depth distribution of recoil atoms that result from ion implantation onto a substrate covered with a thin surface layer. The calculation includes first order recoils considering projected range straggles, and lateral straggles of recoils but neglecting lateral straggles of projectiles. Projectile range distributions at intermediate energies in the surface layer are deduced from look-up tables of known range statistics. A great saving of computing time and human effort is thus attained in comparison with existing procedures. The method is used to calculate recoil profiles of oxygen from implantation of arsenic through SiO₂ and of nitrogen from implantation of phosphorus

73 NUCLEAR AND HIGH-ENERGY PHYSICS

through Si₃N₄ films on silicon. The calculated recoil profiles are in good agreement with results obtained by other investigators using the Boltzmann transport equation and they also compare very well with available experimental results in the literature. The deviation between calculated and experimental results is discussed in relation to lateral straggles. From this discussion, a range of surface layer thickness for which the method applies is recommended. Author

73

NUCLEAR AND HIGH-ENERGY PHYSICS

Includes elementary and nuclear particles; and reactor theory.

A86-22890* Systems Science and Software, La Jolla, Calif. **ENERGY BROADENING DUE TO SPACE-CHARGE OSCILLATIONS IN HIGH CURRENT ELECTRON BEAMS**

I. KATZ, G. A. JONGEWARD, D. E. PARKS (Systems Science and Software, La Jolla, CA), D. L. REASONER (NASA, Marshall Space Flight Center, Huntsville, AL), and C. K. PURVIS (NASA, Lewis Research Center, Cleveland, OH) Geophysical Research Letters (ISSN 0094-8276), vol. 13, Jan. 1986, p. 64-67. refs (Contract F19628-82-C-0081; NAS3-23881)

During electron beam accelerator operation on Spacelab I, substantial fluxes of electrons were observed with energies greater than the initial beam energy. Numerical calculations are performed for the emission of an unneutralized, one-dimensional electron beam. These calculations show clearly that space charge oscillations, which are associated with the charge buildup on the emitter, strongly modify the beam and cause the returning beam particles to have a distribution of kinetic energies ranging from half to over twice the initial energy. Author

74

OPTICS

Includes light phenomena; and optical devices.

A86-11995* John Carroll Univ., Cleveland, Ohio. **ALL-FIBRE SENSING LOOP USING PULSE-MODULATED LIGHT-EMITTING DIODE**

G. ADAMOVSKY (John Carroll University, Cleveland, OH) Electronics Letters (ISSN 0013-5194), vol. 21, Sept. 25, 1985, p. 922, 923. (Contract NAG3-366)

A sensing system is presented which includes a pulse-modulated light-emitting diode (LED) and an all-fibre-optic loop generating a reference signal in the time domain. The basic principle of operation and parameters are introduced, and some properties of such a system are experimentally examined using a microbend sensor. Author

A86-15263* Babcock and Wilcox Co., Alliance, Ohio. **THERMAL DEPENDENCE OF STRESS-INDUCED BIREFRINGENCE IN SINGLE MODE OPTICAL FIBERS**

J. W. BERTHOLD, III and L. B. THOMPSON (Babcock and Wilcox Co., Research and Development Div., Alliance, OH) IN: Fiber optic and laser sensors II; Proceedings of the Meeting, Arlington, VA, May 1, 2, 1984. Bellingham, WA, SPIE - The International Society for Optical Engineering, 1984, p. 63-67. refs (Contract NAS3-23712)

Measurements of the change in stress-induced birefringence with temperature in single mode optical fibers are reported. The fibers examined include those with low residual stress birefringence that have circular and elliptical cores. A section of each fiber was

placed under constant load with weights and heated inside a furnace. Polarized light was coupled into and out of the fiber ends outside the furnace. Two mutually perpendicular polarization components were analyzed and detected at the fiber output end. Changes in the detected signal levels were monitored as a function of the temperature of the single mode fiber stressed under constant load. Discussion of results and applications to localized stress measurements at high temperatures are presented. Author

A86-17421* Bell Telephone Labs., Inc., Allentown, Pa. **PERFORMANCE OF DIRECT AND ITERATIVE ALGORITHMS ON AN OPTICAL SYSTOLIC PROCESSOR**

A. K. GHOSH (AT&T Bell Laboratories, Allentown, PA), D. CASASANT, and C. P. NEUMAN (Carnegie-Mellon University, Pittsburgh, PA) Applied Optics (ISSN 0003-6935), vol. 24, Nov. 15, 1985, p. 3883-3892. refs (Contract NAG3-5; NAG1-575)

The frequency-multiplexed optical linear algebra processor (OLAP) is treated in detail with attention to its performance in the solution of systems of linear algebraic equations (LAEs). General guidelines suitable for most OLAPs, including digital-optical processors, are advanced concerning system and component error source models, guidelines for appropriate use of direct and iterative algorithms, the dominant error sources, and the effect of multiple simultaneous error sources. Specific results are advanced on the quantitative performance of both direct and iterative algorithms in the solution of systems of LAEs and in the solution of nonlinear matrix equations. Acoustic attenuation is found to dominate iterative algorithms and detector noise to dominate direct algorithms. The effect of multiple spatial errors is found to be additive. A theoretical expression for the amount of acoustic attenuation allowed is advanced and verified. Simulations and experimental data are included. Author

A86-31565*# National Aeronautics and Space Administration. Lewis Research Center, Cleveland, Ohio.

DIFFRACTION EFFECTS AND SPECIAL ADVANTAGES IN ELECTRONIC HETERODYNE MOIRE DEFLECTOMETRY

J. STRICKER (NASA, Lewis Research Center, Cleveland, OH) Applied Optics (ISSN 0003-6935), vol. 25, March 15, 1986, p. 895-902. refs

Effects of diffraction on the performance of electronic heterodyne readout of moire fringes are investigated. The sensitivity, accuracy, and resolution of the system are calculated, and it is shown that these features are significantly improved compared with the conventional intensity moire readout technique. The sensitivity of the system can be tripled without changing the distance between gratings. The system was evaluated experimentally by measuring the refractive-index derivatives of a weak phase object consisting of a large KD(asterisk)P crystal. Effects of nonlinear fringe modulation were studied both theoretically and experimentally. It is shown that in this case the electronic phase is not linearly related to the fringe shift, and calibration of the system is necessary. Author

A86-48352* Carnegie-Mellon Univ., Pittsburgh, Pa. **SPACE AND FREQUENCY-MULTIPLEXED OPTICAL LINEAR ALGEBRA PROCESSOR - FABRICATION AND INITIAL TESTS**

D. CASASANT (Carnegie-Mellon University, Pittsburgh, PA) and J. JACKSON (Westinghouse Electric Corp., Baltimore, MD) Applied Optics (ISSN 0003-6935), vol. 25, July 15, 1986, p. 2258-2263. refs

(Contract NAG3-5; AF-AFOSR-84-0239; NAG1-575)

A new optical linear algebra processor architecture is described. Space and frequency-multiplexing are used to accommodate bipolar and complex-valued data. A fabricated laboratory version of this processor is described, the electronic support system used is discussed, and initial test data obtained on it are presented. Author

N86-15113*# Babcock and Wilcox Co., Alliance, Ohio. Research and Development Div.

DEVELOPMENT OF OPTICAL DIAPHRAGM DEFLECTION SENSORS Final Report

W. L. GHERING, D. VARSHNEYA, L. A. JEFFERS, R. T. BAILEY, and J. W. BERTHOLD Jun. 1985 49 p

(Contract NAS3-23712)

(NASA-CR-175008; NAS 1.26:175008; RDD:85:4101-12-01:01)

Avail: NTIS HC A03/MF A01 CSCL 20F

The objective of this project was to develop high-temperature pressure sensors using non-metallic components and optical sensing methods. The sensors are to operate over a temperature range from room temperature approx. 20C to 540C, to respond to internal pressure up to 690 kPa, to respond to external pressure up to 690 kPa, and to withstand external overpressure of 2070 kPa. Project tasks include evaluating sensing techniques and sensor systems. These efforts include materials and sensing method selection, sensor design, sensor fabrication, and sensor testing. Sensors are tested as a function of temperature, pressure, overpressure, and vibration. The project results show that high-temperature pressure sensors based on glass components and optical sensing methods are feasible. The microbend optical diaphragm deflection sensor exhibits the required sensitivity and stability for use as a pressure sensor with temperature compensation. For the microbend sensor, the 95% confidence level deviation of input pressure from the pressure calculated from the overall temperature-compensated calibration equation is 3.7% of full scale. The limitations of the sensors evaluated are primarily due to the restricted temperature range of suitable commercially available optical fibers and the problems associated with glass-to-metal pressure sealing over the entire testing temperature range.

Author

N86-22390*# National Aeronautics and Space Administration. Lewis Research Center, Cleveland, Ohio.

OPTICAL ELEMENTS FORMED BY COMPRESSED GASES: ANALYSIS AND POTENTIAL APPLICATIONS

W. L. HOWES 1986 24 p refs

(NASA-TP-2555; E-2561; NAS 1.60:2555) Avail: NTIS HC

A02/MF A01 CSCL 20F

Spherical, cylindrical, and conical shock waves are optically analogous to gas lenses. The geometrical optics of these shock configurations are analyzed as they pertain to flow visualization instruments, particularly the rainbow schlieren apparatus and single-pass interferometers. It is proposed that a lens or mirror formed by gas compressed between plastic sheets has potential as a fluid visualization test object; as the objective mirror in a very large space-based telescope, communication antenna, or energy collector; as the objective mirror in inexpensive commercial telescopes; and as a component in fluid visualization apparatuses.

Author

N86-28729*# General Electric Co., Cincinnati, Ohio. Aircraft Engine Business Group.

1700 DEG C OPTICAL TEMPERATURE SENSOR Final Report

P. W. MOSSEY, W. M. SHAFFERNOCKER, and A. R. MULUKUTLA Jul. 1986 168 p

(Contract NAS3-24085)

(NASA-CR-175108; NAS 1.26:175108; R86AEB267) Avail: NTIS HC A08/MF A01 CSCL 20F

A new gas temperature sensor was developed that shows promise of sufficient ruggedness to be useful as a gas turbine temperature sensor. The sensor is in the form of a single-crystal aluminum oxide ceramic, ground to a cone shape and given an emissive coating. A lens and an optical fiber conduct the thermally emitted light to a remote and near-infrared photodetector assembly. Being optically coupled and passive, the sensor is highly immune to all types of electrical interference. Candidate sensors were analyzed for optical sensor performance, heat transfer characteristics, stress from gas loading. This led to the selection of the conical shape as the most promising for the gas turbine environment. One uncoated and two coated sensing elements were prepared for testing. Testing was conducted to an indicated 1750

C in a propane-air flame. Comparison with the referee optical pyrometer shows an accuracy of ± 25 C at 1700 C for this initial development. One hundred cycles from room temperature to 1700 C left the sapphire cone intact, but some loss of the platinum, 6% rhodium coating was observed. Several areas for improving the overall performance and durability are identified.

Author

75

PLASMA PHYSICS

Includes magnetohydrodynamics and plasma fusion.

A86-11001*# Michigan State Univ., East Lansing.

MEASUREMENTS OF ENERGY DISTRIBUTION AND WALL TEMPERATURE IN FLOWING HYDROGEN MICROWAVE PLASMA SYSTEMS

R. CHAPMAN, M. FINZEL, and M. C. HAWLEY (Michigan State University, East Lansing) AIAA, DGLR, and JSASS, International Electric Propulsion Conference, 18th, Alexandria, VA, Sept. 30-Oct. 2, 1985. 18 p. refs

(Contract NSG-3299)

(AIAA PAPER 85-2052)

An electrothermal propulsion concept utilizing a microwave plasma system as the mechanism to convert electromagnetic energy into translational energy of the flowing gas is being investigated. A calorimetric experimental system has been designed and built enclosing the microwave plasma system to accurately determine the net energy transferred to the flowing gas. For a flow rate of 8900 micromoles/sec, a pressure of 7.4 torr, and an absorbed power level of 80 W, an energy transfer efficiency of 50 percent has been measured. A heat transfer model that characterizes the energy transfer processes in the plasma is developed. A wall temperature for the plasma system is calculated.

Author

A86-16254*# National Aeronautics and Space Administration. Lewis Research Center, Cleveland, Ohio.

RADICAL MOLECULE AND ION-MOLECULE MECHANISMS IN THE POLYMERIZATION OF HYDROCARBONS AND CHLOROSILANES IN R.F. PLASMAS AT LOW PRESSURES (BELOW 1.0 TORR)

R. AVNI (NASA, Lewis Research Center, Cleveland, OH), U. CARMI, A. INSPEKTOR, and I. ROSENTHAL (Atomic Energy Commission, Negev Nuclear Research Centre, Beersheba, Israel) IN: Metallurgical coatings 1984; Proceedings of the Eleventh International Conference, San Diego, CA, April 9-13, 1984. Volume 1. Lausanne, Switzerland, Elsevier Sequoia, S.A., 1984, p. 231-241. Previously announced in STAR as N84-21329. refs

The ion-molecule and the radical-molecule mechanisms are responsible for the dissociation of hydrocarbons, and chlorosilane monomers and the formation of polymerized species, respectively, in the plasma state of a RF discharge. In the plasma, of a mixture of monomer with Ar, the rate determining step for both dissociation and polymerization is governed by an ion-molecular type interaction. Additions of H₂ or NH₃ to the monomer Ar(+) mixture transforms the rate determining step from an ion-molecular interaction to a radical-molecule type interaction for both monomer dissociation and polymerization processes.

Author

N86-15122* Carnegie-Mellon Univ., Pittsburgh, Pa. Dept. of Mechanical Engineering.
FUNDAMENTAL STUDIES ON A HEAT DRIVEN LAMP Final Report, 1 Sep. 1983 - 1 Sep. 1984
 J. L. LAWLESS 1985 40 p refs
 (Contract NAG3-437)
 (NASA-CR-176381; NAS 1.26:176381) Avail: NTIS HC A03/MF A01 CSDL 201

A detailed theoretical study of a heat-driven lamp has been performed. This lamp uses a plasma produced in a thermionic diode. The light is produced by the resonance transition of cesium. An important result of this study is that up to 30% of the input heat is predicted to be converted to light in this device. This is a major improvement over ordinary thermionic energy converters in which only approx. 1% is converted to resonance radiation. Efficiencies and optimum inter-electrode spacings have been found as a function of cathode temperature and the radiative escape factor. The theory developed explains the operating limits of the device. Author

76

SOLID-STATE PHYSICS

Includes superconductivity.

A86-16268* Nebraska Univ., Lincoln.
OPTICAL AND INTERFACIAL ELECTRONIC PROPERTIES OF DIAMOND-LIKE CARBON FILMS

J. A. WOOLLAM, V. NATARAJAN, J. LAMB, A. A. KHAN, G. BU-ABBUD (Nebraska University, Lincoln), B. BANKS, J. POUCH, D. A. GULINO, S. DOMITZ, D. C. LIU (NASA, Lewis Research Center, Cleveland, OH) et al. IN: Metallurgical coatings 1984; Proceedings of the Eleventh International Conference, San Diego, CA, April 9-13, 1984. Volume 2. Lausanne, Switzerland, Elsevier Sequoia, S.A., 1984, p. 121-126. NASA-supported research. refs

Hard, semitransparent carbon films were prepared on oriented polished crystal wafers of silicon, indium phosphide and gallium arsenide, as well as on KBr and quartz. Properties of the films were determined using IR and visible absorption spectroscopy, ellipsometry, conductance-capacitance spectroscopy and alpha particle-proton recoil spectroscopy. Preparation techniques include RF plasma decomposition of methane (and other hydrocarbons), ion beam sputtering, and dual-ion-beam sputter deposition. Optical energy band gaps as large as 2.7 eV and extinction coefficients lower than 0.1 at long wavelengths are found. Electronic state densities at the interface with silicon as low as 10 to the 10th states/eV sq cm per were found. Author

A86-18567* Rensselaer Polytechnic Inst., Troy, N.Y.
THE EFFECT OF PROCESSING CONDITIONS ON THE GAAS/PLASMA-GROWN INSULATOR INTERFACE
 F. I. HSHIEH, J. M. BORREGO, and S. K. GHANDHI (Rensselaer Polytechnic Institute, Troy, NY) Journal of Applied Physics (ISSN 0021-8979), vol. 59, Jan. 1, 1986, p. 1-4. refs
 (Contract NAG3-175)

The effect of processing conditions on the interface state density was evaluated from C-V measurements on metal-oxide-semiconductor capacitors. The optimum processing conditions for the minimum surface state density was found to be related to the postoxidation annealing temperature and time, and was independent of chemical treatments prior to oxidation. Annealing at the optimum condition (i.e., at 350 C for 1 h in either nitrogen or hydrogen gas, with or without an aluminum pattern on the oxide) reduces the fast surface state density by about one order of magnitude. By using a nitrogen/oxygen plasma, the static dielectric constant of the oxide decreased as the N/O ratio was increased, and nitrogen was incorporated into the oxide. In addition, the fast surface state density was reduced as a result of this nitridation process. Author

A86-28076* Oregon Graduate Center for Study and Research, Beaverton.

THE EFFECT OF OXYGEN PRESSURE ON VOLATILITY AND MORPHOLOGY OF LAB6 SINGLE CRYSTAL CATHODES

P. R. DAVIS, G. A. SCHWIND, and L. W. SWANSON (Oregon Graduate Center, Beaverton) Journal of Vacuum Science and Technology B (ISSN 0734-211X), vol. 4, Jan.-Feb. 1986, p. 112-115. refs
 (Contract AF-AFOSR-83-0105; NAG3-434; F19628-84-K-0026)

The effect of oxygen pressure on the volatility and morphology of single crystal LaB6 cathodes, heated to different temperatures, was investigated. At a temperature of 1600 K, an increase of oxygen pressure from 1 x 10 to the -8th torr to 1 x 10 to the -6th torr has led to a 100-fold enhancement in cathode volatility. The enhancement effect of oxygen pressure diminished with increasing temperature: at a cathode operating temperature of 1900 K, the volatility enhancement due to the same oxygen pressure was negligible. It was shown that the faceting frequently observed during evaporation of conically shaped emitters is due to a crystallographic anisotropy of the oxidation rate of LaB6. No facet formation occurs during evaporation at oxygen pressures below -110 to the -8th torr. I.S.

A86-37075* City Coll. of the City Univ. of New York.
INFRARED-PHOTOINDUCED-ABSORPTION STUDIES IN SOLUBLE TRANS-POLYACETYLENE

R. DORSINVILLE, R. TUBINO, S. KRIMCHANSKY, R. R. ALFANO, J. L. BIRMAN (City College, New York) et al. Physical Review B, 3rd Series (ISSN 0163-1829), vol. 32, Sept. 15, 1985, p. 3377-3380. Research supported by the City University of New York, and USAF. refs
 (Contract NAG3-130; NSF DMR-83-03981)

The observation of photoinduced excitations in trans-polyacetylene in its liquid form in the frequency range from 2000 to 6000/cm is reported on. These measurements strongly suggest that transpolyacetylene is capable of supporting charged solitons even in solution. Author

A86-37441* National Aeronautics and Space Administration. Lewis Research Center, Cleveland, Ohio.

COMPUTER SIMULATION OF THIN-FILM NUCLEATION AND GROWTH - THE MULTILAYER MODE

J. SALIK (NASA, Lewis Research Center, Cleveland, OH) Journal of Applied Physics (ISSN 0021-8979), vol. 59, May 15, 1986, p. 3454-3457. refs

The computer simulation of thin-film nucleation and growth, which was previously performed for the case of single monolayer, has been extended to the case of multilayer growth. The simulation results show that the kinetics of multilayer growth is nearly identical to that of monolayer growth. The cluster density resulting from the multilayer mode is similar to that resulting from the monolayer mode at low coverage. At high coverage, multilayer growth results in substantially higher cluster density than that resulting from monolayer growth. Author

A86-47066* National Aeronautics and Space Administration. Lewis Research Center, Cleveland, Ohio.

ION BEAM SPUTTER DEPOSITED ZINC TELLURIDE FILMS

D. A. GULINO (NASA, Lewis Research Center, Cleveland, OH) Journal of Vacuum Science and Technology A (ISSN 0734-2101), vol. 4, May-June 1986, pt. 1, p. 509-513. Previously announced in STAR as N86-11048. refs

Zinc telluride is of interest as a potential electronic device material, particularly as one component in an amorphous superlattice, which is a new class of interesting and potentially useful materials. Some structural and electronic properties of ZnTe films deposited by argon ion beam sputter deposition are described. Films (up to 3000 angstroms thick) were deposited from a ZnTe target. A beam energy of 1000 eV and a current density of 4 mA/sq cm resulted in deposition rates of approximately 70 angstroms/min. The optical band gap was found to be approximately 1.1 eV, indicating an amorphous structure, as compared to a literature value of 2.26 eV for crystalline material.

Intrinsic stress measurements showed a thickness dependence, varying from tensile for thicknesses below 850 angstroms to compressive for larger thicknesses. Room temperature conductivity measurement also showed a thickness dependence, with values ranging from 1.86×10 to the $-6\text{th}/\text{ohm cm}$ for 300 angstrom film to 2.56×10 to the $-1/\text{ohm cm}$ for a 2600 angstrom film. Measurement of the temperature dependence of the conductivity for these films showed complicated behavior which was thickness dependent. Thinner films showed at least two distinct temperature dependent conductivity mechanisms, as described by a Mott-type model. Thicker films showed only one principal conductivity mechanism, similar to what might be expected for a material with more crystalline character. Author

A86-47076* Westinghouse Research and Development Center, Pittsburgh, Pa.

GROWTH AND CHARACTERIZATION OF EPITAXIAL SRF₂ ON INP(100)

S. SINHARROY, R. A. HOFFMAN, J. H. RIEGER (Westinghouse Research and Development Center, Pittsburgh, PA), J. D. WARNER, and K. B. BHASIN (NASA, Lewis Research Center, Cleveland, OH) *Journal of Vacuum Science and Technology A* (ISSN 0734-2101), vol. 4, May-June 1986, pt. 1, p. 897-899. refs

The epitaxial growth of 100-262.5-nm SrF₂ films on n-type and p-type (100)InP in a conventional baked UHV system at base pressure about 200 ptorr, temperature 250-350 C, and growth rate from less than 100 to about 200 pm/s. Substrates are chemomechanically polished, degreased, bombarded with 500-eV Ar ions for 3-4 min at 350 C, and annealed for 23-30 min at 350 C, producing a slightly In-rich (In/P = 1.02) In-island-free surface with a (4 x 1) or (1 x 1) LEED structure. Films grown at 350 C and less than 100 pm/s are found to be smooth and free of cracks in most cases, with a highly faceted (1 x 1) LEED structure. The electrical properties of the SRF₂ films are found to be acceptable only when the ohmic contacts are applied prior to the substrate prior to SRF₂ growth. T.K.

N86-11048*# National Aeronautics and Space Administration, Lewis Research Center, Cleveland, Ohio.

ION BEAM SPUTTER DEPOSITED ZINC TELLURIDE FILMS

D. A. GULINO 1985 19 p refs Proposed for presentation at 32nd Natl. Symp. of the Am. Vacuum Soc., Houston, Tex., 18-22 1985

(NASA-TM-87119; E-2726; NAS 1.15:87119) Avail: NTIS HC A02/MF A01 CSCL 20L

Zinc telluride is of interest as a potential electronic device material, particularly as one component in an amorphous superlattice, which is a new class of interesting and potentially useful materials. Some structural and electronic properties of ZnTe films deposited by argon ion beam sputter deposition are described. Films (up to 3000 angstroms thick) were deposited from a ZnTe target. A beam energy of 1000 eV and a current density of 4 mA/sq. cm. resulted in deposition rates of approximately 70 angstroms/min. The optical band gap was found to be approximately 1.1 eV, indicating an amorphous structure, as compared to a literature value of 2.26 eV for crystalline material. Intrinsic stress measurements showed a thickness dependence, varying from tensile for thicknesses below 850 angstroms to compressive for larger thicknesses. Room temperature conductivity measurement also showed a thickness dependence, with values ranging from 1.86×10 to the $-6/\text{ohm. cm.}$ for 300 angstrom film to 2.56×10 to the $-1/\text{ohm. cm.}$ for a 2600 angstrom film. Measurement of the temperature dependence of the conductivity for these films showed complicated behavior which was thickness dependent. Thinner films showed at least two distinct temperature dependent conductivity mechanisms, as described by a Mott-type model. Thicker films showed only one principal conductivity mechanism, similar to what might be expected for a material with more crystalline character. Author

N86-12134*# National Aeronautics and Space Administration, Lewis Research Center, Cleveland, Ohio.

ELLIPSO-METRIC AND OPTICAL STUDY OF SOME UNCOMMON INSULATOR FILMS ON 3-5 SEMICONDUCTORS

S. A. ALTEROVITZ, J. D. WARNER, D. C. LIU, and J. J. POUCH 1985 18 p refs Presented at the 168th Meeting of the Electrochem. Soc., Las Vegas, Nev., 13-18 Oct. 1985

(NASA-TM-87135; E-2750; NAS 1.15:87135) Avail: NTIS HC A02/MF A01 CSCL 20L

Optical properties of three types of insulating films that show promise in potential applications in the 3-4 semiconductor technology were evaluated, namely a-C:H, BN and CaF₂. The plasma deposited a-C:H shows an amorphous behavior with optical energy gaps of approximately 2 to 2.4 eV. These a-C:H films have higher density and/or hardness, higher refractive index and lower optical energy gaps with increasing energy of the particles in the plasma, while the density of states remains unchanged. These results are in agreement, and give a fine-tuned positive confirmation to an existing conjecture on the nature of a-C:H films (1). Ion beam deposited BN films show amorphous behavior with energy gap of 5 eV. These films are nonstoichiometric (B/N approximately 2) and have refractive index, density and/or hardness which are dependent on the deposition conditions. The epitaxially grown CaF₂ on GaAs films have optical parameters equal to bulk, but evidence of damage was found in the GaAs at the interface. Author

N86-12135*# National Aeronautics and Space Administration, Lewis Research Center, Cleveland, Ohio.

CARBON FILMS GROWN FROM PLASMA ON III-V SEMICONDUCTORS

J. J. POUCH, J. D. WARNER, and D. C. LIU 1985 12 p refs Presented at the 168th Meeting of the Electrochem. Soc., Las Vegas, Nev., 11-17 Oct. 1985

(NASA-TM-87140; E-2766; NAS 1.15:87140) Avail: NTIS HC A02/MF A01 CSCL 09C

Dielectric carbon films were grown on n- and p-type GaAs and InP substrates using plasmas generated at 30 KHz from gaseous hydrocarbons. The effect of gas source, flow rate, and power on film growth were investigated. Methane and n-butane gases were utilized. The flow rate and power ranged from 30 to 50 sccm and 25 to 300 W, respectively. AES measurements show only carbon to be present in the films. The relative Ar ion sputtering rate (3 KeV) of carbon depends on the ratio power/pressure. In addition, the degree of asymmetry associated with the carbon-semiconductor interface is approximately power-independent. SIMS spectra indicate different H-C bonding configurations to be present in the films. Band gaps as high as 3.05 eV are obtained from optical absorption studies. Author

N86-23468*# Illinois Univ., Urbana-Champaign. Dept. of Electrical Engineering.

OPTICAL CONSTANTS OF GAAS-ALGAAS SUPERLATTICES AND MULTIPLE QUANTUM WELLS

K. B. KAHEN and J. P. LEBURTON 1986 24 p refs

(Contract NAG3-507)

(NASA-CR-176717; NAS 1.26:176717) Avail: NTIS HC A02/MF A01 CSCL 20L

The optical properties of GaAs-Al sub x Ga sub 1-xAs superlattices are calculated as a function of the frequency and superlattice structure. The computations are performed using a partition method which combines the vectors k.p method with the pseudopotential technique. The influence of the super-structure on the electronic properties of the systems is accounted for by appropriate quantization conditions. The anisotropy and structure dependence of the dielectric constant result mainly from the contribution of the gamma region while the contributions of the other regions of the Brillouin zone are rather insensitive to the superlattice structure. The superlattice index of refraction values are shown to attain maxima at the various quantized transition energies, where for certain structures, the difference between the refractive indices of the superlattices and its corresponding Al sub x Ga sub 1-xAs alloy can be as large as 2%. In general

76 SOLID-STATE PHYSICS

results are in good agreement with the experimental data.

Author

N86-25267*# National Aeronautics and Space Administration. Lewis Research Center, Cleveland, Ohio.

COMPENSATION IN EPITAXIAL CUBIC SiC FILMS

B. SEGALL (Case Western Univ., Cleveland, Ohio), S. A. ALTEROVITZ, E. J. HAUGLAND, and L. G. MATUS Mar. 1986 12 p refs

(NASA-TM-87269; E-2918; NAS 1.15:87269) Avail: NTIS HC A02/MF A01 CSCL 20L

Hall measurements on four n-type cubic SiC films epitaxially grown by chemical vapor deposition on SiC substrates are reported. The temperature dependent carrier concentrations indicate that the samples are highly compensated. Donor ionization energies, $E_{\text{sub D}}$, are less than one half the values previously reported. The values for $E_{\text{sub D}}$ and the donor concentration $N_{\text{sub D}}$, combined with results for small bulk platelets with nitrogen donors, suggest the relation $E_{\text{sub D}}(N_{\text{sub D}}) = E_{\text{sub D}}(O) - \alpha N_{\text{sub D}}$ for cubic SiC. A curve fit gives α is approx 2.6×10^{-5} meV cm and $E_{\text{sub D}}(O)$ approx 48 meV, which is the generally accepted value of $E_{\text{sub D}}(O)$ for nitrogen donors in cubic SiC.

E.A.K.

N86-25268*# National Aeronautics and Space Administration. Lewis Research Center, Cleveland, Ohio.

AUGER ELECTRON SPECTROSCOPY, SECONDARY ION MASS SPECTROSCOPY AND OPTICAL CHARACTERIZATION OF A-C-H AND BN FILMS

J. J. POUCH, S. A. ALTEROVITZ, and J. D. WARNER 1986 13 p refs Presented at Symposium on Plasma Processing at the Spring Meeting of the Materials Research Society, Palo Alto, Calif., 15-18 Apr. 1986

(NASA-TM-87258; E-2950; NAS 1.15:87258) Avail: NTIS HC A02/MF A01 CSCL 20L

The amorphous dielectrics a-C:H and BN were deposited on III-V semiconductors. Optical band gaps as high as 3 eV were measured for a-C:H generated by C_4H_{10} plasmas; a comparison was made with band gaps obtained from films prepared by CH_4 glow discharges. The ion beam deposited BN films exhibited amorphous behavior with band gaps on the order of 5 eV. Film compositions were studied by Auger electron spectroscopy (AES), x-ray photoelectron spectroscopy (XPS) and secondary ion mass spectrometry (SIMS). The optical properties were characterized by ellipsometry, UV/VIS absorption, and IR reflection and transmission. Etching rates of a-C:H subjected to O_2 discharges were determined.

Author

N86-28759*# Illinois Univ., Urbana-Champaign. Coordinated Science Lab.

THEORETICAL STUDY OF THE TRANSVERSE DIELECTRIC CONSTANT OF SUPERLATTICES AND THEIR ALLOYS Ph.D Thesis

K. B. KAHEN Aug. 1986 95 p

(Contract NAG3-507)

(NASA-CR-177198; NAS 1.26:177198; UIIU-ENG-86-2221)

Avail: NTIS HC A05/MF A01 CSCL 20L

The optical properties of III to V binary and ternary compounds and $\text{GaAs-Al}(x)\text{Ga}(1-x)\text{As}$ superlattices are determined by calculating the real and imaginary parts of the transverse dielectric constant. Emphasis is given to determining the influence of different material and superlattice parameters on the values of the index of refraction and absorption coefficient. In order to calculate the optical properties of a material, it is necessary to compute its electronic band structure. This was accomplished by introducing a partition band structure approach based on a combination of the vector $\mathbf{k} \times$ vector \mathbf{p} and nonlocal pseudopotential techniques. The advantages of this approach are that it is accurate, computationally fast, analytical, and flexible. These last two properties enable incorporation of additional effects into the model, such as disorder scattering, which occurs for alloy materials and excitons. Furthermore, the model is easily extended to more complex structures, for example multiple quantum wells and superlattices.

The results for the transverse dielectric constant and absorption coefficient of bulk III to V compounds compare well with other one-electron band structure models and the calculations show that for small frequencies, the index of refraction is determined mainly by the contribution of the outer regions of the Brillouin zone.

Author

77

THERMODYNAMICS AND STATISTICAL PHYSICS

Includes quantum mechanics; theoretical physics; and Bose and Fermi statistics.

N86-25284*# National Aeronautics and Space Administration. Lewis Research Center, Cleveland, Ohio.

THERMAL DESORPTION STUDY OF PHYSICAL FORCES AT THE PTFE SURFACE

D. R. WHEELER and S. V. PEPPER 1985 15 p refs Presented at the International Conference on Surface and Colloid Chemistry, Potsdam, N.Y., 24-28 Jun. 1985; sponsored by American Chemical Society

(NASA-TM-87090; E-2680; NAS 1.15:87090) Avail: NTIS HC A02/MF A01 CSCL 20C

Thermal desorption spectroscopy (TDS) of the polytetrafluoroethylene (PTFE) surface was successfully employed to study the possible role of physical forces in the enhancement of metal-PTFE adhesion by radiation. The thermal desorption spectra were analyzed without assumptions to yield the activation energy for desorption over a range of xenon coverage from less than 0.1 monolayer to more than 100 monolayers. For multilayer coverage, the desorption is zero-order with an activation energy equal to the sublimation energy of xenon. For submonolayer coverages, the order for desorption from the unirradiated PTFE surface is 0.73 and the activation energy for desorption is between 3.32 and 3.36 kcal/mol; less than the xenon sublimation energy. The effect of irradiation is to increase the activation energy for desorption to as high as 4 kcal/mol at low coverage.

Author

N86-28775*# National Aeronautics and Space Administration. Lewis Research Center, Cleveland, Ohio.

UNIVERSALITY IN THE COMPRESSIVE BEHAVIOR OF SOLIDS

P. VINET, J. FERRANTE, J. R. SMITH (General Motors Research Labs., Warren, Mich.), and J. H. ROSE (Iowa State Univ. of Science and Technology, Ames.) Apr. 1986 11 p

(NASA-TM-87303; E-2702-1; NAS 1.15:87303) Avail: NTIS HC A02/MF A01 CSCL 08M

It was discovered that the isothermal equation of state for solids in compression is a simple, universal form. This single form accurately describes the pressure and bulk modulus as a function of volume for ionic, metallic, covalent, and rare gas solids.

Author

N86-28776*# National Aeronautics and Space Administration. Lewis Research Center, Cleveland, Ohio.

TEMPERATURE EFFECTS ON THE UNIVERSAL EQUATION OF STATE OF SOLIDS

P. VINET, J. FERRANTE, J. R. SMITH (General Motors Research Labs., Warren, Mich.), and J. H. ROSE (Iowa State Univ. of Science and Technology, Ames.) Apr. 1986 29 p

(NASA-TM-87321; E-3001; NAS 1.15:87321) Avail: NTIS HC A03/MF A01 CSCL 08M

Recently it has been argued based on theoretical calculations and experimental data that there is a universal form for the equation of state of solids. This observation was restricted to the range of temperatures and pressures such that there are no phase transitions. The use of this universal relation to estimate pressure-volume relations (i.e., isotherms) required three input parameters at each fixed temperature. It is shown that for many

solids the input data needed to predict high temperature thermodynamical properties can be dramatically reduced. In particular, only four numbers are needed: (1) the zero pressure ($P=0$) isothermal bulk modulus; (2) the $P=0$ pressure derivative; (3) the $P=0$ volume; and (4) the $P=0$ thermal expansion; all evaluated at a single (reference) temperature. Explicit predictions are made for the high temperature isotherms, the thermal expansion as a function of temperature, and the temperature variation of the isothermal bulk modulus and its pressure derivative. These predictions are tested using experimental data for three representative solids: gold, sodium chloride, and xenon. Good agreement between theory and experiment is found. Author

N86-30556*# National Aeronautics and Space Administration. Lewis Research Center, Cleveland, Ohio.

STABILITY OF SURFACE NUCLEATION

J. SALIK Aug. 1986 9 p
(NASA-TM-88806; E-3154; NAS 1.15:88806) Avail: NTIS HC A02/MF A01 CSCL 20H

The growth and decomposition rates of nuclei on a surface are expressed in microscopic terms. A stability factor is defined and employed for the derivation of a criterion for nucleus stability. Simulation results indicate that the stability factor can be used as a measure of the system stability. Author

80

SOCIAL SCIENCES (GENERAL)

Includes educational matters.

N86-13219*# Akron Univ., Ohio. Dept. of Civil Engineering. NASA LERC/AKRON UNIVERSITY GRADUATE COOPERATIVE FELLOWSHIP PROGRAM AND GRADUATE STUDENT RESEARCHERS PROGRAM Interim Report, Nov. 1981 - Oct. 1983

D. G. FERTIS Oct. 1983 59 p refs
(Contract NAG3-50; NGT36-001-800; NGT36-001-801)
(NASA-CR-174826; NAS 1.26:174826; NAUFP-202-3) Avail:
NTIS HC A04/MF A01 CSCL 05I

On June 1, 1980, the University of Akron and the NASA Lewis Research Center (LERC) established a Graduate Cooperative Fellowship Program in the specialized areas of Engine Structural Analysis and Dynamics, Computational Mechanics, Mechanics of Composite Materials, and Structural Optimization, in order to promote and develop requisite technologies in these areas of engine technology. The objectives of this program are consistent with those of the NASA Engine Structure Program in which graduate students of the University of Akron participate by conducting research at Lewis. This report is the second on this grant and summarizes the second and third year research effort, which includes the participation of five graduate students where each student selects one of the above areas as his special field of interest. Each student is required to spend 30 percent of his educational training time at the NASA Lewis Research Center and the balance at the University of Akron. His course work is judiciously selected and tailored to prepare him for research work in his field of interest. A research topic is selected for each student while in residence at the NASA Lewis Research Center, which is also approved by the faculty of the University of Akron as his thesis topic for a Master's and/or a Ph.D. degree. Author

81

ADMINISTRATION AND MANAGEMENT

Includes management planning and research.

A86-24798* National Aeronautics and Space Administration. Lewis Research Center, Cleveland, Ohio.

DEVELOPMENT OF THE POWER SYSTEM FOR THE UNITED STATES' MANNED SPACE STATION

E. E. KEMPKE, JR. (NASA, Lewis Research Center, Cleveland, OH) IN: Intersociety Energy Conversion Engineering Conference, 20th, Miami Beach, FL, August 18-23, 1985, Proceedings. Volume 1. Warrendale, PA, Society of Automotive Engineers, Inc., 1985, p. 1.139-1.144.

The definition and preliminary design study effort for the Space Station Electric Power System is described. The requirements to be met by the Power System, the characteristics of the major technology options being considered, and the approach to be taken in the definition studies are considered. The role of advanced development in the definition process and the specific tasks to be performed in the preliminary design study are reviewed. The NASA approach to managing the complex Power System interfaces across the Space Station is also discussed. C.D.

82

DOCUMENTATION AND INFORMATION SCIENCE

Includes information management; information storage and retrieval technology; technical writing; graphic arts; and micrography.

N86-21427*# National Aeronautics and Space Administration. Lewis Research Center, Cleveland, Ohio.

RESEARCH AND TECHNOLOGY, LEWIS RESEARCH CENTER Annual Report, 1985

1985 57 p
(NASA-TM-87179; NAS 1.15:87179) Avail: NTIS HC A04/MF A01 CSCL 05B

The NASA Lewis Research Center's research and technology accomplishments for fiscal year 1985 are summarized. The report is organized into five major sections covering aeronautics, aerospace technology, spaceflight systems, space station systems, and computational technology support. This organization of the report roughly parallels the organization of the Center into directorates. Where appropriate, subheadings are used to identify special topics under the major headings. Results of all research and technology work performed during the fiscal year are contained in Lewis-published technical reports and presentations prepared either by Lewis scientists and engineers or by contractor personnel. In addition, significant results are presented by university faculty or graduate students in technical sessions and in journals of the technical societies. For the reader who desires more information about a particular subject, the Lewis contact will provide that information or references. In 1985, five Lewis products were selected by Research and Development Magazine for IR-100 awards. All are described and identified. In addition, the Lewis Distinguished Paper for 1984 to 1985, which was selected by the Chief Scientist and a research advisory board, is included and so identified. Author

N86-32336*# National Aeronautics and Space Administration. Lewis Research Center, Cleveland, Ohio.

BIBLIOGRAPHY OF LEWIS RESEARCH CENTER TECHNICAL PUBLICATIONS ANNOUNCED IN 1985

May 1986 307 p

(NASA-TM-87263; E-2960; NAS 1.15:87263) Avail: NTIS HC A14/MF A01 CSCL 05B

This compilation of abstracts describes and indexes the technical reporting that resulted from the scientific and engineering work performed and managed by the Lewis Research Center in 1985. All the publications were announced in the 1985 issues of STAR (Scientific and Technical Aerospace Reports) and/or IAA (International Aerospace Abstracts). Included are research reports, journal articles, conference presentations, patents and patent applications, and theses. Author

85

URBAN TECHNOLOGY AND TRANSPORTATION

Includes applications of space technology to urban problems; technology transfer; technology assessment; and surface and mass transportation.

N86-13236*# National Aeronautics and Space Administration. Lewis Research Center, Cleveland, Ohio.

OVERVIEW OF FREE-PISTON STIRLING TECHNOLOGY AT THE NASA LEWIS RESEARCH CENTER

J. G. SLABY 1985 21 p refs Presented at the 23rd Automotive Technol. Develop. Contractors' Coordination Meeting, Dearborn, Mich., 21-24 Oct. 1985; sponsored by DOE

(Contract DE-AI05-82OR-1005)

(NASA-TM-87156; E-2783; DOE/NASA/1005-7; NAS 1.15:87156)

Avail: NTIS HC A02/MF A01 CSCL 10B

An overview of the National Aeronautics and Space Administration (NASA) Lewis Research Center (Lewis) free-piston Stirling engine activities is presented. These activities include: (1) a generic free-piston Stirling technology project being conducted to develop technologies synergistic to both space power and terrestrial heat pump applications in a cooperative, cost-shared effort with the Department of Energy (DOE/Oak Ridge National Laboratory (ONRL)), and (2) a free-piston Stirling space-power technology demonstration project as part of the SP-100 program being conducted in support of the Department of Defense (DOD), DOE, and NASA/Lewis. The generic technology effort includes extensive parametric testing of a 1 kw free-piston Stirling engine (RE-1000), development and validation of a free-piston Stirling performance computer code, and fabrication and initial testing of an hydraulic output modification for the RE-1000 engine. The space power technology effort, under SP-100, addresses the status of the 25 kWe Space Power Demonstrator Engine (SPDE) including early test results. Author

N86-14106*# National Aeronautics and Space Administration. Lewis Research Center, Cleveland, Ohio.

STIRLING ENGINE SUPPORTING RESEARCH AND TECHNOLOGY Final Report

W. A. TOMAZIC 1985 19 p Presented at the 23rd Automotive Technology Development Contractors' Coordination Meeting, Dearborn, Mich., 21-24 Oct. 1985; sponsored by DOE

(Contract DE-AI01-85CE-50112)

(NASA-TM-87175; DOE/NASA/50112-60; E-2821; NAS

1.15:87175) Avail: NTIS HC A02/MF A01 CSCL 103

The supporting research and technology effort is intended to provide technical support to the current engine program and also to investigate advanced concepts for the next generation of Stirling engines. Technical areas represented are: seals, materials, engine experiments, combustion, system analysis, ceramics, and tribology. A collage of more recent work in each area is presented. Under seals, analysis and some experimental data on the effect

of wear on rod seal performance is presented. The material work described concerns the effect of water content on hydrogen permeation. Results of experiments with the Philips' Advenco engine are presented. A comparison is made of two combustor nozzles, an air atomizing and an ultrasonic atomizing nozzle. A new venture in systems analysis to provide more rigorous Stirling engine simulation is discussed. The results of hydrogen corrosion tests on silicon carbide are presented. Friction and wear tests on candidate materials for engine hot ring tests are discussed. Author

N86-16164*# Massachusetts Inst. of Tech., Cambridge. Automotive Lab.

A COMPUTER SIMULATION OF THE TURBOCHARGED TURBO COMPOUNDED DIESEL ENGINE SYSTEM: A DESCRIPTION OF THE THERMODYNAMIC AND HEAT TRANSFER MODELS Final Report

D. N. ASSANIS, J. E. EKCHIAN, R. M. FRANK, and J. B. HEYWOOD Aug. 1985 106 p refs

(Contract NAG3-340; DE-AI01-80CS-50194)

(NASA-CR-174971; DOE/NASA/0340-1; NAS 1.26:174971)

Avail: NTIS HC A06/MF A01 CSCL 13F

A computer simulation of the turbocharged turbocompounded direct-injection diesel engine system was developed in order to study the performance characteristics of the total system as major design parameters and materials are varied. Quasi-steady flow models of the compressor, turbines, manifolds, intercooler, and ducting are coupled with a multicylinder reciprocator diesel model, where each cylinder undergoes the same thermodynamic cycle. The master cylinder model describes the reciprocator intake, compression, combustion and exhaust processes in sufficient detail to define the mass and energy transfers in each subsystem of the total engine system. Appropriate thermal loading models relate the heat flow through critical system components to material properties and design details. From this information, the simulation predicts the performance gains, and assesses the system design trade-offs which would result from the introduction of selected heat transfer reduction materials in key system components, over a range of operating conditions. Author

N86-16165*# General Electric Co., Philadelphia, Pa. Space Systems Div.

CERAMIC AUTOMOTIVE STIRLING ENGINE STUDY Final Report

S. MUSIKANT, W. CHIU, D. DAROOKA, D. M. MULLINGS, and C. A. JOHNSON Jan. 1985 373 p refs

(Contract DEN3-312; DE-AI01-85CE-50112)

(NASA-CR-174907; DOE/NASA/0312-1; NAS 1.26:174907)

Avail: NTIS HC A16/MF A01 CSCL 13F

A conceptual design study for a Ceramic Automotive Stirling Engine (CASE) is performed. Year 1990 structural ceramic technology is assumed. Structural and performance analyses of the conceptual design are performed as well as a manufacturing and cost analysis. The general conclusions from this study are that such an engine would be 10-26% more efficient over its performance map than the current metal Automotive Stirling Reference Engine (ASRE). Cost of such a ceramic engine is likely to be somewhat higher than that of the ASRE but engine cost is very sensitive to the ultimate cost of the high purity, ceramic powder raw materials required to fabricate high performance parts. When the design study is projected to the year 2000 technology, substantial net efficiency improvements, on the order of 25 to 46% over the ASRE, are computed. Author

N86-17224*# IIT Research Inst., Chicago, Ill. Nonmetallic Materials and Composites.

LONG-TERM STABILITY AND PROPERTIES OF ZIRCONIA CERAMICS FOR HEAVY DUTY DIESEL ENGINE COMPONENTS Final Report

D. C. LARSEN and J. W. ADAMS Sep. 1985 263 p refs
(Contract DEN3-305; DE-AI01-80CS-50194)
(NASA-CR-174943; DOE/NASA/0305-1; NAS 1.26:174943)
Avail: NTIS HC A12/MF A01 CSCL 13F

Physical, mechanical, and thermal properties of commercially available transformation-toughened zirconia are measured. Behavior is related to the material microstructure and phase assemblage. The stability of the materials is assessed after long-term exposure appropriate for diesel engine application. Properties measured included flexure strength, elastic modulus, fracture toughness, creep, thermal shock, thermal expansion, internal friction, and thermal diffusivity. Stability is assessed by measuring the residual property after 1000 hr/1000C static exposure. Additionally static fatigue and thermal fatigue testing is performed. Both yttria-stabilized and magnesia-stabilized materials are compared and contrasted. The major limitations of these materials are short term loss of properties with increasing temperature as the metastable tetragonal phase becomes more stable. Fine grain yttria-stabilized material (TZP) is higher strength and has a more stable microstructure with respect to overaging phenomena. The long-term limitation of Y-TZP is excessive creep deformation. Magnesia-stabilized PSZ has relatively poor stability at elevated temperature. Overaging, decomposition, and/or destabilization effects are observed. The major limitation of Mg-PSZ is controlling unwanted phase changes at elevated temperature.

Author

N86-17226*# American Trucking Associations, Inc., Alexandria, Va.

FUTURE HEAVY DUTY TRUCKING ENGINE REQUIREMENTS Final Report

L. W. STRAWHORN and V. A. SUSKI Mar. 1985 166 p refs
(Contract NAG3-457; DE-AI01-80CS-50194)
(NASA-CR-174996; DOE/NASA/0457-1; NAS 1.26:174996)
Avail: NTIS HC A08/MF A01 CSCL 13F

Developers of advanced heavy duty diesel engines are engaged in probing the opportunities presented by new materials and techniques. This process is technology driven, but there is neither assurance that the eventual users of the engines so developed will be comfortable with them nor, indeed, that those consumers will continue to exist in either the same form, or numbers as they do today. To ensure maximum payoff of research dollars, the equipment development process must consider user needs. This study defines motor carrier concerns, cost tolerances, and the engine parameters which match the future projected industry needs. The approach taken to do that is to be explained and the results presented. The material to be given comes basically from a survey of motor carrier fleets. It provides indications of the role of heavy duty vehicles in the 1998 period and their desired maintenance and engine performance parameters.

Author

N86-19264*# National Aeronautics and Space Administration, Lewis Research Center, Cleveland, Ohio.

OVERVIEW OF FREE-PISTON STIRLING SP-100 ACTIVITIES AT THE NASA LEWIS RESEARCH CENTER

J. G. SLABY 1986 25 p refs Prepared for Presentation at the 3rd International Stirling Engine Conference, Rome, Italy, 23-27 Jun. 1986

(Contract DE-AI05-82OR-1005)
(NASA-TM-87224; E-2834; DOE/NASA/1005-8; NAS 1.15:87224)
Avail: NTIS HC A02/MF A01 CSCL 10B

An overview of the National Aeronautics and Space Administration (NASA) Lewis Research Center (LeRC) SP-100 free-piston Stirling engine activities is presented. These activities are being conducted in support of the Department of Defense (DOD), Department of Energy (DOE), and NASA. The space-power technology effort, under SP-100, addresses the status of the 25 kW Space Power Demonstrator Engine (SPDE). Another facet of

the SP-100 project covers the status of an endurance test. Dynamic balancing of the SPDE engine is discussed along with a summary covering the parametric results of a study showing the relationship between power-converter specific weight and efficiency both as a function of Stirling engine heater to cooler temperature ratio. Design parameters and conceptual design features are presented for a 25 kW_e, single-cylinder free-piston Stirling space-power converter. And finally, a description of a hydrodynamic gas bearing concept is presented.

Author

N86-21456*# Westinghouse Research and Development Center, Pittsburgh, Pa.

DESIGN AND EVALUATION OF FLUIDIZED BED HEAT RECOVERY FOR DIESEL ENGINE SYSTEMS

J. R. HAMM, R. A. NEWBY, E. J. VIDT, and T. E. LIPPERT Jul. 1985 228 p refs

(Contract DEN3-345; DE-AI01-80CS-50194)
(NASA-CR-174898; DOE/NASA-0345-1; NAS 1.26:174898)
Avail: NTIS HC A11/MF A01 CSCL 13F

The potential of utilizing fluidized bed heat exchangers in place of conventional counter-flow heat exchangers for heat recovery from adiabatic diesel engine exhaust gas streams was studied. Fluidized bed heat recovery systems were evaluated in three different heavy duty transport applications: (1) heavy duty diesel truck; (2) diesel locomotives; and (3) diesel marine pushboat. The three applications are characterized by differences in overall power output and annual utilization. For each application, the exhaust gas source is a turbocharged-adiabatic diesel core. Representative subposed exhaust gas heat utilization power cycles were selected for conceptual design efforts including design layouts and performance estimates for the fluidized bed heat recovery heat exchangers. The selected power cycles were: organic rankine with RC-1 working fluid, turbocompound power turbine with steam injection, and stirling engine. Fuel economy improvement predictions are used in conjunction with capital cost estimates and fuel price data to determine payback times for the various cases.

E.A.K.

N86-21457*# National Aeronautics and Space Administration, Lewis Research Center, Cleveland, Ohio.

AUTOMOTIVE STIRLING SUMMARY AND OVERVIEW Final Report

W. K. TABATA and R. K. SHALTENS Oct. 1985 12 p Presented at the 23rd Automotive Technology Development Contractors Coordination Meeting, Dearborn, Mich., 21-24 Oct., 1985; sponsored by DOE

(Contract DE-AI01-85CE-50112)
(NASA-TM-87177; E-2825; DOE/NASA-50112-61; NAS 1.15:87177) Avail: NTIS HC A02/MF A01 CSCL 13F

Government funded studies for adapting the Stirling engine to an automotive application started in 1971. The initial studies were to reduce exhaust emissions and were later broadened to include fuel economy and alternate fuels. With the passage of the Automotive Propulsion Research and Development Act of 1978, the studies matured into the current Automotive Stirling Engine (ASE) Program. After eight years of development effort, the accomplishments of the ASE Program are reviewed to assess the outlook for program success at its scheduled completion in September 1987. One important goal of the ASE Program is the transfer of Stirling engine technology to the USA. The technology transfer to the ASE Program team members was accomplished. To expand the transfer in the USA, various activities were initiated to make available the developed automotive Stirling engine technology to other U.S. industries, including nonautomotive.

Author

N86-22451*# General Electric Co., Philadelphia, Pa.
TRANSFORMATION TOUGHENED CERAMICS FOR THE HEAVY DUTY DIESEL ENGINE TECHNOLOGY PROGRAM, PHASE 2 Final Report, Aug. 1984 - Jul. 1985
 S. MUSIKANT, S. C. SAMANTA, P. ARCHITETTO, and E. FEINGOLD 1 Dec. 1985 86 p refs
 (Contract DEN3-339; DE-AI-80CS-50194)
 (NASA-CR-175054; NAS 1.26:175054) Avail: NTIS HC A05/MF A01 CSCL 13F

The objective of this program is to develop an insulating structural ceramic for application in a heavy duty adiabatic diesel engine. The approach is to employ transformation toughening (TT) by additions of zirconia-hafnia solid solution (ZHSS). The feasibility of using ZHSS as a toughening agent in mullite and alumina has been demonstrated in Phase 1 of this work. Based on Phase 1 results, a decision was made to concentrate the Phase 2 effort on process optimization of the TT mullite. A strong factor in that decision was the low thermal conductivity and high thermal shock resistance of the mullite. Results of the Phase 2 effort indicate that optimum toughening of mullite by additions of ZHSS is difficult to achieve due to apparent sensitivity to morphology. The 48 ksi room temperature modulus-of-rupture (MOR) achieved in selected specimens is approximately 50% of the original strength target. The MOR deteriorated to 34 ksi at 800 C. Author

N86-24590*# Integral Technologies, Inc., Westmont, Ill.
METHODS FOR HEAT TRANSFER AND TEMPERATURE FIELD ANALYSIS OF THE INSULATED DIESEL PHASE 2 PROGRESS REPORT Interim Report
 T. MOREL, R. KERLBAR, E. F. FORT, and P. N. BLUMBERG Sep. 1985 319 p refs
 (Contract DEN3-342; DE-AI01-80CS-50194)
 (NASA-CR-175072; DOE/NASA/0342-2; NAS 1.26:175072)
 Avail: NTIS HC A14/MF A01 CSCL 13F

This report describes work done during Phase 2 of a 3 year program aimed at developing a comprehensive heat transfer and thermal analysis methodology for design analysis of insulated diesel engines. The overall program addresses all the key heat transfer issues: (1) spatially and time-resolved convective and radiative in-cylinder heat transfer, (2) steady-state conduction in the overall structure, and (3) cyclical and load/speed temperature transients in the engine structure. During Phase 2, radiation heat transfer model was developed, which accounts for soot formation and burn up. A methodology was developed for carrying out the multi-dimensional finite-element heat conduction calculations within the framework of thermodynamic cycle codes. Studies were carried out using the integrated methodology to address key issues in low heat rejection engines. A wide ranging design analysis matrix was covered, including a variety of insulation strategies, recovery devices and base engine configurations. A single cylinder Cummins engine was installed at Purdue University, and it was brought to a full operational status. The development of instrumentation was continued, concentrating on radiation heat flux detector, total heat flux probe, and accurate pressure-crank angle data acquisition. Author

N86-25302*# Stirling Thermal Motors, Inc., Ann Arbor, Mich.
EXPERIMENTAL ASSESSMENT OF ADVANCED STIRLING COMPONENT CONCEPTS Final Report
 B. ZIPH Oct. 1985 106 p
 (Contract DEN3-351; DE-AI01-77CS-51040)
 (NASA-CR-174994; DOE/NASA/0351-1; NAS 1.26:174994)
 Avail: NTIS HC A06/MF A01 CSCL 10B

The results of an experimental assessment of some advanced Stirling engine component concepts are presented. High performance piston rings, reciprocating oil scrapers and heat pipes with getters and with mechanical couplings were tested. The tests yielded the following results: (1) Bonded, split, pumping piston rings, in preliminary testing, proved a promising concept, exhibiting low leakage and friction losses. Solid piston rings proved impractical in view of their sensitivity to the operating temperature; (2) A babbitt oil scraper in a compliant housing performed well in atmospheric endurance testing. In pressurized tests the scraper

did not perform well as a containment seal. The latter tests suggest modifications which may adapt Ti successfully to that application; and (3) Heat pipe endurance tests indicated the adequacy of simple, inexpensive fabrication and filling procedures. Getters were provided to increase the tolerance of the heat pipes to the presence of air and commercially available couplings were demonstrated to be suitable for heat pipe application. In addition to the above tests, the program also included a design effort for a split shaft applicable to a swashplate driven engine with a pressurized crank-case. The design is aimed, and does accomplish, an increase in component life to more than 10,000 hours. Author

N86-25303*# National Aeronautics and Space Administration. Lewis Research Center, Cleveland, Ohio.
STIRLING POWERED VAN PROGRAM OVERVIEW Final Report
 R. K. SHALTENS 1986 14 p Presented at the International Congress and Exposition, Detroit, Mich., 24-28 Feb. 1986; sponsored by Society of Automotive Engineers Revised (Contract DE-AI01-85CE-50112)
 (NASA-TM-87227; DOE/NASA-50112/62-REV; E-2896; NAS 1.15:87227) Avail: NTIS HC A02/MF A01 CSCL 13F

The Stirling Powered Van Program (SPVP) is a multiyear, multiphase program to evaluate the automotive Stirling engine (ASE) in Air Force vans under realistic conditions. The objective of the SPVP is to transfer to manufacturer and end user(s) (i.e., on the path to commercialization) the second-generation Mod 2 ASE upon completion of the Automotive Stirling Engine Program in 1987. In order to meet this objective, the SPVP must establish Stirling performance, integrity, reliability, durability and maintainability. The ASE program background leading to the van program is reviewed and plans for evaluating the kinematic Stirling engine in Air Force vans examined. Also discussed are the NASA technology transfers to industry that have been accomplished and those which are currently being developed. Author

N86-26261*# National Aeronautics and Space Administration. Lewis Research Center, Cleveland, Ohio.
OVERVIEW OF THE 1986 FREE-PISTON STIRLING SP-100 ACTIVITIES AT THE NASA LEWIS RESEARCH CENTER Final Report
 J. G. SLABY 1986 20 p refs Prepared for presentation at the 21st Intersociety Energy Conversion Engineering Conference, San Diego, Calif., 25-29 Aug. 1986; sponsored by ACS, SAE, ANS, ASME, IEEE, AIAA, and AIChE
 (Contract DE-AI05-82OR-1005)
 (NASA-TM-87305; E-3028; DOE/NASA/1005-9; NAS 1.15:87305)
 Avail: NTIS HC A02/MF A01 CSCL 10B

An overview of the NASA Lewis Research Center SP-100 free-piston Stirling engine activities is presented. These activities include a free-piston Stirling space-power technology feasibility demonstration project as part of the SP-100 program being conducted in support of the Department of Defense (DOD), Department of Energy (DOE), and NASA. The space-power Stirling advanced technology effort, under SP-100, addresses the status of the 25 kWe Space Power Demonstrator Engine (SPDE) including test results. Future space-power projections are presented along with a description of a study that will investigate the feasibility of scaling a single-cylinder free-piston Stirling space-power module to the 150 kW power range. Design parameters and conceptual design features will be presented for a 25 kWe, single-cylinder free-piston Stirling space-power converter. A description of a hydrodynamic gas bearing concept is presented whereby the displacer of a 1 kWe free-piston Stirling engine is modified to demonstrate the bearing concept. And finally the goals of a conceptual design for a 25 kWe Solar Advanced Stirling Conversion System capable of delivering electric power to an electric utility grid are discussed. Author

N86-28017*# Mechanical Technology, Inc., Latham, N. Y.
AUTOMOTIVE STIRLING ENGINE DEVELOPMENT PROGRAM
Semiannual Technical Progress Report, 1 Jan. - 30 Jun. 1984
 N. NIGHTINGALE, A. RICHEY, R. FARRELL, G. RIECKE, W. ERNST, R. HOWARTH, M. CRONIN, M. SIMETKOSKY, and G. SMITH Dec. 1984 103 p
 (Contract DEN3-32; DE-AI01-77CS-51040)
 (NASA-CR-174749; DOE/NASA/0032-80/7; NAS 1.26:174749)
 Avail: NTIS HC A06/MF A01 CSCL 13F

This is the sixth Semiannual Progress Report prepared under the Automotive Stirling Engine Development Program. It covers the twenty-fourth and twenty-fifth quarters of activity after award of the contract. Quarterly Technical Progress Reports related program activities from the first through the thirteenth quarters; thereafter, reporting was changed to a semiannual format. This report summarizes activities performed on Mod I engine characterization and analyses, Mod I Transient Test Bed fuel economy, upgraded Mod I performance and testing, Stirling engine reference engine manufacturing and reduced size studies, components and subsystems, and the study and test of low cost casting alloys. The overall program philosophy is outlined, and data and results are presented.

Author

N86-29731*# National Aeronautics and Space Administration.
 Lewis Research Center, Cleveland, Ohio.
NASA/DOE AUTOMOTIVE STIRLING ENGINE PROJECT:
OVERVIEW 1986 Final Report
 D. G. BEREMAND and R. K. SHALTENS 1986 21 p Prepared for presentation at the 21st Intersociety Energy Conversion Engineering Conference, San Diego, Calif., 25-29 Aug. 1986
 (NASA-TM-87345; DOE/NASA-50112/66; E-3098; NAS 1.15:87345) Avail: NTIS HC A02/MF A01 CSCL 13F

The DOE/NASA Automotive Stirling Engine Project is reviewed and its technical progress and status are presented. Key technologies in materials, seals, and piston rings are progressing well. Seven first-generation engines, and modifications thereto, have accumulated over 15,000 hr of test time, including 1100hr of in-vehicle testing. Results indicate good progress toward the program goals. The first second-generation engine is now undergoing initial testing. It is expected that the program goal of a 30-percent improvement in fuel economy will be achieved in tests of a second-generation engine in a Celebrity vehicle.

Author

N86-29732*# National Aeronautics and Space Administration.
 Lewis Research Center, Cleveland, Ohio.
OVERVIEW OF NASA LEWIS RESEARCH CENTER
FREE-PISTON STIRLING ENGINE TECHNOLOGY ACTIVITIES
APPLICABLE TO SPACE POWER SYSTEMS Final Report
 J. G. SLABY 1986 13 p Proposed for presentation at the 4th Symposium on Space Nuclear Power Systems, Albuquerque, N. Mex., 12-16 Jan. 1987; sponsored by the Institute for Space Nuclear Power Studies
 (Contract DE-AI05-82OR-1005)
 (NASA-TM-88815; DOE/NASA-1005/10; E-3170; NAS 1.15:88815) Avail: NTIS HC A02/MF A01 CSCL 10B

Free piston Stirling technology is applicable for both solar and nuclear powered systems. As such, the Lewis Research Center serves as the project office to manage the newly initiated SP-100 Advanced Technology Program. This five year program provides the technology push for providing significant component and subsystem options for increased efficiency, reliability and survivability, and power output growth at reduced specific mass. One of the major elements of the program is the development of advanced power conversion concepts of which the Stirling cycle is a viable candidate. Under this program the research findings of the 25 kWe opposed piston Space Power Demonstrator Engine (SPDE) are presented. Included in the SPDE discussions are initial differences between predicted and experimental power outputs and power output influenced by variations in regenerators. Projections are made for future space power requirements over the next few decades. And a cursory comparison is presented showing the mass benefits that a Stirling system has over a Brayton

system for the same peak temperature and output power.

Author

N86-30579*# Mechanical Technology, Inc., Latham, N. Y. Stirling Engine Systems Div.
AUTOMOTIVE STIRLING ENGINE DEVELOPMENT PROGRAM
Semiannual Progress Report, 1 Jul. - 31 Dec. 1985
 W. ERNST, A. RICHEY, R. FARRELL, G. RIECKE, G. SMITH, R. HOWARTH, M. CRONIN, M. SIMETKOSKY, and J. MEACHER May 1986 66 p
 (Contract DEN3-32; DE-AI01-85CE-50112)
 (NASA-CR-175045; NAS 1.26:175045; REPT-86ASE507SA9; DOE/NASA-0032/80-7) Avail: NTIS HC A04/MF A01 CSCL 13F

This is the ninth Semiannual Technical Progress Report prepared under the Automotive Stirling Engine Development Program. It covers the twenty-eighth and twenty-ninth quarters of activity after award of the contract. Quarterly Technical Progress Reports related program activities from the first through the thirteenth quarters; thereafter, reporting was changed to a Semiannual format. This report summarizes the study of higher-power kinematic Stirling engines for transportation use, development testing of Mod I Stirling engines, and component development activities. Component development testing included successful conical fuel nozzle testing and functional checkout of Mod II controls and auxiliaries on Mod I engine test beds. Overall program philosophy is outlined and data and test results are presented.

Author

N86-31452*# Sverdrup Technology, Inc., Cleveland, Ohio.
EVALUATION OF A STIRLING ENGINE HEATER BYPASS WITH THE NASA LEWIS NODAL-ANALYSIS PERFORMANCE CODE
Final Report
 T. J. SULLIVAN May 1986 26 p
 (Contract NAS3-24105; DE-AI01-77CS-51040)
 (NASA-CR-179460; DOE/NASA/4105-1; E-3113; NAS 1.26:179460) Avail: NTIS HC A03/MF A01 CSCL 10B

In support of the U.S. Department of Energy's Stirling Engine Highway Vehicle Systems program, the NASA Lewis Research Center investigated whether bypassing the P-40 Stirling engine heater during regenerative cooling would improve engine performance. The Lewis nodal-analysis Stirling engine computer simulation was used for this investigation. Results for the heater-bypass concept showed no significant improvement in the indicated thermal efficiency for the P-40 Stirling engine operating at full-power and part-power conditions. Optimizing the heater tube length produced a small increase in the indicated thermal efficiency with the heater-bypass concept.

Author

N86-33211*# Garrett Turbine Engine Co., Phoenix, Ariz.
ADVANCED GAS TURBINE (AGT) TECHNOLOGY
DEVELOPMENT PROJECT ANNUAL REPORT Interim Progress
Report, Jul. 1984 - Jun. 1985
 Jul. 1986 175 p
 (Contract DEN3-167)
 (NASA-CR-179485; NAS 1.26:179485; DOE/NASA/0167-10; GARRETT-31-3725(10)) Avail: NTIS HC A08/MF A01 CSCL 20A

This report is the tenth in a series of Technical Summary reports for the Advanced Gas Turbine (AGT) Technology Development Project, authorized under NASA Contract DEN3-167, and sponsored by the Department of Energy (DOE). This report was prepared by Garrett Turbine Engine Company, A Division of the Garrett Corporation, and includes information provided by Ford Motor Company, the Carborundum Company, and AiResearch Casting Company. The Project is administered by Mr. Thomas N. Strom, Project Manager, NASA-Lewis Research Center, Cleveland, Ohio. This report covers plans and progress for the period July 1, 1984 through June 30, 1985.

Author

SPACE SCIENCES (GENERAL)

N86-14110*# National Aeronautics and Space Administration. Lewis Research Center, Cleveland, Ohio.

DEVELOPMENT OF THE VOLT-A SHUTTLE EXPERIMENT

W. J. BIFANO, J. M. BOZEK, and D. C. FERGUSON 1985 13 p Presented at the 18th Photovoltaic Specialists Conference, Las Vegas, Nev., 21-25 Oct. 1985; sponsored by IEEE (NASA-TM-87169; E-2807; NAS 1.15:87169) Avail: NTIS HC A02/MF A01 CSCL 12A

The NASA Lewis Research Center (LeRC) is investigating potential problems associated with the operation of high voltage solar cell arrays in the space plasma environment. At high voltages, interactions between the solar array and the space plasma could result in unacceptable levels of electrical discharge (arcing) and/or parasitic losses (current drains from the array to the plasma). The objective of the Voltage Operating Limit Tests (VOLT-A) Shuttle bay experiment is to characterize space plasma/solar cell panel interactions in low earth orbit. VOLT-A consists of an experiment plate subassembly which contains four solar panels, an electronics subassembly and a Langmuir probe subassembly mounted on an MPSS carrier. During a given 8.25 hour data taking period (5-1/2 continuous orbits), the solar panels, which represent state-of-the-art solar cell technologies, will be sequentially subjected to bias voltages in steps ranging from minus 626 V to plus 313 V. Appropriate measurements will be made at each voltage to characterize arcing and parasitic losses. Corresponding measurements of the plasma environment (plasma density, electron temperature and neutral density) will also be made. Data will be recorded on an on-board tape recorder for subsequent data reduction and analysis. Author

ASTROPHYSICS

Includes cosmology; celestial mechanics; space plasmas; and interstellar and interplanetary gases and dust.

N86-25310*# Akron Univ., Ohio. Dept. of Civil Engineering.

EFFECTS OF STATE RECOVERY ON CREEP BUCKLING UNDER VARIABLE LOADING Final Report

D. N. ROBINSON and S. M. ARNOLD Apr. 1986 45 p refs (Contract NAG3-379)

(NASA-CR-175094; NAS 1.26:175094) Avail: NTIS HC A03/MF A01 CSCL 03B

Structural alloys embody internal mechanisms that allow recovery of state with varying stress and elevated temperature, i.e., they can return to a softer state following periods of hardening. Such material behavior is known to strongly influence structural response under some important thermomechanical loadings, for example, that involving thermal ratchetting. The influence of dynamic and thermal recovery on the creep buckling of a column under variable loading is investigated. The column is taken as the idealized (Shanley) sandwich column. The constitutive model, unlike the commonly employed Norton creep model, incorporates a representation of both dynamic and thermal (state) recovery. The material parameters of the constitutive model are chosen to characterize Narloy Z, a representative copper alloy used in thrust nozzle liners of reusable rocket engines. Variable loading histories include rapid cyclic unloading/reloading sequences and intermittent reductions of load for extended periods of time; these are superimposed on a constant load. The calculated results show that state recovery significantly affects creep buckling under

variable loading. Structural alloys embody internal mechanisms that allow recovery of state with varying stress and time. Author

LUNAR AND PLANETARY EXPLORATION

Includes planetology; and manned and unmanned flights.

N86-19274*# National Aeronautics and Space Administration. Lewis Research Center, Cleveland, Ohio.

ELECTROCRYSTALLIZATION IN MICROGRAVITY

C. E. MAY Jan. 1986 22 p refs

(NASA-TM-87202; E-2857; NAS 1.15:87202) Avail: NTIS HC A02/MF A01 CSCL 03B

Electrocrystallization under microgravity conditions is proposed as a potential method of crystallization that would be almost completely free of fluid convection. Such crystallization may result in purer, more perfect, and larger crystals than is possible under normal gravity conditions. Observations made and data collected during the crystallization process under convection-free conditions should add to our knowledge of the crystallization process. The proposed method would allow easy comparison of crystals growth in space with those grown under normal gravity conditions. Nine types of electrocrystallization are presented: an example of each is discussed. Electrocrystallization is compared with the compartmental crystallization method used by 3M Corporation in recent shuttle experiments. Author

N86-30620*# National Aeronautics and Space Administration. Lewis Research Center, Cleveland, Ohio.

FUGACITY AND CONCENTRATION GRADIENTS IN A GRAVITY FIELD

C. E. MAY Jul. 1986 39 p

(NASA-TM-88809; E-3157; NAS 1.15:88809) Avail: NTIS HC A03/MF A01 CSCL 03B

Equations are reviewed which show that at equilibrium fugacity and concentration gradients can exist in gravitational fields. At equilibrium, the logarithm of the ratio of the fugacities of a species at two different locations in a gravitational field is proportional to the difference in the heights of the two locations and the molecular weight of the species. An analogous relation holds for the concentration ratios in a multicomponent system. The ratio is calculated for a variety of examples. The kinetics for the general process are derived, and the time required to approach equilibrium is calculated for several systems. The following special topics are discussed: ionic solutions, polymers, multiphase systems, hydrostatic pressure, osmotic pressure, and solubility gradients in a gravity field. Author

GENERAL

N86-25321*# National Aeronautics and Space Administration. Lewis Research Center, Cleveland, Ohio.

RESEARCH AND COMPETITION: BEST PARTNERS

J. M. SHAW 1986 12 p Presented at the 90th Casting Congress, Minneapolis, Minnesota, 11-15 May 1986; sponsored by the American Foundrymen's Society

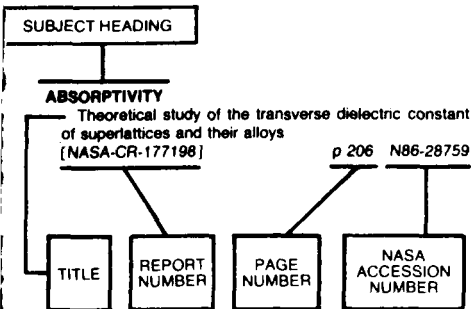
(NASA-TM-87313; E-3044; NAS 1.15:87313) Avail: NTIS HC A02/MF A01 CSCL 05A

NASA's Microgravity Science and Applications Program is directed toward research in the science and technology of processing materials under conditions of low gravity. The objective

is to make a detailed examination of the constraints imposed by gravitational forces on Earth. The program is expected to lead ultimately to the development of new materials and processes in Earth-based commercial applications, adding to this nation's technological base. An important resource that U.S. researchers have readily available to them is the new Microgravity Materials Science Laboratory (MMSL) at NASA Lewis Research Center in Cleveland. A typical scenario for a microgravity materials experiment at Lewis would begin by establishing 1-g baseline data in the MMSL and then proceeding, if it is indicated, to a drop tower or to simulated microgravity conditions in a research aircraft to qualify the project for space flight. A major component of Lewis microgravity materials research work involves the study of metal and alloy solidification fundamentals.

Author

Typical Subject Index Listing



The subject heading is the key to the subject content of the document. Titles, report numbers, and accession numbers of pertinent documents are provided under each subject heading. When the title is insufficiently descriptive of the document content, a title extension has been added, separated from the title by three hyphens. The report number helps to indicate the type of document cited (e.g., NASA report, NASA translation, NASA contractor report). The NASA accession number is the number by which the document abstracts are arranged in this journal and by which the document is sold or requested. The titles, with title extensions if present, are arranged under each subject heading in ascending accession number order. The subject headings have been selected from the latest revision of the *NASA Thesaurus* (NASA SP-7053).

A

ABRASION

Abrasion and deformed layer formation of manganese-zinc ferrite in sliding contact with lapping tapes [NASA-TM-82749] p 104 N86-24838

ABSORPTIVITY

Theoretical study of the transverse dielectric constant of superlattices and their alloys [NASA-CR-177198] p 206 N86-28759

ABSTRACTS

Bibliography of Lewis Research Center technical publications announced in 1985 [NASA-TM-87263] p 208 N86-32336

AC GENERATORS

AC motor and generator requirements for isolated WECS [NASA-CR-176315] p 182 N86-11670

ACCOMMODATION

Robust detection-isolation-accommodation for sensor failures [NASA-CR-174797] p 121 N86-16486

Robust detection, isolation and accommodation for sensor failures [NASA-CR-174825] p 33 N86-30732

ACCUMULATORS

Verification of an improved computational design procedure for TWT-dynamic refocuser-MDC systems for secondary electron emission losses p 119 A86-45194

Secondary-electron-emission losses in multistage depressed collectors and traveling-wave-tube efficiency improvements with carbon collector electrode surfaces [NASA-TP-2622] p 125 N86-32629

ACCURACY

Effect of accuracy of wind power prediction on power system operator [NASA-CR-176300] p 181 N86-11667

ACEE PROGRAM

Subscale-model and full-scale engine mixed-flow exhaust system performance comparison p 18 A86-14528

ACETYLENE

Carbon-rich ceramic composites from ethynyl aromatic precursors [NASA-TM-88812] p 71 N86-29908

ACOUSTIC ATTENUATION

Nondestructive characterization of structural ceramics p 99 A86-37141

Ultrasonic characterization of structural ceramics p 199 N86-22970

ACOUSTIC EMISSION

Analytical Ultrasonics in Materials Research and Testing [NASA-CP-2383] p 164 N86-22962

Wave propagation in anisotropic medium due to an oscillatory point source with application to unidirectional composites [NASA-CR-4001] p 165 N86-27666

ACOUSTIC EXCITATION

Tone excited jets. I - Introduction p 196 A86-16466

Tone excited jets. IV - Acoustic measurements p 196 A86-16469

Tone excited jets. V - A theoretical model and comparison with experiment p 196 A86-16470

An experimental study of tone-excited heated jets p 197 A86-31593

Some unresolved questions on hot-jet mixing control through artificial excitation [AIAA PAPER 86-1956] p 135 A86-45441

Acoustic control of free jet mixing p 135 A86-46314

Shear layer excitation, experiment versus theory [NASA-CR-176604] p 140 N86-20722

ACOUSTIC MEASUREMENT

Tone excited jets. I - Introduction p 196 A86-16466

Tone excited jets. IV - Acoustic measurements p 196 A86-16469

Free jet feasibility study of a thermal acoustic shield concept for AST/VCE application-dual flow. Comprehensive data report. Volume 1: Test nozzles and acoustic data [NASA-CR-174817] p 200 N86-23371

Free-jet feasibility study of a thermal acoustic shield concept for AST/VCE application-dual stream nozzles. Comprehensive data report. Volume 2: Laser velocimeter and suppressor. Base pressure data [NASA-CR-174818] p 201 N86-23372

Ultrasonic stress wave characterization of composite materials [NASA-CR-3976] p 165 N86-27665

A study of the stress wave factor technique for nondestructive evaluation of composite materials [NASA-CR-4002] p 165 N86-28445

Acousto-ultrasonic verification of the strength of filament wound composite material [NASA-TM-88827] p 166 N86-32764

ACOUSTIC MICROSCOPES

Reliability of void detection in structural ceramics by use of scanning laser acoustic microscopy p 163 A86-39027

Reliability of scanning laser acoustic microscopy for detecting internal voids in structural ceramics p 147 A86-46353

Reliability of scanning laser acoustic microscopy for detecting internal voids in structural ceramics [NASA-TM-87222] p 164 N86-16599

Factors that affect reliability of nondestructive detection of flaws in structural ceramics [NASA-TM-87348] p 166 N86-31912

Quantitative void characterization in structural ceramics using scanning laser acoustic microscopy [NASA-TM-88797] p 166 N86-31913

ACOUSTIC PROPAGATION

Time-dependent wave envelope finite difference analysis of sound propagation p 197 A86-20130

A numerical model of acoustic choking. II - Shocked solutions p 197 A86-20795

Non-linear effects in finite amplitude wave propagation through ducts and nozzles p 197 A86-35857

Turbofan aft duct suppressor study program listing and user's guide [NASA-CR-175067] p 30 N86-25357

ACOUSTIC PROPERTIES

An approach to the calculation of the pressure field produced by rigid wide chord dual rotation propellers of high solidity in compressible flow [AIAA PAPER 86-0467] p 198 A86-49566

An analysis of the sound field produced by rigid wide chord dual rotation propellers of high solidity in compressible flow [NASA-TM-87178] p 11 N86-21517

NASA/DOE automotive Stirling engine project: Overview 1986 [NASA-TM-87345] p 211 N86-29731

ACOUSTIC SCATTERING

Scattering of acoustic waves into Tollmien-Schlichting waves by small streamwise variations in surface geometry p 127 A86-17041

ACOUSTIC VELOCITY

Nondestructive characterization of structural ceramics p 99 A86-37141

Ultrasonic characterization of structural ceramics p 199 N86-22970

ACOUSTICS

Quantitative flow characterization with scanning laser acoustic microscopy p 163 A86-45150

Numerical Techniques in Acoustics [NASA-CP-2404] p 198 N86-12007

Quantitative flow characterization with scanning laser acoustic microscopy p 200 N86-22983

Modeling the effects of wind tunnel wall absorption on the acoustic radiation characteristics of propellers [NASA-TM-87333] p 201 N86-29630

ACOUSTO-OPTICS

Performance of direct and iterative algorithms on an optical systolic processor p 202 A86-17421

ACTIVATION ENERGY

Compressive creep behavior of alloys based on B2 FeAl [NASA-TM-87293] p 92 N86-28165

ACTIVE CONTROL

Quasi-modal vibration control by means of active control bearings [NASA-TM-87232] p 159 N86-21856

ACTUATORS

Fiber optics for propulsion control systems [ASME PAPER 84-GT-97] p 17 A86-13054

ADA (PROGRAMMING LANGUAGE)

A high-order language for a system of closely coupled processing elements [NASA-CR-177280] p 193 N86-27930

ADAPTIVE FILTERS

Adaptive antenna arrays for weak interfering signals --- in satellite communication p 45 A86-34591

ADDITIVES

Structure and grain coarsening during the sintering of alumina p 98 A86-26341

Strength and microstructure of Si₃N₄ sintered with ZrO₂ additions p 99 A86-36330

Lubricant and additive effects on spur gear fatigue life [ASME PAPER 85-TRIB-14] p 155 A86-43542

Current evaluation of the tripropellant concept [AIAA PAPER 86-1698] p 56 A86-49615

Fatigue crack propagation of nickel-base superalloys at 650 deg C [NASA-TM-87150] p 87 N86-12294

The effect of cobalt content in U-700 type alloys on degradation of aluminate coatings [NASA-TM-87173] p 87 N86-13408

A possible radiation-resistant solar cell geometry using superlattices p 185 A86-17851

Current evaluation of the tripropellant concept [NASA-TP-2602] p 62 N86-28124

Slip casting and extruding shapes of rhenium with metal oxide additives. I: Feasibility demonstration [NASA-CR-174970] p 63 N86-31648

ADHESION

Fundamental tribological properties of ceramics p 95 A86-15230

Characterization and measurement of polymer wear p 100 A86-48405

- Tribological properties of structural ceramics
[NASA-TM-87105] p 100 N86-10341
- Current viewpoints on oxide adherence mechanisms
[NASA-TM-87168] p 87 N86-13409
- Thermal desorption study of physical forces at the PTFE surface
[NASA-TM-87090] p 206 N86-25284
- ADHESION TESTS**
- Fracture toughness tests on plasma-sprayed coatings
p 64 A86-30051
- Tensile adhesion test measurements on plasma-sprayed coatings
p 98 A86-30052
- ADHESIVE BONDING**
- Adhesion and wear resistance of materials
[NASA-TM-87239] p 158 N86-20809
- ADHESIVES**
- High Temperature Polymer Matrix Composites
[NASA-CP-2385] p 68 N86-11260
- ADIABATIC CONDITIONS**
- Design and evaluation of fluidized bed heat recovery for diesel engine systems
[NASA-CR-174898] p 209 N86-21456
- Sliding seal materials for adiabatic engines, phase 2
[NASA-CR-17475] p 105 N86-29042
- ADSORPTION**
- Adsorption of O₂, SO₂, and SO₃ on nickel oxide - Mechanism for sulfate formation p 75 A86-34238
- AEROACOUSTICS**
- Tone excited jets. I - Introduction p 196 A86-16466
- Flow field and near and far sound field of a subsonic jet p 5 A86-35855
- Modeling wind tunnel effects on the radiation characteristics of acoustic sources p 197 A86-41689
- Numerical evaluation of propeller noise including nonlinear effects p 23 A86-41726
- Noise generated by convected gusts interacting with swept airfoil cascades p 198 A86-45492
- [AIAA PAPER 86-1872] p 198 A86-45492
- Development of an impulsive noise source to study the acoustic reflection characteristics of hard-walled wind tunnels p 198 A86-45500
- [AIAA PAPER 86-1887] p 198 A86-45500
- Acoustic reflection contamination measurements in the 16-foot NASA Langley Transonic Wind Tunnel p 198 A86-45501
- [AIAA PAPER 86-1888] p 198 A86-45501
- Laboratory experiments on active suppression of advanced turboprop noise p 199 N86-19125
- [NASA-TM-87129] p 199 N86-19125
- AEROBRAKING**
- Advanced orbit transfer vehicle propulsion system study p 60 N86-24746
- [NASA-CR-174843] p 60 N86-24746
- AEROCAPTURE**
- Advanced orbit transfer vehicle propulsion system study p 60 N86-24746
- [NASA-CR-174843] p 60 N86-24746
- AERODYNAMIC BALANCE**
- Mass balancing of hollow fan blades p 171 A86-48245
- [ASME PAPER 86-GT-195] p 171 A86-48245
- Mass balancing of hollow fan blades p 174 N86-18611
- [NASA-TM-87197] p 174 N86-18611
- AERODYNAMIC CHARACTERISTICS**
- The effect of limiting aerodynamic and structural coupling in models of mistuned bladed disk vibration p 21 A86-26905
- An LU implicit scheme for high speed inlet analysis [AIAA PAPER 86-1520] p 6 A86-42687
- Real gas effects on the numerical simulation of a hypersonic inlet p 6 A86-48324
- Horseshoe vortex formation around a cylinder p 8 A86-48274
- [ASME PAPER 86-GT-246] p 8 A86-48274
- Evaluation of propfan propulsion applied to general aviation p 30 N86-24895
- [NASA-CR-175020] p 30 N86-24895
- Unsteady heat transfer and direct comparison to steady-state measurements in a rotor-wake experiment [NASA-TM-87220] p 142 N86-24934
- A supersonic fan equipped variable cycle engine for a Mach 2.7 supersonic transport p 32 N86-28946
- [NASA-CR-177141] p 32 N86-28946
- AERODYNAMIC COEFFICIENTS**
- Packet flutter and aerodynamic modes for non-homogeneous airfoil cascades in highly distorted, periodic, stationary throughflows p 5 A86-38896
- [AIAA PAPER 86-0848] p 5 A86-38896
- Statistical prediction of dynamic distortion of inlet flow using minimum dynamic measurement. An application to the Melick statistical method and inlet flow dynamic distortion prediction without RMS measurements p 142 N86-24933
- [NASA-CR-176764] p 142 N86-24933
- AERODYNAMIC CONFIGURATIONS**
- Preliminary results of unsteady blade surface pressure measurements for the SR-3 propeller p 8 A86-49625
- [AIAA PAPER 86-1893] p 8 A86-49625

- Preliminary results of unsteady blade surface pressure measurements for the SR-3 propeller p 12 N86-27213
- [NASA-TM-87352] p 12 N86-27213
- AERODYNAMIC DRAG**
- Ice shapes and the resulting drag increase for a NACA 0012 airfoil p 14 A86-14427
- [AIAA PAPER 84-0109] p 14 A86-14427
- In-flight measurements of wing ice shapes and wing section drag increases caused by natural icing conditions p 12 N86-24667
- [NASA-TM-87301] p 12 N86-24667
- Electrodynamic tether technology considerations p 161 N86-27657
- AERODYNAMIC FORCES**
- Unsteady transonic flow over cascade blades p 3 A86-23141
- Forced response analysis of an aerodynamically detuned supersonic turbomachine rotor p 21 A86-26902
- Unsteady forces on counter-rotating propeller blades [AIAA PAPER 86-1804] p 22 A86-37827
- Passive control of aerodynamically forced vibrations of supersonic turbomachine rotors by splitter blades [AIAA PAPER 86-0844] p 22 A86-38892
- Free jet feasibility study of a thermal acoustic shield concept for AST/VCE application-dual flow. Comprehensive data report. Volume 1: Test nozzles and acoustic data p 200 N86-23371
- [NASA-CR-174817] p 200 N86-23371
- Free-jet feasibility study of a thermal acoustic shield concept for AST/VCE application-dual stream nozzles. Comprehensive data report. Volume 2: Laser velocimeter and suppressor. Base pressure data p 201 N86-23372
- [NASA-CR-174818] p 201 N86-23372
- AERODYNAMIC INTERFERENCE**
- Experimental and theoretical study of propeller spinner/shank interference p 13 N86-29773
- [NASA-CR-176954] p 13 N86-29773
- AERODYNAMIC LOADS**
- Three dimensional unsteady aerodynamics and aeroelastic response of advanced turboprops p 22 A86-38894
- [AIAA PAPER 86-0846] p 22 A86-38894
- Structural integrity and durability for Space Shuttle main engine and future reusable space propulsion systems p 55 A86-42682
- [AIAA PAPER 86-1513] p 55 A86-42682
- Structural integrity and durability for Space Shuttle main engine and future reusable space propulsion systems p 61 N86-25408
- [NASA-TM-87280] p 61 N86-25408
- AERODYNAMIC NOISE**
- Influence of airfoil camber on convected gust interaction noise p 198 A86-45493
- [AIAA PAPER 86-1873] p 198 A86-45493
- Propeller noise caused by blade tip radial forces p 23 A86-45504
- [AIAA PAPER 86-1892] p 23 A86-45504
- AERODYNAMIC STABILITY**
- Stability of limit cycles in frictionally damped and aerodynamically unstable rotor stages p 18 A86-19198
- Aerodynamic detuning analysis of an unstalled supersonic turbopfan cascade p 3 A86-22732
- [ASME PAPER 85-GT-192] p 3 A86-22732
- Bifurcation techniques for nonlinear dynamic analysis of compressor stall phenomena p 22 A86-35403
- AERODYNAMIC STALLING**
- Bifurcation techniques for nonlinear dynamic analysis of compressor stall phenomena p 22 A86-35403
- Analysis of fully stalled compressor p 5 A86-38480
- [AIAA PAPER 86-1123] p 5 A86-38480
- Analysis of fully stalled compressor p 11 N86-20357
- [NASA-TM-87254] p 11 N86-20357
- AERODYNAMICS**
- Application of a linearized unsteady aerodynamic analysis to standard cascade configurations p 11 N86-21505
- [NASA-CR-3940] p 11 N86-21505
- AEROELASTICITY**
- Aeroelastic formulations for turbomachines and propellers p 20 A86-24677
- Dynamic characteristics of an assembly of prop-fan blades p 21 A86-32956
- [ASME PAPER 85-GT-134] p 21 A86-32956
- Three dimensional unsteady aerodynamics and aeroelastic response of advanced turboprops p 22 A86-38894
- [AIAA PAPER 86-0846] p 22 A86-38894
- Computational engine structural analysis p 23 A86-48141
- [ASME PAPER 86-GT-70] p 23 A86-48141
- Analytical and experimental investigation of the coupled bladed disk/shaft whirl of a cantilevered turbopfan p 24 A86-48163
- [ASME PAPER 86-GT-98] p 24 A86-48163
- Aeroelastic behavior of low aspect ratio metal and composite blades p 171 A86-48271
- [ASME PAPER 86-GT-243] p 171 A86-48271
- Forced response analysis of an aerodynamically detuned supersonic turbomachine rotor p 9 N86-10019
- [NASA-TM-87093] p 9 N86-10019
- Summary of recent NASA propeller research p 25 N86-11158

- Computational engine structural analysis p 175 N86-19663
- [NASA-TM-87231] p 175 N86-19663
- AERONAUTICAL ENGINEERING**
- Future directions in aeropropulsion technology p 1 A86-11602
- Research and technology, Lewis Research Center p 207 N86-21427
- [NASA-CR-174719] p 207 N86-21427
- Review and critical analysis: Rolling-element bearings for system life and reliability p 159 N86-24991
- [NASA-CR-174710] p 159 N86-24991
- Advanced instrumentation for aeronautical propulsion research p 150 N86-32703
- [NASA-TM-88853] p 150 N86-32703
- AERONAUTICS**
- Upper air forecasting for aviation in the United States p 191 A86-37501
- AEROSOLS**
- Combustion characteristics in the transition region of liquid fuel sprays p 77 N86-20517
- [NASA-CR-176564] p 77 N86-20517
- Criteria for significance of simultaneous presence of both condensable vapors and aerosol particles on mass transfer (deposition) rates p 109 N86-24869
- [NASA-TM-87247] p 109 N86-24869
- Combined fringe and Fabry-Perot laser anemometer for three component velocity measurements in turbine stator cascade facility p 149 N86-24967
- [NASA-TM-87322] p 149 N86-24967
- AEROSPACE ENGINEERING**
- Computational composite mechanics for aerospace propulsion structures p 67 A86-40596
- [AIAA PAPER 86-1190] p 67 A86-40596
- AEROSPACE ENVIRONMENTS**
- Ion beam sputter-deposited thin film coatings for protection of spacecraft polymers in low earth orbit p 95 A86-14428
- [AIAA PAPER 85-0420] p 95 A86-14428
- Influence of melt convection on solid-liquid interface under terrestrial and reduced gravity environments p 38 N86-10083
- Solidification fundamentals p 39 N86-10090
- Mass loss of shuttle space suit orthofabric under simulated ionospheric atomic oxygen bombardment p 192 N86-13899
- [NASA-TM-87149] p 192 N86-13899
- Space Photovoltaic Research and Technology 1985: High Efficiency, Space Environment, and Array Technology p 184 N86-17839
- [NASA-CP-2408] p 184 N86-17839
- A study of Krypton degradation under simulated shuttle environment p 78 N86-28136
- [NASA-CR-176850] p 78 N86-28136
- AEROSPACE SCIENCES**
- Bibliography of Lewis Research Center technical publications announced in 1985 p 208 N86-32336
- [NASA-TM-87263] p 208 N86-32336
- AEROSPACEPLANES**
- Heat transfer in space power and propulsion systems p 53 A86-26492
- AEROTHERMODYNAMICS**
- Combustion research for gas turbine engines p 17 A86-11609
- Heat transfer results and operational characteristics of the NASA Lewis Research Center hot section cascade test facility p 128 A86-22053
- [ASME PAPER 85-GT-82] p 128 A86-22053
- Experimental measurements of heat transfer from an iced surface during artificial and natural cloud icing conditions p 36 A86-39948
- [AIAA PAPER 86-1352] p 36 A86-39948
- Turbine-stage heat transfer - Comparison of short-duration measurements with state-of-the-art predictions p 134 A86-42656
- [AIAA PAPER 86-1465] p 134 A86-42656
- Combustion hot section technology p 25 N86-11512
- AGING (MATERIALS)**
- Effect of solution concentration and aging conditions on PMR-15 resin p 98 A86-33113
- Fracture characteristics of angleplied laminates fabricated from overaged graphite/epoxy prepreg p 70 N86-25417
- [NASA-TM-87266] p 70 N86-25417
- AGING (METALLURGY)**
- Thermal aging effects in refractory metal alloys p 89 N86-16334
- [NASA-TM-87210] p 89 N86-16334
- AILERONS**
- Summary of NASA/DOE Aileron-Control Development Program for Wind Turbines p 190 N86-31983
- [NASA-TM-88811] p 190 N86-31983
- AIR**
- Two dimensional, transient catalytic combustion of CO-air on platinum p 71 A86-10201
- Characterization of real gas properties for space shuttle main engine fuel turbine and performance calculations p 61 N86-27418
- [NASA-CR-175066] p 61 N86-27418

AIR BREATHING BOOSTERS

A parametric study of a gas-generator airturbo ramjet (ATR)
[NASA-TM-88808] p 34 N86-31586

AIR COOLING

Structural analysis of turbine blades using unified constitutive models
[NASA-TM-88807] p 178 N86-28461

AIR DUCTS

Gas flow environmental and heat transfer nonrotating 3D program
p 137 N86-11506

AIR FLOW

Swirling flows in typical combustor geometries
p 128 A86-20370
Concentration distributions in a model combustor
p 133 A86-38575
A stagnation pressure probe for droplet-laden air flow
p 133 A86-39077

AIR JETS

Heat transfer characteristics within an array of impinging jets. Effects of crossflow temperature relative to jet temperature
[NASA-CR-3936] p 139 N86-15625
Lateral jet injection into typical combustor flowfields
[NASA-CR-3997] p 31 N86-28086

AIRCRAFT CONSTRUCTION MATERIALS

Angular particle impingement studies of thermoplastic materials at normal incidence
[ASLE PREPRINT 85-AM-3A-1] p 94 A86-11076
High Temperature Polymer Matrix Composites
[NASA-CP-2385] p 68 N86-11260

AIRCRAFT CONTROL

The measurement of aircraft performance and stability and control after flight through natural icing conditions
[AIAA PAPER 86-9758] p 35 A86-40681
The measurement of aircraft performance and stability and control after flight through natural icing conditions
[NASA-TM-87265] p 35 N86-22582

AIRCRAFT DESIGN

Lubrication and performance of high-speed rolling-element bearings
p 152 A86-19375
Propeller design by optimization
[AIAA PAPER 86-0081] p 19 A86-19678
A numerical method for the design and analysis of counter-rotating propellers
[AIAA PAPER 84-1205] p 19 A86-20369
Evaluation of propfan propulsion applied to general aviation
[NASA-CR-175020] p 30 N86-24695

AIRCRAFT ENGINES

Sensor failure detection for jet engines using analytical redundancy
p 18 A86-14226
Subscale-model and full-scale engine mixed-flow exhaust system performance comparison
p 18 A86-14528
NASA Lewis Research Center/university graduate research program on engine structures
[ASME PAPER 85-GT-159] p 167 A86-22084
Fuel deposit characteristics at low velocity
[ASME PAPER 85-IGT-130] p 107 A86-23922
Forced response analysis of an aerodynamically detuned supersonic turbomachine rotor
p 21 A86-26902
The effect of limiting aerodynamic and structural coupling in models of mistuned bladed disk vibration
p 21 A86-26905
Bifurcation techniques for nonlinear dynamic analysis of compressor stall phenomena
p 22 A86-35403
The STOL performance of a two-engine, USB powered-lift aircraft with cross-shafted fans
[SAE PAPER 851839] p 16 A86-38336
Rotorcraft propulsion for year 2000 plus
[AIAA PAPER 86-1543] p 23 A86-42702
Small engine technology payoffs for future commuter aircraft
[AIAA PAPER 86-1544] p 23 A86-42703
Advanced rotary engine components utilizing fiber reinforced Mg castings
[AIAA PAPER 86-1559] p 67 A86-42712
Transient engine performance with water ingestion
[AIAA PAPER 86-1621] p 23 A86-42755
Mode II fatigue crack growth specimen development
p 171 A86-43566
Stratified charge rotary engine for general aviation
[ASME PAPER 86-GT-181] p 24 A86-48231
Unified constitutive materials model development and evaluation for high-temperature structural analysis applications --- for aircraft gas turbine engines
p 172 A86-49133
Combustion hot section technology
p 25 N86-11512
HOST structural analysis program overview
p 25 N86-11513
Lightweight two-stroke cycle aircraft diesel engine technology enablement program, volume 1
[NASA-CR-174923-VOL-1] p 26 N86-13328

Lightweight two-stroke cycle aircraft diesel engine technology enablement program, volume 2
[NASA-CR-174923-VOL-2] p 26 N86-13329

Lightweight two-stroke cycle aircraft diesel engine technology enablement program, volume 3
[NASA-CR-174923-VOL-3] p 26 N86-13330
Polymer, metal and ceramic matrix composites for advanced aircraft engine applications
[NASA-TM-87132] p 87 N86-13407

Development of optical diaphragm deflection sensors
[NASA-CR-175008] p 203 N86-15113
Laser fringe anemometry for aero engine components
[NASA-TM-88798] p 12 N86-28053
Robust detection, isolation and accommodation for sensor failures
[NASA-CR-174825] p 33 N86-30732
An overview of the Small Engine Component Technology (SECT) studies
[NASA-TM-88796] p 34 N86-31587

AIRCRAFT EQUIPMENT

Designing an electro-impulse de-icing system
[AIAA PAPER 86-0545] p 16 A86-19940
Piezoelectric deicing device
[NASA-CASE-LEW-13773-2] p 122 N86-20671

AIRCRAFT FUELS

Long term deposit formation in aviation turbine fuel at elevated temperature
[AIAA PAPER 86-0525] p 107 A86-19929
Summary of recent NASA propeller research
p 25 N86-11158

Development of LC-13C NMR
[NASA-CR-176656] p 107 N86-21704
Emission FTIR analyses of thin microscopic patches of jet fuel residues deposited on heated metal surfaces
[NASA-CR-176786] p 108 N86-25502
High accuracy fuel flowmeter
[NASA-CR-174869] p 150 N86-31030

AIRCRAFT HAZARDS

Experimental measurements of heat transfer from an iced surface during artificial and natural cloud icing conditions
[AIAA PAPER 86-1352] p 36 A86-39948
The measurement of aircraft performance and stability and control after flight through natural icing conditions
[AIAA PAPER 86-9758] p 35 A86-40681
NASA's aircraft icing analysis program
p 14 A86-49107
A numerical and experimental investigation of electrochemical aircraft deicing
[NASA-CR-175024] p 14 N86-20380
The measurement of aircraft performance and stability and control after flight through natural icing conditions
[NASA-TM-87265] p 35 N86-22582
Calibration of droplet sizing and liquid water content instruments: Survey and analysis
[NASA-CR-175099] p 149 N86-26596
NASA's Aircraft Icing Analysis Program
[NASA-TM-88791] p 15 N86-31548

AIRCRAFT NOISE

The effect of acoustic reflections on combustor noise measurements
p 197 A86-20364
An experimental investigation of reducing advanced turboprop cabin noise by wing shielding
[AIAA PAPER 86-1966] p 16 A86-45449
Current wind tunnel capability and planned improvements at Lewis Research Center
[NASA-TM-87190] p 37 N86-18329
An estimate of the enroute noise of an advanced turboprop airplane
NASA-TM-87302 E-3020 NAS 1.15:87302 HC A02/MF A01
[NASA-TM-87302] p 201 N86-25217
An experimental investigation of reducing advanced turboprop cabin noise by wing shielding
[NASA-TM-87112] p 201 N86-25218

AIRCRAFT PERFORMANCE

The performance characteristics of simulated ice on rotorcraft airfoils
p 14 A86-35656
The STOL performance of a two-engine, USB powered-lift aircraft with cross-shafted fans
[SAE PAPER 851839] p 16 A86-38336
The measurement of aircraft performance and stability and control after flight through natural icing conditions
[AIAA PAPER 86-9758] p 35 A86-40681
The measurement of aircraft performance and stability and control after flight through natural icing conditions
[NASA-TM-87265] p 35 N86-22582

AIRCRAFT POWER SUPPLIES

Transmission line design for a power distribution system at 20 kHz for aircraft
[NASA-CR-3987] p 32 N86-29818

AIRCRAFT SAFETY

Analyses and tests for design of an electro-impulse de-icing system
[NASA-CR-174919] p 15 N86-27268

AIRCRAFT STABILITY

The measurement of aircraft performance and stability and control after flight through natural icing conditions
[AIAA PAPER 86-9758] p 35 A86-40681
The measurement of aircraft performance and stability and control after flight through natural icing conditions
[NASA-TM-87265] p 35 N86-22582

AIRCRAFT STRUCTURES

Aerospace applications of PMR polyimide composites
p 67 A86-27730
Numerical synthesis of tri-variate velocity realizations of turbulence
p 168 A86-28654
Evaluation of capillary reinforced composites
[NASA-CR-175061] p 70 N86-24760

AIRCRAFT WAKES

An experimental investigation of propeller wakes using a laser Doppler velocimeter
[AIAA PAPER 86-0080] p 18 A86-19677

AIRFOIL PROFILES

Boundary layer measurements on an airfoil in cascade using laser Doppler anemometry
[AIAA PAPER 86-0072] p 145 A86-19670
Packet flutter and aerodynamic modes for non-homogenous airfoil cascades in highly distorted, periodic, stationary throughflows
[AIAA PAPER 86-0848] p 5 A86-38896

AIRFOILS

High-temperature thermocouple and heat flux gauge using a unique thin film-hardware hot junction
[ASME PAPER 85-GT-18] p 145 A86-13059
Local heat-transfer measurements on a large scale-model turbine blade airfoil using a composite of a heater element and liquid crystals
[ASME PAPER 85-GT-59] p 126 A86-13061
Ice shapes and the resulting drag increase for a NACA 0012 airfoil
[AIAA PAPER 84-0109] p 14 A86-14427
Unsteady pressure measurements on a biconvex airfoil in a transonic oscillating cascade
[ASME PAPER 85-GT-212] p 3 A86-22731
An experimental method for measuring droplet impingement efficiency on two- and three-dimensional bodies
[AIAA PAPER 86-0406] p 131 A86-26630
Gas side heat transfer
p 138 N86-11507
Preliminary design of a supersonic cruise aircraft high-pressure turbine
[NASA-CR-174878] p 26 N86-14272
Turbine vane external heat transfer. Volume 1: Analytical and experimental evaluation of surface heat transfer distributions with leading edge showerhead film cooling
[NASA-CR-174827] p 29 N86-21546
Effect of a rotor wake on the local heat transfer on the forward half of a circular cylinder
[NASA-TM-87234] p 140 N86-21794
Thermal barrier coating life prediction model development
[NASA-CR-175087] p 103 N86-22713
In-flight measurements of wing ice shapes and wing section drag increases caused by natural icing conditions
[NASA-TM-87301] p 12 N86-24667
Life prediction and constitutive models for engine hot section anisotropic materials program
[NASA-CR-174952] p 165 N86-25003
Structural tailoring of engine blades (STAEBL) theoretical manual
[NASA-CR-175112] p 31 N86-27283
Structural tailoring of engine blades (STAEBL) user's manual
[NASA-CR-175113] p 31 N86-27284
The boundary layer on compressor cascade blades
[NASA-CR-177279] p 143 N86-27607
Experimental evaluation of two turning vane designs for high-speed corner of 0.1-scale model of NASA Lewis Research Center's proposed altitude wind tunnel
[NASA-TP-2570] p 38 N86-28101
Structural analysis of turbine blades using unified constitutive models
[NASA-TM-88807] p 178 N86-28461
Aerodynamic data banks for Clark-Y, NACA 4-digit and NACA 16-series airfoil families
[NASA-CR-176883] p 13 N86-30693

ALGEBRA

Space and frequency-multiplexed optical linear algebra processor - Fabrication and initial tests
p 202 A86-48352

ALGORITHMS

Linearization of digital derived rate algorithm for use in linear stability analysis
p 47 A86-35338
Acceleration of convergence of vector sequences
p 195 A86-49850
Robust detection-isolation-accommodation for sensor failures
[NASA-CR-174797] p 121 N86-16486

- Aerodynamic properties of turbulent combustion fields
[NASA-CR-175005] p 28 N86-20393
- A real-time simulation evaluation of an advanced detection, isolation and accommodation algorithm for sensor failures in turbine engines
[NASA-TM-87289] p 30 N86-24697
- Theoretical analysis of the electrical aspects of the basic electro-impulse problem in aircraft de-icing applications
[NASA-CR-176808] p 17 N86-26330
- Spectrum orbit utilization program technical manual SOUP5 Version 3.8
[NASA-CR-174944] p 116 N86-26489
- Spectrum Orbit Utilization Program documentation: SOUP5 version 3.8 user's manual, volume 1, chapters 1 through 5
[NASA-CR-174889] p 193 N86-27927
- Solution of elliptic partial differential equations by fast Poisson solvers using a local relaxation factor. 1: One-step method
[NASA-TP-2529] p 195 N86-28661
- Physical and numerical sources of computational inefficiency in integration of chemical kinetic rate equations: Etiology, treatment and prognosis
[NASA-TP-2590] p 195 N86-28662
- HYTESS 2: A Hypothetical Turbofan Engine Simplified Simulation with multivariable control and sensor analytical redundancy
[NASA-TM-87344] p 124 N86-30068
- Compliance matrices for cracked bodies
[NASA-CR-179478] p 179 N86-30236
- ALIPHATIC COMPOUNDS**
Improved perfluoroalkylether fluid development
[NASA-TM-87276] p 104 N86-25474
- ALKALINE BATTERIES**
Evaluation parameters for the alkaline fuel cell oxygen electrode
[NASA-TM-87155] p 77 N86-12268
- ALKYL COMPOUNDS**
Analysis of a spacecraft instrument ball bearing assembly lubricated by a perfluoroalkylether
[NASA-TM-87260] p 50 N86-21575
- The preparation of new perfluoroether fluids exhibiting excellent thermal-oxidative stabilities
[NASA-TM-87284] p 105 N86-25475
- ALKYLATION**
Improved perfluoroalkylether fluid development
[NASA-TM-87276] p 104 N86-25474
- ALLOYS**
Constructing multicomponent phase diagrams by overlapping ZPF lines --- Zero Phase Fraction Line for improved mechanical and corrosion properties
p 83 N86-44038
- Alloys based on NiAl for high temperature applications
p 84 N86-47261
- The development and prevention of channel segregation during alloy solidification
p 38 N86-10086
- Constitutive modeling for isotropic materials (HOST)
[NASA-CR-174980] p 172 N86-10589
- Life prediction and constitutive behavior
p 173 N86-11520
- Tensile behavior of Fe-40Al alloys with B and Zr additions
[NASA-TM-87290] p 91 N86-25453
- Low-cycle thermal fatigue
[NASA-TM-87225] p 177 N86-26651
- Effects of a high mean stress on the high cycle fatigue life of PWA 1480 and correlation of data by linear elastic fracture mechanics
[NASA-CR-175057] p 177 N86-27689
- Effects of surface chemistry on hot corrosion life
[NASA-CR-179471] p 32 N86-28087
- ALTERNATING CURRENT**
A 20 kilohertz space station power system
[NASA-TM-88801] p 62 N86-28122
- ALTITUDE SIMULATION**
Wind tunnel turning vanes of modern design
[AIAA PAPER 86-0044] p 36 N86-19654
- Wind tunnel turning vanes of modern design
[NASA-TM-87146] p 37 N86-12239
- Progress in the Lewis Research Center Altitude Wind Tunnel (AWT) Modeling Program
[NASA-TM-87194] p 37 N86-16233
- ALTITUDE TESTS**
Experimental evaluation of two turning vane designs for high-speed corner of 0.1-scale model of NASA Lewis Research Center's proposed altitude wind tunnel
[NASA-TP-2570] p 38 N86-28101
- ALUMINATES**
Alloys based on NiAl for high temperature applications
p 84 N86-47261
- ALUMINUM**
Optimization of the Ni-Cr-Al-Y/ZrO₂-Y₂O₃ thermal barrier system
p 82 N86-31746
- The mechanism of erosion of metallic materials under cavitation attack
[NASA-TM-87133] p 156 N86-10552

ALUMINUM ALLOYS

- Erosion of aluminum 6061-T6 under cavitation attack in mineral oil and water
p 79 N86-13801
- Modeling degradation and failure of Ni-Cr-Al overlay coatings
p 80 N86-16276
- The effects of grain size on the flow and fracture of long-range ordered alloys
p 84 N86-47243
- High temperature properties of equiatomic FeAl with ternary additions
p 84 N86-47252
- Rapidly solidified NiAl and FeAl
p 84 N86-47263
- High temperature oxidation of beta-NiAl
p 85 N86-47266
- A study of spectrum fatigue crack propagation in two aluminum alloys. I - Spectrum simplification. II - Influence of microstructures
p 85 N86-48973
- The plastic compressibility of 7075-T651 aluminum-alloy plate
p 85 N86-49690
- The influence of grain size and composition on slow plastic flow in FeAl between 1100 and 1400 K
p 86 N86-50279
- Current viewpoints on oxide adherence mechanisms
[NASA-TM-87168] p 87 N86-13409
- High temperature dispersion strengthening of NiAl
[NASA-CR-175073] p 90 N86-22688
- A preliminary study of ester oxidation on an aluminum surface using chemiluminescence
[NASA-TM-87242] p 103 N86-24835
- ALUMINUM COMPOUNDS**
The B2 aluminides as alternative materials
p 84 N86-47259
- Tensile behavior of Fe-40Al alloys with B and Zr additions
[NASA-TM-87290] p 91 N86-25453
- ALUMINUM GALLIUM ARSENIDES**
Cryogenic operation of pseudomorphic AlGaAs/InGaAs single-quantum-well MODFETs
p 117 N86-11998
- High transconductance InGaAs/AlGaAs pseudomorphic modulation-doped field-effect transistors
p 117 N86-18814
- Dc and microwave characteristics of a high current double interface GaAs/InGaAs/AlGaAs pseudomorphic modulation-doped field-effect transistor
p 118 N86-36009
- Determination of carrier saturation velocity in high-performance In(y)Ga(1-y)As/Al(x)Ga(1-x)As modulation-doped field-effect transistors (with y between 0 and 0.2)
p 118 N86-37295
- High-frequency noise of In(y)Ga(1-y)As/Al(x)Ga(1-x)As MODFETs and comparison to GaAs/Al(x)Ga(1-x)As MODFETs
p 119 N86-43914
- High-efficiency AlGaAs-GaAs Cassegrainian concentrator cells
p 185 N86-17845
- Theoretical study of the transverse dielectric constant of superlattices and their alloys
[NASA-CR-177198] p 206 N86-28759
- ALUMINUM OXIDES**
Fundamental tribological properties of ceramics
p 95 N86-15230
- Pretreatment effects on the morphology and properties of aluminum oxide thermally grown on NiCoCrAlY
p 97 N86-17495
- Interaction of sulfuric acid corrosion and mechanical wear of iron
p 81 N86-20436
- Structure and grain coarsening during the sintering of alumina
p 98 N86-26341
- The effect of cobalt content in U-700 type alloys on degradation of aluminide coatings
[NASA-TM-87173] p 87 N86-13408
- Current viewpoints on oxide adherence mechanisms
[NASA-TM-87168] p 87 N86-13409
- The evolution and growth of Al₂O₃ scales on beta-NiAl
[NASA-CR-175097] p 92 N86-27444
- AMBIENT TEMPERATURE**
Surface fatigue life and failure characteristics of EX-53, CBS 1000M, and AISI 9310 gear materials
[NASA-TP-2513] p 157 N86-12609
- AMORPHOUS MATERIALS**
Composition and properties of the so-called 'diamond-like' amorphous carbon films
p 96 N86-16255
- Mechanical-contact-induced transformation from the amorphous to the partially crystalline state in metallic glass
p 80 N86-16257
- Ion beam sputter deposited zinc telluride films
p 204 N86-47066
- Ion beam sputter deposited zinc telluride films
[NASA-TM-87119] p 205 N86-11048
- Ellipsometric and optical study of some uncommon insulator films on 3-5 semiconductors
[NASA-TM-87135] p 205 N86-12134
- Abrasion and deformed layer formation of manganese-zinc ferrite in sliding contact with lapping tapes
[NASA-TM-87249] p 104 N86-24838

- Auger electron spectroscopy, secondary ion mass spectroscopy and optical characterization of a-C-H and BN films
[NASA-TM-87258] p 206 N86-25268
- AMPLIFIER DESIGN**
Ka-band monolithic gain control amplifier
p 119 N86-41343
- AMPLITUDE MODULATION**
Time domain referencing in intensity modulation fiber optic sensing systems
[NASA-CR-175109] p 17 N86-24691
- AMPLITUDES**
The use of an optical data acquisition system for bladed disk vibration analysis
p 146 N86-26909
- Forced response analysis of an aerodynamically detuned supersonic turbomachine rotor
[NASA-TM-87093] p 9 N86-10019
- ANALYSIS (MATHEMATICS)**
Progressive damage, fracture predictions and post mortem correlations for fiber composites
[NASA-TM-87101] p 68 N86-10290
- ANECHOIC CHAMBERS**
Current wind tunnel capability and planned improvements at Lewis Research Center
[NASA-TM-87190] p 37 N86-18329
- ANGLE OF ATTACK**
A numerical analysis applied to high angle of attack three-dimensional inlets
[AIAA PAPER 86-1527] p 6 N86-42760
- Preliminary results of unsteady blade surface pressure measurements for the SR-3 propeller
[AIAA PAPER 86-1893] p 8 N86-49625
- A numerical analysis applied to high angle of attack three-dimensional inlets
[NASA-TM-87298] p 11 N86-24658
- Preliminary results of unsteady blade surface pressure measurements for the SR-3 propeller
[NASA-TM-87352] p 12 N86-27213
- ANGULAR DISTRIBUTION**
Joint research effort on vibrations of twisted plates, phase 1: Final results
[NASA-RP-1150] p 172 N86-10579
- ANGULAR VELOCITY**
Spin analysis of concentrated traction contacts
[ASME PAPER 84-DET-99] p 155 N86-45257
- ANIONS**
Simulation of lubricating behavior of a thioether liquid lubricant by an electrochemical method
p 97 N86-20437
- ANISOTROPIC MEDIA**
Stress waves in transversely isotropic media: The homogeneous problem
[NASA-CR-39977] p 164 N86-25002
- ANISOTROPY**
Orientation and temperature dependence of some mechanical properties of the single-crystal nickel-base superalloy Rene N4. III - Tension-compression anisotropy
p 86 N86-50323
- Anisotropic constitutive model for nickel base single crystal alloys: Development and finite element implementation
[NASA-CR-175015] p 176 N86-21952
- ANNEALING**
Effect of multiple strain-anneal cycles on the 1000 C creep behaviour of gamma/gamma prime-alpha
p 82 N86-30610
- ANNULAR DUCTS**
Turbofan aft duct suppressor study program listing and user's guide
[NASA-CR-175067] p 30 N86-25357
- ANNULI**
A comparison of experimental and theoretical results for leakage, pressure gradients, and rotordynamic coefficients for tapered annular gas seal
[NASA-CR-179709] p 162 N86-32742
- ANODES**
Method and apparatus for rebalancing a REDOX flow cell system
[NASA-CASE-LEW-14127-1] p 122 N86-20680
- ANODIZING**
The effect of processing conditions on the GaAs/plasma-grown insulator interface
p 204 N86-18567
- ANTENNA ARRAYS**
MMIC antenna technology development in the 30/20 gigahertz band
[AIAA PAPER 86-0666] p 45 N86-29628
- Optical techniques to feed and control GaAs MMIC modules for phased array antenna applications
[AIAA PAPER 86-0687] p 110 N86-29638
- Adaptive antenna arrays for weak interfering signals --- in satellite communication
p 45 N86-34591
- A dual frequency microstrip antenna for Ka band
[NASA-TM-87124] p 111 N86-10380
- Characterization of MMIC devices for active array antennas
p 111 N86-11401

- Circularly polarized microstrip antennas p 112 N86-11407
- Optical techniques to feed and control GaAs MMIC modules for phased array antenna applications [NASA-TM-87218] p 113 N86-16458
- MMIC antenna technology development in the 30/20 gigahertz band [NASA-TM-87192] p 46 N86-17368
- Optically controlled phased array antenna concepts using GaAs monolithic microwave integrated circuits [NASA-TM-87229] p 123 N86-21757
- Mutual coupling effects in antenna arrays, volume 1 [NASA-CR-176699] p 114 N86-22782
- ANTENNA COMPONENTS**
- Characterization of MMIC devices for active array antennas p 111 N86-11401
- ANTENNA DESIGN**
- Technology for satellite power conversion [NASA-CR-176554] p 186 N86-19742
- ANTENNA FEEDS**
- Input impedance of a probe-fed circular microstrip antenna with thick substrate p 120 A86-46638
- A dual frequency microstrip antenna for Ka band [NASA-TM-87124] p 111 N86-10380
- ANTENNA RADIATION PATTERNS**
- Strategy for reflector pattern calculation - Let the computer do the work p 110 A86-39542
- Input impedance of a probe-fed circular microstrip antenna with thick substrate p 120 A86-46638
- A numerical method for approximating antenna surfaces defined by discrete surface points [NASA-TM-87125] p 111 N86-10381
- Strategy for reflector pattern calculation: Let the computer do the work p 112 N86-12485
- Secondary pattern computation of an arbitrarily shaped main reflector [NASA-TM-87162] p 112 N86-14477
- Secondary pattern computation of an offset reflector antenna [NASA-TM-87160] p 112 N86-14479
- Compensation of reflector surface distortions using conjugate field matching [NASA-TM-87198] p 113 N86-16461
- The role of service areas in the optimization of FSS orbital and frequency assignments [NASA-CR-176488] p 46 N86-18341
- Computation of the radiation characteristics of a generalized phased array [NASA-TM-87185] p 114 N86-18586
- Technology for satellite power conversion [NASA-CR-176554] p 186 N86-19742
- Near-field spillover from a subreflector: Theory and experiment [NASA-TM-88763] p 115 N86-25650
- Near-field testing of the 30 GHz TRW proof-of-concept multibeam antenna [NASA-TM-87357] p 124 N86-27578
- A simple circular-polarized antenna: Circular waveguide horn coated with lossy magnetic material [NASA-CR-177092] p 116 N86-30039
- Near-field spillover from a subreflector: Theory and experiment [NASA-TM-88818] p 116 N86-32598
- ANTENNAS**
- Satellite voice broadcast system study, volume 2 [NASA-CR-174905] p 115 N86-24877
- ANTIFRICTION BEARINGS**
- Spin analysis of concentrated traction contacts [ASME PAPER 84-DET-99] p 155 A86-45257
- Instability in Rotating Machinery [NASA-CP-2409] p 161 N86-30160
- ANTIMISTING FUELS**
- Atomization and combustion characteristics of antimisting fuels using JT8D and air-boost injectors [ASME PAPER 86-GT-223] p 24 A86-48257
- APERTURES**
- Characterization of MMIC devices for active array antennas p 111 N86-11401
- APPLICATIONS PROGRAMS (COMPUTERS)**
- Turbofan aft duct suppressor study program listing and user's guide [NASA-CR-175067] p 30 N86-25357
- Spectrum Orbit Utilization Program documentation: SOUP5 version 3.8 user's manual, volume 1, chapters 1 through 5 [NASA-CR-174889] p 193 N86-27927
- Integrated research in constitutive modelling at elevated temperatures, part 2 [NASA-CR-177233] p 178 N86-28455
- Performance of oil pumping rings: An analytical and experimental study [NASA-CR-175083] p 144 N86-31000
- NASA's Aircraft Icing Analysis Program [NASA-TM-88791] p 15 N86-31548
- ICAN: A versatile code for predicting composite properties [NASA-TM-87334] p 71 N86-31664
- APPROXIMATION**
- A fundamental study of smoldering with emphasis on experimental design for zero-g p 41 N86-10162
- A numerical method for approximating antenna surfaces defined by discrete surface points [NASA-TM-87125] p 111 N86-10381
- ARC DISCHARGES**
- Hollow cathodes in high pressure arc discharges --- for arcjet thrusters [AIAA PAPER 85-2035] p 50 A86-14446
- Threshold determining mechanisms for discharges in high voltage solar arrays [AIAA PAPER 86-0364] p 52 A86-19834
- ARC JET ENGINES**
- Electrode erosion in arc discharges at atmospheric pressure [AIAA PAPER 85-2018] p 50 A86-14445
- Hollow cathodes in high pressure arc discharges --- for arcjet thrusters [AIAA PAPER 85-2035] p 50 A86-14446
- An experimental study of energy loss mechanisms and efficiency considerations in the low power dc arcjet [AIAA PAPER 85-2017] p 53 A86-37062
- Experimental performance of a 1-kilowatt arcjet thruster [AIAA PAPER 85-2033] p 54 A86-37063
- Low power dc arcjet operation with hydrogen/nitrogen propellant mixtures [AIAA PAPER 86-1505] p 55 A86-42676
- NASA electrothermal auxiliary propulsion technology [AIAA PAPER 86-1703] p 55 A86-42799
- Power electronics for a 1-kilowatt arcjet thruster [AIAA PAPER 86-1507] p 56 A86-49613
- Experimental performance of a 1-kilowatt arcjet thruster [NASA-TM-87131] p 57 N86-10281
- An experimental study of energy loss mechanisms and efficiency consideration in the low power dc arcjet [NASA-TM-87123] p 57 N86-11224
- NASA electrothermal auxiliary propulsion technology [NASA-TM-87281] p 60 N86-24749
- Lower power dc arcjet operations with hydrogen hydrogen/nitrogen propellant mixtures [NASA-TM-87279] p 61 N86-25407
- Power electronics for a 1-kilowatt arc jet thruster [NASA-TM-87340] p 61 N86-25409
- ARCHITECTURE (COMPUTERS)**
- Performance evaluation of a simulated data-flow computer with low-resolution actors p 194 A86-32051
- ARGON**
- Effect of argon and hydrogen on deposition of silicon from tetrochlorosilane in cold plasmas [NASA-TM-87219] p 65 N86-17472
- AROMATIC COMPOUNDS**
- A ceramic matrix composite based on polymerization and pyrolysis of ethynylated aromatics p 65 A86-13169
- The high-temperature oxidation of aromatic hydrocarbons p 75 A86-40834
- ARRAYS**
- Development program on a cold cathode electron gun [NASA-CR-174792] p 121 N86-14499
- Heat transfer characteristics within an array of impinging jets. Effects of crossflow temperature relative to jet temperature [NASA-CR-3936] p 139 N86-15625
- Development of a microprocessor controller for stand-alone photovoltaic power systems [NASA-CR-174723] p 187 N86-21979
- ASPECT RATIO**
- Joint research effort on vibrations of twisted plates, phase 1: Final results [NASA-RP-1150] p 172 N86-10579
- ASYMPTOTIC METHODS**
- Propagation and stability of wavelike solutions of finite difference equations with variable coefficients p 194 A86-20033
- ATMOSPHERIC CIRCULATION**
- A note on the finite differencing of the linearized primitive equations' lower boundary condition p 191 A86-28963
- ATMOSPHERIC COMPOSITION**
- Simultaneous measurements of carbon monoxide and ozone in the NASA Global Atmospheric Sampling Program (GASP) p 191 A86-48620
- ATMOSPHERIC PRESSURE**
- Electrode erosion in arc discharges at atmospheric pressure [AIAA PAPER 85-2018] p 50 A86-14445
- The high-temperature oxidation of aromatic hydrocarbons p 75 A86-40834
- Application of an atmospheric pressure sampling mass spectrometer to chlorination reactions [NASA-TM-87270] p 91 N86-24813
- ATMOSPHERIC TURBULENCE**
- Numerical synthesis of tri-variate velocity realizations of turbulence p 168 A86-28654
- ATOM CONCENTRATION**
- Calculation of recoil implantation profiles using known range statistics p 201 A86-11391
- ATOMIC RECOMBINATION**
- Mass loss of shuttle space suit orthofabric under simulated ionospheric atomic oxygen bombardment [NASA-TM-87149] p 192 N86-13899
- ATOMIZERS**
- High Weber number SMD correlations for pressure atomizers --- Sauter Mean Diameter [ASME PAPER 85-GT-37] p 128 A86-22026
- Formation and characterization of simulated small droplet icing clouds [AIAA PAPER 86-0409] p 145 A86-22700
- Effect of elevated temperature and pressure on sprays from simplex swirl atomizers [ASME PAPER 85-GT-58] p 130 A86-22735
- Formation and characterization of simulated small droplet icing clouds [NASA-TM-87180] p 148 N86-14554
- ATOMIZING**
- Characterization of simulated small-droplet fuel sprays [AIAA PAPER 86-1725] p 135 A86-42813
- Atomization and combustion characteristics of antimisting fuels using JT8D and air-boost injectors [ASME PAPER 86-GT-223] p 24 A86-48257
- Undercooling and solidification behavior in the InSb-Sb system [NASA-CR-175013] p 88 N86-14355
- Characterization of simulated small-droplet fuel sprays [NASA-TM-87286] p 148 N86-24961
- Role of fuel chemical properties on combustor radiative heat load [NASA-CR-177096] p 108 N86-30023
- ATTENUATION**
- Ultrasonic evaluation of mechanical properties of thick, multilayered, filament wound composites [NASA-TM-87088] p 163 N86-10561
- ATTENUATION COEFFICIENTS**
- Scaling attenuation data characterizes changes in material microstructure p 197 A86-26542
- ATTITUDE CONTROL**
- Operating characteristics of a 0.87 kW-hr flywheel energy storage module p 152 A86-24864
- AUGER SPECTROSCOPY**
- Angle-resolved Auger electron spectra induced by neon ion impact on aluminum p 76 A86-43456
- Binary collision model for neon Auger spectra from neon ion bombardment of the aluminum surface p 76 A86-43457
- The beta-SiC(100) surface studied by low energy electron diffraction, Auger electron spectroscopy, and electron energy loss spectra p 77 A86-49864
- Ellipsometric surface analysis of wear tracks produced by different lubricants [NASA-TM-87142] p 87 N86-12293
- AUTOCLAVING**
- Properties of autoclaved Gr/PI composites made from improved tack PMR-15 prepreg p 68 N86-11276
- AUTOMATIC PILOTS**
- Centaur engine gimbal friction characteristics under simulated thrust load [NASA-TM-87335] p 44 N86-31621
- AUTOMOBILE ENGINES**
- Operational maintenance data base development for kinematic Stirling engines [ASME PAPER 85-DGP-20] p 151 A86-14467
- Life cycle cost assessment of future low heat rejection engines [SAE PAPER 860444] p 153 A86-37048
- Creep rupture behavior of Stirling engine materials [NASA-TM-87209] p 88 N86-15380
- Ceramic automotive Stirling engine study [NASA-CR-174907] p 208 N86-16165
- Alloy chemistry and microstructural control to meet the demands of the automotive Stirling engine [NASA-TM-87250] p 89 N86-20541
- Automotive Stirling summary and overview [NASA-TM-87177] p 209 N86-21457
- Stirling Powered Van Program overview [NASA-TM-87227] p 210 N86-25303
- Automotive Stirling Engine Development Program [NASA-CR-174749] p 211 N86-28017
- Automotive Stirling engine development program [NASA-CR-175045] p 211 N86-30579
- Evaluation of a Stirling engine heater bypass with the NASA Lewis nodal-analysis performance code [NASA-CR-179460] p 211 N86-31452

AUTOMOBILES

Research and development of neat alcohol fuel usage in automobiles

[NASA-CR-174813] p 108 N86-27480

AUTOREGRESSIVE PROCESSES

Numerical synthesis of tri-variate velocity realizations of turbulence

[NASA-CR-174813] p 168 A86-28654

AUXILIARY PROPULSION

A long-life 50 lbf H₂/O₂ thruster for Space Station auxiliary propulsion

[AIAA PAPER 86-1404] p 55 A86-42617

Low power dc arcjet operation with hydrogen/nitrogen propellant mixtures

[AIAA PAPER 86-1505] p 55 A86-42676

Advanced technology payoffs for future rotorcraft, commuter aircraft, cruise missile, and APU propulsion systems

[AIAA PAPER 86-1545] p 16 A86-42704

LOX/LH₂ vane pump for auxiliary propulsion systems

[AIAA PAPER 86-1545] p 58 N86-17397

A bibliography of electrothermal thruster technology, 1984

[NASA-TM-86998] p 60 N86-21578

Lower power dc arcjet operations with hydrogen hydrogen/nitrogen propellant mixtures

[NASA-TM-87279] p 61 N86-25407

Proven, long-life hydrogen/oxygen thrust chambers for space station propulsion

[NASA-TM-88822] p 64 N86-32522

AVERAGE

Model equation for simulating flows in multistage turbomachinery

[ASME PAPER 85-GT-226] p 2 A86-22123

AXIAL FLOW

Characteristics of an axisymmetric sudden expansion flow

[NASA-CR-176278] p 151 N86-11465

Rotor wake characteristics of a transonic axial flow fan

[NASA-TM-87073] p 13 N86-28055

AXIAL FLOW PUMPS

Fluid machines: Expanding the limits, past and future

[NASA-TM-87161] p 26 N86-12227

AXIAL FLOW TURBINES

Through-flow modeling of axial turbomachinery

[ASME PAPER 85-IGT-42] p 3 A86-23854

AXIAL LOADS

The plastic compressibility of 7075-T651 aluminum-alloy plate

[NASA-TM-87073] p 85 A86-49690

Axial and torsional fatigue behavior of Waspaloy

[NASA-CR-175052] p 91 N86-25454

J-integral estimates for cracks in infinite bodies

[NASA-CR-179474] p 178 N86-28467

AXISYMMETRIC FLOW

A three-dimensional axisymmetric calculation procedure for turbulent flows in a radial vaneless diffuser

[ASME PAPER 85-GT-133] p 3 A86-22733

Inverse design of axisymmetric flow passages using compressible viscous flow theory

[NASA-TM-87161] p 4 A86-26412

Characteristics of an axisymmetric sudden expansion flow

[NASA-CR-176278] p 151 N86-11465

B**BACKSCATTERING**

Three component velocity measurements using Fabry-Perot interferometer

[NASA-CR-174813] p 145 A86-16378

BACKWARD FACING STEPS

Numerical simulation of a turbulent flame stabilized behind a rearward-facing step

[NASA-TM-87161] p 73 A86-22774

Triple-velocity products in a channel with a backward-facing step

[NASA-TM-87161] p 133 A86-41725

BALANCING

Method and apparatus for rebalancing a REDOX flow cell system

[NASA-CASE-LEW-14127-1] p 122 N86-20680

BALL BEARINGS

Ellipsometric surface analysis of wear tracks produced by different lubricants

[ASLE PREPRINT 85-TA-5A-2] p 151 A86-11018

Optical and other properties changes of M-50 bearing steel surfaces for different lubricants and additives prior to scuffing

[ASLE PREPRINT 85-TA-5A-2] p 97 A86-20435

Operating characteristics of a 0.87 kW-hr flywheel energy storage module

[NASA-TM-87260] p 152 A86-24864

Analysis of a spacecraft instrument ball bearing assembly lubricated by a perfluoroalkylether

[NASA-TM-87260] p 50 N86-21575

Review and critical analysis: Rolling-element bearings for system life and reliability

[NASA-CR-174710] p 159 N86-24991

SSME long-life bearings

[NASA-CR-179455] p 160 N86-27643

Evaluation of a hybrid hydrostatic bearing for cryogenic turbopump application

[NASA-TM-87255] p 83 N86-31649

BANDPASS FILTERS

Characteristics of an axisymmetric sudden expansion flow

[NASA-CR-176278] p 151 N86-11465

BANDWIDTH

Circularly polarized microstrip antennas

[NASA-TM-87255] p 112 N86-11407

BARRIER LAYERS

Advanced thermal barrier system bond coatings for use on nickel-, cobalt- and iron-base alloy substrates

[NASA-TM-86892] p 85 A86-49856

BARS

Thermal-mechanical fatigue crack growth in Inconel X-750

[NASA-CR-174723] p 81 A86-20982

BATTERY CHARGERS

Development of a microprocessor controller for stand-alone photovoltaic power systems

[NASA-CR-174723] p 187 N86-21979

BEAMS (RADIATION)

Characteristics of an axisymmetric sudden expansion flow

[NASA-CR-176278] p 151 N86-11465

Textured carbon on copper: A novel surface with extremely low secondary electron emission characteristics

[NASA-TP-2543] p 101 N86-15394

BEAMS (SUPPORTS)

Joint research effort on vibrations of twisted plates, phase 1: Final results

[NASA-RP-1150] p 172 N86-10579

BEARINGS

Parameter sensitivity in the dynamics of rotor-bearing systems

[ASME PAPER 85-DET-35] p 154 A86-38620

Mode II fatigue crack growth specimen development

[ASME PAPER 85-DET-10] p 171 A86-43566

Fatigue life analysis of a turboprop reduction gearbox

[ASME PAPER 85-DET-10] p 155 A86-45256

Quasi-modal vibration control by means of active control bearings

[NASA-TM-87232] p 159 N86-21856

Passive eddy-current damping as a means of vibration control in cryogenic turbomachinery

[NASA-TP-2562] p 44 N86-24722

Improved fracture toughness corrosion-resistant bearing material

[NASA-CR-174990] p 162 N86-32743

BEND TESTS

Correlation of processing and sintering variables with the strength and radiography of silicon nitride

[NASA-TM-87251] p 106 N86-31729

BENDING

The predicted effect of aerodynamic detuning on coupled bending-torsion unstalled supersonic flutter

[NASA-TM-87240] p 11 N86-21513

BENDING MOMENTS

Compliant hydrodynamic fluid journal bearing

[NASA-CASE-LEW-13670-1] p 158 N86-19606

BENDING VIBRATION

Nonlinear bending-torsional vibration and stability of rotating, pretwisted, precone blades including Coriolis effects

[NASA-TM-87207] p 175 N86-17789

BENZENE

Analysis of a thioether lubricant by infrared Fourier microemission spectrophotometry

[NASA-TM-87195] p 102 N86-16379

Ignition delay times of benzene and toluene with oxygen in argon mixtures

[NASA-TM-87312] p 78 N86-25431

BIBLIOGRAPHIES

Bibliography of Lewis Research Center technical publications announced in 1985

[NASA-TM-87263] p 208 N86-32336

BINARY ALLOYS

Dendritic solidification in a binary alloy melt: Steady-state versus morphological stability theories

[NASA-TM-87293] p 42 N86-10261

Compressive creep behavior of alloys based on B2 FeAl

[NASA-TM-87293] p 92 N86-28165

BINARY SYSTEMS (MATERIALS)

Estimated heats of fusion of fluoride salt mixtures suitable for thermal energy storage applications

[NASA-TM-87320] p 190 N86-31982

BINDING

Thermal-mechanical fatigue test apparatus for metal matrix composites and joint attachments

[NASA-TM-87187] p 88 N86-15378

BIPOLAR TRANSISTORS

Nondestructive characterization of RBSOA of high-power bipolar transistors --- Reverse-bias safe operating area

[NASA-TM-87320] p 118 A86-35718

Programmable, automated transistor test system

[NASA-TP-2554] p 123 N86-21755

BIPOLARITY

Bipolar nickel-hydrogen battery development

[NASA-TM-86892] p 180 A86-24823

Life cycle test results of a bipolar nickel hydrogen battery

[NASA-TM-86892] p 180 A86-24824

BIREFRINGENCE

Thermal dependence of stress-induced birefringence in single mode optical fibers

[NASA-TM-86892] p 202 A86-15263

The determination of the direction of the optic axis of uniaxial crystalline materials

[NASA-TM-86892] p 148 N86-22915

BLADE SLAP NOISE

Numerical evaluation of propeller noise including nonlinear effects

[AIAA PAPER 86-1893] p 8 A86-49625

Preliminary results of calculating propeller noise including acoustic nonlinear effects

[NASA-TM-87352] p 12 N86-27213

BLADE TIPS

Laser Doppler velocimeter measurement in the tip region of a compressor rotor

[AIAA PAPER 86-1892] p 23 A86-45504

Propeller noise caused by blade tip radial forces

Three-dimensional fluid flow phenomena in the blade end wall corner region

[ASME PAPER 86-GT-179] p 7 A86-48229

Ramp-integration technique for capacitance-type blade-tip clearance measurement

[NASA-TM-87241] p 149 N86-24964

BLADES

A numerical method of calculating propeller noise including acoustic nonlinear effects

[NASA-TM-88800] p 161 N86-30206

BODY CENTERED CUBIC LATTICES

The beta-SiC(100) surface studied by low energy electron diffraction, Auger electron spectroscopy, and electron energy loss spectra

[NASA-TM-87241] p 77 A86-49864

BOOMS (EQUIPMENT)

Feasibility study of a discrete bearing/roller drive rotary joint for the space station

[ASME PAPER 85-DET-12] p 152 A86-22748

BORON

Effect of boron on tensile properties of B2 BeAl

[NASA-CR-175074] p 89 N86-21856

BORON NITRIDES

Tribological properties of boron nitride synthesized by ion beam deposition

[NASA-TM-87258] p 96 A86-17479

Auger electron spectroscopy, secondary ion mass spectroscopy and optical characterization of a-C-H and BN films

[NASA-TM-87258] p 206 N86-25288

BOUNDARY ELEMENT METHOD

Stress analysis of gas turbine engine structures using the boundary element method

[NASA-CP-2404] p 169 A86-34444

Advanced three-dimensional dynamic analysis by boundary element methods

[NASA-CP-2404] p 169 A86-34445

BOUNDARY INTEGRAL METHOD

Numerical Techniques in Acoustics

[NASA-CP-2404] p 198 N86-12007

BOUNDARY LAYER EQUATIONS

Calculation of three-dimensional boundary layers on rotating turbine blades

[NASA-TM-87345] p 131 A86-28696

NASA/DOE automotive Stirling engine project: Overview 1986

[NASA-TM-87345] p 211 N86-29731

BOUNDARY LAYER FLOW

Scattering of acoustic waves into Tollmien-Schlichting waves by small streamwise variations in surface geometry

[AIAA PAPER 86-0575] p 127 A86-17041

Temperature and velocity profiles in sooting free boundary layer flames

[ASME PAPER 85-GT-174] p 73 A86-19962

End-wall and profile losses in a low-speed axial flow compressor rotor

[ASME PAPER 85-GT-174] p 20 A86-22090

Backward boundary layers in downward flame spread

[NASA-TM-87279] p 73 A86-22793

Coupling conditions for integrating boundary layer and rotational inviscid flow

[NASA-CR-177279] p 133 A86-41721

Contributions to the understanding of large-scale coherent structures in developing free turbulent shear flows

[NASA-CR-177279] p 142 N86-24932

The boundary layer on compressor cascade blades

[NASA-CR-177279] p 143 N86-27607

BOUNDARY LAYER SEPARATION

Low Reynolds number separation bubble research at UTRC

[NASA-CR-177279] p 126 A86-16311

- Three-dimensional inviscid analysis of radial-turbine flow and a limited comparison with experimental data p 4 A86-28702
- Three-dimensional inviscid analysis of radial turbine flow and a limited comparison with experimental data [NASA-TM-87091] p 9 N86-10017
- BOUNDARY LAYER STABILITY**
Entrainment region phenomena for a large plane shear layer p 132 A86-30211
- BOUNDARY LAYER TRANSITION**
Heat transfer and fluid mechanics measurements in transitional boundary layer flows [ASME PAPER 85-GT-113] p 126 A86-13068
A review and analysis of boundary layer transition data for turbine application [ASME PAPER 85-GT-83] p 129 A86-22054
Entrainment region phenomena for a large plane shear layer p 132 A86-30211
- BOUNDARY LAYERS**
Comparison of calculated and experimental cascade performance for controlled-diffusion compressor stator blading [NASA-TM-87167] p 27 N86-16219
Low Reynolds's number boundary layers in a disturbed environment [NASA-CR-175031] p 139 N86-17665
Experiments for the determination of convective diffusion heat/mass transfer to burner rig test targets comparable in size to jet stream diameter [NASA-TM-87196] p 139 N86-18646
Criteria for significance of simultaneous presence of both condensable vapors and aerosol particles on mass transfer (deposition) rates [NASA-TM-87247] p 109 N86-24869
- BOUNDARY VALUE PROBLEMS**
Analysis of an externally radially crack ring segment subject to three-point radial loading p 167 A86-20710
Boundary perturbation method for free boundary problem in convectively cooled continuous casting p 131 A86-28649
An embedding method for the steady Euler equations p 194 A86-30814
Effect of triangular element orientation on finite element solutions of the Helmholtz equation [NASA-TM-87351] p 201 N86-32247
- BOXES**
Hybrid deployable/erectable solar dynamic box truss system [AIAA PAPER 86-0955] p 47 A86-38883
- BRAGG ANGLE**
Characteristics of an axisymmetric sudden expansion flow [NASA-CR-176278] p 151 N86-11465
- BRANCHING (MATHEMATICS)**
Bifurcation techniques for nonlinear dynamic analysis of compressor stall phenomena p 22 A86-35403
- BRAYTON CYCLE**
Design tradeoffs for a Space Station solar-Brayton power system p 53 A86-24790
Liquid droplet radiator program at the NASA Lewis Research Center [ASME PAPER 86-HT-15] p 48 A86-49621
Liquid droplet radiator program at the NASA Lewis Research Center [NASA-TM-87139] p 48 N86-12246
Technology for Brayton-cycle powerplants using solar and nuclear energy [NASA-TP-2558] p 60 N86-21577
- BROADCASTING**
Engineering calculations for communications satellite systems planning [NASA-CR-176555] p 114 N86-19493
Broadcasting satellite service synthesis using gradient and cyclic coordinate search procedures [NASA-CR-176708] p 114 N86-23781
Satellite voice broadcast. Volume 1: Executive summary [NASA-CR-175016] p 115 N86-24875
Satellite voice broadcast. Volume 2: System study [NASA-CR-175017] p 115 N86-24876
Satellite voice broadcast system study, volume 2 [NASA-CR-174905] p 115 N86-24877
Satellite voice broadcast system study. Volume 1: Executive summary [NASA-CR-174904] p 115 N86-24878
Spectrum Orbit Utilization Program documentation: SOUP5 version 3.8 user's manual, volume 1, chapters 1 through 5 [NASA-CR-174889] p 193 N86-27927
- BROMIDES**
Theoretical and experimental flow cell studies of a hydrogen-bromine fuel cell, part 1 [NASA-CR-177165] p 189 N86-29409
- BROMINATION**
The milling of pristine and brominated P-100 graphite fibers [NASA-TM-88828] p 106 N86-32573
- BROMINE**
Environmental stability of intercalated graphite fibers p 98 A86-31825
A comparison of the bromination dynamics of pitch-based and vapor-grown graphite fibers [NASA-TM-87275] p 103 N86-21683
- BRONZES**
The mechanism of erosion of metallic materials under cavitation attack [NASA-TM-87133] p 156 N86-10552
- BUBBLE TECHNIQUE**
Theoretical modeling of the vapor cavitation in dynamically loaded journal bearings [ASME PAPER 85-TRIB-51] p 130 A86-24496
Theoretical modeling of the vapor cavitation in dynamically loaded journal bearings [NASA-TM-87076] p 137 N86-10463
- BUBBLES**
Mass transport phenomena between bubbles and dissolved gases in liquids under reduced gravity conditions p 39 N86-10110
Thermocapillary and diffusocapillary migration of a fluid drop p 40 N86-10128
- BULK MODULUS**
Universality in the compressive behavior of solids [NASA-TM-87303] p 206 N86-28775
Temperature effects on the universal equation of state of solids [NASA-TM-87321] p 206 N86-28776
- BUOYANCY**
Effects of buoyancy on gas jet diffusion flames - Experiment and theory [IAF PAPER 85-288] p 72 A86-15804
Buoyancy effects on smoldering combustion [IAF PAPER 85-289] p 72 A86-15805
Buoyancy effects upon vapor flame and explosion processes p 41 N86-10161
Fundamental studies of droplet combustion at reduced gravity p 42 N86-10165
- BURNERS**
Ribbon-burner simulation of T-700 turbine shroud for ceramic-lined seals research p 18 A86-15225
Burner rig corrosion of SiC at 1000 C p 99 A86-36328
Determination of convective diffusion heat/mass transfer rates to burner rig test targets comparable in size to cross-stream jet diameter [ASME PAPER 86-GT-68] p 136 A86-48140
Burner liner thermal/structural load modelling p 173 N86-11514
Component-specific modeling p 25 N86-11515
Validation of structural analysis methods using burner liner cyclic rig test data p 173 N86-11518
Determination of convective diffusion heat/mass transfer rates to burner rig test targets comparable in size to cross-stream jet diameter [NASA-TM-87176] p 138 N86-13678
Experiments for the determination of convective diffusion heat/mass transfer to burner rig test targets comparable in size to jet stream diameter [NASA-TM-87196] p 139 N86-18646
Burner liner thermal-structural load modeling [NASA-CR-174892] p 176 N86-21932
Experimental verification of corrosive vapor deposition rate theory in high velocity burner rigs [NASA-TM-87287] p 141 N86-22890
- BURNING RATE**
Effect of gravity on laminar premixed gas combustion. I - Flammability limits and burning velocities p 72 A86-12413
A fundamental study of smoldering with emphasis on experimental design for zero-g p 41 N86-10162
- C**
- CALCIUM FLUORIDES**
Characterization of the tribological coating composition 77 wt % CaF₂ - 23 wt % Li F fused to IN-750 alloy [NASA-TM-87342] p 105 N86-27452
- CALIBRATING**
Calibration of droplet sizing and liquid water content instruments: Survey and analysis [NASA-CR-175099] p 149 N86-26596
High accuracy fuel flowmeter [NASA-CR-174869] p 150 N86-31030
- CAMBERED WINGS**
Influence of airfoil camber on convected gust interaction noise [AIAA PAPER 86-1873] p 198 A86-45493
- CAMS**
Constitutive modelling of lubricants in concentrated contacts at high slide to roll ratios [NASA-CR-175029] p 158 N86-17748
- CANTILEVER MEMBERS**
Influence of rotation and pretwist on cantilever fan blade flutter p 17 A86-11686
Analytical and experimental investigation of the coupled bladed disk/shaft whirl of a cantilevered turbofan [ASME PAPER 86-GT-98] p 24 A86-48163
- CANTILEVER PLATES**
Joint research effort on vibrations of twisted plates, phase 1: Final results [NASA-RP-1150] p 172 N86-10579
- CAPACITANCE SWITCHES**
Ramp-integration technique for capacitance-type blade-tip clearance measurement [NASA-TM-87241] p 149 N86-24964
- CAPACITANCE-VOLTAGE CHARACTERISTICS**
Resonant power processors. II - Methods of control p 117 A86-14482
- CAPACITORS**
The effect of processing conditions on the GaAs/plasma-grown insulator interface p 204 A86-18567
- CAPILLARY FLOW**
Oscillatory thermocapillary flows p 129 A86-22413
Convective and absolute instability of a viscous liquid jet p 132 A86-34377
Energy stability of thermocapillary convection in models of the float zone process p 40 N86-10123
Thermocapillary and diffusocapillary migration of a fluid drop p 40 N86-10128
Evaluation of capillary reinforced composites [NASA-CR-175061] p 70 N86-24760
- CARBON**
Composition and properties of the so-called 'diamond-like' amorphous carbon films p 96 A86-16255
Optical and interfacial electronic properties of diamond-like carbon films p 204 A86-16268
Thin film growth rate effects for primary ion beam deposited diamondlike carbon films p 100 A86-47068
Diamondlike carbon films on semiconductors for insulated-gate technology p 120 A86-47077
Surface modification strategies for (100)3C-SiC p 76 A86-47083
TWT efficiency enhancement with textured carbon surfaces on copper MDC electrodes --- multistage depressed collectors p 120 A86-49617
Dual-ion-beam deposition of carbon films with diamond-like properties p 65 A86-49855
Carbon films grown from plasma on III-V semiconductors [NASA-TM-87140] p 205 N86-12135
Textured carbon on copper: A novel surface with extremely low secondary electron emission characteristics [NASA-TP-2543] p 101 N86-15394
Auger electron spectroscopy, secondary ion mass spectroscopy and optical characterization of a-C-H and BN films [NASA-TM-87258] p 206 N86-25268
Textured carbon surfaces on copper by sputtering [NASA-CASE-LEW-14130-1] p 109 N86-32587
- CARBON FIBER REINFORCED PLASTICS**
Tetraglycidyl epoxy resins and graphite fiber composites cured with flexibilized aromatic diamines p 67 A86-36999
PMR polyimides from solutions containing mixed endcaps p 100 N86-11263
All-aromatic biphenylene end-capped polyquinoline and polyimide matrix resins p 100 N86-11267
Replacement of MDA with more oxidatively stable diamines in PMR-polyimides p 101 N86-11275
- CARBON FIBERS**
Environmental stability of intercalated graphite fibers p 98 A86-31825
Negative magnetoresistance of pitch-based carbon fibers Temperature and pressure dependence p 99 A86-35702
- CARBON MONOXIDE**
Two dimensional, transient catalytic combustion of CO-air on platinum p 71 A86-10201
Carbon monoxide production in low energy oxygen ion bombardment of pyrolytic graphite and Kapton surfaces p 76 A86-47078
Simultaneous measurements of carbon monoxide and ozone in the NASA Global Atmospheric Sampling Program (GASP) p 191 A86-48620
- CARBON 13**
Development of LC-13C NMR [NASA-CR-176656] p 107 N86-21704

CARBURIZING

- Protective coatings of metal surfaces by cold plasma treatment
[NASA-TM-87152] p 157 N86-11475
Improved fracture toughness corrosion-resistant bearing material
[NASA-CR-174990] p 162 N86-32743

CARRIER MOBILITY

- Minority-carrier mobility anomalies in low-resistivity silicon solar cells p 181 A86-49215

CARRIER TO NOISE RATIOS

- Calculation of allowable orbital spacings for the fixed-satellite service
[NASA-CR-176273] p 43 N86-11212

CARRIER TRANSPORT (SOLID STATE)

- Determination of carrier saturation velocity in high-performance In(y)Ga(1-y)As/Al(x)Ga(1-x)As modulation-doped field-effect transistors (with y between 0 and 0.2) p 118 A86-37295

CASCADE FLOW

- Boundary layer measurements on an airfoil in cascade using laser Doppler anemometry
[AIAA PAPER 86-0072] p 145 A86-19670
An implicit LU scheme for the Euler equations applied to arbitrary cascades --- new method of factoring p 2 A86-20131
Calculations of two and three-dimensional transonic cascade flow fields using the Navier-Stokes equations
[ASME PAPER 85-GT-66] p 2 A86-22046
Unsteady pressure measurements on a biconvex airfoil in a transonic oscillating cascade
[ASME PAPER 85-GT-212] p 3 A86-22731
Unsteady transonic flow over cascade blades p 3 A86-23141
Unsteady transonic flow in cascades p 4 A86-24693
The effects of strong shock loading on coupled bending-torsion flutter of tuned and mistuned cascades p 20 A86-26893
Calculation of three-dimensional boundary layers on rotating turbine blades p 131 A86-26896
Packet flutter and aerodynamic modes for non-homogenous airfoil cascades in highly distorted, periodic, stationary throughflows
[AIAA PAPER 86-0848] p 5 A86-38896
Computation of viscous flows in turbomachinery cascades with a space-marching method p 5 A86-39089
A comparison of computational methods for three-dimensional, turbulent turbomachinery flow fields
[AIAA PAPER 86-1599] p 6 A86-42740
Noise generated by convected gusts interacting with swept airfoil cascades
[AIAA PAPER 86-1872] p 198 A86-45492
Computation of three-dimensional, rotational flow through turbomachinery blade rows for improved aerodynamic design studies
[ASME PAPER 86-GT-26] p 7 A86-48117
On the application of a linearized unsteady potential-flow analysis to fan-tip cascades
[ASME PAPER 86-GT-87] p 7 A86-48153
Preliminary results of unsteady blade surface pressure measurements for the SR-3 propeller
[AIAA PAPER 86-1893] p 8 A86-49625
A FORTRAN computer code for calculating flows in multiple-blade-element cascades
[NASA-TM-87104] p 9 N86-13295
Comparison of calculated and experimental cascade performance for controlled-diffusion compressor stator blading
[NASA-TM-87167] p 27 N86-16219
Viscous compressible flow direct and inverse computation and illustrations
[NASA-CR-175037] p 28 N86-20391
Application of a linearized unsteady aerodynamic analysis to standard cascade configurations
[NASA-CR-3940] p 11 N86-21505
Preliminary results of unsteady blade surface pressure measurements for the SR-3 propeller
[NASA-TM-87352] p 12 N86-27213
The boundary layer on compressor cascade blades
[NASA-CR-177279] p 143 N86-27607
Experimental evaluation of two turning vane designs for high-speed corner of 0.1-scale model of NASA Lewis Research Center's proposed altitude wind tunnel
[NASA-TP-2570] p 38 N86-28101

CASCADE WIND TUNNELS

- Wind tunnel turning vanes of modern design
[AIAA PAPER 86-0044] p 36 A86-19654
A novel centrifugal diffuser test device
[ASME PAPER 85-IGT-135] p 3 A86-23927
Wind tunnel turning vanes of modern design
[NASA-TM-87146] p 37 N86-12239

CASSEGRAIN ANTENNAS

- Near-field testing of the 30 GHz TRW proof-of-concept multibeam antenna
[NASA-TM-87357] p 124 N86-27578

CASSEGRAIN OPTICS

- High-efficiency AlGaAs-GaAs Cassegrainian concentrator cells p 185 N86-17845

CASTING

- Boundary perturbation method for free boundary problem in convectively cooled continuous casting p 131 A86-28649
Low-cost single-crystal turbine blades, volume 2
[NASA-CR-174652] p 29 N86-23598

CASTINGS

- Advanced rotary engine components utilizing fiber reinforced Mg castings
[AIAA PAPER 86-1559] p 67 A86-42712

CATALYSTS

- Negative electrode catalyst for the iron chromium redox energy storage system
[NASA-CASE-LEW-14028-1] p 186 N86-19721
Assessment of commercially available and experimental hydrogen electrodes
[NASA-TM-87264] p 187 N86-23035

CATALYTIC ACTIVITY

- Two dimensional, transient catalytic combustion of CO-air on platinum p 71 A86-10201

CATASTROPHE THEORY

- Bifurcation techniques for nonlinear dynamic analysis of compressor stall phenomena p 22 A86-35403

CATHODE RAY TUBES

- Thermionic noise measurements for on-line dispenser cathode diagnostics for linear beam microwave tubes
[NASA-CR-175105] p 124 N86-28323

CATHODES

- Electrode erosion in arc discharges at atmospheric pressure
[AIAA PAPER 85-2018] p 50 A86-14445
The effect of oxygen pressure on volatility and morphology of LaB6 single crystal cathodes p 204 A86-28076

- Develop and test fuel cell powered on-site integrated total energy systems: Phase 3, full-scale power plant development
[NASA-CR-174948] p 182 N86-12757

- Develop and test fuel cell powered on-site integrated total energy systems: Phase 3, full-scale power plant development
[NASA-CR-174998] p 182 N86-12758
Fundamental studies on a heat driven lamp
[NASA-CR-176381] p 204 N86-15122

- Method and apparatus for rebalancing a REDOX flow cell system
[NASA-CASE-LEW-14127-1] p 122 N86-20680

CAVITATION CORROSION

- Erosion of aluminum 6061-T6 under cavitation attack in mineral oil and water p 79 A86-13801
Erosion of phosphor bronze under cavitation attack in a mineral oil p 81 A86-23324

CAVITATION FLOW

- An experimental investigation and some analytical considerations concerning the vaporous/gaseous cavity characteristics of an eccentric shaft seal or bearing p 130 A86-24463

- Theoretical modeling of the vapor cavitation in dynamically loaded journal bearings
[ASME PAPER 85-TRIB-51] p 130 A86-24496

- Theoretical modeling of the vapor cavitation in dynamically loaded journal bearings
[NASA-TM-87076] p 137 N86-10463

- The mechanism of erosion of metallic materials under cavitation attack
[NASA-TM-87133] p 156 N86-10552

- Theoretical and experimental comparison of vapor cavitation in dynamically loaded journal bearings
[NASA-TM-87121] p 137 N86-11425

- Two-phase flows and heat transfer within systems with ambient pressure above the thermodynamic critical pressure
[NASA-TM-87228] p 140 N86-19558

- Feasibility study for convertible engine torque converter
[NASA-CR-175082] p 33 N86-30733

CAVITY VAPOR GENERATORS

- Theoretical and experimental comparison of vapor cavitation, in dynamically loaded journal bearings
[NASA-TM-87121] p 137 N86-11425

CENTAUR LAUNCH VEHICLE

- NASA Lewis Research Center low-gravity fluid management technology program p 44 A86-32906
Linearization of digital derived rate algorithm for use in linear stability analysis p 47 A86-35338
Modal test/analysis correlation for Centaur G Prime launch vehicle
[AIAA PAPER 86-1002] p 43 A86-38943

- NASA Lewis Research Center low-gravity fluid management technology program
[NASA-TM-87145] p 44 N86-11218

- Centaur engine gimbal friction characteristics under simulated thrust load
[NASA-TM-87335] p 44 N86-31621

CENTRAL PROCESSING UNITS

- The baseband processor in future satellite communication systems p 109 A86-21882
Error-source effects in a high-accuracy optical finite-element processor p 192 A86-31571
Space and frequency-multiplexed optical linear algebra processor - Fabrication and initial tests p 202 A86-48352

- Bit error rate testing of a proof-of-concept model baseband processor
[NASA-TM-87206] p 46 N86-18343

CENTRIFUGAL COMPRESSORS

- A novel centrifugal diffuser test device
[ASME PAPER 85-IGT-135] p 3 A86-23927
Effect of area ratio on the performance of a 5.5:1 pressure ratio centrifugal impeller
[ASME PAPER 86-GT-303] p 8 A86-48315

- Effect of area ratio on the performance of a 5.5:1 pressure ratio centrifugal impeller
[NASA-TM-87237] p 10 N86-19290

- Extended parametric representation of compressor fans and turbines. Volume 1: CMGEN user's manual
[NASA-CR-174645] p 159 N86-23936

- Extended parametric representation of compressor fans and turbines. Volume 2: Part user's manual (parametric turbine)
[NASA-CR-174646] p 159 N86-23937

- Extended parametric representation of compressor fans and turbines. Volume 3: MODFAN user's manual (parametric modulating flow fan)
[NASA-CR-174647] p 159 N86-23938

CENTRIFUGAL PUMPS

- AC motor and generator requirements for isolated WECS
[NASA-CR-176315] p 182 N86-11670

- Fluid machines: Expanding the limits, past and future
[NASA-TM-87161] p 26 N86-12227

- Small centrifugal pumps for low-thrust rocket engines
[NASA-CR-174913] p 162 N86-32741

CERAMIC COATINGS

- Finite element analysis of residual stress in plasma-sprayed ceramic p 95 A86-15226
Character of laser-glazed, plasma-sprayed zirconia coatings on stainless steel substrata p 95 A86-15229

- Neutron and X-ray diffraction of plasma-sprayed zirconia-yttria thermal barrier coatings p 96 A86-16269

- Performance of thermal barrier coatings in high heat flux environments p 80 A86-16272

- Tribological properties of boron nitride synthesized by ion beam deposition p 96 A86-17479

- Fracture toughness tests on plasma-sprayed coatings p 64 A86-30051

- Tensile adhesion test measurements on plasma-sprayed coatings p 98 A86-30052

- Inelastic high-temperature thermomechanical response of ceramic coated gas turbine seals p 169 A86-37799

- Thin film growth rate effects for primary ion beam deposited diamondlike carbon films p 100 A86-47068

- Protective coatings of metal surfaces by cold plasma treatment
[NASA-TM-87152] p 157 N86-11475

- Thermomechanical design criteria for ceramic-coated surfaces
[NASA-TM-87328] p 143 N86-25726

CERAMIC MATRIX COMPOSITES

- A ceramic matrix composite based on polymerization and pyrolysis of ethynylated aromatics p 65 A86-13169

- Factors influencing the ball milling of Si3N4 in water p 95 A86-15239

- Film and interstitial formation of metals in plasma-sprayed ceramics p 96 A86-17484

- Polymer, metal and ceramic matrix composites for advanced aircraft engine applications
[NASA-TM-87132] p 87 N86-13407

- Carbon-rich ceramic composites from ethynyl aromatic precursors
[NASA-TM-88812] p 71 N86-29908

CERAMICS

- Densification and properties of alpha-silicon carbide p 94 A86-12416

- Ribbon-burner simulation of T-700 turbine shroud for ceramic-lined seals research p 18 A86-15225

- Experimental study of ceramic-coated tip seals for turbojet engines p 152 A86-15227

- Fundamental tribological properties of ceramics p 95 A86-15230

- Properties of silicon suspensions and slip-cast bodies p 95 A86-15238

- Deposition stress effects on the life of thermal barrier coatings on burner rigs p 96 A86-16271
- Fabrication of ceramic substrate-reinforced and free forms by mandrel plasma spraying metal-ceramic composites p 64 A86-17483
- Sintered alpha silicon carbide ceramics for high temperature structural application - Status review and recent developments [ASME PAPER 85-IGT-127] p 97 A86-23921
- NDE of advanced ceramics p 163 A86-35575
- Nondestructive characterization of structural ceramics p 99 A86-37141
- Fabrication of ceramic components for advanced gas turbine engines [SAE PAPER 851786] p 154 A86-38310
- Methods for improving reliability in ceramic turbine rotors [SAE PAPER 851788] p 154 A86-38312
- Reliability of void detection in structural ceramics by use of scanning laser acoustic microscopy p 163 A86-39027
- Reliability of scanning laser acoustic microscopy for detecting internal voids in structural ceramics p 147 A86-46353
- NDE of structural ceramics [ASME PAPER 86-GT-279] p 163 A86-48298
- Microgravity Materials Science Laboratory p 42 N86-10173
- Tribological properties of structural ceramics [NASA-TM-87105] p 100 N86-10341
- Probability of detection of internal voids in structural ceramics using microfocus radiography [NASA-TM-87164] p 164 N86-13749
- SCARE: A post-processor program to MSC/NASTRAN for the reliability analysis of structural ceramic components [NASA-TM-87188] p 174 N86-14688
- A computer simulation of the turbocharged turbo compounded diesel engine system: A description of the thermodynamic and heat transfer models [NASA-CR-174971] p 208 N86-16164
- Ceramic automotive Stirling engine study [NASA-CR-174907] p 208 N86-16165
- NDE of structural ceramics [NASA-TM-87186] p 164 N86-16598
- Reliability of scanning laser acoustic microscopy for detecting internal voids in structural ceramics [NASA-TM-87222] p 164 N86-16599
- Long-term stability and properties of zirconia ceramics for heavy duty diesel engine components [NASA-CR-174943] p 209 N86-17224
- Rocket thrust chamber thermal barrier coatings [NASA-CR-175022] p 59 N86-20497
- Ultrasonic characterization of structural ceramics p 199 N86-22970
- Adequacy of surface analytical tools for studying the tribology of ceramics [NASA-TM-87308] p 104 N86-24837
- Tribology of selected ceramics at temperatures to 900 deg C [NASA-TM-87267] p 105 N86-25476
- Sliding seal materials for adiabatic engines, phase 2 [NASA-CR-179475] p 105 N86-29042
- Correlation of processing and sintering variables with the strength and radiography of silicon nitride [NASA-TM-87251] p 106 N86-31729
- Factors that affect reliability of nondestructive detection of flaws in structural ceramics [NASA-TM-87348] p 166 N86-31912
- Quantitative void characterization in structural ceramics using scanning laser acoustic microscopy [NASA-TM-88797] p 166 N86-31913
- Advanced Gas Turbine (AGT) Technology Development Project annual report [NASA-CR-179485] p 211 N86-33211
- CERMETS**
- Slip casting and extruding shapes of rhenium with metal oxide additives. 1: Feasibility demonstration [NASA-CR-174970] p 63 N86-31648
- CESIUM PLASMA**
- Fundamental studies on a heat driven lamp [NASA-CR-176381] p 204 N86-15122
- CHANNEL FLOW**
- Inverse design of axisymmetric flow passages using compressible viscous flow theory p 4 A86-26412
- The development and prevention of channel segregation during alloy solidification p 38 N86-10086
- Channel flow modeling of impingement cooling of a rotating turbine blade [NASA-CR-177206] p 31 N86-27285
- CHANNELS (DATA TRANSMISSION)**
- Bit error rate testing of a proof-of-concept model baseband processor [NASA-TM-87206] p 46 N86-18343
- CHAOS**
- Is Navier-Stokes turbulence chaotic? p 137 A86-50275
- CHARACTERISTICS**
- Experimental rotordynamic coefficient results for teeth-on-rotor and teeth-on-stator labyrinth gas seals [ASME PAPER 86-GT-12] p 156 A86-48109
- CHARACTERIZATION**
- High Temperature Polymer Matrix Composites [NASA-CP-2385] p 68 N86-11260
- The synthesis, characterization and thermal chemistry of modified norbornenyl PMR endcaps p 100 N86-11266
- Characterization methodology for PMR-15 p 65 N86-11272
- CHARGE DISTRIBUTION**
- Radiation damage in high-resistivity silicon solar cells p 185 N86-17856
- CHARRING**
- A fundamental study of smoldering with emphasis on experimental design for zero-g p 41 N86-10162
- CHEMICAL ANALYSIS**
- Composition and properties of the so-called 'diamond-like' amorphous carbon films p 96 A86-16255
- Development of LC-13C NMR [NASA-CR-176656] p 107 N86-21704
- CHEMICAL ATTACK**
- Erosion of aluminum 6061-T6 under cavitation attack in mineral oil and water p 79 A86-13801
- Mechanism of Na₂SO₄-induced corrosion of molybdenum containing nickel-base superalloys at high temperatures. I - Corrosion in atmospheres containing O₂ only. II - Corrosion in O₂ + SO₂ atmospheres p 83 A86-37238
- A study of Kapton degradation under simulated shuttle environment [NASA-CR-176850] p 78 N86-28136
- CHEMICAL COMPOSITION**
- Composition and properties of the so-called 'diamond-like' amorphous carbon films p 96 A86-16255
- Optimization of the Ni-Cr-Al-Y/ZrO₂-Y₂O₃ thermal barrier system p 82 A86-31746
- The influence of grain size and composition on slow plastic flow in FeAl between 1100 and 1400 K p 86 A86-50279
- Composition optimization of self-lubricating chromium carbide-based composite coatings for use to 760 deg C [NASA-TM-87261] p 103 N86-20568
- Particle size reduction of Si₃N₄ with Si₃N₄ milling hardware [NASA-TM-86864-REV] p 104 N86-24839
- Emission FTIR analyses of thin microscopic patches of jet fuel residues deposited on heated metal surfaces [NASA-CR-176786] p 108 N86-25502
- CHEMICAL ENGINEERING**
- Microgravity Polymers [NASA-CP-2392] p 105 N86-28194
- CHEMICAL PROPERTIES**
- Fundamental studies of droplet combustion at reduced gravity p 42 N86-10165
- Role of fuel chemical properties on combustor radiative heat load [NASA-CR-177096] p 108 N86-30023
- Effect of an oxygen plasma on the physical and chemical properties of several fluids for the liquid droplet radiator [NASA-TM-88839] p 49 N86-31634
- CHEMICAL PROPULSION**
- Primary propulsion of electrothermal, ion, and chemical systems for space-based radar orbit transfer [AIAA PAPER 85-1477] p 50 A86-14431
- CHEMICAL REACTIONS**
- Simulation of lubricating behavior of a thioether liquid lubricant by an electrochemical method p 97 A86-20437
- Direct numerical simulations of chemically reacting turbulent mixing layers p 130 A86-25567
- The reactions of cobalt, iron and nickel in SO₂ atmospheres Similarities and differences p 75 A86-40677
- Direct numerical simulations of a reacting mixing layer with chemical heat release p 76 A86-41711
- Physical and numerical sources of computational inefficiency in integration of chemical kinetic rate equations: Etiology, treatment and prognosis [NASA-TP-2590] p 195 N86-28662
- CHEMILUMINESCENCE**
- A preliminary study of ester oxidation on an aluminum surface using chemiluminescence [NASA-TM-87242] p 103 N86-24835
- CHEMISTRY**
- Characterization and measurement of polymer wear p 100 A86-48405
- CHLORINATION**
- Application of an atmospheric pressure sampling mass spectrometer to chlorination reactions [NASA-TM-87270] p 91 N86-24813
- CHLOROETHYLENE**
- Shock-tube pyrolysis of chlorinated hydrocarbons - Formation of soot p 75 A86-35126
- CHLOROSILANES**
- Radical molecule and ion-molecule mechanisms in the polymerization of hydrocarbons and chlorosilanes in R.F. plasmas at low pressures (below 1.0 Torr) p 203 A86-16254
- Effect of argon and hydrogen on deposition of silicon from tetrachlorosilane in cold plasmas [NASA-TM-87219] p 65 N86-17472
- CHROMIUM**
- Optimization of the Ni-Cr-Al-Y/ZrO₂-Y₂O₃ thermal barrier system p 82 A86-31746
- Negative electrode catalyst for the iron chromium redox energy storage system [NASA-CASE-LEW-14028-1] p 186 N86-19721
- CHROMIUM ALLOYS**
- Modeling degradation and failure of Ni-Cr-Al overlay coatings p 80 A86-16276
- Orientation and temperature dependence of some mechanical properties of the single-crystal nickel-base superalloy Rene N4. III - Tension-compression anisotropy p 86 A86-50323
- Current viewpoints on oxide adherence mechanisms [NASA-TM-87168] p 87 N86-13409
- Anisotropic constitutive model for nickel base single crystal alloys: Development and finite element implementation [NASA-CR-175015] p 176 N86-21952
- CHROMIUM CARBIDES**
- Composition optimization of self-lubricating chromium carbide-based composite coatings for use to 760 deg C [NASA-TM-87261] p 103 N86-20568
- A new chromium carbide-based tribological coating for use to 900 deg C with particular reference to the Stirling engine [NASA-TM-87274] p 103 N86-21682
- CHROMIUM STEELS**
- Frictional and structural characterization of ion-nitrided low and high chromium steels p 81 A86-17477
- Improved fracture toughness corrosion-resistant bearing material [NASA-CR-174990] p 162 N86-32743
- CIRCUIT BREAKERS**
- Design of high-voltage, high-power, solid state remote power controllers for aerospace applications p 122 N86-17456
- CIRCUIT PROTECTION**
- Design of high-voltage, high-power, solid state remote power controllers for aerospace applications p 122 N86-17456
- CIRCULAR CYLINDERS**
- Effect of free stream turbulence on flow separation p 125 A86-11676
- Effect of a rotor wake on the local heat transfer on the forward half of a circular cylinder [NASA-TM-87234] p 140 N86-21794
- CIRCULAR POLARIZATION**
- Circularly polarized microstrip antennas p 112 N86-11407
- A simple circular-polarized antenna: Circular waveguide horn coated with lossy magnetic material [NASA-CR-177092] p 116 N86-30039
- CIRCULAR TUBES**
- On the modeling of low-Reynolds-number turbulence [NASA-CR-3994] p 32 N86-28089
- CIRCULAR WAVEGUIDES**
- Normal modes in an overmoded circular waveguide coated with lossy material p 119 A86-44078
- The role of service areas in the optimization of FSS orbital and frequency assignments [NASA-CR-176488] p 46 N86-18341
- CIVIL AVIATION**
- Evaluation of propfan propulsion applied to general aviation [NASA-CR-175020] p 30 N86-24695
- CLEARANCES**
- Ramp-integration technique for capacitance-type blade-tip clearance measurement [NASA-TM-87241] p 149 N86-24964
- CLEAVAGE**
- Tensile behavior of Fe-40Al alloys with B and Zr additions [NASA-TM-87290] p 91 N86-25453
- CLOSURE LAW**
- Prediction of heat release effects on a mixing layer [AIAA PAPER 86-0058] p 129 A86-22676
- A model for closing the inviscid form of the average-passage equation system [ASME PAPER 86-GT-227] p 8 A86-48261

- A model for closing the inviscid form of the average-passage equation system
[NASA-TM-87199] p 10 N86-14224
- Prediction of heat release effects on a mixing layer
[NASA-CR-175044] p 142 N86-23857
- CLOSURES**
- A comparison of three algebraic stress closures for combustor flow calculations
[ASME PAPER 85-WA/FE-3] p 132 A86-38388
- CLOUD GLACIATION**
- Experimental measurements of heat transfer from an iced surface during artificial and natural cloud icing conditions
[AIAA PAPER 86-1352] p 36 A86-39948
- Heat transfer and pressure drop performance of a finned-tube heat exchanger proposed for use in the NASA Lewis Altitude Wind Tunnel
[NASA-TM-87151] p 138 N86-13677
- CLOUDS**
- Formation and characterization of simulated small droplet icing clouds
[AIAA PAPER 86-0409] p 145 A86-22700
- Particle cloud combustion experiment
p 41 N86-10160
- Formation and characterization of simulated small droplet icing clouds
[NASA-TM-87180] p 148 N86-14554
- Flame propagation and extinction in particle clouds
[NASA-CR-177304] p 78 N86-27434
- CMOS**
- Development of a microprocessor controller for stand-alone photovoltaic power systems
[NASA-CR-174723] p 187 N86-21979
- COATING**
- Textured carbon surfaces on copper by sputtering
[NASA-CASE-LEW-14130-1] p 109 N86-32587
- COATINGS**
- Dual-ion-beam deposition of carbon films with diamond-like properties
p 65 A86-49855
- The effect of cobalt content in U-700 type alloys on degradation of aluminide coatings
[NASA-TM-87173] p 87 N86-13408
- How to evaluate solid lubricant films using a pin-on-disk tribometer
[NASA-TM-87236] p 102 N86-19465
- Stability of surface nucleation
[NASA-TM-88806] p 207 N86-30556
- COAXIAL FLOW**
- Mass and momentum turbulent transport experiments with swirling confined coaxial jets. II
[AIAA PAPER 86-1665] p 134 A86-42780
- Buoyancy effects upon vapor flame and explosion processes
p 41 N86-10161
- Influence of large-scale motion on turbulent transport for confined coaxial jets. Volume 2: Navier-Stokes calculations of swirling and nonswirling confined coaxial jets
[NASA-CR-175036] p 28 N86-20390
- Influence of large-scale motion on turbulent transport for confined coaxial jets. Volume 1: Analytical analysis of the experimental data using conditional sampling
[NASA-CR-175035] p 29 N86-20395
- COBALT**
- The reactions of cobalt, iron and nickel in SO₂ atmospheres. Similarities and differences
p 75 A86-40677
- The response of cobalt-free Udimet 700 type alloy to modified heat treatments
p 85 A86-48037
- The effect of cobalt content in U-700 type alloys on degradation of aluminide coatings
[NASA-TM-87173] p 87 N86-13408
- Thermal-fatigue and oxidation resistance of cobalt-modified Udimet 700 alloy
[NASA-TP-2591] p 178 N86-28464
- The effect of variations of cobalt content on the cyclic oxidation resistance of selected Ni-base superalloys
[NASA-TM-87297] p 93 N86-31702
- COBALT ALLOYS**
- Slow plastic strain rate compressive flow in binary CoAl intermetallics
p 79 A86-11478
- Dislocations in extruded Co-49.3 at. pct Al
p 83 A86-45091
- Corrosion of nickel and cobalt base alloys in sulfate melts at 750 deg C
[NASA-CR-175111] p 91 N86-24817
- The low cycle fatigue behavior of a plasma-sprayed coating material
[NASA-TM-87318] p 92 N86-31699
- CODERS**
- Wavelength-division multiplexed digital optical position transducer
p 145 A86-20798
- CODING**
- Progressive damage, fracture predictions and post mortem correlations for fiber composites
[NASA-TM-87101] p 68 N86-10290
- Structural tailoring of engine blades (STAEBL) user's manual
[NASA-CR-175113] p 31 N86-27284
- Application of a personal computer for the uncoupled vibration analysis of wind turbine blade and counterweight assemblies
[NASA-CR-175090] p 188 N86-28511
- Physical and numerical sources of computational inefficiency in integration of chemical kinetic rate equations: Etiology, treatment and prognosis
[NASA-TP-2590] p 195 N86-28662
- COEFFICIENT OF FRICTION**
- Comparison of the contact stress and friction behavior of SiC and ZrO₂ materials
p 95 A86-15237
- COGENERATION**
- Develop and test fuel cell powered on-site integrated total energy systems
[NASA-CR-174951] p 188 N86-25877
- COKE**
- Long term deposit formation in aviation turbine fuel at elevated temperature
[AIAA PAPER 86-0525] p 107 A86-19929
- COLD CATHODES**
- Development program on a cold cathode electron gun
[NASA-CR-174792] p 121 N86-14499
- COLD GAS**
- Resistojet operation with various propellants
[AIAA PAPER 85-1158] p 107 A86-37074
- COLD PLASMAS**
- Protective coatings of metal surfaces by cold plasma treatment
[NASA-TM-87152] p 157 N86-11475
- Effect of argon and hydrogen on deposition of silicon from tetrachlorosilane in cold plasmas
[NASA-TM-87219] p 65 N86-17472
- COLD WEATHER TESTS**
- Research and development of neat alcohol fuel usage in automobiles
[NASA-CR-174813] p 108 N86-27460
- COLLIMATION**
- Lens collimation and testing using a Twyman-Green interferometer with a self-pumped phase-conjugating mirror
p 146 A86-29280
- COLLISION RATES**
- Rapid evaluation of ion thruster lifetime using optical emission spectroscopy
[AIAA PAPER 85-2011] p 51 A86-17851
- Rapid evaluation of ion thruster lifetime using optical emission spectroscopy
[NASA-TM-87103] p 56 N86-10280
- COLLOCATION**
- Analysis of an externally radially crack ring segment subject to three-point radial loading
p 167 A86-20710
- COMBUSTIBLE FLOW**
- Periodic oscillations observed in swirling flows with and without combustion
p 73 A86-22755
- Numerical simulation of a turbulent flame stabilized behind a rearward-facing step
p 73 A86-22774
- Backward boundary layers in downward flame spread
p 73 A86-22793
- Formation and inflammation of a turbulent jet
p 130 A86-23131
- Direct numerical simulations of chemically reacting turbulent mixing layers
p 130 A86-25567
- Theory of interactive combustion of counterflow premixed flames
p 74 A86-32752
- Visualization of flows in a motored rotary combustion engine using holographic interferometry
[NASA-TM-88804] p 33 N86-31583
- COMBUSTION**
- Symposium (International) on Combustion, 20th, University of Michigan, Ann Arbor, MI, August 12-17, 1984, Proceedings
p 73 A86-22751
- New integration techniques for chemical kinetic rate equations. II - Accuracy comparison
[ASME PAPER 85-GT-30] p 75 A86-32958
- Buoyancy effects upon vapor flame and explosion processes
p 41 N86-10161
- Fundamental studies of droplet combustion at reduced gravity
p 42 N86-10165
- Characteristics of an axisymmetric sudden expansion flow
[NASA-CR-176278] p 151 N86-11465
- Turbine Engine Hot Section Technology (HOST)
[NASA-CP-2289] p 172 N86-11495
- Combustion hot section technology
p 25 N86-11512
- Aerodynamic properties of turbulent combustion fields
[NASA-CR-175005] p 28 N86-20393
- Combustion characteristics in the transition region of liquid fuel sprays
[NASA-CR-176584] p 77 N86-20517
- COMBUSTION CHAMBERS**
- Combustion research for gas turbine engines
p 17 A86-11609
- Concentration distributions in cylindrical combustors
p 126 A86-11937
- The effect of acoustic reflections on combustor noise measurements
p 197 A86-20364
- Swirling flows in typical combustor geometries
p 128 A86-20370
- Evaluation of fuel preparation systems for lean premixing-prevaporizing combustors
[ASME PAPER 85-GT-137] p 19 A86-22081
- Prediction of the structure of fuel sprays in gas turbine combustors
[AIAA PAPER 86-0450] p 20 A86-26636
- A comparison of three algebraic stress closures for combustor flow calculations
[ASME PAPER 85-WA/FE-3] p 132 A86-38388
- Concentration distributions in a model combustor
p 133 A86-38575
- Characterization of simulated small-droplet fuel sprays
[AIAA PAPER 86-1725] p 135 A86-42813
- Toward improved durability in advanced combustors and turbines - Progress in prediction of thermomechanical loads
[ASME PAPER 86-GT-172] p 24 A86-48224
- Small gas turbine combustor experimental study - Compliant metal/ceramic liner and performance evaluation
[AIAA PAPER 86-1452] p 25 A86-49611
- Perspectives on dilution jet mixing - in creating temperature patterns at combustor exits in gas turbine engines
[AIAA PAPER 86-1611] p 25 A86-49614
- Turbine engine Hot Section Technology (HOST) project
p 173 N86-11496
- Dynamic gas temperature measurement system
p 147 N86-11499
- Demonstration test of burner liner strain measurement systems: Interim results
p 173 N86-11501
- Combustion hot section technology
p 25 N86-11512
- Validation of structural analysis methods using burner liner cyclic rig test data
p 173 N86-11518
- HOST liner cyclic facilities
p 173 N86-11519
- Phenomenological study of the behavior of some silica formers in a high velocity jet fuel burner
[NASA-TM-87127] p 157 N86-14613
- Combustor flame flashback
[NASA-CR-174961] p 183 N86-14727
- Prediction of the structure of fuel sprays in gas turbine combustors
[NASA-CR-175028] p 27 N86-16218
- Thermomechanical cyclic hardening behavior of Hastelloy-X
[NASA-CR-174999] p 174 N86-16610
- Experiments for the determination of convective diffusion heat/mass transfer to burner rig test targets comparable in size to jet stream diameter
[NASA-TM-87196] p 139 N86-18646
- A two-dimensional numerical study of the flow inside the combustion chambers of a motored rotary engine
[NASA-TM-87212] p 10 N86-19289
- Demonstration test of burner liner strain measuring system
[NASA-CR-174743] p 148 N86-21817
- Burner liner thermal-structural load modeling
[NASA-CR-174892] p 176 N86-21932
- Dilution jet mixing program, supplementary report
[NASA-CR-175043] p 141 N86-23856
- Characterization of simulated small-droplet fuel sprays
[NASA-TM-87288] p 148 N86-24961
- Lateral jet injection into typical combustor flowfields
[NASA-CR-3997] p 31 N86-28086
- Longitudinal mode combustion instabilities of a high-pressure fuel-rich LOX/RP-1 preburner
p 165 N86-28250
- Role of fuel chemical properties on combustor radiative heat load
[NASA-CR-177096] p 108 N86-30023
- Small gas turbine combustor experimental study: Compliant metal/ceramic liner and performance evaluation
[NASA-TM-87304] p 33 N86-31582
- Visualization of flows in a motored rotary combustion engine using holographic interferometry
[NASA-TM-88804] p 33 N86-31583
- COMBUSTION CHEMISTRY**
- Dynamic features of combustion
p 72 A86-12925
- New integration techniques for chemical kinetic rate equations. I - Efficiency comparison
p 75 A86-38090
- COMBUSTION EFFICIENCY**
- Ignition characteristics of rich n-heptane fuel sprays in the transition region
[ASME PAPER 85-WA/HT-46] p 107 A86-38393
- The behavior of fuel-lean premixed flames in a standard flammability limit tube under controlled gravity conditions
[NASA-CR-177132] p 78 N86-28139

- Small gas turbine combustor experimental study:
Compliant metal/ceramic liner and performance
evaluation
[NASA-TM-87304] p 33 N86-31582
- COMBUSTION PHYSICS**
- Effect of gravity on laminar premixed gas combustion.
I - Flammability limits and burning velocities
p 72 A86-12413
- Effect of gravity on laminar premixed gas combustion.
II - Ignition and extinction phenomena
p 72 A86-12414
- Dynamic features of combustion p 72 A86-12925
- Buoyancy effects on smoldering combustion
[IAF PAPER 85-289] p 72 A86-15805
- An experimental investigation on flame interaction and
the existence of negative flame speeds
p 74 A86-22816
- Spray atomization and combustion
[AIAA PAPER 86-0136] p 131 A86-26606
- New integration techniques for chemical kinetic rate
equations. I - Efficiency comparison p 75 A86-38090
- Particle cloud combustion experiment
p 41 N86-10160
- COMBUSTION PRODUCTS**
- Influence of temperature and hydroxyl concentration on
incipient soot formation in premixed flames
p 74 A86-29070
- COMBUSTION STABILITY**
- Longitudinal mode combustion instabilities of a
high-pressure fuel-rich LOX/RP-1 preburner
p 56 A86-49640
- Combustor flame flashback
[NASA-CR-174961] p 183 N86-14727
- Longitudinal mode combustion instabilities of a
high-pressure fuel-rich LOX/RP-1 preburner
p 185 N86-28250
- COMBUSTION TEMPERATURE**
- A fundamental study of smoldering with emphasis on
experimental design for zero-g p 41 N86-10162
- COMMERCIAL SPACECRAFT**
- Evaluation of spacecraft technology programs (effects
on communication satellite business ventures), volume 1
[NASA-CR-174978] p 112 N86-16451
- Evaluation of spacecraft technology programs (effects
on communication satellite business ventures), volume 2
[NASA-CR-174979] p 113 N86-16452
- COMMUNICATION**
- Research and technology, Lewis Research Center
[NASA-TM-87179] p 207 N86-21427
- COMMUNICATION EQUIPMENT**
- The baseband processor in future satellite
communication systems p 109 A86-21882
- COMMUNICATION NETWORKS**
- The baseband processor in future satellite
communication systems p 109 A86-21882
- Application of intersatellite links to domestic satellite
systems
[AIAA PAPER 86-0604] p 44 A86-29580
- Impact of the 1985 Space World Administrative Radio
Conference on frequency/orbit planning and use
[AIAA PAPER 86-0634] p 110 A86-49567
- Application of intersatellite links to domestic satellite
systems
[NASA-TM-87215] p 46 N86-16249
- Engineering calculations for communications satellite
systems planning
[NASA-CR-176555] p 114 N86-19493
- Impact of the 1985 Space World Administrative Radio
Conference on frequency/orbit planning and use
[NASA-TM-87285] p 115 N86-24881
- ACTS Experiments Program
[NASA-TM-88820] p 47 N86-31625
- COMMUNICATION SATELLITES**
- The role of service areas in the optimization of FSS
orbital and frequency assignments
[AIAA PAPER 86-0636] p 45 A86-29599
- Technology achievements and projections for
communication satellites of the future
[AIAA PAPER 86-0649] p 109 A86-29611
- Testing of 30-GHz low noise receivers
[AIAA PAPER 86-0654] p 45 A86-29616
- Simulated performance of the NASA 30/20 GHz test
transponder using multi-H phase coded modulation
[AIAA PAPER 86-0717] p 110 A86-29656
- On the effectiveness of onboard processing
[AIAA PAPER 86-0721] p 45 A86-29659
- An analysis of bidirectional use of frequencies for
satellite communications
[AIAA PAPER 86-0635] p 110 A86-29664
- Hard ACTS to follow --- NASA Advanced
Communications Technology Satellite
p 46 A86-35318
- Impact of the 1985 Space World Administrative Radio
Conference on frequency/orbit planning and use
[AIAA PAPER 86-0634] p 110 A86-49567
- An analysis of bi-directional use of frequencies for
satellite communications
[AIAA PAPER 86-0635] p 111 A86-49568
- Testing of 30-GHz low noise receivers
[NASA-TM-87171] p 112 N86-13627
- Secondary pattern computation of an arbitrarily shaped
main reflector
[NASA-TM-87162] p 112 N86-14477
- Evaluation of spacecraft technology programs (effects
on communication satellite business ventures), volume 1
[NASA-CR-174978] p 112 N86-16451
- Evaluation of spacecraft technology programs (effects
on communication satellite business ventures), volume 2
[NASA-CR-174979] p 113 N86-16452
- Technology achievements and projections for
communication satellites of the future
[NASA-TM-87201] p 113 N86-17595
- Bit error rate testing of a proof-of-concept model
baseband processor
[NASA-TM-87206] p 46 N86-18343
- An analysis of bi-directional use of frequencies for
satellite communications
[NASA-TM-87226] p 114 N86-18585
- Engineering calculations for communications satellite
systems planning
[NASA-CR-176555] p 114 N86-19493
- Broadcasting satellite service synthesis using gradient
and cyclic coordinate search procedures
[NASA-CR-176708] p 114 N86-23781
- Satellite voice broadcast. Volume 1: Executive
summary
[NASA-CR-175016] p 115 N86-24875
- Satellite voice broadcast. Volume 2: System study
[NASA-CR-175017] p 115 N86-24876
- Impact of the 1985 Space World Administrative Radio
Conference on frequency/orbit planning and use
[NASA-TM-87285] p 115 N86-24881
- Spectrum orbit utilization program technical manual
SOUPs Version 3.8
[NASA-CR-174944] p 116 N86-26489
- Communications platform payload definition study
[NASA-CR-174986] p 49 N86-27402
- Communications platform payload definition study,
executive summary
[NASA-CR-174985] p 49 N86-27407
- Spectrum Orbit Utilization Program documentation:
SOUPs version 3.8 user's manual, volume 1, chapters 1
through 5
[NASA-CR-174889] p 193 N86-27927
- COMMUNITIES**
- Some design philosophy for reducing the community
noise of advanced counter-rotation propellers
[NASA-TM-87099] p 199 N86-4007
- COMPACTING**
- Structure and grain coarsening during the sintering of
alumina p 98 A86-26341
- COMPARISON**
- Comparison of calculated and experimental cascade
performance for controlled-diffusion compressor stator
blading
[NASA-TM-87167] p 27 N86-16219
- COMPONENT RELIABILITY**
- Oxidizer heat exchanger component testing
[NASA-CR-179487] p 62 N86-29901
- COMPOSITE MATERIALS**
- A new ply model for interlaminar stress analysis
p 66 A86-20629
- High Temperature Polymer Matrix Composites
[NASA-CP-2385] p 68 N86-11260
- Polymer, metal and ceramic matrix composites for
advanced aircraft engine applications
[NASA-TM-87132] p 87 N86-13407
- Analytical Ultrasonics in Materials Research and
Testing
[NASA-CP-2383] p 164 N86-22962
- Analytical ultrasonics for evaluation of composite
materials response. Part 2: Generation and detection
p 200 N86-22973
- Simplified composite micromechanics for predicting
microstresses
[NASA-TM-87295] p 70 N86-24759
- Evaluation of capillary reinforced composites
[NASA-CR-175061] p 70 N86-24760
- Ultrasonic stress wave characterization of composite
materials
[NASA-CR-3976] p 165 N86-27665
- A study of the stress wave factor technique for
nondestructive evaluation of composite materials
[NASA-CR-4002] p 165 N86-28445
- Acousto-ultrasonic verification of the strength of filament
wound composite material
[NASA-TM-88827] p 166 N86-32764
- COMPOSITE STRUCTURES**
- Factors influencing the ultrasonic stress wave factor
evaluation of composite material structures
p 168 A86-34257
- Composite sandwich thermostructural behavior -
Computational simulation
[AIAA PAPER 86-0948] p 170 A86-38842
- Computational composite mechanics for aerospace
propulsion structures
[AIAA PAPER 86-1190] p 67 A86-40596
- Aeroelastic behavior of low aspect ratio metal and
composite blades
[ASME PAPER 86-GT-243] p 171 A86-48271
- COMPRESSIBILITY**
- The plastic compressibility of 7075-T651 aluminum-alloy
plate p 85 A86-49690
- A model for the influence of pressure on the bulk modulus
and the influence of temperature on the solidification
pressure for liquid lubricants
[NASA-TM-87230] p 140 N86-19555
- Compressive creep behavior of alloys based on B2
FeAl
[NASA-TM-87293] p 92 N86-28165
- Universality in the compressive behavior of solids
[NASA-TM-87303] p 206 N86-28775
- COMPRESSIBLE FLOW**
- Inverse design of axisymmetric flow passages using
compressible viscous flow theory p 4 A86-26412
- Recent skin friction techniques for compressible flows
[AIAA PAPER 86-1099] p 147 A86-38460
- An approach to the calculation of the pressure field
produced by rigid wide chord dual rotation propellers of
high solidity in compressible flow
[AIAA PAPER 86-0467] p 198 A86-49566
- Viscous compressible flow direct and inverse
computation and illustrations
[NASA-CR-175037] p 28 N86-20391
- An analysis for the sound field produced by rigid wide
chord dual rotation propellers of high solidity in
compressible flow
[NASA-TM-87178] p 11 N86-21517
- COMPRESSION LOADS**
- Orientation and temperature dependence of some
mechanical properties of the single-crystal nickel-base
superalloy Rene N4. III - Tension-compression
anisotropy p 86 A86-50323
- COMPRESSION TESTS**
- Slow plastic strain rate compressive flow in binary CoAl
intermetallics p 79 A86-11478
- COMPRESSIVE STRENGTH**
- Longitudinal compressive failure modes in fiber
composites End attachment effects on ITRI type test
specimens p 66 A86-19999
- COMPRESSOR BLADES**
- Boundary layer measurements on an airfoil in cascade
using laser Doppler anemometry
[AIAA PAPER 86-0072] p 145 A86-19670
- Comparison of calculated and experimental cascade
performance for controlled-diffusion compressor stator
blading
[NASA-TM-87167] p 27 N86-16219
- Structural tailoring of engine blades (STAEBL)
theoretical manual
[NASA-CR-175112] p 31 N86-27283
- Structural tailoring of engine blades (STAEBL) user's
manual
[NASA-CR-175113] p 31 N86-27284
- The boundary layer on compressor cascade blades
[NASA-CR-177279] p 143 N86-27607
- Rotor wake characteristics of a transonic axial flow
fan
[NASA-TM-87073] p 13 N86-28055
- COMPRESSOR ROTORS**
- End-wall and profile losses in a low-speed axial flow
compressor rotor
[ASME PAPER 85-GT-174] p 20 A86-22090
- Analysis of fully stalled compressor
[AIAA PAPER 86-1123] p 5 A86-38480
- Laser Doppler velocimeter measurement in the tip region
of a compressor rotor p 5 A86-39064
- Three-dimensional boundary layer on a compressor rotor
blade at peak pressure rise coefficient
[ASME PAPER 86-GT-186] p 7 A86-48236
- Analysis of fully stalled compressor
[NASA-TM-87254] p 11 N86-20357
- Extended parametric representation of compressor fans
and turbines. Volume 1: CMGEN user's manual
[NASA-CR-174645] p 159 N86-23936
- Extended parametric representation of compressor fans
and turbines. Volume 2: Part user's manual (parametric
turbine)
[NASA-CR-174646] p 159 N86-23937
- Extended parametric representation of compressor fans
and turbines. Volume 3: MODFAN user's manual
(parametric modulating flow fan)
[NASA-CR-174647] p 159 N86-23938
- Thermodynamic evaluation of transonic compressor
rotors using the finite volume approach
[NASA-CR-176840] p 143 N86-26546

COMPRESSORS

Bifurcation techniques for nonlinear dynamic analysis of compressor stall phenomena p 22 A86-35403
Comparison of calculated and experimental cascade performance for controlled-diffusion compressor stator blading

[NASA-TM-87167] p 27 N86-16219

COMPUTATION

Progressive damage, fracture predictions and post mortem correlations for fiber composites

[NASA-TM-87101] p 68 N86-10290

Secondary pattern computation of an offset reflector antenna

[NASA-TM-87160] p 112 N86-14479

Comparison of calculated and experimental cascade performance for controlled-diffusion compressor stator blading

[NASA-TM-87167] p 27 N86-16219

Partitioning and packing mathematical simulation models for calculation on parallel computers

[NASA-TM-87170] p 193 N86-19008

Increasing processor utilization during parallel computation rundown

[NASA-TM-87349] p 192 N86-26914

Physical and numerical sources of computational inefficiency in integration of chemical kinetic rate equations: Etiology, treatment and prognosis

[NASA-TP-2590] p 195 N86-28662

COMPUTATIONAL FLUID DYNAMICS

Combustion research for gas turbine engines

p 17 A86-11609

Effect of free stream turbulence on flow separation

p 125 A86-11676

Numerical and experimental investigation of nonswirling and swirling confined jets

[AIAA PAPER 86-0040] p 127 A86-19651

Numerical simulation of unsteady flow in an axisymmetric shear layer

[AIAA PAPER 86-0202] p 127 A86-19746

An implicit LU scheme for the Euler equations applied to arbitrary cascades --- new method of factoring

p 2 A86-20131

Swirling flows in typical combustor geometries

p 128 A86-20370

Accelerated solution of the steady Euler equations

p 2 A86-20942

Multi-grid technique for the solution of incompressible Navier-Stokes equations

p 128 A86-21029

NASA Lewis Research Center/university graduate research program on engine structures

[ASME PAPER 85-GT-159] p 167 A86-22084

A theory of post-stall transients in axial compression systems. I - Development of equations

[ASME PAPER 85-GT-171] p 19 A86-22088

Modeling the 3-D flow effects on deviation angle for axial compressor middle stages

[ASME PAPER 85-GT-189] p 2 A86-22102

Model equation for simulating flows in multistage turbomachinery

[ASME PAPER 85-GT-226] p 2 A86-22123

Oscillatory thermocapillary flows

p 129 A86-22413

Simplex finite element analysis of viscous incompressible flow with penalty function formulation

p 129 A86-22615

Computation of turbulent rotating channel flow with an algebraic Reynolds stress model

[AIAA PAPER 86-0214] p 130 A86-22682

Formation and inflammation of a turbulent jet

p 130 A86-23131

Unsteady transonic flow in cascades

p 4 A86-24693

Direct numerical simulations of chemically reacting turbulent mixing layers

p 130 A86-25567

Inverse design of axisymmetric flow passages using compressible viscous flow theory

p 4 A86-26412

Three dimensional flow phenomena in fluid machinery; Proceedings of the Winter Annual Meeting, Miami Beach, FL, November 17-22, 1985

p 4 A86-28682

Calculation of three-dimensional boundary layers on rotating turbine blades

p 131 A86-28696

Theory of interactive combustion of counterflow premixed flames

p 74 A86-32752

A comparison of three algebraic stress closures for combustor flow calculations

[ASME PAPER 85-WA/FE-3] p 132 A86-38388

Parametric effects of CFL number and artificial smoothing on numerical solutions using implicit approximate factorization algorithm

[AIAA PAPER 86-1059] p 132 A86-38427

An efficient method for solving the steady Euler equations

[AIAA PAPER 86-1079] p 132 A86-38442

Computation of viscous flows in turbomachinery cascades with a space-marching method

p 5 A86-39089

A new approach for solving the three-dimensional steady Euler equations. I - General theory p 133 A86-41242

Direct numerical simulations of a reacting mixing layer with chemical heat release

p 76 A86-41711

Transonic potential flow in hyperbolic nozzles

p 5 A86-41723

An LU implicit scheme for high speed inlet analysis

[AIAA PAPER 86-1520] p 6 A86-42687

Improved Euler analysis of advanced turboprop propeller flows

[AIAA PAPER 86-1521] p 6 A86-42688

Numerical analysis of some supersonic viscous flows related to inlet and nozzle systems

[AIAA PAPER 86-1597] p 134 A86-42738

Assessment of a parabolic analysis for axisymmetric internal flows in rocket and turbomachinery ducts

[AIAA PAPER 86-1598] p 134 A86-42739

A comparison of computational methods for three-dimensional, turbulent turbomachinery flow fields

[AIAA PAPER 86-1599] p 6 A86-42740

A numerical analysis applied to high angle of attack three-dimensional inlets

[AIAA PAPER 86-1527] p 6 A86-42760

A space-marching method for viscous incompressible internal flows

p 135 A86-43037

Turbulent two-phase flow in annular seals

[ASLE PREPRINT 86-AM-4G-3] p 156 A86-45391

Finite element simulation of temperature dependent free surface flows

p 136 A86-47012

Computation of three-dimensional, rotational flow through turbomachinery blade rows for improved aerodynamic design studies

[ASME PAPER 86-GT-26] p 7 A86-48117

Validation of viscous and inviscid computational methods for turbomachinery components

[ASME PAPER 86-GT-42] p 7 A86-48126

On the application of a linearized unsteady potential-flow analysis to fan-tip cascades

[ASME PAPER 86-GT-87] p 7 A86-48153

Application of a computational model for vortex generators in subsonic internal flows

[AIAA PAPER 86-1458] p 8 A86-49612

Local equilibrium assumption for round jet calculations

p 136 A86-49829

Is Navier-Stokes turbulence chaotic?

p 137 A86-50275

Validation of viscous and inviscid computational methods for turbomachinery components

[NASA-TM-87193] p 10 N86-16194

Mean velocity and turbulence measurements in a 90 deg curved duct with thin inlet boundary layer

[NASA-CR-174811] p 139 N86-16518

Viscous compressible flow direct and inverse computation and illustrations

[NASA-CR-175037] p 28 N86-20391

An LU implicit scheme for high speed inlet analysis

[NASA-CR-175098] p 11 N86-23563

A numerical analysis applied to high angle of attack three-dimensional inlets

[NASA-TM-87298] p 11 N86-24658

Application of a computational model for vortex generators in subsonic internal flows

[NASA-TM-87327] p 143 N86-26545

On the modeling of low-Reynolds-number turbulence

[NASA-CR-3994] p 32 N86-28089

Experimental and theoretical study of propeller spinner/shank interference

[NASA-CR-176954] p 13 N86-29773

Numerical simulation of the flowfield over ice accretion shapes

[NASA-CR-176960] p 144 N86-30093

Thermodynamic evaluation of transonic compressor rotors using the finite volume approach

[NASA-CR-176947] p 32 N86-30731

COMPUTATIONAL GRIDS

Multi-grid technique for the solution of incompressible Navier-Stokes equations

p 128 A86-21029

A mesh re-zoning technique for finite element simulations of metal forming processes

p 153 A86-36298

A two-dimensional numerical study of the flow inside the combustion chambers of a motored rotary engine

[NASA-TM-87212] p 10 N86-19289

Effect of triangular element orientation on finite element solutions of the Helmholtz equation

[NASA-TM-87351] p 201 N86-32247

COMPUTER AIDED DESIGN

Structural tailoring of SSME turbopump blades

(SSME/STAEBL) --- Structural Tailoring of Engine Blades

[AIAA PAPER 86-0847] p 54 A86-38895

Verification of computer-aided designs of traveling-wave tubes utilizing novel dynamic refocusers and graphite electrodes for the multistage depressed collector

[NASA-TP-2524] p 121 N86-13643

Burner liner thermal-structural load modeling

[NASA-CR-174892] p 176 N86-21932

Burner liner thermal/structural load modeling: TRANCITS program user's manual

[NASA-CR-174891] p 142 N86-24931

Generation of spiral bevel gears with zero kinematic errors and computer aided tooth contact analysis

[NASA-TM-87273] p 160 N86-25793

Dynamic loading on parallel shaft gears

[NASA-CR-179473] p 161 N86-28433

Performance of oil pumping rings: An analytical and experimental study

[NASA-CR-175083] p 144 N86-31000

COMPUTER GRAPHICS

Study of journal bearing dynamics using 3-dimensional motion picture graphics

[NASA-TM-87205] p 140 N86-18647

COMPUTER PROGRAMMING

Simulating a small turboshaft engine in real-time multiprocessor simulator (RTMPS) environment

[NASA-TM-87216] p 27 N86-16221

COMPUTER PROGRAMS

DEAN - A program for Dynamic Engine Analysis

[AIAA PAPER 85-1354] p 18 A86-14430

Modeling dilution of jet flowfields

p 128 A86-20362

An experimental method for measuring droplet impingement efficiency on two- and three-dimensional bodies

[AIAA PAPER 86-0406] p 131 A86-26630

An investigation of the transient thermal analysis of spur gears

[ASME PAPER 84-DET-92] p 155 A86-40683

Dynamic stress analysis of smooth and notched fiber composite flexural specimens

p 67 A86-41070

Fast approach for calculating film thicknesses and pressures in elastohydrodynamically lubricated contacts at high loads

[ASME PAPER 85-TRIB-42] p 155 A86-43541

Validation of viscous and inviscid computational methods for turbomachinery components

[ASME PAPER 86-GT-42] p 7 A86-48126

Progressive damage, fracture predictions and post mortem correlations for fiber composites

[NASA-TM-87101] p 68 N86-10290

A numerical method of calculating propeller noise including acoustic nonlinear effects

p 199 N86-12011

A FORTRAN computer code for calculating flows in multiple-blade-element cascades

[NASA-TM-87104] p 9 N86-13295

Secondary pattern computation of an offset reflector antenna

[NASA-TM-87160] p 112 N86-14479

Thermal-mechanical fatigue test apparatus for metal matrix composites and joint attachments

[NASA-TM-87187] p 88 N86-15378

Validation of viscous and inviscid computational methods for turbomachinery components

[NASA-TM-87193] p 10 N86-16194

LOX/LH2 vane pump for auxiliary propulsion systems

p 58 N86-17397

A numerical and experimental investigation of electrochemical aircraft deicing

[NASA-CR-175024] p 14 N86-20380

Integrated Composite Analyzer (ICAN): Users and programmers manual

[NASA-TP-2515] p 69 N86-21614

A computer program to calculate the resistivity of a thin film deposited on a conductive substrate from four-point probe measurements

[NASA-TM-87262] p 193 N86-22150

Mutual coupling effects in antenna arrays, volume 1

[NASA-CR-176699] p 114 N86-22782

SSME fuelside preburner two-dimensional analysis

[NASA-TM-87299] p 44 N86-23616

Theoretical analysis of the electrical aspects of the basic electro-impulse problem in aircraft de-icing applications

[NASA-CR-176808] p 17 N86-26330

Computational simulation of progressive fracture in fiber composites

[NASA-TM-87341] p 71 N86-26376

Spectrum orbit utilization program technical manual SOUP5 Version 3.8

[NASA-CR-174944] p 116 N86-26489

Structural tailoring of engine blades (STAEBL) user's manual

[NASA-CR-175113] p 31 N86-27284

Spectrum Orbit Utilization Program documentation: SOUP5 version 3.8 user's manual, volume 2, appendices A through G

[NASA-CR-174890] p 193 N86-27928

Application of a personal computer for the uncoupled vibration analysis of wind turbine blade and counterweight assemblies

[NASA-CR-175090] p 188 N86-28511

- Physical and numerical sources of computational inefficiency in integration of chemical kinetic rate equations: Etiology, treatment and prognosis [NASA-TP-2590] p 195 N86-28662
- COMPUTER SYSTEMS DESIGN**
Theoretical and software considerations for general dynamic analysis using multilevel substructured models [NASA-CR-176822] p 195 N86-26067
- COMPUTER SYSTEMS PERFORMANCE**
The effects of syntactic complexity on the human-computer interaction p 192 A86-36172
- COMPUTER SYSTEMS SIMULATION**
Performance evaluation of a simulated data-flow computer with low-resolution actors p 194 A86-32051
- COMPUTER TECHNIQUES**
Computer aided derivation of equations for composite mechanics problems and finite element analyses [AIAA PAPER 86-1016] p 170 A86-38873
- COMPUTERIZED SIMULATION**
DEAN - A program for Dynamic Engine Analysis [AIAA PAPER 85-1354] p 18 A86-14430
Resonant power processors. I - State plane analysis p 117 A86-14481
A structural dynamics investigation related to EIDI applications --- Electro-Impulse Deicing [AIAA PAPER 86-0550] p 16 A86-19942
Development and application of dynamic simulations of a subsonic wind tunnel p 36 A86-24745
Test results of a 40 kW Stirling engine and comparison with the NASA-Lewis computer code predictions p 181 A86-24889
Computer simulation of thin-film nucleation and growth - The multilayer mode p 204 A86-37441
Composite sandwich thermostructural behavior - Computational simulation p 170 A86-38842
Generation of spiral bevel gears with zero kinematical errors and computer aided simulation of their meshing and contact p 154 A86-40656
Computational simulation of liquid rocket injector anomalies p 55 A86-42633
Computational engine structural analysis [ASME PAPER 86-GT-70] p 23 A86-48141
Gas flow environmental and heat transfer nonrotating 3D program p 137 N86-11506
Overview of free-piston Stirling technology at the NASA Lewis Research Center p 208 N86-13236
SCARE: A post-processor program to MSC/NASTRAN for the reliability analysis of structural ceramic components p 174 N86-14688
A computer simulation of the turbocharged turbo compounded diesel engine system: A description of the thermodynamic and heat transfer models [NASA-CR-174971] p 208 N86-16164
High-efficiency AlGaAs-GaAs Cassegrainian concentrator cells p 185 N86-17845
Development and application of dynamic simulations of a subsonic wind tunnel p 43 N86-18338
Partitioning and packing mathematical simulation models for calculation on parallel computers [NASA-TM-87170] p 193 N86-19008
Computational engine structural analysis [NASA-TM-87231] p 175 N86-19663
A real-time simulation evaluation of an advanced detection. Isolation and accommodation algorithm for sensor failures in turbine engines [NASA-TM-87289] p 30 N86-24697
System life and reliability modeling for helicopter transmissions [NASA-CR-3967] p 159 N86-24990
Power conversion distribution system using a resonant high-frequency AC link [NASA-CR-176804] p 123 N86-25694
Computational simulation of progressive fracture in fiber composites [NASA-TM-87341] p 71 N86-26376
A lumped parameter mathematical model for simulation of subsonic wind tunnels [NASA-TM-87324] p 196 N86-27036
Hardware configuration for a real-time multiprocessor simulator [NASA-TM-88802] p 194 N86-28651
HYTESS 2: A Hypothetical Turbofan Engine Simplified Simulation with multivariable control and sensor analytical redundancy [NASA-TM-87344] p 124 N86-30068
Aerodynamic data banks for Clark-Y, NACA 4-digit and NACA 16-series airfoil families [NASA-CR-176883] p 13 N86-30693
Measurements in liquid fuel sprays [NASA-CR-177088] p 144 N86-30960
- Evaluation of a Stirling engine heater bypass with the NASA Lewis nodal-analysis performance code [NASA-CR-179460] p 211 N86-31452
NASA's Aircraft Icing Analysis Program [NASA-TM-88791] p 15 N86-31548
Fiber composite sandwich thermostructural behavior: Computational simulation [NASA-TM-88787] p 71 N86-31663
A sensor failure simulator for control system reliability studies [NASA-TM-87271] p 124 N86-31792
Design considerations for advanced battery concepts [NASA-TM-87319] p 190 N86-31981
- CONCENTRATION (COMPOSITION)**
Criteria for significance of simultaneous presence of both condensable vapors and aerosol particles on mass transfer (deposition) rates [NASA-TM-87247] p 109 N86-24869
Fugacity and concentration gradients in a gravity field [NASA-TM-88809] p 212 N86-30620
The effect of variations of cobalt content on the cyclic oxidation resistance of selected Ni-base superalloys [NASA-TM-87297] p 93 N86-31702
- CONCENTRATORS**
Performance of Hughes GaAs concentrator cells under 1-MeV electron irradiation p 185 N86-17860
- CONDENSATION**
Structure-to-glass transition temperature relationships in high temperature stable condensation polyimides [NASA-TM-87113] p 101 N86-12311
- CONDUCTIVE HEAT TRANSFER**
Analysis of the transient behavior of rubbing components [NASA-CR-176546] p 102 N86-19464
- CONFERENCES**
New directions in lubrication, materials, wear, and surface interactions - Tribology in the 80's --- Book p 152 A86-18700
Symposium (International) on Combustion, 20th, University of Michigan, Ann Arbor, MI, August 12-17, 1984, Proceedings p 73 A86-22751
Vibrations of blades and bladed disk assemblies; Proceedings of the Tenth Biennial Conference on Mechanical Vibration and Noise, Cincinnati, OH, September 10-13, 1985 p 20 A86-26901
Analytical Ultrasonics in Materials Research and Testing [NASA-CP-2383] p 164 N86-22962
- CONFIGURATION INTERACTION**
Some design philosophy for reducing the community noise of advanced counter-rotation propellers [NASA-TM-87099] p 199 N86-14007
- CONJUGATION**
Compensation of reflector surface distortions using conjugate field matching [NASA-TM-87198] p 113 N86-16461
- CONSTITUTIVE EQUATIONS**
Unified constitutive materials model development and evaluation for high-temperature structural analysis applications --- for aircraft gas turbine engines p 172 A86-49133
Anisotropic constitutive model for nickel base single crystal alloys: Development and finite element implementation [NASA-CR-175015] p 176 N86-21952
Integrated research in constitutive modelling at elevated temperatures, part 1 [NASA-CR-177237] p 179 N86-30227
- CONSTRAINTS**
Locally bound constrained Newton-Raphson solution algorithms --- for modeling kinematic and material nonlinearity p 171 A86-43771
Constrained hierarchical least square nonlinear equation solvers --- for indefinite stiffness and large structural deformations p 171 A86-43774
Research and competition: Best partners [NASA-TM-87313] p 212 N86-25321
Structural tailoring of engine blades (STAEBL) theoretical manual [NASA-CR-175112] p 31 N86-27283
- CONSTRUCTION**
Summary of tower designs for large horizontal axis wind turbines [NASA-TM-87166] p 186 N86-18776
- CONTACT RESISTANCE**
Lubrication of nonconformal contacts [NASA-TM-87120] p 138 N86-13679
- CONTAINERLESS MELTS**
Solidification fundamentals p 39 N86-10090
Containerless processing of undercooled melts p 39 N86-10093
- CONTAMINANTS**
Compatibility of grain-stabilized platinum with candidate propellants for resistojets [AIAA PAPER 85-2014] p 51 A86-17835
- Compatibility of grain-stabilized platinum with candidate propellants for resistojets [NASA-TM-87118] p 56 N86-10279
- CONTINENTAL SHELVES**
Wilson study cycles: Research relative to ocean geodynamic cycles [NASA-CR-176560] p 192 N86-21092
- CONTINUUM MECHANICS**
Probabilistic finite elements for transient analysis in nonlinear continua p 168 A86-28653
Constrained hierarchical least square nonlinear equation solvers --- for indefinite stiffness and large structural deformations p 171 A86-43774
- CONTOURS**
Application of a computational model for vortex generators in subsonic internal flows [AIAA PAPER 86-1458] p 8 A86-49612
Application of a computational model for vortex generators in subsonic internal flows [NASA-TM-87327] p 143 N86-26545
- CONTRAROTATING PROPELLERS**
A numerical method for the design and analysis of counter-rotating propellers [AIAA PAPER 84-1205] p 19 A86-20369
Unsteady forces on counter-rotating propeller blades [AIAA PAPER 86-1804] p 22 A86-37827
Some design philosophy for reducing the community noise of advanced counter-rotation propellers [NASA-TM-87099] p 199 N86-14007
- CONTROL EQUIPMENT**
Advanced on-site power plant development technology program [NASA-CR-174709] p 187 N86-25040
Robust detection, isolation and accommodation for sensor failures [NASA-CR-174825] p 33 N86-30732
A sensor failure simulator for control system reliability studies [NASA-TM-87271] p 124 N86-31792
- CONTROL SIMULATION**
A sensor failure simulator for control system reliability studies [NASA-TM-87271] p 124 N86-31792
- CONVECTION**
Determination of convective diffusion heat/mass transfer rates to burner rig test targets comparable in size to cross-stream jet diameter [ASME PAPER 86-GT-68] p 136 A86-48140
Surface tension induced instabilities in reduced gravity: The Benard problem p 40 N86-10117
Determination of convective diffusion heat/mass transfer rates to burner rig test targets comparable in size to cross-stream jet diameter [NASA-TM-87176] p 138 N86-13678
- CONVECTIVE FLOW**
Oscillatory thermocapillary flows p 129 A86-22413
Electrocrystallization in microgravity [NASA-TM-87202] p 212 N86-19274
Diffusion flame extinction in slow convective flow under microgravity environment [NASA-TM-88799] p 144 N86-28378
- CONVECTIVE HEAT TRANSFER**
Deposit formation and heat-transfer characteristics of hydrocarbon rocket fuels p 106 A86-10028
Thermophoretically augmented mass transfer rates to solid walls across laminar boundary layers p 128 A86-20150
Boundary perturbation method for free boundary problem in convectively cooled continuous casting p 131 A86-28649
Free boundary shape of a convectively cooled solidified region p 131 A86-29029
Ignition and flame spread above liquid fuel pools p 41 N86-10163
Experiments for the determination of convective diffusion heat/mass transfer to burner rig test targets comparable in size to jet stream diameter [NASA-TM-87196] p 139 N86-18646
- CONVERGENCE**
Acceleration of convergence of vector sequences p 195 A86-49850
- CONVERTERS**
State-plane analysis of parallel resonant converter p 119 A86-40431
- COOLANTS**
Effect of an oxygen plasma on the physical and chemical properties of several fluids for the liquid droplet radiator [NASA-TM-88839] p 49 N86-31634
- COOLING**
Fabrication of ceramic substrate-reinforced and free forms by mandrel plasma spraying metal-ceramic composites p 64 A86-17483
Design principles for nickel-hydrogen cells and batteries p 179 A86-24799

- Performance analysis of radiation cooled dc transmission lines for high power space systems
p 117 A86-24811
- Boundary perturbation method for free boundary problem in convectively cooled continuous casting
p 131 A86-28649
- Free boundary shape of a convectively cooled solidified region
p 131 A86-29029
- Small gas turbine combustor experimental study - Compliant metal/ceramic liner and performance evaluation
[AIAA PAPER 86-1452] p 25 A86-49611
- Containerless processing of undercooled melts
p 39 N86-10093
- Preliminary design of a supersonic cruise aircraft high-pressure turbine
[NASA-CR-174878] p 26 N86-14272
- Heat transfer to two-phase air/water mixtures flowing in small tubes with inlet disequilibrium
[NASA-CR-175076] p 141 N86-22892
- Channel flow modeling of impingement cooling of a rotating turbine blade
[NASA-CR-177206] p 31 N86-27285
- Small gas turbine combustor experimental study: Compliant metal/ceramic liner and performance evaluation
[NASA-TM-87304] p 33 N86-31582
- COOLING FINs**
- Heat transfer and pressure drop performance of a finned-tube heat exchanger proposed for use in the NASA Lewis Altitude Wind Tunnel
[NASA-TM-87151] p 138 N86-13677
- COPOLYMERIZATION**
- Chemical control of rate and onset temperature of nadimide polymerization
p 101 N86-11271
- COPPER**
- The mechanism of erosion of metallic materials under cavitation attack
[NASA-TM-87133] p 156 N86-10552
- Textured carbon on copper: A novel surface with extremely low secondary electron emission characteristics
[NASA-TP-2543] p 101 N86-15394
- Ultrasonic verification of microstructural changes due to heat treatment
p 200 N86-22977
- Nonlinear damage analysis: Postulate and evaluation
[NASA-CR-168171] p 177 N86-26652
- COPPER ALLOYS**
- Erosion of phosphor bronze under cavitation attack in a mineral oil
p 81 A86-23324
- An experimental data base for material selection and design of high-speed, high-pressure, oxygen turbomachinery
p 58 N86-17387
- COPPER CHLORIDES**
- Environmental stability of intercalated graphite fibers
p 98 A86-31825
- Graphite fiber intercalation: Basic properties of copper chloride intercalated fibers
[NASA-TM-87217] p 65 N86-18442
- COPPER OXIDES**
- Textured carbon surfaces on copper by sputtering
[NASA-CASE-LEW-14130-1] p 109 N86-32587
- CORIOLIS EFFECT**
- Vibration and buckling of rotating, pretwisted, preconed beams including Coriolis effects
p 168 A86-26910
- Nonlinear bending-torsional vibration and stability of rotating, pretwisted, preconed blades including Coriolis effects
[NASA-TM-87207] p 175 N86-17789
- CORNER FLOW**
- Three-dimensional fluid flow phenomena in the blade end wall corner region
[ASME PAPER 86-GT-179] p 7 A86-48229
- CORRELATION**
- Uniform engine testing program phase 7: NASA Lewis Research Center second entry
[NASA-TM-87272] p 31 N86-28085
- CORROSION**
- Surface effects of corrosive media on hardness, friction, and wear of materials
p 94 A86-10825
- Interaction of sulfuric acid corrosion and mechanical wear of iron
p 81 A86-20436
- The reactions of cobalt, iron and nickel in SO₂ atmospheres Similarities and differences
p 75 A86-40677
- Corrosion of nickel and cobalt base alloys in sulfate melts at 750 deg C
[NASA-CR-175111] p 91 N86-24817
- CORROSION PREVENTION**
- Oxidation protecting coatings for polymers
[NASA-CASE-LEW-14072-3] p 105 N86-26434
- CORROSION RESISTANCE**
- The effects of metals and inhibitors on thermal oxidative degradation reactions of unbranched perfluoroalkyl ethers
p 99 A86-40682
- Improved fracture toughness corrosion-resistant bearing material
[NASA-CR-174990] p 162 N86-32743
- CORROSION TESTS**
- Na₂SO₄ induced corrosion of nickel at high temperature
p 83 A86-37073
- Mechanism of Na₂SO₄-induced corrosion of molybdenum containing nickel-base superalloys at high temperatures. I - Corrosion in atmospheres containing O₂ only. II - Corrosion in O₂ + SO₂ atmospheres
p 83 A86-37238
- Compatibility experiments of facilities, materials, and propellants for electrothermal thrusters
p 59 N86-17426
- CORRUGATING**
- A simple circular-polarized antenna: Circular waveguide horn coated with lossy magnetic material
[NASA-CR-177092] p 116 N86-30039
- COST ANALYSIS**
- Ceramic automotive Stirling engine study
[NASA-CR-174907] p 208 N86-16165
- Summary of tower designs for large horizontal axis wind turbines
[NASA-TM-87166] p 186 N86-18776
- Structural tailoring of engine blades (STAEBL) user's manual
[NASA-CR-175113] p 31 N86-27284
- Communications platform payload definition study
[NASA-CR-174986] p 49 N86-27402
- Communications platform payload definition study, executive summary
[NASA-CR-174985] p 49 N86-27407
- COST EFFECTIVENESS**
- Evaluation of propan propulsion applied to general aviation
[NASA-CR-175020] p 30 N86-24695
- A 20 kilohertz space station power system
[NASA-TM-88801] p 62 N86-28122
- COST ESTIMATES**
- Life cycle cost assessment of future low heat rejection engines
[SAE PAPER 860444] p 153 A86-37048
- COST REDUCTION**
- An overview of the Small Engine Component Technology (SECT) studies
[NASA-TM-88796] p 34 N86-31587
- COUNTER ROTATION**
- Some design philosophy for reducing the community noise of advanced counter-rotation propellers
[NASA-TM-87099] p 199 N86-14007
- COUNTERBALANCES**
- Application of a personal computer for the uncoupled vibration analysis of wind turbine blade and counterweight assemblies
[NASA-CR-175090] p 188 N86-28511
- COUNTERFLOW**
- Theory of interactive combustion of counterflow premixed flames
p 74 A86-32752
- COUPLED MODES**
- The predicted effect of aerodynamic detuning on coupled bending-torsion unstalled supersonic flutter
[NASA-TM-87240] p 11 N86-21513
- COUPLING**
- Linear dynamic coupling in geared rotor systems
[ASME PAPER 85-DET-11] p 154 A86-38617
- CRACK CLOSURE**
- Influence of load interactions on crack growth as related to state of stress and crack closure
[NASA-TM-87117] p 86 N86-12292
- Closure of fatigue cracks at high strains
[NASA-CR-175021] p 175 N86-17788
- Variables controlling fatigue crack growth of short cracks
[NASA-TM-87208] p 90 N86-21661
- Influence of fatigue crack wake length and state of stress on crack closure
[NASA-TM-87292] p 90 N86-22686
- The evolution and growth of Al₂O₃ scales on beta-NiAl
[NASA-CR-175097] p 92 N86-27444
- CRACK GEOMETRY**
- Wide-range displacement expressions for standard fracture mechanics specimens
p 166 A86-20706
- CRACK INITIATION**
- Three-dimensional hybrid-stress finite element analysis of composite laminates with cracks and cutouts
p 167 A86-26896
- Fatigue crack propagation of nickel-base superalloys at 650 deg C
[NASA-TM-87150] p 87 N86-12294
- Simplified cyclic structural analyses of SSME turbine blades
[NASA-TM-87214] p 175 N86-16615
- Fatigue crack growth under general-yielding cyclic-loading
[NASA-CR-175049] p 176 N86-21951
- Cyclic creep analysis from elastic finite-element solutions
[NASA-TM-87213] p 176 N86-25822
- Low-cycle thermal fatigue
[NASA-TM-87225] p 177 N86-26651
- Nonlinear damage analysis: Postulate and evaluation
[NASA-CR-168171] p 177 N86-26652
- Structural analysis of turbine blades using unified constitutive models
[NASA-TM-88807] p 178 N86-28461
- Compliance matrices for cracked bodies
[NASA-CR-179478] p 179 N86-30236
- Test program to provide confidence in liquid oxygen cooling of hydrocarbon fueled rocket thrust chambers
[NASA-TM-88816] p 62 N86-31646
- CRACK PROPAGATION**
- Failure analysis of plasma-sprayed thermal barrier coatings
p 80 A86-18270
- Thermal-mechanical fatigue crack growth in Inconel X-750
p 81 A86-20982
- Shear fatigue crack growth - A literature survey
p 167 A86-24219
- Fracture mechanics applied to nonisothermal fatigue crack growth
p 81 A86-28951
- The crack layer approach to toughness characterization in steel
p 82 A86-30010
- Effect of grain-boundary crystallization on the high-temperature strength of silicon nitride
p 98 A86-33495
- Strength and microstructure of Si₃N₄ sintered with ZrO₂ additions
p 99 A86-36330
- Dynamic delamination crack propagation in a graphite/epoxy laminate
p 68 A86-43010
- Mode II fatigue crack growth specimen development
p 171 A86-43566
- Fatigue crack growth under general-yielding cyclic-loading
p 171 A86-44339
- A study of spectrum fatigue crack propagation in two aluminum alloys. I - Spectrum simplification. II - Influence of microstructures
p 85 A86-48973
- Orientation and temperature dependence of some mechanical properties of the single-crystal nickel-base superalloy Rene N4. II - Low cycle fatigue behavior
p 86 A86-50322
- Creep-fatigue behavior of NiCoCrAlY coated PWA 1480 superalloy single crystals
[NASA-TM-87110] p 86 N86-10311
- Influence of load interactions on crack growth as related to state of stress and crack closure
[NASA-TM-87117] p 86 N86-12292
- Fatigue crack propagation of nickel-base superalloys at 650 deg C
[NASA-TM-87150] p 87 N86-12294
- Fractured toughness of Si₃N₄ measured with short bar chevron-notched specimens
[NASA-TM-87153] p 101 N86-13495
- Structure-property characterization of rheocast and VADER processed IN-100 superalloy
[NASA-CR-175014] p 88 N86-14354
- Closure of fatigue cracks at high strains
[NASA-CR-175021] p 175 N86-17788
- Estimating the R-curve from residual strength data
[NASA-TM-87182] p 175 N86-18750
- Grain boundary oxidation and oxidation accelerated fatigue crack nucleation and propagation
[NASA-CR-175050] p 89 N86-20542
- Variables controlling fatigue crack growth of short cracks
[NASA-TM-87208] p 90 N86-21661
- Fatigue crack growth under general-yielding cyclic-loading
[NASA-CR-175049] p 176 N86-21951
- Simplified composite micromechanics for predicting microstresses
[NASA-TM-87295] p 70 N86-24759
- Thermal-mechanical fatigue behavior of nickel-base superalloys
[NASA-CR-175048] p 91 N86-24818
- Axial and torsional fatigue behavior of Waspaloy
[NASA-CR-175052] p 91 N86-25454
- Fatigue crack layer propagation in silicon-iron
[NASA-CR-175115] p 177 N86-25851
- Low-cycle thermal fatigue
[NASA-TM-87225] p 177 N86-26651
- Effects of a high mean stress on the high cycle fatigue life of PWA 1480 and correlation of data by linear elastic fracture mechanics
[NASA-CR-175057] p 177 N86-27689
- CRACK TIPS**
- Analysis of an externally radially crack ring segment subject to three-point radial loading
p 167 A86-20710
- Re-examination of cumulative fatigue damage analysis: An engineering perspective
[NASA-TM-87325] p 177 N86-27680

CRACKING (FRACTURING)

- SCARE: A post-processor program to MSC/NASTRAN for the reliability analysis of structural ceramic components
[NASA-TM-87188] p 174 N86-14688
Compliance matrices for cracked bodies
[NASA-CR-179478] p 179 N86-30236

CRACKS

- Wide-range weight functions for the strip with a single edge crack p 167 A86-20709
J-integral estimates for cracks in infinite bodies
[NASA-CR-179474] p 178 N86-28467

CREEP ANALYSIS

- Fatigue crack propagation of nickel-base superalloys at 650 deg C p 87 N86-12294
Cyclic creep analysis from elastic finite-element solutions
[NASA-TM-87213] p 176 N86-25822

CREEP BUCKLING

- Effects of state recovery on creep buckling under variable loading
[NASA-CR-175094] p 212 N86-25310

CREEP PROPERTIES

- Constitutive modeling of cyclic plasticity and creep, using an internal time concept p 170 A86-41673
Creep-fatigue behavior of NiCoCrAlY coated PWA 1480 superalloy single crystals p 86 N86-10311
Creep fatigue life prediction for engine hot section materials (isotropic) p 174 N86-11521
An update of the total-strain version of SRP
[NASA-TP-2499] p 87 N86-12295
Time dependency of strainrange partitioning life relationships p 174 N86-13755
Development of constitutive models for cyclic plasticity and creep behavior of super alloys at high temperature
[NASA-CR-176418] p 88 N86-14356
Compressive creep behavior of alloys based on B2 FeAl p 92 N86-28165
Integrated research in constitutive modelling at elevated temperatures, part 2 p 178 N86-28455
Microstructure-property relationships in directionally solidified single crystal nickel-base superalloys
[NASA-TM-88788] p 93 N86-31700
Creep properties of PWC-11 base metal and weldments as affected by heat treatment p 93 N86-32557
[NASA-TM-88842]

CREEP RUPTURE STRENGTH

- Creep-rupture and fractographic analysis of Stirling engine superalloys tested in air and 15 MPa hydrogen p 82 A86-30041
High-pressure creep tests p 84 A86-46564
Creep rupture behavior of Stirling engine materials
[NASA-TM-87209] p 88 N86-15380
Creep-rupture behavior of iron superalloys in high-pressure hydrogen
[NASA-CR-175027] p 89 N86-17531
Heat treatment for superalloy
[NASA-CASE-LEW-14262-1] p 92 N86-26414

CREEP STRENGTH

- Alloys based on NiAl for high temperature applications p 84 A86-47261

CREEP TESTS

- Effect of multiple strain-anneal cycles on the 1000 C creep behaviour of gamma/gamma prime-alpha p 82 A86-30610
High-pressure creep tests p 84 A86-46564
Constitutive modeling for isotropic materials (HOST)
[NASA-CR-174980] p 172 N86-10589
Creep properties of PWC-11 base metal and weldments as affected by heat treatment p 93 N86-32557
[NASA-TM-88842]

CRITICAL PRESSURE

- Two-phase flows within systems with ambient pressure p 161 N86-30167

CROSS CORRELATION

- Measurement of ultrasonic velocity using phase-slope and cross-correlation methods p 162 A86-13192

CROSS COUPLING

- An analysis of cross-coupling of a multicomponent jet engine test stand using finite element modeling techniques
[NASA-CR-176424] p 37 N86-15323

CROSS FLOW

- Effect of free stream turbulence on flow separation p 125 A86-11676
Multispark flow visualization of lateral jet injection into a swirling cross flow p 1 A86-14561
Hot-wire measurements of a single lateral jet injected into swirling crossflow
[AIAA PAPER 86-0055] p 127 A86-19661

- An analytical model for the vorticity associated with a transverse jet p 4 A86-28538
Vortex modeling of single and multiple dilution jet mixing in a cross flow p 135 A86-46318
Perspectives on dilution jet mixing --- in creating temperature patterns at combustor exits in gas turbine engines p 25 A86-49614
[AIAA PAPER 86-1611]

- Turbine blade and vane heat flux sensor development, phase 2 p 26 N86-12226
[NASA-CR-174995]
Heat transfer characteristics within an array of impinging jets. Effects of crossflow temperature relative to jet temperature p 139 N86-15625
[NASA-CR-3936]

CROSSLINKING

- Replacement of MDA with more oxidatively stable diamines in PMR-polyimides p 101 N86-11275
The correlation of low-velocity impact resistance of graphite-fiber-reinforced composites with matrix properties p 71 N86-27426
[NASA-TM-87337]

CRUISE MISSILES

- Advanced technology payoffs for future rotorcraft, commuter aircraft, cruise missile, and APU propulsion systems p 16 A86-42704
[AIAA PAPER 86-1545]
Year 2000 small engine technology payoffs in cruise missiles p 23 A86-42705
[AIAA PAPER 86-1546]

CRYOGENIC EQUIPMENT

- Cryogenic operation of pseudomorphic AlGaAs/InGaAs single-quantum-well MODFETs p 117 A86-11998
Evaluation of a hybrid hydrostatic bearing for cryogenic turbopump application p 63 N86-31649
[NASA-TM-87255]
The noncavitating performance and life of a small vane-type positive displacement pump in liquid hydrogen
[NASA-TM-87347] p 63 N86-31651

CRYOGENIC FLUID STORAGE

- NASA Lewis Research Center low-gravity fluid management technology program p 44 A86-32906
Cryogenic Fluid Management Facility p 108 A86-37053
LH2 on-orbit storage tank support trunnion design and verification p 53 A86-37054
NASA Lewis Research Center low-gravity fluid management technology program p 44 N86-11218
[NASA-TM-87145]

CRYOGENIC FLUIDS

- NASA Lewis Research Center low-gravity fluid management technology program p 44 A86-32906
NASA Lewis Research Center low-gravity fluid management technology program p 44 N86-11218
[NASA-TM-87145]
SSME long-life bearings p 160 N86-27643
[NASA-CR-179455]

CRYOGENIC ROCKET PROPELLANTS

- Effect of subcooling on the on-orbit pressurization rate of cryogenic propellant tankage p 54 A86-39877
[AIAA PAPER 86-1253]
Small, two-stage, partial-admission turbine p 57 N86-17386
An experimental data base for material selection and design of high-speed, high-pressure, oxygen turbomachinery p 58 N86-17387
Oxidizer heat exchanger component testing
[NASA-CR-179487] p 62 N86-29901

CRYOGENIC WIND TUNNELS

- Experimental and analytical investigation of a freezing point depressant fluid ice protection system p 12 N86-27186
[NASA-CR-174758]

CRYOGENICS

- Mannating orbital transfer vehicle propulsion p 50 A86-14429
[AIAA PAPER 85-1226]
High-frequency noise of In(y)Ga(1-y)As/Al(x)Ga(1-x)As MODFETs and comparison to GaAs/Al(x)Ga(1-x)As MODFETs p 119 A86-43914
Passive eddy-current damping as a means of vibration control in cryogenic turbomachinery p 44 N86-24722
[NASA-TP-2562]

CRYSTAL DISLOCATIONS

- Dislocations in extruded Co-49.3 at. pct Al p 83 A86-45091

CRYSTAL GROWTH

- Computer simulation of thin-film nucleation and growth - The multilayer mode p 204 A86-37441
Transport processes in solution crystal growth p 39 N86-10107
Energy stability of thermocapillary convection in models of the float zone process p 40 N86-10123
Experimental and theoretical analysis of chemical vapor deposition with prediction of gravity effects p 41 N86-10132
Microgravity Materials Science Laboratory p 42 N86-10173

- Electrocrystallization in microgravity p 212 N86-19274
[NASA-TM-87202]
Low-cost single-crystal turbine blades, volume 2 p 29 N86-23598
[NASA-CR-174652]

CRYSTAL LATTICES

- Temperature dependence of gamma-gamma prime lattice mismatch in nickel-base superalloys p 81 A86-21849

CRYSTAL OPTICS

- The determination of the direction of the optic axis of uniaxial crystalline materials p 148 N86-22915
[NASA-TM-86892]

CRYSTAL STRUCTURE

- Frictional and morphological properties of Au-MoS2 films sputtered from a compact target p 152 A86-16258
High temperature properties of equiatomic FeAl with ternary additions p 84 A86-47252
The influence of grain size and composition on slow plastic flow in FeAl between 1100 and 1400 K p 86 A86-50279

- The continuing battle against defects in nickel-base superalloys p 93 N86-31701
[NASA-TM-87343]

- Effect of crystallographical and geometrical changes of a ferrite head on magnetic signals during the sliding process with magnetic tape p 106 N86-31728
[NASA-TM-87277]

CRYSTAL SURFACES

- Surface modification strategies for (100)3C-SiC p 76 A86-47083
The beta-SiC(100) surface studied by low energy electron diffraction, Auger electron spectroscopy, and electron energy loss spectra p 77 A86-49864

CRYSTALLINITY

- Abrasion and deformed layer formation of manganese-zinc ferrite in sliding contact with lapping tapes p 104 N86-24838
[NASA-TM-87249]

CRYSTALLITES

- Characterization of the tribological coating composition 77 wt % CaF2 - 23 wt % Li F fused to IN-750 alloy p 105 N86-27452
[NASA-TM-87342]

CRYSTALLIZATION

- Mechanical-contact-induced transformation from the amorphous to the partially crystalline state in metallic glass p 80 A86-16257
Effect of grain-boundary crystallization on the high-temperature strength of silicon nitride p 98 A86-33495

- Undercooling and solidification behavior in the InSb-Sb system p 88 N86-14355
[NASA-CR-175013]

- Electrocrystallization in microgravity p 212 N86-19274
[NASA-TM-87202]
Determination of solid mass fraction in partially frozen hydrocarbon fuels p 108 N86-28261
[NASA-CR-179472]

CUMULATIVE DAMAGE

- The crack layer approach to toughness characterization in steel p 82 A86-30010
Progressive fracture of fiber composites p 67 A86-35809

CURING

- Tetraglycidyl epoxy resins and graphite fiber composites cured with flexibilized aromatic diamines p 67 A86-36999

- PMR polyimides from solutions containing mixed endcaps p 100 N86-11263
Chemical control of rate and onset temperature of nadimide polymerization p 101 N86-11271
Characterization methodology for PMR-15 p 65 N86-11272

- Replacement of MDA with more oxidatively stable diamines in PMR-polyimides p 101 N86-11275
The 371 deg C mechanical properties of graphite/polyimide composites p 69 N86-12256
[NASA-TM-87122]

CURRENT CONVERTERS (AC TO DC)

- Input current shaped ac-to-dc converters
[NASA-CR-176438] p 121 N86-15544
Input-current shaped ac to dc converters
[NASA-CR-176787] p 123 N86-25693
Description of a 20 Kiloherzt power distribution system
[NASA-TM-87346] p 34 N86-31584

CURRENT DISTRIBUTION

- Description of a 20 Kiloherzt power distribution system
[NASA-TM-87346] p 34 N86-31584

CYCLIC LOADS

- Mode II fatigue crack growth specimen development p 171 A86-43566
Fatigue crack growth under general-yielding cyclic-loading p 171 A86-44339
Thermomechanical cyclic hardening behavior of Hastelloy-X p 174 N86-16610
[NASA-CR-174999]

- Cyclic structural analyses of anisotropic turbine blades for reusable space propulsion systems p 58 N86-17404
- Closure of fatigue cracks at high strains [NASA-CR-175021] p 175 N86-17788
- Fatigue crack growth under general-yielding cyclic-loading [NASA-CR-175049] p 176 N86-21951
- Cyclic creep analysis from elastic finite-element solutions [NASA-TM-87213] p 176 N86-25822
- Experimental evaluation criteria for constitutive models of time dependent cyclic plasticity [NASA-CR-176821] p 176 N86-25850
- Low-cycle thermal fatigue [NASA-TM-87225] p 177 N86-26651
- Ultrasonic stress wave characterization of composite materials [NASA-CR-3976] p 165 N86-27665
- Effects of a high mean stress on the high cycle fatigue life of PWA 1480 and correlation of data by linear elastic fracture mechanics [NASA-CR-175057] p 177 N86-27689
- Structural analysis of turbine blades using unified constitutive models [NASA-TM-88907] p 178 N86-28461
- CYLINDERS**
- Horseshoe vortex formation around a cylinder [ASME PAPER 86-GT-246] p 8 A86-48274
- Measurements of a turbulent horseshoe vortex formed around a cylinder [NASA-CR-3986] p 13 N86-28063
- CYLINDRICAL CHAMBERS**
- Concentration distributions in cylindrical combustors p 126 A86-11937
- CYLINDRICAL COORDINATES**
- Hybrid solid element with a traction-free cylindrical surface p 169 A86-34462

D

- DAMAGE**
- Progressive damage, fracture predictions and post mortem correlations for fiber composites [NASA-TM-87101] p 68 N86-10290
- DAMAGE ASSESSMENT**
- Nonlinear damage analysis: Postulate and evaluation [NASA-CR-168171] p 177 N86-26652
- Ultrasonic stress wave characterization of composite materials [NASA-CR-3976] p 165 N86-27665
- Re-examination of cumulative fatigue damage analysis: An engineering perspective [NASA-TM-87325] p 177 N86-27680
- DAMPING**
- Passive eddy-current damping as a means of vibration control in cryogenic turbomachinery [NASA-TP-2562] p 44 N86-24722
- DATA ACQUISITION**
- Measurement of the density of base fluids at pressures 0.422 to 2.20 GPa [NASA-TM-87114] p 156 N86-10551
- Measurements in liquid fuel sprays [NASA-CR-177088] p 144 N86-30960
- DATA BASE MANAGEMENT SYSTEMS**
- Spectrum orbit utilization program technical manual SOUP5 Version 3.8 [NASA-CR-174944] p 116 N86-28489
- DATA BASES**
- Operational maintenance data base development for kinematic Stirling engines [ASME PAPER 85-DGP-20] p 151 A86-14467
- Advanced turboprop vibratory characteristics [NASA-CR-174708] p 30 N86-24693
- Aerodynamic data banks for Clark-Y, NACA 4-digit and NACA 16-series airfoil families [NASA-CR-176883] p 13 N86-30693
- DATA FLOW ANALYSIS**
- Performance evaluation of a simulated data-flow computer with low-resolution actors p 194 A86-32051
- DECAY RATES**
- Rapid evaluation of ion thruster lifetime using optical emission spectroscopy [AIAA PAPER 85-2011] p 51 A86-17851
- Rapid evaluation of ion thruster lifetime using optical emission spectroscopy [NASA-TM-87103] p 56 N86-10280
- DEFECTS**
- Reliability of void detection in structural ceramics by use of scanning laser acoustic microscopy p 163 A86-39027
- Quantitative flaw characterization with scanning laser acoustic microscopy p 163 A86-45150
- Quantitative flaw characterization with scanning laser acoustic microscopy p 200 N86-22983

- The continuing battle against defects in nickel-base superalloys [NASA-TM-87343] p 93 N86-31701
- DEFLECTION**
- A comparison of electronic heterodyne moire deflectometry and electronic heterodyne holographic interferometry for flow measurements [SAE PAPER 851896] p 146 A86-38359
- DEFORMATION**
- Creep of chemically vapour deposited SiC fibres p 66 A86-21486
- The tensile and fatigue deformation structures in a single crystal Ni-base superalloy p 83 A86-35697
- A comparison of electronic heterodyne moire deflectometry and electronic heterodyne holographic interferometry for flow measurements [SAE PAPER 851896] p 146 A86-38359
- Bounding solutions of geometrically nonlinear viscoelastic problems [AIAA PAPER 86-0943] p 170 A86-38838
- Bounding solutions of geometrically nonlinear viscoelastic problems [NASA-CR-176219] p 195 N86-10860
- Fundamental studies of low velocity impact resistance of graphite fiber reinforced polymer matrix composites [NASA-TM-88886] p 69 N86-23661
- Yielding and deformation behavior of the single crystal nickel-base superalloy PWA 1480 [NASA-CR-175100] p 91 N86-25455
- Re-examination of cumulative fatigue damage analysis: An engineering perspective [NASA-TM-87325] p 177 N86-27680
- DEGRADATION**
- All-aromatic biphenylene end-capped polyquinoline and polyimide matrix resins p 100 N86-11267
- The effect of cobalt content in U-700 type alloys on degradation of aluminide coatings [NASA-TM-87173] p 87 N86-13408
- Mass loss of shuttle space suit orthofabric under simulated ionospheric atomic oxygen bombardment [NASA-TM-87149] p 192 N86-13899
- A thin film degradation study of a fluorinated polyether liquid lubricant using an HPLC method [NASA-TM-87221] p 77 N86-19417
- Analytical determination of propeller performance degradation due to ice accretion [NASA-CR-175092] p 15 N86-23577
- A study of Kapton degradation under simulated shuttle environment [NASA-CR-176850] p 78 N86-28136
- Effect of crystallographical and geometrical changes of a ferrite head on magnetic signals during the sliding process with magnetic tape [NASA-TM-87277] p 106 N86-31728
- DEICERS**
- A structural dynamics investigation related to EIDI applications --- Electro-Impulse Deicing [AIAA PAPER 86-0550] p 16 A86-19942
- NASA's aircraft icing analysis program p 14 A86-49107
- Piezoelectric deicing device [NASA-CASE-LEW-13773-2] p 122 N86-20671
- Analyses and tests for design of an electro-impulse de-icing system [NASA-CR-174919] p 15 N86-27268
- De-icing of the altitude wind tunnel turning vanes by electro-magnetic impulse [NASA-CR-177260] p 38 N86-27291
- NASA's Aircraft Icing Analysis Program [NASA-TM-88791] p 15 N86-31548
- DEICING**
- Designing an electro-impulse de-icing system [AIAA PAPER 86-0545] p 16 A86-19940
- A numerical and experimental investigation of electrochemical aircraft deicing [NASA-CR-175024] p 14 N86-20380
- Evaluation of capillary reinforced composites [NASA-CR-175061] p 70 N86-24760
- Theoretical analysis of the electrical aspects of the basic electro-impulse problem in aircraft de-icing applications [NASA-CR-176808] p 17 N86-26330
- Calibration of droplet sizing and liquid water content instruments: Survey and analysis [NASA-CR-175099] p 149 N86-26596
- Analyses and tests for design of an electro-impulse de-icing system [NASA-CR-174919] p 15 N86-27268
- DELAMINATING**
- A new ply model for interlaminar stress analysis p 66 A86-20629
- Dynamic delamination crack propagation in a graphite/epoxy laminate p 68 A86-43010

DELAY

- Methane oxidation behind reflected shock waves: Ignition delay times measured by pressure and flame band emission [NASA-TM-87268] p 77 N86-21635
- DENDRITIC CRYSTALS**
- The development and prevention of channel segregation during alloy solidification p 38 N86-10086
- Dendritic solidification in a binary alloy melt: Steady-state versus morphological stability theories p 42 N86-10261
- DENSIFICATION**
- Densification and properties of alpha-silicon carbide p 94 A86-12416
- DENSITY (MASS/VOLUME)**
- Light scattering tests of fundamental theories of transport properties in the critical region p 39 N86-10113
- Universality in the compressive behavior of solids [NASA-TM-87303] p 206 N86-28775
- DENSITY DISTRIBUTION**
- Vortex modeling of single and multiple dilution jet mixing in a cross flow p 135 A86-46318
- Flammability limits of gases under low gravity conditions p 42 N86-10164
- Correlation of processing and sintering variables with the strength and radiography of silicon nitride [NASA-TM-87251] p 106 N86-31729
- DENSITY MEASUREMENT**
- The plastic compressibility of 7075-T651 aluminum-alloy plate p 85 A86-49690
- Improved consolidation of silicon carbide [NASA-TM-87243] p 104 N86-24836
- DEPLOYMENT**
- Hybrid deployable/erectable solar dynamic box truss system [AIAA PAPER 86-0955] p 47 A86-38883
- DEPOLYMERIZATION**
- Effect of an oxygen plasma on the physical and chemical properties of several fluids for the liquid droplet radiator [NASA-TM-88839] p 49 N86-31634
- DEPOSITION**
- Dual-ion-beam deposition of carbon films with diamond-like properties p 65 A86-49855
- HOST liner cyclic facilities p 173 N86-11519
- Effect of argon and hydrogen on deposition of silicon from tetrochlorosilane in cold plasmas [NASA-TM-87219] p 65 N86-17472
- A computer program to calculate the resistivity of a thin film deposited on a conductive substrate from four-point probe measurements [NASA-TM-87262] p 193 N86-22150
- Numerical simulation of the flowfield over ice accretion shapes [NASA-CR-176960] p 144 N86-30093
- DEPOSITS**
- Long term deposit formation in aviation turbine fuel at elevated temperature [AIAA PAPER 86-0525] p 107 A86-19929
- Fuel deposit characteristics at low velocity [ASME PAPER 85-IGT-130] p 107 A86-23922
- Emission FTIR analyses of thin microscopic patches of jet fuel residues deposited on heated metal surfaces [NASA-CR-176786] p 108 N86-25502
- DERIVATION**
- Computer aided derivation of equations for composite mechanics problems and finite element analyses [AIAA PAPER 86-1016] p 170 A86-38873
- DESIGN ANALYSIS**
- Velocity and temperature decay characteristics of inverted-profile jets [AIAA PAPER 86-0312] p 2 A86-22693
- Inverse design of axisymmetric flow passages using compressible viscous flow theory p 4 A86-26412
- Rotary transformer design with fixed magnetizing and/or leakage inductances p 119 A86-40462
- Design considerations for advanced battery concepts [AIAA PAPER 86-1164] p 181 A86-40579
- High Temperature Polymer Matrix Composites [NASA-CP-2385] p 68 N86-11260
- Preliminary measurement of the noise from the 2/9 scale model of the Large-scale Advanced Propfan (LAP) propeller, SR-7A [NASA-TM-87116] p 199 N86-14006
- Velocity and temperature decay characteristics of inverted-profile jets [NASA-TM-87159] p 9 N86-14223
- Preliminary design of a supersonic cruise aircraft high-pressure turbine [NASA-CR-174878] p 26 N86-14272
- Gearing [NASA-RP-1152] p 157 N86-14612
- Onsite 40-kilowatt fuel cell power plant manufacturing and field test program [NASA-CR-174988] p 185 N86-18773

- Variable-reluctance motor drives for electric vehicle propulsion
[NASA-CR-176586] p 122 N86-20700
- Heat transfer to two-phase air/water mixtures flowing in small tubes with inlet disequilibrium
[NASA-CR-175076] p 141 N86-22892
- Extended parametric representation of compressor fans and turbines. Volume 1: CMGEN user's manual
[NASA-CR-174645] p 159 N86-23936
- Extended parametric representation of compressor fans and turbines. Volume 3: MODFAN user's manual (parametric modulating flow fan)
[NASA-CR-174647] p 159 N86-23938
- Designing a 25-kilowatt high frequency series resonant
[NASA-CR-176774] p 123 N86-24906
- Thermomechanical design criteria for ceramic-coated surfaces
[NASA-TM-87328] p 143 N86-25726
- Large-Scale Advanced Prop-Fan (LAP) pitch change actuator and control design report
[NASA-CR-174788] p 31 N86-27282
- Structural tailoring of engine blades (STAEBL) theoretical manual
[NASA-CR-175112] p 31 N86-27283
- Structural tailoring of engine blades (STAEBL) user's manual
[NASA-CR-175113] p 31 N86-27284
- New methodology for shaft design based on life expectancy
[NASA-TM-87354] p 161 N86-27661
- MOD-5A wind turbine generator program design report: Volume 1: Executive Summary
[NASA-CR-174734] p 188 N86-27708
- Transmission line design for a power distribution system at 20 kHz for aircraft
[NASA-CR-3987] p 32 N86-29818
- Double-injection, deep-impurity switch development
[NASA-CR-174936] p 124 N86-30073
- Design and initial testing of a one-bladed 30-meter-diameter rotor on the NASA/DOE mod-O wind turbine
[NASA-TM-88810] p 189 N86-30251
- Feasibility study for convertible engine torque converter
[NASA-CR-175082] p 33 N86-30733
- Design considerations for advanced battery concepts
[NASA-TM-87319] p 190 N86-31981
- DESORPTION**
- Thermal desorption study of physical forces at the PTFE surface
[NASA-TM-87090] p 206 N86-25284
- DESTRUCTIVE TESTS**
- Wide-range displacement expressions for standard fracture mechanics specimens p 166 N86-20706
- DETECTION**
- Radiographic detectability limits for seeded voids in sintered silicon carbide and silicon nitride
p 162 N86-31745
- Application of FDI metrics to detection and isolation of sensor failures in turbine engines p 21 N86-35400
- Reliability of scanning laser acoustic microscopy for detecting internal voids in structural ceramics
p 147 N86-46353
- Robust detection-isolation-accommodation for sensor failures
[NASA-CR-174797] p 121 N86-16486
- Reliability of scanning laser acoustic microscopy for detecting internal voids in structural ceramics
[NASA-TM-87222] p 164 N86-16599
- A real-time simulation evaluation of an advanced detection, isolation and accommodation algorithm for sensor failures in turbine engines
[NASA-TM-87289] p 30 N86-24697
- DIAMINES**
- Tetraglycidyl epoxy resins and graphite fiber composites cured with flexibilized aromatic diamines
p 67 N86-36999
- Replacement of MDA with more oxidatively stable diamines in PMR-polyimides p 101 N86-11275
- DIAMONDS**
- Thin film growth rate effects for primary ion beam deposited diamondlike carbon films p 100 N86-47068
- Diamondlike carbon films on semiconductors for insulated-gate technology p 120 N86-47077
- DIAPHRAGMS (MECHANICS)**
- Development of optical diaphragm deflection sensors
[NASA-CR-175008] p 203 N86-15113
- DICHROISM**
- Characteristics of an axisymmetric sudden expansion flow
[NASA-CR-176278] p 151 N86-11465
- DIELECTRICS**
- Input impedance of a probe-fed circular microstrip antenna with thick substrate p 120 N86-46638
- Diamondlike carbon films on semiconductors for insulated-gate technology p 120 N86-47077
- Auger electron spectroscopy, secondary ion mass spectroscopy and optical characterization of a-C-H and BN films
[NASA-TM-87258] p 206 N86-25268
- DIELS-ALDER REACTIONS**
- Chemical control of rate and onset temperature of nadimide polymerization p 101 N86-11271
- DIES**
- Improved consolidation of silicon carbide
[NASA-TM-87243] p 104 N86-24836
- DIESEL ENGINES**
- Life cycle cost assessment of future low heat rejection engines
[SAE PAPER 860444] p 153 N86-37048
- Lightweight two-stroke cycle aircraft diesel engine technology enablement program, volume 1
[NASA-CR-174923-VOL-1] p 26 N86-13328
- Lightweight two-stroke cycle aircraft diesel engine technology enablement program, volume 2
[NASA-CR-174923-VOL-2] p 26 N86-13329
- Lightweight two-stroke cycle aircraft diesel engine technology enablement program, volume 3
[NASA-CR-174923-VOL-3] p 26 N86-13330
- A computer simulation of the turbocharged turbo compounded diesel engine system: A description of the thermodynamic and heat transfer models
[NASA-CR-174971] p 208 N86-16164
- Long-term stability and properties of zirconia ceramics for heavy duty diesel engine components
[NASA-CR-174943] p 209 N86-17224
- Future heavy duty trucking engine requirements
[NASA-CR-174996] p 209 N86-17226
- Design and evaluation of fluidized bed heat recovery for diesel engine systems
[NASA-CR-174898] p 209 N86-21456
- Transformation toughened ceramics for the heavy duty diesel engine technology program, phase 2
[NASA-CR-175054] p 210 N86-22451
- Methods for heat transfer and temperature field analysis of the insulated diesel phase 2 progress report
[NASA-CR-175072] p 210 N86-24590
- Preliminary evaluation of a compound cycle engine for shipboard gensets
[NASA-CR-179451] p 180 N86-26629
- Sliding seal materials for adiabatic engines, phase 2
[NASA-CR-179475] p 105 N86-29042
- DIFFERENTIAL EQUATIONS**
- New integration techniques for chemical kinetic rate equations. II - Accuracy comparison
[ASME PAPER 85-GT-30] p 75 N86-32958
- DIFRACTION PROPAGATION**
- Quantitative flow characterization with scanning laser acoustic microscopy p 163 N86-45150
- Quantitative flow characterization with scanning laser acoustic microscopy p 200 N86-22983
- DIFFUSERS**
- A novel centrifugal diffuser test device
[ASME PAPER 85-IGT-135] p 3 N86-23927
- Comparison of analytical and experimental performance of a wind-tunnel diffuser section
[NASA-TM-88795] p 13 N86-31537
- DIFFUSION**
- Interdiffusional effects between tungsten fibers and an iron-nickel-base alloy p 66 N86-14718
- Determination of convective diffusion heat/mass transfer rates to burner rig test targets comparable in size to cross-stream jet diameter
[ASME PAPER 86-GT-68] p 136 N86-48140
- Application of a computational model for vortex generators in subsonic internal flows
[AIAA PAPER 86-1458] p 8 N86-49612
- Determination of convective diffusion heat/mass transfer rates to burner rig test targets comparable in size to cross-stream jet diameter
[NASA-TM-87176] p 138 N86-13678
- Comparison of calculated and experimental cascade performance for controlled-diffusion compressor stator blading
[NASA-TM-87167] p 27 N86-16219
- Experiments for the determination of convective diffusion heat/mass transfer to burner rig test targets comparable in size to jet stream diameter
[NASA-TM-87196] p 139 N86-18646
- Application of a computational model for vortex generators in subsonic internal flows
[NASA-TM-87327] p 143 N86-26545
- The evolution and growth of Al₂O₃ scales on beta-NiAl
[NASA-CR-175097] p 92 N86-27444
- DIFFUSION FLAMES**
- Effects of buoyancy on gas jet diffusion flames - Experiment and theory
[IAF PAPER 85-288] p 72 N86-15804
- Temperature and velocity profiles in sooting free boundary layer flames
[AIAA PAPER 86-0575] p 73 N86-19962
- Drop-turbulence interactions in a diffusion flame
p 73 N86-20139
- Effects of preferential diffusion on the burning intensity of curved flames p 73 N86-22813
- Buoyancy effects upon vapor flame and explosion processes p 41 N86-10161
- Diffusion flame extinction in slow convective flow under microgravity environment
[NASA-TM-88799] p 144 N86-28378
- DIFFUSION PUMPS**
- Liquid belt radiator design study
[NASA-CR-174901] p 57 N86-16259
- DIFFUSION THEORY**
- Grid-free simulation of diffusion using random walk methods p 196 N86-16521
- DIFFUSIVITY**
- The reactions of cobalt, iron and nickel in SO₂ atmospheres Similarities and differences p 75 N86-40677
- DIGITAL FILTERS**
- Numerical synthesis of tri-variate velocity realizations of turbulence p 168 N86-28654
- Linearization of digital derived rate algorithm for use in linear stability analysis p 47 N86-35338
- DIGITAL SIMULATION**
- Error-source effects in a high-accuracy optical finite-element processor p 192 N86-31571
- Simulating a small turboshaft engine in real-time multiprocessor simulator (RTMPS) environment
[NASA-TM-87216] p 27 N86-16221
- DIGITAL SYSTEMS**
- Fiber optics for propulsion control systems
[ASME PAPER 84-GT-97] p 17 N86-13054
- HYTESS 2: A Hypothetical Turbofan Engine Simplified Simulation with multivariable control and sensor analytical redundancy
[NASA-TM-87344] p 124 N86-30068
- DIGITAL TRANSDUCERS**
- Wavelength-division multiplexed digital optical position transducer p 145 N86-20798
- DILUTION**
- Modeling dilution of jet flowfields p 128 N86-20362
- Dilution jet mixing program, supplementary report
[NASA-CR-175043] p 141 N86-23856
- Perspectives on dilution jet mixing
[NASA-TM-87294] p 35 N86-32432
- DIMENSIONAL MEASUREMENT**
- Polarization modulated ellipsometry
[NASA-CR-177264] p 149 N86-26599
- DIMENSIONAL STABILITY**
- Fiber composite sandwich thermostructural behavior: Computational simulation
[NASA-TM-88787] p 71 N86-31663
- DIMENSIONLESS NUMBERS**
- A fundamental study of smoldering with emphasis on experimental design for zero-g p 41 N86-10162
- DIRECT CURRENT**
- Performance analysis of radiation cooled dc transmission lines for high power space systems
p 117 N86-24811
- Low power dc arcjet operation with hydrogen/nitrogen propellant mixtures
[AIAA PAPER 86-1505] p 55 N86-42676
- Power electronics for a 1-kilowatt arcjet thruster
[AIAA PAPER 86-1507] p 56 N86-49613
- Lower power dc arcjet operations with hydrogen hydrogen/nitrogen propellant mixtures
[NASA-TM-87279] p 61 N86-25407
- Power electronics for a 1-kilowatt arc jet thruster
[NASA-TM-87340] p 61 N86-25409
- DIRECTIONAL SOLIDIFICATION (CRYSTALS)**
- Dendritic solidification in a binary alloy melt: Steady-state versus morphological stability theories
p 42 N86-10261
- Microstructure-property relationships in directionally solidified single crystal nickel-base superalloys
[NASA-TM-88788] p 93 N86-31700
- DISPENSERS**
- Thermionic noise measurements for on-line dispenser cathode diagnostics for linear beam microwave tubes
[NASA-CR-175105] p 124 N86-28323
- DISPENSING**
- Turbulent dispersion of the icing cloud from spray nozzles used in icing tunnels
[NASA-TM-87316] p 34 N86-31588
- DISPERSIONS**
- Effect of stress on ultrasonic pulses in fiber reinforced composites p 200 N86-22975
- Analysis of the Gas Particle Radiator (GPR)
[NASA-TM-88786] p 63 N86-31652
- DISPLACEMENT**
- Wide-range displacement expressions for standard fracture mechanics specimens p 166 N86-20706

- Wave propagation in anisotropic medium due to an oscillatory point source with application to unidirectional composites
[NASA-CR-4001] p 165 N86-27866
- Parametric study of beam refraction problems across laser anemometer windows
[NASA-TM-87350] p 150 N86-31857
- DISPLACEMENT MEASUREMENT**
- A study of the stress wave factor technique for nondestructive evaluation of composite materials
[NASA-CR-4002] p 165 N86-28445
- Advanced optical measuring systems for measuring the properties of fluids and structures
[NASA-TM-88829] p 150 N86-31859
- DISSOLVED GASES**
- Mass transport phenomena between bubbles and dissolved gases in liquids under reduced gravity conditions p 39 N86-10110
- DISSOLVING**
- Molten salt corrosion of SiC: Pitting mechanism
[NASA-TM-87143] p 101 N86-12310
- DISTRIBUTION FUNCTIONS**
- Determination of grain size distribution function using two-dimensional Fourier transforms of tone pulse encoded images
[NASA-TM-88790] p 166 N86-31065
- DOCUMENTATION**
- Documentation of ice shapes accreted on the main rotor of a UH-1H helicopter in level flight
[NASA-CR-175088] p 15 N86-22559
- Bibliography of Lewis Research Center technical publications announced in 1985
[NASA-TM-87263] p 208 N86-32336
- DOMAINS**
- Time domain referencing in intensity modulation fiber optic sensing systems
[NASA-CR-175109] p 17 N86-24691
- DONOR MATERIALS**
- Compensation in epitaxial cubic SiC films
[NASA-TM-87269] p 206 N86-25267
- DOPED CRYSTALS**
- The effect of a defective BSF layer on solar cell open circuit voltage --- Back Surface Field p 179 N86-12673
- DOPES**
- Lithium counterdoped silicon solar cell
[NASA-CASE-LEW-14177-1] p 190 N86-32875
- DOPPLER EFFECT**
- Filter induced errors in laser anemometry using counter-processor p 146 N86-34431
- DOWNLINKING**
- Spacecraft multibeam antenna system for 30/20 GHz
[NASA-CR-174654] p 116 N86-31760
- DOWNWASH**
- Some design philosophy for reducing the community noise of advanced counter-rotation propellers
[NASA-TM-87099] p 199 N86-14007
- DROP SIZE**
- Effect of elevated temperature and pressure on sprays from simplex swirl atomizers
[ASME PAPER 85-GT-58] p 130 N86-22735
- Study of ice accretion on icing wind tunnel components
[AIAA PAPER 86-0290] p 36 N86-26620
- Analysis of the effects of fuel spray characteristics on NO(x) formation
[ASME PAPER 85-WA/HT-47] p 107 N86-38394
- Oxides of nitrogen emissions from the combustion of monodisperse liquid fuel sprays
[NASA-CR-176373] p 191 N86-14770
- Study of ice accretion on icing wind tunnel components
[NASA-TM-87095] p 37 N86-16232
- Measurements in liquid fuel sprays
[NASA-CR-177088] p 144 N86-30960
- DROP TESTS**
- Graphite/PMR polyimide composites with improved toughness p 66 N86-21731
- Ignition and flame spread above liquid fuel pools p 41 N86-10163
- DROPS (LIQUIDS)**
- Structure of nonevaporating sprays. II - Drop and turbulence properties p 125 N86-11237
- Drop-turbulence interactions in a diffusion flame p 73 N86-20139
- Experimental study of the spray characteristics of a research airblast atomizer
[ASME PAPER 85-GT-229] p 129 N86-22125
- Formation and characterization of simulated small droplet icing clouds
[AIAA PAPER 86-0409] p 145 N86-22700
- Spray atomization and combustion
[AIAA PAPER 86-0136] p 131 N86-26606
- Analysis of the effects of fuel spray characteristics on NO(x) formation
[ASME PAPER 85-WA/HT-47] p 107 N86-38394

- Liquid droplet radiator thermal characteristics
[AIAA PAPER 86-1162] p 133 N86-40578
- Characterization of simulated small-droplet fuel sprays
[AIAA PAPER 86-1725] p 135 N86-42813
- Liquid droplet radiator program at the NASA Lewis Research Center
[ASME PAPER 86-HT-15] p 48 N86-49621
- Fundamental studies of droplet combustion at reduced gravity p 42 N86-10165
- Liquid droplet radiator program at the NASA Lewis Research Center
[NASA-TM-87139] p 48 N86-12246
- Formation and characterization of simulated small droplet icing clouds
[NASA-TM-87180] p 148 N86-14554
- Organosiloxane working fluids for the liquid droplet radiator
[NASA-CR-175033] p 102 N86-16381
- Effect of liquid droplets on turbulence in a round gaseous jet
[NASA-CR-175063] p 29 N86-23597
- Characterization of simulated small-droplet fuel sprays
[NASA-TM-87286] p 148 N86-24961
- Calibration of droplet sizing and liquid water content instruments: Survey and analysis
[NASA-CR-175099] p 149 N86-26596
- DRY FRICTION**
- Influence of friction dampers on torsional blade flutter
[ASME PAPER 85-GT-170] p 21 N86-32957
- Frequency domain solutions to multi-degree-of-freedom, dry friction damped systems under periodic excitation p 170 N86-39485
- DUCTED FLOW**
- Numerical and experimental investigation of nonswirling and swirling confined jets
[AIAA PAPER 86-0040] p 127 N86-19651
- Modeling dilution of jet flowfields p 128 N86-20362
- Non-linear effects in finite amplitude wave propagation through ducts and nozzles p 197 N86-35857
- Assessment of a parabolic analysis for axisymmetric internal flows in rocket and turbomachinery ducts
[AIAA PAPER 86-1598] p 134 N86-42739
- A space-marching method for viscous incompressible internal flows p 135 N86-43037
- Computation of turbulent flows on rotating bodies and ducts p 135 N86-46307
- Flow visualization of secondary flows in three curve ducts
[ASME PAPER 86-GT-166] p 136 N86-48218
- Gas flow environmental and heat transfer nonrotating 3D program p 137 N86-11506
- Thermodynamic evaluation of transonic compressor rotors using the finite volume approach p 27 N86-16220
- Mean velocity and turbulence measurements in a 90 deg curved duct with thin inlet boundary layer
[NASA-CR-174811] p 139 N86-16518
- NASA/DOE automotive Stirling engine project: Overview 1986
[NASA-TM-87345] p 211 N86-29731
- Thermodynamic evaluation of transonic compressor rotors using the finite volume approach
[NASA-CR-176947] p 32 N86-30731
- DUCTILITY**
- The effects of grain size on the flow and fracture of long-range ordered alloys p 84 N86-47243
- Tensile behavior of Fe-40Al alloys with B and Zr additions
[NASA-TM-87290] p 91 N86-25453
- DURABILITY**
- Structural integrity and durability for Space Shuttle main engine and future reusable space propulsion systems
[AIAA PAPER 86-1513] p 55 N86-42682
- Gas side heat transfer p 138 N86-11507
- Structural integrity and durability for Space Shuttle main engine and future reusable space propulsion systems
[NASA-TM-87280] p 61 N86-25408
- DYNAMIC CHARACTERISTICS**
- Modal test/analysis correlation for Centaur G Prime launch vehicle
[AIAA PAPER 86-1002] p 43 N86-38943
- Reliability and mass analysis of dynamic power conversion systems with parallel of standby redundancy
[NASA-TM-87189] p 57 N86-16258
- Review and evaluation of recent developments in melic inlet dynamic flow distortion prediction and computer program documentation and user's manual estimating maximum instantaneous inlet flow distortion from steady-state total pressure measurements with full, limited, or no dynamic data
[NASA-CR-176765] p 143 N86-24955
- DYNAMIC LOADS**
- Theoretical modeling of the vapor cavitation in dynamically loaded journal bearings
[ASME PAPER 85-TRIB-51] p 130 N86-24496

- Torsional vibrations and dynamic loads in a basic planetary gear system p 156 N86-47354
- Theoretical modeling of the vapor cavitation in dynamically loaded journal bearings
[NASA-TM-87076] p 137 N86-10463
- Study of journal bearing dynamics using 3-dimensional motion picture graphics
[NASA-TM-87205] p 140 N86-18647
- Dynamic loading on parallel shaft gears
[NASA-CR-179473] p 161 N86-28433
- DYNAMIC MODELS**
- Development and application of dynamic simulations of a subsonic wind tunnel
[NASA-TM-87211] p 43 N86-18338
- Burner liner thermal/structural load modeling: TRANCITS program user's manual
[NASA-CR-174891] p 142 N86-24931
- DYNAMIC RESPONSE**
- The dynamics of a flexible bladed disc on a flexible rotor in a two-rotor system p 20 N86-25743
- Dynamic response of film thickness in spiral-groove face seals
[NASA-TP-2544] p 27 N86-15313
- Extensions of the Ritz-Galerkin method for the forced, damped vibrations of structural elements p 176 N86-21909
- Dynamic loading on parallel shaft gears
[NASA-CR-179473] p 161 N86-28433
- DYNAMIC STRUCTURAL ANALYSIS**
- A structural dynamics investigation related to EIDI applications --- Electro-Impulse Deicing p 16 N86-19942
- Aeroelastic formulations for turbomachines and propellers p 20 N86-24677
- Hierarchical implicit dynamic least-square solution algorithm p 167 N86-26689
- The effects of strong shock loading on coupled bending-torsion flutter of tuned and mistuned cascades p 20 N86-26893
- Vibrations of blades and bladed disk assemblies; Proceedings of the Tenth Biennial Conference on Mechanical Vibration and Noise, Cincinnati, OH, September 10-13, 1985 p 20 N86-26901
- The effect of limiting aerodynamic and structural coupling in models of mistuned bladed disk vibration p 21 N86-26905
- Probabilistic finite elements for transient analysis in nonlinear continua p 168 N86-28653
- Efficient algorithms for use in probabilistic finite element analysis p 168 N86-28655
- Dynamic characteristics of an assembly of prop-fan blades
[ASME PAPER 85-GT-134] p 21 N86-32956
- Advanced three-dimensional dynamic analysis by boundary element methods p 169 N86-34445
- Parameter sensitivity in the dynamics of rotor-bearing systems
[ASME PAPER 85-DET-35] p 154 N86-38620
- NASA LeRC/Akron University Graduate Cooperative Fellowship Program and Graduate Student Researchers Program p 207 N86-13219
- An analysis of cross-coupling of a multicomponent jet engine test stand using finite element modeling techniques
[NASA-CR-176424] p 37 N86-15323
- Extensions of the Ritz-Galerkin method for the forced, damped vibrations of structural elements p 176 N86-21909
- Advanced turboprop vibratory characteristics
[NASA-CR-174708] p 30 N86-24693
- Burner liner thermal/structural load modeling: TRANCITS program user's manual
[NASA-CR-174891] p 142 N86-24931
- Theoretical and software considerations for general dynamic analysis using multilevel substructured models
[NASA-CR-176822] p 195 N86-28067
- Identification of differences between finite element analysis and experimental vibration data
[NASA-TM-87336] p 149 N86-27617
- Structural dynamic measurement practices for turbomachinery at the NASA Lewis Research Center
[NASA-TM-88857] p 35 N86-32433
- DYNAMICAL SYSTEMS**
- Hierarchical implicit dynamic least-square solution algorithm p 167 N86-26689
- Polynomial nonlinear dynamical systems - A residual sensitivity method for model reduction p 194 N86-35386
- Linear dynamic coupling in geared rotor systems
[ASME PAPER 85-DET-11] p 154 N86-38617
- DYNAMICS**
- A comparison of experimental and theoretical results for leakage, pressure gradients, and rotordynamic coefficients for tapered annular gas seal
[NASA-CR-179709] p 162 N86-32742

E

EARTH (PLANET)

- Research and competition: Best partners
[NASA-TM-87313] p 212 N86-25321

EARTH IONOSPHERE

- Mass loss of shuttle space suit orthofabric under simulated ionospheric atomic oxygen bombardment
[NASA-TM-87149] p 192 N86-13899

EARTH ORBITAL ENVIRONMENTS

- Circuit transients due to negative bias arcs-III — on solar cell power systems in low earth orbit
[AIAA PAPER 86-0366] p 52 A86-19835
- Bipolar nickel-hydrogen battery development
p 180 A86-24823

- Organosiloxane working fluids for the liquid droplet radiator
[NASA-CR-175033] p 102 N86-16381

EARTH ORBITS

- Development of the VOLT-A shuttle experiment
[NASA-TM-87189] p 212 N86-14110
- Radiation exposure and performance of multiple burn LEO-GEO orbit transfer trajectories p 43 N86-17417
- The voltage threshold for arcing for solar cells in LEO: Flight and ground test results
[NASA-TM-87259] p 62 N86-28125

EARTH PLANETARY STRUCTURE

- Wilson study cycles: Research relative to ocean geodynamic cycles
[NASA-CR-178560] p 192 N86-21082

ECONOMIC ANALYSIS

- Evaluation of spacecraft technology programs (effects on communication satellite business ventures), volume 1
[NASA-CR-174978] p 112 N86-16451

EDDY CURRENTS

- Passive eddy-current damping as a means of vibration control in cryogenic turbomachinery
[NASA-TP-2562] p 44 N86-24722

EDGE DISLOCATIONS

- Orientation and temperature dependence of some mechanical properties of the single-crystal nickel-base superalloy Rene N4. I - Tensile behavior
p 86 A86-50321

EDGES

- Wide-range weight functions for the strip with a single edge crack
p 167 A86-20709

EDUCATION

- NASA Lewis Research Center/university graduate research program on engine structures
[ASME PAPER 85-GT-159] p 167 A86-22084

EFFECTS

- Effect of argon and hydrogen on deposition of silicon from tetrachlorosilane in cold plasmas
[NASA-TM-87219] p 65 N86-17472

EFFICIENCY

- An experimental method for measuring droplet impingement efficiency on two- and three-dimensional bodies
[AIAA PAPER 86-0406] p 131 A86-26630
- Efficiency of nonstandard and high contact ratio involute spur gears
[ASME PAPER 84-DET-172] p 155 A86-45255
- Space Photovoltaic Research and Technology 1985: High Efficiency, Space Environment, and Array Technology
[NASA-CP-2408] p 184 N86-17839
- A 20 kilohertz space station power system
[NASA-TM-88801] p 62 N86-28122

EIGENVALUES

- Theoretical and software considerations for general dynamic analysis using multilevel substructured models
[NASA-CR-176822] p 195 N86-26067

EJECTORS

- Forced mixer lobes in ejector designs
[AIAA PAPER 86-1614] p 134 A86-42752

ELASTIC BENDING

- Influence of third-degree geometric nonlinearities on the vibration and stability of pretwisted, precone, rotating blades
[NASA-TM-87307] p 179 N86-31920

ELASTIC DEFORMATION

- Fundamental tribological properties of ceramics
p 95 A86-15230
- Analysis of large, non-isothermal elastic-visco-plastic deformations
[NASA-CR-178220] p 172 N86-10588
- Lubrication of nonconformal contacts
[NASA-TM-87120] p 138 N86-13679
- Formulation of the nonlinear analysis of shell-like structures, subjected to time-dependent mechanical and thermal loading
[NASA-CR-177194] p 178 N86-28462

ELASTIC PROPERTIES

- Existence and stability, and discrete BB and rank conditions, for general mixed-hybrid finite elements in elasticity
p 169 A86-34464

The 371 deg C mechanical properties of graphite/polyimide composites
[NASA-TM-87122] p 69 N86-12256

Simplified cyclic structural analyses of SSME turbine blades
[NASA-TM-87214] p 175 N86-16615

Constitutive modelling of lubricants in concentrated contacts at high slide to roll ratios
[NASA-CR-175029] p 158 N86-17748

Cyclic creep analysis from elastic finite-element solutions
[NASA-TM-87213] p 176 N86-25822

Effects of a high mean stress on the high cycle fatigue life of PWA 1480 and correlation of data by linear elastic fracture mechanics
[NASA-CR-175057] p 177 N86-27689

ELASTIC WAVES

Wave propagation in anisotropic medium due to an oscillatory point source with application to unidirectional composites
[NASA-CR-4001] p 165 N86-27666

ELASTODYNAMICS

Optical and other properties changes of M-50 bearing steel surfaces for different lubricants and additives prior to scuffing
p 97 A86-20435

ELASTOHYDRODYNAMICS

Ellipsometric surface analysis of wear tracks produced by different lubricants
[ASLE PREPRINT 85-TC-5A-2] p 151 A86-11016

Operating aspects of an oil pumping ring seal
[ASME PAPER 85-TRIB-29] p 153 A86-34010

Fast approach for calculating film thicknesses and pressures in elastohydrodynamically lubricated contacts at high loads
[ASME PAPER 85-TRIB-42] p 155 A86-43541

Measurement of the density of base fluids at pressures 0.422 to 2.20 GPa
[NASA-TM-87114] p 156 N86-10551

A model for the influence of pressure on the bulk modulus and the influence of temperature on the solidification pressure for liquid lubricants
[NASA-TM-87230] p 140 N86-19555

Starvation effects on the hydrodynamic lubrication of rigid nonconformal contacts in combined rolling and normal motion
[NASA-TM-87174] p 140 N86-19556

ELASTOPLASTICITY

J-integral estimates for cracks in infinite bodies
[NASA-CR-179474] p 178 N86-28467

ELASTOSTATICS

Efficient algorithms for use in probabilistic finite element analysis
p 168 A86-28655

ELECTRIC ARCS

Threshold determining mechanisms for discharges in high voltage solar arrays
[AIAA PAPER 86-0364] p 52 A86-19834

Circuit transients due to negative bias arcs-III — on solar cell power systems in low earth orbit
[AIAA PAPER 86-0366] p 52 A86-19835

The voltage threshold for arcing for solar cells in LEO: Flight and ground test results
[NASA-TM-87259] p 62 N86-28125

ELECTRIC BATTERIES

Photovoltaic-powered vaccine refrigerator: Freezer systems field test results
[NASA-TM-86972-REV] p 181 N86-11666

ELECTRIC CHARGE

KOH concentration effect on the cycle life of nickel-hydrogen cells
p 180 A86-24802

ELECTRIC CONTACTS

Surface modification strategies for (100)3C-SiC
p 76 A86-47083

ELECTRIC CURRENT

Current collection from the space plasma through defects in solar array insulation
p 52 A86-18042

Theoretical analysis of the electrical aspects of the basic electro-impulse problem in aircraft de-icing applications
[NASA-CR-176808] p 17 N86-26330

ELECTRIC DISCHARGES

KOH concentration effect on the cycle life of nickel-hydrogen cells
p 180 A86-24802

The role of unneutralized surface ions in negative potential arcing
p 118 A86-25525

ELECTRIC ENERGY STORAGE

Cycling performance of the iron-chromium redox energy storage system
p 180 A86-24849

Input-current shaped ac to dc converters
[NASA-CR-176787] p 123 N86-25693

ELECTRIC EQUIPMENT

Photovoltaic systems in remote locations: An experience summary
[NASA-TM-87106] p 181 N86-10643

ELECTRIC FIELDS

Radiation damage in high-resistivity silicon solar cells
p 185 N86-17856

ELECTRIC FILTERS

Input current shaped ac-to-dc converters
[NASA-CR-176438] p 121 N86-15544

ELECTRIC GENERATORS

A mathematical model for the doubly-fed wound rotor generator. II
p 119 A86-39472

Photovoltaic systems in remote locations: An experience summary
[NASA-TM-87106] p 181 N86-10643

Technology for Bayton-cycle powerplants using solar and nuclear energy
[NASA-TP-2558] p 60 N86-21577

ELECTRIC MOTOR VEHICLES

Variable-reluctance motor drives for electric vehicle propulsion
[NASA-CR-178566] p 122 N86-20700

ELECTRIC POTENTIAL

The role of unneutralized surface ions in negative potential arcing
p 118 A86-25525

Voltage-controlling mechanisms in low-resistivity silicon solar cells - A unified approach
p 120 A86-45195

Verification of computer-aided designs of traveling-wave tubes utilizing novel dynamic refocusers and graphite electrodes for the multistage depressed collector
[NASA-TP-2524] p 121 N86-13643

Principles for system level electrochemistry
[NASA-TM-87283] p 187 N86-25039

A mathematical approach for evaluating nickel-hydrogen cells
[NASA-TM-88803] p 78 N86-31680

ELECTRIC POWER

Ceramic thermal barrier coatings for electric utility gas turbine engines
[NASA-TM-87288] p 90 N86-22687

ELECTRIC POWER PLANTS

Description and test results of a variable speed, constant frequency generating system
[NASA-TM-87181] p 121 N86-16487

Advanced on-site power plant development technology program
[NASA-CR-174709] p 187 N86-25040

ELECTRIC POWER SUPPLIES

Development of the power system for the United States' Manned Space Station
p 207 A86-24798

Performance and endurance tests of a multipropellant resistojet for space station auxiliary propulsion
[AIAA PAPER 86-1435] p 55 A86-42640

Space station 20-kHz power management and distribution system
[NASA-TM-87314] p 60 N86-24747

Performance and endurance tests of a multipropellant resistojet for space station auxiliary propulsion
[NASA-TM-87278] p 60 N86-24748

Input-current shaped ac to dc converters
[NASA-CR-176787] p 123 N86-25693

ELECTRIC POWER TRANSMISSION

Inverter design for high frequency power distribution
p 117 A86-24831

ELECTRIC PROPULSION

Primary propulsion of electrothermal, ion, and chemical systems for space-based radar orbit transfer
[AIAA PAPER 85-1477] p 50 A86-14431

NASA electric propulsion technology
[AIAA PAPER 85-1999] p 51 A86-17831

An experimental study of energy loss mechanisms and efficiency considerations in the low power dc arcjet
[AIAA PAPER 85-2017] p 53 A86-37062

Experimental performance of a 1-kilowatt arcjet thruster
[AIAA PAPER 85-2033] p 54 A86-37063

Experimental performance of a 1-kilowatt arcjet thruster
[NASA-TM-87131] p 57 N86-10281

An experimental study of energy loss mechanisms and efficiency consideration in the low power dc arcjet
[NASA-TM-87123] p 57 N86-11224

A bibliography of electrothermal thruster technology, 1984
[NASA-TM-86998] p 60 N86-21578

ELECTRIC PULSES

Designing an electro-impulse de-icing system
[AIAA PAPER 86-0545] p 16 A86-19940

De-icing of the altitude wind tunnel turning vanes by electro-magnetic impulse
[NASA-CR-177260] p 38 N86-27291

ELECTRICAL FAULTS

Mass spectrometric studies of the electrical breakdown of thin polymer films
p 100 A86-47070

ELECTRICAL IMPEDANCE

Input impedance of a probe-fed circular microstrip antenna with thick substrate
p 120 A86-46638

ELECTRICAL INSULATION

Numerical methods for analyzing electromagnetic scattering
[NASA-CR-176141] p 111 N86-10377

ELECTRICAL MEASUREMENT

Convenient mounting method for electrical measurements of thin samples p 120 A86-46649
AC motor and generator requirements for isolated WECS

[NASA-CR-176315] p 182 N86-11670
The role of service areas in the optimization of FSS orbital and frequency assignments
[NASA-CR-176488] p 46 N86-18341
Apparatus for electrical measurements of thin films from 77 to 1000 K
[NASA-TM-87256] p 148 N86-24959

ELECTRICAL PROPERTIES

Optical and interfacial electronic properties of diamond-like carbon films p 204 A86-16268

ELECTRICAL RESISTANCE

High temperature static strain sensor development program p 148 N86-11500
Demonstration test of burner liner strain measurement systems: Interim results p 173 N86-11501

ELECTRICAL RESISTIVITY

Voltage-controlling mechanisms in low-resistivity silicon solar cells - A unified approach p 120 A86-45195
Radiation damage in high-resistivity silicon solar cells p 185 N86-17856

A computer program to calculate the resistivity of a thin film deposited on a conductive substrate from four-point probe measurements
[NASA-TM-87262] p 193 N86-22150

The milling of pristine and brominated P-100 graphite fibers
[NASA-TM-88828] p 106 N86-32573

ELECTROCATALYSTS

Transmission electron microscopic examination of phosphoric acid fuel cell components

p 74 A86-23352
Develop and test fuel cell powered on-site integrated total energy systems: Phase 3, full-scale power plant development
[NASA-CR-174948] p 182 N86-12757
Develop and test fuel cell powered on-site integrated total energy systems: Phase 3, full-scale power plant development
[NASA-CR-174998] p 182 N86-12758

ELECTROCHEMICAL CELLS

Simulation of lubricating behavior of a thioether liquid lubricant by an electrochemical method

p 97 A86-20437
Cycling performance of the iron-chromium redox energy storage system p 180 A86-24849
Method and apparatus for rebalancing a REDOX flow cell system

[NASA-CASE-LEW-14127-1] p 122 N86-20680
Principles for system level electrochemistry

[NASA-TM-87283] p 187 N86-25039
Advanced on-site power plant development technology program

[NASA-CR-175007] p 189 N86-29411

ELECTROCHEMISTRY

Electrocrystallization in microgravity
[NASA-TM-87202] p 212 N86-19274

Lightweight nickel electrode for nickel hydrogen cells and batteries
[NASA-TM-87253] p 186 N86-21978
Principles for system level electrochemistry
[NASA-TM-87283] p 187 N86-25039

ELECTRODE MATERIALS

KOH concentration effect on the cycle life of nickel-hydrogen cells p 180 A86-24802

Effect of impregnation method on cycle life of the nickel electrode
[NASA-TM-87326] p 190 N86-31980

ELECTRODEPOSITION

Film and interstitial formation of metals in plasma-sprayed ceramics p 96 A86-17484

Long life nickel electrodes for a nickel-hydrogen cell: Cycle life tests
[NASA-CR-174815] p 188 N86-25046

ELECTRODES

Electrode erosion in arc discharges at atmospheric pressure
[AIAA PAPER 85-2018] p 50 A86-14445

Bipolar nickel-hydrogen battery development p 180 A86-24823

An experimental study of energy loss mechanisms and efficiency considerations in the low power dc arcjet
[AIAA PAPER 85-2017] p 53 A86-37062

An experimental study of energy loss mechanisms and efficiency consideration in the low power dc arcjet
[NASA-TM-87123] p 57 N86-11224

Evaluation parameters for the alkaline fuel cell oxygen electrode
[NASA-TM-87155] p 77 N86-12268

Verification of computer-aided designs of traveling-wave tubes utilizing novel dynamic refocusers and graphite electrodes for the multistage depressed collector
[NASA-TP-2524] p 121 N86-13643

Structure-property characterization of rheocast and VADER processed IN-100 superalloy
[NASA-CR-175014] p 88 N86-14354

Negative electrode catalyst for the iron chromium redox energy storage system
[NASA-CASE-LEW-14028-1] p 186 N86-19721

Assessment of commercially available and experimental hydrogen electrodes
[NASA-TM-87264] p 187 N86-23035

Long life nickel electrodes for a nickel-hydrogen cell: Cycle life tests
[NASA-CR-174815] p 188 N86-25046

Effect of impregnation method on cycle life of the nickel electrode
[NASA-TM-87326] p 190 N86-31980

Secondary-electron-emission losses in multistage depressed collectors and traveling-wave-tube efficiency improvements with carbon collector electrode surfaces
[NASA-TP-2622] p 125 N86-32629

ELECTRODYNAMICS

Analyses and tests for design of an electro-impulse de-icing system
[NASA-CR-174919] p 15 N86-27268

Electrodynamic tether technology considerations p 161 N86-27657

ELECTROHYDRODYNAMICS

Electrohydrodynamics p 41 N86-10130

ELECTROLYTES

Bipolar nickel-hydrogen battery development p 180 A86-24823

Develop and test fuel cell powered on-site integrated total energy systems: Phase 3, full-scale power plant development
[NASA-CR-174948] p 182 N86-12757

Advanced on-site power plant development technology program
[NASA-CR-174709] p 187 N86-25040

ELECTROMAGNETIC ACCELERATION

Rail accelerators for space transportation: An experimental investigation
[NASA-TP-2571] p 62 N86-28123

ELECTROMAGNETIC INTERACTIONS

Electrodynamic tether technology considerations p 161 N86-27657

ELECTROMAGNETIC INTERFERENCE

Calculation of allowable orbital spacings for the fixed-satellite service
[NASA-CR-176273] p 43 N86-11212

Broadcasting satellite service synthesis using gradient and cyclic coordinate search procedures
[NASA-CR-176708] p 114 N86-23781

ELECTROMAGNETIC MEASUREMENT

Nondestructive techniques for characterizing mechanical properties of structural materials - An overview
[ASME PAPER 86-GT-75] p 163 A86-48143

Nondestructive techniques for characterizing mechanical properties of structural materials: An overview
[NASA-TM-87203] p 164 N86-19636

ELECTROMAGNETIC NOISE

Fiber optics for propulsion control systems
[ASME PAPER 84-GT-97] p 17 A86-13054

ELECTROMAGNETIC PULSES

Fiber optics for propulsion control systems
[ASME PAPER 84-GT-97] p 17 A86-13054

A structural dynamics investigation related to EIDI applications --- Electro-Impulse Deicing
[AIAA PAPER 86-0550] p 16 A86-19942

ELECTROMAGNETIC SCATTERING

Numerical methods for analyzing electromagnetic scattering
[NASA-CR-176141] p 111 N86-10377

ELECTROMAGNETISM

Strategy for reflector pattern calculation - Let the computer do the work p 110 A86-39542

Strategy for reflector pattern calculation: Let the computer do the work
[NASA-TM-87137] p 112 N86-12485

Analyses and tests for design of an electro-impulse de-icing system
[NASA-CR-174919] p 15 N86-27268

ELECTRON ACCELERATION

Energy broadening due to space-charge oscillations in high current electron beams --- SEPAC payload experiment on Spacelab 1 p 202 A86-22890

ELECTRON BEAM WELDING

Creep properties of PWC-11 base metal and weldments as affected by heat treatment
[NASA-TM-88842] p 93 N86-32557

ELECTRON BEAMS

Energy broadening due to space-charge oscillations in high current electron beams --- SEPAC payload experiment on Spacelab 1 p 202 A86-22890

Development program on a cold cathode electron gun
[NASA-CR-174792] p 121 N86-14499

ELECTRON DENSITY (CONCENTRATION)

Improvement of ion thruster design
[NASA-CR-177223] p 61 N86-27419

ELECTRON DIFFRACTION

The beta-SiC(100) surface studied by low energy electron diffraction, Auger electron spectroscopy, and electron energy loss spectra p 77 A86-49864

ELECTRON EMISSION

Hollow cathodes in high pressure arc discharges --- for arcjet thrusters
[AIAA PAPER 85-2035] p 50 A86-14446

Energy broadening due to space-charge oscillations in high current electron beams --- SEPAC payload experiment on Spacelab 1 p 202 A86-22890

Angle-resolved Auger electron spectra induced by neon ion impact on aluminum p 76 A86-43456

Verification of an improved computational design procedure for TWT-dynamic refocuser-MDC systems with secondary electron emission losses p 119 A86-45194

Verification of computer-aided designs of traveling-wave tubes utilizing novel dynamic refocusers and graphite electrodes for the multistage depressed collector
[NASA-TP-2524] p 121 N86-13643

Textured carbon on copper: A novel surface with extremely low secondary electron emission characteristics
[NASA-TP-2543] p 101 N86-15394

Textured carbon surfaces on copper by sputtering
[NASA-CASE-LEW-14130-1] p 109 N86-32587

Secondary-electron-emission losses in multistage depressed collectors and traveling-wave-tube efficiency improvements with carbon collector electrode surfaces
[NASA-TP-2622] p 125 N86-32629

ELECTRON ENERGY

Improvement of ion thruster design
[NASA-CR-177223] p 61 N86-27419

ELECTRON GUNS

Development program on a cold cathode electron gun
[NASA-CR-174792] p 121 N86-14499

ELECTRON IRRADIATION

Performance of Hughes GaAs concentrator cells under 1-MeV electron irradiation p 185 N86-17860

ELECTRON MICROSCOPY

Transmission electron microscopic examination of phosphoric acid fuel cell components

p 74 A86-23352

ELECTRON PLASMA

Threshold determining mechanisms for discharges in high voltage solar arrays
[AIAA PAPER 86-0364] p 52 A86-19834

ELECTRON SCATTERING

Negative magnetoresistance of pitch-based carbon fibers Temperature and pressure dependence p 99 A86-35702

ELECTRON SPECTROSCOPY

The beta-SiC(100) surface studied by low energy electron diffraction, Auger electron spectroscopy, and electron energy loss spectra p 77 A86-49864

ELECTRONIC EQUIPMENT

Space and frequency-multiplexed optical linear algebra processor - Fabrication and initial tests p 202 A86-48352

Power electronics for a 1-kilowatt arcjet thruster
[AIAA PAPER 86-1507] p 56 A86-49613

Power electronics for a 1-kilowatt arc jet thruster
[NASA-TM-87340] p 61 N86-25409

ELECTRONIC EQUIPMENT TESTS

Radiofrequency testing of satellite segment of simulated 30/20 GHz satellite communications system
[NASA-TM-87163] p 114 N86-19494

ELECTROTHERMAL ENGINES

Measurements of energy distribution and wall temperature in flowing hydrogen microwave plasma systems
[AIAA PAPER 85-2052] p 203 A86-11001

Measurement of energy distribution in flowing hydrogen microwave plasmas p 52 A86-18041

Compatibility experiments of facilities, materials, and propellants for electrothermal thrusters p 59 N86-17426

A bibliography of electrothermal thruster technology, 1984
[NASA-TM-86998] p 60 N86-21578

ELLIPSOIDAL METERS

Ellipsometric surface analysis of wear tracks produced by different lubricants
[ASLE PREPRINT 85-TC-5A-2] p 151 A86-11016

Ellipsometric surface analysis of wear tracks produced by different lubricants
[NASA-TM-87142] p 87 N86-12293

- Polarization modulated ellipsometry
[NASA-CR-177264] p 149 N86-26599
- ELLIPTIC DIFFERENTIAL EQUATIONS**
Solution of elliptic partial differential equations by fast Poisson solvers using a local relaxation factor. 1: One-step method
[NASA-TP-2529] p 195 N86-28661
- ELLIPTIC FUNCTIONS**
Solution of elliptic partial differential equations by fast Poisson solvers using a local relaxation factor. 1: One-step method
[NASA-TP-2529] p 195 N86-28661
- ELLIPTICITY**
The role of service areas in the optimization of FSS orbital and frequency assignments
[NASA-CR-176488] p 46 N86-18341
- EMBRIEMENT**
Thermal aging effects in refractory metal alloys
[NASA-TM-87210] p 89 N86-16334
- EMISSION**
Research and development of neat alcohol fuel usage in automobiles
[NASA-CR-174813] p 108 N86-27460
- EMISSION SPECTRA**
Development program on a cold cathode electron gun
[NASA-CR-174792] p 121 N86-14499
Methane oxidation behind reflected shock waves: Ignition delay times measured by pressure and flame band emission
[NASA-TM-87268] p 77 N86-21635
- EMISSIVITY**
Liquid belt radiator design study
[NASA-CR-174901] p 57 N86-16259
Analysis of the Gas Particle Radiator (GPR)
[NASA-TM-88786] p 63 N86-31652
- ENERGY CONSERVATION**
Polymer, metal and ceramic matrix composites for advanced aircraft engine applications
[NASA-TM-87132] p 87 N86-13407
- ENERGY CONVERSION**
Reliability and mass analysis of dynamic power conversion systems with parallel of standby redundancy
[NASA-TM-87189] p 57 N86-16258
Design and evaluation of fluidized bed heat recovery for diesel engine systems
[NASA-CR-174898] p 209 N86-21456
- ENERGY CONVERSION EFFICIENCY**
Overview of the 1985 NASA Lewis Research Center SP-100 free-piston Stirling engine activities
p 153 N86-24884
A 25.5 percent AMO gallium arsenide grating solar cell
[NASA-TM-87134] p 182 N86-11671
Gallium arsenide solar cell efficiency: Problems and potential
p 184 N86-17843
N/P GaAs concentrator solar cells with an improved grid and busbar contact design
p 184 N86-17844
Develop and test fuel cell powered on-site integrated total energy systems
[NASA-CR-174951] p 188 N86-25877
Overview of the 1986 free-piston Stirling SP-100 activities at the NASA Lewis Research Center
[NASA-TM-87305] p 210 N86-26261
Space solar cell research: Problems and potential
[NASA-TM-88833] p 125 N86-31793
Potential high efficiency solar cells: Applications from space photovoltaic research
[NASA-TM-88832] p 125 N86-32627
- ENERGY DISSIPATION**
End-wall and profile losses in a low-speed axial flow compressor rotor
[ASME PAPER 85-GT-174] p 20 A86-22090
An experimental study of energy loss mechanisms and efficiency considerations in the low power dc arcjet
[AIAA PAPER 85-2017] p 53 A86-37062
An experimental study of energy loss mechanisms and efficiency consideration in the low power dc arcjet
[NASA-TM-87123] p 57 N86-11224
Effect of liquid droplets on turbulence in a round gaseous jet
[NASA-CR-175063] p 29 N86-23597
- ENERGY DISTRIBUTION**
Measurements of energy distribution and wall temperature in flowing hydrogen microwave plasma systems
[AIAA PAPER 85-2052] p 203 A86-11001
Measurement of energy distribution in flowing hydrogen microwave plasmas
p 52 A86-18041
Space station power management and distribution
p 59 N86-17869
- ENERGY GAPS (SOLID STATE)**
A possible radiation-resistant solar cell geometry using superlattices
p 185 N86-17851
Analysis of optically controlled microwave/millimeter wave device structures
[NASA-TM-87246] p 123 N86-24907
- ENERGY STORAGE**
Design tradeoffs for a Space Station solar-Brayton power system
p 53 A86-24790
Operating characteristics of a 0.87 kW-hr flywheel energy storage module
p 152 A86-24864
Negative electrode catalyst for the iron chromium redox energy storage system
[NASA-CASE-LEW-14028-1] p 186 N86-19721
Theoretical and experimental flow cell studies of a hydrogen-bromine fuel cell, part 1
[NASA-CR-177165] p 189 N86-29409
- ENERGY TECHNOLOGY**
A preliminary study of the modified Ericsson for space power
p 180 A86-24840
- ENGINE AIRFRAME INTEGRATION**
Evaluation of propeller/nacelle interactions in the PTA program
[AIAA PAPER 86-1552] p 6 A86-42709
- ENGINE ANALYZERS**
DEAN - A program for Dynamic Engine Analysis
[AIAA PAPER 85-1354] p 18 A86-14430
- ENGINE CONTROL**
Sensor failure detection for jet engines using analytical redundancy
p 18 A86-14226
A sensor failure simulator for control system reliability studies
[NASA-TM-87271] p 124 N86-31792
- ENGINE COOLANTS**
Test program to provide confidence in liquid oxygen cooling of hydrocarbon fueled rocket thrust chambers
[NASA-TM-88816] p 62 N86-31646
- ENGINE DESIGN**
Operational maintenance data base development for kinematic Stirling engines
[ASME PAPER 85-DGP-20] p 151 A86-14467
Lubrication and performance of high-speed rolling-element bearings
p 152 A86-19375
Evaluation of fuel preparation systems for lean premixing-prevaporizing combustors
[ASME PAPER 85-GT-137] p 19 A86-22081
Modeling the 3-D flow effects on deviation angle for axial compressor middle stages
[ASME PAPER 85-GT-189] p 2 A86-22102
Liquid fueled external heating system for STM4-120 Stirling engine
p 180 A86-24888
Three-dimensional inviscid flow in mixers. I - Mixer analysis using a Cartesian grid
p 5 A86-39090
Rotorcraft propulsion for year 2000 plus
[AIAA PAPER 86-1543] p 23 A86-42702
Small engine technology payoffs for future commuter aircraft
[AIAA PAPER 86-1544] p 23 A86-42703
Computation of three-dimensional, rotational flow through turbomachinery blade rows for improved aerodynamic design studies
[ASME PAPER 86-GT-26] p 7 A86-48117
Analytical and experimental investigation of the coupled bladed disk/shaft whirl of a cantilevered turbofan
[ASME PAPER 86-GT-98] p 24 A86-48163
Stratified charge rotary engine for general aviation
[ASME PAPER 86-GT-181] p 24 A86-48231
Small gas turbine combustor experimental study - Compliant metal/ceramic liner and performance evaluation
[AIAA PAPER 86-1452] p 25 A86-49611
Perspectives on dilution jet mixing --- in creating temperature patterns at combustor exits in gas turbine engines
[AIAA PAPER 86-1611] p 25 A86-49614
NASA LeRC/Akron University Graduate Cooperative Fellowship Program and Graduate Student Researchers Program
[NASA-CR-174826] p 207 N86-13219
Stirling engine supporting research and technology
[NASA-TM-87175] p 208 N86-14106
Design optimization for a space based, reusable orbit transfer vehicle
p 48 N86-17418
A supersonic fan equipped variable cycle engine for a Mach 2.7 supersonic transport
[NASA-CR-177141] p 32 N86-28946
Overview of NASA Lewis Research Center free-piston Stirling engine technology activities applicable to space power systems
[NASA-TM-88815] p 211 N86-29732
Aeropropulsion opportunities for the 21st century
[NASA-TM-88817] p 34 N86-31585
A parametric study of a gas-generator air turbo ramjet (ATR)
[NASA-TM-88808] p 34 N86-31586
An overview of the Small Engine Component Technology (SECT) studies
[NASA-TM-88796] p 34 N86-31587
- ENGINE FAILURE**
Sensor failure detection for jet engines using analytical redundancy
p 18 A86-14226
- ENGINE INLETS**
An LU implicit scheme for high speed inlet analysis
[AIAA PAPER 86-1520] p 6 A86-42687
A numerical analysis applied to high angle of attack three-dimensional inlets
[AIAA PAPER 86-1527] p 6 A86-42760
An iterative finite element-integral technique for predicting sound radiation from turbofan inlets in steady flight
p 198 A86-49806
Particle trajectory computation on a 3-dimensional engine inlet
[NASA-CR-175023] p 14 N86-20379
SSME fuelside preburner two-dimensional analysis
[NASA-TM-87299] p 44 N86-23616
A numerical analysis applied to high angle of attack three-dimensional inlets
[NASA-TM-87298] p 11 N86-24658
- ENGINE MONITORING INSTRUMENTS**
Sensor failure detection for jet engines using analytical redundancy
p 18 A86-14226
Robust detection, isolation, and accommodation for sensor failures --- in jet engine control systems
p 21 A86-35402
- ENGINE NOISE**
The effect of acoustic reflections on combustor noise measurements
p 197 A86-20364
Development of an impulsive noise source to study the acoustic reflection characteristics of hard-walled wind tunnels
[AIAA PAPER 86-1887] p 198 A86-45500
Propeller noise caused by blade tip radial forces
[AIAA PAPER 86-1892] p 23 A86-45504
An iterative finite element-integral technique for predicting sound radiation from turbofan inlets in steady flight
p 198 A86-49806
Current wind tunnel capability and planned improvements at Lewis Research Center
[NASA-TM-87190] p 37 N86-18329
Turbofan aft duct suppressor study program listing and user's guide
[NASA-CR-175067] p 30 N86-25357
- ENGINE PARTS**
Sintered alpha silicon carbide ceramics for high temperature structural application - Status review and recent developments
[ASME PAPER 85-IGT-127] p 97 A86-23921
Probabilistic structural analysis for space propulsion system components
p 168 A86-28659
Stress analysis of gas turbine engine structures using the boundary element method
p 169 A86-34444
Fabrication of ceramic components for advanced gas turbine engines
[SAE PAPER 851786] p 154 A86-38310
Probabilistic structural analysis methods for critical SSME propulsion components
[AIAA PAPER 86-1188] p 54 A86-40595
Computational composite mechanics for aerospace propulsion structures
[AIAA PAPER 86-1190] p 67 A86-40596
High-pressure creep tests
p 84 A86-46564
Stress and deformation modeling of multiple rotary combustion engine trochoid housings
[SAE PAPER 860614] p 156 A86-49624
Turbine Engine Hot Section Technology (HOST)
[NASA-CP-2289] p 172 N86-11495
High temperature static strain sensor development program
p 148 N86-11500
Stirling engine supporting research and technology
[NASA-TM-87175] p 208 N86-14106
Phenomenological study of the behavior of some silica formers in a high velocity jet fuel burner
[NASA-TM-87127] p 157 N86-14613
Automotive Stirling engine development program
[NASA-CR-175045] p 211 N86-30579
An overview of the Small Engine Component Technology (SECT) studies
[NASA-TM-88796] p 34 N86-31587
Thermal stress minimized, two component, turbine shroud seal
[NASA-CASE-LEW-14212-1] p 162 N86-32740
- ENGINE TESTS**
Subscale-model and full-scale engine mixed-flow exhaust system performance comparison
p 18 A86-14528
Test results of a 40 kW Stirling engine and comparison with the NASA-Lewis computer code predictions
p 181 A86-24889
RE-1000 free-piston Stirling engine update
p 153 A86-24890
Transient engine performance with water ingestion
[AIAA PAPER 86-1621] p 23 A86-42755
Computational engine structural analysis
[ASME PAPER 86-GT-70] p 23 A86-48141
RE-1000 free-piston Stirling engine update
[NASA-TM-87126] p 182 N86-11668

- Stirling engine supporting research and technology
[NASA-TM-87175] p 208 N86-14106
Small, two-stage, partial-admission turbine
p 57 N86-17386
- Computational engine structural analysis
[NASA-TM-87231] p 175 N86-19663
Advanced Gas Turbine (AGT) technology report
[NASA-CR-175018] p 158 N86-20808
Summary of investigations of engine response to distorted inlet conditions
[NASA-TM-87317] p 30 N86-26336
Preliminary evaluation of a compound cycle engine for shipboard gensets
[NASA-CR-179451] p 160 N86-26629
Research and development of neat alcohol fuel usage in automobiles
[NASA-CR-174813] p 108 N86-27460
Automotive Stirling Engine Development Program
[NASA-CR-174749] p 211 N86-28017
Uniform engine testing program phase 7: NASA Lewis Research Center second entry
[NASA-TM-87272] p 31 N86-28085
Longitudinal mode combustion instabilities of a high-pressure fuel-rich LOX/RP-1 preburner
p 165 N86-28250
Automotive Stirling engine development program
[NASA-CR-175045] p 211 N86-30579
A parametric study of a gas-generator air turbo ramjet (ATR)
[NASA-TM-88808] p 34 N86-31586
- ENGINEERING DRAWINGS**
Mod-5A wind turbine generator program design report. Volume 2: Conceptual and preliminary design, book 1
[NASA-CR-174735-VOL-2-BK-1] p 183 N86-15722
Mod-5A wind turbine generator program design report. Volume 2: Conceptual and preliminary design, book 2
[NASA-CR-174735-VOL-2-BK-2] p 183 N86-15723
Mod-5A wind turbine generator program design report. Volume 3: Final design and system description, book 1
[NASA-CR-174735-VOL-3-BK-1] p 183 N86-15724
Mod-5A wind turbine generator program design report. Volume 3: Final design and system description, book 2
[NASA-CR-174735-VOL-3-BK-2] p 183 N86-15725
Mod-5A wind turbine generator program design report. Volume 4: Drawings and specifications, book 1
[NASA-CR-174735-VOL-4-BK-1] p 183 N86-15726
Mod-5A wind turbine generator program design report. Volume 4: Drawings and specifications, book 2
[NASA-CR-174735-VOL-4-BK-2] p 184 N86-15727
Mod-5A wind turbine generator program design report. Volume 4: Drawings and specifications, book 3
[NASA-CR-174735-VOL-4-BK-3] p 184 N86-15728
Mod-5A wind turbine generator program design report. Volume 4: Drawings and specifications, book 4
[NASA-CR-174735-VOL-4-BK-4] p 184 N86-15729
Mod-5A wind turbine generator program design report. Volume 4: Drawings and specifications, book 5
[NASA-CR-174735-VOL-4-BK-5] p 184 N86-15730
- ENGINES**
Overview of free-piston Stirling technology at the NASA Lewis Research Center
[NASA-TM-87156] p 208 N86-13236
Tribology of selected ceramics at temperatures to 900 deg C
[NASA-TM-87267] p 105 N86-25476
- ENTRAINMENT**
Entrainment region phenomena for a large plane shear layer
p 132 A86-30211
- ENVIRONMENT EFFECTS**
High Temperature Polymer Matrix Composites
[NASA-CP-2385] p 68 N86-11260
- ENVIRONMENT SIMULATION**
Ribbon-burner simulation of T-700 turbine shroud for ceramic-lined seals research
p 18 A86-15225
- ENVIRONMENTAL CONTROL**
Space Station benefits from ECLS - Propulsion system synergism
[AIAA PAPER 86-1407] p 47 A86-42619
- ENVIRONMENTAL TESTS**
Creep-rupture and fractographic analysis of Stirling engine superalloys tested in air and 15 MPa hydrogen
p 82 A86-30041
Centaur engine gimbal friction characteristics under simulated thrust load
[NASA-TM-87335] p 44 N86-31621
Effect of an oxygen plasma on the physical and chemical properties of several fluids for the liquid droplet radiator
[NASA-TM-88839] p 49 N86-31634
- EPITAXY**
Growth and characterization of epitaxial SrF₂ on InP(100)
p 205 A86-47076
Compensation in epitaxial cubic SiC films
[NASA-TM-87269] p 206 N86-25267
- EPOXY MATRIX COMPOSITES**
LH2 on-orbit storage tank support trunnion design and verification
p 53 A86-37054
- The correlation of low-velocity impact resistance of graphite-fiber-reinforced composites with matrix properties
[NASA-TM-87337] p 71 N86-27426
- EPOXY RESINS**
Tetraglycidyl epoxy resins and graphite fiber composites cured with flexibilized aromatic diamines
p 67 A86-38999
- The correlation of low-velocity impact resistance of graphite-fiber-reinforced composites with matrix properties
[NASA-TM-87337] p 71 N86-27426
- EQUATIONS OF MOTION**
Vibration analysis of rotating turbomachinery blades by an improved finite difference method
p 18 A86-14338
- EQUATIONS OF STATE**
A lumped parameter mathematical model for simulation of subsonic wind tunnels
[NASA-TM-87324] p 196 N86-27036
Universality in the compressive behavior of solids
[NASA-TM-87303] p 206 N86-28775
Temperature effects on the universal equation of state of solids
[NASA-TM-87321] p 206 N86-28776
- EQUILIBRIUM**
Fugacity and concentration gradients in a gravity field
[NASA-TM-88809] p 212 N86-30620
- EQUILIBRIUM FLOW**
Local equilibrium assumption for round jet calculations
p 136 A86-49829
- EXHAUST SPECIFICATIONS**
High accuracy fuel flowmeter
[NASA-CR-174869] p 150 N86-31030
- EROSION**
Angular particle impingement studies of thermoplastic materials at normal incidence
[ASLE PREPRINT 85-AM-3A-1] p 94 A86-11076
Electrode erosion in arc discharges at atmospheric pressure
[AIAA PAPER 85-2018] p 50 A86-14445
Rapid evaluation of ion thruster lifetime using optical emission spectroscopy
[AIAA PAPER 85-2011] p 51 A86-17851
Erosion of phosphor bronze under cavitation attack in a mineral oil
p 81 A86-23324
An experimental study of energy loss mechanisms and efficiency considerations in the low power dc arcjet
[AIAA PAPER 85-2017] p 53 A86-37082
Rapid evaluation of ion thruster lifetime using optical emission spectroscopy
[NASA-TM-87103] p 56 N86-10280
The mechanism of erosion of metallic materials under cavitation attack
[NASA-TM-87133] p 156 N86-10552
An experimental study of energy loss mechanisms and efficiency consideration in the low power dc arcjet
[NASA-TM-87123] p 57 N86-11224
- ERROR ANALYSIS**
Error-source effects in a high-accuracy optical finite-element processor
p 192 A86-31571
- ERRORS**
Filter induced errors in laser anemometry using counter-processor
p 146 A86-34431
- ESTERS**
Ellipsometric surface analysis of wear tracks produced by different lubricants
[NASA-TM-87142] p 87 N86-12293
A preliminary study of ester oxidation on an aluminum surface using chemiluminescence
[NASA-TM-87242] p 103 N86-24835
- ESTIMATES**
Potential for use of indium phosphide solar cells in the space radiation environment
[NASA-TM-87157] p 121 N86-13645
Development of a microprocessor controller for stand-alone photovoltaic power systems
[NASA-CR-174723] p 187 N86-21979
- ESTIMATING**
Estimating the R-curve from residual strength data
[NASA-TM-87182] p 175 N86-18750
- ESTIMATORS**
Robust detection, isolation and accommodation for sensor failures
[NASA-CR-174825] p 33 N86-30732
- ETCHING**
Dry etching of beta-SiC in CF₄ and CF₄ + O₂ mixtures
p 76 A86-47069
Ion beam sputter etching
[NASA-CASE-LEW-13899-1] p 109 N86-20587
- ETHERS**
Analysis of a spacecraft instrument ball bearing assembly lubricated by a perfluoroalkylether
[NASA-TM-87260] p 50 N86-21575
The preparation of new perfluoroether fluids exhibiting excellent thermal-oxidative stabilities
[NASA-TM-87284] p 105 N86-25475
- EULER EQUATIONS OF MOTION**
Development of an explicit multigrid algorithm for quasi-three-dimensional viscous flows in turbomachinery
[AIAA PAPER 86-0032] p 1 A86-19644
An implicit LU scheme for the Euler equations applied to arbitrary cascades --- new method of factoring
p 2 A86-20131
Accelerated solution of the steady Euler equations
p 2 A86-20942
An embedding method for the steady Euler equations
p 194 A86-30814
Parametric effects of CFL number and artificial smoothing on numerical solutions using implicit approximate factorization algorithm
[AIAA PAPER 86-1059] p 132 A86-38427
An efficient method for solving the steady Euler equations
[AIAA PAPER 86-1079] p 132 A86-38442
A new approach for solving the three-dimensional steady Euler equations. I - General theory
p 133 A86-41242
Improved Euler analysis of advanced turboprop propeller flows
[AIAA PAPER 86-1521] p 6 A86-42688
Development of an explicit multigrid algorithm for quasi-three-dimensional viscous flows in turbo-machinery
[NASA-TM-87128] p 1 N86-11146
An LU implicit scheme for high speed inlet analysis
[NASA-CR-175098] p 11 N86-23563
- EUTECTIC ALLOYS**
Effect of multiple strain-anneal cycles on the 1000 C creep behaviour of gamma/gamma prime-alpha
p 82 A86-30610
Undercooling and solidification behavior in the InSb-Sb system
[NASA-CR-175013] p 88 N86-14355
- EUTECTICS**
Estimated heats of fusion of fluoride salt mixtures suitable for thermal energy storage applications
[NASA-TM-87320] p 190 N86-31982
- EVALUATION**
Nondestructive techniques for characterizing mechanical properties of structural materials - An overview
[ASME PAPER 86-GT-75] p 163 A86-48143
Ultrasonic evaluation of mechanical properties of thick, multilayered, filament wound composites
[NASA-TM-87088] p 163 N86-10561
Lateral dampers for thrust bearings
[NASA-CR-174924] p 157 N86-11474
The effect of cobalt content in U-700 type alloys on degradation of aluminate coatings
[NASA-TM-87173] p 87 N86-13408
Preliminary measurement of the noise from the 2/9 scale model of the Large-scale Advanced Propfan (LAP) propeller, SR-7A
[NASA-TM-87116] p 199 N86-14006
Nondestructive techniques for characterizing mechanical properties of structural materials: An overview
[NASA-TM-87203] p 164 N86-19636
A real-time simulation evaluation of an advanced detection, isolation and accommodation algorithm for sensor failures in turbine engines
[NASA-TM-87289] p 30 N86-24697
Stirling Powered Van Program overview
[NASA-TM-87227] p 210 N86-25303
Experimental evaluation of two turning vane designs for high-speed corner of 0.1-scale model of NASA Lewis Research Center's proposed altitude wind tunnel
[NASA-TP-2570] p 38 N86-28101
- EXCITATION**
Rapid evaluation of ion thruster lifetime using optical emission spectroscopy
[AIAA PAPER 85-2011] p 51 A86-17851
Rapid evaluation of ion thruster lifetime using optical emission spectroscopy
[NASA-TM-87103] p 56 N86-10280
- EXHAUST EMISSION**
HOST liner cyclic facilities
p 173 N86-11519
- EXHAUST FLOW SIMULATION**
Subscale-model and full-scale engine mixed-flow exhaust system performance comparison
p 18 A86-14528
- EXHAUST GASES**
Design and evaluation of fluidized bed heat recovery for diesel engine systems
[NASA-CR-174898] p 209 N86-21456
Theoretical study on the effect of the design of small (milli-Newton) thruster jets on molecular contamination for the space station
[NASA-CR-177263] p 48 N86-26358
- EXHAUST SYSTEMS**
Turbofan aft duct suppressor study program listing and user's guide
[NASA-CR-175067] p 30 N86-25357

EXISTENCE THEOREMS

- Existence and stability, and discrete BB and rank conditions, for general mixed-hybrid finite elements in elasticity p 169 N86-34464

EXOTHERMIC REACTIONS

- Dynamic features of combustion p 72 A86-12925
Chemical control of rate and onset temperature of nadimide polymerization p 101 N86-11271
Low-cost single-crystal turbine blades, volume 2 [NASA-CR-174652] p 29 N86-23598

EXPERIMENT DESIGN

- Ignition and flame spread above liquid fuel pools p 41 N86-10163
Broadcasting satellite service synthesis using gradient and cyclic coordinate search procedures [NASA-CR-176708] p 114 N86-23781
ACTS Experiments Program [NASA-TM-88820] p 47 N86-31625

EXPERIMENTATION

- An experimental investigation of reducing advanced turboprop cabin noise by wing shielding [AIAA PAPER 86-1966] p 16 A86-45449
Progressive damage, fracture predictions and post mortem correlations for fiber composites [NASA-TM-87101] p 68 N86-10290
Measurement of the density of base fluids at pressures 0.422 to 2.20 GPa [NASA-TM-87114] p 156 N86-10551
Comparison of calculated and experimental cascade performance for controlled-diffusion compressor stator blading [NASA-TM-87167] p 27 N86-16219
An experimental investigation of reducing advanced turboprop cabin noise by wing shielding [NASA-TM-87112] p 201 N86-25218
Identification of differences between finite element analysis and experimental vibration data [NASA-TM-87336] p 149 N86-27617
Experimental evaluation of two turning vane designs for high-speed corner of 0.1-scale model of NASA Lewis Research Center's proposed altitude wind tunnel [NASA-TP-2570] p 38 N86-28101

EXPOSURE

- Time dependency of strainrange partitioning life relationships [NASA-CR-174946] p 174 N86-13755

EXTERNAL COMBUSTION ENGINES

- Evaluation of a Stirling engine heater bypass with the NASA Lewis nodal-analysis performance code [NASA-CR-174960] p 211 N86-31452

EXTINCTION

- A fundamental study of smoldering with emphasis on experimental design for zero-g p 41 N86-10162
Flammability limits of gases under low gravity conditions p 42 N86-10164
Fundamental studies of droplet combustion at reduced gravity p 42 N86-10165
Flame propagation and extinction in particle clouds [NASA-CR-177304] p 78 N86-27434

EXTINGUISHING

- Theory of interactive combustion of counterflow premixed flames p 74 A86-32752
Diffusion flame extinction in slow convective flow under microgravity environment p 144 N86-28378

EXTREMELY HIGH FREQUENCIES

- Ka-band monolithic gain control amplifier p 119 A86-41343

EXTRUDING

- Dislocations in extruded Co-49.3 at. pct Al p 83 A86-45091
Tensile behavior of Fe-40Al alloys with B and Zr additions [NASA-TM-87290] p 91 N86-25453
Slip casting and extruding shapes of rhenium with metal oxide additives. 1: Feasibility demonstration [NASA-CR-174970] p 63 N86-31648

F**FABRICATION**

- Effect of substituted phenylnadimides on processing and properties of PMR polyimide composites p 94 A86-13179
Fabrication of ceramic components for advanced gas turbine engines [SAE PAPER 851786] p 154 A86-38310
A 10,000 hour life multipropellant engine for Space Station applications [AIAA PAPER 86-1403] p 54 A86-42616
Space and frequency-multiplexed optical linear algebra processor - Fabrication and initial tests p 202 A86-48352

- Designing a 25-kilowatt high frequency series resonant [NASA-CR-176774] p 123 N86-24906
Fracture characteristics of angleplied laminates fabricated from overaged graphite/epoxy prepreg [NASA-TM-87266] p 70 N86-25417
Double-injection, deep-impurity switch development [NASA-CR-174936] p 124 N86-30073
FABRY-PEROT INTERFEROMETERS
Fibre-optic thermometer using semiconductor-etalon sensor p 146 A86-32046
Combined fringe and Fabry-Perot laser anemometer for three component velocity measurements in turbine stator cascade facility [NASA-TM-87322] p 149 N86-24967

FACE CENTERED CUBIC LATTICES

- Temperature dependence of gamma-gamma prime lattice mismatch in nickel-base superalloys p 81 A86-21849
Effect of multiple strain-anneal cycles on the 1000 C creep behaviour of gamma/gamma prime-alpha p 82 A86-30610

FACTORIZATION

- An implicit LU scheme for the Euler equations applied to arbitrary cascades --- new method of factoring p 2 A86-20131
Parametric effects of CFL number and artificial smoothing on numerical solutions using implicit approximate factorization algorithm [AIAA PAPER 86-1059] p 132 A86-38427

FAILURE

- Effects of a high mean stress on the high cycle fatigue life of PWA 1480 and correlation of data by linear elastic fracture mechanics [NASA-CR-175057] p 177 N86-27689

FAILURE ANALYSIS

- Failure analysis of plasma-sprayed thermal barrier coatings p 80 A86-16270
Deposition stress effects on the life of thermal barrier coatings on burner rigs p 96 A86-16271
Methods for improving reliability in ceramic turbine rotors [SAE PAPER 851788] p 154 A86-38312
Mode II fatigue crack growth specimen development p 171 A86-43566
Turbine Engine Hot Section Technology (HOST) [NASA-CP-2289] p 172 N86-11495
Surface fatigue life and failure characteristics of EX-53, CBS 1000M, and AISI 9310 gear materials [NASA-TP-2513] p 157 N86-12609
SCARE: A post-processor program to MSC/NASTRAN for the reliability analysis of structural ceramic components [NASA-TM-87188] p 174 N86-17588
Robust detection-isolation-accommodation for sensor failures [NASA-CR-174797] p 121 N86-16486
Yielding and deformation behavior of the single crystal nickel-base superalloy PWA 1480 [NASA-CR-175100] p 91 N86-25455
Re-examination of cumulative fatigue damage analysis: An engineering perspective [NASA-TM-87325] p 177 N86-27680
HYTESS 2: A Hypothetical Turbofan Engine Simplified Simulation with multivariable control and sensor analytical redundancy [NASA-TM-87344] p 124 N86-30068
A sensor failure simulator for control system reliability studies [NASA-TM-87271] p 124 N86-31792

FAILURE MODES

- Longitudinal compressive failure modes in fiber composites End attachment effects on ITRI type test specimens p 66 A86-19999
Nondestructive characterization of RBSOA of high-power bipolar transistors --- Reverse-bias safe operating area p 118 A86-35718
Mode II fatigue crack growth specimen development p 171 A86-43566
Thermal barrier coating life prediction model development [NASA-CR-175087] p 103 N86-22713
A real-time simulation evaluation of an advanced detection, isolation and accommodation algorithm for sensor failures in turbine engines [NASA-TM-87289] p 30 N86-24697
Computational simulation of progressive fracture in fiber composites [NASA-TM-87341] p 71 N86-26376
The correlation of low-velocity impact resistance of graphite-fiber-reinforced composites with matrix properties [NASA-TM-87337] p 71 N86-27426
Ultrasonic stress wave characterization of composite materials [NASA-CR-3976] p 165 N86-27665

- Re-examination of cumulative fatigue damage analysis: An engineering perspective [NASA-TM-87325] p 177 N86-27680

FAN BLADES

- Influence of rotation and pretwist on cantilever fan blade flutter p 17 A86-11686
Study of ice accretion on icing wind tunnel components [AIAA PAPER 86-0290] p 36 A86-26620
Dynamic characteristics of an assembly of prop-fan blades [ASME PAPER 85-GT-134] p 21 A86-32956
On the application of a linearized unsteady potential-flow analysis to fan-tip cascades [ASME PAPER 86-GT-87] p 7 A86-48153
Mass balancing of hollow fan blades [ASME PAPER 86-GT-195] p 171 A86-48245
Study of ice accretion on icing wind tunnel components [NASA-TM-87095] p 37 N86-16232
Mass balancing of hollow fan blades [NASA-TM-87197] p 174 N86-16611
Rotor wake characteristics of a transonic axial flow fan [NASA-TM-87073] p 13 N86-28055

FANS

- Feasibility study for convertible engine torque converter [NASA-CR-175082] p 33 N86-30733

FAST FOURIER TRANSFORMATIONS

- Secondary pattern computation of an arbitrarily shaped main reflector [NASA-TM-87162] p 112 N86-14477

FATIGUE (MATERIALS)

- Fatigue crack growth under general-yielding cyclic-loading p 171 A86-44339
Turbine Engine Hot Section Technology (HOST) [NASA-CP-2289] p 172 N86-11495
Influence of load interactions on crack growth as related to state of stress and crack closure [NASA-TM-87117] p 86 N86-12292
Fatigue crack propagation of nickel-base superalloys at 650 deg C [NASA-TM-87150] p 87 N86-12294
An update of the total-strain version of SRP [NASA-TP-2499] p 87 N86-12295
Design of traction drives [NASA-RP-1154] p 157 N86-13734
Time dependency of strainrange partitioning life relationships [NASA-CR-174946] p 174 N86-13755
Closure of fatigue cracks at high strains [NASA-CR-175021] p 175 N86-17788
Grain boundary oxidation and oxidation accelerated fatigue crack nucleation and propagation [NASA-CR-175050] p 89 N86-20542
Fatigue crack growth under general-yielding cyclic-loading [NASA-CR-175049] p 176 N86-21951
Anisotropic constitutive model for nickel base single crystal alloys: Development and finite element implementation [NASA-CR-175015] p 176 N86-21952
Influence of fatigue crack wake length and state of stress on crack closure [NASA-TM-87292] p 90 N86-22686
Thermal-mechanical fatigue behavior of nickel-base superalloys [NASA-CR-175048] p 91 N86-24818
Fatigue crack layer propagation in silicon-iron [NASA-CR-175115] p 177 N86-25851
Low-cycle thermal fatigue [NASA-TM-87225] p 177 N86-26651
Micromechanisms of thermomechanical fatigue: A comparison with isothermal fatigue [NASA-TM-87331] p 92 N86-28164
Improved fracture toughness corrosion-resistant bearing material [NASA-CR-174990] p 162 N86-32743
FATIGUE LIFE
Thermal-mechanical fatigue crack growth in Inconel X-750 p 81 A86-20982
Fatigue life analysis of a turboprop reduction gearbox [ASME PAPER 85-DET-10] p 155 A86-45256
A study of spectrum fatigue crack propagation in two aluminum alloys. I - Spectrum simplification. II - Influence of microstructures p 85 A86-48973
Validation of structural analysis methods using burner liner cyclic rig test data p 173 N86-11518
Life prediction and constitutive behavior p 173 N86-11520
Creep fatigue life prediction for engine hot section materials (isotropic) p 174 N86-11521
Surface fatigue life and failure characteristics of EX-53, CBS 1000M, and AISI 9310 gear materials [NASA-TP-2513] p 157 N86-12609

- Effect on interference fits on roller bearing fatigue life [NASA-TM-87165] p 158 N86-19616
Nonlinear damage analysis: Postulate and evaluation [NASA-CR-168171] p 177 N86-26652
New methodology for shaft design based on life expectancy [NASA-TM-87354] p 161 N86-27661
Re-examination of cumulative fatigue damage analysis: An engineering perspective [NASA-TM-87325] p 177 N86-27680
Effects of a high mean stress on the high cycle fatigue life of PWA 1480 and correlation of data by linear elastic fracture mechanics [NASA-CR-175057] p 177 N86-27689
Thermal-fatigue and oxidation resistance of cobalt-modified Udimet 700 alloy [NASA-TP-2591] p 178 N86-28464

FATIGUE TESTS

- Fracture mechanics applied to nonisothermal fatigue crack growth p 81 A86-28951
Lubricant and additive effects on spur gear fatigue life [ASME PAPER 85-TRIB-14] p 155 A86-43542
The cyclic stress-strain behavior of a nickel-base superalloy at 650 C p 83 A86-45715
Orientation and temperature dependence of some mechanical properties of the single-crystal nickel-base superalloy Rene N4. II - Low cycle fatigue behavior p 86 A86-50322
Creep-fatigue behavior of NiCoCrAlY coated PWA 1480 superalloy single crystals [NASA-TM-87110] p 86 N86-10311
Thermal-mechanical fatigue test apparatus for metal matrix composites and joint attachments [NASA-TM-87187] p 88 N86-15378
New methodology for shaft design based on life expectancy [NASA-TM-87354] p 161 N86-27661
The low cycle fatigue behavior of a plasma-sprayed coating material [NASA-TM-87318] p 92 N86-31699

FEASIBILITY ANALYSIS

- Technology achievements and projections for communication satellites of the future [AIAA PAPER 86-0649] p 109 A86-29611
Technology achievements and projections for communication satellites of the future [NASA-TM-87201] p 113 N86-17595
Free jet feasibility study of a thermal acoustic shield concept for AST/VCE application-dual flow. Comprehensive data report. Volume 1: Test nozzles and acoustic data [NASA-CR-174817] p 200 N86-23371
Free-jet feasibility study of a thermal acoustic shield concept for AST/VCE application-dual stream nozzles. Comprehensive data report. Volume 2: Laser velocimeter and suppressor. Base pressure data [NASA-CR-174818] p 201 N86-23372

FEEDBACK CONTROL

- Nonlinear optimal control with tensors - Some computational issues p 194 A86-35419
Quasi-modal vibration control by means of active control bearings [NASA-TM-87232] p 159 N86-21856
A lumped parameter mathematical model for simulation of subsonic wind tunnels [NASA-TM-87324] p 196 N86-27036

FERRITES

- Fundamental tribological properties of ceramics p 95 A86-15230
Abrasion and deformed layer formation of manganese-zinc ferrite in sliding contact with lapping tapes [NASA-TM-87249] p 104 N86-24838
Effect of crystallographical and geometrical changes of a ferrite head on magnetic signals during the sliding process with magnetic tape [NASA-TM-87277] p 106 N86-31728

FIBER COMPOSITES

- Longitudinal compressive failure modes in fiber composites End attachment effects on IITRI type test specimens p 66 A86-19999
Designing for fiber composite structural durability in hygrothermomechanical environments p 67 A86-27734
Tribological paroperties of graphite-fiber-reinforced, partially fluorinated polyimide composites p 98 A86-34177
Progressive fracture of fiber composites p 67 A86-35809
Computer aided derivation of equations for composite mechanics problems and finite element analyses [AIAA PAPER 86-1016] p 170 A86-38873
Dynamic stress analysis of smooth and notched fiber composite flexural specimens p 67 A86-41070
PMR polyimides from solutions containing mixed endcaps p 100 N86-11263

- Integrated Composite Analyzer (ICAN): Users and programmers manual [NASA-TP-2515] p 69 N86-21614

- A comparison of the bromination dynamics of pitch-based and vapor-grown graphite fibers [NASA-TM-87275] p 103 N86-21683

- Computational simulation of progressive fracture in fiber composites [NASA-TM-87341] p 71 N86-26376

- The correlation of low-velocity impact resistance of graphite-fiber-reinforced composites with matrix properties [NASA-TM-87337] p 71 N86-27426

- Structure-to-property relationships in addition cured polymers 2: Resin Tg composite initial mechanical properties of norbornenyl cured polyimide resins [NASA-TM-88794] p 105 N86-29041

- Fiber composite sandwich thermostructural behavior: Computational simulation [NASA-TM-88787] p 71 N86-31663

- ICAN: A versatile code for predicting composite properties [NASA-TM-87334] p 71 N86-31664

FIBER OPTICS

- All-fibre sensing loop using pulse-modulated light-emitting diode p 202 A86-11995
Fiber optics for propulsion control systems [ASME PAPER 84-GT-97] p 17 A86-13054
Thermal dependence of stress-induced birefringence in single mode optical fibers p 202 A86-15263
Wavelength-division multiplexed digital optical position transducer p 145 A86-20798
Optical techniques to feed and control GaAs MMIC modules for phased array antenna applications [AIAA PAPER 86-0687] p 110 A86-29638
Fibre-optic thermometer using semiconductor-etalon sensor p 146 A86-32046
Development of optical diaphragm deflection sensors [NASA-CR-175008] p 203 N86-15113
Optical techniques to feed and control GaAs MMIC modules for phased array antenna applications [NASA-TM-87218] p 113 N86-16458
Time domain referencing in intensity modulation fiber optic sensing systems [NASA-CR-175109] p 17 N86-24691
1700 deg C optical temperature sensor [NASA-CR-175108] p 203 N86-28729

FIBER ORIENTATION

- A comparison of the bromination dynamics of pitch-based and vapor-grown graphite fibers [NASA-TM-87275] p 103 N86-21683

FIBER REINFORCED COMPOSITES

- A ceramic matrix composite based on polymerization and pyrolysis of ethynylated aromatics p 65 A86-13169
Three-dimensional hybrid-stress finite element analysis of composite laminates with cracks and cutouts p 167 A86-26896
Aerospace applications of PMR polyimide composites p 67 A86-27730
Advanced rotary engine components utilizing fiber reinforced Mg castings [AIAA PAPER 86-1559] p 67 A86-42712
Properties of autoclaved Gr/PI composites made from improved tack PMR-15 prepreg p 68 N86-11276
Surface protection of graphite fabric/PMR-15 composites subjected to thermal oxidation p 68 N86-11281

- Interlaminar fracture toughness: Three-dimensional finite element modeling for end-notch and mixed-mode flexure [NASA-TM-87138] p 69 N86-14316

- Effect of stress on ultrasonic pulses in fiber reinforced composites p 200 N86-22975

- Fundamental studies of low velocity impact resistance of graphite fiber reinforced polymer matrix composites [NASA-TM-86886] p 69 N86-23661

- A unique set of micromechanics equations for high temperature metal matrix composites [NASA-TM-87154] p 70 N86-24757

- Stress waves in transversely isotropic media: The homogeneous problem [NASA-CR-3977] p 164 N86-25002

- Nickel-hydrogen separator development [NASA-TM-87332] p 188 N86-26677

- Ultrasonic stress wave characterization of composite materials [NASA-CR-3976] p 165 N86-27865

- Wave propagation in anisotropic medium due to an oscillatory point source with application to unidirectional composites [NASA-CR-4001] p 165 N86-27866

FIBERS

- Creep of chemically vapour deposited SiC fibres p 66 A86-21486

- Graphite fiber intercalation: Basic properties of copper chloride intercalated fibers [NASA-TM-87217] p 65 N86-1844
Nickel-hydrogen separator development [NASA-TM-87332] p 188 N86-2667
The milling of pristine and brominated P-100 graphite fibers [NASA-TM-88828] p 106 N86-3257

FIELD EFFECT TRANSISTORS

- Cryogenic operation of pseudomorphic AlGaAs/InGaAs single-quantum-well MODFETs p 117 A86-1199
High transconductance InGaAs/AlGaAs pseudomorphic modulation-doped field-effect transistors p 117 A86-1881
Dc and microwave characteristics of a high current double interface GaAs/InGaAs/AlGaAs pseudomorphic modulation-doped field-effect transistor p 118 A86-3600

- Determination of carrier saturation velocity in high-performance In(y)Ga(1-y)As/Al(x)Ga(1-x)As modulation-doped field-effect transistors (with y between 0 and 0.2) p 118 A86-3729

- High-frequency noise of In(y)Ga(1-y)As/Al(x)Ga(1-x)As MODFETs and comparison to GaAs/Al(x)Ga(1-x)As MODFETs p 119 A86-43914

- Growth and characterization of epitaxial SrF2 or InP(100) p 205 A86-47071

- Test results for 20-GHz GaAs FET spacecraft power amplifier [NASA-TM-87072] p 111 N86-10378

- Hybrid power semiconductor [NASA-CASE-LEW-13922-1] p 122 N86-20678
Programmable, automated transistor test system [NASA-TP-2554] p 123 N86-21751

FIELD STRENGTH

- Electrohydrodynamics p 41 N86-10138

FILAMENT WINDING

- Ultrasonic evaluation of mechanical properties of thick multilayered, filament wound composites [NASA-TM-87088] p 163 N86-10561
Acousto-ultrasonic verification of the strength of filament wound composite material [NASA-TM-88827] p 166 N86-32764

FILE MAINTENANCE (COMPUTERS)

- Spectrum orbit utilization program technical manual SOUPs Version 3.8 [NASA-CR-174844] p 116 N86-26486

FILM COOLING

- Heat transfer results and operational characteristics of the NASA Lewis Research Center hot section cascade test facility [ASME PAPER 85-GT-82] p 128 A86-22053

- Film cooling on a convex wall: Heat transfer and hydrodynamic measurements for full and partial coverage [NASA-CR-174964] p 137 N86-10461

- Turbine vane external heat transfer. Volume 1: Analytical and experimental evaluation of surface heat transfer distributions with leading edge showerhead film cooling [NASA-CR-174827] p 29 N86-21546

FILM THICKNESS

- Fast approach for calculating film thicknesses and pressures in elastohydrodynamically lubricated contacts at high loads [ASME PAPER 85-TRIB-42] p 155 A86-43541

- Dynamic response of film thickness in spiral-groove face seals [NASA-TP-2544] p 27 N86-15313

- Polarization modulated ellipsometry [NASA-CR-177264] p 149 N86-26599

FINITE DIFFERENCE THEORY

- Vibration analysis of rotating turbomachinery blades by an improved finite difference method p 18 A86-14338

- Propagation and stability of wavelike solutions of finite difference equations with variable coefficients p 194 A86-20033

- Time-dependent wave envelope finite difference analysis of sound propagation p 197 A86-20130

- Vibration and buckling of rotating, pretwisted, precond beams including Coriolis effects p 168 A86-26910

- A note on the finite differencing of the linearized primitive equations' lower boundary condition p 191 A86-28963

- A computer analysis program for interfacing thermal and structural codes p 193 A86-36861

- A numerical and experimental investigation of electrochemical aircraft deicing [NASA-CR-175024] p 14 N86-20380

FINITE ELEMENT METHOD

- Finite elements based on consistently assumed stresses and displacements p 166 A86-18123
Simplex finite element analysis of viscous incompressible flow with penalty function formulation p 129 A86-22615

- Hierarchical implicit dynamic least-square solution algorithm p 167 A86-26689
- Three-dimensional hybrid-stress finite element analysis of composite laminates with cracks and cutouts p 167 A86-26896
- Designing for fiber composite structural durability in hygrothermomechanical environments p 67 A86-27734
- Probabilistic finite elements for transient analysis in nonlinear continua p 168 A86-28653
- Efficient algorithms for use in probabilistic finite element analysis p 168 A86-28655
- Error-source effects in a high-accuracy optical finite-element processor p 192 A86-31571
- Iterative methods for mixed finite element equations p 169 A86-34481
- Hybrid solid element with a traction-free cylindrical surface p 169 A86-34462
- Existence and stability, and discrete BB and rank conditions, for general mixed-hybrid finite elements in elasticity p 169 A86-34464
- A mesh re-zoning technique for finite element simulations of metal forming processes p 153 A86-36298
- A computer analysis program for interfacing thermal and structural codes p 193 A86-36861
- Computer aided derivation of equations for composite mechanics problems and finite element analyses [AIAA PAPER 86-1016] p 170 A86-38873
- An investigation of the transient thermal analysis of spur gears [ASME PAPER 84-DET-92] p 155 A86-40683
- Locally bound constrained Newton-Raphson solution algorithms --- for modeling kinematic and material nonlinearity p 171 A86-43771
- Finite element simulation of temperature dependent free surface flows p 136 A86-47012
- An iterative finite element-integral technique for predicting sound radiation from turbofan inlets in steady flight p 198 A86-49806
- Joint research effort on vibrations of twisted plates, phase 1: Final results [NASA-RP-1150] p 172 A86-10579
- Burner liner thermal/structural load modelling p 173 A86-11514
- Numerical Techniques in Acoustics [NASA-CP-2404] p 198 A86-12007
- Interlaminar fracture toughness: Three-dimensional finite element modeling for end-notch and mixed-mode flexure [NASA-TM-87138] p 69 A86-14316
- An analysis of cross-coupling of a multicomponent jet engine test stand using finite element modeling techniques [NASA-TM-176424] p 37 A86-15323
- Analysis of the transient behavior of rubbing components [NASA-CR-176546] p 102 A86-19464
- Rocket thrust chamber thermal barrier coatings [NASA-CR-175022] p 59 A86-20497
- A unique set of micromechanics equations for high temperature metal matrix composites [NASA-TM-87154] p 70 A86-24757
- Cyclic creep analysis from elastic finite-element solutions [NASA-TM-87213] p 176 A86-25822
- Theoretical and software considerations for general dynamic analysis using multilevel substructured models [NASA-CR-176822] p 195 A86-26067
- Computational simulation of progressive fracture in fiber composites [NASA-TM-87341] p 71 A86-26376
- Identification of differences between finite element analysis and experimental vibration data [NASA-TM-87336] p 149 A86-27617
- Modeling the effects of wind tunnel wall absorption on the acoustic radiation characteristics of propellers [NASA-TM-87333] p 201 A86-29630
- Effect of triangular element orientation on finite element solutions of the Helmholtz equation [NASA-TM-87351] p 201 A86-32247
- FINITE VOLUME METHOD**
- Thermodynamic evaluation of transonic compressor rotors using the finite volume approach [NASA-CR-176428] p 27 A86-16220
- Thermodynamic evaluation of transonic compressor rotors using the finite volume approach [NASA-CR-176840] p 143 A86-26546
- Thermodynamic evaluation of transonic compressor rotors using the finite volume approach [NASA-CR-176947] p 32 A86-30731
- FIRE PREVENTION**
- Ignition and flame spread above liquid fuel pools p 41 A86-10163
- FIRING (IGNITING)**
- Spontaneous ignition delay characteristics of hydrocarbon fuel-air mixtures [NASA-CR-175064] p 29 A86-21545
- FLAME PROPAGATION**
- Effects of buoyancy on gas jet diffusion flames - Experiment and theory [IAF PAPER 85-288] p 72 A86-15804
- Temperature and velocity profiles in sooting free boundary layer flames [AIAA PAPER 86-0575] p 73 A86-19962
- Drop-turbulence interactions in a diffusion flame p 73 A86-20139
- Prediction of heat release effects on a mixing layer [AIAA PAPER 86-0058] p 129 A86-22676
- Backward boundary layers in downward flame spread p 73 A86-22793
- Effects of preferential diffusion on the burning intensity of curved flames p 73 A86-22813
- On the determination of laminar flame speeds from stretched flames p 74 A86-22814
- An experimental investigation on flame interaction and the existence of negative flame speeds p 74 A86-22816
- Formation and inflammation of a turbulent jet p 130 A86-23131
- Particle cloud combustion experiment p 41 A86-10160
- A fundamental study of smoldering with emphasis on experimental design for zero-g p 41 A86-10162
- Ignition and flame spread above liquid fuel pools p 41 A86-10163
- Flammability limits of gases under low gravity conditions p 42 A86-10164
- Aerodynamic properties of turbulent combustion fields [NASA-CR-175005] p 28 A86-20393
- Prediction of heat release effects on a mixing layer [NASA-CR-175044] p 142 A86-23857
- Flame propagation and extinction in particle clouds [NASA-CR-177304] p 78 A86-27434
- The behavior of fuel-lean premixed flames in a standard flammability limit tube under controlled gravity conditions [NASA-CR-177132] p 78 A86-28139
- FLAME SPECTROSCOPY**
- Methane oxidation behind reflected shock waves: Ignition delay times measured by pressure and flame band emission [NASA-TM-87268] p 77 A86-21635
- FLAME STABILITY**
- Numerical simulation of a turbulent flame stabilized behind a rearward-facing step p 73 A86-22774
- Buoyancy effects upon vapor flame and explosion processes p 41 A86-10161
- Flammability limits of gases under low gravity conditions p 42 A86-10164
- FLAME TEMPERATURE**
- Temperature and velocity profiles in sooting free boundary layer flames [AIAA PAPER 86-0575] p 73 A86-19962
- Effects of preferential diffusion on the burning intensity of curved flames p 73 A86-22813
- Influence of temperature and hydroxyl concentration on incipient soot formation in premixed flames p 74 A86-29070
- FLAMMABILITY**
- Effect of gravity on laminar premixed gas combustion. I - Flammability limits and burning velocities p 72 A86-12413
- Flammability limits of gases under low gravity conditions p 42 A86-10164
- FLAMMABLE GASES**
- Flammability limits of gases under low gravity conditions p 42 A86-10164
- FLASHBACK**
- Combustor flame flashback [NASA-CR-174961] p 183 A86-14727
- FLAT PLATES**
- Relaminarization of the boundary layer over a flat plate in shock tube experiments [AIAA PAPER 86-1238] p 133 A86-39865
- Low Reynolds number boundary layers in a disturbed environment [NASA-CR-175031] p 139 A86-17665
- FLEXIBLE BODIES**
- The dynamics of a flexible bladed disc on a flexible rotor in a two-rotor system p 20 A86-25743
- FLEXIBLE SPACECRAFT**
- Frequency domain solutions to multi-degree-of-freedom, dry friction damped systems under periodic excitation p 170 A86-39485
- FLEXING**
- Graphite/PMR polyimide composites with improved toughness p 66 A86-21731
- FLIGHT CHARACTERISTICS**
- The aerodynamics of rotor blades with ice shapes accreted in hover and in level flight p 5 A86-35655
- Polymer, metal and ceramic matrix composites for advanced aircraft engine applications [NASA-TM-87132] p 87 A86-13407
- FLIGHT CONDITIONS**
- MERIT - A new approach to upper air forecasting for aviation p 191 A86-17962
- FLIGHT SAFETY**
- Performance degradation of helicopters due to icing - A review p 16 A86-35668
- FLIGHT SIMULATION**
- A high-order language for a system of closely coupled processing elements [NASA-CR-177280] p 193 A86-27930
- FLIGHT TESTS**
- Uniform engine testing program phase 7: NASA Lewis Research Center second entry [NASA-TM-87272] p 31 A86-28085
- The voltage threshold for arcing for solar cells in LEO: Flight and ground test results [NASA-TM-87259] p 62 A86-28125
- ACTS Experiments Program [NASA-TM-88820] p 47 A86-31625
- FLOW CHARACTERISTICS**
- Applications of variational principles in computing rotational flows p 128 A86-20951
- A numerical simulation of the inviscid flow through a counter-rotating propeller [NASA-TM-87200] p 10 A86-16195
- FLOW COEFFICIENTS**
- Semiempirical method of determining flow coefficients for pitot rake mass flow rate measurements [NASA-TM-87144] p 9 A86-14219
- FLOW DISTORTION**
- Packet flutter and aerodynamic modes for non-homogeneous airfoil cascades in highly distorted, periodic, stationary throughflows [AIAA PAPER 86-0848] p 5 A86-38896
- Horseshoe vortex formation around a cylinder [ASME PAPER 86-GT-246] p 8 A86-48274
- Statistical prediction of dynamic distortion of inlet flow using minimum dynamic measurement. An application to the Melick statistical method and inlet flow dynamic distortion prediction without RMS measurements [NASA-CR-176764] p 142 A86-24933
- Review and evaluation of recent developments in melt inlet dynamic flow distortion prediction and computer program documentation and user's manual estimating maximum instantaneous inlet flow distortion from steady-state total pressure measurements with full, limited, or no dynamic data [NASA-CR-176765] p 143 A86-24955
- Summary of investigations of engine response to distorted inlet conditions [NASA-TM-87317] p 30 A86-26336
- FLOW DISTRIBUTION**
- Modeling dilution of jet flowfields p 128 A86-20362
- Steady inviscid three-dimensional flows p 128 A86-20952
- Calculations of two and three-dimensional transonic cascade flow fields using the Navier-Stokes equations [ASME PAPER 85-GT-66] p 2 A86-22046
- A three-dimensional axisymmetric calculation procedure for turbulent flows in a radial vaneless diffuser [ASME PAPER 85-GT-133] p 3 A86-22733
- Through-flow modeling of axial turbomachinery [ASME PAPER 85-IGT-42] p 3 A86-23854
- Calculation of three-dimensional boundary layers on rotating turbine blades p 131 A86-28696
- An experimental study of tone-excited heated jets p 197 A86-31593
- Flow field and near and far sound field of a subsonic jet p 5 A86-35855
- An experimental study of energy loss mechanisms and efficiency considerations in the low power dc arcjet [AIAA PAPER 85-2017] p 53 A86-37062
- Turbine-stage heat transfer - Comparison of short-duration measurements with state-of-the-art predictions [AIAA PAPER 86-1485] p 134 A86-42656
- Structural integrity and durability for Space Shuttle main engine and future reusable space propulsion systems [AIAA PAPER 86-1513] p 55 A86-26882
- Improved Euler analysis of advanced turboprop propeller flows [AIAA PAPER 86-1521] p 6 A86-42688
- A comparison of computational methods for three-dimensional, turbulent turbomachinery flow fields [AIAA PAPER 86-1599] p 6 A86-42740
- Three-dimensional flow field measurements in a radial inflow turbine scroll using LDV [ASME PAPER 86-GT-122] p 7 A86-48181
- A model for closing the inviscid form of the average-passage equation system [ASME PAPER 86-GT-227] p 8 A86-48261

- Effect of area ratio on the performance of a 5.5:1 pressure ratio centrifugal impeller
[ASME PAPER 86-GT-303] p 8 A86-48315
- Summary of recent NASA propeller research
p 25 N86-11158
- An experimental study of energy loss mechanisms and efficiency consideration in the low power dc arcjet
[NASA-TM-87123] p 57 N86-11224
- Assessment of a 3-D boundary layer code to predict heat transfer and flow losses in a turbine
p 138 N86-11508
- A FORTRAN computer code for calculating flows in multiple-blade-element cascades
[NASA-TM-87104] p 9 N86-13295
- A model for closing the inviscid form of the average-passage equation system
[NASA-TM-87199] p 10 N86-14224
- Effect of area ratio on the performance of a 5.5:1 pressure ratio centrifugal impeller
[NASA-TM-87237] p 10 N86-19290
- Particle trajectory computation on a 3-dimensional engine inlet
[NASA-CR-175023] p 14 N86-20379
- Measurements of a single lateral jet injected into swirling crossflow
[NASA-CR-175040] p 28 N86-20392
- Aerodynamic properties of turbulent combustion fields
[NASA-CR-175005] p 28 N86-20393
- Experiments on opposed lateral jets injected into swirling crossflow
[NASA-CR-175041] p 29 N86-20394
- Method and apparatus for rebalancing a REDOX flow cell system
[NASA-CASE-LEW-14127-1] p 122 N86-20680
- Shear layer excitation, experiment versus theory
[NASA-CR-176604] p 140 N86-20722
- SSME fuelside preburner two-dimensional analysis
[NASA-TM-87299] p 44 N86-23616
- Statistical prediction of dynamic distortion of inlet flow using minimum dynamic measurement. An application to the Melick statistical method and inlet flow dynamic distortion prediction without RMS measurements
[NASA-CR-176764] p 142 N86-24833
- Structural integrity and durability for Space Shuttle main engine and future reusable space propulsion systems
[NASA-TM-87280] p 61 N86-25408
- The boundary layer on compressor cascade blades
[NASA-CR-177279] p 143 N86-27607
- Application of laser anemometry to turbomachinery flow field measurements
p 160 N86-27640
- Laser fringe anemometry for aero engine components
[NASA-TM-88798] p 12 N86-28053
- Measurements of a turbulent horseshoe vortex formed around a cylinder
[NASA-CR-3986] p 13 N86-28063
- Lateral jet injection into typical combustor flowfields
[NASA-CR-3997] p 31 N86-28086
- Numerical simulation of the flowfield over ice accretion shapes
[NASA-CR-176960] p 144 N86-30093
- Comparison of analytical and experimental performance of a wind-tunnel diffuser section
[NASA-TM-88795] p 13 N86-31537
- Visualization of flows in a motored rotary combustion engine using holographic interferometry
[NASA-TM-88804] p 33 N86-31583
- FLOW EQUATIONS**
- An implicit LU scheme for the Euler equations applied to arbitrary cascades — new method of factoring
p 2 A86-20131
- A theory of post-stall transients in axial compression systems. I - Development of equations
[ASME PAPER 85-GT-171] p 19 A86-22088
- A theory of post-stall transients in axial compression systems. II - Application
[ASME PAPER 85-GT-172] p 19 A86-22089
- A model for closing the inviscid form of the average-passage equation system
[ASME PAPER 86-GT-227] p 8 A86-48261
- A model for closing the inviscid form of the average-passage equation system
[NASA-TM-87199] p 10 N86-14224
- Improvement of the second- and third-moment modeling of turbulence: A study of Reynolds-stress closure model
[NASA-CR-176478] p 139 N86-18519
- NASA/DOE automotive Stirling engine project: Overview 1986
[NASA-TM-87345] p 211 N86-29731
- Thermodynamic evaluation of transonic compressor rotors using the finite volume approach
[NASA-CR-176947] p 32 N86-30731
- FLOW GEOMETRY**
- Free shear flows - Organized structures and effects of excitation
[AIAA PAPER 86-0235] p 131 A86-26614

FLOW MEASUREMENT

- Concentration distributions in cylindrical combustors
p 126 A86-11937
- Scalar and momentum turbulent transport experiments with swirling and nonswirling flows
p 126 A86-11938
- Tone excited jets. III - Flow measurements
p 127 A86-16468
- Numerical and experimental investigation of nonswirling and swirling confined jets
[AIAA PAPER 86-0040] p 127 A86-19651
- Boundary layer measurements on an airfoil in cascade using laser Doppler anemometry
[AIAA PAPER 86-0072] p 145 A86-19670
- An experimental investigation of propeller wakes using a laser Doppler velocimeter
[AIAA PAPER 86-0080] p 18 A86-19677
- Simultaneous measurements of velocity and pressure fields in subsonic and supersonic flows through image-intensified detection of laser-induced fluorescence
[AIAA PAPER 86-0161] p 145 A86-19726
- Oscillatory thermocapillary flows
p 129 A86-22413
- An experimental investigation and some analytical considerations concerning the vaporous/gaseous cavity characteristics of an eccentric shaft seal or bearing
p 130 A86-24463
- Accuracy and directional sensitivity of the single-wire technique
p 146 A86-28541
- Implementation of a new type of time-of-flight laser anemometer
p 146 A86-29755
- An experimental study of tone-excited heated jets
p 197 A86-31593
- Recent skin friction techniques for compressible flows
[AIAA PAPER 86-1099] p 147 A86-38460
- Laser anemometry for hot section applications
p 151 N86-11503
- Semiempirical method of determining flow coefficients for pitot rake mass flow rate measurements
[NASA-TM-87144] p 9 N86-14219
- Application of laser anemometry to turbomachinery flow field measurements
p 160 N86-27640
- High accuracy fuel flowmeter
[NASA-CR-174869] p 150 N86-31030
- Parametric study of beam refraction problems across laser anemometer windows
[NASA-TM-87350] p 150 N86-31857
- Advanced optical measuring systems for measuring the properties of fluids and structures
[NASA-TM-88829] p 150 N86-31859
- FLOW STABILITY**
- Periodic oscillations observed in swirling flows with and without combustion
p 73 A86-22755
- Interaction of flows with the crystal-melt interface
p 132 A86-29419
- Convective and absolute instability of a viscous liquid jet
p 132 A86-34377
- Extended parametric representation of compressor fans and turbines. Volume 1: CMGEN user's manual
[NASA-CR-174645] p 159 N86-23936
- Extended parametric representation of compressor fans and turbines. Volume 3: MODFAN user's manual (parametric modulating flow fan)
[NASA-CR-174647] p 159 N86-23938
- FLOW THEORY**
- Free shear flows - Organized structures and effects of excitation
[AIAA PAPER 86-0235] p 131 A86-26614
- A new approach for solving the three-dimensional steady Euler equations. I - General theory
p 133 A86-41242
- FLOW VELOCITY**
- Three component velocity measurements using Fabry-Perot interferometer
p 145 A86-16378
- Temperature and velocity profiles in sooting free boundary layer flames
[AIAA PAPER 86-0575] p 73 A86-19962
- On the determination of laminar flame speeds from stretched flames
p 74 A86-22814
- Triple-velocity products in a channel with a backward-facing step
p 133 A86-41725
- Plume characteristics of single-stream and dual-flow conventional and inverted-profile nozzles at equal thrust
[AIAA PAPER 86-1809] p 8 A86-49585
- Characteristics of an axisymmetric sudden expansion flow
[NASA-CR-176278] p 151 N86-11465
- Laser anemometry for hot section applications
p 151 N86-11503
- Semiempirical method of determining flow coefficients for pitot rake mass flow rate measurements
[NASA-TM-87144] p 9 N86-14219
- Dilution jet mixing program, phase 3
[NASA-CR-174884] p 142 N86-24938
- Plume characteristics of single-stream and dual-flow conventional and inverted-profile nozzles at equal thrust
[NASA-TM-87323] p 12 N86-26285

FLOW VISUALIZATION

- Multispark flow visualization of lateral jet injection into a swirling cross flow
p 1 A86-14561
- Unsteady pressure measurements on a biconvex airfoil in a transonic oscillating cascade
[ASME PAPER 85-GT-212] p 3 A86-22731
- Entrainment region phenomena for a large plane shear layer
p 132 A86-30211
- Flow visualization of secondary flows in three curve ducts
[ASME PAPER 86-GT-166] p 136 A86-48218
- Three-dimensional fluid flow phenomena in the blade end wall corner region
[ASME PAPER 86-GT-179] p 7 A86-48229
- Development of seeding techniques for small supersonic wind tunnel
p 147 N86-11452
- Optical elements formed by compressed gases: Analysis and potential applications
[NASA-TP-2555] p 203 N86-22390
- Beam-modulation methods in quantitative and flow visualization holographic interferometry
[NASA-TM-87306] p 148 N86-24958
- The boundary layer on compressor cascade blades
[NASA-CR-177279] p 143 N86-27607
- Lateral jet injection into typical combustor flowfields
[NASA-CR-3997] p 31 N86-28086
- Visualization of flows in a motored rotary combustion engine using holographic interferometry
[NASA-TM-88804] p 33 N86-31583
- Advanced optical measuring systems for measuring the properties of fluids and structures
[NASA-TM-88829] p 150 N86-31859
- FLOWMETERS**
- High accuracy fuel flowmeter
[NASA-CR-174869] p 150 N86-31030
- FLUID DYNAMICS**
- Fluid management and its role in the future of Space Station
[AIAA PAPER 86-2301] p 47 A86-49553
- Surface tension induced instabilities in reduced gravity: The Benard problem
p 40 N86-10117
- Experimental and theoretical analysis of chemical vapor deposition with prediction of gravity effects
p 41 N86-10132
- Measurement of the density of base fluids at pressures 0.422 to 2.20 GPa
[NASA-TM-87114] p 156 N86-10551
- Advanced research and technology program for advanced high pressure oxygen-hydrogen rocket propulsion
p 58 N86-17405
- Advanced seals for Liquid Oxygen (LOX) turbopumps
p 157 N86-17408
- Dilution jet mixing program, phase 3
[NASA-CR-174884] p 142 N86-24938
- Improved perfluoroalkylether fluid development
[NASA-TM-87276] p 104 N86-25474
- A lumped parameter mathematical model for simulation of subsonic wind tunnels
[NASA-TM-87324] p 196 N86-27036
- Two-phase flows within systems with ambient pressure
p 161 N86-30167
- FLUID FILMS**
- Operating aspects of an oil pumping ring seal
[ASME PAPER 85-TRIB-29] p 153 A86-34010
- Advanced seals for Liquid Oxygen (LOX) turbopumps
p 157 N86-17408
- FLUID FLOW**
- Fluid flow and fuel-air mixing in a motored two-dimensional Wankel rotary engine
[AIAA PAPER 86-1556] p 134 A86-42711
- Three-dimensional fluid flow phenomena in the blade end wall corner region
[ASME PAPER 86-GT-179] p 7 A86-48229
- Transport processes in solution crystal growth
p 39 N86-10107
- Surface-tension driven convection
p 40 N86-10124
- Flammability limits of gases under low gravity conditions
p 42 N86-10164
- Electrocrystallization in microgravity
[NASA-TM-87202] p 212 N86-19274
- A lumped parameter mathematical model for simulation of subsonic wind tunnels
[NASA-TM-87324] p 196 N86-27036
- Experimental and analytical investigation of a freezing point depressant fluid ice protection system
[NASA-CR-174758] p 12 N86-27186
- FLUID INJECTION**
- Hot-wire measurements of a single lateral jet injected into swirling crossflow
[AIAA PAPER 86-0055] p 127 A86-19661
- Vortex modeling of single and multiple dilution jet mixing in a cross flow
p 135 A86-46318
- Flow and atomization in flashing injectors
p 136 A86-49442

SUBJECT INDEX

FLUID JETS

- Convective and absolute instability of a viscous liquid jet p 132 A86-34377

FLUID MANAGEMENT

- Cryogenic Fluid Management Facility p 108 A86-37053
Effect of subcooling on the on-orbit pressurization rate of cryogenic propellant tankage [AIAA PAPER 86-1253] p 54 A86-39877
Fluid management and its role in the future of Space Station [AIAA PAPER 86-2301] p 47 A86-49553

FLUID MECHANICS

- Heat transfer and fluid mechanics measurements in transitional boundary layer flows [ASME PAPER 85-GT-113] p 126 A86-13068
Three component velocity measurements using Fabry-Perot interferometer p 145 A86-16378
Three dimensional flow phenomena in fluid machinery: Proceedings of the Winter Annual Meeting, Miami Beach, FL, November 17-22, 1985 p 4 A86-28682
Surface-tension driven convection p 40 N86-10124
Thermocapillary motion research p 40 N86-10125
Transport processes research p 40 N86-10129
Fluid machines: Expanding the limits, past and future [NASA-TM-87161] p 26 N86-12227
Advanced research and technology program for advanced high pressure oxygen-hydrogen rocket propulsion p 58 N86-17405

FLUID PRESSURE

- Analysis of a two row hydrostatic journal bearing with variable properties, inertia effects and surface roughness p 153 A86-30599

FLUID-SOLID INTERACTIONS

- Interaction of flows with the crystal-melt interface p 132 A86-29419

FLUIDIZED BED PROCESSORS

- Design and evaluation of fluidized bed heat recovery for diesel engine systems [NASA-CR-174898] p 209 N86-21456

FLUORIDES

- Estimated heats of fusion of fluoride salt mixtures suitable for thermal energy storage applications [NASA-TM-87320] p 190 N86-31982

FLUOROAMINES

- Low-wear partially fluorinated polyimides p 94 A86-11175

FLUOROCARBONS

- Dry etching of beta-SiC in CF₄ and CF₄ + O₂ mixtures p 76 A86-47069

FLUTTER

- Aerodynamic detuning analysis of an unstalled supersonic turbofan cascade [ASME PAPER 85-GT-192] p 3 A86-22732
The effects of strong shock loading on coupled bending-torsion flutter of tuned and mistuned cascades p 20 A86-26893
Application of a linearized unsteady aerodynamic analysis to standard cascade configurations [NASA-CR-3940] p 11 N86-21505

FLUTTER ANALYSIS

- Influence of rotation and pretwist on cantilever fan blade flutter p 17 A86-11686
Packet flutter and aerodynamic modes for non-homogeneous airfoil cascades in highly distorted, periodic, stationary throughflows [AIAA PAPER 86-0848] p 5 A86-38896
Mass balancing of hollow fan blades [ASME PAPER 86-GT-195] p 171 A86-48245
Mass balancing of hollow fan blades [NASA-TM-87197] p 174 N86-16611
Experimental classical flutter results of a composite advanced turboprop model [NASA-TM-88792] p 178 N86-29271

FLYWHEELS

- Operating characteristics of a 0.87 kW-hr flywheel energy storage module p 152 A86-24864

FOCI

- Near-field spillover from a subreflector: Theory and experiment [NASA-TM-88763] p 115 N86-25650

FOCUSING

- Verification of an improved computational design procedure for TWT-dynamic refocuser-MDC systems with secondary electron emission losses p 119 A86-45194

FORCED VIBRATION

- Forced response analysis of an aerodynamically detuned supersonic turbomachine rotor p 21 A86-26902
Extensions of the Ritz-Galerkin method for the forced, damped vibrations of structural elements p 176 N86-21909

FORMING TECHNIQUES

- Factors influencing the ball milling of Si₃N₄ in water p 95 A86-15239

- A mesh re-zoning technique for finite element simulations of metal forming processes p 153 A86-36298

FORTAN

- Reliability of void detection in structural ceramics by use of scanning laser acoustic microscopy p 163 A86-39027

- A FORTRAN computer code for calculating flows in multiple-blade-element cascades [NASA-TM-87104] p 9 N86-13295

FORWARD SCATTERING

- Characteristics of an axisymmetric sudden expansion flow [NASA-CR-176278] p 151 N86-11465

FOULING

- Experiments for the determination of convective diffusion heat/mass transfer to burner rig test targets comparable in size to jet stream diameter [NASA-TM-87196] p 139 N86-18646

FOURIER TRANSFORMATION

- Characterization methodology for PMR-15 p 65 N86-11272
Secondary pattern computation of an offset reflector antenna [NASA-TM-87160] p 112 N86-14479
Analysis of a thioether lubricant by infrared Fourier microemission spectrophotometry [NASA-TM-87195] p 102 N86-16379
Determination of grain size distribution function using two-dimensional Fourier transforms of tone pulse encoded images [NASA-TM-88790] p 166 N86-31065

FOURIER-BESSEL TRANSFORMATIONS

- Strategy for reflector pattern calculation - Let the computer do the work p 110 A86-39542
Strategy for reflector pattern calculation: Let the computer do the work [NASA-TM-87137] p 112 N86-12485

FRACTOGRAPHY

- Creep-rupture and fractographic analysis of Stirling engine superalloys tested in air and 15 MPa hydrogen p 82 A86-30041
A study of spectrum fatigue crack propagation in two aluminum alloys. I - Spectrum simplification. II - Influence of microstructures p 85 A86-48973

FRACTURE MECHANICS

- Failure analysis of plasma-sprayed thermal barrier coatings p 80 A86-16270
Wide-range displacement expressions for standard fracture mechanics specimens p 166 A86-20706
Wide-range weight functions for the strip with a single edge crack p 167 A86-20709
Fracture mechanics applied to nonisothermal fatigue crack growth p 81 A86-26351
Progressive fracture of fiber composites p 67 A86-35809
Burner rig corrosion of SiC at 1000 C p 99 A86-36328
Quantitative flaw characterization with scanning laser acoustic microscopy p 163 A86-45150
Rapidly solidified NiAl and FeAl p 84 A86-47263
Progressive damage, fracture predictions and post mortem correlations for fiber composites [NASA-TM-87101] p 68 N86-10290
SCARE: A post-processor program to MSC/NASTRAN for the reliability analysis of structural ceramic components [NASA-TM-87188] p 174 N86-14688
Estimating the R-curve from residual strength data [NASA-TM-87182] p 175 N86-18750
Variables controlling fatigue crack growth of short cracks [NASA-TM-87208] p 90 N86-21661
Quantitative flaw characterization with scanning laser acoustic microscopy p 200 N86-22983
Fatigue crack layer propagation in silicon-iron [NASA-CR-175115] p 177 N86-25851
Computational simulation of progressive fracture in fiber composites [NASA-TM-87341] p 71 N86-26376
Effects of a high mean stress on the high cycle fatigue life of PWA 1480 and correlation of data by linear elastic fracture mechanics [NASA-CR-175057] p 177 N86-27689

FRACTURE STRENGTH

- Comparison of the contact stress and friction behavior of SiC and ZrO₂ materials p 95 A86-15237
The crack layer approach to toughness characterization in steel p 82 A86-30010
Fracture toughness tests on plasma-sprayed coatings p 64 A86-30051
Tensile adhesion test measurements on plasma-sprayed coatings p 98 A86-30052
Dynamic stress analysis of smooth and notched fiber composite flexural specimens p 67 A86-41070

FREQUENCY ASSIGNMENT

- Dynamic delamination crack propagation in a graphite/epoxy laminate p 68 A86-43010
Fractured toughness of Si₃N₄ measured with short bar chevron-notched specimens [NASA-TM-87153] p 101 N86-13495

- Interlaminar fracture toughness: Three-dimensional finite element modeling for end-notch and mixed-mode flexure [NASA-TM-87138] p 69 N86-14316

- Transformation toughened ceramics for the heavy duty diesel engine technology program, phase 2 [NASA-CR-175054] p 210 N86-22451

- Fracture characteristics of angleplated laminates fabricated from overaged graphite/epoxy prepreg [NASA-TM-87266] p 70 N86-25417

- Concepts for interrelating ultrasonic attenuation, microstructure and fracture toughness in polycrystalline solids [NASA-TM-87339] p 165 N86-25812

- Correlation of processing and sintering variables with the strength and radiography of silicon nitride [NASA-TM-87251] p 106 N86-31729

- Improved fracture toughness corrosion-resistant bearing material [NASA-CR-174990] p 162 N86-32743

- Acousto-ultrasonic verification of the strength of filament wound composite material [NASA-TM-88827] p 166 N86-32764

FRACTURES (MATERIALS)

- Fundamental tribological properties of ceramics p 95 A86-15230
Fundamental studies of low velocity impact resistance of graphite fiber reinforced polymer matrix composites [NASA-TM-86886] p 69 N86-23661

FRACTURING

- Designing for fiber composite structural durability in hygrothermomechanical environments p 67 A86-27734

- Progressive damage, fracture predictions and post mortem correlations for fiber composites [NASA-TM-87101] p 68 N86-10290

- Surface fatigue life and failure characteristics of EX-53, CBS 1000M, and AISI 9310 gear materials [NASA-TP-2513] p 157 N86-12609

FREE BOUNDARIES

- Boundary perturbation method for free boundary problem in convectively cooled continuous casting p 131 A86-28649

- Free boundary shape of a convectively cooled solidified region p 131 A86-29029

- Free surface phenomena under low- and zero-gravity conditions p 39 N86-10108

FREE CONVECTION

- Surface temperature distribution along a thin liquid layer due to thermocapillary convection [IAF PAPER 85-282] p 126 A86-15800
Energy stability of thermocapillary convection in models of the float zone process p 40 N86-10123

FREE FLOW

- Effect of free stream turbulence on flow separation p 125 A86-11676

- Preliminary results of a study of the relationship between free stream turbulence and stagnation region heat transfer [ASME PAPER 85-GT-84] p 129 A86-22055

- Free shear flows - Organized structures and effects of excitation [AIAA PAPER 86-0235] p 131 A86-26614

- Entrainment region phenomena for a large plane shear layer p 132 A86-30211

FREE JETS

- Three component velocity measurements using Fabry-Perot interferometer p 145 A86-16378
Numerical simulation of unsteady flow in an axisymmetric shear layer [AIAA PAPER 86-0202] p 127 A86-19746

- Acoustic control of free jet mixing p 135 A86-46314

FREE RADICALS

- Chemical control of rate and onset temperature of nadimide polymerization p 101 N86-11271

FREEZING

- Determination of solid mass fraction in partially frozen hydrocarbon fuels [NASA-CR-179472] p 108 N86-28261

FREON

- SSME long-life bearings [NASA-CR-179455] p 160 N86-27643

FREQUENCIES

- Transfer function concept for ultrasonic characterization of material microstructures p 200 N86-22980

FREQUENCY ASSIGNMENT

- The role of service areas in the optimization of FSS orbital and frequency assignments [AIAA PAPER 86-0636] p 45 A86-29599

- Impact of the 1985 space World Administrative Radio Conference on frequency/orbit planning and use [AIAA PAPER 86-0634] p 110 N86-49567
- The role of service areas in the optimization of FSS orbital and frequency assignments [NASA-CR-176488] p 46 N86-18341
- Broadcasting satellite service synthesis using gradient and cyclic coordinate search procedures [NASA-CR-176708] p 114 N86-23781
- Impact of the 1985 Space World Administrative Radio Conference on frequency/orbit planning and use [NASA-TM-87285] p 115 N86-24881
- FREQUENCY DIVIDERS**
- 10-30 GHz monolithic GaAs travelling-wave divider/combiner p 118 N86-34882
- FREQUENCY MEASUREMENT**
- Thermoviscoplastic nonlinear constitutive relationships for structural analysis of high temperature metal matrix composites [NASA-TM-87291] p 70 N86-24756
- FREQUENCY MODULATION**
- Range finding using frequency-modulated laser diode p 147 N86-39521
- FREQUENCY REUSE**
- Calculation of allowable orbital spacings for the fixed-satellite service [NASA-CR-176273] p 43 N86-11212
- FREQUENCY SHIFT**
- Characteristics of an axisymmetric sudden expansion flow [NASA-CR-176278] p 151 N86-11465
- FRETTING CORROSION**
- Selected fretting-wear-resistant coatings for Ti-6 pct Al-4 pct V alloy p 97 N86-24856
- FRICTION**
- Surface effects of corrosive media on hardness, friction, and wear of materials p 94 N86-10825
- Fundamental tribological properties of ceramics p 95 N86-15230
- Frictional and morphological properties of Au-MoS₂ films sputtered from a compact target p 152 N86-16258
- Tribological properties of boron nitride synthesized by ion beam deposition p 96 N86-17479
- Optical and other properties changes of M-50 bearing steel surfaces for different lubricants and additives prior to scuffing p 97 N86-20435
- Characterization and measurement of polymer wear p 100 N86-48405
- Tribological characteristics of gold films deposited on metals by ion plating and vapor deposition p 85 N86-49600
- Tribological properties of structural ceramics [NASA-TM-87105] p 100 N86-10341
- Constitutive modelling of lubricants in concentrated contacts at high slide to roll ratios [NASA-CR-175029] p 158 N86-17748
- Adhesion and wear resistance of materials [NASA-TM-87239] p 158 N86-20809
- Tribology of selected ceramics at temperatures to 900 deg C [NASA-TM-87267] p 105 N86-25476
- FRICTION FACTOR**
- Centaur engine gimbal friction characteristics under simulated thrust load [NASA-TM-87335] p 44 N86-31621
- FRICTION MEASUREMENT**
- Recent skin friction techniques for compressible flows [AIAA PAPER 86-1099] p 147 N86-38460
- FRICTION REDUCTION**
- Lubricant and additive effects on spur gear fatigue life [ASME PAPER 85-TRIB-14] p 155 N86-43542
- FUEL CELL POWER PLANTS**
- Onsite 40-kilowatt fuel cell power plant manufacturing and field test program [NASA-CR-174988] p 185 N86-18773
- Develop and test fuel cell powered on-site integrated total energy systems [NASA-CR-174951] p 188 N86-25877
- Advanced on-site power plant development technology program [NASA-CR-175007] p 189 N86-29411
- Gas cooled fuel cell systems technology development [NASA-CR-175047] p 190 N86-31984
- FUEL CELLS**
- Onsite 40-kilowatt fuel cell power plant manufacturing and field test program [NASA-CR-174988] p 185 N86-18773
- Advanced on-site power plant development technology program [NASA-CR-174709] p 187 N86-25040
- Develop and test fuel cell powered on-site integrated total energy systems [NASA-CR-174951] p 188 N86-25877
- Theoretical and experimental flow cell studies of a hydrogen-bromine fuel cell, part 1 [NASA-CR-177165] p 189 N86-29409
- Advanced on-site power plant development technology program [NASA-CR-175007] p 189 N86-29411
- FUEL COMBUSTION**
- Two dimensional, transient catalytic combustion of CO-air on platinum p 71 N86-10201
- On the determination of laminar flame speeds from stretched flames p 74 N86-22814
- Ignition characteristics of rich n-heptane fuel sprays in the transition region [ASME PAPER 85-WA/HT-46] p 107 N86-38393
- Analysis of the effects of fuel spray characteristics on NO(x) formation [ASME PAPER 85-WA/HT-47] p 107 N86-38394
- Combustor flame flashback [NASA-CR-174961] p 183 N86-14727
- Oxides of nitrogen emissions from the combustion of monodisperse liquid fuel sprays [NASA-CR-176373] p 191 N86-14770
- Ignition delay times of benzene and toluene with oxygen in argon mixtures [NASA-TM-87312] p 78 N86-25431
- Role of fuel chemical properties on combustor radiative heat load [NASA-CR-177096] p 108 N86-30023
- Small gas turbine combustor experimental study: Compliant metal/ceramic liner and performance evaluation [NASA-TM-87304] p 33 N86-31582
- FUEL CONSUMPTION**
- Method for improving the fuel efficiency of a gas turbine engine [NASA-CASE-LEW-13142-2] p 28 N86-20389
- A supersonic fan equipped variable cycle engine for a Mach 2.7 supersonic transport [NASA-CR-177141] p 32 N86-28946
- Aerodynamic data banks for Clark-Y, NACA 4-digit and NACA 16-series airfoil families [NASA-CR-176883] p 13 N86-30693
- FUEL CONTAMINATION**
- Fuel deposit characteristics at low velocity [ASME PAPER 85-IGT-130] p 107 N86-23922
- FUEL CONTROL**
- Polymer, metal and ceramic matrix composites for advanced aircraft engine applications [NASA-TM-87132] p 87 N86-13407
- FUEL CORROSION**
- Emission FTIR analyses of thin microscopic patches of jet fuel residues deposited on heated metal surfaces [NASA-CR-178786] p 108 N86-25502
- FUEL INJECTION**
- Experimental study of the spray characteristics of a research airblast atomizer [ASME PAPER 85-GT-229] p 129 N86-22125
- Fluid flow and fuel-air mixing in a motored two-dimensional Wankel rotary engine [AIAA PAPER 86-1556] p 134 N86-42711
- Atomization and combustion characteristics of antimisting fuels using JT8D and air-boost injectors [ASME PAPER 86-GT-223] p 24 N86-48257
- Lightweight two-stroke cycle aircraft diesel engine technology enablement program, volume 1 [NASA-CR-174923-VOL-1] p 26 N86-13328
- Lightweight two-stroke cycle aircraft diesel engine technology enablement program, volume 2 [NASA-CR-174923-VOL-2] p 26 N86-13329
- Lightweight two-stroke cycle aircraft diesel engine technology enablement program, volume 3 [NASA-CR-174923-VOL-3] p 26 N86-13330
- Role of fuel chemical properties on combustor radiative heat load [NASA-CR-177096] p 108 N86-30023
- FUEL PUMPS**
- The noncavitating performance and life of a small vane-type positive displacement pump in liquid hydrogen [NASA-TM-87347] p 63 N86-31651
- Small centrifugal pumps for low-thrust rocket engines [NASA-CR-174913] p 162 N86-32741
- FUEL SPRAYS**
- Drop-turbulence interactions in a diffusion flame p 73 N86-20139
- High Weber number SMD correlations for pressure atomizers — Sauter Mean Diameter [ASME PAPER 85-GT-37] p 128 N86-22026
- Effect of elevated temperature and pressure on sprays from simplex swirl atomizers [ASME PAPER 85-GT-58] p 130 N86-22735
- Prediction of the structure of fuel sprays in gas turbine combustors [AIAA PAPER 86-0450] p 20 N86-26636
- Ignition characteristics of rich n-heptane fuel sprays in the transition region [ASME PAPER 85-WA/HT-46] p 107 N86-38393
- Analysis of the effects of fuel spray characteristics on NO(x) formation [ASME PAPER 85-WA/HT-47] p 107 N86-38394
- Characterization of simulated small-droplet fuel sprays [AIAA PAPER 86-1725] p 135 N86-42813
- Transition region ignition characteristics of n-heptane fuel sprays [NASA-CR-176364] p 77 N86-14331
- Prediction of the structure of fuel sprays in gas turbine combustors [NASA-CR-175028] p 27 N86-16218
- Combustion characteristics in the transition region of liquid fuel sprays [NASA-CR-176584] p 77 N86-20517
- Characterization of simulated small-droplet fuel sprays [NASA-TM-87286] p 148 N86-24961
- FUEL SYSTEMS**
- Evaluation of fuel preparation systems for lean premixing-prevaporizing combustors [ASME PAPER 85-GT-137] p 19 N86-22081
- Method for improving the fuel efficiency of a gas turbine engine [NASA-CASE-LEW-13142-2] p 28 N86-20389
- Characterization of real gas properties for space shuttle main engine fuel turbine and performance calculations [NASA-CR-175066] p 61 N86-27418
- Research and development of neat alcohol fuel usage in automobiles [NASA-CR-174813] p 108 N86-27460
- FUEL TANK PRESSURIZATION**
- Effect of subcooling on the on-orbit pressurization rate of cryogenic propellant tankage [AIAA PAPER 86-1253] p 54 N86-39877
- FUEL TESTS**
- Deposit formation and heat-transfer characteristics of hydrocarbon rocket fuels p 106 N86-10028
- Fuel deposit characteristics at low velocity [ASME PAPER 85-IGT-130] p 107 N86-23922
- FUEL-AIR RATIO**
- Evaluation of fuel preparation systems for lean premixing-prevaporizing combustors [ASME PAPER 85-GT-137] p 19 N86-22081
- On the determination of laminar flame speeds from stretched flames p 74 N86-22814
- Fluid flow and fuel-air mixing in a motored two-dimensional Wankel rotary engine [AIAA PAPER 86-1556] p 134 N86-42711
- Ignition delay times of benzene and toluene with oxygen in argon mixtures [NASA-TM-87312] p 78 N86-25431
- The behavior of fuel-lean premixed flames in a standard flammability limit tube under controlled gravity conditions [NASA-CR-177132] p 78 N86-28139
- FUNCTIONAL DESIGN SPECIFICATIONS**
- Mod-5A wind turbine generator program design report. Volume 2: Conceptual and preliminary design, book 1 [NASA-CR-174735-VOL-2-BK-1] p 183 N86-15722
- Mod-5A wind turbine generator program design report. Volume 2: Conceptual and preliminary design, book 2 [NASA-CR-174735-VOL-2-BK-2] p 183 N86-15723
- Mod-5A wind turbine generator program design report. Volume 3: Final design and system description, book 1 [NASA-CR-174735-VOL-3-BK-1] p 183 N86-15724
- Mod-5A wind turbine generator program design report. Volume 3: Final design and system description, book 2 [NASA-CR-174735-VOL-3-BK-2] p 183 N86-15725
- Mod-5A wind turbine generator program design report. Volume 4: Drawings and specifications, book 1 [NASA-CR-174735-VOL-4-BK-1] p 183 N86-15726
- Mod-5A wind turbine generator program design report. Volume 4: Drawings and specifications, book 2 [NASA-CR-174735-VOL-4-BK-2] p 184 N86-15727
- Mod-5A wind turbine generator program design report. Volume 4: Drawings and specifications, book 3 [NASA-CR-174735-VOL-4-BK-3] p 184 N86-15728
- Mod-5A wind turbine generator program design report. Volume 4: Drawings and specifications, book 4 [NASA-CR-174735-VOL-4-BK-4] p 184 N86-15729
- Mod-5A wind turbine generator program design report. Volume 4: Drawings and specifications, book 5 [NASA-CR-174735-VOL-4-BK-5] p 184 N86-15730
- FURNACES**
- Role of molybdenum in the Na sub 2SO sub 4 induced corrosion of superalloys at high temperatures [NASA-TM-87235] p 90 N86-21658
- G**
- GALERKIN METHOD**
- A theory of post-stall transients in axial compression systems. I - Development of equations [ASME PAPER 85-GT-171] p 19 N86-22088
- Extensions of the Ritz-Galerkin method for the forced, damped vibrations of structural elements p 176 N86-21909
- Effect of triangular element orientation on finite element solutions of the Helmholtz equation [NASA-TM-87351] p 201 N86-32247

GALLIUM ARSENIDES

- The effect of processing conditions on the GaAs/plasma-grown insulator interface p 204 A86-18567
- MMIC antenna technology development in the 30/20 gigahertz band
[AIAA PAPER 86-0666] p 45 A86-29628
- 10-30 GHz monolithic GaAs travelling-wave divider/combiner p 118 A86-34882
- Test results for 20-GHz GaAs FET spacecraft power amplifier
[NASA-TM-87072] p 111 N86-10379
- A 25.5 percent AMO gallium arsenide grating solar cell
[NASA-TM-87134] p 182 N86-11671
- Carbon films grown from plasma on III-V semiconductors
[NASA-TM-87140] p 205 N86-12135
- Monolithic optical integrated control circuitry for GaAs MMIC-based phased arrays
[NASA-TM-87183] p 113 N86-16457
- MMIC antenna technology development in the 30/20 gigahertz band
[NASA-TM-87192] p 46 N86-17368
- Gallium arsenide solar cell efficiency: Problems and potential p 184 N86-17843
- N/P GaAs concentrator solar cells with an improved grid and busbar contact design p 184 N86-17844
- High-efficiency AlGaAs-GaAs Cassegrainian concentrator cells p 185 N86-17845
- A possible radiation-resistant solar cell geometry using superlattices p 185 N86-17851
- Performance of Hughes GaAs concentrator cells under 1-MeV electron irradiation p 185 N86-17860
- Optically controlled phased array antenna concepts using GaAs monolithic microwave integrated circuits
[NASA-TM-87229] p 123 N86-21757
- Indium phosphide solar cells: status and prospects for use in space p 123 N86-26520
- GAS BEARINGS**
- Dynamic response of film thickness in spiral-groove face seals
[NASA-TP-2544] p 27 N86-15313
- Compliant hydrodynamic fluid journal bearing
[NASA-CASE-LEW-13670-1] p 158 N86-19606
- GAS CHROMATOGRAPHY**
- Characterization methodology for PMR-15 p 65 N86-11272
- GAS COOLING**
- Gas cooled fuel cell systems technology development
[NASA-CR-175047] p 190 N86-31984
- GAS DYNAMICS**
- Time-dependent wave envelope finite difference analysis of sound propagation p 197 A86-20130
- Advanced research and technology program for advanced high pressure oxygen-hydrogen rocket propulsion p 58 N86-17405
- Optical elements formed by compressed gases: Analysis and potential applications
[NASA-TP-2555] p 203 N86-22390
- GAS EVOLUTION**
- Carbon monoxide production in low energy oxygen ion bombardment of pyrolytic graphite and Kapton surfaces p 76 A86-47078
- GAS GENERATORS**
- A parametric study of a gas-generator air turbo ramjet (ATR)
[NASA-TM-88808] p 34 N86-31586
- GAS INJECTION**
- Multispark flow visualization of lateral jet injection into a swirling cross flow p 1 A86-14561
- Mass transport phenomena between bubbles and dissolved gases in liquids under reduced gravity conditions p 39 N86-10110
- GAS IONIZATION**
- Radical molecule and ion-molecule mechanisms in the polymerization of hydrocarbons and chlorosilanes in R.F. plasmas at low pressures (below 1.0 Torr) p 203 A86-16254
- Frictional and structural characterization of ion-nitrided low and high chromium steels p 81 A86-17477
- GAS JETS**
- Effects of buoyancy on gas jet diffusion flames - Experiment and theory
[IAF PAPER 85-288] p 72 A86-15804
- Effect of liquid droplets on turbulence in a round gaseous jet
[NASA-CR-175063] p 29 N86-23597
- GAS MIXTURES**
- Two dimensional, transient catalytic combustion of CO-air on platinum p 71 A86-10201
- A two-dimensional numerical study of the flow inside the combustion chambers of a motored rotary engine
[NASA-TM-87212] p 10 N86-19289

GAS PRESSURE

- The effect of oxygen pressure on volatility and morphology of LaB6 single crystal cathodes p 204 A86-28076
- GAS STREAMS**
- Experiments for the determination of convective diffusion heat/mass transfer to burner rig test targets comparable in size to jet stream diameter
[NASA-TM-87196] p 139 N86-18646
- GAS TEMPERATURE**
- Further development of the dynamic gas temperature measurement system
[AIAA PAPER 86-1648] p 147 A86-42770
- Dynamic gas temperature measurement system p 147 N86-11499
- 1700 deg C optical temperature sensor
[NASA-CR-175108] p 203 N86-28729
- Research instrumentation for hot section components of turbine engines
[NASA-TM-88851] p 150 N86-32702
- GAS TURBINE ENGINES**
- Combustion research for gas turbine engines p 17 A86-11609
- Sensor failure detection for jet engines using analytical redundancy p 18 A86-14226
- Stability of limit cycles in frictionally damped and aerodynamically unstable rotor stages p 18 A86-19198
- A review and analysis of boundary layer transition data for turbine application
[ASME PAPER 85-GT-83] p 129 A86-22054
- Prediction of the structure of fuel sprays in gas turbine combustors
[AIAA PAPER 86-0450] p 20 A86-26636
- Studies on the hot corrosion of a nickel-base superalloy, Udmet 700 p 82 A86-29722
- Aerodynamic and structural detuning of supersonic turbomachine rotors p 21 A86-31595
- Stress analysis of gas turbine engine structures using the boundary element method p 169 A86-34444
- The application of LQR synthesis techniques to the turbohaft engine control problem --- Linear Quadratic Regulator p 22 A86-35614
- Inelastic high-temperature thermomechanical response of ceramic coated gas turbine seals p 169 A86-37799
- Fabrication of ceramic components for advanced gas turbine engines
[SAE PAPER 851786] p 154 A86-38310
- Processing study of injection molding of silicon nitride for engine applications
[SAE PAPER 851787] p 154 A86-38311
- Advanced technology payoffs for future rotorcraft, commuter aircraft, cruise missile, and APU propulsion systems
[AIAA PAPER 86-1545] p 16 A86-42704
- Year 2000 small engine technology payoffs in cruise missiles
[AIAA PAPER 86-1546] p 23 A86-42705
- Further development of the dynamic gas temperature measurement system
[AIAA PAPER 86-1648] p 147 A86-42770
- Unified constitutive materials model development and evaluation for high-temperature structural analysis applications --- for aircraft gas turbine engines p 172 A86-49133
- Small gas turbine combustor experimental study - Compliant metal/ceramic liner and performance evaluation
[AIAA PAPER 86-1452] p 25 A86-49611
- Perspectives on dilution jet mixing --- in creating temperature patterns at combustor exits in gas turbine engines
[AIAA PAPER 86-1611] p 25 A86-49614
- Constitutive modeling for isotropic materials (HOST)
[NASA-CR-174980] p 172 N86-10589
- Turbine Engine Hot Section Technology (HOST)
[NASA-CP-2289] p 172 N86-11495
- Dynamic gas temperature measurement system p 147 N86-11499
- High temperature static strain sensor development program p 148 N86-11500
- Demonstration test of burner liner strain measurement systems: Interim results p 173 N86-11501
- Turbine heat transfer p 137 N86-11505
- Gas side heat transfer p 138 N86-11507
- Combustion hot section technology p 25 N86-11512
- HOST structural analysis program overview p 25 N86-11513
- Burner liner thermal/structural load modelling p 173 N86-11514
- Component-specific modeling p 25 N86-11515
- HOST liner cyclic facilities p 173 N86-11519
- Life prediction and constitutive behavior p 173 N86-11520

- Creep fatigue life prediction for engine hot section materials (isotropic) p 174 N86-11521
- Phenomenological study of the behavior of some silica formers in a high velocity jet fuel burner
[NASA-TM-87127] p 157 N86-14613
- Prediction of the structure of fuel sprays in gas turbine combustors
[NASA-CR-175028] p 27 N86-16218
- Comparison of calculated and experimental cascade performance for controlled-diffusion compressor stator blading
[NASA-TM-87167] p 27 N86-16219
- Small, two-stage, partial-admission turbine p 57 N86-17386
- Compliant hydrodynamic fluid journal bearing
[NASA-CASE-LEW-13670-1] p 158 N86-19606
- Method for improving the fuel efficiency of a gas turbine engine
[NASA-CASE-LEW-13142-2] p 28 N86-20389
- Technology for Brayton-cycle powerplants using solar and nuclear energy
[NASA-TP-2558] p 60 N86-21577
- Ceramic thermal barrier coatings for electric utility gas turbine engines
[NASA-CR-87288] p 90 N86-22687
- Life prediction and constitutive models for engine hot section anisotropic materials program
[NASA-CR-174952] p 165 N86-25003
- Emission FTIR analyses of thin microscopic patches of jet fuel residues deposited on heated metal surfaces
[NASA-CR-176786] p 108 N86-25502
- Lateral jet injection into typical combustor flowfields
[NASA-CR-3997] p 31 N86-28086
- Small gas turbine combustor experimental study: Compliant metal/ceramic liner and performance evaluation
[NASA-TM-87304] p 33 N86-31582
- An overview of the Small Engine Component Technology (SECT) studies
[NASA-TM-88796] p 34 N86-31587
- A sensor failure simulator for control system reliability studies
[NASA-TM-87271] p 124 N86-31792
- Perspectives on dilution jet mixing
[NASA-TM-87294] p 35 N86-32432
- Thermal stress minimized, two component, turbine shroud seal
[NASA-CASE-LEW-14212-1] p 162 N86-32740
- Advanced Gas Turbine (AGT) Technology Development Project annual report
[NASA-CR-179485] p 211 N86-33211
- GAS TURBINES**
- Heat transfer results and operational characteristics of the NASA Lewis Research Center hot section cascade test facility
[ASME PAPER 85-GT-82] p 128 A86-22053
- NASA Lewis Research Center/university graduate research program on engine structures
[ASME PAPER 85-GT-159] p 167 A86-22084
- Methods for improving reliability in ceramic turbine rotors
[SAE PAPER 851788] p 154 A86-38312
- Heat-flux measurements for the rotor of a full-stage turbine. I - Time-averaged results
[ASME PAPER 86-GT-77] p 24 A86-48145
- Heat-flux measurements for the rotor of a full-stage turbine. II - Description of analysis technique and typical time-resolved measurements
[ASME PAPER 86-GT-78] p 24 A86-48146
- Heat transfer characteristics within an array of impinging jets. Effects of crossflow temperature relative to jet temperature
[NASA-CR-3936] p 139 N86-15625
- Advanced Gas Turbine (AGT) technology report
[NASA-CR-175018] p 158 N86-20808
- Thermal barrier coating life prediction model development
[NASA-CR-175087] p 103 N86-22713
- Heat transfer to two-phase air/water mixtures flowing in small tubes with inlet disequilibrium
[NASA-CR-175076] p 141 N86-22892
- Dilution jet mixing program, phase 3
[NASA-CR-174884] p 142 N86-24938
- Tribology of selected ceramics at temperatures to 900 deg C
[NASA-TM-87267] p 105 N86-25476
- The boundary layer on compressor cascade blades
[NASA-CR-177279] p 143 N86-27607
- Effects of surface chemistry on hot corrosion life
[NASA-CR-179471] p 32 N86-28087
- Micromechanisms of thermomechanical fatigue: A comparison with isothermal fatigue
[NASA-TM-87331] p 92 N86-28164
- 1700 deg C optical temperature sensor
[NASA-CR-175108] p 203 N86-28729

GAS-METAL INTERACTIONS

- Adsorption of O₂, SO₂, and SO₃, on nickel oxide - Mechanism for sulfate formation p 75 A86-34238
Angle-resolved Auger electron spectra induced by neon ion impact on aluminum p 76 A86-43456

GASEOUS ROCKET PROPELLANTS

- Resistojet operation with various propellants [AIAA PAPER 85-1158] p 107 A86-37074
A long-life 50 lbf H₂/O₂ thruster for Space Station auxiliary propulsion [AIAA PAPER 86-1404] p 55 A86-42617

GASKETS

- Sliding seal materials for adiabatic engines, phase 2 [NASA-CR-179475] p 105 N86-29042

GATES (CIRCUITS)

- A new very high voltage semiconductor switch p 119 A86-40449

GEAR TEETH

- Linear dynamic coupling in geared rotor systems [ASME PAPER 85-DET-11] p 154 A86-38617
Efficiency of nonstandard and high contact ratio involute spur gears [ASME PAPER 84-DET-172] p 155 A86-45255
Surface fatigue life and failure characteristics of EX-53, CBS 1000M, and AISI 9310 gear materials [NASA-TP-2513] p 157 N86-12609
Generation of spiral bevel gears with zero kinematical errors and computer aided tooth contact analysis [NASA-TM-87273] p 160 N86-25793
Dynamic loading on parallel shaft gears [NASA-CR-179473] p 161 N86-28433

GEARS

- Life and reliability modeling of bevel gear reductions [ASME PAPER 85-DE-7] p 151 A86-14466
Generation of spiral bevel gears with zero kinematical errors and computer aided simulation of their meshing and contact p 154 A86-40656
Generated spiral bevel gears - Optimal machine-tool settings and tooth contact analysis [SAE PAPER 851573] p 154 A86-40678
An investigation of the transient thermal analysis of spur gears [ASME PAPER 84-DET-92] p 155 A86-40683
Lubricant and additive effects on spur gear fatigue life [ASME PAPER 85-TRIB-14] p 155 A86-43542
Efficiency of nonstandard and high contact ratio involute spur gears [ASME PAPER 84-DET-172] p 155 A86-45255
Fatigue life analysis of a turboprop reduction gearbox [ASME PAPER 85-DET-10] p 155 A86-45256
Torsional vibrations and dynamic loads in a basic planetary gear system p 156 A86-47354
Surface fatigue life and failure characteristics of EX-53, CBS 1000M, and AISI 9310 gear materials [NASA-TP-2513] p 157 N86-12609
Gearing [NASA-RP-1152] p 157 N86-14612
Constitutive modelling of lubricants in concentrated contacts at high slide to roll ratios [NASA-CR-175029] p 158 N86-17748
Testing of YUH-61A helicopter transmission in NASA Lewis 2240-kW (3000-hp) facility [NASA-TP-2538] p 160 N86-24992
Generation of spiral bevel gears with zero kinematical errors and computer aided tooth contact analysis [NASA-TM-87273] p 160 N86-25793
Dynamic loading on parallel shaft gears [NASA-CR-179473] p 161 N86-28433
Surface fatigue and failure characteristics of hot forged powder metal AISI 4620, AISI 4640, and machined AISI 4340 steel spur gears [NASA-TM-87330] p 161 N86-31889

GENERAL AVIATION AIRCRAFT

- Advanced technology payoffs for future rotorcraft, commuter aircraft, cruise missile, and APU propulsion systems [AIAA PAPER 86-1545] p 16 A86-42704

GEOMETRICAL ACOUSTICS

- A high frequency analysis of electromagnetic plane wave scattering by perfectly-conducting semi-infinite parallel plate and rectangular waveguides with absorber coated inner walls [NASA-CR-179759] p 116 N86-32600

GEOMETRICAL THEORY OF DIFFRACTION

- Numerical methods for analyzing electromagnetic scattering [NASA-CR-176141] p 111 N86-10377
A high frequency analysis of electromagnetic plane wave scattering by perfectly-conducting semi-infinite parallel plate and rectangular waveguides with absorber coated inner walls [NASA-CR-179759] p 116 N86-32600

GEOMETRY

- Free jet feasibility study of a thermal acoustic shield concept for AST/VCE application-dual flow. Comprehensive data report. Volume 1: Test nozzles and acoustic data [NASA-CR-174817] p 200 N86-23371
Free-jet feasibility study of a thermal acoustic shield concept for AST/VCE application-dual stream nozzles. Comprehensive data report. Volume 2: Laser velocimeter and suppressor. Base pressure data [NASA-CR-174818] p 201 N86-23372

GEOSYNCHRONOUS ORBITS

- Impact of the 1985 Space World Administrative Radio Conference on frequency/orbit planning and use [AIAA PAPER 86-0634] p 110 A86-49567
Calculation of allowable orbital spacings for the fixed-satellite service [NASA-CR-176273] p 43 N86-11212
Radiation exposure and performance of multiple burn LEO-GEO orbit transfer trajectories p 43 N86-17417
Impact of the 1985 Space World Administrative Radio Conference on frequency/orbit planning and use [NASA-TM-87285] p 115 N86-24881
Communication Platform Payload Definition (CPPD) study. Volume 1: Executive summary [NASA-CR-174928] p 49 N86-27403
Communication Platform Payload Definition (CPPD) study. Volume 3: Addendum [NASA-CR-174930] p 49 N86-27405
Communications platform payload definition study, executive summary [NASA-CR-174985] p 49 N86-27407

GERMANIUM COMPOUNDS

- Optical techniques to feed and control GaAs MMIC modules for phased array antenna applications [AIAA PAPER 86-0687] p 110 A86-29638
Optical techniques to feed and control GaAs MMIC modules for phased array antenna applications [NASA-TM-87218] p 113 N86-16458

GERMANIUM DIODES

- Performance and temperature dependencies of proton irradiated n/p GaAs and n/p silicon cells [NASA-TM-87136] p 120 N86-12509

GIBBS FREE ENERGY

- Theory of homogeneous nucleation - A chemical kinetic view p 72 A86-19389

GIMBALS

- Centaur engine gimbal friction characteristics under simulated thrust load [NASA-TM-87335] p 44 N86-31621

GLASS

- Angular particle impingement studies of thermoplastic materials at normal incidence [ASLE PREPRINT 85-AM-3A-1] p 94 A86-11076
Microgravity Materials Science Laboratory p 42 N86-10173
The 371 deg C mechanical properties of graphite/polyimide composites [NASA-TM-87122] p 69 N86-12256
Structure-to-glass transition temperature relationships in high temperature stable condensation polyimides [NASA-TM-87113] p 101 N86-12311
Structure-to-property relationships in addition cured polymers 2: Resin Tg composite initial mechanical properties of norbornenyl cured polyimide resins [NASA-TM-88794] p 105 N86-29041

GLAZES

- Character of laser-glazed, plasma-sprayed zirconia coatings on stainless steel substrata p 95 A86-15229

GLOBAL AIR SAMPLING PROGRAM

- Simultaneous measurements of carbon monoxide and ozone in the NASA Global Atmospheric Sampling Program (GASP) p 191 A86-48620

GLOW DISCHARGES

- Frictional and structural characterization of ion-nitrided low and high chromium steels p 81 A86-17477

GLYCOLS

- Experimental and analytical investigation of a freezing point depressant fluid ice protection system [NASA-CR-174758] p 12 N86-27186

GOLD COATINGS

- Frictional and morphological properties of Au-MoS₂ films sputtered from a compact target p 152 A86-16258
Tribological characteristics of gold films deposited on metals by ion plating and vapor deposition p 85 A86-49600

GOVERNMENT/INDUSTRY RELATIONS

- Evaluation of spacecraft technology programs (effects on communication satellite business ventures), volume 1 [NASA-CR-174978] p 112 N86-16451

GRADIENTS

- Fugacity and concentration gradients in a gravity field [NASA-TM-88809] p 212 N86-30620

GRAIN BOUNDARIES

- Compatibility of grain-stabilized platinum with candidate propellants for resistojets [AIAA PAPER 85-2014] p 51 A86-17835
Structure and grain coarsening during the sintering of alumina p 98 A86-26341
Effect of grain-boundary crystallization on the high-temperature strength of silicon nitride p 98 A86-33495
Compatibility of grain-stabilized platinum with candidate propellants for resistojets [NASA-TM-87118] p 56 N86-10279
Fatigue crack propagation of nickel-base superalloys at 650 deg C [NASA-TM-87150] p 87 N86-12294
Molten salt corrosion of SiC: Pitting mechanism [NASA-TM-87143] p 101 N86-12310
Grain boundary oxidation and oxidation accelerated fatigue crack nucleation and propagation [NASA-CR-175050] p 89 N86-20542
Effect of boron on tensile properties of B2 BeAl [NASA-CR-175074] p 89 N86-21656
Tensile behavior of Fe-40Al alloys with B and Zr additions [NASA-TM-87290] p 91 N86-25453
The evolution and growth of Al₂O₃ scales on beta-NiAl [NASA-CR-175097] p 92 N86-27444
The continuing battle against defects in nickel-base superalloys [NASA-TM-87343] p 93 N86-31701

GRAIN SIZE

- Scaling attenuation data characterizes changes in material microstructure p 197 A86-26542
Dislocations in extruded Co-49.3 at. pct Al p 83 A86-45091
The effects of grain size on the flow and fracture of long-range ordered alloys p 84 A86-47243
The influence of grain size and composition on slow plastic flow in FeAl between 1100 and 1400 K p 86 A86-50279
Fatigue crack propagation of nickel-base superalloys at 650 deg C [NASA-TM-87150] p 87 N86-12294
Ultrasonic verification of microstructural changes due to heat treatment p 200 N86-22977
Determination of grain size distribution function using two-dimensional Fourier transforms of tone pulse encoded images [NASA-TM-88790] p 166 N86-31065

GRANTS

- NASA LeRC/Akron University Graduate Cooperative Fellowship Program and Graduate Student Researchers Program [NASA-CR-174826] p 207 N86-13219

GRANULAR MATERIALS

- Compatibility of grain-stabilized platinum with candidate propellants for resistojets [AIAA PAPER 85-2014] p 51 A86-17835
Compatibility of grain-stabilized platinum with candidate propellants for resistojets [NASA-TM-87118] p 56 N86-10279
Tensile behavior of Fe-40Al alloys with B and Zr additions [NASA-TM-87290] p 91 N86-25453

GRAPHITE

- Environmental stability of intercalated graphite fibers p 98 A86-31825
Tribological properties of graphite-fiber-reinforced, partially fluorinated polyimide composites p 98 A86-34177
Advanced rotary engine components utilizing fiber reinforced Mg castings [AIAA PAPER 86-1559] p 67 A86-42712
Verification of computer-aided designs of traveling-wave tubes utilizing novel dynamic refocusers and graphite electrodes for the multistage depressed collector [NASA-TP-2524] p 121 N86-13643
Graphite fiber intercalation: Basic properties of copper chloride intercalated fibers [NASA-TM-87217] p 65 N86-18442
A comparison of the bromination dynamics of pitch-based and vapor-grown graphite fibers [NASA-TM-87275] p 103 N86-21683
Fundamental studies of low velocity impact resistance of graphite fiber reinforced polymer matrix composites [NASA-TM-86886] p 69 N86-23661
Sputtered cadmium oxide as a surface pretreatment for graphite solid lubricant films [NASA-TM-87300] p 104 N86-25473
The correlation of low-velocity impact resistance of graphite-fiber-reinforced composites with matrix properties [NASA-TM-87337] p 71 N86-27426

- A study of Kapton degradation under simulated shuttle environment
[NASA-CR-178850] p 78 N86-28136
- Structure-to-property relationships in addition cured polymers 2: Resin Tg composite initial mechanical properties of norbornenyl cured polyimide resins
[NASA-TM-88794] p 105 N86-29041
- Carbon-rich ceramic composites from ethynyl aromatic precursors
[NASA-TM-88812] p 71 N86-29908
- The milling of pristine and brominated P-100 graphite fibers
[NASA-TM-88828] p 106 N86-32573
- Secondary-electron-emission losses in multistage depressed collectors and traveling-wave-tube efficiency improvements with carbon collector electrode surfaces
[NASA-TP-2622] p 125 N86-32629
- GRAPHITE-EPOXY COMPOSITES**
- Factors influencing the ultrasonic stress wave factor evaluation of composite material structures
p 168 A86-34257
- Progressive fracture of fiber composites
p 67 A86-35809
- Tetraglycidyl epoxy resins and graphite fiber composites cured with flexibilized aromatic diamines
p 67 A86-36999
- Dynamic delamination crack propagation in a graphite/epoxy laminate
p 68 A86-43010
- Progressive damage, fracture predictions and post mortem correlations for fiber composites
[NASA-TM-87101] p 68 N86-10290
- Ultrasonic evaluation of mechanical properties of thick, multilayered, filament wound composites
[NASA-TM-87088] p 163 N86-10561
- Effect of stress on ultrasonic pulses in fiber reinforced composites
p 200 N86-22975
- Fracture characteristics of angleplied laminates fabricated from overaged graphite/epoxy prepreg
[NASA-TM-87266] p 70 N86-25417
- GRAPHITE-POLYIMIDE COMPOSITES**
- Graphite/PMR polyimide composites with improved toughness
p 66 A86-21731
- Aerospace applications of PMR polyimide composites
p 67 A86-27730
- PMR polyimides from solutions containing mixed endcaps
p 100 N86-11263
- Properties of autoclaved Gr/Pi composites made from improved tack PMR-15 prepreg
p 68 N86-11276
- Rheological, processing, and 371 deg C mechanical properties of Celion 8000/N-phenylnadimide modified PMR composites
p 68 N86-11278
- The 371 deg C mechanical properties of graphite/polyimide composites
[NASA-TM-87122] p 69 N86-12256
- Specimen geometry effects on graphite/PMR-15 composites during thermo-oxidative aging
[NASA-TM-87204] p 69 N86-17477
- GRATINGS (SPECTRA)**
- Diffraction effects and special advantages in electronic heterodyne moire deflectometry
p 202 A86-31565
- GRAVITATION**
- Fugacity and concentration gradients in a gravity field
[NASA-TM-88809] p 212 N86-30620
- GRAVITATIONAL EFFECTS**
- Effect of gravity on laminar premixed gas combustion. I - Flammability limits and burning velocities
p 72 A86-12413
- Effect of gravity on laminar premixed gas combustion. II - Ignition and extinction phenomena
p 72 A86-12414
- Research and competition: Best partners
[NASA-TM-87313] p 212 N86-25321
- The behavior of fuel-lean premixed flames in a standard flammability limit tube under controlled gravity conditions
[NASA-CR-177132] p 78 N86-28139
- Microgravity Polymers
[NASA-CP-2392] p 105 N86-28194
- GRINDING (COMMINUTION)**
- Particle size reduction of Si3N4 with Si3N4 milling hardware
[NASA-TM-88664-REV] p 104 N86-24839
- GRINDING (MATERIAL REMOVAL)**
- Factors influencing the ball milling of Si3N4 in water
p 95 A86-15239
- Parametric evaluation of ball milling of SiC in water
p 96 A86-15240
- GROOVES**
- Dynamic response of film thickness in spiral-groove face seals
[NASA-TP-2544] p 27 N86-15313
- GROUND STATIONS**
- Calculation of allowable orbital spacings for the fixed-satellite service
[NASA-CR-176273] p 43 N86-11212

GROUND TESTS

- Development and application of dynamic simulations of a subsonic wind tunnel
[NASA-TM-87211] p 43 N86-18338
- Uniform engine testing program phase 7: NASA Lewis Research Center second entry
[NASA-TM-87272] p 31 N86-28085
- GROUP VELOCITY**
- Stress waves in transversely isotropic media: The homogeneous problem
[NASA-CR-3977] p 164 N86-25002
- GUIDE VANES**
- Wind tunnel turning vanes of modern design
[AIAA PAPER 86-0044] p 36 A86-19654
- Wind tunnel turning vanes of modern design
[NASA-TM-87146] p 37 N86-12239
- GUSTS**
- Noise generated by convected gusts interacting with swept airfoil cascades
[AIAA PAPER 86-1872] p 198 A86-45492
- Forced response analysis of an aerodynamically detuned supersonic turbomachine rotor
[NASA-TM-87093] p 9 N86-10019

H**HALL EFFECT**

- Characterisation of plasma in a rail gun
p 118 A86-26051

HARDENING (MATERIALS)

- Thermomechanical cyclic hardening behavior of Hastelloy-X
[NASA-CR-174999] p 174 N86-18610

HARMONIC ANALYSIS

- Frequency domain solutions to multi-degree-of-freedom, dry friction damped systems under periodic excitation
p 170 A86-39485
- On the equivalence of the incremental harmonic balance method and the harmonic balance-Newton Raphson method
p 170 A86-40695

HASTELLOY (TRADEMARK)

- Fracture mechanics applied to nonisothermal fatigue crack growth
p 81 A86-28951
- Elevated temperature biaxial fatigue
[NASA-CR-175009] p 174 N86-11526
- Thermomechanical cyclic hardening behavior of Hastelloy-X
[NASA-CR-174999] p 174 N86-18610

HEAT EXCHANGERS

- Study of ice accretion on icing wind tunnel components
[AIAA PAPER 86-0290] p 36 A86-26620
- NASA Lewis Research Center low-gravity fluid management technology program
p 44 A86-32906
- NASA Lewis Research Center low-gravity fluid management technology program
[NASA-TM-87145] p 44 N86-11218
- Heat transfer and pressure drop performance of a finned-tube heat exchanger proposed for use in the NASA Lewis Altitude Wind Tunnel
[NASA-TM-87151] p 138 N86-13677
- Study of ice accretion on icing wind tunnel components
[NASA-TM-87095] p 37 N86-16232
- Design and evaluation of fluidized bed heat recovery for diesel engine systems
[NASA-CR-174898] p 209 N86-21456
- Advanced on-site power plant development technology program
[NASA-CR-174709] p 187 N86-25040
- Oxidizer heat exchanger component testing
[NASA-CR-179487] p 62 N86-29901

HEAT FLUX

- High-temperature thermocouple and heat flux gauge using a unique thin film-hardware hot junction
[ASME PAPER 85-GT-18] p 145 A86-13059
- Performance of thermal barrier coatings in high heat flux environments
p 80 A86-16272
- Heat-flux measurements for the rotor of a full-stage turbine. I - Time-averaged results
[ASME PAPER 86-GT-77] p 24 A86-48145
- Heat-flux measurements for the rotor of a full-stage turbine. II - Description of analysis technique and typical time-resolved measurements
[ASME PAPER 86-GT-78] p 24 A86-48146
- Turbine blade and vane heat flux sensor development, phase 2
[NASA-CR-174995] p 26 N86-12226
- Research instrumentation for hot section components of turbine engines
[NASA-TM-88851] p 150 N86-32702
- HEAT GENERATION**
- Prediction of heat release effects on a mixing layer
[AIAA PAPER 86-0058] p 129 A86-22676

- Generated spiral bevel gears - Optimal machine-tool settings and tooth contact analysis
[SAE PAPER 851573] p 154 A86-40678
- Prediction of heat release effects on a mixing layer
[NASA-CR-175044] p 142 N86-23857
- HEAT MEASUREMENT**
- Research instrumentation for hot section components of turbine engines
[NASA-TM-88851] p 150 N86-32702
- HEAT OF FORMATION**
- Direct numerical simulations of a reacting mixing layer with chemical heat release
p 76 A86-41711
- HEAT OF FUSION**
- Estimated heats of fusion of fluoride salt mixtures suitable for thermal energy storage applications
[NASA-TM-87320] p 190 N86-31982
- HEAT PIPES**
- Heat pipe radiator technology for space power systems
[AIAA PAPER 86-1300] p 47 A86-39907
- Experimental assessment of advanced Stirling component concepts
[NASA-CR-174994] p 210 N86-25302
- HEAT RADIATORS**
- Heat pipe radiator technology for space power systems
[AIAA PAPER 86-1300] p 47 A86-39907
- Liquid droplet radiator program at the NASA Lewis Research Center
[ASME PAPER 86-HT-15] p 48 A86-49621
- Liquid droplet radiator program at the NASA Lewis Research Center
[NASA-TM-87139] p 48 N86-12246
- Liquid belt radiator design study
[NASA-CR-174901] p 57 N86-16259
- Methods for heat transfer and temperature field analysis of the insulated diesel phase 2 progress report
[NASA-CR-175072] p 210 N86-24590
- HEAT RESISTANT ALLOYS**
- The influence of cobalt, tantalum, and tungsten on the microstructure of single crystal nickel-base superalloys
p 79 A86-12995
- The influence of cobalt, tantalum, and tungsten on the elevated temperature mechanical properties of single crystal nickel-base superalloys
p 79 A86-12996
- The development of gamma-gamma-prime lamellar structures in a nickel-base superalloy during elevated temperature mechanical testing
p 79 A86-14719
- Pretreatment effects on the morphology and properties of aluminum oxide thermally grown on NiCoCrAlY
p 97 A86-17495
- Temperature dependence of gamma-gamma prime lattice mismatch in nickel-base superalloys
p 81 A86-21849
- Studies on the hot corrosion of a nickel-base superalloy, Udimet 700
p 82 A86-29722
- Creep-rupture and fractographic analysis of Stirling engine superalloys tested in air and 15 MPa hydrogen
p 82 A86-30041
- Impact wear of iron rich superalloys
p 82 A86-34687
- The tensile and fatigue deformation structures in a single crystal Ni-base superalloy
p 83 A86-35697
- Mechanism of Na2SO4-induced corrosion of molybdenum containing nickel-base superalloys at high temperatures. I - Corrosion in atmospheres containing O2 only. II - Corrosion in O2 + SO2 atmospheres
p 83 A86-37238
- Toward improved durability in advanced combustors and turbines - Progress in prediction of thermomechanical loads
[ASME PAPER 86-GT-172] p 24 A86-48224
- Orientation and temperature dependence of some mechanical properties of the single-crystal nickel-base superalloy Rene N4. I - Tensile behavior
p 86 A86-50321
- Orientation and temperature dependence of some mechanical properties of the single-crystal nickel-base superalloy Rene N4. II - Low cycle fatigue behavior
p 86 A86-50322
- Orientation and temperature dependence of some mechanical properties of the single-crystal nickel-base superalloy Rene N4. III - Tension-compression anisotropy
p 86 A86-50323
- Fatigue crack propagation of nickel-base superalloys at 650 deg C
[NASA-TM-87150] p 87 N86-12294
- The effect of cobalt content in U-700 type alloys on degradation of aluminate coatings
[NASA-TM-87173] p 87 N86-13408
- Structure-property characterization of rheocast and VADER processed IN-100 superalloy
[NASA-CR-175014] p 88 N86-14354
- Development of constitutive models for cyclic plasticity and creep behavior of super alloys at high temperature
[NASA-CR-176418] p 88 N86-14356

- Creep rupture behavior of Stirling engine materials [NASA-TM-87209] p 88 N86-15380
- Simplified cyclic structural analyses of SSME turbine blades [NASA-TM-87214] p 175 N86-16615
- Creep-rupture behavior of iron superalloys in high-pressure hydrogen [NASA-CR-175027] p 89 N86-17531
- Role of molybdenum in the Na sub 2SO sub 4 induced corrosion of superalloys at high temperatures [NASA-TM-87235] p 90 N86-21658
- Anisotropic constitutive model for nickel base single crystal alloys: Development and finite element implementation [NASA-CR-175015] p 176 N86-21952
- Low-cost single-crystal turbine blades, volume 2 [NASA-CR-174652] p 29 N86-23598
- Thermal-mechanical fatigue behavior of nickel-base superalloys [NASA-CR-175048] p 91 N86-24818
- Life prediction and constitutive models for engine hot section anisotropic materials program [NASA-CR-174952] p 165 N86-25003
- Yielding and deformation behavior of the single crystal nickel-base superalloy PWA 1480 [NASA-CR-175100] p 91 N86-25455
- Heat treatment for superalloy [NASA-CASE-LEW-14262-1] p 92 N86-26414
- Micromechanisms of thermomechanical fatigue: A comparison with isothermal fatigue [NASA-TM-87331] p 92 N86-26164
- Thermal-fatigue and oxidation resistance of cobalt-modified Udimet 700 alloy [NASA-TP-2591] p 178 N86-28464
- Integrated research in constitutive modelling at elevated temperatures, part 1 [NASA-CR-177237] p 179 N86-30227
- Microstructure-property relationships in directionally solidified single crystal nickel-base superalloys [NASA-TM-88788] p 93 N86-31700
- The continuing battle against defects in nickel-base superalloys [NASA-TM-87343] p 93 N86-31701
- The effect of variations of cobalt content on the cyclic oxidation resistance of selected Ni-base superalloys [NASA-TM-87297] p 93 N86-31702

HEAT SHIELDING

- Free jet feasibility study of a thermal acoustic shield concept for AST/VCE application-dual flow. Comprehensive data report. Volume 1: Test nozzles and acoustic data [NASA-CR-174817] p 200 N86-23371
- Free-jet feasibility study of a thermal acoustic shield concept for AST/VCE application-dual stream nozzles. Comprehensive data report. Volume 2: Laser velocimeter and suppressor. Base pressure data [NASA-CR-174818] p 201 N86-23372

HEAT STORAGE

- Estimated heats of fusion of fluoride salt mixtures suitable for thermal energy storage applications [NASA-TM-87320] p 190 N86-31982

HEAT TRANSFER

- High-temperature thermocouple and heat flux gauge using a unique thin film hardware hot junction [ASME PAPER 85-GT-18] p 145 A86-13059
- Local heat-transfer measurements on a large scale-model turbine blade airfoil using a composite of a heater element and liquid crystals [ASME PAPER 85-GT-59] p 126 A86-13061
- Heat transfer and fluid mechanics measurements in transitional boundary layer flows [ASME PAPER 85-GT-113] p 126 A86-13068
- Manrating orbital transfer vehicle propulsion [AIAA PAPER 85-1226] p 50 A86-14429
- Ribbon-burner simulation of T-700 turbine shroud for ceramic-lined seals research p 18 A86-15225
- Experimental study of ceramic-coated tip seals for turbojet engines p 152 A86-15227
- Heat transfer results and operational characteristics of the NASA Lewis Research Center hot section cascade test facility [ASME PAPER 85-GT-82] p 128 A86-22053
- A review and analysis of boundary layer transition data for turbine application [ASME PAPER 85-GT-83] p 129 A86-22054
- Preliminary results of a study of the relationship between free stream turbulence and stagnation region heat transfer [ASME PAPER 85-GT-84] p 129 A86-22055
- Heat transfer in space power and propulsion systems p 53 A86-26492
- A computer analysis program for interfacing thermal and structural codes p 193 A86-36861
- Effect of subcooling on the on-orbit pressurization rate of cryogenic propellant tankage [AIAA PAPER 86-1253] p 54 A86-39877

- Turbine-stage heat transfer - Comparison of short-duration measurements with state-of-the-art predictions [AIAA PAPER 86-1465] p 134 A86-42656
- Determination of convective diffusion heat/mass transfer rates to burner rig test targets comparable in size to cross-stream jet diameter [ASME PAPER 86-GT-68] p 136 A86-48140
- Toward improved durability in advanced combustors and turbines - Progress in prediction of thermomechanical loads [ASME PAPER 86-GT-172] p 24 A86-48224
- Fluid management and its role in the future of Space Station [AIAA PAPER 86-2301] p 47 A86-49553
- Fundamental studies of droplet combustion at reduced gravity p 42 N86-10165
- Film cooling on a convex wall: Heat transfer and hydrodynamic measurements for full and partial coverage [NASA-CR-174964] p 137 N86-10461
- Assessment of a 3-D boundary layer code to predict heat transfer and flow losses in a turbine p 138 N86-11508
- HOST structural analysis program overview p 25 N86-11513
- Burner liner thermal/structural load modelling p 173 N86-11514
- Component-specific modeling p 25 N86-11515
- Heat transfer and pressure drop performance of a finned-tube heat exchanger proposed for use in the NASA Lewis Altitude Wind Tunnel [NASA-TM-87151] p 138 N86-13677
- Determination of convective diffusion heat/mass transfer rates to burner rig test targets comparable in size to cross-stream jet diameter [NASA-TM-87176] p 138 N86-13678
- Heat transfer characteristics within an array of impinging jets. Effects of crossflow temperature relative to jet temperature [NASA-CR-3936] p 139 N86-15625
- A computer simulation of the turbocharged turbo compounded diesel engine system: A description of the thermodynamic and heat transfer models [NASA-CR-174971] p 208 N86-16164
- Liquid belt radiator design study [NASA-CR-174901] p 57 N86-16259
- Improvement of the second- and third-moment modeling of turbulence: A study of Reynolds-stress closure model [NASA-CR-176478] p 139 N86-16519
- Two-phase flows and heat transfer within systems with ambient pressure above the thermodynamic critical pressure [NASA-TM-87228] p 140 N86-19558
- Burner liner thermal-structural load modeling [NASA-CR-174892] p 176 N86-21932
- Heat transfer to two-phase air/water mixtures flowing in small tubes with inlet disequilibrium [NASA-CR-175076] p 141 N86-22892
- Evaluation of capillary reinforced composites [NASA-CR-175061] p 70 N86-24760
- Unsteady heat transfer and direct comparison to steady-state measurements in a rotor-wake experiment [NASA-TM-87220] p 142 N86-24934
- Numerical simulation of the flowfield over ice accretion shapes [NASA-CR-176960] p 144 N86-30093
- Modeling of zero gravity venting: Studies of two-phase heat transfer under reduced gravity [NASA-CR-179662] p 144 N86-31826

HEAT TRANSFER COEFFICIENTS

- Local heat-transfer measurements on a large scale-model turbine blade airfoil using a composite of a heater element and liquid crystals [ASME PAPER 85-GT-59] p 126 A86-13061
- Turbine blade and vane heat flux sensor development, phase 2 [NASA-CR-174995] p 26 N86-12226
- Turbine vane external heat transfer. Volume 1: Analytical and experimental evaluation of surface heat transfer distributions with leading edge showerhead film cooling [NASA-CR-174827] p 29 N86-21546
- Effect of a rotor wake on the local heat transfer on the forward half of a circular cylinder [NASA-TM-87234] p 140 N86-21794
- Channel flow modeling of impingement cooling of a rotating turbine blade [NASA-CR-177206] p 31 N86-27285

HEAT TRANSMISSION

- Turbine Engine Hot Section Technology (HOST) [NASA-CP-2289] p 172 N86-11495
- Gas flow environmental and heat transfer nonrotating 3D program p 137 N86-11506
- Gas side heat transfer p 138 N86-11507

HEAT TREATMENT

- Creep of chemically vapour deposited SiC fibres p 66 A86-21486
- Effect of grain-boundary crystallization on the high-temperature strength of silicon nitride p 98 A86-33491
- Constructing multicomponent phase diagrams by overlapping ZPF lines - Zero Phase Fraction Line for improved mechanical and corrosion properties p 83 A86-44031
- The response of cobalt-free Udimet 700 type alloy to modified heat treatments p 85 A86-48031
- Specimen geometry effects on graphite/PMR-11 composites during thermo-oxidative aging [NASA-TM-87204] p 69 N86-17471
- High temperature dispersion strengthening of NiAl [NASA-CR-175073] p 90 N86-22681
- Ultrasonic verification of microstructural changes due to heat treatment p 200 N86-22971
- Heat treatment for superalloy [NASA-CASE-LEW-14262-1] p 92 N86-26414
- Creep properties of PWC-11 base metal and weldments as affected by heat treatment [NASA-TM-88842] p 93 N86-32557

HEATING

- Method for improving the fuel efficiency of a gas turbine engine [NASA-CASE-LEW-13142-2] p 28 N86-20386

HEATING EQUIPMENT

- Liquid fueled external heating system for STM4-120 Stirling engine p 180 A86-24886
- A numerical and experimental investigation of electrochemical aircraft deicing [NASA-CR-175024] p 14 N86-20381

HELICAL FLOW

- Preliminary measurement of the noise from the 2/9 scale model of the Large-scale Advanced Propfan (LAP) propeller, SR-7A [NASA-TM-87116] p 199 N86-14000

HELICOPTER DESIGN

- System life and reliability modeling for helicopter transmissions [NASA-CR-3967] p 159 N86-24990

HELICOPTER ENGINES

- The application of LQR synthesis techniques to the turboshaft engine control problem - Linear Quadratic Regulator p 22 A86-35614
- Preliminary evaluation of a compound cycle engine for shipboard gensets [NASA-CR-179451] p 160 N86-26621

HELICOPTER PERFORMANCE

- The aerodynamics of rotor blades with ice shapes accreted in hover and in level flight p 5 A86-35651
- Performance degradation of helicopters due to icing: A review p 16 A86-35661
- Wind tunnel tests of rotor blade sections with replication of ice formations accreted in hover [NASA-CR-175089] p 15 N86-22551

HELICOPTERS

- Documentation of ice shapes accreted on the main rotor of a UH-1H helicopter in level flight [NASA-CR-175088] p 15 N86-22551
- Testing of YUH-61A helicopter transmission in NASA/Lewis 2240-kW (3000-hp) facility [NASA-TP-2538] p 160 N86-24992

HELMHOLTZ EQUATIONS

- Effect of triangular element orientation on finite element solutions of the Helmholtz equation [NASA-TM-87351] p 201 N86-32247

HEPTANES

- Ignition characteristics of rich n-heptane fuel sprays in the transition region [ASME PAPER 85-WA/HT-46] p 107 A86-38393
- Transition region ignition characteristics of n-heptane fuel sprays [NASA-CR-176364] p 77 N86-14331

HERMETIC SEALS

- Experimental stiffness of tapered bore seals [ASME PAPER 85-DET-12] p 152 A86-22746
- Development of optical diaphragm deflection sensors [NASA-CR-175008] p 203 N86-15111

HETERODYNING

- A comparison of electronic heterodyne moiré deflectometry and electronic heterodyne holographic interferometry for flow measurements [SAE PAPER 851896] p 146 A86-38356
- Beam-modulation methods in quantitative and flow visualization holographic interferometry [NASA-TM-87306] p 148 N86-24956

HETEROJUNCTION DEVICES

- Cryogenic operation of pseudomorphic AlGaAs/InGaAs single-quantum-well MODFETs p 117 A86-11996
- Determination of carrier saturation velocity in high-performance In(y)Ga(1-y)As/Al(x)Ga(1-x)As modulation-doped field-effect transistors (with y between 0 and 0.2) p 118 A86-37295

- High-frequency noise of In(y)Ga(1-y)As/Al(x)Ga(1-x)As
MODFETs and comparison to GaAs/Al(x)Ga(1-x)As
MODFETs p 119 A86-43914
- HETEROJUNCTIONS**
High transconductance InGaAs/AlGaAs pseudomorphic
modulation-doped field-effect transistors p 117 A86-18814
- Performance and temperature dependencies of proton
irradiated n/p GaAs and n/p silicon cells
[NASA-TM-87136] p 120 N86-12509
- HIGH ALTITUDE**
Heat transfer and pressure drop performance of a
finned-tube heat exchanger proposed for use in the NASA
Lewis Altitude Wind Tunnel
[NASA-TM-87151] p 138 N86-13677
- HIGH ENERGY PROPELLANTS**
Current evaluation of the tripropellant concept
[AIAA PAPER 86-1698] p 56 A86-49615
Current evaluation of the tripropellant concept
[NASA-TP-2602] p 62 N86-28124
- HIGH FREQUENCIES**
Space station 20-kHz power management and
distribution system
[NASA-TM-87314] p 60 N86-24747
Power conversion distribution system using a resonant
high-frequency AC link
[NASA-CR-176804] p 123 N86-25694
A 20 kilohertz space station power system
[NASA-TM-88801] p 62 N86-28122
- HIGH LEVEL LANGUAGES**
A high-order language for a system of closely coupled
processing elements
[NASA-CR-177280] p 193 N86-27930
- HIGH PRESSURE**
Hollow cathodes in high pressure arc discharges --- for
arcjet thrusters
[AIAA PAPER 85-2035] p 50 A86-14446
Measurement of the density of base fluids at pressures
0.422 to 2.20 GPa
[NASA-TM-87114] p 156 N86-10551
Lightweight two-stroke cycle aircraft diesel engine
technology enablement program, volume 1
[NASA-CR-174923-VOL-1] p 26 N86-13328
Lightweight two-stroke cycle aircraft diesel engine
technology enablement program, volume 2
[NASA-CR-174923-VOL-2] p 26 N86-13329
Lightweight two-stroke cycle aircraft diesel engine
technology enablement program, volume 3
[NASA-CR-174923-VOL-3] p 26 N86-13330
Preliminary design of a supersonic cruise aircraft
high-pressure turbine
[NASA-CR-174878] p 26 N86-14272
Creep-rupture behavior of iron superalloys in
high-pressure hydrogen
[NASA-CR-175027] p 89 N86-17531
- HIGH SPEED**
Lubrication and performance of high-speed
rolling-element bearings p 152 A86-19375
- HIGH SPEED PHOTOGRAPHY**
Theoretical and experimental comparison of vapor
cavitation in dynamically loaded journal bearings
[NASA-TM-87121] p 137 N86-11425
- HIGH TEMPERATURE**
The high-temperature oxidation of aromatic
hydrocarbons p 75 A86-40834
Constitutive modeling for isotropic materials (HOST)
[NASA-CR-174980] p 172 N86-10589
All-aromatic biphenylene end-capped polyquinoline and
polyimide matrix resins p 100 N86-11267
Rheological, processing, and 371 deg C mechanical
properties of Celion 6000/N-phenylindamide modified
PMR composites p 68 N86-11278
Turbine Engine Hot Section Technology (HOST)
[NASA-CP-2289] p 172 N86-11495
Turbine engine Hot Section Technology (HOST)
project p 173 N86-11496
Dynamic gas temperature measurement system
p 147 N86-11499
Turbine heat transfer p 137 N86-11505
Structure-to-glass transition temperature relationships in
high temperature stable condensation polyimides
[NASA-TM-87113] p 101 N86-12311
Modifications of system for elevated temperature tensile
testing and stress-strain measurement of metal matrix
composites
[NASA-TM-87172] p 65 N86-13370
Development of optical diaphragm deflection sensors
[NASA-CR-175008] p 203 N86-15113
Thermal aging effects in refractory metal alloys
[NASA-TM-87210] p 89 N86-16334
Negative electrode catalyst for the iron chromium redox
energy storage system
[NASA-CASE-LEW-14028-1] p 186 N86-19721
High temperature dispersion strengthening of NiAl
[NASA-CR-175073] p 90 N86-22688
- Application of an atmospheric pressure sampling mass
spectrometer to chlorination reactions
[NASA-TM-87270] p 91 N86-24813
Effects of state recovery on creep buckling under
variable loading
[NASA-CR-175094] p 212 N86-25310
- HIGH TEMPERATURE ENVIRONMENTS**
Performance of thermal barrier coatings in high heat
flux environments p 80 A86-16272
High temperature properties of equiatomic FeAl with
ternary additions p 84 A86-47252
High temperature oxidation of beta-NiAl
p 85 A86-47266
Unified constitutive materials model development and
evaluation for high-temperature structural analysis
applications --- for aircraft gas turbine engines
p 172 A86-49133
- HIGH TEMPERATURE GASES**
Determination of convective diffusion heat/mass
transfer rates to burner rig test targets comparable in size
to cross-stream jet diameter
[ASME PAPER 86-GT-68] p 136 A86-48140
Determination of convective diffusion heat/mass
transfer rates to burner rig test targets comparable in size
to cross-stream jet diameter
[NASA-TM-87176] p 138 N86-13678
- HIGH TEMPERATURE TESTS**
The development of gamma-gamma-prime lamellar
structures in a nickel-base superalloy during elevated
temperature mechanical testing p 79 A86-14719
Effect of multiple strain-anneal cycles on the 1000 C
creep behaviour of gamma/gamma prime-alpha
p 82 A86-30610
Effect of grain-boundary crystallization on the
high-temperature strength of silicon nitride
p 98 A86-33495
The cyclic stress-strain behavior of a nickel-base
superalloy at 650 C p 83 A86-45715
High-pressure creep tests p 84 A86-46564
Surface protection of graphite fabric/PMR-15
composites subjected to thermal oxidation
p 68 N86-11281
Compatibility experiments of facilities, materials, and
propellants for electrothermal thrusters
p 59 N86-17426
- HIGH VACUUM**
Vacuum chamber pressure effects on thrust
measurements p 59 N86-17425
- HIGH VOLTAGES**
A new very high voltage semiconductor switch
p 119 A86-40449
Development of the VOLT-A shuttle experiment
[NASA-TM-87169] p 212 N86-14110
Design of high-voltage, high-power, solid state remote
power controllers for aerospace applications
p 122 N86-17456
- HISTORIES**
Heat-flux measurements for the rotor of a full-stage
turbine. II - Description of analysis technique and typical
time-resolved measurements
[ASME PAPER 86-GT-78] p 24 A86-48146
- HOLLOW CATHODES**
Hollow cathodes in high pressure arc discharges --- for
arcjet thrusters
[AIAA PAPER 85-2035] p 50 A86-14446
Heaterless ignition of inert gas ion thruster hollow
cathodes
[AIAA PAPER 85-2008] p 51 A86-17833
- HOLOGRAPHIC INTERFEROMETRY**
A comparison of electronic heterodyne moire
deflectometry and electronic heterodyne holographic
interferometry for flow measurements
[SAE PAPER 851896] p 146 A86-38359
Beam-modulation methods in quantitative and flow
visualization holographic interferometry
[NASA-TM-87306] p 148 N86-24958
Visualization of flows in a motored rotary combustion
engine using holographic interferometry
[NASA-TM-88804] p 33 N86-31583
Advanced optical measuring systems for measuring the
properties of fluids and structures
[NASA-TM-88829] p 150 N86-31859
- HOLOGRAPHY**
Nondestructive techniques for characterizing
mechanical properties of structural materials - An
overview
[ASME PAPER 86-GT-75] p 163 A86-48143
Nondestructive techniques for characterizing
mechanical properties of structural materials: An
overview
[NASA-TM-87203] p 164 N86-19636
Beam-modulation methods in quantitative and flow
visualization holographic interferometry
[NASA-TM-87306] p 148 N86-24958
- Advanced optical measuring systems for measuring the
properties of fluids and structures
[NASA-TM-88829] p 150 N86-31859
- HOMOJUNCTIONS**
Performance and temperature dependencies of proton
irradiated n/p GaAs and n/p silicon cells
[NASA-TM-87136] p 120 N86-12509
- HONEYCOMB STRUCTURES**
Fiber composite sandwich thermostructural behavior:
Computational simulation
[NASA-TM-88787] p 71 N86-31663
- HORIZONTAL ORIENTATION**
Design and initial testing of a one-bladed
30-meter-diameter rotor on the NASA/DOE mod-O wind
turbine
[NASA-TM-88810] p 189 N86-30251
- HOT CORROSION**
Kinetics and mechanism of corrosion of SiC by molten
salts p 97 A86-20992
Studies on the hot corrosion of a nickel-base superalloy,
Udimet 700 p 82 A86-29722
Burner rig corrosion of SiC at 1000 C
p 99 A86-36328
Na₂SO₄ induced corrosion of nickel at high
temperature p 83 A86-37073
Mechanism of Na₂SO₄-induced corrosion of
molybdenum containing nickel-base superalloys at high
temperatures. I - Corrosion in atmospheres containing O₂
only. II - Corrosion in O₂ + SO₂ atmospheres
p 83 A86-37238
Experiments for the determination of convective
diffusion heat/mass transfer to burner rig test targets
comparable in size to jet stream diameter
[NASA-TM-87196] p 139 N86-18646
Role of molybdenum in the Na sub 2SO sub 4 induced
corrosion of superalloys at high temperatures
[NASA-TM-87235] p 90 N86-21658
Experimental verification of corrosive vapor deposition
rate theory in high velocity burner rigs
[NASA-TM-87287] p 141 N86-22890
Research and development of neat alcohol fuel usage
in automobiles
[NASA-CR-174813] p 108 N86-27460
Effects of surface chemistry on hot corrosion life
[NASA-CR-179471] p 32 N86-28087
- HOT PRESSING**
Fractured toughness of Si₃N₄ measured with short bar
chevron-notched specimens
[NASA-TM-87153] p 101 N86-13495
- HOT SURFACES**
Structural analysis of turbine blades using unified
constitutive models
[NASA-TM-88807] p 178 N86-28461
Research instrumentation for hot section components
of turbine engines
[NASA-TM-88851] p 150 N86-32702
- HOT WORKING**
Slow plastic strain rate compressive flow in binary CoAl
intermetallics p 79 A86-11478
- HOT-WIRE ANEMOMETERS**
Hot-wire measurements of a single lateral jet injected
into swirling crossflow
[AIAA PAPER 86-0055] p 127 A86-19661
Analysis of the uncertainties in velocity measurements
with triple hot-wire probes p 130 A86-24468
Accuracy and directional sensitivity of the single-wire
technique p 146 A86-28541
- HOT-WIRE FLOWMETERS**
Concentration distributions in a model combustor
p 133 A86-38575
- HOUSINGS**
Stress and deformation modeling of multiple rotary
combustion engine trochoid housings
[SAE PAPER 860614] p 156 A86-49624
- HOVERING**
The aerodynamics of rotor blades with ice shapes
accreted in hover and in level flight p 5 A86-35655
- HYBRID CIRCUITS**
Hybrid power semiconductor
[NASA-CASE-LEW-13922-1] p 122 N86-20672
- HYDRAULIC CONTROL**
Large-Scale Advanced Prop-Fan (LAP) pitch change
actuator and control design report
[NASA-CR-174788] p 31 N86-27282
- HYDRAULIC EQUIPMENT**
Fluid machines: Expanding the limits, past and future
[NASA-TM-87161] p 26 N86-12227
- HYDRAZINE ENGINES**
Resistojet operation with various propellants
[AIAA PAPER 85-1158] p 107 A86-37074
- HYDROCARBON COMBUSTION**
Ignition characteristics of rich n-heptane fuel sprays in
the transition region
[ASME PAPER 85-WA/HT-46] p 107 A86-38393

HYDROCARBON FUELS

- Deposit formation and heat-transfer characteristics of hydrocarbon rocket fuels p 106 A86-10028
Effects of preferential diffusion on the burning intensity of curved flames p 73 A86-22813
Fuel deposit characteristics at low velocity [ASME PAPER 85-IGT-130] p 107 A86-23922
Determination of solid mass fraction in partially frozen hydrocarbon fuels [NASA-CR-178472] p 108 N86-28261

HYDROCARBONS

- Radical molecule and ion-molecule mechanisms in the polymerization of hydrocarbons and chlorosilanes in R.F. plasmas at low pressures (below 1.0 Torr) p 203 A86-18254
The high-temperature oxidation of aromatic hydrocarbons p 75 A86-40834

HYDROCHLORIDES

- Method and apparatus for rebalancing a REDOX flow cell system [NASA-CASE-LEW-14127-1] p 122 N86-20680

HYDRODYNAMICS

- Theoretical and experimental comparison of vapor cavitation in dynamically loaded journal bearings [NASA-TM-87121] p 137 N86-11425
Piezoviscous effects in nonconformal contacts lubricated hydrodynamically [NASA-TM-87141] p 141 N86-21797
Overview of the 1986 free-piston Stirling SP-100 activities at the NASA Lewis Research Center [NASA-TM-87305] p 210 N86-26261

HYDROGEN

- Develop and test fuel cell powered on-site integrated total energy systems: Phase 3, full-scale power plant development [NASA-CR-174998] p 182 N86-12758
Effect of argon and hydrogen on deposition of silicon from tetrachlorosilane in cold plasmas [NASA-TM-87219] p 65 N86-17472
Creep-rupture behavior of iron superalloys in high-pressure hydrogen [NASA-CR-175027] p 89 N86-17531

HYDROGEN EMBRITTLEMENT

- Creep-rupture and fractographic analysis of Stirling engine superalloys tested in air and 15 MPa hydrogen p 82 A86-30041
High-pressure creep tests p 84 A86-46564
Thermal aging effects in refractory metal alloys [NASA-TM-87210] p 89 N86-16334

HYDROGEN FUELS

- Low power dc arcjet operation with hydrogen/nitrogen propellant mixtures [AIAA PAPER 86-1505] p 55 A86-42676
Creep rupture behavior of Stirling engine materials [NASA-TM-87209] p 88 N86-15380
Lower power dc arcjet operations with hydrogen hydrogen/nitrogen propellant mixtures [NASA-TM-87279] p 61 N86-25407
Characterization of real gas properties for space shuttle main engine fuel turbine and performance calculations [NASA-CR-175066] p 61 N86-27418

HYDROGEN OXYGEN ENGINES

- Status of advanced orbital transfer propulsion [IAF PAPER 85-184] p 51 A86-17850
A long-life 50 lbf H₂/O₂ thruster for Space Station auxiliary propulsion [AIAA PAPER 86-1404] p 55 A86-42617
Advanced research and technology program for advanced high pressure oxygen-hydrogen rocket propulsion p 58 N86-17405
The noncavitating performance and life of a small vane-type positive displacement pump in liquid hydrogen [NASA-TM-87347] p 63 N86-31651
Proven, long-life hydrogen/oxygen thrust chambers for space station propulsion [NASA-CR-88822] p 64 N86-32522

HYDROGEN OXYGEN FUEL CELLS

- Evaluation parameters for the alkaline fuel cell oxygen electrode [NASA-TM-87155] p 77 N86-12268

HYDROGEN PLASMA

- Frictional and structural characterization of ion-nitrided low and high chromium steels p 81 A86-17477
Measurement of energy distribution in flowing hydrogen microwave plasmas p 52 A86-18041

HYDROGEN-BASED ENERGY

- Theoretical and experimental flow cell studies of a hydrogen-bromine fuel cell, part 1 [NASA-CR-177165] p 189 N86-29409

HYDROSTATIC PRESSURE

- SSME long-life bearings [NASA-CR-179455] p 160 N86-27643

HYDROSTATICS

- Analysis of a two row hydrostatic journal bearing with variable properties, inertia effects and surface roughness p 153 A86-30599

HYDROTHERMAL STRESS ANALYSIS

- Designing for fiber composite structural durability in hydrothermomechanical environments p 67 A86-27734

- Fiber composite sandwich thermostructural behavior: Computational simulation [NASA-TM-88787] p 71 N86-31663

HYDROXYL RADICALS

- Influence of temperature and hydroxyl concentration on incipient soot formation in premixed flames p 74 A86-29070

HYGRAL PROPERTIES

- Designing for fiber composite structural durability in hydrothermomechanical environments p 67 A86-27734

- Composite sandwich thermostructural behavior - Computational simulation [AIAA PAPER 86-0948] p 170 A86-38842

- Fiber composite sandwich thermostructural behavior: Computational simulation [NASA-TM-88787] p 71 N86-31663

HYPERSONIC INLETS

- Real gas effects on the numerical simulation of a hypersonic inlet p 6 A86-46324

HYPERSONIC WIND TUNNELS

- Current wind tunnel capability and planned improvements at Lewis Research Center [AIAA PAPER 86-0728] p 36 A86-24727

HYPERVELOCITY IMPACT

- Computational engine structural analysis [ASME PAPER 86-GT-70] p 23 A86-48141
Computational engine structural analysis [NASA-TM-87231] p 175 N86-19663

HYPERVELOCITY LAUNCHERS

- Rail accelerators for space transportation: An experimental investigation [NASA-TP-2571] p 62 N86-28123

ICE FORMATION

- Ice shapes and the resulting drag increase for a NACA 0012 airfoil [AIAA PAPER 84-0109] p 14 A86-14427
Formation and characterization of simulated small droplet icing clouds [AIAA PAPER 86-0409] p 145 A86-22700
Study of ice accretion on icing wind tunnel components [AIAA PAPER 86-0290] p 36 A86-26620
The aerodynamics of rotor blades with ice shapes accreted in hover and in level flight p 5 A86-35655
The performance characteristics of simulated ice on rotorcraft airfoils p 14 A86-35656
Performance degradation of helicopters due to icing - A review p 16 A86-35668
Experimental measurements of heat transfer from an iced surface during artificial and natural cloud icing conditions [AIAA PAPER 86-1352] p 36 A86-39948
The measurement of aircraft performance and stability and control after flight through natural icing conditions [AIAA PAPER 86-9758] p 35 A86-40681
NASA's aircraft icing analysis program p 14 A86-49107

- Heat transfer and pressure drop performance of a finned-tube heat exchanger proposed for use in the NASA Lewis Altitude Wind Tunnel [NASA-TM-87151] p 138 N86-13677
Formation and characterization of simulated small droplet icing clouds [NASA-TM-87180] p 148 N86-14554
Study of ice accretion on icing wind tunnel components [NASA-TM-87095] p 37 N86-16232

- Particle trajectory computation on a 3-dimensional engine inlet [NASA-CR-175023] p 14 N86-20379
Wind tunnel tests of rotor blade sections with replications of ice formations accreted in hover [NASA-CR-175089] p 15 N86-22558
Documentation of ice shapes accreted on the main rotor of a UH-1H helicopter in level flight [NASA-CR-175088] p 15 N86-22559

- The measurement of aircraft performance and stability and control after flight through natural icing conditions [NASA-TM-87265] p 35 N86-22582
Analytical determination of propeller performance degradation due to ice accretion [NASA-CR-175092] p 15 N86-23577

- In-flight measurements of wing ice shapes and wing section drag increases caused by natural icing conditions [NASA-TM-87301] p 12 N86-24667

- Evaluation of capillary reinforced composites [NASA-CR-175061] p 70 N86-24760
Calibration of droplet sizing and liquid water content instruments: Survey and analysis [NASA-CR-175099] p 149 N86-26596
Experimental and analytical investigation of a freezing point depressant fluid ice protection system [NASA-CR-174758] p 12 N86-27186
Numerical simulation of the flowfield over ice accretion shapes [NASA-CR-176960] p 144 N86-30093
Measurements in liquid fuel sprays [NASA-CR-177088] p 144 N86-30960
NASA's Aircraft Icing Analysis Program [NASA-TM-88791] p 15 N86-31548
In-flight photogrammetric measurement of wing ice accretions [NASA-TM-87191] p 17 N86-31562
Turbulent dispersion of the icing cloud from spray nozzles used in icing tunnels [NASA-TM-87316] p 34 N86-31588

ICE NUCLEI

- In-flight measurements of wing ice shapes and wing section drag increases caused by natural icing conditions [NASA-TM-87301] p 12 N86-24667

ICE PREVENTION

- Experimental and analytical investigation of a freezing point depressant fluid ice protection system [NASA-CR-174758] p 12 N86-27186
Analyses and tests for design of an electro-impulse de-icing system [NASA-CR-174919] p 15 N86-27268
De-icing of the altitude wind tunnel turning vanes by electro-magnetic impulse [NASA-CR-177260] p 38 N86-27291
NASA's Aircraft Icing Analysis Program [NASA-TM-88791] p 15 N86-31548

IGNITION

- Ignition and flame spread above liquid fuel pools p 41 N86-10163
Combustion characteristics in the transition region of liquid fuel sprays [NASA-CR-176564] p 77 N86-20517
Spontaneous ignition delay characteristics of hydrocarbon fuel-air mixtures [NASA-CR-175064] p 29 N86-21545
Methane oxidation behind reflected shock waves: Ignition delay times measured by pressure and flame band emission [NASA-TM-87268] p 77 N86-21635
Ignition delay times of benzene and toluene with oxygen in argon mixtures [NASA-TM-87312] p 78 N86-25431

IGNITION LIMITS

- Effect of gravity on laminar premixed gas combustion. II - Ignition and extinction phenomena p 72 A86-12414

IGNITION SYSTEMS

- Fundamental studies of droplet combustion at reduced gravity p 42 N86-10165

IGNITION TEMPERATURE

- The high-temperature oxidation of aromatic hydrocarbons p 75 A86-40834
A fundamental study of smoldering with emphasis on experimental design for zero-g p 41 N86-10162

IMAGE ANALYSIS

- Determination of grain size distribution function using two-dimensional Fourier transforms of tone pulse encoded images [NASA-TM-88790] p 166 N86-31065

IMIDES

- Chemical control of rate and onset temperature of nadimide polymerization p 101 N86-11271

IMPACT LOADS

- Impact wear of iron rich superalloys p 82 A86-34687
Fundamental studies of low velocity impact resistance of graphite fiber reinforced polymer matrix composites [NASA-TM-86886] p 69 N86-23661

IMPACT RESISTANCE

- Computational engine structural analysis [ASME PAPER 86-GT-70] p 23 A86-48141
Computational engine structural analysis [NASA-TM-87231] p 175 N86-19663
Fundamental studies of low velocity impact resistance of graphite fiber reinforced polymer matrix composites [NASA-TM-86886] p 69 N86-23661
The correlation of low-velocity impact resistance of graphite-fiber-reinforced composites with matrix properties [NASA-TM-87337] p 71 N86-27426

IMPACT TESTS

- Dynamic delamination crack propagation in a graphite/epoxy laminate p 68 A86-43010

IMPELLERS

- Effect of area ratio on the performance of a 5.5:1 pressure ratio centrifugal impeller
[ASME PAPER 86-GT-303] p 8 A86-48315
- Effect of area ratio on the performance of a 5.5:1 pressure ratio centrifugal impeller
[NASA-TM-87237] p 10 N86-19290

IMPIGEMENT

- An experimental method for measuring droplet impingement efficiency on two- and three-dimensional bodies
[AIAA PAPER 86-0406] p 131 A86-26630
- Textured carbon on copper: A novel surface with extremely low secondary electron emission characteristics
[NASA-TP-2543] p 101 N86-15394

IMPREGNATING

- Effect of impregnation method on cycle life of the nickel electrode
[NASA-TM-87326] p 190 N86-31980

IMPROVEMENT

- Wind tunnel turning vanes of modern design
[AIAA PAPER 86-0044] p 36 A86-19654
- Wind tunnel turning vanes of modern design
[NASA-TM-87146] p 37 N86-12239

IMPURITIES

- Double-injection, deep-impurity switch development
[NASA-CR-174936] p 124 N86-30073

INCOMPRESSIBLE FLOW

- Multi-grid technique for the solution of incompressible Navier-Stokes equations p 128 A86-21029
- Simplex finite element analysis of viscous incompressible flow with penalty function formulation p 129 A86-22615
- A comparison of three algebraic stress closures for combustor flow calculations
[ASME PAPER 85-WA/FE-3] p 132 A86-38388
- A space-marching method for viscous incompressible internal flows p 135 A86-43037
- Mean velocity and turbulence measurements in a 90 deg curved duct with thin inlet boundary layer
[NASA-CR-174811] p 139 N86-16518
- Analytical determination of propeller performance degradation due to ice accretion
[NASA-CR-175092] p 15 N86-23577

INCONEL (TRADEMARK)

- Thermal-mechanical fatigue crack growth in Inconel X-750 p 81 A86-20982

INDIUM ANTIMONIDES

- Undercooling and solidification behavior in the InSb-Sb system
[NASA-CR-175013] p 88 N86-14355

INDIUM ARSENIDES

- Cryogenic operation of pseudomorphic AlGaAs/InGaAs single-quantum-well MODFETs p 117 A86-11998
- High transconductance InGaAs/AlGaAs pseudomorphic modulation-doped field-effect transistors p 117 A86-18814
- Determination of carrier saturation velocity in high-performance In(y)Ga(1-y)As/Al(x)Ga(1-x)As modulation-doped field-effect transistors (with y between 0 and 0.2) p 118 A86-37295

INDIUM PHOSPHIDES

- Growth and characterization of epitaxial SrF₂ on InP(100) p 205 A86-47076
- Potential for use of indium phosphide solar cells in the space radiation environment
[NASA-TM-87157] p 121 N86-13645
- Indium phosphide solar cells: status and prospects for use in space
[NASA-TM-87315] p 123 N86-26520

INDUCTANCE

- Rotary transformer design with fixed magnetizing and/or leakage inductances p 119 A86-40462

INELASTIC STRESS

- Inelastic high-temperature thermomechanical response of ceramic coated gas turbine seals p 169 A86-37799
- Analysis of large, non-isothermal elastic-visco-plastic deformations
[NASA-CR-176220] p 172 N86-10588
- Nonlinear damage analysis: Postulate and evaluation
[NASA-CR-168171] p 177 N86-26652

INFRARED ABSORPTION

- Infrared-photoinduced-absorption studies in soluble trans-polyacetylene p 204 A86-37075

INFRARED SPECTROMETERS

- Characterization methodology for PMR-15 p 65 N86-11272

INFRARED SPECTROPHOTOMETERS

- Analysis of a thioether lubricant by infrared Fourier microemission spectrophotometry
[NASA-TM-87195] p 102 N86-16379

INGESTION (ENGINES)

- Transient engine performance with water ingestion
[AIAA PAPER 86-1621] p 23 A86-42755

INGOTS

- Structure-property characterization of rheocast and VADER processed IN-100 superalloy
[NASA-CR-175014] p 88 N86-14354

INHIBITORS

- The effects of metals and inhibitors on thermal oxidative degradation reactions of unbranched perfluoroalkyl ethers p 99 A86-40682

INJECTION

- A new very high voltage semiconductor switch p 119 A86-40449
- Double-injection, deep-impurity switch development
[NASA-CR-174936] p 124 N86-30073

INJECTION MOLDING

- Processing study of injection molding of silicon nitride for engine applications
[SAE PAPER 851787] p 154 A86-38311
- PMR polyimides from solutions containing mixed endcaps p 100 N86-11263

INJECTORS

- Computational simulation of liquid rocket injector anomalies
[AIAA PAPER 86-1424] p 55 A86-42633
- Flow and atomization in flashing injectors p 136 A86-49442
- Longitudinal mode combustion instabilities of a high-pressure fuel-rich LOX/RP-1 preburner p 165 N86-28250

INLET FLOW

- Aerodynamic detuning analysis of an unstalled supersonic turbofan cascade
[ASME PAPER 85-GT-192] p 3 A86-22732
- Relaminarization of the boundary layer over a flat plate in shock tube experiments
[AIAA PAPER 86-1238] p 133 A86-39865
- Turbine-stage heat transfer - Comparison of short-duration measurements with state-of-the-art predictions
[AIAA PAPER 86-1465] p 134 A86-42656
- An LU implicit scheme for high speed inlet analysis
[AIAA PAPER 86-1520] p 6 A86-42687
- Numerical analysis of some supersonic viscous flows related to inlet and nozzle systems
[AIAA PAPER 86-1597] p 134 A86-42738
- A numerical analysis applied to high angle of attack three-dimensional inlets
[AIAA PAPER 86-1527] p 6 A86-42760
- Three-dimensional flow field measurements in a radial inflow turbine scroll using LDV
[ASME PAPER 86-GT-122] p 7 A86-48181
- Starvation effects on the hydrodynamic lubrication of rigid nonconformal contacts in combined rolling and normal motion
[NASA-TM-87174] p 140 N86-19556
- Particle trajectory computation on a 3-dimensional engine inlet
[NASA-CR-175023] p 14 N86-20379
- An LU implicit scheme for high speed inlet analysis
[NASA-CR-175098] p 11 N86-23563
- A numerical analysis applied to high angle of attack three-dimensional inlets
[NASA-TM-87298] p 11 N86-24658
- Statistical prediction of dynamic distortion of inlet flow using minimum dynamic measurement. An application to the Melick statistical method and inlet flow dynamic distortion prediction without RMS measurements
[NASA-CR-176764] p 142 N86-24933
- Review and evaluation of recent developments in melic inlet dynamic flow distortion prediction and computer program documentation and user's manual estimating maximum instantaneous inlet flow distortion from steady-state total pressure measurements with full, limited, or no dynamic data
[NASA-CR-176765] p 143 N86-24955
- Summary of investigations of engine response to distorted inlet conditions
[NASA-TM-87317] p 30 N86-26336

INLET PRESSURE

- Two-phase flows and heat transfer within systems with ambient pressure above the thermodynamic critical pressure
[NASA-TM-87228] p 140 N86-19558

INLET TEMPERATURE

- Summary of investigations of engine response to distorted inlet conditions
[NASA-TM-87317] p 30 N86-26336
- 1700 deg C optical temperature sensor
[NASA-CR-175108] p 203 N86-28729

INPUT

- Input current shaped ac-to-dc converters
[NASA-CR-176438] p 121 N86-15544

INSTRUMENT COMPENSATION

- Compensation of reflector surface distortions using conjugate field matching
[NASA-TM-87198] p 113 N86-16461

INSTRUMENT ORIENTATION

- Accuracy and directional sensitivity of the single-wire technique p 146 A86-28541

INSTRUMENT PACKAGES

- HOST instrumentation R and D program overview p 147 N86-11497

INSTRUMENTS

- 1700 deg C optical temperature sensor
[NASA-CR-175108] p 203 N86-28729

INSULATION

- Current collection from the space plasma through defects in solar array insulation p 52 A86-18042

INSULATORS

- Ellipsometric and optical study of some uncommon insulator films on 3-5 semiconductors
[NASA-TM-87135] p 205 N86-12134

INTAKE SYSTEMS

- Evaluation of capillary reinforced composites
[NASA-CR-175061] p 70 N86-24760

INTEGRAL EQUATIONS

- Compliance matrices for cracked bodies
[NASA-CR-179478] p 179 N86-30236

INTEGRATED CIRCUITS

- Optical techniques to feed and control GaAs MMIC modules for phased array antenna applications
[AIAA PAPER 86-0687] p 110 A86-29638
- 10-30 GHz monolithic GaAs travelling-wave divider/combiner p 118 A86-34882
- Ka-band monolithic gain control amplifier p 119 A86-41343
- Characterization of MMIC devices for active array antennas p 111 N86-11401
- Monolithic optical integrated control circuitry for GaAs MMIC-based phased arrays p 113 N86-16457
- Optical techniques to feed and control GaAs MMIC modules for phased array antenna applications
[NASA-TM-87218] p 113 N86-16458
- Compensation of reflector surface distortions using conjugate field matching p 113 N86-16461
- Computation of the radiation characteristics of a generalized phased array
[NASA-TM-87185] p 114 N86-18586
- Ion beam sputter etching
[NASA-CASE-LEW-13899-1] p 109 N86-20587
- Optically controlled phased array antenna concepts using GaAs monolithic microwave integrated circuits
[NASA-TM-87229] p 123 N86-21757
- Analysis of optically controlled microwave/millimeter wave device structures
[NASA-TM-87246] p 123 N86-24907
- MMIC devices for active phased array antennas
[NASA-CR-176990] p 116 N86-30037

INTERACTIONAL AERODYNAMICS

- Numerical study of three-dimensional turbulent flow interactions between blockage models and wind tunnels including longitudinally slotted test sections
[AIAA PAPER 85-5017] p 1 A86-11065
- End-wall and profile losses in a low-speed axial flow compressor rotor
[ASME PAPER 85-GT-174] p 20 A86-22090
- Evaluation of propeller/nacelle interactions in the PTA program
[AIAA PAPER 86-1552] p 6 A86-42709
- Noise generated by convected gusts interacting with swept airfoil cascades
[AIAA PAPER 86-1872] p 198 A86-45492
- Influence of airfoil camber on convected gust interaction noise
[AIAA PAPER 86-1873] p 198 A86-45493

INTERCALATION

- Environmental stability of intercalated graphite fibers p 98 A86-31825
- Graphite fiber intercalation: Basic properties of copper chloride intercalated fibers p 65 N86-18442
- A comparison of the bromination dynamics of pitch-based and vapor-grown graphite fibers
[NASA-TM-87275] p 103 N86-21683
- The milling of pristine and brominated P-100 graphite fibers
[NASA-TM-88828] p 106 N86-32573

INTERFACE STABILITY

- Dendritic solidification in a binary alloy melt: Steady-state versus morphological stability theories p 42 N86-10261

INTERFACES

- Tribological characteristics of gold films deposited on metals by ion plating and vapor deposition p 85 A86-49600
- Burner liner thermal-structural load modeling
[NASA-CR-174892] p 176 N86-21932

INTERFACIAL TENSION

- Tribological properties of boron nitride synthesized by ion beam deposition p 96 A86-17479

- Contact angle and surface tension measurements of a five-ring polyphenyl ether p 98 A86-34179
Finite element simulation of temperature dependent free surface flows p 136 A86-47012
Surface tension induced instabilities in reduced gravity: The Benard problem p 40 N86-10117
Surface-tension driven convection p 40 N86-10124
Thermocapillary motion research p 40 N86-10125
Thermocapillary and diffusocapillary migration of a fluid drop p 40 N86-10128

INTERFERENCE

- Adaptive antenna arrays for weak interfering signals --- in satellite communication p 45 A86-34591

INTERFEROMETERS

- Lens collimation and testing using a Twyman-Green interferometer with a self-pumped phase-conjugating mirror p 146 A86-29280
Optical elements formed by compressed gases: Analysis and potential applications [NASA-TM-2555] p 203 N86-22390

INTERMETALLICS

- Slow plastic strain rate compressive flow in binary CoAl intermetallics p 79 A86-11478
Dislocations in extruded Co-49.3 at. pct Al p 83 A86-45091
The B2 aluminides as alternative materials p 84 A86-47259
Alloys based on NiAl for high temperature applications p 84 A86-47261
High temperature oxidation of beta-NiAl p 85 A86-47266

INTERNAL COMBUSTION ENGINES

- Lateral dampers for thrust bearings [NASA-CR-174924] p 157 N86-11474
Overview of free-piston Stirling SP-100 activities at the NASA Lewis Research Center [NASA-TM-87224] p 209 N86-19264
Preliminary evaluation of a compound cycle engine for shipboard gensets [NASA-CR-179451] p 180 N86-26629

INTERNAL COMPRESSION INLETS

- Low-speed performance of an axisymmetric, mixed-compression, supersonic inlet with auxiliary inlets [NASA-TP-2557] p 30 N86-24694

INTERNAL FRICTION

- Instability in Rotating Machinery [NASA-CP-2409] p 181 N86-30160

INTERORBITAL TRAJECTORIES

- Radiation exposure and performance of multiple burn LEO-GEO orbit transfer trajectories p 43 N86-17417

INTERPOLATION

- A numerical method for approximating antenna surfaces defined by discrete surface points [NASA-TM-87125] p 111 N86-10381

INTERSTELLAR RADIATION

- Radiation exposure and performance of multiple burn LEO-GEO orbit transfer trajectories p 43 N86-17417

INVERTED CONVERTERS (DC TO AC)

- A 20 kilohertz space station power system [NASA-TM-88801] p 62 N86-28122
Advanced on-site power plant development technology program [NASA-CR-175007] p 189 N86-29411
Description of a 20 Kilohertz power distribution system [NASA-TM-87346] p 34 N86-31584

INVERTERS

- Inverter design for high frequency power distribution p 117 A86-24831
Advanced on-site power plant development technology program [NASA-CR-174709] p 187 N86-25040

INVESTIGATION

- An experimental investigation of reducing advanced turboprop cabin noise by wing shielding [AIAA PAPER 86-1966] p 16 A86-45449
An experimental investigation of reducing advanced turboprop cabin noise by wing shielding [NASA-TM-87112] p 201 N86-25218

INVISCID FLOW

- Development of an explicit multigrid algorithm for quasi-three-dimensional viscous flows in turbomachinery [AIAA PAPER 86-0032] p 1 A86-19644
Applications of variational principles in computing rotational flows p 128 A86-20951
Steady inviscid three-dimensional flows p 128 A86-20952
Three-dimensional inviscid analysis of radial-turbine flow and a limited comparison with experimental data p 4 A86-28702
Three-dimensional inviscid flow in mixers. I - Mixer analysis using a Cartesian grid p 5 A86-39090
Coupling conditions for integrating boundary layer and rotational inviscid flow p 133 A86-41721
An LU implicit scheme for high speed inlet analysis [AIAA PAPER 86-1520] p 6 A86-42687

- Improved Euler analysis of advanced turboprop propeller flows [AIAA PAPER 86-1521] p 6 A86-42688

- Three-dimensional inviscid flow in mixers. II - Analysis of turboprop forced mixers p 6 A86-46316
Validation of viscous and inviscid computational methods for turbomachinery components [ASME PAPER 86-GT-42] p 7 A86-48126

- Three-dimensional inviscid analysis of radial turbine flow and a limited comparison with experimental data [NASA-TM-87091] p 9 N86-10017

- Development of an explicit multigrid algorithm for quasi-three-dimensional viscous flows in turbo-machinery [NASA-TM-87128] p 1 N86-11146

- Validation of viscous and inviscid computational methods for turbomachinery components [NASA-TM-87193] p 10 N86-16194

- A numerical simulation of the inviscid flow through a counter-rotating propeller [NASA-TM-87200] p 10 N86-16195

- Comparison of calculated and experimental cascade performance for controlled-diffusion compressor stator blading [NASA-TM-87167] p 27 N86-16219

- Analytical determination of propeller performance degradation due to ice accretion [NASA-CR-175092] p 15 N86-23577

IODINE COMPOUNDS

- Environmental stability of intercalated graphite fibers p 98 A86-31825

ION BEAMS

- Ion beam sputter-deposited thin film coatings for protection of spacecraft polymers in low earth orbit [AIAA PAPER 85-0420] p 95 A86-14428
Thin film growth rate effects for primary ion beam deposited diamondlike carbon films p 100 A86-47068
Dual-ion-beam deposition of carbon films with diamond-like properties p 85 A86-49855
Ion beam sputter etching [NASA-CASE-LEW-13899-1] p 109 N86-20587
Ion-beam nitriding of steels [NASA-CASE-LEW-14104-2] p 93 N86-32556

ION ENGINES

- Heaterless ignition of inert gas ion thruster hollow cathodes [AIAA PAPER 85-2008] p 51 A86-17833
Improvement of ion thruster design [NASA-CR-177223] p 61 N86-27419
Performance characteristics of ring-cusp thrusters with xenon propellant [NASA-TM-87338] p 63 N86-31650

ION EXCHANGE MEMBRANE ELECTROLYTES

- Method and apparatus for rebalancing a REDOX flow cell system [NASA-CASE-LEW-14127-1] p 122 N86-20680

ION IMPACT

- Carbon monoxide production in low energy oxygen ion bombardment of pyrolytic graphite and Kapton surfaces p 76 A86-47078

ION IMPLANTATION

- Calculation of recoil implantation profiles using known range statistics p 201 A86-11391
Sliding seal materials for adiabatic engines, phase 2 [NASA-CR-179475] p 105 N86-29042

ION IRRADIATION

- Angle-resolved Auger electron spectra induced by neon ion impact on aluminum p 76 A86-43456
Binary collision model for neon Auger spectra from neon ion bombardment of the aluminum surface p 76 A86-43457

- Ion-beam nitriding of steels [NASA-CASE-LEW-14104-2] p 93 N86-32556

ION PLATING

- Metallic glass as a temperature sensor during ion plating p 80 A86-16906
Tribological properties of boron nitride synthesized by ion beam deposition p 96 A86-17479
Tribological characteristics of gold films deposited on metals by ion plating and vapor deposition p 85 A86-49600

ION PROPULSION

- Rapid evaluation of ion thruster lifetime using optical emission spectroscopy [AIAA PAPER 85-2011] p 51 A86-17851
Rapid evaluation of ion thruster lifetime using optical emission spectroscopy [NASA-TM-87103] p 58 N86-10280
Performance characteristics of ring-cusp thrusters with xenon propellant [NASA-TM-87338] p 63 N86-31650

ION SHEATHS

- The role of unneutralized surface ions in negative potential arcing p 118 A86-25525

IONIC MOBILITY

- Electrohydrodynamics p 41 N86-10130

IRON

- Surface effects of corrosive media on hardness, friction, and wear of materials p 94 A86-10825
Interaction of sulfuric acid corrosion and mechanical wear of iron p 81 A86-20438
The reactions of cobalt, iron and nickel in SO₂ atmospheres Similarities and differences p 75 A86-40677

- The mechanism of erosion of metallic materials under cavitation attack [NASA-TM-87133] p 156 N86-10552

- Negative electrode catalyst for the iron chromium redox energy storage system [NASA-CASE-LEW-14028-1] p 186 N86-19721

IRON ALLOYS

- Interdiffusional effects between tungsten fibers and an iron-nickel-base alloy p 68 A86-14718
Impact wear of iron rich superalloys p 82 A86-34687

- High temperature properties of equiatomic FeAl with ternary additions p 84 A86-47252
The influence of grain size and composition on slow plastic flow in FeAl between 1100 and 1400 K p 86 A86-50279

- Creep rupture behavior of Stirling engine materials [NASA-TM-87209] p 88 N86-15380
Creep-rupture behavior of iron superalloys in high-pressure hydrogen [NASA-CR-175027] p 89 N86-17531

- Alloy chemistry and microstructural control to meet the demands of the automotive Stirling engine [NASA-TM-87250] p 89 N86-20541
Fatigue crack layer propagation in silicon-iron [NASA-CR-175115] p 177 N86-25851

IRON CHLORIDES

- Environmental stability of intercalated graphite fibers p 98 A86-31825

IRON COMPOUNDS

- Tensile behavior of Fe-40Al alloys with B and Zr additions [NASA-TM-87290] p 91 N86-25453

IRRADIATION

- Thermal desorption study of physical forces at the PTFE surface [NASA-TM-87090] p 206 N86-25284

ISOLATION

- Robust detection-isolation-accommodation for sensor failures [NASA-CR-174797] p 121 N86-16486

ISOMERIZATION

- The synthesis, characterization and thermal chemistry of modified norbornenyl PMR endcaps p 100 N86-11266

ISOPARAMETRIC FINITE ELEMENTS

- Burner liner thermal/structural load modeling: TRANCITS program user's manual [NASA-CR-174891] p 142 N86-24931

ISOTROPIC MEDIA

- Constitutive modeling for isotropic materials (HOST) [NASA-CR-174960] p 172 N86-10589
Wave propagation in anisotropic medium due to an oscillatory point source with application to unidirectional composites [NASA-CR-4001] p 165 N86-27666

ITERATIVE SOLUTION

- Performance of direct and iterative algorithms on an optical systolic processor p 202 A86-17421
Iterative methods for mixed finite element equations p 169 A86-34461
An iterative finite element-integral technique for predicting sound radiation from turboprop inlets in steady flight p 198 A86-49806

- Integrated research in constitutive modelling at elevated temperatures, part 2 [NASA-CR-177233] p 178 N86-28455

- Solution of elliptic partial differential equations by fast Poisson solvers using a local relaxation factor. 1: One-step method [NASA-TP-2529] p 195 N86-28661

J**J INTEGRAL**

- Closure of fatigue cracks at high strains [NASA-CR-175021] p 175 N86-17788
J-integral estimates for cracks in infinite bodies [NASA-CR-179474] p 178 N86-28467

JET AIRCRAFT

- A high-order language for a system of closely coupled processing elements [NASA-CR-177280] p 193 N86-27930

JET AIRCRAFT NOISE

- Tone excited jets. I - Introduction p 196 A86-16466
Tone excited jets. IV - Acoustic measurements p 196 A86-16469

- Flow field and near and far sound field of a subsonic jet p 5 A86-35855
- Laboratory experiments on active suppression of advanced turboprop noise
[NASA-TM-87129] p 199 N86-19125
- Free jet feasibility study of a thermal acoustic shield concept for AST/VCE application-dual flow. Comprehensive data report. Volume 1: Test nozzles and acoustic data
[NASA-CR-174817] p 200 N86-23371
- Free-jet feasibility study of a thermal acoustic shield concept for AST/VCE application-dual stream nozzles. Comprehensive data report. Volume 2: Laser velocimeter and suppressor. Base pressure data
[NASA-CR-174818] p 201 N86-23372
- JET ENGINE FUELS**
- Determination of solid mass fraction in partially frozen hydrocarbon fuels
[NASA-CR-179472] p 108 N86-28261
- Jet fuel viscosity at low temperatures with notes on n-alkaline crystals
[NASA-CR-174911] p 15 N86-30022
- JET ENGINES**
- Fabrication of ceramic substrate-reinforced and free forms by mandrel plasma spraying metal-ceramic composites p 64 A86-17483
- Transient engine performance with water ingestion
[AIAA PAPER 86-1621] p 23 A86-42755
- An analysis of cross-coupling of a multicomponent jet engine test stand using finite element modeling techniques
[NASA-CR-176424] p 37 N86-15323
- Demonstration test of burner liner strain measuring system
[NASA-CR-174743] p 148 N86-21817
- Evaluation of capillary reinforced composites
[NASA-CR-175061] p 70 N86-24760
- JET EXHAUST**
- Plume characteristics of single-stream and dual-flow conventional and inverted-profile nozzles at equal thrust
[AIAA PAPER 86-1809] p 8 A86-49585
- Plume characteristics of single-stream and dual-flow conventional and inverted-profile nozzles at equal thrust
[NASA-TM-87323] p 12 N86-26285
- JET FLAPS**
- Velocity and temperature decay characteristics of inverted-profile jets
[AIAA PAPER 86-0312] p 2 A86-22693
- Velocity and temperature decay characteristics of inverted-profile jets
[NASA-TM-87159] p 9 N86-14223
- JET FLOW**
- Tone excited jets. III - Flow measurements
[NASA-TM-87159] p 9 N86-14223
- Tone excited jets. V - A theoretical model and comparison with experiment p 196 A86-16470
- Numerical and experimental investigation of nonswirling and swirling confined jets
[AIAA PAPER 86-0040] p 127 A86-19651
- Modeling dilution of jet flowfields p 128 A86-20362
- Velocity and temperature decay characteristics of inverted-profile jets
[AIAA PAPER 86-0312] p 2 A86-22693
- Mass and momentum turbulent transport experiments with swirling confined coaxial jets. II
[AIAA PAPER 86-1665] p 134 A86-42780
- Plume characteristics of single-stream and dual-flow conventional and inverted-profile nozzles at equal thrust
[AIAA PAPER 86-1809] p 8 A86-49585
- Buoyancy effects upon vapor flame and explosion processes p 41 N86-10161
- Velocity and temperature decay characteristics of inverted-profile jets
[NASA-TM-87159] p 9 N86-14223
- Influence of large-scale motion on turbulent transport for confined coaxial jets. Volume 2: Navier-Stokes calculations of swirling and nonswirling confined coaxial jets
[NASA-CR-175036] p 28 N86-20390
- Influence of large-scale motion on turbulent transport for confined coaxial jets. Volume 1: Analytical analysis of the experimental data using conditional sampling
[NASA-CR-175035] p 29 N86-20395
- Dilution jet mixing program, phase 3
[NASA-CR-174884] p 142 N86-24938
- Plume characteristics of single-stream and dual-flow conventional and inverted-profile nozzles at equal thrust
[NASA-TM-87323] p 12 N86-26285
- JET IMPINGEMENT**
- Heat transfer characteristics within an array of impinging jets. Effects of crossflow temperature relative to jet temperature
[NASA-CR-3936] p 139 N86-15625
- Channel flow modeling of impingement cooling of a rotating turbine blade
[NASA-CR-177206] p 31 N86-27285

JET MIXING FLOW

- Concentration distributions in cylindrical combustors
[NASA-CR-176220] p 172 N86-10588
- An analytical model for the vorticity associated with a transverse jet p 4 A86-28538
- An experimental study of tone-excited heated jets
[NASA-CR-177194] p 178 N86-28462
- Concentration distributions in a model combustor
[NASA-CR-177194] p 178 N86-28462
- Forced mixer lobes in ejector designs
[AIAA PAPER 86-1614] p 134 A86-42752
- Some unresolved questions on hot-jet mixing control through artificial excitation
[AIAA PAPER 86-1956] p 135 A86-45441
- Acoustic control of free jet mixing p 135 A86-46314
- Vortex modeling of single and multiple dilution jet mixing in a cross flow p 135 A86-46318
- Perspectives on dilution jet mixing --- in creating temperature patterns at combustor exits in gas turbine engines
[AIAA PAPER 86-1611] p 25 A86-49614
- Dilution jet mixing program, supplementary report
[NASA-CR-175043] p 141 N86-23856
- Perspectives on dilution jet mixing
[NASA-TM-87294] p 35 N86-32432
- JET NOZZLES**
- High Weber number SMD correlations for pressure atomizers --- Sauter Mean Diameter
[ASME PAPER 85-GT-37] p 128 A86-22026
- JET PROPULSION**
- Aeropropulsion opportunities for the 21st century
[NASA-TM-88817] p 34 N86-31585
- JET THRUST**
- Experimental performance of a 1-kilowatt arcjet thruster
[AIAA PAPER 85-2033] p 54 A86-37063
- Experimental performance of a 1-kilowatt arcjet thruster
[NASA-TM-87131] p 57 N86-10281
- JOINING**
- Demonstrated results of welded and soldered interconnections p 185 N86-17866
- JOINTS (JUNCTIONS)**
- Improved stud configurations for attaching laminated wood wind turbine blades
[NASA-TM-87109] p 172 N86-10582
- Thermal-mechanical fatigue test apparatus for metal matrix composites and joint attachments
[NASA-TM-87187] p 88 N86-15378
- Feasibility study of a discrete bearing/roller drive rotary joint for the space station
[NASA-TM-88800] p 161 N86-30206
- JOURNAL BEARINGS**
- An experimental investigation and some analytical considerations concerning the vaporous/gaseous cavity characteristics of an eccentric shaft seal or bearing
[NASA-TM-87255] p 130 A86-24463
- Theoretical modeling of the vapor cavitation in dynamically loaded journal bearings
[ASME PAPER 85-TRIB-51] p 130 A86-24496
- Analysis of a two row hydrostatic journal bearing with variable properties, inertia effects and surface roughness p 153 A86-30599
- Theoretical modeling of the vapor cavitation in dynamically loaded journal bearings
[NASA-TM-87076] p 137 N86-10463
- Theoretical and experimental comparison of vapor cavitation in dynamically loaded journal bearings
[NASA-TM-87121] p 137 N86-11425
- Study of journal bearing dynamics using 3-dimensional motion picture graphics
[NASA-TM-87205] p 140 N86-18647
- Compliant hydrodynamic fluid journal bearing
[NASA-CASE-LEW-13670-1] p 158 N86-19606
- Evaluation of a hybrid hydrostatic bearing for cryogenic turbopump application
[NASA-TM-87255] p 63 N86-31649

K**KAPTON (TRADEMARK)**

- Carbon monoxide production in low energy oxygen ion bombardment of pyrolytic graphite and Kapton surfaces
[NASA-CR-3976] p 165 N86-27665
- A study of Kapton degradation under simulated shuttle environment
[NASA-CR-176850] p 78 N86-28136
- KINEMATICS**
- Generated spiral bevel gears - Optimal machine-tool settings and tooth contact analysis
[SAE PAPER 851573] p 154 A86-40678
- Spin analysis of concentrated traction contacts
[ASME PAPER 84-DET-99] p 155 A86-45257

- Analysis of large, non-isothermal elastic-visco-plastic deformations
[NASA-CR-176220] p 172 N86-10588
- Formulation of the nonlinear analysis of shell-like structures, subjected to time-dependent mechanical and thermal loading
[NASA-CR-177194] p 178 N86-28462
- KINETICS**
- Rapid evaluation of ion thruster lifetime using optical emission spectroscopy
[AIAA PAPER 85-2011] p 51 A86-17851
- Rapid evaluation of ion thruster lifetime using optical emission spectroscopy
[NASA-TM-87103] p 56 N86-10280
- Formulation of the nonlinear analysis of shell-like structures, subjected to time-dependent mechanical and thermal loading
[NASA-CR-177194] p 178 N86-28462

L**LABORATORIES**

- Microgravity Materials Science Laboratory
[NASA-CR-176220] p 42 N86-10173

LABYRINTH SEALS

- Experimental rotordynamic coefficient results for teeth-on-rotor and teeth-on-stator labyrinth gas seals
[ASME PAPER 86-GT-12] p 156 A86-48109

LAGRANGE MULTIPLIERS

- Finite elements based on consistently assumed stresses and displacements p 166 A86-18123

LAMELLA (METALLURGY)

- The development of gamma-gamma-prime lamellar structures in a nickel-base superalloy during elevated temperature mechanical testing p 79 A86-14719

LAMINAR BOUNDARY LAYER

- Thermophoretically augmented mass transfer rates to solid walls across laminar boundary layers
[NASA-TM-87103] p 56 N86-10280

- Relaminarization of the boundary layer over a flat plate in shock tube experiments
[AIAA PAPER 86-1238] p 133 A86-39865

LAMINAR FLOW

- Low Reynolds number separation bubble research at UTRC p 126 A86-16311
- A review and analysis of boundary layer transition data for turbine application
[ASME PAPER 85-GT-83] p 129 A86-22054
- On the determination of laminar flame speeds from stretched flames p 74 A86-22814
- Thermodynamic evaluation of transonic compressor rotors using the finite volume approach
[NASA-CR-176947] p 32 N86-30731

LAMINATES

- A new ply model for interlaminar stress analysis
[NASA-TM-87138] p 69 N86-14316
- Three-dimensional hybrid-stress finite element analysis of composite laminates with cracks and cutouts
[NASA-TM-87266] p 70 N86-25417
- Progressive fracture of fiber composites
[NASA-TM-87088] p 163 N86-10561
- Dynamic delamination crack propagation in a graphite/epoxy laminate p 68 N86-11281
- Ultrasonic evaluation of mechanical properties of thick, multilayered, filament wound composites
[NASA-TM-87088] p 163 N86-10561
- Surface protection of graphite fabric/PMR-15 composites subjected to thermal oxidation p 68 N86-11281
- Interlaminar fracture toughness: Three-dimensional finite element modeling for end-notch and mixed-mode flexure
[NASA-TM-87138] p 69 N86-14316
- Fracture characteristics of angle-ply laminates fabricated from overaged graphite/epoxy prepreg
[NASA-TM-87266] p 70 N86-25417
- Computational simulation of progressive fracture in fiber composites
[NASA-TM-87341] p 71 N86-26376
- Ultrasonic stress wave characterization of composite materials
[NASA-CR-3976] p 165 N86-27665
- Fiber composite sandwich thermostructural behavior: Computational simulation
[NASA-TM-88787] p 71 N86-31663
- ICAN: A versatile code for predicting composite properties
[NASA-TM-87334] p 71 N86-31664
- LANTHANUM COMPOUNDS**
- The effect of oxygen pressure on volatility and morphology of LaB₆ single crystal cathodes
[NASA-CR-177206] p 31 N86-27285

LARGE SPACE STRUCTURES

Frequency domain solutions to multi-degree-of-freedom, dry friction damped systems under periodic excitation

p 170 A86-39485

Satellite voice broadcast. Volume 1: Executive summary

[NASA-CR-175016] p 115 N86-24875

Satellite voice broadcast. Volume 2: System study

[NASA-CR-175017] p 115 N86-24876

Satellite voice broadcast system study, volume 2

[NASA-CR-174905] p 115 N86-24877

Contributions to the understanding of large-scale coherent structures in developing free turbulent shear flows

[NASA-CR-176772] p 142 N86-24932

LASER ANEMOMETERS

Implementation of a new type of time-of-flight laser anemometer

p 146 A86-28755

Filter induced errors in laser anemometry using counter-processor

p 146 A86-34431

Development of seeding techniques for small supersonic wind tunnel

p 147 N86-11452

Laser anemometry for hot section applications

p 151 N86-11503

Combined fringe and Fabry-Perot laser anemometer for three component velocity measurements in turbine stator cascade facility

[NASA-TM-87322] p 149 N86-24967

Application of laser anemometry to turbomachinery flow field measurements

p 160 N86-27640

Laser fringe anemometry for aero engine components

[NASA-TM-88798] p 12 N86-28053

Parametric study of beam refraction problems across laser anemometer windows

[NASA-TM-87350] p 150 N86-31857

LASER APPLICATIONS

Calibration of droplet sizing and liquid water content instruments: Survey and analysis

[NASA-CR-175099] p 149 N86-26596

Application of laser anemometry to turbomachinery flow field measurements

p 160 N86-27640

Advanced optical measuring systems for measuring the properties of fluids and structures

[NASA-TM-88829] p 150 N86-31859

LASER DOPPLER VELOCIMETERS

Boundary layer measurements on an airfoil in cascade using laser Doppler anemometry

[AIAA PAPER 86-0072] p 145 A86-19670

An experimental investigation of propeller wakes using a laser Doppler velocimeter

[AIAA PAPER 86-0080] p 18 A86-19677

Laser Doppler velocimeter measurement in the tip region of a compressor rotor

p 5 A86-39064

Three-dimensional flow field measurements in a radial inflow turbine scroll using LDV

[ASME PAPER 86-GT-122] p 7 A86-48181

Laser velocimeter measurements in shrouded and unshrouded radial flow pump impellers

[ASME PAPER 86-GT-129] p 136 A86-48187

Characteristics of an axisymmetric sudden expansion flow

[NASA-CR-176278] p 151 N86-11465

The boundary layer on compressor cascade blades

[NASA-CR-177279] p 143 N86-27607

LASER INDUCED FLUORESCENCE

Simultaneous measurements of velocity and pressure fields in subsonic and supersonic flows through image-intensified detection of laser-induced fluorescence

[AIAA PAPER 86-0181] p 145 A86-19726

LASER INTERFEROMETRY

A study of the stress wave factor technique for nondestructive evaluation of composite materials

[NASA-CR-4002] p 165 N86-28445

LASER MICROSCOPY

Quantitative flow characterization with scanning laser acoustic microscopy

p 163 A86-45150

Reliability of scanning laser acoustic microscopy for detecting internal voids in structural ceramics

p 147 A86-46353

Reliability of scanning laser acoustic microscopy for detecting internal voids in structural ceramics

[NASA-TM-87222] p 164 N86-18599

Quantitative flow characterization with scanning laser acoustic microscopy

p 200 N86-22983

Factors that affect reliability of nondestructive detection of flaws in structural ceramics

[NASA-TM-87348] p 166 N86-31912

Quantitative void characterization in structural ceramics using scanning laser acoustic microscopy

[NASA-TM-88797] p 166 N86-31913

LASER PROPULSION

Radiation energy receiver for solar propulsion systems

p 52 A86-18043

LASER RANGE FINDERS

Range finding using frequency-modulated laser diode

p 147 A86-39521

LC CIRCUITS

Input current shaped ac-to-dc converters

[NASA-CR-176438] p 121 N86-15544

LEADING EDGES

Turbine vane external heat transfer. Volume 1: Analytical and experimental evaluation of surface heat transfer distributions with leading edge showerhead film cooling

[NASA-CR-174827] p 29 N86-21546

Effect of a rotor wake on the local heat transfer on the forward half of a circular cylinder

[NASA-TM-87234] p 140 N86-21794

LEAKAGE

Theory versus experiment for the rotordynamic coefficients of annular gas seals. I - Test facility and apparatus

[ASME PAPER 85-TRIB-1] p 152 A86-24481

A comparison of experimental and theoretical results for leakage, pressure gradients, and rotordynamic coefficients for tapered annular gas seal

[NASA-CR-179709] p 162 N86-32742

LEAST SQUARES METHOD

Hierarchical implicit dynamic least-square solution algorithm

p 167 A86-26889

Constrained hierarchical least square nonlinear equation solvers --- for indefinite stiffness and large structural deformations

p 171 A86-43774

LENS ANTENNAS

Optimized three-dimensional lenses for wide-angle scanning

p 109 A86-19184

LENS DESIGN

Optimized three-dimensional lenses for wide-angle scanning

p 109 A86-19184

Lens collimation and testing using a Twyman-Green interferometer with a self-pumped phase-conjugating mirror

p 146 A86-29280

LENSES

Optical elements formed by compressed gases: Analysis and potential applications

[NASA-TP-2555] p 203 N86-22390

LIFE (DURABILITY)

Life and reliability modeling of bevel gear reductions

[ASME PAPER 85-DE-7] p 151 A86-14466

Fabrication of ceramic substrate-reinforced and free forms by mandrel plasma spraying metal-ceramic composites

p 64 A86-17483

Compatibility of grain-stabilized platinum with candidate propellants for resistojets

[AIAA PAPER 85-2014] p 51 A86-17835

KOH concentration effect on the cycle life of nickel-hydrogen cells

p 180 A86-24802

NASA electrothermal auxiliary propulsion technology

[AIAA PAPER 86-1703] p 55 A86-42799

Fatigue life analysis of a turboprop reduction gearbox

[ASME PAPER 85-DET-10] p 155 A86-45256

Toward improved durability in advanced combustors and turbines - Progress in prediction of thermomechanical loads

[ASME PAPER 86-GT-172] p 24 A86-48224

Compatibility of grain-stabilized platinum with candidate propellants for resistojets

[NASA-TM-87118] p 56 N86-10279

Time dependency of strainrange partitioning life relationships

[NASA-CR-174946] p 174 N86-13755

Adhesion and wear resistance of materials

[NASA-TM-87239] p 158 N86-20809

Automotive Stirling summary and overview

[NASA-TM-87177] p 209 N86-21457

Lightweight nickel electrode for nickel hydrogen cells and batteries

[NASA-TM-87253] p 186 N86-21978

Thermal barrier coating life prediction model development

[NASA-CR-175087] p 103 N86-22713

Assessment of commercially available and experimental hydrogen electrodes

[NASA-TM-87264] p 187 N86-23035

NASA electrothermal auxiliary propulsion technology

[NASA-TM-87281] p 80 N86-24749

System life and reliability modeling for helicopter transmissions

[NASA-CR-3967] p 159 N86-24990

Long life nickel electrodes for a nickel-hydrogen cell: Cycle life tests

[NASA-CR-174815] p 188 N86-25046

Nonlinear damage analysis: Postulate and evaluation

[NASA-CR-168171] p 177 N86-26852

Re-examination of cumulative fatigue damage analysis: An engineering perspective

[NASA-TM-87325] p 177 N86-27680

Effects of surface chemistry on hot corrosion life

[NASA-CR-179471] p 32 N86-28087

Structural analysis of turbine blades using unified constitutive models

[NASA-TM-86807] p 178 N86-28481

Effect of impregnation method on cycle life of the nickel electrode

[NASA-TM-87326] p 190 N86-31980

LIFE CYCLE COSTS

Life cycle cost assessment of future low heat rejection engines

[SAE PAPER 860444] p 153 A86-37048

Year 2000 small engine technology payoffs in cruise missiles

[AIAA PAPER 86-1546] p 23 A86-42705

Satellite voice broadcast. Volume 1: Executive summary

[NASA-CR-175016] p 115 N86-24875

LIFE SUPPORT SYSTEMS

Space Station benefits from ECLS - Propulsion system synergism

[AIAA PAPER 86-1407] p 47 A86-42619

LIGHT BEAMS

Parametric study of beam refraction problems across laser anemometer windows

[NASA-TM-87350] p 150 N86-31857

LIGHT EMITTING DIODES

All-fibre sensing loop using pulse-modulated light-emitting diode

p 202 A86-11995

LIGHT MODULATION

All-fibre sensing loop using pulse-modulated light-emitting diode

p 202 A86-11995

LIGHT SCATTERING

Light scattering tests of fundamental theories of transport properties in the critical region

p 39 N86-10113

LIGHT TRANSMISSION

Diffraction effects and special advantages in electronic heterodyne moire deflectometry

p 202 A86-31565

Reassessment of the theory of stimulated Raman scattering

p 150 A86-40662

LINEAR EQUATIONS

Space and frequency-multiplexed optical linear algebra processor - Fabrication and initial tests

p 202 A86-48352

LINEAR FILTERS

Linearization of digital derived rate algorithm for use in linear stability analysis

p 47 A86-35338

LINEAR PROGRAMMING

The role of service areas in the optimization of FSS orbital and frequency assignments

[NASA-CR-176488] p 46 N86-18341

LINEAR RECEIVERS

Testing of 30-GHz low noise receivers

[AIAA PAPER 86-0854] p 45 A86-29616

Testing of 30-GHz low noise receivers

[NASA-TM-87171] p 112 N86-13627

LINEAR SYSTEMS

Linear dynamic coupling in geared rotor systems

[ASME PAPER 85-DET-11] p 154 A86-38617

Effects of a high mean stress on the high cycle fatigue life of PWA 1480 and correlation of data by linear elastic fracture mechanics

[NASA-CR-175057] p 177 N86-27689

LINEAR TRANSFORMATIONS

Performance of direct and iterative algorithms on an optical systolic processor

p 202 A86-17421

LINEARITY

Linearized traveling wave amplifier with hard limiter characteristics

[NASA-CASE-LEW-13981-2] p 122 N86-21742

Identification of differences between finite element analysis and experimental vibration data

[NASA-TM-87336] p 149 N86-27617

LINEARIZATION

Application of a linearized unsteady aerodynamic analysis to standard cascade configurations

[NASA-CR-3940] p 11 N86-21505

LININGS

Small gas turbine combustor experimental study - Compliant metal/ceramic liner and performance evaluation

[AIAA PAPER 86-1452] p 25 A86-49611

Burner liner thermal/structural load modelling

p 173 N86-11514

Component-specific modeling

p 25 N86-11515

Validation of structural analysis methods using burner liner cyclic rig test data

p 173 N86-11518

Thermomechanical cyclic hardening behavior of Hastelloy-X

[NASA-CR-174999] p 174 N86-18610

Burner liner thermal-structural load modeling

[NASA-CR-174892] p 176 N86-21932

Small gas turbine combustor experimental study: Compliant metal/ceramic liner and performance evaluation

[NASA-TM-87304] p 33 N86-31582

LIQUID ATOMIZATION

Spray atomization and combustion

[AIAA PAPER 86-0136] p 131 A86-26606

- Flow and atomization in flashing injectors
p 136 A86-48442
- LIQUID BEARINGS**
Evaluation of a hybrid hydrostatic bearing for cryogenic turbopump application
[NASA-TM-87255] p 63 N86-31649
- LIQUID CHROMATOGRAPHY**
Characterization methodology for PMR-15
p 65 N86-11272
A thin film degradation study of a fluorinated polyether liquid lubricant using an HPLC method
[NASA-TM-87221] p 77 N86-19417
Development of LC-13C NMR
[NASA-CR-176656] p 107 N86-21704
- LIQUID COOLING**
Test program to provide confidence in liquid oxygen cooling of hydrocarbon fueled rocket thrust chambers
[NASA-TM-88816] p 62 N86-31646
- LIQUID FLOW**
Convective and absolute instability of a viscous liquid jet
p 132 A86-34377
Flow and atomization in flashing injectors
p 136 A86-48442
- LIQUID FUELS**
Liquid fueled external heating system for STM4-120 Stirling engine
p 180 A86-24888
Ignition and flame spread above liquid fuel pools
p 41 N86-10163
Combustion characteristics in the transition region of liquid fuel sprays
[NASA-CR-176564] p 77 N86-20517
Measurements in liquid fuel sprays
[NASA-CR-177088] p 144 N86-30960
- LIQUID HYDROGEN**
LH2 on-orbit storage tank support trunnion design and verification
p 53 A86-37054
Effect of subcooling on the on-orbit pressurization rate of cryogenic propellant tankage
[AIAA PAPER 86-1253] p 54 A86-39877
Creep rupture behavior of Stirling engine materials
[NASA-TM-87209] p 88 N86-15380
An experimental data base for material selection and design of high-speed, high-pressure, oxygen turbomachinery
p 58 N86-17387
SSME long-life bearings
[NASA-CR-179455] p 160 N86-27643
The noncavitating performance and life of a small vane-type positive displacement pump in liquid hydrogen
[NASA-TM-87347] p 63 N86-31651
- LIQUID NITROGEN**
SSME long-life bearings
[NASA-CR-179455] p 160 N86-27643
- LIQUID OXYGEN**
Turbulent two-phase flow in annular seals
[ASLE PREPRINT 86-AM-4G-3] p 156 A86-45391
An experimental data base for material selection and design of high-speed, high-pressure, oxygen turbomachinery
p 58 N86-17387
Advanced seals for Liquid Oxygen (LOX) turbopumps
p 157 N86-17408
SSME long-life bearings
[NASA-CR-179455] p 160 N86-27643
Test program to provide confidence in liquid oxygen cooling of hydrocarbon fueled rocket thrust chambers
[NASA-TM-88816] p 62 N86-31646
- LIQUID PROPELLANT ROCKET ENGINES**
Computational simulation of liquid rocket injector anomalies
[AIAA PAPER 86-1424] p 55 A86-42633
Orbital transfer vehicle engine integration study
[NASA-CR-174842] p 59 N86-20493
- LIQUID ROCKET PROPELLANTS**
Deposit formation and heat-transfer characteristics of hydrocarbon rocket fuels
p 106 A86-10028
Current evaluation of the tripropellant concept
[AIAA PAPER 86-1698] p 56 A86-49615
Current evaluation of the tripropellant concept
[NASA-TP-2602] p 62 N86-28124
- LIQUID SURFACES**
Surface temperature distribution along a thin liquid layer due to thermocapillary convection
[IAF PAPER 85-282] p 126 A86-15800
Free surface phenomena under low- and zero-gravity conditions
p 39 N86-10108
- LIQUID-SOLID INTERFACES**
Interaction of flows with the crystal-melt interface
p 132 A86-29419
Operating aspects of an oil pumping ring seal
[ASME PAPER 85-TRIB-29] p 153 A86-34010
Finite element simulation of temperature dependent free surface flows
p 136 A86-47012
Influence of melt convection on solid-liquid interface under terrestrial and reduced gravity environments
p 38 N86-10083
The development and prevention of channel segregation during alloy solidification
p 38 N86-10086
- LIQUID-VAPOR INTERFACES**
Theory of homogeneous nucleation - A chemical kinetic view
p 72 A86-19389
Liquid-vapor interface locations in a spheroidal container under low gravity
[NASA-TM-87147] p 141 N86-23854
Modeling of zero gravity venting: Studies of two-phase heat transfer under reduced gravity
[NASA-CR-179662] p 144 N86-31826
- LIQUIDS**
Mass transport phenomena between bubbles and dissolved gases in liquids under reduced gravity conditions
p 39 N86-10110
Light scattering tests of fundamental theories of transport properties in the critical region
p 39 N86-10113
- LITHIUM**
Lithium counterdoped silicon solar cell
[NASA-CASE-LEW-14177-1] p 190 N86-32875
- LITHIUM FLUORIDES**
Estimated heats of fusion of fluoride salt mixtures suitable for thermal energy storage applications
[NASA-TM-87320] p 190 N86-31982
- LITHOSPHERE**
Wilson study cycles: Research relative to ocean geodynamic cycles
[NASA-CR-176560] p 192 N86-21092
- LOAD DISTRIBUTION (FORCES)**
A study of spectrum fatigue crack propagation in two aluminum alloys. I - Spectrum simplification. II - Influence of microstructures
p 85 A86-48973
- LOAD TESTS**
Longitudinal compressive failure modes in fiber composites End attachment effects on IITRI type test specimens
p 66 A86-19999
Shear fatigue crack growth - A literature survey
p 167 A86-24219
Instability in Rotating Machinery
[NASA-CP-2409] p 161 N86-30160
- LOADS (FORCES)**
Theoretical and experimental comparison of vapor cavitation in dynamically loaded journal bearings
[NASA-TM-87121] p 137 N86-11425
Surface fatigue life and failure characteristics of EX-53, CBS 1000M, and AISI 9310 gear materials
[NASA-TP-2513] p 157 N86-12609
Modifications of system for elevated temperature tensile testing and stress-strain measurement of metal matrix composites
[NASA-TM-87172] p 65 N86-13370
Fractured toughness of Si3N4 measured with short bar chevron-notched specimens
[NASA-TM-87153] p 101 N86-13495
Burner liner thermal-structural load modeling
[NASA-CR-174892] p 176 N86-21932
Simplified composite micromechanics for predicting microstresses
[NASA-TM-87295] p 70 N86-24759
Burner liner thermal/structural load modeling: TRANCITS program user's manual
[NASA-CR-174891] p 142 N86-24931
Effects of state recovery on creep buckling under variable loading
[NASA-CR-175094] p 212 N86-25310
New methodology for shaft design based on life expectancy
[NASA-TM-87354] p 161 N86-27661
Integrated research in constitutive modelling at elevated temperatures, part 2
[NASA-CR-177233] p 178 N86-28455
- LONG TERM EFFECTS**
Long term deposit formation in aviation turbine fuel at elevated temperature
[AIAA PAPER 86-0525] p 107 A86-19929
- LOSSES**
Development of the VOLT-A shuttle experiment
[NASA-TM-87169] p 212 N86-14110
- LOSSY MEDIA**
Normal modes in an overmoded circular waveguide coated with lossy material
p 119 A86-44078
A simple circular-polarized antenna: Circular waveguide horn coated with lossy magnetic material
[NASA-CR-177092] p 116 N86-30039
- LOW NOISE**
Testing of 30-GHz low noise receivers
[AIAA PAPER 86-0654] p 45 A86-29616
Testing of 30-GHz low noise receivers
[NASA-TM-87171] p 112 N86-13627
- LOW REYNOLDS NUMBER**
Low Reynolds number separation bubble research at UTRC
p 126 A86-16311
- LOW SPEED**
Fundamental studies of low velocity impact resistance of graphite fiber reinforced polymer matrix composites
[NASA-TM-88886] p 69 N86-23661
- Low-speed performance of an axisymmetric, mixed-compression, supersonic inlet with auxiliary inlets
[NASA-TP-2557] p 30 N86-24694
- LOW SPEED WIND TUNNELS**
A novel centrifugal diffuser test device
[ASME PAPER 85-IGT-135] p 3 A86-23927
Low Reynolds number boundary layers in a disturbed environment
[NASA-CR-175031] p 139 N86-17665
- LOW TEMPERATURE**
Jet fuel viscosity at low temperatures with notes on n-alkaline crystals
[NASA-CR-174911] p 15 N86-30022
- LOW THRUST**
Small centrifugal pumps for low-thrust rocket engines
[NASA-CR-174913] p 162 N86-32741
- LOW THRUST PROPULSION**
An analysis of low-thrust, resistojet reboost for the Space Station
[AIAA PAPER 85-2042] p 51 A86-14447
LOX/LH2 vane pump for auxiliary propulsion systems
p 58 N86-17397
Theoretical study on the effect of the design of small (milli-Newton) thruster jets on molecular contamination for the space station
[NASA-CR-177263] p 48 N86-26358
- LUBRICANT TESTS**
An experimental investigation and some analytical considerations concerning the vaporous/gaseous cavity characteristics of an eccentric shaft seal or bearing
p 130 A86-24463
- LUBRICANTS**
Ellipsometric surface analysis of wear tracks produced by different lubricants
[ASLE PREPRINT 85-TC-5A-2] p 151 A86-11016
Simulation of lubricating behavior of a thioether liquid lubricant by an electrochemical method
p 97 A86-20437
Tribological properties of graphite-fiber-reinforced, partially fluorinated polyimide composites
p 98 A86-34177
Contact angle and surface tension measurements of a five-ring polyphenyl ether
p 98 A86-34179
Lubricant and additive effects on spur gear fatigue life
[ASME PAPER 85-TRIB-14] p 155 A86-43542
Ellipsometric surface analysis of wear tracks produced by different lubricants
[NASA-TM-87142] p 87 N86-12293
Analysis of a thioether lubricant by infrared Fourier microemission spectrophotometry
[NASA-TM-87195] p 102 N86-16379
Constitutive modelling of lubricants in concentrated contacts at high slide to roll ratios
[NASA-CR-175029] p 158 N86-17748
A thin film degradation study of a fluorinated polyether liquid lubricant using an HPLC method
[NASA-TM-87221] p 77 N86-19417
How to evaluate solid lubricant films using a pin-on-disk tribometer
[NASA-TM-87236] p 102 N86-19465
A model for the influence of pressure on the bulk modulus and the influence of temperature on the solidification pressure for liquid lubricants
[NASA-TM-87230] p 140 N86-19555
A preliminary study of ester oxidation on an aluminum surface using chemiluminescence
[NASA-TM-87242] p 103 N86-24835
The preparation of new perfluoroether fluids exhibiting excellent thermal-oxidative stabilities
[NASA-TM-87284] p 105 N86-25475
- LUBRICATING OILS**
Optical and other properties changes of M-50 bearing steel surfaces for different lubricants and additives prior to scuffing
p 97 A86-20435
Operating aspects of an oil pumping ring seal
[ASME PAPER 85-TRIB-29] p 153 A86-34010
Liquid belt radiator design study
[NASA-CR-174901] p 57 N86-16259
- LUBRICATION**
Fundamental tribological properties of ceramics
p 95 A86-15230
New directions in lubrication, materials, wear, and surface interactions - Tribology in the 80's - Book
p 152 A86-18700
Lubrication and performance of high-speed rolling-element bearings
p 152 A86-19375
Fast approach for calculating film thicknesses and pressures in elastohydrodynamically lubricated contacts at high loads
[ASME PAPER 85-TRIB-42] p 155 A86-43541
Measurement of the density of base fluids at pressures 0.422 to 2.20 GPa
[NASA-TM-87114] p 156 N86-10551
Lubrication of nonconformal contacts
[NASA-TM-87120] p 138 N86-13679

- Design of traction drives
[NASA-RP-1154] p 157 N86-13734
Starvation effects on the hydrodynamic lubrication of rigid nonconformal contacts in combined rolling and normal motion
[NASA-TM-87174] p 140 N86-19556
Analysis of a spacecraft instrument ball bearing assembly lubricated by a perfluoroalkylether
[NASA-TM-87280] p 50 N86-21575
A new chromium carbide-based tribological coating for use to 900 deg C with particular reference to the Stirling engine
[NASA-TM-87274] p 103 N86-21882
Piezoviscous effects in nonconformal contacts lubricated hydrodynamically
[NASA-TM-87141] p 141 N86-21797

M

- MACH NUMBER**
Preliminary measurement of the noise from the 2/9 scale model of the Large-scale Advanced Propfan (LAP) propeller, SR-7A
[NASA-TM-87116] p 199 N86-14006
Progress in the Lewis Research Center Altitude Wind Tunnel (AWT) Modeling Program
[NASA-TM-87194] p 37 N86-16233
Current wind tunnel capability and planned improvements at Lewis Research Center
[NASA-TM-87190] p 37 N86-18329
- MACHINE TOOLS**
Generated spiral bevel gears - Optimal machine-tool settings and tooth contact analysis
[SAE PAPER 851573] p 154 A86-40678
Lubrication of nonconformal contacts
[NASA-TM-87120] p 138 N86-13679
- MAGNESIUM ALLOYS**
Advanced rotary engine components utilizing fiber reinforced Mg castings
[AIAA PAPER 86-1559] p 67 A86-42712
- MAGNESIUM OXIDES**
Surface effects of corrosive media on hardness, friction, and wear of materials p 94 A86-10825
- MAGNETIC FIELD CONFIGURATIONS**
Improvement of ion thruster design
[NASA-CR-177223] p 61 N86-27419
- MAGNETIC INDUCTION**
Theoretical analysis of the electrical aspects of the basic electro-impulse problem in aircraft de-icing applications
[NASA-CR-176808] p 17 N86-26330
- MAGNETIC MATERIALS**
A simple circular-polarized antenna: Circular waveguide horn coated with lossy magnetic material
[NASA-CR-177092] p 116 N86-30039
- MAGNETIC SIGNALS**
Effect of crystallographical and geometrical changes of a ferrite head on magnetic signals during the sliding process with magnetic tape
[NASA-TM-87277] p 106 N86-31728
- MAGNETIC TAPES**
Abrasion and deformed layer formation of manganese-zinc ferrite in sliding contact with lapping tapes
[NASA-TM-87249] p 104 N86-24838
Effect of crystallographical and geometrical changes of a ferrite head on magnetic signals during the sliding process with magnetic tape
[NASA-TM-87277] p 106 N86-31728
- MAGNETOHYDRODYNAMIC FLOW**
Measurement of energy distribution in flowing hydrogen microwave plasmas p 52 A86-18041
- MAGNETOHYDRODYNAMICS**
NASA electrothermal auxiliary propulsion technology
[AIAA PAPER 86-1703] p 55 A86-42799
NASA electrothermal auxiliary propulsion technology
[NASA-TM-87281] p 60 N86-24749
- MAGNETORESISTIVITY**
Negative magnetoresistance of pitch-based carbon fibers Temperature and pressure dependence p 99 A86-35702
- MAGNETS**
Improvement of ion thruster design
[NASA-CR-177223] p 61 N86-27419
- MAINTENANCE**
Operational maintenance data base development for kinematic Stirling engines
[ASME PAPER 85-DGP-20] p 151 A86-14467
- MAN MACHINE SYSTEMS**
The effects of syntactic complexity on the human-computer interaction p 192 A86-36172
- MAN-COMPUTER INTERFACE**
The effects of syntactic complexity on the human-computer interaction p 192 A86-36172

- MANGANESE**
Abrasion and deformed layer formation of manganese-zinc ferrite in sliding contact with lapping tapes
[NASA-TM-87249] p 104 N86-24838
- MANUFACTURING**
Ceramic automotive Stirling engine study
[NASA-CR-174907] p 208 N86-16185
Nickel-hydrogen separator development
[NASA-TM-87332] p 188 N86-26677
- MASKS**
Ion beam sputter etching
[NASA-CASE-LEW-13899-1] p 109 N86-20587
- MASS DISTRIBUTION**
Mass balancing of hollow fan blades
[ASME PAPER 86-GT-195] p 171 A86-48245
Mass balancing of hollow fan blades
[NASA-TM-87197] p 174 N86-18611
Graphite fiber intercalation: Basic properties of copper chloride intercalated fibers
[NASA-TM-87217] p 65 N86-18442
- MASS FLOW**
Analysis of a two row hydrostatic journal bearing with variable properties, inertia effects and surface roughness p 153 A86-30599
- MASS SPECTROSCOPY**
Characterization methodology for PMR-15 p 65 N86-11272
- MASS TRANSFER**
Scalar and momentum turbulent transport experiments with swirling and nonswirling flows p 126 A86-11938
Thermophoretically augmented mass transfer rates to solid walls across laminar boundary layers p 128 A86-20150
Mass and momentum turbulent transport experiments with swirling confined coaxial jets. II
[AIAA PAPER 86-1665] p 134 A86-42780
Determination of convective diffusion heat/mass transfer rates to burner rig test targets comparable in size to cross-stream jet diameter
[ASME PAPER 86-GT-68] p 136 A86-48140
Mass transport phenomena between bubbles and dissolved gases in liquids under reduced gravity conditions p 39 N86-10110
Fundamental studies of droplet combustion at reduced gravity p 42 N86-10165
Determination of convective diffusion heat/mass transfer rates to burner rig test targets comparable in size to cross-stream jet diameter
[NASA-TM-87176] p 138 N86-13678
Experiments for the determination of convective diffusion heat/mass transfer to burner rig test targets comparable in size to jet stream diameter
[NASA-TM-87196] p 139 N86-18646
Influence of large-scale motion on turbulent transport for confined coaxial jets. Volume 1: Analytical analysis of the experimental data using conditional sampling
[NASA-CR-175035] p 29 N86-20395
- MATERIALS HANDLING**
Characterization and measurement of polymer wear p 100 A86-48405
Microgravity Materials Science Laboratory p 42 N86-10173
- MATERIALS RECOVERY**
Fluid management and its role in the future of Space Station
[AIAA PAPER 86-2301] p 47 A86-49553
- MATERIALS SCIENCE**
New directions in lubrication, materials, wear, and surface interactions - Tribology in the 80's - Book p 152 A86-18700
- MATERIALS TESTS**
Scaling attenuation data characterizes changes in material microstructure p 197 A86-26542
Factors influencing the ultrasonic stress wave factor evaluation of composite material structures p 168 A86-34257
Characterization and measurement of polymer wear p 100 A86-48405
- MATHEMATICAL MODELS**
Modeling degradation and failure of Ni-Cr-Al overlay coatings p 80 A86-16276
Three component velocity measurements using Fabry-Perot interferometer p 145 A86-18378
A numerical model of acoustic choking. II - Shocked solutions p 197 A86-20795
Computation of turbulent rotating channel flow with an algebraic Reynolds stress model p 130 A86-22682
Through-flow modeling of axial turbomachinery
[ASME PAPER 85-IGT-42] p 3 A86-23854
Unsteady transonic flow in cascades p 4 A86-24693
Polynomic nonlinear dynamical systems - A residual sensitivity method for model reduction p 194 A86-35386

- Passive control of aerodynamically forced vibrations of supersonic turbomachine rotors by splitter blades
[AIAA PAPER 86-0844] p 22 A86-38892
Vortex modeling of single and multiple dilution jet mixing in a cross flow p 135 A86-48318
A model for closing the inviscid form of the average-passage equation system
[ASME PAPER 86-GT-227] p 8 A86-48261
Ignition and flame spread above liquid fuel pools p 41 N86-10163
Dendritic solidification in a binary alloy melt: Steady-state versus morphological stability theories p 42 N86-10261
Component-specific modeling p 25 N86-11515
A model for closing the inviscid form of the average-passage equation system p 10 N86-14224
Interlaminar fracture toughness: Three-dimensional finite element modeling for end-notch and mixed-mode flexure p 69 N86-14316
A computer simulation of the turbocharged turbo compounded diesel engine system: A description of the thermodynamic and heat transfer models
[NASA-CR-174971] p 208 N86-16164
A numerical simulation of the inviscid flow through a counter-rotating propeller
[NASA-TM-87200] p 10 N86-16195
Improvement of the second- and third-moment modeling of turbulence: A study of Reynolds-stress closure model
[NASA-CR-176478] p 139 N86-18519
Specimen geometry effects on graphite/PMR-15 composites during thermo-oxidative aging
[NASA-TM-87204] p 69 N86-17477
Development and application of dynamic simulations of a subsonic wind tunnel
[NASA-TM-87211] p 43 N86-18338
Study of journal bearing dynamics using 3-dimensional motion picture graphics p 140 N86-18647
Mutual coupling effects in antenna arrays, volume 1
[NASA-CR-176699] p 114 N86-22782
Effect of liquid droplets on turbulence in a round gaseous jet p 29 N86-23597
A unique set of micromechanics equations for high temperature metal matrix composites
[NASA-TM-87154] p 70 N86-24757
Dilution jet mixing program, phase 3 p 142 N86-24938
Yielding and deformation behavior of the single crystal nickel-base superalloy PWA 1480
[NASA-CR-175100] p 91 N86-25455
Concepts for interrelating ultrasonic attenuation, microstructure and fracture toughness in polycrystalline solids p 185 N86-25812
Theoretical analysis of the electrical aspects of the basic electro-impulse problem in aircraft de-icing applications
[NASA-CR-176808] p 17 N86-26330
Spectrum orbit utilization program technical manual SOUP5 Version 3.8
[NASA-CR-174944] p 116 N86-26489
A lumped parameter mathematical model for simulation of subsonic wind tunnels p 196 N86-27036
Spectrum Orbit Utilization Program documentation: SOUP5 version 3.8 user's manual, volume 1, chapters 1 through 5 p 193 N86-27927
Laser fringe anemometry for aero engine components
[NASA-TM-88798] p 12 N86-28053
On the modeling of low-Reynolds-number turbulence
[NASA-CR-3994] p 32 N86-28089
Integrated research in constitutive modelling at elevated temperatures, part 2 p 178 N86-28455
Formulation of the nonlinear analysis of shell-like structures, subjected to time-dependent mechanical and thermal loading
[NASA-CR-177194] p 178 N86-28462
Experimental and theoretical study of propeller spinner/shank interference p 13 N86-29773
Integrated research in constitutive modelling at elevated temperatures, part 1 p 179 N86-30227
Performance of oil pumping rings: An analytical and experimental study
[NASA-CR-175083] p 144 N86-31000
Comparison of analytical and experimental performance of a wind-tunnel diffuser section p 13 N86-31537
A mathematical approach for evaluating nickel-hydrogen cells
[NASA-TM-88803] p 78 N86-31680

- Design considerations for advanced battery concepts
[NASA-TM-87319] p 190 N86-31981
- MATRIX MATERIALS**
- High Temperature Polymer Matrix Composites
[NASA-CP-2385] p 68 N86-11260
- Surface protection of graphite fabric/PMR-15 composites subjected to thermal oxidation
p 68 N86-11281
- MATRIX THEORY**
- Performance of direct and iterative algorithms on an optical systolic processor p 202 A86-17421
- MEASURING INSTRUMENTS**
- High-temperature thermocouple and heat flux gauge using a unique thin film hardware hot junction
[ASME PAPER 85-GT-18] p 145 A86-13059
- How to evaluate solid lubricant films using a pin-on-disk tribometer
[NASA-TM-87236] p 102 N86-19465
- Ramp-integration technique for capacitance-type blade-tip clearance measurement
[NASA-TM-87241] p 149 N86-24964
- Calibration of droplet sizing and liquid water content instruments: Survey and analysis
[NASA-CR-175099] p 149 N86-26596
- Laser fringe anemometry for aero engine components
[NASA-TM-88798] p 12 N86-28053
- Advanced instrumentation for aeronautical propulsion research
[NASA-TM-88853] p 150 N86-32703
- MECHANICAL DRIVES**
- Generation of spiral bevel gears with zero kinematical errors and computer aided simulation of their meshing and contact
p 154 A86-40656
- Design of traction drives
[NASA-RP-1154] p 157 N86-13734
- Gearing
[NASA-RP-1152] p 157 N86-14612
- MECHANICAL MEASUREMENT**
- Advanced instrumentation for aeronautical propulsion research
[NASA-TM-88853] p 150 N86-32703
- MECHANICAL PROPERTIES**
- Densification and properties of alpha-silicon carbide
p 94 A86-12416
- The influence of cobalt, tantalum, and tungsten on the elevated temperature mechanical properties of single crystal nickel-base superalloys p 79 A86-12996
- Effect of substituted phenylindimides on processing and properties of PMR polyimide composites
p 94 A86-13179
- Effect of grain-boundary crystallization on the high-temperature strength of silicon nitride
p 98 A86-33495
- Strength and microstructure of Si₃N₄ sintered with ZrO₂ additions
p 99 A86-36330
- Tetraglycidyl epoxy resins and graphite fiber composites cured with flexibilized aromatic diamines
p 67 A86-36999
- Fabrication of ceramic components for advanced gas turbine engines
[SAE PAPER 851786] p 154 A86-38310
- Processing study of injection molding of silicon nitride for engine applications
[SAE PAPER 851787] p 154 A86-38311
- Composite sandwich thermostructural behavior - Computational simulation
[AIAA PAPER 86-0948] p 170 A86-38842
- Generated spiral bevel gears - Optimal machine-tool settings and tooth contact analysis
[SAE PAPER 851573] p 154 A86-40678
- High temperature properties of equiatomic FeAl with ternary additions
p 84 A86-47252
- Orientation and temperature dependence of some mechanical properties of the single-crystal nickel-base superalloy Rene N4. I - Tensile behavior
p 86 A86-50321
- Orientation and temperature dependence of some mechanical properties of the single-crystal nickel-base superalloy Rene N4. II - Low cycle fatigue behavior
p 86 A86-50322
- Ultrasonic evaluation of mechanical properties of thick, multilayered, filament wound composites
[NASA-TM-87088] p 163 N86-10561
- The 371 deg C mechanical properties of graphite/polyimide composites
[NASA-TM-87122] p 69 N86-12256
- Long-term stability and properties of zirconia ceramics for heavy duty diesel engine components
[NASA-CR-174943] p 209 N86-17224
- High temperature dispersion strengthening of NiAl
[NASA-CR-175073] p 90 N86-22688
- The correlation of low-velocity impact resistance of graphite-fiber-reinforced composites with matrix properties
[NASA-TM-87337] p 71 N86-27426
- Formulation of the nonlinear analysis of shell-like structures, subjected to time-dependent mechanical and thermal loading
[NASA-CR-177194] p 178 N86-28462
- MMIC devices for active phased array antennas
[NASA-CR-176990] p 116 N86-30037
- ICAN: A versatile code for predicting composite properties
[NASA-TM-87334] p 71 N86-31664
- Acousto-ultrasonic verification of the strength of filament wound composite material
[NASA-TM-88827] p 166 N86-32764
- MELT SPINNING**
- Rapidly solidified NiAl and FeAl p 84 A86-47263
- Undercooled and rapidly quenched Ni-Mo alloys
[NASA-TM-87257] p 90 N86-21859
- MELTS (CRYSTAL GROWTH)**
- Interaction of flows with the crystal-melt interface
p 132 A86-29419
- Influence of melt convection on solid-liquid interface under terrestrial and reduced gravity environments
p 38 N86-10083
- Solidification fundamentals p 39 N86-10090
- Containerless processing of undercooled melts
p 39 N86-10093
- Dendritic solidification in a binary alloy melt: Steady-state versus morphological stability theories
p 42 N86-10261
- MEMBRANES**
- Theoretical and experimental flow cell studies of a hydrogen-bromine fuel cell, part 1
[NASA-CR-177165] p 189 N86-29409
- MENTAL PERFORMANCE**
- The effects of syntactic complexity on the human-computer interaction
p 192 A86-36172
- MESSAGE PROCESSING**
- The baseband processor in future satellite communication systems
p 109 A86-21882
- METAL BONDING**
- Advanced thermal barrier system bond coatings for use on nickel-, cobalt- and iron-base alloy substrates
p 85 A86-49856
- METAL COATINGS**
- Modeling degradation and failure of Ni-Cr-Al overlay coatings
p 80 A86-16276
- Film and interstitial formation of metals in plasma-sprayed ceramics
p 96 A86-17484
- Pretreatment effects on the morphology and properties of aluminum oxide thermally grown on NiCoCrAlY
p 97 A86-17495
- The use of silver in self-lubricating coatings for extreme temperatures
p 99 A86-44425
- The low cycle fatigue behavior of a plasma-sprayed coating material
[NASA-TM-87318] p 92 N86-31699
- METAL CRYSTALS**
- The influence of cobalt, tantalum, and tungsten on the elevated temperature mechanical properties of single crystal nickel-base superalloys
p 79 A86-12996
- METAL FATIGUE**
- Optical and other properties changes of M-50 bearing steel surfaces for different lubricants and additives prior to scuffing
p 97 A86-20435
- Thermal-mechanical fatigue crack growth in Inconel X-750
p 81 A86-20982
- Shear fatigue crack growth - A literature survey
p 167 A86-24219
- Fracture mechanics applied to nonisothermal fatigue crack growth
p 81 A86-28951
- The tensile and fatigue deformation structures in a single crystal Ni-base superalloy
p 83 A86-35697
- Elevated temperature biaxial fatigue
[NASA-CR-175009] p 174 N86-11526
- Axial and torsional fatigue behavior of Waspaloy
[NASA-CR-175052] p 91 N86-25454
- Low-cycle thermal fatigue
[NASA-TM-87225] p 177 N86-26651
- The low cycle fatigue behavior of a plasma-sprayed coating material
[NASA-TM-87318] p 92 N86-31699
- Surface fatigue and failure characteristics of hot forged powder metal AISI 4620, AISI 4640, and machined AISI 4340 steel spur gears
[NASA-TM-87330] p 161 N86-31889
- METAL FIBERS**
- Interdiffusional effects between tungsten fibers and an iron-nickel-base alloy
p 66 A86-14718
- Thermal-mechanical fatigue test apparatus for metal matrix composites and joint attachments
[NASA-TM-87187] p 88 N86-15378
- METAL MATRIX COMPOSITES**
- Interdiffusional effects between tungsten fibers and an iron-nickel-base alloy
p 66 A86-14718
- Modifications of system for elevated temperature tensile testing and stress-strain measurement of metal matrix composites
[NASA-TM-87172] p 65 N86-13370
- Polymer, metal and ceramic matrix composites for advanced aircraft engine applications
[NASA-TM-87132] p 87 N86-13407
- Thermal-mechanical fatigue test apparatus for metal matrix composites and joint attachments
[NASA-TM-87187] p 88 N86-15378
- Thermoviscoplastic nonlinear constitutive relationships for structural analysis of high temperature metal matrix composites
[NASA-TM-87291] p 70 N86-24756
- A unique set of micromechanics equations for high temperature metal matrix composites
[NASA-TM-87154] p 70 N86-24757
- METAL OXIDE SEMICONDUCTORS**
- The effect of processing conditions on the GaAs/plasma-grown insulator interface
p 204 A86-18567
- Technology for satellite power conversion
[NASA-CR-176777] p 187 N86-25042
- METAL OXIDES**
- Oxidation protecting coatings for polymers
[NASA-CASE-LEW-14072-3] p 105 N86-26434
- Slip casting and extruding shapes of rhenium with metal oxide additives. 1: Feasibility demonstration
[NASA-CR-174970] p 63 N86-31648
- Apparatus for producing oxidation protection coatings for polymers
[NASA-CASE-LEW-14072-2] p 106 N86-32569
- METAL PLATES**
- Optical and other properties changes of M-50 bearing steel surfaces for different lubricants and additives prior to scuffing
p 97 A86-20435
- The plastic compressibility of 7075-T651 aluminum-alloy plate
p 85 A86-49690
- METAL PROPELLANTS**
- Compatibility of grain-stabilized platinum with candidate propellants for resistojets
[AIAA PAPER 85-2014] p 51 A86-17835
- Current evaluation of the tripropellant concept
[AIAA PAPER 86-1698] p 56 A86-49615
- Compatibility of grain-stabilized platinum with candidate propellants for resistojets
[NASA-TM-87118] p 56 N86-10279
- Current evaluation of the tripropellant concept
[NASA-TP-2602] p 62 N86-28124
- METAL SURFACES**
- Surface effects of corrosive media on hardness, friction, and wear of materials
p 94 A86-10825
- Binary collision model for neon Auger spectra from neon ion bombardment of the aluminum surface
p 76 A86-43457
- Protective coatings of metal surfaces by cold plasma treatment
[NASA-TM-87152] p 157 N86-11475
- Validation of structural analysis methods using burner liner cyclic rig test data
p 173 N86-11518
- Ion-beam nitriding of steels
[NASA-CASE-LEW-14104-2] p 93 N86-32556
- METAL WORKING**
- A mesh re-zoning technique for finite element simulations of metal forming processes
p 153 A86-36298
- Slip casting and extruding shapes of rhenium with metal oxide additives. 1: Feasibility demonstration
[NASA-CR-174970] p 63 N86-31648
- METAL-METAL BONDING**
- Current viewpoints on oxide adherence mechanisms
[NASA-TM-87168] p 87 N86-13409
- METALLIC GLASSES**
- Mechanical-contact-induced transformation from the amorphous to the partially crystalline state in metallic glass
p 80 A86-16257
- Metallic glass as a temperature sensor during ion plating
p 80 A86-16906
- METALLIZING**
- The mechanism of erosion of metallic materials under cavitation attack
[NASA-TM-87133] p 156 N86-10552
- METALLOGRAPHY**
- Determination of grain size distribution function using two-dimensional Fourier transforms of tone pulse encoded images
[NASA-TM-88790] p 166 N86-31065
- METALS**
- Current evaluation of the tripropellant concept
[AIAA PAPER 86-1698] p 56 A86-49615
- Microgravity Materials Science Laboratory
p 42 N86-10173
- Method and apparatus for rebalancing a REDOX flow cell system
[NASA-CASE-LEW-14127-1] p 122 N86-20680

Application of an atmospheric pressure sampling mass spectrometer to chlorination reactions
[NASA-TM-87270] p 91 N86-24813

Current evaluation of the tripropellant concept
[NASA-TP-2602] p 62 N86-28124

METEOROLOGICAL SERVICES
Upper air forecasting for aviation in the United States
p 191 A86-37501

METHANE
Shock-tube pyrolysis of chlorinated hydrocarbons - Formation of soot p 75 A86-35126
Flammability limits of gases under low gravity conditions p 42 N86-10164
Methane oxidation behind reflected shock waves: Ignition delay times measured by pressure and flame band emission
[NASA-TM-87268] p 77 N86-21635

METHOD OF MOMENTS
Mutual coupling effects in antenna arrays, volume 1
[NASA-CR-176699] p 114 N86-22782

METHYL ALCOHOL
Research and development of neat alcohol fuel usage in automobiles
[NASA-TM-174813] p 108 N86-27460

METHYL CHLORIDE
Shock-tube pyrolysis of chlorinated hydrocarbons - Formation of soot p 75 A86-35126

MICROCOMPUTERS
Hardware configuration for a real-time multiprocessor simulator
[NASA-TM-88802] p 194 N86-28651

MICROCRACKS
Erosion of phosphor bronze under cavitation attack in a mineral oil p 81 A86-23324
Closure of fatigue cracks at high strains
[NASA-CR-175021] p 175 N86-17788

MICROFIBERS
Simplified composite micromechanics for predicting microstresses
[NASA-TM-87295] p 70 N86-24759

MICROHARDNESS
Surface effects of corrosive media on hardness, friction, and wear of materials p 94 A86-10825
Frictional and structural characterization of ion-nitrided low and high chromium steels p 81 A86-17477

MICROMECHANICS
A unique set of micromechanics equations for high temperature metal matrix composites
[NASA-TM-87154] p 70 N86-24757
Simplified composite micromechanics for predicting microstresses
[NASA-TM-87295] p 70 N86-24759
ICAN: A versatile code for predicting composite properties
[NASA-TM-87334] p 71 N86-31664

MICROPARTICLES
Angular particle impingement studies of thermoplastic materials at normal incidence
[ASLE PREPRINT 85-AM-3A-1] p 94 A86-11076

MICROPROCESSORS
Development of a microprocessor controller for stand-alone photovoltaic power systems
[NASA-CR-174723] p 187 N86-21979

MICROSCOPY
Development program on a cold cathode electron gun
[NASA-CR-174792] p 121 N86-14499

MICROSTRIP TRANSMISSION LINES
Input impedance of a probe-fed circular microstrip antenna with thick substrate p 120 A86-46638
A dual frequency microstrip antenna for Ka band
[NASA-TM-87124] p 111 N86-10380
Circularly polarized microstrip antennas p 112 N86-11407
MMIC devices for active phased array antennas
[NASA-CR-176990] p 116 N86-30037

MICROSTRUCTURE
The influence of cobalt, tantalum, and tungsten on the microstructure of single crystal nickel-base superalloys p 79 A86-12995
Frictional and morphological properties of Au-MoS₂ films sputtered from a compact target p 152 A86-16258
Transmission electron microscopic examination of phosphoric acid fuel cell components p 74 A86-23352
Scaling attenuation data characterizes changes in material microstructure p 197 A86-26542
Strength and microstructure of Si₃N₄ sintered with ZrO₂ additions p 99 A86-36330
Nondestructive characterization of structural ceramics p 99 A86-37141
The development and prevention of channel segregation during alloy solidification p 38 N86-10086
Progressive damage, fracture predictions and post mortem correlations for fiber composites
[NASA-TM-87101] p 68 N86-10290

Thermal aging effects in refractory metal alloys
[NASA-TM-87210] p 89 N86-18334

Long-term stability and properties of zirconia ceramics for heavy duty diesel engine components
[NASA-CR-174943] p 209 N86-17224

Alloy chemistry and microstructural control to meet the demands of the automotive Stirling engine
[NASA-TM-87250] p 89 N86-20541

Ion beam sputter etching
[NASA-CASE-LEW-13899-1] p 109 N86-20587

Variables controlling fatigue crack growth of short cracks
[NASA-TM-87208] p 90 N86-21661

Ultrasonic characterization of structural ceramics p 199 N86-22970

Ultrasonic verification of microstructural changes due to heat treatment p 200 N86-22977

Transfer function concept for ultrasonic characterization of material microstructures p 200 N86-22980

Thermoviscoplastic nonlinear constitutive relationships for structural analysis of high temperature metal matrix composites
[NASA-TM-87291] p 70 N86-24756

Concepts for interrelating ultrasonic attenuation, microstructure and fracture toughness in polycrystalline solids
[NASA-TM-87338] p 165 N86-25812

Carbon-rich ceramic composites from ethynyl aromatic precursors
[NASA-TM-88812] p 71 N86-29908

Determination of grain size distribution function using two-dimensional Fourier transforms of tone pulse encoded images
[NASA-TM-88790] p 166 N86-31065

Microstructure-property relationships in directionally solidified single crystal nickel-base superalloys
[NASA-TM-88788] p 93 N86-31700

The continuing battle against defects in nickel-base superalloys
[NASA-TM-87343] p 93 N86-31701

Improved fracture toughness corrosion-resistant bearing material
[NASA-CR-174990] p 162 N86-32743

MICROWAVE AMPLIFIERS
Textured carbon on copper: A novel surface with extremely low secondary electron emission characteristics
[NASA-TP-2543] p 101 N86-15394

MICROWAVE ANTENNAS
Input impedance of a probe-fed circular microstrip antenna with thick substrate p 120 A86-46638
Characterization of MMIC devices for active array antennas p 111 N86-11401

MICROWAVE ATTENUATION
Normal modes in an overmoded circular waveguide coated with lossy material p 119 A86-44078

MICROWAVE CIRCUITS
Characterization of MMIC devices for active array antennas p 111 N86-11401
Compensation of reflector surface distortions using conjugate field matching
[NASA-TM-87198] p 113 N86-18461
Computation of the radiation characteristics of a generalized phased array
[NASA-TM-87185] p 114 N86-18586
Optically controlled phased array antenna concepts using GaAs monolithic microwave integrated circuits
[NASA-TM-87229] p 123 N86-21757

MICROWAVE EQUIPMENT
10-30 GHz monolithic GaAs travelling-wave divider/combiner p 118 A86-34882
Analysis of optically controlled microwave/millimeter wave device structures
[NASA-TM-87246] p 123 N86-24907

MICROWAVE FREQUENCIES
Radiofrequency testing of satellite segment of simulated 30/20 GHz satellite communications system
[NASA-TM-87163] p 114 N86-19494

MICROWAVE SENSORS
Time domain referencing in intensity modulation fiber optic sensing systems
[NASA-CR-175109] p 17 N86-24691

MICROWAVES
Measurement of energy distribution in flowing hydrogen microwave plasmas p 52 A86-18041
Monolithic optical integrated control circuitry for GaAs MMIC-based phased arrays
[NASA-TM-87183] p 113 N86-16457
MMIC devices for active phased array antennas
[NASA-CR-176990] p 116 N86-30037

MIDLATITUDE ATMOSPHERE
A note on the finite differencing of the linearized primitive equations' lower boundary condition p 191 A86-28963

MILITARY OPERATIONS
Review and critical analysis: Rolling-element bearings for system life and reliability
[NASA-CR-174710] p 159 N86-24891

MILLIMETER WAVES
Dc and microwave characteristics of a high current double interface GaAs/InGaAs/AlGaAs pseudomorphic modulation-doped field-effect transistor p 118 A86-36009
Circularly polarized microstrip antennas p 112 N86-11407
Analysis of optically controlled microwave/millimeter wave device structures
[NASA-TM-87246] p 123 N86-24907

MILLING (MACHINING)
Factors influencing the ball milling of Si₃N₄ in water p 95 A86-15239
Parametric evaluation of ball milling of SiC in water p 96 A86-15240
Particle size reduction of Si₃N₄ with Si₃N₄ milling hardware
[NASA-TM-86864-REV] p 104 N86-24839
The milling of pristine and brominated P-100 graphite fibers
[NASA-TM-88828] p 106 N86-32573

MINERAL OILS
Erosion of aluminum 6061-T6 under cavitation attack in mineral oil and water p 79 A86-13801
Erosion of phosphor bronze under cavitation attack in a mineral oil p 81 A86-23324
The mechanism of erosion of metallic materials under cavitation attack
[NASA-TM-87133] p 156 N86-10552

MINORITY CARRIERS
Minority-carrier mobility anomalies in low-resistivity silicon solar cells p 181 A86-49215

MIRRORS
Lens collimation and testing using a Twyman-Green interferometer with a self-pumped phase-conjugating mirror p 146 A86-29280

MIS (SEMICONDUCTORS)
Growth and characterization of epitaxial SrF₂ on InP(100) p 205 A86-47076
Diamondlike carbon films on semiconductors for insulated-gate technology p 120 A86-47077

MISALIGNMENT
Generation of spiral bevel gears with zero kinematical errors and computer aided tooth contact analysis
[NASA-TM-87273] p 160 N86-25793

MISSION PLANNING
Tethered nuclear power for the space station p 53 A86-24808
Orbital transfer vehicle engine integration study p 58 N86-17416

MIXERS
Three-dimensional inviscid flow in mixers. I - Mixer analysis using a Cartesian grid p 5 A86-39090
Three-dimensional inviscid flow in mixers. II - Analysis of turbofan forced mixers p 6 A86-46316

MIXING
Particle cloud combustion experiment p 41 N86-10160
Dilution jet mixing program, phase 3
[NASA-CR-174884] p 142 N86-24938

MODAL RESPONSE
Modal test/analysis correlation for Centaur G Prime launch vehicle
[AIAA PAPER 86-1002] p 43 A86-38943
Quasi-modal vibration control by means of active control bearings
[NASA-TM-87232] p 159 N86-21856
Theoretical and software considerations for general dynamic analysis using multilevel substructured models
[NASA-CR-176822] p 195 N86-26067
Identification of differences between finite element analysis and experimental vibration data
[NASA-TM-87338] p 149 N86-27617

MODELS
Theoretical modeling of the vapor cavitation in dynamically loaded journal bearings
[ASME PAPER 85-TRIB-51] p 130 A86-24496
Application of a computational model for vortex generators in subsonic internal flows
[AIAA PAPER 86-1458] p 8 A86-49612
Thermocapillary motion research p 40 N86-10125
Electrohydrodynamics p 41 N86-10130
Experimental and theoretical analysis of chemical vapor deposition with prediction of gravity effects p 41 N86-10132
Theoretical modeling of the vapor cavitation in dynamically loaded journal bearings
[NASA-TM-87076] p 137 N86-10463
Constitutive modeling for isotropic materials (HOST)
[NASA-CR-174980] p 172 N86-10589
Chemical control of rate and onset temperature of nadimide polymerization p 101 N86-11271

- Laser anemometry for hot section applications p 151 N86-11503
- Overview of free-piston Stirling technology at the NASA Lewis Research Center p 208 N86-13236 [NASA-TM-87156]
- Progress in the Lewis Research Center Altitude Wind Tunnel (AWT) Modeling Program [NASA-TM-87194] p 37 N86-16233
- Constitutive modelling of lubricants in concentrated contacts at high slide to roll ratios [NASA-CR-175029] p 158 N86-17748
- Extended parametric representation of compressor fans and turbines. Volume 1: CMGEN user's manual [NASA-CR-174645] p 159 N86-23936
- Extended parametric representation of compressor fans and turbines. Volume 2: Part user's manual (parametric turbine) [NASA-CR-174646] p 159 N86-23937
- Extended parametric representation of compressor fans and turbines. Volume 3: MODFAN user's manual (parametric modulating flow fan) [NASA-CR-174647] p 159 N86-23938
- Application of a computational model for vortex generators in subsonic internal flows [NASA-TM-87327] p 143 N86-26545
- Experimental classical flutter results of a composite advanced turboprop model [NASA-TM-88792] p 178 N86-29271
- MODULARITY**
- Orbit Transfer Rocket Engine Technology Program: Advanced engine study, task D.1/D.3 [NASA-CR-175084] p 61 N86-26369
- MODULATORS**
- Characteristics of an axisymmetric sudden expansion flow [NASA-CR-176278] p 151 N86-11465
- MODULES**
- Operating characteristics of a 0.87 kW-hr flywheel energy storage module p 152 A86-24864
- MODULUS OF ELASTICITY**
- Modifications of system for elevated temperature tensile testing and stress-strain measurement of metal matrix composites [NASA-TM-87172] p 65 N86-13370
- Compliance matrices for cracked bodies [NASA-CR-179478] p 179 N86-30236
- MOIRE EFFECTS**
- A comparison of electronic heterodyne moire deflectometry and electronic heterodyne holographic interferometry for flow measurements [SAE PAPER 851896] p 146 A86-38359
- MOIRE FRINGES**
- Diffraction effects and special advantages in electronic heterodyne moire deflectometry p 202 A86-31565
- MOLECULAR BEAM EPITAXY**
- Dc and microwave characteristics of a high current double interface GaAs/InGaAs/AlGaAs pseudomorphic modulation-doped field-effect transistor p 118 A86-36009
- MOLECULAR ORBITALS**
- Gallium arsenide solar cell efficiency: Problems and potential p 184 N86-17843
- High-efficiency AlGaAs-GaAs Cassegrainian concentrator cells p 185 N86-17845
- MOLECULAR WEIGHT**
- Fugacity and concentration gradients in a gravity field [NASA-TM-88809] p 212 N86-30620
- MOLTEN SALTS**
- Kinetics and mechanism of corrosion of SiC by molten salts p 97 A86-20992
- Molten salt corrosion of SiC: Pitting mechanism [NASA-TM-87143] p 101 N86-12310
- MOLYBDENUM**
- Rapid evaluation of ion thruster lifetime using optical emission spectroscopy [AIAA PAPER 85-2011] p 51 A86-17851
- Rapid evaluation of ion thruster lifetime using optical emission spectroscopy [NASA-TM-87103] p 56 N86-10280
- The mechanism of erosion of metallic materials under cavitation attack [NASA-TM-87133] p 156 N86-10552
- Phenomenological study of the behavior of some silica formers in a high velocity jet fuel burner [NASA-TM-87127] p 157 N86-14613
- Role of molybdenum in the Na sub 2SO sub 4 induced corrosion of superalloys at high temperatures [NASA-TM-87235] p 90 N86-21658
- MOLYBDENUM ALLOYS**
- Undercooled and rapidly quenched Ni-Mo alloys [NASA-TM-87257] p 90 N86-21659
- MOLYBDENUM DISULFIDES**
- Frictional and morphological properties of Au-MoS2 films sputtered from a compact target p 152 A86-16258
- MOMENTUM TRANSFER**
- Scalar and momentum turbulent transport experiments with swirling and nonswirling flows p 126 A86-11938
- Mass and momentum turbulent transport experiments with swirling confined coaxial jets. II [AIAA PAPER 86-1665] p 134 A86-42780
- Influence of large-scale motion on turbulent transport for confined coaxial jets. Volume 1: Analytical analysis of the experimental data using conditional sampling [NASA-CR-175035] p 29 N86-20395
- MONOMERS**
- Graphite/PMR polyimide composites with improved toughness p 66 A86-21731
- PMR polyimides from solutions containing mixed endcaps p 100 N86-11263
- The synthesis, characterization and thermal chemistry of modified norbornenyl PMR endcaps p 100 N86-11266
- Characterization methodology for PMR-15 p 65 N86-11272
- Replacement of MDA with more oxidatively stable diamines in PMR-polyimides p 101 N86-11275
- Structure-to-property relationships in addition cured polymers 2: Resin Tg composite initial mechanical properties of norbornenyl cured polyimide resins [NASA-TM-88794] p 105 N86-29041
- Carbon-rich ceramic composites from ethynyl aromatic precursors [NASA-TM-88812] p 71 N86-29908
- MORPHOLOGY**
- Frictional and morphological properties of Au-MoS2 films sputtered from a compact target p 152 A86-16258
- Pretreatment effects on the morphology and properties of aluminum oxide thermally grown on NiCoCrAlY p 97 A86-17495
- Tribological properties of graphite-fiber-reinforced, partially fluorinated polyimide composites p 98 A86-34177
- Dendritic solidification in a binary alloy melt: Steady-state versus morphological stability theories p 42 N86-10261
- The evolution and growth of Al2O3 scales on beta-NiAl [NASA-CR-175097] p 92 N86-27444
- MOTION PICTURES**
- Study of journal bearing dynamics using 3-dimensional motion picture graphics [NASA-TM-87205] p 140 N86-18647
- MOTION STABILITY**
- Linearization of digital derived rate algorithm for use in linear stability analysis p 47 A86-35338
- MOUNTING**
- Convenient mounting method for electrical measurements of thin samples p 120 A86-46649
- Apparatus for electrical measurements of thin films from 77 to 1000 K [NASA-TM-87256] p 148 N86-24959
- MULTIBEAM ANTENNAS**
- Near-field testing of the 30 GHz TRW proof-of-concept multibeam antenna [NASA-TM-87357] p 124 N86-27578
- Spacecraft multibeam antenna system for 30/20 GHz [NASA-CR-174654] p 116 N86-31760
- MULTIENGINE VEHICLES**
- The STOL performance of a two-engine, USB powered-lift aircraft with cross-shafted fans [SAE PAPER 851839] p 16 A86-38336
- MULTIPLE BEAM INTERVAL SCANNERS**
- MMIC antenna technology development in the 30/20 gigahertz band [AIAA PAPER 86-0666] p 45 A86-29628
- MMIC antenna technology development in the 30/20 gigahertz band [NASA-TM-87192] p 46 N86-17368
- MULTIPROCESSING (COMPUTERS)**
- Performance evaluation of a simulated data-flow computer with low-resolution actors p 194 A86-32051
- Simulating a small turboshaft engine in real-time multiprocessor simulator (RTMPS) environment [NASA-TM-87216] p 27 N86-18621
- N**
- N-TYPE SEMICONDUCTORS**
- Carbon films grown from plasma on III-V semiconductors [NASA-TM-87140] p 205 N86-12135
- NACELLES**
- Evaluation of propeller/nacelle interactions in the PTA program [AIAA PAPER 86-1552] p 6 A86-42709
- NASA PROGRAMS**
- NASA electric propulsion technology [AIAA PAPER 85-1999] p 51 A86-17831
- MERIT - A new approach to upper air forecasting for aviation p 191 A86-17982
- NASA's aircraft icing analysis program p 14 A86-49107
- NASA LeRC/Akron University Graduate Cooperative Fellowship Program and Graduate Student Researchers Program [NASA-CR-174826] p 207 N86-13219
- NASA's Aircraft Icing Analysis Program [NASA-TM-88791] p 15 N86-31548
- Potential high efficiency solar cells: Applications from space photovoltaic research [NASA-TM-88832] p 125 N86-32627
- NASA SPACE PROGRAMS**
- Space station power system p 50 A86-12676
- Space power systems - 'Spacecraft 2000' p 53 A86-24836
- Spacecraft 2000 [AIAA PAPER 86-0616] p 38 A86-29586
- NAVIER-STOKES EQUATION**
- Development of an explicit multigrid algorithm for quasi-three-dimensional viscous flows in turbomachinery [AIAA PAPER 86-0032] p 1 A86-19644
- Calculation of three-dimensional, viscous flow through turbomachinery blade passage by parabolic marching p 2 A86-20372
- Multi-grid technique for the solution of incompressible Navier-Stokes equations p 128 A86-21029
- Calculations of two and three-dimensional transonic cascade flow fields using the Navier-Stokes equations [ASME PAPER 85-GT-66] p 2 A86-22046
- Model equation for simulating flows in multistage turbomachinery [ASME PAPER 85-GT-226] p 2 A86-22123
- Assessment of a parabolic analysis for axisymmetric internal flows in rocket and turbomachinery ducts [AIAA PAPER 86-1598] p 134 A86-42739
- Is Navier-Stokes turbulence chaotic? p 137 A86-50275
- Development of an explicit multigrid algorithm for quasi-three-dimensional viscous flows in turbo-machinery [NASA-TM-87128] p 1 N86-11146
- Influence of large-scale motion on turbulent transport for confined coaxial jets. Volume 2: Navier-Stokes calculations of swirling and nonswirling confined coaxial jets [NASA-CR-175036] p 28 N86-20390
- Aerodynamic properties of turbulent combustion fields [NASA-CR-175005] p 28 N86-20393
- Diffusion flame extinction in slow convective flow under microgravity environment [NASA-TM-88799] p 144 N86-28378
- Numerical simulation of the flowfield over ice accretion shapes [NASA-CR-176960] p 144 N86-30093
- NEAR FIELDS**
- Computation of the radiation characteristics of a generalized phased array [NASA-TM-87185] p 114 N86-18586
- Near-field spillover from a subreflector: Theory and experiment [NASA-TM-88763] p 115 N86-25650
- Near-field testing of the 30 GHz TRW proof-of-concept multibeam antenna [NASA-TM-87357] p 124 N86-27578
- Near-field spillover from a subreflector: Theory and experiment [NASA-TM-88818] p 116 N86-32598
- NEGATIVE CONDUCTANCE**
- Circuit transients due to negative bias arcs-II --- on solar cell power systems in low earth orbit [AIAA PAPER 86-0366] p 52 A86-19835
- NEON**
- Binary collision model for neon Auger spectra from neon ion bombardment of the aluminum surface p 76 A86-43457
- NETWORK ANALYSIS**
- Resonant power processors. I - State plane analysis p 117 A86-14481
- Circuit transients due to negative bias arcs-II --- on solar cell power systems in low earth orbit [AIAA PAPER 86-0366] p 52 A86-19835
- NETWORK SYNTHESIS**
- Inverter design for high frequency power distribution p 117 A86-24831
- NEUTRON DIFFRACTION**
- Neutron and X-ray diffraction of plasma-sprayed zirconia-ytria thermal barrier coatings p 96 A86-16269
- NEWTON-RAPHSON METHOD**
- On the equivalence of the incremental harmonic balance method and the harmonic balance-Newton Raphson method p 170 A86-40695
- Locally bound constrained Newton-Raphson solution algorithms --- for modeling kinematic and material nonlinearity p 171 A86-43771

NICKEL

- Surface effects of corrosive media on hardness, friction, and wear of materials p 94 A86-10825
- Optimization of the Ni-Cr-Al-Y/ZrO₂-Y₂O₃ thermal barrier system p 82 A86-31746
- The reactions of cobalt, iron and nickel in SO₂ atmospheres Similarities and differences p 75 A86-40677
- An update of the total-strain version of SRP [NASA-TP-2499] p 87 N86-12295
- Ultrasonic verification of microstructural changes due to heat treatment p 200 N86-22977
- NICKEL ALLOYS**
- The influence of cobalt, tantalum, and tungsten on the microstructure of single crystal nickel-base superalloys p 79 A86-12995
- The influence of cobalt, tantalum, and tungsten on the elevated temperature mechanical properties of single crystal nickel-base superalloys p 79 A86-12996
- Interdiffusion effects between tungsten fibers and an iron-nickel-base alloy p 66 A86-14718
- The development of gamma-gamma-prime lamellar structures in a nickel-base superalloy during elevated temperature mechanical testing p 79 A86-14719
- Modeling degradation and failure of Ni-Cr-Al overlay coatings p 80 A86-16276
- Temperature dependence of gamma-gamma prime lattice mismatch in nickel-base superalloys p 81 A86-21849
- Studies on the hot corrosion of a nickel-base superalloy, Udimet 700 p 82 A86-29722
- The tensile and fatigue deformation structures in a single crystal Ni-base superalloy p 83 A86-35697
- Na₂SO₄ induced corrosion of nickel at high temperature p 83 A86-37073
- Mechanism of Na₂SO₄-induced corrosion of molybdenum containing nickel-base superalloys at high temperatures. I - Corrosion in atmospheres containing O₂ only. II - Corrosion in O₂ + SO₂ atmospheres p 83 A86-37238
- The cyclic stress-strain behavior of a nickel-base superalloy at 650 C p 83 A86-45715
- High temperature oxidation of beta-NiAl p 85 A86-47266
- Orientation and temperature dependence of some mechanical properties of the single-crystal nickel-base superalloy Rene N4. I - Tensile behavior p 86 A86-50321
- Orientation and temperature dependence of some mechanical properties of the single-crystal nickel-base superalloy Rene N4. II - Low cycle fatigue behavior p 86 A86-50322
- Fatigue crack propagation of nickel-base superalloys at 650 deg C [NASA-TM-87150] p 87 N86-12294
- Current viewpoints on oxide adherence mechanisms [NASA-TM-87168] p 87 N86-13409
- Simplified cyclic structural analyses of SSME turbine blades [NASA-TM-87214] p 175 N86-16615
- An experimental data base for material selection and design of high-speed, high-pressure, oxygen turbomachinery p 58 N86-17387
- Undercooled and rapidly quenched Ni-Mo alloys [NASA-TM-87257] p 90 N86-21659
- Anisotropic constitutive model for nickel base single crystal alloys: Development and finite element implementation [NASA-CR-175015] p 176 N86-21952
- High temperature dispersion strengthening of NiAl [NASA-CR-175073] p 90 N86-22688
- Corrosion of nickel and cobalt base alloys in sulfate melts at 750 deg C [NASA-CR-175111] p 91 N86-24817
- Yielding and deformation behavior of the single crystal nickel-base superalloy PWA 1480 [NASA-CR-175100] p 91 N86-25455
- Heat treatment for superalloy [NASA-CASE-LEW-14262-1] p 92 N86-26414
- The evolution and growth of Al₂O₃ scales on beta-NiAl [NASA-CR-175097] p 92 N86-27444
- Characterization of the tribological coating composition 77 wt % CaF₂ - 23 wt % Li F fused to IN-750 alloy [NASA-TM-87342] p 105 N86-27452
- Thermal-fatigue and oxidation resistance of cobalt-modified Udimet 700 alloy [NASA-TP-2591] p 178 N86-28464
- The low cycle fatigue behavior of a plasma-sprayed coating material [NASA-TM-87318] p 92 N86-31699
- Microstructure-property relationships in directionally solidified single crystal nickel-base superalloys [NASA-TM-88788] p 93 N86-31700

- The continuing battle against defects in nickel-base superalloys [NASA-TM-87343] p 93 N86-31701
- The effect of variations of cobalt content on the cyclic oxidation resistance of selected Ni-base superalloys [NASA-TM-87297] p 93 N86-31702
- NICKEL COMPOUNDS**
- Alloys based on NiAl for high temperature applications p 84 A86-47261
- NICKEL HYDROGEN BATTERIES**
- Design principles for nickel-hydrogen cells and batteries p 179 A86-24799
- Initial performance of advanced designs for IPV nickel-hydrogen cells p 179 A86-24800
- KOH concentration effect on the cycle life of nickel-hydrogen cells p 180 A86-24802
- Bipolar nickel-hydrogen battery development p 180 A86-24823
- Life cycle test results of a bipolar nickel hydrogen battery p 180 A86-24824
- Lightweight nickel electrode for nickel hydrogen cells and batteries [NASA-TM-87253] p 186 N86-21978
- Assessment of commercially available and experimental hydrogen electrodes [NASA-TM-87264] p 187 N86-23035
- Long life nickel electrodes for a nickel-hydrogen cell: Cycle life tests [NASA-CR-174815] p 188 N86-25046
- Oxygen recombination in individual pressure vessel nickel-hydrogen batteries [NASA-CASE-LEW-13822-1] p 188 N86-25874
- Nickel-hydrogen separator development [NASA-TM-87332] p 188 N86-26677
- A mathematical approach for evaluating nickel-hydrogen cells [NASA-TM-88803] p 78 N86-31680
- Parametric and cycle tests of a 40-A-hr bipolar nickel-hydrogen battery [NASA-TM-88793] p 189 N86-31879
- Effect of impregnation method on cycle life of the nickel electrode [NASA-TM-87326] p 190 N86-31980
- NICKEL OXIDES**
- Adsorption of O₂, SO₂, and SO₃ on nickel oxide - Mechanism for sulfate formation p 75 A86-34238
- NIOBIUM**
- Technology for satellite power conversion [NASA-CR-176777] p 187 N86-25042
- Characterization of the tribological coating composition 77 wt % CaF₂ - 23 wt % Li F fused to IN-750 alloy [NASA-TM-87342] p 105 N86-27452
- NIOBIUM ALLOYS**
- Thermal aging effects in refractory metal alloys [NASA-TM-87210] p 89 N86-16334
- Creep properties of PWC-11 base metal and weldments as affected by heat treatment [NASA-TM-88842] p 93 N86-32557
- NITRIC OXIDE**
- Analysis of the effects of fuel spray characteristics on NO(x) formation [ASME PAPER 85-WA/HT-47] p 107 A86-38394
- NITRIDING**
- Protective coatings of metal surfaces by cold plasma treatment [NASA-TM-87152] p 157 N86-11475
- Ion-beam nitriding of steels [NASA-CASE-LEW-14104-2] p 93 N86-32556
- NITROGEN**
- Electrode erosion in arc discharges at atmospheric pressure [AIAA PAPER 85-2018] p 50 A86-14445
- Low power dc arcjet operation with hydrogen/nitrogen propellant mixtures [AIAA PAPER 86-1505] p 55 A86-42676
- All-aromatic biphenylene end-capped polyquinoline and polyimide matrix resins p 100 N86-11267
- Lower power dc arcjet operations with hydrogen hydrogen/nitrogen propellant mixtures [NASA-TM-87279] p 61 N86-25407
- NITROGEN OXIDES**
- Oxides of nitrogen emissions from the combustion of monodisperse liquid fuel sprays [NASA-CR-176373] p 191 N86-14770
- NITROGEN PLASMA**
- Frictional and structural characterization of ion-nitrided low and high chromium steels p 81 A86-17477
- NOISE (SOUND)**
- Generated spiral bevel gears - Optimal machine-tool settings and tooth contact analysis [SAE PAPER 851573] p 154 A86-40678
- Numerical Techniques in Acoustics [NASA-CP-2404] p 198 N86-12007

- Preliminary measurement of the noise from the 2/9 scale model of the Large-scale Advanced Propfan (LAP) propeller, SR-7A [NASA-TM-87116] p 199 N86-14006
- An estimate of the enroute noise of an advanced turboprop airplane NASA-TM-87302 E-3020 NAS 1.15:87302 HC A02/MF A01 [NASA-TM-87302] p 201 N86-25217
- NOISE INTENSITY**
- An estimate of the enroute noise of an advanced turboprop airplane NASA-TM-87302 E-3020 NAS 1.15:87302 HC A02/MF A01 [NASA-TM-87302] p 201 N86-25217
- NOISE MEASUREMENT**
- Tone excited jets. IV - Acoustic measurements p 196 A86-16489
- The effect of acoustic reflections on combustor noise measurements p 197 A86-20364
- High-frequency noise of In(y)Ga(1-y)As/Al(x)Ga(1-x)As MODFETs and comparison to GaAs/Al(x)Ga(1-x)As MODFETs p 119 A86-43914
- Thermionic noise measurements for on-line dispenser cathode diagnostics for linear beam microwave tubes [NASA-CR-175105] p 124 N86-28323
- NOISE PREDICTION**
- An iterative finite element-integral technique for predicting sound radiation from turbofan inlets in steady flight p 198 A86-49806
- Numerical Techniques in Acoustics [NASA-CP-2404] p 198 N86-12007
- NOISE PREDICTION (AIRCRAFT)**
- Modeling wind tunnel effects on the radiation characteristics of acoustic sources p 197 A86-41689
- Numerical evaluation of propeller noise including nonlinear effects p 23 A86-41726
- Influence of airfoil camber on convected gust interaction noise [AIAA PAPER 86-1873] p 198 A86-45493
- A numerical method of calculating propeller noise including acoustic nonlinear effects p 199 N86-12011
- NOISE REDUCTION**
- Noise generated by convected gusts interacting with swept airfoil cascades [AIAA PAPER 86-1872] p 198 A86-45492
- Preliminary measurement of the noise from the 2/9 scale model of the Large-scale Advanced Propfan (LAP) propeller, SR-7A [NASA-TM-87116] p 199 N86-14006
- Some design philosophy for reducing the community noise of advanced counter-rotation propellers [NASA-TM-87099] p 199 N86-14007
- Laboratory experiments on active suppression of advanced turboprop noise [NASA-TM-87129] p 199 N86-19125
- Turbofan aft duct suppressor study program listing and user's guide [NASA-CR-175067] p 30 N86-25357
- Generation of spiral bevel gears with zero kinematical errors and computer aided tooth contact analysis [NASA-TM-87273] p 160 N86-25793
- NOISE SPECTRA**
- An estimate of the enroute noise of an advanced turboprop airplane NASA-TM-87302 E-3020 NAS 1.15:87302 HC A02/MF A01 [NASA-TM-87302] p 201 N86-25217
- NONDESTRUCTIVE TESTS**
- Measurement of ultrasonic velocity using phase-slope and cross-correlation methods p 162 A86-13192
- NDE of advanced ceramics p 163 A86-35575
- Nondestructive characterization of RBSOA of high-power bipolar transistors --- Reverse-bias safe operating area p 118 A86-35718
- Nondestructive characterization of structural ceramics p 99 A86-37141
- Reliability of void detection in structural ceramics by use of scanning laser acoustic microscopy p 163 A86-39027
- Nondestructive techniques for characterizing mechanical properties of structural materials - An overview [ASME PAPER 86-GT-75] p 163 A86-48143
- NDE of structural ceramics [ASME PAPER 86-GT-279] p 163 A86-48298
- NDE of structural ceramics [NASA-TM-87186] p 164 N86-16598
- Nondestructive techniques for characterizing mechanical properties of structural materials: An overview [NASA-TM-87203] p 164 N86-19636
- Analytical Ultrasonics in Materials Research and Testing [NASA-CP-2383] p 164 N86-22962
- Ultrasonic characterization of structural ceramics p 199 N86-22970
- Ultrasonic verification of microstructural changes due to heat treatment p 200 N86-22977

- Transfer function concept for ultrasonic characterization of material microstructures p 200 N86-22980
- Stress waves in transversely isotropic media: The homogeneous problem [NASA-CR-3977] p 164 N86-25002
- Concepts for interrelating ultrasonic attenuation, microstructure and fracture toughness in polycrystalline solids [NASA-TM-87339] p 165 N86-25812
- Ultrasonic stress wave characterization of composite materials [NASA-CR-3976] p 165 N86-27665
- Wave propagation in anisotropic medium due to an oscillatory point source with application to unidirectional composites [NASA-CR-4001] p 165 N86-27666
- A study of the stress wave factor technique for nondestructive evaluation of composite materials [NASA-CR-4002] p 165 N86-28445
- Factors that affect reliability of nondestructive detection of flaws in structural ceramics [NASA-TM-87348] p 166 N86-31912
- Quantitative void characterization in structural ceramics using scanning laser acoustic microscopy [NASA-TM-88797] p 166 N86-31913
- Acousto-ultrasonic verification of the strength of filament wound composite material [NASA-TM-88827] p 166 N86-32764
- NONISOTHERMAL PROCESSES**
- Fracture mechanics applied to nonisothermal fatigue crack growth p 81 A86-28951
- Analysis of large, non-isothermal elastic-visco-plastic deformations [NASA-CR-176220] p 172 N86-10588
- NONLINEAR EQUATIONS**
- Constrained hierarchical least square nonlinear equation solvers --- for indefinite stiffness and large structural deformations p 171 A86-43774
- NONLINEAR SYSTEMS**
- Polynomial nonlinear dynamical systems - A residual sensitivity method for model reduction p 194 A86-35386
- Nonlinear optimal control with tensors - Some computational issues p 194 A86-35419
- Constitutive modeling for isotropic materials (HOST) [NASA-CR-174980] p 172 N86-10589
- Structural analysis of turbine blades using unified constitutive models [NASA-TM-88807] p 178 N86-28461
- Influence of third-degree geometric nonlinearities on the vibration and stability of pretwisted, precone, rotating blades [NASA-TM-87307] p 179 N86-31920
- NONLINEARITY**
- Bounding solutions of geometrically nonlinear viscoelastic problems [AIAA PAPER 86-0943] p 170 A86-38838
- Analysis of large, non-isothermal elastic-visco-plastic deformations [NASA-CR-176220] p 172 N86-10588
- Bounding solutions of geometrically nonlinear viscoelastic problems [NASA-CR-176219] p 195 N86-10860
- Simplified cyclic structural analyses of SSM turbine blades [NASA-TM-87214] p 175 N86-16615
- Nonlinear bending-torsional vibration and stability of rotating, pretwisted, precone blades including Coriolis effects [NASA-TM-87207] p 175 N86-17789
- Integrated research in constitutive modelling at elevated temperatures, part 2 [NASA-CR-177233] p 178 N86-28455
- Influence of third-degree geometric nonlinearities on the vibration and stability of pretwisted, precone, rotating blades [NASA-TM-87307] p 179 N86-31920
- NONUNIFORM FLOW**
- Packet flutter and aerodynamic modes for non-homogeneous airfoil cascades in highly distorted, periodic, stationary throughflows [AIAA PAPER 86-0848] p 5 A86-38896
- NOTCH SENSITIVITY**
- Fractured toughness of Si3N4 measured with short bar chevron-notched specimens [NASA-TM-87153] p 101 N86-13495
- NOTCH STRENGTH**
- Experimental evaluation criteria for constitutive models of time dependent cyclic plasticity [NASA-CR-176821] p 176 N86-25850
- NOTCH TESTS**
- Mode II fatigue crack growth specimen development p 171 A86-43566
- Fractured toughness of Si3N4 measured with short bar chevron-notched specimens [NASA-TM-87153] p 101 N86-13495
- NOZZLE DESIGN**
- Velocity and temperature decay characteristics of inverted-profile jets [AIAA PAPER 86-0312] p 2 A86-22693
- Forced mixer lobes in ejector designs [AIAA PAPER 86-1614] p 134 A86-42752
- Velocity and temperature decay characteristics of inverted-profile jets [NASA-TM-87159] p 9 N86-14223
- Free jet feasibility study of a thermal acoustic shield concept for AST/VCE application-dual flow. Comprehensive data report. Volume 1: Test nozzles and acoustic data [NASA-CR-174817] p 200 N86-23371
- Free-jet feasibility study of a thermal acoustic shield concept for AST/VCE application-dual stream nozzles. Comprehensive data report. Volume 2: Laser velocimeter and suppressor. Base pressure data [NASA-CR-174818] p 201 N86-23372
- Theoretical study on the effect of the design of small (milli-Newton) thruster jets on molecular contamination for the space station [NASA-CR-177263] p 48 N86-26358
- NOZZLE EFFICIENCY**
- Experimental performance of a 1-kilowatt arcjet thruster [AIAA PAPER 85-2033] p 54 A86-37063
- Experimental performance of a 1-kilowatt arcjet thruster [NASA-TM-87131] p 57 N86-10281
- NOZZLE FLOW**
- Non-linear effects in finite amplitude wave propagation through ducts and nozzles p 197 A86-35857
- Transonic potential flow in hyperbolic nozzles p 5 A86-41723
- Numerical analysis of some supersonic viscous flows related to inlet and nozzle systems [AIAA PAPER 86-1597] p 134 A86-42738
- Theoretical study on the effect of the design of small (milli-Newton) thruster jets on molecular contamination for the space station [NASA-CR-177263] p 48 N86-26358
- NOZZLE GEOMETRY**
- High Weber number SMD correlations for pressure atomizers --- Sauter Mean Diameter [ASME PAPER 85-GT-37] p 128 A86-22026
- Transonic potential flow in hyperbolic nozzles p 5 A86-41723
- Variable area radial turbine fabrication and test program [NASA-CR-175091] p 32 N86-28947
- NOZZLE INSERTS**
- Low power dc arcjet operation with hydrogen/nitrogen propellant mixtures [AIAA PAPER 86-1505] p 55 A86-42676
- Lower power dc arcjet operations with hydrogen hydrogen/nitrogen propellant mixtures [NASA-TM-87279] p 61 N86-25407
- NOZZLE THRUST COEFFICIENTS**
- An analysis of cross-coupling of a multicomponent jet engine test stand using finite element modeling techniques [NASA-CR-176424] p 37 N86-15323
- NUCLEAR AUXILIARY POWER UNITS**
- Reliability and mass analysis of dynamic power conversion systems with parallel of standby redundancy [NASA-TM-87189] p 57 N86-16258
- NUCLEAR ELECTRIC PROPULSION**
- Tethered nuclear power for the space station p 53 A86-24808
- NUCLEAR MAGNETIC RESONANCE**
- Development of LC-13C NMR [NASA-CR-176656] p 107 N86-21704
- NUCLEAR PROPULSION**
- Technology for Brayton-cycle powerplants using solar and nuclear energy [NASA-TP-2558] p 60 N86-21577
- NUCLEATION**
- Theory of homogeneous nucleation - A chemical kinetic view p 72 A86-19389
- Computer simulation of thin-film nucleation and growth - The multilayer mode p 204 A86-37441
- Undercooling and solidification behavior in the InSb-Sb system [NASA-CR-175013] p 88 N86-14355
- Grain boundary oxidation and oxidation accelerated fatigue crack nucleation and propagation [NASA-CR-175050] p 89 N86-20542
- Stability of surface nucleation [NASA-TM-88806] p 207 N86-30556
- NUMERICAL ANALYSIS**
- Computation of the radiation characteristics of a generalized phased array [NASA-TM-87185] p 114 N86-18586
- Near-field spillover from a subreflector: Theory and experiment [NASA-TM-88818] p 116 N86-32598
- NUMERICAL CONTROL**
- Variable friction secondary seal for face seals [NASA-CASE-LEW-14170-1] p 160 N86-25790
- NUMERICAL FLOW VISUALIZATION**
- Numerical simulation of unsteady flow in an axisymmetric shear layer [AIAA PAPER 86-0202] p 127 A86-19746
- Coherent structures in a turbulent mixing layer - A comparison between direct numerical simulations and experiments p 132 A86-30218
- NUMERICAL INTEGRATION**
- Integrated research in constitutive modelling at elevated temperatures, part 1 [NASA-CR-177237] p 179 N86-30227
- NUMERICAL STABILITY**
- Propagation and stability of wavelike solutions of finite difference equations with variable coefficients p 194 A86-20033
- Existence and stability, and discrete BB and rank conditions, for general mixed-hybrid finite elements in elasticity p 169 A86-34464
- Locally bound constrained Newton-Raphson solution algorithms --- for modeling kinematic and material nonlinearity p 171 A86-43771
- NUMERICAL WEATHER FORECASTING**
- MERIT - A new approach to upper air forecasting for aviation p 191 A86-17982
- Upper air forecasting for aviation in the United States p 191 A86-37501
- O**
- O RING SEALS**
- Experimental stiffness of tapered bore seals [ASME PAPER 85-DET-12] p 152 A86-22748
- Turbulent two-phase flow in annular seals [ASLE PREPRINT 86-AM-4G-3] p 156 A86-45391
- Variable friction secondary seal for face seals [NASA-CASE-LEW-14170-1] p 160 N86-25790
- Performance of oil pumping rings: An analytical and experimental study [NASA-CR-175083] p 144 N86-31000
- OBATE SPHEROIDS**
- Liquid-vapor interface locations in a spheroidal container under low gravity [NASA-TM-87147] p 141 N86-23854
- OILS**
- Surface tension induced instabilities in reduced gravity: The Benard problem p 40 N86-10117
- ON-LINE SYSTEMS**
- Thermionic noise measurements for on-line dispenser cathode diagnostics for linear beam microwave tubes [NASA-CR-175105] p 124 N86-28323
- ONBOARD DATA PROCESSING**
- On the effectiveness of onboard processing [AIAA PAPER 86-0721] p 45 A86-29659
- Bit error rate testing of a proof-of-concept model baseband processor [NASA-TM-87206] p 46 N86-18343
- OPEN CIRCUIT VOLTAGE**
- The effect of a defective BSF layer on solar cell open circuit voltage --- Back Surface Field p 179 A86-12673
- A 25.5 percent AMO gallium arsenide grating solar cell [NASA-TM-87134] p 182 N86-11671
- Theoretical and experimental flow cell studies of a hydrogen-bromine fuel cell, part 1 [NASA-CR-177165] p 189 N86-29409
- OPERATING TEMPERATURE**
- Turbine Engine Hot Section Technology (HOST) [NASA-CP-2289] p 172 N86-11495
- Turbine engine Hot Section Technology (HOST) project p 173 N86-11496
- Turbine heat transfer p 137 N86-11505
- Gas side heat transfer p 138 N86-11507
- OPERATORS (MATHEMATICS)**
- Model equation for simulating flows in multistage turbomachinery [ASME PAPER 85-GT-226] p 2 A86-22123
- An embedding method for the steady Euler equations p 194 A86-30814
- OPTICAL COMPUTERS**
- Space and frequency-multiplexed optical linear algebra processor - Fabrication and initial tests p 202 A86-48352
- OPTICAL DATA PROCESSING**
- Performance of direct and iterative algorithms on an optical systolic processor p 202 A86-17421
- Error-source effects in a high-accuracy optical finite-element processor p 192 A86-31571

OPTICAL EMISSION SPECTROSCOPY

- Rapid evaluation of ion thruster lifetime using optical emission spectroscopy
[AIAA PAPER 85-2011] p 51 A86-17851
- Rapid evaluation of ion thruster lifetime using optical emission spectroscopy
[NASA-TM-87103] p 56 N86-10280

OPTICAL FILTERS

- Filter induced errors in laser anemometry using counter-processor p 146 A86-34431

OPTICAL HETERODYNING

- Diffraction effects and special advantages in electronic heterodyne moire deflectometry p 202 A86-31565
- Advanced optical measuring systems for measuring the properties of fluids and structures
[NASA-TM-88829] p 150 N86-31859

OPTICAL MEASUREMENT

- Diffraction effects and special advantages in electronic heterodyne moire deflectometry p 202 A86-31565
- The determination of the direction of the optic axis of uniaxial crystalline materials
[NASA-TM-86892] p 148 N86-22915
- A study of the stress wave factor technique for nondestructive evaluation of composite materials
[NASA-CR-4002] p 165 N86-28445
- Advanced optical measuring systems for measuring the properties of fluids and structures
[NASA-TM-88829] p 150 N86-31859

OPTICAL MEASURING INSTRUMENTS

- All-fibre sensing loop using pulse-modulated light-emitting diode p 202 A86-11995
- Development of optical diaphragm deflection sensors
[NASA-CR-175008] p 203 N86-15113
- 1700 deg C optical temperature sensor
[NASA-CR-175108] p 203 N86-28729

OPTICAL PROPERTIES

- Optical and interfacial electronic properties of diamond-like carbon films p 204 A86-16268
- Optical and other properties changes of M-50 bearing steel surfaces for different lubricants and additives prior to scuffing p 97 A86-20435
- Optical techniques to feed and control GaAs MMIC modules for phased array antenna applications
[AIAA PAPER 86-0687] p 110 A86-29638
- Liquid droplet radiator program at the NASA Lewis Research Center
[ASME PAPER 86-HT-15] p 48 A86-49621
- Ellipsometric and optical study of some uncommon insulator films on 3-5 semiconductors
[NASA-TM-87135] p 205 N86-12134
- Liquid droplet radiator program at the NASA Lewis Research Center
[NASA-TM-87139] p 48 N86-12246
- Monolithic optical integrated control circuitry for GaAs MMIC-based phased arrays
[NASA-TM-87183] p 113 N86-16457
- Optical techniques to feed and control GaAs MMIC modules for phased array antenna applications
[NASA-TM-87218] p 113 N86-16458
- Optical constants of GaAs-AlGaAs superlattices and multiple quantum wells
[NASA-CR-176717] p 205 N86-23468
- Superlattices and NiPi structures in new forms of cascade solar cells
[NASA-CR-176718] p 187 N86-24007
- Theoretical study of the transverse dielectric constant of superlattices and their alloys
[NASA-CR-177198] p 206 N86-28759

OPTICS

- The use of an optical data acquisition system for bladed disk vibration analysis p 146 A86-26909

OPTIMAL CONTROL

- Nonlinear optimal control with tensors - Some computational issues p 194 A86-35419

OPTIMIZATION

- The role of service areas in the optimization of FSS orbital and frequency assignments
[AIAA PAPER 86-0636] p 45 A86-29599
- Optimization of the Ni-Cr-Al-Y/ZrO₂-Y₂O₃ thermal barrier system p 82 A86-31746
- Polynomial nonlinear dynamical systems - A residual sensitivity method for model reduction p 194 A86-35386
- Structural tailoring of SSME turbopump blades (SSME/STAEBL) --- Structural Tailoring of Engine Blades
[AIAA PAPER 86-0847] p 54 A86-38895
- Design optimization for a space based, reusable orbit transfer vehicle p 48 N86-17418
- Structural tailoring of engine blades (STAEBL) theoretical manual
[NASA-CR-175112] p 31 N86-27283
- Structural tailoring of engine blades (STAEBL) user's manual
[NASA-CR-175113] p 31 N86-27284

ORBIT SPECTRUM UTILIZATION

- The role of service areas in the optimization of FSS orbital and frequency assignments
[AIAA PAPER 86-0636] p 45 A86-29599
- An analysis of bidirectional use of frequencies for satellite communications
[AIAA PAPER 86-0635] p 110 A86-29664
- Impact of the 1985 Space World Administrative Radio Conference on frequency/orbit planning and use
[AIAA PAPER 86-0634] p 110 A86-49567
- An analysis of bi-directional use of frequencies for satellite communications
[AIAA PAPER 86-0635] p 111 A86-49568
- An analysis of bi-directional use of frequencies for satellite communications
[NASA-TM-87226] p 114 N86-18585
- Impact of the 1985 Space World Administrative Radio Conference on frequency/orbit planning and use
[NASA-TM-87285] p 115 N86-24881
- Communications platform payload definition study
[NASA-CR-174886] p 49 N86-27402
- Spectrum Orbit Utilization Program documentation: SOUP5 version 3.8 user's manual, volume 1, chapters 1 through 5
[NASA-CR-174889] p 193 N86-27927
- Spectrum Orbit Utilization Program documentation: SOUP5 version 3.8 user's manual, volume 2, appendices A through G
[NASA-CR-174890] p 193 N86-27928

ORBIT TRANSFER VEHICLES

- Status of advanced orbital transfer propulsion
[IAF PAPER 85-164] p 51 A86-17850
- Heat transfer in space power and propulsion systems p 53 A86-26492
- Orbital transfer vehicle engine integration study p 58 N86-17418
- Design optimization for a space based, reusable orbit transfer vehicle p 48 N86-17418
- Orbital transfer vehicle engine integration study
[NASA-CR-174842] p 59 N86-20493
- Advanced orbit transfer vehicle propulsion system study
[NASA-CR-174843] p 60 N86-24746
- Orbit Transfer Rocket Engine Technology Program: Advanced engine study, task D.1/D.3
[NASA-CR-175084] p 61 N86-26369

ORBITAL MANEUVERING VEHICLES

- Status of advanced orbital transfer propulsion
[IAF PAPER 85-164] p 51 A86-17850

ORBITAL RENDEZVOUS

- Space station propulsion requirements study
[NASA-CR-174934] p 57 N86-15339

ORBITAL SERVICING

- The role of service areas in the optimization of FSS orbital and frequency assignments
[NASA-CR-176488] p 46 N86-18341

ORBITAL SPACE STATIONS

- Space station power system p 50 A86-12676
- Manrating orbital transfer vehicle propulsion
[AIAA PAPER 85-1226] p 50 A86-14429
- Fluid management and its role in the future of Space Station
[AIAA PAPER 86-2301] p 47 A86-49553
- Theoretical study on the effect of the design of small (milli-Newton) thruster jets on molecular contamination for the space station
[NASA-CR-177263] p 48 N86-26358

ORTHOGONALITY

- Modal test/analysis correlation for Centaur G Prime launch vehicle
[AIAA PAPER 86-1002] p 43 A86-38943

OSCILLATING FLOW

- Oscillatory thermocapillary flows p 129 A86-22413

OSCILLATORS

- Wave propagation in anisotropic medium due to an oscillatory point source with application to unidirectional composites
[NASA-CR-4001] p 165 N86-27666

OVERPRESSURE

- Development of optical diaphragm deflection sensors
[NASA-CR-175008] p 203 N86-15113

OXIDATION

- Ion beam sputter-deposited thin film coatings for protection of spacecraft polymers in low earth orbit
[AIAA PAPER 85-0420] p 95 A86-14428
- Performance of thermal barrier coatings in high heat flux environments p 80 A86-18272
- Modeling degradation and failure of Ni-Cr-Al overlay coatings p 80 A86-18276
- Optimization of the Ni-Cr-Al-Y/ZrO₂-Y₂O₃ thermal barrier system p 82 A86-31746
- Burner rig corrosion of SiC at 1000 C p 99 A86-36328
- The high-temperature oxidation of aromatic hydrocarbons p 75 A86-40834

- Molten salt corrosion of SiC: Pitting mechanism
[NASA-TM-87143] p 101 N86-12310
- Current viewpoints on oxide adherence mechanisms
[NASA-TM-87168] p 87 N86-13409
- Oxidation protection coatings for polymers
[NASA-CASE-LEW-14072-1] p 102 N86-19458
- Grain boundary oxidation and oxidation accelerated fatigue crack nucleation and propagation
[NASA-CR-175050] p 89 N86-20542
- Methane oxidation behind reflected shock waves: Ignition delay times measured by pressure and flame band emission
[NASA-TM-87268] p 77 N86-21835
- A preliminary study of ester oxidation on an aluminum surface using chemiluminescence
[NASA-TM-87242] p 103 N86-24835
- Technology for satellite power conversion
[NASA-CR-176777] p 187 N86-25042
- Ignition delay times of benzene and toluene with oxygen in argon mixtures
[NASA-TM-87312] p 78 N86-25431
- Improved perfluoroalkylether fluid development
[NASA-TM-87276] p 104 N86-25474
- The preparation of new perfluoroether fluids exhibiting excellent thermal-oxidative stabilities
[NASA-TM-87284] p 105 N86-25475
- Oxidation protecting coatings for polymers
[NASA-CASE-LEW-14072-3] p 105 N86-26434
- Low-cycle thermal fatigue
[NASA-TM-87225] p 177 N86-26651
- The evolution and growth of Al₂O₃ scales on beta-NiAl
[NASA-CR-175097] p 92 N86-27444
- Thermal-fatigue and oxidation resistance of cobalt-modified Udumet 700 alloy
[NASA-TP-2591] p 178 N86-28464

OXIDATION RESISTANCE

- High temperature oxidation of beta-NiAl p 85 A86-47266
- All-aromatic biphenylene end-capped polyquinoline and polyimide matrix resins p 100 N86-11267
- Replacement of MDA with more oxidatively stable diamines in PMR-polyimides p 101 N86-11275
- Specimen geometry effects on graphite/PMR-15 composites during thermo-oxidative aging
[NASA-TM-87204] p 69 N86-17477
- High temperature resistant polyimide from tetra ester, diamine, diester and N-arylnadimide
[NASA-CASE-LEW-13864-1] p 102 N86-19457
- The effect of variations of cobalt content on the cyclic oxidation resistance of selected Ni-base superalloys
[NASA-TM-87297] p 93 N86-31702
- Apparatus for producing oxidation protection coatings for polymers
[NASA-CASE-LEW-14072-2] p 106 N86-32569

OXIDATION-REDUCTION REACTIONS

- Cycling performance of the iron-chromium redox energy storage system p 180 A86-24849

OXIDE FILMS

- Ion beam sputter-deposited thin film coatings for protection of spacecraft polymers in low earth orbit
[AIAA PAPER 85-0420] p 95 A86-14428
- Pretreatment effects on the morphology and properties of aluminum oxide thermally grown on NiCoCrAlY
[NASA-TM-87168] p 87 N86-17495
- Current viewpoints on oxide adherence mechanisms
[NASA-TM-87168] p 87 N86-13409
- Oxidation protection coatings for polymers
[NASA-CASE-LEW-14072-1] p 102 N86-19458
- Oxidation protecting coatings for polymers
[NASA-CASE-LEW-14072-3] p 105 N86-26434
- Apparatus for producing oxidation protection coatings for polymers
[NASA-CASE-LEW-14072-2] p 106 N86-32569

OXIDES

- Corrosion of nickel and cobalt base alloys in sulfate melts at 750 deg C
[NASA-CR-175111] p 91 N86-24817

OXYGEN

- Mass loss of shuttle space suit orthofabric under simulated ionospheric atomic oxygen bombardment
[NASA-TM-87149] p 192 N86-13899
- Oxygen recombination in individual pressure vessel nickel-hydrogen batteries
[NASA-CASE-LEW-13822-1] p 188 N86-25874

OXYGEN ATOMS

- Effect of an oxygen plasma on the physical and chemical properties of several fluids for the liquid droplet radiator
[NASA-TM-88839] p 49 N86-31634

OXYGEN IONS

- Adsorption of O₂, SO₂, and SO₃ on nickel oxide - Mechanism for sulfate formation p 75 A86-34238
- Carbon monoxide production in low energy oxygen ion bombardment of pyrolytic graphite and Kapton surfaces p 76 A86-47078

OXYGEN TENSION

Na₂SO₄ induced corrosion of nickel at high temperature p 83 A86-37073

OZONOMETRY

Simultaneous measurements of carbon monoxide and ozone in the NASA Global Atmospheric Sampling Program (GASP) p 191 A86-48620

P

P-N JUNCTIONS

Performance and temperature dependencies of proton irradiated n/p GaAs and n/p silicon cells [NASA-TM-87136] p 120 N86-12509

P-TYPE SEMICONDUCTORS

Carbon films grown from plasma on III-V semiconductors [NASA-TM-87140] p 205 N86-12135

PALMGREN-MINER RULE

Re-examination of cumulative fatigue damage analysis: An engineering perspective [NASA-TM-87325] p 177 N86-27680

PANEL METHOD (FLUID DYNAMICS)

Unsteady forces on counter-rotating propeller blades [AIAA PAPER 86-1804] p 22 A86-37827
A numerical analysis applied to high angle of attack three-dimensional inlets [AIAA PAPER 86-1527] p 6 A86-42760
A numerical analysis applied to high angle of attack three-dimensional inlets [NASA-TM-87298] p 11 N86-24658

PARABOLIC ANTENNAS

Calculation of allowable orbital spacings for the fixed-satellite service [NASA-CR-176273] p 43 N86-11212

PARABOLIC DIFFERENTIAL EQUATIONS

Assessment of a parabolic analysis for axisymmetric internal flows in rocket and turbomachinery ducts [AIAA PAPER 86-1598] p 134 A86-42739

PARALLEL PLATES

A high frequency analysis of electromagnetic plane wave scattering by perfectly-conducting semi-infinite parallel plate and rectangular waveguides with absorber coated inner walls [NASA-CR-179759] p 116 N86-32600

PARALLEL PROCESSING (COMPUTERS)

Simulating a small turboshaft engine in real-time multiprocessor simulator (RTMPS) environment [NASA-TM-87216] p 27 N86-16221
Partitioning and packing mathematical simulation models for calculation on parallel computers [NASA-TM-87170] p 193 N86-19008
Increasing processor utilization during parallel computation rundown [NASA-TM-87349] p 192 N86-26914
Hardware configuration for a real-time multiprocessor simulator [NASA-TM-88802] p 194 N86-28651

PARAMETERIZATION

Parameter sensitivity in the dynamics of rotor-bearing systems [ASME PAPER 85-DET-35] p 154 A86-38620
Extended parametric representation of compressor fans and turbines. Volume 1: CMGEN user's manual [NASA-CR-174645] p 159 N86-23936
Extended parametric representation of compressor fans and turbines. Volume 2: Part user's manual (parametric turbine) [NASA-CR-174646] p 159 N86-23937
Extended parametric representation of compressor fans and turbines. Volume 3: MODFAN user's manual (parametric modulating flow fan) [NASA-CR-174647] p 159 N86-23938

PARITY

Robust detection-isolation-accommodation for sensor failures [NASA-CR-174797] p 121 N86-16486

PARTIAL DIFFERENTIAL EQUATIONS

Solution of elliptic partial differential equations by fast Poisson solvers using a local relaxation factor. 1: One-step method [NASA-TP-2529] p 195 N86-28661

PARTICLE COLLISIONS

Binary collision model for neon Auger spectra from neon ion bombardment of the aluminum surface p 76 A86-43457

PARTICLE MOTION

Grid-free simulation of diffusion using random walk methods p 196 A86-16521

PARTICLE SIZE DISTRIBUTION

Thermophoretically augmented mass transfer rates to solid walls across laminar boundary layers p 128 A86-20150
Characterization of simulated small-droplet fuel sprays [AIAA PAPER 86-1725] p 135 A86-42813

Criteria for significance of simultaneous presence of both condensable vapors and aerosol particles on mass transfer (deposition) rates

[NASA-TM-87247] p 109 N86-24869
Characterization of simulated small-droplet fuel sprays [NASA-TM-87286] p 148 N86-24961

PARTICLE TRAJECTORIES

An experimental method for measuring droplet impingement efficiency on two- and three-dimensional bodies [AIAA PAPER 86-0406] p 131 A86-26630
Particle trajectory computation on a 3-dimensional engine inlet [NASA-CR-175023] p 14 N86-20379

PARTICLES

Particle cloud combustion experiment p 41 N86-10160
Criteria for significance of simultaneous presence of both condensable vapors and aerosol particles on mass transfer (deposition) rates [NASA-TM-87247] p 109 N86-24869
Flame propagation and extinction in particle clouds [NASA-CR-177304] p 78 N86-27434

PAYLOADS

Modal test/analysis correlation for Centaur G Prime launch vehicle [AIAA PAPER 86-1002] p 43 A86-38943

PENALTY FUNCTION

Simplex finite element analysis of viscous incompressible flow with penalty function formulation p 129 A86-22615

PERFLUORO COMPOUNDS

The effects of metals and inhibitors on thermal oxidative degradation reactions of unbranched perfluoroalkyl ethers p 99 A86-40682
Analysis of a spacecraft instrument ball bearing assembly lubricated by a perfluoroalkylether [NASA-TM-87260] p 50 N86-21575
The preparation of new perfluoroether fluids exhibiting excellent thermal-oxidative stabilities [NASA-TM-87284] p 105 N86-25475

PERFLUOROALKANE

Improved perfluoroalkylether fluid development [NASA-TM-87276] p 104 N86-25474

PERFORMANCE

Life cycle test results of a bipolar nickel hydrogen battery p 180 A86-24824

PERFORMANCE PREDICTION

Test results of a 40 kW Stirling engine and comparison with the NASA-Lewis computer code predictions p 181 A86-24889
The performance characteristics of simulated ice on rotorcraft airfoils p 14 A86-35656
An investigation of the transient thermal analysis of spur gears [ASME PAPER 84-DET-92] p 155 A86-40683
Performance and temperature dependencies of proton irradiated n/p GaAs and n/p silicon cells [NASA-TM-87136] p 120 N86-12509
Theoretical and experimental flow cell studies of a hydrogen-bromine fuel cell, part 1 [NASA-CR-177165] p 189 N86-29409
Aerodynamic data banks for Clark-Y, NACA 4-digit and NACA 16-series airfoil families [NASA-CR-176883] p 13 N86-30693

PERFORMANCE TESTS

10 kW solar array switching unit performance test results p 118 A86-24844
RE-1000 free-piston Stirling engine update p 153 A86-24890
Resistojet operation with various propellants [AIAA PAPER 85-1158] p 107 A86-37074
A long-life 50 lbf H₂/O₂ thruster for Space Station auxiliary propulsion [AIAA PAPER 86-1404] p 55 A86-42617
Atomization and combustion characteristics of antimisting fuels using JT8D and air-boost injectors [ASME PAPER 86-GT-223] p 24 A86-48257
Test results for 20-GHz GaAs FET spacecraft power amplifier [NASA-TM-87072] p 111 N86-10379
RE-1000 free-piston Stirling engine update [NASA-TM-87126] p 182 N86-11668
Evaluation parameters for the alkaline fuel cell oxygen electrode [NASA-TM-87155] p 77 N86-12268
Develop and test fuel cell powered on-site integrated total energy systems: Phase 3, full-scale power plant development [NASA-CR-174948] p 182 N86-12757
Develop and test fuel cell powered on-site integrated total energy systems: Phase 3, full-scale power plant development [NASA-CR-174998] p 182 N86-12758
Ceramic automotive Stirling engine study [NASA-CR-174907] p 208 N86-16165

LOX/LH₂ vane pump for auxiliary propulsion systems p 58 N86-17397

Onsite 40-kilowatt fuel cell power plant manufacturing and field test program [NASA-CR-174988] p 185 N86-18773

Development and testing of tip devices for horizontal axis wind turbines [NASA-CR-174991] p 185 N86-18774

Programmable, automated transistor test system [NASA-TP-2554] p 123 N86-21755

Designing a 25-kilowatt high frequency series resonant [NASA-CR-176774] p 123 N86-24906

Stirling Powered Van Program overview [NASA-TM-87227] p 210 N86-25303

Evaluation of a hybrid hydrostatic bearing for cryogenic turbopump application [NASA-TM-87255] p 63 N86-31649

The noncavitating performance and life of a small vane-type positive displacement pump in liquid hydrogen [NASA-TM-87347] p 63 N86-31651

Parametric and cycle tests of a 40-A-hr bipolar nickel-hydrogen battery [NASA-TM-88793] p 189 N86-31979

PERIODIC VARIATIONS

Periodic oscillations observed in swirling flows with and without combustion p 73 A86-22755

PERMITTIVITY

Theoretical study of the transverse dielectric constant of superlattices and their alloys [NASA-CR-177198] p 206 N86-28759

PERSONAL COMPUTERS

Application of a personal computer for the uncoupled vibration analysis of wind turbine blade and counterweight assemblies [NASA-CR-175090] p 188 N86-28511

PERTURBATION THEORY

Boundary perturbation method for free boundary problem in convectively cooled continuous casting p 131 A86-28649

PHASE CHANGE MATERIALS

Estimated heats of fusion of fluoride salt mixtures suitable for thermal energy storage applications [NASA-TM-87320] p 190 N86-31982

PHASE CONJUGATION

Lens collimation and testing using a Twyman-Green interferometer with a self-pumped phase-conjugating mirror p 146 A86-29280

PHASE DETECTORS

Range finding using frequency-modulated laser diode p 147 A86-39521

PHASE DIAGRAMS

Constructing multicomponent phase diagrams by overlapping ZPF lines --- Zero Phase Fraction Line for improved mechanical and corrosion properties p 83 A86-44038

PHASE MODULATION

Simulated performance of the NASA 30/20 GHz test transponder using multi-H phase coded modulation [AIAA PAPER 86-0717] p 110 A86-29656

PHASE SHIFT

Laboratory experiments on active suppression of advanced turboprop noise [NASA-TM-87129] p 199 N86-19125

PHASE TRANSFORMATIONS

Neutron and X-ray diffraction of plasma-sprayed zirconia-yttria thermal barrier coatings p 96 A86-16269

The effects of grain size on the flow and fracture of long-range ordered alloys p 84 A86-47243
High temperature oxidation of beta-NiAl p 85 A86-47266

Measurement of the density of base fluids at pressures 0.422 to 2.20 GPa [NASA-TM-87114] p 156 N86-10551

Long-term stability and properties of zirconia ceramics for heavy duty diesel engine components [NASA-CR-174943] p 209 N86-17224

PHASE VELOCITY

Stress waves in transversely isotropic media: The homogeneous problem [NASA-CR-3977] p 164 N86-25002

PHASED ARRAYS

Optical techniques to feed and control GaAs MMIC modules for phased array antenna applications [AIAA PAPER 86-0687] p 110 A86-29638

Monolithic optical integrated control circuitry for GaAs MMIC-based phased arrays [NASA-TM-87183] p 113 N86-16457

Optical techniques to feed and control GaAs MMIC modules for phased array antenna applications [NASA-TM-87218] p 113 N86-16458

Computation of the radiation characteristics of a generalized phased array [NASA-TM-87185] p 114 N86-18586

- Satellite voice broadcast system study, volume 2
[NASA-CR-174905] p 115 N86-24877
- PHENYLS**
Effect of substituted phenylindimides on processing and properties of PMR polyimide composites p 94 A86-13179
Chemical control of rate and onset temperature of nadimide polymerization p 101 N86-11271
Rheological, processing, and 371 deg C mechanical properties of Celion 6000/N-phenylindimide modified PMR composites p 88 N86-11278
- PHOSPHORIC ACID FUEL CELLS**
Transmission electron microscopic examination of phosphoric acid fuel cell components p 74 A86-23352
Develop and test fuel cell powered on-site integrated total energy systems: Phase 3, full-scale power plant development [NASA-CR-174948] p 182 N86-12757
Develop and test fuel cell powered on-site integrated total energy systems: Phase 3, full-scale power plant development [NASA-CR-174998] p 182 N86-12758
Gas cooled fuel cell systems technology development [NASA-CR-175047] p 190 N86-31984
- PHOSPHORUS**
The mechanism of erosion of metallic materials under cavitation attack [NASA-TM-87133] p 156 N86-10552
- PHOTOABSORPTION**
Infrared-photoinduced-absorption studies in soluble trans-polyacetylene p 204 A86-37075
- PHOTOACOUSTIC MICROSCOPY**
NDE of structural ceramics [ASME PAPER 86-GT-279] p 163 A86-48298
NDE of structural ceramics [NASA-TM-87186] p 164 N86-16598
- PHOTOCHEMICAL REACTIONS**
Research and development of neat alcohol fuel usage in automobiles [NASA-CR-174813] p 108 N86-27460
- PHOTOGRAMMETRY**
In-flight photogrammetric measurement of wing ice accretions [NASA-TM-87191] p 17 N86-31562
- PHOTOGRAPHY**
Fundamental studies of droplet combustion at reduced gravity p 42 N86-10165
- PHOTOMULTIPLIER TUBES**
Characteristics of an axisymmetric sudden expansion flow [NASA-CR-176278] p 151 N86-11465
- PHOTOVOLTAIC CELLS**
Photovoltaic systems in remote locations: An experience summary [NASA-TM-87106] p 181 N86-10643
Photovoltaic-powered vaccine refrigerator: Freezer systems field test results [NASA-TM-86972-REV] p 181 N86-11666
Space Photovoltaic Research and Technology 1985: High Efficiency, Space Environment, and Array Technology [NASA-CP-2408] p 184 N86-17839
Superlattices and NiPi structures in new forms of cascade solar cells [NASA-CR-176718] p 187 N86-24007
Potential high efficiency solar cells: Applications from space photovoltaic research [NASA-TM-88832] p 125 N86-32627
- PHOTOVOLTAIC CONVERSION**
Space Station Power System Advanced Development p 52 A86-24778
Development of a microprocessor controller for stand-alone photovoltaic power systems [NASA-CR-174723] p 187 N86-21979
Space solar cell research: Problems and potential [NASA-TM-88833] p 125 N86-31793
Electrical power system for the U.S. space station [NASA-TM-88856] p 64 N86-32520
The space station power system [NASA-TM-88847] p 64 N86-32521
- PHOTOVOLTAIC EFFECT**
Photovoltaic systems in remote locations: An experience summary [NASA-TM-87106] p 181 N86-10643
- PHYSICAL PROPERTIES**
Composition and properties of the so-called 'diamond-like' amorphous carbon films p 96 A86-16255
- PIEZOELECTRIC GAGES**
Piezoviscous effects in nonconformal contacts lubricated hydrodynamically [NASA-TM-87141] p 141 N86-21797
- PIEZOELECTRIC TRANSDUCERS**
Piezoelectric deicing device [NASA-CASE-LEW-13773-2] p 122 N86-20671

PIEZOELECTRICITY

- Analytical ultrasonics for evaluation of composite materials response. Part 2: Generation and detection p 200 N86-22973

PILOT TRAINING

- The effects of syntactic complexity on the human-computer interaction p 192 A86-36172

PIPE FLOW

- A model for closing the inviscid form of the average-passage equation system [ASME PAPER 86-GT-227] p 8 A86-48261
A model for closing the inviscid form of the average-passage equation system [NASA-TM-87199] p 10 N86-14224

PIPES (TUBES)

- HOST liner cyclic facilities p 173 N86-11519

PISTON ENGINES

- Overview of the 1985 NASA Lewis Research Center SP-100 free-piston Stirling engine activities p 153 A86-24884
RE-1000 free-piston Stirling engine update p 153 A86-24890
RE-1000 free-piston Stirling engine update [NASA-TM-87126] p 182 N86-11668
Lightweight two-stroke cycle aircraft diesel engine technology enablement program, volume 1 [NASA-CR-174923-VOL-1] p 26 N86-13328
Lightweight two-stroke cycle aircraft diesel engine technology enablement program, volume 2 [NASA-CR-174923-VOL-2] p 26 N86-13329
Lightweight two-stroke cycle aircraft diesel engine technology enablement program, volume 3 [NASA-CR-174923-VOL-3] p 26 N86-13330

PISTONS

- Experimental assessment of advanced Stirling component concepts [NASA-CR-174994] p 210 N86-25302
Overview of the 1986 free-piston Stirling SP-100 activities at the NASA Lewis Research Center [NASA-TM-87305] p 210 N86-26261

PITOT TUBES

- Semiempirical method of determining flow coefficients for pitot rake mass flow rate measurements [NASA-TM-87144] p 9 N86-14219

PITTING

- Molten salt corrosion of SiC: Pitting mechanism [NASA-TM-87143] p 101 N86-12310

PLANE STRAIN

- Fractured toughness of Si3N4 measured with short bar chevron-notched specimens [NASA-TM-87153] p 101 N86-13495

PLANE WAVES

- NASA/DOE automotive Stirling engine project: Overview 1986 [NASA-TM-87345] p 211 N86-29731
A high frequency analysis of electromagnetic plane wave scattering by perfectly-conducting semi-infinite parallel plate and rectangular waveguides with absorber coated inner walls [NASA-CR-179759] p 116 N86-32600

PLANETARY WAVES

- A note on the finite differencing of the linearized primitive equations' lower boundary condition p 191 A86-28963

PLASMA ACCELERATION

- Characterisation of plasma in a rail gun p 118 A86-26051

PLASMA CONDUCTIVITY

- Characterisation of plasma in a rail gun p 118 A86-26051

PLASMA CURRENTS

- Electrodynamic tether technology considerations p 161 N86-27857

PLASMA DENSITY

- Threshold determining mechanisms for discharges in high voltage solar arrays [AIAA PAPER 86-0364] p 52 A86-19834
The voltage threshold for arcing for solar cells in LEO: Flight and ground test results [NASA-TM-87259] p 62 N86-28125

PLASMA DIODES

- Auger electron spectroscopy, secondary ion mass spectroscopy and optical characterization of a-C-H and BN films [NASA-TM-87258] p 206 N86-25268

PLASMA DISPLAY DEVICES

- Frictional and structural characterization of ion-nitrided low and high chromium steels p 81 A86-17477

PLASMA ETCHING

- Dry etching of beta-SiC in CF4 and CF4 + O2 mixtures p 76 A86-47069

PLASMA INTERACTIONS

- The role of unneutralized surface ions in negative potential arcing p 118 A86-25525

- Effect of an oxygen plasma on the physical and chemical properties of several fluids for the liquid droplet radiator [NASA-TM-88839] p 49 N86-31634

PLASMA JETS

- Deposition stress effects on the life of thermal barrier coatings on burner rigs p 96 A86-16271

PLASMA PROPULSION

- Measurements of energy distribution and wall temperature in flowing hydrogen microwave plasma systems [AIAA PAPER 85-2052] p 203 A86-11001
Rail accelerators for space transportation: An experimental investigation [NASA-TP-2571] p 62 N86-28123

PLASMA SPRAYING

- Finite element analysis of residual stress in plasma-sprayed ceramic p 95 A86-15226
Character of laser-glazed, plasma-sprayed zirconia coatings on stainless steel substrata p 95 A86-15229
Optical and interfacial electronic properties of diamond-like carbon films p 204 A86-16268
Neutron and X-ray diffraction of plasma-sprayed zirconia-yttria thermal barrier coatings p 96 A86-16269
Failure analysis of plasma-sprayed thermal barrier coatings p 80 A86-16270
Deposition stress effects on the life of thermal barrier coatings on burner rigs p 96 A86-16271
Film and interstitial formation of metals in plasma-sprayed ceramics p 96 A86-17484
Selected fretting-wear-resistant coatings for Ti-6 pct Al-4 pct V alloy p 97 A86-24956
Fracture toughness tests on plasma-sprayed coatings p 64 A86-30051

- Tensile adhesion test measurements on plasma-sprayed coatings p 98 A86-30052

- Creep-fatigue behavior of NiCoCrAlY coated PWA 1480 superalloy single crystals [NASA-TM-87110] p 86 N86-10311

- A new chromium carbide-based tribological coating for use to 900 deg C with particular reference to the Stirling engine [NASA-TM-87274] p 103 N86-21682

- The low cycle fatigue behavior of a plasma-sprayed coating material [NASA-TM-87318] p 92 N86-31699

PLASMA TEMPERATURE

- Characterisation of plasma in a rail gun p 118 A86-26051

PLASMAS (PHYSICS)

- Radical molecule and ion-molecule mechanisms in the polymerization of hydrocarbons and chlorosilanes in R.F. plasmas at low pressures (below 1.0 Torr) p 203 A86-16254

- Improvement of ion thruster design [NASA-CR-177223] p 61 N86-27419

PLASTIC DEFORMATION

- Shear fatigue crack growth - A literature survey p 167 A86-24219
Constitutive modeling of cyclic plasticity and creep, using an internal time concept p 170 A86-41673
Effect of boron on tensile properties of B2 BeAl [NASA-CR-175074] p 89 N86-21656
Experimental evaluation criteria for constitutive models of time dependent cyclic plasticity [NASA-CR-176821] p 176 N86-25850
Fatigue crack layer propagation in silicon-iron [NASA-CR-175115] p 177 N86-25851

PLASTIC FLOW

- Slow plastic strain rate compressive flow in binary CoAl intermetallics p 79 A86-11478
The influence of grain size and composition on slow plastic flow in FeAl between 1100 and 1400 K p 86 A86-50279

PLASTIC PROPERTIES

- The plastic compressibility of 7075-T651 aluminum-alloy plate p 85 A86-49690
Development of constitutive models for cyclic plasticity and creep behavior of super alloys at high temperature [NASA-CR-176418] p 88 N86-14356

PLATE (STRUCTURAL MEMBERS)

- Low-cycle thermal fatigue [NASA-TM-87225] p 177 N86-26651

PLATES (TECTONICS)

- Experimental assessment of advanced Stirling component concepts [NASA-CR-174994] p 210 N86-25302

PLATES (TECTONICS)

- Wilson study cycles: Research relative to ocean geodynamic cycles [NASA-CR-176560] p 192 N86-21092

PLATINUM

- Two dimensional, transient catalytic combustion of CO-air on platinum p 71 A86-10201

PLATINUM ALLOYS

Compatibility experiments of facilities, materials, and propellants for electrothermal thrusters p 59 N86-17426

PLATINUM COMPOUNDS

Compatibility of grain-stabilized platinum with candidate propellants for resistojets [AIAA PAPER 85-2014] p 51 A86-17835
Compatibility of grain-stabilized platinum with candidate propellants for resistojets [NASA-TM-871118] p 56 N86-10279

PLUMES

Plume characteristics of single-stream and dual-flow conventional and inverted-profile nozzles at equal thrust [AIAA PAPER 86-1809] p 8 A86-49585
Plume characteristics of single-stream and dual-flow conventional and inverted-profile nozzles at equal thrust [NASA-TM-87323] p 12 N86-26285

PLY ORIENTATION

A new ply model for interlaminar stress analysis p 66 A86-20629
Progressive fracture of fiber composites p 67 A86-35809

PNEUMATIC EQUIPMENT

Method for improving the fuel efficiency of a gas turbine engine [NASA-CASE-LEW-13142-2] p 28 N86-20389

POLARIZATION (WAVES)

Polarization modulated ellipsometry [NASA-CR-177264] p 149 N86-26599

POLLUTION TRANSPORT

Criteria for significance of simultaneous presence of both condensable vapors and aerosol particles on mass transfer (deposition) rates [NASA-TM-87247] p 109 N86-24869

POLYACETYLENE

Infrared-photoinduced-absorption studies in soluble trans-polyacetylene p 204 A86-37075

POLYCRYSTALS

Dislocations in extruded Co-49.3 at. pct Al p 83 A86-45091
The mechanism of erosion of metallic materials under cavitation attack [NASA-TM-87133] p 156 N86-10552
Ultrasonic verification of microstructural changes due to heat treatment p 200 N86-22977
Transfer function concept for ultrasonic characterization of material microstructures p 200 N86-22980
Abrasion and deformed layer formation of manganese-zinc ferrite in sliding contact with lapping tapes [NASA-TM-87249] p 104 N86-24838
Concepts for interrelating ultrasonic attenuation, microstructure and fracture toughness in polycrystalline solids [NASA-TM-87339] p 165 N86-25812

POLYETHER RESINS

A thin film degradation study of a fluorinated polyether liquid lubricant using an HPLC method [NASA-TM-87221] p 77 N86-19417

POLYIMIDE RESINS

Graphite/PMR polyimide composites with improved toughness p 66 A86-21731
PMR polyimides from solutions containing mixed endcaps p 100 N86-11263
All-aromatic biphenylene end-capped polyquinoline and polyimide matrix resins p 100 N86-11267
Characterization methodology for PMR-15 p 65 N86-11272
Replacement of MDA with more oxidatively stable diamines in PMR-polyimides p 101 N86-11275
The 371 deg C mechanical properties of graphite/polyimide composites p 69 N86-12256
High temperature resistant polyimide from tetra ester, diamine, diester and N-arylnadimide [NASA-CASE-LEW-13864-1] p 102 N86-19457
Structure-to-property relationships in addition cured polymers 2: Resin Tg composite initial mechanical properties of norbornenyl cured polyimide resins [NASA-TM-88794] p 105 N86-29041

POLYIMIDES

Low-wear partially fluorinated polyimides p 94 A86-11175
Effect of substituted phenylnadimides on processing and properties of PMR polyimide composites p 94 A86-13179
Ion beam sputter-deposited thin film coatings for protection of spacecraft polymers in low earth orbit [AIAA PAPER 85-0420] p 95 A86-14428
Graphite/PMR polyimide composites with improved toughness p 66 A86-21731
Aerospace applications of PMR polyimide composites p 67 A86-27730
Effect of solution concentration and aging conditions on PMR-15 resin p 98 A86-33113

Tribological paroperties of graphite-fiber-reinforced, partially fluorinated polyimide composites p 98 A86-34177

Structure-to-glass transition temperature relationships in high temperature stable condensation polyimides [NASA-TM-87113] p 101 N86-12311
Oxidation protecting coatings for polymers [NASA-CASE-LEW-14072-3] p 105 N86-26434
Feasibility study of a discrete bearing/roller drive rotary joint for the space station [NASA-TM-88800] p 161 N86-30206

POLYMER CHEMISTRY

Structure-to-glass transition temperature relationships in high temperature stable condensation polyimides [NASA-TM-87113] p 101 N86-12311
Microgravity Polymers [NASA-CP-2392] p 105 N86-28194

POLYMER MATRIX COMPOSITES

Aerospace applications of PMR polyimide composites p 67 A86-27730
The synthesis, characterization and thermal chemistry of modified norbornenyl PMR endcaps p 100 N86-11266
Properties of autoclaved Gr/PI composites made from improved tack PMR-15 prepreg p 68 N86-11276
Rheological, processing, and 371 deg C mechanical properties of Celcon 6000/N-phenylnadimide modified PMR composites p 68 N86-11278
Mass loss of shuttle space suit orthofabric under simulated ionospheric atomic oxygen bombardment [NASA-TM-87149] p 192 N86-13899

POLYMER PHYSICS

Microgravity Polymers [NASA-CP-2392] p 105 N86-28194

POLYMERIC FILMS

Mass spectrometric studies of the electrical breakdown of thin polymer films p 100 A86-47070

POLYMERIZATION

A ceramic matrix composite based on polymerization and pyrolysis of ethynylated aromatics p 65 A86-13169
Radical molecule and ion-molecule mechanisms in the polymerization of hydrocarbons and chlorosilanes in R.F. plasmas at low pressures (below 1.0 Torr) p 203 A86-16254
Graphite/PMR polyimide composites with improved toughness p 66 A86-21731
PMR polyimides from solutions containing mixed endcaps p 100 N86-11263
The synthesis, characterization and thermal chemistry of modified norbornenyl PMR endcaps p 100 N86-11266
Chemical control of rate and onset temperature of nadimide polymerization p 101 N86-11271
Characterization methodology for PMR-15 p 65 N86-11272
Structure-to-property relationships in addition cured polymers 2: Resin Tg composite initial mechanical properties of norbornenyl cured polyimide resins [NASA-TM-88794] p 105 N86-29041
Carbon-rich ceramic composites from ethynyl aromatic precursors [NASA-TM-88812] p 71 N86-29908

POLYMERS

Tribological paroperties of graphite-fiber-reinforced, partially fluorinated polyimide composites p 98 A86-34177
Characterization and measurement of polymer wear p 100 A86-48405
Oxidation protecting coatings for polymers [NASA-CASE-LEW-14072-3] p 105 N86-26434

POLYNOMIALS

Lubrication of nonconformal contacts [NASA-TM-87120] p 138 N86-13679

POLYPHENYL ETHER

Contact angle and surface tension measurements of a five-ring polyphenyl ether p 98 A86-34179

POLYTETRAFLUOROETHYLENE

Thermal desorption study of physical forces at the PTFE surface [NASA-TM-87090] p 206 N86-25284

POROSITY

Molten salt corrosion of SiC: Pitting mechanism [NASA-TM-87143] p 101 N86-12310

POROUS MATERIALS

Buoyancy effects on smoldering combustion [IAF PAPER 85-289] p 72 A86-15805

POTASSIUM HYDROXIDES

KOH concentration effect on the cycle life of nickel-hydrogen cells p 180 A86-24802

POTENTIAL FLOW

Transonic potential flow in hyperbolic nozzles p 5 A86-41723
A numerical analysis applied to high angle of attack three-dimensional inlets [AIAA PAPER 86-1527] p 6 A86-42760

On the application of a linearized unsteady potential-flow analysis to fan-tip cascades [ASME PAPER 86-GT-87] p 7 A86-48153

Application of a linearized unsteady aerodynamic analysis to standard cascade configurations [NASA-CR-3940] p 11 N86-21505

A numerical analysis applied to high angle of attack three-dimensional inlets [NASA-TM-87298] p 11 N86-24658

POWDER (PARTICLES)

Properties of silicon suspensions and slip-cast bodies p 95 A86-15238
Factors influencing the ball milling of Si3N4 in water p 95 A86-15239
Particle size reduction of Si3N4 with Si3N4 milling hardware [NASA-TM-86864-REV] p 104 N86-24839

POWDER METALLURGY

Fabrication of ceramic substrate-reinforced and free forms by mandrel plasma spraying metal-ceramic composites p 64 A86-17483
Fabrication of ceramic components for advanced gas turbine engines [SAE PAPER 851786] p 154 A86-38310
Alloys based on NiAl for high temperature applications p 84 A86-47261
Effect of boron on tensile properties of B2 BaAl [NASA-CR-175074] p 89 N86-21656
Tensile behavior of Fe-40Al alloys with B and Zr additions [NASA-TM-87290] p 91 N86-25453
Surface fatigue and failure characteristics of hot forged powder metal AISI 4620, AISI 4640, and machined AISI 4340 steel spur gears [NASA-TM-87330] p 161 N86-31889

POWER AMPLIFIERS

Test results for 20-GHz GaAs FET spacecraft power amplifier [NASA-TM-87072] p 111 N86-10379

POWER CONDITIONING

Resonant power processors. I - State plane analysis p 117 A86-14481
Space Station Power System Advanced Development p 52 A86-24778
State-plane analysis of parallel resonant converter p 119 A86-40431
Description of a 20 Kiloherzt power distribution system [NASA-TM-87346] p 34 N86-31584

POWER CONVERTERS

Resonant power processors. I - State plane analysis p 117 A86-14481
Resonant power processors. II - Methods of control p 117 A86-14482
Inverter design for high frequency power distribution p 117 A86-24831
Power electronics for a 1-kilowatt arcjet thruster [AIAA PAPER 86-1507] p 56 A86-49613
Technology for satellite power conversion [NASA-CR-176554] p 186 N86-19742
Space station 20-kHz power management and distribution system [NASA-TM-87314] p 60 N86-24747
Power electronics for a 1-kilowatt arc jet thruster [NASA-TM-87340] p 61 N86-25409
Power conversion distribution system using a resonant high-frequency AC link [NASA-CR-176804] p 123 N86-25694

POWER EFFICIENCY

An experimental study of energy loss mechanisms and efficiency considerations in the low power dc arcjet [AIAA PAPER 85-2017] p 53 A86-37062
An experimental study of energy loss mechanisms and efficiency consideration in the low power dc arcjet [NASA-TM-87123] p 57 N86-11224
Space station power management and distribution p 59 N86-17869

Linearized traveling wave amplifier with hard limiter characteristics [NASA-CASE-LEW-13981-2] p 122 N86-21742
Overview of NASA Lewis Research Center free-piston Stirling engine technology activities applicable to space power systems [NASA-TM-88815] p 211 N86-29732

POWER GAIN

Ka-band monolithic gain control amplifier p 119 A86-41343

POWER SUPPLY CIRCUITS

Inverter design for high frequency power distribution p 117 A86-24831

POWERED LIFT AIRCRAFT

The STOL performance of a two-engine, USB powered-lift aircraft with cross-shafted fans [SAE PAPER 851839] p 16 A86-38336

PREBURNERS

- Longitudinal mode combustion instabilities of a high-pressure fuel-rich LOX/PP-1 preburner p 56 A86-49640
- SSME fuelside preburner two-dimensional analysis [NASA-TM-87299] p 44 A86-23616
- Longitudinal mode combustion instabilities of a high-pressure fuel-rich LOX/PP-1 preburner p 165 A86-28250

PREDICTION ANALYSIS TECHNIQUES

- Heat transfer and fluid mechanics measurements in transitional boundary layer flows [ASME PAPER 85-GT-113] p 126 A86-13068
- Computation of viscous flows in turbomachinery cascades with a space-marching method p 5 A86-39089
- Efficiency of nonstandard and high contact ratio involute spur gears [ASME PAPER 84-DET-172] p 155 A86-45255
- Effect of accuracy of wind power prediction on power system operator [NASA-CR-176300] p 181 A86-11667
- An update of the total-strain version of SRP [NASA-TP-2499] p 87 A86-12295
- Rocket thrust chamber thermal barrier coatings [NASA-CR-175022] p 59 A86-20497
- Life prediction and constitutive models for engine hot section anisotropic materials program [NASA-CR-174952] p 165 A86-25003
- Computational simulation of progressive fracture in fiber composites [NASA-TM-87341] p 71 A86-26376
- Effects of surface chemistry on hot corrosion life [NASA-CR-179471] p 32 A86-28087
- Micromechanisms of thermomechanical fatigue: A comparison with isothermal fatigue [NASA-TM-87331] p 92 A86-28164
- Experimental and theoretical study of propeller spinner/shank interference [NASA-CR-176954] p 13 A86-29773

PREDICTIONS

- Progressive damage, fracture predictions and post mortem correlations for fiber composites [NASA-TM-87101] p 68 A86-10290
- Gas side heat transfer p 138 A86-11507
- Life prediction and constitutive behavior p 173 A86-11520
- Creep fatigue life prediction for engine hot section materials (isotropic) p 174 A86-11521
- Preliminary measurement of the noise from the 2/9 scale model of the Large-scale Advanced Propfan (LAP) propeller, SR-7A [NASA-TM-87116] p 199 A86-14006
- Ceramic automotive Stirling engine study [NASA-CR-174907] p 208 A86-16165
- Future heavy duty trucking engine requirements [NASA-CR-174996] p 209 A86-17226
- Satellite voice broadcast. Volume 1: Executive summary [NASA-CR-175016] p 115 A86-24875
- Communication Platform Payload Definition (CPPD) study. Volume 1: Executive summary [NASA-CR-174928] p 49 A86-27403
- Communication Platform Payload Definition (CPPD) study. Volume 2: Technical report [NASA-CR-174929] p 49 A86-27404
- Communication Platform Payload Definition (CPPD) study. Volume 3: Addendum [NASA-CR-174930] p 49 A86-27405
- Structural analysis of turbine blades using unified constitutive models [NASA-TM-88807] p 178 A86-28461
- Formulation of the nonlinear analysis of shell-like structures, subjected to time-dependent mechanical and thermal loading [NASA-CR-177194] p 178 A86-28462

PRELAUNCH TESTS

- Modal test/analysis correlation for Centaur G Prime launch vehicle [AIAA PAPER 86-1002] p 43 A86-38943

PREMIXED FLAMES

- Effect of gravity on laminar premixed gas combustion. I - Flammability limits and burning velocities p 72 A86-12413
- Effect of gravity on laminar premixed gas combustion. II - Ignition and extinction phenomena p 72 A86-12414
- Numerical simulation of a turbulent flame stabilized behind a rearward-facing step p 73 A86-22774
- An experimental investigation on flame interaction and the existence of negative flame speeds p 74 A86-22816
- Influence of temperature and hydroxyl concentration on incipient soot formation in premixed flames p 74 A86-29070

- Theory of interactive combustion of counterflow premixed flames p 74 A86-32752
- The behavior of fuel-lean premixed flames in a standard flammability limit tube under controlled gravity conditions [NASA-CR-177132] p 78 A86-28139

PREMIXING

- Evaluation of fuel preparation systems for lean premixing-prevaporizing combustors [ASME PAPER 85-GT-137] p 19 A86-22081
- Combustor flame flashback [NASA-CR-174961] p 183 A86-14727

PREPREGS

- Replacement of MDA with more oxidatively stable diamines in PMR-polyimides p 101 A86-11275
- Fracture characteristics of angleplied laminates fabricated from overaged graphite/epoxy prepreg [NASA-TM-87266] p 70 A86-25417

PRESSING (FORMING)

- Improved consolidation of silicon carbide [NASA-TM-87243] p 104 A86-24836

PRESSURE

- Piezoviscous effects in nonconformal contacts lubricated hydrodynamically [NASA-TM-87141] p 141 A86-21797

PRESSURE DEPENDENCE

- Negative magnetoresistance of pitch-based carbon fibers Temperature and pressure dependence p 99 A86-35702
- Spontaneous ignition delay characteristics of hydrocarbon fuel-air mixtures [NASA-CR-175064] p 29 A86-21545

PRESSURE DISTRIBUTION

- Simultaneous measurements of velocity and pressure fields in subsonic and supersonic flows through image-intensified detection of laser-induced fluorescence [AIAA PAPER 86-0161] p 145 A86-19726

PRESSURE EFFECTS

- Effect of elevated temperature and pressure on sprays from simplex swirl atomizers [ASME PAPER 85-GT-58] p 130 A86-22735
- The effect of oxygen pressure on volatility and morphology of LaB6 single crystal cathodes p 204 A86-28076

- Fast approach for calculating film thicknesses and pressures in elastohydrodynamically lubricated contacts at high loads [ASME PAPER 85-TRIB-42] p 155 A86-43541

PRESSURE GRADIENTS

- Heat transfer and pressure drop performance of a finned-tube heat exchanger proposed for use in the NASA Lewis Altitude Wind Tunnel [NASA-TM-87151] p 138 A86-13677
- A comparison of experimental and theoretical results for leakage, pressure gradients, and rotordynamic coefficients for tapered annular gas seal [NASA-CR-179709] p 162 A86-32742

PRESSURE MEASUREMENT

- Unsteady pressure measurements on a biconvex airfoil in a transonic oscillating cascade [ASME PAPER 85-GT-212] p 3 A86-22731
- A stagnation pressure probe for droplet-laden air flow p 133 A86-39077
- Development of optical diaphragm deflection sensors [NASA-CR-175008] p 203 A86-15113

PRESSURE OSCILLATIONS

- A numerical method of calculating propeller noise including acoustic nonlinear effects p 199 A86-12011

PRESSURE RATIO

- Effect of area ratio on the performance of a 5.5:1 pressure ratio centrifugal impeller [ASME PAPER 86-GT-303] p 8 A86-48315
- Effect of area ratio on the performance of a 5.5:1 pressure ratio centrifugal impeller [NASA-TM-87237] p 10 A86-19290

PRESSURE RECOVERY

- Effect of area ratio on the performance of a 5.5:1 pressure ratio centrifugal impeller [ASME PAPER 86-GT-303] p 8 A86-48315
- Effect of area ratio on the performance of a 5.5:1 pressure ratio centrifugal impeller [NASA-TM-87237] p 10 A86-19290

PRESSURE REDUCTION

- Modeling of zero gravity venting: Studies of two-phase heat transfer under reduced gravity [NASA-CR-179662] p 144 A86-31826

PRESSURE SENSORS

- A stagnation pressure probe for droplet-laden air flow p 133 A86-39077
- Development of optical diaphragm deflection sensors [NASA-CR-175008] p 203 A86-15113

PRESSURE VESSELS

- Initial performance of advanced designs for IPV nickel-hydrogen cells p 179 A86-24800
- Oxygen recombination in individual pressure vessel nickel-hydrogen batteries [NASA-CASE-LEW-13822-1] p 188 A86-25874

PRESTRESSING

- Influence of rotation and pretwist on cantilever fan blade flutter p 17 A86-11686
- Vibration and buckling of rotating, pretwisted, precone beams including Coriolis effects p 168 A86-26910
- Nonlinear bending-torsional vibration and stability of rotating, pretwisted, precone blades including Coriolis effects [NASA-TM-87207] p 175 A86-17789

PRIMITIVE EQUATIONS

- A note on the finite differencing of the linearized primitive equations' lower boundary condition p 191 A86-28963

PROBABILITY THEORY

- Probabilistic finite elements for transient analysis in nonlinear continua p 168 A86-28653
- Efficient algorithms for use in probabilistic finite element analysis p 168 A86-28655
- Probabilistic structural analysis for space propulsion system components p 168 A86-28659
- Reliability of void detection in structural ceramics by use of scanning laser acoustic microscopy p 163 A86-39027

- Probabilistic structural analysis methods for critical SSME propulsion components [AIAA PAPER 86-1188] p 54 A86-40595

- SCARE: A post-processor program to MSC/NASTRAN for the reliability analysis of structural ceramic components [NASA-TM-87188] p 174 A86-14688

PROBLEM SOLVING

- New integration techniques for chemical kinetic rate equations. II - Accuracy comparison [ASME PAPER 85-GT-30] p 75 A86-32958

PRODUCT DEVELOPMENT

- Development program on a cold cathode electron gun [NASA-CR-174792] p 121 A86-14499
- Development and testing of tip devices for horizontal axis wind turbines [NASA-CR-174991] p 185 A86-18774

PROP-FAN TECHNOLOGY

- Dynamic characteristics of an assembly of prop-fan blades [ASME PAPER 85-GT-134] p 21 A86-32956
- Numerical evaluation of propeller noise including nonlinear effects p 23 A86-41726
- Evaluation of propeller/nacelle interactions in the PTA program [AIAA PAPER 86-1552] p 6 A86-42709
- Propeller noise caused by blade tip radial forces [AIAA PAPER 86-1892] p 23 A86-45504
- Preliminary measurement of the noise from the 2/9 scale model of the Large-scale Advanced Propfan (LAP) propeller, SR-7A [NASA-TM-87116] p 199 A86-14006
- Advanced turboprop vibratory characteristics [NASA-CR-174708] p 30 A86-24693
- Evaluation of propfan propulsion applied to general aviation [NASA-CR-175020] p 30 A86-24695
- Large-Scale Advanced Prop-Fan (LAP) pitch change actuator and control design report [NASA-CR-174788] p 31 A86-27282
- Experimental classical flutter results of a composite advanced turboprop model [NASA-TM-88792] p 178 A86-29271
- System design and integration of the large-scale advanced prop-fan [NASA-CR-174789] p 13 A86-31536

PROPAGATION MODES

- Shear fatigue crack growth - A literature survey p 167 A86-24219
- Normal modes in an overmoded circular waveguide coated with lossy material p 119 A86-44078

PROPAGATION VELOCITY

- An experimental investigation on flame interaction and the existence of negative flame speeds p 74 A86-22816

PROPELLANT SPRAYS

- Oxides of nitrogen emissions from the combustion of monodisperse liquid fuel sprays [NASA-CR-176373] p 191 A86-14770

PROPELLANT STORAGE

- LH2 on-orbit storage tank support trunnion design and verification p 53 A86-37054

PROPELLANT TANKS

- Effect of subcooling on the on-orbit pressurization rate of cryogenic propellant tankage [AIAA PAPER 86-1253] p 54 A86-39877

PROPELLANT TESTS

- Compatibility experiments of facilities, materials, and propellants for electrothermal thrusters p 59 A86-17426

PROPELLER BLADES

- Dynamic characteristics of an assembly of prop-fan blades p 21 A86-32956
- [ASME PAPER 85-GT-134] p 21 A86-32956
- Unsteady forces on counter-rotating propeller blades [AIAA PAPER 86-1804] p 22 A86-37827
- Numerical evaluation of propeller noise including nonlinear effects p 23 A86-41726
- Propeller noise caused by blade tip radial forces [AIAA PAPER 86-1892] p 23 A86-45504
- Preliminary results of unsteady blade surface pressure measurements for the SR-3 propeller [AIAA PAPER 86-1893] p 8 A86-49625
- Preliminary measurement of the noise from the 2/9 scale model of the Large-scale Advanced Propfan (LAP) propeller, SR-7A [NASA-TM-87116] p 199 N86-14006
- Preliminary results of unsteady blade surface pressure measurements for the SR-3 propeller [NASA-TM-87352] p 12 N86-27213
- Experimental classical flutter results of a composite advanced turboprop model [NASA-TM-88792] p 178 N86-29271
- Influence of third-degree geometric nonlinearities on the vibration and stability of pretwisted, precone, rotating blades [NASA-TM-87307] p 179 N86-31920

PROPELLER EFFICIENCY

- An experimental investigation of propeller wakes using a laser Doppler velocimeter [AIAA PAPER 86-0080] p 18 A86-19677
- An experimental investigation of reducing advanced turboprop cabin noise by wing shielding [AIAA PAPER 86-1966] p 16 A86-45449
- Evaluation of propfan propulsion applied to general aviation [NASA-CR-175020] p 30 N86-24695
- An experimental investigation of reducing advanced turboprop cabin noise by wing shielding [NASA-TM-87112] p 201 N86-25218
- A supersonic fan equipped variable cycle engine for a Mach 2.7 supersonic transport [NASA-CR-177141] p 32 N86-28946
- Aerodynamic data banks for Clark-Y, NACA 4-digit and NACA 16-series airfoil families [NASA-CR-176883] p 13 N86-30693

PROPELLER FANS

- Advanced turboprop vibratory characteristics [NASA-CR-174708] p 30 N86-24693

PROPELLERS

- Propeller design by optimization [AIAA PAPER 86-0081] p 19 A86-19678
 - Aeroelastic formulations for turbomachines and propellers p 20 A86-24677
 - Parametric effects of CFL number and artificial smoothing on numerical solutions using implicit approximate factorization algorithm [AIAA PAPER 86-1059] p 132 A86-38427
 - Evaluation of propeller/nacelle interactions in the PTA program [AIAA PAPER 86-1552] p 6 A86-42709
 - An approach to the calculation of the pressure field produced by rigid wide chord dual rotation propellers of high solidity in compressible flow [AIAA PAPER 86-0467] p 198 A86-49566
 - Summary of recent NASA propeller research p 25 N86-11158
 - A numerical method of calculating propeller noise including acoustic nonlinear effects p 199 N86-12011
 - Some design philosophy for reducing the community noise of advanced counter-rotation propellers [NASA-TM-87099] p 199 N86-14007
 - Laboratory experiments on active suppression of advanced turboprop noise [NASA-TM-87129] p 199 N86-19125
 - An analysis for the sound field produced by rigid wide chord dual rotation propellers of high solidity in compressible flow [NASA-TM-87178] p 11 N86-21517
 - Analytical determination of propeller performance degradation due to ice accretion [NASA-CR-175092] p 15 N86-23577
 - Experimental and theoretical study of propeller spinner/shank interference [NASA-CR-176954] p 13 N86-29773
- PROPULSION**
- Future directions in aeropropulsion technology p 1 A86-11602
 - Compatibility of grain-stabilized platinum with candidate propellants for resistojets [AIAA PAPER 85-2014] p 51 A86-17835
 - Status of advanced orbital transfer propulsion [IAF PAPER 85-164] p 51 A86-17850
 - Compatibility of grain-stabilized platinum with candidate propellants for resistojets [NASA-TM-87118] p 56 N86-10279

PROPULSION SYSTEM CONFIGURATIONS

- Manrating orbital transfer vehicle propulsion [AIAA PAPER 85-1226] p 50 A86-14429
- NASA electric propulsion technology [AIAA PAPER 85-1999] p 51 A86-17831
- Space Station benefits from ECLS - Propulsion system synergism [AIAA PAPER 86-1407] p 47 A86-42619
- Advanced technology payoffs for future rotorcraft, commuter aircraft, cruise missile, and APU propulsion systems [AIAA PAPER 86-1545] p 16 A86-42704
- Progress in the Lewis Research Center Altitude Wind Tunnel (AWT) Modeling Program [NASA-TM-87194] p 37 N86-18233
- Orbital transfer vehicle engine integration study p 58 N86-17416
- Advanced orbit transfer vehicle propulsion system study [NASA-CR-174843] p 60 N86-24746
- Rail accelerators for space transportation: An experimental investigation [NASA-TP-2571] p 62 N86-28123

PROPULSION SYSTEM PERFORMANCE

- Fiber optics for propulsion control systems [ASME PAPER 84-GT-97] p 17 A86-13054
- Subscale-model and full-scale engine mixed-flow exhaust system performance comparison p 18 A86-14528
- Propeller design by optimization [AIAA PAPER 86-0081] p 19 A86-19678
- Probabilistic structural analysis for space propulsion system components p 188 A86-28659
- Experimental performance of a 1-kilowatt arcjet thruster [AIAA PAPER 85-2033] p 54 A86-37063
- NASA electrothermal auxiliary propulsion technology [AIAA PAPER 86-1703] p 55 A86-42799
- Experimental performance of a 1-kilowatt arcjet thruster [NASA-TM-87131] p 57 N86-10281
- Orbital transfer vehicle engine integration study p 58 N86-17416
- Current wind tunnel capability and planned improvements at Lewis Research Center [NASA-TM-87190] p 37 N86-18329
- Development and application of dynamic simulations of a subsonic wind tunnel [NASA-TM-87211] p 43 N86-18338
- Advanced Gas Turbine (AGT) technology report [NASA-CR-175018] p 158 N86-20808
- Evaluation of propfan propulsion applied to general aviation [NASA-CR-175020] p 30 N86-24695
- NASA electrothermal auxiliary propulsion technology [NASA-TM-87281] p 60 N86-24749
- Aeropropulsion opportunities for the 21st century [NASA-TM-88817] p 34 N86-31585
- Performance characteristics of ring-cusp thrusters with xenon propellant [NASA-TM-87338] p 63 N86-31650
- Structural dynamic measurement practices for turbomachinery at the NASA Lewis Research Center [NASA-TM-88857] p 35 N86-32433
- Advanced instrumentation for aeronautical propulsion research [NASA-TM-88853] p 150 N86-32703

PROPULSIVE EFFICIENCY

- Manrating orbital transfer vehicle propulsion [AIAA PAPER 85-1226] p 50 A86-14429
- Current wind tunnel capability and planned improvements at Lewis Research Center [NASA-TM-87190] p 37 N86-18329
- Aeropropulsion opportunities for the 21st century [NASA-TM-88817] p 34 N86-31585

PROTECTIVE COATINGS

- Ion beam sputter-deposited thin film coatings for protection of spacecraft polymers in low earth orbit [AIAA PAPER 85-0420] p 95 A86-14428
- Performance of thermal barrier coatings in high heat flux environments p 80 A86-16272
- Pretreatment effects on the morphology and properties of aluminum oxide thermally grown on NiCoCrAlY p 97 A86-17495
- Selected fretting-wear-resistant coatings for Ti-6 pct Al-4 pct V alloy p 97 A86-24956
- Turbine Engine Hot Section Technology (HOST) [NASA-CP-2289] p 172 N86-11495
- Oxidation protection coatings for polymers [NASA-CASE-LEW-14072-1] p 102 N86-19458
- Adhesion and wear resistance of materials [NASA-TM-87239] p 158 N86-20809
- Life prediction and constitutive models for engine hot section anisotropic materials program [NASA-CR-174952] p 165 N86-25003

- Oxidation protecting coatings for polymers [NASA-CASE-LEW-14072-3] p 105 N86-26434
- Characterization of the tribological coating composition 77 wt % CaF₂ - 23 wt % Li F fused to IN-750 alloy [NASA-TM-87342] p 105 N86-27452
- Effects of surface chemistry on hot corrosion life [NASA-CR-179471] p 32 N86-28087
- Thermal-fatigue and oxidation resistance of cobalt-modified Udimet 700 alloy [NASA-TP-2591] p 178 N86-28464
- Feasibility study of a discrete bearing/roller drive rotary joint for the space station [NASA-TM-88800] p 161 N86-30206
- Apparatus for producing oxidation protection coatings for polymers [NASA-CASE-LEW-14072-2] p 106 N86-32569

PROTON IRRADIATION

- Performance and temperature dependencies of proton irradiated n/p GaAs and n/p silicon cells [NASA-TM-87136] p 120 N86-12509
- Potential for use of indium phosphide solar cells in the space radiation environment [NASA-TM-87157] p 121 N86-13645

PROTOTYPES

- Theoretical analysis of the electrical aspects of the basic electro-impulse problem in aircraft de-icing applications [NASA-CR-176808] p 17 N86-26330
- High accuracy fuel flowmeter [NASA-CR-174869] p 150 N86-31030

PROVING

- Validation of viscous and inviscid computational methods for turbomachinery components [ASME PAPER 86-GT-42] p 7 A86-48126
- Validation of viscous and inviscid computational methods for turbomachinery components [NASA-TM-87193] p 10 N86-16194
- Near-field testing of the 30 GHz TRW proof-of-concept multibeam antenna [NASA-TM-87357] p 124 N86-27578
- Some design philosophy for reducing the community noise of advanced counter-rotation propellers [NASA-TM-87099] p 199 N86-14007

PULSE DURATION MODULATION

- Resonant power processors. II - Methods of control p 117 A86-14482
- Power electronics for a 1-kilowatt arcjet thruster [AIAA PAPER 86-1507] p 56 A86-49613
- Power electronics for a 1-kilowatt arc jet thruster [NASA-TM-87340] p 61 N86-25409

PULSE MODULATION

- All-fibre sensing loop using pulse-modulated light-emitting diode p 202 A86-11995
- Power conversion distribution system using a resonant high-frequency AC link [NASA-CR-176804] p 123 N86-25694

PUMP IMPELLERS

- Laser velocimeter measurements in shrouded and unshrouded radial flow pump impellers [ASME PAPER 86-GT-129] p 136 A86-48187

PUMP SEALS

- Operating aspects of an oil pumping ring seal [ASME PAPER 85-TRIB-29] p 153 A86-34010
- Performance of oil pumping rings: An analytical and experimental study [NASA-CR-175083] p 144 N86-31000

PUMPS

- LOX/LH₂ vane pump for auxiliary propulsion systems p 58 N86-17397

PYROLYSIS

- A ceramic matrix composite based on polymerization and pyrolysis of ethynylated aromatics p 65 A86-13169
- Shock-tube pyrolysis of chlorinated hydrocarbons - Formation of soot p 75 A86-35126

PYROLYTIC GRAPHITE

- Carbon monoxide production in low energy oxygen ion bombardment of pyrolytic graphite and Kapton surfaces p 76 A86-47078

Q**QUALITY CONTROL**

- High Temperature Polymer Matrix Composites [NASA-CP-2385] p 68 N86-11260
- Review and critical analysis: Rolling-element bearings for system life and reliability [NASA-CR-174710] p 159 N86-24991

QUANTUM MECHANICS

- Reassessment of the theory of stimulated Raman scattering p 150 A86-40662

QUANTUM WELLS

- Cryogenic operation of pseudomorphic AlGaAs/InGaAs single-quantum-well MODFETs p 117 A86-11998

Dc and microwave characteristics of a high current double interface GaAs/InGaAs/AlGaAs pseudomorphic modulation-doped field-effect transistor

p 118 A86-38009

Optical constants of GaAs-AlGaAs superlattices and multiple quantum wells
[NASA-CR-176717]

p 205 N86-23468

QUINOLINE

All-aromatic biphenylene end-capped polyquinoline and polyimide matrix resins

p 100 N86-11267

R

RADAR ABSORBERS

Normal modes in an overmoded circular waveguide coated with lossy material

p 119 A86-44078

RADAR ANTENNAS

Near-field spillover from a subreflector: Theory and experiment

[NASA-TM-88763] p 115 N86-25650

RADIAL FLOW

Three-dimensional inviscid analysis of radial-turbine flow and a limited comparison with experimental data

p 4 A86-28702

Three-dimensional flow field measurements in a radial inflow turbine scroll using LDV

[ASME PAPER 86-GT-122] p 7 A86-48181

Laser velocimeter measurements in shrouded and unshrouded radial flow pump impellers

[ASME PAPER 86-GT-129] p 136 A86-48187

Three-dimensional inviscid analysis of radial turbine flow and a limited comparison with experimental data

[NASA-TM-87091] p 9 N86-10017

Characteristics of an axisymmetric sudden expansion flow

[NASA-CR-176278] p 151 N86-11465

Variable area radial turbine fabrication and test program

[NASA-CR-175091] p 32 N86-28947

RADIANT HEATING

Radiation energy receiver for solar propulsion systems

p 52 A86-18043

RADIATION ABSORPTION

Modeling the effects of wind tunnel wall absorption on the acoustic radiation characteristics of propellers

[NASA-TM-87333] p 201 N86-29630

RADIATION DAMAGE

Radiation damage in high-resistivity silicon solar cells

p 185 N86-17856

Indium phosphide solar cells: status and prospects for use in space

[NASA-TM-87315] p 123 N86-26520

Lithium counterdoped silicon solar cell

[NASA-CASE-LEW-14177-1] p 190 N86-32875

RADIATION DISTRIBUTION

Normal modes in an overmoded circular waveguide coated with lossy material

p 119 A86-44078

RADIATION DOSAGE

Radiation exposure and performance of multiple burn LEO-GEO orbit transfer trajectories

p 43 N86-17417

RADIATION EFFECTS

Potential for use of indium phosphide solar cells in the space radiation environment

[NASA-TM-87157] p 121 N86-13645

RADIATION TOLERANCE

A possible radiation-resistant solar cell geometry using superlattices

p 185 N86-17851

Lithium counterdoped silicon solar cell

[NASA-CASE-LEW-14177-1] p 190 N86-32875

RADIATIVE HEAT TRANSFER

Performance analysis of radiation cooled dc transmission lines for high power space systems

p 117 A86-24811

Methods for heat transfer and temperature field analysis of the insulated diesel phase 2 progress report

[NASA-CR-175072] p 210 N86-24590

Role of fuel chemical properties on combustor radiative heat load

[NASA-CR-177096] p 108 N86-30023

Analysis of the Gas Particle Radiator (GPR)

[NASA-TM-88786] p 63 N86-31652

RADIATIVE TRANSFER

Fundamental studies on a heat driven lamp

[NASA-CR-176381] p 204 N86-15122

RADIO FREQUENCIES

Linearized traveling wave amplifier with hard limiter characteristics

[NASA-CASE-LEW-13981-2] p 122 N86-21742

RADIO FREQUENCY INTERFERENCE

An analysis of bi-directional use of frequencies for satellite communications

[AIAA PAPER 86-0635] p 110 A86-29664

An analysis of bi-directional use of frequencies for satellite communications

[AIAA PAPER 86-0635] p 111 A86-49568

An analysis of bi-directional use of frequencies for satellite communications

[NASA-TM-87226] p 114 N86-18585

Spectrum Orbit Utilization Program documentation: SOUP5 version 3.8 user's manual, volume 1, chapters 1 through 5

[NASA-CR-174889] p 193 N86-27927

RADIO TRANSMISSION

Satellite voice broadcast system study. Volume 1: Executive summary

[NASA-CR-174904] p 115 N86-24878

RADIOGRAPHY

Radiographic detectability limits for seeded voids in sintered silicon carbide and silicon nitride

p 162 A86-31745

Nondestructive characterization of structural ceramics

p 99 A86-37141

Nondestructive techniques for characterizing mechanical properties of structural materials - An overview

[ASME PAPER 86-GT-75] p 163 A86-48143

Probability of detection of internal voids in structural ceramics using microfocus radiography

[NASA-TM-87164] p 164 N86-13749

Nondestructive techniques for characterizing mechanical properties of structural materials: An overview

[NASA-TM-87203] p 164 N86-19636

Ultrasonic characterization of structural ceramics

p 199 N86-22970

Factors that affect reliability of nondestructive detection of flaws in structural ceramics

[NASA-TM-87348] p 166 N86-31912

RAILGUN ACCELERATORS

Characterisation of plasma in a rail gun

p 118 A86-26051

Rail accelerators for space transportation: An experimental investigation

[NASA-TP-2571] p 62 N86-28123

RAMAN SPECTRA

Reassessment of the theory of stimulated Raman scattering

p 150 A86-40662

RANDOM LOADS

Efficient algorithms for use in probabilistic finite element analysis

p 168 A86-28655

Effects of state recovery on creep buckling under variable loading

[NASA-CR-175094] p 212 N86-25310

RANDOM WALK

Grid-free simulation of diffusion using random walk methods

p 196 A86-18521

RANKING

Existence and stability, and discrete BB and rank conditions, for general mixed-hybrid finite elements in elasticity

p 169 A86-34464

RAPID QUENCHING (METALLURGY)

Rapidly solidified NiAl and FeAl

p 84 A86-47263

Undercooled and rapidly quenched Ni-Mo alloys

[NASA-TM-87257] p 90 N86-21659

RARE GASES

Heaterless ignition of inert gas ion thruster hollow cathodes

[AIAA PAPER 85-2008] p 51 A86-17833

RAY TRACING

Parametric study of beam refraction problems across laser anemometer windows

[NASA-TM-87350] p 150 N86-31857

REACTION BONDING

Radiographic detectability limits for seeded voids in sintered silicon carbide and silicon nitride

p 162 A86-31745

REACTION KINETICS

Buoyancy effects on smoldering combustion

[IAF PAPER 85-289] p 72 A86-15805

Theory of homogeneous nucleation - A chemical kinetic view

p 72 A86-19389

Kinetics and mechanism of corrosion of SiC by molten salts

p 97 A86-20992

New integration techniques for chemical kinetic rate equations. II - Accuracy comparison

[ASME PAPER 85-GT-30] p 75 A86-32958

New integration techniques for chemical kinetic rate equations. I - Efficiency comparison

p 75 A86-38090

Fundamental studies of droplet combustion at reduced gravity

p 42 N86-10165

Diffusion flame extinction in slow convective flow under microgravity environment

[NASA-TM-88799] p 144 N86-28378

Physical and numerical sources of computational inefficiency in integration of chemical kinetic rate equations: Etiology, treatment and prognosis

[NASA-TP-2590] p 195 N86-28662

REAL GASES

Real gas effects on the numerical simulation of a hypersonic inlet

p 6 A86-46324

Characterization of real gas properties for space shuttle main engine fuel turbine and performance calculations

[NASA-CR-175068] p 61 N86-27418

REAL TIME OPERATION

Development and testing of tip devices for horizontal axis wind turbines

[NASA-CR-174991] p 185 N86-18774

A real-time simulation evaluation of an advanced detection, isolation and accommodation algorithm for sensor failures in turbine engines

[NASA-TM-87289] p 30 N86-24697

A high-order language for a system of closely coupled processing elements

[NASA-CR-177280] p 193 N86-27930

Hardware configuration for a real-time multiprocessor simulator

[NASA-TM-88802] p 194 N86-28651

REATTACHED FLOW

Triple-velocity products in a channel with a backward-facing step

p 133 A86-41725

Turbulence energy and diffusion transport in a separating and reattaching flow

[AIAA PAPER 86-1724] p 135 A86-42812

RECOIL ATOMS

Calculation of recoil implantation profiles using known range statistics

p 201 A86-11391

RECOMBINATION REACTIONS

A possible radiation-resistant solar cell geometry using superlattices

p 185 N86-17851

Oxygen recombination in individual pressure vessel nickel-hydrogen batteries

[NASA-CASE-LEW-13822-1] p 188 N86-25874

RECORDING HEADS

Effect of crystallographical and geometrical changes of a ferrite head on magnetic signals during the sliding process with magnetic tape

[NASA-TM-87277] p 106 N86-31728

RECTANGULAR WAVEGUIDES

A high frequency analysis of electromagnetic plane wave scattering by perfectly-conducting semi-infinite parallel plate and rectangular waveguides with absorber coated inner walls

[NASA-CR-179759] p 116 N86-32600

REDOX CELLS

Cycling performance of the iron-chromium redox energy storage system

p 180 A86-24849

Negative electrode catalyst for the iron chromium redox energy storage system

[NASA-CASE-LEW-14028-1] p 186 N86-19721

Method and apparatus for rebalancing a REDOX flow cell system

[NASA-CASE-LEW-14127-1] p 122 N86-20680

REDUCED GRAVITY

Effects of buoyancy on gas jet diffusion flames - Experiment and theory

[IAF PAPER 85-288] p 72 A86-15804

NASA Lewis Research Center low-gravity fluid management technology program

p 44 A86-32906

Effect of subcooling on the on-orbit pressurization rate of cryogenic propellant tankage

[AIAA PAPER 86-1253] p 54 A86-39877

Solidification fundamentals

p 39 N86-10090

Transport processes in solution crystal growth

p 39 N86-10107

Free surface phenomena under low- and zero-gravity conditions

p 39 N86-10108

Mass transport phenomena between bubbles and dissolved gases in liquids under reduced gravity conditions

p 39 N86-10110

Light scattering tests of fundamental theories of transport properties in the critical region

p 39 N86-10113

Surface tension induced instabilities in reduced gravity: The Benard problem

p 40 N86-10117

Surface-tension driven convection

p 40 N86-10124

Thermocapillary motion research

p 40 N86-10125

Thermocapillary and diffusocapillary migration of a fluid drop

p 40 N86-10128

Transport processes research

p 40 N86-10129

Experimental and theoretical analysis of chemical vapor deposition with prediction of gravity effects

p 41 N86-10132

Buoyancy effects upon vapor flame and explosion processes

p 41 N86-10161

A fundamental study of smoldering with emphasis on experimental design for zero-g

p 41 N86-10162

Ignition and flame spread above liquid fuel pools

p 41 N86-10163

Flammability limits of gases under low gravity conditions

p 42 N86-10164

Fundamental studies of droplet combustion at reduced gravity

p 42 N86-10165

Microgravity Materials Science Laboratory

p 42 N86-10173

NASA Lewis Research Center low-gravity fluid management technology program [NASA-TM-87145] p 44 N86-11218

Orbital transfer vehicle engine integration study p 58 N86-17416

Liquid-vapor interface locations in a spheroidal container under low gravity [NASA-TM-87147] p 141 N86-23854

Flame propagation and extinction in particle clouds [NASA-CR-177304] p 78 N86-27434

Microgravity Polymers [NASA-CP-2392] p 105 N86-28194

Diffusion flame extinction in slow convective flow under microgravity environment [NASA-TM-88799] p 144 N86-28378

Modeling of zero gravity venting: Studies of two-phase heat transfer under reduced gravity [NASA-CR-179662] p 144 N86-31826

REDUCTION

Life and reliability modeling of bevel gear reductions [ASME PAPER 85-DE-7] p 151 A86-14466

REDUNDANCY

Sensor failure detection for jet engines using analytical redundancy p 18 A86-14226

Robust detection-isolation-accommodation for sensor failures [NASA-CR-174797] p 121 N86-16486

REFLECTOR ANTENNAS

Near-field spillover from a subreflector: Theory and experiment [NASA-TM-88763] p 115 N86-25650

REFLECTORS

Strategy for reflector pattern calculation - Let the computer do the work p 110 A86-39542

A numerical method for approximating antenna surfaces defined by discrete surface points [NASA-TM-87125] p 111 N86-10381

Strategy for reflector pattern calculation: Let the computer do the work [NASA-TM-87137] p 112 N86-12485

Secondary pattern computation of an arbitrarily shaped main reflector [NASA-TM-87162] p 112 N86-14477

Compensation of reflector surface distortions using conjugate field matching [NASA-TM-87198] p 113 N86-16461

REFRACTION

Parametric study of beam refraction problems across laser anemometer windows [NASA-TM-87350] p 150 N86-31857

REFRACTIVITY

A comparison of electronic heterodyne moire deflectometry and electronic heterodyne holographic interferometry for flow measurements [SAE PAPER 851896] p 146 A86-38359

Theoretical study of the transverse dielectric constant of superlattices and their alloys [NASA-CR-177198] p 206 N86-28759

REFRACTORY COATINGS

The low cycle fatigue behavior of a plasma-sprayed coating material [NASA-TM-87318] p 92 N86-31699

REFRACTORY MATERIALS

Sintered alpha silicon carbide ceramics for high temperature structural application - Status review and recent developments [ASME PAPER 85-IGT-127] p 97 A86-23921

High temperature resistant polyimide from tetra ester, diamine, diester and N-arylnadimide [NASA-CASE-LEW-13864-1] p 102 N86-19457

Advanced Gas Turbine (AGT) Technology Development Project annual report [NASA-CR-179485] p 211 N86-33211

REFRACTORY METAL ALLOYS

Thermal aging effects in refractory metal alloys [NASA-TM-87210] p 89 N86-16334

REFRIGERATORS

Photovoltaic-powered vaccine refrigerator: Freezer systems field test results [NASA-TM-86972-REV] p 181 N86-11666

REGENERATIVE FUEL CELLS

Design of a regenerative fuel cell system for Space Station p 53 A86-24857

REGENERATORS

An overview of the Small Engine Component Technology (SECT) studies [NASA-TM-88796] p 34 N86-31587

REINFORCING FIBERS

Rheological, processing, and 371 deg C mechanical properties of Celion 6000/N-phenylnadimide modified PMR composites p 68 N86-11278

Thermal-mechanical fatigue test apparatus for metal matrix composites and joint attachments [NASA-TM-87187] p 88 N86-15378

RELAY SATELLITES

Satellite voice broadcast system study. Volume 1: Executive summary [NASA-CR-174904] p 115 N86-24878

RELIABILITY

Life and reliability modeling of bevel gear reductions [ASME PAPER 85-DE-7] p 151 A86-14466

Reliability of scanning laser acoustic microscopy for detecting internal voids in structural ceramics p 147 A86-46353

Reliability of scanning laser acoustic microscopy for detecting internal voids in structural ceramics [NASA-TM-87222] p 164 N86-16599

Assessment of commercially available and experimental hydrogen electrodes [NASA-TM-87264] p 187 N86-23035

System life and reliability modeling for helicopter transmissions [NASA-CR-3967] p 159 N86-24990

New methodology for shaft design based on life expectancy [NASA-TM-87354] p 161 N86-27661

RELIABILITY ANALYSIS

Reliability and mass analysis of dynamic power conversion systems with parallel of standby redundancy [NASA-TM-87189] p 57 N86-16258

A sensor failure simulator for control system reliability studies [NASA-TM-87271] p 124 N86-31792

Factors that affect reliability of nondestructive detection of flaws in structural ceramics [NASA-TM-87348] p 166 N86-31912

RELIABILITY ENGINEERING

Methods for improving reliability in ceramic turbine rotors [SAE PAPER 851788] p 154 A86-38312

Orbit Transfer Rocket Engine Technology Program: Advanced engine study, task D.1/D.3 [NASA-CR-175084] p 61 N86-26369

RELUCTANCE

Variable-reluctance motor drives for electric vehicle propulsion [NASA-CR-176566] p 122 N86-20700

REMOTE REGIONS

Photovoltaic systems in remote locations: An experience summary [NASA-TM-87106] p 181 N86-10643

REPLACING

Replacement of MDA with more oxidatively stable diamines in PMR-polyimides p 101 N86-11275

REPLENISHMENT

Develop and test fuel cell powered on-site integrated total energy systems: Phase 3, full-scale power plant development [NASA-CR-174948] p 182 N86-12757

Develop and test fuel cell powered on-site integrated total energy systems: Phase 3, full-scale power plant development [NASA-CR-174998] p 182 N86-12758

RESEARCH AND DEVELOPMENT

Spacecraft 2000 [AIAA PAPER 86-0616] p 38 A86-29586

Technology achievements and projections for communication satellites of the future [AIAA PAPER 86-0649] p 109 A86-29611

Stratified charge rotary engine for general aviation [ASME PAPER 86-GT-181] p 24 A86-48231

Fluid management and its role in the future of Space Station [AIAA PAPER 86-2301] p 47 A86-49553

HOST instrumentation R and D program overview p 147 N86-11497

Technology achievements and projections for communication satellites of the future [NASA-TM-87201] p 113 N86-17595

Research and technology, Lewis Research Center [NASA-TM-87179] p 207 N86-21427

Automotive Stirling Engine Development Program [NASA-CR-174749] p 211 N86-28017

RESEARCH FACILITIES

Progress in the Lewis Research Center Altitude Wind Tunnel (AWT) modeling program [AIAA PAPER 86-0757] p 36 A86-24744

Development and application of dynamic simulations of a subsonic wind tunnel [AIAA PAPER 86-0758] p 36 A86-24745

NASA Lewis Research Center low-gravity fluid management technology program p 44 A86-32906

NASA Lewis Research Center low-gravity fluid management technology program [NASA-TM-87145] p 44 N86-11218

RESEARCH MANAGEMENT

Uniform engine testing program phase 7: NASA Lewis Research Center second entry [NASA-TM-87272] p 31 N86-28085

Advanced instrumentation for aeronautical propulsion research [NASA-TM-88853] p 150 N86-32703

RESIDUAL STRENGTH

Estimating the R-curve from residual strength data [NASA-TM-87182] p 175 N86-18750

RESIDUAL STRESS

Finite element analysis of residual stress in plasma-sprayed ceramic p 95 A86-15226

Nonlinear damage analysis: Postulate and evaluation [NASA-CR-168171] p 177 N86-26652

New methodology for shaft design based on life expectancy [NASA-TM-87354] p 161 N86-27661

RESIN MATRIX COMPOSITES

All-aromatic biphenylene end-capped polyquinoline and polyimide matrix resins p 100 N86-11267

Replacement of MDA with more oxidatively stable diamines in PMR-polyimides p 101 N86-11275

The 371 deg C mechanical properties of graphite/polyimide composites [NASA-TM-87122] p 69 N86-12256

Polymer, metal and ceramic matrix composites for advanced aircraft engine applications [NASA-TM-87132] p 87 N86-13407

RESISTANCE

Estimating the R-curve from residual strength data [NASA-TM-87182] p 175 N86-18750

RESISTOJET ENGINES

An analysis of low-thrust, resistojets to boost for the Space Station [AIAA PAPER 85-2042] p 51 A86-14447

Compatibility of grain-stabilized platinum with candidate propellants for resistojets [AIAA PAPER 85-2014] p 51 A86-17835

Resistojet operation with various propellants [AIAA PAPER 85-1158] p 107 A86-37074

A 10,000 hour life multipropellant engine for Space Station applications [AIAA PAPER 86-1403] p 54 A86-42616

Performance and endurance tests of a multipropellant resistojets for space station auxiliary propulsion [AIAA PAPER 86-1435] p 55 A86-42640

NASA electrothermal auxiliary propulsion technology [AIAA PAPER 86-1703] p 55 A86-42799

Compatibility of grain-stabilized platinum with candidate propellants for resistojets [NASA-TM-87118] p 56 N86-10279

Compatibility experiments of facilities, materials, and propellants for electrothermal thrusters p 59 N86-17426

A bibliography of electrothermal thruster technology, 1984 [NASA-TM-86998] p 60 N86-21578

Performance and endurance tests of a multipropellant resistojets for space station auxiliary propulsion [NASA-TM-87278] p 60 N86-24748

NASA electrothermal auxiliary propulsion technology [NASA-TM-87281] p 60 N86-24749

Theoretical study on the effect of the design of small (milli-Newton) thruster jets on molecular contamination for the space station [NASA-CR-177263] p 48 N86-26358

RESONANCE

Designing a 25-kilowatt high frequency series resonant [NASA-CR-176774] p 123 N86-24906

RESONANCE FLUORESCENCE

Fundamental studies on a heat driven lamp [NASA-CR-176381] p 204 N86-15122

RESONANT FREQUENCIES

Resonant power processors. II - Methods of control p 117 A86-14482

The use of an optical data acquisition system for bladed disk vibration analysis p 146 A86-26909

Power conversion distribution system using a resonant high-frequency AC link [NASA-CR-176804] p 123 N86-25694

RETARDANTS

Chemical control of rate and onset temperature of nadimide polymerization p 101 N86-11271

REUSABLE ROCKET ENGINES

Design optimization for a space based, reusable orbit transfer vehicle p 48 N86-17418

REUSABLE SPACECRAFT

Cyclic structural analyses of anisotropic turbine blades for reusable space propulsion systems p 58 N86-17404

Advanced research and technology program for advanced high pressure oxygen-hydrogen rocket propulsion p 58 N86-17405

REVERBERATION

Reverberation effects on directionality and response of stationary monopole and dipole sources in a wind tunnel [ASME PAPER 85-WA/NCA-1] p 197 A86-22747

REVERSED FLOW

A long-life 50 lbf H₂/O₂ thruster for Space Station auxiliary propulsion
[AIAA PAPER 86-1404] p 55 A86-42617

REYNOLDS EQUATION

Contributions to the understanding of large-scale coherent structures in developing free turbulent shear flows
[NASA-CR-176772] p 142 N86-24932

REYNOLDS NUMBER

A review and analysis of boundary layer transition data for turbine application
[ASME PAPER 85-GT-83] p 129 A86-22054
Comparison of calculated and experimental cascade performance for controlled-diffusion compressor stator blading
[NASA-TM-87167] p 27 N86-16219
Mean velocity and turbulence measurements in a 90 deg curved duct with thin inlet boundary layer
[NASA-CR-174811] p 139 N86-16518
Low Reynolds's number boundary layers in a disturbed environment
[NASA-CR-175031] p 139 N86-17665
On the modeling of low-Reynolds-number turbulence
[NASA-CR-3994] p 32 N86-28089

REYNOLDS STRESS

Prediction of heat release effects on a mixing layer
[AIAA PAPER 86-0058] p 129 A86-22676
Computation of turbulent rotating channel flow with an algebraic Reynolds stress model
[AIAA PAPER 86-0214] p 130 A86-22682
A comparison of three algebraic stress closures for combustor flow calculations
[ASME PAPER 85-WA/FE-3] p 132 A86-38388
Triple-velocity products in a channel with a backward-facing step
p 133 A86-41725
Improvement of the second- and third-moment modeling of turbulence: A study of Reynolds-stress closure model
[NASA-CR-176478] p 139 N86-16519
Prediction of heat release effects on a mixing layer
[NASA-CR-175044] p 142 N86-23857
On the modeling of low-Reynolds-number turbulence
[NASA-CR-3994] p 32 N86-28089

RHENIUM

Compatibility experiments of facilities, materials, and propellants for electrothermal thrusters
p 59 N86-17426
Slip casting and extruding shapes of rhenium with metal oxide additives. 1: Feasibility demonstration
[NASA-CR-174970] p 63 N86-31648

RIGID STRUCTURES

Starvation effects on the hydrodynamic lubrication of rigid nonconformal contacts in combined rolling and normal motion
[NASA-TM-87174] p 140 N86-19556

RING STRUCTURES

Analysis of an externally radially crack ring segment subject to three-point radial loading
p 167 A86-20710
Operating aspects of an oil pumping ring seal
[ASME PAPER 85-TRIB-29] p 153 A86-34010

RITZ AVERAGING METHOD

Extensions of the Ritz-Galerkin method for the forced, damped vibrations of structural elements
p 176 N86-21909

ROBUSTNESS (MATHEMATICS)

Application of FDI metrics to detection and isolation of sensor failures in turbine engines
p 21 A86-35400
Robust detection, isolation, and accommodation for sensor failures --- in jet engine control systems
p 21 A86-35402

Robust detection-isolation-accommodation for sensor failures
[NASA-CR-174797] p 121 N86-16486

Robust detection, isolation and accommodation for sensor failures
[NASA-CR-174825] p 33 N86-30732

ROCKET ENGINE CASES

Ultrasonic evaluation of mechanical properties of thick, multilayered, filament wound composites
[NASA-TM-87088] p 163 N86-10561

ROCKET ENGINE DESIGN

A 10,000 hour life multipropellant engine for Space Station applications
[AIAA PAPER 86-1403] p 54 A86-42616
Longitudinal mode combustion instabilities of a high-pressure fuel-rich LOX/RP-1 preburner
p 56 A86-49640
An experimental data base for material selection and design of high-speed, high-pressure, oxygen turbomachinery
p 58 N86-17387
Orbital transfer vehicle engine integration study
[NASA-CR-174842] p 59 N86-20493
Orbit Transfer Rocket Engine Technology Program: Advanced engine study, task D.1/D.3
[NASA-CR-175084] p 61 N86-26369

ROCKET ENGINES

Assessment of a parabolic analysis for axisymmetric internal flows in rocket and turbomachinery ducts
[AIAA PAPER 86-1598] p 134 A86-42739
Characterization of real gas properties for space shuttle main engine fuel turbine and performance calculations
[NASA-CR-175066] p 61 N86-27418
Longitudinal mode combustion instabilities of a high-pressure fuel-rich LOX/RP-1 preburner
p 165 N86-28250
Oxidizer heat exchanger component testing
[NASA-CR-179487] p 62 N86-29901
Test program to provide confidence in liquid oxygen cooling of hydrocarbon fueled rocket thrust chambers
[NASA-TM-88816] p 62 N86-31646
Small centrifugal pumps for low-thrust rocket engines
[NASA-CR-174913] p 162 N86-32741

ROCKET OXIDIZERS

Oxidizer heat exchanger component testing
[NASA-CR-179487] p 62 N86-29901

ROCKET PROPELLANTS

Radiation energy receiver for solar propulsion systems
p 52 A86-18043
Performance and endurance tests of a multipropellant resistojel for space station auxiliary propulsion
[AIAA PAPER 86-1435] p 55 A86-42640
Performance and endurance tests of a multipropellant resistojel for space station auxiliary propulsion
[NASA-TM-87278] p 60 N86-24748

ROCKET THRUST

Heaterless ignition of inert gas ion thruster hollow cathodes
[AIAA PAPER 85-2008] p 51 A86-17833
Thermomechanical design criteria for ceramic-coated surfaces
[NASA-TM-87328] p 143 N86-25726
ROLLER BEARINGS
Lubrication and performance of high-speed rolling-element bearings
p 152 A86-19375
Effect on interference fits on roller bearing fatigue life
[NASA-TM-87165] p 158 N86-19616
Review and critical analysis: Rolling-element bearings for system life and reliability
[NASA-CR-174710] p 159 N86-24991
Feasibility study of a discrete bearing/roller drive rotary joint for the space station
[NASA-TM-88800] p 161 N86-30206

ROLLING CONTACT LOADS

Traction forces at solid-lubricated rolling/sliding contacts
[ASLE PREPRINT 85-AM-4E-2] p 151 A86-11091
Surface fatigue life and failure characteristics of EX-53, CBS 1000M, and AISI 9310 gear materials
[NASA-TP-2513] p 157 N86-12809
Constitutive modelling of lubricants in concentrated contacts at high slide to roll ratios
[NASA-CR-175029] p 158 N86-17748

ROLLING MOMENTS

Starvation effects on the hydrodynamic lubrication of rigid nonconformal contacts in combined rolling and normal motion
[NASA-TM-87174] p 140 N86-19556

ROOM TEMPERATURE

PMR polyimides from solutions containing mixed endcaps
p 100 N86-11263
Replacement of MDA with more oxidatively stable diamines in PMR-polyimides
p 101 N86-11275
Development of optical diaphragm deflection sensors
[NASA-CR-175008] p 203 N86-15113

ROTARY ENGINES

Fluid flow and fuel-air mixing in a motored two-dimensional Wankel rotary engine
[AIAA PAPER 86-1556] p 134 A86-42711
Stratified charge rotary engine for general aviation
[ASME PAPER 86-GT-181] p 24 A86-48231
Stress and deformation modeling of multiple rotary combustion engine trochoid housings
[SAE PAPER 860614] p 156 A86-49624
A two-dimensional numerical study of the flow inside the combustion chambers of a motored rotary engine
[NASA-TM-87212] p 10 N86-19289
Visualization of flows in a motored rotary combustion engine using holographic interferometry
[NASA-TM-88804] p 33 N86-31583

ROTARY STABILITY

Instability in Rotating Machinery
[NASA-CP-2409] p 161 N86-30160
Two-phase flows within systems with ambient pressure
p 161 N86-30167
Influence of third-degree geometric nonlinearities on the vibration and stability of pretwisted, precone, rotating blades
[NASA-TM-87307] p 179 N86-31920

ROTARY WING AIRCRAFT

Rotorcraft propulsion for year 2000 plus
[AIAA PAPER 86-1543] p 23 A86-42702

Small engine technology payoffs for future commuter aircraft
[AIAA PAPER 86-1544] p 23 A86-42703
Variable area radial turbine fabrication and test program
[NASA-CR-175091] p 32 N86-28947

ROTARY WINGS

Vortex generators as a means for increasing rotor performance
p 4 A86-24920
Documentation of ice shapes accreted on the main rotor of a UH-1H helicopter in level flight
[NASA-CR-175088] p 15 N86-22559

ROTATING BODIES

Influence of rotation and pretwist on cantilever fan blade flutter
p 17 A86-11686
Computation of turbulent flows on rotating bodies and ducts
p 135 A86-46307

ROTATING DISKS

Vibrations of blades and bladed disk assemblies; Proceedings of the Tenth Biennial Conference on Mechanical Vibration and Noise, Cincinnati, OH, September 10-13, 1985
p 20 A86-26901
The effect of limiting aerodynamic and structural coupling in models of mistuned bladed disk vibration
p 21 A86-26905
Analytical and experimental investigation of the coupled bladed disk/shaft whirl of a cantilevered turbofan
[ASME PAPER 86-GT-98] p 24 A86-48163

ROTATING ELECTRICAL MACHINES

Rotary transformer design with fixed magnetizing and/or leakage inductances
p 119 A86-40482

ROTATING ENVIRONMENTS

Laser fringe anemometry for aero engine components
[NASA-TM-88798] p 12 N86-28053

ROTATING FLUIDS

Applications of variational principles in computing rotational flows
p 128 A86-20951
Computation of turbulent rotating channel flow with an algebraic Reynolds stress model
[AIAA PAPER 86-0214] p 130 A86-22682

ROTATING SHAFTS

An experimental investigation and some analytical considerations concerning the vaporous/gaseous cavity characteristics of an eccentric shaft seal or bearing
p 130 A86-24463
Analytical and experimental investigation of the coupled bladed disk/shaft whirl of a cantilevered turbofan
[ASME PAPER 86-GT-98] p 24 A86-48163

ROTATING STALLS

A theory of post-stall transients in axial compression systems. II - Application
[ASME PAPER 85-GT-172] p 19 A86-22089

ROTATION

Theoretical modeling of the vapor cavitation in dynamically loaded journal bearings
[ASME PAPER 85-TRIB-51] p 130 A86-24496
Linearization of digital derived rate algorithm for use in linear stability analysis
p 47 A86-35338
Theoretical modeling of the vapor cavitation in dynamically loaded journal bearings
[NASA-TM-87076] p 137 N86-10463
Nonlinear bending-torsional vibration and stability of rotating, pretwisted, precone blades including Coriolis effects
[NASA-TM-87207] p 175 N86-17789
Channel flow modeling of impingement cooling of a rotating turbine blade
[NASA-CR-177206] p 31 N86-27285
Feasibility study of a discrete bearing/roller drive rotary joint for the space station
[NASA-TM-88800] p 161 N86-30206
A comparison of experimental and theoretical results for leakage, pressure gradients, and rotordynamic coefficients for tapered annular gas seal
[NASA-CR-179709] p 162 N86-32742

ROTOR AERODYNAMICS

Stability of limit cycles in frictionally damped and aerodynamically unstable rotor stages
p 18 A86-19196
Theory versus experiment for the rotordynamic coefficients of annular gas seals. I - Test facility and apparatus
[ASME PAPER 85-TRIB-1] p 152 A86-24481
Aeroelastic formulations for turbomachines and propellers
p 20 A86-24677
Operating characteristics of a 0.87 kW-hr flywheel energy storage module
p 152 A86-24884
Vortex generators as a means for increasing rotor performance
p 4 A86-24920
Forced response analysis of an aerodynamically detuned supersonic turbomachine rotor
p 21 A86-26902
Aerodynamic and structural detuning of supersonic turbomachine rotors
p 21 A86-31595
The aerodynamics of rotor blades with ice shapes accreted in hover and in level flight
p 5 A86-35655

Computation of three-dimensional, rotational flow through turbomachinery blade rows for improved aerodynamic design studies
[ASME PAPER 86-GT-26] p 7 A86-48117

Validation of viscous and inviscid computational methods for turbomachinery components
[ASME PAPER 86-GT-42] p 7 A86-48126

Validation of viscous and inviscid computational methods for turbomachinery components
[NASA-TM-87193] p 10 N86-16194

Passive eddy-current damping as a means of vibration control in cryogenic turbomachinery
[NASA-TP-2562] p 44 N86-24722

Application of a personal computer for the uncoupled vibration analysis of wind turbine blade and counterweight assemblies
[NASA-CR-175090] p 188 N86-28511

ROTOR BLADES
Summary of NASA/DOE Aileron-Control Development Program for Wind Turbines
[NASA-TM-88811] p 190 N86-31983

ROTOR BLADES (TURBOMACHINERY)
Ice shapes and the resulting drag increase for a NACA 0012 airfoil
[AIAA PAPER 84-0109] p 14 A86-14427

Calculation of three-dimensional, viscous flow through turbomachinery blade passage by parabolic marching
p 2 A86-20372

Aerodynamic detuning analysis of an unstalled supersonic turbofan cascade
[ASME PAPER 85-GT-192] p 3 A86-22732

The dynamics of a flexible bladed disc on a flexible rotor in a two-rotor system
p 20 A86-25743

Vibration and buckling of rotating, pretwisted, precone beams including Coriolis effects
p 168 A86-26910

Influence of friction dampers on torsional blade flutter
[ASME PAPER 85-GT-170] p 21 A86-32957

Passive control of aerodynamically forced vibrations of supersonic turbomachine rotors by splitter blades
[AIAA PAPER 86-0844] p 22 A86-38892

Forced response analysis of an aerodynamically detuned supersonic turbomachine rotor
[NASA-TM-87093] p 9 N86-10019

Development and testing of tip devices for horizontal axis wind turbines
[NASA-CR-174991] p 185 N86-18774

Mod-2 wind turbine field operations experiment
[NASA-TM-87233] p 186 N86-18775

The predicted effect of aerodynamic detuning on coupled bending-torsion unstalled supersonic flutter
[NASA-TM-87240] p 11 N86-21513

Wind tunnel tests of rotor blade sections with replications of ice formations accreted in hover
[NASA-CR-175089] p 15 N86-22558

A supersonic fan equipped variable cycle engine for a Mach 2.7 supersonic transport
[NASA-CR-177141] p 32 N86-28946

Design and initial testing of a one-bladed 30-meter-diameter rotor on the NASA/DOE mod-O wind turbine
[NASA-TM-88810] p 189 N86-30251

ROTOR SPEED
Methods for improving reliability in ceramic turbine rotors
[SAE PAPER 851788] p 154 A86-38312

Parameter sensitivity in the dynamics of rotor-bearing systems
[ASME PAPER 85-DET-35] p 154 A86-38620

ROTORCRAFT AIRCRAFT
The performance characteristics of simulated ice on rotorcraft airfoils
p 14 A86-35656

Advanced technology payoffs for future rotorcraft, commuter aircraft, cruise missile, and APU propulsion systems
[AIAA PAPER 86-1545] p 16 A86-42704

ROTORS
The use of an optical data acquisition system for bladed disk vibration analysis
p 146 A86-26909

Three-dimensional inviscid analysis of radial-turbine flow and a limited comparison with experimental data
p 4 A86-28702

Linear dynamic coupling in geared rotor systems
[ASME PAPER 85-DET-11] p 154 A86-38617

A mathematical model for the doubly-fed wound rotor generator. II
p 119 A86-39472

Experimental rotordynamic coefficient results for teeth-on-rotor and teeth-on-stator labyrinth gas seals
[ASME PAPER 86-GT-12] p 156 A86-48109

Three-dimensional inviscid analysis of radial turbine flow and a limited comparison with experimental data
[NASA-TM-87091] p 9 N86-10017

Thermodynamic evaluation of transonic compressor rotors using the finite volume approach
[NASA-CR-176428] p 27 N86-16220

Development and testing of tip devices for horizontal axis wind turbines
[NASA-CR-174991] p 185 N86-18774

Unsteady heat transfer and direct comparison to steady-state measurements in a rotor-wake experiment
[NASA-TM-87220] p 142 N86-24934

MOD-5A wind turbine generator program design report: Volume 1: Executive Summary
[NASA-CR-174734] p 188 N86-27708

Laser fringe anemometry for aero engine components
[NASA-TM-88798] p 12 N86-28053

Structural dynamic measurement practices for turbomachinery at the NASA Lewis Research Center
[NASA-TM-88857] p 35 N86-32433

RUBBER COATINGS
Sputtered cadmium oxide as a surface pretreatment for graphite solid lubricant films
[NASA-TM-87300] p 104 N86-25473

RUN TIME (COMPUTERS)
An efficient method for solving the steady Euler equations
[AIAA PAPER 86-1079] p 132 A86-38442

Increasing processor utilization during parallel computation rundown
[NASA-TM-87349] p 192 N86-26914

S

SAFETY
A 20 kiloHertz space station power system
[NASA-TM-88801] p 62 N86-28122

SAFETY FACTORS
Space Station benefits from ECLS - Propulsion system synergism
[AIAA PAPER 86-1407] p 47 A86-42619

SALT SPRAY TESTS
Experimental verification of corrosive vapor deposition rate theory in high velocity burner rigs
[NASA-TM-87287] p 141 N86-22890

SALTS
Estimated heats of fusion of fluoride salt mixtures suitable for thermal energy storage applications
[NASA-TM-87320] p 190 N86-31982

SAMPLES
Apparatus for electrical measurements of thin films from 77 to 1000 K
[NASA-TM-87256] p 148 N86-24959

SANDWICH STRUCTURES
Composite sandwich thermostructural behavior - Computational simulation
[AIAA PAPER 86-0948] p 170 A86-38842

Fiber composite sandwich thermostructural behavior: Computational simulation
[NASA-TM-88787] p 71 N86-31663

SAPPHIRE
The determination of the direction of the optic axis of uniaxial crystalline materials
[NASA-TM-88892] p 148 N86-22915

SATELLITE ANTENNAS
A dual frequency microstrip antenna for Ka band
[NASA-TM-87124] p 111 N86-10380

Bit error rate testing of a proof-of-concept model baseband processor
[NASA-TM-87206] p 46 N86-18343

Computation of the radiation characteristics of a generalized phased array
[NASA-TM-87185] p 114 N86-18586

Spacecraft multibeam antenna system for 30/20 GHz
[NASA-CR-174654] p 116 N86-31760

SATELLITE COMMUNICATION
The baseband processor in future satellite communication systems
p 109 A86-21882

ACTS Experiments Program
[NASA-TM-88820] p 47 N86-31625

SATELLITE DESIGN
Hard ACTS to follow --- NASA Advanced Communications Technology Satellite
p 46 A86-35318

Communications platform payload definition study, executive summary
[NASA-CR-174985] p 49 N86-27407

SATELLITE NETWORKS
Application of intersatellite links to domestic satellite systems
[AIAA PAPER 86-0604] p 44 A86-29580

Impact of the 1985 space World Administrative Radio Conference on frequency/orbit planning and use
[AIAA PAPER 86-0634] p 110 A86-49567

Application of intersatellite links to domestic satellite systems
[NASA-TM-87215] p 46 N86-16249

Satellite voice broadcast system study, volume 2
[NASA-CR-174905] p 115 N86-24877

Impact of the 1985 Space World Administrative Radio Conference on frequency/orbit planning and use
[NASA-TM-87285] p 115 N86-24881

SATELLITE ORBITS
The role of service areas in the optimization of FSS orbital and frequency assignments
[NASA-CR-176488] p 46 N86-18341

Engineering calculations for communications satellite systems planning
[NASA-CR-176555] p 114 N86-19493

SATELLITE SOLAR POWER STATIONS
Space solar cell research: Problems and potential
[NASA-TM-88833] p 125 N86-31793

SATELLITE TRANSMISSION
The role of service areas in the optimization of FSS orbital and frequency assignments
[AIAA PAPER 86-0636] p 45 A86-29599

Simulated performance of the NASA 30/20 GHz test transponder using multi-H phase coded modulation
[AIAA PAPER 86-0717] p 110 A86-29656

On the effectiveness of onboard processing
[AIAA PAPER 86-0721] p 45 A86-29659

Hard ACTS to follow --- NASA Advanced Communications Technology Satellite
p 46 A86-35318

Satellite voice broadcast system study, Volume 1: Executive summary
[NASA-CR-174904] p 115 N86-24878

Communications platform payload definition study
[NASA-CR-174986] p 49 N86-27402

Spectrum Orbit Utilization Program documentation: SOUP5 version 3.8 user's manual, volume 1, chapters 1 through 5
[NASA-CR-174889] p 193 N86-27927

SCALE (CORROSION)
Current viewpoints on oxide adherence mechanisms
[NASA-TM-87168] p 87 N86-13409

The evolution and growth of Al₂O₃ scales on beta-NiAl
[NASA-CR-175097] p 92 N86-27444

SCALE MODELS
Preliminary measurement of the noise from the 2/9 scale model of the Large-scale Advanced Propfan (LAP) propeller, SR-7A
[NASA-TM-87116] p 199 N86-14006

SCALING LAWS
Scaling attenuation data characterizes changes in material microstructure
p 197 A86-26542

Ignition and flame spread above liquid fuel pools
p 41 N86-10163

SCANNING
Optimized three-dimensional lenses for wide-angle scanning
p 109 A86-19184

SCATTERING
Ultrasonic evaluation of mechanical properties of thick, multilayered, filament wound composites
[NASA-TM-87088] p 163 N86-10561

SCATTERING CROSS SECTIONS
Characteristics of an axisymmetric sudden expansion flow
[NASA-CR-176278] p 151 N86-11465

SCAVENGING
Lightweight two-stroke cycle aircraft diesel engine technology enablement program, volume 1
[NASA-CR-174923-VOL-1] p 26 N86-13328

Lightweight two-stroke cycle aircraft diesel engine technology enablement program, volume 2
[NASA-CR-174923-VOL-2] p 26 N86-13329

Lightweight two-stroke cycle aircraft diesel engine technology enablement program, volume 3
[NASA-CR-174923-VOL-3] p 26 N86-13330

SCHLIEREN PHOTOGRAPHY
Optical elements formed by compressed gases: Analysis and potential applications
[NASA-TP-2555] p 203 N86-22390

Advanced optical measuring systems for measuring the properties of fluids and structures
[NASA-TM-88829] p 150 N86-31859

SCINTILLATION
Unsteady pressure measurements on a biconvex airfoil in a transonic oscillating cascade
[ASME PAPER 85-GT-212] p 3 A86-22731

SCORING
An investigation of the transient thermal analysis of spur gears
[ASME PAPER 84-DET-92] p 155 A86-40683

SEALS (STOPPERS)
Ribon-burner simulation of T-700 turbine shroud for ceramic-lined seals research
p 18 A86-15225

Experimental study of ceramic-coated tip seals for turbojet engines
p 152 A86-15227

Experimental stiffness of tapered bore seals
[ASME PAPER 85-DET-12] p 152 A86-22748

- Theory versus experiment for the rotordynamic coefficients of annular gas seals. I - Test facility and apparatus
[ASME PAPER 85-TRIB-1] p 152 A86-24481
Inelastic high-temperature thermomechanical response of ceramic coated gas turbine seals p 169 A86-37799
Dynamic response of film thickness in spiral-groove face seals
[NASA-TP-2544] p 27 N86-15313
Advanced seals for Liquid Oxygen (LOX) turbopumps p 157 N86-17408
Experimental assessment of advanced Stirling component concepts p 210 N86-25302
[NASA-CR-174994]
Sliding seal materials for adiabatic engines, phase 2 [NASA-TM-179475] p 105 N86-29042
Thermal stress minimized, two component, turbine shroud seal
[NASA-CASE-LEW-14212-1] p 162 N86-32740
A comparison of experimental and theoretical results for leakage, pressure gradients, and rotordynamic coefficients for tapered annular gas seal
[NASA-CR-179709] p 162 N86-32742
- SECONDARY EMISSION**
Textured carbon on copper: A novel surface with extremely low secondary electron emission characteristics
[NASA-TP-2543] p 101 N86-15394
Textured carbon surfaces on copper by sputtering
[NASA-CASE-LEW-14130-1] p 109 N86-32587
Secondary-electron-emission losses in multistage depressed collectors and traveling-wave-tube efficiency improvements with carbon collector electrode surfaces
[NASA-TP-2622] p 125 N86-32629
- SECONDARY FLOW**
A new approach for solving the three-dimensional steady Euler equations. I - General theory p 133 A86-41242
Flow visualization of secondary flows in three curve ducts
[ASME PAPER 86-GT-166] p 136 A86-48218
- SELF SEALING**
Experimental stiffness of tapered bore seals
[ASME PAPER 85-DET-12] p 152 A86-22748
- SEMICONDUCTING FILMS**
Growth and characterization of epitaxial SrF₂ on InP(100) p 205 A86-47076
Diamondlike carbon films on semiconductors for insulated-gate technology p 120 A86-47077
Carbon films grown from plasma on III-V semiconductors p 205 N86-12135
- SEMICONDUCTOR DEVICES**
Fibre-optic thermometer using semiconductor-etalon sensor p 146 A86-32046
A new very high voltage semiconductor switch p 119 A86-40449
Analysis of optically controlled microwave/millimeter wave device structures
[NASA-TM-87246] p 123 N86-24907
Auger electron spectroscopy, secondary ion mass spectroscopy and optical characterization of a-C-H and BN films
[NASA-TM-87258] p 206 N86-25268
- SEMICONDUCTOR DIODES**
Technology for satellite power conversion
[NASA-CR-176777] p 187 N86-25042
- SEMICONDUCTOR PLASMAS**
The effect of processing conditions on the GaAs/plasma-grown insulator interface p 204 A86-18567
- SEMICONDUCTORS (MATERIALS)**
Optical techniques to feed and control GaAs MMIC modules for phased array antenna applications
[AIAA PAPER 86-0687] p 110 A86-29638
Surface modification strategies for (100)3C-SiC p 76 A86-47083
Energy stability of thermocapillary convection in models of the float zone process p 40 N86-10123
Ellipsometric and optical study of some uncommon insulator films on 3-5 semiconductors
[NASA-TM-87135] p 205 N86-12134
Optical techniques to feed and control GaAs MMIC modules for phased array antenna applications
[NASA-TM-87218] p 113 N86-16458
- SENSITIVITY**
RE-1000 free-piston Stirling engine update p 153 A86-24890
Radiographic detectability limits for seeded voids in sintered silicon carbide and silicon nitride p 162 A86-31745
RE-1000 free-piston Stirling engine update
[NASA-TM-87126] p 182 N86-11668
- SENSORS**
Fiber optics for propulsion control systems
[ASME PAPER 84-GT-97] p 17 A86-13054
- Application of FDI metrics to detection and isolation of sensor failures in turbine engines p 21 A86-35400
Robust detection, isolation, and accommodation for sensor failures --- in jet engine control systems p 21 A86-35402
A sensor failure simulator for control system reliability studies
[NASA-TM-87271] p 124 N86-31792
- SEPARATED FLOW**
Effect of free stream turbulence on flow separation p 125 A86-11676
Low Reynolds number separation bubble research at UTRC p 126 A86-16311
Applications of variational principles in computing rotational flows p 128 A86-20951
Spray atomization and combustion
[AIAA PAPER 86-0136] p 131 A86-26606
Prediction of the structure of fuel sprays in gas turbine combustors
[AIAA PAPER 86-0450] p 20 A86-26636
Triple-velocity products in a channel with a backward-facing step p 133 A86-41725
A numerical analysis applied to high angle of attack three-dimensional inlets
[AIAA PAPER 86-1527] p 6 A86-42780
Turbulence energy and diffusion transport in a separating and reattaching flow
[AIAA PAPER 86-1724] p 135 A86-42812
Application of a computational model for vortex generators in subsonic internal flows
[AIAA PAPER 86-1458] p 8 A86-49612
Prediction of the structure of fuel sprays in gas turbine combustors
[NASA-CR-175028] p 27 N86-16218
Vacuum chamber pressure effects on thrust measurements p 59 N86-17425
A numerical analysis applied to high angle of attack three-dimensional inlets
[NASA-TM-87298] p 11 N86-24658
Application of a computational model for vortex generators in subsonic internal flows
[NASA-TM-87327] p 143 N86-26545
- SEPARATION**
Current viewpoints on oxide adherence mechanisms
[NASA-TM-87168] p 87 N86-13409
- SEPARATORS**
Nickel-hydrogen separator development
[NASA-TM-87332] p 188 N86-26677
- SERVICE LIFE**
Design principles for nickel-hydrogen cells and batteries p 179 A86-24799
Life cycle test results of a bipolar nickel hydrogen battery p 180 A86-24824
Long-term stability and properties of zirconia ceramics for heavy duty diesel engine components
[NASA-CR-174943] p 209 N86-17224
Long life nickel electrodes for a nickel-hydrogen cell: Cycle life tests
[NASA-CR-174815] p 188 N86-25046
New methodology for shaft design based on life expectancy
[NASA-TM-87354] p 161 N86-27661
Micromechanisms of thermomechanical fatigue: A comparison with isothermal fatigue
[NASA-TM-87331] p 92 N86-28164
The noncavitating performance and life of a small vane-type positive displacement pump in liquid hydrogen
[NASA-TM-87347] p 63 N86-31651
A mathematical approach for evaluating nickel-hydrogen cells
[NASA-TM-88803] p 78 N86-31680
- SHAFTS (MACHINE ELEMENTS)**
LH2 on-orbit storage tank support trunnion design and verification p 53 A86-37054
Experimental assessment of advanced Stirling component concepts
[NASA-CR-174994] p 210 N86-25302
New methodology for shaft design based on life expectancy
[NASA-TM-87354] p 161 N86-27661
Dynamic loading on parallel shaft gears
[NASA-CR-179473] p 161 N86-28433
Structural dynamic measurement practices for turbomachinery at the NASA Lewis Research Center
[NASA-TM-88857] p 35 N86-32433
- SHAPES**
Documentation of ice shapes accreted on the main rotor of a UH-1H helicopter in level flight
[NASA-CR-175088] p 15 N86-22559
- SHEAR FLOW**
Finite-amplitude steady waves in plane viscous shear flows
[AD-A165461] p 127 A86-19419
Steady inviscid three-dimensional flows p 128 A86-20952
- Free shear flows - Organized structures and effects of excitation
[AIAA PAPER 86-0235] p 131 A86-26614
Influence of large-scale motion on turbulent transport for confined coaxial jets. Volume 2: Navier-Stokes calculations of swirling and nonswirling confined coaxial jets
[NASA-CR-175036] p 28 N86-20390
Contributions to the understanding of large-scale coherent structures in developing free turbulent shear flows
[NASA-CR-176772] p 142 N86-24932
- SHEAR LAYERS**
Numerical simulation of unsteady flow in an axisymmetric shear layer
[AIAA PAPER 86-0202] p 127 A86-19748
Entrainment region phenomena for a large plane shear layer p 132 A86-30211
Triple-velocity products in a channel with a backward-facing step p 133 A86-41725
Influence of large-scale motion on turbulent transport for confined coaxial jets. Volume 2: Navier-Stokes calculations of swirling and nonswirling confined coaxial jets
[NASA-CR-175036] p 28 N86-20390
Influence of large-scale motion on turbulent transport for confined coaxial jets. Volume 1: Analytical analysis of the experimental data using conditional sampling
[NASA-CR-175035] p 29 N86-20395
Shear layer excitation, experiment versus theory
[NASA-CR-176604] p 140 N86-20722
- SHEAR PROPERTIES**
Constitutive modelling of lubricants in concentrated contacts at high slide to roll ratios
[NASA-CR-175029] p 158 N86-17748
Fiber composite sandwich thermostructural behavior: Computational simulation
[NASA-TM-88787] p 71 N86-31663
- SHEAR STRENGTH**
Graphite/PMR polyimide composites with improved toughness p 66 A86-21731
Ultrasonic evaluation of mechanical properties of thick, multilayered, filament wound composites
[NASA-TM-87088] p 163 N86-10561
Replacement of MDA with more oxidatively stable diamines in PMR-polyimides p 101 N86-11275
The 371 deg C mechanical properties of graphite/polyimide composites
[NASA-TM-87122] p 69 N86-12256
Specimen geometry effects on graphite/PMR-15 composites during thermo-oxidative aging
[NASA-TM-87204] p 69 N86-17477
- SHEAR STRESS**
Shear fatigue crack growth - A literature survey p 167 A86-24219
Effect on interference fits on roller bearing fatigue life
[NASA-TM-87185] p 158 N86-19618
Simplified composite micromechanics for predicting microstresses
[NASA-TM-87295] p 70 N86-24759
- SHELLS (STRUCTURAL FORMS)**
Joint research effort on vibrations of twisted plates, phase 1: Final results
[NASA-RP-1150] p 172 N86-10579
- SHIELDING**
An experimental investigation of reducing advanced turboprop cabin noise by wing shielding
[AIAA PAPER 86-1966] p 16 A86-45449
An experimental investigation of reducing advanced turboprop cabin noise by wing shielding
[NASA-TM-87112] p 201 N86-25218
- SHIPS**
Preliminary evaluation of a compound cycle engine for shipboard gensets
[NASA-CR-178451] p 160 N86-26629
- SHOCK TUBES**
Shock-tube pyrolysis of chlorinated hydrocarbons - Formation of soot p 75 A86-35126
Relaminarization of the boundary layer over a flat plate in shock tube experiments
[AIAA PAPER 86-1238] p 133 A86-39865
Methane oxidation behind reflected shock waves: Ignition delay times measured by pressure and flame band emission
[NASA-TM-87268] p 77 N86-21635
- SHOCK WAVE ATTENUATION**
A numerical model of acoustic choking. II - Shocked solutions p 197 A86-20795
- SHOCK WAVE INTERACTION**
Relaminarization of the boundary layer over a flat plate in shock tube experiments
[AIAA PAPER 86-1238] p 133 A86-39865
- SHOCK WAVES**
The effects of strong shock loading on coupled bending-torsion flutter of tuned and mistuned cascades p 20 A86-26893

Thermodynamic evaluation of transonic compressor rotors using the finite volume approach
[NASA-CR-176428] p 27 N86-16220

SHORT TAKEOFF AIRCRAFT
Velocity and temperature decay characteristics of inverted-profile jets
[AIAA PAPER 86-0312] p 2 A86-22693
The STOL performance of a two-engine, USB powered-lift aircraft with cross-shafted fans
[SAE PAPER 851839] p 16 A86-38336
Velocity and temperature decay characteristics of inverted-profile jets
[NASA-TM-87159] p 9 N86-14223
In-flight measurements of wing ice shapes and wing section drag increases caused by natural icing conditions
[NASA-TM-87301] p 12 N86-24667

SHROUDED NOZZLES
Variable area radial turbine fabrication and test program
[NASA-CR-175091] p 32 N86-28947

SHROUDED TURBINES
Ribon-burner simulation of T-700 turbine shroud for ceramic-lined seals research p 18 A86-15225
Vibration characteristics of mistuned shrouded blade assemblies
[ASME PAPER 85-GT-115] p 19 A86-22068
Thermal stress minimized, two component, turbine shroud seal
[NASA-CASE-LEW-14212-1] p 162 N86-32740

SHROUDS
Thermal stress minimized, two component, turbine shroud seal
[NASA-CASE-LEW-14212-1] p 162 N86-32740

SIDELobe REDUCTION
Adaptive antenna arrays for weak interfering signals --- in satellite communication p 45 A86-34591

SIGNAL ENCODING
Error-source effects in a high-accuracy optical finite-element processor p 192 A86-31571

SIGNAL PROCESSING
Power conversion distribution system using a resonant high-frequency AC link
[NASA-CR-176804] p 123 N86-25694
Effect of crystallographical and geometrical changes of a ferrite head on magnetic signals during the sliding process with magnetic tape
[NASA-TM-87277] p 106 N86-31728

SIGNAL TO NOISE RATIOS
Adaptive antenna arrays for weak interfering signals --- in satellite communication p 45 A86-34591

SILICON
Properties of silicon suspensions and slip-cast bodies p 95 A86-15238
Minority-carrier mobility anomalies in low-resistivity silicon solar cells p 181 A86-49215
Surface tension induced instabilities in reduced gravity: The Benard problem p 40 N86-10117
Potential for use of indium phosphide solar cells in the space radiation environment
[NASA-TM-87157] p 121 N86-13645
Development of optical diaphragm deflection sensors
[NASA-CR-175008] p 203 N86-15113
Technology for satellite power conversion
[NASA-CR-176777] p 187 N86-25042
Indium phosphide solar cells: status and prospects for use in space
[NASA-TM-87315] p 123 N86-26520
Double-injection, deep-impurity switch development
[NASA-CR-174936] p 124 N86-30073

SILICON ALLOYS
Fatigue crack layer propagation in silicon-iron
[NASA-CR-175115] p 177 N86-25851

SILICON CARBIDES
Densification and properties of alpha-silicon carbide p 94 A86-12416
Fundamental tribological properties of ceramics p 95 A86-15230
Comparison of the contact stress and friction behavior of SiC and ZrO₂ materials p 95 A86-15237
Parametric evaluation of ball milling of SiC in water p 96 A86-15240
Kinetics and mechanism of corrosion of SiC by molten salts p 97 A86-20992
Creep of chemically vapour deposited SiC fibres p 66 A86-21486
Sintered alpha silicon carbide ceramics for high temperature structural application - Status review and recent developments
[ASME PAPER 85-IGT-127] p 97 A86-23921
Radiographic detectability limits for seeded voids in sintered silicon carbide and silicon nitride p 162 A86-31745
Burner rig corrosion of SiC at 1000 C p 99 A86-36328

Nondestructive characterization of structural ceramics p 99 A86-37141
Reliability of void detection in structural ceramics by use of scanning laser acoustic microscopy p 163 A86-39027
Dry etching of beta-SiC in CF₄ and CF₄ + O₂ mixtures p 76 A86-47069
Surface modification strategies for (100)3C-SiC p 76 A86-47083
The beta-SiC(100) surface studied by low energy electron diffraction, Auger electron spectroscopy, and electron energy loss spectra p 77 A86-49864
Molten salt corrosion of SiC: Pitting mechanism
[NASA-TM-87143] p 101 N86-12310
Ultrasonic characterization of structural ceramics p 199 N86-22970
Improved consolidation of silicon carbide
[NASA-TM-87243] p 104 N86-24836
Compensation in epitaxial cubic SiC films
[NASA-TM-87269] p 206 N86-25267
Carbon-rich ceramic composites from ethynyl aromatic precursors p 71 N86-29908
Factors that affect reliability of nondestructive detection of flaws in structural ceramics p 166 N86-31912
[NASA-TM-87348]

SILICON COMPOUNDS
Effect of argon and hydrogen on deposition of silicon from tetrachlorosilane in cold plasmas
[NASA-TM-87219] p 65 N86-17472

SILICON NITRIDES
Factors influencing the ball milling of Si₃N₄ in water p 95 A86-15239
Radiographic detectability limits for seeded voids in sintered silicon carbide and silicon nitride p 162 A86-31745
Effect of grain-boundary crystallization on the high-temperature strength of silicon nitride p 98 A86-33495
Strength and microstructure of Si₃N₄ sintered with ZrO₂ additions p 99 A86-36330
Nondestructive characterization of structural ceramics p 99 A86-37141
Processing study of injection molding of silicon nitride for engine applications
[SAE PAPER 851787] p 154 A86-38311
Reliability of void detection in structural ceramics by use of scanning laser acoustic microscopy p 163 A86-39027
Fractured toughness of Si₃N₄ measured with short bar chevron-notched specimens
[NASA-TM-87153] p 101 N86-13495
Phenomenological study of the behavior of some silica formers in a high velocity jet fuel burner
[NASA-TM-87127] p 157 N86-14613
Ultrasonic characterization of structural ceramics p 199 N86-22970
Particle size reduction of Si₃N₄ with Si₃N₄ milling hardware
[NASA-TM-86864-REV] p 104 N86-24839
Correlation of processing and sintering variables with the strength and radiography of silicon nitride
[NASA-TM-87251] p 106 N86-31729
Factors that affect reliability of nondestructive detection of flaws in structural ceramics p 166 N86-31912
[NASA-TM-87348]
Quantitative void characterization in structural ceramics using scanning laser acoustic microscopy p 166 N86-31913
[NASA-TM-88797]

SILOXANES
Organosiloxane working fluids for the liquid droplet radiator
[NASA-CR-175033] p 102 N86-16381

SIMULATION
Simulation of lubricating behavior of a thioether liquid lubricant by an electrochemical method p 97 A86-20437
Chemical control of rate and onset temperature of nadimide polymerization p 101 N86-11271
Current wind tunnel capability and planned improvements at Lewis Research Center
[NASA-TM-87190] p 37 N86-18329

SIMULATORS
HOST liner cyclic facilities p 173 N86-11519

SINGLE CRYSTALS
The influence of cobalt, tantalum, and tungsten on the microstructure of single crystal nickel-base superalloys p 79 A86-12995
The influence of cobalt, tantalum, and tungsten on the elevated temperature mechanical properties of single crystal nickel-base superalloys p 79 A86-12996
The tensile and fatigue deformation structures in a single crystal Ni-base superalloy p 83 A86-35697
Negative magnetoresistance of pitch-based carbon fibers Temperature and pressure dependence p 99 A86-35702

The cyclic stress-strain behavior of a nickel-base superalloy at 650 C p 83 A86-45715
Dry etching of beta-SiC in CF₄ and CF₄ + O₂ mixtures p 76 A86-47069
Orientation and temperature dependence of some mechanical properties of the single-crystal nickel-base superalloy Rene N4. I - Tensile behavior p 86 A86-50321
Orientation and temperature dependence of some mechanical properties of the single-crystal nickel-base superalloy Rene N4. III - Tension-compression anisotropy p 86 A86-50323
Creep-fatigue behavior of NiCoCrAlY coated PWA 1480 superalloy single crystals
[NASA-TM-87110] p 86 N86-10311
Anisotropic constitutive model for nickel base single crystal alloys: Development and finite element implementation
[NASA-CR-175015] p 176 N86-21952
Low-cost single-crystal turbine blades, volume 2
[NASA-CR-174652] p 29 N86-23598
Abrasion and deformed layer formation of manganese-zinc ferrite in sliding contact with lapping tapes p 104 N86-24838
Life prediction and constitutive models for engine hot section anisotropic materials program
[NASA-CR-174952] p 165 N86-25003
Effects of a high mean stress on the high cycle fatigue life of PWA 1480 and correlation of data by linear elastic fracture mechanics p 177 N86-27689
[NASA-CR-175057]
Microstructure-property relationships in directionally solidified single crystal nickel-base superalloys
[NASA-TM-88788] p 93 N86-31700

SINTERING
Densification and properties of alpha-silicon carbide p 94 A86-12416
Structure and grain coarsening during the sintering of alumina p 98 A86-26341
Strength and microstructure of Si₃N₄ sintered with ZrO₂ additions p 99 A86-36330
Reliability of void detection in structural ceramics by use of scanning laser acoustic microscopy p 163 A86-39027
Molten salt corrosion of SiC: Pitting mechanism
[NASA-TM-87143] p 101 N86-12310
Probability of detection of internal voids in structural ceramics using microfocus radiography p 164 N86-13749
[NASA-TM-87164]
Improved consolidation of silicon carbide
[NASA-TM-87243] p 104 N86-24836
Slip casting and extruding shapes of rhenium with metal oxide additives. 1: Feasibility demonstration
[NASA-CR-174970] p 63 N86-31648
Correlation of processing and sintering variables with the strength and radiography of silicon nitride
[NASA-TM-87251] p 106 N86-31729

SIZE DETERMINATION
Quantitative void characterization in structural ceramics using scanning laser acoustic microscopy
[NASA-TM-88797] p 166 N86-31913

SIZE DISTRIBUTION
Experimental study of the spray characteristics of a research airblast atomizer
[ASME PAPER 85-GT-229] p 129 A86-22125
Measurements in liquid fuel sprays
[NASA-CR-177088] p 144 N86-30960
Determination of grain size distribution function using two-dimensional Fourier transforms of tone pulse encoded images
[NASA-TM-88790] p 166 N86-31065

SKIN FRICTION
Recent skin friction techniques for compressible flows
[AIAA PAPER 86-1099] p 147 A86-38460

SLIDING CONTACT
Traction forces at solid-lubricated rolling/sliding contacts
[ASLE PREPRINT 85-AM-4E-2] p 151 A86-11091
Comparison of the contact stress and friction behavior of SiC and ZrO₂ materials p 95 A86-15237

SLIDING FRICTION
Comparison of the contact stress and friction behavior of SiC and ZrO₂ materials p 95 A86-15237
Mechanical-contact-induced transformation from the amorphous to the partially crystalline state in metallic glass p 80 A86-16257
Interaction of sulfuric acid corrosion and mechanical wear of iron p 81 A86-20436
Selected fretting-wear-resistant coatings for Ti-6 pct Al-4 pct V alloy p 97 A86-24956
Constitutive modelling of lubricants in concentrated contacts at high slide to roll ratios
[NASA-CR-175029] p 158 N86-17748

- Analysis of the transient behavior of rubbing components
[NASA-CR-176546] p 102 N86-19464
- Sliding seal materials for adiabatic engines, phase 2
[NASA-CR-179475] p 105 N86-29042
- SLIP CASTING**
- Properties of silicon suspensions and slip-cast bodies
p 95 A86-15238
- Slip casting and extruding shapes of rhenium with metal oxide additives. 1: Feasibility demonstration
[NASA-CR-174970] p 63 N86-31648
- SLOTTED WIND TUNNELS**
- Numerical study of three-dimensional turbulent flow interactions between blockage models and wind tunnels including longitudinally slotted test sections
[AIAA PAPER 85-5017] p 1 A86-11065
- SMOG**
- Research and development of neat alcohol fuel usage in automobiles
[NASA-CR-174813] p 108 N86-27460
- SODIUM**
- Experimental verification of corrosive vapor deposition rate theory in high velocity burner rigs
[NASA-TM-87287] p 141 N86-22890
- SODIUM CARBONATES**
- Kinetics and mechanism of corrosion of SiC by molten salts
p 97 A86-20992
- SODIUM FLUORIDES**
- Estimated heats of fusion of fluoride salt mixtures suitable for thermal energy storage applications
[NASA-TM-87320] p 190 N86-31982
- SODIUM SILICATES**
- Molten salt corrosion of SiC: Pitting mechanism
[NASA-TM-87143] p 101 N86-12310
- SODIUM SULFATES**
- Kinetics and mechanism of corrosion of SiC by molten salts
p 97 A86-20992
- Na₂SO₄ induced corrosion of nickel at high temperature
p 83 A86-37073
- Mechanism of Na₂SO₄-induced corrosion of molybdenum containing nickel-base superalloys at high temperatures. I - Corrosion in atmospheres containing O₂ only. II - Corrosion in O₂ + SO₂ atmospheres
p 83 A86-37238
- SODIUM SULFUR BATTERIES**
- Design considerations for advanced battery concepts
[AIAA PAPER 86-1164] p 181 A86-40579
- Design considerations for advanced battery concepts
[NASA-TM-87319] p 190 N86-31981
- SOFTWARE ENGINEERING**
- Programmable, automated transistor test system
[NASA-TP-2554] p 123 N86-21755
- Spectrum orbit utilization program technical manual SOUP5 Version 3.8
[NASA-CR-174944] p 116 N86-26489
- Integrated research in constitutive modelling at elevated temperatures, part 1
[NASA-CR-177237] p 179 N86-30227
- SOLAR ARRAYS**
- Current collection from the space plasma through defects in solar array insulation
p 52 A86-18042
- Threshold determining mechanisms for discharges in high voltage solar arrays
[AIAA PAPER 86-0364] p 52 A86-19834
- Circuit transients due to negative bias arcs-II --- on solar cell power systems in low earth orbit
[AIAA PAPER 86-0366] p 52 A86-19835
- 10 kW solar array switching unit performance test results
p 118 A86-24844
- The role of unneutralized surface ions in negative potential arcing
p 118 A86-25525
- Space Photovoltaic Research and Technology 1985: High Efficiency, Space Environment, and Array Technology
[NASA-CP-2408] p 184 N86-17839
- Indium phosphide solar cells: status and prospects for use in space
[NASA-TM-87315] p 123 N86-26520
- SOLAR CELLS**
- The effect of a defective BSF layer on solar cell open circuit voltage --- Back Surface Field
p 179 A86-12673
- Circuit transients due to negative bias arcs-II --- on solar cell power systems in low earth orbit
[AIAA PAPER 86-0366] p 52 A86-19835
- Space Station Power System Advanced Development
p 52 A86-24778
- Voltage-controlling mechanisms in low-resistivity silicon solar cells - A unified approach
p 120 A86-45195
- Minority-carrier mobility anomalies in low-resistivity silicon solar cells
p 181 A86-49215
- A 25.5 percent AMO gallium arsenide grating solar cell
[NASA-TM-87134] p 182 N86-11671
- Performance and temperature dependencies of proton irradiated n/p GaAs and n/p silicon cells
[NASA-TM-87136] p 120 N86-12509
- Potential for use of indium phosphide solar cells in the space radiation environment
[NASA-TM-87157] p 121 N86-13645
- Development of the VOLT-A shuttle experiment
[NASA-TM-87169] p 212 N86-14110
- Space Photovoltaic Research and Technology 1985: High Efficiency, Space Environment, and Array Technology
[NASA-CP-2408] p 184 N86-17839
- Gallium arsenide solar cell efficiency: Problems and potential
p 184 N86-17843
- N/P GaAs concentrator solar cells with an improved grid and busbar contact design
p 184 N86-17844
- High-efficiency AlGaAs-GaAs Cassegrainian concentrator cells
p 185 N86-17845
- A possible radiation-resistant solar cell geometry using superlattices
p 185 N86-17851
- Radiation damage in high-resistivity silicon solar cells
p 185 N86-17856
- Performance of Hughes GaAs concentrator cells under 1-MeV electron irradiation
p 185 N86-17860
- Demonstrated results of welded and soldered interconnections
p 185 N86-17866
- Superlattices and NiPi structures in new forms of cascade solar cells
[NASA-CR-176718] p 187 N86-24007
- Indium phosphide solar cells: status and prospects for use in space
[NASA-TM-87315] p 123 N86-26520
- The voltage threshold for arcing for solar cells in LEO: Flight and ground test results
[NASA-TM-87259] p 62 N86-28125
- Space solar cell research: Problems and potential
[NASA-TM-88833] p 125 N86-31793
- Potential high efficiency solar cells: Applications from space photovoltaic research
[NASA-TM-88832] p 125 N86-32627
- Lithium counterdoped silicon solar cell
[NASA-CASE-LEW-14177-1] p 190 N86-32875
- SOLAR COLLECTORS**
- N/P GaAs concentrator solar cells with an improved grid and busbar contact design
p 184 N86-17844
- High-efficiency AlGaAs-GaAs Cassegrainian concentrator cells
p 185 N86-17845
- Performance of Hughes GaAs concentrator cells under 1-MeV electron irradiation
p 185 N86-17860
- SOLAR DYNAMIC POWER SYSTEMS**
- Electrical power system for the U.S. space station
[NASA-TM-88856] p 64 N86-32520
- The space station power system
[NASA-TM-88847] p 64 N86-32521
- SOLAR ENERGY**
- Technology for Brayton-cycle powerplants using solar and nuclear energy
[NASA-TP-2558] p 60 N86-21577
- SOLAR ENERGY CONVERSION**
- N/P GaAs concentrator solar cells with an improved grid and busbar contact design
p 184 N86-17844
- Potential high efficiency solar cells: Applications from space photovoltaic research
[NASA-TM-88832] p 125 N86-32627
- SOLAR FLUX**
- Compensation of reflector surface distortions using conjugate field matching
[NASA-TM-87198] p 113 N86-16461
- SOLAR GENERATORS**
- Design tradeoffs for a Space Station solar-Brayton power system
p 53 A86-24790
- Hybrid deployable/erectable solar dynamic box truss system
[AIAA PAPER 86-0955] p 47 A86-38883
- Solar dynamic power for the Space Station
[AIAA PAPER 86-1299] p 54 A86-39906
- Development of a microprocessor controller for stand-alone photovoltaic power systems
[NASA-CR-174723] p 187 N86-21979
- SOLAR POWER SATELLITES**
- Solar dynamic power for the Space Station
[AIAA PAPER 86-1299] p 54 A86-39906
- SOLAR PROPULSION**
- Radiation energy receiver for solar propulsion systems
p 52 A86-18043
- SOLDERED JOINTS**
- Demonstrated results of welded and soldered interconnections
p 185 N86-17866
- SOLID ELECTRODES**
- TWT efficiency enhancement with textured carbon surfaces on copper MDC electrodes --- multistage depressed collectors
p 120 A86-49617
- SOLID LUBRICANTS**
- Traction forces at solid-lubricated rolling/sliding contacts
[ASLE PREPRINT 85-AM-4E-2] p 151 A86-11091
- Low-wear partially fluorinated polyimides
p 94 A86-11175
- The use of silver in self-lubricating coatings for extreme temperatures
p 99 A86-44425
- Sputtered cadmium oxide as a surface pretreatment for graphite solid lubricant films
[NASA-TM-87300] p 104 N86-25473
- Tribology of selected ceramics at temperatures to 900 deg C
[NASA-TM-87267] p 105 N86-25476
- Sliding seal materials for adiabatic engines, phase 2
[NASA-CR-179475] p 105 N86-29042
- SOLID MECHANICS**
- Hybrid solid element with a traction-free cylindrical surface
p 169 A86-34462
- SOLID SOLUTIONS**
- Structure and grain coarsening during the sintering of alumina
p 98 A86-26341
- SOLID STATE**
- Temperature effects on the universal equation of state of solids
[NASA-TM-87321] p 206 N86-28776
- SOLID STATE DEVICES**
- A new very high voltage semiconductor switch
p 119 A86-40449
- SOLID SURFACES**
- Thermophoretically augmented mass transfer rates to solid walls across laminar boundary layers
p 128 A86-20150
- SOLID SUSPENSIONS**
- Properties of silicon suspensions and slip-cast bodies
p 95 A86-15238
- SOLID-SOLID INTERFACES**
- The effect of processing conditions on the GaAs/plasma-grown insulator interface
p 204 A86-18567
- SOLIDIFICATION**
- Free boundary shape of a convectively cooled solidified region
p 131 A86-29029
- Influence of melt convection on solid-liquid interface under terrestrial and reduced gravity environments
p 38 N86-10083
- The development and prevention of channel segregation during alloy solidification
p 38 N86-10086
- Solidification fundamentals
p 39 N86-10090
- Containerless processing of undercooled melts
p 39 N86-10093
- Microgravity Materials Science Laboratory
p 42 N86-10173
- Measurement of the density of base fluids at pressures 0.422 to 2.20 GPa
[NASA-TM-87114] p 156 N86-10551
- Structure-property characterization of rheocast and VADER processed IN-100 superalloy
[NASA-CR-175014] p 88 N86-14354
- Undercooling and solidification behavior in the InSb-Sb system
[NASA-CR-175013] p 88 N86-14355
- A model for the influence of pressure on the bulk modulus and the influence of temperature on the solidification pressure for liquid lubricants
[NASA-TM-87230] p 140 N86-19555
- Determination of solid mass fraction in partially frozen hydrocarbon fuels
[NASA-CR-179472] p 108 N86-28261
- SOLIDS**
- Measurement of ultrasonic velocity using phase-slope and cross-correlation methods
p 162 A86-13192
- Reliability of void detection in structural ceramics by use of scanning laser acoustic microscopy
p 163 A86-39027
- Universality in the compressive behavior of solids
[NASA-TM-87303] p 206 N86-28775
- SOLITARY WAVES**
- Infrared-photoinduced-absorption studies in soluble trans-polyacetylene
p 204 A86-37075
- SOLUTES**
- Electrohydrodynamics
p 41 N86-10130
- SOOT**
- Temperature and velocity profiles in sooting free boundary layer flames
[AIAA PAPER 86-0575] p 73 A86-19962
- Influence of temperature and hydroxyl concentration on incipient soot formation in premixed flames
p 74 A86-29070
- Shock-tube pyrolysis of chlorinated hydrocarbons - Formation of soot
p 75 A86-35126
- SOUND FIELDS**
- Flow field and near and far sound field of a subsonic jet
p 5 A86-35855
- An approach to the calculation of the pressure field produced by rigid wide chord dual rotation propellers of high solidity in compressible flow
[AIAA PAPER 86-0487] p 198 A86-49566

An iterative finite element-integral technique for predicting sound radiation from turbofan inlets in steady flight p 198 A86-49806

An analysis for the sound field produced by rigid wide cord dual rotation propellers of high solidarity in compressible flow [NASA-TM-87178] p 11 N86-21517

SOUND PRESSURE

Numerical Techniques in Acoustics [NASA-CP-2404] p 198 N86-12007

SOUND PROPAGATION

The effect of acoustic reflections on combustor noise measurements p 197 A86-20364

SOUND WAVES

Non-linear effects in finite amplitude wave propagation through ducts and nozzles p 197 A86-35857

Development of an impulsive noise source to study the acoustic reflection characteristics of hard-walled wind tunnels [AIAA PAPER 86-1887] p 198 A86-45500

Acoustic reflection contamination measurements in the 16-foot NASA Langley Transonic Wind Tunnel [AIAA PAPER 86-1888] p 198 A86-45501

Modeling the effects of wind tunnel wall absorption on the acoustic radiation characteristics of propellers [NASA-TM-87333] p 201 N86-29630

SPACE BASED RADAR

Primary propulsion of electrothermal, ion, and chemical systems for space-based radar orbit transfer [AIAA PAPER 85-1477] p 50 A86-14431

SPACE CHARGE

Energy broadening due to space-charge oscillations in high current electron beams --- SEPAC payload experiment on Spacelab 1 p 202 A86-22890

Thermionic noise measurements for on-line dispenser cathode diagnostics for linear beam microwave tubes [NASA-CR-175105] p 124 N86-28323

SPACE COMMERCIALIZATION

Accommodation requirements for microgravity science and applications research on space station [NASA-CR-175038] p 42 N86-18334

Research and competition: Best partners [NASA-TM-87313] p 212 N86-25321

SPACE COMMUNICATION

The baseband processor in future satellite communication systems p 109 A86-21882

An analysis of bidirectional use of frequencies for satellite communications [AIAA PAPER 86-0635] p 110 A86-29664

An analysis of bi-directional use of frequencies for satellite communications [AIAA PAPER 86-0635] p 111 A86-49568

Compensation of reflector surface distortions using conjugate field matching [NASA-TM-87198] p 113 N86-16461

An analysis of bi-directional use of frequencies for satellite communications [NASA-TM-87226] p 114 N86-18585

SPACE ERECTABLE STRUCTURES

Hybrid deployable/erectable solar dynamic box truss system [AIAA PAPER 86-0955] p 47 A86-38883

SPACE MAINTENANCE

Orbit Transfer Rocket Engine Technology Program: Advanced engine study, task D.1/D.3 [NASA-CR-175084] p 61 N86-26369

SPACE MANUFACTURING

Thermocapillary and diffusocapillary migration of a fluid drop p 40 N86-10128

Accommodation requirements for microgravity science and applications research on space station [NASA-CR-175038] p 42 N86-18334

SPACE MISSIONS

Power electronics for a 1-kilowatt arcjet thruster [AIAA PAPER 86-1507] p 56 A86-49613

Power electronics for a 1-kilowatt arc jet thruster [NASA-TM-87340] p 61 N86-25409

SPACE PLASMAS

Current collection from the space plasma through defects in solar array insulation p 52 A86-18042

Development of the VOLT-A shuttle experiment [NASA-TM-87169] p 212 N86-14110

SPACE PLATFORMS

Communication Platform Payload Definition (CPPD) study, Volume 2: Technical report [NASA-CR-174929] p 49 N86-27404

SPACE POWER REACTORS

Thermal aging effects in refractory metal alloys [NASA-TM-87210] p 89 N86-16334

Overview of the 1986 free-piston Stirling SP-100 activities at the NASA Lewis Research Center [NASA-TM-87305] p 210 N86-26261

Overview of NASA Lewis Research Center free-piston Stirling engine technology activities applicable to space power systems [NASA-TM-88815] p 211 N86-29732

SPACE POWER UNIT REACTORS

Overview of the 1985 NASA Lewis Research Center SP-100 free-piston Stirling engine activities p 153 A86-24884

SPACE PROCESSING APPLICATIONS ROCKET

Accommodation requirements for microgravity science and applications research on space station [NASA-CR-175038] p 42 N86-18334

SPACE SHUTTLE MAIN ENGINE

Probabilistic structural analysis for space propulsion system components p 168 A86-28659

Analysis of a two row hydrostatic journal bearing with variable properties, inertia effects and surface roughness p 153 A86-30599

Structural tailoring of SSME turbopump blades (SSME/STAEBL) --- Structural Tailoring of Engine Blades [AIAA PAPER 86-0847] p 54 A86-38895

Probabilistic structural analysis methods for critical SSME propulsion components [AIAA PAPER 86-1188] p 54 A86-40595

Structural integrity and durability for Space Shuttle main engine and future reusable space propulsion systems [AIAA PAPER 86-1513] p 55 A86-42682

Simplified cyclic structural analyses of SSME turbine blades [NASA-TM-87214] p 175 N86-16615

SSME fuelside preburner two-dimensional analysis [NASA-TM-87299] p 44 N86-23616

Structural integrity and durability for Space Shuttle main engine and future reusable space propulsion systems [NASA-TM-87280] p 61 N86-25408

Characterization of real gas properties for space shuttle main engine fuel turbine and performance calculations [NASA-CR-175068] p 61 N86-27418

SPACE SHUTTLE PAYLOADS

Cryogenic Fluid Management Facility p 108 A86-37053

Communication Platform Payload Definition (CPPD) study, Volume 1: Executive summary [NASA-CR-174928] p 49 N86-27403

Communication Platform Payload Definition (CPPD) study, Volume 3: Addendum [NASA-CR-174930] p 49 N86-27405

SPACE SHUTTLES

NASA Lewis Research Center low-gravity fluid management technology program p 44 A86-32906

Structural integrity and durability for Space Shuttle main engine and future reusable space propulsion systems [AIAA PAPER 86-1513] p 55 A86-42682

NASA Lewis Research Center low-gravity fluid management technology program [NASA-TM-87145] p 44 N86-11218

Advanced research and technology program for advanced high pressure oxygen-hydrogen rocket propulsion p 58 N86-17405

Structural integrity and durability for Space Shuttle main engine and future reusable space propulsion systems [NASA-TM-87280] p 61 N86-25408

SPACE STATION POWER SUPPLIES

Space station power system p 50 A86-12676

Space Station Power System Advanced Development p 52 A86-24778

Design tradeoffs for a Space Station solar-Brayton power system p 53 A86-24790

Development of the power system for the United States' Manned Space Station p 207 A86-24798

Tethered nuclear power for the space station p 53 A86-24808

Design of a regenerative fuel cell system for Space Station p 53 A86-24857

Heat transfer in space power and propulsion systems p 53 A86-26492

Hybrid deployable/erectable solar dynamic box truss system [AIAA PAPER 86-0955] p 47 A86-38883

Solar dynamic power for the Space Station [AIAA PAPER 86-1299] p 54 A86-39906

A 20 kilohertz space station power system [NASA-TM-88801] p 62 N86-28122

Parametric and cycle tests of a 40-A-hr bipolar nickel-hydrogen battery [NASA-TM-88793] p 189 N86-31979

SPACE STATION PROPULSION

A 10,000 hour life multipropellant engine for Space Station applications [AIAA PAPER 86-1403] p 54 A86-42616

A long-life 50 lbf H₂/O₂ thruster for Space Station auxiliary propulsion [AIAA PAPER 86-1404] p 55 A86-42617

Theoretical study on the effect of the design of small (milli-Newton) thruster jets on molecular contamination for the space station [NASA-CR-177263] p 48 N86-26358

SPACE STATIONS

An analysis of low-thrust, resistojet rebost for the Space Station [AIAA PAPER 85-2042] p 51 A86-14447

Compatibility of grain-stabilized platinum with candidate propellants for resistojets [AIAA PAPER 85-2014] p 51 A86-17835

Space Station Power System Advanced Development p 52 A86-24778

Design tradeoffs for a Space Station solar-Brayton power system p 53 A86-24790

Development of the power system for the United States' Manned Space Station p 207 A86-24798

Tethered nuclear power for the space station p 53 A86-24808

Performance analysis of radiation cooled dc transmission lines for high power space systems p 117 A86-24811

Design of a regenerative fuel cell system for Space Station p 53 A86-24857

The role of unneutralized surface ions in negative potential arcing p 118 A86-25525

Heat transfer in space power and propulsion systems p 53 A86-26492

Space Station benefits from ECLS - Propulsion system synergism [AIAA PAPER 86-1407] p 47 A86-42619

Performance and endurance tests of a multipropellant resistojet for space station auxiliary propulsion [AIAA PAPER 86-1435] p 55 A86-42640

NASA electrothermal auxiliary propulsion technology [AIAA PAPER 86-1703] p 55 A86-42799

Compatibility of grain-stabilized platinum with candidate propellants for resistojets [NASA-TM-87118] p 56 N86-10279

Space station propulsion requirements study [NASA-CR-174934] p 57 N86-15339

Advanced research and technology program for advanced high pressure oxygen-hydrogen rocket propulsion p 58 N86-17405

Accommodation requirements for microgravity science and applications research on space station [NASA-CR-175038] p 42 N86-18334

Space station 20-kHz power management and distribution system [NASA-TM-87314] p 60 N86-24747

Performance and endurance tests of a multipropellant resistojet for space station auxiliary propulsion [NASA-TM-87278] p 60 N86-24748

NASA electrothermal auxiliary propulsion technology [NASA-TM-87281] p 60 N86-24749

A 20 kilohertz space station power system [NASA-TM-88801] p 62 N86-28122

Feasibility study of a discrete bearing/roller drive rotary joint for the space station [NASA-TM-88800] p 161 N86-30206

Electrical power system for the U.S. space station [NASA-TM-88856] p 64 N86-32520

The space station power system [NASA-TM-88847] p 64 N86-32521

Proven, long-life hydrogen/oxygen thrust chambers for space station propulsion [NASA-TM-88822] p 64 N86-32522

SPACE SUITS

Mass loss of shuttle space suit orthofabric under simulated ionospheric atomic oxygen bombardment [NASA-TM-87149] p 192 N86-13899

SPACE TRANSPORTATION

Rail accelerators for space transportation: An experimental investigation [NASA-TP-2571] p 62 N86-28123

SPACEBORNE EXPERIMENTS

Cryogenic Fluid Management Facility p 108 A86-37053

SPACECRAFT ANTENNAS

MMIC antenna technology development in the 30/20 gigahertz band [AIAA PAPER 86-0666] p 45 A86-29628

A numerical method for approximating antenna surfaces defined by discrete surface points [NASA-TM-87125] p 111 N86-10381

MMIC antenna technology development in the 30/20 gigahertz band [NASA-TM-87192] p 46 N86-17368

SPACECRAFT COMMUNICATION

MMIC antenna technology development in the 30/20 gigahertz band [AIAA PAPER 86-0666] p 45 A86-29628

Adaptive antenna arrays for weak interfering signals --- in satellite communication p 45 A86-34591

MMIC antenna technology development in the 30/20 gigahertz band [NASA-TM-87192] p 46 N86-17368

Bit error rate testing of a proof-of-concept model baseband processor [NASA-TM-87206] p 46 N86-18343

- Radiofrequency testing of satellite segment of simulated 30/20 GHz satellite communications system
[NASA-TM-87163] p 114 N86-19494
- Communication Platform Payload Definition (CPPD) study. Volume 1: Executive summary
[NASA-CR-174928] p 49 N86-27403
- Communication Platform Payload Definition (CPPD) study. Volume 2: Technical report
[NASA-CR-174929] p 49 N86-27404
- Communication Platform Payload Definition (CPPD) study. Volume 3: Addendum
[NASA-CR-174930] p 49 N86-27405
- Communications platform payload definition study, executive summary
[NASA-TM-174985] p 49 N86-27407
- Spacecraft multibeam antenna system for 30/20 GHz
[NASA-CR-174654] p 116 N86-31760
- SPACECRAFT CONSTRUCTION MATERIALS**
- Ion beam sputter-deposited thin film coatings for protection of spacecraft polymers in low earth orbit
[AIAA PAPER 85-0420] p 95 A86-14428
- A 10,000 hour life multipropellant engine for Space Station applications
[AIAA PAPER 86-1403] p 54 A86-42616
- Oxidation protecting coatings for polymers
[NASA-CASE-LEW-14072-3] p 105 N86-26434
- ICAN: A versatile code for predicting composite properties
[NASA-TM-87334] p 71 N86-31664
- SPACECRAFT CONTAMINATION**
- Theoretical study on the effect of the design of small (milli-Newton) thruster jets on molecular contamination for the space station
[NASA-CR-177263] p 48 N86-26358
- SPACECRAFT DESIGN**
- Spacecraft 2000
[AIAA PAPER 86-0616] p 38 A86-29586
- Orbital transfer vehicle engine integration study
p 58 N86-17416
- Design optimization for a space based, reusable orbit transfer vehicle
p 48 N86-17418
- Advanced orbit transfer vehicle propulsion system study
[NASA-CR-174843] p 60 N86-24746
- SPACECRAFT ENVIRONMENTS**
- Accommodation requirements for microgravity science and applications research on space station
[NASA-CR-175038] p 42 N86-18334
- SPACECRAFT EQUIPMENT**
- Analysis of a spacecraft instrument ball bearing assembly lubricated by a perfluoroalkylether
[NASA-TM-87260] p 50 N86-21575
- SPACECRAFT POWER SUPPLIES**
- Space station power system
p 50 A86-12676
- Current collection from the space plasma through defects in solar array insulation
p 52 A86-18042
- Space Station Power System Advanced Development
p 52 A86-24778
- Design tradeoffs for a Space Station solar-Brayton power system
p 53 A86-24790
- Development of the power system for the United States' Manned Space Station
p 207 A86-24798
- Design principles for nickel-hydrogen cells and batteries
p 179 A86-24799
- Tethered nuclear power for the space station
p 53 A86-24808
- Performance analysis of radiation cooled dc transmission lines for high power space systems
p 117 A86-24811
- Bipolar nickel-hydrogen battery development
p 180 A86-24823
- Space power systems - 'Spacecraft 2000'
p 53 A86-24836
- A preliminary study of the modified Ericsson for space power
p 180 A86-24840
- Design of a regenerative fuel cell system for Space Station
p 53 A86-24857
- Heat transfer in space power and propulsion systems
p 53 A86-26492
- Heat pipe radiator technology for space power systems
[AIAA PAPER 86-1300] p 47 A86-39907
- Liquid droplet radiator program at the NASA Lewis Research Center
[ASME PAPER 86-HT-15] p 48 A86-49621
- Liquid droplet radiator program at the NASA Lewis Research Center
[NASA-TM-87139] p 48 N86-12246
- Reliability and mass analysis of dynamic power conversion systems with parallel of standby redundancy
[NASA-TM-87189] p 57 N86-16258
- Evaluation of spacecraft technology programs (effects on communication satellite business ventures), volume 2
[NASA-CR-174979] p 113 N86-16452

- Design of high-voltage, high-power, solid state remote power controllers for aerospace applications
p 122 N86-17456
- Space Photovoltaic Research and Technology 1985: High Efficiency, Space Environment, and Array Technology
[NASA-CP-2408] p 184 N86-17839
- N/P GaAs concentrator solar cells with an improved grid and bushbar contact design
p 184 N86-17844
- Performance of Hughes GaAs concentrator cells under 1-MeV electron irradiation
p 185 N86-17860
- Space station power management and distribution
p 59 N86-17869
- Overview of free-piston Stirling SP-100 activities at the NASA Lewis Research Center
[NASA-TM-87224] p 209 N86-19264
- Technology for satellite power conversion
[NASA-CR-176554] p 186 N86-19742
- Assessment of commercially available and experimental hydrogen electrodes
[NASA-TM-87264] p 187 N86-23035
- Principles for system level electrochemistry
[NASA-TM-87283] p 187 N86-25039
- Technology for satellite power conversion
[NASA-CR-176777] p 187 N86-25042
- Space solar cell research: Problems and potential
[NASA-TM-88833] p 125 N86-31793
- Parametric and cycle tests of a 40-A-hr bipolar nickel-hydrogen battery
[NASA-TM-88793] p 189 N86-31979
- Electrical power system for the U.S. space station
[NASA-TM-88856] p 64 N86-32520
- The space station power system
[NASA-TM-88847] p 64 N86-32521
- Potential high efficiency solar cells: Applications from space photovoltaic research
[NASA-TM-88832] p 125 N86-32627
- SPACECRAFT PROPULSION**
- An analysis of low-thrust, resistojet reboost for the Space Station
[AIAA PAPER 85-2042] p 51 A86-14447
- Measurement of energy distribution in flowing hydrogen microwave plasmas
p 52 A86-18041
- Radiation energy receiver for solar propulsion systems
p 52 A86-18043
- Heat transfer in space power and propulsion systems
p 53 A86-26492
- Space station propulsion requirements study
[NASA-CR-174934] p 57 N86-15339
- Evaluation of spacecraft technology programs (effects on communication satellite business ventures), volume 2
[NASA-CR-174979] p 113 N86-16452
- Cyclic structural analyses of anisotropic turbine blades for reusable space propulsion systems
p 58 N86-17404
- Performance characteristics of ring-cusp thrusters with xenon propellant
[NASA-TM-87338] p 63 N86-31650
- SPACECRAFT RADIATORS**
- A preliminary study of the modified Ericsson for space power
p 180 A86-24840
- Liquid droplet radiator thermal characteristics
[AIAA PAPER 86-1162] p 133 A86-40578
- Liquid belt radiator design study
[NASA-CR-174901] p 57 N86-16259
- Organosiloxane working fluids for the liquid droplet radiator
[NASA-CR-175033] p 102 N86-16381
- Effect of an oxygen plasma on the physical and chemical properties of several fluids for the liquid droplet radiator
[NASA-TM-88839] p 49 N86-31634
- Analysis of the Gas Particle Radiator (GPR)
[NASA-TM-88786] p 63 N86-31652
- SPACECRAFT STRUCTURES**
- Aerospace applications of PMR polyimide composites
p 67 A86-27730
- Structural integrity and durability for Space Shuttle main engine and future reusable space propulsion systems
[AIAA PAPER 86-1513] p 55 A86-42682
- Polymer, metal and ceramic matrix composites for advanced aircraft engine applications
[NASA-TM-87132] p 87 N86-13407
- Structural integrity and durability for Space Shuttle main engine and future reusable space propulsion systems
[NASA-TM-87280] p 61 N86-25408
- SPARK IGNITION**
- Ignition characteristics of rich n-heptane fuel sprays in the transition region
[ASME PAPER 85-WA/HT-46] p 107 A86-38393
- Transition region ignition characteristics of n-heptane fuel sprays
[NASA-CR-176364] p 77 N86-14331
- SPATIAL MARCHING**
- Computation of viscous flows in turbomachinery cascades with a space-marching method
p 5 A86-39089

- A space-marching method for viscous incompressible internal flows
p 135 A86-43037
- SPATIAL RESOLUTION**
- Polarization modulated ellipsometry
[NASA-CR-177264] p 149 N86-26599
- SPECIFIC IMPULSE**
- Performance and endurance tests of a multipropellant resistojet for space station auxiliary propulsion
[AIAA PAPER 86-1435] p 55 A86-42640
- Current evaluation of the tripropellant concept
[AIAA PAPER 86-1698] p 56 A86-49615
- Performance and endurance tests of a multipropellant resistojet for space station auxiliary propulsion
[NASA-TM-87278] p 60 N86-24748
- Current evaluation of the tripropellant concept
[NASA-TP-2602] p 62 N86-28124
- SPECIMEN GEOMETRY**
- Mode II fatigue crack growth specimen development
p 171 A86-43586
- Specimen geometry effects on graphite/PMR-15 composites during thermo-oxidative aging
[NASA-TM-87204] p 69 N86-17477
- SPECTROSCOPY**
- Light scattering tests of fundamental theories of transport properties in the critical region
p 39 N86-10113
- Characterization methodology for PMR-15
p 65 N86-11272
- SPEED CONTROL**
- Summary of NASA/DOE Aileron-Control Development Program for Wind Turbines
[NASA-TM-88811] p 190 N86-31983
- SPIN**
- Spin analysis of concentrated traction contacts
[ASME PAPER 84-DET-99] p 155 A86-45257
- SPINEL**
- The evolution and growth of Al₂O₃ scales on beta-NiAl
[NASA-CR-175097] p 92 N86-27444
- SPIRAL WRAPPING**
- Generated spiral bevel gears - Optimal machine-tool settings and tooth contact analysis
[SAE PAPER 851573] p 154 A86-40678
- SPIRALS**
- Generation of spiral bevel gears with zero kinematical errors and computer aided simulation of their meshing and contact
p 154 A86-40656
- SPLASHING**
- Experimental assessment of advanced Stirling component concepts
[NASA-CR-174994] p 210 N86-25302
- SPONTANEOUS COMBUSTION**
- Spontaneous ignition delay characteristics of hydrocarbon fuel-air mixtures
[NASA-CR-175064] p 29 N86-21545
- SPRAY CHARACTERISTICS**
- Structure of nonevaporating sprays. II - Drop and turbulence properties
p 125 A86-11237
- Spray atomization and combustion
[AIAA PAPER 86-0136] p 131 A86-26606
- Analysis of the effects of fuel spray characteristics on NO(x) formation
[ASME PAPER 85-WA/HT-47] p 107 A86-38394
- Atomization and combustion characteristics of antimisting fuels using JT8D and air-boost injectors
[ASME PAPER 86-GT-223] p 24 A86-48257
- SPRAY NOZZLES**
- Experimental study of the spray characteristics of a research airblast atomizer
[ASME PAPER 85-GT-229] p 129 A86-22125
- Turbulent dispersion of the icing cloud from spray nozzles used in icing tunnels
[NASA-TM-87316] p 34 N86-31588
- SPRAYED COATINGS**
- Fracture toughness tests on plasma-sprayed coatings
p 64 A86-30051
- Tensile adhesion test measurements on plasma-sprayed coatings
p 98 A86-30052
- The low cycle fatigue behavior of a plasma-sprayed coating material
[NASA-TM-87318] p 92 N86-31699
- SPRAYERS**
- High Weber number SMD correlations for pressure atomizers - Sauter Mean Diameter
[ASME PAPER 85-GT-37] p 128 A86-22026
- Heat transfer and pressure drop performance of a finned-tube heat exchanger proposed for use in the NASA Lewis Altitude Wind Tunnel
[NASA-TM-87151] p 138 N86-13677
- SPRAYING**
- Measurements in liquid fuel sprays
[NASA-CR-177088] p 144 N86-30960
- SPUTTERING**
- Ion beam sputter-deposited thin film coatings for protection of spacecraft polymers in low earth orbit
[AIAA PAPER 85-0420] p 95 A86-14428

- Frictional and morphological properties of Au-MoS₂ films sputtered from a compact target p 152 A86-16258
- Rapid evaluation of ion thruster lifetime using optical emission spectroscopy [AIAA PAPER 85-2011] p 51 A86-17851
- Dual-ion-beam deposition of carbon films with diamond-like properties p 65 A86-49855
- Rapid evaluation of ion thruster lifetime using optical emission spectroscopy [NASA-TM-87103] p 56 N86-10280
- Oxidation protection coatings for polymers [NASA-CASE-LEW-14072-1] p 102 N86-19458
- Ion beam sputter etching [NASA-CASE-LEW-13899-1] p 109 N86-20587
- Sputtered cadmium oxide as a surface pretreatment for graphite solid lubricant films [NASA-TM-87300] p 104 N86-25473
- Textured carbon surfaces on copper by sputtering [NASA-CASE-LEW-14130-1] p 109 N86-32587
- SQUEEZE FILMS**
- Starvation effects on the hydrodynamic lubrication of rigid nonconformal contacts in combined rolling and normal motion [NASA-TM-87174] p 140 N86-19556
- STABILITY**
- Organosiloxane working fluids for the liquid droplet radiator [NASA-CR-175033] p 102 N86-16381
- Long-term stability and properties of zirconia ceramics for heavy duty diesel engine components [NASA-CR-174943] p 209 N86-17224
- Nonlinear bending-torsional vibration and stability of rotating, pretwisted, precone blades including Coriolis effects [NASA-TM-87207] p 175 N86-17789
- Variable friction secondary seal for face seals [NASA-CASE-LEW-14170-1] p 160 N86-25790
- Stability of surface nucleation [NASA-TM-88806] p 207 N86-30556
- STABILITY TESTS**
- Environmental stability of intercalated graphite fibers p 98 A86-31825
- STABLE OSCILLATIONS**
- Stability of limit cycles in frictionally damped and aerodynamically unstable rotor stages p 18 A86-19198
- STACKS**
- Advanced on-site power plant development technology program [NASA-CR-175007] p 189 N86-29411
- STAGNATION POINT**
- Preliminary results of a study of the relationship between free stream turbulence and stagnation region heat transfer [ASME PAPER 85-GT-84] p 129 A86-22055
- STAGNATION PRESSURE**
- A stagnation pressure probe for droplet-laden air flow p 133 A86-39077
- STAINLESS STEELS**
- Character of laser-glazed, plasma-sprayed zirconia coatings on stainless steel substrata p 95 A86-15229
- An experimental data base for material selection and design of high-speed, high-pressure, oxygen turbomachinery p 58 N86-17387
- STANDING WAVE RATIOS**
- 10-30 GHz monolithic GaAs travelling-wave divider/combiner p 118 A86-34882
- STATIC CHARACTERISTICS**
- Application of a personal computer for the uncoupled vibration analysis of wind turbine blade and counterweight assemblies [NASA-CR-175090] p 188 N86-28511
- STATISTICAL ANALYSIS**
- Factors influencing the ball milling of Si₃N₄ in water p 95 A86-15239
- Reliability of void detection in structural ceramics by use of scanning laser acoustic microscopy p 163 A86-39027
- Probability of detection of internal voids in structural ceramics using microfocus radiography [NASA-TM-87164] p 164 N86-13749
- STATISTICAL DISTRIBUTIONS**
- Statistical prediction of dynamic distortion of inlet flow using minimum dynamic measurement. An application to the Melick statistical method and inlet flow dynamic distortion prediction without RMS measurements [NASA-CR-176764] p 142 N86-24933
- STATISTICAL MECHANICS**
- Theory of homogeneous nucleation - A chemical kinetic view p 72 A86-19389
- NASA LeRC/Akron University Graduate Cooperative Fellowship Program and Graduate Student Researchers Program [NASA-CR-174826] p 207 N86-13219

STATOR BLADES

- Noise generated by convected gusts interacting with swept airfoil cascades [AIAA PAPER 86-1872] p 198 A86-45492

STATORS

- A mathematical model for the doubly-fed wound rotor generator. II p 119 A86-39472
- Experimental rotordynamic coefficient results for teeth-on-rotor and teeth-on-stator labyrinth gas seals [ASME PAPER 86-GT-12] p 156 A86-48109
- Comparison of calculated and experimental cascade performance for controlled-diffusion compressor stator blading [NASA-TM-87167] p 27 N86-16219
- Combined fringe and Fabry-Perot laser anemometer for three component velocity measurements in turbine stator cascade facility [NASA-TM-87322] p 149 N86-24967

STEADY FLOW

- Accelerated solution of the steady Euler equations p 2 A86-20942
- Steady inviscid three-dimensional flows p 128 A86-20952
- A new approach for solving the three-dimensional steady Euler equations. I - General theory p 133 A86-41242
- A space-marching method for viscous incompressible internal flows p 135 A86-43037
- Turbulent two-phase flow in annular seals [ASLE PREPRINT 86-AM-4G-3] p 156 A86-45391

STEADY STATE

- Rapid evaluation of ion thruster lifetime using optical emission spectroscopy [AIAA PAPER 85-2011] p 51 A86-17851
- An efficient method for solving the steady Euler equations [AIAA PAPER 86-1079] p 132 A86-38442
- Power electronics for a 1-kilowatt arcjet thruster [AIAA PAPER 86-1507] p 56 A86-49613
- Dendritic solidification in a binary alloy melt: Steady-state versus morphological stability theories p 42 N86-10261
- Rapid evaluation of ion thruster lifetime using optical emission spectroscopy [NASA-TM-87103] p 56 N86-10280
- Power electronics for a 1-kilowatt arc jet thruster [NASA-TM-87340] p 61 N86-25409

STEAM

- Characterization of real gas properties for space shuttle main engine fuel turbine and performance calculations [NASA-CR-175066] p 61 N86-27418

STEELS

- Optical and other properties changes of M-50 bearing steel surfaces for different lubricants and additives prior to scuffing p 97 A86-20435
- The crack layer approach to toughness characterization in steel p 82 A86-30010
- Surface fatigue life and failure characteristics of EX-53, CBS 1000M, and AISI 9310 gear materials [NASA-TP-2513] p 157 N86-12609
- Surface fatigue and failure characteristics of hot forged powder metal AISI 4620, AISI 4640, and machined AISI 4340 steel spur gears [NASA-TM-87330] p 161 N86-31889
- Ion-beam nitriding of steels [NASA-CASE-LEW-14104-2] p 93 N86-32556

STIFFNESS

- Experimental stiffness of tapered bore seals [ASME PAPER 85-DET-12] p 152 A86-22748
- SSME long-life bearings [NASA-CR-179455] p 160 N86-27643

STIFFNESS MATRIX

- Finite elements based on consistently assumed stresses and displacements p 166 A86-18123

STIMULATED EMISSION

- Reassessment of the theory of stimulated Raman scattering p 150 A86-40662

STIRLING CYCLE

- Operational maintenance data base development for kinematic Stirling engines [ASME PAPER 85-DGP-20] p 151 A86-14467
- Overview of the 1985 NASA Lewis Research Center SP-100 free-piston Stirling engine activities p 153 A86-24884
- Liquid fueled external heating system for STM4-120 Stirling engine p 180 A86-24888
- Test results of a 40 kW Stirling engine and comparison with the NASA-Lewis computer code predictions p 181 A86-24889
- RE-1000 free-piston Stirling engine update p 153 A86-24890
- Creep-rupture and fractographic analysis of Stirling engine superalloys tested in air and 15 MPa hydrogen p 82 A86-30041
- High-pressure creep tests p 84 A86-46564

- Liquid droplet radiator program at the NASA Lewis Research Center [ASME PAPER 86-HT-15] p 48 A86-49621
- RE-1000 free-piston Stirling engine update [NASA-TM-87126] p 182 N86-11668
- Liquid droplet radiator program at the NASA Lewis Research Center [NASA-TM-87139] p 48 N86-12246
- Overview of free-piston Stirling technology at the NASA Lewis Research Center [NASA-TM-87156] p 208 N86-13236
- Stirling engine supporting research and technology [NASA-TM-87175] p 208 N86-14106
- Creep rupture behavior of Stirling engine materials [NASA-TM-87209] p 88 N86-15380
- Ceramic automotive Stirling engine study [NASA-CR-174907] p 208 N86-16165
- Overview of free-piston Stirling SP-100 activities at the NASA Lewis Research Center [NASA-TM-87224] p 209 N86-19264
- Alloy chemistry and microstructural control to meet the demands of the automotive Stirling engine [NASA-TM-87250] p 89 N86-20541
- Automotive Stirling summary and overview [NASA-TM-87177] p 209 N86-21457
- A new chromium carbide-based tribological coating for use to 900 deg C with particular reference to the Stirling engine [NASA-TM-87274] p 103 N86-21682
- Experimental assessment of advanced Stirling component concepts [NASA-CR-174994] p 210 N86-25302
- Stirling Powered Van Program overview [NASA-TM-87227] p 210 N86-25303
- Tribology of selected ceramics at temperatures to 900 deg C [NASA-TM-87267] p 105 N86-25476
- Overview of the 1986 free-piston Stirling SP-100 activities at the NASA Lewis Research Center [NASA-TM-87305] p 210 N86-26261
- Automotive Stirling Engine Development Program [NASA-CR-174749] p 211 N86-28017
- Overview of NASA Lewis Research Center free-piston Stirling engine technology activities applicable to space power systems [NASA-TM-88815] p 211 N86-29732
- Automotive Stirling engine development program [NASA-CR-175045] p 211 N86-30579
- Evaluation of a Stirling engine heater bypass with the NASA Lewis nodal-analysis performance code [NASA-CR-179460] p 211 N86-31452
- STIRLING ENGINES**
- Operational maintenance data base development for kinematic Stirling engines [ASME PAPER 85-DGP-20] p 151 A86-14467
- Overview of the 1985 NASA Lewis Research Center SP-100 free-piston Stirling engine activities p 153 A86-24884
- Liquid fueled external heating system for STM4-120 Stirling engine p 180 A86-24888
- Test results of a 40 kW Stirling engine and comparison with the NASA-Lewis computer code predictions p 181 A86-24889
- RE-1000 free-piston Stirling engine update p 153 A86-24890
- Creep-rupture and fractographic analysis of Stirling engine superalloys tested in air and 15 MPa hydrogen p 82 A86-30041
- RE-1000 free-piston Stirling engine update [NASA-TM-87126] p 182 N86-11668
- Stirling engine supporting research and technology [NASA-TM-87175] p 208 N86-14106
- Creep rupture behavior of Stirling engine materials [NASA-TM-87209] p 88 N86-15380
- Ceramic automotive Stirling engine study [NASA-CR-174907] p 208 N86-16165
- Alloy chemistry and microstructural control to meet the demands of the automotive Stirling engine [NASA-TM-87250] p 89 N86-20541
- A new chromium carbide-based tribological coating for use to 900 deg C with particular reference to the Stirling engine [NASA-TM-87274] p 103 N86-21682
- Automotive Stirling Engine Development Program [NASA-CR-174749] p 211 N86-28017
- NASA/DOE automotive Stirling engine project: Overview 1986 [NASA-TM-87345] p 211 N86-29731
- Overview of NASA Lewis Research Center free-piston Stirling engine technology activities applicable to space power systems [NASA-TM-88815] p 211 N86-29732
- Automotive Stirling engine development program [NASA-CR-175045] p 211 N86-30579

STOICHIOMETRY

Graphite fiber intercalation: Basic properties of copper chloride intercalated fibers
[NASA-TM-87217] p 65 N86-18442

STORAGE BATTERIES

Development of a microprocessor controller for stand-alone photovoltaic power systems
[NASA-CR-174723] p 187 N86-21979

STORAGE STABILITY

Photovoltaic-powered vaccine refrigerator: Freezer systems field test results
[NASA-TM-86972-REV] p 181 N86-11666

STORAGE TANKS

LH2 on-orbit storage tank support trunnion design and verification p 53 A86-37054

STRAIN ENERGY METHODS

Fracture toughness tests on plasma-sprayed coatings p 64 A86-30051

STRAIN GAGES

High temperature static strain sensor development program p 148 N86-11500
Demonstration test of burner liner strain measurement systems: Interim results p 173 N86-11501
Demonstration test of burner liner strain measuring system
[NASA-CR-174743] p 148 N86-21817

STRAIN MEASUREMENT

Closure of fatigue cracks at high strains
[NASA-CR-175021] p 175 N86-17788
Demonstration test of burner liner strain measuring system
[NASA-CR-174743] p 148 N86-21817

STRAIN RATE

Slow plastic strain rate compressive flow in binary CoAl intermetallics p 79 A86-11478
Effect of multiple strain-anneal cycles on the 1000 C creep behaviour of gamma/gamma prime-alpha p 82 A86-30610

An update of the total-strain version of SRP
[NASA-TP-2499] p 87 N86-12295

Time dependency of strainrange partitioning life relationships
[NASA-CR-174946] p 174 N86-13755

STRATEGIC MATERIALS

The B2 aluminides as alternative materials p 84 A86-47259

STREAK PHOTOGRAPHY

Flow visualization of secondary flows in three curve ducts
[ASME PAPER 86-GT-166] p 136 A86-48218

STRESS ANALYSIS

Finite element analysis of residual stress in plasma-sprayed ceramic p 95 A86-15226
Thermal dependence of stress-induced birefringence in single mode optical fibers p 202 A86-15263
Finite elements based on consistently assumed stresses and displacements p 166 A86-18123
A new ply model for interlaminar stress analysis p 66 A86-20629

Analysis of an externally radially crack ring segment subject to three-point radial loading p 167 A86-20710
Stress analysis of gas turbine engine structures using the boundary element method p 169 A86-34444

Hybrid solid element with a traction-free cylindrical surface p 169 A86-34462

Dynamic stress analysis of smooth and notched fiber composite flexural specimens p 67 A86-41070

Stress and deformation modeling of multiple rotary combustion engine trochoid housings
[SAE PAPER 860614] p 156 A86-49624

Burner liner thermal/structural load modelling p 173 N86-11514

Component-specific modeling p 25 N86-11515

Effect on interference fits on roller bearing fatigue life
[NASA-TM-87165] p 158 N86-19616

Burner liner thermal-structural load modeling
[NASA-CR-174892] p 176 N86-21932

Thermomechanical design criteria for ceramic-coated surfaces
[NASA-TM-87328] p 143 N86-25726

On the modeling of low-Reynolds-number turbulence
[NASA-CR-3994] p 32 N86-28089

J-integral estimates for cracks in infinite bodies
[NASA-CR-179474] p 178 N86-28467

ICAN: A versatile code for predicting composite properties
[NASA-TM-87334] p 71 N86-31664

STRESS CONCENTRATION
Influence of load interactions on crack growth as related to state of stress and crack closure
[NASA-TM-87117] p 86 N86-12292

A unique set of micromechanics equations for high temperature metal matrix composites
[NASA-TM-87154] p 70 N86-24757

Experimental evaluation criteria for constitutive models of time dependent cyclic plasticity
[NASA-CR-176821] p 176 N86-25850

STRESS INTENSITY FACTORS
Analysis of an externally radially crack ring segment subject to three-point radial loading p 167 A86-20710
Influence of fatigue crack wake length and state of stress on crack closure
[NASA-TM-87282] p 90 N86-22686

STRESS MEASUREMENT
Deposition stress effects on the life of thermal barrier coatings on burner rigs p 96 A86-18271
High temperature static strain sensor development program p 148 N86-11500
Demonstration test of burner liner strain measurement systems: Interim results p 173 N86-11501

STRESS RELAXATION
Constitutive modeling for isotropic materials (HOST)
[NASA-CR-174980] p 172 N86-10589
Effects of state recovery on creep buckling under variable loading
[NASA-CR-175094] p 212 N86-25310
Cyclic creep analysis from elastic finite-element solutions
[NASA-TM-87213] p 176 N86-25822

STRESS WAVES
Factors influencing the ultrasonic stress wave factor evaluation of composite material structures p 168 A86-34257
Ultrasonic evaluation of mechanical properties of thick, multilayered, filament wound composites
[NASA-TM-87088] p 163 N86-10561
Effect of stress on ultrasonic pulses in fiber reinforced composites p 200 N86-22975
Stress waves in transversely isotropic media: The homogeneous problem
[NASA-CR-3977] p 164 N86-25002
Ultrasonic stress wave characterization of composite materials
[NASA-CR-3976] p 165 N86-27665
A study of the stress wave factor technique for nondestructive evaluation of composite materials
[NASA-CR-4002] p 165 N86-28445

STRESS-STRAIN DIAGRAMS
Simplified cyclic structural analyses of SSME turbine blades
[NASA-TM-87214] p 175 N86-16615

STRESS-STRAIN RELATIONSHIPS
The cyclic stress-strain behavior of a nickel-base superalloy at 650 C p 83 A86-45715
Life prediction and constitutive behavior p 173 N86-11520
Modifications of system for elevated temperature tensile testing and stress-strain measurement of metal matrix composites
[NASA-TM-87172] p 65 N86-13370
Cyclic structural analyses of anisotropic turbine blades for reusable space propulsion systems p 58 N86-17404
Experimental evaluation criteria for constitutive models of time dependent cyclic plasticity
[NASA-CR-176821] p 176 N86-25850
Structural analysis of turbine blades using unified constitutive models
[NASA-TM-88807] p 178 N86-28461
J-integral estimates for cracks in infinite bodies
[NASA-CR-179474] p 178 N86-28467

STRESS-STRAIN-TIME RELATIONS
Constitutive modeling of cyclic plasticity and creep, using an internal time concept p 170 A86-41673
Experimental evaluation criteria for constitutive models of time dependent cyclic plasticity
[NASA-CR-176821] p 176 N86-25850

STRONTIUM FLUORIDES
Growth and characterization of epitaxial SrF2 on InP(100) p 205 A86-47076

STRUCTURAL ANALYSIS
NASA Lewis Research Center/university graduate research program on engine structures
[ASME PAPER 85-GT-159] p 167 A86-22084
Hierarchical implicit dynamic least-square solution algorithm p 167 A86-26689
Vibration and buckling of rotating, pretwisted, precone beams including Coriolis effects p 168 A86-26910
Stress analysis of gas turbine engine structures using the boundary element method p 169 A86-34444
Iterative methods for mixed finite element equations p 169 A86-34461
A computer analysis program for interfacing thermal and structural codes p 193 A86-36861
Computer aided derivation of equations for composite mechanics problems and finite element analyses
[AIAA PAPER 86-1016] p 170 A86-38873
Probabilistic structural analysis methods for critical SSME propulsion components
[AIAA PAPER 86-1188] p 54 A86-40595

Computational composite mechanics for aerospace propulsion structures
[AIAA PAPER 86-1190] p 67 A86-405
Computational engine structural analysis
[ASME PAPER 86-GT-70] p 23 A86-481
Unified constitutive materials model development a evaluation for high-temperature structural analysis applications --- for aircraft gas turbine engines p 172 A86-491
Constitutive modeling for isotropic materials (HOST)
[NASA-CR-174980] p 172 N86-105
Turbine Engine Hot Section Technology (HOST)
[NASA-CP-2289] p 172 N86-114
HOST structural analysis program overview p 25 N86-115
Burner liner thermal/structural load modelling p 173 N86-115
Component-specific modeling p 25 N86-115
Validation of structural analysis methods using burner cyclic rig test data p 173 N86-115
NASA LeRC/Akron University Graduate Cooperative Fellowship Program and Graduate Student Research Program
[NASA-CR-174826] p 207 N86-132
Ceramic automotive Stirling engine study
[NASA-CR-174907] p 208 N86-1611
Simplified cyclic structural analyses of SSME turbine blades
[NASA-TM-87214] p 175 N86-166
Cyclic structural analyses of anisotropic turbine blades for reusable space propulsion systems p 58 N86-1741
Summary of tower designs for large horizontal axis wind turbines
[NASA-TM-87186] p 186 N86-187
Computational engine structural analysis
[NASA-TM-87231] p 175 N86-196
Integrated Composite Analyzer (ICAN): Users and programmers manual p 69 N86-2161
Advanced orbit transfer vehicle propulsion system study
[NASA-CR-174843] p 60 N86-2474
Structural analysis of turbine blades using unified constitutive models
[NASA-TM-88807] p 178 N86-2841
Fiber composite sandwich thermostructural behavior
Computational simulation
[NASA-TM-86787] p 71 N86-3164

STRUCTURAL DESIGN
Structural tailoring of SSME turbopump blades (SSME/STAEBL) --- Structural Tailoring of Engine Blades
[AIAA PAPER 86-0847] p 54 A86-3881
Advanced on-site power plant development technology program p 187 N86-2504
Nickel-hydrogen separator development
[NASA-TM-87332] p 188 N86-2667
A lumped parameter mathematical model for simulation of subsonic wind tunnels p 196 N86-2703
Large-Scale Advanced Prop-Fan (LAP) pitch change actuator and control design report
[NASA-CR-174788] p 31 N86-2726
The voltage threshold for arcing for solar cells in LEI Flight and ground test results
[NASA-TM-87259] p 62 N86-2812
High accuracy fuel flowmeter
[NASA-CR-174869] p 150 N86-3103

STRUCTURAL DESIGN CRITERIA
Analysis of fully stalled compressor
[AIAA PAPER 86-1123] p 5 A86-3848
Computational engine structural analysis
[ASME PAPER 86-GT-70] p 23 A86-4814
NASA LeRC/Akron University Graduate Cooperative Fellowship Program and Graduate Student Research Program
[NASA-CR-174826] p 207 N86-1321
Compliant hydrodynamic fluid journal bearing
[NASA-CASE-LEW-13670-1] p 158 N86-1960
Computational engine structural analysis
[NASA-TM-87231] p 175 N86-1966
Analysis of fully stalled compressor
[NASA-TM-87254] p 11 N86-2035
Advanced orbit transfer vehicle propulsion system study
[NASA-CR-174843] p 60 N86-2474

STRUCTURAL FAILURE
Structural integrity and durability for Space Shuttle main engine and future reusable space propulsion system
[AIAA PAPER 86-1513] p 55 A86-4268
Progressive damage, fracture predictions and post mortem correlations for fiber composites
[NASA-TM-87101] p 68 N86-10294

Structural integrity and durability for Space Shuttle main engine and future reusable space propulsion systems [NASA-TM-87280] p 61 N86-25408

Surface fatigue and failure characteristics of hot forged powder metal AISI 4620, AISI 4640, and machined AISI 4340 steel spur gears [NASA-TM-87330] p 161 N86-31889

STRUCTURAL MEMBERS

Modifications of system for elevated temperature tensile testing and stress-strain measurement of metal matrix composites [NASA-TM-87172] p 65 N86-13370

Extensions of the Ritz-Galerkin method for the forced, damped vibrations of structural elements p 176 N86-21909

STRUCTURAL RELIABILITY

Structural integrity and durability for Space Shuttle main engine and future reusable space propulsion systems [AIAA PAPER 86-1513] p 55 A86-42682

Structural integrity and durability for Space Shuttle main engine and future reusable space propulsion systems [NASA-TM-87280] p 61 N86-25408

STRUCTURAL STABILITY

Probabilistic structural analysis for space propulsion system components p 168 A86-28659

Aeroelastic behavior of low aspect ratio metal and composite blades [ASME PAPER 86-GT-243] p 171 A86-48271

STRUCTURAL VIBRATION

Vibration analysis of rotating turbomachinery blades by an improved finite difference method p 18 A86-14338

Vibration characteristics of mistuned shrouded blade assemblies [ASME PAPER 85-GT-115] p 19 A86-22068

The dynamics of a flexible bladed disc on a flexible rotor in a two-rotor system p 20 A86-25743

Vibrations of blades and bladed disk assemblies; Proceedings of the Tenth Biennial Conference on Mechanical Vibration and Noise, Cincinnati, OH, September 10-13, 1985 p 20 A86-26901

On the equivalence of the incremental harmonic balance method and the harmonic balance-Newton Raphson method p 170 A86-40695

Influence of third-degree geometric nonlinearities on the vibration and stability of pretwisted, precone, rotating blades [NASA-TM-87307] p 179 N86-31920

STUDS (STRUCTURAL MEMBERS)

Improved stud configurations for attaching laminated wood wind turbine blades [NASA-TM-87109] p 172 N86-10582

SUBCRITICAL FLOW

Two-phase flows and heat transfer within systems with ambient pressure above the thermodynamic critical pressure [NASA-TM-87228] p 140 N86-19558

SUBREFLECTORS

Near-field spillover from a subreflector: Theory and experiment [NASA-TM-88763] p 115 N86-25650

SUBSONIC FLOW

Simultaneous measurements of velocity and pressure fields in subsonic and supersonic flows through image-intensified detection of laser-induced fluorescence [AIAA PAPER 86-0161] p 145 A86-19726

Flow field and near and far sound field of a subsonic jet p 5 A86-35855

Application of a computational model for vortex generators in subsonic internal flows [AIAA PAPER 86-1458] p 8 A86-49612

Application of a computational model for vortex generators in subsonic internal flows [NASA-TM-87327] p 143 N86-26545

SUBSONIC WIND TUNNELS

Progress in the Lewis Research Center Altitude Wind Tunnel (AWT) modeling program [AIAA PAPER 86-0757] p 36 A86-24744

Development and application of dynamic simulations of a subsonic wind tunnel [AIAA PAPER 86-0758] p 36 A86-24745

Progress in the Lewis Research Center Altitude Wind Tunnel (AWT) Modeling Program [NASA-TM-87194] p 37 N86-16233

Development and application of dynamic simulations of a subsonic wind tunnel [NASA-TM-87211] p 43 N86-18338

A lumped parameter mathematical model for simulation of subsonic wind tunnels [NASA-TM-87324] p 196 N86-27036

SUBSTITUTES

The B2 aluminides as alternative materials p 84 A86-47259

SUBSTRATES

Optical and interfacial electronic properties of diamond-like carbon films p 204 A86-16268

Neutron and X-ray diffraction of plasma-sprayed zirconia-yttria thermal barrier coatings p 96 A86-16269

Deposition stress effects on the life of thermal barrier coatings on burner rigs p 96 A86-16271

Metallic glass as a temperature sensor during ion plating p 80 A86-16906

Tribological characteristics of gold films deposited on metals by ion plating and vapor deposition p 85 A86-49600

Textured carbon on copper: A novel surface with extremely low secondary electron emission characteristics [NASA-TP-2543] p 101 N86-15394

A computer program to calculate the resistivity of a thin film deposited on a conductive substrate from four-point probe measurements [NASA-TM-87262] p 193 N86-22150

SUBSTRUCTURES

Theoretical and software considerations for general dynamic analysis using multilevel substructured models [NASA-CR-176822] p 195 N86-26067

SULFATES

Adsorption of O₂, SO₂, and SO₃, on nickel oxide - Mechanism for sulfate formation p 75 A86-34238

Corrosion of nickel and cobalt base alloys in sulfate melts at 750 deg C [NASA-CR-175111] p 91 N86-24817

SULFUR OXIDES

Adsorption of O₂, SO₂, and SO₃, on nickel oxide - Mechanism for sulfate formation p 75 A86-34238

SULFURIC ACID

Interaction of sulfuric acid corrosion and mechanical wear of iron p 81 A86-20436

SUPERCARGERS

Lightweight two-stroke cycle aircraft diesel engine technology enablement program, volume 1 [NASA-CR-174923-VOL-1] p 26 N86-13328

Lightweight two-stroke cycle aircraft diesel engine technology enablement program, volume 2 [NASA-CR-174923-VOL-2] p 26 N86-13329

Lightweight two-stroke cycle aircraft diesel engine technology enablement program, volume 3 [NASA-CR-174923-VOL-3] p 26 N86-13330

A computer simulation of the turbocharged turbo compounded diesel engine system: A description of the thermodynamic and heat transfer models [NASA-CR-174971] p 208 N86-16164

SUPERCritical PRESSURES

Two-phase flows and heat transfer within systems with ambient pressure above the thermodynamic critical pressure [NASA-TM-87228] p 140 N86-19558

SUPERLATTICES

A possible radiation-resistant solar cell geometry using superlattices p 185 N86-17851

Optical constants of GaAs-AlGaAs superlattices and multiple quantum wells [NASA-CR-176717] p 205 N86-23468

Superlattices and NiPi structures in new forms of cascade solar cells [NASA-CR-176718] p 187 N86-24007

Theoretical study of the transverse dielectric constant of superlattices and their alloys [NASA-CR-177198] p 206 N86-28759

SUPERSONIC AIRCRAFT

Low-speed performance of an axisymmetric, mixed-compression, supersonic inlet with auxiliary inlets [NASA-TP-2557] p 30 N86-24694

SUPERSONIC COMPRESSORS

Mass balancing of hollow fan blades [ASME PAPER 86-GT-195] p 171 A86-48245

Mass balancing of hollow fan blades [NASA-TM-87197] p 174 N86-16611

SUPERSONIC CRUISE AIRCRAFT RESEARCH

Preliminary design of a supersonic cruise aircraft high-pressure turbine [NASA-CR-174878] p 26 N86-14272

SUPERSONIC FLOW

Simultaneous measurements of velocity and pressure fields in subsonic and supersonic flows through image-intensified detection of laser-induced fluorescence [AIAA PAPER 86-0161] p 145 A86-19726

Numerical analysis of some supersonic viscous flows related to inlet and nozzle systems [AIAA PAPER 86-1597] p 134 A86-42738

Forced response analysis of an aerodynamically detuned supersonic turbomachine rotor [NASA-TM-87093] p 9 N86-10019

SUPERSONIC FLUTTER

Aerodynamic and structural detuning of supersonic turbomachine rotors p 21 A86-31595

Influence of friction dampers on torsional blade flutter [ASME PAPER 85-GT-170] p 21 A86-32957

The predicted effect of aerodynamic detuning on coupled bending-torsion unstalled supersonic flutter [NASA-TM-87240] p 11 N86-21513

SUPERSONIC INLETS

Low-speed performance of an axisymmetric, mixed-compression, supersonic inlet with auxiliary inlets [NASA-TP-2557] p 30 N86-24694

SUPERSONIC SPEED

Preliminary measurement of the noise from the 2/9 scale model of the Large-scale Advanced Propfan (LAP) propeller, SR-7A [NASA-TM-87116] p 199 N86-14006

SUPERSONIC TURBINES

Forced response analysis of an aerodynamically detuned supersonic turbomachine rotor p 21 A86-26902

Passive control of aerodynamically forced vibrations of supersonic turbomachine rotors by splitter blades [AIAA PAPER 86-0844] p 22 A86-38892

SUPERSONIC WIND TUNNELS

Current wind tunnel capability and planned improvements at Lewis Research Center [AIAA PAPER 86-0728] p 36 A86-24727

Development of seeding techniques for small supersonic wind tunnel p 147 N86-11452

Current wind tunnel capability and planned improvements at Lewis Research Center [NASA-TM-87190] p 37 N86-18329

SUPPORTS

Summary of tower designs for large horizontal axis wind turbines [NASA-TM-87166] p 186 N86-18776

SUPPRESSORS

Free jet feasibility study of a thermal acoustic shield concept for AST/VCE application-dual flow. Comprehensive data report. Volume 1: Test nozzles and acoustic data [NASA-CR-174817] p 200 N86-23371

SURFACE DISTORTION

Compensation of reflector surface distortions using conjugate field matching [NASA-TM-87198] p 113 N86-16461

SURFACE FINISHING

Reliability of void detection in structural ceramics by use of scanning laser acoustic microscopy p 163 A86-39027

TWT efficiency enhancement with textured carbon surfaces on copper MDC electrodes -- multistage depressed collectors p 120 A86-49617

Sputtered cadmium oxide as a surface pretreatment for graphite solid lubricant films [NASA-TM-87300] p 104 N86-25473

Ion-beam nitriding of steels [NASA-CASE-LEW-14104-2] p 93 N86-32556

Textured carbon surfaces on copper by sputtering [NASA-CASE-LEW-14130-1] p 109 N86-32587

SURFACE GEOMETRY

Scattering of acoustic waves into Tollmien-Schlichting waves by small streamwise variations in surface geometry p 127 A86-17041

SURFACE LAYERS

The effect of a defective BSF layer on solar cell open circuit voltage -- Back Surface Field p 179 A86-12673

Comparison of calculated and experimental cascade performance for controlled-diffusion compressor stator blading [NASA-TM-87167] p 27 N86-16219

SURFACE PROPERTIES

Ellipsometric surface analysis of wear tracks produced by different lubricants [ASLE PREPRINT 85-TC-5A-2] p 151 A86-11016

Tribological properties of boron nitride synthesized by ion beam deposition p 96 A86-17479

New directions in lubrication, materials, wear, and surface interactions - Tribology in the 80's -- Book p 152 A86-18700

Ellipsometric surface analysis of wear tracks produced by different lubricants [NASA-TM-87142] p 87 N86-12293

Current viewpoints on oxide adherence mechanisms [NASA-TM-87168] p 87 N86-13409

Textured carbon on copper: A novel surface with extremely low secondary electron emission characteristics [NASA-TP-2543] p 101 N86-15394

Ion beam sputter etching [NASA-CASE-LEW-13899-1] p 109 N86-20587

Adequacy of surface analytical tools for studying the tribology of ceramics [NASA-TM-87308] p 104 N86-24837

Stability of surface nucleation [NASA-TM-88806] p 207 N86-30556

T

SURFACE REACTIONS

- Mechanical-contact-induced transformation from the amorphous to the partially crystalline state in metallic glass p 80 A86-16257
- Compatibility of grain-stabilized platinum with candidate propellants for resistojets p 51 A86-17835
- Compatibility of grain-stabilized platinum with candidate propellants for resistojets p 56 N86-10279
- Surface fatigue life and failure characteristics of EX-53, CBS 1000M, and AISI 9310 gear materials p 157 N86-12609
- Effects of surface chemistry on hot corrosion life p 32 N86-28087
- A study of Kapton degradation under simulated shuttle environment p 78 N86-28136
- SURFACE ROUGHNESS**
- Erosion of phosphor bronze under cavitation attack in a mineral oil p 81 A86-23324
- Quantitative flaw characterization with scanning laser acoustic microscopy p 163 A86-45150
- Lubrication of nonconformal contacts p 138 N86-13679
- Quantitative flaw characterization with scanning laser acoustic microscopy p 200 N86-22983
- Numerical simulation of the flowfield over ice accretion shapes p 144 N86-30093
- SURFACE ROUGHNESS EFFECTS**
- Analysis of a two row hydrostatic journal bearing with variable properties, inertia effects and surface roughness p 153 A86-30599
- Quantitative flaw characterization with scanning laser acoustic microscopy p 163 A86-45150
- Quantitative flaw characterization with scanning laser acoustic microscopy p 200 N86-22983
- SURFACE TEMPERATURE**
- Surface temperature distribution along a thin liquid layer due to thermocapillary convection p 126 A86-15800
- Metallic glass as a temperature sensor during ion plating p 80 A86-16906
- Fabrication of ceramic substrate-reinforced and free forms by mandrel plasma spraying metal-ceramic composites p 64 A86-17483
- An investigation of the transient thermal analysis of spur gears p 155 A86-40683
- Research instrumentation for hot section components of turbine engines p 150 N86-32702
- SURGES**
- A theory of post-stall transients in axial compression systems. I - Development of equations p 19 A86-22088
- A theory of post-stall transients in axial compression systems. II - Application p 19 A86-22089
- Summary of investigations of engine response to distorted inlet conditions p 30 N86-26336
- SWEEP EFFECT**
- Noise generated by convected gusts interacting with swept airfoil cascades p 198 A86-45492
- SWIRLING**
- Scalar and momentum turbulent transport experiments with swirling and nonswirling flows p 126 A86-11938
- Multispark flow visualization of lateral jet injection into a swirling cross flow p 1 A86-14581
- Numerical and experimental investigation of nonswirling and swirling confined jets p 127 A86-19651
- Swirling flows in typical combustor geometries p 128 A86-20370
- Periodic oscillations observed in swirling flows with and without combustion p 73 A86-22755
- Concentration distributions in a model combustor p 133 A86-38575
- Mass and momentum turbulent transport experiments with swirling confined coaxial jets. II p 134 A86-42780
- Influence of large-scale motion on turbulent transport for confined coaxial jets. Volume 2: Navier-Stokes calculations of swirling and nonswirling confined coaxial jets p 28 N86-20390
- Experiments on opposed lateral jets injected into swirling crossflow p 29 N86-20394
- SWITCHES**
- A new very high voltage semiconductor switch p 119 A86-40449

- Double-injection, deep-impurity switch development p 124 N86-30073
- SWITCHING CIRCUITS**
- 10 kW solar array switching unit performance test results p 118 A86-24844
- Design of high-voltage, high-power, solid state remote power controllers for aerospace applications p 122 N86-17456
- Hybrid power semiconductor p 122 N86-20672
- SWITCHING THEORY**
- Theoretical modeling of the vapor cavitation in dynamically loaded journal bearings p 130 A86-24496
- Theoretical modeling of the vapor cavitation in dynamically loaded journal bearings p 137 N86-10463
- SYNCHRONOUS PLATFORMS**
- Communications platform payload definition study p 49 N86-27402
- Communication Platform Payload Definition (CPPD) study. Volume 1: Executive summary p 49 N86-27403
- Communication Platform Payload Definition (CPPD) study. Volume 2: Technical report p 49 N86-27404
- Communication Platform Payload Definition (CPPD) study. Volume 3: Addendum p 49 N86-27405
- Communications platform payload definition study, executive summary p 49 N86-27407
- SYNCHRONOUS SATELLITES**
- Calculation of allowable orbital spacings for the fixed-satellite service p 43 N86-11212
- Communication Platform Payload Definition (CPPD) study. Volume 2: Technical report p 49 N86-27404
- Communication Platform Payload Definition (CPPD) study. Volume 3: Addendum p 49 N86-27405
- Communications platform payload definition study, executive summary p 49 N86-27407
- SYNTAX**
- The effects of syntactic complexity on the human-computer interaction p 192 A86-36172
- SYNTHESIS (CHEMISTRY)**
- The synthesis, characterization and thermal chemistry of modified norbornenyl PMR endcaps p 100 N86-11266
- SYSTEM EFFECTIVENESS**
- System life and reliability modeling for helicopter transmissions p 159 N86-24990
- SYSTEM FAILURES**
- Application of FDI metrics to detection and isolation of sensor failures in turbine engines p 21 A86-35400
- Robust detection, isolation, and accommodation for sensor failures --- in jet engine control systems p 21 A86-35402
- Robust detection, isolation and accommodation for sensor failures p 33 N86-30732
- SYSTEMS ANALYSIS**
- Photovoltaic-powered vaccine refrigerator: Freezer systems field test results p 181 N86-11666
- Communications platform payload definition study p 49 N86-27402
- SYSTEMS ENGINEERING**
- Designing an electro-impulse de-icing system p 16 A86-19940
- Design of a regenerative fuel cell system for Space Station p 53 A86-24857
- Engineering calculations for communications satellite systems planning p 114 N86-19493
- Research and technology, Lewis Research Center p 207 N86-21427
- System design and integration of the large-scale advanced prop-fan p 13 N86-31536
- Aeropropulsion opportunities for the 21st century p 34 N86-31585
- SYSTEMS MANAGEMENT**
- Development of a microprocessor controller for stand-alone photovoltaic power systems p 187 N86-21979

TANKS (CONTAINERS)

- Liquid-vapor interface locations in a spheroidal container under low gravity p 141 N86-23855

TANTALUM ALLOYS

- Thermal aging effects in refractory metal alloys p 89 N86-16333

TARS

- A fundamental study of smoldering with emphasis on experimental design for zero-g p 41 N86-10161

TASK COMPLEXITY

- The effects of syntactic complexity on the human-computer interaction p 192 A86-36172

TECHNOLOGICAL FORECASTING

- Space power systems - 'Spacecraft 2000' p 53 A86-24833

Spacecraft 2000

- [AIAA PAPER 86-0616] p 38 A86-29588

TECHNOLOGY ASSESSMENT

- NASA electric propulsion technology p 51 A86-17833

- Current wind tunnel capability and planned improvements at Lewis Research Center p 36 A86-24722

- Application of intersatellite links to domestic satellite systems p 44 A86-29588

- [AIAA PAPER 86-0604] p 38 A86-29588

- Technology achievements and projections for communication satellites of the future p 109 A86-29611

- Year 2000 small engine technology payoffs in cruise missiles p 23 A86-42701

- [AIAA PAPER 86-1546] p 157 N86-14612

- Gearing p 46 N86-16241

- Application of intersatellite links to domestic satellite systems p 113 N86-17591

- [NASA-TM-87215] p 49 N86-27402

- Technology achievements and projections for communication satellites of the future p 49 N86-27402

- [NASA-TM-87201] p 49 N86-27402

- Communications platform payload definition study, executive summary p 49 N86-27402

- [NASA-CR-174986] p 34 N86-31587

- Gas cooled fuel cell systems technology development p 190 N86-31984

- [NASA-CR-175047] p 209 N86-21457

- TECHNOLOGY TRANSFER**

- Automotive Stirling summary and overview p 209 N86-21457

- [NASA-TM-87177] p 209 N86-21457

- TECHNOLOGY UTILIZATION**

- Application of intersatellite links to domestic satellite systems p 44 A86-29588

- [AIAA PAPER 86-0604] p 46 N86-16245

- Application of intersatellite links to domestic satellite systems p 115 N86-24875

- [NASA-TM-87215] p 115 N86-24875

- Satellite voice broadcast. Volume 1: Executive summary p 115 N86-24875

- [NASA-CR-175016] p 115 N86-24875

- Satellite voice broadcast. Volume 2: System study p 115 N86-24875

- [NASA-CR-175017] p 115 N86-24875

- Communication Platform Payload Definition (CPPD) study. Volume 1: Executive summary p 49 N86-27403

- [NASA-CR-174928] p 49 N86-27403

- Communication Platform Payload Definition (CPPD) study. Volume 2: Technical report p 49 N86-27404

- [NASA-CR-174929] p 49 N86-27404

- Communication Platform Payload Definition (CPPD) study. Volume 3: Addendum p 49 N86-27405

- [NASA-CR-174930] p 49 N86-27405

- ACTS Experiments Program p 47 N86-31625

- [NASA-TM-88820] p 47 N86-31625

- TEMPERATURE CONTROL**

- Advanced thermal barrier system bond coatings for use on nickel-, cobalt- and iron-base alloy substrates p 85 A86-49856

- Chemical control of rate and onset temperature of nadimide polymerization p 101 N86-11271

- TEMPERATURE DEPENDENCE**

- Thermal dependence of stress-induced birefringence in single mode optical fibers p 202 A86-15263

- Temperature dependence of gamma-gamma prime lattice mismatch in nickel-base superalloys p 81 A86-21849

- Negative magnetoresistance of pitch-based carbon fibers Temperature and pressure dependence p 99 A86-35702

- Finite element simulation of temperature dependent free surface flows p 136 A86-47012
- The effects of grain size on the flow and fracture of long-range ordered alloys p 84 A86-47243
- Orientation and temperature dependence of some mechanical properties of the single-crystal nickel-base superalloy Rene N4. II - Low cycle fatigue behavior p 86 A86-50322
- Orientation and temperature dependence of some mechanical properties of the single-crystal nickel-base superalloy Rene N4. III - Tension-compression anisotropy p 86 A86-50323
- Performance and temperature dependencies of proton irradiated n/p GaAs and n/p silicon cells [NASA-TM-87136] p 120 N86-12509
- Compensation in epitaxial cubic SiC films [NASA-TM-87269] p 206 N86-25267
- The low cycle fatigue behavior of a plasma-sprayed coating material [NASA-TM-87318] p 92 N86-31699
- TEMPERATURE DISTRIBUTION**
- Surface temperature distribution along a thin liquid layer due to thermocapillary convection [IAF PAPER 85-282] p 126 A86-15800
- Perspectives on dilution jet mixing --- in creating temperature patterns at combustor exits in gas turbine engines [AIAA PAPER 86-1611] p 25 A86-49614
- Analysis of the transient behavior of rubbing components [NASA-CR-176546] p 102 N86-19464
- Burner liner thermal-structural load modeling [NASA-CR-174892] p 176 N86-21932
- Dilution jet mixing program, supplementary report [NASA-CR-175043] p 141 N86-23856
- Dilution jet mixing program, phase 3 [NASA-CR-174884] p 142 N86-24938
- TEMPERATURE EFFECTS**
- Effect of elevated temperature and pressure on sprays from simplex swirl atomizers [ASME PAPER 85-GT-58] p 130 A86-22735
- An experimental study of tone-excited heated jets p 197 A86-31593
- Nondestructive characterization of RBSCA of high-power bipolar transistors --- Reverse-bias safe operating area p 118 A86-35718
- Characterization methodology for PMR-15 p 65 N86-11272
- Compensation of reflector surface distortions using conjugate field matching [NASA-TM-87198] p 113 N86-16461
- Demonstrated results of welded and soldered interconnections p 185 N86-17866
- A model for the influence of pressure on the bulk modulus and the influence of temperature on the solidification pressure for liquid lubricants [NASA-TM-87230] p 140 N86-19555
- A unique set of micromechanics equations for high temperature metal matrix composites [NASA-TM-87154] p 70 N86-24757
- Corrosion of nickel and cobalt base alloys in sulfate melts at 750 deg C [NASA-CR-175111] p 91 N86-24817
- Emission FTIR analyses of thin microscopic patches of jet fuel residues deposited on heated metal surfaces [NASA-TM-176786] p 108 N86-25502
- Micromechanisms of thermomechanical fatigue: A comparison with isothermal fatigue [NASA-TM-87331] p 92 N86-28164
- Integrated research in constitutive modelling at elevated temperatures, part 2 [NASA-CR-177233] p 178 N86-28455
- Temperature effects on the universal equation of state of solids [NASA-TM-87321] p 206 N86-28776
- Integrated research in constitutive modelling at elevated temperatures, part 1 [NASA-CR-177237] p 179 N86-30227
- TEMPERATURE GRADIENTS**
- Oscillatory thermocapillary flows p 129 A86-22413
- An investigation of the transient thermal analysis of spur gears [ASME PAPER 84-DET-92] p 155 A86-40683
- Thermocapillary motion research p 40 N86-10125
- Analysis of large, non-isothermal elastic-visco-plastic deformations [NASA-CR-176220] p 172 N86-10588
- TEMPERATURE MEASUREMENT**
- Further development of the dynamic gas temperature measurement system [AIAA PAPER 86-1648] p 147 A86-42770
- Dynamic gas temperature measurement system p 147 N86-11499
- TEMPERATURE MEASURING INSTRUMENTS**
- HOST instrumentation R and D program overview p 147 N86-11497
- TEMPERATURE PROFILES**
- Plume characteristics of single-stream and dual-flow conventional and inverted-profile nozzles at equal thrust [AIAA PAPER 86-1809] p 8 A86-49585
- Flammability limits of gases under low gravity conditions p 42 N86-10164
- Plume characteristics of single-stream and dual-flow conventional and inverted-profile nozzles at equal thrust [NASA-TM-87323] p 12 N86-26285
- TEMPERATURE SENSORS**
- Metallic glass as a temperature sensor during ion plating p 80 A86-16906
- Fibre-optic thermometer using semiconductor-etalon sensor p 146 A86-32046
- 1700 deg C optical temperature sensor [NASA-CR-175108] p 203 N86-28729
- TENSILE PROPERTIES**
- Effect of boron on tensile properties of B2 BeAl [NASA-CR-175074] p 89 N86-21656
- Influence of fatigue crack wake length and state of stress on crack closure [NASA-TM-87292] p 90 N86-22686
- Tensile behavior of Fe-40Al alloys with B and Zr additions [NASA-TM-87290] p 91 N86-25453
- TENSILE STRENGTH**
- Modifications of system for elevated temperature tensile testing and stress-strain measurement of metal matrix composites [NASA-TM-87172] p 65 N86-13370
- Heat treatment for superalloy [NASA-CASE-LEW-14262-1] p 92 N86-26414
- TENSILE STRESS**
- Orientation and temperature dependence of some mechanical properties of the single-crystal nickel-base superalloy Rene N4. III - Tension-compression anisotropy p 86 A86-50323
- Theoretical and experimental comparison of vapor cavitation in dynamically loaded journal bearings [NASA-TM-87121] p 137 N86-11425
- Effect of stress on ultrasonic pulses in fiber reinforced composites p 200 N86-22975
- TENSILE TESTS**
- Graphite/PMR polyimide composites with improved toughness p 66 A86-21731
- Tensile adhesion test measurements on plasma-sprayed coatings p 98 A86-30052
- The tensile and fatigue deformation structures in a single crystal Ni-base superalloy p 83 A86-35697
- A study of spectrum fatigue crack propagation in two aluminum alloys. I - Spectrum simplification. II - Influence of microstructures p 85 A86-48973
- Orientation and temperature dependence of some mechanical properties of the single-crystal nickel-base superalloy Rene N4. I - Tensile behavior p 86 A86-50321
- Constitutive modeling for isotropic materials (HOST) [NASA-CR-174980] p 172 N86-10589
- Yielding and deformation behavior of the single crystal nickel-base superalloy PWA 1480 [NASA-CR-175100] p 91 N86-25455
- TENSORS**
- Nonlinear optimal control with tensors - Some computational issues p 194 A86-35419
- TERNARY SYSTEMS**
- Estimated heats of fusion of fluoride salt mixtures suitable for thermal energy storage applications [NASA-TM-87320] p 190 N86-31982
- TEST CHAMBERS**
- Fundamental studies of droplet combustion at reduced gravity p 42 N86-10165
- TEST EQUIPMENT**
- Apparatus for electrical measurements of thin films from 77 to 1000 K [NASA-TM-87256] p 148 N86-24959
- TEST FACILITIES**
- Heat transfer results and operational characteristics of the NASA Lewis Research Center hot section cascade test facility [ASME PAPER 85-GT-82] p 128 A86-22053
- Theory versus experiment for the rotordynamic coefficients of annular gas seals. I - Test facility and apparatus [ASME PAPER 85-TRIB-1] p 152 A86-24481
- Cryogenic Fluid Management Facility p 108 A86-37053
- HOST liner cyclic facilities p 173 N86-11519
- Uniform engine testing program phase 7: NASA Lewis Research Center second entry [NASA-TM-87272] p 31 N86-28085
- TEST STANDS**
- An analysis of cross-coupling of a multicomponent jet engine test stand using finite element modeling techniques [NASA-CR-176424] p 37 N86-15323
- Simplified cyclic structural analyses of SSME turbine blades [NASA-TM-87214] p 175 N86-16615
- TETHERING**
- Space station propulsion requirements study [NASA-CR-174934] p 57 N86-15339
- TETHERLINES**
- Electrodynamic tether technology considerations p 161 N86-27657
- TEXTURES**
- Textured carbon on copper: A novel surface with extremely low secondary electron emission characteristics [NASA-TP-2543] p 101 N86-15394
- THERMAL ANALYSIS**
- Composite sandwich thermostructural behavior - Computational simulation [AIAA PAPER 86-0948] p 170 A86-38842
- Liquid droplet radiator thermal characteristics [AIAA PAPER 86-1162] p 133 A86-40578
- An investigation of the transient thermal analysis of spur gears [ASME PAPER 84-DET-92] p 155 A86-40683
- The synthesis, characterization and thermal chemistry of modified norbornenyl PMR endcaps p 100 N86-11266
- THERMAL CONTROL COATINGS**
- Neutron and X-ray diffraction of plasma-sprayed zirconia-ytria thermal barrier coatings p 96 A86-18269
- Failure analysis of plasma-sprayed thermal barrier coatings p 80 A86-16270
- Optimization of the Ni-Cr-Al-Y/ZrO₂-Y₂O₃ thermal barrier system p 82 A86-31746
- Advanced thermal barrier system bond coatings for use on nickel-, cobalt- and iron-base alloy substrates p 85 A86-49856
- Rocket thrust chamber thermal barrier coatings [NASA-CR-175022] p 59 N86-20497
- Ceramic thermal barrier coatings for electric utility gas turbine engines [NASA-TM-87288] p 90 N86-22687
- Thermal barrier coating life prediction model development [NASA-CR-175087] p 103 N86-22713
- THERMAL CYCLING TESTS**
- Fracture mechanics applied to nonisothermal fatigue crack growth p 81 A86-28951
- The cyclic stress-strain behavior of a nickel-base superalloy at 650 C p 83 A86-45715
- Thermal-mechanical fatigue test apparatus for metal matrix composites and joint attachments [NASA-TM-87187] p 88 N86-15378
- Demonstrated results of welded and soldered interconnections p 185 N86-17866
- THERMAL DEGRADATION**
- Modeling degradation and failure of Ni-Cr-Al overlay coatings p 80 A86-16276
- The effects of metals and inhibitors on thermal oxidative degradation reactions of unbranched perfluoroalkyl ethers p 99 A86-40682
- Thermal aging effects in refractory metal alloys [NASA-TM-87210] p 89 N86-16334
- THERMAL DIFFUSION**
- Thermophoretically augmented mass transfer rates to solid walls across laminar boundary layers p 128 A86-20150
- THERMAL DIFFUSIVITY**
- Improved perfluoroalkyl ether fluid development [NASA-TM-87276] p 104 N86-25474
- THERMAL ENERGY**
- Method for improving the fuel efficiency of a gas turbine engine [NASA-CASE-LEW-13142-2] p 28 N86-20389
- THERMAL EXPANSION**
- Temperature effects on the universal equation of state of solids [NASA-TM-87321] p 206 N86-28776
- Fiber composite sandwich thermostructural behavior: Computational simulation [NASA-TM-88787] p 71 N86-31663
- THERMAL FATIGUE**
- Thermal-mechanical fatigue crack growth in Inconel X-750 p 81 A86-20982
- Elevated temperature biaxial fatigue [NASA-TM-175009] p 174 N86-11526
- Thermal-mechanical fatigue behavior of nickel-base superalloys [NASA-CR-175048] p 91 N86-24818
- Low-cycle thermal fatigue [NASA-TM-87225] p 177 N86-26651
- Thermal-fatigue and oxidation resistance of cobalt-modified Udimet 700 alloy [NASA-TP-2591] p 178 N86-28464

THERMAL PROTECTION

Thermal stress minimized, two component, turbine shroud seal
[NASA-CASE-LEW-14212-1] p 162 N86-32740

THERMAL RESISTANCE

Performance of thermal barrier coatings in high heat flux environments p 80 A86-16272
The 371 deg C mechanical properties of graphite/polyimide composites
[NASA-TM-87122] p 69 N86-12256

THERMAL STABILITY

Graphite/PMR polyimide composites with improved toughness p 66 A86-21731
All-aromatic biphenylene end-capped polyquinoline and polyimide matrix resins p 100 N86-11267
Replacement of MDA with more oxidatively stable diamines in PMR-polyimides p 101 N86-11275
Specimen geometry effects on graphite/PMR-15 composites during thermo-oxidative aging
[NASA-TM-87204] p 69 N86-17477
High temperature resistant polyimide from tetra ester, diamine, diester and N-arylnadimide
[NASA-CASE-LEW-13864-1] p 102 N86-19457

THERMAL STRESSES

Inelastic high-temperature thermomechanical response of ceramic coated gas turbine seals p 169 A86-37799
Toward improved durability in advanced combustors and turbines - Progress in prediction of thermomechanical loads
[ASME PAPER 86-GT-172] p 24 A86-48224

HOST structural analysis program overview
p 25 N86-11513

Burner liner thermal/structural load modelling
p 173 N86-11514
Validation of structural analysis methods using burner liner cyclic rig test data
p 173 N86-11518

Low-cycle thermal fatigue
[NASA-TM-87225] p 177 N86-26651
Thermal stress minimized, two component, turbine shroud seal

[NASA-CASE-LEW-14212-1] p 162 N86-32740

THERMIONIC CATHODES

Thermionic noise measurements for on-line dispenser cathode diagnostics for linear beam microwave tubes
[NASA-CR-175105] p 124 N86-28323

THERMIONIC CONVERTERS

Fundamental studies on a heat driven lamp
[NASA-CR-176381] p 204 N86-15122

THERMIONIC DIODES

Fundamental studies on a heat driven lamp
[NASA-CR-176381] p 204 N86-15122

THERMIONIC POWER GENERATION

Fundamental studies on a heat driven lamp
[NASA-CR-176381] p 204 N86-15122

THERMOCOUPLES

High-temperature thermocouple and heat flux gauge using a unique thin film-hardware hot junction
[ASME PAPER 85-GT-18] p 145 A86-13059

Further development of the dynamic gas temperature measurement system
[AIAA PAPER 86-1648] p 147 A86-42770

A numerical and experimental investigation of electrochemical aircraft deicing
[NASA-CR-175024] p 14 N86-20380

THERMODYNAMIC CYCLES

A preliminary study of the modified Ericsson for space power
p 180 A86-24840

Overview of free-piston Stirling SP-100 activities at the NASA Lewis Research Center
[NASA-TM-87224] p 209 N86-19264

Methods for heat transfer and temperature field analysis of the insulated diesel phase 2 progress report
[NASA-CR-175072] p 210 N86-24590

Cyclic creep analysis from elastic finite-element solutions
[NASA-TM-87213] p 176 N86-25822

THERMODYNAMIC EFFICIENCY

Preliminary evaluation of a compound cycle engine for shipboard gensets
[NASA-CR-179451] p 160 N86-26629

THERMODYNAMIC PROPERTIES

Thermodynamic evaluation of transonic compressor rotors using the finite volume approach
[NASA-CR-176428] p 27 N86-16220

Long-term stability and properties of zirconia ceramics for heavy duty diesel engine components
[NASA-CR-174943] p 209 N86-17224

Thermoviscoplastic nonlinear constitutive relationships for structural analysis of high temperature metal matrix composites
[NASA-TM-87291] p 70 N86-24756

Thermodynamic evaluation of transonic compressor rotors using the finite volume approach
[NASA-CR-176840] p 143 N86-26546

Characterization of real gas properties for space shuttle main engine fuel turbine and performance calculations
[NASA-CR-175068] p 61 N86-27418

Formulation of the nonlinear analysis of shell-like structures, subjected to time-dependent mechanical and thermal loading
[NASA-CR-177194] p 178 N86-28462

THERMODYNAMICS

Designing for fiber composite structural durability in hygrothermomechanical environments
p 67 A86-27734

Component-specific modeling
p 25 N86-11515
Thermal-mechanical fatigue test apparatus for metal matrix composites and joint attachments
[NASA-TM-87187] p 88 N86-15378

A computer simulation of the turbocharged turbo compounded diesel engine system: A description of the thermodynamic and heat transfer models
[NASA-CR-174971] p 208 N86-18164

Thermal-mechanical fatigue behavior of nickel-base superalloys
[NASA-CR-175048] p 91 N86-24818

Improved perfluoroalkylether fluid development
[NASA-TM-87276] p 104 N86-25474

Two-phase flows within systems with ambient pressure
p 161 N86-30167

Integrated research in constitutive modelling at elevated temperatures, part 1
[NASA-CR-177237] p 179 N86-30227

THERMOGRAVIMETRY

A ceramic matrix composite based on polymerization and pyrolysis of ethynylated aromatics
p 65 A86-13169

THERMOMECHANICAL TREATMENT

Thermomechanical design criteria for ceramic-coated surfaces
[NASA-TM-87328] p 143 N86-25726

THERMOMETERS

Fibre-optic thermometer using semiconductor-etalon sensor
p 146 A86-32048

THERMOPLASTIC RESINS

Angular particle impingement studies of thermoplastic materials at normal incidence
[ASLE PREPRINT 85-AM-3A-1] p 94 A86-11076

The correlation of low-velocity impact resistance of graphite-fiber-reinforced composites with matrix properties
[NASA-TM-87337] p 71 N86-27426

THERMOPLASTICITY

Inelastic high-temperature thermomechanical response of ceramic coated gas turbine seals
p 169 A86-37799

THERMOSETTING RESINS

Effect of solution concentration and aging conditions on PMR-15 resin
p 98 A86-33113

THERMOVISCOELASTICITY

Thermomechanical cyclic hardening behavior of Hastelloy-X
[NASA-CR-174999] p 174 N86-16610

Thermoviscoplastic nonlinear constitutive relationships for structural analysis of high temperature metal matrix composites
[NASA-TM-87291] p 70 N86-24756

THICKNESS

Ion beam sputter deposited zinc telluride films
p 204 A86-47066

Ion beam sputter deposited zinc telluride films
[NASA-TM-87119] p 205 N86-11048

THICKNESS RATIO

Joint research effort on vibrations of twisted plates, phase 1: Final results
[NASA-RP-11150] p 172 N86-10579

THIN AIRFOILS

System design and integration of the large-scale advanced prop-fan
[NASA-CR-174789] p 13 N86-31536

THIN BODIES

Convenient mounting method for electrical measurements of thin samples
p 120 A86-48649

THIN FILMS

High-temperature thermocouple and heat flux gauge using a unique thin film-hardware hot junction
[ASME PAPER 85-GT-18] p 145 A86-13059

Ion beam sputter-deposited thin film coatings for protection of spacecraft polymers in low earth orbit
[AIAA PAPER 85-0420] p 95 A86-14428

Composition and properties of the so-called 'diamond-like' amorphous carbon films
p 96 A86-16255

Frictional and morphological properties of Au-MoS₂ films sputtered from a compact target
p 152 A86-16258

Optical and interfacial electronic properties of diamond-like carbon films
p 204 A86-16268

Computer simulation of thin-film nucleation and growth - The multilayer mode
p 204 A86-37441

Ion beam sputter deposited zinc telluride films
p 204 A86-47066

Thin film growth rate effects for primary ion beam deposited diamondlike carbon films
p 100 A86-47004

Dry etching of beta-SiC in CF₄ and CF₄ + C₂H₆ mixtures
p 76 A86-47064

Mass spectrometric studies of the electrical breakdown of thin polymer films
p 100 A86-47070

Diamondlike carbon films on semiconductors for insulated-gate technology
p 120 A86-47070

TWT efficiency enhancement with textured carbon surfaces on copper MDC electrodes - multistage depressed collectors
p 120 A86-49616

Dual-ion-beam deposition of carbon films with diamond-like properties
p 85 A86-49855

Ion beam sputter deposited zinc telluride films
[NASA-TM-87119] p 205 N86-11048

Ellipsometric and optical study of some uncommon insulator films on 3-5 semiconductors
[NASA-TM-87135] p 205 N86-12131

A thin film degradation study of a fluorinated polyether liquid lubricant using an HPLC method
[NASA-TM-87221] p 77 N86-19411

How to evaluate solid lubricant films using a pin-on-disk tribometer
[NASA-TM-87236] p 102 N86-19468

A computer program to calculate the resistivity of a thin film deposited on a conductive substrate from four-point probe measurements
[NASA-TM-87262] p 193 N86-22155

Apparatus for electrical measurements of thin films from 77 to 1000 K
[NASA-TM-87256] p 148 N86-24955

Sputtered cadmium oxide as a surface pretreatment for graphite solid lubricant films
[NASA-TM-87300] p 104 N86-25477

Polarization modulated ellipsometry
[NASA-CR-177264] p 149 N86-26589

Feasibility study of a discrete bearing/roller drive rotor joint for the space station
[NASA-TM-88800] p 161 N86-30200

Stability of surface nucleation
[NASA-TM-88806] p 207 N86-30555

THIN WALLED SHELLS

Fabrication of ceramic substrate-reinforced and free forms by mandrel plasma spraying metal-ceramic composites
p 64 A86-17488

Formulation of the nonlinear analysis of shell-like structures, subjected to time-dependent mechanical and thermal loading
[NASA-CR-177194] p 178 N86-28462

THREE DIMENSIONAL BODIES

Optimized three-dimensional lenses for wide-angle scanning
p 109 A86-19181

Advanced three-dimensional dynamic analysis by boundary element methods
p 169 A86-34444

THREE DIMENSIONAL BOUNDARY LAYER

Calculation of three-dimensional boundary layers on rotating turbine blades
p 131 A86-28699

Computation of turbulent flows on rotating bodies and ducts
p 135 A86-46300

Three-dimensional boundary layer on a compressor rotor blade at peak pressure rise coefficient
[ASME PAPER 86-GT-186] p 7 A86-48233

Assessment of a 3-D boundary layer code to predict heat transfer and flow losses in a turbine
p 138 N86-11500

Mean velocity and turbulence measurements in a 90 deg curved duct with thin inlet boundary layer
[NASA-CR-174811] p 139 N86-16511

THREE DIMENSIONAL COMPOSITES

Three-dimensional hybrid-stress finite element analysis of composite laminates with cracks and cutouts
p 167 A86-26891

THREE DIMENSIONAL FLOW

Numerical study of three-dimensional turbulent flow interactions between blockage models and wind tunnels including longitudinally slotted test sections
[AIAA PAPER 85-5017] p 1 A86-11068

Calculation of three-dimensional, viscous flow through turbomachinery blade passage by parabolic marching
p 2 A86-20372

Steady inviscid three-dimensional flows
p 128 A86-20952

Modeling the 3-D flow effects on deviation angle for axial compressor middle stages
[ASME PAPER 85-GT-189] p 2 A86-22102

Three dimensional flow phenomena in fluid machinery: Proceedings of the Winter Annual Meeting, Miami Beach, FL, November 17-22, 1985
p 4 A86-28682

Three-dimensional inviscid analysis of radial-turbine flow and a limited comparison with experimental data
p 4 A86-28702

Three-dimensional inviscid flow in mixers. I - Mixer analysis using a Cartesian grid
p 5 A86-3909C

A new approach for solving the three-dimensional steady Euler equations. I - General theory
p 133 A86-41242

- A comparison of computational methods for three-dimensional, turbulent turbomachinery flow fields [AIAA PAPER 86-1599] p 6 A86-42740
- Three-dimensional inviscid flow in mixers. II - Analysis of turbofan forced mixers p 6 A86-46316
- Computation of three-dimensional, rotational flow through turbomachinery blade rows for improved aerodynamic design studies [ASME PAPER 86-GT-26] p 7 A86-48117
- Validation of viscous and inviscid computational methods for turbomachinery components [ASME PAPER 86-GT-42] p 7 A86-48126
- Three-dimensional flow field measurements in a radial inflow turbine scroll using LDV [ASME PAPER 86-GT-122] p 7 A86-48181
- Three-dimensional fluid flow phenomena in the blade end wall corner region [ASME PAPER 86-GT-179] p 7 A86-48229
- Three-dimensional inviscid analysis of radial turbine flow and a limited comparison with experimental data [NASA-TM-87091] p 9 N86-10017
- Gas flow environmental and heat transfer nonrotating 3D program p 137 N86-11506
- Validation of viscous and inviscid computational methods for turbomachinery components [NASA-TM-87193] p 10 N86-16194
- Thermodynamic evaluation of transonic compressor rotors using the finite volume approach [NASA-CR-176428] p 27 N86-16220
- THREE DIMENSIONAL MOTION**
- Three dimensional unsteady aerodynamics and aeroelastic response of advanced turboprops [AIAA PAPER 86-0846] p 22 A86-38894
- THRESHOLD VOLTAGE**
- Threshold determining mechanisms for discharges in high voltage solar arrays [AIAA PAPER 86-0364] p 52 A86-19834
- THRUST**
- Experimental and theoretical study of propeller spinner/shank interference [NASA-CR-176954] p 13 N86-29773
- THRUST BEARINGS**
- Lateral dampers for thrust bearings [NASA-CR-174924] p 157 N86-11474
- THRUST CHAMBERS**
- Rapid evaluation of ion thruster lifetime using optical emission spectroscopy [AIAA PAPER 85-2011] p 51 A86-17851
- Rapid evaluation of ion thruster lifetime using optical emission spectroscopy [NASA-TM-87103] p 56 N86-10280
- Rocket thrust chamber thermal barrier coatings [NASA-CR-175022] p 59 N86-20497
- Thermomechanical design criteria for ceramic-coated surfaces [NASA-TM-87328] p 143 N86-25726
- Test program to provide confidence in liquid oxygen cooling of hydrocarbon fueled rocket thrust chambers [NASA-TM-88816] p 62 N86-31646
- Proven, long-life hydrogen/oxygen thrust chambers for space station propulsion [NASA-TM-88822] p 64 N86-32522
- THRUST LOADS**
- Centaur engine gimbal friction characteristics under simulated thrust load [NASA-TM-87335] p 44 N86-31621
- THRUST MEASUREMENT**
- Vacuum chamber pressure effects on thrust measurements p 59 N86-17425
- THRUST VECTOR CONTROL**
- An analysis of cross-coupling of a multicomponent jet engine test stand using finite element modeling techniques [NASA-CR-176424] p 37 N86-15323
- Centaur engine gimbal friction characteristics under simulated thrust load [NASA-TM-87335] p 44 N86-31621
- THRUST-WEIGHT RATIO**
- Polymer, metal and ceramic matrix composites for advanced aircraft engine applications [NASA-TM-87132] p 87 N86-13407
- TILT ROTOR AIRCRAFT**
- Feasibility study for convertible engine torque converter [NASA-CR-175082] p 33 N86-30733
- TIME**
- Time domain referencing in intensity modulation fiber optic sensing systems [NASA-CR-175109] p 17 N86-24691
- TIME DEPENDENCE**
- Time-dependent wave envelope finite difference analysis of sound propagation p 197 A86-20130
- Time dependency of strainrange partitioning life relationships [NASA-CR-174946] p 174 N86-13755
- TIME MARCHING**
- Thermodynamic evaluation of transonic compressor rotors using the finite volume approach [NASA-CR-176428] p 27 N86-16220
- Thermodynamic evaluation of transonic compressor rotors using the finite volume approach [NASA-CR-176840] p 143 N86-26546
- TIME OF FLIGHT SPECTROMETERS**
- Implementation of a new type of time-of-flight laser anemometer p 146 A86-29755
- Mass spectrometric studies of the electrical breakdown of thin polymer films p 100 A86-47070
- TIME SHARING**
- The effects of syntactic complexity on the human-computer interaction p 192 A86-36172
- TIME TEMPERATURE PARAMETER**
- Heat-flux measurements for the rotor of a full-stage turbine. II - Description of analysis technique and typical time-resolved measurements [ASME PAPER 86-GT-78] p 24 A86-48146
- TIP SPEED**
- Preliminary measurement of the noise from the 2/9 scale model of the Large-scale Advanced Propfan (LAP) propeller, SR-7A [NASA-TM-87116] p 199 N86-14006
- Laboratory experiments on active suppression of advanced turbo-prop noise [NASA-TM-87129] p 199 N86-19125
- TIP VANES**
- Development and testing of tip devices for horizontal axis wind turbines [NASA-CR-174991] p 185 N86-18774
- TITANIUM**
- Characterization of the tribological coating composition 77 wt % CaF₂ - 23 wt % Li F fused to IN-750 alloy [NASA-TM-87342] p 105 N86-27452
- TITANIUM ALLOYS**
- Selected fretting-wear-resistant coatings for Ti-6 pct Al-4 pct V alloy p 97 A86-24956
- Aeroelastic behavior of low aspect ratio metal and composite blades [ASME PAPER 86-GT-243] p 171 A86-48271
- TOLLMEIN-SCHLICHTING WAVES**
- Scattering of acoustic waves into Tollmien-Schlichting waves by small streamwise variations in surface geometry p 127 A86-17041
- TOLUENE**
- Ignition delay times of benzene and toluene with oxygen in argon mixtures [NASA-TM-87312] p 78 N86-25431
- TOPOGRAPHY**
- Nonlinear damage analysis: Postulate and evaluation [NASA-CR-168171] p 177 N86-26652
- TORQUE**
- Experimental and theoretical study of propeller spinner/shank interference [NASA-CR-176954] p 13 N86-29773
- TORQUE CONVERTERS**
- Feasibility study for convertible engine torque converter [NASA-CR-175082] p 33 N86-30733
- TORSION**
- The predicted effect of aerodynamic detuning on coupled bending-torsion unstalled supersonic flutter [NASA-TM-87240] p 11 N86-21513
- Influence of third-degree geometric nonlinearities on the vibration and stability of pretwisted, precone, rotating blades [NASA-TM-87307] p 179 N86-31920
- TORSIONAL VIBRATION**
- Aerodynamic and structural detuning of supersonic turbomachine rotors p 21 A86-31595
- Influence of friction dampers on torsional blade flutter [ASME PAPER 85-GT-170] p 21 A86-32957
- Torsional vibrations and dynamic loads in a basic planetary gear system p 156 A86-47354
- Nonlinear bending-torsional vibration and stability of rotating, pretwisted, precone blades including Coriolis effects [NASA-TM-87207] p 175 N86-17789
- TOUGHNESS**
- Graphite/PMR polyimide composites with improved toughness p 66 A86-21731
- Transformation toughened ceramics for the heavy duty diesel engine technology program, phase 2 [NASA-CR-175054] p 210 N86-22451
- The correlation of low-velocity impact resistance of graphite-fiber-reinforced composites with matrix properties [NASA-TM-87337] p 71 N86-27426
- TOWERS**
- Summary of tower designs for large horizontal axis wind turbines [NASA-TM-87166] p 186 N86-18776
- TRACTION**
- Traction forces at solid-lubricated rolling/sliding contacts [ASLE PREPRINT 85-AM-4E-2] p 151 A86-11091
- Spin analysis of concentrated traction contacts [ASME PAPER 84-DET-99] p 155 A86-45257
- Design of traction drives [NASA-RP-1154] p 157 N86-13734
- TRAILING EDGE FLAPS**
- Summary of NASA/DOE Aileron-Control Development Program for Wind Turbines [NASA-TM-88811] p 190 N86-31983
- TRAJECTORY CONTROL**
- Resonant power processors. II - Methods of control p 117 A86-14482
- TRANSCONDUCTANCE**
- Determination of carrier saturation velocity in high-performance In(y)Ga(1-y)As/Al(x)Ga(1-x)As modulation-doped field-effect transistors (with y between 0 and 0.2) p 118 A86-37295
- TRANSDUCERS**
- Unsteady pressure measurements on a biconvex airfoil in a transonic oscillating cascade [ASME PAPER 85-GT-212] p 3 A86-22731
- Preliminary results of unsteady blade surface pressure measurements for the SR-3 propeller [AIAA PAPER 86-1893] p 8 A86-49625
- Preliminary results of unsteady blade surface pressure measurements for the SR-3 propeller [NASA-TM-87352] p 12 N86-27213
- TRANSFER FUNCTIONS**
- Transfer function concept for ultrasonic characterization of material microstructures p 200 N86-22980
- A lumped parameter mathematical model for simulation of subsonic wind tunnels [NASA-TM-87324] p 196 N86-27036
- TRANSFER ORBITS**
- Manrating orbital transfer vehicle propulsion [AIAA PAPER 85-1226] p 50 A86-14429
- Primary propulsion of electrothermal, ion, and chemical systems for space-based radar orbit transfer [AIAA PAPER 85-1477] p 50 A86-14431
- An analysis of low-thrust, resistojet reboost for the Space Station [AIAA PAPER 85-2042] p 51 A86-14447
- Radiation exposure and performance of multiple burn LEO-GEO orbit transfer trajectories p 43 N86-17417
- TRANSFORMATIONS (MATHEMATICS)**
- Bounding solutions of geometrically nonlinear viscoelastic problems [AIAA PAPER 86-0943] p 170 A86-38838
- Bounding solutions of geometrically nonlinear viscoelastic problems [NASA-CR-176219] p 195 N86-10860
- TRANSFORMERS**
- Rotary transformer design with fixed magnetizing and/or leakage inductances p 119 A86-40462
- TRANSIENT RESPONSE**
- Probabilistic finite elements for transient analysis in nonlinear continua p 168 A86-28653
- Advanced three-dimensional dynamic analysis by boundary element methods p 169 A86-34445
- A fundamental study of smoldering with emphasis on experimental design for zero-g p 41 N86-10162
- Compensation in epitaxial cubic SiC films [NASA-TM-87269] p 206 N86-25267
- TRANSISTOR AMPLIFIERS**
- Nondestructive characterization of RBOSOA of high-power bipolar transistors --- Reverse-bias safe operating area p 118 A86-35718
- TRANSISTOR CIRCUITS**
- Designing a 25-kilowatt high frequency series resonant [NASA-CR-176774] p 123 N86-24906
- TRANSITION FLOW**
- Low Reynold's number boundary layers in a disturbed environment [NASA-CR-175031] p 139 N86-17665
- TRANSITION POINTS**
- Ignition characteristics of rich n-heptane fuel sprays in the transition region [ASME PAPER 85-WA/HT-46] p 107 A86-38393
- TRANSITION TEMPERATURE**
- The 371 deg C mechanical properties of graphite/polyimide composites p 69 N86-12256
- Structure-to-glass transition temperature relationships in high temperature stable condensation polyimides [NASA-TM-87113] p 101 N86-12311
- Structure-to-property relationships in addition cured polymers 2: Resin Tg composite initial mechanical properties of norbornenyl cured polyimide resins [NASA-TM-88794] p 105 N86-29041

TRANSMISSION LINES

Performance analysis of radiation cooled dc transmission lines for high power space systems

p 117 A86-24811

Transmission line design for a power distribution system at 20 kHz for aircraft

[NASA-CR-3987] p 32 N86-29818

TRANSMISSIONS (MACHINE ELEMENTS)

Torsional vibrations and dynamic loads in a basic planetary gear system

p 156 A86-47354

System life and reliability modeling for helicopter transmissions

[NASA-CR-3967] p 159 N86-24990

Testing of YUH-61A helicopter transmission in NASA Lewis 2240-kW (3000-hp) facility

[NASA-TP-2538] p 160 N86-24992

Generation of spiral bevel gears with zero kinematical errors and computer aided tooth contact analysis

[NASA-TM-87273] p 160 N86-25793

New methodology for shaft design based on life expectancy

[NASA-TM-87354] p 161 N86-27661

TRANSMISSIVITY

Particle cloud combustion experiment

p 41 N86-10160

TRANSONIC COMPRESSORS

Thermodynamic evaluation of transonic compressor rotors using the finite volume approach

[NASA-CR-176428] p 27 N86-16220

Thermodynamic evaluation of transonic compressor rotors using the finite volume approach

[NASA-CR-176840] p 143 N86-26546

TRANSONIC FLOW

Accelerated solution of the steady Euler equations

p 2 A86-20942

Applications of variational principles in computing rotational flows

p 128 A86-20951

Calculations of two and three-dimensional transonic cascade flow fields using the Navier-Stokes equations

[ASME PAPER 85-GT-66] p 2 A86-22046

Unsteady transonic flow over cascade blades

p 3 A86-23141

Unsteady transonic flow in cascades

p 4 A86-24693

Transonic potential flow in hyperbolic nozzles

p 5 A86-41723

Validation of viscous and inviscid computational methods for turbomachinery components

[ASME PAPER 86-GT-42] p 7 A86-48126

Validation of viscous and inviscid computational methods for turbomachinery components

[NASA-TM-87193] p 10 N86-16194

An LU implicitly scheme for high speed inlet analysis

[NASA-CR-175098] p 11 N86-23563

Rotor wake characteristics of a transonic axial flow fan

[NASA-TM-87073] p 13 N86-28055

TRANSONIC SPEED

Unsteady transonic flow in cascades

p 4 A86-24693

TRANSONIC WIND TUNNELS

Development of an impulsive noise source to study the acoustic reflection characteristics of hard-walled wind tunnels

[AIAA PAPER 86-1887] p 198 A86-45500

Acoustic reflection contamination measurements in the 16-foot NASA Langley Transonic Wind Tunnel

[AIAA PAPER 86-1888] p 198 A86-45501

TRANSPARENCE

Optical and interfacial electronic properties of diamond-like carbon films

p 204 A86-16268

TRANSPONDERS

Simulated performance of the NASA 30/20 GHz test transponder using multi-H phase coded modulation

[AIAA PAPER 86-0717] p 110 A86-29656

TRANSPORT AIRCRAFT

Evaluation of propeller/nacelle interactions in the PTA program

[AIAA PAPER 86-1552] p 6 A86-42709

In-flight measurements of wing ice shapes and wing section drag increases caused by natural icing conditions

[NASA-TM-87301] p 12 N86-24667

TRANSPORT PROPERTIES

High transconductance InGaAs/AlGaAs pseudomorphic modulation-doped field-effect transistors

p 117 A86-18814

Mass and momentum turbulent transport experiments with swirling confined coaxial jets. II

[AIAA PAPER 86-1665] p 134 A86-42780

Light scattering tests of fundamental theories of transport properties in the critical region

p 39 N86-10113

Transport processes research

p 40 N86-10129

Improvement of the second- and third-moment modeling of turbulence: A study of Reynolds-stress closure model

[NASA-CR-176478] p 139 N86-18519

Experiments for the determination of convective diffusion heat/mass transfer to burner rig test targets comparable in size to jet stream diameter

[NASA-TM-87196] p 139 N86-18646

Characterization of real gas properties for space shuttle main engine fuel turbine and performance calculations

[NASA-CR-175066] p 61 N86-27418

TRANSPORT THEORY

Transport processes in solution crystal growth

p 39 N86-10107

Transport processes research

p 40 N86-10129

TRANSPORTATION

Future heavy duty trucking engine requirements

[NASA-CR-174996] p 209 N86-17226

TRAVELING WAVE TUBES

Verification of an improved computational design procedure for TWT-dynamic refocuser-MDC systems with secondary electron emission losses

p 119 A86-45194

TWT efficiency enhancement with textured carbon surfaces on copper MDC electrodes -- multistage depressed collectors

p 120 A86-49617

Verification of computer-aided designs of traveling-wave tubes utilizing novel dynamic refocusers and graphite electrodes for the multistage depressed collector

[NASA-TP-2524] p 121 N86-13643

Textured carbon on copper: A novel surface with extremely low secondary electron emission characteristics

[NASA-TP-2543] p 101 N86-15394

Linearized traveling wave amplifier with hard limiter characteristics

[NASA-CASE-LEW-13981-2] p 122 N86-21742

Thermionic noise measurements for on-line dispenser cathode diagnostics for linear beam microwave tubes

[NASA-CR-175105] p 124 N86-28323

Secondary-electron-emission losses in multistage depressed collectors and traveling-wave-tube efficiency improvements with carbon collector electrode surfaces

[NASA-TP-2622] p 125 N86-32629

TRAVELING WAVES

10-30 GHz monolithic GaAs travelling-wave divider/combiner

p 118 A86-34882

TRIBOLOGY

Low-wear partially fluorinated polyimides

p 94 A86-11175

Tribological properties of boron nitride synthesized by ion beam deposition

p 96 A86-17479

New directions in lubrication, materials, wear, and surface interactions - Tribology in the 80's -- Book

p 152 A86-18700

Tribological properties of graphite-fiber-reinforced, partially fluorinated polyimide composites

p 98 A86-34177

The use of silver in self-lubricating coatings for extreme temperatures

p 99 A86-44425

Tribological characteristics of gold films deposited on metals by ion plating and vapor deposition

p 85 A86-49600

Tribological properties of structural ceramics

[NASA-TM-87105] p 100 N86-10341

How to evaluate solid lubricant films using a pin-on-disk tribometer

[NASA-TM-87236] p 102 N86-19465

Adequacy of surface analytical tools for studying the tribology of ceramics

[NASA-TM-87308] p 104 N86-24837

Tribology of selected ceramics at temperatures to 900 deg C

[NASA-TM-87267] p 105 N86-25476

Characterization of the tribological coating composition 77 wt % CaF₂ - 23 wt % Li F fused to IN-750 alloy

[NASA-TM-87342] p 105 N86-27452

TRIODES

Textured carbon surfaces on copper by sputtering

[NASA-CASE-LEW-14130-1] p 109 N86-32587

TRUCKS

Future heavy duty trucking engine requirements

[NASA-CR-174996] p 209 N86-17226

Stirling Powered Van Program overview

[NASA-TM-87227] p 210 N86-25303

TRUSSES

Hybrid deployable/erectable solar dynamic box truss system

[AIAA PAPER 86-0955] p 47 A86-38883

TUNABLE LASERS

Range finding using frequency-modulated laser diode

p 147 A86-39521

TUNGSTEN

Interdiffusional effects between tungsten fibers and an iron-nickel-base alloy

p 66 A86-14718

Thermal-mechanical fatigue test apparatus for metal matrix composites and joint attachments

[NASA-TM-87187] p 88 N86-15378

TUNING

Vibration characteristics of mistuned shrouded bl assemblies

[ASME PAPER 85-GT-115] p 19 A86-2

The predicted effect of aerodynamic detuning coupled bending-torsion unstalled supersonic flutter

[NASA-TM-87240] p 11 N86-2

TURBINE BLADES

Local heat-transfer measurements on a 1/4 scale-model turbine blade airfoil using a composite heater element and liquid crystals

[ASME PAPER 85-GT-59] p 126 A86-1

Preliminary results of a study of the relationship between free stream turbulence and stagnation region transfer

[ASME PAPER 85-GT-84] p 129 A86-22

Vibrations of blades and bladed disk assembly

Proceedings of the Tenth Biennial Conference

Mechanical Vibration and Noise, Cincinnati, September 10-13, 1985

p 20 A86-26

The effect of limiting aerodynamic and structural coupling in models of mistuned bladed disk vibration

p 21 A86-26

Calculation of three-dimensional boundary layers rotating turbine blades

p 131 A86-28

Three-dimensional inviscid analysis of radial-turbine and a limited comparison with experimental data

p 4 A86-28

Studies on the hot corrosion of a nickel-base superalloy

Udimet 700 p 82 A86-29

Aerodynamic and structural detuning of supersonic turbomachine rotors

p 21 A86-31

Na₂SO₄ induced corrosion of nickel at 1100°C

p 83 A86-37

Structural tailoring of SSME turbopump blades (SSME/STAEBL) -- Structural Tailoring of Engine Blades

[AIAA PAPER 86-0847] p 54 A86-38

Relaminarization of the boundary layer over a flat plate in shock tube experiments

[AIAA PAPER 86-1236] p 133 A86-39

Heat-flux measurements for the rotor of a full-scale turbine. I - Time-averaged results

[ASME PAPER 86-GT-77] p 24 A86-48

Three-dimensional flow field measurements in a radial inflow turbine scroll using LDV

[ASME PAPER 86-GT-122] p 7 A86-48

Aeroelastic behavior of low aspect ratio metal composite blades

[ASME PAPER 86-GT-243] p 171 A86-48

Three-dimensional inviscid analysis of radial turbine and a limited comparison with experimental data

[NASA-TM-87091] p 9 N86-10

Film cooling on a convex wall: Heat transfer and hydrodynamic measurements for full and partial coverage

[NASA-CR-174964] p 137 N86-10

Joint research effort on vibrations of twisted blades: phase 1: Final results

[NASA-RP-1150] p 172 N86-10

Improved stud configurations for attaching laminar wood wind turbine blades

[NASA-TM-87109] p 172 N86-10

Assessment of a 3-D boundary layer code to predict heat transfer and flow losses in a turbine

p 138 N86-11

Life prediction and constitutive behavior

p 173 N86-11

Turbine blade and vane heat flux sensor development phase 2

[NASA-CR-174995] p 26 N86-122

Simplified cyclic structural analyses of SSME turbine blades

[NASA-TM-87214] p 175 N86-186

Cyclic structural analyses of anisotropic turbine blades for reusable space propulsion systems

p 58 N86-174

Low-cost single-crystal turbine blades, volume 2

[NASA-CR-174652] p 29 N86-235

Thermoviscoplastic nonlinear constitutive relationships for structural analysis of high temperature metal matrix composites

[NASA-TM-87291] p 70 N86-247

Structural tailoring of engine blades (STAEBL) user manual

[NASA-CR-175113] p 31 N86-272

Channel flow modeling of impingement cooling of rotating turbine blade

[NASA-CR-177206] p 31 N86-272

Structural analysis of turbine blades using unified constitutive models

[NASA-TM-88807] p 178 N86-284

Application of a personal computer for the uncoupled vibration analysis of wind turbine blade and counterweight assemblies

[NASA-CR-175080] p 188 N86-285

Design and initial testing of a one-bladed 30-meter-diameter rotor on the NASA/DOE mod-O wind turbine
[NASA-TM-88810] p 189 N86-30251

System design and integration of the large-scale advanced prop-fan
[NASA-CR-174789] p 13 N86-31536

Summary of NASA/DOE Aileron-Control Development Program for Wind Turbines
[NASA-TM-88811] p 190 N86-31983

Structural dynamic measurement practices for turbomachinery at the NASA Lewis Research Center
[NASA-TM-88857] p 35 N86-32433

TURBINE ENGINES

Long term deposit formation in aviation turbine fuel at elevated temperature
[AIAA PAPER 86-0525] p 107 A86-19929

Application of FDI metrics to detection and isolation of sensor failures in turbine engines p 21 A86-35400

Toward improved durability in advanced combustors and turbines - Progress in prediction of thermomechanical loads
[ASME PAPER 86-GT-172] p 24 A86-48224

Film cooling on a convex wall: Heat transfer and hydrodynamic measurements for full and partial coverage
[NASA-CR-174964] p 137 N86-10461

Turbine engine Hot Section Technology (HOST) project p 173 N86-11496

HOST instrumentation R and D program overview p 147 N86-11497

Assessment of a 3-D boundary layer code to predict heat transfer and flow losses in a turbine p 138 N86-11508

Preliminary design of a supersonic cruise aircraft high-pressure turbine
[NASA-CR-174878] p 26 N86-14272

Simulating a small turboshaft engine in real-time multiprocessor simulator (RTMPS) environment
[NASA-TM-87216] p 27 N86-16221

A real-time simulation evaluation of an advanced detection, isolation and accommodation algorithm for sensor failures in turbine engines
[NASA-TM-87289] p 30 N86-24697

Combined fringe and Fabry-Perot laser anemometer for three component velocity measurements in turbine stator cascade facility
[NASA-TM-87322] p 149 N86-24967

Structural tailoring of engine blades (STAEBL) theoretical manual p 31 N86-27283

Uniform engine testing program phase 7: NASA Lewis Research Center second entry
[NASA-TM-87272] p 31 N86-28085

Variable area radial turbine fabrication and test program
[NASA-CR-175091] p 32 N86-28947

Research instrumentation for hot section components of turbine engines
[NASA-TM-88851] p 150 N86-32702

TURBINE EXHAUST NOZZLES

Plume characteristics of single-stream and dual-flow conventional and inverted-profile nozzles at equal thrust
[AIAA PAPER 86-1809] p 8 A86-49585

Plume characteristics of single-stream and dual-flow conventional and inverted-profile nozzles at equal thrust
[NASA-TM-87323] p 12 N86-26285

TURBINE PUMPS

Structural tailoring of SSME turbopump blades (SSME/STAEBL) --- Structural Tailoring of Engine Blades
[AIAA PAPER 86-0847] p 54 A86-38895

Advanced seals for Liquid Oxygen (LOX) turbopumps p 157 N86-17408

Passive eddy-current damping as a means of vibration control in cryogenic turbomachinery
[NASA-TP-2562] p 44 N86-24722

Characterization of real gas properties for space shuttle main engine fuel turbine and performance calculations
[NASA-CR-175066] p 61 N86-27418

SSME long-life bearings
[NASA-CR-179455] p 160 N86-27643

Evaluation of a hybrid hydrostatic bearing for cryogenic turbopump application
[NASA-TM-87255] p 63 N86-31649

TURBINE WHEELS

The dynamics of a flexible bladed disc on a flexible rotor in a two-rotor system p 20 A86-25743

Turbine-stage heat transfer - Comparison of short-duration measurements with state-of-the-art predictions
[AIAA PAPER 86-1465] p 134 A86-42656

Heat-flux measurements for the rotor of a full-stage turbine. I - Time-averaged results
[ASME PAPER 86-GT-77] p 24 A86-48145

Heat-flux measurements for the rotor of a full-stage turbine. II - Description of analysis technique and typical time-resolved measurements
[ASME PAPER 86-GT-78] p 24 A86-48146

TURBINES

Extended parametric representation of compressor fans and turbines. Volume 2: Part user's manual (parametric turbine)
[NASA-CR-174646] p 159 N86-23937

Two-phase flows within systems with ambient pressure p 161 N86-30167

TURBOCOMPRESSORS

A theory of post-stall transients in axial compression systems. I - Development of equations
[ASME PAPER 85-GT-171] p 19 A86-22088

A theory of post-stall transients in axial compression systems. II - Application
[ASME PAPER 85-GT-172] p 19 A86-22089

End-wall and profile losses in a low-speed axial flow compressor rotor
[ASME PAPER 85-GT-174] p 20 A86-22090

Modeling the 3-D flow effects on deviation angle for axial compressor middle stages
[ASME PAPER 85-GT-189] p 2 A86-22102

Three-dimensional boundary layer on a compressor rotor blade at peak pressure rise coefficient
[ASME PAPER 86-GT-186] p 7 A86-48236

Fluid machines: Expanding the limits, past and future
[NASA-TM-87161] p 26 N86-12227

TURBOFAN AIRCRAFT

Aerodynamic detuning analysis of an unstalled supersonic turbofan cascade
[ASME PAPER 85-GT-192] p 3 A86-22732

The STOL performance of a two-engine, USB powered-lift aircraft with cross-shafted fans
[SAE PAPER 851839] p 16 A86-38336

TURBOFAN ENGINES

DEAN - A program for Dynamic Engine Analysis
[AIAA PAPER 85-1354] p 18 A86-14430

The dynamics of a flexible bladed disc on a flexible rotor in a two-rotor system p 20 A86-25743

Three-dimensional inviscid flow in mixers. I - Mixer analysis using a Cartesian grid p 5 A86-39090

Three-dimensional inviscid flow in mixers. II - Analysis of turbofan forced mixers p 6 A86-46316

An iterative finite element-integral technique for predicting sound radiation from turbofan inlets in steady flight p 198 A86-49806

A real-time simulation evaluation of an advanced detection, isolation and accommodation algorithm for sensor failures in turbine engines
[NASA-TM-87289] p 30 N86-24697

Turbofan aft duct suppressor study program listing and user's guide
[NASA-CR-175067] p 30 N86-25357

A supersonic fan equipped variable cycle engine for a Mach 2.7 supersonic transport
[NASA-CR-177141] p 32 N86-28946

HYTESSE 2: A Hypothetical Turbofan Engine Simplified Simulation with multivariable control and sensor analytical redundancy
[NASA-TM-87344] p 124 N86-30068

Feasibility study for convertible engine torque converter
[NASA-CR-175082] p 33 N86-30733

An overview of the Small Engine Component Technology (SECT) studies
[NASA-TM-88796] p 34 N86-31587

TURBOFANS

Analytical and experimental investigation of the coupled bladed disk/shaft whirl of a cantilevered turbofan
[ASME PAPER 86-GT-98] p 24 A86-48163

Modeling the effects of wind tunnel wall absorption on the acoustic radiation characteristics of propellers
[NASA-TM-87333] p 201 N86-29630

TURBOJET ENGINE CONTROL

Robust detection, isolation, and accommodation for sensor failures --- in jet engine control systems p 21 A86-35402

The application of LQR synthesis techniques to the turboshaft engine control problem --- Linear Quadratic Regulator p 22 A86-35614

TURBOJET ENGINES

Experimental study of ceramic-coated tip seals for turbojet engines p 152 A86-15227

TURBOMACHINE BLADES

Vibration analysis of rotating turbomachinery blades by an improved finite difference method p 18 A86-14338

Vibration characteristics of mistuned shrouded blade assemblies
[ASME PAPER 85-GT-115] p 19 A86-22068

Model equation for simulating flows in multistage turbomachinery
[ASME PAPER 85-GT-226] p 2 A86-22123

Unsteady transonic flow over cascade blades p 3 A86-23141

Unsteady transonic flow in cascades p 4 A86-24693

The effects of strong shock loading on coupled bending-torsion flutter of tuned and mistuned cascades p 20 A86-26893

TURBOMACHINERY

Future directions in aeropropulsion technology p 1 A86-11602

Development of an explicit multigrid algorithm for quasi-three-dimensional viscous flows in turbomachinery
[AIAA PAPER 86-0032] p 1 A86-19644

Model equation for simulating flows in multistage turbomachinery
[ASME PAPER 85-GT-226] p 2 A86-22123

Aeroelastic formulations for turbomachines and propellers p 20 A86-24677

The use of an optical data acquisition system for bladed disk vibration analysis p 146 A86-26909

Computation of viscous flows in turbomachinery cascades with a space-marching method p 5 A86-39089

Assessment of a parabolic analysis for axisymmetric internal flows in rocket and turbomachinery ducts
[AIAA PAPER 86-1598] p 134 A86-42739

A comparison of computational methods for three-dimensional, turbulent turbomachinery flow fields
[AIAA PAPER 86-1599] p 6 A86-42740

Computation of three-dimensional, rotational flow through turbomachinery blade rows for improved aerodynamic design studies
[ASME PAPER 86-GT-26] p 7 A86-48117

A model for closing the inviscid form of the average-passage equation system
[ASME PAPER 86-GT-227] p 8 A86-48261

Development of an explicit multigrid algorithm for quasi-three-dimensional viscous flows in turbomachinery
[NASA-TM-87128] p 1 N86-11146

Laser anemometry for hot section applications p 151 N86-11503

A FORTRAN computer code for calculating flows in multiple-blade-element cascades
[NASA-TM-87104] p 9 N86-13295

A model for closing the inviscid form of the average-passage equation system
[NASA-TM-87199] p 10 N86-14224

Compliant hydrodynamic fluid journal bearing
[NASA-CASE-LEW-13670-1] p 158 N86-19606

Ramp-integration technique for capacitance-type blade-tip clearance measurement
[NASA-TM-87241] p 149 N86-24964

Application of laser anemometry to turbomachinery flow field measurements p 160 N86-27640

Laser fringe anemometry for aero engine components
[NASA-TM-88798] p 12 N86-28053

Instability in Rotating Machinery
[NASA-CP-2409] p 161 N86-30160

Structural dynamic measurement practices for turbomachinery at the NASA Lewis Research Center
[NASA-TM-88857] p 35 N86-32433

TURBOPROP AIRCRAFT

Three dimensional unsteady aerodynamics and aeroelastic response of advanced turboprops
[AIAA PAPER 86-0846] p 22 A86-38894

An experimental investigation of reducing advanced turboprop cabin noise by wing shielding
[AIAA PAPER 86-1966] p 16 A86-45449

Acoustic reflection contamination measurements in the 16-foot NASA Langley Transonic Wind Tunnel
[AIAA PAPER 86-1888] p 198 A86-45501

Summary of recent NASA propeller research p 25 N86-11158

Laboratory experiments on active suppression of advanced turboprop noise
[NASA-TM-87129] p 199 N86-19125

An estimate of the enroute noise of an advanced turboprop airplane NASA-TM-87302 E-3020 NAS 1.15:87302 HC A02/MF A01
[NASA-TM-87302] p 201 N86-25217

An experimental investigation of reducing advanced turboprop cabin noise by wing shielding
[NASA-TM-87112] p 201 N86-25218

TURBOPROP ENGINES

Improved Euler analysis of advanced turboprop propeller flows
[AIAA PAPER 86-1521] p 6 A86-42688

Rotorcraft propulsion for year 2000 plus
[AIAA PAPER 86-1543] p 23 A86-42702

Small engine technology payoffs for future commuter aircraft
[AIAA PAPER 86-1544] p 23 A86-42703

Fatigue life analysis of a turboprop reduction gearbox
[ASME PAPER 85-DET-10] p 155 A86-45256

Development of an impulsive noise source to study the acoustic reflection characteristics of hard-walled wind tunnels
[AIAA PAPER 86-1887] p 198 A86-45500

- A numerical simulation of the inviscid flow through a counter-rotating propeller
[NASA-TM-87200] p 10 N86-16195
- Experimental classical flutter results of a composite advanced turboprop model
[NASA-TM-88792] p 178 N86-29271
- System design and integration of the large-scale advanced prop-fan
[NASA-CR-1747n4] p 13 N86-31536
- An overview of the Small Engine Component Technology (SECT) studies
[NASA-TM-88796] p 34 N86-31587

TURBORAMJET ENGINES

- A parametric study of a gas-generator air turbo ramjet (ATR)
[NASA-TM-88808] p 34 N86-31586

TURBOSHAFTS

- The application of LQR synthesis techniques to the turboshaft engine control problem --- Linear Quadratic Regulator
p 22 A86-35614
- Simulating a small turboshaft engine in real-time multiprocessor simulator (RTMPS) environment
[NASA-TM-87216] p 27 N86-16221
- Thermomechanical design criteria for ceramic-coated surfaces
[NASA-TM-87328] p 143 N86-25726

TURBULENCE

- Numerical and experimental investigation of nonswirling and swirling confined jets
[AIAA PAPER 86-0040] p 127 A86-19651
- Film cooling on a convex wall: Heat transfer and hydrodynamic measurements for full and partial coverage
[NASA-CR-174964] p 137 N86-10461
- Effect of liquid droplets on turbulence in a round gaseous jet
[NASA-CR-175063] p 29 N86-23597
- Review and evaluation of recent developments in helix inlet dynamic flow distortion prediction and computer program documentation and user's manual estimating maximum instantaneous inlet flow distortion from steady-state total pressure measurements with full, limited, or no dynamic data
[NASA-CR-176765] p 143 N86-24955

TURBULENCE EFFECTS

- Effect of free stream turbulence on flow separation
p 125 A86-11676
- Numerical synthesis of tri-variate velocity realizations of turbulence
p 168 A86-28654
- Buoyancy effects upon vapor flame and explosion processes
p 41 N86-10161

TURBULENT BOUNDARY LAYER

- Boundary layer measurements on an airfoil in cascade using laser Doppler anemometry
[AIAA PAPER 86-0072] p 145 A86-19670
- Direct numerical simulations of chemically reacting turbulent mixing layers
p 130 A86-25567
- Three-dimensional boundary layer on a compressor rotor blade at peak pressure rise coefficient
[ASME PAPER 86-GT-186] p 7 A86-48236
- Influence of large-scale motion on turbulent transport for confined coaxial jets. Volume 1: Analytical analysis of the experimental data using conditional sampling
[NASA-CR-175035] p 29 N86-20395
- Measurements of a turbulent horseshoe vortex formed around a cylinder
[NASA-CR-3986] p 13 N86-28063

TURBULENT DIFFUSION

- Turbulence energy and diffusion transport in a separating and reattaching flow
[AIAA PAPER 86-1724] p 135 A86-42812

TURBULENT FLOW

- Numerical study of three-dimensional turbulent flow interactions between blockage models and wind tunnels including longitudinally slotted test sections
[AIAA PAPER 85-5017] p 1 A86-11065
- Structure of nonevaporating sprays. II - Drop and turbulence properties
p 125 A86-11237
- Scalar and momentum turbulent transport experiments with swirling and nonswirling flows
p 126 A86-11938
- Heat transfer and fluid mechanics measurements in transitional boundary layer flows
[ASME PAPER 85-GT-113] p 126 A86-13068
- Drop-turbulence interactions in a diffusion flame
p 73 A86-20139
- Swirling flows in typical combustor geometries
p 128 A86-20370
- Calculations of two and three-dimensional transonic cascade flow fields using the Navier-Stokes equations
[ASME PAPER 85-GT-66] p 2 A86-22046
- A review and analysis of boundary layer transition data for turbine application
[ASME PAPER 85-GT-83] p 129 A86-22054

- Preliminary results of a study of the relationship between free stream turbulence and stagnation region heat transfer
[ASME PAPER 85-GT-84] p 129 A86-22055
- Prediction of heat release effects on a mixing layer
[AIAA PAPER 86-0058] p 129 A86-22676
- Computation of turbulent rotating channel flow with an algebraic Reynolds stress model
[AIAA PAPER 86-0214] p 130 A86-22682
- A three-dimensional axisymmetric calculation procedure for turbulent flows in a radial vaneless diffuser
[ASME PAPER 85-GT-133] p 3 A86-22733
- Periodic oscillations observed in swirling flows with and without combustion
p 73 A86-22755
- Numerical simulation of a turbulent flame stabilized behind a rearward-facing step
p 73 A86-22774
- Spray atomization and combustion
[AIAA PAPER 86-0136] p 131 A86-26606
- Accuracy and directional sensitivity of the single-wire technique
p 146 A86-28541
- Implementation of a new type of time-of-flight laser anemometer
p 146 A86-29755
- Theory of interactive combustion of counterflow premixed flames
p 74 A86-32752
- A comparison of three algebraic stress closures for combustor flow calculations
[ASME PAPER 85-WA/FE-3] p 132 A86-38388
- Triple-velocity products in a channel with a backward-facing step
p 133 A86-41725
- Mass and momentum turbulent transport experiments with swirling confined coaxial jets. II
[AIAA PAPER 86-1665] p 134 A86-42780
- Turbulence energy and diffusion transport in a separating and reattaching flow
[AIAA PAPER 86-1724] p 135 A86-42812
- Turbulent two-phase flow in annular seals
[ASLE PREPRINT 86-AM-4G-3] p 156 A86-45391
- Computation of turbulent flows on rotating bodies and ducts
p 135 A86-46307
- Is Navier-Stokes turbulence chaotic?
p 137 A86-50275
- Semiempirical method of determining flow coefficients for pilot rake mass flow rate measurements
[NASA-TM-87144] p 9 N86-14219
- Improvement of the second- and third-moment modeling of turbulence: A study of Reynolds-stress closure model
[NASA-CR-176478] p 139 N86-16519
- Low Reynolds number boundary layers in a disturbed environment
[NASA-CR-175031] p 139 N86-17665
- Measurements of a single lateral jet injected into swirling crossflow
[NASA-CR-175040] p 28 N86-20392
- Shear layer excitation, experiment versus theory
[NASA-CR-176804] p 140 N86-20722
- Prediction of heat release effects on a mixing layer
[NASA-CR-175044] p 142 N86-23857
- Contributions to the understanding of large-scale coherent structures in developing free turbulent shear flows
[NASA-CR-176772] p 142 N86-24932
- Measurements of a turbulent horseshoe vortex formed around a cylinder
[NASA-CR-3986] p 13 N86-28063
- On the modeling of low-Reynolds-number turbulence
[NASA-CR-3994] p 32 N86-28089
- Thermodynamic evaluation of transonic compressor rotors using the finite volume approach
[NASA-CR-176947] p 32 N86-30731
- Turbulent dispersion of the icing cloud from spray nozzles used in icing tunnels
[NASA-TM-87316] p 34 N86-31588

TURBULENT JETS

- Multispark flow visualization of lateral jet injection into a swirling cross flow
p 1 A86-14561
- Tone excited jets. III - Flow measurements
p 127 A86-16468
- Tone excited jets. V - A theoretical model and comparison with experiment
p 196 A86-16470
- Hot-wire measurements of a single lateral jet injected into swirling crossflow
[AIAA PAPER 86-0055] p 127 A86-19661
- Formation and inflammation of a turbulent jet
p 130 A86-23131
- An analytical model for the vorticity associated with a transverse jet
p 4 A86-28538
- Local equilibrium assumption for round jet calculations
p 136 A86-49829
- Experiments on opposed lateral jets injected into swirling crossflow
[NASA-CR-175041] p 29 N86-20394

TURBULENT MIXING

- Concentration distributions in cylindrical combustors
p 126 A86-11837
- Prediction of heat release effects on a mixing layer
[AIAA PAPER 86-0058] p 129 A86-22676

- Direct numerical simulations of chemically reacting turbulent mixing layers
p 130 A86-251
- Coherent structures in a turbulent mixing layer: comparison between direct numerical simulations and experiments
p 132 A86-301
- Some unresolved questions on hot-jet mixing controlled through artificial excitation
[AIAA PAPER 86-1956] p 135 A86-451
- Measurements of a single lateral jet injected into swirling crossflow
[NASA-CR-175040] p 28 N86-201
- Experiments on opposed lateral jets injected into swirling crossflow
[NASA-CR-175041] p 29 N86-201
- Prediction of heat release effects on a mixing layer
[NASA-CR-175044] p 142 N86-231

TURBULENT WAKES

- Measurements of a single lateral jet injected into swirling crossflow
[NASA-CR-175040] p 28 N86-201

TWISTING

- Influence of rotation and pretwist on cantilever fan blade flutter
p 17 A86-1116
- Joint research effort on vibrations of twisted plate phase 1: Final results
[NASA-RP-1150] p 172 N86-101

TWO DIMENSIONAL BOUNDARY LAYER

- Turbine vane external heat transfer. Volume 1: Analytical and experimental evaluation of surface heat transfer distributions with leading edge showerhead cooling
[NASA-CR-174827] p 29 N86-211

TWO DIMENSIONAL FLOW

- Finite-amplitude steady waves in plane viscous shear flows
[AD-A165461] p 127 A86-194
- An analytical model for the vorticity associated with transverse jet
p 4 A86-285
- A two-dimensional numerical study of the flow inside the combustion chambers of a motored rotary engine
[NASA-TM-87212] p 10 N86-192
- Thermodynamic evaluation of transonic compressor rotors using the finite volume approach
[NASA-CR-176947] p 32 N86-307

TWO PHASE FLOW

- Prediction of the structure of fuel sprays in gas turbine combustors
[AIAA PAPER 86-0450] p 20 A86-266
- A stagnation pressure probe for droplet-laden air flow
p 133 A86-39C
- Computational simulation of liquid rocket injection anomalies
[AIAA PAPER 86-1424] p 55 A86-426
- Turbulent two-phase flow in annular seals
[ASLE PREPRINT 86-AM-4G-3] p 156 A86-453
- Prediction of the structure of fuel sprays in gas turbine combustors
[NASA-CR-175028] p 27 N86-162
- Two-phase flows and heat transfer within systems with ambient pressure above the thermodynamic critical pressure
[NASA-TM-87228] p 140 N86-195
- Heat transfer to two-phase air/water mixtures flowing in small tubes with inlet disequilibrium
[NASA-CR-175078] p 141 N86-228
- Two-phase flows within systems with ambient pressure
p 161 N86-3011
- Modeling of zero gravity venting: Studies of two-phase heat transfer under reduced gravity
[NASA-CR-179662] p 144 N86-318

TWO REFLECTOR ANTENNAS

- Near-field testing of the 30 GHz TRW proof-of-concept multibeam antenna
[NASA-TM-87357] p 124 N86-2751

TWO STAGE TURBINES

- Small, two-stage, partial-admission turbine
p 57 N86-1731

U**UDIMET ALLOYS**

- The response of cobalt-free Udimet 700 type alloy to modified heat treatments
p 85 A86-480C
- Thermal-fatigue and oxidation resistance of cobalt-modified Udimet 700 alloy
[NASA-TP-2591] p 178 N86-2846

ULTRAHIGH VACUUM

- Surface modification strategies for (100)3C-SiC
p 76 A86-4706

ULTRASONIC FLAW DETECTION

- Scaling attenuation data characterizes changes in material microstructure
p 197 A86-2654
- Factors influencing the ultrasonic stress wave factor evaluation of composite material structures
p 168 A86-342E

- Factors that affect reliability of nondestructive detection of flaws in structural ceramics
[NASA-TM-87348] p 166 N86-31912
- Quantitative void characterization in structural ceramics using scanning laser acoustic microscopy
[NASA-TM-88797] p 166 N86-31913
- ULTRASONIC RADIATION**
- Nondestructive characterization of structural ceramics
[NASA-TM-88797] p 99 A86-37141
- Analytical Ultrasonics in Materials Research and Testing
[NASA-CP-2383] p 164 N86-22962
- Ultrasonic characterization of structural ceramics
p 199 N86-22970
- Effect of stress on ultrasonic pulses in fiber reinforced composites
p 200 N86-22975
- Ultrasonic verification of microstructural changes due to heat treatment
p 200 N86-22977
- ULTRASONIC TESTS**
- Nondestructive techniques for characterizing mechanical properties of structural materials - An overview
[ASME PAPER 86-GT-75] p 163 A86-48143
- Ultrasonic evaluation of mechanical properties of thick, multilayered, filament wound composites
[NASA-TM-87088] p 163 N86-10561
- Nondestructive techniques for characterizing mechanical properties of structural materials: An overview
[NASA-TM-87203] p 164 N86-19636
- Stress waves in transversely isotropic media: The homogeneous problem
[NASA-CR-3977] p 164 N86-25002
- Ultrasonic stress wave characterization of composite materials
[NASA-CR-3976] p 165 N86-27665
- A study of the stress wave factor technique for nondestructive evaluation of composite materials
[NASA-CR-4002] p 165 N86-28445
- Factors that affect reliability of nondestructive detection of flaws in structural ceramics
[NASA-TM-87348] p 166 N86-31912
- Acousto-ultrasonic verification of the strength of filament wound composite material
[NASA-TM-88827] p 166 N86-32764
- ULTRASONIC WAVE TRANSDUCERS**
- Ultrasonic evaluation of mechanical properties of thick, multilayered, filament wound composites
[NASA-TM-87088] p 163 N86-10561
- ULTRASONICS**
- Measurement of ultrasonic velocity using phase-slope and cross-correlation methods
p 162 A86-13192
- Nondestructive characterization of structural ceramics
p 99 A86-37141
- Reliability of void detection in structural ceramics by use of scanning laser acoustic microscopy
p 163 A86-39027
- NDE of structural ceramics
[ASME PAPER 86-GT-279] p 163 A86-48298
- NDE of structural ceramics
[NASA-TM-87186] p 164 N86-16598
- Analytical Ultrasonics in Materials Research and Testing
[NASA-CP-2383] p 164 N86-22962
- Ultrasonic characterization of structural ceramics
p 199 N86-22970
- Analytical ultrasonics for evaluation of composite materials response. Part 2: Generation and detection
p 200 N86-22973
- Effect of stress on ultrasonic pulses in fiber reinforced composites
p 200 N86-22975
- Ultrasonic verification of microstructural changes due to heat treatment
p 200 N86-22977
- Transfer function concept for ultrasonic characterization of material microstructures
p 200 N86-22980
- Concepts for interrelating ultrasonic attenuation, microstructure and fracture toughness in polycrystalline solids
[NASA-TM-87339] p 165 N86-25812
- Wave propagation in anisotropic medium due to an oscillatory point source with application to unidirectional composites
[NASA-CR-4001] p 165 N86-27666
- UNCOUPLED MODES**
- Application of a personal computer for the uncoupled vibration analysis of wind turbine blade and counterweight assemblies
[NASA-CR-175090] p 188 N86-28511
- UNIVERSITIES**
- NASA Lewis Research Center/university graduate research program on engine structures
[ASME PAPER 85-GT-159] p 167 A86-22084
- UNSTEADY FLOW**
- Numerical simulation of unsteady flow in an axisymmetric shear layer
[AIAA PAPER 86-0202] p 127 A86-19746

- Unsteady transonic flow over cascade blades
p 3 A86-23141
- Aeroelastic formulations for turbomachines and propellers
p 20 A86-24677
- Unsteady transonic flow in cascades
p 4 A86-24693
- Three dimensional unsteady aerodynamics and aeroelastic response of advanced turboprops
[AIAA PAPER 86-0846] p 22 A86-38894
- Fluid flow and fuel-air mixing in a motored two-dimensional Wankel rotary engine
[AIAA PAPER 86-1556] p 134 A86-42711
- On the application of a linearized unsteady potential-flow analysis to fan-tip cascades
[ASME PAPER 86-GT-87] p 7 A86-48153
- Preliminary results of unsteady blade surface pressure measurements for the SR-3 propeller
[AIAA PAPER 86-1893] p 8 A86-49625
- Application of a linearized unsteady aerodynamic analysis to standard cascade configurations
[NASA-CR-3940] p 11 N86-21505
- Preliminary results of unsteady blade surface pressure measurements for the SR-3 propeller
[NASA-TM-87352] p 12 N86-27213
- UNSTEADY STATE**
- Unsteady forces on counter-rotating propeller blades
[AIAA PAPER 86-1804] p 22 A86-37827
- UPPER ATMOSPHERE**
- Upper air forecasting for aviation in the United States
p 191 A86-37501
- UPPER STAGE ROCKET ENGINES**
- Centaur engine gimbal friction characteristics under simulated thrust load
[NASA-TM-87335] p 44 N86-31621
- UPWASH**
- Some design philosophy for reducing the community noise of advanced counter-rotation propellers
[NASA-TM-87099] p 199 N86-14007
- USER MANUALS (COMPUTER PROGRAMS)**
- Integrated Composite Analyzer (ICAN): Users and programmers manual
[NASA-TP-2515] p 69 N86-21614
- Burner liner thermal/structural load modeling: TRANCITS program user's manual
[NASA-CR-174891] p 142 N86-24931
- Turbofan aft duct suppressor study program listing and user's guide
[NASA-CR-175067] p 30 N86-25357
- Structural tailoring of engine blades (STAEBL) theoretical manual
[NASA-CR-175112] p 31 N86-27283
- Spectrum Orbit Utilization Program documentation: SOUP5 version 3.8 user's manual, volume 1, chapters 1 through 5
[NASA-CR-174889] p 193 N86-27927
- Spectrum Orbit Utilization Program documentation: SOUP5 version 3.8 user's manual, volume 2, appendices A through G
[NASA-CR-174890] p 193 N86-27928
- USER REQUIREMENTS**
- Future heavy duty trucking engine requirements
[NASA-CR-174996] p 209 N86-17226
- Extended parametric representation of compressor fans and turbines. Volume 1: CMGEN user's manual
[NASA-CR-174645] p 159 N86-23936
- Extended parametric representation of compressor fans and turbines. Volume 2: Part user's manual (parametric turbine)
[NASA-CR-174646] p 159 N86-23937
- Extended parametric representation of compressor fans and turbines. Volume 3: MODFAN user's manual (parametric modulating flow fan)
[NASA-CR-174647] p 159 N86-23938
- Structural tailoring of engine blades (STAEBL) user's manual
[NASA-CR-175113] p 31 N86-27284
- UTILITIES**
- Photovoltaic systems in remote locations: An experience summary
[NASA-TM-87106] p 181 N86-10643
- Ceramic thermal barrier coatings for electric utility gas turbine engines
[NASA-TM-87288] p 90 N86-22687

V

- VACCINES**
- Photovoltaic-powered vaccine refrigerator: Freezer systems field test results
[NASA-TM-86972-REV] p 181 N86-11666
- VACUUM**
- Mass spectrometric studies of the electrical breakdown of thin polymer films
p 100 A86-47070

VACUUM MELTING

- Structure-property characterization of rheocast and VADER processed IN-100 superalloy
[NASA-CR-175014] p 88 N86-14354

VANELESS DIFFUSERS

- A three-dimensional axisymmetric calculation procedure for turbulent flows in a radial vaneless diffuser
[ASME PAPER 85-GT-133] p 3 A86-22733

VANES

- Wind tunnel turning vanes of modern design
[AIAA PAPER 86-0044] p 36 A86-19654
- Preliminary results of a study of the relationship between free stream turbulence and stagnation region heat transfer
[ASME PAPER 85-GT-84] p 129 A86-22055
- Studies on the hot corrosion of a nickel-base superalloy, Udimet 700
p 82 A86-29722
- Turbine blade and vane heat flux sensor development, phase 2
[NASA-CR-174995] p 26 N86-12226
- Wind tunnel turning vanes of modern design
[NASA-TM-87146] p 37 N86-12239
- LOX/LH2 vane pump for auxiliary propulsion systems
p 58 N86-17397

- De-icing of the altitude wind tunnel turning vanes by electro-magnetic impulse
[NASA-CR-177260] p 38 N86-27291
- Lateral jet injection into typical combustor flowfields
[NASA-CR-3997] p 31 N86-28086
- Experimental evaluation of two turning vane designs for high-speed corner of 0.1-scale model of NASA Lewis Research Center's proposed altitude wind tunnel
[NASA-TP-2570] p 38 N86-28101
- Variable area radial turbine fabrication and test program
[NASA-CR-175091] p 32 N86-28947

VAPOR DEPOSITION

- Creep of chemically vapour deposited SiC fibres
p 66 A86-21486
- Thin film growth rate effects for primary ion beam deposited diamondlike carbon films
p 100 A86-47068
- Experimental and theoretical analysis of chemical vapor deposition with prediction of gravity effects
p 41 N86-10132
- Experimental verification of corrosive vapor deposition rate theory in high velocity burner rigs
[NASA-TM-87287] p 141 N86-22890
- Compensation in epitaxial cubic SiC films
[NASA-TM-87269] p 206 N86-25267
- VAPOR PHASE EPITAXY**
- Experimental and theoretical analysis of chemical vapor deposition with prediction of gravity effects
p 41 N86-10132

VAPOR PHASES

- Prediction of the structure of fuel sprays in gas turbine combustors
[AIAA PAPER 86-0450] p 20 A86-26636
- Fundamental studies of droplet combustion at reduced gravity
p 42 N86-10165
- Prediction of the structure of fuel sprays in gas turbine combustors
[NASA-CR-175028] p 27 N86-16218
- Physical and numerical sources of computational inefficiency in integration of chemical kinetic rate equations: Etiology, treatment and prognosis
[NASA-TP-2590] p 195 N86-28662

VAPOR PRESSURE

- Liquid belt radiator design study
[NASA-CR-174901] p 57 N86-16259
- Organosiloxane working fluids for the liquid droplet radiator
[NASA-CR-175033] p 102 N86-16381

VAPORS

- Application of an atmospheric pressure sampling mass spectrometer to chlorination reactions
[NASA-TM-87270] p 91 N86-24813
- Criteria for significance of simultaneous presence of both condensable vapors and aerosol particles on mass transfer (deposition) rates
[NASA-TM-87247] p 109 N86-24869

VARIABLEITY

- Variable-reluctance motor drives for electric vehicle propulsion
[NASA-CR-176566] p 122 N86-20700

VARIABLE CYCLE ENGINES

- Free jet feasibility study of a thermal acoustic shield concept for AST/VCE application-dual flow. Comprehensive data report. Volume 1: Test nozzles and acoustic data
[NASA-CR-174817] p 200 N86-23371
- Free-jet feasibility study of a thermal acoustic shield concept for AST/VCE application-dual stream nozzles. Comprehensive data report. Volume 2: Laser velocimeter and suppressor. Base pressure data
[NASA-CR-174818] p 201 N86-23372

VARIABLE GEOMETRY STRUCTURES

Variable area radial turbine fabrication and test program
[NASA-CR-175091] p 32 N86-28947

VARIABLE PITCH PROPELLERS

Large-Scale Advanced Prop-Fan (LAP) pitch change actuator and control design report
[NASA-CR-174788] p 31 N86-27282

VARIABLE STREAM CONTROL ENGINES

Preliminary design of a supersonic cruise aircraft high-pressure turbine
[NASA-CR-174878] p 26 N86-14272

VARIATIONAL PRINCIPLES

Applications of variational principles in computing rotational flows p 128 N86-20951

VECTORS (MATHEMATICS)

Acceleration of convergence of vector sequences p 195 N86-49850
Optical constants of GaAs-AlGaAs superlattices and multiple quantum wells
[NASA-CR-176717] p 205 N86-23468

VELOCITY

Ultrasonic evaluation of mechanical properties of thick, multilayered, filament wound composites
[NASA-TM-87088] p 163 N86-10561
Experimental verification of corrosive vapor deposition rate theory in high velocity burner rigs
[NASA-TM-87287] p 141 N86-22890

VELOCITY DISTRIBUTION

Simultaneous measurements of velocity and pressure fields in subsonic and supersonic flows through image-intensified detection of laser-induced fluorescence
[AIAA PAPER 86-0161] p 145 N86-19726
Numerical synthesis of tri-variate velocity realizations of turbulence p 168 N86-28554
Concentration distributions in a model combustor p 133 N86-38575
Laser velocimeter measurements in shrouded and unshrouded radial flow pump impellers
[ASME PAPER 86-GT-129] p 136 N86-48187
Improvement of the second- and third-moment modeling of turbulence: A study of Reynolds-stress closure model
[NASA-CR-176478] p 139 N86-16519
Dilution jet mixing program, supplementary report
[NASA-CR-175043] p 141 N86-23856

VELOCITY ERRORS

Analysis of the uncertainties in velocity measurements with triple hot-wire probes p 130 N86-24468

VELOCITY MEASUREMENT

Measurement of ultrasonic velocity using phase-slope and cross-correlation methods p 162 N86-13192
Analysis of the uncertainties in velocity measurements with triple hot-wire probes p 130 N86-24468
Laser Doppler velocimeter measurement in the tip region of a compressor rotor p 5 N86-39064

VENTING

Modeling of zero gravity venting: Studies of two-phase heat transfer under reduced gravity
[NASA-CR-179662] p 144 N86-31826

VERSATILITY

A 20 kilohertz space station power system
[NASA-TM-88801] p 62 N86-28122

VIBRATION

Generated spiral bevel gears - Optimal machine-tool settings and tooth contact analysis
[SAE PAPER 851573] p 154 N86-40678
Numerical Techniques in Acoustics
[NASA-CP-2404] p 198 N86-12007
Quasi-modal vibration control by means of active control bearings
[NASA-TM-87232] p 159 N86-21856
Testing of YUH-61A helicopter transmission in NASA Lewis 2240-kW (3000-hp) facility
[NASA-TP-2538] p 160 N86-24992

VIBRATION DAMPING

Influence of friction dampers on torsional blade flutter
[ASME PAPER 85-GT-170] p 21 N86-32957
Parameter sensitivity in the dynamics of rotor-bearing systems
[ASME PAPER 85-DET-35] p 154 N86-38620
Passive control of aerodynamically forced vibrations of supersonic turbomachine rotors by splitter blades
[AIAA PAPER 86-0844] p 22 N86-38892
Frequency domain solutions to multi-degree-of-freedom, dry friction damped systems under periodic excitation p 170 N86-39485
Lateral dampers for thrust bearings
[NASA-CR-174924] p 157 N86-11474
Extensions of the Ritz-Galerkin method for the forced, damped vibrations of structural elements p 176 N86-21909
Variable friction secondary seal for face seals
[NASA-CASE-LEW-14170-1] p 160 N86-25790
SSME long-life bearings
[NASA-CR-179455] p 160 N86-27643

VIBRATION MEASUREMENT

Joint research effort on vibrations of twisted plates, phase 1: Final results
[NASA-RP-1150] p 172 N86-10579

Thermoviscoplastic nonlinear constitutive relationships for structural analysis of high temperature metal matrix composites

[NASA-TM-87291] p 70 N86-24756
Identification of differences between finite element analysis and experimental vibration data
[NASA-TM-87336] p 149 N86-27617
Application of a personal computer for the uncoupled vibration analysis of wind turbine blade and counterweight assemblies
[NASA-CR-175090] p 188 N86-28511
Instability in Rotating Machinery
[NASA-CP-2409] p 161 N86-30180
Advanced optical measuring systems for measuring the properties of fluids and structures
[NASA-TM-88829] p 150 N86-31859

VIBRATION MODE

The use of an optical data acquisition system for bladed disk vibration analysis p 146 N86-26909
Application of a personal computer for the uncoupled vibration analysis of wind turbine blade and counterweight assemblies
[NASA-CR-175090] p 188 N86-28511

VIBRATION TESTS

Dynamic characteristics of an assembly of prop-fan blades
[ASME PAPER 85-GT-134] p 21 N86-32956
Nondestructive techniques for characterizing mechanical properties of structural materials - An overview
[ASME PAPER 86-GT-75] p 163 N86-48143
Nondestructive techniques for characterizing mechanical properties of structural materials: An overview p 164 N86-19636
[NASA-TM-87203] p 184 N86-19636

VIBRATIONAL STRESS

Advanced turboprop vibratory characteristics
[NASA-CR-174708] p 30 N86-24693

VISCOELASTICITY

Bounding solutions of geometrically nonlinear viscoelastic problems
[AIAA PAPER 86-0943] p 170 N86-38838
Bounding solutions of geometrically nonlinear viscoelastic problems
[NASA-CR-176219] p 195 N86-10860

VISCOPLASTICITY

Effects of state recovery on creep buckling under variable loading
[NASA-CR-175094] p 212 N86-25310
Integrated research in constitutive modelling at elevated temperatures, part 2
[NASA-CR-177233] p 178 N86-28455

VISCOSITY

Organosiloxane working fluids for the liquid droplet radiator
[NASA-CR-175033] p 102 N86-16391
Constitutive modelling of lubricants in concentrated contacts at high slide to roll ratios
[NASA-CR-175029] p 158 N86-17748
Piezoviscous effects in nonconformal contacts lubricated hydrodynamically
[NASA-TM-87141] p 141 N86-21797
The preparation of new perfluoroether fluids exhibiting excellent thermal-oxidative stabilities
[NASA-TM-87284] p 105 N86-25475
Jet fuel viscosity at low temperatures with notes on n-alkane crystals
[NASA-CR-174911] p 15 N86-30022

VISCOUS DAMPING

Identification of differences between finite element analysis and experimental vibration data
[NASA-TM-87336] p 149 N86-27617

VISCOUS FLOW

Finite-amplitude steady waves in plane viscous shear flows
[AD-A185461] p 127 N86-19419
Development of an explicit multigrid algorithm for quasi-three-dimensional viscous flows in turbomachinery
[AIAA PAPER 86-0032] p 1 N86-19644
Calculation of three-dimensional, viscous flow through turbomachinery blade passage by parabolic marching p 2 N86-20372
Model equation for simulating flows in multistage turbomachinery
[ASME PAPER 85-GT-226] p 2 N86-22123
Simplex finite element analysis of viscous incompressible flow with penalty function formulation p 129 N86-22615
Inverse design of axisymmetric flow passages using compressible viscous flow theory p 4 N86-26412
Convective and absolute instability of a viscous liquid jet p 132 N86-34377

Computation of viscous flows in turbomachinery cascades with a space-marching method p 5 N86-39089

Numerical analysis of some supersonic viscous flows related to inlet and nozzle systems
[AIAA PAPER 86-1597] p 134 N86-42738

A space-marching method for viscous incompressible internal flows p 135 N86-43037

Validation of viscous and inviscid computational methods for turbomachinery components
[ASME PAPER 86-GT-42] p 7 N86-48126

Application of a computational model for vortex generators in subsonic internal flows
[AIAA PAPER 86-1458] p 8 N86-49612

Development of an explicit multigrid algorithm for quasi-three-dimensional viscous flows in turbomachinery
[NASA-TM-87128] p 1 N86-11146

Validation of viscous and inviscid computational methods for turbomachinery components
[NASA-TM-87193] p 10 N86-16194

Viscous compressible flow direct and inverse computation and illustrations
[NASA-CR-175037] p 28 N86-20391

Application of a computational model for vortex generators in subsonic internal flows
[NASA-TM-87327] p 143 N86-26545

Thermodynamic evaluation of transonic compressor rotors using the finite volume approach
[NASA-CR-176947] p 32 N86-30731

VOICE OF AMERICA

Satellite voice broadcast system study, volume 2
[NASA-CR-174905] p 115 N86-24877

Satellite voice broadcast system study, Volume 1: Executive summary
[NASA-CR-174904] p 115 N86-24878

VOID RATIO

All-aromatic biphenylene end-capped polyquinoline and polyimide matrix resins p 100 N86-11267

VOIDS

Reliability of void detection in structural ceramics by use of scanning laser acoustic microscopy p 163 N86-39027

Reliability of scanning laser acoustic microscopy for detecting internal voids in structural ceramics p 147 N86-46353

The 371 deg C mechanical properties of graphite/polyimide composites
[NASA-TM-87122] p 69 N86-12256

Probability of detection of internal voids in structural ceramics using microfocus radiography
[NASA-TM-87164] p 164 N86-13749

Reliability of scanning laser acoustic microscopy for detecting internal voids in structural ceramics
[NASA-TM-87222] p 164 N86-16599

Factors that affect reliability of nondestructive detection of flaws in structural ceramics
[NASA-TM-87348] p 168 N86-31912

Quantitative void characterization in structural ceramics using scanning laser acoustic microscopy
[NASA-TM-88797] p 166 N86-31913

VOLT-AMPERE CHARACTERISTICS

High transconductance InGaAs/AlGaAs pseudomorphic modulation-doped field-effect transistors p 117 N86-18814

Dc and microwave characteristics of a high current double interface GaAs/InGaAs/AlGaAs pseudomorphic modulation-doped field-effect transistor p 118 N86-36009

VOLTAGE CONVERTERS (DC TO DC)

Designing a 25-kilowatt high frequency series resonant
[NASA-CR-176774] p 123 N86-24906

VOLTAGE REGULATORS

10 kW solar array switching unit performance test results p 118 N86-24844

State-plane analysis of parallel resonant converter p 119 N86-40431

Input-current shaped ac to dc converters
[NASA-CR-176787] p 123 N86-25693

VOLTMETERS

Evaluation parameters for the alkaline fuel cell oxygen electrode
[NASA-TM-87155] p 77 N86-12268

VOLUMETRIC ANALYSIS

Measurement of the density of base fluids at pressures 0.422 to 2.20 GPa
[NASA-TM-87114] p 156 N86-10551

VORTEX GENERATORS

Vortex generators as a means for increasing rotor performance p 4 N86-24920

Application of a computational model for vortex generators in subsonic internal flows
[AIAA PAPER 86-1458] p 8 N86-49612

Application of a computational model for vortex generators in subsonic internal flows
[NASA-TM-87327] p 143 N86-26545

VORTEX SHEDDING

- Rotor wake characteristics of a transonic axial flow fan
[NASA-TM-87073] p 13 N86-28055

VORTICES

- Numerical simulation of a turbulent flame stabilized behind a rearward-facing step p 73 A86-22774
Formation and inflammation of a turbulent jet p 130 A86-23131
Coherent structures in a turbulent mixing layer - A comparison between direct numerical simulations and experiments p 132 A86-30218
An experimental study of energy loss mechanisms and efficiency considerations in the low power dc arcjet [AIAA PAPER 85-2017] p 53 A86-37062
Coupling conditions for integrating boundary layer and rotational inviscid flow p 133 A86-41721
Propeller noise caused by blade tip radial forces [AIAA PAPER 86-1892] p 23 A86-45504
Vortex modeling of single and multiple dilution jet mixing in a cross flow p 135 A86-46318
Laser velocimeter measurements in shrouded and unshrouded radial flow pump impellers [ASME PAPER 86-GT-129] p 136 A86-48187
Horseshoe vortex formation around a cylinder [ASME PAPER 86-GT-246] p 8 A86-48274
An experimental study of energy loss mechanisms and efficiency consideration in the low power dc arcjet [NASA-TM-87123] p 57 N86-11224
Some design philosophy for reducing the community noise of advanced counter-rotation propellers [NASA-TM-87099] p 199 N86-14007
Shear layer excitation, experiment versus theory [NASA-CR-176604] p 140 N86-20722
Effect of a rotor wake on the local heat transfer on the forward half of a circular cylinder [NASA-TM-8734] p 140 N86-21794
Review and evaluation of recent developments in melic inlet dynamic flow distortion prediction and computer program documentation and user's manual estimating maximum instantaneous inlet flow distortion from steady-state total pressure measurements with full, limited, or no dynamic data [NASA-CR-176765] p 143 N86-24955
Measurements of a turbulent horseshoe vortex formed around a cylinder [NASA-CR-3986] p 13 N86-28063
- VORTICITY**
Steady inviscid three-dimensional flows p 128 A86-20952
An analytical model for the vorticity associated with a transverse jet p 4 A86-28538

W**WAFERS**

- Lithium counterdoped silicon solar cell [NASA-CASE-LEW-14177-1] p 190 N86-32875

WAKES

- Some design philosophy for reducing the community noise of advanced counter-rotation propellers [NASA-TM-87099] p 199 N86-14007
Unsteady heat transfer and direct comparison to steady-state measurements in a rotor-wake experiment [NASA-TM-87220] p 142 N86-24934
Rotor wake characteristics of a transonic axial flow fan [NASA-TM-87073] p 13 N86-28055

WALL FLOW

- End-wall and profile losses in a low-speed axial flow compressor rotor [ASME PAPER 85-GT-174] p 20 A86-22090
Modeling the 3-D flow effects on deviation angle for axial compressor middle stages [ASME PAPER 85-GT-189] p 2 A86-22102
Three-dimensional fluid flow phenomena in the blade end wall corner region [ASME PAPER 86-GT-179] p 7 A86-48229

WALL TEMPERATURE

- Measurements of energy distribution and wall temperature in flowing hydrogen microwave plasma systems [AIAA PAPER 85-2052] p 203 A86-11001
High-temperature thermocouple and heat flux gauge using a unique thin film-hardware hot junction [ASME PAPER 85-GT-18] p 145 A86-13059

WANKEL ENGINES

- Fluid flow and fuel-air mixing in a motored two-dimensional Wankel rotary engine [AIAA PAPER 86-1556] p 134 A86-42711

WASPALLOY

- Axial and torsional fatigue behavior of Waspalloy [NASA-CR-175052] p 91 N86-25454

WASTE DISPOSAL

- Shock-tube pyrolysis of chlorinated hydrocarbons - Formation of soot p 75 A86-35126

WASTE ENERGY UTILIZATION

- Method for improving the fuel efficiency of a gas turbine engine [NASA-CASE-LEW-13142-2] p 28 N86-20389

WATER

- Erosion of aluminum 6061-T6 under cavitation attack in mineral oil and water p 79 A86-13801
Factors influencing the ball milling of Si3N4 in water p 95 A86-15239
Parametric evaluation of ball milling of SiC in water p 96 A86-15240

WATER INJECTION

- Transient engine performance with water ingestion [AIAA PAPER 86-1621] p 23 A86-42755

WAVE AMPLIFICATION

- Wave propagation in anisotropic medium due to an oscillatory point source with application to unidirectional composites [NASA-CR-4001] p 165 N86-27666

WAVE ATTENUATION

- Numerical methods for analyzing electromagnetic scattering [NASA-CR-176141] p 111 N86-10377
Effect of stress on ultrasonic pulses in fiber reinforced composites p 200 N86-22975
Ultrasonic verification of microstructural changes due to heat treatment p 200 N86-22977
Transfer function concept for ultrasonic characterization of material microstructures p 200 N86-22980

WAVE EQUATIONS

- Propagation and stability of wavelike solutions of finite difference equations with variable coefficients p 194 A86-20033
Reverberation effects on directionality and response of stationary monopole and dipole sources in a wind tunnel [ASME PAPER 85-WA/NCA-1] p 197 A86-22747

WAVE EXCITATION

- Analytical ultrasonics for evaluation of composite materials response. Part 2: Generation and detection p 200 N86-22973

WAVE GENERATION

- Analytical ultrasonics for evaluation of composite materials response. Part 2: Generation and detection p 200 N86-22973

WAVE PROPAGATION

- Measurement of ultrasonic velocity using phase-slope and cross-correlation methods p 162 A86-13192
Finite-amplitude steady waves in plane viscous shear flows [AD-A165461] p 127 A86-19419
Propagation and stability of wavelike solutions of finite difference equations with variable coefficients p 194 A86-20033
Non-linear effects in finite amplitude wave propagation through ducts and nozzles p 197 A86-35857
Dynamic stress analysis of smooth and notched fiber composite flexural specimens p 67 A86-41070
Analytical Ultrasonics in Materials Research and Testing [NASA-CP-2383] p 164 N86-22962
Wave propagation in anisotropic medium due to an oscillatory point source with application to unidirectional composites [NASA-CR-4001] p 165 N86-27666
NASA/DOE automotive Stirling engine project: Overview 1986 [NASA-TM-87345] p 211 N86-29731
Effect of triangular element orientation on finite element solutions of the Helmholtz equation [NASA-TM-87351] p 201 N86-32247

WAVE REFLECTION

- Development of an impulsive noise source to study the acoustic reflection characteristics of hard-walled wind tunnels [AIAA PAPER 86-1887] p 198 A86-45500
Acoustic reflection contamination measurements in the 16-foot NASA Langley Transonic Wind Tunnel [AIAA PAPER 86-1888] p 198 A86-45501

WAVE SCATTERING

- A high frequency analysis of electromagnetic plane wave scattering by perfectly-conducting semi-infinite parallel plate and rectangular waveguides with absorber coated inner walls [NASA-CR-179759] p 116 N86-32600

WAVEFORMS

- Input current shaped ac-to-dc converters [NASA-CR-176438] p 121 N86-15544

WAVEGUIDE ANTENNAS

- A simple circular-polarized antenna: Circular waveguide horn coated with lossy magnetic material [NASA-CR-177092] p 116 N86-30039

WAVEGUIDES

- Numerical methods for analyzing electromagnetic scattering [NASA-CR-176141] p 111 N86-10377
MMIC devices for active phased array antennas [NASA-CR-176990] p 116 N86-30037

WAVELENGTH DIVISION MULTIPLEXING

- Wavelength-division multiplexed digital optical position transducer p 145 A86-20798

WAVELENGTHS

- Time domain referencing in intensity modulation fiber optic sensing systems [NASA-CR-175109] p 17 N86-24691

WEAR

- Surface effects of corrosive media on hardness, friction, and wear of materials p 94 A86-10825
Ellipsometric surface analysis of wear tracks produced by different lubricants [ASLE PREPRINT 85-TC-5A-2] p 151 A86-11016
Low-wear partially fluorinated polyimides p 94 A86-11175
Fundamental tribological properties of ceramics p 95 A86-15230
Mechanical-contact-induced transformation from the amorphous to the partially crystalline state in metallic glass p 80 A86-16257
Frictional and morphological properties of Au-MoS2 films sputtered from a compact target p 152 A86-16258
New directions in lubrication, materials, wear, and surface interactions - Tribology in the 80's - Book p 152 A86-18700
Interaction of sulfuric acid corrosion and mechanical wear of iron p 81 A86-20436
Characterization and measurement of polymer wear p 100 A86-48405
Tribological characteristics of gold films deposited on metals by ion plating and vapor deposition p 85 A86-49600
Tribological properties of structural ceramics [NASA-TM-87105] p 100 N86-10341
Ellipsometric surface analysis of wear tracks produced by different lubricants [NASA-TM-87142] p 87 N86-12293
How to evaluate solid lubricant films using a pin-on-disk tribometer [NASA-TM-87236] p 102 N86-19465
Composition optimization of self-lubricating chromium carbide-based composite coatings for use to 760 deg C [NASA-TM-87261] p 103 N86-20568
Tribology of selected ceramics at temperatures to 900 deg C [NASA-TM-87267] p 105 N86-25476
Research and development of neat alcohol fuel usage in automobiles [NASA-CR-174813] p 108 N86-27460
Sliding seal materials for adiabatic engines, phase 2 [NASA-CR-179475] p 105 N86-29042
- WEAR INHIBITORS**
Lubricant and additive effects on spur gear fatigue life [ASME PAPER 85-TRIB-14] p 155 A86-43542
- WEAR RESISTANCE**
Selected fretting-wear-resistant coatings for Ti-6 pct Al-4 pct V alloy p 97 A86-24956
Impact wear of iron rich superalloys p 82 A86-34687
Adhesion and wear resistance of materials [NASA-TM-87239] p 158 N86-20809
- WEAR TESTS**
Lubricant and additive effects on spur gear fatigue life [ASME PAPER 85-TRIB-14] p 155 A86-43542
Abrasion and deformed layer formation of manganese-zinc ferrite in sliding contact with lapping tapes [NASA-TM-87249] p 104 N86-24838
Evaluation of a hybrid hydrostatic bearing for cryogenic turbopump application [NASA-TM-87255] p 63 N86-31649
- WEIGHT REDUCTION**
Lightweight nickel electrode for nickel hydrogen cells and batteries [NASA-TM-87253] p 186 N86-21978
- WEIGHTING FUNCTIONS**
Wide-range weight functions for the strip with a single edge crack p 167 A86-20709
- WEIGHTLESSNESS**
Influence of melt convection on solid-liquid interface under terrestrial and reduced gravity environments p 38 N86-10083
Accommodation requirements for microgravity science and applications research on space station [NASA-CR-175038] p 42 N86-18334
Electrocrystallization in microgravity [NASA-TM-87202] p 212 N86-19274
Liquid-vapor interface locations in a spheroidal container under low gravity [NASA-TM-87147] p 141 N86-23854

- Research and competition: Best partners
[NASA-TM-87313] p 212 N86-25321
- WELDED JOINTS**
Demonstrated results of welded and soldered interconnections p 185 N86-17866
- WETTABILITY**
Contact angle and surface tension measurements of a five-ring polyphenyl ether p 98 A86-34179
Liquid belt radiator design study
[NASA-CR-174901] p 57 N86-16259
- WETTING**
Factors influencing the ball milling of Si₃N₄ in water p 95 A86-15239
- WIDE ANGLE LENSES**
Optimized three-dimensional lenses for wide-angle scanning p 109 A86-19184
- WIND (METEOROLOGY)**
Description and test results of a variable speed, constant frequency generating system
[NASA-TM-87181] p 121 N86-16487
- WIND TUNNEL APPARATUS**
Study of ice accretion on icing wind tunnel components
[AIAA PAPER 86-0290] p 36 A86-26620
Study of ice accretion on icing wind tunnel components
[NASA-TM-87095] p 37 N86-16232
De-icing of the altitude wind tunnel turning vanes by electro-magnetic impulse
[NASA-CR-177260] p 38 N86-27291
Comparison of analytical and experimental performance of a wind-tunnel diffuser section
[NASA-TM-88795] p 13 N86-31537
- WIND TUNNEL DRIVES**
Study of ice accretion on icing wind tunnel components
[AIAA PAPER 86-0290] p 36 A86-26620
Study of ice accretion on icing wind tunnel components
[NASA-TM-87095] p 37 N86-16232
- WIND TUNNEL MODELS**
Progress in the Lewis Research Center Altitude Wind Tunnel (AWT) modeling program
[AIAA PAPER 86-0757] p 36 A86-24744
Modeling wind tunnel effects on the radiation characteristics of acoustic sources p 197 A86-41689
- WIND TUNNEL NOZZLES**
Study of ice accretion on icing wind tunnel components
[AIAA PAPER 86-0290] p 36 A86-26620
Study of ice accretion on icing wind tunnel components
[NASA-TM-87095] p 37 N86-16232
- WIND TUNNEL TESTS**
Numerical study of three-dimensional turbulent flow interactions between blockage models and wind tunnels including longitudinally slotted test sections
[AIAA PAPER 85-5017] p 1 A86-11065
Reverberation effects on directionality and response of stationary monopole and dipole sources in a wind tunnel
[ASME PAPER 85-WA/NCA-1] p 197 A86-22747
A novel centrifugal diffuser test device
[ASME PAPER 85-IGT-135] p 3 A86-23927
Current wind tunnel capability and planned improvements at Lewis Research Center
[AIAA PAPER 86-0728] p 36 A86-24727
Study of ice accretion on icing wind tunnel components
[AIAA PAPER 86-0290] p 36 A86-26620
Modeling wind tunnel effects on the radiation characteristics of acoustic sources p 197 A86-41689
Preliminary measurement of the noise from the 2/9 scale model of the Large-scale Advanced Propfan (LAP) propeller, SR-7A
[NASA-TM-87116] p 199 N86-14006
Study of ice accretion on icing wind tunnel components
[NASA-TM-87095] p 37 N86-16232
Progress in the Lewis Research Center Altitude Wind Tunnel (AWT) Modeling Program
[NASA-TM-87194] p 37 N86-16233
Current wind tunnel capability and planned improvements at Lewis Research Center
[NASA-TM-87190] p 37 N86-18329
Development and application of dynamic simulations of a subsonic wind tunnel
[NASA-TM-87211] p 43 N86-18338
Wind tunnel tests of rotor blade sections with replications of ice formations accreted in hover
[NASA-CR-175089] p 15 N86-22558
Experimental and analytical investigation of a freezing point depressant fluid ice protection system
[NASA-CR-174758] p 12 N86-27186
Measurements of a turbulent horseshoe vortex formed around a cylinder
[NASA-CR-3986] p 13 N86-28063
- Lateral jet injection into typical combustor flowfields
[NASA-CR-3997] p 31 N86-28066
Experimental evaluation of two turning vane designs for high-speed corner of 0.1-scale model of NASA Lewis Research Center's proposed altitude wind tunnel
[NASA-TP-2570] p 38 N86-28101
Turbulent dispersion of the icing cloud from spray nozzles used in icing tunnels
[NASA-TM-87318] p 34 N86-31588
Summary of NASA/DOE Aileron-Control Development Program for Wind Turbines
[NASA-TM-88811] p 190 N86-31983
- WIND TUNNEL WALLS**
Reverberation effects on directionality and response of stationary monopole and dipole sources in a wind tunnel
[ASME PAPER 85-WA/NCA-1] p 197 A86-22747
Modeling wind tunnel effects on the radiation characteristics of acoustic sources p 197 A86-41689
Modeling the effects of wind tunnel wall absorption on the acoustic radiation characteristics of propellers
[NASA-TM-87333] p 201 N86-29630
- WIND TUNNELS**
Wind tunnel turning vanes of modern design
[AIAA PAPER 86-0044] p 36 A86-19654
Wind tunnel turning vanes of modern design
[NASA-TM-87146] p 37 N86-12239
Heat transfer and pressure drop performance of a finned-tube heat exchanger proposed for use in the NASA Lewis Altitude Wind Tunnel
[NASA-TM-87151] p 138 N86-13677
De-icing of the altitude wind tunnel turning vanes by electro-magnetic impulse
[NASA-CR-177260] p 38 N86-27291
Comparison of analytical and experimental performance of a wind-tunnel diffuser section
[NASA-TM-88795] p 13 N86-31537
- WIND TURBINES**
Vortex generators as a means for increasing rotor performance p 4 A86-24920
Improved stud configurations for attaching laminated wood wind turbine blades
[NASA-TM-87109] p 172 N86-10582
Effect of accuracy of wind power prediction on power system operator
[NASA-CR-176300] p 181 N86-11667
Mod-5A wind turbine generator program design report. Volume 2: Conceptual and preliminary design, book 1
[NASA-CR-174735-VOL-2-BK-1] p 183 N86-15722
Mod-5A wind turbine generator program design report. Volume 2: Conceptual and preliminary design, book 2
[NASA-CR-174735-VOL-2-BK-2] p 183 N86-15723
Mod-5A wind turbine generator program design report. Volume 3: Final design and system description, book 1
[NASA-CR-174735-VOL-3-BK-1] p 183 N86-15724
Mod-5A wind turbine generator program design report. Volume 3: Final design and system description, book 2
[NASA-CR-174735-VOL-3-BK-2] p 183 N86-15725
Mod-5A wind turbine generator program design report. Volume 4: Drawings and specifications, book 1
[NASA-CR-174735-VOL-4-BK-1] p 183 N86-15726
Mod-5A wind turbine generator program design report. Volume 4: Drawings and specifications, book 2
[NASA-CR-174735-VOL-4-BK-2] p 184 N86-15727
Mod-5A wind turbine generator program design report. Volume 4: Drawings and specifications, book 3
[NASA-CR-174735-VOL-4-BK-3] p 184 N86-15728
Mod-5A wind turbine generator program design report. Volume 4: Drawings and specifications, book 4
[NASA-CR-174735-VOL-4-BK-4] p 184 N86-15729
Mod-5A wind turbine generator program design report. Volume 4: Drawings and specifications, book 5
[NASA-CR-174735-VOL-4-BK-5] p 184 N86-15730
Description and test results of a variable speed, constant frequency generating system
[NASA-TM-87181] p 121 N86-16487
Mod-2 wind turbine field operations experiment
[NASA-TM-87233] p 186 N86-18775
Design and initial testing of a one-bladed 30-meter-diameter rotor on the NASA/DOE mod-O wind turbine
[NASA-TM-88810] p 189 N86-30251
- WINDPOWERED GENERATORS**
Mod-5A wind turbine generator program design report. Volume 2: Conceptual and preliminary design, book 1
[NASA-CR-174735-VOL-2-BK-1] p 183 N86-15722
Mod-5A wind turbine generator program design report. Volume 2: Conceptual and preliminary design, book 2
[NASA-CR-174735-VOL-2-BK-2] p 183 N86-15723
Mod-5A wind turbine generator program design report. Volume 3: Final design and system description, book 1
[NASA-CR-174735-VOL-3-BK-1] p 183 N86-15724
Mod-5A wind turbine generator program design report. Volume 3: Final design and system description, book 2
[NASA-CR-174735-VOL-3-BK-2] p 183 N86-15725
Mod-5A wind turbine generator program design report. Volume 4: Drawings and specifications, book 1
[NASA-CR-174735-VOL-4-BK-1] p 183 N86-15726
Mod-5A wind turbine generator program design report. Volume 4: Drawings and specifications, book 2
[NASA-CR-174735-VOL-4-BK-2] p 184 N86-15727
Mod-5A wind turbine generator program design report. Volume 4: Drawings and specifications, book 3
[NASA-CR-174735-VOL-4-BK-3] p 184 N86-15728
Mod-5A wind turbine generator program design report. Volume 4: Drawings and specifications, book 4
[NASA-CR-174735-VOL-4-BK-4] p 184 N86-15729
Mod-5A wind turbine generator program design report. Volume 4: Drawings and specifications, book 5
[NASA-CR-174735-VOL-4-BK-5] p 184 N86-15730
Mod-5A wind turbine generator program design report. Volume 1: Executive Summary
[NASA-CR-174734] p 188 N86-27708
- Application of a personal computer for the uncoupled vibration analysis of wind turbine blade and counterweight assemblies
[NASA-CR-175090] p 188 N86-28511
Design and initial testing of a one-bladed 30-meter-diameter rotor on the NASA/DOE mod-O wind turbine
[NASA-TM-88810] p 189 N86-30251
- Summary of NASA/DOE Aileron-Control Development Program for Wind Turbines
[NASA-TM-88811] p 190 N86-31983
- WIND VANES**
Study of ice accretion on icing wind tunnel components
[AIAA PAPER 86-0290] p 36 A86-26620
Study of ice accretion on icing wind tunnel components
[NASA-TM-87095] p 37 N86-16232
- WINDING**
A mathematical model for the doubly-fed wound rotor generator. II p 119 A86-39474
- WINDOWS (APERTURES)**
Parametric study of beam refraction problems across laser anemometer windows
[NASA-TM-87350] p 150 N86-31857
- WINDPOWER UTILIZATION**
Effect of accuracy of wind power prediction on power system operator
[NASA-CR-176300] p 181 N86-11667
AC motor and generator requirements for isolatex WECS
[NASA-CR-176315] p 182 N86-11670
Mod-5A wind turbine generator program design report. Volume 2: Conceptual and preliminary design, book 1
[NASA-CR-174735-VOL-2-BK-1] p 183 N86-15722
Mod-5A wind turbine generator program design report. Volume 2: Conceptual and preliminary design, book 2
[NASA-CR-174735-VOL-2-BK-2] p 183 N86-15723
Mod-5A wind turbine generator program design report. Volume 3: Final design and system description, book 1
[NASA-CR-174735-VOL-3-BK-1] p 183 N86-15724
Mod-5A wind turbine generator program design report. Volume 3: Final design and system description, book 2
[NASA-CR-174735-VOL-3-BK-2] p 183 N86-15725
Mod-5A wind turbine generator program design report. Volume 4: Drawings and specifications, book 1
[NASA-CR-174735-VOL-4-BK-1] p 183 N86-15726
Mod-5A wind turbine generator program design report. Volume 4: Drawings and specifications, book 2
[NASA-CR-174735-VOL-4-BK-2] p 184 N86-15727
Mod-5A wind turbine generator program design report. Volume 4: Drawings and specifications, book 3
[NASA-CR-174735-VOL-4-BK-3] p 184 N86-15728
Mod-5A wind turbine generator program design report. Volume 4: Drawings and specifications, book 4
[NASA-CR-174735-VOL-4-BK-4] p 184 N86-15729
Mod-5A wind turbine generator program design report. Volume 4: Drawings and specifications, book 5
[NASA-CR-174735-VOL-4-BK-5] p 184 N86-15730
Description and test results of a variable speed, constant frequency generating system
[NASA-TM-87181] p 121 N86-16487
Mod-2 wind turbine field operations experiment
[NASA-TM-87233] p 186 N86-18775
Design and initial testing of a one-bladed 30-meter-diameter rotor on the NASA/DOE mod-O wind turbine
[NASA-TM-88810] p 189 N86-30251
- WINDPOWERED GENERATORS**
Mod-5A wind turbine generator program design report. Volume 2: Conceptual and preliminary design, book 1
[NASA-CR-174735-VOL-2-BK-1] p 183 N86-15722
Mod-5A wind turbine generator program design report. Volume 2: Conceptual and preliminary design, book 2
[NASA-CR-174735-VOL-2-BK-2] p 183 N86-15723
Mod-5A wind turbine generator program design report. Volume 3: Final design and system description, book 1
[NASA-CR-174735-VOL-3-BK-1] p 183 N86-15724
Mod-5A wind turbine generator program design report. Volume 3: Final design and system description, book 2
[NASA-CR-174735-VOL-3-BK-2] p 183 N86-15725
Mod-5A wind turbine generator program design report. Volume 4: Drawings and specifications, book 1
[NASA-CR-174735-VOL-4-BK-1] p 183 N86-15726
Mod-5A wind turbine generator program design report. Volume 4: Drawings and specifications, book 2
[NASA-CR-174735-VOL-4-BK-2] p 184 N86-15727
Mod-5A wind turbine generator program design report. Volume 4: Drawings and specifications, book 3
[NASA-CR-174735-VOL-4-BK-3] p 184 N86-15728
Mod-5A wind turbine generator program design report. Volume 4: Drawings and specifications, book 4
[NASA-CR-174735-VOL-4-BK-4] p 184 N86-15729
Mod-5A wind turbine generator program design report. Volume 4: Drawings and specifications, book 5
[NASA-CR-174735-VOL-4-BK-5] p 184 N86-15730
Mod-5A wind turbine generator program design report. Volume 1: Executive Summary
[NASA-CR-174734] p 188 N86-27708
- WING CAMBER**
Influence of airfoil camber on convected gust interaction noise
[AIAA PAPER 86-1873] p 198 A86-45493

WING FLAPS

Velocity and temperature decay characteristics of inverted-profile jets
[AIAA PAPER 86-0312] p 2 A86-22693

Velocity and temperature decay characteristics of inverted-profile jets
[NASA-TM-87159] p 9 N86-14223

WING LOADING

Influence of airfoil camber on convected gust interaction noise
[AIAA PAPER 86-1873] p 198 A86-45493

WING NACELLE CONFIGURATIONS

Evaluation of propeller/nacelle interactions in the PTA program
[AIAA PAPER 86-1552] p 6 A86-42709

WINGLETS

Development and testing of tip devices for horizontal axis wind turbines
[NASA-CR-174991] p 185 N86-18774

WINGS

An experimental investigation of reducing advanced turboprop cabin noise by wing shielding
[AIAA PAPER 86-1966] p 16 A86-45449

Piezoelectric deicing device
[NASA-CASE-LEW-13773-2] p 122 N86-20671

An experimental investigation of reducing advanced turboprop cabin noise by wing shielding
[NASA-TM-87112] p 201 N86-25218

In-flight photogrammetric measurement of wing ice accretions
[NASA-TM-87191] p 17 N86-31562

WOOD

Improved stud configurations for attaching laminated wood wind turbine blades
[NASA-TM-87109] p 172 N86-10582

WORK FUNCTIONS

Thermionic noise measurements for on-line dispenser cathode diagnostics for linear beam microwave tubes
[NASA-CR-175105] p 124 N86-28323

WORKING FLUIDS

Organosiloxane working fluids for the liquid droplet radiator
[NASA-CR-175033] p 102 N86-16381

Effect of an oxygen plasma on the physical and chemical properties of several fluids for the liquid droplet radiator
[NASA-TM-88639] p 49 N86-31634

X**X RAY ANALYSIS**

NDE of structural ceramics
[ASME PAPER 86-GT-279] p 163 A86-48298

NDE of structural ceramics
[NASA-TM-87186] p 164 N86-16598

X RAY DENSITY MEASUREMENT

Correlation of processing and sintering variables with the strength and radiography of silicon nitride
[NASA-TM-87251] p 106 N86-31729

X RAY DIFFRACTION

Neutron and X-ray diffraction of plasma-sprayed zirconia-yttria thermal barrier coatings
p 96 A86-16269

X RAY INSPECTION

Factors that affect reliability of nondestructive detection of flaws in structural ceramics
[NASA-TM-87348] p 166 N86-31912

XENON

Light scattering tests of fundamental theories of transport properties in the critical region
p 39 N86-10113

Performance characteristics of ring-cusp thrusters with xenon propellant
[NASA-TM-87338] p 63 N86-31650

Y**YIELD STRENGTH**

The effects of grain size on the flow and fracture of long-range ordered alloys
p 84 A86-47243

Modifications of system for elevated temperature tensile testing and stress-strain measurement of metal matrix composites
[NASA-TM-87172] p 65 N86-13370

Simplified cyclic structural analyses of SSME turbine blades
[NASA-TM-87214] p 175 N86-16615

Yielding and deformation behavior of the single crystal nickel-base superalloy PWA 1480
[NASA-CR-175100] p 91 N86-25455

YTTERBIUM

Optimization of the Ni-Cr-Al-Y/ZrO₂-Y₂O₃ thermal barrier system
p 82 A86-31746

YTTRIUM

Compatibility experiments of facilities, materials, and propellants for electrothermal thrusters
p 59 N86-17426

Z**ZINC**

Abrasion and deformed layer formation of manganese-zinc ferrite in sliding contact with lapping tapes
[NASA-TM-87249] p 104 N86-24838

ZINC TELLURIDES

Ion beam sputter deposited zinc telluride films
p 204 A86-47066

Ion beam sputter deposited zinc telluride films
[NASA-TM-87119] p 205 N86-11048

ZIRCONIUM COMPOUNDS

Long-term stability and properties of zirconia ceramics for heavy duty diesel engine components
[NASA-CR-174943] p 209 N86-17224

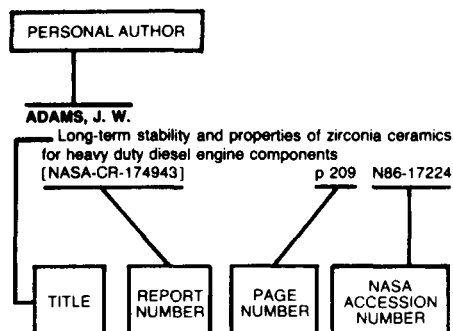
ZIRCONIUM OXIDES

Character of laser-glazed, plasma-sprayed zirconia coatings on stainless steel substrata
p 95 A86-15229

Comparison of the contact stress and friction behavior of SiC and ZrO₂ materials
p 95 A86-15237

PERSONAL AUTHOR INDEX

Typical Personal Author Index Listing



Listings in this index are arranged alphabetically by personal author. The NASA accession number denotes the number by which the citation is identified.

A

ABDELWAHAB, M.

Summary of investigations of engine response to distorted inlet conditions p 30 N86-26336
[NASA-TM-87317]
Uniform engine testing program phase 7: NASA Lewis Research Center second entry
[NASA-TM-87272] p 31 N86-28085

ACETO, L. D.

Preliminary design of a supersonic cruise aircraft high-pressure turbine
[NASA-CR-174878] p 26 N86-14272

ACOSTA, R.

Strategy for reflector pattern calculation - Let the computer do the work p 110 N86-39542
A numerical method for approximating antenna surfaces defined by discrete surface points
[NASA-TM-87125] p 111 N86-10381
Near-field spillover from a subreflector: Theory and experiment
[NASA-TM-88763] p 115 N86-25650
Near-field spillover from a subreflector: Theory and experiment
[NASA-TM-88818] p 116 N86-32598

ACOSTA, R. J.

Secondary pattern computation of an arbitrarily shaped main reflector
[NASA-TM-87162] p 112 N86-14477
Secondary pattern computation of an offset reflector antenna
[NASA-TM-87160] p 112 N86-14479
Compensation of reflector surface distortions using conjugate field matching
[NASA-TM-87198] p 113 N86-16461
Computation of the radiation characteristics of a generalized phased array
[NASA-TM-87185] p 114 N86-18586

ACOSTA, W. A.

Experimental study of the spray characteristics of a research airblast atomizer
[ASME PAPER 85-GT-229] p 129 N86-22125
Small gas turbine combustor experimental study - Compliant metal/ceramic liner and performance evaluation
[AIAA PAPER 86-1452] p 25 N86-49611

Small gas turbine combustor experimental study: Compliant metal/ceramic liner and performance evaluation
[NASA-TM-87304] p 33 N86-31582

ACOSTA, R.

Strategy for reflector pattern calculation: Let the computer do the work
[NASA-TM-87137] p 112 N86-12485

ADAMCZYK, J. H.

A numerical simulation of the inviscid flow through a counter-rotating propeller
[NASA-TM-87200] p 10 N86-16195

ADAMCZYK, J. J.

Steady inviscid three-dimensional flows p 128 N86-20952
Model equation for simulating flows in multistage turbomachinery
[ASME PAPER 85-GT-226] p 2 N86-22123
Unsteady transonic flow over cascade blades p 3 N86-23141
Unsteady transonic flow in cascades p 4 N86-24693

A new approach for solving the three-dimensional steady Euler equations. I - General theory p 133 N86-41242
A model for closing the inviscid form of the average-passage equation system
[ASME PAPER 86-GT-227] p 8 N86-48261
A model for closing the inviscid form of the average-passage equation system
[NASA-TM-87199] p 10 N86-14224

ADAMOVSKY, G.

All-fibre sensing loop using pulse-modulated light-emitting diode p 202 N86-11995
Time domain referencing in intensity modulation fiber optic sensing systems
[NASA-CR-175109] p 17 N86-24691

ADAMS, J. W.

Long-term stability and properties of zirconia ceramics for heavy duty diesel engine components
[NASA-CR-174943] p 209 N86-17224

ADAMS, M. L.

Analysis of a two row hydrostatic journal bearing with variable properties, inertia effects and surface roughness
p 153 N86-30599

AGGARWAL, B. B.

Traction forces at solid-lubricated rolling/sliding contacts
[ASLE PREPRINT 85-AM-4E-2] p 151 N86-11091

AHMA, S.

Advanced three-dimensional dynamic analysis by boundary element methods p 169 N86-34445

AHMED, S. A.

Concentration distributions in cylindrical combustors p 126 N86-11937
Concentration distributions in a model combustor p 133 N86-38575

AHUJA, K. K.

Tone excited jets. I - Introduction p 196 N86-16466
Tone excited jets. III - Flow measurements p 127 N86-16468
Tone excited jets. IV - Acoustic measurements p 196 N86-16469
An experimental study of tone-excited heated jets p 197 N86-31593
Some unresolved questions on hot-jet mixing control through artificial excitation
[AIAA PAPER 86-1956] p 135 N86-45441
Development of an impulsive noise source to study the acoustic reflection characteristics of hard-walled wind tunnels
[AIAA PAPER 86-1887] p 198 N86-45500
Acoustic reflection contamination measurements in the 16-foot NASA Langley Transonic Wind Tunnel
[AIAA PAPER 86-1888] p 198 N86-45501
Acoustic control of free jet mixing p 135 N86-46314

AIELLO, R. A.

Composite sandwich thermostructural behavior - Computational simulation
[AIAA PAPER 86-0948] p 170 N86-38842
Fiber composite sandwich thermostructural behavior: Computational simulation
[NASA-TM-88787] p 71 N86-31663

AKAY, H. U.

Applications of variational principles in computing rotational flows p 128 N86-20951

AKHTER, M. M.

Robust detection, isolation, and accommodation for sensor failures p 21 N86-35402
Robust detection, isolation and accommodation for sensor failures
[NASA-CR-174825] p 33 N86-30732

AKIN, L. S.

An investigation of the transient thermal analysis of spur gears
[ASME PAPER 84-DET-92] p 155 N86-40683

ALBRIGHT, A. E.

Experimental and analytical investigation of a freezing point depressant fluid ice protection system
[NASA-CR-174758] p 12 N86-27186

ALEXOVICH, R. E.

MMIC antenna technology development in the 30/20 gigahertz band
[AIAA PAPER 86-0666] p 45 N86-29628
MMIC antenna technology development in the 30/20 gigahertz band
[NASA-TM-87192] p 46 N86-17368

ALFANO, R. R.

Infrared-photoinduced-absorption studies in soluble trans-polyacetylene p 204 N86-37075

ALI, S. K.

Entrainment region phenomena for a large plane shear layer p 132 N86-30211

ALJABRI, A. S.

Evaluation of propeller/nacelle interactions in the PTA program
[AIAA PAPER 86-1552] p 6 N86-42709

ALLAIRE, P. E.

Simplex finite element analysis of viscous incompressible flow with penalty function formulation p 129 N86-22615

ALLEN, D.

Test results of a 40 kW Stirling engine and comparison with the NASA-Lewis computer code predictions p 181 N86-24889

ALLEN, D. H.

Integrated research in constitutive modelling at elevated temperatures, part 2
[NASA-CR-177233] p 178 N86-28455

Integrated research in constitutive modelling at elevated temperatures, part 1
[NASA-CR-177237] p 179 N86-30227

ALLEN, G. P.

Ribbon-burner simulation of T-700 turbine shroud for ceramic-lined seals research p 18 N86-15225

ALSTON, W. B.

Effect of substituted phenylhydrazines on processing and properties of PMR polyimide composites p 94 N86-13179

All-aromatic biphenylene end-capped polyquinoline and polyimide matrix resins p 100 N86-11267

Replacement of MDA with more oxidatively stable diamines in PMR-polyimides p 101 N86-11275

Structure-to-glass transition temperature relationships in high temperature stable condensation polyimides
[NASA-TM-87113] p 101 N86-12311

Structure-to-property relationships in addition cured polymers 2: Resin Tg composite initial mechanical properties of norbornenyl cured polyimide resins
[NASA-TM-88794] p 105 N86-29041

ALTENKIRCH, R. A.

Backward boundary layers in downward flame spread p 73 N86-22793

ALTEROVITZ, S. A.

Ellipsometric and optical study of some uncommon insulator films on 3-5 semiconductors
[NASA-TM-87135] p 205 N86-12134

Compensation in epitaxial cubic SiC films
[NASA-TM-87269] p 206 N86-25267

Auger electron spectroscopy, secondary ion mass spectroscopy and optical characterization of a-C-H and BN films
[NASA-TM-87258] p 206 N86-25268

- AMANO, R. S.**
Triple-velocity products in a channel with a backward-facing step p 133 A86-41725
Turbulence energy and diffusion transport in a separating and reattaching flow [AIAA PAPER 86-1724] p 135 A86-42812
Improvement of the second- and third-moment modeling of turbulence: A study of Reynolds-stress closure model [NASA-CR-176478] p 139 N86-16519
- ANDERSON, A. B.**
Adsorption of O₂, SO₂, and SO₃ on nickel oxide - Mechanism for sulfate formation p 75 A86-34238
- ANDERSON, G. G.**
High temperature properties of equiatomic FeAl with ternary additions p 84 A86-47252
- ANDERSON, N. E.**
Efficiency of nonstandard and high contact ratio involute spur gears [ASME PAPER 84-DET-172] p 155 A86-45255
- ANDERSON, O. L.**
Calculation of three-dimensional boundary layers on rotating turbine blades p 131 A86-28696
Assessment of a parabolic analysis for axisymmetric internal flows in rocket and turbomachinery ducts [AIAA PAPER 86-1598] p 134 A86-42739
- ANDERSON, W. J.**
Review and critical analysis: Rolling-element bearings for system life and reliability [NASA-CR-174710] p 159 N86-24991
- ANDRACCHIO, C. A.**
High-temperature thermocouple and heat flux gauge using a unique thin film hardware hot junction [ASME PAPER 85-GT-18] p 145 A86-13059
- ANG, J. A.**
Temperature and velocity profiles in sooting free boundary layer flames [AIAA PAPER 86-0575] p 73 A86-19962
- ANGUS, J. C.**
Composition and properties of the so-called 'diamond-like' amorphous carbon films p 96 A86-16255
Dual-ion-beam deposition of carbon films with diamond-like properties p 65 A86-49855
- ANTOLOVICH, S. D.**
A study of spectrum fatigue crack propagation in two aluminum alloys. I - Spectrum simplification. II - Influence of microstructures p 85 A86-48973
- ANZIC, G.**
Optical techniques to feed and control GaAs MMIC modules for phased array antenna applications [AIAA PAPER 86-0687] p 110 A86-29638
Optical techniques to feed and control GaAs MMIC modules for phased array antenna applications [NASA-TM-87218] p 113 N86-16458
- AOKI, K.**
Multispark flow visualization of lateral jet injection into a swirling cross flow p 1 A86-14561
- APELIAN, D.**
Structure-property characterization of rheocast and VADER processed IN-100 superalloy [NASA-CR-175014] p 88 N86-14354
- APPLEWHITE, A. Z.**
Bipolar nickel-hydrogen battery development p 180 A86-24823
- ARCHER, J. S.**
Solar dynamic power for the Space Station [AIAA PAPER 86-1299] p 54 A86-39906
- ARCHITETTO, P.**
Transformation toughened ceramics for the heavy duty diesel engine technology program, phase 2 [NASA-CR-175054] p 210 N86-22451
- ARMSTRONG, E. S.**
Test program to provide confidence in liquid oxygen cooling of hydrocarbon fueled rocket thrust chambers [NASA-TM-88816] p 62 N86-31646
- ARNOLD, S. M.**
Effects of state recovery on creep buckling under variable loading [NASA-CR-175094] p 212 N86-25310
- ARON, P. R.**
Angle-resolved Auger electron spectra induced by neon ion impact on aluminum p 76 A86-43456
Characterization and measurement of polymer wear p 100 A86-48405
- ARPASI, D. J.**
Development and application of dynamic simulations of a subsonic wind tunnel [AIAA PAPER 86-0758] p 36 A86-24745
Simulating a small turboshaft engine in real-time multiprocessor simulator (RTMPS) environment [NASA-TM-87216] p 27 N86-16221
Development and application of dynamic simulations of a subsonic wind tunnel [NASA-TM-87211] p 43 N86-18338

- Partitioning and packing mathematical simulation models for calculation on parallel computers [NASA-TM-87170] p 193 N86-19008
- ASAKA, Y.**
Effects of preferential diffusion on the burning intensity of curved flames p 73 A86-22813
- ASKEW, J. W.**
Centaur engine gimbal friction characteristics under simulated thrust load [NASA-TM-87335] p 44 N86-31821
- ASLANIDIS, I.**
Alloys based on NiAl for high temperature applications p 84 A86-47261
- ASSANIS, D. N.**
A computer simulation of the turbocharged turbo compounded diesel engine system: A description of the thermodynamic and heat transfer models [NASA-CR-174971] p 208 N86-16164
- ASTON, G.**
NASA electric propulsion technology [AIAA PAPER 85-1999] p 51 A86-17831
- ATKINSON, W. H.**
Turbine blade and vane heat flux sensor development, phase 2 [NASA-CR-174995] p 26 N86-12226
- ATLURI, S. N.**
Existence and stability, and discrete BB and rank conditions, for general mixed-hybrid finite elements in elasticity p 169 A86-34464
Constitutive modeling of cyclic plasticity and creep, using an internal time concept p 170 A86-41673
- AUGUST, R.**
Torsional vibrations and dynamic loads in a basic planetary gear system p 156 A86-47354
- AVILA, R. E.**
Calculation of recoil implantation profiles using known range statistics p 201 A86-11391
- AVNI, R.**
Radical molecule and ion-molecule mechanisms in the polymerization of hydrocarbons and chlorosilanes in R.F. plasmas at low pressures (below 1.0 Torr) p 203 A86-16254
Effect of argon and hydrogen on deposition of silicon from tetrachlorosilane in cold plasmas [NASA-TM-87219] p 65 N86-17472
- AWKER, R. W.**
Evaluation of propan propulsion applied to general aviation [NASA-CR-175020] p 30 N86-24695
- AYDELOTT, J. C.**
NASA Lewis Research Center low-gravity fluid management technology program p 44 A86-32906
Effect of subcooling on the on-orbit pressurization rate of cryogenic propellant tankage [AIAA PAPER 86-1253] p 54 A86-39877
NASA Lewis Research Center low-gravity fluid management technology program [NASA-TM-87145] p 44 N86-11218

B

- BAAKLINI, G. Y.**
Radiographic detectability limits for seeded voids in sintered silicon carbide and silicon nitride p 162 A86-31745
Reliability of void detection in structural ceramics by use of scanning laser acoustic microscopy p 163 A86-39027
Reliability of scanning laser acoustic microscopy for detecting internal voids in structural ceramics p 147 A86-46353
Probability of detection of internal voids in structural ceramics using microfocus radiography [NASA-TM-87164] p 164 N86-13749
Reliability of scanning laser acoustic microscopy for detecting internal voids in structural ceramics [NASA-TM-87222] p 164 N86-16599
Ultrasonic characterization of structural ceramics p 199 N86-22970
Effect of stress on ultrasonic pulses in fiber reinforced composites p 200 N86-22975
Correlation of processing and sintering variables with the strength and radiography of silicon nitride [NASA-TM-87251] p 106 N86-31729
Factors that affect reliability of nondestructive detection of flaws in structural ceramics [NASA-TM-87348] p 166 N86-31912
Quantitative void characterization in structural ceramics using scanning laser acoustic microscopy [NASA-TM-88797] p 166 N86-31913
- BACHTELL, E. E.**
Satellite voice broadcast. Volume 1: Executive summary [NASA-CR-175016] p 115 N86-24875
- Satellite voice broadcast. Volume 2: System study [NASA-CR-175017] p 115 N86-24876
- BADDOUR, M. F.**
A dual frequency microstrip antenna for Ka band [NASA-TM-87124] p 111 N86-10380
- BAGWELL, J. W.**
Technology achievements and projections for communication satellites of the future [AIAA PAPER 86-0649] p 109 A86-29811
Technology achievements and projections for communication satellites of the future [NASA-TM-87201] p 113 N86-17595
- BAHADORI, M. Y.**
Effects of buoyancy on gas jet diffusion flames - Experiment and theory [IAF PAPER 85-288] p 72 A86-15804
- BAILEY, R.**
High temperature static strain sensor development program p 148 N86-11500
- BAILEY, R. T.**
Development of optical diaphragm deflection sensors [NASA-CR-175008] p 203 N86-15113
- BAILEY, W. J.**
Cryogenic Fluid Management Facility p 108 A86-37053
LH2 on-orbit storage tank support trunnion design and verification p 53 A86-37054
- BALLARINI, R.**
Compliance matrices for cracked bodies [NASA-CR-179478] p 179 N86-30236
- BAMBERGER, E. N.**
Improved fracture toughness corrosion-resistant bearing material [NASA-CR-174990] p 162 N86-32743
- BANERJEE, P. K.**
Stress analysis of gas turbine engine structures using the boundary element method p 169 A86-34444
Advanced three-dimensional dynamic analysis by boundary element methods p 169 A86-34445
- BANKS, A.**
Apparatus for producing oxidation protection coatings for polymers [NASA-CASE-LEW-14072-2] p 106 N86-32569
- BANKS, B.**
Optical and interfacial electronic properties of diamond-like carbon films p 204 A86-16268
- BANKS, B. A.**
Ion beam sputter-deposited thin film coatings for protection of spacecraft polymers in low earth orbit [AIAA PAPER 85-0420] p 95 A86-14428
Diamondlike carbon films on semiconductors for insulated-gate technology p 120 A86-47077
Oxidation protection coatings for polymers [NASA-CASE-LEW-14072-1] p 102 N86-19458
Ion beam sputter etching [NASA-CASE-LEW-13899-1] p 109 N86-20587
Piezoelectric deicing device [NASA-CASE-LEW-13773-2] p 122 N86-20671
Oxidation protecting coatings for polymers [NASA-CASE-LEW-14072-3] p 105 N86-26434
- BARAONA, C. R.**
Space station power system p 50 A86-12676
Space Station Power System Advanced Development p 52 A86-24778
The space station power system [NASA-TM-88847] p 64 N86-32521
- BARBER, T. J.**
Three-dimensional inviscid flow in mixers. I - Mixer analysis using a Cartesian grid p 5 A86-39090
Three-dimensional inviscid flow in mixers. II - Analysis of turbulent forced mixers p 6 A86-46316
- BARNETT, A. M.**
N/P GaAs concentrator solar cells with an improved grid and busbar contact design p 184 N86-17844
- BARR, F. A.**
Slip casting and extruding shapes of rhenium with metal oxide additives. I: Feasibility demonstration [NASA-CR-174970] p 63 N86-31648
- BARRANGER, J. P.**
Ramp-integration technique for capacitance-type blade-tip clearance measurement [NASA-TM-87241] p 149 N86-24964
- BARRETT, C. A.**
The effect of variations of cobalt content on the cyclic oxidation resistance of selected Ni-base superalloys [NASA-TM-87297] p 93 N86-31702
- BARROW, B. J.**
Thermal-fatigue and oxidation resistance of cobalt-modified Udmet 700 alloy [NASA-TP-2591] p 178 N86-28464
- BARTEL, H. W.**
Development of an impulsive noise source to study the acoustic reflection characteristics of hard-walled wind tunnels [AIAA PAPER 86-1887] p 198 A86-45500

- Acoustic reflection contamination measurements in the 16-foot NASA Langley Transonic Wind Tunnel
[AIAA PAPER 86-1888] p 198 A86-45501
- BARTOLOTTA, P. A.**
Thermomechanical cyclic hardening behavior of Hastelloy-X
[NASA-CR-174999] p 174 N86-16610
- BARTON, J. M.**
Improved Euler analysis of advanced turboprop propeller flows
[AIAA PAPER 86-1521] p 6 A86-42688
- BASKLINI, G. Y.**
Nondestructive characterization of structural ceramics
p 99 A86-37141
- BASU, P.**
The effect of limiting aerodynamic and structural coupling in models of mistuned bladed disk vibration
p 21 A86-26905
- BATAKIS, A. P.**
Rocket thrust chamber thermal barrier coatings
[NASA-CR-175022] p 59 N86-20497
- BAUMBICK, R. J.**
Fiber optics for propulsion control systems
[ASME PAPER 84-GT-97] p 17 A86-13054
- BAUMEISTER, K. J.**
Time-dependent wave envelope finite difference analysis of sound propagation p 197 A86-20130
Reverberation effects on directionality and response of stationary monopole and dipole sources in a wind tunnel
[ASME PAPER 85-WA/NCA-1] p 197 A86-22747
Modeling wind tunnel effects on the radiation characteristics of acoustic sources p 197 A86-41689
Numerical Techniques in Acoustics
[NASA-CP-2404] p 198 N86-12007
Modeling the effects of wind tunnel wall absorption on the acoustic radiation characteristics of propellers
[NASA-TM-87333] p 201 N86-29630
Effect of triangular element orientation on finite element solutions of the Helmholtz equation
[NASA-TM-87351] p 201 N86-32247
- BEATTY, P. A.**
Turbulent two-phase flow in annular seals
[ASLE PREPRINT 86-AM-4G-3] p 156 A86-45391
- BECHERT, D. W.**
Shear layer excitation, experiment versus theory
[NASA-CR-176604] p 140 N86-20722
- BEHEIM, G.**
Wavelength-division multiplexed digital optical position transducer p 145 A86-20798
Fibre-optic thermometer using semiconductor-etalon sensor p 146 A86-32046
Range finding using frequency-modulated laser diode p 147 A86-39521
- BELLINA, J. J., JR.**
Surface modification strategies for (100)3C-SiC
p 76 A86-47083
- BELLOWS, R. S.**
Interdiffusional effects between tungsten fibers and an iron-nickel-base alloy p 66 A86-14718
- BELYTSCHKO, T.**
Probabilistic finite elements for transient analysis in nonlinear continua p 168 A86-28653
- BENDIKSEN, O. O.**
Vibration characteristics of mistuned shrouded blade assemblies
[ASME PAPER 85-GT-115] p 19 A86-22068
Aeroelastic behavior of low aspect ratio metal and composite blades
[ASME PAPER 86-GT-243] p 171 A86-48271
- BENNETT, J. C.**
Scalar and momentum turbulent transport experiments with swirling and nonswirling flows p 126 A86-11938
Numerical and experimental investigation of nonswirling and swirling confined jets
[AIAA PAPER 86-0040] p 127 A86-19651
Influence of large-scale motion on turbulent transport for confined coaxial jets. Volume 1: Analytical analysis of the experimental data using conditional sampling
[NASA-CR-175035] p 29 N86-20395
- BERNARD, T. J.**
Real gas effects on the numerical simulation of a hypersonic inlet p 6 A86-46324
- BENSTEIN, E. H.**
Year 2000 small engine technology payoffs in cruise missiles
[AIAA PAPER 86-1546] p 23 A86-42705
- BENTS, D. J.**
Tethered nuclear power for the space station
p 53 A86-24808
- BEREMAND, D. G.**
NASA/DOE automotive Stirling engine project: Overview 1986
[NASA-TM-87345] p 211 N86-29731
- BERENYI, S. G.**
Lightweight two-stroke cycle aircraft diesel engine technology enablement program, volume 1
[NASA-CR-174923-VOL-1] p 26 N86-13328
Lightweight two-stroke cycle aircraft diesel engine technology enablement program, volume 2
[NASA-CR-174923-VOL-2] p 26 N86-13329
Lightweight two-stroke cycle aircraft diesel engine technology enablement program, volume 3
[NASA-CR-174923-VOL-3] p 26 N86-13330
- BERGER, J. H.**
Wind tunnel tests of rotor blade sections with replications of ice formations accreted in hover
[NASA-CR-175089] p 15 N86-22558
- BERGSTROEM, S. I.**
Measurement of the density of base fluids at pressures 0.422 to 2.20 GPa
[NASA-TM-87114] p 156 N86-10551
- BERKOPEC, F. D.**
NASA electric propulsion technology
[AIAA PAPER 85-1999] p 51 A86-17831
- BERLAD, A. L.**
Particle cloud combustion experiment
p 41 N86-10160
Flame propagation and extinction in particle clouds
[NASA-CR-177304] p 78 N86-27434
- BERNDT, C. C.**
Neutron and X-ray diffraction of plasma-sprayed zirconia-yttria thermal barrier coatings
p 96 A86-16269
Failure analysis of plasma-sprayed thermal barrier coatings p 80 A86-16270
Performance of thermal barrier coatings in high heat flux environments p 80 A86-16272
Fracture toughness tests on plasma-sprayed coatings p 64 A86-30051
Tensile adhesion test measurements on plasma-sprayed coatings p 98 A86-30052
- BERNER, J.**
A preliminary study of the modified Ericsson for space power p 180 A86-24840
- BERNHART, W. D.**
A structural dynamics investigation related to EIDI applications
[AIAA PAPER 86-0550] p 16 A86-19942
Analyses and tests for design of an electro-impulse de-icing system
[NASA-CR-174919] p 15 N86-27268
- BERTHOLD, J. W.**
Development of optical diaphragm deflection sensors
[NASA-CR-175008] p 203 N86-13113
- BERTHOLD, J. W., III**
Thermal dependence of stress-induced birefringence in single mode optical fibers p 202 A86-15263
- BERTLES, C. R.**
Communications platform payload definition study
[NASA-CR-174986] p 49 N86-27402
Communications platform payload definition study, executive summary
[NASA-CR-174985] p 49 N86-27407
- BESSENDOORFF, M.**
The crack layer approach to toughness characterization in steel p 82 A86-30010
- BETTADAPUR, S. S.**
Satellite voice broadcast. Volume 1: Executive summary
[NASA-CR-175016] p 115 N86-24875
Satellite voice broadcast. Volume 2: System study
[NASA-CR-175017] p 115 N86-24876
- BHASIN, K. B.**
Optical techniques to feed and control GaAs MMIC modules for phased array antenna applications
[AIAA PAPER 86-0687] p 110 A86-29638
Dry etching of beta-SiC in CF₄ and CF₄ + O₂ mixtures p 76 A86-47069
Growth and characterization of epitaxial SrF₂ on InP(100) p 205 A86-47076
Monolithic optical integrated control circuitry for GaAs MMIC-based phased arrays
[NASA-TM-87183] p 113 N86-16457
Optical techniques to feed and control GaAs MMIC modules for phased array antenna applications
[NASA-TM-87218] p 113 N86-16458
Optically controlled phased array antenna concepts using GaAs monolithic microwave integrated circuits
[NASA-TM-87229] p 123 N86-21757
Analysis of optically controlled microwave/millimeter wave device structures
[NASA-TM-87246] p 123 N86-24907
- BHATTACHARYYA, S.**
Creep-rupture and fractographic analysis of Stirling engine superalloys tested in air and 15 MPa hydrogen
p 82 A86-30041
High-pressure creep tests p 84 A86-46564
- Creep-rupture behavior of iron superalloys in high-pressure hydrogen
[NASA-CR-175027] p 89 N86-17531
- BIAGLOW, J. A.**
Effect of elevated temperature and pressure on sprays from simplex swirl atomizers
[ASME PAPER 85-GT-58] p 130 A86-22735
- BIERSCHENK, T. R.**
The preparation of new perfluoroether fluids exhibiting excellent thermal-oxidative stabilities
[NASA-TM-87284] p 105 N86-25475
- BIESIADNY, T. J.**
Experimental study of ceramic-coated tip seals for turbojet engines p 152 A86-15227
Summary of investigations of engine response to distorted inlet conditions
[NASA-TM-87317] p 30 N86-26336
Uniform engine testing program phase 7: NASA Lewis Research Center second entry
[NASA-TM-87272] p 31 N86-28085
- BIFANO, W. J.**
Development of the VOLT-A shuttle experiment
[NASA-TM-87169] p 212 N86-14110
- BILL, R. C.**
Selected fretting-wear-resistant coatings for Ti-6 pct Al-4 pct V alloy p 97 A86-24956
Micromechanisms of thermomechanical fatigue: A comparison with isothermal fatigue
[NASA-TM-87331] p 92 N86-28164
- BIRMAN, J. L.**
Infrared-photoinduced-absorption studies in soluble trans-polyacetylene p 204 A86-37075
- BIROL, Y.**
Fatigue crack layer propagation in silicon-iron
[NASA-CR-175115] p 177 N86-25851
- BIZON, P. T.**
Thermal-fatigue and oxidation resistance of cobalt-modified Udimet 700 alloy
[NASA-TP-2591] p 178 N86-28464
- BLACK, J. D.**
Fatigue life analysis of a turboprop reduction gearbox
[ASME PAPER 85-DET-10] p 155 A86-45256
- BLAKNEY, D. F.**
Tone excited jets. IV - Acoustic measurements
p 196 A86-16469
- BLECH, R. A.**
Hardware configuration for a real-time multiprocessor simulator
[NASA-TM-88802] p 194 N86-28651
- BLOOMFIELD, H. S.**
Reliability and mass analysis of dynamic power conversion systems with parallel of standby redundancy
[NASA-TM-87189] p 57 N86-16258
- BLUMBERG, P. N.**
Methods for heat transfer and temperature field analysis of the insulated diesel phase 2 progress report
[NASA-CR-175072] p 210 N86-24590
- BOBER, L. J.**
Numerical evaluation of propeller noise including nonlinear effects p 23 A86-41726
Improved Euler analysis of advanced turboprop propeller flows
[AIAA PAPER 86-1521] p 6 A86-42688
An approach to the calculation of the pressure field produced by rigid wide chord dual rotation propellers of high solidity in compressible flow
[AIAA PAPER 86-0467] p 198 A86-49566
Summary of recent NASA propeller research
p 25 N86-11158
An analysis for the sound field produced by rigid wide chord dual rotation propellers of high solidity in compressible flow
[NASA-TM-87178] p 11 N86-21517
- BOBULA, G. A.**
The application of LQR synthesis techniques to the turboshaft engine control problem p 22 A86-35614
- BODNER, S. R.**
Constitutive modeling for isotropic materials (HOST)
[NASA-CR-174980] p 172 N86-10589
- BOECKER, W. D. G.**
Sintered alpha silicon carbide ceramics for high temperature structural application - Status review and recent developments
[ASME PAPER 85-IGT-127] p 97 A86-23921
- BOJAN, V. J.**
Mass spectrometric studies of the electrical breakdown of thin polymer films p 100 A86-47070
- BOLDMAN, D. R.**
Unsteady pressure measurements on a biconvex airfoil in a transonic oscillating cascade
[ASME PAPER 85-GT-212] p 3 A86-22731
Three-dimensional fluid flow phenomena in the blade end wall corner region
[ASME PAPER 86-GT-179] p 7 A86-48229

- Experimental evaluation of two turning vane designs for high-speed corner of 0.1-scale model of NASA Lewis Research Center's proposed altitude wind tunnel [NASA-TP-2570] p 38 N86-28101
- Comparison of analytical and experimental performance of a wind-tunnel diffuser section [NASA-TM-88795] p 13 N86-31537
- BORRERO, J. M.**
- The effect of processing conditions on the GaAs/plasma-grown insulator interface p 204 A86-18567
- BOVENKERK, R. L.**
- Traction forces at solid-lubricated rolling/sliding contacts [ASLE PREPRINT 85-AM-4E-2] p 151 A86-11091
- BOWDITCH, D. N.**
- Current wind tunnel capability and planned improvements at Lewis Research Center [AIAA PAPER 86-0728] p 36 A86-24727
- Current wind tunnel capability and planned improvements at Lewis Research Center [NASA-TM-87190] p 37 N86-18329
- BOWLES, K. J.**
- Graphite/PMR polyimide composites with improved toughness p 66 A86-21731
- Specimen geometry effects on graphite/PMR-15 composites during thermo-oxidative aging [NASA-TM-87204] p 69 N86-17477
- Fundamental studies of low velocity impact resistance of graphite fiber reinforced polymer matrix composites [NASA-TM-86886] p 69 N86-23661
- The correlation of low-velocity impact resistance of graphite-fiber-reinforced composites with matrix properties [NASA-TM-87337] p 71 N86-27426
- BOYNTON, J. L.**
- Small, two-stage, partial-admission turbine p 57 N86-17386
- BOZEK, J. M.**
- Development of the VOLT-A shuttle experiment [NASA-TM-87169] p 212 N86-14110
- BOZZOLA, R.**
- Computation of three-dimensional, rotational flow through turbomachinery blade rows for improved aerodynamic design studies [ASME PAPER 86-GT-26] p 7 A86-48117
- BRABBS, T.**
- Ignition delay times of benzene and toluene with oxygen in argon mixtures [NASA-TM-87312] p 78 N86-25431
- BRABBS, T. A.**
- Methane oxidation behind reflected shock waves: Ignition delay times measured by pressure and flame band emission [NASA-TM-87268] p 77 N86-21635
- BRACCO, F. V.**
- Two dimensional, transient catalytic combustion of CO-air on platinum p 71 A86-10201
- BRADLEY, S. A.**
- Stress and deformation modeling of multiple rotary combustion engine trochoid housings [SAE PAPER 860614] p 156 A86-49624
- BRADY, F. J.**
- A mathematical model for the doubly-fed wound rotor generator. II p 119 A86-39472
- Description and test results of a variable speed, constant frequency generating system [NASA-TM-87181] p 121 N86-16487
- BRAITHWAITE, W. M.**
- Summary of investigations of engine response to distorted inlet conditions [NASA-TM-87317] p 30 N86-26336
- Uniform engine testing program phase 7: NASA Lewis Research Center second entry [NASA-TM-87272] p 31 N86-28085
- BRANDHORST, H. W., JR.**
- Lithium counterdoped silicon solar cell [NASA-CASE-LEW-14177-1] p 190 N86-32875
- BRAUN, M. J.**
- An experimental investigation and some analytical considerations concerning the vaporous/gaseous cavity characteristics of an eccentric shaft seal or bearing p 130 A86-24463
- Analysis of a two row hydrostatic journal bearing with variable properties, inertia effects and surface roughness p 153 A86-30599
- Two-phase flows and heat transfer within systems with ambient pressure above the thermodynamic critical pressure [NASA-TM-87228] p 140 N86-19558
- Thermomechanical design criteria for ceramic-coated surfaces [NASA-TM-87328] p 143 N86-25726
- Two-phase flows within systems with ambient pressure p 161 N86-30167
- BRAUSCH, J. F.**
- Free jet feasibility study of a thermal acoustic shield concept for AST/VCE application-dual flow. Comprehensive data report. Volume 1: Test nozzles and acoustic data [NASA-CR-174817] p 200 N86-23371
- Free-jet feasibility study of a thermal acoustic shield concept for AST/VCE application-dual stream nozzles. Comprehensive data report. Volume 2: Laser velocimeter and suppressor. Base pressure data [NASA-CR-174818] p 201 N86-23372
- BRENNAN, S. M.**
- Space Station benefits from ECLS - Propulsion system synergism [AIAA PAPER 86-1407] p 47 A86-42619
- Space station propulsion requirements study [NASA-CR-174934] p 57 N86-15339
- BREWE, D. E.**
- Theoretical modeling of the vapor cavitation in dynamically loaded journal bearings [ASME PAPER 85-TRIB-51] p 130 A86-24496
- Theoretical modeling of the vapor cavitation in dynamically loaded journal bearings [NASA-TM-87076] p 137 N86-10463
- Theoretical and experimental comparison of vapor cavitation in dynamically loaded journal bearings [NASA-TM-87121] p 137 N86-11425
- Study of journal bearing dynamics using 3-dimensional motion picture graphics [NASA-TM-87205] p 140 N86-18647
- Starvation effects on the hydrodynamic lubrication of rigid nonconformal contacts in combined rolling and normal motion [NASA-TM-87174] p 140 N86-19556
- Piezoviscous effects in nonconformal contacts lubricated hydrodynamically [NASA-TM-87141] p 141 N86-21797
- BREZINSKY, K.**
- The high-temperature oxidation of aromatic hydrocarbons p 75 A86-40834
- BRIKMANIS, C. K.**
- Life and reliability modeling of bevel gear reductions [ASME PAPER 85-DE-7] p 151 A86-14466
- System life and reliability modeling for helicopter transmissions [NASA-CR-3967] p 159 N86-24990
- BRINKER, D.**
- A possible radiation-resistant solar cell geometry using superlattices p 185 N86-17851
- BRINKER, D. J.**
- Indium phosphide solar cells: status and prospects for use in space [NASA-TM-87315] p 123 N86-26520
- BRITTON, D. L.**
- Lightweight nickel electrode for nickel hydrogen cells and batteries [NASA-TM-87253] p 186 N86-21978
- BROCKWELL, J. L.**
- Mass transport phenomena between bubbles and dissolved gases in liquids under reduced gravity conditions p 39 N86-10110
- BRODIE, I.**
- Thermionic noise measurements for on-line dispenser cathode diagnostics for linear beam microwave tubes [NASA-CR-175105] p 124 N86-28323
- BRONDUM, D. C.**
- Numerical and experimental investigation of nonswirling and swirling confined jets [AIAA PAPER 86-0040] p 127 A86-19651
- Influence of large-scale motion on turbulent transport for confined coaxial jets. Volume 1: Analytical analysis of the experimental data using conditional sampling [NASA-CR-175035] p 29 N86-20395
- BROOK, R. J.**
- Structure and grain coarsening during the sintering of alumina p 98 A86-26341
- BROUWERS, A. P.**
- Lightweight two-stroke cycle aircraft diesel engine technology enablement program, volume 1 [NASA-CR-174923-VOL-1] p 26 N86-13328
- Lightweight two-stroke cycle aircraft diesel engine technology enablement program, volume 2 [NASA-CR-174923-VOL-2] p 26 N86-13329
- Lightweight two-stroke cycle aircraft diesel engine technology enablement program, volume 3 [NASA-CR-174923-VOL-3] p 26 N86-13330
- BROWN, G. V.**
- Nonlinear bending-torsional vibration and stability of rotating, pretwisted, precone blades including Coriolis effects [NASA-TM-87207] p 175 N86-17789
- BROWN, K. W.**
- Structural tailoring of engine blades (STAEBL) theoretical manual [NASA-CR-175112] p 31 N86-27283
- Structural tailoring of engine blades (STAEBL) user's manual [NASA-CR-175113] p 31 N86-27284
- BROWN, S. D.**
- Character of laser-glazed, plasma-sprayed zirconia coatings on stainless steel substrata p 95 A86-15229
- BROWN, W. H.**
- Non-linear effects in finite amplitude wave propagation through ducts and nozzles p 197 A86-35857
- Some unresolved questions on hot-jet mixing control through artificial excitation [AIAA PAPER 86-1956] p 135 A86-45441
- Acoustic control of free jet mixing p 135 A86-46314
- BROWNING, L.**
- Research and development of neat alcohol fuel usage in automobiles [NASA-CR-174813] p 108 N86-27460
- BROWNING, R.**
- Current viewpoints on oxide adherence mechanisms [NASA-TM-87168] p 87 N86-13409
- BRUCE, A. J.**
- Determination of solid mass fraction in partially frozen hydrocarbon fuels [NASA-CR-179472] p 108 N86-28261
- BRUNO, C.**
- Two dimensional, transient catalytic combustion of CO-air on platinum p 71 A86-10201
- BRUTON, W. M.**
- A lumped parameter mathematical model for simulation of subsonic wind tunnels [NASA-TM-87324] p 196 N86-27036
- BU-ABBUD, G.**
- Optical and interfacial electronic properties of diamond-like carbon films p 204 A86-16268
- BUCH, R. R.**
- Organosiloxane working fluids for the liquid droplet radiator [NASA-CR-175033] p 102 N86-16381
- BUCKLEY, D. H.**
- Surface effects of corrosive media on hardness, friction, and wear of materials p 94 A86-10825
- Angular particle impingement studies of thermoplastic materials at normal incidence [ASLE PREPRINT 85-AM-3A-1] p 94 A86-11076
- Erosion of aluminum 6061-T6 under cavitation attack in mineral oil and water p 79 A86-13801
- Fundamental tribological properties of ceramics p 95 A86-15230
- Mechanical-contact-induced transformation from the amorphous to the partially crystalline state in metallic glass p 80 A86-16257
- Metallic glass as a temperature sensor during ion plating p 80 A86-16906
- Tribological properties of boron nitride synthesized by ion beam deposition p 96 A86-17479
- Interaction of sulfuric acid corrosion and mechanical wear of iron p 81 A86-20436
- Erosion of phosphor bronze under cavitation attack in a mineral oil p 81 A86-23324
- Characterization and measurement of polymer wear p 100 A86-48405
- Tribological characteristics of gold films deposited on metals by ion plating and vapor deposition p 85 A86-49600
- Tribological properties of structural ceramics [NASA-TM-87105] p 100 N86-10341
- The mechanism of erosion of metallic materials under cavitation attack [NASA-TM-87133] p 156 N86-10552
- Adhesion and wear resistance of materials [NASA-TM-87239] p 158 N86-20809
- Analysis of a spacecraft instrument ball bearing assembly lubricated by a perfluoralkylether [NASA-TM-87260] p 50 N86-21575
- Abrasion and deformed layer formation of manganese-zinc ferrite in sliding contact with lapping tapes [NASA-TM-87249] p 104 N86-24838
- Effect of crystallographical and geometrical changes of a ferrite head on magnetic signals during the sliding process with magnetic tape [NASA-TM-87277] p 106 N86-31728
- BUDDHAYARAJU, J.**
- Heat transfer and fluid mechanics measurements in transitional boundary layer flows [ASME PAPER 85-GT-113] p 126 A86-13068
- BUDHANI, R.**
- Pretreatment effects on the morphology and properties of aluminum oxide thermally grown on NiCoCrAlY p 97 A86-17495
- BUFFUM, D. H.**
- Unsteady pressure measurements on a biconvex airfoil in a transonic oscillating cascade [ASME PAPER 85-GT-212] p 3 A86-22731

- BUGAJSKI, D.**
Polynomial nonlinear dynamical systems - A residual sensitivity method for model reduction p 194 A86-35386
- BUGGELE, A. E.**
Unsteady pressure measurements on a biconvex airfoil in a transonic oscillating cascade [ASME PAPER 85-GT-212] p 3 A86-22731
- BUGGELN, R. C.**
Numerical analysis of some supersonic viscous flows related to inlet and nozzle systems [AIAA PAPER 86-1597] p 134 A86-42738
- BUNSHAH, R. F.**
Pretreatment effects on the morphology and properties of aluminum oxide thermally grown on NiCoCrAlY p 97 A86-17495
- BUR, M. J.**
An analysis of low-thrust, resistojet reboost for the Space Station [AIAA PAPER 85-2042] p 51 A86-14447
- BURATYNSKI, E. K.**
An implicit LU scheme for the Euler equations applied to arbitrary cascades p 2 A86-20131
- BURCAT, A.**
Ignition delay times of benzene and toluene with oxygen in argon mixtures [NASA-TM-87312] p 78 N86-25431
- BURKARDT, L. A.**
Uniform engine testing program phase 7: NASA Lewis Research Center second entry [NASA-TM-87272] p 31 N86-28085
- BURLEY, R. R.**
Progress in the Lewis Research Center Altitude Wind Tunnel (AWT) modeling program [AIAA PAPER 86-0757] p 36 A86-24744
Progress in the Lewis Research Center Altitude Wind Tunnel (AWT) Modeling Program [NASA-TM-87194] p 37 N86-18233
- BURNSIDE, O. H.**
Probabilistic structural analysis for space propulsion system components p 168 A86-28659
- BURRIN, R. H.**
Tone excited jets. III - Flow measurements p 127 A86-16468
Development of an impulsive noise source to study the acoustic reflection characteristics of hard-walled wind tunnels [AIAA PAPER 86-1887] p 198 A86-45500
Acoustic reflection contamination measurements in the 16-foot NASA Langley Transonic Wind Tunnel [AIAA PAPER 86-1888] p 198 A86-45501
- BUSBEY, B. C.**
The effects of strong shock loading on coupled bending-torsion flutter of tuned and mistuned cascades p 20 A86-26893
- BUTNER, M. F.**
SSME long-life bearings [NASA-CR-179455] p 180 N86-27643
- BUZEK, B. C.**
Effect of multiple strain-anneal cycles on the 1000 C creep behaviour of gamma/gamma prime-alpha p 82 A86-30610
- BUZZARD, R. J.**
Mode II fatigue crack growth specimen development p 171 A86-43566
- C**
- CAHILL, J. E.**
Evaluation of capillary reinforced composites [NASA-CR-175061] p 70 N86-24780
- CAIRELLI, J.**
Test results of a 40 kW Stirling engine and comparison with the NASA-Lewis computer code predictions p 181 A86-24889
- CALDERBANK, J. C.**
Preliminary design of a supersonic cruise aircraft high-pressure turbine [NASA-CR-174878] p 26 N86-14272
- CAMBA, J., III**
Aerodynamic data banks for Clark-Y, NACA 4-digit and NACA 16-series airfoil families [NASA-CR-176883] p 13 N86-30693
- CAMPBELL, D. P.**
Technology for satellite power conversion [NASA-CR-176554] p 186 N86-19742
Technology for satellite power conversion [NASA-CR-176777] p 187 N86-25042
- CANN, G. L.**
A 10,000 hour life multipropellant engine for Space Station applications [AIAA PAPER 86-1403] p 54 A86-42616
- CARLSON, A. W.**
Heat pipe radiator technology for space power systems [AIAA PAPER 86-1300] p 47 A86-39907
- CARLSON, R. L.**
Analysis of large, non-isothermal elastic-visco-plastic deformations [NASA-CR-176220] p 172 N86-10588
Formulation of the nonlinear analysis of shell-like structures, subjected to time-dependent mechanical and thermal loading [NASA-CR-177194] p 178 N86-28462
- CARMU, U.**
Radical molecule and ion-molecule mechanisms in the polymerization of hydrocarbons and chlorosilanes in R.F. plasmas at low pressures (below 1.0 Torr) p 203 A86-16254
- CARNEY, K. S.**
Joint research effort on vibrations of twisted plates, phase 1: Final results [NASA-RP-1150] p 172 N86-10579
- CARNEY, M. J.**
NASA Lewis Research Center low-gravity fluid management technology program p 44 A86-32906
NASA Lewis Research Center low-gravity fluid management technology program [NASA-TM-87145] p 44 N86-11218
Liquid-vapor interface locations in a spheroidal container under low gravity [NASA-TM-87147] p 141 N86-23854
- CARPENTER, R. T.**
Improvement of ion thruster design [NASA-CR-177223] p 61 N86-27419
- CARROLL, D. R.**
The baseband processor in future satellite communication systems p 109 A86-21882
On the effectiveness of onboard processing [AIAA PAPER 86-0721] p 45 A86-29659
- CARVALHO, P.**
Large-Scale Advanced Prop-Fan (LAP) pitch change actuator and control design report [NASA-CR-174788] p 31 N86-27282
- CASASANT, D.**
Performance of direct and iterative algorithms on an optical systolic processor p 202 A86-17421
Space and frequency-multiplexed optical linear algebra processor - Fabrication and initial tests p 202 A86-48352
- CASASANT, D. P.**
Error-source effects in a high-accuracy optical finite-element processor p 192 A86-31571
- CASSENTI, B. N.**
Constitutive modeling for isotropic materials (HOST) [NASA-CR-174980] p 172 N86-10589
- CASTOR, J. G.**
Preliminary evaluation of a compound cycle engine for shipboard gensets [NASA-CR-179451] p 180 N86-26629
- CATALDO, R. L.**
Life cycle test results of a bipolar nickel hydrogen battery p 180 A86-24824
Parametric and cycle tests of a 40-A-hr bipolar nickel-hydrogen battery [NASA-TM-88793] p 189 N86-31979
- CATHCART, J. A.**
Advanced orbit transfer vehicle propulsion system study [NASA-CR-174843] p 60 N86-24746
- CAUGHEY, D. A.**
An implicit LU scheme for the Euler equations applied to arbitrary cascades p 2 A86-20131
Transonic potential flow in hyperbolic nozzles p 5 A86-41723
- CAULFIELD, T.**
Interdiffusional effects between tungsten fibers and an iron-nickel-base alloy p 66 A86-14718
- CAWLEY, J. D.**
Phenomenological study of the behavior of some silica formers in a high velocity jet fuel burner [NASA-TM-87127] p 157 N86-14613
- CELESTINA, M. L.**
A model for closing the inviscid form of the average-passage equation system [ASME PAPER 86-GT-227] p 8 A86-48261
A model for closing the inviscid form of the average-passage equation system [NASA-TM-87199] p 10 N86-14224
A numerical simulation of the inviscid flow through a counter-rotating propeller [NASA-TM-87200] p 10 N86-16195
- CERNANSKY, N. P.**
Ignition characteristics of rich n-heptane fuel sprays in the transition region [ASME PAPER 85-WA/HT-46] p 107 A86-38393
- Analysis of the effects of fuel spray characteristics on NO(x) formation [ASME PAPER 85-WA/HT-47] p 107 A86-38394
Transition region ignition characteristics of n-heptane fuel sprays [NASA-CR-176364] p 77 N86-14331
Combustion characteristics in the transition region of liquid fuel sprays [NASA-CR-176564] p 77 N86-20517
- CHAI, A. T.**
Transport processes in solution crystal growth p 39 N86-10107
Surface tension induced instabilities in reduced gravity: The Benard problem p 40 N86-10117
Thermocapillary motion research p 40 N86-10125
- CHAI, A.-T.**
Surface temperature distribution along a thin liquid layer due to thermocapillary convection [IAF PAPER 85-282] p 126 A86-15800
- CHAMBERLIN, R.**
Subscale-model and full-scale engine mixed-flow exhaust system performance comparison p 18 A86-14528
- CHAMIS, C. C.**
Longitudinal compressive failure modes in fiber composites End attachment effects on IITRI type test specimens p 66 A86-19999
NASA Lewis Research Center/university graduate research program on engine structures [ASME PAPER 85-GT-159] p 167 A86-22084
Designing for fiber composite structural durability in hydrothermomechanical environments p 67 A86-27734
Composite sandwich thermostructural behavior - Computational simulation [AIAA PAPER 86-0948] p 170 A86-38842
Computer aided derivation of equations for composite mechanics problems and finite element analyses [AIAA PAPER 86-1016] p 170 A86-38873
Structural tailoring of SSME turbopump blades (SSME/STAEPL) [AIAA PAPER 86-0847] p 54 A86-38895
Probabilistic structural analysis methods for critical SSME propulsion components [AIAA PAPER 86-1188] p 54 A86-40595
Computational composite mechanics for aerospace propulsion structures [AIAA PAPER 86-1190] p 67 A86-40596
Dynamic stress analysis of smooth and notched fiber composite flexural specimens p 67 A86-41070
Computational engine structural analysis [ASME PAPER 86-GT-70] p 23 A86-48141
Interlaminar fracture toughness: Three-dimensional finite element modeling for end-notch and mixed-mode flexure [NASA-TM-87138] p 69 N86-14316
Computational engine structural analysis [NASA-TM-87231] p 175 N86-19663
Integrated Composite Analyzer (ICAN): Users and programmers manual [NASA-TP-2515] p 69 N86-21614
Thermoviscoplastic nonlinear constitutive relationships for structural analysis of high temperature metal matrix composites [NASA-TM-87291] p 70 N86-24756
A unique set of micromechanics equations for high temperature metal matrix composites [NASA-TM-87154] p 70 N86-24757
Simplified composite micromechanics for predicting microstresses [NASA-TM-87295] p 70 N86-24759
Fracture characteristics of angleplied laminates fabricated from overaged graphite/epoxy prepreg [NASA-TM-87286] p 70 N86-25417
Computational simulation of progressive fracture in fiber composites [NASA-TM-87341] p 71 N86-26376
Fiber composite sandwich thermostructural behavior: Computational simulation [NASA-TM-88787] p 71 N86-31663
ICAN: A versatile code for predicting composite properties [NASA-TM-87334] p 71 N86-31664
- CHAN, K. S.**
Constitutive modeling for isotropic materials (HOST) [NASA-CR-174980] p 172 N86-10589
- CHANG, A. T.**
Influence of rotation and pretwist on cantilever fan blade flutter p 17 A86-11686
- CHANG, S. C.**
Solution of elliptic partial differential equations by fast Poisson solvers using a local relaxation factor. 1: One-step method [NASA-TP-2529] p 195 N86-28661

- CHANG, S.-C.**
Steady inviscid three-dimensional flows p 128 A86-20952
A new approach for solving the three-dimensional steady Euler equations. I - General theory p 133 A86-41242
- CHANG, S.-H.**
An embedding method for the steady Euler equations p 194 A86-30814
- CHAPMAN, R.**
Measurements of energy distribution and wall temperature in flowing hydrogen microwave plasma systems [AIAA PAPER 85-2052] p 203 A86-11001
Measurement of energy distribution in flowing hydrogen microwave plasmas p 52 A86-18041
- CHARLESTON, J. A.**
Assessment of commercially available and experimental hydrogen electrodes [NASA-TM-87264] p 187 N86-23035
- CHECHILE, R. A.**
The effects of syntactic complexity on the human-computer interaction p 192 A86-36172
- CHEN, C. H.**
Character of laser-glazed, plasma-sprayed zirconia coatings on stainless steel substrata p 95 A86-15229
Diffusion flame extinction in slow convective flow under microgravity environment [NASA-TM-88799] p 144 N86-28378
- CHEN, D. Y.**
Formation and inflammation of a turbulent jet p 130 A86-23131
Nondestructive characterization of RB50A of high-power bipolar transistors p 118 A86-35718
Hybrid power semiconductor [NASA-CASE-LEW-13922-1] p 122 N86-20872
- CHEN, J.**
Modal test/analysis correlation for Centaur G Prime launch vehicle [AIAA PAPER 86-1002] p 43 A86-38943
- CHEN, L.-D.**
Flow and atomization in flashing injectors p 136 A86-49442
- CHEN, W. J.**
Parameter sensitivity in the dynamics of rotor-bearing systems [ASME PAPER 85-DET-35] p 154 A86-38620
- CHEN, Y. S.**
Statistical prediction of dynamic distortion of inlet flow using minimum dynamic measurement. An application to the Melick statistical method and inlet flow dynamic distortion prediction without RMS measurements [NASA-CR-176764] p 142 N86-24933
- CHENG, J. J. A.**
Structure-property characterization of rheocast and VADER processed IN-100 superalloy [NASA-CR-175014] p 88 N86-14354
- CHENG, J.-C.**
A mesh re-zoning technique for finite element simulations of metal forming processes p 153 A86-38298
- CHERRETTE, A. R.**
Near-field spillover from a subreflector: Theory and experiment [NASA-TM-88763] p 115 N86-25650
Near-field spillover from a subreflector: Theory and experiment [NASA-TM-88818] p 116 N86-32598
- CHIGIER, N.**
Measurements in liquid fuel sprays [NASA-CR-177088] p 144 N86-30960
- CHILDS, D. W.**
Theory versus experiment for the rotordynamic coefficients of annular gas seals. I - Test facility and apparatus [ASME PAPER 85-TRIB-1] p 152 A86-24481
Experimental rotordynamic coefficient results for teeth-on-rotor and teeth-on-stator labyrinth gas seals [ASME PAPER 86-GT-12] p 156 A86-48109
A comparison of experimental and theoretical results for leakage, pressure gradients, and rotordynamic coefficients for tapered annular gas seal [NASA-CR-179709] p 182 N86-32742
- CHIMA, R. V.**
Development of an explicit multigrid algorithm for quasi-three-dimensional viscous flows in turbomachinery [AIAA PAPER 86-0032] p 1 A86-19844
Development of an explicit multigrid algorithm for quasi-three-dimensional viscous flows in turbo-machinery [NASA-TM-87128] p 1 N86-11146
- CHIU, W.**
Ceramic automotive Stirling engine study [NASA-CR-174907] p 208 N86-16185
- CHOO, Y. K.**
Three-dimensional inviscid analysis of radial-turbine flow and a limited comparison with experimental data p 4 A86-28702
- Three-dimensional inviscid analysis of radial turbine flow and a limited comparison with experimental data [NASA-TM-87091] p 9 N86-10017
- CHORIN, A. J.**
Numerical simulation of a turbulent flame stabilized behind a rearward-facing step p 73 A86-22774
- CHRIST, R. M.**
Development of seeding techniques for small supersonic wind tunnel p 147 N86-11452
- CHUANG, S. L.**
Numerical methods for analyzing electromagnetic scattering [NASA-CR-176141] p 111 N86-10377
- CHUANG, S.-L.**
Normal modes in an overmoded circular waveguide coated with lossy material p 119 A86-44078
- CHUBB, D. L.**
Analysis of the Gas Particle Radiator (GPR) [NASA-TM-88786] p 63 N86-31852
- CHUDNOVSKY, A.**
The crack layer approach to toughness characterization in steel p 82 A86-30010
Fatigue crack layer propagation in silicon-iron [NASA-CR-175115] p 177 N86-25851
- CHUNG, B. T. F.**
Thermomechanical design criteria for ceramic-coated surfaces [NASA-TM-87328] p 143 N86-25726
- CIEPLUCH, C. C.**
Progress in the Lewis Research Center Altitude Wind Tunnel (AWT) modeling program [AIAA PAPER 86-0757] p 36 A86-24744
Progress in the Lewis Research Center Altitude Wind Tunnel (AWT) Modeling Program [NASA-TM-87194] p 37 N86-16233
- CIVINKAS, K. C.**
Turbine-stage heat transfer - Comparison of short-duration measurements with state-of-the-art predictions [AIAA PAPER 86-1465] p 134 A86-42656
- CIVINSKAS, K. C.**
Three-dimensional inviscid analysis of radial-turbine flow and a limited comparison with experimental data p 4 A86-28702
Three-dimensional inviscid analysis of radial turbine flow and a limited comparison with experimental data [NASA-TM-87091] p 9 N86-10017
- CLARK, B. J.**
Preliminary results of unsteady blade surface pressure measurements for the SR-3 propeller [AIAA PAPER 86-1893] p 8 A86-49625
Preliminary results of unsteady blade surface pressure measurements for the SR-3 propeller [NASA-TM-87352] p 12 N86-27213
- CLARK, D. A.**
Effect of area ratio on the performance of a 5.5:1 pressure ratio centrifugal impeller [ASME PAPER 86-GT-303] p 8 A86-48315
Effect of area ratio on the performance of a 5.5:1 pressure ratio centrifugal impeller [NASA-TM-87237] p 10 N86-19290
- CLARK, R.**
A possible radiation-resistant solar cell geometry using superlattices p 185 N86-17851
- CLAUS, R. W.**
Combustion research for gas turbine engines p 17 A86-11609
SSME fuelside preburner two-dimensional analysis [NASA-TM-87299] p 44 N86-23616
- CLOPP, H. W.**
Communications platform payload definition study [NASA-CR-174986] p 49 N86-27402
Communications platform payload definition study, executive summary [NASA-CR-174985] p 49 N86-27407
- COE, H. H.**
Lubrication and performance of high-speed rolling-element bearings p 152 A86-19375
Effect on interference fits on roller bearing fatigue life [NASA-TM-87165] p 158 N86-19618
- COFFINBERRY, G. A.**
Method for improving the fuel efficiency of a gas turbine engine [NASA-CASE-LEW-13142-2] p 28 N86-20389
- COHEN, L. M.**
Simultaneous measurements of velocity and pressure fields in subsonic and supersonic flows through image-intensified detection of laser-induced fluorescence [AIAA PAPER 86-0161] p 145 A86-19726
- COHEN, S.**
Fuel deposit characteristics at low velocity [ASME PAPER 85-IGT-130] p 107 A86-23922
- COLE, G. L.**
Development and application of dynamic simulations of a subsonic wind tunnel [AIAA PAPER 86-0758] p 36 A86-24745
- Development and application of dynamic simulations of a subsonic wind tunnel [NASA-TM-87211] p 43 N86-18338
A lumped parameter mathematical model for simulation of subsonic wind tunnels [NASA-TM-87324] p 196 N86-27036
- COLEMAN, E.**
Dilution jet mixing program, phase 3 [NASA-CR-174884] p 142 N86-24938
- COLES, C. E.**
Liquid droplet radiator program at the NASA Lewis Research Center [ASME PAPER 86-HT-15] p 48 A86-49621
Liquid droplet radiator program at the NASA Lewis Research Center [NASA-TM-87139] p 48 N86-12246
Effect of an oxygen plasma on the physical and chemical properties of several fluids for the liquid droplet radiator [NASA-TM-88839] p 49 N86-31834
- COLES, D.**
Free surface phenomena under low- and zero-gravity conditions p 39 N86-10108
- COLLIN, R. E.**
Mutual coupling effects in antenna arrays, volume 1 [NASA-CR-176899] p 114 N86-22782
- COLLINS, W. R.**
A high-order language for a system of closely coupled processing elements [NASA-CR-177280] p 193 N86-27930
- CONCUS, P.**
Free surface phenomena under low- and zero-gravity conditions p 39 N86-10108
- CONNOLLY, D. J.**
Optical techniques to feed and control GaAs MMIC modules for phased array antenna applications [AIAA PAPER 86-0687] p 110 A86-29638
Optical techniques to feed and control GaAs MMIC modules for phased array antenna applications [NASA-TM-87218] p 113 N86-16458
- CONROY, M. J.**
Testing of 30-GHz low noise receivers [AIAA PAPER 86-0654] p 45 A86-29616
Testing of 30-GHz low noise receivers [NASA-TM-87171] p 112 N86-13627
- CONTOLATIS, T.**
Ka-band monolithic gain control amplifier p 119 A86-41343
- CONVERSE, G. L.**
Extended parametric representation of compressor fans and turbines. Volume 1: CMGEN user's manual [NASA-CR-174645] p 159 N86-23936
Extended parametric representation of compressor fans and turbines. Volume 3: MODFAN user's manual (parametric modulating flow fan) [NASA-CR-174647] p 159 N86-23938
- COOPER, L. P.**
Manrating orbital transfer vehicle propulsion [AIAA PAPER 85-1226] p 50 A86-14429
Status of advanced orbital transfer propulsion [IAF PAPER 85-164] p 51 A86-17850
- COOPER, T. W.**
Advanced orbit transfer vehicle propulsion system study [NASA-CR-174843] p 60 N86-24746
- CORRIEL, S. R.**
Interaction of flows with the crystal-melt interface p 132 A86-29419
- CORNELL, C. C.**
Experimental and theoretical study of propeller spinner/shank interference [NASA-CR-176954] p 13 N86-29773
- CORRIGAN, R. D.**
Vortex generators as a means for increasing rotor performance p 4 A86-24920
Design and initial testing of a one-bladed 30-meter-diameter rotor on the NASA/DOE mod-O wind turbine [NASA-TM-88810] p 169 N86-30251
- CORRINGRATO, R. M.**
Advanced orbit transfer vehicle propulsion system study [NASA-CR-174843] p 60 N86-24746
- COSTI, T.**
Effect of accuracy of wind power prediction on power system operator [NASA-CR-176300] p 181 N86-11667
- COTTERELL, E. M.**
Determination of solid mass fraction in partially frozen hydrocarbon fuels [NASA-CR-179472] p 108 N86-28261
- COVERSE, G. L.**
Extended parametric representation of compressor fans and turbines. Volume 2: Part user's manual (parametric turbine) [NASA-CR-174646] p 159 N86-23937

- COWELL, L. H.**
Spontaneous ignition delay characteristics of hydrocarbon fuel-air mixtures
[NASA-CR-175064] p 29 N86-21545
- COY, J. J.**
Life and reliability modeling of bevel gear reductions
[ASME PAPER 85-DE-7] p 151 A86-14486
Generation of spiral bevel gears with zero kinematical errors and computer aided simulation of their meshing and contact
p 154 A86-40656
Generated spiral bevel gears - Optimal machine-tool settings and tooth contact analysis
[SAE PAPER 851573] p 154 A86-40678
Fatigue life analysis of a turboprop reduction gearbox
[ASME PAPER 85-DET-10] p 155 A86-45256
Gearing
[NASA-RP-1152] p 157 N86-14612
Generation of spiral bevel gears with zero kinematical errors and computer aided tooth contact analysis
[NASA-TM-87273] p 160 N86-25793
- COYNER, J. V.**
Satellite voice broadcast. Volume 1: Executive summary
[NASA-CR-175016] p 115 N86-24875
Satellite voice broadcast. Volume 2: System study
[NASA-CR-175017] p 115 N86-24876
- COYNER, J. V., JR.**
Hybrid deployable/erectable solar dynamic box truss system
[AIAA PAPER 86-0955] p 47 A86-38883
- CRAIG, J. E.**
Visualization of flows in a motored rotary combustion engine using holographic interferometry
[NASA-TM-88804] p 33 N86-31583
- CRAWFORD, J. T.**
Robust detection-isolation-accommodation for sensor failures
[NASA-CR-174797] p 121 N86-16486
- CRAWFORD, R. A.**
Mean velocity and turbulence measurements in a 90 deg curved duct with thin inlet boundary layer
[NASA-CR-174811] p 139 N86-16518
- CRAWLEY, E. F.**
Aeroelastic formulations for turbomachines and propellers
p 20 A86-24677
Analytical and experimental investigation of the coupled bladed disk/shaft whirl of a cantilevered turbofan
[ASME PAPER 86-GT-98] p 24 A86-48163
- CRIMP, M.**
Effect of boron on tensile properties of B2 BeAl
[NASA-CR-175074] p 89 N86-21656
- CRIMP, M. A.**
Rapidly solidified NiAl and FeAl
p 84 A86-47263
- CRONAU, S. T.**
Advanced orbit transfer vehicle propulsion system study
[NASA-CR-174843] p 60 N86-24746
- CRONIN, M.**
Automotive Stirling Engine Development Program
[NASA-CR-174749] p 211 N86-28017
Automotive Stirling engine development program
[NASA-CR-175045] p 211 N86-30579
- CUNNINGHAM, R. E.**
Passive eddy-current damping as a means of vibration control in cryogenic turbomachinery
[NASA-TP-2562] p 44 N86-24722
- CURRAN, F. M.**
Hollow cathodes in high pressure arc discharges
[AIAA PAPER 85-2035] p 50 A86-14448
An experimental study of energy loss mechanisms and efficiency considerations in the low power dc arcjet
[AIAA PAPER 85-2017] p 53 A86-37062
Low power dc arcjet operation with hydrogen/nitrogen propellant mixtures
[AIAA PAPER 86-1505] p 55 A86-42676
An experimental study of energy loss mechanisms and efficiency consideration in the low power dc arcjet
[NASA-TM-87123] p 57 N86-11224
Lower power dc arcjet operations with hydrogen hydrogen/nitrogen propellant mixtures
[NASA-TM-87279] p 61 N86-25407
- CURREN, A. N.**
TWT efficiency enhancement with textured carbon surfaces on copper MDC electrodes
p 120 A86-49617
Textured carbon on copper: A novel surface with extremely low secondary electron emission characteristics
[NASA-TP-2543] p 101 N86-15394
Textured carbon surfaces on copper by sputtering
[NASA-CASE-LEW-14130-1] p 109 N86-32587
- CURTIS, H. B.**
Performance of Hughes GaAs concentrator cells under 1-MeV electron irradiation
p 185 N86-17860
- CUTLER, M. J.**
Large-Scale Advanced Prop-Fan (LAP) pitch change actuator and control design report
[NASA-CR-174788] p 31 N86-27282
- CYR, M. A.**
Turbine blade and vane heat flux sensor development, phase 2
[NASA-CR-174995] p 26 N86-12226

D

- DADONE, L.**
Performance degradation of helicopters due to icing - A review
p 16 A86-35668
- DAME, L. T.**
Anisotropic constitutive model for nickel base single crystal alloys: Development and finite element implementation
[NASA-CR-175015] p 176 N86-21952
- DANIS, A. M.**
Ignition characteristics of rich n-heptane fuel sprays in the transition region
[ASME PAPER 85-WA/HT-46] p 107 A86-38393
Transition region ignition characteristics of n-heptane fuel sprays
[NASA-CR-176364] p 77 N86-14331
- DAROOKA, D.**
Ceramic automotive Stirling engine study
[NASA-CR-174907] p 208 N86-16165
- DASO, E. O.**
Parametric effects of CFL number and artificial smoothing on numerical solutions using implicit approximate factorization algorithm
[AIAA PAPER 86-1059] p 132 A86-38427
- DAVID, J. W.**
Linear dynamic coupling in geared rotor systems
[ASME PAPER 85-DET-11] p 154 A86-38617
- DAVIDIAN, K.**
Computational simulation of liquid rocket injector anomalies
[AIAA PAPER 86-1424] p 55 A86-42633
- DAVIDOVITZ, M.**
Input impedance of a probe-fed circular microstrip antenna with thick substrate
p 120 A86-46638
- DAVIDSON, J.**
Spectrum orbit utilization program technical manual SOUP5 Version 3.8
[NASA-CR-174944] p 116 N86-26489
Spectrum Orbit Utilization Program documentation: SOUP5 version 3.8 user's manual, volume 1, chapters 1 through 5
[NASA-CR-174889] p 193 N86-27927
Spectrum Orbit Utilization Program documentation: SOUP5 version 3.8 user's manual, volume 2, appendices A through G
[NASA-CR-174890] p 193 N86-27928
- DAVIS, P. R.**
The effect of oxygen pressure on volatility and morphology of LaB6 single crystal cathodes
p 204 A86-28076
- DAVIS, R. F.**
Dry etching of beta-SiC in CF4 and CF4 + O2 mixtures
p 76 A86-47069
- DAVIS, V. A.**
Threshold determining mechanisms for discharges in high voltage solar arrays
[AIAA PAPER 86-0364] p 52 A86-19834
- DAYAN, M.**
The beta-SiC(100) surface studied by low energy electron diffraction, Auger electron spectroscopy, and electron energy loss spectra
p 77 A86-49884
- DAYTON, J. A., JR.**
Verification of an improved computational design procedure for TWT-dynamic refocuser-MDC systems with secondary electron emission losses
p 119 A86-45194
Verification of computer-aided designs of traveling-wave tubes utilizing novel dynamic refocusers and graphite electrodes for the multistage depressed collector
[NASA-TP-2524] p 121 N86-13643
- DE LOS REYES, G.**
The application of LQR synthesis techniques to the turbohaft engine control problem
p 22 A86-35614
- DEADMORE, D.**
Tribology of selected ceramics at temperatures to 900 deg C
[NASA-TM-87267] p 105 N86-25476
- DEADMORE, D. L.**
Characterization of the tribological coating composition 77 wt % CaF2 - 23 wt % Li F fused to IN-750 alloy
[NASA-TM-87342] p 105 N86-27452
- DECK, R. T.**
Reassessment of the theory of stimulated Raman scattering
p 150 A86-40662
- DECKER, A.**
Beam-modulation methods in quantitative and flow visualization holographic interferometry
[NASA-TM-87306] p 148 N86-24958
- DECKER, A. J.**
A comparison of electronic heterodyne moire deflectometry and electronic heterodyne holographic interferometry for flow measurements
[SAE PAPER 851896] p 148 A86-38359
Advanced optical measuring systems for measuring the properties of fluids and structures
[NASA-TM-88829] p 150 N86-31859
- DEISSLER, R. G.**
Is Navier-Stokes turbulence chaotic?
p 137 A86-50275
- DELAAT, J. C.**
A real-time simulation evaluation of an advanced detection. Isolation and accommodation algorithm for sensor failures in turbine engines
[NASA-TM-87289] p 30 N86-24697
A sensor failure simulator for control system reliability studies
[NASA-TM-87271] p 124 N86-31792
- DELLACORTE, C.**
Composition optimization of self-lubricating chromium carbide-based composite coatings for use to 780 deg C
[NASA-TM-87261] p 103 N86-20568
- DELOMBARD, R.**
Minority-carrier mobility anomalies in low-resistivity silicon solar cells
p 181 A86-49215
- DELVIGS, P.**
Tetraglycidyl epoxy resins and graphite fiber composites cured with flexibilized aromatic diamines
p 67 A86-36999
PMR polyimides from solutions containing mixed endcaps
p 100 N86-11263
The 371 deg C mechanical properties of graphite/polyimide composites
[NASA-TM-87122] p 69 N86-12256
- DEMASI, J. T.**
Thermal barrier coating life prediction model development
[NASA-CR-175087] p 103 N86-22713
- DENNIS, R. E.**
Low-cost single-crystal turbine blades, volume 2
[NASA-CR-174652] p 28 N86-23598
- DENNON, S. R.**
Review and evaluation of recent developments in melic inlet dynamic flow distortion prediction and computer program documentation and user's manual estimating maximum instantaneous inlet flow distortion from steady-state total pressure measurements with full, limited, or no dynamic data
[NASA-CR-176765] p 143 N86-24955
- DERNER, W. J.**
Review and critical analysis: Rolling-element bearings for system life and reliability
[NASA-CR-174710] p 159 N86-24991
- DESALVO, G. C.**
N/P GaAs concentrator solar cells with an improved grid and busbar contact design
p 184 N86-17844
- DESHANDEY, C. V.**
Pretreatment effects on the morphology and properties of aluminum oxide thermally grown on NiCoCrAlY
p 97 A86-17495
- DEUTSCH, S.**
The boundary layer on compressor cascade blades
[NASA-CR-177279] p 143 N86-27607
- DEWITT, K. J.**
Mass transport phenomena between bubbles and dissolved gases in liquids under reduced gravity conditions
p 39 N86-10110
- DIAMANT, E. S.**
Solar dynamic power for the Space Station
[AIAA PAPER 86-1299] p 54 A86-39906
- DIAS, J. B.**
Efficient algorithms for use in probabilistic finite element analysis
p 168 A86-28655
- DIAZ, J. O.**
Modifications of system for elevated temperature tensile testing and stress-strain measurement of metal matrix composites
[NASA-TM-87172] p 65 N86-13370
- DICARLO, J. A.**
Creep of chemically vapour deposited SiC fibres
p 66 A86-21486
Polymer, metal and ceramic matrix composites for advanced aircraft engine applications
[NASA-TM-87132] p 87 N86-13407
- DIEM-KIRSOP, P. S.**
Liquid droplet radiator thermal characteristics
[AIAA PAPER 86-1182] p 133 A86-40578
Liquid droplet radiator program at the NASA Lewis Research Center
[ASME PAPER 86-HT-15] p 48 A86-49621

- Liquid droplet radiator program at the NASA Lewis Research Center
[NASA-TM-87139] p 48 N86-12246
- DILLEHAY, M. E.**
The milling of pristine and brominated P-100 graphite fibers
[NASA-TM-88828] p 106 N86-32573
- DIRUSSO, E.**
Dynamic response of film thickness in spiral-groove face seals
[NASA-TP-2544] p 27 N86-15313
Variable friction secondary seal for face seals
[NASA-CASE-LEW-14170-1] p 160 N86-25790
- DISIMILE, P. J.**
Entrainment region phenomena for a large plane shear layer
p 132 N86-30211
- DITTMAR, J. H.**
An experimental investigation of reducing advanced turboprop cabin noise by wing shielding
[AIAA PAPER 86-1966] p 16 N86-45449
Preliminary measurement of the noise from the 2/9 scale model of the Large-scale Advanced Propfan (LAP) propeller, SR-7A
[NASA-TM-87116] p 199 N86-14006
Some design philosophy for reducing the community noise of advanced counter-rotation propellers
[NASA-TM-87099] p 199 N86-14007
Laboratory experiments on active suppression of advanced turboprop noise
[NASA-TM-87129] p 199 N86-19125
An estimate of the enroute noise of an advanced turboprop airplane NASA-TM-87302 E-3020 NAS 1.15:87302 HC A02/MF A01
[NASA-TM-87302] p 201 N86-25217
An experimental investigation of reducing advanced turboprop cabin noise by wing shielding
[NASA-TM-87112] p 201 N86-25218
- DODDS, R. H., JR.**
Theoretical and software considerations for general dynamic analysis using multilevel substructured models
[NASA-CR-176822] p 195 N86-26067
- DODDS, W. J.**
Evaluation of fuel preparation systems for lean premixing-prevaporizing combustors
[ASME PAPER 85-GT-137] p 19 N86-22081
- DODGE, L. G.**
Effect of elevated temperature and pressure on sprays from simplex swirl atomizers
[ASME PAPER 85-GT-58] p 130 N86-22735
- DOERR, H. J.**
Pretreatment effects on the morphology and properties of aluminum oxide thermally grown on NiCoCrAlY
p 87 N86-17495
- DOMITZ, S.**
Optical and interfacial electronic properties of diamond-like carbon films
p 204 N86-16268
- DONOVAN, R. M.**
Space Station benefits from ECLS - Propulsion system synergism
[AIAA PAPER 86-1407] p 47 N86-42619
- DORN, H. C.**
Development of LC-13C NMR
[NASA-TM-176656] p 107 N86-21704
- DORSINVILLE, R.**
Infrared-photoinduced-absorption studies in soluble trans-polyacetylene
p 204 N86-37075
- DOSANJH, S.**
Buoyancy effects on smoldering combustion
[IAF PAPER 85-289] p 72 N86-15805
- DOUGHERTY, D.**
Inelastic high-temperature thermomechanical response of ceramic coated gas turbine seals
p 169 N86-37799
- DOWELL, E. H.**
Frequency domain solutions to multi-degree-of-freedom, dry friction damped systems under periodic excitation
p 170 N86-39485
- DOWLING, N. E.**
Closure of fatigue cracks at high strains
[NASA-CR-175021] p 175 N86-17788
J-integral estimates for cracks in infinite bodies
[NASA-CR-179474] p 178 N86-28467
- DOYCHAK, J. K.**
The evolution and growth of Al₂O₃ scales on beta-NiAl
[NASA-CR-175097] p 92 N86-27444
- DRESHFIELD, R. L.**
The continuing battle against defects in nickel-base superalloys
[NASA-TM-87343] p 93 N86-31701
- DRIGGERS, T.**
Communication Platform Payload Definition (CPPD) study. Volume 2: Technical report
[NASA-CR-174929] p 49 N86-27404
Communication Platform Payload Definition (CPPD) study. Volume 3: Addendum
[NASA-CR-174930] p 49 N86-27405
- DRING, R. P.**
Through-flow modeling of axial turbomachinery
[ASME PAPER 85-IGT-42] p 3 N86-23854
- DROSKE, J. P.**
All-aromatic biphenylene end-capped polyquinoline and polyimide matrix resins
p 100 N86-11267
- DUCHARME, E. H.**
Analytical and experimental investigation of the coupled bladed disk/shaft whirl of a cantilevered turbofan
[ASME PAPER 86-GT-98] p 24 N86-48183
- DUKE, J. C., JR.**
Factors influencing the ultrasonic stress wave factor evaluation of composite material structures
p 168 N86-34257
Analytical ultrasonics for evaluation of composite materials response. Part 2: Generation and detection
p 200 N86-22973
Ultrasonic stress wave characterization of composite materials
[NASA-CR-3976] p 165 N86-27665
A study of the stress wave factor technique for nondestructive evaluation of composite materials
[NASA-CR-4002] p 165 N86-28445
- DUNN, M. G.**
Turbine-stage heat transfer - Comparison of short-duration measurements with state-of-the-art predictions
[AIAA PAPER 86-1465] p 134 N86-42656
Heat-flux measurements for the rotor of a full-stage turbine. I - Time-averaged results
[ASME PAPER 86-GT-77] p 24 N86-48145
Heat-flux measurements for the rotor of a full-stage turbine. II - Description of analysis technique and typical time-resolved measurements
[ASME PAPER 86-GT-78] p 24 N86-48146
- DUNNING, J. W., JR.**
Heat transfer in space power and propulsion systems
p 53 N86-26492
- DUTTA, S.**
Densification and properties of alpha-silicon carbide
p 94 N86-12416
- E**
- EBERHARDT, R. H.**
Cryogenic Fluid Management Facility
p 108 N86-37053
- EBERT, L. J.**
The influence of cobalt, tantalum, and tungsten on the microstructure of single crystal nickel-base superalloys
p 79 N86-12995
The influence of cobalt, tantalum, and tungsten on the elevated temperature mechanical properties of single crystal nickel-base superalloys
p 79 N86-12996
The development of gamma-gamma-prime lamellar structures in a nickel-base superalloy during elevated temperature mechanical testing
p 79 N86-14719
- EBIHARA, B. T.**
Secondary-electron-emission losses in multistage depressed collectors and traveling-wave-tube efficiency improvements with carbon collector electrode surfaces
[NASA-TP-2622] p 125 N86-32629
- ECER, A.**
Applications of variational principles in computing rotational flows
p 128 N86-20951
- ECK, T. G.**
Carbon monoxide production in low energy oxygen ion bombardment of pyrolytic graphite and Kapton surfaces
p 76 N86-47078
A study of Kapton degradation under simulated shuttle environment
[NASA-CR-176850] p 78 N86-28136
- ECKERLE, W. A.**
Horseshoe vortex formation around a cylinder
[ASME PAPER 86-GT-246] p 8 N86-48274
Measurements of a turbulent horseshoe vortex formed around a cylinder
[NASA-CR-3986] p 13 N86-28063
- EDELMAN, R. B.**
Effects of buoyancy on gas jet diffusion flames - Experiment and theory
[IAF PAPER 85-288] p 72 N86-15804
Buoyancy effects upon vapor flame and explosion processes
p 41 N86-10161
- EDGERTON, R. H.**
Liquid droplet radiator thermal characteristics
[AIAA PAPER 86-1162] p 133 N86-40578
- EDWARDS, D. E.**
Low Reynolds number separation bubble research at UTRC
p 126 N86-16311
- EDWARDS, R. V.**
Implementation of a new type of time-of-flight laser anemometer
p 146 N86-29755
- EHRESMAN, C. M.**
A stagnation pressure probe for droplet-laden air flow
p 133 N86-39077
- EKCHIAN, J. E.**
A computer simulation of the turbocharged turbo compounded diesel engine system: A description of the thermodynamic and heat transfer models
[NASA-CR-174971] p 208 N86-16164
- EKSTEDT, E. E.**
Evaluation of fuel preparation systems for lean premixing-prevaporizing combustors
[ASME PAPER 85-GT-137] p 19 N86-22081
- EL-BAYOUMY, L. E.**
An investigation of the transient thermal analysis of spur gears
[ASME PAPER 84-DET-92] p 155 N86-40683
- ELANGOVAR, R.**
An experimental method for measuring droplet impingement efficiency on two- and three-dimensional bodies
[AIAA PAPER 86-0406] p 131 N86-26630
- ELGHOBASHI, S. E.**
Effect of liquid droplets on turbulence in a round gaseous jet
[NASA-CR-175063] p 29 N86-23597
- ELMORE, D. L.**
Further development of the dynamic gas temperature measurement system
[AIAA PAPER 86-1648] p 147 N86-42770
Dynamic gas temperature measurement system
p 147 N86-11499
- ELROD, D.**
Theory versus experiment for the rotordynamic coefficients of annular gas seals. I - Test facility and apparatus
[ASME PAPER 85-TRIB-1] p 152 N86-24481
- ELROD, D. A.**
A comparison of experimental and theoretical results for leakage, pressure gradients, and rotordynamic coefficients for tapered annular gas seal
[NASA-CR-179709] p 162 N86-32742
- EMAMI-NAEINI, A.**
Robust detection, isolation, and accommodation for sensor failures
p 21 N86-35402
Robust detection, isolation and accommodation for sensor failures
[NASA-CR-174825] p 33 N86-30732
- ENGELMAN, M. S.**
Finite element simulation of temperature dependent free surface flows
p 136 N86-47012
- ENGELHART, M.**
A bibliography of electrothermal thruster technology, 1984
[NASA-TM-86996] p 60 N86-21578
- ENGLISH, R. E.**
Technology for Brayton-cycle powerplants using solar and nuclear energy
[NASA-TP-2558] p 60 N86-21577
- ENGLUND, D. R.**
HOST instrumentation R and D program overview
p 147 N86-11497
Research instrumentation for hot section components of turbine engines
[NASA-TM-88851] p 150 N86-32702
- ENGST, B.**
Circularly polarized microstrip antennas
p 112 N86-11407
- ENSIGN, C. R.**
Toward improved durability in advanced combustors and turbines - Progress in prediction of thermomechanical loads
[ASME PAPER 86-GT-172] p 24 N86-48224
Turbine engine Hot Section Technology (HOST) project
p 173 N86-11496
- ENSWORTH, C. B. F.**
Design and initial testing of a one-bladed 30-meter-diameter rotor on the NASA/DOE mod-O wind turbine
[NASA-TM-88810] p 189 N86-30251
- ENVIA, E.**
Noise generated by convected gusts interacting with swept airfoil cascades
[AIAA PAPER 86-1872] p 198 N86-45492
- EPSTEIN, A.**
Rotor wake characteristics of a transonic axial flow fan
[NASA-TM-87073] p 13 N86-28055
- ERCEGOVAC, M. D.**
Performance evaluation of a simulated data-flow computer with low-resolution actors
p 194 N86-32051
- ERCEGOVIC, B. A.**
Heat pipe radiator technology for space power systems
[AIAA PAPER 86-1300] p 47 N86-39907

- ERCEGOVIC, D. B.**
Combustion hot section technology p 25 N86-11512
- ERICKSON, C.**
Orbit Transfer Rocket Engine Technology Program:
Advanced engine study, task D.1/D.3
[NASA-CR-175084] p 61 N86-26389
- ERNST, W.**
Automotive Stirling Engine Development Program
[NASA-CR-174749] p 211 N86-28017
Automotive Stirling engine development program
[NASA-CR-175045] p 211 N86-30579
- ERWIN, J. R.**
A novel centrifugal diffuser test device
[ASME PAPER 85-IGT-135] p 3 A86-23927
- ESPANOLA, S.**
Research and development of neat alcohol fuel usage
in automobiles
[NASA-CR-174813] p 108 N86-27480
- ETERNO, J. S.**
Application of FDI metrics to detection and isolation of
sensor failures in turbine engines p 21 A86-35400
Robust detection-isolation-accommodation for sensor
failures
[NASA-CR-174797] p 121 N86-16486
- EUSEPI, M. W.**
Performance of oil pumping rings: An analytical and
experimental study
[NASA-CR-175083] p 144 N86-31000
- EVERSMAN, W.**
A numerical model of acoustic choking. II - Shocked
solutions p 197 A86-20795
Modeling wind tunnel effects on the radiation
characteristics of acoustic sources p 197 A86-41689
Modeling the effects of wind tunnel wall absorption on
the acoustic radiation characteristics of propellers
[NASA-TM-87333] p 201 N86-29630
- F**
- FADOUL, J. R.**
Improved stud configurations for attaching laminated
wood wind turbine blades
[NASA-TM-87109] p 172 N86-10582
- FAETH, G. M.**
Structure of nonevaporating sprays. II - Drop and
turbulence properties p 125 A86-11237
Drop-turbulence interactions in a diffusion flame
p 73 A86-20139
Spray atomization and combustion
[AIAA PAPER 86-0136] p 131 A86-26606
Flow and atomization in flashing injectors
p 136 A86-49442
- FANG, J. J.**
Longitudinal mode combustion instabilities of a
high-pressure fuel-rich LOX/RP-1 preburner
p 56 A86-49640
Longitudinal mode combustion instabilities of a
high-pressure fuel-rich LOX/RP-1 preburner
p 165 N86-28250
- FARR, E.**
Characterization of MMIC devices for active array
antennas p 111 N86-11401
- FARRELL, C. E.**
Satellite voice broadcast. Volume 1: Executive
summary
[NASA-CR-175018] p 115 N86-24875
Satellite voice broadcast. Volume 2: System study
[NASA-CR-175017] p 115 N86-24876
- FARRELL, R.**
Automotive Stirling Engine Development Program
[NASA-CR-174749] p 211 N86-28017
Automotive Stirling engine development program
[NASA-CR-175045] p 211 N86-30579
- FARSHCHI, M.**
Prediction of heat release effects on a mixing layer
[AIAA PAPER 86-0058] p 129 A86-22676
Prediction of heat release effects on a mixing layer
[NASA-CR-175044] p 142 N86-23857
- FAYMON, K. A.**
Space power systems - 'Spacecraft 2000'
p 53 A86-24836
Spacecraft 2000
[AIAA PAPER 86-0618] p 38 A86-29586
- FEINGOLD, E.**
Transformation toughened ceramics for the heavy duty
diesel engine technology program, phase 2
[NASA-CR-175054] p 210 N86-22451
- FERET, J. M.**
Gas cooled fuel cell systems technology development
[NASA-CR-175047] p 190 N86-31984
- FERGUSON, D. C.**
Development of the VOLT-A shuttle experiment
[NASA-TM-87169] p 212 N86-14110

- The voltage threshold for arcing for solar cells in LEO:
Flight and ground test results
[NASA-TM-87259] p 62 N86-28125
- FERNANDEZ-PELLO, A. C.**
Buoyancy effects on smoldering combustion
[IAF PAPER 85-289] p 72 A86-15805
A fundamental study of smoldering with emphasis on
experimental design for zero-g p 41 N86-10162
- FERRANTE, J.**
Surface modification strategies for (100)3C-SiC
p 76 A86-47083
Universality in the compressive behavior of solids
[NASA-TM-87303] p 206 N86-28775
Temperature effects on the universal equation of state
of solids
[NASA-TM-87321] p 206 N86-28776
- FERRELL, G. B.**
Multiphase flow visualization of lateral jet injection into
a swirling cross flow p 1 A86-14561
- FERRI, A. A.**
Frequency domain solutions to multi-degree-of-freedom,
dry friction damped systems under periodic excitation
p 170 A86-39485
On the equivalence of the incremental harmonic balance
method and the harmonic balance-Newton Raphson
method p 170 A86-40695
- FERTIS, D. G.**
NASA LaRC/Akron University Graduate Cooperative
Fellowship Program and Graduate Student Researchers
Program
[NASA-CR-174826] p 207 N86-13219
- FESTER, D. A.**
LH2 on-orbit storage tank support trunnion design and
verification p 53 A86-37054
- FEYOCK, S.**
A high-order language for a system of closely coupled
processing elements
[NASA-CR-177280] p 193 N86-27930
- FINKE, R. C.**
Piezoelectric deicing device
[NASA-CASE-LEW-13773-2] p 122 N86-20671
- FINN, R.**
Free surface phenomena under low- and zero-gravity
conditions p 39 N86-10108
- FINZEL, M.**
Measurements of energy distribution and wall
temperature in flowing hydrogen microwave plasma
systems
[AIAA PAPER 85-2052] p 203 A86-11001
Measurement of energy distribution in flowing hydrogen
microwave plasmas p 52 A86-18041
- FISCHER, R.**
High transconductance InGaAs/AlGaAs pseudomorphic
modulation-doped field-effect transistors
p 117 A86-18814
- FISCHMAN, G. S.**
Character of laser-glazed, plasma-sprayed zirconia
coatings on stainless steel substrata p 95 A86-15229
- FISHER, D. M.**
Variables controlling fatigue crack growth of short
cracks
[NASA-TM-87208] p 90 N86-21661
Influence of fatigue crack wake length and state of stress
on crack closure
[NASA-TM-87292] p 90 N86-22686
- FISHMAN, J.**
Evaluation of spacecraft technology programs (effects
on communication satellite business ventures), volume 1
[NASA-CR-174978] p 112 N86-16451
Evaluation of spacecraft technology programs (effects
on communication satellite business ventures), volume 2
[NASA-CR-174979] p 113 N86-16452
- FISZDON, J. P.**
Heat transfer to two-phase air/water mixtures flowing
in small tubes with inlet disequilibrium
[NASA-CR-175076] p 141 N86-22892
- FITZGERALD, K. F.**
Liquid belt radiator design study
[NASA-CR-174901] p 57 N86-16259
- FLACK, R. D.**
Laser velocimeter measurements in shrouded and
unshrouded radial flow pump impellers
[ASME PAPER 86-GT-129] p 136 A86-48187
Flow visualization of secondary flows in three curve
ducts
[ASME PAPER 86-GT-166] p 136 A86-48218
- FLECK, G. W.**
10 kW solar array switching unit performance test
results p 118 A86-24844
- FLEETER, S.**
Aerodynamic detuning analysis of an unstalled
supersonic turbofan cascade
[ASME PAPER 85-GT-192] p 3 A86-22732
Forced response analysis of an aerodynamically
detuned supersonic turbomachine rotor
p 21 A86-26902

- Aerodynamic and structural detuning of supersonic
turbomachine rotors p 21 A86-31595
- Passive control of aerodynamically forced vibrations of
supersonic turbomachine rotors by splitter blades
[AIAA PAPER 86-0844] p 22 A86-38892
Forced response analysis of an aerodynamically
detuned supersonic turbomachine rotor
[NASA-TM-87093] p 9 N86-10019
The predicted effect of aerodynamic detuning on
coupled bending-torsion unstalled supersonic flutter
[NASA-TM-87240] p 11 N86-21513
- FLEISCHMAN, R. M.**
The effects of syntactic complexity on the
human-computer interaction p 192 A86-36172
- FLEMING, D. P.**
Experimental stiffness of tapered bore seals
[ASME PAPER 85-DET-12] p 152 A86-22748
Quasi-modal vibration control by means of active control
bearings
[NASA-TM-87232] p 159 N86-21856
- FLEMING, R. J.**
The performance characteristics of simulated ice on
rotorcraft airfoils p 14 A86-35656
- FLOOD, D. J.**
Space solar cell research: Problems and potential
[NASA-TM-88833] p 125 N86-31793
Potential high efficiency solar cells: Applications from
space photovoltaic research
[NASA-TM-88832] p 125 N86-32627
- FLORENTINO, A. J.**
Atomization and combustion characteristics of
antimisting fuels using JT8D and air-boost injectors
[ASME PAPER 86-GT-223] p 24 A86-48257
- FLORSCHUETZ, L. W.**
Heat transfer characteristics within an array of impinging
jets. Effects of crossflow temperature relative to jet
temperature
[NASA-CR-3936] p 139 N86-15825
Heat transfer to two-phase air/water mixtures flowing
in small tubes with inlet disequilibrium
[NASA-CR-175076] p 141 N86-22892
- FORCE, D. A.**
Verification of an improved computational design
procedure for TWT-dynamic refocuser-MDC systems with
secondary electron emission losses p 119 A86-45194
Verification of computer-aided designs of traveling-wave
tubes utilizing novel dynamic refocusers and graphite
electrodes for the multistage depressed collector
[NASA-TP-2524] p 121 N86-13643
- FORD, C. W.**
High-efficiency AlGaAs-GaAs Cassegrainian
concentrator cells p 185 N86-17845
- FORD, W. F.**
Acceleration of convergence of vector sequences
p 195 A86-49850
- FORESTIERI, A. F.**
Space station power system p 50 A86-12676
Space Station Power System Advanced Development
p 52 A86-24778
- FORGIE, S. C.**
Advanced orbit transfer vehicle propulsion system
study
[NASA-CR-174843] p 60 N86-24746
- FORKOSH, M.**
10 kW solar array switching unit performance test
results p 118 A86-24844
- FORT, E. F.**
Methods for heat transfer and temperature field analysis
of the insulated diesel phase 2 progress report
[NASA-CR-175072] p 210 N86-24590
- FORTE, T. P.**
Nonlinear damage analysis: Postulate and evaluation
[NASA-CR-168171] p 177 N86-26652
- FOSS, J. F.**
Entrainment region phenomena for a large plane shear
layer p 132 A86-30211
- FRALICK, G. C.**
Reassessment of the theory of stimulated Raman
scattering p 150 A86-40662
A computer program to calculate the resistivity of a thin
film deposited on a conductive substrate from four-point
probe measurements
[NASA-TM-87262] p 193 N86-22150
- FRANK, R. M.**
A computer simulation of the turbocharged turbo
compounded diesel engine system: A description of the
thermodynamic and heat transfer models
[NASA-CR-174971] p 208 N86-16164
- FREDERICK, G. R.**
Summary of tower designs for large horizontal axis wind
turbines
[NASA-TM-87166] p 186 N86-18776
- FREED, A. D.**
The plastic compressibility of 7075-T651 aluminum-alloy
plate p 85 A86-49690

G

FREEDMAN, M. R.

- Factors influencing the ball milling of Si₃N₄ in water
p 95 A86-15239
- Parametric evaluation of ball milling of SiC in water
p 96 A86-15240
- Improved consolidation of silicon carbide
[NASA-TM-87243] p 104 N86-24836
- Particle size reduction of Si₃N₄ with Si₃N₄ milling hardware
[NASA-TM-86864-REV] p 104 N86-24839

FREEDMAN, R.

- In-flight measurements of wing ice shapes and wing section drag increases caused by natural icing conditions
[NASA-TM-87301] p 12 N86-24667

FREEMAN, W. G.

- Spontaneous ignition delay characteristics of hydrocarbon fuel-air mixtures
[NASA-CR-175064] p 29 N86-21545

FREEMAN, P. D.

- Lightweight two-stroke cycle aircraft diesel engine technology enablement program, volume 1
[NASA-CR-174923-VOL-1] p 26 N86-13328
- Lightweight two-stroke cycle aircraft diesel engine technology enablement program, volume 2
[NASA-CR-174923-VOL-2] p 26 N86-13329
- Lightweight two-stroke cycle aircraft diesel engine technology enablement program, volume 3
[NASA-CR-174923-VOL-3] p 26 N86-13330

FRENKLACH, M.

- Shock-tube pyrolysis of chlorinated hydrocarbons - Formation of soot
p 75 A86-35126

FREUND, G. A., JR.

- An experimental method for measuring droplet impingement efficiency on two- and three-dimensional bodies
[AIAA PAPER 86-0406] p 131 A86-26630

FRIEDBERG, R. A.

- Designing an electro-impulse de-icing system
[AIAA PAPER 86-0545] p 16 A86-19940
- Analyses and tests for design of an electro-impulse de-icing system
[NASA-CR-174919] p 15 N86-27268

FRITSCH, K.

- Wavelength-division multiplexed digital optical position transducer
p 145 A86-20798
- Range finding using frequency-modulated laser diode
p 147 A86-39521

FRITTS, S. D.

- Theoretical and experimental flow cell studies of a hydrogen-bromine fuel cell, part 1
[NASA-CR-177165] p 189 N86-29409

FRONEK, D. L.

- Heat transfer results and operational characteristics of the NASA Lewis Research Center hot section cascade test facility
[ASME PAPER 85-GT-82] p 128 A86-22053

FROTA, M. N.

- Analysis of the uncertainties in velocity measurements with triple hot-wire probes
p 130 A86-24468

FRYXELL, R. E.

- Effects of surface chemistry on hot corrosion life
[NASA-CR-179471] p 32 N86-28087

FUJIKAWA, G.

- Bit error rate testing of a proof-of-concept model baseband processor
[NASA-TM-87206] p 46 N86-18343

FULTON, G. B.

- Advanced turboprop vibratory characteristics
[NASA-CR-174708] p 30 N86-24693

FUNG, C. D.

- Calculation of recoil implantation profiles using known range statistics
p 201 A86-11391

FURST, R. B.

- Small centrifugal pumps for low-thrust rocket engines
[NASA-CR-174913] p 162 N86-32741

FURUHAMA, K.

- Film cooling on a convex wall: Heat transfer and hydrodynamic measurements for full and partial coverage
[NASA-CR-174964] p 137 N86-10461

FUSARO, R. L.

- Low-wear partially fluorinated polyimides
p 94 A86-11175
- Tribological properties of graphite-fiber-reinforced, partially fluorinated polyimide composites
p 98 A86-34177
- How to evaluate solid lubricant films using a pin-on-disk tribometer
[NASA-TM-87236] p 102 N86-19465
- Sputtered cadmium oxide as a surface pretreatment for graphite solid lubricant films
[NASA-TM-87300] p 104 N86-25473

GABE, T. P.

- The tensile and fatigue deformation structures in a single crystal Ni-base superalloy
p 83 A86-35697
- The cyclic stress-strain behavior of a nickel-base superalloy at 650 C
p 83 A86-45715
- Orientation and temperature dependence of some mechanical properties of the single-crystal nickel-base superalloy Rene N4. I - Tensile behavior
p 86 A86-50321

- Orientation and temperature dependence of some mechanical properties of the single-crystal nickel-base superalloy Rene N4. II - Low cycle fatigue behavior
p 86 A86-50322

- Orientation and temperature dependence of some mechanical properties of the single-crystal nickel-base superalloy Rene N4. III - Tension-compression anisotropy
p 86 A86-50323

- Fatigue crack propagation of nickel-base superalloys at 650 deg C
[NASA-TM-87150] p 87 N86-12294

- The low cycle fatigue behavior of a plasma-sprayed coating material
[NASA-TM-87318] p 92 N86-31699

GAELICK, C.

- Evaluation of spacecraft technology programs (effects on communication satellite business ventures), volume 1
[NASA-CR-174978] p 112 N86-16451

GAHN, R. F.

- Cycling performance of the iron-chromium redox energy storage system
p 180 A86-24849
- Negative electrode catalyst for the iron chromium redox energy storage system
[NASA-CASE-LEW-14028-1] p 186 N86-19721

- Method and apparatus for rebalancing a REDOX flow cell system
[NASA-CASE-LEW-14127-1] p 122 N86-20680

GAIER, J. R.

- Environmental stability of intercalated graphite fibers
p 98 A86-31825

- A comparison of the bromination dynamics of pitch-based and vapor-grown graphite fibers
[NASA-TM-87275] p 103 N86-21683

- The milling of pristine and brominated P-100 graphite fibers
[NASA-TM-88828] p 106 N86-32573

GALLAGHER, J. J.

- Technology for satellite power conversion
[NASA-CR-176554] p 186 N86-19742

- Technology for satellite power conversion
[NASA-CR-176777] p 187 N86-25042

GALLARDO, V. C.

- The dynamics of a flexible bladed disc on a flexible rotor in a two-rotor system
p 20 A86-25743

GAMMON, R. W.

- Light scattering tests of fundamental theories of transport properties in the critical region
p 39 N86-10113

GARLICK, R. G.

- Temperature dependence of gamma-gamma prime lattice mismatch in nickel-base superalloys
p 81 A86-21849

GAUDIOT, J. L.

- Performance evaluation of a simulated data-flow computer with low-resolution actors
p 194 A86-32051

GAUGLER, R. E.

- A review and analysis of boundary layer transition data for turbine application
[ASME PAPER 85-GT-83] p 129 A86-22054

GAWRYLOWICZ, H. T.

- Structural integrity and durability for Space Shuttle main engine and future reusable space propulsion systems
[AIAA PAPER 86-1513] p 55 A86-42682

- Structural integrity and durability for Space Shuttle main engine and future reusable space propulsion systems
[NASA-TM-87280] p 61 N86-25408

GAYDA, J.

- The tensile and fatigue deformation structures in a single crystal Ni-base superalloy
p 83 A86-35697
- Orientation and temperature dependence of some mechanical properties of the single-crystal nickel-base superalloy Rene N4. I - Tensile behavior
p 86 A86-50321

- Orientation and temperature dependence of some mechanical properties of the single-crystal nickel-base superalloy Rene N4. II - Low cycle fatigue behavior
p 86 A86-50322

- Orientation and temperature dependence of some mechanical properties of the single-crystal nickel-base superalloy Rene N4. III - Tension-compression anisotropy
p 86 A86-50323

- Creep-fatigue behavior of NiCoCrAlY coated PWA 1480 superalloy single crystals
[NASA-TM-87110] p 86 N86-10311

- Fatigue crack propagation of nickel-base superalloys at 650 deg C
[NASA-TM-87150] p 87 N86-12294

- The low cycle fatigue behavior of a plasma-sprayed coating material
[NASA-TM-87318] p 92 N86-31699

GAYDOS, D.

- Compressive creep behavior of alloys based on B2 FeAl
[NASA-TM-87293] p 92 N86-28165

GAYDOS, D. J.

- Rapidly solidified NiAl and FeAl
p 84 A86-47263

- Tensile behavior of Fe-40Al alloys with B and Zr additions
[NASA-TM-87290] p 91 N86-25453

GEDDES, J.

- Ka-band monolithic gain control amplifier
p 119 A86-41343

GEDYMIN, J. S.

- Dc and microwave characteristics of a high current double interface GaAs/InGaAs/AlGaAs pseudomorphic modulation-doped field-effect transistor
p 118 A86-36009

GEIL, T.

- Gas flow environmental and heat transfer nonrotating 3D program
p 137 N86-11506

GELDER, T. F.

- Wind tunnel turning vanes of modern design
[AIAA PAPER 86-0044] p 36 A86-19654

- Wind tunnel turning vanes of modern design
[NASA-TM-87146] p 37 N86-12239

GENERAZIO, E. R.

- Scaling attenuation data characterizes changes in material microstructure
p 197 A86-26542

- Quantitative flaw characterization with scanning laser acoustic microscopy
p 163 A86-45150

- Ultrasonic verification of microstructural changes due to heat treatment
p 200 N86-22977

- Quantitative flaw characterization with scanning laser acoustic microscopy
p 200 N86-22983

- Determination of grain size distribution function using two-dimensional Fourier transforms of tone pulse encoded images
[NASA-TM-88790] p 166 N86-31065

- Quantitative void characterization in structural ceramics using scanning laser acoustic microscopy
[NASA-TM-88797] p 166 N86-31913

GEORGE, W. K.

- Heat-flux measurements for the rotor of a full-stage turbine. II - Description of analysis technique and typical time-resolved measurements
[ASME PAPER 86-GT-78] p 24 A86-48146

GERTZ, J.

- Rotor wake characteristics of a transonic axial flow fan
[NASA-TM-87073] p 13 N86-28055

GHANDHI, S. K.

- The effect of processing conditions on the GaAs/plasma-grown insulator interface
p 204 A86-18567

GHERING, W. L.

- Development of optical diaphragm deflection sensors
[NASA-CR-175008] p 203 N86-15113

GHIA, K. N.

- Multi-grid technique for the solution of incompressible Navier-Stokes equations
p 128 A86-21029

GHIA, U.

- Multi-grid technique for the solution of incompressible Navier-Stokes equations
p 128 A86-21029

GHONIEM, A. F.

- Grid-free simulation of diffusion using random walk methods
p 196 A86-16521

- Numerical simulation of a turbulent flame stabilized behind a rearward-facing step
p 73 A86-22774

- Formation and inflammation of a turbulent jet
p 130 A86-23131

GHOSH, A. K.

- Performance of direct and iterative algorithms on an optical systolic processor
p 202 A86-17421

GHOSH, M. K.

- Starvation effects on the hydrodynamic lubrication of rigid nonconformal contacts in combined rolling and normal motion
[NASA-TM-87174] p 140 N86-19556

GIEN, P. H.

- A structural dynamics investigation related to EIDI applications
[AIAA PAPER 86-0550] p 16 A86-19942

GIFFIN, R. G.

- Extended parametric representation of compressor fans and turbines. Volume 1: CMGEN user's manual
[NASA-CR-174645] p 159 N86-23936

GILES, M. B.

- Propagation and stability of wavelike solutions of finite difference equations with variable coefficients
p 194 A86-20033

- GINTY, C. A.**
Progressive fracture of fiber composites p 67 A86-35809
Fracture characteristics of angleplied laminates fabricated from overaged graphite/epoxy prepreg [NASA-TM-87266] p 70 N86-25417
ICAN: A versatile code for predicting composite properties [NASA-TM-87334] p 71 N86-31664
- GIOVANNETTI, A. J.**
Deposit formation and heat-transfer characteristics of hydrocarbon rocket fuels p 106 A86-10028
Long term deposit formation in aviation turbine fuel at elevated temperature [AIAA PAPER 86-0525] p 107 A86-19929
Fuel deposit characteristics at low velocity [ASME PAPER 85-IGT-130] p 107 A86-23922
- GLADDEN, H. J.**
Heat transfer results and operational characteristics of the NASA Lewis Research Center hot section cascade test facility [ASME PAPER 85-GT-82] p 128 A86-22053
- GLASGOW, T. K.**
Undercooled and rapidly quenched Ni-Mo alloys [NASA-TM-87257] p 90 N86-21659
- GLASS, T. E.**
Development of LC-13C NMR [NASA-CR-176656] p 107 N86-21704
- GLASSMAN, A. J.**
Future directions in aeropropulsion technology p 1 A86-11602
- GLICKSMAN, M. E.**
Interaction of flows with the crystal-melt interface p 132 A86-29419
Influence of melt convection on solid-liquid interface under terrestrial and reduced gravity environments p 38 N86-10083
- GODDARD, D.**
Advanced rotary engine components utilizing fiber reinforced Mg castings [AIAA PAPER 86-1559] p 67 A86-42712
- GOODYKOONTZ, J.**
Velocity and temperature decay characteristics of inverted-profile jets [NASA-TM-87159] p 9 N86-14223
- GODETT, T. M.**
Liquid fueled external heating system for STM4-120 Stirling engine p 180 A86-24888
- GODLEWSKI, M. P.**
Voltage-controlling mechanisms in low-resistivity silicon solar cells - A unified approach p 120 A86-45195
A 25.5 percent AMO gallium arsenide grating solar cell [NASA-TM-87134] p 182 N86-11671
Gallium arsenide solar cell efficiency: Problems and potential p 184 N86-17843
- GOEKOGLU, S. A.**
Determination of convective diffusion heat/mass transfer rates to burner rig test targets comparable in size to cross-stream jet diameter [NASA-TM-87176] p 138 N86-13678
Experiments for the determination of convective diffusion heat/mass transfer to burner rig test targets comparable in size to jet stream diameter [NASA-TM-87196] p 139 N86-18646
Criteria for significance of simultaneous presence of both condensable vapors and aerosol particles on mass transfer (deposition) rates [NASA-TM-87247] p 109 N86-24869
- GOEL, P.**
Triple-velocity products in a channel with a backward-facing step p 133 A86-41725
Turbulence energy and diffusion transport in a separating and reattaching flow [AIAA PAPER 86-1724] p 135 A86-42812
Improvement of the second- and third-moment modeling of turbulence: A study of Reynolds-stress closure model [NASA-CR-176478] p 139 N86-16519
- GOKOGLU, S. A.**
Thermophoretically augmented mass transfer rates to solid walls across laminar boundary layers p 128 A86-20150
Determination of convective diffusion heat/mass transfer rates to burner rig test targets comparable in size to cross-stream jet diameter [ASME PAPER 86-GT-68] p 136 A86-48140
Experimental verification of corrosive vapor deposition rate theory in high velocity burner rigs [NASA-TM-87287] p 141 N86-22890
- GOLDMAN, L. J.**
Three component velocity measurements using Fabry-Perot interferometer p 145 A86-16378
Combined fringe and Fabry-Perot laser anemometer for three component velocity measurements in turbine stator cascade facility [NASA-TM-87322] p 149 N86-24967
- GOLDSTEIN, M. E.**
Scattering of acoustic waves into Tollmien-Schlichting waves by small streamwise variations in surface geometry p 127 A86-17041
Convective and absolute instability of a viscous liquid jet p 132 A86-34377
- GONSALVEZ, D. J.**
The role of service areas in the optimization of FSS orbital and frequency assignments [AIAA PAPER 86-0636] p 45 A86-29599
The role of service areas in the optimization of FSS orbital and frequency assignments [NASA-CR-176488] p 46 N86-18341
Engineering calculations for communications satellite systems planning [NASA-CR-176555] p 114 N86-19493
Broadcasting satellite service synthesis using gradient and cyclic coordinate search procedures [NASA-CR-176708] p 114 N86-23781
- GONZALEZ-SANABRIA, O. D.**
Design principles for nickel-hydrogen cells and batteries p 179 A86-24799
Nickel-hydrogen separator development [NASA-TM-87332] p 188 N86-26677
- GOODYKOONTZ, J.**
Velocity and temperature decay characteristics of inverted-profile jets [AIAA PAPER 86-0312] p 2 A86-22693
- GOODYKOONTZ, J. H.**
Plume characteristics of single-stream and dual-flow conventional and inverted-profile nozzles at equal thrust [AIAA PAPER 86-1809] p 8 A86-49585
Plume characteristics of single-stream and dual-flow conventional and inverted-profile nozzles at equal thrust [NASA-TM-87323] p 12 N86-26285
- GORADIA, C.**
A possible radiation-resistant solar cell geometry using superlattices p 185 N86-17851
Radiation damage in high-resistivity silicon solar cells p 185 N86-17856
- GORDON, L. H.**
Mod-2 wind turbine field operations experiment [NASA-TM-87233] p 186 N86-18775
- GORLA, R. S. R.**
Effect of free stream turbulence on flow separation p 125 A86-11676
- GORLAND, S. H.**
Radiation exposure and performance of multiple burn LEO-GEO orbit transfer trajectories p 43 N86-17417
- GOUKER, M. A.**
Technology for satellite power conversion [NASA-CR-176554] p 186 N86-19742
Technology for satellite power conversion [NASA-CR-176777] p 187 N86-25042
- GOULDIN, F. C.**
Periodic oscillations observed in swirling flows with and without combustion p 73 A86-22755
- GOUSY, R. G.**
Forced mixer lobes in ejector designs [AIAA PAPER 86-1614] p 134 A86-42752
- GOVINDAN, T. R.**
Computation of viscous flows in turbomachinery cascades with a space-marching method p 5 A86-39089
- GRADY, J. E.**
Dynamic delamination crack propagation in a graphite/epoxy laminate p 68 A86-43010
- GRAHAM, R. E.**
Linearization of digital derived rate algorithm for use in linear stability analysis p 47 A86-35338
- GRANT, H.**
High temperature static strain sensor development program p 148 N86-11500
- GRANT, H. P.**
Demonstration test of burner liner strain measurement systems: Interim results p 173 N86-11501
- GRATZ, R. F.**
Structure-to-glass transition temperature relationships in high temperature stable condensation polyimides [NASA-TM-87113] p 101 N86-12311
- GRAVES, J. A.**
Undercooling and solidification behavior in the InSb-Sb system [NASA-CR-175013] p 88 N86-14355
- GREENBURG, J. S.**
Evaluation of spacecraft technology programs (effects on communication satellite business ventures), volume 1 [NASA-CR-174978] p 112 N86-16451
Evaluation of spacecraft technology programs (effects on communication satellite business ventures), volume 2 [NASA-CR-174979] p 113 N86-16452
- GREISING, J.**
In-flight measurements of wing ice shapes and wing section drag increases caused by natural icing conditions [NASA-TM-87301] p 12 N86-24667
- GREITZER, E. M.**
A theory of post-stall transients in axial compression systems. I - Development of equations [ASME PAPER 85-GT-171] p 19 A86-22088
A theory of post-stall transients in axial compression systems. II - Application [ASME PAPER 85-GT-172] p 19 A86-22089
- GRIFFIN, J. H.**
Stability of limit cycles in frictionally damped and aerodynamically unstable rotor stages p 18 A86-19198
The effect of limiting aerodynamic and structural coupling in models of mistuned bladed disk vibration p 21 A86-26905
Influence of friction dampers on torsional blade flutter [ASME PAPER 85-GT-170] p 21 A86-32957
- GRILL, A.**
Protective coatings of metal surfaces by cold plasma treatment [NASA-TM-87152] p 157 N86-11475
Effect of argon and hydrogen on deposition of silicon from tetrachlorosilane in cold plasmas [NASA-TM-87219] p 65 N86-17472
- GRISAFFE, S. J.**
Microgravity Materials Science Laboratory p 42 N86-10173
- GRISNIK, S. P.**
Compatibility of grain-stabilized platinum with candidate propellants for resistojets [AIAA PAPER 85-2014] p 51 A86-17835
Compatibility of grain-stabilized platinum with candidate propellants for resistojets [NASA-TM-87118] p 56 N86-10279
Vacuum chamber pressure effects on thrust measurements p 59 N86-17425
Compatibility experiments of facilities, materials, and propellants for electrothermal thrusters p 59 N86-17426
- GROBSTEIN, T. L.**
Creep properties of PWC-11 base metal and weldments as affected by heat treatment [NASA-TM-88842] p 93 N86-32557
- GROESBECK, D. E.**
Progress in the Lewis Research Center Altitude Wind Tunnel (AWT) modeling program [AIAA PAPER 86-0757] p 36 A86-24744
Progress in the Lewis Research Center Altitude Wind Tunnel (AWT) Modeling Program [NASA-TM-87194] p 37 N86-16233
- GROSECLOSE, L. E.**
Methods for improving reliability in ceramic turbine rotors [SAE PAPER 851788] p 154 A86-38312
- GROSS, B.**
Wide-range displacement expressions for standard fracture mechanics specimens p 166 A86-20706
Analysis of an externally radially crack ring segment subject to three-point radial loading p 167 A86-20710
Mode II fatigue crack growth specimen development p 171 A86-43566
- GRUBER, R. P.**
Power electronics for a 1-kilowatt arcjet thruster [AIAA PAPER 86-1507] p 56 A86-49613
Power electronics for a 1-kilowatt arc jet thruster [NASA-TM-87340] p 61 N86-25409
- GULINO, D. A.**
Optical and interfacial electronic properties of diamond-like carbon films p 204 A86-16268
Ion beam sputter deposited zinc telluride films p 204 A86-47066
Ion beam sputter deposited zinc telluride films [NASA-TM-87119] p 205 N86-11048
Effect of an oxygen plasma on the physical and chemical properties of several fluids for the liquid droplet radiator [NASA-TM-88839] p 49 N86-31634
- GUPTA, H.**
Constructing multicomponent phase diagrams by overlapping ZPF lines p 83 A86-44038
- GUPTA, I. J.**
Adaptive antenna arrays for weak interfering signals p 45 A86-34591
- GURURANGAN, R.**
Research and development of neat alcohol fuel usage in automobiles [NASA-CR-174813] p 108 N86-27480
- GUSTAFSON, E.**
Heat pipe radiator technology for space power systems [AIAA PAPER 86-1300] p 47 A86-39907
- GYATT, G. W.**
Development and testing of tip devices for horizontal axis wind turbines [NASA-CR-174991] p 185 N86-18774

GYEKENYESI, J. P.

- SCARE: A post-processor program to MSC/NASTRAN for the reliability analysis of structural ceramic components
[NASA-TM-87188] p 174 N86-14688

H

HADY, W. F.

- Low-wear partially fluorinated polyimides
p 94 A86-11175

- Tribological properties of graphite-fiber-reinforced, partially fluorinated polyimide composites
p 98 A86-34177

- Stratified charge rotary engine for general aviation
[ASME PAPER 86-GT-181] p 24 A86-48231

HAGEDORN, N. H.

- Cycling performance of the iron-chromium redox energy storage system
p 180 A86-24849

- Negative electrode catalyst for the iron chromium redox energy storage system
[NASA-CASE-LEW-14028-1] p 186 N86-19721

HAISLER, W. E.

- Development of constitutive models for cyclic plasticity and creep behavior of super alloys at high temperature
[NASA-CR-178418] p 88 N86-14356

- Integrated research in constitutive modelling at elevated temperatures, part 2
[NASA-CR-177233] p 178 N86-28455

- Integrated research in constitutive modelling at elevated temperatures, part 1
[NASA-CR-177237] p 179 N86-30227

HALASE, J. F.

- Evaluation of capillary reinforced composites
[NASA-CR-175061] p 70 N86-24760

HALES, C.

- High-pressure creep tests
p 84 A86-46564

HALFORD, G. R.

- Life prediction and constitutive behavior
p 173 N86-11520

- An update of the total-strain version of SRP
[NASA-TP-2499] p 87 N86-12295

- Low-cycle thermal fatigue
[NASA-TM-87225] p 177 N86-26651

- Re-examination of cumulative fatigue damage analysis: An engineering perspective
[NASA-TM-87325] p 177 N86-27680

- Structural analysis of turbine blades using unified constitutive models
[NASA-TM-88807] p 178 N86-28461

HALL, A. M.

- Bipolar nickel-hydrogen battery development
p 180 A86-24823

HALLINAN, G. J.

- Electrical power system for the U.S. space station
[NASA-TM-88856] p 64 N86-32520

HALTHORE, R. N.

- Periodic oscillations observed in swirling flows with and without combustion
p 73 A86-22755

HAMAKER, H. C.

- High-efficiency AlGaAs-GaAs Cassegrainian concentrator cells
p 185 N86-17845

HAMBOURGER, P. D.

- Negative magnetoresistance of pitch-based carbon fibers: Temperature and pressure dependence
p 99 A86-35702

HAMED, A.

- Three dimensional flow phenomena in fluid machinery; Proceedings of the Winter Annual Meeting, Miami Beach, FL, November 17-22, 1985
p 4 A86-28682

- Three-dimensional flow field measurements in a radial inflow turbine scroll using LDV
[ASME PAPER 86-GT-122] p 7 A86-48181

HAMKINS, C. P.

- Laser velocimeter measurements in shrouded and unshrouded radial flow pump impellers
[ASME PAPER 86-GT-129] p 136 A86-48187

HAMM, J. R.

- Design and evaluation of fluidized bed heat recovery for diesel engine systems
[NASA-CR-174898] p 209 N86-21456

HAMM, R.

- Advanced seals for Liquid Oxygen (LOX) turbopumps
p 157 N86-17408

HAMROCK, B. J.

- Fast approach for calculating film thicknesses and pressures in elastohydrodynamically lubricated contacts at high loads
[ASME PAPER 85-TRIB-42] p 155 A86-43541

- Measurement of the density of base fluids at pressures 0.422 to 2.20 GPa
[NASA-TM-87114] p 156 N86-10551

- Theoretical and experimental comparison of vapor cavitation in dynamically loaded journal bearings
[NASA-TM-87121] p 137 N86-11425

- Starvation effects on the hydrodynamic lubrication of rigid nonconformal contacts in combined rolling and normal motion
[NASA-TM-87174] p 140 N86-19556

- Piezoviscous effects in nonconformal contacts lubricated hydrodynamically
[NASA-TM-87141] p 141 N86-21797

HANDSCHUH, R. F.

- Phenomenological study of the behavior of some silica formers in a high velocity jet fuel burner
[NASA-TM-87127] p 157 N86-14613

- Thermal stress minimized, two component, turbine shroud seal
[NASA-CASE-LEW-14212-1] p 182 N86-32740

HANKEY, W. L.

- Numerical simulation of unsteady flow in an axisymmetric shear layer
[AIAA PAPER 86-0202] p 127 A86-19746

HANNUN, N. P.

- Evaluation of a hybrid hydrostatic bearing for cryogenic turbopump application
[NASA-TM-87255] p 63 N86-31649

HANSEN, I. G.

- Space station 20-kHz power management and distribution system
[NASA-TM-87314] p 80 N86-24747

- A 20 kilohertz space station power system
[NASA-TM-88801] p 62 N86-28122

- Description of a 20 Kilohertz power distribution system
[NASA-TM-87346] p 34 N86-31584

HANSMAN, R. J., JR.

- Experimental measurements of heat transfer from an iced surface during artificial and natural cloud icing conditions
[AIAA PAPER 86-1352] p 36 A86-39948

HANSON, B.

- AC motor and generator requirements for isolated WECS
[NASA-CR-176315] p 182 N86-11670

HANSON, D. B.

- Propeller noise caused by blade tip radial forces
[AIAA PAPER 86-1892] p 23 A86-45504

HANSON, M. K.

- Documentation of ice shapes accreted on the main rotor of a UH-1H helicopter in level flight
[NASA-CR-175088] p 15 N86-22559

HANSON, M. P.

- Surface protection of graphite fabric/PMR-15 composites subjected to thermal oxidation
p 68 N86-11281

HANSON, R. K.

- Simultaneous measurements of velocity and pressure fields in subsonic and supersonic flows through image-intensified detection of laser-induced fluorescence
[AIAA PAPER 86-0161] p 145 A86-19726

HARDER, M. J.

- Advanced orbit transfer vehicle propulsion system study
[NASA-CR-174843] p 60 N86-24746

HARDY, T. L.

- Electrode erosion in arc discharges at atmospheric pressure
[AIAA PAPER 85-2018] p 50 A86-14445

- Hollow cathodes in high pressure arc discharges
[AIAA PAPER 85-2035] p 50 A86-14446

- A bibliography of electrothermal thruster technology, 1984
[NASA-TM-86998] p 60 N86-21578

HARF, F. H.

- The response of cobalt-free Udmet 700 type alloy to modified heat treatments
p 85 A86-48037

- Heat treatment for superalloy
[NASA-CASE-LEW-14262-1] p 92 N86-26414

HARLOFF, G. J.

- Characterization of real gas properties for space shuttle main engine fuel turbine and performance calculations
[NASA-CR-175066] p 61 N86-27418

HARRIS, D. H.

- The effects of metals and inhibitors on thermal oxidative degradation reactions of unbranched perfluoroalkyl ethers
p 99 A86-40682

HARRIS, M. M.

- Influence of temperature and hydroxyl concentration on incipient soot formation in premixed flames
p 74 A86-29070

HARSHA, P. T.

- Buoyancy effects upon vapor flame and explosion processes
p 41 N86-10161

HART, R. E.

- Voltage-controlling mechanisms in low-resistivity silicon solar cells - A unified approach
p 120 A86-45195

HART, R. E., JR.

- Performance and temperature dependencies of proton irradiated n/p GaAs and n/p silicon cells
[NASA-TM-87136] p 120 N86-12509

- Potential for use of indium phosphide solar cells in the space radiation environment
[NASA-TM-87157] p 121 N86-13845

- Demonstrated results of welded and soldered interconnections
p 185 N86-17866

HARTMANN, M. J.

- Fluid machines: Expanding the limits, past and future
[NASA-TM-87161] p 26 N86-12227

- Advanced instrumentation for aeronautical propulsion research
[NASA-TM-88853] p 150 N86-32703

HATHAWAY, M. D.

- Rotor wake characteristics of a transonic axial flow fan
[NASA-TM-87073] p 13 N86-28055

HAUGLAND, E. J.

- Compensation in epitaxial cubic SiC films
[NASA-TM-87269] p 206 N86-25267

HAWKES, T. A.

- Communications platform payload definition study
[NASA-CR-174986] p 49 N86-27402

- Communications platform payload definition study, executive summary
[NASA-CR-174985] p 49 N86-27407

HAWLEY, M. C.

- Measurements of energy distribution and wall temperature in flowing hydrogen microwave plasma systems
[AIAA PAPER 85-2052] p 203 A86-11001

- Measurement of energy distribution in flowing hydrogen microwave plasmas
p 52 A86-18041

HAYAKAWA, M.

- Free shear flows - Organized structures and effects of excitation
[AIAA PAPER 86-0235] p 131 A86-26614

HAYKIN, T.

- Transient engine performance with water ingestion
[AIAA PAPER 86-1621] p 23 A86-42755

HAZARIKA, B. K.

- Three-dimensional fluid flow phenomena in the blade end wall corner region
[ASME PAPER 86-GT-179] p 7 A86-48229

HEATH, B. R.

- Low-cost single-crystal turbine blades, volume 2
[NASA-CR-174852] p 29 N86-23598

HEBSUR, M. G.

- Creep-fatigue behavior of NiCoCrAlY coated PWA 1480 superalloy single crystals
[NASA-TM-87110] p 86 N86-10311

HECKEL, R. W.

- Modeling degradation and failure of Ni-Cr-Al overlay coatings
p 80 A86-16276

HECKERT, B.

- A 10,000 hour life multipropellant engine for Space Station applications
[AIAA PAPER 86-1403] p 54 A86-42616

HEIDELBERG, L. J.

- Preliminary results of unsteady blade surface pressure measurements for the SR-3 propeller
[AIAA PAPER 86-1893] p 8 A86-49625

- Preliminary results of unsteady blade surface pressure measurements for the SR-3 propeller
[NASA-TM-87352] p 12 N86-27213

HEINE, C.

- Generated spiral bevel gears - Optimal machine-tool settings and tooth contact analysis
[SAE PAPER 851573] p 154 A86-40678

- Generation of spiral bevel gears with zero kinematical errors and computer aided tooth contact analysis
[NASA-TM-87273] p 160 N86-25793

HELLAWELL, A.

- The development and prevention of channel segregation during alloy solidification
p 38 N86-10086

HEMANN, J. H.

- Effect of stress on ultrasonic pulses in fiber reinforced composites
p 200 N86-22975

HEMKER, K. J.

- Orientation and temperature dependence of some mechanical properties of the single-crystal nickel-base superalloy Rene N4. III - Tension-compression anisotropy
p 86 A86-50323

HEMMINGER, J. A.

- LOX/LH2 vane pump for auxiliary propulsion systems
p 58 N86-17397

- Advanced seals for Liquid Oxygen (LOX) turbopumps
p 157 N86-17408

- The noncavitating performance and life of a small vane-type positive displacement pump in liquid hydrogen
[NASA-TM-87347] p 63 N86-31651

HENDERSON, R. A.

- Theoretical analysis of the electrical aspects of the basic electro-impulse problem in aircraft de-icing applications
[NASA-CR-176808] p 17 N86-26330

HENDERSON, T.

Dc and microwave characteristics of a high current double interface GaAs/InGaAs/AlGaAs pseudomorphic modulation-doped field-effect transistor

p 118 A86-38009

High-frequency noise of In(y)Ga(1-y)As/Al(x)Ga(1-x)As MODFETs and comparison to GaAs/Al(x)Ga(1-x)As MODFETs

p 119 A86-43914

HENDERSON, T. S.

Determination of carrier saturation velocity in high-performance In(y)Ga(1-y)As/Al(x)Ga(1-x)As modulation-doped field-effect transistors (with y between 0 and 0.2)

p 118 A86-37295

HENDRICKS, B.

Inelastic high-temperature thermomechanical response of ceramic coated gas turbine seals

p 169 A86-37799

HENDRICKS, R. C.

Ribbon-burner simulation of T-700 turbine shroud for ceramic-lined seals research

p 18 A86-15225

Finite element analysis of residual stress in plasma-sprayed ceramic

p 95 A86-15226

Experimental study of ceramic-coated tip seals for turbojet engines

p 152 A86-15227

Fabrication of ceramic substrate-reinforced and free forms by mandrel plasma spraying metal-ceramic composites

p 64 A86-17483

Film and interstitial formation of metals in plasma-sprayed ceramics

p 96 A86-17484

An experimental investigation and some analytical considerations concerning the vaporous/gaseous cavity characteristics of an eccentric shaft seal or bearing

p 130 A86-24463

Heat transfer in space power and propulsion systems

p 53 A86-26492

Two-phase flows and heat transfer within systems with ambient pressure above the thermodynamic critical pressure

[NASA-TM-87228] p 140 A86-19558

Thermomechanical design criteria for ceramic-coated surfaces

[NASA-TM-87328] p 143 A86-25726

Two-phase flows within systems with ambient pressure

p 161 A86-30167

HENNEKE, E. G., II

Analytical ultrasonics for evaluation of composite materials response. Part 2: Generation and detection

p 200 A86-22973

Ultrasonic stress wave characterization of composite materials

[NASA-CR-3976] p 165 A86-27665

A study of the stress wave factor technique for nondestructive evaluation of composite materials

[NASA-CR-4002] p 165 A86-28445

HERBELL, T. P.

Factors influencing the ball milling of Si₃N₄ in water

p 95 A86-15239

Parametric evaluation of ball milling of SiC in water

p 96 A86-15240

Particle size reduction of Si₃N₄ with Si₃N₄ milling hardware

[NASA-TM-86864-REV] p 104 A86-24839

HERMAN, H.

Neutron and X-ray diffraction of plasma-sprayed zirconia-yttria thermal barrier coatings

p 96 A86-16269

HERRING, J.

Three dimensional flow phenomena in fluid machinery; Proceedings of the Winter Annual Meeting, Miami Beach, FL, November 17-22, 1985

p 4 A86-28682

HESS, K.

Superlattices and NIPi structures in new forms of cascade solar cells

[NASA-CR-176718] p 187 A86-24007

HESELINK, L.

Free surface phenomena under low- and zero-gravity conditions

p 39 A86-10108

HEYWOOD, J. B.

A computer simulation of the turbocharged turbo compounded diesel engine system: A description of the thermodynamic and heat transfer models

[NASA-CR-174971] p 208 A86-16164

HIBNER, D. H.

Lateral dampers for thrust bearings

[NASA-CR-174924] p 157 A86-11474

HICKS, Y. R.

Visualization of flows in a motored rotary combustion engine using holographic interferometry

[NASA-TM-88804] p 33 A86-31583

HILL, M.

Fluid management and its role in the future of Space Station

[AIAA PAPER 86-2301] p 47 A86-49553

HILLER, B.

Simultaneous measurements of velocity and pressure fields in subsonic and supersonic flows through image-intensified detection of laser-induced fluorescence

[AIAA PAPER 86-0161] p 145 A86-19726

HINCKEL, J. N.

Relaminarization of the boundary layer over a flat plate in shock tube experiments

[AIAA PAPER 86-1238] p 133 A86-39865

HINES, B.

Orbit Transfer Rocket Engine Technology Program: Advanced engine study, task D.1/D.3

[NASA-CR-175084] p 61 A86-26369

HINGST, W. R.

Development of seeding techniques for small supersonic wind tunnel

p 147 A86-11452

HIPPENSTEELE, S. A.

High-temperature thermocouple and heat flux gauge using a unique thin film-hardware hot junction

[ASME PAPER 85-GT-18] p 145 A86-13059

Local heat-transfer measurements on a large scale-model turbine blade airfoil using a composite of a heater element and liquid crystals

[ASME PAPER 85-GT-59] p 126 A86-13061

HOBERECHT, M. A.

Design of a regenerative fuel cell system for Space Station

p 53 A86-24857

HOCHSTEIN, J. I.

NASA Lewis Research Center low-gravity fluid management technology program

p 44 A86-32906

Effect of subcooling on the on-orbit pressurization rate of cryogenic propellant tankage

[AIAA PAPER 86-1253] p 54 A86-39877

NASA Lewis Research Center low-gravity fluid management technology program

[NASA-TM-87145] p 44 A86-11218

HOFFMAN, R. A.

Growth and characterization of epitaxial SrF₂ on InP(100)

p 205 A86-47076

HOFFMAN, R. W.

Carbon monoxide production in low energy oxygen ion bombardment of pyrolytic graphite and Kapton surfaces

p 76 A86-47078

A study of Kapton degradation under simulated shuttle environment

[NASA-CR-176850] p 78 A86-28136

HOLANDA, R.

High-temperature thermocouple and heat flux gauge using a unique thin film-hardware hot junction

[ASME PAPER 85-GT-18] p 145 A86-13059

HOLDEMAN, J. D.

Modeling dilution of jet flowfields

p 128 A86-20362

Perspectives on dilution jet mixing

[AIAA PAPER 86-1611] p 25 A86-49614

Perspectives on dilution jet mixing

[NASA-TM-87294] p 35 A86-32432

HOLKA, D.

Variables controlling fatigue crack growth of short cracks

[NASA-TM-87208] p 90 A86-21661

HOLLAND, C.

Thermionic noise measurements for on-line dispenser cathode diagnostics for linear beam microwave tubes

[NASA-CR-175105] p 124 A86-28323

HOLLAND, C. E.

Development program on a cold cathode electron gun

[NASA-CR-174792] p 121 A86-14499

HOLLAND, L. R.

Accommodation requirements for microgravity science and applications research on space station

[NASA-CR-175038] p 42 A86-18334

HOLMES, P.

Performance of oil pumping rings: An analytical and experimental study

[NASA-CR-175083] p 144 A86-31000

HOPKINS, C.

Evaluation of spacecraft technology programs (effects on communication satellite business ventures), volume 1

[NASA-CR-174978] p 112 A86-16451

Evaluation of spacecraft technology programs (effects on communication satellite business ventures), volume 2

[NASA-CR-174979] p 113 A86-16452

HOPKINS, D. A.

Thermoviscoplastic nonlinear constitutive relationships for structural analysis of high temperature metal matrix composites

[NASA-TM-87291] p 70 A86-24756

A unique set of micromechanics equations for high temperature metal matrix composites

[NASA-TM-87154] p 70 A86-24757

HORNKOHL, J. O.

Mean velocity and turbulence measurements in a 90 deg curved duct with thin inlet boundary layer

[NASA-CR-174811] p 139 A86-16518

HOROWITZ, S. J.

An iterative finite element-integral technique for predicting sound radiation from turbofan inlets in steady flight

p 198 A86-49806

HORSTEIN, M.

Satellite voice broadcast system study, volume 2

[NASA-CR-174905] p 115 A86-24877

Satellite voice broadcast system study. Volume 1: Executive summary

[NASA-CR-174904] p 115 A86-24878

HORTON, C. C.

Carbon monoxide production in low energy oxygen ion bombardment of pyrolytic graphite and Kapton surfaces

p 76 A86-47078

HOUPERT, L. G.

Fast approach for calculating film thicknesses and pressures in elastohydrodynamically lubricated contacts at high loads

[ASME PAPER 85-TRIB-42] p 155 A86-43541

HOVENAC, E. C.

Calibration of droplet sizing and liquid water content instruments: Survey and analysis

[NASA-CR-175099] p 149 A86-26596

HOWARTH, R.

Automotive Stirling Engine Development Program

[NASA-CR-174749] p 211 A86-28017

Automotive Stirling engine development program

[NASA-CR-175045] p 211 A86-30579

HOWES, W. L.

Lens collimation and testing using a Twyman-Green interferometer with a self-pumped phase-conjugating mirror

p 146 A86-29280

Optical elements formed by compressed gases: Analysis and potential applications

[NASA-TP-2555] p 203 A86-22390

HOYNIK, D.

Aerodynamic detuning analysis of an unstalled supersonic turbofan cascade

[ASME PAPER 85-GT-192] p 3 A86-22732

Forced response analysis of an aerodynamically detuned supersonic turbomachine rotor

p 21 A86-26902

Aerodynamic and structural detuning of supersonic turbomachine rotors

p 21 A86-31595

Passive control of aerodynamically forced vibrations of supersonic turbomachine rotors by splitter blades

[AIAA PAPER 86-0844] p 22 A86-38892

Forced response analysis of an aerodynamically detuned supersonic turbomachine rotor

[NASA-TM-87093] p 9 A86-10019

The predicted effect of aerodynamic detuning on coupled bending-torsion unstalled supersonic flutter

[NASA-TM-87240] p 11 A86-21513

HSIHIEH, F. I.

The effect of processing conditions on the GaAs/plasma-grown insulator interface

p 204 A86-18567

HSIAO, C. C.

Numerical simulation of a turbulent flame stabilized behind a rearward-facing step

p 73 A86-22774

Aerodynamic properties of turbulent combustion fields

[NASA-CR-175005] p 28 A86-20393

HSU, J. P.

Shock-tube pyrolysis of chlorinated hydrocarbons - Formation of soot

p 75 A86-35126

HUBBELL, T. E., JR.

Ion-beam nitriding of steels

[NASA-CASE-LEW-14104-2] p 93 A86-32556

HUFF, R. G.

The effect of acoustic reflections on combustor noise measurements

p 197 A86-20364

HUGHES, W. F.

Turbulent two-phase flow in annular seals

[ASLE PREPRINT 86-AM-4G-3] p 156 A86-45391

HULL, D. R.

Measurement of ultrasonic velocity using phase-slope and cross-correlation methods

p 162 A86-13192

HULSE, C.

High temperature static strain sensor development program

p 148 A86-11500

HUMES, R. L.

In-flight photogrammetric measurement of wing ice accretions

[NASA-TM-87191] p 17 A86-31562

HUNG, C. C.

Strategy for reflector pattern calculation - Let the computer do the work

p 110 A86-39542

Strategy for reflector pattern calculation: Let the computer do the work

[NASA-TM-87137] p 112 A86-12485

HUNTER, A. B.

Characterization methodology for PMR-15

p 65 A86-11272

HUNTER, E. M.

- Communication Platform Payload Definition (CPPD) study. Volume 1: Executive summary [NASA-CR-174928] p 49 N86-27403
- Communication Platform Payload Definition (CPPD) study. Volume 2: Technical report [NASA-CR-174929] p 49 N86-27404
- Communication Platform Payload Definition (CPPD) study. Volume 3: Addendum [NASA-CR-174930] p 49 N86-27405

HUNTRESS, A. R.

- Organosiloxane working fluids for the liquid droplet radiator [NASA-CR-175033] p 102 N86-16381

HURWITZ, F. I.

- A ceramic matrix composite based on polymerization and pyrolysis of ethynylated aromatics p 65 A86-13169
- Carbon-rich ceramic composites from ethynyl aromatic precursors [NASA-TM-88812] p 71 N86-28908

HUSAIN, H. S.

- Free shear flows - Organized structures and effects of excitation [AIAA PAPER 86-0235] p 131 A86-26614

HUSSAIN, A. K. F.

- Free shear flows - Organized structures and effects of excitation [AIAA PAPER 86-0235] p 131 A86-26614

HUSSAIN, A. K. M. F.

- Coherent structures in a turbulent mixing layer - A comparison between direct numerical simulations and experiments p 132 A86-30218

HUSTON, R. L.

- Dynamic loading on parallel shaft gears [NASA-CR-178473] p 161 N86-28433

HUTH, B. P.

- System design and integration of the large-scale advanced prop-fan [NASA-CR-174789] p 13 N86-31536

HWANG, B. C.

- A comparison of three algebraic stress closures for combustor flow calculations [ASME PAPER 85-WA/FE-3] p 132 A86-38388
- Local equilibrium assumption for round jet calculations p 136 A86-49829

HWANG, C.-C.

- Three dimensional unsteady aerodynamics and aeroelastic response of advanced turboprops [AIAA PAPER 86-0846] p 22 A86-38894

HWANG, D. P.

- A numerical analysis applied to high angle of attack three-dimensional inlets [AIAA PAPER 86-1527] p 6 A86-42760
- A numerical analysis applied to high angle of attack three-dimensional inlets [NASA-TM-87298] p 11 N86-24658

HWANG, S. Y.

- Cyclic creep analysis from elastic finite-element solutions [NASA-TM-87213] p 176 N86-25822

HYLTON, L. D.

- Gas side heat transfer p 138 N86-11507
- Turbine vane external heat transfer. Volume 1: Analytical and experimental evaluation of surface heat transfer distributions with leading edge showerhead film cooling [NASA-CR-174827] p 29 N86-21546

IDE, R. F.

- The measurement of aircraft performance and stability and control after flight through natural icing conditions [AIAA PAPER 86-9758] p 35 A86-40681
- The measurement of aircraft performance and stability and control after flight through natural icing conditions [NASA-TM-87265] p 35 N86-22582

IKAI, S.

- Effects of preferential diffusion on the burning intensity of curved flames p 73 A86-22813

INGEBO, R. D.

- Formation and characterization of simulated small droplet icing clouds [AIAA PAPER 86-0409] p 145 A86-22700
- Characterization of simulated small-droplet fuel sprays [AIAA PAPER 86-1725] p 135 A86-42813
- Formation and characterization of simulated small droplet icing clouds [NASA-TM-87180] p 148 N86-14554
- Characterization of simulated small-droplet fuel sprays [NASA-TM-87286] p 148 N86-24961

INSPEKTOR, A.

- Radical molecule and ion-molecule mechanisms in the polymerization of hydrocarbons and chlorosilanes in R.F. plasmas at low pressures (below 1.0 Torr) p 203 A86-16254

IRVINE, T. B.

- Progressive fracture of fiber composites p 67 A86-35809
- Hybrid deployable/erectable solar dynamic box truss system [AIAA PAPER 86-0955] p 47 A86-38883

IRWIN, A. S.

- Review and critical analysis: Rolling-element bearings for system life and reliability [NASA-CR-174710] p 159 N86-24991

ISHIGAKI, H.

- Surface effects of corrosive media on hardness, friction, and wear of materials p 94 A86-10825

IYER, N. S.

- Closure of fatigue cracks at high strains [NASA-CR-175021] p 175 N86-17788

J

JACKSON, J.

- Space and frequency-multiplexed optical linear algebra processor - Fabrication and initial tests p 202 A86-48352

JACKSON, T. W.

- Accuracy and directional sensitivity of the single-wire technique p 146 A86-28541

JACOBSON, B. A.

- Theoretical and experimental comparison of vapor cavitation in dynamically loaded journal bearings [NASA-TM-87121] p 137 N86-11425

JACOBSON, B. O.

- Measurement of the density of base fluids at pressures 0.422 to 2.20 GPa [NASA-TM-87114] p 156 N86-10551
- A model for the influence of pressure on the bulk modulus and the influence of temperature on the solidification pressure for liquid lubricants [NASA-TM-87230] p 140 N86-19555

JACOBSON, N. S.

- Kinetics and mechanism of corrosion of SiC by molten salts p 97 A86-20992
- Burner rig corrosion of SiC at 1000 C p 99 A86-36328

- The reactions of cobalt, iron and nickel in SO₂ atmospheres. Similarities and differences p 75 A86-40677

JACOBSON, N. S.

- Molten salt corrosion of SiC: Pitting mechanism [NASA-TM-87143] p 101 N86-12310
- Application of an atmospheric pressure sampling mass spectrometer to chlorination reactions [NASA-TM-87270] p 91 N86-24813

JACOBSON, T. P.

- Tribology of selected ceramics at temperatures to 900 deg C [NASA-TM-87267] p 105 N86-25476

JACOMIN, D.

- A note on the finite differencing of the linearized primitive equations' lower boundary condition p 191 A86-28963

JAMESON, A.

- An LU implicit scheme for high speed inlet analysis [AIAA PAPER 86-1520] p 6 A86-42687
- An LU implicit scheme for high speed inlet analysis [NASA-CR-175098] p 11 N86-23563

JANARDAN, B. A.

- Free jet feasibility study of a thermal acoustic shield concept for AST/VCE application-dual flow. Comprehensive data report. Volume 1: Test nozzles and acoustic data [NASA-CR-174817] p 200 N86-23371

- Free-jet feasibility study of a thermal acoustic shield concept for AST/VCE application-dual stream nozzles. Comprehensive data report. Volume 2: Laser velocimeter and suppressor. Base pressure data [NASA-CR-174818] p 201 N86-23372

JANKOWSKI, D. F.

- Energy stability of thermocapillary convection in models of the float zone process p 40 N86-10123

JANSSEN, J. M.

- Heat transfer to two-phase air/water mixtures flowing in small tubes with inlet disequilibrium [NASA-CR-175076] p 141 N86-22892

JAWORSKE, D. A.

- Graphite fiber intercalation: Basic properties of copper chloride intercalated fibers [NASA-TM-87217] p 65 N86-18442

JAWORSKIE, D. A.

- Environmental stability of intercalated graphite fibers p 98 A86-31825

JEFFERS, L. A.

- Development of optical diaphragm deflection sensors [NASA-CR-175008] p 203 N86-15113

JENG, Y. R.

- Lubrication of nonconformal contacts [NASA-TM-87120] p 138 N86-13679
- Piezoviscous effects in nonconformal contacts lubricated hydrodynamically [NASA-TM-87141] p 141 N86-21797

JENSEN, K. A.

- Textured carbon on copper: A novel surface with extremely low secondary electron emission characteristics [NASA-TP-2543] p 101 N86-15394
- Textured carbon surfaces on copper by sputtering [NASA-CASE-LEW-14130-1] p 109 N86-32587

JI, H.-C.

- Effect of subcooling on the on-orbit pressurization rate of cryogenic propellant tankage [AIAA PAPER 86-1253] p 54 A86-39877

JIRBERG, R. J.

- On the effectiveness of onboard processing [AIAA PAPER 86-0721] p 45 A86-29659

JOHNS, R. H.

- Computational engine structural analysis [ASME PAPER 86-GT-70] p 23 A86-48141
- HOST structural analysis program overview p 25 N86-11513

- Computational engine structural analysis [NASA-TM-87231] p 175 N86-19663

JOHNSON, B. V.

- Scalar and momentum turbulent transport experiments with swirling and nonswirling flows p 128 A86-11938
- Mass and momentum turbulent transport experiments with swirling confined coaxial jets. II [AIAA PAPER 86-1665] p 134 A86-42780

JOHNSON, C. A.

- Ceramic automotive Stirling engine study [NASA-CR-174907] p 208 N86-16165

JOHNSON, G. M.

- Accelerated solution of the steady Euler equations p 2 A86-20942
- An embedding method for the steady Euler equations p 194 A86-30814

JOHNSON, J. A.

- Cycling performance of the iron-chromium redox energy storage system p 180 A86-24849

JOHNSTON, J. P.

- Film cooling on a convex wall: Heat transfer and hydrodynamic measurements for full and partial coverage [NASA-CR-174964] p 137 N86-10461

JOHNSTON, W. A.

- Coupling conditions for integrating boundary layer and rotational inviscid flow p 133 A86-41721

JONES, W. H.

- Increasing processor utilization during parallel computation shutdown [NASA-TM-87349] p 192 N86-26914

JONES, W. R., JR.

- Ellipsometric surface analysis of wear tracks produced by different lubricants [ASLE PREPRINT 85-TC-SA-2] p 151 A86-11016

- Optical and other properties changes of M-50 bearing steel surfaces for different lubricants and additives prior to scuffing p 97 A86-20435

- Contact angle and surface tension measurements of a five-ring polyphenyl ether p 98 A86-34179
- The effects of metals and inhibitors on thermal oxidative degradation reactions of unbranched perfluoroalkyl ethers p 99 A86-40682

- Ellipsometric surface analysis of wear tracks produced by different lubricants [NASA-TM-87142] p 87 N86-12293

- Analysis of a thioether lubricant by infrared Fourier microemission spectrophotometry [NASA-TM-87195] p 102 N86-16379

- Analysis of a spacecraft instrument ball bearing assembly lubricated by a perfluoroalkylether [NASA-TM-87260] p 50 N86-21575

- A preliminary study of ester oxidation on an aluminum surface using chemiluminescence [NASA-TM-87242] p 103 N86-24835

- Improved perfluoroalkylether fluid development [NASA-TM-87276] p 104 N86-25474

- The preparation of new perfluoroether fluids exhibiting excellent thermal-oxidative stabilities [NASA-TM-87284] p 105 N86-25475

JONGEWARD, G. A.

- Threshold determining mechanisms for discharges in high voltage solar arrays [AIAA PAPER 86-0364] p 52 A86-19834

- Energy broadening due to space-charge oscillations in high current electron beams p 202 A86-22890

- The role of unneutralized surface ions in negative potential arcing p 118 A86-25525

- JORASCH, R.**
Communication Platform Payload Definition (CPPD) study, Volume 2: Technical report
[NASA-CR-174929] p 49 N86-27404
Communication Platform Payload Definition (CPPD) study, Volume 3: Addendum
[NASA-CR-174930] p 49 N86-27405
- JORDAN, E. H.**
Fracture mechanics applied to nonisothermal fatigue crack growth p 81 N86-28951
Elevated temperature biaxial fatigue
[NASA-CR-175009] p 174 N86-11526
- JORDAN, J. L.**
The measurement of aircraft performance and stability and control after flight through natural icing conditions
[NASA-TM-87265] p 35 N86-22582
- JOSHI, M. C.**
Turbofan aft duct suppressor study program listing and user's guide
[NASA-CR-175067] p 30 N86-25357
- JOSHI, N. D.**
Flame propagation and extinction in particle clouds
[NASA-CR-177304] p 78 N86-27434
- JOSLYN, H. D.**
Through-flow modeling of axial turbomachinery
[ASME PAPER 85-IGT-42] p 3 A86-23854
- JOU, W.-H.**
Propeller design by optimization
[AIAA PAPER 86-0081] p 19 A86-19678
Direct numerical simulations of a reacting mixing layer with chemical heat release p 76 A86-41711
- JOVANOVIC, M. M.**
Nondestructive characterization of RBSOA of high-power bipolar transistors p 118 A86-35718
- JUHASZ, A.**
A preliminary study of the modified Ericsson for space power p 180 A86-24840
- JUHASZ, A. J.**
Reliability and mass analysis of dynamic power conversion systems with parallel of standby redundancy
[NASA-TM-87189] p 57 N86-16258
- JUHASZ, N.**
In-flight measurements of wing ice shapes and wing section drag increases caused by natural icing conditions
[NASA-TM-87301] p 12 N86-24667
- JUHLKE, T. J.**
The preparation of new perfluoroether fluids exhibiting excellent thermal-oxidative stabilities
[NASA-TM-87284] p 105 N86-25475
- JUSTICE, D. W.**
A simple circular-polarized antenna: Circular waveguide horn coated with lossy magnetic material
[NASA-CR-177092] p 116 N86-30039
- K**
- KAHLER, H.**
Small engine technology payoffs for future commuter aircraft
[AIAA PAPER 86-1544] p 23 A86-42703
- KAHEN, K. B.**
Optical constants of GaAs-AlGaAs superlattices and multiple quantum wells p 205 N86-23468
Theoretical study of the transverse dielectric constant of superlattices and their alloys
[NASA-CR-177198] p 206 N86-28759
- KALLURI, S.**
Time dependency of strainrange partitioning life relationships
[NASA-CR-174946] p 174 N86-13755
- KAMOTANI, Y.**
Oscillatory thermocapillary flows p 129 A86-22413
Surface-tension driven convection p 40 N86-10124
- KANIC, P.**
Oxidizer heat exchanger component testing
[NASA-CR-179487] p 62 N86-29901
- KAO, T.**
Communications platform payload definition study
[NASA-CR-174986] p 49 N86-27402
Communications platform payload definition study, executive summary
[NASA-CR-174985] p 49 N86-27407
- KAPLAN, M.**
Evaluation of spacecraft technology programs (effects on communication satellite business ventures), volume 1
[NASA-CR-174978] p 112 N86-16451
Evaluation of spacecraft technology programs (effects on communication satellite business ventures), volume 2
[NASA-CR-174979] p 113 N86-16452
- KAPOOR, V. J.**
Diamondlike carbon films on semiconductors for insulated-gate technology p 120 A86-47077
- KAPP, J. A.**
Wide-range displacement expressions for standard fracture mechanics specimens p 166 A86-20706
- KARAGOZIAN, A. R.**
An analytical model for the vorticity associated with a transverse jet p 4 A86-28538
Vortex modeling of single and multiple dilution jet mixing in a cross flow p 135 A86-46318
- KASCAK, T. J.**
MMIC antenna technology development in the 30/20 gigahertz band
[AIAA PAPER 86-0666] p 45 A86-29628
Monolithic optical integrated control circuitry for GaAs MMIC-based phased arrays p 113 N86-16457
[NASA-TM-87183] p 113 N86-16457
MMIC antenna technology development in the 30/20 gigahertz band
[NASA-TM-87192] p 46 N86-17368
- KASUBA, R.**
Torsional vibrations and dynamic loads in a basic planetary gear system p 156 A86-47354
- KATSANIS, T.**
Calculation of three-dimensional, viscous flow through turbomachinery blade passage by parabolic marching p 2 A86-20372
- KATZ, I.**
Threshold determining mechanisms for discharges in high voltage solar arrays
[AIAA PAPER 86-0364] p 52 A86-19834
Energy broadening due to space-charge oscillations in high current electron beams p 202 A86-22890
The role of unneutralized surface ions in negative potential arcing p 118 A86-25525
- KAUFMAN, A.**
Develop and test fuel cell powered on-site integrated total energy systems: Phase 3, full-scale power plant development
[NASA-CR-174948] p 182 N86-12757
Develop and test fuel cell powered on-site integrated total energy systems: Phase 3, full-scale power plant development
[NASA-CR-174998] p 182 N86-12758
Simplified cyclic structural analyses of SSME turbine blades
[NASA-TM-87214] p 175 N86-16615
Cyclic structural analyses of anisotropic turbine blades for reusable space propulsion systems p 58 N86-17404
Cyclic creep analysis from elastic finite-element solutions
[NASA-TM-87213] p 176 N86-25822
Develop and test fuel cell powered on-site integrated total energy systems
[NASA-CR-174951] p 188 N86-25877
Structural analysis of turbine blades using unified constitutive models
[NASA-TM-88807] p 178 N86-28461
- KAUFMAN, D. L.**
Development of a microprocessor controller for stand-alone photovoltaic power systems
[NASA-CR-174723] p 187 N86-21979
- KAUFMAN, H. R.**
Current collection from the space plasma through defects in solar array insulation p 52 A86-18042
- KAUFMAN, R. M.**
Turbine vane external heat transfer. Volume 1: Analytical and experimental evaluation of surface heat transfer distributions with leading edge showerhead film cooling
[NASA-CR-174827] p 29 N86-21546
- KAUTZ, H. E.**
Measurement of ultrasonic velocity using phase-slope and cross-correlation methods p 162 A86-13192
Ultrasonic evaluation of mechanical properties of thick, multilayered, filament wound composites
[NASA-TM-87088] p 163 N86-10561
Transfer function concept for ultrasonic characterization of material microstructures p 200 N86-22980
Acousto-ultrasonic verification of the strength of filament wound composite material
[NASA-TM-88827] p 166 N86-32764
- KAWA, H.**
The preparation of new perfluoroether fluids exhibiting excellent thermal-oxidative stabilities
[NASA-TM-87284] p 105 N86-25475
- KAYS, W. M.**
Film cooling on a convex wall: Heat transfer and hydrodynamic measurements for full and partial coverage
[NASA-CR-174964] p 137 N86-10461
- KAZA, K. R. V.**
Vibration analysis of rotating turbomachinery blades by an improved finite difference method p 18 A86-14338
The effects of strong shock loading on coupled bending-torsion flutter of tuned and mistuned cascades p 20 A86-26893
- Vibration and buckling of rotating, pretwisted, precone beams including Coriolis effects p 168 A86-26910
Nonlinear bending-torsional vibration and stability of rotating, pretwisted, precone blades including Coriolis effects
[NASA-TM-87207] p 175 N86-17789
Experimental classical flutter results of a composite advanced turboprop model
[NASA-TM-88792] p 178 N86-29271
Influence of third-degree geometric nonlinearities on the vibration and stability of pretwisted, precone, rotating blades
[NASA-TM-87307] p 179 N86-31920
- KEITH, T. G., JR.**
The effects of strong shock loading on coupled bending-torsion flutter of tuned and mistuned cascades p 20 A86-26893
Operating aspects of an oil pumping ring seal
[ASME PAPER 85-TRIB-29] p 153 A86-34010
- KEMP, F. S.**
Advanced on-site power plant development technology program
[NASA-CR-175007] p 189 N86-29411
- KEMPKER, E. E., JR.**
Development of the power system for the United States' Manned Space Station p 207 A86-24798
- KENDALL, B. R. F.**
Mass spectrometric studies of the electrical breakdown of thin polymer films p 100 A86-47070
- KENNEDY, J. B.**
High Weber number SMD correlations for pressure atomizers
[ASME PAPER 85-GT-37] p 128 A86-22026
Atomization and combustion characteristics of antimisting fuels using JT8D and air-boost injectors
[ASME PAPER 86-GT-223] p 24 A86-48257
- KERCZEWSKI, R.**
Radiofrequency testing of satellite segment of simulated 30/20 GHz satellite communications system
[NASA-TM-87163] p 114 N86-19494
- KERCZEWSKI, R. J.**
Testing of 30-GHz low noise receivers
[AIAA PAPER 86-0654] p 45 A86-29616
Testing of 30-GHz low noise receivers
[NASA-TM-87171] p 112 N86-13627
- KERLBAR, R.**
Methods for heat transfer and temperature field analysis of the insulated diesel phase 2 progress report
[NASA-CR-175072] p 210 N86-24590
- KERSCHEN, E. J.**
Noise generated by convected gusts interacting with swept airfoil cascades
[AIAA PAPER 86-0654] p 198 A86-45492
Influence of airfoil camber on convected gust interaction noise
[AIAA PAPER 86-1873] p 198 A86-45493
- KERSLAKE, W. R.**
Rail accelerators for space transportation: An experimental investigation
[NASA-TP-2571] p 62 N86-28123
- KETCHUM, W. J.**
Orbital transfer vehicle engine integration study p 58 N86-17416
Orbital transfer vehicle engine integration study
[NASA-CR-174842] p 59 N86-20493
- KETTERSON, A.**
Cryogenic operation of pseudomorphic AlGaAs/InGaAs single-quantum-well MODFETs p 117 A86-11998
High transconductance InGaAs/AlGaAs pseudomorphic modulation-doped field-effect transistors p 117 A86-18814
- KHAN, A. A.**
Optical and interfacial electronic properties of diamond-like carbon films p 204 A86-16268
- KIDD, W. S. F.**
Wilson study cycles: Research relative to ocean geodynamic cycles
[NASA-CR-176560] p 192 N86-21092
- KIELB, R. E.**
Vibrations of blades and bladed disk assemblies; Proceedings of the Tenth Biennial Conference on Mechanical Vibration and Noise, Cincinnati, OH, September 10-13, 1985 p 20 A86-26901
Dynamic characteristics of an assembly of prop-fan blades
[ASME PAPER 85-GT-134] p 21 A86-32956
Influence of friction dampers on torsional blade flutter
[ASME PAPER 85-GT-170] p 21 A86-32957
Mass balancing of hollow fan blades
[ASME PAPER 86-GT-195] p 171 A86-48245
Joint research effort on vibrations of twisted plates, phase 1: Final results
[NASA-RP-1150] p 172 N86-10579
Mass balancing of hollow fan blades
[NASA-TM-87197] p 174 N86-16611

KIERNAN, M. T.

A study of the stress wave factor technique for nondestructive evaluation of composite materials
[NASA-CR-4002] p 165 N86-28445

KIKUCHI, N.

A mesh re-zoning technique for finite element simulations of metal forming processes
p 153 A86-36298

KIM, C. N.

Vortex modeling of single and multiple dilution jet mixing in a cross flow
p 135 A86-46318

KIM, J. J.

An experimental method for measuring droplet impingement efficiency on two- and three-dimensional bodies
[AIAA PAPER 86-0406] p 131 A86-26630

Particle trajectory computation on a 3-dimensional engine inlet
[NASA-CR-175023] p 14 N86-20379

KIM, Y.-N.

Numerical analysis of some supersonic viscous flows related to inlet and nozzle systems
[AIAA PAPER 86-1597] p 134 A86-42738

KING, G. B.

Influence of temperature and hydroxyl concentration on incipient soot formation in premixed flames
p 74 A86-29070

KING, R. J.

Inverter design for high frequency power distribution
p 117 A86-24831

Rotary transformer design with fixed magnetizing and/or leakage inductances
p 119 A86-40462

KIRALY, L. J.

Structural dynamic measurement practices for turbomachinery at the NASA Lewis Research Center
[NASA-TM-88857] p 35 N86-32433

KIRBY, M. S.

Experimental measurements of heat transfer from an iced surface during artificial and natural cloud icing conditions
[AIAA PAPER 86-1352] p 36 A86-39948

KIRCHGESSNER, T. A.

Uniform engine testing program phase 7: NASA Lewis Research Center second entry
[NASA-TM-87272] p 31 N86-28085

KIRTLEY, K. R.

A comparison of computational methods for three-dimensional, turbulent turbomachinery flow fields
[AIAA PAPER 86-1599] p 6 A86-42740

KISER, J. D.

Factors influencing the ball milling of Si3N4 in water
p 95 A86-15239

Parametric evaluation of ball milling of SiC in water
p 96 A86-15240

Radiographic detectability limits for seeded voids in sintered silicon carbide and silicon nitride
p 162 A86-31745

Reliability of void detection in structural ceramics by use of scanning laser acoustic microscopy
p 163 A86-39027

Particle size reduction of Si3N4 with Si3N4 milling hardware
[NASA-TM-86864-REV] p 104 N86-24839

KLANN, G. A.

Experimental study of ceramic-coated tip seals for turbojet engines
p 152 A86-15227

KLANN, J. L.

Design tradeoffs for a Space Station solar-Brayton power system
p 53 A86-24790

KLEM, J.

Cryogenic operation of pseudomorphic AlGaAs/InGaAs single-quantum-well MODFETs
p 117 A86-11998

High transconductance InGaAs/AlGaAs pseudomorphic modulation-doped field-effect transistors
p 117 A86-18814

Dc and microwave characteristics of a high current double interface GaAs/InGaAs/AlGaAs pseudomorphic modulation-doped field-effect transistor
p 118 A86-36009

KLEWICKI, C. L.

Entrainment region phenomena for a large plane shear layer
p 132 A86-30211

KLIMA, S. J.

NDE of advanced ceramics
p 163 A86-35575

Nondestructive characterization of structural ceramics
p 99 A86-37141

Reliability of void detection in structural ceramics by use of scanning laser acoustic microscopy
p 163 A86-39027

Nondestructive techniques for characterizing mechanical properties of structural materials - An overview
[ASME PAPER 86-GT-75] p 163 A86-48143

NDE of structural ceramics
[ASME PAPER 86-GT-279] p 163 A86-48298

NDE of structural ceramics

[NASA-TM-87186] p 164 N86-18598

Nondestructive techniques for characterizing mechanical properties of structural materials: An overview
[NASA-TM-87203] p 164 N86-19636

Ultrasonic characterization of structural ceramics
p 199 N86-22970

Factors that affect reliability of nondestructive detection of flaws in structural ceramics
[NASA-TM-87348] p 166 N86-31912

KMIEC, T.

Oxidizer heat exchanger component testing
[NASA-CR-179487] p 62 N86-29901

Bipolar nickel-hydrogen battery development
p 180 A86-24823

KOLECKI, J. C.

Electrodynamic tether technology considerations
p 161 N86-27657

KOO, J. J.

Channel flow modeling of impingement cooling of a rotating turbine blade
[NASA-CR-177206] p 31 N86-27285

KOPP, W.

Cryogenic operation of pseudomorphic AlGaAs/InGaAs single-quantum-well MODFETs
p 117 A86-11998

Dc and microwave characteristics of a high current double interface GaAs/InGaAs/AlGaAs pseudomorphic modulation-doped field-effect transistor
p 118 A86-36009

Determination of carrier saturation velocity in high-performance In(y)Ga(1-y)As/Al(x)Ga(1-x)As modulation-doped field-effect transistors (with y between 0 and 0.2)
p 118 A86-37295

High-frequency noise of In(y)Ga(1-y)As/Al(x)Ga(1-x)As MODFETs and comparison to GaAs/Al(x)Ga(1-x)As MODFETs
p 119 A86-43914

KORKAN, K. D.

A numerical method for the design and analysis of counter-rotating propellers
[AIAA PAPER 84-1205] p 19 A86-20369

Performance degradation of helicopters due to icing - A review
p 16 A86-35668

Numerical evaluation of propeller noise including nonlinear effects
p 23 A86-41726

A numerical method of calculating propeller noise including acoustic nonlinear effects
p 199 N86-12011

Aerodynamic data banks for Clark-Y, NACA 4-digit and NACA 16-series airfoil families
[NASA-CR-176883] p 13 N86-30693

KOSCHMIEDER, E.

Surface tension induced instabilities in reduced gravity: The Benard problem
p 40 N86-10117

KOSMAHL, H. G.

Verification of an improved computational design procedure for TWT-dynamic refocuser-MDC systems with secondary electron emission losses
p 119 A86-45194

Verification of computer-aided designs of traveling-wave tubes utilizing novel dynamic refocusers and graphite electrodes for the multistage depressed collector
[NASA-TP-2524] p 121 N86-13643

Linearized traveling wave amplifier with hard limiter characteristics
[NASA-CASE-LEW-13981-2] p 122 N86-21742

KOYCHAK, J. K.

High temperature oxidation of beta-NiAl
p 85 A86-47266

KRAFT, R. E.

Turbofan aft duct suppressor study program listing and user's guide
[NASA-CR-175067] p 30 N86-25357

KRATZER, R.

Improved perfluoroalkylether fluid development
[NASA-TM-87276] p 104 N86-25474

KRATZER, R. H.

The effects of metals and inhibitors on thermal oxidative degradation reactions of unbranched perfluoroalkyl ethers
p 99 A86-40682

KRAUSS, O.

AC motor and generator requirements for isolated WECS
[NASA-CR-176315] p 182 N86-11670

KRIMCHANSKY, S.

Infrared-photoinduced-absorption studies in soluble trans-polyacetylene
p 204 A86-37075

KROSEL, S. M.

A lumped parameter mathematical model for simulation of subsonic wind tunnels
[NASA-TM-87324] p 196 N86-27036

KSIENSKI, A. A.

Adaptive antenna arrays for weak interfering signals
p 45 A86-34591

KUCHAR, A. P.

Subscale-model and full-scale engine mixed-flow exhaust system performance comparison
p 18 A86-14528

KUNATH, R. R.

Optical techniques to feed and control GaAs MMIC modules for phased array antenna applications
[AIAA PAPER 86-0687] p 110 A86-29638

Optical techniques to feed and control GaAs MMIC modules for phased array antenna applications
[NASA-TM-87218] p 113 N86-16458

Optically controlled phased array antenna concepts using GaAs monolithic microwave integrated circuits
[NASA-TM-87229] p 123 N86-21757

KUNATH, R. R., JR.

Near-field testing of the 30 GHz TRW proof-of-concept multibeam antenna
[NASA-TM-87357] p 124 N86-27578

KUNIK, W. G.

Real gas effects on the numerical simulation of a hypersonic inlet
p 6 A86-46324

Application of a computational model for vortex generators in subsonic internal flows
[AIAA PAPER 86-1458] p 8 A86-49612

Application of a computational model for vortex generators in subsonic internal flows
[NASA-TM-87327] p 143 N86-26545

KWASNY, R.

Effects of a high mean stress on the high cycle fatigue life of PWA 1480 and correlation of data by linear elastic fracture mechanics
[NASA-CR-175057] p 177 N86-27689

KWATRA, S. C.

Simulated performance of the NASA 30/20 GHz test transponder using multi-H phase coded modulation
[AIAA PAPER 86-0717] p 110 A86-29656

L
LACKNEY, J.

Hierarchical implicit dynamic least-square solution algorithm
p 167 A86-26689

Constrained hierarchical least square nonlinear equation solvers
p 171 A86-43774

LAGOW, R. J.

The preparation of new perfluoroether fluids exhibiting excellent thermal-oxidative stabilities
[NASA-TM-87284] p 105 N86-25475

LAGRAFF, J. E.

Unsteady heat transfer and direct comparison to steady-state measurements in a rotor-wake experiment
[NASA-TM-87220] p 142 N86-24934

LAI, C. L.

Oscillatory thermocapillary flows
p 129 A86-22413

LAI, C.-L.

Surface temperature distribution along a thin liquid layer due to thermocapillary convection
[IAF PAPER 85-282] p 126 A86-15800

LAKSHMINARAYANA, B.

End-wall and profile losses in a low-speed axial flow compressor rotor
[ASME PAPER 85-GT-174] p 20 A86-22090

Computation of turbulent rotating channel flow with an algebraic Reynolds stress model
[AIAA PAPER 86-0214] p 130 A86-22682

Laser Doppler velocimeter measurement in the tip region of a compressor rotor
p 5 A86-39064

Computation of viscous flows in turbomachinery cascades with a space-marching method
p 5 A86-39089

A comparison of computational methods for three-dimensional, turbulent turbomachinery flow fields
[AIAA PAPER 86-1599] p 6 A86-42740

A space-marching method for viscous incompressible internal flows
p 135 A86-43037

Computation of turbulent flows on rotating bodies and ducts
p 135 A86-46307

Three-dimensional boundary layer on a compressor rotor blade at peak pressure rise coefficient
[ASME PAPER 86-GT-186] p 7 A86-48236

LAM, P. T.

Strategy for reflector pattern calculation - Let the computer do the work
p 110 A86-39542

Strategy for reflector pattern calculation: Let the computer do the work
[NASA-TM-87137] p 112 N86-12485

Near-field spillover from a subreflector: Theory and experiment
[NASA-TM-88763] p 115 N86-25650

Near-field spillover from a subreflector: Theory and experiment
[NASA-TM-88818] p 116 N86-32598

- LAM, P. T. C.**
Secondary pattern computation of an arbitrarily shaped main reflector
[NASA-CR-87162] p 112 N86-14477
- LAMB, J.**
Optical and interfacial electronic properties of diamond-like carbon films p 204 A86-16268
- LAMOUREUX, J.**
High-pressure creep tests p 84 A86-46564
- LANG, J. H.**
Variable-reluctance motor drives for electric vehicle propulsion
[NASA-CR-176586] p 122 N86-20700
- LANGSTON, L. S.**
Horseshoe vortex formation around a cylinder
[ASME PAPER 86-GT-246] p 8 A86-48274
Measurements of a turbulent horseshoe vortex formed around a cylinder
[NASA-CR-3986] p 13 N86-28063
- LANKFORD, J.**
Sliding seal materials for adiabatic engines, phase 2
[NASA-CR-179475] p 105 N86-29042
- LARKIN, T. R.**
Rotorcraft propulsion for year 2000 plus
[AIAA PAPER 86-1543] p 23 A86-42702
- LARSEN, D. C.**
Long-term stability and properties of zirconia ceramics for heavy duty diesel engine components
[NASA-CR-174943] p 209 N86-17224
- LAUSSOW, E. S.**
Experimental study of ceramic-coated tip seals for turbojet engines p 152 A86-15227
- LAUER, J. L.**
Ellipsometric surface analysis of wear tracks produced by different lubricants
[ASLE PREPRINT 85-TC-5A-2] p 151 A86-11016
- LAUER, J. L.**
Optical and other properties changes of M-50 bearing steel surfaces for different lubricants and additives prior to scuffing p 97 A86-20435
Ellipsometric surface analysis of wear tracks produced by different lubricants
[NASA-TM-87142] p 87 N86-12293
Analysis of a thioether lubricant by infrared Fourier microemission spectrophotometry
[NASA-TM-87195] p 102 N86-16379
Emission FTIR analyses of thin microscopic patches of jet fuel residues deposited on heated metal surfaces
[NASA-CR-176786] p 108 N86-25502
Polarization modulated ellipsometry
[NASA-CR-177264] p 149 N86-26599
- LAURENDEAU, N. M.**
Influence of temperature and hydroxyl concentration on incipient soot formation in premixed flames p 74 A86-29070
- LAUVER, R. W.**
Effect of substituted phenylindimides on processing and properties of PMR polyimide composites p 94 A86-13179
Chemical control of rate and onset temperature of nadimide polymerization p 101 N86-11271
- LAW, C. K.**
Effects of preferential diffusion on the burning intensity of curved flames p 73 A86-22813
On the determination of laminar flame speeds from stretched flames p 74 A86-22814
An experimental investigation on flame interaction and the existence of negative flame speeds p 74 A86-22816
Theory of interactive combustion of counterflow premixed flames p 74 A86-32752
- LAWLESS, J. L.**
Fundamental studies on a heat driven lamp
[NASA-CR-176381] p 204 N86-15122
- LAWRENCE, C.**
The use of an optical data acquisition system for bladed disk vibration analysis p 146 A86-26909
Dynamic characteristics of an assembly of prop-fan blades
[ASME PAPER 85-GT-134] p 21 A86-32956
Nonlinear bending-torsional vibration and stability of rotating, pretwisted, precone blades including Coriolis effects
[NASA-TM-87207] p 175 N86-17789
Identification of differences between finite element analysis and experimental vibration data
[NASA-TM-87336] p 149 N86-27617
- LAWSON, I.**
Entrainment region phenomena for a large plane shear layer p 132 A86-30211
- LAXMANAN, V.**
Solidification fundamentals p 39 N86-10090
- LAYMANAN, V.**
Dendritic solidification in a binary alloy melt: Steady-state versus morphological stability theories p 42 N86-10261
- LEBURTON, J. P.**
Optical constants of GaAs-AlGaAs superlattices and multiple quantum wells
[NASA-CR-176717] p 205 N86-23468
Superlattices and NiPi structures in new forms of cascade solar cells
[NASA-CR-176718] p 187 N86-24007
- LEE, C. S.**
Normal modes in an overmoded circular waveguide coated with lossy material p 119 A86-44078
Numerical methods for analyzing electromagnetic scattering
[NASA-CR-176141] p 111 N86-10377
A simple circular-polarized antenna: Circular waveguide horn coated with lossy magnetic material
[NASA-CR-177092] p 116 N86-30039
- LEE, C.-M.**
Advanced rotary engine components utilizing fiber reinforced Mg castings
[AIAA PAPER 86-1559] p 67 A86-42712
Stress and deformation modeling of multiple rotary combustion engine trochoid housings
[SAE PAPER 860614] p 156 A86-48624
- LEE, D. Y.**
Visualization of flows in a motored rotary combustion engine using holographic interferometry
[NASA-TM-88804] p 33 N86-31583
- LEE, F. C.**
Resonant power processors. I - State plane analysis p 117 A86-14481
Resonant power processors. II - Methods of control p 117 A86-14482
Nondestructive characterization of RBSOA of high-power bipolar transistors p 118 A86-35718
State-plane analysis of parallel resonant converter p 119 A86-40431
- LEE, J. D.**
The aerodynamics of rotor blades with ice shapes accreted in hover and in level flight p 5 A86-35655
The performance characteristics of simulated ice on rotorcraft airfoils p 14 A86-35656
Wind tunnel tests of rotor blade sections with replications of ice formations accreted in hover
[NASA-CR-175089] p 15 N86-22558
Documentation of ice shapes accreted on the main rotor of a UH-1H helicopter in level flight
[NASA-CR-175088] p 15 N86-22559
- LEE, R. Q.**
A dual frequency microstrip antenna for Ka band
[NASA-TM-87124] p 111 N86-10380
A numerical method for approximating antenna surfaces defined by discrete surface points
[NASA-TM-87125] p 111 N86-10381
- LEE, R. Q. H.**
Circularly polarized microstrip antennas p 112 N86-11407
- LEE, S. S.**
Wave propagation in anisotropic medium due to an oscillatory point source with application to unidirectional composites
[NASA-CR-4001] p 165 N86-27666
- LEE, S. W.**
Numerical methods for analyzing electromagnetic scattering
[NASA-CR-176141] p 111 N86-10377
Strategy for reflector pattern calculation: Let the computer do the work p 112 N86-12485
Secondary pattern computation of an arbitrarily shaped main reflector
[NASA-TM-87162] p 112 N86-14477
Near-field spillover from a subreflector: Theory and experiment
[NASA-TM-88763] p 115 N86-25650
A simple circular-polarized antenna: Circular waveguide horn coated with lossy magnetic material
[NASA-CR-177092] p 116 N86-30039
Near-field spillover from a subreflector: Theory and experiment
[NASA-TM-88818] p 116 N86-32598
- LEE, S.-W.**
Strategy for reflector pattern calculation - Let the computer do the work p 110 A86-39542
Normal modes in an overmoded circular waveguide coated with lossy material p 119 A86-44078
- LEESE, G. E.**
Effects of surface chemistry on hot corrosion life
[NASA-TM-179471] p 32 N86-28087
- LEFEBVRE, A. H.**
Spontaneous ignition delay characteristics of hydrocarbon fuel-air mixtures
[NASA-CR-175064] p 29 N86-21545
- LEFFEL, K. L.**
A numerical and experimental investigation of electrochemical aircraft deicing
[NASA-CR-175024] p 14 N86-20380
- LEGER, G. S.**
Wide-range displacement expressions for standard fracture mechanics specimens p 166 A86-20706
- LEIB, S. J.**
Convective and absolute instability of a viscous liquid jet p 132 A86-34377
- LEIBECKI, H. F.**
Design considerations for advanced battery concepts
[AIAA PAPER 86-1164] p 181 A86-40579
A mathematical approach for evaluating nickel-hydrogen cells
[NASA-TM-88803] p 78 N86-31680
Design considerations for advanced battery concepts
[NASA-TM-87319] p 190 N86-31981
- LEIS, B. N.**
Nonlinear damage analysis: Postulate and evaluation
[NASA-CR-168171] p 177 N86-26652
- LEISSA, A. W.**
Joint research effort on vibrations of twisted plates, phase 1: Final results
[NASA-RP-1150] p 172 N86-10579
Extensions of the Ritz-Galerkin method for the forced, damped vibrations of structural elements p 176 N86-21909
- LEONARD, R. F.**
Radiofrequency testing of satellite segment of simulated 30/20 GHz satellite communications system
[NASA-TM-87163] p 114 N86-19494
- LEONARDO, M.**
A stagnation pressure probe for droplet-laden air flow p 133 A86-39077
- LEPICOVSKY, J.**
Tone excited jets. III - Flow measurements p 127 A86-16468
An experimental study of tone-excited heated jets p 197 A86-31593
Some unresolved questions on hot-jet mixing control through artificial excitation
[AIAA PAPER 86-1956] p 135 A86-45441
Acoustic control of free jet mixing p 135 A86-46314
- LEPISTO, J. W.**
10 kW solar array switching unit performance test results p 118 A86-24844
- LESIEUTRE, D. J.**
Unsteady forces on counter-rotating propeller blades
[AIAA PAPER 86-1804] p 22 A86-37827
- LEVINE, S. R.**
Deposition stress effects on the life of thermal barrier coatings on burner rigs p 96 A86-16271
- LEVIS, C. A.**
The role of service areas in the optimization of FSS orbital and frequency assignments
[AIAA PAPER 86-0636] p 45 A86-29599
Calculation of allowable orbital spacings for the fixed-satellite service
[NASA-CR-176273] p 43 N86-11212
The role of service areas in the optimization of FSS orbital and frequency assignments
[NASA-CR-176488] p 46 N86-18341
Engineering calculations for communications satellite systems planning
[NASA-CR-176555] p 114 N86-19493
Broadcasting satellite service synthesis using gradient and cyclic coordinate search procedures
[NASA-CR-176708] p 114 N86-23781
- LEVY, R.**
Numerical study of three-dimensional turbulent flow interactions between blockage models and wind tunnels including longitudinally slotted test sections
[AIAA PAPER 85-5017] p 1 A86-11065
- LEWICKI, D. G.**
Life and reliability modeling of bevel gear reductions
[ASME PAPER 85-DE-7] p 151 A86-14466
Fatigue life analysis of a turboprop reduction gearbox
[ASME PAPER 85-DET-10] p 155 A86-45256
- LEWIS, C. R.**
High-efficiency AlGaAs-GaAs Cassegrainian concentrator cells p 185 N86-17845
- LIEBERT, C. H.**
High-temperature thermocouple and heat flux gauge using a unique thin film hardware hot junction
[ASME PAPER 85-GT-18] p 145 A86-13059
- LILLEY, D. G.**
Multispark flow visualization of lateral jet injection into a swirling cross flow p 1 A86-14561
Hot-wire measurements of a single lateral jet injected into swirling crossflow
[AIAA PAPER 86-0055] p 127 A86-19661
Swirling flows in typical combustor geometries p 128 A86-20370
Accuracy and directional sensitivity of the single-wire technique p 146 A86-28541
Measurements of a single lateral jet injected into swirling crossflow
[NASA-CR-175040] p 28 N86-20392

- Experiments on opposed lateral jets injected into swirling crossflow
[NASA-CR-175041] p 29 N86-20394
- Lateral jet injection into typical combustor flowfields
[NASA-CR-3997] p 31 N86-28086
- LIM, H. S.**
KOH concentration effect on the cycle life of nickel-hydrogen cells p 180 A86-24802
Long life nickel electrodes for a nickel-hydrogen cell: Cycle life tests
[NASA-CR-174815] p 188 N86-25046
- LIN, H. H. (EDWARD)**
Dynamic loading on parallel shaft gears
[NASA-CR-179473] p 161 N86-28433
- LIN, S.-J.**
Numerical study of three-dimensional turbulent flow interactions between blockage models and wind tunnels including longitudinally slotted test sections
[AIAA PAPER 85-5017] p 1 A86-11065
- LINASK, I.**
Life prediction and constitutive models for engine hot section anisotropic materials program
[NASA-CR-174952] p 165 N86-25003
- LINDBERG, L. J.**
Comparison of the contact stress and friction behavior of SiC and ZrO₂ materials p 95 A86-15237
- LINDHOLM, U. S.**
Constitutive modeling for isotropic materials (HOST)
[NASA-CR-174980] p 172 N86-10589
- LIU, M.-S.**
An efficient method for solving the steady Euler equations
[AIAA PAPER 86-1079] p 132 A86-38442
- LIPO, T. A.**
Power conversion distribution system using a resonant high-frequency AC link
[NASA-CR-174804] p 123 N86-25694
- LIPPERT, T. E.**
Design and evaluation of fluidized bed heat recovery for diesel engine systems
[NASA-CR-174896] p 209 N86-21456
- LISSAMAN, P. B. S.**
Development and testing of tip devices for horizontal axis wind turbines
[NASA-CR-174991] p 185 N86-18774
- LITTLE, J. K.**
Ribbon-burner simulation of T-700 turbine shroud for ceramic-lined seals research p 18 A86-15225
- LITTLE, R. R.**
Application of a personal computer for the uncoupled vibration analysis of wind turbine blade and counterweight assemblies
[NASA-CR-175090] p 188 N86-28511
- LITVIN, F. L.**
Generation of spiral bevel gears with zero kinematical errors and computer aided simulation of their meshing and contact p 154 A86-40656
Generated spiral bevel gears - Optimal machine-tool settings and tooth contact analysis
[SAE PAPER 851573] p 154 A86-40678
Generation of spiral bevel gears with zero kinematical errors and computer aided tooth contact analysis
[NASA-TM-87273] p 160 N86-25793
- LIU, D. C.**
Optical and interfacial electronic properties of diamond-like carbon films p 204 A86-16288
Ellipsometric and optical study of some uncommon insulator films on 3-5 semiconductors
[NASA-TM-87135] p 205 N86-12134
Carbon films grown from plasma on III-V semiconductors
[NASA-TM-87140] p 205 N86-12135
- LIU, F.**
Fabrication of ceramic components for advanced gas turbine engines
[SAE PAPER 851786] p 154 A86-38310
- LIU, H. W.**
Shear fatigue crack growth - A literature survey p 167 A86-24219
Fatigue crack growth under general-yielding cyclic-loading p 171 A86-44339
Grain boundary oxidation and oxidation accelerated fatigue crack nucleation and propagation
[NASA-CR-175050] p 89 N86-20542
Fatigue crack growth under general-yielding cyclic-loading
[NASA-CR-175049] p 176 N86-21951
- LIU, J. T. C.**
Contributions to the understanding of large-scale coherent structures in developing free turbulent shear flows
[NASA-CR-176772] p 142 N86-24932
- LIU, W. K.**
Probabilistic finite elements for transient analysis in nonlinear continua p 168 A86-28653

- LO, Y. T.**
Input impedance of a probe-fed circular microstrip antenna with thick substrate p 120 A86-46638
Numerical methods for analyzing electromagnetic scattering
[NASA-CR-176141] p 111 N86-10377
Circularly polarized microstrip antennas p 112 N86-11407
- LOCK, J. A.**
The determination of the direction of the optic axis of uniaxial crystalline materials
[NASA-TM-86892] p 148 N86-22915
- LOEWENTHAL, S. H.**
Operating characteristics of a 0.87 kW-hr flywheel energy storage module p 152 A86-24864
Efficiency of nonstandard and high contact ratio involute spur gears
[ASME PAPER 84-DET-172] p 155 A86-45255
Spin analysis of concentrated traction contacts
[ASME PAPER 84-DET-99] p 155 A86-45257
Design of traction drives
[NASA-RP-1154] p 157 N86-13734
New methodology for shaft design based on life expectancy
[NASA-TM-87354] p 161 N86-27661
Feasibility study of a discrete bearing/roller drive rotary joint for the space station
[NASA-TM-88800] p 161 N86-30206
- LOOMIS, W. R.**
New directions in lubrication, materials, wear, and surface interactions - Tribology in the 80's p 152 A86-18700
- LOUIS, J. F.**
A preliminary study of the modified Ericsson for space power p 180 A86-24840
- LYCHUK, W. M.**
Stress and deformation modeling of multiple rotary combustion engine trochoid housings
[SAE PAPER 860614] p 156 A86-49624
- LYMAN, V.**
Evaluation of propeller/nacelle interactions in the PTA program
[AIAA PAPER 86-1552] p 6 A86-42709
- LYONS, V. J.**
Temperature and velocity profiles in sooting free boundary layer flames
[AIAA PAPER 86-0575] p 73 A86-19962

M

- MACBAIN, J. C.**
Joint research effort on vibrations of twisted plates, phase 1: Final results
[NASA-RP-1150] p 172 N86-10579
- MACDONALD, J. R.**
Composition and properties of the so-called 'diamond-like' amorphous carbon films p 98 A86-16255
- MACKAY, R. A.**
The development of gamma-gamma-prime lamellar structures in a nickel-base superalloy during elevated temperature mechanical testing p 79 A86-14719
Temperature dependence of gamma-gamma prime lattice mismatch in nickel-base superalloys p 81 A86-21849
Microstructure-property relationships in directionally solidified single crystal nickel-base superalloys
[NASA-TM-88788] p 93 N86-31700
- MAFFEO, R.**
Burner liner thermal-structural load modeling
[NASA-CR-174892] p 176 N86-21932
Burner liner thermal/structural load modeling: TRANCITS program user's manual
[NASA-CR-174891] p 142 N86-24931
- MAFFEO, R. J.**
A computer analysis program for interfacing thermal and structural codes p 193 A86-36881
Burner liner thermal/structural load modeling p 173 N86-11514
- MAJUMDAR, S.**
Effects of a high mean stress on the high cycle fatigue life of PWA 1480 and correlation of data by linear elastic fracture mechanics
[NASA-CR-175057] p 177 N86-27689
- MALAK, M. F.**
Three-dimensional flow field measurements in a radial inflow turbine scroll using LDV
[ASME PAPER 86-GT-122] p 7 A86-48181
- MALHOTRA, V.**
The synthesis, characterization and thermal chemistry of modified norbornenyl PMR endcaps p 100 N86-11266
- MANDELL, M. J.**
The role of unneutralized surface ions in negative potential arcing p 118 A86-25525
- MANDERSCHIED, J. M.**
Simplified cyclic structural analyses of SSME turbine blades
[NASA-TM-87214] p 175 N86-16611
Cyclic structural analyses of anisotropic turbine blades for reusable space propulsion systems p 58 N86-17404
- MANI, A.**
Probabilistic finite elements for transient analysis in nonlinear continua p 168 A86-28653
- MANORY, R.**
Protective coatings of metal surfaces by cold plasma treatment
[NASA-TM-87152] p 157 N86-11479
- MANORY, R. R.**
Effect of argon and hydrogen on deposition of silicon from tetrochlorosilane in cold plasmas
[NASA-TM-87219] p 65 N86-17472
- MANSON, S. S.**
Time dependency of strainrange partitioning life relationships
[NASA-CR-174946] p 174 N86-13755
Re-examination of cumulative fatigue damage analysis: An engineering perspective
[NASA-TM-87325] p 177 N86-27686
- MANTENIEKS, M. A.**
Rapid evaluation of ion thruster lifetime using optical emission spectroscopy
[AIAA PAPER 85-2011] p 51 A86-17851
Rapid evaluation of ion thruster lifetime using optical emission spectroscopy
[NASA-TM-87103] p 56 N86-10280
- MANTRAVADI, N.**
Compressive creep behavior of alloys based on B2 FeAl
[NASA-TM-87293] p 92 N86-28165
- MANZO, M. A.**
Design principles for nickel-hydrogen cells and batteries p 179 A86-24796
- MAO, C. P.**
Measurements in liquid fuel sprays
[NASA-CR-177088] p 144 N86-30966
- MARCHAND, N.**
Thermal-mechanical fatigue crack growth in Inconel X-750 p 81 A86-20982
Thermal-mechanical fatigue behavior of nickel-base superalloys
[NASA-CR-175048] p 91 N86-24818
- MAREK, C. J.**
Turbulent dispersion of the icing cloud from spray nozzles used in icing tunnels
[NASA-TM-87316] p 34 N86-31586
- MAREK, J. A.**
Progress in the Lewis Research Center Altitude Wind Tunnel (AWT) modeling program
[AIAA PAPER 86-0757] p 36 A86-24744
- MAREK, J. C.**
Progress in the Lewis Research Center Altitude Wind Tunnel (AWT) Modeling Program
[NASA-TM-87194] p 37 N86-16233
- MARGLE, J. M.**
Temperature and velocity profiles in sooting free boundary layer flames
[AIAA PAPER 86-0575] p 73 A86-19962
- MARQUES, E. R. C.**
Stress waves in transversely isotropic media: The homogeneous problem
[NASA-CR-3977] p 164 N86-25002
Wave propagation in anisotropic medium due to an oscillatory point source with application to unidirectional composites
[NASA-CR-4001] p 165 N86-27686
- MARSIK, S. J.**
Structural integrity and durability for Space Shuttle main engine and future reusable space propulsion systems
[AIAA PAPER 86-1513] p 55 A86-42682
Advanced research and technology program for advanced high pressure oxygen-hydrogen rocket propulsion p 58 N86-17405
Structural integrity and durability for Space Shuttle main engine and future reusable space propulsion systems
[NASA-TM-87280] p 61 N86-25406
- MARTIN, C. H.**
Broadcasting satellite service synthesis using gradient and cyclic coordinate search procedures
[NASA-CR-176708] p 114 N86-23781
- MARTIN, J. F.**
Experimental evaluation criteria for constitutive models of time dependent cyclic plasticity
[NASA-CR-176821] p 176 N86-25850
- MARTINEZ, A.**
Orbit Transfer Rocket Engine Technology Program: Advanced engine study, task D.1/D.3
[NASA-CR-175084] p 61 N86-26368

- MARKER, N.**
Ellipsometric surface analysis of wear tracks produced by different lubricants p 151 A86-11016
[ASLE PREPRINT 85-TC-5A-2]
Optical and other properties changes of M-50 bearing steel surfaces for different lubricants and additives prior to scuffing p 97 A86-20435
Ellipsometric surface analysis of wear tracks produced by different lubricants p 87 N86-12293
[NASA-TM-87142]
Polarization modulated ellipsometry p 149 N86-28599
[NASA-CR-177264]
- MASSELINK, W. T.**
Cryogenic operation of pseudomorphic AlGaAs/InGaAs single-quantum-well MODFETs p 117 A86-11998
High transconductance InGaAs/AlGaAs pseudomorphic modulation-doped field-effect transistors p 117 A86-18814
Determination of carrier saturation velocity in high-performance In(y)Ga(1-y)As/Al(x)Ga(1-x)As modulation-doped field-effect transistors (with y between 0 and 0.2) p 118 A86-37295
- MATAGA, T. G.**
Temperature and velocity profiles in sooting free boundary layer flames p 73 A86-19962
[AIAA PAPER 86-0575]
- MATHES, J. B.**
Transmission line design for a power distribution system at 20 kHz for aircraft p 32 N86-29818
[NASA-CR-3987]
- MATULA, R. A.**
Shock-tube pyrolysis of chlorinated hydrocarbons - Formation of soot p 75 A86-35126
- MATUS, L. G.**
Convenient mounting method for electrical measurements of thin samples p 120 A86-46649
Apparatus for electrical measurements of thin films from 77 to 1000 K p 148 N86-24959
[NASA-TM-87256]
Compensation in epitaxial cubic SiC films p 206 N86-25267
[NASA-TM-87269]
- MAY, C. E.**
Electrocrystallization in microgravity p 212 N86-19274
[NASA-TM-87202]
Fugacity and concentration gradients in a gravity field p 212 N86-30620
[NASA-TM-88809]
- MCALLISTER, J. G.**
Advanced orbit transfer vehicle propulsion system study p 60 N86-24748
[NASA-TM-174843]
- MCCLEER, P. J.**
AC motor and generator requirements for isolated WECS p 182 N86-11670
[NASA-CR-176315]
- MCDANIELS, D. L.**
Polymer, metal and ceramic matrix composites for advanced aircraft engine applications p 87 N86-13407
[NASA-TM-87132]
- MCDONALD, G.**
Ribbon-burner simulation of T-700 turbine shroud for ceramic-lined seals research p 18 A86-15225
Finite element analysis of residual stress in plasma-sprayed ceramic p 95 A86-15226
Experimental study of ceramic-coated tip seals for turbojet engines p 152 A86-15227
Fabrication of ceramic substrate-reinforced and free forms by mandrel plasma spraying metal-ceramic composites p 64 A86-17483
Film and interstitial formation of metals in plasma-sprayed ceramics p 96 A86-17484
Thermomechanical design criteria for ceramic-coated surfaces p 143 N86-25726
[NASA-TM-87328]
- MCDONALD, H.**
Numerical and experimental investigation of nonswirling and swirling confined jets p 127 A86-19851
[AIAA PAPER 86-0040]
Calculations of two and three-dimensional transonic cascade flow fields using the Navier-Stokes equations [ASME PAPER 85-GT-86] p 2 A86-22046
Numerical analysis of some supersonic viscous flows related to inlet and nozzle systems p 134 A86-42738
[AIAA PAPER 86-1597]
Influence of large-scale motion on turbulent transport for confined coaxial jets. Volume 2: Navier-Stokes calculations of swirling and nonswirling confined coaxial jets p 28 N86-20390
[NASA-CR-175036]
- MCDONALD, T. J.**
Wind tunnel tests of rotor blade sections with replications of ice formations accreted in hover p 15 N86-22558
[NASA-CR-175089]
- MCFADDEN, G. B.**
Interaction of flows with the crystal-melt interface p 132 A86-29419
- MC FARLAND, E. R.**
Wind tunnel turning vanes of modern design p 36 A86-19854
[AIAA PAPER 86-0044]
Wind tunnel turning vanes of modern design p 37 N86-12239
[NASA-TM-87146]
A FORTRAN computer code for calculating flows in multiple-blade-element cascades p 9 N86-13295
[NASA-TM-87104]
- MCKNIGHT, R.**
In-flight measurements of wing ice shapes and wing section drag increases caused by natural icing conditions p 12 N86-24667
[NASA-TM-87301]
- MCKNIGHT, R. C.**
The measurement of aircraft performance and stability and control after flight through natural icing conditions [AIAA PAPER 86-9758] p 35 A86-40681
The measurement of aircraft performance and stability and control after flight through natural icing conditions [NASA-TM-87265] p 35 N86-22582
In-flight photogrammetric measurement of wing ice accretions p 17 N86-31562
[NASA-TM-87191]
- MC MURRY, C. B.**
Hot-wire measurements of a single lateral jet injected into swirling crossflow p 127 A86-19861
[AIAA PAPER 86-0055]
Experiments on opposed lateral jets injected into swirling crossflow p 29 N86-20394
[NASA-CR-175041]
- MC MURTRY, C. H.**
Sintered alpha silicon carbide ceramics for high temperature structural application - Status review and recent developments p 97 A86-23921
[ASME PAPER 85-IGT-127]
- MC MURTRY, P. A.**
Direct numerical simulations of a reacting mixing layer with chemical heat release p 76 A86-41711
- MEACHER, J.**
Automotive Stirling engine development program p 211 N86-30579
[NASA-CR-175045]
- MEADER, C. B.**
Simulated performance of the NASA 30/20 GHz test transponder using multi-H phase coded modulation p 110 A86-29856
[AIAA PAPER 86-0717]
- MEADOR, M. A.**
A preliminary study of ester oxidation on an aluminum surface using chemiluminescence p 103 N86-24835
[NASA-TM-87242]
- MEHANDRU, S. P.**
Adsorption of O₂, SO₂, and SO₃ on nickel oxide - Mechanism for sulfate formation p 75 A86-34238
- MEHMED, O.**
Experimental classical flutter results of a composite advanced turboprop model p 178 N86-29271
[NASA-TM-868792]
- MEHRA, R. K.**
Bifurcation techniques for nonlinear dynamic analysis of compressor stall phenomena p 22 A86-35403
- MEIJER, R. J.**
Liquid fueled external heating system for STM4-120 Stirling engine p 180 A86-24888
- MELCHER, K. J.**
DEAN - A program for Dynamic Engine Analysis p 18 A86-14430
[AIAA PAPER 85-1354]
A sensor failure simulator for control system reliability studies p 124 N86-31792
[NASA-TM-87271]
- MENGLE, V. G.**
Packet flutter and aerodynamic modes for non-homogenous airfoil cascades in highly distorted, periodic, stationary throughflows p 5 A86-38896
[AIAA PAPER 86-0848]
- MENON, S.**
Coherent structures in a turbulent mixing layer - A comparison between direct numerical simulations and experiments p 132 A86-30218
- MERRILL, W. C.**
Sensor failure detection for jet engines using analytical redundancy p 18 A86-14226
A real-time simulation evaluation of an advanced detection, isolation and accommodation algorithm for sensor failures in turbine engines p 30 N86-24697
[NASA-TM-87289]
HYTESS 2: A Hypothetical Turbofan Engine Simplified Simulation with multivariable control and sensor analytical redundancy p 124 N86-30068
[NASA-TM-87344]
A sensor failure simulator for control system reliability studies p 124 N86-31792
[NASA-TM-87271]
- MERTE, H., JR.**
Modeling of zero gravity venting: Studies of two-phase heat transfer under reduced gravity p 144 N86-31826
[NASA-CR-179662]
- METCALFE, R. W.**
Direct numerical simulations of chemically reacting turbulent mixing layers p 130 A86-25567
Coherent structures in a turbulent mixing layer - A comparison between direct numerical simulations and experiments p 132 A86-30218
Direct numerical simulations of a reacting mixing layer with chemical heat release p 76 A86-41711
- METZ, R. N.**
Circuit transients due to negative bias arcs-II p 52 A86-19835
[AIAA PAPER 86-0366]
- MEYER, S. D.**
Evaluation of a hybrid hydrostatic bearing for cryogenic turbopump application p 63 N86-31649
[NASA-TM-87255]
- MEYER, T. G.**
Life prediction and constitutive models for engine hot section anisotropic materials program p 165 N86-25003
[NASA-CR-174952]
- MEYERS, A.**
Specimen geometry effects on graphite/PMR-15 composites during thermo-oxidative aging p 69 N86-17477
[NASA-TM-87204]
- MEYERS, G. J.**
Fracture mechanics applied to nonisothermal fatigue crack growth p 81 A86-28951
- MEYN, E. H.**
The use of an optical data acquisition system for bladed disk vibration analysis p 146 A86-26909
- MIESKOWSKI, D. M.**
Effect of grain-boundary crystallization on the high-temperature strength of silicon nitride p 98 A86-33495
Strength and microstructure of Si₃N₄ sintered with ZrO₂ additions p 99 A86-38330
- MIKKELSEN, K.**
In-flight measurements of wing ice shapes and wing section drag increases caused by natural icing conditions p 12 N86-24667
[NASA-TM-87301]
- MIKKELSEN, K. L.**
The measurement of aircraft performance and stability and control after flight through natural icing conditions [AIAA PAPER 86-9758] p 35 A86-40681
The measurement of aircraft performance and stability and control after flight through natural icing conditions [NASA-TM-87265] p 35 N86-22582
- MIKKELSON, D. C.**
Summary of recent NASA propeller research p 25 N86-11158
- MILINAZZO, F. A.**
Finite-amplitude steady waves in plane viscous shear flows p 127 A86-19419
[AD-A185461]
- MILLARD, M. L.**
Improved consolidation of silicon carbide p 104 N86-24836
[NASA-TM-87243]
- MILLER, D. L.**
Shock-tube pyrolysis of chlorinated hydrocarbons - Formation of soot p 75 A86-35126
- MILLER, D. R.**
Summary of NASA/DOE Aileron-Control Development Program for Wind Turbines p 190 N86-31983
[NASA-TM-88811]
- MILLER, E. F.**
An analysis of bidirectional use of frequencies for satellite communications p 110 A86-29664
[AIAA PAPER 86-0635]
Impact of the 1985 Space World Administrative Radio Conference on frequency/orbit planning and use p 110 A86-49567
[AIAA PAPER 86-0834]
An analysis of bi-directional use of frequencies for satellite communications p 111 A86-49568
[AIAA PAPER 86-0635]
An analysis of bi-directional use of frequencies for satellite communications p 114 N86-18585
[NASA-TM-87226]
Impact of the 1985 Space World Administrative Radio Conference on frequency/orbit planning and use p 115 N86-24861
[NASA-TM-87285]
- MILLER, J. D.**
Graphite fiber intercalation: Basic properties of copper chloride intercalated fibers p 65 N86-18442
[NASA-TM-87217]
- MILLER, J. E.**
An analysis of bidirectional use of frequencies for satellite communications p 110 A86-29664
[AIAA PAPER 86-0635]
An analysis of bi-directional use of frequencies for satellite communications p 111 A86-49568
[AIAA PAPER 86-0635]
An analysis of bi-directional use of frequencies for satellite communications p 114 N86-18585
[NASA-TM-87226]

- MILLER, R. A.**
Failure analysis of plasma-sprayed thermal barrier coatings p 80 A86-18270
Performance of thermal barrier coatings in high heat flux environments p 80 A86-18272
Ceramic thermal barrier coatings for electric utility gas turbine engines [NASA-TM-87288] p 90 N86-22687
- MILLER, T. L.**
Analytical determination of propeller performance degradation due to ice accretion [NASA-CR-175092] p 15 N86-23577
- MILLER, W. L.**
Mass loss of shuttle space suit orthofabric under simulated ionospheric atomic oxygen bombardment [NASA-TM-87149] p 192 N86-13899
- MILLIGAN, W. W., JR.**
Yielding and deformation behavior of the single crystal nickel-base superalloy PWA 1480 [NASA-CR-175100] p 91 N86-25455
- MILLNER, A. R.**
Development of a microprocessor controller for stand-alone photovoltaic power systems [NASA-CR-174723] p 187 N86-21979
- MILNER, E. J.**
Simulating a small turboshaft engine in real-time multiprocessor simulator (RTMPS) environment [NASA-TM-87216] p 27 N86-18221
Partitioning and packing mathematical simulation models for calculation on parallel computers [NASA-TM-87170] p 193 N86-19008
- MINER, R. V.**
The tensile and fatigue deformation structures in a single crystal Ni-base superalloy p 83 A86-35697
Orientation and temperature dependence of some mechanical properties of the single-crystal nickel-base superalloy Rene N4. I - Tensile behavior p 86 A86-50321
Orientation and temperature dependence of some mechanical properties of the single-crystal nickel-base superalloy Rene N4. II - Low cycle fatigue behavior p 86 A86-50322
Orientation and temperature dependence of some mechanical properties of the single-crystal nickel-base superalloy Rene N4. III - Tension-compression anisotropy p 86 A86-50323
Creep-fatigue behavior of NiCoCrAlY coated PWA 1480 superalloy single crystals [NASA-TM-87110] p 86 N86-10311
Fatigue crack propagation of nickel-base superalloys at 650 deg C [NASA-TM-87150] p 87 N86-12294
- MINER, R. V., JR.**
The low cycle fatigue behavior of a plasma-sprayed coating material [NASA-TM-87318] p 92 N86-31699
- MINZHONG, Z.**
Fatigue crack growth under general-yielding cyclic-loading p 171 A86-44339
Fatigue crack growth under general-yielding cyclic-loading [NASA-CR-175049] p 176 N86-21951
- MIRDAMADI, M.**
Axial and torsional fatigue behavior of Waspaloy [NASA-CR-175052] p 91 N86-25454
- MIRTTICH, M.**
Thin film growth rate effects for primary ion beam deposited diamondlike carbon films p 100 A86-47068
- MIRTTICH, M. J.**
Ion beam sputter-deposited thin film coatings for protection of spacecraft polymers in low earth orbit [AIAA PAPER 85-0420] p 95 A86-14428
Composition and properties of the so-called 'diamond-like' amorphous carbon films p 96 A86-16255
Diamondlike carbon films on semiconductors for insulated-gate technology p 120 A86-47077
Dual-ion-beam deposition of carbon films with diamond-like properties p 65 A86-49855
Oxidation protection coatings for polymers [NASA-CASE-LEW-14072-1] p 102 N86-19458
Oxidation protecting coatings for polymers [NASA-CASE-LEW-14072-3] p 105 N86-26434
Apparatus for producing oxidation protection coatings for polymers [NASA-CASE-LEW-14072-2] p 106 N86-32569
- MISRA, A. K.**
Studies on the hot corrosion of a nickel-base superalloy, Udmet 700 p 82 A86-28722
Na₂SO₄ induced corrosion of nickel at high temperature p 83 A86-37073
Mechanism of Na₂SO₄-induced corrosion of molybdenum containing nickel-base superalloys at high temperatures. I - Corrosion in atmospheres containing O₂ only. II - Corrosion in O₂ + SO₂ atmospheres p 83 A86-37238
- Role of molybdenum in the Na sub 2SO sub 4 sub 4 induced corrosion of superalloys at high temperatures [NASA-TM-87235] p 90 N86-21658
Corrosion of nickel and cobalt base alloys in sulfate melts at 750 deg C [NASA-CR-175111] p 91 N86-24817
Estimated heats of fusion of fluoride salt mixtures suitable for thermal energy storage applications [NASA-TM-87320] p 190 N86-31982
- MITCHELL, A. M.**
Testing of YUH-61A helicopter transmission in NASA Lewis 2240-kW (3000-hp) facility [NASA-TP-2538] p 160 N86-24992
- MITCHELL, G. A.**
Summary of recent NASA propeller research p 25 N86-11158
- MITCHELL, L. D.**
Linear dynamic coupling in geared rotor systems [ASME PAPER 85-DET-11] p 154 A86-38617
- MITCHELL, T. E.**
High temperature oxidation of beta-NiAl p 85 A86-47266
- MITTRA, R.**
Characterization of MMIC devices for active array antennas p 111 N86-11401
MMIC devices for active phased array antennas [NASA-CR-176990] p 116 N86-30037
- MIYOSHI, K.**
Surface effects of corrosive media on hardness, friction, and wear of materials p 94 A86-10825
Fundamental tribological properties of ceramics p 95 A86-15230
Mechanical-contact-induced transformation from the amorphous to the partially crystalline state in metallic glass p 80 A86-18257
Metallic glass as a temperature sensor during ion plating p 80 A86-16906
Tribological properties of boron nitride synthesized by ion beam deposition p 96 A86-17479
Interaction of sulfuric acid corrosion and mechanical wear of iron p 81 A86-20436
Tribological characteristics of gold films deposited on metals by ion plating and vapor deposition p 85 A86-49600
Tribological properties of structural ceramics [NASA-TM-87105] p 100 N86-10341
Abrasion and deformed layer formation of manganese-zinc ferrite in sliding contact with lapping tapes [NASA-TM-87249] p 104 N86-24838
Tribology of selected ceramics at temperatures to 900 deg C [NASA-TM-87267] p 105 N86-25476
Effect of crystallographical and geometrical changes of a ferrite head on magnetic signals during the sliding process with magnetic tape [NASA-TM-87277] p 106 N86-31728
- MIZOMOTO, M.**
Effects of preferential diffusion on the burning intensity of curved flames p 73 A86-22813
- MOFFAT, R. J.**
Analysis of the uncertainties in velocity measurements with triple hot-wire probes p 130 A86-24468
Film cooling on a convex wall: Heat transfer and hydrodynamic measurements for full and partial coverage [NASA-CR-174964] p 137 N86-10461
- MOKADAM, D. R.**
Analytical and experimental investigation of the coupled bladed disk/shaft whirl of a cantilevered turbofan [ASME PAPER 86-GT-98] p 24 A86-48163
- MOLDOVER, M. R.**
Light scattering tests of fundamental theories of transport properties in the critical region p 39 N86-10113
- MOLLER, J. C.**
Heat-flux measurements for the rotor of a full-stage turbine. II - Description of analysis technique and typical time-resolved measurements [ASME PAPER 86-GT-78] p 24 A86-48146
- MOLONEY, M.**
High transconductance InGaAs/AlGaAs pseudomorphic modulation-doped field-effect transistors p 117 A86-18814
- MONGIA, H. C.**
Rotorcraft propulsion for year 2000 plus [AIAA PAPER 86-1543] p 23 A86-42702
- MOORE, F. K.**
A theory of post-stall transients in axial compression systems. I - Development of equations [ASME PAPER 85-GT-171] p 19 A86-22088
A theory of post-stall transients in axial compression systems. II - Application [ASME PAPER 85-GT-172] p 19 A86-22089
- MOORE, J.**
Thermodynamic evaluation of transonic compressor rotors using the finite volume approach [NASA-CR-176428] p 27 N86-18220
Thermodynamic evaluation of transonic compressor rotors using the finite volume approach [NASA-CR-176840] p 143 N86-26546
Thermodynamic evaluation of transonic compressor rotors using the finite volume approach [NASA-CR-176947] p 32 N86-30731
- MOORE, J. G.**
Thermodynamic evaluation of transonic compressor rotors using the finite volume approach [NASA-CR-176428] p 27 N86-18220
- MOORE, R. D.**
Wind tunnel turning vanes of modern design [AIAA PAPER 88-0044] p 38 A86-19854
Wind tunnel turning vanes of modern design [NASA-TM-87146] p 37 N86-12239
Experimental evaluation of two turning vane designs for high-speed corner of 0.1-scale model of NASA Lewis Research Center's proposed altitude wind tunnel [NASA-TP-2570] p 38 N86-28101
Comparison of analytical and experimental performance of a wind-tunnel diffuser section [NASA-TM-88795] p 13 N86-31537
- MOORE, T. J.**
Creep properties of PWC-11 base metal and weldments as affected by heat treatment [NASA-TM-88842] p 93 N86-32557
- MORALES, W.**
Simulation of lubricating behavior of a thioether liquid lubricant by an electrochemical method p 97 A86-20437
Analysis of a thioether lubricant by infrared Fourier microemission spectrophotometry [NASA-TM-87195] p 102 N86-16379
A thin film degradation study of a fluorinated polyether liquid lubricant using an HPLC method [NASA-TM-87221] p 77 N86-19417
Analysis of a spacecraft instrument ball bearing assembly lubricated by a perfluoroalkylether [NASA-TM-87260] p 50 N86-21575
A preliminary study of ester oxidation on an aluminum surface using chemiluminescence [NASA-TM-87242] p 103 N86-24835
- MOREA, S. F.**
Advanced research and technology program for advanced high pressure oxygen-hydrogen rocket propulsion p 58 N86-17405
- MOREHOUSE, K. A.**
Effect of a rotor wake on the local heat transfer on the forward half of a circular cylinder [NASA-TM-87234] p 140 N86-21794
Unsteady heat transfer and direct comparison to steady-state measurements in a rotor-wake experiment [NASA-TM-87220] p 142 N86-24934
- MOREL, T.**
Methods for heat transfer and temperature field analysis of the insulated diesel phase 2 progress report [NASA-CR-175072] p 210 N86-24590
- MORENO, V.**
Creep fatigue life prediction for engine hot section materials (isotropic) p 174 N86-11521
- MORIN, B. L.**
Forced mixer lobes in ejector designs [AIAA PAPER 86-1814] p 134 A86-42752
- MORIN, T.**
Measurement of energy distribution in flowing hydrogen microwave plasmas p 52 A86-18041
- MORKOC, H.**
Cryogenic operation of pseudomorphic AlGaAs/InGaAs single-quantum-well MODFETs p 117 A86-11998
Determination of carrier saturation velocity in high-performance In(y)Ga(1-y)As/Al(x)Ga(1-x)As modulation-doped field-effect transistors (with y between 0 and 0.2) p 118 A86-37295
High-frequency noise of In(y)Ga(1-y)As/Al(x)Ga(1-x)As MODFETs and comparison to GaAs/Al(x)Ga(1-x)As MODFETs p 119 A86-43914
- MORRAL, J. E.**
Constructing multicomponent phase diagrams by overlapping ZPF lines p 83 A86-44038
- MORREN, W. E.**
Performance and endurance tests of a multipropellant resistojel for space station auxiliary propulsion [AIAA PAPER 86-1435] p 55 A86-42640
Performance and endurance tests of a multipropellant resistojel for space station auxiliary propulsion [NASA-TM-87278] p 80 N86-24748
- MORRIS, P. J.**
Tone excited jets. V - A theoretical model and comparison with experiment p 196 A86-16470
Acoustic control of free jet mixing p 135 A86-46314

- MORRIS, P. M.**
Aerodynamic data banks for Clark-Y, NACA 4-digit and NACA 16-series airfoil families
[NASA-CR-176883] p 13 N86-30693
- MOSCARELLO, R.**
Locally bound constrained Newton-Raphson solution algorithms
p 171 A86-43771
- MOSSADEGH, R.**
Determination of solid mass fraction in partially frozen hydrocarbon fuels
[NASA-CR-179472] p 108 N86-28261
- MOSSEY, P. W.**
1700 deg C optical temperature sensor
[NASA-CR-175108] p 203 N86-28729
- MOSTAFA, A. A.**
Effect of liquid droplets on turbulence in a round gaseous jet
[NASA-CR-175083] p 29 N86-23597
- MOUNT-CAMPBELL, C.**
Engineering calculations for communications satellite systems planning
[NASA-CR-176555] p 114 N86-19493
- MOUNT-CAMPBELL, C. A.**
Broadcasting satellite service synthesis using gradient and cyclic coordinate search procedures
[NASA-CR-176708] p 114 N86-23781
- MOUNT, R. E.**
Stratified charge rotary engine for general aviation
[ASME PAPER 86-GT-181] p 24 A86-48231
- MOY, L.**
Hard ACTS to follow
p 46 A86-35318
- MOY, L. L.**
On the effectiveness of onboard processing
[AIAA PAPER 86-0721] p 45 A86-29659
- MOYNIHAN, C. T.**
Determination of solid mass fraction in partially frozen hydrocarbon fuels
[NASA-CR-179472] p 108 N86-28261
- MOYNIHAN, M. E.**
Lightweight two-stroke cycle aircraft diesel engine technology enablement program, volume 1
[NASA-CR-174923-VOL-1] p 26 N86-13328
Lightweight two-stroke cycle aircraft diesel engine technology enablement program, volume 2
[NASA-CR-174923-VOL-2] p 26 N86-13329
Lightweight two-stroke cycle aircraft diesel engine technology enablement program, volume 3
[NASA-CR-174923-VOL-3] p 26 N86-13330
- MUELLER, E. H.**
N/P GaAs concentrator solar cells with an improved grid and bushbar contact design
p 184 N86-17844
- MULAC, R. A.**
A model for closing the inviscid form of the average-passage equation system
[ASME PAPER 86-GT-227] p 8 A86-48261
A model for closing the inviscid form of the average-passage equation system
[NASA-TM-87199] p 10 N86-14224
A numerical simulation of the inviscid flow through a counter-rotating propeller
[NASA-TM-87200] p 10 N86-16195
- MULARZ, E. J.**
Combustion research for gas turbine engines
p 17 A86-11609
- MULLEN, R. L.**
Finite element analysis of residual stress in plasma-sprayed ceramic
p 95 A86-15226
Film and interstitial formation of metals in plasma-sprayed ceramics
p 96 A86-17484
Analysis of a two row hydrostatic journal bearing with variable properties, inertia effects and surface roughness
p 153 A86-30599
Analysis of the transient behavior of rubbing components
[NASA-CR-176548] p 102 N86-19464
Two-phase flows and heat transfer within systems with ambient pressure above the thermodynamic critical pressure
[NASA-TM-87228] p 140 N86-19558
Thermomechanical design criteria for ceramic-coated surfaces
[NASA-TM-87328] p 143 N86-25726
Two-phase flows within systems with ambient pressure
p 161 N86-30167
- MULLER, G. L.**
Three-dimensional inviscid flow in mixers. I - Mixer analysis using a Cartesian grid
p 5 A86-39090
Three-dimensional inviscid flow in mixers. II - Analysis of turbofan forced mixers
p 6 A86-46316
- MULLINGS, D. M.**
Ceramic automotive Stirling engine study
[NASA-CR-174907] p 208 N86-16165
- MULUKUTLA, A. R.**
1700 deg C optical temperature sensor
[NASA-CR-175108] p 203 N86-28729
- MURMAN, E. M.**
Three-dimensional inviscid flow in mixers. I - Mixer analysis using a Cartesian grid
p 5 A86-39090
Three-dimensional inviscid flow in mixers. II - Analysis of turbofan forced mixers
p 6 A86-46316
- MURPHY, B. T.**
SSME long-life bearings
[NASA-CR-179455] p 160 N86-27643
- MURTHY, K. N. S.**
Laser Doppler velocimeter measurement in the tip region of a compressor rotor
p 5 A86-39064
- MURTHY, P. L. N.**
Composite sandwich thermostructural behavior - Computational simulation
[AIAA PAPER 86-0948] p 170 A86-38842
Dynamic stress analysis of smooth and notched fiber composite flexural specimens
p 67 A86-41070
Interlaminar fracture toughness: Three-dimensional finite element modeling for end-notch and mixed-mode flexure
[NASA-TM-87138] p 89 N86-14316
Integrated Composite Analyzer (ICAN): Users and programmers manual
[NASA-TP-2515] p 69 N86-21614
Fiber composite sandwich thermostructural behavior: Computational simulation
[NASA-TM-88787] p 71 N86-31663
- MURTHY, S. N. B.**
A stagnation pressure probe for droplet-laden air flow
p 133 A86-39077
Transient engine performance with water ingestion
[AIAA PAPER 86-1621] p 23 A86-42755
- MUSIKANT, S.**
Ceramic automotive Stirling engine study
[NASA-CR-174907] p 208 N86-16165
Transformation toughened ceramics for the heavy duty diesel engine technology program, phase 2
[NASA-CR-175054] p 210 N86-22451
- MYERS, G.**
Dilution jet mixing program, phase 3
[NASA-CR-174884] p 142 N86-24938
- MYERS, M. R.**
Influence of airfoil camber on convected gust interaction noise
[AIAA PAPER 86-1873] p 198 A86-45493
- N**
- NAGAMATSU, H. T.**
Relaminarization of the boundary layer over a flat plate in shock tube experiments
[AIAA PAPER 86-1238] p 133 A86-39865
- NAGTEGAAL, J. C.**
Efficient algorithms for use in probabilistic finite element analysis
p 168 A86-28655
Iterative methods for mixed finite element equations
p 169 A86-34461
- NAHM, A. H.**
Improved fracture toughness corrosion-resistant bearing material
[NASA-CR-174990] p 162 N86-32743
- NAHRA, H. K.**
Ion beam sputter-deposited thin film coatings for protection of spacecraft polymers in low earth orbit
[AIAA PAPER 85-0420] p 95 A86-14428
- NAKAHARA, J.**
Improved perfluoroalkylether fluid development
[NASA-TM-87276] p 104 N86-25474
- NAKAHARA, J. H.**
The effects of metals and inhibitors on thermal oxidative degradation reactions of unbranched perfluoroalkyl ethers
p 99 A86-40682
- NAKANISHI, S.**
Experimental performance of a 1-kilowatt arcjet thruster
[AIAA PAPER 85-2033] p 54 A86-37063
Low power dc arcjet operation with hydrogen/nitrogen propellant mixtures
[AIAA PAPER 86-1505] p 55 A86-42676
Experimental performance of a 1-kilowatt arcjet thruster
[NASA-TM-87131] p 57 N86-10281
Lower power dc arcjet operations with hydrogen hydrogen/nitrogen propellant mixtures
[NASA-TM-87279] p 61 N86-25407
- NAKAZAWA, S.**
Iterative methods for mixed finite element equations
p 169 A86-34461
- NAMER, I.**
Ignition characteristics of rich n-heptane fuel sprays in the transition region
[ASME PAPER 85-WA/HT-46] p 107 A86-38393
Transition region ignition characteristics of n-heptane fuel sprays
[NASA-CR-176364] p 77 N86-14331
- Combustion characteristics in the transition region of liquid fuel sprays
[NASA-CR-176584] p 77 N86-20517
- NATARAJAN, V.**
Optical and interfacial electronic properties of diamond-like carbon films
p 204 A86-16268
- NATHAL, M. V.**
The influence of cobalt, tantalum, and tungsten on the microstructure of single crystal nickel-base superalloys
p 79 A86-12995
The influence of cobalt, tantalum, and tungsten on the elevated temperature mechanical properties of single crystal nickel-base superalloys
p 79 A86-12996
Temperature dependence of gamma-gamma prime lattice mismatch in nickel-base superalloys
p 81 A86-21849
Tensile behavior of Fe-40Al alloys with B and Zr additions
[NASA-TM-87290] p 91 N86-25453
Microstructure-property relationships in directionally solidified single crystal nickel-base superalloys
[NASA-TM-88788] p 93 N86-31700
- NEITZEL, G. P.**
Energy stability of thermocapillary convection in models of the float zone process
p 40 N86-10123
- NELSON, C. E.**
Theory versus experiment for the rotordynamic coefficients of annular gas seals. I - Test facility and apparatus
[ASME PAPER 85-TRIB-1] p 152 A86-24481
- NELSON, H. D.**
Parametric sensitivity in the dynamics of rotor-bearing systems
[ASME PAPER 85-DET-35] p 154 A86-38620
- NESBITT, J. A.**
Modeling degradation and failure of Ni-Cr-Al overlay coatings
p 80 A86-16276
- NEUMAN, C. P.**
Performance of direct and iterative algorithms on an optical systolic processor
p 202 A86-17421
- NEWBY, R. A.**
Design and evaluation of fluidized bed heat recovery for diesel engine systems
[NASA-CR-174898] p 209 N86-21456
- NEWELL, R. E.**
Simultaneous measurements of carbon monoxide and ozone in the NASA Global Atmospheric Sampling Program (GASP)
p 191 A86-48620
- NEWTON, J.**
Ice shapes and the resulting drag increase for a NACA 0012 airfoil
[AIAA PAPER 84-0109] p 14 A86-14427
- NEWTON, J. E.**
Study of ice accretion on icing wind tunnel components
[AIAA PAPER 86-0290] p 36 A86-26620
Study of ice accretion on icing wind tunnel components
[NASA-TM-87095] p 37 N86-16232
- NG, W.-F.**
Real gas effects on the numerical simulation of a hypersonic inlet
p 6 A86-46324
- NGUYEN, H. L.**
Fluid flow and fuel-air mixing in a motored two-dimensional Wankel rotary engine
[AIAA PAPER 86-1556] p 134 A86-42711
- NGUYEN, T. T.**
Vortex modeling of single and multiple dilution jet mixing in a cross flow
p 135 A86-46318
- NICHOLSON, S.**
Thermodynamic evaluation of transonic compressor rotors using the finite volume approach
[NASA-CR-176428] p 27 N86-16220
Thermodynamic evaluation of transonic compressor rotors using the finite volume approach
[NASA-CR-176840] p 143 N86-26546
Thermodynamic evaluation of transonic compressor rotors using the finite volume approach
[NASA-CR-176947] p 32 N86-30731
- NICKS, C.**
Theory versus experiment for the rotordynamic coefficients of annular gas seals. I - Test facility and apparatus
[ASME PAPER 85-TRIB-1] p 152 A86-24481
- NIEDZWIECKI, R. W.**
An overview of the Small Engine Component Technology (SECT) studies
[NASA-TM-88796] p 34 N86-31587
- NIGHTINGALE, N.**
Automotive Stirling Engine Development Program
[NASA-CR-174749] p 211 N86-28017
- NIKJOOY, M.**
A comparison of three algebraic stress closures for combustor flow calculations
[ASME PAPER 85-WA/FE-3] p 132 A86-38388

- NIR, D.**
Thin film growth rate effects for primary ion beam deposited diamondlike carbon films p 100 A86-47068
- NISSLEY, D. M.**
Life prediction and constitutive models for engine hot section anisotropic materials program [NASA-CR-174952] p 165 N86-25003
- NIX, W. D.**
Dislocations in extruded Co-49.3 at pct Al p 83 A86-45091
- NOH, H. M.**
A high frequency analysis of electromagnetic plane wave scattering by perfectly-conducting semi-infinite parallel plate and rectangular waveguides with absorber coated inner walls [NASA-CR-179759] p 116 N86-32600
- NONAMI, K.**
Quasi-modal vibration control by means of active control bearings [NASA-TM-87232] p 159 N86-21856
- NORED, D. L.**
Electrical power system for the U.S. space station [NASA-TM-88856] p 64 N86-32520
- NORGREN, C. T.**
Small gas turbine combustor experimental study - Compliant metal/ceramic liner and performance evaluation [AIAA PAPER 86-1452] p 25 A86-49611
Small gas turbine combustor experimental study: Compliant metal/ceramic liner and performance evaluation [NASA-TM-87304] p 33 N86-31582
- NORRIS, P. P.**
Life prediction and constitutive models for engine hot section anisotropic materials program [NASA-CR-174952] p 165 N86-25003
- NOURINEJAD, J.**
Mean velocity and turbulence measurements in a 90 deg curved duct with thin inlet boundary layer [NASA-CR-174811] p 139 N86-16518
- NOWOTNY, H.**
Impact wear of iron rich superalloys p 82 A86-34687
Constructing multicomponent phase diagrams by overlapping ZPF lines p 83 A86-44038
- NTONE, F.**
Inverse design of axisymmetric flow passages using compressible viscous flow theory p 4 A86-26412
Viscous compressible flow direct and inverse computation and illustrations [NASA-CR-175037] p 28 N86-20391
- O**
- OBERLE, L. A.**
Filter induced errors in laser anemometry using counter-processor p 146 A86-34431
- OBERLE, L. G.**
Laser anemometry for hot section applications p 151 N86-11503
A computer program to calculate the resistivity of a thin film deposited on a conductive substrate from four-point probe measurements [NASA-TM-87262] p 193 N86-22150
A sensor failure simulator for control system reliability studies [NASA-TM-87271] p 124 N86-31792
- OBRIEN, J. E.**
Unsteady heat transfer and direct comparison to steady-state measurements in a rotor-wake experiment [NASA-TM-87220] p 142 N86-24934
- OLSEN, W.**
Ice shapes and the resulting drag increase for a NACA 0012 airfoil [AIAA PAPER 84-0109] p 14 A86-14427
Study of ice accretion on icing wind tunnel components [AIAA PAPER 86-0290] p 36 A86-26620
Study of ice accretion on icing wind tunnel components [NASA-TM-87095] p 37 N86-16232
- OLSEN, W. A., JR.**
Turbulent dispersion of the icing cloud from spray nozzles used in icing tunnels [NASA-TM-87316] p 34 N86-31588
- ONG, L. H.**
Hot-wire measurements of a single lateral jet injected into swirling crossflow [AIAA PAPER 86-0055] p 127 A86-19661
Measurements of a single lateral jet injected into swirling crossflow [NASA-CR-175040] p 28 N86-20392
- OPPENHEIM, A. K.**
Dynamic features of combustion p 72 A86-12925
- Numerical simulation of a turbulent flame stabilized behind a rearward-facing step p 73 A86-22774
Formation and inflammation of a turbulent jet p 130 A86-23131
Aerodynamic properties of turbulent combustion fields [NASA-CR-175005] p 28 N86-20393
- ORANGE, T. W.**
Wide-range weight functions for the strip with a single edge crack p 167 A86-20709
Estimating the R-curve from residual strength data [NASA-TM-87182] p 175 N86-18750
- ORSZAG, S. A.**
Direct numerical simulations of chemically reacting turbulent mixing layers p 130 A86-25567
- ORUGANTI, R.**
Resonant power processors. I - State plane analysis p 117 A86-14481
Resonant power processors. II - Methods of control p 117 A86-14482
State-plane analysis of parallel resonant converter p 119 A86-40431
- OSHIDA, Y.**
Grain boundary oxidation and oxidation accelerated fatigue crack nucleation and propagation [NASA-CR-175050] p 89 N86-20542
- OSTRACH, S.**
Oscillatory thermocapillary flows p 129 A86-22413
Surface-tension driven convection p 40 N86-10124
- OSULLIVAN, J. A.**
Nonlinear optimal control with tensors - Some computational issues p 184 A86-35419
- OSWALD, F. B.**
Testing of YUH-61A helicopter transmission in NASA Lewis 2240-kW (3000-hp) facility [NASA-TP-2538] p 160 N86-24992
- OTTEY, H. R.**
Spectrum orbit utilization program technical manual SOUP5 Version 3.8 [NASA-CR-174944] p 116 N86-26489
Spectrum Orbit Utilization Program documentation: SOUP5 version 3.8 user's manual, volume 1, chapters 1 through 5 [NASA-CR-174889] p 193 N86-27927
Spectrum Orbit Utilization Program documentation: SOUP5 version 3.8 user's manual, volume 2, appendices A through G [NASA-CR-174890] p 193 N86-27928
- OWEN, A. K.**
Parametric study of beam refraction problems across laser anemometer windows [NASA-TM-87350] p 150 N86-31857
- P**
- PACIOREK, K.**
Improved perfluoroalkylether fluid development [NASA-TM-87276] p 104 N86-25474
- PACIOREK, K. J. L.**
The effects of metals and inhibitors on thermal oxidative degradation reactions of unbranched perfluoroalkyl ethers p 99 A86-40682
- PADOVAN, J.**
Hierarchical implicit dynamic least-square solution algorithm p 167 A86-26689
Inelastic high-temperature thermomechanical response of ceramic coated gas turbine seals p 169 A86-37799
Locally bound constrained Newton-Raphson solution algorithms p 171 A86-43771
Constrained hierarchical least square nonlinear equation solvers p 171 A86-43774
Thermomechanical design criteria for ceramic-coated surfaces [NASA-TM-87328] p 143 N86-25726
- PAGE, R. J.**
Slip casting and extruding shapes of rhenium with metal oxide additives. 1: Feasibility demonstration [NASA-CR-174970] p 63 N86-31648
- PAGNI, P. J.**
Buoyancy effects on smoldering combustion [IAF PAPER 85-289] p 72 A86-15805
Temperature and velocity profiles in sooting free boundary layer flames [AIAA PAPER 86-0575] p 73 A86-19962
A fundamental study of smoldering with emphasis on experimental design for zero-g p 41 N86-10162
- PAIK, D. K.**
Low Reynold's number boundary layers in a disturbed environment [NASA-CR-175031] p 139 N86-17665
- PALKO, R. L.**
In-flight photogrammetric measurement of wing ice accretions [NASA-TM-87191] p 17 N86-31562
- PALMER, R. W.**
Verification of an improved computational design procedure for TWT-dynamic refocuser-MDC systems with secondary electron emission losses p 119 A86-45194
Verification of computer-aided designs of traveling-wave tubes utilizing novel dynamic refocusers and graphite electrodes for the multistage depressed collector [NASA-TP-2524] p 121 N86-13643
- PALMOUR, J. W.**
Dry etching of beta-SiC in CF₄ and CF₄ + O₂ mixtures p 76 A86-47069
- PAPADAKIS, M.**
An experimental method for measuring droplet impingement efficiency on two- and three-dimensional bodies [AIAA PAPER 86-0406] p 131 A86-26630
- PARENTE, A. M.**
Stratified charge rotary engine for general aviation [ASME PAPER 86-GT-181] p 24 A86-48231
- PARK, G. L.**
AC motor and generator requirements for isolated WECS [NASA-CR-176315] p 182 N86-11670
- PARK, M.**
Transonic potential flow in hyperbolic nozzles p 5 A86-41723
- PARKER, R. J.**
Operating characteristics of a 0.87 kW-hr flywheel energy storage module p 152 A86-24864
Evaluation of propeller/nacelle interactions in the PTA program [AIAA PAPER 86-1552] p 6 A86-42709
- PARKS, D. E.**
Threshold determining mechanisms for discharges in high voltage solar arrays [AIAA PAPER 86-0364] p 52 A86-19834
Energy broadening due to space-charge oscillations in high current electron beams p 202 A86-22890
The role of unneutralized surface ions in negative potential arcing p 118 A86-25525
- PARSONS, M. L.**
Rapid evaluation of ion thruster lifetime using optical emission spectroscopy [AIAA PAPER 85-2011] p 51 A86-17851
Rapid evaluation of ion thruster lifetime using optical emission spectroscopy [NASA-TM-87103] p 56 N86-10280
- PASSERELLO, C. E.**
Stress and deformation modeling of multiple rotary combustion engine trochoid housings [SAE PAPER 860614] p 156 A86-49624
- PATER, R. H.**
Rheological, processing, and 371 deg C mechanical properties of Celion 6000/N-phenylnadimide modified PMR composites p 68 N86-11278
High temperature resistant polyimide from tetra ester, diamine, diester and N-arylnadimide [NASA-CASE-LEW-13864-1] p 102 N86-19457
- PATHAK, P. H.**
A high frequency analysis of electromagnetic plane wave scattering by perfectly-conducting semi-infinite parallel plate and rectangular waveguides with absorber coated inner walls [NASA-CR-179759] p 116 N86-32600
- PATHARE, V.**
Alloys based on NiAl for high temperature applications p 84 A86-47261
- PATRICK, W. P.**
Low Reynolds number separation bubble research at UTRC p 126 A86-16311
- PATTERSON, M. J.**
Performance characteristics of ring-cusp thrusters with xenon propellant [NASA-TM-87338] p 63 N86-31650
- PATTIPATI, K. R.**
Application of FDI metrics to detection and isolation of sensor failures in turbine engines p 21 A86-35400
Robust detection-isolation-accommodation for sensor failures [NASA-CR-174797] p 121 N86-16486
- PEBLER, A.**
Transmission electron microscopic examination of phosphoric acid fuel cell components p 74 A86-23352
- PEFLEY, R. K.**
Research and development of neat alcohol fuel usage in automobiles [NASA-CR-174813] p 108 N86-27460
- PELLOUX, R. M.**
Thermal-mechanical fatigue crack growth in Inconel X-750 p 81 A86-20982
Thermal-mechanical fatigue behavior of nickel-base superalloys [NASA-CR-175048] p 91 N86-24818

- PELTON, A. R.**
Dislocations in extruded Co-49.3 at. pct Al
p 83 A86-45091
- PENG, C. K.**
Dc and microwave characteristics of a high current double interface GaAs/InGaAs/AlGaAs pseudomorphic modulation-doped field-effect transistor
p 118 A86-36009
High-frequency noise of In(y)Ga(1-y)As/Al(x)Ga(1-x)As MODFETs and comparison to GaAs/Al(x)Ga(1-x)As MODFETs
p 119 A86-43914
- PENKO, P. F.**
An analysis of low-thrust, resistojet reboost for the Space Station
[AIAA PAPER 85-2042] p 51 A86-14447
Vacuum chamber pressure effects on thrust measurements
p 59 N86-17425
- PEPPER, S. V.**
Angle-resolved Auger electron spectra induced by neon ion impact on aluminum
p 76 A86-43456
Binary collision model for neon Auger spectra from neon ion bombardment of the aluminum surface
p 76 A86-43457
Thermal desorption study of physical forces at the PTFE surface
[NASA-TM-87090] p 206 N86-25284
- PEREPEZKO, J. H.**
Containerless processing of undercooled melts
p 39 N86-10093
- PETERMAN, W.**
Creep-rupture behavior of iron superalloys in high-pressure hydrogen
[NASA-CR-175027] p 89 N86-17531
- PETERS, C. E.**
Mean velocity and turbulence measurements in a 90 deg curved duct with thin inlet boundary layer
[NASA-CR-174811] p 139 N86-16518
- PETERSEN, D. R.**
Life cycle cost assessment of future low heat rejection engines
[SAE PAPER 860444] p 153 A86-37048
- PETERSON, J.**
Buoyancy effects on smoldering combustion
[IAF PAPER 85-289] p 72 A86-15805
- PETERSON, T.**
Fluid management and its role in the future of Space Station
[AIAA PAPER 86-2301] p 47 A86-49553
- PETERSON, T. T.**
Thermocapillary motion research
p 40 N86-10125
- PETRASEK, D. W.**
Thermal-mechanical fatigue test apparatus for metal matrix composites and joint attachments
[NASA-TM-87187] p 88 N86-15378
- PFEL, W. H.**
The application of LQR synthesis techniques to the turbofan engine control problem
p 22 A86-35614
- PIAN, T. H. H.**
Finite elements based on consistently assumed stresses and displacements
p 166 A86-18123
Hybrid solid element with a traction-free cylindrical surface
p 169 A86-34462
- PIERCE, L. A.**
Effect of grain-boundary crystallization on the high-temperature strength of silicon nitride
p 98 A86-33495
- PINKUS, O.**
Performance of oil pumping rings: An analytical and experimental study
[NASA-CR-175083] p 144 N86-31000
- PLATZ, S. J.**
The measurement of aircraft performance and stability and control after flight through natural icing conditions
[NASA-TM-87265] p 35 N86-22582
- PLAYLE, S. C.**
A numerical method for the design and analysis of counter-rotating propellers
[AIAA PAPER 84-1205] p 19 A86-20369
- PONCHAK, D. S.**
Application of intersatellite links to domestic satellite systems
[AIAA PAPER 86-0604] p 44 A86-29580
Application of intersatellite links to domestic satellite systems
[NASA-TM-87215] p 46 N86-16249
- PONCHAK, G. E.**
Monolithic optical integrated control circuitry for GaAs MMIC-based phased arrays
[NASA-TM-87183] p 113 N86-16457
- PONTANO, B. A.**
Communications platform payload definition study
[NASA-CR-174986] p 49 N86-27402
Communications platform payload definition study, executive summary
[NASA-CR-174985] p 49 N86-27407
- POPOVSKI, P.**
Three-dimensional boundary layer on a compressor rotor blade at peak pressure rise coefficient
[ASME PAPER 86-GT-186] p 7 A86-48236
- PORADA, T. W.**
Linearization of digital derived rate algorithm for use in linear stability analysis
p 47 A86-35338
- POUGARE, M.**
Computation of viscous flows in turbomachinery cascades with a space-marching method
p 5 A86-39089
A space-marching method for viscous incompressible internal flows
p 135 A86-43037
- POUCH, J.**
Optical and interfacial electronic properties of diamond-like carbon films
p 204 A86-16268
- POUCH, J. J.**
Ellipsometric and optical study of some uncommon insulator films on 3-5 semiconductors
[NASA-TM-87135] p 205 N86-12134
Carbon films grown from plasma on III-V semiconductors
[NASA-TM-87140] p 205 N86-12135
Auger electron spectroscopy, secondary ion mass spectroscopy and optical characterization of a-C-H and BN films
[NASA-TM-87258] p 206 N86-25268
- POUGARE, M.**
Computation of turbulent flows on rotating bodies and ducts
p 135 A86-46307
- POVINELLI, L.**
Three dimensional flow phenomena in fluid machinery; Proceedings of the Winter Annual Meeting, Miami Beach, FL, November 17-22, 1985
p 4 A86-28682
- POVINELLI, L. A.**
Computation of three-dimensional, rotational flow through turbomachinery blade rows for improved aerodynamic design studies
[ASME PAPER 86-GT-26] p 7 A86-48117
Validation of viscous and inviscid computational methods for turbomachinery components
[ASME PAPER 86-GT-42] p 7 A86-48126
Validation of viscous and inviscid computational methods for turbomachinery components
[NASA-TM-87193] p 10 N86-16194
- POWER, G. D.**
Assessment of a parabolic analysis for axisymmetric internal flows in rocket and turbomachinery ducts
[AIAA PAPER 86-1598] p 134 A86-42739
- PRAKASH, S.**
Pretreatment effects on the morphology and properties of aluminum oxide thermally grown on NiCoCrAlY
p 97 A86-17495
- PRATT, D. T.**
Physical and numerical sources of computational inefficiency in integration of chemical kinetic rate equations: Etiology, treatment and prognosis
[NASA-TP-2590] p 195 N86-28662
- PRESLER, A. F.**
Liquid droplet radiator program at the NASA Lewis Research Center
[ASME PAPER 86-HT-15] p 48 A86-49621
Liquid droplet radiator program at the NASA Lewis Research Center
[NASA-TM-87139] p 48 N86-12246
- PRESZ, W. M., JR.**
Forced mixer lobes in ejector designs
[AIAA PAPER 86-1614] p 134 A86-42752
- PRICE, A. O.**
Free jet feasibility study of a thermal acoustic shield concept for AST/VCE application-dual flow. Comprehensive data report. Volume 1: Test nozzles and acoustic data
[NASA-CR-174817] p 200 N86-23371
Free-jet feasibility study of a thermal acoustic shield concept for AST/VCE application-dual stream nozzles. Comprehensive data report. Volume 2: Laser velocimeter and suppressor. Base pressure data
[NASA-CR-174818] p 201 N86-23372
- PRICE, H. G.**
Proven, long-life hydrogen/oxygen thrust chambers for space station propulsion
[NASA-TM-88822] p 64 N86-32522
- PROCTOR, M. P.**
Combustor flame flashback
[NASA-CR-174961] p 183 N86-14727
- PRZEKWAŚ, A. J.**
Computational simulation of liquid rocket injector anomalies
[AIAA PAPER 86-1424] p 55 A86-42633
- PUDICK, S.**
Develop and test fuel cell powered on-site integrated total energy systems: Phase 3, full-scale power plant development
[NASA-CR-174948] p 182 N86-12757
- Develop and test fuel cell powered on-site integrated total energy systems: Phase 3, full-scale power plant development
[NASA-CR-174996] p 182 N86-12758
- PUGMIRE, T. K.**
A 10,000 hour life multipropellant engine for Space Station applications
[AIAA PAPER 86-1403] p 54 A86-42616
- PULLMAN, B.**
Research and development of neat alcohol fuel usage in automobiles
[NASA-CR-174813] p 108 N86-27460
- PUMPHREY, R.**
Advanced rotary engine components utilizing fiber reinforced Mg castings
[AIAA PAPER 86-1559] p 67 A86-42712
- PURVIS, C. K.**
Energy broadening due to space-charge oscillations in high current electron beams
p 202 A86-22890
- Q**
- QIU, H.**
Theory of homogeneous nucleation - A chemical kinetic view
p 72 A86-19389
- QUENTMEYER, R. J.**
Fabrication of ceramic substrate-reinforced and free forms by mandrel plasma spraying metal-ceramic composites
p 64 A86-17483
- QUEZDOU, M. B.**
Analysis of the transient behavior of rubbing components
[NASA-CR-176546] p 102 N86-19484
- R**
- RADHAKRISHNAN, K.**
New integration techniques for chemical kinetic rate equations. II - Accuracy comparison
[ASME PAPER 85-GT-30] p 75 A86-32958
New integration techniques for chemical kinetic rate equations. I - Efficiency comparison
p 75 A86-38090
Physical and numerical sources of computational inefficiency in integration of chemical kinetic rate equations: Etiology, treatment and prognosis
[NASA-TP-2590] p 195 N86-28662
- RAE, W. J.**
Turbine-stage heat transfer - Comparison of short-duration measurements with state-of-the-art predictions
[AIAA PAPER 86-1465] p 134 A86-42656
Heat-flux measurements for the rotor of a full-stage turbine. II - Description of analysis technique and typical time-resolved measurements
[ASME PAPER 86-GT-78] p 24 A86-48146
- RAJ, R.**
Three-dimensional fluid flow phenomena in the blade end wall corner region
[ASME PAPER 86-GT-179] p 7 A86-48229
- RAJAN, M.**
Parameter sensitivity in the dynamics of rotor-bearing systems
[ASME PAPER 85-DET-35] p 154 A86-38620
- RAMACHANDRA, S. M.**
An approach to the calculation of the pressure field produced by rigid wide chord dual rotation propellers of high solidity in compressible flow
[AIAA PAPER 86-0467] p 198 A86-49566
An analysis for the sound field produced by rigid wide chord dual rotation propellers of high solidity in compressible flow
[NASA-TM-87178] p 11 N86-21517
- RAMACHANDRAN, K.**
Mean velocity and turbulence measurements in a 90 deg curved duct with thin inlet boundary layer
[NASA-CR-174811] p 139 N86-16518
- RAMINS, P.**
Verification of an improved computational design procedure for TWT-dynamic refocuser-MDC systems with secondary electron emission losses
p 119 A86-45194
TWT efficiency enhancement with textured carbon surfaces on copper MDC electrodes
p 120 A86-49617
Verification of computer-aided designs of traveling-wave tubes utilizing novel dynamic refocusers and graphite electrodes for the multistage depressed collector
[NASA-TP-2524] p 121 N86-13643
Secondary-electron-emission losses in multistage depressed collectors and traveling-wave-tube efficiency improvements with carbon collector electrode surfaces
[NASA-TP-2622] p 125 N86-32629
- RAMSAY, S. M.**
Three-dimensional inviscid flow in mixers. I - Mixer analysis using a Cartesian grid
p 5 A86-39090

- Three-dimensional inviscid flow in mixers. II - Analysis of turbofan forced mixers p 6 A86-46316
- RANAUDO, R.**
In-flight measurements of wing ice shapes and wing section drag increases caused by natural icing conditions [NASA-TM-87301] p 12 N86-24667
- RANAUDO, R. J.**
The measurement of aircraft performance and stability and control after flight through natural icing conditions [AIAA PAPER 86-9758] p 35 A86-40681
The measurement of aircraft performance and stability and control after flight through natural icing conditions [NASA-TM-87265] p 35 N86-22582
- RAO VALSETTY, R.**
A new ply model for interlaminar stress analysis p 66 A86-20629
- RAO, B. C. S.**
Erosion of aluminum 6061-T6 under cavitation attack in mineral oil and water p 79 A86-13801
Erosion of phosphor bronze under cavitation attack in a mineral oil p 81 A86-23324
The mechanism of erosion of metallic materials under cavitation attack [NASA-TM-87133] p 156 N86-10552
- RAO, P. V.**
Angular particle impingement studies of thermoplastic materials at normal incidence [ASLE PREPRINT 85-AM-3A-1] p 94 A86-11076
- RAPPAPORT, C. M.**
Optimized three-dimensional lenses for wide-angle scanning p 109 A86-19184
- RATAJCZAK, A. F.**
Photovoltaic systems in remote locations: An experience summary [NASA-TM-87106] p 181 N86-10643
Photovoltaic-powered vaccine refrigerator: Freezer systems field test results [NASA-TM-86972-REV] p 181 N86-11866
- RAULT, D. F. G.**
Radiation energy receiver for solar propulsion systems p 52 A86-18043
- RAY, P. K.**
Characterisation of plasma in a rail gun p 118 A86-26051
- RAZAVI, H. C.**
Bifurcation techniques for nonlinear dynamic analysis of compressor stall phenomena p 22 A86-35403
- REASONER, D. L.**
Energy broadening due to space-charge oscillations in high current electron beams p 202 A86-22890
- REBELLO, C. J.**
Factors influencing the ultrasonic stress wave factor evaluation of composite material structures p 168 A86-34257
- REDD, L.**
Design optimization for a space based, reusable orbit transfer vehicle p 48 N86-17418
- REEHORST, A. L.**
The measurement of aircraft performance and stability and control after flight through natural icing conditions [AIAA PAPER 86-9758] p 35 A86-40681
The measurement of aircraft performance and stability and control after flight through natural icing conditions [NASA-TM-87265] p 35 N86-22582
- REGAN, C. A.**
The determination of the direction of the optic axis of uniaxial crystalline materials [NASA-TM-86892] p 148 N86-22915
- REHFELD, L. W.**
A new ply model for interlaminar stress analysis p 68 A86-20629
- REILLY, C. H.**
The role of service areas in the optimization of FSS orbital and frequency assignments [AIAA PAPER 86-0636] p 45 A86-29599
The role of service areas in the optimization of FSS orbital and frequency assignments [NASA-CR-176488] p 46 N86-18341
Engineering calculations for communications satellite systems planning [NASA-CR-176555] p 114 N86-19493
Broadcasting satellite service synthesis using gradient and cyclic coordinate search procedures [NASA-CR-176708] p 114 N86-23781
- RENGSTORFF, G. W. P.**
Surface effects of corrosive media on hardness, friction, and wear of materials p 94 A86-10825
Interaction of sulfuric acid corrosion and mechanical wear of iron p 81 A86-20436
- RESHOTKO, E.**
Low Reynold's number boundary layers in a disturbed environment [NASA-CR-175031] p 139 N86-17665
- RICE, J. G.**
Simplex finite element analysis of viscous incompressible flow with penalty function formulation p 129 A86-22615
- RICE, S. L.**
Impact wear of iron rich superalloys p 82 A86-34687
- RICHERSON, D. W.**
Comparison of the contact stress and friction behavior of SiC and ZrO2 materials p 95 A86-15237
- RICHEY, A.**
Operational maintenance data base development for kinematic Stirling engines [ASME PAPER 85-DGP-20] p 151 A86-14467
Automotive Stirling Engine Development Program [NASA-CR-174749] p 211 N86-28017
Automotive Stirling engine development program [NASA-CR-175045] p 211 N86-30579
- RICHTER, G. P.**
A long-life 50 lbf H2/O2 thruster for Space Station auxiliary propulsion [AIAA PAPER 86-1404] p 55 A86-42617
Proven, long-life hydrogen/oxygen thrust chambers for space station propulsion [NASA-TM-88822] p 64 N86-32522
- RIECKE, G.**
Automotive Stirling Engine Development Program [NASA-CR-174749] p 211 N86-28017
Automotive Stirling engine development program [NASA-CR-175045] p 211 N86-30579
- RIEGER, J. H.**
Growth and characterization of epitaxial SrF2 on InP(100) p 205 A86-47076
- RIEGER, N. F.**
Vibrations of blades and bladed disk assemblies; Proceedings of the Tenth Biennial Conference on Mechanical Vibration and Noise, Cincinnati, OH, September 10-13, 1985 p 20 A86-26901
- RIEKER, L. L.**
Design of a regenerative fuel cell system for Space Station p 53 A86-24857
- RIFF, R.**
Analysis of large, non-isothermal elastic-visco-plastic deformations [NASA-CR-176220] p 172 N86-10588
Formulation of the nonlinear analysis of shell-like structures, subjected to time-dependent mechanical and thermal loading [NASA-CR-177194] p 178 N86-28462
- RIGSBEE, J. M.**
Character of laser-glazed, plasma-sprayed zirconia coatings on stainless steel substrata p 95 A86-15229
- RILEY, B. R.**
Theoretical study on the effect of the design of small (milli-Newton) thruster jets on molecular contamination for the space station [NASA-CR-177263] p 48 N86-26358
- RILEY, J. J.**
Direct numerical simulations of chemically reacting turbulent mixing layers p 130 A86-25567
Direct numerical simulations of a reacting mixing layer with chemical heat release p 76 A86-41711
- RITCHIEY, W. M.**
The synthesis, characterization and thermal chemistry of modified norbornenyl PMR endcaps p 100 N86-11266
- RIZK, M. H.**
Propeller design by optimization [AIAA PAPER 86-0081] p 19 A86-19678
- ROBACK, R.**
Scalar and momentum turbulent transport experiments with swirling and nonswirling flows p 126 A86-11938
Mass and momentum turbulent transport experiments with swirling confined coaxial jets. II [AIAA PAPER 86-1665] p 134 A86-42780
- ROBERTS, G. D.**
Effect of solution concentration and aging conditions on PMR-15 resin p 98 A86-33113
- ROBERTS, M. L.**
Component-specific modeling p 25 N86-11515
- ROBERTS, T. E.**
Spacecraft multibeam antenna system for 30/20 GHz [NASA-CR-174854] p 116 N86-31760
- ROBERTS, W. B.**
Modeling the 3-D flow effects on deviation angle for axial compressor middle stages [ASME PAPER 85-GT-189] p 2 A86-22102
- ROBERTSON, T. F.**
Methane oxidation behind reflected shock waves: Ignition delay times measured by pressure and flame band emission [NASA-TM-87268] p 77 N86-21635
- ROBINSON, D. N.**
Effects of state recovery on creep buckling under variable loading [NASA-CR-175094] p 212 N86-25310
- ROBINSON, R. S.**
Current collection from the space plasma through defects in solar array insulation p 52 A86-18042
- ROBINSON, W. W.**
Further development of the dynamic gas temperature measurement system [AIAA PAPER 86-1648] p 147 A86-42770
Dynamic gas temperature measurement system p 147 N86-11499
- ROBSON, R. R.**
Designing a 25-kilowatt high frequency series resonant [NASA-CR-176774] p 123 N86-24906
- ROCK, B. A.**
Rapid evaluation of ion thruster lifetime using optical emission spectroscopy [AIAA PAPER 85-2011] p 51 A86-17851
Rapid evaluation of ion thruster lifetime using optical emission spectroscopy [NASA-TM-87103] p 56 N86-10280
- ROCK, S. M.**
Robust detection, isolation, and accommodation for sensor failures p 21 A86-35402
Robust detection, isolation and accommodation for sensor failures [NASA-CR-174825] p 33 N86-30732
- ROGO, C.**
Variable area radial turbine fabrication and test program [NASA-CR-175091] p 32 N86-28947
- ROHDE, J. E.**
Turbine heat transfer p 137 N86-11505
- ROHRER, V. S.**
Mass spectrometric studies of the electrical breakdown of thin polymer films p 100 A86-47070
- ROMAN, R. F.**
Textured carbon surfaces on copper by sputtering [NASA-CASE-LEW-14130-1] p 109 N86-32587
- RONNEY, P. D.**
Effect of gravity on laminar premixed gas combustion. I - Flammability limits and burning velocities p 72 A86-12413
Effect of gravity on laminar premixed gas combustion. II - Ignition and extinction phenomena p 72 A86-12414
- RORABAUGH, M. E.**
Processing study of injection molding of silicon nitride for engine applications [SAE PAPER 851787] p 154 A86-38311
- ROSE, J. H.**
Universality in the compressive behavior of solids [NASA-TM-87303] p 206 N86-28775
Temperature effects on the universal equation of state of solids [NASA-TM-87321] p 206 N86-28776
- ROSE, T.**
Modal test/analysis correlation for Centaur G Prime launch vehicle [AIAA PAPER 86-1002] p 43 A86-38943
- ROSEN, M. C.**
Simplex finite element analysis of viscous incompressible flow with penalty function formulation p 129 A86-22615
- ROSENTHAL, I.**
Radical molecule and ion-molecule mechanisms in the polymerization of hydrocarbons and chlorosilanes in R.F. plasmas at low pressures (below 1.0 Torr) p 203 A86-16254
- ROSFJORD, T. J.**
Role of fuel chemical properties on combustor radiative heat load [NASA-CR-177096] p 108 N86-30023
- ROSNER, D. E.**
Thermophoretically augmented mass transfer rates to solid walls across laminar boundary layers p 128 A86-20150
- ROSS, R.**
De-icing of the altitude wind tunnel turning vanes by electro-magnetic impulse [NASA-CR-177260] p 38 N86-27291
- ROSTAFINSKI, W.**
Analysis of fully stalled compressor [AIAA PAPER 86-1123] p 5 A86-38480
Analysis of fully stalled compressor [NASA-TM-87254] p 11 N86-20357
- ROTH, D. J.**
Radiographic detectability limits for seeded voids in sintered silicon carbide and silicon nitride p 162 A86-31745
Reliability of void detection in structural ceramics by use of scanning laser acoustic microscopy p 163 A86-39027
Quantitative flaw characterization with scanning laser acoustic microscopy p 163 A86-45150

- Reliability of scanning laser acoustic microscopy for detecting internal voids in structural ceramics
[NASA-TM-87164] p 147 A86-48353
- Probability of detection of internal voids in structural ceramics using microfocus radiography
[NASA-TM-87164] p 164 N86-13749
- Reliability of scanning laser acoustic microscopy for detecting internal voids in structural ceramics
[NASA-TM-87222] p 164 N86-16599
- Quantitative flaw characterization with scanning laser acoustic microscopy p 200 N86-22983
- Factors that affect reliability of nondestructive detection of flaws in structural ceramics
[NASA-TM-87348] p 166 N86-31912
- Quantitative void characterization in structural ceramics using scanning laser acoustic microscopy
[NASA-TM-88797] p 166 N86-31913
- RUBINSTEIN, R.**
Structural tailoring of SSME turbopump blades (SSME/STAEBL)
[AIAA PAPER 86-0847] p 54 A86-38895
- RUDMAN, T. J.**
Advanced orbit transfer vehicle propulsion system study
[NASA-CR-174843] p 60 N86-24746
- RUPPRECHT, S. D.**
Flow and atomization in flashing injectors
p 136 A86-49442
- RUSSEL, W. B.**
Transport processes research p 40 N86-10129
- RUSSELL, L. M.**
Local heat-transfer measurements on a large scale-model turbine blade airfoil using a composite of a heater element and liquid crystals
[ASME PAPER 85-GT-59] p 126 A86-13061
- RUSSELL, P. G.**
Bipolar nickel-hydrogen battery development
p 180 A86-24823
- RUTLEDGE, S. K.**
Ion beam sputter-deposited thin film coatings for protection of spacecraft polymers in low earth orbit
[AIAA PAPER 85-0420] p 95 A86-14428
- Ion beam sputter etching
[NASA-CASE-LEW-13899-1] p 109 N86-20587
- S**
- SACKS, M. D.**
Properties of silicon suspensions and slip-cast bodies
p 95 A86-15238
- SADLER, G. G.**
DEAN - A program for Dynamic Engine Analysis
[AIAA PAPER 85-1354] p 18 A86-14430
- A sensor failure simulator for control system reliability studies
[NASA-TM-87271] p 124 N86-31792
- SADOSKI, D. M.**
The effects of syntactic complexity on the human-computer interaction p 192 A86-36172
- SAFFMAN, P. G.**
Finite-amplitude steady waves in plane viscous shear flows
[AD-A165461] p 127 A86-19419
- SAIN, M.**
Polynomic nonlinear dynamical systems - A residual sensitivity method for model reduction
p 194 A86-35386
- SAIN, M. K.**
Nonlinear optimal control with tensors - Some computational issues p 194 A86-35419
- SAITO, N.**
Research and development of neat alcohol fuel usage in automobiles
[NASA-CR-174813] p 108 N86-27460
- SALEM, J. A.**
Fractured toughness of Si₃N₄ measured with short bar chevron-notched specimens
[NASA-TM-87153] p 101 N86-13495
- SALIK, J.**
Computer simulation of thin-film nucleation and growth - The multilayer mode p 204 A86-37441
- Stability of surface nucleation
[NASA-TM-88806] p 207 N86-30556
- Ion-beam nitriding of steels
[NASA-CASE-LEW-14104-2] p 93 N86-32556
- SALIKUDDIN, M.**
An experimental study of tone-excited heated jets
p 197 A86-31593
- Non-linear effects in finite amplitude wave propagation through ducts and nozzles p 197 A86-35857
- Development of an impulsive noise source to study the acoustic reflection characteristics of hard-walled wind tunnels
[AIAA PAPER 86-1887] p 198 A86-45500
- Acoustic reflection contamination measurements in the 16-foot NASA Langley Transonic Wind Tunnel
[AIAA PAPER 86-1888] p 198 A86-45501
- SALTSMAN, J. F.**
An update of the total-strain version of SRP
[NASA-TP-2499] p 87 N86-12295
- Structural analysis of turbine blades using unified constitutive models
[NASA-TM-88807] p 178 N86-28461
- SALZMAN, J.**
Fluid management and its role in the future of Space Station
[AIAA PAPER 86-2301] p 47 A86-49553
- SAMANTA, S. C.**
Transformation toughened ceramics for the heavy duty diesel engine technology program, phase 2
[NASA-CR-175054] p 210 N86-22451
- SANDERCOCK, D. M.**
Modeling the 3-D flow effects on deviation angle for axial compressor middle stages
[ASME PAPER 85-GT-189] p 2 A86-22102
- Fluid machines: Expanding the limits, past and future
[NASA-TM-87161] p 26 N86-12227
- SANDERS, W. A.**
Effect of grain-boundary crystallization on the high-temperature strength of silicon nitride
p 98 A86-33495
- Strength and microstructure of Si₃N₄ sintered with ZrO₂ additions p 99 A86-36330
- Correlation of processing and sintering variables with the strength and radiography of silicon nitride
[NASA-TM-87251] p 106 N86-31729
- SANDOR, B. I.**
The plastic compressibility of 7075-T651 aluminum-alloy plate p 85 A86-49690
- SANGER, N. L.**
Comparison of calculated and experimental cascade performance for controlled-diffusion compressor stator blading
[NASA-TM-87167] p 27 N86-16219
- SANI, R. L.**
Finite element simulation of temperature dependent free surface flows p 136 A86-47012
- Thermocapillary and diffusocapillary migration of a fluid drop p 40 N86-10128
- SANTORO, G. J.**
Determination of convective diffusion heat/mass transfer rates to burner rig test targets comparable in size to cross-stream jet diameter
[ASME PAPER 86-GT-68] p 136 A86-48140
- Determination of convective diffusion heat/mass transfer rates to burner rig test targets comparable in size to cross-stream jet diameter
[NASA-TM-87178] p 138 N86-13678
- Experiments for the determination of convective diffusion heat/mass transfer to burner rig test targets comparable in size to jet stream diameter
[NASA-TM-87196] p 139 N86-18646
- Experimental verification of corrosive vapor deposition rate theory in high velocity burner rigs
[NASA-TM-87287] p 141 N86-22890
- SANZ, G. M.**
Flow visualization of secondary flows in three curve ducts
[ASME PAPER 86-GT-166] p 136 A86-48218
- SANZ, J. M.**
Wind tunnel turning vanes of modern design
[AIAA PAPER 86-0044] p 36 A86-19654
- Wind tunnel turning vanes of modern design
[NASA-TM-87146] p 37 N86-12239
- SARIQUL, N.**
Computer aided derivation of equations for composite mechanics problems and finite element analyses
[AIAA PAPER 86-1016] p 170 A86-38873
- SARMA, G. R.**
Ramp-integration technique for capacitance-type blade-tip clearance measurement
[NASA-TM-87241] p 149 N86-24964
- SARRAFZADEH-KHOEE, A.**
A study of the stress wave factor technique for nondestructive evaluation of composite materials
[NASA-CR-4002] p 165 N86-28445
- SARV, H.**
Analysis of the effects of fuel spray characteristics on NO(x) formation
[ASME PAPER 85-WA/HT-47] p 107 A86-38394
- Oxides of nitrogen emissions from the combustion of monodisperse liquid fuel sprays
[NASA-CR-176373] p 191 N86-14770
- SAUNDERS, N. T.**
Future directions in aeropropulsion technology
p 1 A86-11602
- SAUNIER, P.**
10-30 GHz monolithic GaAs travelling-wave divider/combiner p 118 A86-34882
- SAVAGE, M.**
Life and reliability modeling of bevel gear reductions
[ASME PAPER 85-DE-7] p 151 A86-14466
- Fatigue life analysis of a turboprop reduction gearbox
[ASME PAPER 85-DET-10] p 155 A86-45256
- System life and reliability modeling for helicopter transmissions
[NASA-CR-3967] p 159 N86-24990
- SAVILLE, D. A.**
Transport processes research p 40 N86-10129
- Electrohydrodynamics p 41 N86-10130
- SAVINELL, R. F.**
Theoretical and experimental flow cell studies of a hydrogen-bromine fuel cell, part 1
[NASA-CR-177165] p 189 N86-29409
- SAVINO, J. M.**
Vortex generators as a means for increasing rotor performance p 4 A86-24820
- Summary of tower designs for large horizontal axis wind turbines
[NASA-TM-87166] p 186 N86-18776
- SAWITZ, P.**
Spectrum orbit utilization program technical manual SOUP5 Version 3.8
[NASA-CR-174944] p 116 N86-26489
- Spectrum Orbit Utilization Program documentation: SOUP5 version 3.8 user's manual, volume 1, chapters 1 through 5
[NASA-CR-174889] p 193 N86-27927
- Spectrum Orbit Utilization Program documentation: SOUP5 version 3.8 user's manual, volume 2, appendices A through G
[NASA-CR-174890] p 193 N86-27928
- SCHAEFER, J. H.**
A sensor failure simulator for control system reliability studies
[NASA-TM-87271] p 124 N86-31792
- SCHARRER, J.**
Theory versus experiment for the rotordynamic coefficients of annular gas seals. I - Test facility and apparatus
[ASME PAPER 85-TRIB-1] p 152 A86-24481
- SCHARRER, J. K.**
Experimental rotordynamic coefficient results for teeth-on-rotor and teeth-on-stator labyrinth gas seals
[ASME PAPER 86-GT-12] p 156 A86-48109
- SCHATZ, M. F.**
Heaterless ignition of inert gas ion thruster hollow cathodes
[AIAA PAPER 85-2008] p 51 A86-17833
- SCHER, D.**
Small, two-stage, partial-admission turbine
p 57 N86-17386
- SCHIFFELLE, G. W.**
Properties of silicon suspensions and slip-cast bodies
p 95 A86-15238
- SCHERTLER, R. J.**
ACTS Experiments Program
[NASA-TM-88820] p 47 N86-31625
- SCHUEERMAN, C. M.**
Creep rupture behavior of Stirling engine materials
[NASA-TM-87209] p 88 N86-15380
- SCHINSTOCK, W. C.**
The measurement of aircraft performance and stability and control after flight through natural icing conditions
[NASA-TM-87265] p 35 N86-22582
- SCHLUETER, R. A.**
Effect of accuracy of wind power prediction on power system operator
[NASA-CR-176300] p 181 N86-11667
- SCHMIDT, R. J.**
Theoretical and software considerations for general dynamic analysis using multilevel substructured models
[NASA-CR-176822] p 195 N86-26067
- SCHNEIDER, W.**
Small engine technology payoffs for future commuter aircraft
[AIAA PAPER 86-1544] p 23 A86-42703
- SCHOCK, H. J.**
A two-dimensional numerical study of the flow inside the combustion chambers of a motored rotary engine
[NASA-TM-87212] p 10 N86-19289
- The determination of the direction of the optic axis of uniaxial crystalline materials
[NASA-TM-86892] p 148 N86-22915
- Visualization of flows in a motored rotary combustion engine using holographic interferometry
[NASA-TM-88804] p 33 N86-31583
- SCHOENMAN, L.**
An experimental data base for material selection and design of high-speed, high-pressure, oxygen turbomachinery
p 58 N86-17387
- SCHRAG, R. L.**
Theoretical analysis of the electrical aspects of the basic electro-impulse problem in aircraft de-icing applications
[NASA-CR-176808] p 17 N86-26330

- Analyses and tests for design of an electro-impulse de-icing system
[NASA-CR-174919] p 15 N86-27268
- SCHREIBER, J.**
RE-1000 free-piston Stirling engine update
p 153 A86-24890
- SCHREIBER, J. G.**
RE-1000 free-piston Stirling engine update
[NASA-TM-87126] p 182 N86-11668
- SCHUBEN, D.**
Jet fuel viscosity at low temperatures with notes on n-alkaline crystals
[NASA-CR-174911] p 15 N86-30022
- SCHULLER, F. T.**
Lubrication and performance of high-speed rolling-element bearings p 152 A86-19375
Testing of YUH-61A helicopter transmission in NASA Lewis 2240-kW (3000-hp) facility
[NASA-TP-2538] p 160 N86-24992
Feasibility study of a discrete bearing/roller drive rotary joint for the space station
[NASA-TM-88800] p 161 N86-30206
- SCHULSON, E. M.**
The effects of grain size on the flow and fracture of long-range ordered alloys p 84 A86-47243
- SCHULTZ, D.**
HOST liner cyclic facilities p 173 N86-11519
- SCHULTZ, K. P.**
Numerical synthesis of tri-variate velocity realizations of turbulence p 168 A86-28654
- SCHULZ, H. D.**
A novel centrifugal diffuser test device
[ASME PAPER 85-IGT-135] p 3 A86-23927
- SCHUMANN, L.**
A novel centrifugal diffuser test device
[ASME PAPER 85-IGT-135] p 3 A86-23927
- SCHUMANN, L. F.**
A three-dimensional axisymmetric calculation procedure for turbulent flows in a radial vaneless diffuser
[ASME PAPER 85-GT-133] p 3 A86-22733
Effect of area ratio on the performance of a 5.5:1 pressure ratio centrifugal impeller
[ASME PAPER 86-GT-303] p 8 A86-48315
Effect of area ratio on the performance of a 5.5:1 pressure ratio centrifugal impeller
[NASA-TM-87237] p 10 N86-19290
- SCHWARTZ, R. A.**
Large-Scale Advanced Prop-Fan (LAP) pitch change actuator and control design report
[NASA-CR-174788] p 31 N86-27282
- SCHWARZE, G. E.**
Performance analysis of radiation cooled dc transmission lines for high power space systems
p 117 A86-24811
- SCHWEIKHARD, W. G.**
An analysis of cross-coupling of a multicomponent jet engine test stand using finite element modeling techniques
[NASA-CR-176424] p 37 N86-15323
Statistical prediction of dynamic distortion of inlet flow using minimum dynamic measurement. An application to the Melick statistical method and inlet flow dynamic distortion prediction without RMS measurements
[NASA-CR-176764] p 142 N86-24933
Review and evaluation of recent developments in melic inlet dynamic flow distortion prediction and computer program documentation and user's manual estimating maximum instantaneous inlet flow distortion from steady-state total pressure measurements with full, limited, or no dynamic data
[NASA-CR-176765] p 143 N86-24955
- SCHWIND, G. A.**
The effect of oxygen pressure on volatility and morphology of LaB6 single crystal cathodes
p 204 A86-28076
- SCIBBE, H. W.**
Operating characteristics of a 0.87 kW-hr flywheel energy storage module p 152 A86-24864
Lubricant and additive effects on spur gear fatigue life
[ASME PAPER 85-TRIB-14] p 155 A86-43542
- SCOTT, J. N.**
Numerical simulation of unsteady flow in an axisymmetric shear layer
[AIAA PAPER 86-0202] p 127 A86-19746
Numerical simulation of the flowfield over ice accretion shapes
[NASA-CR-176960] p 144 N86-30093
- SCOTT, W. F.**
Spacecraft multibeam antenna system for 30/20 GHz
[NASA-CR-174654] p 116 N86-31760
- SEASHOLTZ, R. G.**
Three component velocity measurements using Fabry-Perot interferometer p 145 A86-16378
Filter induced errors in laser anemometry using counter-processor p 146 A86-34431
- Laser anemometry for hot section applications
p 151 N86-11503
- Combined fringe and Fabry-Perot laser anemometer for three component velocity measurements in turbine stator cascade facility
[NASA-TM-87322] p 149 N86-24967
- SEGALL, B.**
Compensation in epitaxial cubic SiC films
[NASA-TM-87269] p 206 N86-25267
- SEIDEL, R. C.**
Development and application of dynamic simulations of a subsonic wind tunnel
[AIAA PAPER 86-0758] p 36 A86-24745
Development and application of dynamic simulations of a subsonic wind tunnel
[NASA-TM-87211] p 43 N86-18338
- SENNEFF, J. M.**
A long-life 50 lb H₂/O₂ thruster for Space Station auxiliary propulsion
[AIAA PAPER 86-1404] p 55 A86-42617
- SERAFINI, T. T.**
Aerospace applications of PMR polyimide composites
p 67 A86-27730
Surface protection of graphite fabric/PMR-15 composites subjected to thermal oxidation
p 68 N86-11281
Polymer, metal and ceramic matrix composites for advanced aircraft engine applications
[NASA-TM-87132] p 87 N86-13407
- SEROVY, G. K.**
Modeling the 3-D flow effects on deviation angle for axial compressor middle stages
[ASME PAPER 85-GT-189] p 2 A86-22102
- SETTLES, G. S.**
Recent skin friction techniques for compressible flows
[AIAA PAPER 86-1099] p 147 A86-38460
- SHAFFERNOCKER, W. M.**
1700 deg C optical temperature sensor
[NASA-CR-175108] p 203 N86-28729
- SHAKER, F.**
Modal test/analysis correlation for Centaur G Prime launch vehicle
[AIAA PAPER 86-1002] p 43 A86-38943
- SHALKHAUSER, K. A.**
Test results for 20-GHz GaAs FET spacecraft power amplifier
[NASA-TM-87072] p 111 N86-10379
- SHALTENS, R. K.**
Automotive Stirling summary and overview
[NASA-TM-87177] p 209 N86-21457
Stirling Powered Van Program overview
[NASA-TM-87227] p 210 N86-25303
NASA/DOE automotive Stirling engine project: Overview 1986
[NASA-TM-87345] p 211 N86-29731
- SHAMROTH, S. J.**
Calculations of two and three-dimensional transonic cascade flow fields using the Navier-Stokes equations
[ASME PAPER 85-GT-66] p 2 A86-22046
- SHAMSEDDIN, H.**
Rotary transformer design with fixed magnetizing and/or leakage inductances p 119 A86-40462
- SHANKAR, N. R.**
Neutron and X-ray diffraction of plasma-sprayed zirconia-yttria thermal barrier coatings p 96 A86-16269
- SHANNON, J. L., JR.**
Analysis of an externally radially crack ring segment subject to three-point radial loading p 167 A86-20710
Fractured toughness of Si3N4 measured with short bar chevron-notched specimens
[NASA-TM-87153] p 101 N86-13495
- SHAPIRO, W.**
Advanced seals for Liquid Oxygen (LOX) turbopumps
p 157 N86-17408
- SHAW, J. M.**
Research and competition: Best partners
[NASA-TM-87313] p 212 N86-25321
- SHAW, L. M.**
Unsteady pressure measurements on a biconvex airfoil in a transonic oscillating cascade
[ASME PAPER 85-GT-212] p 3 A86-22731
- SHAW, N. J.**
Structure and grain coarsening during the sintering of alumina p 98 A86-26341
- SHAW, R.**
Ice shapes and the resulting drag increase for a NACA 0012 airfoil
[AIAA PAPER 84-0109] p 14 A86-14427
- SHAW, R. J.**
The aerodynamics of rotor blades with ice shapes accreted in hover and in level flight p 5 A86-35655
The performance characteristics of simulated ice on rotorcraft airfoils p 14 A86-35656
Performance degradation of helicopters due to icing - A review p 16 A86-35668
- NASA's aircraft icing analysis program
p 14 A86-49107
- NASA's Aircraft Icing Analysis Program
[NASA-CR-398791] p 15 N86-31544
- SHAWVER, J. W.**
Transmission line design for a power distribution system at 20 kHz for aircraft
[NASA-CR-3987] p 32 N86-29818
- SHEFFLER, K. D.**
Thermal barrier coating life prediction mode development
[NASA-CR-175087] p 103 N86-22713
- SHERMAN, F. S.**
Grid-free simulation of diffusion using random walk methods p 196 A86-16521
- SHERMAN, M.**
High temperature dispersion strengthening of NIAI
[NASA-CR-175073] p 90 N86-22688
- SHIH, T. I. P.**
A two-dimensional numerical study of the flow inside the combustion chambers of a motored rotary engine
[NASA-TM-87212] p 10 N86-19289
- SHIH, T. I.-P.**
Fluid flow and fuel-air mixing in a motored two-dimensional Wankel rotary engine
[AIAA PAPER 86-1556] p 134 A86-42711
- SHILLER, P. J.**
Composition and properties of the so-called 'diamond-like' amorphous carbon films p 96 A86-16255
- SHREEVE, R. P.**
A novel centrifugal diffuser test device
[ASME PAPER 85-IGT-135] p 3 A86-23927
Comparison of calculated and experimental cascade performance for controlled-diffusion compressor stator blading
[NASA-TM-87167] p 27 N86-16219
- SHUEN, J. S.**
Prediction of the structure of fuel sprays in gas turbine combustors
[NASA-CR-175028] p 27 N86-16218
- SHUEN, J.-S.**
Structure of nonevaporating sprays. II - Drop and turbulence properties p 125 A86-11237
Drop-turbulence interactions in a diffusion flame p 73 A86-20139
Prediction of the structure of fuel sprays in gas turbine combustors
[AIAA PAPER 86-0450] p 20 A86-26636
- SHYNE, R. J.**
Experimental evaluation of two turning vane designs for high-speed corner of 0.1-scale model of NASA Lewis Research Center's proposed altitude wind tunnel
[NASA-TP-2570] p 38 N86-28101
Comparison of analytical and experimental performance of a wind-tunnel diffuser section
[NASA-TM-88795] p 13 N86-31537
- SIDI, A.**
Acceleration of convergence of vector sequences
p 195 A86-49850
- SIEGEL, R.**
Boundary perturbation method for free boundary problem in convectively cooled continuous casting
p 131 A86-28649
Free boundary shape of a convectively cooled solidified region p 131 A86-29029
- SIGARI, G.**
Effect of accuracy of wind power prediction on power system operator
[NASA-CR-176300] p 181 N86-11667
- SIGMAN, R. K.**
An iterative finite element-integral technique for predicting sound radiation from turbofan inlets in steady flight p 198 A86-49806
- SILVER, D.**
Uniform engine testing program phase 7: NASA Lewis Research Center second entry
[NASA-TM-87272] p 31 N86-28085
- SIMETKOSKY, M.**
Automotive Stirling Engine Development Program
[NASA-CR-174749] p 211 N86-28017
Automotive Stirling engine development program
[NASA-CR-175045] p 211 N86-30579
- SIMITSES, G. J.**
Bounding solutions of geometrically nonlinear viscoelastic problems
[AIAA PAPER 86-0943] p 170 A86-38838
Analysis of large, non-isothermal elastic-visco-plastic deformations
[NASA-CR-176220] p 172 N86-10588
Bounding solutions of geometrically nonlinear viscoelastic problems
[NASA-CR-176219] p 195 N86-10860

- Formulation of the nonlinear analysis of shell-like structures, subjected to time-dependent mechanical and thermal loading
[NASA-CR-177194] p 178 N86-28462
- SIMON, T. W.**
Heat transfer and fluid mechanics measurements in transitional boundary layer flows
[ASME PAPER 85-GT-113] p 126 A86-13068
- SIMONEAU, R. J.**
Preliminary results of a study of the relationship between free stream turbulence and stagnation region heat transfer
[ASME PAPER 85-GT-84] p 129 A86-22055
Heat transfer in space power and propulsion systems p 53 A86-26492
Unsteady heat transfer and direct comparison to steady-state measurements in a rotor-wake experiment
[NASA-TM-87220] p 142 N86-24934
- SIMONEU, R. J.**
Effect of a rotor wake on the local heat transfer on the forward half of a circular cylinder
[NASA-TM-87234] p 140 N86-21794
- SIMONS, R. N.**
Analysis of optically controlled microwave/millimeter wave device structures
[NASA-TM-87246] p 123 N86-24907
- SINCLAIR, J. H.**
Longitudinal compressive failure modes in fiber composites End attachment effects on ITRI type test specimens p 66 A86-19999
- SINGER, J.**
Evaluation parameters for the alkaline fuel cell oxygen electrode
[NASA-TM-87155] p 77 N86-12268
- SINGH, B.**
Year 2000 small engine technology payoffs in cruise missiles
[AIAA PAPER 86-1546] p 23 A86-42705
- SINGHAL, A. K.**
Computational simulation of liquid rocket injector anomalies
[AIAA PAPER 86-1424] p 55 A86-42633
- SINGHAL, S. P.**
Neutron and X-ray diffraction of plasma-sprayed zirconia-yttria thermal barrier coatings p 96 A86-16269
- SINGNOI, W. N.**
An analysis of cross-coupling of a multicomponent jet engine test stand using finite element modeling techniques
[NASA-CR-176424] p 37 N86-15323
- SINHA, A.**
Stability of limit cycles in frictionally damped and aerodynamically unstable rotor stages p 18 A86-19198
Influence of friction dampers on torsional blade flutter
[ASME PAPER 85-GT-170] p 21 A86-32957
- SINHA, N.**
Two dimensional, transient catalytic combustion of CO-air on platinum p 71 A86-10201
- SINHAROV, S.**
Growth and characterization of epitaxial SrF₂ on InP(100) p 205 A86-47076
- SIRIGNANO, W. A.**
Ignition and flame spread above liquid fuel pools p 41 N86-10163
- SISTO, F.**
Influence of rotation and pretwist on cantilever fan blade flutter p 17 A86-11686
- SITARAM, N.**
End-wall and profile losses in a low-speed axial flow compressor rotor
[ASME PAPER 85-GT-174] p 20 A86-22090
- SLABY, J. G.**
Overview of the 1985 NASA Lewis Research Center SP-100 free-piston Stirling engine activities p 153 A86-24884
Overview of free-piston Stirling technology at the NASA Lewis Research Center p 208 N86-13236
Overview of free-piston Stirling SP-100 activities at the NASA Lewis Research Center p 209 N86-19264
Overview of the 1986 free-piston Stirling SP-100 activities at the NASA Lewis Research Center p 210 N86-26261
Overview of NASA Lewis Research Center free-piston Stirling engine technology activities applicable to space power systems p 211 N86-29732
- SLINEY, H. E.**
The use of silver in self-lubricating coatings for extreme temperatures p 99 A86-44425
Composition optimization of self-lubricating chromium carbide-based composite coatings for use to 760 deg C
[NASA-TM-87261] p 103 N86-20568
- A new chromium carbide-based tribological coating for use to 900 deg C with particular reference to the Stirling engine
[NASA-TM-87274] p 103 N86-21682
Adequacy of surface analytical tools for studying the tribology of ceramics
[NASA-TM-87308] p 104 N86-24837
Tribology of selected ceramics at temperatures to 900 deg C
[NASA-TM-87267] p 105 N86-25476
Characterization of the tribological coating composition 77 wt % CaF₂ - 23 wt % Li F fused to IN-750 alloy
[NASA-TM-87342] p 105 N86-27452
- SMETANA, J.**
MMIC antenna technology development in the 30/20 gigahertz band
[AIAA PAPER 86-0666] p 45 A86-29628
Characterization of MMIC devices for active array antennas p 111 N86-11401
MMIC antenna technology development in the 30/20 gigahertz band
[NASA-TM-87182] p 46 N86-17368
- SMIALEK, J. L.**
Burner rig corrosion of SiC at 1000 C p 99 A86-36328
High temperature oxidation of beta-NiAl p 85 A86-47266
Molten salt corrosion of SiC: Pitting mechanism
[NASA-TM-87143] p 101 N86-12310
Current viewpoints on oxide adherence mechanisms
[NASA-TM-87168] p 87 N86-13409
- SMITH, D. A.**
Acceleration of convergence of vector sequences p 195 A86-49850
- SMITH, G.**
Operational maintenance data base development for kinematic Stirling engines
[ASME PAPER 85-DGP-20] p 151 A86-14467
Automotive Stirling Engine Development Program
[NASA-CR-174749] p 211 N86-28017
Automotive Stirling engine development program
[NASA-CR-175045] p 211 N86-30579
- SMITH, J. R.**
Universality in the compressive behavior of solids
[NASA-TM-87303] p 206 N86-28775
Temperature effects on the universal equation of state of solids
[NASA-TM-87321] p 206 N86-28776
- SMITH, P. J.**
Operating aspects of an oil pumping ring seal
[ASME PAPER 85-TRIB-29] p 153 A86-34010
- SMITHRICK, J. J.**
Initial performance of advanced designs for IPV nickel-hydrogen cells p 179 A86-24800
Oxygen recombination in individual pressure vessel nickel-hydrogen batteries
[NASA-CASE-LEW-13822-1] p 188 N86-25874
Effect of impregnation method on cycle life of the nickel electrode
[NASA-TM-87326] p 190 N86-31980
- SMYTHE, M.**
Improved perfluoroalkylether fluid development
[NASA-TM-87276] p 104 N86-25474
- SMYTHE, M. E.**
The effects of metals and inhibitors on thermal oxidative degradation reactions of unbranched perfluoroalkyl ethers p 99 A86-40682
- SNOW, D. W.**
Stress analysis of gas turbine engine structures using the boundary element method p 169 A86-34444
- SNYDER, C.**
Ignition delay times of benzene and toluene with oxygen in argon mixtures
[NASA-TM-87312] p 78 N86-25431
- SNYDER, C. A.**
A parametric study of a gas-generator airturbo ramjet (ATR)
[NASA-TM-88808] p 34 N86-31586
- SO, R. M. C.**
Concentration distributions in cylindrical combustors p 126 A86-11937
A comparison of three algebraic stress closures for combustor flow calculations
[ASME PAPER 85-WA/FE-3] p 132 A86-38388
Concentration distributions in a model combustor p 133 A86-38575
Local equilibrium assumption for round jet calculations p 136 A86-49829
On the modeling of low-Reynolds-number turbulence
[NASA-CR-3994] p 32 N86-28069
- SOCKOL, P. M.**
Coupling conditions for integrating boundary layer and rotational inviscid flow p 133 A86-41721
- SOEDER, R. H.**
Summary of investigations of engine response to distorted inlet conditions
[NASA-TM-87317] p 30 N86-26336
- SOHRAB, S. H.**
An experimental investigation on flame interaction and the existence of negative flame speeds p 74 A86-22816
Theory of interactive combustion of counterflow premixed flames p 74 A86-32752
- SOKOLOV, V.**
Ka-band monolithic gain control amplifier p 119 A86-41343
- SOKOLOWSKI, D. E.**
Toward improved durability in advanced combustors and turbines - Progress in prediction of thermomechanical loads
[ASME PAPER 86-GT-172] p 24 A86-48224
Turbine engine Hot Section Technology (HOST) project p 173 N86-11496
- SOLIDUM, E.**
Fabrication of ceramic components for advanced gas turbine engines
[SAE PAPER 851786] p 154 A86-38310
- SOLOMON, A. S. P.**
Structure of nonevaporating sprays. II - Drop and turbulence properties p 125 A86-11237
Drop-turbulence interactions in a diffusion flame p 73 A86-20139
Flow and atomization in flashing injectors p 136 A86-49442
- SOOD, P. K.**
Power conversion distribution system using a resonant high-frequency AC link
[NASA-CR-176804] p 123 N86-25694
- SOSOKA, D. J.**
Study of journal bearing dynamics using 3-dimensional motion picture graphics
[NASA-TM-87205] p 140 N86-18647
- SOUTH, W. K.**
Evaluation of capillary reinforced composites
[NASA-CR-175061] p 70 N86-24760
- SOVEY, J. S.**
A 10,000 hour life multipropellant engine for Space Station applications
[AIAA PAPER 86-1403] p 54 A86-42616
Performance and endurance tests of a multipropellant resistojet for space station auxiliary propulsion
[AIAA PAPER 86-1435] p 55 A86-42640
Vacuum chamber pressure effects on thrust measurements p 59 N86-17425
Compatibility experiments of facilities, materials, and propellants for electrothermal thrusters p 59 N86-17426
Oxidation protection coatings for polymers
[NASA-CASE-LEW-14072-1] p 102 N86-19458
A bibliography of electrothermal thruster technology, 1984 p 60 N86-21578
Performance and endurance tests of a multipropellant resistojet for space station auxiliary propulsion
[NASA-TM-87278] p 60 N86-24748
Oxidation protecting coatings for polymers
[NASA-CASE-LEW-14072-3] p 105 N86-26434
Apparatus for producing oxidation protection coatings for polymers
[NASA-CASE-LEW-14072-2] p 106 N86-32569
- SPADACCINI, L. J.**
Deposit formation and heat-transfer characteristics of hydrocarbon rocket fuels p 106 A86-10028
- SPALVINS, T.**
Frictional and morphological properties of Au-MoS₂ films sputtered from a compact target p 152 A86-16258
Metallic glass as a temperature sensor during ion plating p 80 A86-16906
Frictional and structural characterization of ion-nitrided low and high chromium steels p 81 A86-17477
Tribological properties of boron nitride synthesized by ion beam deposition p 96 A86-17479
Tribological characteristics of gold films deposited on metals by ion plating and vapor deposition p 85 A86-49600
- SPANOS, P.-T. D.**
Numerical synthesis of tri-variate velocity realizations of turbulence p 168 A86-28654
- SPEAR, K. E.**
Experimental and theoretical analysis of chemical vapor deposition with prediction of gravity effects p 41 N86-10132
- SPENCE, R. L.**
Application of intersatellite links to domestic satellite systems
[AIAA PAPER 86-0604] p 44 A86-29580
Application of intersatellite links to domestic satellite systems
[NASA-TM-87215] p 46 N86-16249

- SPICA, P. W.**
Evaluation of a hybrid hydrostatic bearing for cryogenic turbopump application [NASA-TM-87255] p 63 N86-31649
- SPINDT, C. A.**
Development program on a cold cathode electron gun [NASA-CR-174792] p 121 N86-14499
- SPRAWLEY, J. E.**
Analysis of an externally radially crack ring segment subject to three-point radial loading p 187 N86-20710
Mode II fatigue crack growth specimen development p 171 N86-43566
- SRINIVASAN, A. V.**
Dynamic characteristics of an assembly of prop-fan blades [ASME PAPER 85-GT-134] p 21 N86-32956
Advanced turboprop vibratory characteristics [NASA-CR-174708] p 30 N86-24893
- SRINIVASAN, M.**
Sintered alpha silicon carbide ceramics for high temperature structural application - Status review and recent developments [ASME PAPER 85-IGT-127] p 97 N86-23921
- SRINIVASAN, R.**
Modeling dilution of jet flowfields p 128 N86-20362
Perspectives on dilution jet mixing [AIAA PAPER 86-1611] p 25 N86-49614
Dilution jet mixing program, supplementary report [NASA-CR-175043] p 141 N86-23856
Dilution jet mixing program, phase 3 [NASA-CR-174884] p 142 N86-24938
Perspectives on dilution jet mixing [NASA-TM-87294] p 35 N86-32432
- SRINIVASAN, V.**
Evaluation parameters for the alkaline fuel cell oxygen electrode [NASA-TM-87155] p 77 N86-12268
- STAHL, B.**
Shear layer excitation, experiment versus theory [NASA-CR-176604] p 140 N86-20722
- STAIGER, P. J.**
Primary propulsion of electrothermal, ion, and chemical systems for space-based radar orbit transfer [AIAA PAPER 85-1477] p 50 N86-14431
An analysis of low-thrust, resistojet reboost for the Space Station [AIAA PAPER 85-2042] p 51 N86-14447
Design tradeoffs for a Space Station solar-Brayton power system p 53 N86-24790
- STALLONE, M. J.**
The dynamics of a flexible bladed disc on a flexible rotor in a two-rotor system p 20 N86-25743
- STATON, D. V.**
Rotorcraft propulsion for year 2000 plus [AIAA PAPER 86-1543] p 23 N86-42702
- STEARNS, C. A.**
Burner rig corrosion of SiC at 1000 C p 99 N86-36328
- STECURA, S.**
Optimization of the Ni-Cr-Al-Y/ZrO₂-Y₂O₃ thermal barrier system p 82 N86-31748
Advanced thermal barrier system bond coatings for use on nickel-, cobalt- and iron-base alloy substrates p 85 N86-49856
- STEGEMAN, J.**
Fluid flow and fuel-air mixing in a motored two-dimensional Wankel rotary engine [AIAA PAPER 86-1556] p 134 N86-42711
- STEINBERG, R.**
MERIT - A new approach to upper air forecasting for aviation p 191 N86-17982
Upper air forecasting for aviation in the United States p 191 N86-37501
- STEINHOFF, J.**
Gas flow environmental and heat transfer nonrotating 3D program p 137 N86-11506
Mean velocity and turbulence measurements in a 90 deg curved duct with thin inlet boundary layer [NASA-CR-174811] p 139 N86-18518
- STEPHENS, J. R.**
The B2 aluminides as alternative materials p 84 N86-47259
Creep rupture behavior of Stirling engine materials [NASA-TM-87209] p 88 N86-15380
Thermal aging effects in refractory metal alloys [NASA-TM-87210] p 89 N86-16334
Alloy chemistry and microstructural control to meet the demands of the automotive Stirling engine [NASA-TM-87250] p 89 N86-20541
- STETSON, K. A.**
Demonstration test of burner liner strain measurement systems: Interim results p 173 N86-11501
Demonstration test of burner liner strain measuring system [NASA-CR-174743] p 148 N86-21817
- STEVENS, G. H.**
Simulated performance of the NASA 30/20 GHz test transponder using multi-H phase coded modulation [AIAA PAPER 86-0717] p 110 N86-29656
- STEVENS, V. C.**
The STOL performance of a two-engine, USB powered-lift aircraft with cross-shafted fans [SAE PAPER 851839] p 16 N86-38336
- STEVENSON, W. H.**
Characteristics of an axisymmetric sudden expansion flow [NASA-CR-176278] p 151 N86-11465
- STILLE, J. K.**
All-aromatic biphenylene end-capped polyquinoline and polyimide matrix resins p 100 N86-11267
- STILLWELL, R. P.**
Current collection from the space plasma through defects in solar array insulation p 52 N86-18042
- STINCHCOMB, W. W.**
Ultrasonic stress wave characterization of composite materials [NASA-CR-3978] p 165 N86-27665
- STINESPRING, C. D.**
Experimental and theoretical analysis of chemical vapor deposition with prediction of gravity effects p 41 N86-10132
- STOFFER, L. J.**
Evaluation of capillary reinforced composites [NASA-CR-175061] p 70 N86-24760
- STOLTZFUS, J. M.**
An experimental data base for material selection and design of high-speed, high-pressure, oxygen turbomachinery p 58 N86-17387
- STONE, J. R.**
NASA electric propulsion technology [AIAA PAPER 85-1999] p 51 N86-17831
NASA electrothermal auxiliary propulsion technology [AIAA PAPER 86-1703] p 55 N86-42799
NASA electrothermal auxiliary propulsion technology [NASA-TM-87281] p 60 N86-24749
- STONEBACK, V. W.**
Advanced orbit transfer vehicle propulsion system study [NASA-CR-174843] p 60 N86-24746
- STORM, R. S.**
Sintered alpha silicon carbide ceramics for high temperature structural application - Status review and recent developments [ASME PAPER 85-IGT-127] p 97 N86-23921
- STOUFFER, D. C.**
Anisotropic constitutive model for nickel base single crystal alloys: Development and finite element implementation [NASA-CR-175015] p 176 N86-21952
- STOVER, J. B.**
Bit error rate testing of a proof-of-concept model baseband processor [NASA-TM-87206] p 46 N86-18343
- STRACK, W. C.**
Aeropropulsion opportunities for the 21st century [NASA-TM-88817] p 34 N86-31585
- STRANGE, R. L.**
Turbine blade and vane heat flux sensor development, phase 2 [NASA-CR-174995] p 26 N86-12226
- STRANGMAN, T. E.**
Low-cost single-crystal turbine blades, volume 2 [NASA-CR-174852] p 29 N86-23598
- STRAUHOORN, L. W.**
Future heavy duty trucking engine requirements [NASA-CR-174998] p 209 N86-17226
- STRAZISAR, A. J.**
Application of laser anemometry to turbomachinery flow field measurements p 160 N86-27640
Laser fringe anemometry for aero engine components [NASA-TM-88798] p 12 N86-28053
Rotor wake characteristics of a transonic axial flow fan [NASA-TM-87073] p 13 N86-28055
- STREHLOW, R. A.**
Flammability limits of gases under low gravity conditions p 42 N86-10164
The behavior of fuel-lean premixed flames in a standard flammability limit tube under controlled gravity conditions [NASA-CR-177132] p 78 N86-28139
- STRICKER, J.**
Diffraction effects and special advantages in electronic heterodyne moire deflectometry p 202 N86-31565
A comparison of electronic heterodyne moire deflectometry and electronic heterodyne holographic interferometry for flow measurements [SAE PAPER 851896] p 148 N86-38359
- STUART, T. A.**
Rotary transformer design with fixed magnetizing and/or leakage inductances p 119 N86-40462
- STUBSTAD, J. M.**
Bounding solutions of geometrically nonlinear viscoelastic problems [AIAA PAPER 86-0943] p 170 N86-38838
Bounding solutions of geometrically nonlinear viscoelastic problems [NASA-CR-176219] p 195 N86-10660
- STULTZ, J. E.**
Composition and properties of the so-called 'diamond-like' amorphous carbon films p 96 N86-16255
- STURMAN, J. C.**
Design of high-voltage, high-power, solid state remote power controllers for aerospace applications p 122 N86-17456
- STURMAN, J. L.**
Rail accelerators for space transportation: An experimental investigation [NASA-TP-2571] p 62 N86-28123
- SU, C. C.**
Heat transfer characteristics within an array of impinging jets. Effects of crossflow temperature relative to jet temperature [NASA-CR-3936] p 139 N86-15625
- SUBRAHMANYAM, K. B.**
Vibration analysis of rotating turbomachinery blades by an improved finite difference method p 18 N86-14338
Vibration and buckling of rotating, pretwisted, precone beams including Coriolis effects p 168 N86-26910
Nonlinear bending-torsional vibration and stability of rotating, pretwisted, precone blades including Coriolis effects [NASA-TM-87207] p 175 N86-17789
Influence of third-degree geometric nonlinearities on the vibration and stability of pretwisted, precone, rotating blades [NASA-TM-87307] p 179 N86-31920
- SUBRAMANIAN, S. V.**
Computation of three-dimensional, rotational flow through turbomachinery blade rows for improved aerodynamic design studies [ASME PAPER 86-GT-26] p 7 N86-48117
- SUENIK, C. N.**
The synthesis, characterization and thermal chemistry of modified norbornenyl PMR endcaps p 100 N86-11266
- SULLIVAN, J. P.**
An experimental investigation of propeller wakes using a laser Doppler velocimeter [AIAA PAPER 86-0080] p 18 N86-19677
Unsteady forces on counter-rotating propeller blades [AIAA PAPER 86-1804] p 22 N86-37827
- SULLIVAN, T.**
An analysis of bidirectional use of frequencies for satellite communications [AIAA PAPER 86-0635] p 110 N86-29664
An analysis of bi-directional use of frequencies for satellite communications [AIAA PAPER 86-0635] p 111 N86-49568
An analysis of bi-directional use of frequencies for satellite communications [NASA-TM-87226] p 114 N86-18585
- SULLIVAN, T. J.**
Evaluation of a Stirling engine heater bypass with the NASA Lewis nodal-analysis performance code [NASA-CR-179460] p 211 N86-31452
- SUMMERS, R. L.**
Convenient mounting method for electrical measurements of thin samples p 120 N86-46649
Apparatus for electrical measurements of thin films from 77 to 1000 K [NASA-TM-87256] p 148 N86-24959
- SUN, C. T.**
Dynamic delamination crack propagation in a graphite/epoxy laminate p 68 N86-43010
- SUNDAR, R. M.**
An experimental investigation of propeller wakes using a laser Doppler velocimeter [AIAA PAPER 86-0080] p 18 N86-19677
- SUNDBERG, G. R.**
A new very high voltage semiconductor switch p 119 N86-40449
Space station 20-kHz power management and distribution system [NASA-TM-87314] p 60 N86-24747
- SUNDBURG, G. R.**
Programmable, automated transistor test system [NASA-TP-2554] p 123 N86-21755
- SURAMPUDI, S. P.**
Unsteady transonic flow over cascade blades p 3 N86-23141
Unsteady transonic flow in cascades p 4 N86-24693
- SUSKI, V. A.**
Future heavy duty trucking engine requirements [NASA-CR-174998] p 209 N86-17226

- SUTTON, R. F.**
Small, two-stage, partial-admission turbine
p 57 N86-17386
- SWANSON, G. A.**
Life prediction and constitutive models for engine hot section anisotropic materials program
[NASA-CR-174952] p 165 N86-25003
- SWANSON, L. W.**
The effect of oxygen pressure on volatility and morphology of LaB₆ single crystal cathodes
p 204 A86-28076
- SWARTZ, C. K.**
Voltage-controlling mechanisms in low-resistivity silicon solar cells - A unified approach p 120 A86-45195
Performance and temperature dependencies of proton irradiated n/p GaAs and n/p silicon cells
[NASA-TM-87136] p 120 N86-12509
Potential for use of indium phosphide solar cells in the space radiation environment
[NASA-TM-87157] p 121 N86-13645
Radiation damage in high-resistivity silicon solar cells
p 185 N86-17856
Performance of Hughes GaAs concentrator cells under 1-MeV electron irradiation p 185 N86-17860
- SWEC, D. M.**
Ion beam sputter-deposited thin film coatings for protection of spacecraft polymers in low earth orbit
[AIAA PAPER 85-0420] p 95 A86-14428
Dual-ion-beam deposition of carbon films with diamond-like properties p 65 A86-49855
- SZAFIR, D. R.**
Lateral dampers for thrust bearings
[NASA-CR-174924] p 157 N86-11474
- SZETELA, E. J.**
Deposit formation and heat-transfer characteristics of hydrocarbon rocket fuels p 106 A86-10028
Long term deposit formation in aviation turbine fuel at elevated temperature
[AIAA PAPER 86-0525] p 107 A86-19929
Fuel deposit characteristics at low velocity
[ASME PAPER 85-IGT-130] p 107 A86-23922
- SZUCH, J. R.**
Development and application of dynamic simulations of a subsonic wind tunnel
[AIAA PAPER 86-0758] p 36 A86-24745
Development and application of dynamic simulations of a subsonic wind tunnel
[NASA-TM-87211] p 43 N86-18338
A lumped parameter mathematical model for simulation of subsonic wind tunnels
[NASA-TM-87324] p 196 N86-27036
- ## T
- TABAKOFF, W.**
Three-dimensional flow field measurements in a radial inflow turbine scroll using LDV
[ASME PAPER 86-GT-122] p 7 A86-48181
- TABATA, W. K.**
Automotive Stirling summary and overview
[NASA-TM-87177] p 209 N86-21457
- TAM, C. K. W.**
Tone excited jets. V - A theoretical model and comparison with experiment p 196 A86-16470
- TAM, L. T.**
Computational simulation of liquid rocket injector anomalies
[AIAA PAPER 86-1424] p 55 A86-42633
- TANAKA, K.**
Abrasion and deformed layer formation of manganese-zinc ferrite in sliding contact with lapping tapes
[NASA-TM-87249] p 104 N86-24838
Effect of crystallographical and geometrical changes of a ferrite head on magnetic signals during the sliding process with magnetic tape
[NASA-TM-87277] p 106 N86-31728
- TANNA, H. K.**
Tone excited jets. I - Introduction p 196 A86-16466
- TAULBEE, D. B.**
Turbine-stage heat transfer - Comparison of short-duration measurements with state-of-the-art predictions
[AIAA PAPER 86-1465] p 134 A86-42656
- TAVARES, T. S.**
A supersonic fan equipped variable cycle engine for a Mach 2.7 supersonic transport
[NASA-CR-177141] p 32 N86-28946
- TAYLOR, B. K.**
Error-source effects in a high-accuracy optical finite-element processor p 192 A86-31571
- TEAGAN, W. P.**
Liquid belt radiator design study
[NASA-CR-174901] p 57 N86-16259
- TELESMAN, J.**
A study of spectrum fatigue crack propagation in two aluminum alloys. I - Spectrum simplification. II - Influence of microstructures p 85 A86-48973
Influence of load interactions on crack growth as related to state of stress and crack closure
[NASA-TM-87117] p 86 N86-12292
Variables controlling fatigue crack growth of short cracks
[NASA-TM-87208] p 90 N86-21661
Influence of fatigue crack wake length and state of stress on crack closure
[NASA-TM-87292] p 90 N86-22686
- TEREN, F.**
Space station power management and distribution
p 59 N86-17869
- TEVAARWERK, J. L.**
Constitutive modelling of lubricants in concentrated contacts at high slide to roll ratios
[NASA-CR-175029] p 158 N86-17748
- TEWARI, S. N.**
Undercooled and rapidly quenched Ni-Mo alloys
[NASA-TM-87257] p 90 N86-21659
- THALLER, L. H.**
Design principles for nickel-hydrogen cells and batteries p 179 A86-24799
Design considerations for advanced battery concepts
[AIAA PAPER 86-1164] p 181 A86-40579
Principles for system level electrochemistry
[NASA-TM-87283] p 187 N86-25039
Design considerations for advanced battery concepts
[NASA-TM-87319] p 190 N86-31981
- THOMAS, R. E.**
The baseband processor in future satellite communication systems p 109 A86-21882
- THOMPSON, W. T., JR.**
Propagation and stability of wavelike solutions of finite difference equations with variable coefficients
p 194 A86-20033
- THOMPSON, H. D.**
Characteristics of an axisymmetric sudden expansion flow
[NASA-CR-176278] p 151 N86-11465
- THOMPSON, L. B.**
Thermal dependence of stress-induced birefringence in single mode optical fibers p 202 A86-15263
- THOMPSON, R.**
Validation of structural analysis methods using burner liner cyclic rig test data p 173 N86-11518
- THOMPSON, R. L.**
A computer analysis program for interfacing thermal and structural codes p 193 A86-36861
Unified constitutive materials model development and evaluation for high-temperature structural analysis applications p 172 A86-49133
- TIAN, Z.**
Hybrid solid element with a traction-free cylindrical surface p 169 A86-34462
- TIDONA, R. J.**
Combustion characteristics in the transition region of liquid fuel sprays
[NASA-CR-176564] p 77 N86-20517
- TIEN, J. K.**
Interdiffusional effects between tungsten fibers and an iron-nickel-base alloy p 66 A86-14718
- TIEN, J. S.**
Combustor flame flashback
[NASA-CR-174961] p 183 N86-14727
- TITRAN, R. H.**
Creep-rupture and fractographic analysis of Stirling engine superalloys tested in air and 15 MPa hydrogen
p 82 A86-30041
High temperature properties of equiatomic FeAl with ternary additions p 84 A86-47252
Alloys based on NiAl for high temperature applications p 84 A86-47261
Creep rupture behavior of Stirling engine materials
[NASA-TM-87209] p 88 N86-15380
Compressive creep behavior of alloys based on B2 FeAl
[NASA-TM-87293] p 92 N86-28165
Creep properties of PWC-11 base metal and weldments as affected by heat treatment
[NASA-TM-88842] p 93 N86-32557
- TOMAZIC, W. A.**
Stirling engine supporting research and technology
[NASA-TM-87175] p 208 N86-14106
- TONG, M.**
Structural analysis of turbine blades using unified constitutive models
[NASA-TM-88807] p 178 N86-28461
- TONG, M. T.**
Unified constitutive materials model development and evaluation for high-temperature structural analysis applications p 172 A86-49133
- TOPP, D. A.**
Passive control of aerodynamically forced vibrations of supersonic turbomachine rotors by splitter blades
[AIAA PAPER 86-0844] p 22 A86-38892
- TORRES, F. J.**
Local heat-transfer measurements on a large scale-model turbine blade airflow using a composite of a heater element and liquid crystals
[ASME PAPER 85-GT-59] p 126 A86-13061
- TOTH, J. M., JR.**
LH2 on-orbit storage tank support trunnion design and verification p 53 A86-37054
- TOWNSEND, D. P.**
An investigation of the transient thermal analysis of spur gears
[ASME PAPER 84-DET-92] p 155 A86-40683
Lubricant and additive effects on spur gear fatigue life
[ASME PAPER 85-TRIB-14] p 155 A86-43542
Surface fatigue life and failure characteristics of EX-53, CBS 1000M, and AISI 9310 gear materials
[NASA-TP-2513] p 157 N86-12609
Gearing
[NASA-RP-1152] p 157 N86-14612
Surface fatigue and failure characteristics of hot forged powder metal AISI 4620, AISI 4640, and machined AISI 4340 steel spur gears
[NASA-TM-87330] p 161 N86-31889
- TREFFNY, C. J.**
Semiempirical method of determining flow coefficients for pitot rake mass flow rate measurements
[NASA-TM-87144] p 9 N86-14219
Low-speed performance of an axisymmetric, mixed-compression, supersonic inlet with auxiliary inlets
[NASA-TP-2557] p 30 N86-24694
- TRUBERT, M.**
Modal test/analysis correlation for Centaur G Prime launch vehicle
[AIAA PAPER 86-1002] p 43 A86-38943
- TRUONG, L. V.**
Programmable, automated transistor test system
[NASA-TP-2554] p 123 N86-21755
- TSENG, H. Q.**
10-30 GHz monolithic GaAs travelling-wave divider/combiner p 118 A86-34882
- TSO, J.**
Free shear flows - Organized structures and effects of excitation
[AIAA PAPER 86-0235] p 131 A86-26614
- TSUNG, W. J.**
Generation of spiral bevel gears with zero kinematical errors and computer aided tooth contact analysis
[NASA-TM-87273] p 160 N86-25793
- TSUNG, W.-J.**
Generation of spiral bevel gears with zero kinematical errors and computer aided simulation of their meshing and contact p 154 A86-40656
Generated spiral bevel gears - Optimal machine-tool settings and tooth contact analysis
[SAE PAPER 851573] p 154 A86-40678
- TUBINO, R.**
Infrared-photoinduced-absorption studies in soluble trans-polyacetylene p 204 A86-37075
- TURK, M. A.**
Advanced technology payoffs for future rotorcraft, commuter aircraft, cruise missile, and APU propulsion systems
[AIAA PAPER 86-1545] p 16 A86-42704
- TURNER, D. A.**
Methods for improving reliability in ceramic turbine rotors
[SAE PAPER 851788] p 154 A86-38312
- TURNER, E. R.**
Turbine vane external heat transfer. Volume 1: Analytical and experimental evaluation of surface heat transfer distributions with leading edge showerhead film cooling
[NASA-CR-174827] p 29 N86-21546
- ## U
- UHRAN, M. L.**
Accommodation requirements for microgravity science and applications research on space station
[NASA-CR-175038] p 42 N86-18334
- ULBRIGHT, T. E.**
LOX/LH2 vane pump for auxiliary propulsion systems
p 58 N86-17397
The noncavitating performance and life of a small vane-type positive displacement pump in liquid hydrogen
[NASA-TM-87347] p 63 N86-31651
- UMSTATTER, H. L.**
Visualization of flows in a motored rotary combustion engine using holographic interferometry
[NASA-TM-88804] p 33 N86-31583

USAB, W. J., JR.

- On the application of a linearized unsteady potential-flow analysis to fan-tip cascades p 7 A86-48153
[ASME PAPER 86-GT-87]
Application of a linearized unsteady aerodynamic analysis to standard cascade configurations p 11 N86-21505
[NASA-CR-3940]

V

VALERO, N. A.

- Vibration characteristics of mistuned shrouded blade assemblies p 19 A86-22068
[ASME PAPER 85-GT-115]

VALGORA, M. E.

- Space Station Power System Advanced Development p 52 A86-24778

VALLESE, F. J.

- Variable-reluctance motor drives for electric vehicle propulsion p 122 N86-20700
[NASA-CR-176566]

VANCO, M. R.

- An overview of the Small Engine Component Technology (SECT) studies p 34 N86-31587
[NASA-TM-88796]

VANFOSSEN, G. J.

- Heat transfer and pressure drop performance of a finned-tube heat exchanger proposed for use in the NASA Lewis Altitude Wind Tunnel p 138 N86-13677
[NASA-TM-87151]

VANFOSSEN, G. J., JR.

- Preliminary results of a study of the relationship between free stream turbulence and stagnation region heat transfer p 129 A86-22055
[ASME PAPER 85-GT-84]

VANNUCCI, R. D.

- Graphite/PMR polyimide composites with improved toughness p 66 A86-21731
Effect of solution concentration and aging conditions on PMR-15 resin p 98 A86-33113
Properties of autoclaved Gr/PI composites made from improved tack PMR-15 prepreg p 68 N86-11276

VANOVERBEKE, T. J.

- SSME fuelside preburner two-dimensional analysis p 44 N86-23616
[NASA-TM-87299]

VARDE, U.

- The synthesis, characterization and thermal chemistry of modified norbornenyl PMR endcaps p 100 N86-11266

VARSHNEYA, D.

- Development of optical diaphragm deflection sensors p 203 N86-15113
[NASA-CR-175008]

VARY, A.

- Measurement of ultrasonic velocity using phase-slope and cross-correlation methods p 162 A86-13192
Nondestructive techniques for characterizing mechanical properties of structural materials - An overview p 163 A86-48143
[ASME PAPER 86-GT-75]
NDE of structural ceramics p 163 A86-48298
[ASME PAPER 86-GT-279]
NDE of structural ceramics p 164 N86-16598
[NASA-TM-87186]
Nondestructive techniques for characterizing mechanical properties of structural materials: An overview p 164 N86-19636
[NASA-TM-87203]
Analytical Ultrasonics in Materials Research and Testing p 164 N86-22962
[NASA-CP-2383]
Transfer function concept for ultrasonic characterization of material microstructures p 200 N86-22980
Concepts for interrelating ultrasonic attenuation, microstructure and fracture toughness in polycrystalline solids p 165 N86-25812
[NASA-TM-87339]

VATSA, V. N.

- Assessment of a 3-D boundary layer code to predict heat transfer and flow losses in a turbine p 138 N86-11508

VEDHA-NAYAGAM, M.

- Backward boundary layers in downward flame spread p 73 A86-22793

VEDULA, K.

- Alloys based on NiAl for high temperature applications p 84 A86-47261
Effect of boron on tensile properties of B2 BeAl p 89 N86-21656
[NASA-CR-175074]
High temperature dispersion strengthening of NiAl p 90 N86-22688
[NASA-CR-175073]
Compressive creep behavior of alloys based on B2 FeAl p 92 N86-28165
[NASA-TM-87293]

VEDULA, K. M.

- High temperature properties of equiatomic FeAl with ternary additions p 84 A86-47252

VERDON, J. M.

- On the application of a linearized unsteady potential-flow analysis to fan-tip cascades p 7 A86-48153
[ASME PAPER 86-GT-87]
Application of a linearized unsteady aerodynamic analysis to standard cascade configurations p 11 N86-21505
[NASA-CR-3940]

VERNON, R.

- Fluid management and its role in the future of Space Station p 47 A86-49553
[AIAA PAPER 86-2301]

VERZWEVELT, S. A.

- KOH concentration effect on the cycle life of nickel-hydrogen cells p 180 A86-24802
Long life nickel electrodes for a nickel-hydrogen cell: Cycle life tests p 188 N86-25046
[NASA-CR-174815]

VIDT, E. J.

- Design and evaluation of fluidized bed heat recovery for diesel engine systems p 209 N86-21456
[NASA-CR-174898]

VILMANN, C. R.

- Stress and deformation modeling of multiple rotary combustion engine trochoid housings p 156 A86-49624
[SAE PAPER 860614]

VINET, P.

- A model for the influence of pressure on the bulk modulus and the influence of temperature on the solidification pressure for liquid lubricants p 140 N86-19555
[NASA-TM-87230]
Universality in the compressive behavior of solids p 206 N86-28775
[NASA-TM-87303]
Temperature effects on the universal equation of state of solids p 206 N86-28776
[NASA-TM-87321]

VIRSHUP, G. F.

- High-efficiency AlGaAs-GaAs Cassegrainian concentrator cells p 185 N86-17845

VOGAN, J. W.

- Rocket thrust chamber thermal barrier coatings p 59 N86-20497
[NASA-CR-175022]

VOGEL, P.

- Emission FTIR analyses of thin microscopic patches of jet fuel residues deposited on heated metal surfaces p 108 N86-25502
[NASA-CR-176786]

VOIGT, R. C.

- Orientation and temperature dependence of some mechanical properties of the single-crystal nickel-base superalloy Rene N4. I - Tensile behavior p 86 A86-50321

VON GLAHN, U.

- Velocity and temperature decay characteristics of inverted-profile jets p 2 A86-22693
[AIAA PAPER 86-0312]

VON GLAHN, U. H.

- Plume characteristics of single-stream and dual-flow conventional and inverted-profile nozzles at equal thrust p 8 A86-49585
[AIAA PAPER 86-1809]

VON LAVANTE, E.

- A numerical method for the design and analysis of counter-rotating propellers p 19 A86-20369
[AIAA PAPER 84-1205]
Numerical evaluation of propeller noise including nonlinear effects p 23 A86-41726

VONGLAHN, U.

- Velocity and temperature decay characteristics of inverted-profile jets p 9 N86-14223
[NASA-TM-87159]

VONGLAHN, U. H.

- Plume characteristics of single-stream and dual-flow conventional and inverted-profile nozzles at equal thrust p 12 N86-26285
[NASA-TM-87323]

VU, B. T.

- Periodic oscillations observed in swirling flows with and without combustion p 73 A86-22755

W

WACHMAN, H. Y.

- Effect of gravity on laminar premixed gas combustion. I - Flammability limits and burning velocities p 72 A86-12413

WADA, B.

- Modal test/analysis correlation for Centaur G Prime launch vehicle p 43 A86-38943
[AIAA PAPER 86-1002]

WALKER, K. P.

- Constitutive modeling for isotropic materials (HOST) p 172 N86-10589
[NASA-CR-174980]
Life prediction and constitutive models for engine hot section anisotropic materials program p 165 N86-25003
[NASA-CR-174952]

WALKINGTON, N. J.

- A numerical model of acoustic choking. II - Shocked solutions p 197 A86-20795

WALLACE, J. F.

- Solidification fundamentals p 39 N86-10090

WALLET, T. M.

- Dry etching of beta-SiC in CF₄ and CF₄ + O₂ mixtures p 76 A86-47069

WALOWIT, J. A.

- Performance of oil pumping rings: An analytical and experimental study p 144 N86-31000
[NASA-CR-175083]

WANG, C. L.

- Develop and test fuel cell powered on-site integrated total energy systems: Phase 3, full-scale power plant development p 182 N86-12757
[NASA-CR-174948]
Develop and test fuel cell powered on-site integrated total energy systems: Phase 3, full-scale power plant development p 182 N86-12758
[NASA-CR-174998]

WANG, C. W.

- The role of service areas in the optimization of FSS orbital and frequency assignments p 46 N86-18341
[NASA-CR-176488]
Engineering calculations for communications satellite systems planning p 114 N86-19493
[NASA-CR-176555]
Broadcasting satellite service synthesis using gradient and cyclic coordinate search procedures p 114 N86-23781
[NASA-CR-176708]

WANG, C.-W.

- The role of service areas in the optimization of FSS orbital and frequency assignments p 45 A86-29599
[AIAA PAPER 86-0636]

WANG, J. S.

- Development of LC-13C NMR p 107 N86-21704
[NASA-CR-176656]

WANG, S. S.

- Three-dimensional hybrid-stress finite element analysis of composite laminates with cracks and cutouts p 167 A86-26896

WANG, S.-Y.

- Primary propulsion of electrothermal, ion, and chemical systems for space-based radar orbit transfer p 50 A86-14431
[AIAA PAPER 85-1477]

WANG, T.

- Heat transfer and fluid mechanics measurements in transitional boundary layer flows p 126 A86-13068
[ASME PAPER 85-GT-113]

WARFIELD, M.

- A comparison of computational methods for three-dimensional, turbulent turbomachinery flow fields p 6 A86-42740
[AIAA PAPER 86-1599]

WARFIELD, M. J.

- Computation of turbulent rotating channel flow with an algebraic Reynolds stress model p 130 A86-22682
[AIAA PAPER 86-0214]

WARNER, J. D.

- Growth and characterization of epitaxial SrF₂ on InP(100) p 205 A86-47076

- Ellipsometric and optical study of some uncommon insulator films on 3-5 semiconductors p 205 N86-12134
[NASA-TM-87135]

- Carbon films grown from plasma on III-V semiconductors p 205 N86-12135
[NASA-TM-87140]

- Auger electron spectroscopy, secondary ion mass spectroscopy and optical characterization of a-C-H and BN films p 206 N86-25268
[NASA-TM-87258]

WARREN, E. L.

- Compliant hydrodynamic fluid journal bearing p 158 N86-19806
[NASA-CASE-LEW-13670-1]

WASSERBAUER, C.

- Velocity and temperature decay characteristics of inverted-profile jets p 2 A86-22693
[AIAA PAPER 86-0312]

- Velocity and temperature decay characteristics of inverted-profile jets p 9 N86-14223
[NASA-TM-87159]

WASSERBAUER, J. W.

- Low-speed performance of an axisymmetric, mixed-compression, supersonic inlet with auxiliary inlets p 30 N86-24694
[NASA-TP-2557]

WATANABE, O.

- Constitutive modeling of cyclic plasticity and creep, using an internal time concept p 170 A86-41673

WATKINS, W. B.

- Further development of the dynamic gas temperature measurement system p 147 A86-42770
[AIAA PAPER 86-1648]

- Dynamic gas temperature measurement system p 147 N86-11499

- WATSON, J. W.**
Deposition stress effects on the life of thermal barrier coatings on burner rigs p 96 A86-16271
- WAYNE, S. F.**
Impact wear of iron rich superalloys p 82 A86-34687
- WEAR, W. O.**
Accommodation requirements for microgravity science and applications research on space station [NASA-CR-175038] p 42 N86-18334
- WEBER, R. M.**
Constitutive modeling for isotropic materials (HOST) [NASA-CR-174980] p 172 N86-10589
- WEI, W.**
Sliding seal materials for adiabatic engines, phase 2 [NASA-CR-179475] p 105 N86-29042
- WEIKLE, D. H.**
Laser anemometry for hot section applications p 151 N86-11503
- WEINBERG, B.**
AC motor and generator requirements for isolated WECS [NASA-CR-178315] p 182 N86-11670
- WEINBERG, B. C.**
Numerical and experimental investigation of nonswirling and swirling confined jets [AIAA PAPER 86-0040] p 127 A86-19651
Calculations of two and three-dimensional transonic cascade flow fields using the Navier-Stokes equations [ASME PAPER 85-GT-66] p 2 A86-22046
Influence of large-scale motion on turbulent transport for confined coaxial jets. Volume 2: Navier-Stokes calculations of swirling and nonswirling confined coaxial jets [NASA-CR-175036] p 28 N86-20390
- WEINBERG, I.**
Performance and temperature dependencies of proton irradiated n/p GaAs and n/p silicon cells [NASA-TM-87136] p 120 N86-12509
Potential for use of indium phosphide solar cells in the space radiation environment [NASA-TM-87157] p 121 N86-13645
Radiation damage in high-resistivity silicon solar cells p 185 N86-17856
Indium phosphide solar cells: status and prospects for use in space [NASA-TM-87315] p 123 N86-26520
Lithium counterdoped silicon solar cell [NASA-CASE-LEW-14177-1] p 190 N86-32875
- WEISS, J. L.**
Application of FDI metrics to detection and isolation of sensor failures in turbine engines p 21 A86-35400
Robust detection-isolation-accommodation for sensor failures [NASA-CR-174797] p 121 N86-16486
- WEIZER, V. G.**
The effect of a defective BSF layer on solar cell open circuit voltage p 179 A86-12673
Voltage-controlling mechanisms in low-resistivity silicon solar cells - A unified approach p 120 A86-45195
Minority-carrier mobility anomalies in low-resistivity silicon solar cells p 181 A86-49215
A 25.5 percent AMO gallium arsenide grating solar cell [NASA-TM-87134] p 182 N86-11671
Gallium arsenide solar cell efficiency: Problems and potential p 184 N86-17843
- WELSCH, G.**
Fatigue crack layer propagation in silicon-iron [NASA-CR-175115] p 177 N86-25851
- WELSCH, G. E.**
The cyclic stress-strain behavior of a nickel-base superalloy at 650 C p 83 A86-45715
- WERNET, M. P.**
Implementation of a new type of time-of-flight laser anemometer p 146 A86-29755
- WERTH, J.**
Develop and test fuel cell powered on-site integrated total energy systems: Phase 3, full-scale power plant development [NASA-CR-174948] p 182 N86-12757
Develop and test fuel cell powered on-site integrated total energy systems: Phase 3, full-scale power plant development [NASA-CR-174998] p 182 N86-12758
Develop and test fuel cell powered on-site integrated total energy systems [NASA-CR-174951] p 188 N86-25877
- WERTHEN, J. G.**
High-efficiency AlGaAs-GaAs Cassegrainian concentrator cells p 185 N86-17845
- WESTFALL, L. J.**
Thermal-mechanical fatigue test apparatus for metal matrix composites and joint attachments [NASA-TM-87187] p 88 N86-15378
- WHALEN, M. V.**
Compatibility of grain-stabilized platinum with candidate propellants for resistojets [AIAA PAPER 85-2014] p 51 A86-17835
Performance and endurance tests of a multipropellant resistojets for space station auxiliary propulsion [AIAA PAPER 86-1435] p 55 A86-42640
Compatibility of grain-stabilized platinum with candidate propellants for resistojets [NASA-TM-87118] p 56 N86-10279
Vacuum chamber pressure effects on thrust measurements p 59 N86-17425
Compatibility experiments of facilities, materials, and propellants for electrothermal thrusters p 59 N86-17426
Performance and endurance tests of a multipropellant resistojets for space station auxiliary propulsion [NASA-TM-87278] p 60 N86-24748
- WHEELER, D. R.**
Thermal desorption study of physical forces at the PTFE surface [NASA-TM-87090] p 206 N86-25284
- WHEELER, R. L., III**
Two-phase flows within systems with ambient pressure p 161 N86-30167
- WHELAN, J. A.**
Develop and test fuel cell powered on-site integrated total energy systems: Phase 3, full-scale power plant development [NASA-CR-174948] p 182 N86-12757
Develop and test fuel cell powered on-site integrated total energy systems: Phase 3, full-scale power plant development [NASA-CR-174998] p 182 N86-12758
- WHERLEY, B. L.**
The behavior of fuel-lean premixed flames in a standard flammability limit tube under controlled gravity conditions [NASA-CR-177132] p 78 N86-28139
- WHITE, C.**
Dilution jet mixing program, supplementary report [NASA-CR-175043] p 141 N86-23856
Dilution jet mixing program, phase 3 [NASA-CR-174884] p 142 N86-24938
- WHITE, J. F., III**
Aeroelastic behavior of low aspect ratio metal and composite blades [ASME PAPER 86-GT-243] p 171 A86-48271
- WHITE, K. A., III**
Liquid droplet radiator program at the NASA Lewis Research Center [ASME PAPER 86-HT-15] p 48 A86-49621
Liquid droplet radiator program at the NASA Lewis Research Center [NASA-TM-87139] p 48 N86-12246
- WHITE, P. R.**
Application of a personal computer for the uncoupled vibration analysis of wind turbine blade and counterweight assemblies [NASA-CR-175090] p 188 N86-28511
- WHITMAN, W.**
Advanced rotary engine components utilizing fiber reinforced Mg castings [AIAA PAPER 86-1559] p 67 A86-42712
- WHITSON, D. W.**
Double-injection, deep-impurity switch development [NASA-CR-174936] p 124 N86-30073
- WHITTENBERGER, J. D.**
Slow plastic strain rate compressive flow in binary CoAl intermetallics p 79 A86-11478
Effect of multiple strain-anneal cycles on the 1000 C creep behaviour of gamma/gamma prime-alpha p 82 A86-30610
The influence of grain size and composition on slow plastic flow in FeAl between 1100 and 1400 K p 86 A86-50279
Estimated heats of fusion of fluoride salt mixtures suitable for thermal energy storage applications [NASA-TM-87320] p 190 N86-31982
- WHYTE, W. A., JR.**
An analysis of bidirectional use of frequencies for satellite communications [AIAA PAPER 86-0635] p 110 A86-29664
An analysis of bi-directional use of frequencies for satellite communications [AIAA PAPER 86-0635] p 111 A86-49568
An analysis of bi-directional use of frequencies for satellite communications [NASA-TM-87226] p 114 N86-18585
- WILKINSON, C. L.**
Space station propulsion requirements study [NASA-CR-174934] p 57 N86-15339
- WILLIAMS, A. D.**
Hardware configuration for a real-time multiprocessor simulator [NASA-TM-88802] p 194 N86-28651
- WILLIAMS, F. A.**
Fundamental studies of droplet combustion at reduced gravity p 42 N86-10165
- WILLIAMS, F. W.**
Boundary layer measurements on an airfoil in cascade using laser Doppler anemometry [AIAA PAPER 86-0072] p 145 A86-19670
- WILLIAMS, J. H., JR.**
Stress waves in transversely isotropic media: The homogeneous problem [NASA-CR-3977] p 164 N86-25002
Wave propagation in anisotropic medium due to an oscillatory point source with application to unidirectional composites [NASA-CR-4001] p 165 N86-27666
- WILLIAMS, M. H.**
Three dimensional unsteady aerodynamics and aeroelastic response of advanced turboprops [AIAA PAPER 86-0846] p 22 A86-38894
- WILLSKY, A. S.**
Application of FDI metrics to detection and isolation of sensor failures in turbine engines p 21 A86-35400
Robust detection-isolation-accommodation for sensor failures [NASA-CR-174797] p 121 N86-16486
- WILSON, M. D.**
Turbine vane external heat transfer. Volume 1: Analytical and experimental evaluation of surface heat transfer distributions with leading edge showerhead film cooling [NASA-CR-174827] p 29 N86-21546
- WILSON, R. B.**
Stress analysis of gas turbine engine structures using the boundary element method p 169 A86-34444
- WILSON, S. B., III**
The STOL performance of a two-engine, USB powered-lift aircraft with cross-shafted fans [SAE PAPER 851839] p 16 A86-38336
- WINTUCKY, W. T.**
Preliminary evaluation of a compound cycle engine for shipboard gensets [NASA-CR-179451] p 160 N86-26629
An overview of the Small Engine Component Technology (SECT) studies [NASA-TM-88796] p 34 N86-31587
- WIRTH, G.**
Effect of multiple strain-anneal cycles on the 1000 C creep behaviour of gamma/gamma prime-alpha p 82 A86-30610
- WOLFF, F. J.**
A 20 kilohertz space station power system [NASA-TM-88801] p 62 N86-28122
- WOOD, J. R.**
Effect of area ratio on the performance of a 5.5:1 pressure ratio centrifugal impeller [ASME PAPER 86-GT-303] p 8 A86-48315
Effect of area ratio on the performance of a 5.5:1 pressure ratio centrifugal impeller [NASA-TM-87237] p 10 N86-19290
- WOODWARD, S. H.**
Heat-flux measurements for the rotor of a full-stage turbine. II - Description of analysis technique and typical time-resolved measurements [ASME PAPER 86-GT-78] p 24 A86-48146
- WOOLLAM, J. A.**
Optical and interfacial electronic properties of diamond-like carbon films p 204 A86-16268
- WORRELL, W. L.**
The reactions of cobalt, iron and nickel in SO₂ atmospheres Similarities and differences p 75 A86-40677
- WU, C. K.**
On the determination of laminar flame speeds from stretched flames p 74 A86-22814
- WU, M.-F.**
Simultaneous measurements of carbon monoxide and ozone in the NASA Global Atmospheric Sampling Program (GASP) p 191 A86-48620

X

- XUE, W.-M.**
Existence and stability, and discrete BB and rank conditions, for general mixed-hybrid finite elements in elasticity p 169 A86-34464

Y

- YAMAMOTO, O.**
Improved Euler analysis of advanced turboprop propeller flows [AIAA PAPER 86-1521] p 6 A86-42688

YAMAMURA, Y.

- The role of service areas in the optimization of FSS orbital and frequency assignments
[AIAA PAPER 86-0636] p 45 A86-29599
- Calculation of allowable orbital spacings for the fixed-satellite service
[NASA-CR-176273] p 43 N86-11212
- The role of service areas in the optimization of FSS orbital and frequency assignments
[NASA-CR-176488] p 46 N86-18341
- Engineering calculations for communications satellite systems planning
[NASA-CR-176555] p 114 N86-19493

YANEY, D. L.

- Dislocations in extruded Co-49.3 at. pct Al
p 83 A86-45091

YANG, C. H.

- Theory of homogeneous nucleation - A chemical kinetic view
p 72 A86-19389

YANG, R.-J.

- Calculations of two and three-dimensional transonic cascade flow fields using the Navier-Stokes equations
[ASME PAPER 85-GT-86] p 2 A86-22046

YANG, S. L.

- A two-dimensional numerical study of the flow inside the combustion chambers of a motored rotary engine
[NASA-TM-87212] p 10 N86-19289

YANG, T. T.

- Viscous compressible flow direct and inverse computation and illustrations
[NASA-CR-175037] p 28 N86-20391

YANG, T.-T.

- Inverse design of axisymmetric flow passages using compressible viscous flow theory p 4 A86-26412

YE, Z. Y.

- An experimental investigation on flame interaction and the existence of negative flame speeds p 74 A86-22816

- Theory of interactive combustion of counterflow premixed flames p 74 A86-32752

YEH, F. C.

- Heat transfer results and operational characteristics of the NASA Lewis Research Center hot section cascade test facility
[ASME PAPER 85-GT-82] p 128 A86-22053

YEH, H. C.

- Processing study of injection molding of silicon nitride for engine applications
[SAE PAPER 851787] p 154 A86-38311

YOO, G. J.

- On the modeling of low-Reynolds-number turbulence
[NASA-CR-3994] p 32 N86-28089

YOON, S.

- An LU implicit scheme for high speed inlet analysis
[AIAA PAPER 86-1520] p 6 A86-42687
- An LU implicit scheme for high speed inlet analysis
[NASA-CR-175098] p 11 N86-23563

YOUNG, T. H.

- Extensions of the Ritz-Galerkin method for the forced, damped vibrations of structural elements p 176 N86-21909

YURKOVICH, S.

- Polynomial nonlinear dynamical systems - A residual sensitivity method for model reduction p 194 A86-35386

Z**ZAFRAN, S.**

- Resistojet operation with various propellants
[AIAA PAPER 85-1158] p 107 A86-37074

ZAGHLOUL, A. I.

- Optimized three-dimensional lenses for wide-angle scanning p 109 A86-19184

ZAHIRI, F.

- Axial and torsional fatigue behavior of Waspaloy
[NASA-CR-175052] p 91 N86-25454

ZAKRAJSEK, R. J.

- Near-field testing of the 30 GHz TRW proof-of-concept multibeam antenna
[NASA-TM-87357] p 124 N86-27578

ZAMAN, K. B. M. Q.

- Free shear flows - Organized structures and effects of excitation
[AIAA PAPER 86-0235] p 131 A86-26614
- Flow field and near and far sound field of a subsonic jet p 5 A86-35855

ZAMRIK, S.

- Axial and torsional fatigue behavior of Waspaloy
[NASA-CR-175052] p 91 N86-25454

ZANA, L. M.

- Rail accelerators for space transportation: An experimental investigation
[NASA-TP-2571] p 62 N86-28123

ZAPLATYNSKY, I.

- The effect of cobalt content in U-700 type alloys on degradation of aluminide coatings
[NASA-TM-87173] p 87 N86-13408

ZARETSKY, E. V.

- Lubrication and performance of high-speed rolling-element bearings p 152 A86-18375
- Operating characteristics of a 0.87 kW-hr flywheel energy storage module p 152 A86-24864
- Lubricant and additive effects on spur gear fatigue life
[ASME PAPER 85-TRIB-14] p 155 A86-43542
- Design of traction drives
[NASA-RP-1154] p 157 N86-13734
- Gearing
[NASA-RP-1152] p 157 N86-14612
- Effect on interference fits on roller bearing fatigue life
[NASA-TM-87185] p 158 N86-19616

ZEINER, P. K.

- Advanced technology payoffs for future rotorcraft, commuter aircraft, cruise missile, and APU propulsion systems
[AIAA PAPER 86-1545] p 16 A86-42704

ZELBY, L. W.

- Transmission line design for a power distribution system at 20 kHz for aircraft
[NASA-CR-3987] p 32 N86-29818

ZELLER, M. V.

- Surface modification strategies for (100)3C-SiC
p 76 A86-47083

ZHANG, J.

- End-wall and profile losses in a low-speed axial flow compressor rotor
[ASME PAPER 85-GT-174] p 20 A86-22090

ZHANG, Q.-Z.

- Structure of nonevaporating sprays. II - Drop and turbulence properties p 125 A86-11237

ZIENKIEWICZ, O. C.

- Iterative methods for mixed finite element equations p 169 A86-34461

ZIERKE, W. C.

- The boundary layer on compressor cascade blades
[NASA-CR-177279] p 143 N86-27607

ZINN, B. T.

- An iterative finite element-integral technique for predicting sound radiation from turbofan inlets in steady flight p 198 A86-49806

ZIPH, B.

- Liquid fueled external heating system for STM4-120 Stirling engine p 180 A86-24888
- Experimental assessment of advanced Stirling component concepts
[NASA-CR-174994] p 210 N86-25302

ZOLA, C. A.

- The STOL performance of a two-engine, USB powered-lift aircraft with cross-shafted fans
[SAE PAPER 851839] p 16 A86-38336

ZUMWALT, G. W.

- Designing an electro-impulse de-icing system
[AIAA PAPER 86-0545] p 16 A86-19940
- An experimental method for measuring droplet impingement efficiency on two- and three-dimensional bodies
[AIAA PAPER 86-0406] p 131 A86-26630
- Analyses and tests for design of an electro-impulse de-icing system
[NASA-CR-174919] p 15 N86-27268
- De-icing of the altitude wind tunnel turning vanes by electro-magnetic impulse
[NASA-CR-177260] p 38 N86-27291

ZURAWSKI, R. L.

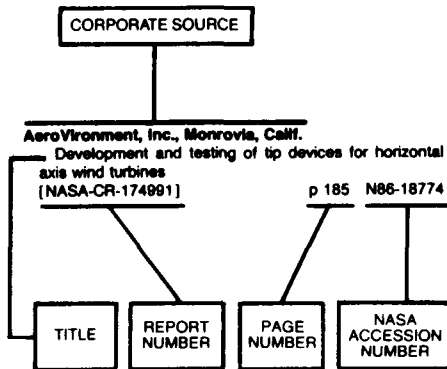
- Current evaluation of the tripropellant concept
[AIAA PAPER 86-1898] p 58 A86-49615
- Current evaluation of the tripropellant concept
[NASA-TP-2602] p 62 N86-28124

ZUSMAN, F. S.

- Spectrum orbit utilization program technical manual SOUP5 Version 3.8
[NASA-CR-174944] p 116 N86-26489
- Spectrum Orbit Utilization Program documentation: SOUP5 version 3.8 user's manual, volume 1, chapters 1 through 5 p 193 N86-27927
- Spectrum Orbit Utilization Program documentation: SOUP5 version 3.8 user's manual, volume 2, appendices A through G p 193 N86-27928
- [NASA-CR-174890]

CORPORATE SOURCE INDEX

Typical Corporate Source Index Listing



Listings in this index are arranged alphabetically by corporate source. The title of the document provides the user with a brief description of the subject matter. The report number helps to indicate the type of document cited (e.g., NASA report, translation, NASA contractor report). The NASA accession number denotes the number by which the citation is identified. The titles are arranged under each corporate source in ascending accession number order.

A

- Aerodyne Research, Inc., Billerica, Mass.**
Experimental and theoretical analysis of chemical vapor deposition with prediction of gravity effects p 41 N86-10132
- Aerojet Technical Systems Co., Sacramento, Calif.**
Longitudinal mode combustion instabilities of a high-pressure fuel-rich LOX/RP-1 preburner p 56 A86-49640
Longitudinal mode combustion instabilities of a high-pressure fuel-rich LOX/RP-1 preburner p 165 N86-28250
- Aerojet TechSystems Co., Sacramento, Calif.**
Orbital transfer vehicle engine integration study p 58 N86-17416
- Aerospace Corp., El Segundo, Calif.**
Coupling conditions for integrating boundary layer and rotational inviscid flow p 133 A86-41721
- AeroVironment, Inc., Monrovia, Calif.**
Development and testing of tip devices for horizontal axis wind turbines [NASA-CR-174991] p 185 N86-18774
- AlResearch Casting Co., Torrance, Calif.**
Fabrication of ceramic components for advanced gas turbine engines [SAE PAPER 851786] p 154 A86-38310
Processing study of injection molding of silicon nitride for engine applications [SAE PAPER 851787] p 154 A86-38311
- Akron Univ., Ohio.**
Life and reliability modeling of bevel gear reductions [ASME PAPER 85-DE-7] p 151 A86-14466
An experimental investigation and some analytical considerations concerning the vaporous/gaseous cavity characteristics of an eccentric shaft seal or bearing p 130 A86-24483
Hierarchical implicit dynamic least-square solution algorithm p 167 A86-26689

- Analysis of a two row hydrostatic journal bearing with variable properties, inertia effects and surface roughness p 153 A86-30599
Inelastic high-temperature thermomechanical response of ceramic coated gas turbine seals p 169 A86-37799
Locally bound constrained Newton-Raphson solution algorithms p 171 A86-43771
Constrained hierarchical least square nonlinear equation solvers p 171 A86-43774
Fatigue life analysis of a turboprop reduction gearbox [ASME PAPER 85-DET-10] p 155 A86-45256
NASA LeRC/Akron University Graduate Cooperative Fellowship Program and Graduate Student Researchers Program [NASA-CR-174826] p 207 N86-13219
Thermomechanical cyclic hardening behavior of Hastelloy-X [NASA-CR-174999] p 174 N86-16610
System life and reliability modeling for helicopter transmissions [NASA-CR-3967] p 159 N86-24990
Effects of state recovery on creep buckling under variable loading [NASA-CR-175094] p 212 N86-25310
Theoretical and experimental flow cell studies of a hydrogen-bromine fuel cell, part 1 [NASA-CR-177165] p 189 N86-29409
Jet fuel viscosity at low temperatures with notes on n-alkaline crystals [NASA-CR-174911] p 15 N86-30022
- Alphatech, Inc., Burlington, Mass.**
Application of FDI metrics to detection and isolation of sensor failures in turbine engines p 21 A86-35400
Robust detection-isolation-accommodation for sensor failures [NASA-CR-174797] p 121 N86-16486
- American Trucking Associations, Inc., Alexandria, Va.**
Future heavy duty trucking engine requirements [NASA-CR-174996] p 209 N86-17226
- Ames Lab., Iowa.**
Dislocations in extruded Co-49.3 at. pct Al p 83 A86-45091
- Analex Corp., Cleveland, Ohio.**
Testing of 30-GHz low noise receivers [AIAA PAPER 86-0654] p 45 A86-29616
Low power dc arcjet operation with hydrogen/nitrogen propellant mixtures [AIAA PAPER 86-1505] p 55 A86-42676
Verification of an improved computational design procedure for TWT-dynamic refocuser-MDC systems with secondary electron emission losses p 119 A86-45194
- Argonne National Lab., Ill.**
Effects of a high mean stress on the high cycle fatigue life of PWA 1480 and correlation of data by linear elastic fracture mechanics [NASA-CR-175057] p 177 N86-27689
- Arizona State Univ., Tempe.**
Concentration distributions in cylindrical combustors p 126 A86-11937
Rapid evaluation of ion thruster lifetime using optical emission spectroscopy [AIAA PAPER 85-2011] p 51 A86-17851
A comparison of three algebraic stress closures for combustor flow calculations [ASME PAPER 85-WA/FE-3] p 132 A86-38388
Concentration distributions in a model combustor p 133 A86-38575
Parameter sensitivity in the dynamics of rotor-bearing systems [ASME PAPER 85-DET-35] p 154 A86-38620
Local equilibrium assumption for round jet calculations p 136 A86-49829
Energy stability of thermocapillary convection in models of the float zone process p 40 N86-10123
Heat transfer characteristics within an array of impinging jets. Effects of crossflow temperature relative to jet temperature [NASA-CR-3936] p 139 N86-15625
Heat transfer to two-phase air/water mixtures flowing in small tubes with inlet disequilibrium [NASA-CR-175076] p 141 N86-22892

- On the modeling of low-Reynolds-number turbulence [NASA-CR-3994] p 32 N86-28089
- Arizona Univ., Tucson.**
Noise generated by convected gusts interacting with swept airfoil cascades [AIAA PAPER 86-1872] p 198 A86-45492
Influence of airfoil camber on convected gust interaction noise [AIAA PAPER 86-1873] p 198 A86-45493
- Army Armament Research and Development Command, Watervliet, N. Y.**
Wide-range displacement expressions for standard fracture mechanics specimens p 166 A86-20706
- Army Aviation Research and Development Command, Cleveland, Ohio.**
Small gas turbine combustor experimental study - Compliant metal/ceramic liner and performance evaluation [AIAA PAPER 86-1452] p 25 A86-49611
Theoretical and experimental comparison of vapor cavitation in dynamically loaded journal bearings [NASA-TM-87121] p 137 N86-11425
Micromechanisms of thermomechanical fatigue: A comparison with isothermal fatigue [NASA-TM-87331] p 92 N86-28164
Structure-to-property relationships in addition cured polymers 2: Resin Tg composite initial mechanical properties of norbornenyl cured polyimide resins [NASA-TM-88794] p 105 N86-29041
- Army Propulsion Lab., Cleveland, Ohio.**
Combustion research for gas turbine engines p 17 A86-11609
DEAN - A program for Dynamic Engine Analysis [AIAA PAPER 85-1354] p 18 A86-14430
Experimental study of ceramic-coated tip seals for turbojet engines p 152 A86-15227
Experimental study of the spray characteristics of a research airblast atomizer [ASME PAPER 85-GT-229] p 129 A86-22125
Theoretical modeling of the vapor cavitation in dynamically loaded journal bearings [ASME PAPER 85-TRIB-51] p 130 A86-24496
Three-dimensional inviscid analysis of radial-turbine flow and a limited comparison with experimental data p 4 A86-28702
The application of LQR synthesis techniques to the turboshaft engine control problem p 22 A86-35614
Generation of spiral bevel gears with zero kinematical errors and computer aided simulation of their meshing and contact p 154 A86-40656
Generated spiral bevel gears - Optimal machine-tool settings and tooth contact analysis [SAE PAPER 851573] p 154 A86-40678
Efficiency of nonstandard and high contact ratio involute spur gears [ASME PAPER 84-DET-172] p 155 A86-45255
Fatigue life analysis of a turboprop reduction gearbox [ASME PAPER 85-DET-10] p 155 A86-45256
Effect of area ratio on the performance of a 5.5:1 pressure ratio centrifugal impeller [ASME PAPER 86-GT-303] p 8 A86-48315
- Army Research and Technology Labs., Cleveland, Ohio.**
Effect of substituted phenylindimides on processing and properties of PMR polyimide composites p 94 A86-13179
Life and reliability modeling of bevel gear reductions [ASME PAPER 85-DE-7] p 151 A86-14466
A three-dimensional axisymmetric calculation procedure for turbulent flows in a radial vaneless diffuser [ASME PAPER 85-GT-133] p 3 A86-22733
- Arnold Engineering Development Center, Arnold Air Force Station, Tenn.**
Ribbon-burner simulation of T-700 turbine shroud for ceramic-lined seals research p 18 A86-15225
- Avco Corp., Stratford, Conn.**
Computation of three-dimensional, rotational flow through turbomachinery blade rows for improved aerodynamic design studies [ASME PAPER 86-GT-26] p 7 A86-48117

Avco Lycoming Div., Stratford, Conn.

- Small engine technology payoffs for future commuter aircraft
[AIAA PAPER 86-1544] p 23 A86-42703
- Avco Lycoming Div., Williamsport, Pa.**
Stratified charge rotary engine for general aviation
[ASME PAPER 86-GT-181] p 24 A86-48231

B

Babcock and Wilcox Co., Alliance, Ohio.

- Thermal dependence of stress-induced birefringence in single mode optical fibers p 202 A86-15263
- Development of optical diaphragm deflection sensors
[NASA-CR-175008] p 203 A86-15113

Battelle Columbus Labs., Ohio.

- Nonlinear damage analysis: Postulate and evaluation
[NASA-CR-168171] p 177 A86-26652

Beech Aircraft Corp., Wichita, Kans.

- Evaluation of propfan propulsion applied to general aviation
[NASA-CR-175020] p 30 A86-24695

Bell Telephone Labs., Inc., Allentown, Pa.

- Performance of direct and iterative algorithms on an optical systolic processor p 202 A86-17421

Boeing Aerospace Co., Huntsville, Ala.

- Space Station benefits from ECLS - Propulsion system synergism
[AIAA PAPER 86-1407] p 47 A86-42619

Boeing Aerospace Co., Seattle, Wash.

- Characterization methodology for PMR-15
p 65 A86-11272

- Space station propulsion requirements study
[NASA-CR-174934] p 57 A86-15339

Boeing Military Airplane Development, Wichita, Kans.

- An experimental method for measuring droplet impingement efficiency on two- and three-dimensional bodies
[AIAA PAPER 86-0406] p 131 A86-26630

Boeing Vertol Co., Philadelphia, Pa.

- Performance degradation of helicopters due to icing - A review p 16 A86-35668

Brown Univ., Providence, R. I.

- Contributions to the understanding of large-scale coherent structures in developing free turbulent shear flows
[NASA-CR-176772] p 142 A86-24932

C

California Inst. of Tech., Pasadena.

- Finite-amplitude steady waves in plane viscous shear flows
[AD-A165461] p 127 A86-19419
- Input current shaped ac-to-dc converters
[NASA-CR-176438] p 121 A86-15544
- Input-current shaped ac to dc converters
[NASA-CR-176787] p 123 A86-25693

California State Univ., Long Beach.

- An investigation of the transient thermal analysis of spur gears
[ASME PAPER 84-DET-92] p 155 A86-40683

California Univ., Berkeley.

- Dynamic features of combustion p 72 A86-12925
- Buoyancy effects on smoldering combustion
[IAF PAPER 85-289] p 72 A86-15805
- Grid-free simulation of diffusion using random walk methods p 196 A86-16521
- Temperature and velocity profiles in sooting free boundary layer flames
[AIAA PAPER 86-0575] p 73 A86-19962
- Numerical simulation of a turbulent flame stabilized behind a rearward-facing step p 73 A86-22774
- Formation and inflammation of a turbulent jet p 130 A86-23131

- Free surface phenomena under low- and zero-gravity conditions p 39 A86-10108
- A fundamental study of smoldering with emphasis on experimental design for zero-g p 41 A86-10162

- Aerodynamic properties of turbulent combustion fields
[NASA-CR-175005] p 28 A86-20393

- California Univ., Berkeley. Lawrence Berkeley Lab.**
Dynamic features of combustion p 72 A86-12925

California Univ., Irvine.

- Effect of liquid droplets on turbulence in a round gaseous jet
[NASA-CR-175063] p 29 A86-23597

California Univ., Los Angeles.

- Pretreatment effects on the morphology and properties of aluminum oxide thermally grown on NiCoCrAlY
p 97 A86-17495

- An analytical model for the vorticity associated with a transverse jet p 4 A86-28538

- Performance evaluation of a simulated data-flow computer with low-resolution actors p 194 A86-32051
- Packet flutter and aerodynamic modes for non-homogeneous airfoil cascades in highly distorted, periodic, stationary throughflows
[AIAA PAPER 86-0648] p 5 A86-38896
- Vortex modeling of single and multiple dilution jet mixing in a cross flow p 135 A86-46318

California Univ., San Diego.

- Flame propagation and extinction in particle clouds
[NASA-CR-177304] p 78 A86-27434

California Univ., San Diego, La Jolla.

- Particle cloud combustion experiment p 41 A86-10160

Calspan Corp., Buffalo, N. Y.

- Turbine-stage heat transfer - Comparison of short-duration measurements with state-of-the-art predictions
[AIAA PAPER 86-1485] p 134 A86-42856

- Heat-flux measurements for the rotor of a full-stage turbine. I - Time-averaged results
[ASME PAPER 86-GT-77] p 24 A86-48145

- Heat-flux measurements for the rotor of a full-stage turbine. II - Description of analysis technique and typical time-resolved measurements
[ASME PAPER 86-GT-78] p 24 A86-48146

Cambridge Univ. (England).

- High-pressure creep tests p 84 A86-46564

Carnegie-Mellon Univ., Pittsburgh, Pa.

- Performance of direct and iterative algorithms on an optical systolic processor p 202 A86-17421

- Stability of limit cycles in frictionally damped and aerodynamically unstable rotor stages p 18 A86-19198

- The effect of limiting aerodynamic and structural coupling in models of mistuned bladed disk vibration p 21 A86-26905

- Error-source effects in a high-accuracy optical finite-element processor p 192 A86-31571

- Influence of friction dampers on torsional blade flutter
[ASME PAPER 85-GT-170] p 21 A86-32957

- Turbulent two-phase flow in annular seals
[ASLE PREPRINT 86-AM-4G-3] p 156 A86-45391

- Space and frequency-multiplexed optical linear algebra processor - Fabrication and initial tests p 202 A86-48352

- Ignition and flame spread above liquid fuel pools p 41 A86-10163

- Fundamental studies on a heat driven lamp
[NASA-CR-176381] p 204 A86-15122

- Measurements in liquid fuel sprays
[NASA-CR-177088] p 144 A86-30960

Case Western Reserve Univ., Cleveland, Ohio.

- Calculation of recoil implantation profiles using known range statistics p 201 A86-11391

- The influence of cobalt, tantalum, and tungsten on the microstructure of single crystal nickel-base superalloys p 79 A86-12995

- The influence of cobalt, tantalum, and tungsten on the elevated temperature mechanical properties of single crystal nickel-base superalloys p 79 A86-12996

- The development of gamma-gamma-prime lamellar structures in a nickel-base superalloy during elevated temperature mechanical testing p 79 A86-14719

- Finite element analysis of residual stress in plasma-sprayed ceramic p 95 A86-15226

- Composition and properties of the so-called 'diamond-like' amorphous carbon films p 86 A86-16255

- Film and interstitial formation of metals in plasma-sprayed ceramics p 86 A86-17484

- Oscillatory thermocapillary flows p 129 A86-22413

- Implementation of a new type of time-of-flight laser anemometer p 146 A86-29755

- The crack layer approach to toughness characterization in steel p 82 A86-30010

- Analysis of a two row hydrostatic journal bearing with variable properties, inertia effects and surface roughness p 153 A86-30599

- Adsorption of O₂, SO₂, and SO₃ on nickel oxide - Mechanism for sulfate formation p 75 A86-34238

- The cyclic stress-strain behavior of a nickel-base superalloy at 650 C p 83 A86-45715

- Carbon monoxide production in low energy oxygen ion bombardment of pyrolytic graphite and Kapton surfaces p 76 A86-47078

- High temperature properties of equiatomic FeAl with ternary additions p 84 A86-47252

- Alloys based on NiAl for high temperature applications p 84 A86-47261

- Rapidly solidified NiAl and FeAl p 84 A86-47263

- High temperature oxidation of beta-NiAl p 85 A86-47268

- Dual-ion-beam deposition of carbon films with diamond-like properties p 65 A86-49855

- Solidification fundamentals p 39 A86-10090

- Surface-tension driven convection p 40 A86-10124

- The synthesis, characterization and thermal chemistry of modified norbornenyl PMR endcaps p 100 A86-11266

- Time dependency of strainrange partitioning life relationships
[NASA-CR-174946] p 174 A86-137555

- Combustor flame flashback
[NASA-CR-174061] p 183 A86-14727

- Low Reynold's number boundary layers in a disturbed environment
[NASA-CR-175031] p 139 A86-17665

- Analysis of the transient behavior of rubbing components
[NASA-CR-176546] p 102 A86-19484

- Effect of boron on tensile properties of B2 BeAl
[NASA-CR-175074] p 89 A86-21656

- High temperature dispersion strengthening of NiAl
[NASA-CR-175073] p 90 A86-22688

- Mutual coupling effects in antenna arrays, volume 1
[NASA-CR-176699] p 114 A86-22782

- Corrosion of nickel and cobalt base alloys in sulfate melts at 750 deg C
[NASA-CR-175111] p 91 A86-24817

- Fatigue crack layer propagation in silicon-iron
[NASA-CR-175115] p 177 A86-25851

- The evolution and growth of Al₂O₃ scales on beta-NiAl
[NASA-CR-175097] p 92 A86-27444

- A study of Kapton degradation under simulated shuttle environment
[NASA-CR-176850] p 78 A86-28136

Centro Tecnico Aeroespacial, San Jose dos Campos (Brazil).

- Relaminarization of the boundary layer over a flat plate in shock tube experiments
[AIAA PAPER 86-1238] p 133 A86-39865

CHAM of North America, Inc., Huntsville, Ala.

- Computational simulation of liquid rocket injector anomalies
[AIAA PAPER 86-1424] p 55 A86-42633

Chinese Academy of Sciences, Peking.

- On the determination of laminar flame speeds from stretched flames p 74 A86-22814

- Hybrid solid element with a traction-free cylindrical surface p 169 A86-34482

Cincinnati Univ., Ohio.

- Multi-grid technique for the solution of incompressible Navier-Stokes equations p 128 A86-21029

- Three dimensional flow phenomena in fluid machinery: Proceedings of the Winter Annual Meeting, Miami Beach, FL, November 17-22, 1985 p 4 A86-28682

- Diamondlike carbon films on semiconductors for insulated-gate technology p 120 A86-47077

- Three-dimensional flow field measurements in a radial inflow turbine scroll using LDV
[ASME PAPER 86-GT-122] p 7 A86-48181

- Anisotropic constitutive model for nickel base single crystal alloys: Development and finite element implementation
[NASA-CR-175015] p 176 A86-21952

- Dynamic loading on parallel shaft gears
[NASA-CR-179473] p 181 A86-28433

City Coll. of the City Univ. of New York.

- Infrared-photoinduced-absorption studies in soluble trans-polyacetylene p 204 A86-37075

- Three-dimensional fluid flow phenomena in the blade end wall corner region
[ASME PAPER 86-GT-179] p 7 A86-48229

Clemson Univ., S.C.

- Heat transfer and fluid mechanics measurements in transitional boundary layer flows
[ASME PAPER 85-GT-113] p 126 A86-13068

- Inverse design of axisymmetric flow passages using compressible viscous flow theory p 4 A86-26412

- Viscous compressible flow direct and inverse computation and illustrations
[NASA-CR-175037] p 28 A86-20391

Cleveland State Univ., Ohio.

- Effect of free stream turbulence on flow separation p 125 A86-11676

- Ion beam sputter-deposited thin film coatings for protection of spacecraft polymers in low earth orbit
[AIAA PAPER 85-0420] p 95 A86-14428

- Unsteady transonic flow in cascades p 4 A86-24693

- An embedding method for the steady Euler equations p 194 A86-30814

- Negative magnetoresistance of pitch-based carbon fibers Temperature and pressure dependence p 99 A86-35702

- Composite sandwich thermostructural behavior - Computational simulation
[AIAA PAPER 86-0948] p 170 A86-38842

- Reliability of void detection in structural ceramics by use of scanning laser acoustic microscopy p 163 A86-39027
- Torsional vibrations and dynamic loads in a basic planetary gear system p 156 A86-47354
- Compliance matrices for cracked bodies [NASA-CR-179478] p 179 N86-30236
- Colby Coll., Waterville, Maine.**
- Circuit transients due to negative bias arcs-II [AIAA PAPER 86-0366] p 52 A86-19835
- College of William and Mary, Williamsburg, Va.**
- A high-order language for a system of closely coupled processing elements [NASA-CR-177280] p 193 N86-27930
- Colorado State Univ., Fort Collins.**
- Current collection from the space plasma through defects in solar array insulation p 52 A86-18042
- Colorado Univ., Boulder.**
- Finite element simulation of temperature dependent free surface flows p 136 A86-47012
- Thermocapillary and diffusocapillary migration of a fluid drop p 40 N86-10128
- Columbia Univ., New York.**
- Interdiffusional effects between tungsten fibers and an iron-nickel-base alloy p 66 A86-14718
- Communications Satellite Corp., Clarksburg, Md.**
- Optimized three-dimensional lenses for wide-angle scanning p 109 A86-19184
- Connecticut Univ., Storrs.**
- Scalar and momentum turbulent transport experiments with swirling and nonswirling flows p 126 A86-11938
- Numerical and experimental investigation of nonswirling and swirling confined jets [AIAA PAPER 86-0040] p 127 A86-19651
- Fracture mechanics applied to nonisothermal fatigue crack growth p 81 A86-28951
- Impact wear of iron rich superalloys p 82 A86-34687
- Constructing multicomponent phase diagrams by overlapping ZPF lines p 83 A86-44038
- Horseshoe vortex formation around a cylinder [ASME PAPER 86-GT-246] p 8 A86-48274
- Elevated temperature biaxial fatigue [NASA-CR-175009] p 174 N86-11526
- Influence of large-scale motion on turbulent transport for confined coaxial jets. Volume 1: Analytical analysis of the experimental data using conditional sampling [NASA-CR-175035] p 29 N86-20395
- Cornell Univ., Ithaca, N.Y.**
- An implicit LU scheme for the Euler equations applied to arbitrary cascades p 2 A86-20131
- A theory of post-stall transients in axial compression systems. I - Development of equations [ASME PAPER 85-GT-171] p 19 A86-22088
- A theory of post-stall transients in axial compression systems. II - Application [ASME PAPER 85-GT-172] p 19 A86-22089
- Periodic oscillations observed in swirling flows with and without combustion p 73 A86-22755
- Transonic potential flow in hyperbolic nozzles p 5 A86-41723
- D**
- Dana Corp., Fort Wayne, Ind.**
- Generated spiral bevel gears - Optimal machine-tool settings and tooth contact analysis [SAE PAPER 851573] p 154 A86-40678
- Dartmouth Coll., Hanover, N.H.**
- The effects of grain size on the flow and fracture of long-range ordered alloys p 84 A86-47243
- Dayton Univ., Ohio.**
- Numerical simulation of unsteady flow in an axisymmetric shear layer [AIAA PAPER 86-0202] p 127 A86-19746
- Numerical simulation of the flowfield over ice accretion shapes [NASA-CR-176960] p 144 N86-30093
- Delaware Univ., Newark.**
- N/P GaAs concentrator solar cells with an improved grid and busbar contact design p 184 N86-17844
- Detroit Diesel Allison, Mich.**
- Gas side heat transfer p 138 N86-11507
- Detroit Diesel Allison, Indianapolis, Ind.**
- Life cycle cost assessment of future low heat rejection engines [SAE PAPER 860444] p 153 A86-37048
- Feasibility study for convertible engine torque converter [NASA-CR-175082] p 33 N86-30733
- Deutsche Forschungs- und Versuchsanstalt fuer Luft- und Raumfahrt, Cologne (West Germany).**
- Effect of multiple strain-anneal cycles on the 1000 C creep behaviour of gamma/gamma prime-alpha p 82 A86-30610

- Deutsche Forschungs- und Versuchsanstalt fuer Luft- und Raumfahrt, Goettingen (West Germany).**
- Shear layer excitation, experiment versus theory [NASA-CR-176604] p 140 N86-20722
- Douglas Aircraft Co., Inc., Long Beach, Calif.**
- Turbofan aft duct suppressor study program listing and user's guide [NASA-CR-175067] p 30 N86-25357
- Dow Corning Corp., Midland, Mich.**
- Organosiloxane working fluids for the liquid droplet radiator [NASA-CR-175033] p 102 N86-16381
- Drexel Univ., Philadelphia, Pa.**
- Ignition characteristics of rich n-heptane fuel sprays in the transition region [ASME PAPER 85-WA/HT-46] p 107 A86-38393
- Analysis of the effects of fuel spray characteristics on NO(x) formation [ASME PAPER 85-WA/HT-47] p 107 A86-38394
- Transition region ignition characteristics of n-heptane fuel sprays [NASA-CR-176364] p 77 N86-14331
- Structure-property characterization of rheocast and VADER processed IN-100 superalloy [NASA-CR-175014] p 88 N86-14354
- Oxides of nitrogen emissions from the combustion of monodisperse liquid fuel sprays [NASA-CR-176373] p 191 N86-14770
- Combustion characteristics in the transition region of liquid fuel sprays [NASA-CR-176564] p 77 N86-20517
- Duke Univ., Durham, N.C.**
- Frequency domain solutions to multi-degree-of-freedom, dry friction damped systems under periodic excitation p 170 A86-39485
- Acceleration of convergence of vector sequences p 195 A86-49850
- Dynalysis of Princeton, N.J.**
- Three dimensional flow phenomena in fluid machinery; Proceedings of the Winter Annual Meeting, Miami Beach, FL, November 17-22, 1985 p 4 A86-28682

E

- Embry-Riddle Aeronautical Univ., Daytona Beach, Fla.**
- An experimental investigation of propeller wakes using a laser Doppler velocimeter [AIAA PAPER 86-0080] p 18 A86-19677
- Engelhard Corp., Edison, N.J.**
- Develop and test fuel cell powered on-site integrated total energy systems: Phase 3, full-scale power plant development [NASA-CR-174948] p 182 N86-12757
- Develop and test fuel cell powered on-site integrated total energy systems: Phase 3, full-scale power plant development [NASA-CR-174998] p 182 N86-12758
- Develop and test fuel cell powered on-site integrated total energy systems [NASA-CR-174951] p 188 N86-25877
- Evansville Univ., Ind.**
- Theoretical study on the effect of the design of small (milli-Newton) thruster jets on molecular contamination for the space station [NASA-CR-177263] p 48 N86-26358

F

- Florida State Univ., Tallahassee.**
- Tone excited jets. V - A theoretical model and comparison with experiment p 196 A86-16470
- Florida Univ., Gainesville.**
- Properties of silicon suspensions and slip-cast bodies p 95 A86-15238
- Fluid flow and fuel-air mixing in a motored two-dimensional Wankel rotary engine [AIAA PAPER 86-1556] p 134 A86-42711
- Flow Application Research, Fremont, Calif.**
- Modeling the 3-D flow effects on deviation angle for axial compressor middle stages [ASME PAPER 85-GT-189] p 2 A86-22102
- Flow Research, Inc., Kent, Wash.**
- Propeller design by optimization [AIAA PAPER 86-0081] p 19 A86-19678
- Direct numerical simulations of chemically reacting turbulent mixing layers p 130 A86-25567
- Coherent structures in a turbulent mixing layer - A comparison between direct numerical simulations and experiments p 132 A86-30218
- Direct numerical simulations of a reacting mixing layer with chemical heat release p 76 A86-41711

- Fluidyne Engineering Corp., Columbus, Ohio.**
- Documentation of ice shapes accreted on the main rotor of a UH-1H helicopter in level flight [NASA-CR-175088] p 15 N86-22559
- Ford Aerospace and Communications Corp., Palo Alto, Calif.**
- Bipolar nickel-hydrogen battery development p 180 A86-24823
- Communication Platform Payload Definition (CPPD) study. Volume 1: Executive summary [NASA-CR-174828] p 49 N86-27403
- Communication Platform Payload Definition (CPPD) study. Volume 2: Technical report [NASA-CR-174829] p 49 N86-27404
- Communication Platform Payload Definition (CPPD) study. Volume 3: Addendum [NASA-CR-174830] p 49 N86-27405
- Spacecraft multibeam antenna system for 30/20 GHz [NASA-CR-174854] p 116 N86-31760

G

- Garrett Turbine Engine Co., Phoenix, Ariz.**
- Comparison of the contact stress and friction behavior of SiC and ZrO₂ materials p 95 A86-15237
- Modeling dilution of jet flowfields p 128 A86-20362
- Advanced technology payoffs for future rotorcraft, commuter aircraft, cruise missile, and APU propulsion systems [AIAA PAPER 86-1545] p 16 A86-42704
- Perspectives on dilution jet mixing [AIAA PAPER 86-1611] p 25 A86-49614
- Low-cost single-crystal turbine blades, volume 2 [NASA-CR-174852] p 29 N86-23588
- Dilution jet mixing program, supplementary report [NASA-CR-175043] p 141 N86-23856
- Dilution jet mixing program, phase 3 [NASA-CR-174884] p 142 N86-24938
- Preliminary evaluation of a compound cycle engine for shipboard gensets [NASA-CR-174851] p 160 N86-26629
- Advanced Gas Turbine (AGT) Technology Development Project annual report [NASA-CR-179485] p 211 N86-33211
- General Dynamics/Convair, San Diego, Calif.**
- Orbital transfer vehicle engine integration study p 58 N86-17416
- Orbital transfer vehicle engine integration study [NASA-CR-174842] p 59 N86-20493
- General Electric Co., Cincinnati, Ohio.**
- Subscale-model and full-scale engine mixed-flow exhaust system performance comparison p 18 A86-14528
- Evaluation of fuel preparation systems for lean premixing-prevaporizing combustors [ASME PAPER 85-GT-137] p 19 A86-22081
- The dynamics of a flexible bladed disc on a flexible rotor in a two-rotor system p 20 A86-25743
- A computer analysis program for interfacing thermal and structural codes p 193 A86-36861
- Burner liner thermal/structural load modelling p 173 N86-11514
- Component-specific modeling p 25 N86-11515
- Method for improving the fuel efficiency of a gas turbine engine [NASA-CASE-LEW-13142-2] p 28 N86-20389
- Burner liner thermal-structural load modelling [NASA-CR-174892] p 176 N86-21932
- Free jet feasibility study of a thermal acoustic shield concept for AST/VCE application-dual flow. Comprehensive data report. Volume 1: Test nozzles and acoustic data [NASA-CR-174817] p 200 N86-23371
- Free-jet feasibility study of a thermal acoustic shield concept for AST/VCE application-dual stream nozzles. Comprehensive data report. Volume 2: Laser velocimeter and suppressor. Base pressure data [NASA-CR-174818] p 201 N86-23372
- Extended parametric representation of compressor fans and turbines. Volume 1: CMGEN user's manual [NASA-CR-174845] p 159 N86-23936
- Extended parametric representation of compressor fans and turbines. Volume 2: Part user's manual (parametric turbine) [NASA-CR-174846] p 159 N86-23937
- Extended parametric representation of compressor fans and turbines. Volume 3: MODFAN user's manual (parametric modulating flow fan) [NASA-CR-174847] p 159 N86-23938
- Evaluation of capillary reinforced composites [NASA-CR-175061] p 70 N86-24780
- Burner liner thermal/structural load modeling: TRANCITS program user's manual [NASA-CR-174891] p 142 N86-24931

- Effects of surface chemistry on hot corrosion life
[NASA-CR-179471] p 32 N86-28087
- 1700 deg C optical temperature sensor
[NASA-CR-175108] p 203 N86-28729
- Improved fracture toughness corrosion-resistant bearing material
[NASA-CR-174990] p 162 N86-32743
- General Electric Co., Lynn, Mass.**
The application of LQR synthesis techniques to the turbohaft engine control problem p 22 A86-35614
- General Electric Co., Philadelphia, Pa.**
Mod-5A wind turbine generator program design report. Volume 2: Conceptual and preliminary design, book 1
[NASA-CR-174735-VOL-2-BK-1] p 183 N86-15722
- Mod-5A wind turbine generator program design report. Volume 2: Conceptual and preliminary design, book 2
[NASA-CR-174735-VOL-2-BK-2] p 183 N86-15723
- Mod-5A wind turbine generator program design report. Volume 3: Final design and system description, book 1
[NASA-CR-174735-VOL-3-BK-1] p 183 N86-15724
- Mod-5A wind turbine generator program design report. Volume 3: Final design and system description, book 2
[NASA-CR-174735-VOL-3-BK-2] p 183 N86-15725
- Mod-5A wind turbine generator program design report. Volume 4: Drawings and specifications, book 1
[NASA-CR-174735-VOL-4-BK-1] p 183 N86-15726
- Mod-5A wind turbine generator program design report. Volume 4: Drawings and specifications, book 2
[NASA-CR-174735-VOL-4-BK-2] p 184 N86-15727
- Mod-5A wind turbine generator program design report. Volume 4: Drawings and specifications, book 3
[NASA-CR-174735-VOL-4-BK-3] p 184 N86-15728
- Mod-5A wind turbine generator program design report. Volume 4: Drawings and specifications, book 4
[NASA-CR-174735-VOL-4-BK-4] p 184 N86-15729
- Mod-5A wind turbine generator program design report. Volume 4: Drawings and specifications, book 5
[NASA-CR-174735-VOL-4-BK-5] p 184 N86-15730
- Ceramic automotive Stirling engine study
[NASA-CR-174907] p 208 N86-16165
- Transformation toughened ceramics for the heavy duty diesel engine technology program, phase 2
[NASA-CR-175054] p 210 N86-22451
- MOD-5A wind turbine generator program design report: Volume 1: Executive Summary
[NASA-CR-174734] p 188 N86-27708
- General Electric Co., Wilmington, Mass.**
High accuracy fuel flowmeter
[NASA-CR-174869] p 150 N86-31030
- General Motors Corp., Indianapolis, Ind.**
Formation and inflammation of a turbulent jet
p 130 A86-23131
- Methods for improving reliability in ceramic turbine rotors
[SAE PAPER 851788] p 154 A86-38312
- Rotorcraft propulsion for year 2000 plus
[AIAA PAPER 86-1543] p 23 A86-42702
- Fatigue life analysis of a turboprop reduction gearbox
[ASME PAPER 85-DET-10] p 155 A86-45256
- Advanced Gas Turbine (AGT) technology report
[NASA-CR-175018] p 158 N86-20808
- Turbine vane external heat transfer. Volume 1: Analytical and experimental evaluation of surface heat transfer distributions with leading edge showerhead film cooling
[NASA-CR-174827] p 29 N86-21548
- General Tire and Rubber Co., Akron, Ohio.**
Inelastic high-temperature thermomechanical response of ceramic coated gas turbine seals p 169 A86-37799
- Georgia Inst. of Tech., Atlanta.**
Existence and stability, and discrete BB and rank conditions, for general mixed-hybrid finite elements in elasticity p 169 A86-34464
- Bounding solutions of geometrically nonlinear viscoelastic problems
[AIAA PAPER 86-0943] p 170 A86-38838
- On the equivalence of the incremental harmonic balance method and the harmonic balance-Newton Raphson method p 170 A86-40695
- Constitutive modeling of cyclic plasticity and creep, using an internal time concept p 170 A86-41673
- A study of spectrum fatigue crack propagation in two aluminum alloys. I - Spectrum simplification. II - Influence of microstructures p 85 A86-48973
- An iterative finite element-integral technique for predicting sound radiation from turbofan inlets in steady flight p 198 A86-49806
- Analysis of large, non-isothermal elastic-visco-plastic deformations
[NASA-CR-176220] p 172 N86-10588
- Bounding solutions of geometrically nonlinear viscoelastic problems
[NASA-CR-176219] p 195 N86-10860
- Technology for satellite power conversion
[NASA-CR-176554] p 186 N86-19742

- Technology for satellite power conversion
[NASA-CR-176777] p 187 N86-25042
- Yielding and deformation behavior of the single crystal nickel-base superalloy PWA 1480
[NASA-CR-175100] p 91 N86-25455
- Formulation of the nonlinear analysis of shell-like structures, subjected to time-dependent mechanical and thermal loading
[NASA-CR-177194] p 178 N86-28482
- Goodyear Aerospace Corp., Akron, Ohio.**
Operating characteristics of a 0.87 kW-hr flywheel energy storage module p 152 A86-24864
- Grumman Aerospace Corp., Bethpage, N.Y.**
Heat pipe radiator technology for space power systems
[AIAA PAPER 86-1300] p 47 A86-39907
- Guelph Univ. (Ontario).**
Composition and properties of the so-called 'diamond-like' amorphous carbon films p 96 A86-16255
- H**
- Hamilton Standard, Windsor Locks, Conn.**
Large-Scale Advanced Prop-Fan (LAP) pitch change actuator and control design report
[NASA-CR-174788] p 31 N86-27282
- System design and integration of the large-scale advanced prop-fan
[NASA-CR-174789] p 13 N86-31536
- Harvard Univ., Cambridge, Mass.**
A note on the finite differencing of the linearized primitive equations' lower boundary condition p 191 A86-28963
- Honeywell, Inc., Bloomington, Minn.**
Ka-band monolithic gain control amplifier p 119 A86-41343
- Honeywell Systems and Research Center, Minneapolis, Minn.**
Polynomic nonlinear dynamical systems - A residual sensitivity method for model reduction p 194 A86-35388
- Houston Univ., Tex.**
Free shear flows - Organized structures and effects of excitation
[AIAA PAPER 86-0235] p 131 A86-26614
- Coherent structures in a turbulent mixing layer - A comparison between direct numerical simulations and experiments p 132 A86-30218
- Howmet Turbine Components Corp., White Hall, Mich.**
Experimental study of ceramic-coated tip seals for turbojet engines p 152 A86-15227
- Hughes Research Labs., Malibu, Calif.**
K₂H concentration effect on the cycle life of nickel-hydrogen cells p 180 A86-24802
- Long life nickel electrodes for a nickel-hydrogen cell: Cycle life tests
[NASA-CR-174815] p 188 N86-25048
- Hughes Research Labs., Torrance, Calif.**
Designing a 25-kilowatt high frequency series resonant
[NASA-CR-176774] p 123 N86-24906
- I**
- IIT Research Inst., Chicago, Ill.**
Creep-rupture and fractographic analysis of Stirling engine superalloys tested in air and 15 MPa hydrogen
p 82 A86-30041
- High-pressure creep tests p 84 A86-46564
- Long-term stability and properties of zirconia ceramics for heavy duty diesel engine components
[NASA-CR-174943] p 209 N86-17224
- Creep-rupture behavior of iron superalloys in high-pressure hydrogen
[NASA-CR-175027] p 89 N86-17531
- Illinois Inst. of Tech., Chicago.**
Finite element simulation of temperature dependent free surface flows p 136 A86-47012
- Illinois Univ., Chicago.**
Generation of spiral bevel gears with zero kinematical errors and computer aided simulation of their meshing and contact p 154 A86-40656
- Generated spiral bevel gears - Optimal machine-tool settings and tooth contact analysis
[SAE PAPER 851573] p 154 A86-40678
- Illinois Univ., Urbana.**
Cryogenic operation of pseudomorphic AlGaAs/InGaAs single-quantum-well MODFETs p 117 A86-11998
- Character of laser-glazed, plasma-sprayed zirconia coatings on stainless steel substrata p 95 A86-15229
- High transconductance InGaAs/AlGaAs pseudomorphic modulation-doped field-effect transistors p 117 A86-18814

- Three-dimensional hybrid-stress finite element analysis of composite laminates with cracks and cutouts p 187 A86-26888
- Determination of carrier saturation velocity high-performance In(y)Ga(1-y)As/Al(x)Ga(1-x) modulation-doped field-effect transistors (with y between 0 and 0.2) p 118 A86-37212
- Strategy for reflector pattern calculation - Let the computer do the work p 110 A86-39555
- High-frequency noise of In(y)Ga(1-y)As/Al(x)Ga(1-x) MODFETs and comparison to GaAs/Al(x)Ga(1-x) MODFETs p 119 A86-43999
- Normal modes in an overmoded circular waveguide coated with lossy material p 119 A86-44001
- Input impedance of a probe-fed circular microstrip antenna with thick substrate p 120 A86-46666
- Flammability limits of gases under low gravity conditions p 42 N86-10111
- Numerical methods for analyzing electromagnetic scattering
[NASA-CR-176141] p 111 N86-10373
- The behavior of fuel-lean premixed flames in a standard flammability limit tube under controlled gravity conditions
[NASA-CR-177132] p 78 N86-28111
- MMIC devices for active phased array antennas
[NASA-CR-176990] p 116 N86-30001
- Illinois Univ., Urbana-Champaign.**
Dc and microwave characteristics of a high current double interface GaAs/InGaAs/AlGaAs pseudomorphic modulation-doped field-effect transistor p 118 A86-38066
- Optical constants of GaAs-AlGaAs superlattices and multiple quantum wells
[NASA-CR-176717] p 205 N86-23466
- Superlattices and NiPi structures in new forms cascade solar cells
[NASA-CR-176718] p 187 N86-24066
- Theoretical study of the transverse dielectric constants of superlattices and their alloys
[NASA-CR-177198] p 206 N86-28711
- A simple circular-polarized antenna: Circular waveguide horn coated with lossy magnetic material
[NASA-CR-177092] p 116 N86-30001
- Integral Technologies, Inc., Westmont, Ill.**
Methods for heat transfer and temperature field analysis of the insulated diesel phase 2 progress report
[NASA-CR-175072] p 210 N86-24555
- Iowa State Univ. of Science and Technology, Ames.**
Modeling the 3-D flow effects on deviation angle of axial compressor middle stages
[ASME PAPER 85-GT-189] p 2 A86-22111
- Iowa Univ., Iowa City.**
Improvement of ion thruster design
[NASA-CR-177223] p 61 N86-27411
- Irwin (Arthur S.) Co., Inc., Bemus Point, N.Y.**
Review and critical analysis: Rolling-element bearing for system life and reliability
[NASA-CR-174710] p 159 N86-24999
- Israel Atomic Energy Commission, BeerSheva.**
Radical molecule and ion-molecule mechanisms in the polymerization of hydrocarbons and chlorosilanes in R₂ plasmas at low pressures (below 1.0 Torr) p 203 A86-16231
- J**
- Jet Propulsion Lab., California Inst. of Tech., Pasadena.**
NASA electric propulsion technology
[AIAA PAPER 85-1899] p 51 A86-17831
- Modal test/analysis correlation for Centaur G Prime launch vehicle
[AIAA PAPER 86-1002] p 43 A86-38941
- John Carroll Univ., Cleveland, Ohio.**
All-fibre sensing loop using pulse-modulated light-emitting diode p 202 A86-11999
- Wavelength-division multiplexed digital optical position transducer p 145 A86-20779
- Range finding using frequency-modulated laser diode p 147 A86-39522
- Time domain referencing in intensity modulation fiber optic sensing systems
[NASA-CR-175109] p 17 N86-24699
- John Deere Technologies International, Inc., Wood-Ridge, N.J.**
Stratified charge rotary engine for general aviation
[ASME PAPER 86-GT-181] p 24 A86-48231

K

Kansas Univ., Lawrence.

Orientation and temperature dependence of some mechanical properties of the single-crystal nickel-base superalloy Rene N4. I - Tensile behavior

p 86 A86-50321

Experimental and analytical investigation of a freezing point depressant fluid ice protection system

[NASA-CR-174758] p 12 N86-27186

Kansas Univ. Center for Research, Inc., Lawrence.

An analysis of cross-coupling of a multicomponent jet engine test stand using finite element modeling techniques

[NASA-CR-178424] p 37 N86-15323

Statistical prediction of dynamic distortion of inlet flow using minimum dynamic measurement. An application to the Melick statistical method and inlet flow dynamic distortion prediction without RMS measurements

[NASA-CR-176764] p 142 N86-24933

Review and evaluation of recent developments in melic inlet dynamic flow distortion prediction and computer program documentation and user's manual estimating maximum instantaneous inlet flow distortion from steady-state total pressure measurements with full, limited, or no dynamic data

[NASA-CR-176765] p 143 N86-24955

Theoretical and software considerations for general dynamic analysis using multilevel substructured models

[NASA-CR-176822] p 195 N86-26067

Kelo Univ., Yokohama (Japan).

Effects of preferential diffusion on the burning intensity of curved flames

p 73 A86-22813

Kentucky Univ., Lexington.

Backward boundary layers in downward flame spread

p 73 A86-22793

Klein, Schanzlin und Becker A.G., Frankenthal (West Germany).

Laser velocimeter measurements in shrouded and unshrouded radial flow pump impellers

[ASME PAPER 86-GT-129] p 136 A86-48187

Kohman Systems Research, Inc., Lawrence, Kans.

The measurement of aircraft performance and stability and control after flight through natural icing conditions

[NASA-TM-87265] p 35 N86-22582

L

Leeds Univ. (England).

Structure and grain coarsening during the sintering of alumina

p 98 A86-26341

Little (Arthur D.), Inc., Cambridge, Mass.

Liquid belt radiator design study

[NASA-CR-174901] p 57 N86-16259

Lockheed Engineering and Management Services Co., Inc., Houston, Tex.

Numerical synthesis of tri-variate velocity realizations of turbulence

p 168 A86-28654

Lockheed-Georgia Co., Marietta.

Tone excited jets. I - Introduction

p 196 A86-16466

Tone excited jets. III - Flow measurements

p 127 A86-16468

Tone excited jets. IV - Acoustic measurements

p 196 A86-16469

An experimental study of tone-excited heated jets

p 197 A86-31593

Non-linear effects in finite amplitude wave propagation through ducts and nozzles

p 197 A86-35857

Evaluation of propeller/nacelle interactions in the PTA program

[AIAA PAPER 86-1552] p 6 A86-42709

Some unresolved questions on hot-jet mixing control through artificial excitation

[AIAA PAPER 86-1956] p 135 A86-45441

Development of an impulsive noise source to study the acoustic reflection characteristics of hard-walled wind tunnels

[AIAA PAPER 86-1887] p 198 A86-45500

Acoustic reflection contamination measurements in the 16-foot NASA Langley Transonic Wind Tunnel

[AIAA PAPER 86-1888] p 198 A86-45501

Acoustic control of free jet mixing

p 135 A86-46314

Lockheed Missiles and Space Co., Sunnyvale, Calif.

Strategy for reflector pattern calculation - Let the computer do the work

p 110 A86-39542

Louisiana State Univ., Baton Rouge.

Shock-tube pyrolysis of chlorinated hydrocarbons - Formation of soot

p 75 A86-35126

M

M/A-COM, Inc., Vienna, Va.

Simulated performance of the NASA 30/20 GHz test transponder using multi-H phase coded modulation

[AIAA PAPER 86-0717] p 110 A86-29656

MARC Analysis Research Corp., Palo Alto, Calif.

Efficient algorithms for use in probabilistic finite element analysis

p 168 A86-28655

Iterative methods for mixed finite element equations

p 169 A86-34461

Martin Marietta Aerospace, Denver, Colo.

Hybrid deployable/erectable solar dynamic box truss system

[AIAA PAPER 86-0955] p 47 A86-38883

Design optimization for a space based, reusable orbit transfer vehicle

p 48 A86-17418

Advanced orbit transfer vehicle propulsion system study

[NASA-CR-174843] p 60 N86-24746

Satellite voice broadcast. Volume 1: Executive summary

[NASA-CR-175016] p 115 N86-24875

Satellite voice broadcast. Volume 2: System study

[NASA-CR-175017] p 115 N86-24876

Martin Marietta Corp., Denver, Colo.

Cryogenic Fluid Management Facility

p 108 A86-37053

LH2 on-orbit storage tank support trunion design and verification

p 53 A86-37054

Maryland Univ., College Park.

Accuracy and directional sensitivity of the single-wire technique

p 146 A86-28541

Light scattering tests of fundamental theories of transport properties in the critical region

p 39 N86-10113

Massachusetts Inst. of Tech., Cambridge.

Effect of gravity on laminar premixed gas combustion. I - Flammability limits and burning velocities

p 72 A86-12413

Effect of gravity on laminar premixed gas combustion. II - Ignition and extinction phenomena

p 72 A86-12414

Grid-free simulation of diffusion using random walk methods

p 196 A86-16521

Finite elements based on consistently assumed stresses and displacements

p 166 A86-18123

Optimized three-dimensional lenses for wide-angle scanning

p 109 A86-19184

Propagation and stability of wavelike solutions of finite difference equations with variable coefficients

p 194 A86-20033

Thermal-mechanical fatigue crack growth in Inconel X-750

p 81 A86-20982

A theory of post-stall transients in axial compression systems. I - Development of equations

[ASME PAPER 85-GT-171] p 19 A86-22088

A theory of post-stall transients in axial compression systems. II - Application

[ASME PAPER 85-GT-172] p 19 A86-22089

Numerical simulation of a turbulent flame stabilized behind a rearward-facing step

p 73 A86-22774

Formation and inflammation of a turbulent jet

p 130 A86-23131

Aeroelastic formulations for turbomachines and propellers

p 20 A86-24677

A preliminary study of the modified Ericsson for space power

p 180 A86-24840

Hybrid solid element with a traction-free cylindrical surface

p 169 A86-34462

Three-dimensional inviscid flow in mixers. I - Mixer analysis using a Cartesian grid

p 5 A86-39090

Experimental measurements of heat transfer from an iced surface during artificial and natural cloud icing conditions

[AIAA PAPER 86-1352] p 36 A86-39948

Three-dimensional inviscid flow in mixers. II - Analysis of turbofan forced mixers

p 6 A86-46316

Analytical and experimental investigation of the coupled bladed disk/shaft whirl of a cantilevered turbofan

[ASME PAPER 86-GT-98] p 24 A86-48163

Simultaneous measurements of carbon monoxide and ozone in the NASA Global Atmospheric Sampling Program (GASP)

p 191 A86-48620

A computer simulation of the turbocharged turbo compounded diesel engine system: A description of the thermodynamic and heat transfer models

[NASA-CR-174971] p 208 N86-16164

Variable-reluctance motor drives for electric vehicle propulsion

[NASA-CR-176586] p 122 N86-20700

Thermal-mechanical fatigue behavior of nickel-base superalloys

[NASA-CR-175048] p 91 N86-24818

Stress waves in transversely isotropic media: The homogeneous problem

[NASA-CR-3977] p 164 N86-25002

Channel flow modeling of impingement cooling of a rotating turbine blade

[NASA-CR-177206] p 31 N86-27285

Wave propagation in anisotropic medium due to an oscillatory point source with application to unidirectional composites

[NASA-CR-4001] p 165 N86-27666

A supersonic fan equipped variable cycle engine for a Mach 2.7 supersonic transport

[NASA-CR-177141] p 32 N86-28946

Advanced rotary engine components utilizing fiber reinforced Mg castings

[AIAA PAPER 86-1559] p 67 A86-42712

Radiation energy receiver for solar propulsion systems

[NASA-CR-177141] p 52 A86-18043

Material Concepts, Inc., Columbus, Ohio.

Operational maintenance data base development for kinematic Stirling engines

[ASME PAPER 85-DGP-20] p 151 A86-14487

Automotive Stirling Engine Development Program

[NASA-CR-174749] p 211 N86-28017

Automotive Stirling engine development program

[NASA-CR-175045] p 211 N86-30579

Performance of oil pumping rings: An analytical and experimental study

[NASA-CR-175083] p 144 N86-31000

Michigan State Univ., East Lansing.

Measurements of energy distribution and wall temperature in flowing hydrogen microwave plasma systems

[AIAA PAPER 85-2052] p 203 A86-11001

Measurement of energy distribution in flowing hydrogen microwave plasmas

p 52 A86-18041

Entrainment region phenomena for a large plane shear layer

p 132 A86-30211

Effect of accuracy of wind power prediction on power system operator

[NASA-CR-176300] p 181 N86-11667

AC motor and generator requirements for isolated WECS

[NASA-CR-176315] p 182 N86-11670

Experimental evaluation criteria for constitutive models of time dependent cyclic plasticity

[NASA-CR-176821] p 176 N86-25850

Michigan Technological Univ., Houghton.

Modeling degradation and failure of Ni-Cr-Al overlay coatings

p 80 A86-16276

Stress and deformation modeling of multiple rotary combustion engine trochoid housings

[SAE PAPER 860614] p 156 A86-49624

The development and prevention of channel segregation during alloy solidification

p 38 N86-10086

Michigan Univ., Ann Arbor.

Spray atomization and combustion

[AIAA PAPER 86-0136] p 131 A86-26606

A mesh re-zoning technique for finite element simulations of metal forming processes

p 153 A86-36298

Modeling of zero gravity venting: Studies of two-phase heat transfer under reduced gravity

[NASA-CR-179662] p 144 N86-31826

Minnesota Univ., Minneapolis.

Heat transfer and fluid mechanics measurements in transitional boundary layer flows

[ASME PAPER 85-GT-113] p 126 A86-13068

Missouri Univ., Rolla.

A numerical model of acoustic choking. II - Shocked solutions

p 197 A86-20795

Modeling wind tunnel effects on the radiation characteristics of acoustic sources

p 197 A86-41889

Motorola, Inc., Scottsdale, Ariz.

The baseband processor in future satellite communication systems

[AIAA PAPER 86-0721] p 45 A86-29659

On the effectiveness of onboard processing

[AIAA PAPER 86-0721] p 45 A86-29659

Hard ACTS to follow

p 46 A86-35318

N

National Aeronautics and Space Administration, Washington, D.C.

Structural integrity and durability for Space Shuttle main engine and future reusable space propulsion systems

[AIAA PAPER 86-1513] p 55 A86-42682

National Aeronautics and Space Administration. Ames Research Center, Moffett Field, Calif.

The STOL performance of a two-engine, USB powered-lift aircraft with cross-shafted fans
[SAE PAPER 85-1839] p 16 A86-38336

National Aeronautics and Space Administration.

Goddard Space Flight Center, Greenbelt, Md.
Simultaneous measurements of carbon monoxide and ozone in the NASA Global Atmospheric Sampling Program (GASP) p 191 A86-48620

National Aeronautics and Space Administration.

Marshall Space Flight Center, Huntsville, Ala.
Energy broadening due to space-charge oscillations in high current electron beams p 202 A86-22890

National Aeronautics and Space Administration. White Sands Test Facility, N. Mex.

An experimental data base for material selection and design of high-speed, high-pressure, oxygen turbomachinery p 58 N86-17387

National Bureau of Standards, Gaithersburg, Md.

Interaction of flows with the crystal-melt interface p 132 A86-29419

National Bureau of Standards, Washington, D.C.

Neutron and X-ray diffraction of plasma-sprayed zirconia-yttria thermal barrier coatings p 96 A86-16269

National Technical Systems, Hartwood, Va.

Factors influencing the ultrasonic stress wave factor evaluation of composite material structures p 168 A86-34257

Naval Postgraduate School, Monterey, Calif.

A novel centrifugal diffuser test device
[ASME PAPER 85-IGT-135] p 3 A86-23927

Naval Ship Research and Development Center, Annapolis, Md.

A comparison of three algebraic stress closures for combustor flow calculations
[ASME PAPER 85-WA/FE-3] p 132 A86-38388
Local equilibrium assumption for round jet calculations p 136 A86-48829

Preliminary evaluation of a compound cycle engine for shipboard gensets
[NASA-CR-179451] p 160 N86-26629

Nebraska Univ., Lincoln.

Optical and interfacial electronic properties of diamond-like carbon films p 204 A86-16268

Nielsen Engineering and Research, Inc., Mountain View, Calif.

Unsteady forces on counter-rotating propeller blades
[AIAA PAPER 86-1804] p 22 A86-37827

North Carolina State Univ., Raleigh.

Linear dynamic coupling in geared rotor systems
[ASME PAPER 85-DET-11] p 154 A86-38617
Dry etching of beta-SiC in CF₄ and CF₄ + O₂ mixtures p 78 A86-47069

Northwestern Univ., Evanston, Ill.

Effects of preferential diffusion on the burning intensity of curved flames p 73 A86-22813
On the determination of laminar flame speeds from stretched flames p 74 A86-22814
An experimental investigation on flame interaction and the existence of negative flame speeds p 74 A86-22816

Probabilistic finite elements for transient analysis in nonlinear continua p 168 A86-28653
Theory of interactive combustion of counterflow premixed flames p 74 A86-32752

Notre Dame Univ., Ind.

Polynomial nonlinear dynamical systems - A residual sensitivity method for model reduction p 194 A86-35386

Nonlinear optimal control with tensors - Some computational issues p 194 A86-35419
Surface modification strategies for (100)3C-SiC p 76 A86-47083

O**Oakland Univ., Rochester, Mich.**

Liquid droplet radiator thermal characteristics
[AIAA PAPER 86-1162] p 133 A86-40578

Ohio State Univ., Columbus.

The role of service areas in the optimization of FSS orbital and frequency assignments
[AIAA PAPER 86-0636] p 45 A86-29599
Adaptive antenna arrays for weak interfering signals p 45 A86-34591

Polynomial nonlinear dynamical systems - A residual sensitivity method for model reduction p 194 A86-35386

The aerodynamics of rotor blades with ice shapes accreted in hover and in level flight p 5 A86-35655
The performance characteristics of simulated ice on rotorcraft airfoils p 14 A86-35656
Computer aided derivation of equations for composite

mechanics problems and finite element analyses

[AIAA PAPER 86-1016] p 170 A86-38873

Calculation of allowable orbital spacings for the fixed-satellite service

[NASA-CR-176273] p 43 N86-11212

The role of service areas in the optimization of FSS orbital and frequency assignments

[NASA-CR-176488] p 46 N86-18341

Engineering calculations for communications satellite systems planning

[NASA-CR-176555] p 114 N86-19493

Extensions of the Ritz-Galerkin method for the forced, damped vibrations of structural elements

p 176 N86-21909

Wind tunnel tests of rotor blade sections with replications of ice formations accreted in hover

[NASA-CR-175089] p 15 N86-22558

Broadcasting satellite service synthesis using gradient and cyclic coordinate search procedures

[NASA-CR-176708] p 114 N86-23781

A high frequency analysis of electromagnetic plane wave scattering by perfectly-conducting semi-infinite parallel plate and rectangular waveguides with absorber coated inner walls

[NASA-CR-179759] p 116 N86-32600

Oklahoma State Univ., Stillwater.

Multipark flow visualization of lateral jet injection into a swirling cross flow

p 1 A86-14561

Hot-wire measurements of a single lateral jet injected into swirling crossflow

[AIAA PAPER 86-0055] p 127 A86-19661

Swirling flows in typical combustor geometries

p 128 A86-20370

Accuracy and directional sensitivity of the single-wire technique

p 146 A86-28541

Measurements of a single lateral jet injected into swirling crossflow

[NASA-CR-175040] p 28 N86-20392

Lateral jet injection into typical combustor flowfields

[NASA-CR-3997] p 31 N86-28086

Oklahoma Univ., Norman.

Experiments on opposed lateral jets injected into swirling crossflow

[NASA-CR-175041] p 29 N86-20394

Transmission line design for a power distribution system at 20 kHz for aircraft

[NASA-CR-3987] p 32 N86-29818

Operations Research, Inc., Landover, Md.

An analysis of bidirectional use of frequencies for satellite communications

[AIAA PAPER 86-0635] p 110 A86-29664

An analysis of bi-directional use of frequencies for satellite communications

[AIAA PAPER 86-0635] p 111 A86-49568

Operations Research, Inc., Rockville, Md.

Spectrum Orbit Utilization Program documentation: SOUP5 version 3.8 user's manual, volume 1, chapters 1 through 5

[NASA-CR-174889] p 193 N86-27927

Spectrum Orbit Utilization Program documentation: SOUP5 version 3.8 user's manual, volume 2, appendices A through G

[NASA-CR-174890] p 193 N86-27928

Operations Research, Inc., Silver Spring, Md.

Spectrum orbit utilization program technical manual SOUP5 Version 3.8

[NASA-CR-174944] p 116 N86-26489

Oregon Graduate Center for Study and Research, Beaverton.

The effect of oxygen pressure on volatility and morphology of LaB₆ single crystal cathodes

p 204 A86-28076

P**Page (R. J.) Co., Santa Ana, Calif.**

Slip casting and extruding shapes of rhenium with metal oxide additives. 1: Feasibility demonstration

[NASA-CR-174970] p 63 N86-31648

Pennsylvania State Univ., State College.

The boundary layer on compressor cascade blades

[NASA-CR-177279] p 143 N86-27607

Pennsylvania State Univ., University Park.

Structure of nonevaporating sprays. II - Drop and turbulence properties

p 125 A86-11237

Tone excited jets. V - A theoretical model and comparison with experiment

p 196 A86-16470

Stability of limit cycles in frictionally damped and aerodynamically unstable rotor stages

p 18 A86-19198

Drop-turbulence interactions in a diffusion flame

p 73 A86-20139

End-wall and profile losses in a low-speed axial flow compressor rotor

[ASME PAPER 85-GT-174] p 20 A86-22090

Computation of turbulent rotating channel flow with algebraic Reynolds stress model

[AIAA PAPER 86-0214] p 130 A86-226

Influence of friction dampers on torsional blade flutter

[ASME PAPER 85-GT-170] p 21 A86-326

Recent skin friction techniques for compressible flow

[AIAA PAPER 86-1099] p 147 A86-384

Laser Doppler velocimeter measurement in the tip region of a compressor rotor

p 5 A86-390

Computation of viscous flows in turbomachine cascades with a space-marching method

p 5 A86-390

A comparison of computational methods for three-dimensional, turbulent turbomachinery flow fields

[AIAA PAPER 86-1599] p 6 A86-427

A space-marching method for viscous incompressible internal flows

p 135 A86-430

Computation of turbulent flows on rotating bodies: ducts

p 135 A86-463

Mass spectrometric studies of the electrical breakdown of thin polymer films

p 100 A86-470

Three-dimensional boundary layer on a compressor rotor blade at peak pressure rise coefficient

[ASME PAPER 86-GT-186] p 7 A86-482

Flow and atomization in flashing injectors

p 136 A86-494

Axial and torsional fatigue behavior of Waspaloy

[NASA-CR-175052] p 91 N86-254

Pennsylvania Univ., Philadelphia.

The reactions of cobalt, iron and nickel in SC atmospheres: Similarities and differences

p 75 A86-406

Pratt and Whitney Aircraft, East Hartford, Conn.

Lateral dampers for thrust bearings

[NASA-CR-174924] p 157 N86-114

Dynamic gas temperature measurement system

p 147 N86-114

Creep fatigue life prediction for engine hot section materials (isotropic)

p 174 N86-115

Preliminary design of a supersonic cruise aircraft high-pressure turbine

[NASA-CR-174878] p 26 N86-142

Thermal barrier coating life prediction model development

[NASA-CR-175087] p 103 N86-2271

Life prediction and constitutive models for engine hot section anisotropic materials program

[NASA-CR-174952] p 165 N86-250

Structural tailoring of engine blades (STAEBL) theoretical manual

[NASA-CR-175112] p 31 N86-272

Structural tailoring of engine blades (STAEBL) user manual

[NASA-CR-175113] p 31 N86-272

Pratt and Whitney Aircraft, West Palm Beach, Fla.

Further development of the dynamic gas temperature measurement system

[AIAA PAPER 86-1648] p 147 A86-427

Oxidizer heat exchanger component testing

[NASA-CR-179487] p 62 N86-299

Pratt and Whitney Aircraft Group, East Hartford, Conn.

Three-dimensional inviscid flow in mixers. II - Analysis of turbofan forced mixers

p 6 A86-4631

Turbine blade and vane heat flux sensor development phase 2

[NASA-CR-174995] p 26 N86-1222

Princeton Synergetics, Inc., N.J.

Evaluation of spacecraft technology programs (effect on communication satellite business ventures), volume 1

[NASA-CR-174978] p 112 N86-1645

Evaluation of spacecraft technology programs (effect on communication satellite business ventures), volume 2

[NASA-CR-174979] p 113 N86-1645

Princeton Univ., N. J.

Vibration characteristics of mistuned shrouded blade assemblies

[ASME PAPER 85-GT-115] p 19 A86-2206

The high-temperature oxidation of aromatic hydrocarbons

p 75 A86-4083

An LU implicit scheme for high speed inlet analysis

[AIAA PAPER 86-1520] p 6 A86-4268

Aeroelastic behavior of low aspect ratio metal and composite blades

[ASME PAPER 86-GT-243] p 171 A86-4827

Transport processes research

p 40 N86-1012

Electrohydrodynamics

p 41 N86-1013

Fundamental studies of droplet combustion at reduced gravity

p 42 N86-1016

Purdue Univ., Indianapolis, Ind.

Applications of variational principles in computer rotational flows

p 128 A86-2096

Purdue Univ., West Lafayette, Ind.

An experimental investigation of propeller wakes using a laser Doppler velocimeter

[AIAA PAPER 86-0080] p 18 A86-1967

Unsteady pressure measurements on a biconvex airfoil

- in a transonic oscillating cascade
[ASME PAPER 85-GT-212] p 3 A86-22731
- Aerodynamic detuning analysis of an unstalled supersonic turbomachine cascade
[ASME PAPER 85-GT-192] p 3 A86-22732
- Forced response analysis of an aerodynamically detuned supersonic turbomachine rotor
p 21 A86-26902
- Influence of temperature and hydroxyl concentration on incipient soot formation in premixed flames
p 74 A86-29070
- Aerodynamic and structural detuning of supersonic turbomachine rotors
p 21 A86-31595
- Unsteady forces on counter-rotating propeller blades
[AIAA PAPER 86-1804] p 22 A86-37827
- Passive control of aerodynamically forced vibrations of supersonic turbomachine rotors by splitter blades
[AIAA PAPER 86-0844] p 22 A86-38892
- Three dimensional unsteady aerodynamics and aeroelastic response of advanced turboprops
[AIAA PAPER 86-0846] p 22 A86-38894
- A stagnation pressure probe for droplet-laden air flow
p 133 A86-39077
- Transient engine performance with water ingestion
[AIAA PAPER 86-1621] p 23 A86-42755
- Dynamic delamination crack propagation in a graphite/epoxy laminate
p 68 A86-43010
- Characteristics of an axisymmetric sudden expansion flow
[NASA-CR-176278] p 151 N86-11465
- The predicted effect of aerodynamic detuning on coupled bending-torsion unstalled supersonic flutter
[NASA-TM-87240] p 11 N86-21513
- Spontaneous ignition delay characteristics of hydrocarbon fuel-air mixtures
[NASA-CR-175064] p 29 N86-21545

R

- RCA Astro-Electronics Div., Princeton, N. J.**
Communications platform payload definition study
[NASA-CR-174986] p 49 N86-27402
- Communications platform payload definition study, executive summary
[NASA-CR-174985] p 49 N86-27407
- Rensselaer Polytechnic Inst., Troy, N.Y.**
Ellipsometric surface analysis of wear tracks produced by different lubricants
[ASLE PREPRINT 85-TC-5A-2] p 151 A86-11016
- The effect of processing conditions on the GaAs/plasma-grown insulator interface
p 204 A86-18567
- Optical and other properties changes of M-50 bearing steel surfaces for different lubricants and additives prior to scuffing
p 97 A86-20435
- Interaction of flows with the crystal-melt interface
p 132 A86-29419
- Relaminarization of the boundary layer over a flat plate in shock tube experiments
[AIAA PAPER 86-1238] p 133 A86-39865
- Influence of melt convection on solid-liquid interface under terrestrial and reduced gravity environments
p 38 N86-10083
- Emission FTIR analyses of thin microscopic patches of jet fuel residues deposited on heated metal surfaces
[NASA-CR-176786] p 108 N86-25502
- Polarization modulated ellipsometry
[NASA-CR-177264] p 149 N86-26599
- Determination of solid mass fraction in partially frozen hydrocarbon fuels
[NASA-CR-179472] p 108 N86-26261
- Rice Univ., Houston, Tex.**
Numerical synthesis of tri-variate velocity realizations of turbulence
p 168 A86-26654
- Rockwell International Corp., Canoga Park, Calif.**
A 10,000 hour life multipropellant engine for Space Station applications
[AIAA PAPER 86-1403] p 54 A86-42616
- Orbit Transfer Rocket Engine Technology Program: Advanced engine study, task D.1/D.3
[NASA-CR-175084] p 61 N86-26369
- SSME long-life bearings
[NASA-CR-179455] p 160 N86-27643
- Small centrifugal pumps for low-thrust rocket engines
[NASA-CR-174913] p 162 N86-32741

S

- Saint Mary's Coll., Notre Dame, Ind.**
Surface modification strategies for (100)3C-SiC
p 76 A86-47083
- Santa Clara Univ., Calif.**
Research and development of neat alcohol fuel usage

- in automobiles
[NASA-CR-174813] p 108 N86-27460
- Science Applications, Inc., Chatsworth, Calif.**
Buoyancy effects upon vapor flame and explosion processes
p 41 N86-10181
- Science Applications International Corp., Chatsworth, Calif.**
Effects of buoyancy on gas jet diffusion flames - Experiment and theory
[IAF PAPER 85-288] p 72 A86-15804
- Science Applications International Corp., Princeton, N.J.**
Two dimensional, transient catalytic combustion of CO-air on platinum
p 71 A86-10201
- Scientific Research Associates, Inc., Glastonbury, Conn.**
Numerical study of three-dimensional turbulent flow interactions between blockage models and wind tunnels including longitudinally slotted test sections
[AIAA PAPER 85-5017] p 1 A86-11065
- Numerical and experimental investigation of nonswirling and swirling confined jets
[AIAA PAPER 86-0040] p 127 A86-19651
- Calculations of two and three-dimensional transonic cascade flow fields using the Navier-Stokes equations
[ASME PAPER 85-GT-66] p 2 A86-22046
- Numerical analysis of some supersonic viscous flows related to inlet and nozzle systems
[AIAA PAPER 86-1597] p 134 A86-42738
- Influence of large-scale motion on turbulent transport for confined coaxial jets. Volume 2: Navier-Stokes calculations of swirling and nonswirling confined coaxial jets
[NASA-CR-175036] p 28 N86-20390
- Scientific Systems, Inc., Cambridge, Mass.**
Bifurcation techniques for nonlinear dynamic analysis of compressor stall phenomena
p 22 A86-35403
- Sikorsky Aircraft, Stratford, Conn.**
The performance characteristics of simulated ice on rotorcraft airfoils
p 14 A86-35656
- SKF Industries, Inc., King of Prussia, Pa.**
Traction forces at solid-lubricated rolling/sliding contacts
[ASLE PREPRINT 85-AM-4E-2] p 151 A86-11091
- SOHIO Engineered Materials Co., Niagara Falls, N.Y.**
Sintered alpha silicon carbide ceramics for high temperature structural application - Status review and recent developments
[ASME PAPER 85-GT-127] p 97 A86-23921
- Solar Turbines International, San Diego, Calif.**
Rocket thrust chamber thermal barrier coatings
[NASA-CR-175022] p 59 N86-20497
- Southwest Research Inst., Houston, Tex.**
Effect of elevated temperature and pressure on sprays from simplex swirl atomizers
[ASME PAPER 85-GT-58] p 130 A86-22735
- Southwest Research Inst., San Antonio, Tex.**
Probabilistic structural analysis for space propulsion system components
p 168 A86-28659
- Constitutive modeling for isotropic materials (HOST)
[NASA-CR-174980] p 172 N86-10589
- Sliding seal materials for adiabatic engines, phase 2
[NASA-CR-179475] p 105 N86-29042
- SRI International Corp., Menlo Park, Calif.**
Development program on a cold cathode electron gun
[NASA-CR-174792] p 121 N86-14499
- Thermionic noise measurements for on-line dispenser cathode diagnostics for linear beam microwave tubes
[NASA-CR-175105] p 124 N86-28323
- Stanford Univ., Calif.**
Simultaneous measurements of velocity and pressure fields in subsonic and supersonic flows through image-intensified detection of laser-induced fluorescence
[AIAA PAPER 86-0161] p 145 A86-19726
- Analysis of the uncertainties in velocity measurements with triple hot-wire probes
p 130 A86-24468
- Dislocations in extruded Co-49.3 at pct Al
p 83 A86-45091
- Film cooling on a convex wall: Heat transfer and hydrodynamic measurements for full and partial coverage
[NASA-CR-174964] p 137 N86-10461
- State Univ. of New York, Albany.**
Wilson study cycles: Research relative to ocean geodynamic cycles
[NASA-CR-176560] p 192 N86-21092
- State Univ. of New York, Buffalo.**
Stress analysis of gas turbine engine structures using the boundary element method
p 169 A86-34444
- Advanced three-dimensional dynamic analysis by boundary element methods
p 169 A86-34445
- State Univ. of New York, Stony Brook.**
Neutron and X-ray diffraction of plasma-sprayed zirconia-yttria thermal barrier coatings
p 96 A86-16269
- Theory of homogeneous nucleation - A chemical kinetic view
p 72 A86-19389

- Stevens Inst. of Tech., Hoboken, N. J.**
Influence of rotation and pretwist on cantilever fan blade flutter
p 17 A86-11686
- Stirling Thermal Motors, Inc., Ann Arbor, Mich.**
Liquid fueled external heating system for STM4-120 Stirling engine
p 180 A86-24888
- Experimental assessment of advanced Stirling component concepts
[NASA-CR-174994] p 210 N86-25302
- Sverdrup Technology, Inc., Cleveland, Ohio.**
Prediction of heat release effects on a mixing layer
[AIAA PAPER 86-0058] p 129 A86-22676
- Test results of a 40 kW Stirling engine and comparison with the NASA-Lewis computer code predictions
p 181 A86-24889
- Prediction of the structure of fuel sprays in gas turbine combustors
[AIAA PAPER 86-0450] p 20 A86-26636
- Parametric effects of CFL number and artificial smoothing on numerical solutions using implicit approximate factorization algorithm
[AIAA PAPER 86-1059] p 132 A86-38427
- An LU implicit scheme for high speed inlet analysis
[AIAA PAPER 86-1520] p 6 A86-42687
- Torsional vibrations and dynamic loads in a basic planetary gear system
p 156 A86-47354
- A model for closing the inviscid form of the average-passage equation system
[ASME PAPER 86-GT-227] p 8 A86-48261
- Unified constitutive materials model development and evaluation for high-temperature structural analysis applications
p 172 A86-49133
- Prediction of the structure of fuel sprays in gas turbine combustors
[NASA-CR-175028] p 27 N86-16218
- An LU implicit scheme for high speed inlet analysis
[NASA-CR-175098] p 11 N86-23563
- Analytical determination of propeller performance degradation due to ice accretion
[NASA-CR-175092] p 15 N86-23577
- Prediction of heat release effects on a mixing layer
[NASA-CR-175044] p 142 N86-23857
- Calibration of droplet sizing and liquid water content instruments: Survey and analysis
[NASA-CR-175099] p 149 N86-26596
- Characterization of real gas properties for space shuttle main engine fuel turbine and performance calculations
[NASA-CR-175066] p 61 N86-27418
- Evaluation of a Stirling engine heater bypass with the NASA Lewis nodal-analysis performance code
[NASA-CR-179460] p 211 N86-31452
- Syracuse Univ., N. Y.**
Shear fatigue crack growth - A literature survey
p 167 A86-24219
- Fatigue crack growth under general-yielding cyclic-loading
p 171 A86-44339
- Grain boundary oxidation and oxidation accelerated fatigue crack nucleation and propagation
[NASA-CR-175050] p 89 N86-20542
- Fatigue crack growth under general-yielding cyclic-loading
[NASA-CR-175049] p 176 N86-21951
- Systems Control Technology, Inc., Palo Alto, Calif.**
Robust detection, isolation, and accommodation for sensor failures
p 21 A86-35402
- Robust detection, isolation and accommodation for sensor failures
[NASA-CR-174825] p 33 N86-30732
- Systems Science and Software, La Jolla, Calif.**
Threshold determining mechanisms for discharges in high voltage solar arrays
[AIAA PAPER 86-0364] p 52 A86-19834
- Energy broadening due to space-charge oscillations in high current electron beams
p 202 A86-22890
- The role of unneutralized surface ions in negative potential arcing
p 118 A86-25525

T

- Technion - Israel Inst. of Tech., Haifa.**
A comparison of electronic heterodyne moire deflectometry and electronic heterodyne holographic interferometry for flow measurements
[SAE PAPER 851896] p 146 A86-38359
- Acceleration of convergence of vector sequences
p 195 A86-49850
- Technion, Inc., Irvine, Calif.**
A 10,000 hour life multipropellant engine for Space Station applications
[AIAA PAPER 86-1403] p 54 A86-42616
- Teledyne CAE, Toledo, Ohio.**
The effects of strong shock loading on coupled bending-torsion flutter of tuned and mistuned cascades
p 20 A86-26893

- Year 2000 small engine technology payoffs in cruise missiles
[AIAA PAPER 86-1546] p 23 A86-42705
- Variable area radial turbine fabrication and test program
[NASA-CR-175091] p 32 N86-28947
- Teledyne Continental Motors, Muskegon, Mich.**
- Lightweight two-stroke cycle aircraft diesel engine technology enablement program, volume 1
[NASA-CR-174923-VOL-1] p 26 N86-13328
- Lightweight two-stroke cycle aircraft diesel engine technology enablement program, volume 2
[NASA-CR-174923-VOL-2] p 26 N86-13329
- Lightweight two-stroke cycle aircraft diesel engine technology enablement program, volume 3
[NASA-CR-174923-VOL-3] p 26 N86-13330
- Tennessee Univ. Space Inst., Tullahoma.**
- Gas flow environmental and heat transfer nonrotating 3D program p 137 N86-11506
- Mean velocity and turbulence measurements in a 90 deg curved duct with thin inlet boundary layer
[NASA-CR-174811] p 139 N86-16518
- Texas A&M Univ., College Station.**
- A numerical method for the design and analysis of counter-rotating propellers
[AIAA PAPER 84-1205] p 19 A86-20369
- Theory versus experiment for the rotordynamic coefficients of annular gas seals. I - Test facility and apparatus
[ASME PAPER 85-TRIB-1] p 152 A86-24481
- Performance degradation of helicopters due to icing - A review p 16 A86-35668
- Numerical evaluation of propeller noise including nonlinear effects p 23 A86-41726
- Experimental rotordynamic coefficient results for teeth-on-rotor and teeth-on-stator labyrinth gas seals
[ASME PAPER 86-GT-12] p 156 A86-48109
- A numerical method of calculating propeller noise including acoustic nonlinear effects p 199 N86-12011
- Development of constitutive models for cyclic plasticity and creep behavior of super alloys at high temperature
[NASA-CR-176418] p 88 N86-14356
- Integrated research in constitutive modelling at elevated temperatures, part 2
[NASA-CR-177233] p 178 N86-28455
- Experimental and theoretical study of propeller spinner/shank interference p 13 N86-29773
- Integrated research in constitutive modelling at elevated temperatures, part 1
[NASA-CR-177237] p 179 N86-30227
- Aerodynamic data banks for Clark-Y, NACA 4-digit and NACA 16-series airfoil families p 13 N86-30693
- A comparison of experimental and theoretical results for leakage, pressure gradients, and rotordynamic coefficients for tapered annular gas seal
[NASA-CR-179709] p 162 N86-32742
- Texas Instruments, Inc., Dallas.**
- 10-30 GHz monolithic GaAs travelling-wave divider/combiner p 118 A86-34882
- Texas Technological Univ., Lubbock.**
- Multipass flow visualization of lateral jet injection into a swirling cross flow p 1 A86-14561
- Textron Bell Aerospace Co., Buffalo, N. Y.**
- A long-life 50 lbf H₂/O₂ thruster for Space Station auxiliary propulsion p 55 A86-42617
- Thermo-Systems, Inc., St. Paul, Minn.**
- Heat transfer and fluid mechanics measurements in transitional boundary layer flows
[ASME PAPER 85-GT-113] p 126 A86-13068
- Toledo Univ., Ohio.**
- Interaction of sulfuric acid corrosion and mechanical wear of iron p 81 A86-20436
- Inverter design for high frequency power distribution p 117 A86-24831
- The effects of strong shock loading on coupled bending-torsion flutter of tuned and mistuned cascades p 20 A86-26893
- Simulated performance of the NASA 30/20 GHz test transponder using multi-H phase coded modulation
[AIAA PAPER 86-0717] p 110 A86-29656
- Operating aspects of an oil pumping ring seal
[ASME PAPER 85-TRIB-29] p 153 A86-34010
- Rotary transformer design with fixed magnetizing and/or leakage inductances p 119 A86-40462
- Reassessment of the theory of stimulated Raman scattering p 150 A86-40662
- Fluid flow and fuel-air mixing in a motored two-dimensional Wankel rotary engine
[AIAA PAPER 86-1558] p 134 A86-42711
- Mass transport phenomena between bubbles and dissolved gases in liquids under reduced gravity conditions p 39 N86-10110

- A numerical and experimental investigation of electrochemical aircraft deicing
[NASA-CR-175024] p 14 N86-20380
- Application of a personal computer for the uncoupled vibration analysis of wind turbine blade and counterweight assemblies
[NASA-CR-175090] p 188 N86-28511
- Transmission Research, Inc., Cleveland, Ohio.**
- Constitutive modelling of lubricants in concentrated contacts at high slide to roll ratios
[NASA-CR-175029] p 158 N86-17748
- TriSolar Corp., Bedford, Mass.**
- Development of a microprocessor controller for stand-alone photovoltaic power systems
[NASA-CR-174723] p 187 N86-21979
- TRW, Inc., Redondo Beach, Calif.**
- Resistojet operation with various propellants
[AIAA PAPER 85-1158] p 107 A86-37074
- Solar dynamic power for the Space Station
[AIAA PAPER 86-1299] p 54 A86-39906
- Satellite voice broadcast system study. Volume 1: Executive summary
[NASA-CR-174904] p 115 N86-24878
- TRW Space Technology Labs., Redondo Beach, Calif.**
- 10 kW solar array switching unit performance test results p 118 A86-24844
- Satellite voice broadcast system study, volume 2
[NASA-CR-174905] p 115 N86-24877
- Tufts Univ., Medford, Mass.**
- The effects of syntactic complexity on the human-computer interaction p 192 A86-36172
- Tuskegee Inst., Ala.**
- Characterisation of plasma in a rail gun p 118 A86-26051

U

- United Technologies Corp., East Hartford, Conn.**
- Stress analysis of gas turbine engine structures using the boundary element method p 169 A86-34444
- Three-dimensional inviscid flow in mixers. I - Mixer analysis using a Cartesian grid p 5 A86-39090
- Atomization and combustion characteristics of antimisting fuels using JT8D and air-boost injectors
[ASME PAPER 86-GT-223] p 24 A86-48257
- Horseshoe vortex formation around a cylinder
[ASME PAPER 86-GT-246] p 8 A86-48274
- United Technologies Corp., South Windsor, Conn.**
- Onsite 40-kilowatt fuel cell power plant manufacturing and field test program p 185 N86-18773
- Advanced on-site power plant development technology program
[NASA-CR-174709] p 187 N86-25040
- Advanced on-site power plant development technology program
[NASA-CR-175007] p 189 N86-29411
- United Technologies Corp., Windsor Locks, Conn.**
- Propeller noise caused by blade tip radial forces
[AIAA PAPER 86-1892] p 23 A86-45504
- United Technologies Research Center, East Hartford, Conn.**
- Deposit formation and heat-transfer characteristics of hydrocarbon rocket fuels p 106 A86-10028
- Scalar and momentum turbulent transport experiments with swirling and nonswirling flows p 126 A86-11938
- Low Reynolds number separation bubble research at UTRC p 126 A86-16311
- Long term deposit formation in aviation turbine fuel at elevated temperature
[AIAA PAPER 86-0525] p 107 A86-19929
- High Weber number SMD correlations for pressure atomizers
[ASME PAPER 85-GT-37] p 128 A86-22026
- Through-flow modeling of axial turbomachinery
[ASME PAPER 85-IGT-42] p 3 A86-23854
- Fuel deposit characteristics at low velocity
[ASME PAPER 85-IGT-130] p 107 A86-23922
- Calculation of three-dimensional boundary layers on rotating turbine blades p 131 A86-28896
- Dynamic characteristics of an assembly of prop-fan blades
[ASME PAPER 85-GT-134] p 21 A86-32958
- Three-dimensional inviscid flow in mixers. I - Mixer analysis using a Cartesian grid p 5 A86-39090
- Assessment of a parabolic analysis for axisymmetric internal flows in rocket and turbomachinery ducts
[AIAA PAPER 86-1598] p 134 A86-42739
- Forced mixer lobes in ejector designs
[AIAA PAPER 86-1614] p 134 A86-42752
- Mass and momentum turbulent transport experiments with swirling confined coaxial jets. II
[AIAA PAPER 86-1665] p 134 A86-42780

V

- Three-dimensional inviscid flow in mixers. II - Analysis of turbofan forced mixers p 6 A86-4631
- On the application of a linearized unsteady potential-flow analysis to fan-tip cascades
[ASME PAPER 86-GT-87] p 7 A86-4815
- High temperature static strain sensor development program p 148 N86-11506
- Demonstration test of burner liner strain measurement systems: Interim results p 173 N86-11506
- Assessment of a 3-D boundary layer code to predict heat transfer and flow losses in a turbine p 138 N86-11506
- Demonstration test of burner liner strain measurement system
[NASA-CR-174743] p 148 N86-21811
- Advanced turboprop vibratory characteristics
[NASA-CR-174708] p 30 N86-24666
- Measurements of a turbulent horseshoe vortex formed around a cylinder
[NASA-CR-3986] p 13 N86-28066
- Role of fuel chemical properties on combustor radiative heat load
[NASA-CR-177096] p 108 N86-30022
- University Coll. of Swansea (Wales).**
- Iterative methods for mixed finite element equations p 169 A86-3446
- University of Central Florida, Orlando.**
- Impact wear of iron rich superalloys p 82 A86-34668
- University of Southern California, Los Angeles.**
- Performance evaluation of a simulated data-flow computer with low-resolution actors p 194 A86-32055

Varian Associates, Palo Alto, Calif.

- High-efficiency AlGaAs-GaAs Cassegrainian concentrator cells p 185 N86-1784
- Virginia Polytechnic Inst. and State Univ., Blacksburg.**
- Resonant power processors. I - State plane analysis p 117 A86-1448
- Resonant power processors. II - Methods of control p 117 A86-1448
- Factors influencing the ultrasonic stress wave factor evaluation of composite material structures p 168 A86-3425
- Nondestructive characterization of RBSOA high-power bipolar transistors p 118 A86-3571
- Linear dynamic coupling in geared rotor systems
[ASME PAPER 85-DET-11] p 154 A86-3861
- State-plane analysis of parallel resonant converter p 119 A86-4043
- Real gas effects on the numerical simulation of hypersonic inlet p 6 A86-4632
- Thermodynamic evaluation of transonic compressor rotors using the finite volume approach
[NASA-CR-176428] p 27 N86-16222
- Closure of fatigue cracks at high strains
[NASA-CR-175021] p 175 N86-17788
- Development of LC-13C NMR
[NASA-CR-176658] p 107 N86-21700
- Analytical ultrasonics for evaluation of composite materials response. Part 2: Generation and detection p 200 N86-22977
- Thermodynamic evaluation of transonic compressor rotors using the finite volume approach
[NASA-CR-176840] p 143 N86-26544
- Ultrasonic stress wave characterization of composite materials
[NASA-CR-3976] p 165 N86-27666
- A study of the stress wave factor technique for nondestructive evaluation of composite materials
[NASA-CR-4002] p 165 N86-28444
- J-integral estimates for cracks in infinite bodies
[NASA-CR-179474] p 178 N86-28461
- Thermodynamic evaluation of transonic compressor rotors using the finite volume approach
[NASA-CR-176947] p 32 N86-30731
- Virginia Univ., Charlottesville.**
- Simplex finite element analysis of viscous incompressible flow with penalty function formulation p 129 A86-22615
- Laser velocimeter measurements in shrouded and unshrouded radial flow pump impellers
[ASME PAPER 86-GT-129] p 136 A86-48187
- Flow visualization of secondary flows in three curved ducts
[ASME PAPER 86-GT-166] p 136 A86-48216

W

Washington Univ., St. Louis, Mo.

- NASA Lewis Research Center low-gravity fluid management technology program p 44 A86-32906

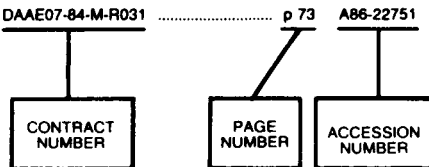
- Effect of subcooling on the on-orbit pressurization rate of cryogenic propellant tankage
[AIAA PAPER 86-1253] p 54 A86-39877
- Westinghouse Electric Corp., Baltimore, Md.**
Space and frequency-multiplexed optical linear algebra processor - Fabrication and initial tests
p 202 A86-48352
- Westinghouse Electric Corp., Pittsburgh, Pa.**
Gas cooled fuel cell systems technology development
[NASA-CR-175047] p 190 N86-31984
- Westinghouse Research and Development Center, Pittsburgh, Pa.**
Transmission electron microscopic examination of phosphoric acid fuel cell components
p 74 A86-23352
- Growth and characterization of epitaxial SrF₂ on InP(100)
p 205 A86-47076
- Design and evaluation of fluidized bed heat recovery for diesel engine systems
[NASA-CR-174898] p 209 N86-21456
- Double-injection, deep-impurity switch development
[NASA-CR-174836] p 124 N86-30073
- Wichita State Univ., Kans.**
An experimental method for measuring droplet impingement efficiency on two- and three-dimensional bodies
[AIAA PAPER 86-0406] p 131 A86-26630
- Particle trajectory computation on a 3-dimensional engine inlet
[NASA-CR-175023] p 14 N86-20379
- Theoretical analysis of the electrical aspects of the basic electro-impulse problem in aircraft de-icing applications
[NASA-CR-176808] p 17 N86-26330
- Analyses and tests for design of an electro-impulse de-icing system
[NASA-CR-174919] p 15 N86-27268
- De-icing of the altitude wind tunnel turning vanes by electro-magnetic impulse
[NASA-CR-177260] p 38 N86-27291
- Wichita Univ., Kans.**
Designing an electro-impulse de-icing system
[AIAA PAPER 86-0545] p 16 A86-19940
- A structural dynamics investigation related to EIDI applications
[AIAA PAPER 86-0550] p 16 A86-19942
- Wisconsin Univ., Madison.**
The plastic compressibility of 7075-T651 aluminum-alloy plate
p 85 A86-49690
- Containerless processing of undercooled melts
p 39 N86-10093
- Undercooling and solidification behavior in the InSb-Sb system
[NASA-CR-175013] p 88 N86-14355
- Power conversion distribution system using a resonant high-frequency AC link
[NASA-CR-176804] p 123 N86-25694
- Wisconsin Univ., Milwaukee.**
Triple-velocity products in a channel with a backward-facing step
p 133 A86-41725
- Turbulence energy and diffusion transport in a separating and reattaching flow
[AIAA PAPER 86-1724] p 135 A86-42812
- Improvement of the second- and third-moment modeling of turbulence: A study of Reynolds-stress closure model
[NASA-CR-176478] p 139 N86-16519
- Wright State Univ., Dayton, Ohio.**
Numerical simulation of unsteady flow in an axisymmetric shear layer
[AIAA PAPER 86-0202] p 127 A86-19746
- Wyle Labs., Inc., Huntsville, Ala.**
Accommodation requirements for microgravity science and applications research on space station
[NASA-CR-175038] p 42 N86-18334

Y

- Yale Univ., New Haven, Conn.**
Thermophoretically augmented mass transfer rates to solid walls across laminar boundary layers
p 128 A86-20150
- Yardney Electric Corp., Pawcatuck, Conn.**
Bipolar nickel-hydrogen battery development
p 180 A86-24823

CONTRACT NUMBER INDEX

Typical Contract Number Index Listing



Listings in this index are arranged alphanumerically by contract number. Under each contract number the NASA accession numbers denoting documents that have been produced as a result of research done under that contract are arranged in ascending order. The NASA accession number denotes the number by which the citation is identified.

DE-AI01-79ET-20485	p 181	N86-10643	DREXEL PROJ. 1098	p 77	N86-20517
	p 181	N86-11866	EPA-CR-809140-10	p 75	A86-35126
	p 187	N86-21979	F19628-82-C-0061	p 202	A86-22890
DE-AI01-80CS-50194	p 208	N86-16164	F19628-84-K-0026	p 204	A86-28076
	p 209	N86-17224	F33515-79-C-2087	p 7	A86-48153
	p 209	N86-17226	F33615-77-C-2083	p 3	A86-23854
	p 209	N86-21456	F33615-78-C-2401	p 133	A86-39077
	p 210	N86-24590	F33615-83-K-5016	p 166	A86-18123
DE-AI01-80ET-17088	p 182	N86-12757	F49620-82-K-0011	p 75	A86-40834
	p 182	N86-12758	F49620-82-K-0020	p 128	A86-20150
	p 188	N86-25877	F49620-82-K-0033	p 152	A86-24481
	p 190	N86-31984		p 156	A86-48109
DE-AI01-85CE-50112	p 208	N86-14106	F49620-83-K-0004	p 145	A86-19726
	p 208	N86-16165	GTRI PROJ. 3244	p 186	N86-19742
	p 89	N86-20541	JPL-956684	p 118	A86-35718
	p 103	N86-20568	NAG-419	p 116	N86-32598
	p 209	N86-21457	NAG1-287	p 132	A86-30211
	p 103	N86-21682	NAG1-379	p 142	N86-24932
	p 210	N86-25303	NAG1-575	p 202	A86-17421
	p 211	N86-30579		p 192	A86-31571
	p 144	N86-31000		p 202	A86-48352
DE-AI01-86CE-50162	p 105	N86-29042	NAG2-86	p 132	A86-30211
DE-AI05-82OR-1005	p 182	N86-11668	NAG3-106	p 200	N86-22975
	p 208	N86-13236	NAG3-11	p 142	N86-24933
	p 209	N86-19264		p 143	N86-24955
	p 210	N86-26261	NAG3-122	p 7	A86-48229
	p 211	N86-29732	NAG3-130	p 204	A86-37075
DE-AI21-80ET-17088	p 187	N86-25040	NAG3-131	p 72	A86-12925
	p 189	N86-29411		p 196	A86-16521
DE-AI31-80ET-17088	p 185	N86-18773		p 73	A86-22774
DE-AT03-76ER-72012	p 127	A86-19419		p 130	A86-23131
DE-FG02-84ER-45148	p 84	A86-47243	NAG3-132	p 28	N86-20393
DE-FG03-84ER-13274	p 74	A86-32752	NAG3-137	p 194	A86-32051
DE-FG05-84ER-13166	p 73	A86-22751	NAG3-137	p 72	A86-12925
DEN3-153	p 183	N86-15722	NAG3-13	p 84	A86-47243
	p 183	N86-15723	NAG3-143	p 108	N86-27460
	p 183	N86-15724	NAG3-147	p 39	N86-10108
	p 183	N86-15725		p 195	N86-28662
	p 183	N86-15726	NAG3-149	p 112	N86-12485
	p 184	N86-15727	NAG3-14	p 88	N86-14354
	p 184	N86-15728	NAG3-157	p 110	A86-29656
	p 184	N86-15729	NAG3-159	p 45	A86-29599
	p 184	N86-15730		p 43	N86-11212
	p 188	N86-27708		p 46	N86-18341
DEN3-167	p 95	A86-15237		p 114	N86-19493
	p 95	A86-15238	NAG3-163	p 114	N86-23781
	p 97	A86-23921	NAG3-164	p 100	N86-11266
	p 154	A86-38310	NAG3-166	p 96	A86-16269
DEN3-168	p 211	N86-33211	NAG3-167	p 156	A86-45391
	p 97	A86-23921		p 136	A86-49829
DEN3-17	p 154	A86-38312	NAG3-16	p 32	N86-28089
DEN3-217	p 158	N86-20808	NAG3-172	p 52	A86-18043
	p 97	A86-23921	NAG3-173	p 165	N86-28445
DEN3-241	p 82	A86-30041	NAG3-175	p 72	A86-12414
	p 84	A86-46564	NAG3-176	p 204	A86-18567
	p 182	N86-12757	NAG3-179	p 29	N86-23597
	p 182	N86-12758	NAG3-180	p 127	A86-19419
	p 188	N86-25877		p 129	A86-22615
DEN3-255	p 185	N86-18773		p 136	A86-48187
DEN3-256	p 144	N86-31000	NAG3-181	p 136	A86-48218
DEN3-289	p 187	N86-25040		p 152	A86-24481
	p 189	N86-29411	NAG3-186	p 162	N86-32742
DEN3-290	p 74	A86-23352	NAG3-190	p 156	A86-47354
	p 190	N86-31984		p 125	A86-11237
DEN3-303	p 84	A86-46564		p 73	A86-20139
DEN3-305	p 209	N86-17224	NAG3-194	p 131	A86-26606
DEN3-310	p 187	N86-21979	NAG3-198	p 128	A86-21029
DEN3-312	p 208	N86-16165	NAG3-19	p 140	N86-20722
DEN3-323	p 151	A86-11091		p 2	A86-20131
DEN3-324	p 95	A86-15237		p 5	A86-41723
DEN3-329	p 153	A86-37048	NAG3-1	p 107	A86-38394
DEN3-32	p 151	A86-14467		p 191	N86-14770
	p 211	N86-28017	NAG3-200	p 24	A86-48163
DEN3-339	p 211	N86-30579	NAG3-201	p 128	A86-20150
DEN3-341	p 185	N86-18774	NAG3-205	p 108	N86-25502
DEN3-342	p 210	N86-24590	NAG3-206	p 61	N86-27419
DEN3-345	p 209	N86-21456	NAG3-210	p 168	A86-28654
DEN3-351	p 210	N86-25302	NAG3-211	p 68	A86-43010
DEN3-352	p 105	N86-29042	NAG3-213	p 108	N86-28261
DEN3-35	p 158	N86-17748	NAG3-222	p 97	A86-20435
DEN3-363	p 89	N86-17531	NAG3-223	p 149	N86-26599
DE0AI01-79ET-20305	p 188	N86-27708		p 82	A86-30010
				p 177	N86-25851

CONTRACT

NAG3-226

CONTRACT NUMBER INDE

NAG3-226	p 29	N86-21545	NAG3-3	p 130	A86-24468	NAG3-560	p 38	N86-10086
NAG3-22	p 151	A86-11016	NAG3-403	p 137	N86-10461	NAG3-563	p 89	N86-21656
	p 87	N86-12293	NAG3-404	p 144	N86-31826	NAG3-566	p 131	A86-26630
NAG3-230	p 139	N86-17665	NAG3-405	p 41	N86-10163		p 14	N86-20379
NAG3-231	p 18	A86-19198		p 117	A86-14481	NAG3-568	p 40	N86-10123
NAG3-232	p 193	N86-27930		p 117	A86-14482	NAG3-570	p 40	N86-10124
NAG3-242	p 16	A86-35668	NAG3-406	p 131	A86-26614	NAG3-571	p 147	A86-39521
NAG3-248	p 83	A86-45091	NAG3-410	p 66	A86-14718	NAG3-574	p 132	A86-30211
NAG3-257	p 122	N86-20700	NAG3-411	p 29	A86-22413	NAG3-576	p 52	A86-19835
NAG3-258	p 73	A86-22793	NAG3-417	p 39	N86-10090	NAG3-578	p 54	A86-39877
NAG3-259	p 41	N86-10130	NAG3-418	p 117	A86-24831	NAG3-580	p 154	A86-38620
NAG3-260	p 126	A86-11937		p 120	A86-46638	NAG3-581	p 134	A86-42656
	p 132	A86-38368	NAG3-419	p 115	N86-25650		p 24	A86-48145
	p 133	A86-38575	NAG3-422	p 184	N86-17844		p 24	A86-48146
	p 136	A86-49829	NAG3-424	p 178	N86-21909	NAG3-593	p 27	N86-16220
NAG3-264	p 91	N86-25454	NAG3-426	p 76	A86-47078		p 143	N86-26546
NAG3-265	p 169	A86-37799		p 78	N86-28136		p 32	N86-30731
NAG3-26	p 7	A86-48181	NAG3-428	p 76	A86-47083	NAG3-5	p 202	A86-17421
NAG3-271	p 82	A86-34687	NAG3-434	p 204	A86-28076		p 192	A86-31571
	p 83	A86-44038	NAG3-436	p 39	N86-10093		p 202	A86-48352
NAG3-273	p 12	N86-27186	NAG3-437	p 204	N86-15122	NAG3-607	p 38	N86-27291
NAG3-280	p 81	A86-20982	NAG3-438	p 175	N86-17788	NAG3-610	p 134	A86-42752
	p 91	N86-24818		p 178	N86-28467	NAG3-613	p 117	A86-11998
NAG3-282	p 188	N86-19742	NAG3-443	p 72	A86-15805		p 117	A86-18814
	p 187	N86-25042		p 41	N86-10162		p 118	A86-36009
NAG3-284	p 16	A86-19940	NAG3-447	p 40	N86-10129		p 118	A86-37295
	p 16	A86-19942	NAG3-451	p 97	A86-17495		p 119	A86-43914
	p 17	N86-26330	NAG3-457	p 209	N86-17226	NAG3-615	p 121	N86-15544
	p 15	N86-27268	NAG3-469	p 134	A86-42656		p 123	N86-25693
NAG3-285	p 145	A86-19726		p 24	A86-48145	NAG3-62	p 133	A86-39077
NAG3-286	p 126	A86-13068	NAG3-46	p 24	A86-48146	NAG3-665	p 144	N86-30093
NAG3-290	p 183	N86-14727	NAG3-470	p 170	A86-41673	NAG3-666	p 36	A86-39948
NAG3-291	p 114	N86-22782	NAG3-471	p 39	N86-10113	NAG3-673	p 142	N86-24932
NAG3-292	p 133	A86-39865	NAG3-473	p 78	N86-27434	NAG3-674	p 48	N86-26358
NAG3-294	p 75	A86-38090	NAG3-475	p 119	A86-44078	NAG3-697	p 32	N86-28946
NAG3-2	p 146	A86-29755		p 111	N86-10377	NAG3-72	p 14	N86-20380
NAG3-303	p 40	N86-10117	NAG3-476	p 116	N86-30039	NAG3-74	p 128	A86-20370
NAG3-304	p 153	A86-30599	NAG3-477	p 118	N86-32600		p 146	A86-28541
NAG3-308	p 19	A86-22068	NAG3-478	p 75	A86-35126	NAG3-76	p 118	A86-26051
	p 171	A86-48271	NAG3-47	p 119	A86-40462	NAG3-85	p 37	N86-15323
NAG3-310	p 75	A86-40834	NAG3-481	p 17	A86-11686	NAG3-8	p 71	A86-10201
NAG3-31	p 88	N86-14356	NAG3-483	p 23	A86-42755	NAG3-89	p 118	A86-35718
NAG3-323	p 168	A86-34257	NAG3-488	p 5	A86-38896	NAG3-9	p 194	A86-20033
	p 200	N86-22973	NAG3-48	p 15	N86-30022	NASA ORDER C-91113-D	p 177	N86-27689
NAG3-328	p 165	N86-27665	NAG3-490	p 180	N86-25793	NASA ORDER H-27954-B	p 132	A86-29419
	p 164	N86-25002	NAG3-491	p 201	A86-11391	NASA ORDER L-814740	p 59	N86-20493
NAG3-32	p 165	N86-27666		p 178	N86-28455	NAS3-14	p 88	N86-14355
NAG3-333	p 195	N86-28067	NAG3-492	p 179	N86-30227	NAS3-160	p 174	N86-11526
	p 38	N86-10063	NAG3-493	p 123	N86-25694	NAS3-181	p 156	A86-48109
	p 192	N86-21092		p 136	A86-47012	NAS3-20073	p 29	N86-23598
NAG3-335	p 31	N86-27285	NAG3-495	p 40	N86-10128	NAS3-20357	p 26	N86-14272
NAG3-337	p 174	N86-13755	NAG3-496	p 95	A86-15229	NAS3-20797	p 197	A86-35857
NAG3-339	p 194	A86-30814		p 85	A86-47266	NAS3-21987	p 196	A86-16466
NAG3-33	p 166	A86-18123	NAG3-499	p 92	N86-27444		p 127	A86-16468
	p 132	A86-29419	NAG3-500	p 22	A86-38894		p 196	A86-16469
NAG3-340	p 169	A86-34482	NAG3-502	p 189	N86-29409	NAS3-22006	p 196	A86-16470
NAG3-341	p 208	N86-16184	NAG3-503	p 151	N86-11485	NAS3-22045	p 19	A86-22081
NAG3-346	p 75	A86-34238	NAG3-507	p 91	N86-25455	NAS3-22110	p 24	A86-48257
NAG3-348	p 169	A86-34484		p 205	N86-23468		p 141	N86-23856
	p 167	A86-24219	NAG3-508	p 187	N86-24007	NAS3-22137	p 142	N86-24938
	p 171	A86-44339	NAG3-50	p 206	N86-28759		p 200	N86-23371
NAG3-34	p 89	N86-20542	NAG3-511	p 32	N86-29818	NAS3-22139	p 201	N86-23372
	p 178	N86-21951	NAG3-516	p 207	N86-13219	NAS3-22218	p 150	N86-31030
NAG3-350	p 19	A86-22088		p 176	N86-21952		p 26	N86-13328
	p 39	N86-10110	NAG3-517	p 170	A86-39485		p 26	N86-13329
	p 127	A86-19651	NAG3-51	p 170	A86-40695	NAS3-22238	p 26	N86-13330
	p 28	N86-20390		p 107	N86-21704		p 180	A86-24802
NAG3-354	p 29	N86-20395	NAG3-521	p 182	A86-38172	NAS3-22257	p 188	N86-25046
	p 19	A86-20369	NAG3-526	p 178	N86-25850	NAS3-22498	p 11	N86-21505
	p 23	A86-41726	NAG3-527	p 2	A86-22102	NAS3-22502	p 116	N86-31760
NAG3-357	p 199	N86-12011	NAG3-527	p 127	A86-19746	NAS3-22508	p 109	A86-21882
	p 196	A86-45492	NAG3-530	p 147	A86-38460	NAS3-22523	p 162	N86-32743
	p 198	A86-45493	NAG3-534	p 182	N86-11670	NAS3-22525	p 65	N86-11272
NAG3-360	p 74	A86-29070		p 170	A86-38838		p 31	N86-27283
NAG3-361	p 73	A86-22813	NAG3-535	p 172	N86-10588	NAS3-22541	p 31	N86-27284
	p 74	A86-22814	NAG3-536	p 195	N86-10860	NAS3-22550	p 191	A86-48620
	p 74	A86-22816	NAG3-538	p 178	N86-28462	NAS3-22647	p 81	A86-28951
NAG3-363	p 74	A86-32752		p 168	A86-28653		p 56	A86-49640
	p 134	A86-42711	NAG3-543	p 45	A86-34591	NAS3-22759	p 165	N86-28250
NAG3-366	p 10	N86-19289	NAG3-546	p 4	A86-26412	NAS3-22761	p 134	A86-42738
	p 202	A86-11995		p 28	N86-20391	NAS3-22763	p 138	N86-11507
NAG3-367	p 17	N86-24691		p 4	A86-28538	NAS3-22766	p 22	A86-35614
NAG3-369	p 21	A86-26905		p 135	A86-46318	NAS3-22771	p 30	N86-25357
NAG3-374	p 102	N86-19464		p 133	A86-41725		p 126	A86-11938
	p 15	N86-22558		p 135	A86-42812	NAS3-22822	p 134	A86-42780
NAG3-379	p 15	N86-22559	NAG3-548	p 139	N86-16519		p 72	A86-15804
	p 174	N86-16610	NAG3-549	p 125	A86-11676		p 41	N86-10161
	p 212	N86-25310		p 1	A86-14561	NAS3-22825	p 177	N86-26652
NAG3-380	p 42	N86-10165		p 127	A86-19661	NAS3-22885	p 116	N86-26489
NAG3-381	p 41	N86-10160		p 28	N86-20392		p 193	N86-27927
NAG3-382	p 107	A86-38393	NAG3-54	p 29	N86-20394	NAS3-23039	p 193	N86-27928
	p 77	N86-14331		p 31	N86-28086		p 5	A86-39090
	p 77	N86-20517	NAG3-551	p 187	A86-26689	NAS3-23051	p 6	A86-46316
NAG3-387	p 90	N86-22688	NAG3-55	p 171	A86-43771		p 23	A86-45504
NAG3-388	p 153	A86-36298		p 119	A86-40431		p 31	N86-27282
NAG3-399	p 181	N86-11667		p 159	N86-24990		p 13	N86-31536

NAS3-23053	p 134	A86-42738	p 132	A86-38427	NSG-3180	p 195	A86-49650	
NAS3-23055	p 159	N86-23936	p 6	A86-42688	NSG-3188	p 161	N86-28433	
	p 159	N86-23937	p 27	N86-16218	NSG-3196	p 52	A86-18042	
	p 159	N86-23938	p 11	N86-23563	NSG-3208	p 19	A86-22088	
NAS3-23154	p 147	N86-11499	p 15	N86-23577		p 19	A86-22089	
NAS3-23157	p 3	A86-23854	p 142	N86-23857	NSG-3212	p 5	A86-39064	
NAS3-23159	p 123	N86-24806	p 149	N86-26596		p 7	A86-48236	
NAS3-23164	p 162	N86-32741	p 61	N86-27418	NSG-3231	p 197	A86-20795	
NAS3-23167	p 128	A86-22026	p 211	N86-31452	NSG-3238	p 8	A86-48274	
	p 108	N86-30023	NAS3-24224	p 1	A86-11065	p 13	N86-28083	
NAS3-23173	p 32	N86-28947		p 134	A86-42738	p 154	A86-38817	
NAS3-23245	p 53	A86-37054	NAS3-24228	p 147	A86-42770	p 79	A86-14719	
NAS3-23250	p 109	A86-19184	NAS3-24229	p 76	A86-41711	p 143	N86-27607	
NAS3-23260	p 157	N86-17408	NAS3-24232	p 115	N86-24877	p 145	A86-19670	
NAS3-23262	p 59	N86-20497		p 115	N86-24878	p 130	A86-22682	
NAS3-23265	p 107	A86-37074	NAS3-24233	p 115	N86-24875	p 5	A86-39089	
NAS3-23272	p 173	N86-11514		p 115	N86-24876	p 6	A86-42740	
	p 176	N86-21932	NAS3-24235	p 49	N86-27403	p 135	A86-43037	
	p 142	N86-24931		p 49	N86-27404	p 135	A86-46307	
NAS3-23278	p 137	N86-11506		p 49	N86-27405	NSG-3267	p 128	A86-21029
	p 139	N86-16518	NAS3-24236	p 49	N86-27402	NSG-3283	p 171	A86-43774
NAS3-23281	p 20	A86-25743		p 49	N86-27407	NSG-3294	p 128	A86-20951
NAS3-23288	p 174	N86-11521	NAS3-24238	p 82	N86-29901	NSG-3299	p 203	A86-11001
NAS3-23344	p 106	A86-10028	NAS3-24261	p 73	A86-22751		p 52	A86-18041
NAS3-23353	p 47	A86-42619	NAS3-24338	p 134	A86-42739	NSG-3301	p 100	A86-47070
	p 57	N86-15339	NAS3-24339	p 8	A86-42709	NSG-3306	p 136	A86-49442
NAS3-23355	p 108	A86-37053		p 198	A86-45500	NSG-330	p 79	A86-12995
	p 53	A86-37054	NAS3-24346	p 198	A86-45501	NSG3-172	p 200	N86-22973
NAS3-23356	p 119	A86-41343	NAS3-24349	p 160	N86-26829	NSG3-387	p 92	N86-28165
NAS3-23520	p 159	N86-24991	NAS3-24385	p 30	N86-24695	N00014-80-C-0517	p 131	A86-26806
NAS3-23531	p 130	A86-25567	NAS3-24386	p 154	A86-38311	N00014-80-C-0870	p 85	A86-15237
	p 132	A86-30218	NAS3-24386	p 70	N86-24780	N00014-82-C-0800	p 132	A86-30218
NAS3-23533	p 30	N86-24693	NAS3-24389	p 168	A86-28655	N00014-82-K-0182	p 76	A86-47089
NAS3-23606	p 195	A86-49850		p 168	A86-28659	N00014-84-C-0354	p 3	A86-23854
NAS3-23623	p 160	N86-27643	NAS3-24400	p 102	N86-16381	N00014-85-C-0148	p 131	A86-26806
NAS3-23629	p 26	N86-12226	NAS3-244	p 80	A86-16278	N00014-85-K-0126	p 131	A86-26814
NAS3-23687	p 25	N86-11515	NAS3-24533	p 19	A86-19678		p 132	A86-30218
NAS3-23690	p 173	N86-11501	NAS3-24541	p 23	A86-42705	N00014-85-K-0205	p 127	A86-19419
	p 148	N86-21817	NAS3-24542	p 23	A86-42702	N00167-79-M-4413	p 128	A86-21029
NAS3-23693	p 126	A86-16311	NAS3-24544	p 16	A86-42704	PASA-NASA/DSB-5710-2-79	p 181	N86-11686
NAS3-23695	p 2	A86-22046	NAS3-24545	p 23	A86-42703	RESEARCH FOUNDATION PROJ.		
	p 138	N86-11507	NAS3-24654	p 42	N86-18334	4246	p 88	N86-14356
	p 29	N86-21546	NAS3-24655	p 54	A86-39908	SRI PROJ. 5723	p 121	N86-14499
NAS3-23696	p 7	A86-48153	NAS3-24685	p 47	A86-39907	SRI PROJ-6923	p 124	N86-28323
NAS3-23697	p 169	A86-34444	NAS3-272	p 13	N86-29773	W-31-109-ENG-38	p 177	N86-27689
	p 169	A86-34445		p 13	N86-30693	W-7405-ENG-48	p 130	A86-23131
	p 169	A86-34461	NAS7-918	p 43	A86-38943	324-01-00	p 104	N86-25474
NAS3-23708	p 197	A86-31593	NATO-343/85	p 142	N86-24932		p 105	N86-25475
	p 135	A86-45441	NCC3-19	p 99	A86-35702	481-01-02	p 64	N86-32522
	p 135	A86-46314	NCC3-22	p 110	A86-29656	481-02-02	p 60	N86-24748
NAS3-23712	p 202	A86-15263	NCC3-27	p 80	A86-16270	481-54-02	p 62	N86-28122
	p 203	N86-15113		p 64	A86-30051	485-40-02	p 64	N86-32521
NAS3-23716	p 131	A86-28696		p 98	A86-30052	500-33-05	p 164	N86-13749
	p 138	N86-11508	NCC3-2	p 72	A86-19389	505-31-04	p 9	N86-10017
NAS3-23720	p 23	A86-45504	NCC3-30	p 138	N86-13679		p 137	N86-10461
NAS3-23722	p 148	N86-11500	NCC3-35	p 78	N86-28139		p 1	N86-11146
NAS3-23770	p 42	N86-10164	NCC3-37	p 144	N86-30960		p 9	N86-13295
NAS3-23772	p 58	N86-17387	NCC3-43	p 82	A86-29722		p 27	N86-16218
	p 58	N86-17416		p 91	N86-24817		p 140	N86-21794
	p 59	N86-20493	NCC3-46	p 179	N86-30236		p 142	N86-24934
NAS3-23773	p 61	N86-26369	NCC3-5	p 188	N86-28511		p 13	N86-28055
NAS3-23776	p 121	N86-14499	NCC3-8	p 116	N86-30037		p 195	N86-28661
NAS3-23777	p 124	N86-28323	NGL-22-007-228	p 191	A86-28963		p 195	N86-28662
NAS3-23781	p 118	A86-34882	NGL-22-009-640	p 36	A86-39948	505-31-42	p 28	N86-20390
NAS3-23790	p 46	A86-35318	NGT-39-009-802	p 130	A86-22682		p 29	N86-20395
NAS3-23858	p 48	N86-17418	NGT36-001-800	p 207	N86-13219		p 29	N86-21545
	p 60	N86-24746	NGT36-001-801	p 207	N86-13219		p 29	N86-23597
NAS3-23876	p 185	N86-17845	NG0530-85-C-0191	p 32	N86-28089		p 108	N86-28261
NAS3-23879	p 180	A86-24823	NSF ATM-82-05638	p 191	A86-28963	505-31-54	p 150	N86-31030
NAS3-23881	p 52	A86-19834	NSF CEE-81-00491	p 22	A86-35403	505-32-32	p 32	N86-28089
	p 202	A86-22890	NSF CPE-81-15163	p 73	A86-22774	505-33-1A	p 68	N86-10290
	p 118	A86-25525		p 130	A86-23131		p 86	N86-10311
NAS3-23882	p 124	N86-30073	NSF CPE-83-02232	p 72	A86-12925		p 87	N86-12294
NAS3-23884	p 63	N86-31648	NSF CPE-84-04811	p 198	A86-18521		p 92	N86-31699
NAS3-23886	p 112	N86-16451	NSF DMR-79-23647	p 75	A86-40677	505-33-22	p 178	N86-28464
	p 113	N86-16452	NSF DMR-83-03981	p 204	A86-37075	505-33-62	p 137	N86-11425
NAS3-23888	p 180	A86-24888	NSF ECS-81-06693	p 201	A86-11391		p 69	N86-12256
NAS3-23889	p 57	N86-16259	NSF ECS-84-04345	p 194	A86-32051		p 87	N86-13407
NAS3-23925	p 172	N86-10589	NSF INT-85-14196	p 142	N86-24932		p 138	N86-13679
NAS3-23926	p 32	N86-28087	NSF MED-80-06806	p 133	A86-39865		p 88	N86-15378
NAS3-23932	p 157	N86-11474	NSF MSM-83-20307	p 142	N86-24932		p 102	N86-16379
NAS3-23934	p 41	N86-10132	NSF MSM-84-10876	p 153	A86-36298		p 141	N86-21797
NAS3-23939	p 165	N86-25003	NSG-3019	p 73	A86-22755	505-33-7A	p 157	N86-13734
NAS3-23944	p 103	N86-22713	NSG-3032	p 20	A86-22090		p 174	N86-16610
NAS3-24078	p 21	A86-35400	NSG-3036	p 198	A86-49806		p 69	N86-21614
	p 121	N86-16486	NSG-3044	p 167	A86-26896	505-33-7B	p 157	N86-14613
	p 21	A86-35402	NSG-3048	p 194	A86-35386		p 174	N86-16611
NAS3-24079	p 33	N86-30732		p 194	A86-35419		p 149	N86-27617
	p 203	N86-28729	NSG-3075	p 139	N86-15625	505-33-7C	p 86	N86-12292
NAS3-24085	p 22	A86-35403		p 141	N86-22692		p 175	N86-17788
NAS3-24089	p 130	A86-22735	NSG-3079	p 20	A86-24677		p 158	N86-19616
NAS3-24090	p 107	A86-19929	NSG-3114	p 73	A86-22793		p 90	N86-21661
NAS3-24091	p 107	A86-23922	NSG-3135	p 18	A86-19677		p 90	N86-22686
	p 33	N86-30733		p 22	A86-37827		p 159	N86-24991
NAS3-24092	p 129	A86-22676	NSG-3139	p 20	A86-26893	505-33-78	p 172	N86-10579
NAS3-24105	p 20	A86-26636	NSG-3156	p 153	A86-34010		p 69	N86-14316

505-34-02

CONTRACT NUMBER INDEX

505-34-02	p 27 N86-15313	505-63-11	p 83 N86-31702	508-51-313	p 57 N86-16251
	p 121 N86-16486		p 174 N86-11526	508-53-01	p 104 N86-2547
505-36-22	p 33 N86-30732		p 87 N86-13408	508-53-1A	p 163 N86-1056
	p 139 N86-17665		p 175 N86-17789		p 164 N86-1659
505-40-14	p 28 N86-20393		p 175 N86-18750		p 164 N86-1963
	p 203 N86-15113		p 175 N86-19683		p 165 N86-2581
505-40-22	p 203 N86-22390		p 90 N86-21658		p 165 N86-2766
	p 15 N86-30022		p 159 N86-21856		p 165 N86-2844
505-40-62	p 26 N86-13328		p 70 N86-24756	508-53-1B	p 156 N86-1055
	p 26 N86-13329		p 70 N86-24757	508-53-12	p 206 N86-2528
	p 26 N86-13330		p 70 N86-24759	508-53-18	p 157 N86-1147
505-40-88	p 148 N86-22915		p 91 N86-24813	508-55-22	p 56 N86-1027
505-40-7A	p 138 N86-13677		p 91 N86-24817		p 57 N86-1028
505-40-74	p 27 N86-16221		p 91 N86-24818		p 57 N86-1122
	p 37 N86-16233		p 109 N86-24889		p 62 N86-2812
	p 43 N86-18338		p 91 N86-25454	508-55-24	p 60 N86-21571
	p 196 N86-27036		p 161 N86-27661	508-55-42	p 182 N86-1167
	p 38 N86-28101		p 92 N86-28164		p 184 N86-17831
505-40-8K	p 32 N86-28947		p 178 N86-28467	508-55-6E	p 182 N86-1166
505-40-90	p 198 N86-12007		p 181 N86-30206	508-55-62B	p 208 N86-1323
	p 9 N86-14223		p 71 N86-31863	508-55-72	p 205 N86-11041
505-41-21	p 124 N86-27578		p 71 N86-31864		p 123 N86-21751
505-42-11	p 62 N86-31646		p 179 N86-31920		p 123 N86-24901
505-42-94	p 157 N86-12609		p 35 N86-32433	508-55-82A	p 57 N86-18258
505-43-52	p 9 N86-14219	505-63-28	p 13 N86-31537	508-58-22	p 111 N86-10381
	p 30 N86-24694	505-63-31	p 71 N86-26376		p 111 N86-10381
505-45-02	p 12 N86-27186	505-63-81	p 65 N86-13370		p 205 N86-12131
505-45-54	p 37 N86-16232		p 140 N86-18647		p 121 N86-13641
	p 15 N86-27268		p 177 N86-25851		p 121 N86-14491
505-45-58	p 199 N86-14006	505-68-1A	p 149 N86-26596		p 101 N86-15394
	p 199 N86-14007	505-68-11	p 14 N86-20379		p 113 N86-16451
	p 199 N86-19125		p 15 N86-22559		p 113 N86-16451
	p 11 N86-21505		p 35 N86-22582		p 113 N86-16461
	p 201 N86-25218		p 15 N86-23577		p 46 N86-17361
505-55-72	p 65 N86-18442		p 12 N86-24667		p 123 N86-21751
505-60-12	p 212 N86-25310		p 15 N86-31548		p 123 N86-24907
505-62-01	p 193 N86-22150		p 17 N86-31582		p 206 N86-25261
	p 17 N86-24691	505-68-51	p 30 N86-26336		p 116 N86-32591
	p 30 N86-24697	505-69-11	p 11 N86-20357	508-60-12	p 87 N86-12291
	p 148 N86-24958		p 15 N86-22558		p 175 N86-16611
	p 148 N86-24959	505-69-41	p 34 N86-31586		p 44 N86-23611
	p 149 N86-24964	505-69	p 141 N86-22892	508-60-42	p 44 N86-24721
	p 149 N86-24967	505-90-01	p 26 N86-12227		p 44 N86-11211
	p 203 N86-28729		p 10 N86-14224		p 63 N86-31641
	p 124 N86-30068		p 10 N86-16195	508-62-21	p 192 N86-26914
	p 124 N86-31792		p 150 N86-32703	508-62-22	p 112 N86-16451
	p 150 N86-31859	508-41-11	p 121 N86-13645		p 113 N86-16451
505-62-11	p 10 N86-19289		p 212 N86-14110	508-62-52	p 112 N86-12481
	p 33 N86-31583		p 123 N86-26520		p 112 N86-14471
505-62-21	p 10 N86-16194		p 63 N86-31852		p 112 N86-14471
	p 27 N86-16219		p 125 N86-31793		p 114 N86-18581
	p 140 N86-19558		p 125 N86-32627	508-62-91	p 12 N86-26281
	p 28 N86-20391		p 166 N86-32764	508-63-01	p 91 N86-25451
	p 77 N86-21635	508-41-21	p 77 N86-12268	508-63-81	p 140 N86-19551
	p 11 N86-23563		p 187 N86-23035		p 140 N86-19551
	p 142 N86-23857		p 187 N86-25039	508-64-12	p 57 N86-15331
	p 148 N86-24961		p 188 N86-26677	523-13-00	p 61 N86-25401
	p 12 N86-28053		p 78 N86-31680	533-04-1A	p 172 N86-10581
	p 13 N86-28063		p 189 N86-31979		p 172 N86-11491
	p 194 N86-28651		p 190 N86-31980		p 28 N86-20391
	p 201 N86-29630		p 190 N86-31981		p 29 N86-20391
505-62-22	p 201 N86-32247	508-41-3A	p 186 N86-21978	533-04-11	p 176 N86-21951
	p 10 N86-19290	508-41-3B	p 190 N86-31982		p 32 N86-29081
	p 143 N86-25726		p 209 N86-19264		p 178 N86-28461
505-62-3A	p 150 N86-31857		p 210 N86-26261	533-04-12	p 138 N86-13671
	p 37 N86-12239		p 211 N86-29732		p 26 N86-14272
505-62-38	p 193 N86-19008	508-41-38	p 93 N86-32557		p 139 N86-15621
	p 37 N86-18329	508-41-4A	p 60 N86-24747		p 89 N86-20541
	p 31 N86-28085	508-41-4B	p 106 N86-32573		p 178 N86-21951
505-62-51	p 159 N86-24990	508-41-4C	p 192 N86-13899		p 141 N86-23851
	p 160 N86-24992		p 62 N86-28125		p 176 N86-25821
	p 161 N86-28433	508-41-42	p 120 N86-12509		p 35 N86-32431
	p 161 N86-31889	508-41-48	p 103 N86-21683		p 150 N86-32701
505-62-61	p 143 N86-26545	508-41-5A	p 48 N86-12246	533-05-01	p 104 N86-24837
505-62-91	p 11 N86-24658		p 102 N86-16381		p 166 N86-31912
505-63-01	p 87 N86-13409		p 49 N86-31634		p 166 N86-31913
	p 88 N86-14354	508-42-11	p 160 N86-27643	533-05-11	p 174 N86-14681
	p 88 N86-14355		p 179 N86-30236		p 105 N86-25476
	p 89 N86-16334	508-42-21	p 60 N86-24746		p 106 N86-31729
	p 139 N86-18646		p 61 N86-26369	533-05-12	p 101 N86-12310
	p 77 N86-19417		p 63 N86-31651	533-13-00	p 91 N86-25455
	p 102 N86-19465	508-42-32	p 60 N86-24749		p 61 N86-27418
	p 50 N86-21575		p 61 N86-25407	533-13-01	p 174 N86-13755
	p 90 N86-22687		p 61 N86-25408	535-03-01	p 11 N86-21513
	p 90 N86-22688		p 63 N86-31650		p 11 N86-21517
	p 103 N86-22713	508-43-01	p 158 N86-20809		p 30 N86-24695
	p 141 N86-22890	508-43-11	p 65 N86-17472		p 201 N86-25217
	p 69 N86-23661		p 104 N86-24838		p 12 N86-27213
	p 103 N86-24835		p 164 N86-25002		p 13 N86-31536
	p 104 N86-24836		p 165 N86-27666	535-03-12	p 178 N86-29271
	p 92 N86-27444		p 71 N86-29906	535-05-01	p 33 N86-31582
	p 105 N86-27452		p 166 N86-31065		p 34 N86-31587
	p 92 N86-28165	508-44-21	p 106 N86-31728	535-05-121	p 101 N86-13495
	p 93 N86-31700		p 124 N86-28323	553-13-00	p 177 N86-27680
	p 93 N86-31701	508-44-22	p 125 N86-32629	643-10-01	p 114 N86-18585
			p 206 N86-25267		p 115 N86-24881

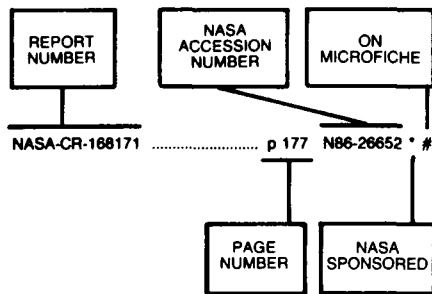
CONTRACT NUMBER INDEX

928-60-02

	p 193	N86-27927
	p 193	N86-27928
643-10-20	p 115	N86-24876
	p 115	N86-24878
650-60-20	p 113	N86-17595
	p 116	N86-31760
650-60-23	p 112	N86-13627
	p 46	N86-16343
	p 114	N86-19494
650-60-26	p 46	N86-16249
674-22-05	p 144	N86-28378
674-25-05	p 90	N86-21659
674-29-05	p 212	N86-19274
	p 105	N86-28194
	p 212	N86-30620
776-33-41	p 172	N86-10582
	p 121	N86-16487
	p 186	N86-18775
	p 186	N86-18776
	p 190	N86-31963
776-52-41	p 181	N86-10643
776-54-01	p 181	N86-11666
776-34-12	p 210	N86-24590
776-35-03	p 89	N86-20541
776-35-13	p 208	N86-14106
	p 88	N86-15380
	p 103	N86-20568
	p 209	N86-21457
	p 103	N86-21682
	p 210	N86-25303
	p 211	N86-29731
	p 211	N86-31452
927-60-01	p 141	N86-23854
928-60-02	p 44	N86-31621

REPORT/ACCESSION NUMBER INDEX

Typical Report Number Index Listing



Listings in this index are arranged alphanumerically by report number. The NASA accession number denotes the number by which the citation is identified. An asterisk (*) indicates that the item is a NASA report. A pound sign (#) indicates that the item is available on microfiche.

AAE-86-3	p 78	N86-28139 * #
AD-A165461	p 127	A86-19419 * #
AIAA PAPER 84-0109	p 14	A86-14427 * #
AIAA PAPER 84-1205	p 19	A86-20369 * #
AIAA PAPER 85-0420	p 95	A86-14428 * #
AIAA PAPER 85-1158	p 107	A86-37074 * #
AIAA PAPER 85-1226	p 50	A86-14429 * #
AIAA PAPER 85-1354	p 18	A86-14430 * #
AIAA PAPER 85-1477	p 50	A86-14431 * #
AIAA PAPER 85-1999	p 51	A86-17831 * #
AIAA PAPER 85-2008	p 51	A86-17833 * #
AIAA PAPER 85-2011	p 51	A86-17851 * #
AIAA PAPER 85-2014	p 51	A86-17835 * #
AIAA PAPER 85-2017	p 53	A86-37062 * #
AIAA PAPER 85-2018	p 50	A86-14445 * #
AIAA PAPER 85-2033	p 54	A86-37063 * #
AIAA PAPER 85-2035	p 50	A86-14446 * #
AIAA PAPER 85-2042	p 51	A86-14447 * #
AIAA PAPER 85-2052	p 203	A86-11001 * #
AIAA PAPER 85-5017	p 1	A86-11065 * #
AIAA PAPER 86-0032	p 1	A86-19644 * #
AIAA PAPER 86-0040	p 127	A86-19651 * #
AIAA PAPER 86-0044	p 36	A86-19654 * #
AIAA PAPER 86-0055	p 127	A86-19661 * #
AIAA PAPER 86-0058	p 129	A86-22676 * #
AIAA PAPER 86-0072	p 145	A86-19670 * #
AIAA PAPER 86-0080	p 18	A86-19677 * #
AIAA PAPER 86-0081	p 19	A86-19678 * #
AIAA PAPER 86-0136	p 131	A86-26606 * #
AIAA PAPER 86-0161	p 145	A86-19726 * #
AIAA PAPER 86-0202	p 127	A86-19746 * #
AIAA PAPER 86-0214	p 130	A86-22682 * #
AIAA PAPER 86-0235	p 131	A86-26614 * #
AIAA PAPER 86-0290	p 36	A86-26620 * #
AIAA PAPER 86-0312	p 2	A86-22693 * #
AIAA PAPER 86-0364	p 52	A86-19834 * #
AIAA PAPER 86-0366	p 52	A86-19835 * #
AIAA PAPER 86-0406	p 131	A86-26630 * #
AIAA PAPER 86-0409	p 145	A86-22700 * #
AIAA PAPER 86-0450	p 20	A86-26636 * #
AIAA PAPER 86-0467	p 198	A86-49566 * #
AIAA PAPER 86-0525	p 107	A86-19929 * #
AIAA PAPER 86-0545	p 16	A86-19940 * #
AIAA PAPER 86-0550	p 16	A86-19942 * #
AIAA PAPER 86-0575	p 73	A86-19962 * #
AIAA PAPER 86-0604	p 44	A86-29580 * #
AIAA PAPER 86-0616	p 38	A86-29586 * #
AIAA PAPER 86-0634	p 110	A86-49567 * #
AIAA PAPER 86-0635	p 110	A86-29664 * #
AIAA PAPER 86-0635	p 111	A86-49568 * #
AIAA PAPER 86-0636	p 45	A86-29599 * #
AIAA PAPER 86-0649	p 109	A86-29611 * #
AIAA PAPER 86-0654	p 45	A86-29616 * #

AIAA PAPER 86-0666	p 45	A86-29628 * #
AIAA PAPER 86-0687	p 110	A86-29638 * #
AIAA PAPER 86-0717	p 110	A86-29656 * #
AIAA PAPER 86-0721	p 45	A86-29659 * #
AIAA PAPER 86-0728	p 36	A86-24727 * #
AIAA PAPER 86-0757	p 36	A86-24744 * #
AIAA PAPER 86-0758	p 36	A86-24745 * #
AIAA PAPER 86-0844	p 22	A86-38892 * #
AIAA PAPER 86-0846	p 22	A86-38894 * #
AIAA PAPER 86-0847	p 54	A86-38895 * #
AIAA PAPER 86-0848	p 5	A86-38896 * #
AIAA PAPER 86-0943	p 170	A86-38838 * #
AIAA PAPER 86-0948	p 170	A86-38842 * #
AIAA PAPER 86-0955	p 47	A86-38883 * #
AIAA PAPER 86-1002	p 43	A86-38943 * #
AIAA PAPER 86-1016	p 130	A86-38873 * #
AIAA PAPER 86-1059	p 132	A86-38427 * #
AIAA PAPER 86-1079	p 132	A86-38442 * #
AIAA PAPER 86-1099	p 147	A86-38460 * #
AIAA PAPER 86-1123	p 5	A86-38480 * #
AIAA PAPER 86-1162	p 133	A86-40578 * #
AIAA PAPER 86-1164	p 181	A86-40579 * #
AIAA PAPER 86-1188	p 54	A86-40595 * #
AIAA PAPER 86-1190	p 67	A86-40596 * #
AIAA PAPER 86-1238	p 133	A86-39865 * #
AIAA PAPER 86-1253	p 54	A86-39877 * #
AIAA PAPER 86-1299	p 54	A86-39906 * #
AIAA PAPER 86-1300	p 47	A86-39907 * #
AIAA PAPER 86-1352	p 36	A86-39948 * #
AIAA PAPER 86-1403	p 54	A86-42616 * #
AIAA PAPER 86-1404	p 55	A86-42617 * #
AIAA PAPER 86-1407	p 47	A86-42619 * #
AIAA PAPER 86-1424	p 55	A86-42633 * #
AIAA PAPER 86-1435	p 55	A86-42640 * #
AIAA PAPER 86-1452	p 25	A86-49611 * #
AIAA PAPER 86-1458	p 8	A86-49612 * #
AIAA PAPER 86-1465	p 134	A86-42656 * #
AIAA PAPER 86-1505	p 55	A86-42676 * #
AIAA PAPER 86-1507	p 56	A86-49613 * #
AIAA PAPER 86-1513	p 55	A86-42682 * #
AIAA PAPER 86-1520	p 6	A86-42687 * #
AIAA PAPER 86-1521	p 6	A86-42688 * #
AIAA PAPER 86-1527	p 6	A86-42760 * #
AIAA PAPER 86-1543	p 23	A86-42702 * #
AIAA PAPER 86-1544	p 23	A86-42703 * #
AIAA PAPER 86-1545	p 16	A86-42704 * #
AIAA PAPER 86-1546	p 23	A86-42705 * #
AIAA PAPER 86-1552	p 6	A86-42709 * #
AIAA PAPER 86-1556	p 134	A86-42711 * #
AIAA PAPER 86-1559	p 67	A86-42712 * #
AIAA PAPER 86-1597	p 134	A86-42738 * #
AIAA PAPER 86-1598	p 134	A86-42739 * #
AIAA PAPER 86-1599	p 6	A86-42740 * #
AIAA PAPER 86-1611	p 25	A86-49614 * #
AIAA PAPER 86-1614	p 134	A86-42752 * #
AIAA PAPER 86-1621	p 23	A86-42755 * #
AIAA PAPER 86-1648	p 147	A86-42770 * #
AIAA PAPER 86-1665	p 134	A86-42780 * #
AIAA PAPER 86-1698	p 56	A86-49615 * #
AIAA PAPER 86-1703	p 55	A86-42799 * #
AIAA PAPER 86-1724	p 135	A86-42812 * #
AIAA PAPER 86-1725	p 135	A86-42813 * #
AIAA PAPER 86-1804	p 22	A86-37827 * #
AIAA PAPER 86-1809	p 8	A86-49585 * #
AIAA PAPER 86-1872	p 198	A86-45492 * #
AIAA PAPER 86-1873	p 198	A86-45493 * #
AIAA PAPER 86-1887	p 198	A86-45500 * #
AIAA PAPER 86-1888	p 198	A86-45501 * #
AIAA PAPER 86-1892	p 23	A86-45504 * #
AIAA PAPER 86-1893	p 8	A86-49625 * #
AIAA PAPER 86-1956	p 135	A86-45441 * #
AIAA PAPER 86-1966	p 16	A86-45449 * #
AIAA PAPER 86-2301	p 47	A86-49553 * #
AIAA PAPER 86-9758	p 35	A86-40681 * #
AIAA-PAPER-86-0362	p 62	N86-28125 * #
AIAA-85-1133	p 13	N86-28055 * #
AIAA-85-2011	p 56	N86-10280 * #
AIAA-85-2014	p 56	N86-10279 * #
AIAA-85-2017	p 57	N86-11224 * #
AIAA-86-0044	p 37	N86-12239 * #
AIAA-86-0312	p 9	N86-14223 * #

AIAA-86-0450	p 27	N86-16218 * #
AIAA-86-1392	p 63	N86-31650 * #
AIAA-86-1438	p 63	N86-31651 * #
AIAA-86-1458	p 143	N86-26545 * #
AIAA-86-1520	p 11	N86-23563 * #
AIAA-86-1542	p 34	N86-31587 * #
AIAA-86-1557	p 33	N86-31583 * #
AIAA-86-1611	p 35	N86-32432 * #
AIAA-86-1627	p 11	N86-24658 * #
AIAA-86-1703	p 60	N86-24749 * #
AIAA-86-1809	p 12	N86-26285 * #
AIAA-86-1876	p 201	N86-29630 * #
AIAA-86-1893	p 12	N86-27213 * #
AIAA-86-9758	p 35	N86-22582 * #
AIAA/GNOS-85-002	p 44	N86-11218 * #
ANL-85-74	p 177	N86-27689 * #
AR-1	p 103	N86-22713 * #
AR-85-1	p 15	N86-27268 * #
AR-86-2	p 17	N86-26330 * #
ASLE PREPRINT 85-AM-3A-1	p 94	A86-11076 * #
ASLE PREPRINT 85-AM-4E-2	p 151	A86-11091 * #
ASLE PREPRINT 85-TC-5A-2	p 151	A86-11016 * #
ASLE PREPRINT 86-AM-4G-3	p 156	A86-45391 * #
ASME PAPER 84-DET-172	p 155	A86-45255 * #
ASME PAPER 84-DET-92	p 155	A86-40683 * #
ASME PAPER 84-DET-99	p 155	A86-45257 * #
ASME PAPER 84-GT-97	p 17	A86-13054 * #
ASME PAPER 85-DE-7	p 151	A86-14466 * #
ASME PAPER 85-DET-10	p 155	A86-45256 * #
ASME PAPER 85-DET-11	p 154	A86-38617 * #
ASME PAPER 85-DET-12	p 152	A86-22748 * #
ASME PAPER 85-DET-35	p 154	A86-38620 * #
ASME PAPER 85-DGP-20	p 151	A86-14467 * #
ASME PAPER 85-GT-113	p 126	A86-13068 * #
ASME PAPER 85-GT-115	p 19	A86-22068 * #
ASME PAPER 85-GT-133	p 3	A86-22733 * #
ASME PAPER 85-GT-134	p 21	A86-32956 * #
ASME PAPER 85-GT-137	p 19	A86-22081 * #
ASME PAPER 85-GT-159	p 167	A86-22084 * #
ASME PAPER 85-GT-170	p 21	A86-32957 * #
ASME PAPER 85-GT-171	p 19	A86-22088 * #
ASME PAPER 85-GT-172	p 19	A86-22089 * #
ASME PAPER 85-GT-174	p 20	A86-22090 * #
ASME PAPER 85-GT-189	p 2	A86-22102 * #
ASME PAPER 85-GT-18	p 145	A86-13059 * #
ASME PAPER 85-GT-192	p 3	A86-22732 * #
ASME PAPER 85-GT-212	p 3	A86-22731 * #
ASME PAPER 85-GT-226	p 2	A86-22123 * #
ASME PAPER 85-GT-229	p 129	A86-22125 * #
ASME PAPER 85-GT-30	p 75	A86-32958 * #
ASME PAPER 85-GT-37	p 128	A86-22026 * #
ASME PAPER 85-GT-58	p 130	A86-22735 * #
ASME PAPER 85-GT-59	p 126	A86-13061 * #
ASME PAPER 85-GT-66	p 2	A86-22046 * #
ASME PAPER 85-GT-82	p 128	A86-22053 * #
ASME PAPER 85-GT-83	p 129	A86-22054 * #
ASME PAPER 85-GT-84	p 129	A86-22055 * #
ASME PAPER 85-IGT-127	p 97	A86-23921 * #
ASME PAPER 85-IGT-130	p 107	A86-23922 * #
ASME PAPER 85-IGT-135	p 3	A86-23927 * #
ASME PAPER 85-IGT-42	p 3	A86-23854 * #
ASME PAPER 85-TRIB-14	p 155	A86-43542 * #
ASME PAPER 85-TRIB-1	p 152	A86-24481 * #
ASME PAPER 85-TRIB-29	p 153	A86-34010 * #
ASME PAPER 85-TRIB-42	p 155	A86-43541 * #
ASME PAPER 85-TRIB-51	p 130	A86-24496 * #
ASME PAPER 85-WA/FE-3	p 132	A86-38368 * #
ASME PAPER 85-WA/HT-46	p 107	A86-38393 * #
ASME PAPER 85-WA/HT-47	p 107	A86-38394 * #
ASME PAPER 85-WA/NCA-1	p 197	A86-22747 * #
ASME PAPER 86-GT-122	p 7	A86-48181 * #
ASME PAPER 86-GT-129	p 136	A86-48187 * #
ASME PAPER 86-GT-12	p 156	A86-48109 * #
ASME PAPER 86-GT-166	p 136	A86-48218 * #
ASME PAPER 86-GT-172	p 24	A86-48224 * #
ASME PAPER 86-GT-179	p 7	A86-48229 * #
ASME PAPER 86-GT-181	p 24	A86-48231 * #
ASME PAPER 86-GT-186	p 7	A86-48236 * #

ASME PAPER 86-GT-195	p 171	A86-48245 *	#	DOE/NASA/20320-67	p 121	N86-16487 *	#	E-2746	p 87	N86-13407 *	#
ASME PAPER 86-GT-223	p 24	A86-48257 *	#	DOE/NASA/20320-68	p 186	N86-18776 *	#	E-2747-1	p 157	N86-11475 *	#
ASME PAPER 86-GT-227	p 8	A86-48261 *	#	DOE/NASA/20320-69	p 186	N86-18775 *	#	E-2748	p 182	N86-11671 *	#
ASME PAPER 86-GT-243	p 171	A86-48271 *	#	DOE/NASA/20485-18	p 181	N86-11686 *	#	E-2749	p 101	N86-13495 *	#
ASME PAPER 86-GT-246	p 8	A86-48274 *	#	DOE/NASA/20485-20	p 181	N86-10643 *	#	E-2750	p 205	N86-12134 *	#
ASME PAPER 86-GT-26	p 7	A86-48117 *	#	DOE/NASA/4105-1	p 211	N86-31452 *	#	E-2751	p 140	N86-21794 *	#
ASME PAPER 86-GT-279	p 163	A86-48298 *	#	DOE/NASA/50112-60	p 208	N86-14106 *	#	E-2753	p 120	N86-12509 *	#
ASME PAPER 86-GT-303	p 8	A86-48315 *	#	DOE/NASA/50112-63	p 89	N86-20541 *	#	E-2754	p 62	N86-28123 *	#
ASME PAPER 86-GT-42	p 7	A86-48126 *	#	DOE/NASA/50112-64	p 103	N86-20568 *	#	E-2755	p 112	N86-12485 *	#
ASME PAPER 86-GT-68	p 136	A86-48140 *	#	DOE/NASA/50112-65	p 103	N86-21682 *	#	E-2756	p 104	N86-24837 *	#
ASME PAPER 86-GT-70	p 23	A86-48141 *	#	DOE/NASA/51044-37	p 88	N86-15380 *	#	E-2757	p 142	N86-24934 *	#
ASME PAPER 86-GT-75	p 163	A86-48143 *	#	DOE/NBB-0067	p 108	N86-27460 *	#	E-2758	p 198	N86-12007 *	#
ASME PAPER 86-GT-77	p 24	A86-48145 *	#	DOT-FAA-CT-86-1	p 14	N86-20379 *	#	E-2761	p 60	N86-21577 *	#
ASME PAPER 86-GT-78	p 24	A86-48146 *	#	DTNSRDC-PASD-CR-1886	p 180	N86-26629 *	#	E-2762	p 44	N86-24722 *	#
ASME PAPER 86-GT-87	p 7	A86-48153 *	#	D180-28264-1	p 57	N86-15339 *	#	E-2765	p 10	N86-16194 *	#
ASME PAPER 86-GT-98	p 24	A86-48163 *	#	E-1816	p 172	N86-11495 *	#	E-2766	p 205	N86-12135 *	#
ASME PAPER 86-HT-15	p 48	A86-49621 *	#	E-2003	p 157	N86-14612 *	#	E-2767	p 141	N86-21797 *	#
ASR-2	p 172	N86-10589 *	#	E-2017	p 71	N86-31664 *	#	E-2768	p 123	N86-21755 *	#
AV-FR-85/802	p 185	N86-18774 *	#	E-2035	p 89	N86-21614 *	#	E-2769	p 87	N86-12293 *	#
AVSCOM-TR-84-C-15	p 157	N86-14612 *	#	E-2143	p 157	N86-13734 *	#	E-2770	p 101	N86-12310 *	#
AVSCOM-TR-86-C-13	p 32	N86-28947 *	#	E-2188	p 68	N86-23661 *	#	E-2771	p 30	N86-24694 *	#
AVSCOM-TR-86-C-20	p 160	N86-26629 *	#	E-2190	p 10	N86-19290 *	#	E-2772	p 9	N86-14219 *	#
CR-R-R85020	p 139	N86-15625 *	#	E-2328-1	p 104	N86-24839 *	#	E-2773	p 88	N86-15378 *	#
CR-R85033	p 32	N86-28089 *	#	E-2364	p 148	N86-22915 *	#	E-2774	p 44	N86-11218 *	#
DE85-017585	p 122	N86-20700 *	#	E-2425	p 68	N86-11260 *	#	E-2775	p 37	N86-12239 *	#
DFVLR-FB-84-26	p 140	N86-20722 *	#	E-2461-1	p 195	N86-28661 *	#	E-2777	p 192	N86-13899 *	#
DOC-84AEPD004-VOL-2-BK-1	p 183	N86-15722 *	#	E-2486	p 164	N86-22962 *	#	E-2778	p 87	N86-12294 *	#
DOC-84AEPD004-VOL-2-BK-2	p 183	N86-15723 *	#	E-2498	p 181	N86-11666 *	#	E-2780	p 70	N86-24757 *	#
DOC-84AEPD004-VOL-3-BK-1	p 183	N86-15724 *	#	E-2516	p 158	N86-19616 *	#	E-2782	p 70	N86-24759 *	#
DOC-84AEPD004-VOL-3-BK-2	p 183	N86-15725 *	#	E-2536	p 60	N86-21578 *	#	E-2783	p 208	N86-13236 *	#
DOC-84AEPD004-VOL-4-BK-1	p 183	N86-15726 *	#	E-2561	p 203	N86-22390 *	#	E-2785	p 121	N86-13645 *	#
DOC-84AEPD004-VOL-4-BK-2	p 184	N86-15727 *	#	E-2566	p 121	N86-13643 *	#	E-2791	p 112	N86-14479 *	#
DOC-84AEPD004-VOL-4-BK-3	p 184	N86-15728 *	#	E-2573	p 111	N86-10379 *	#	E-2793	p 26	N86-12227 *	#
DOC-84AEPD004-VOL-4-BK-4	p 184	N86-15729 *	#	E-2575	p 87	N86-12295 *	#	E-2794	p 139	N86-18646 *	#
DOC-84AEPD004-VOL-4-BK-5	p 184	N86-15730 *	#	E-2576	p 172	N86-10579 *	#	E-2796	p 112	N86-14477 *	#
DOE/CS-54209	p 122	N86-20700 *	#	E-2578	p 157	N86-12609 *	#	E-2797	p 114	N86-19494 *	#
DOE/NASA-0032/80-7	p 211	N86-30579 *	#	E-2587	p 195	N86-28662 *	#	E-2798	p 87	N86-13408 *	#
DOE/NASA-0153/1	p 188	N86-27708 *	#	E-2597	p 182	N86-11668 *	#	E-2800	p 164	N86-13749 *	#
DOE/NASA-0241-12	p 188	N86-25877 *	#	E-2623	p 138	N86-13677 *	#	E-2801	p 180	N86-24992 *	#
DOE/NASA-0241-15	p 182	N86-12757 *	#	E-2626	p 69	N86-14316 *	#	E-2803	p 186	N86-18776 *	#
DOE/NASA-0241-17	p 182	N86-12758 *	#	E-2639-1	p 63	N86-31652 *	#	E-2805	p 27	N86-16219 *	#
DOE/NASA-0256/11	p 144	N86-31000 *	#	E-2644	p 13	N86-28055 *	#	E-2806	p 87	N86-13409 *	#
DOE/NASA-0345-1	p 209	N86-21456 *	#	E-2647	p 103	N86-24835 *	#	E-2807	p 212	N86-14110 *	#
DOE/NASA-1005/10	p 211	N86-29732 *	#	E-2649	p 100	N86-10341 *	#	E-2808	p 193	N86-19008 *	#
DOE/NASA-20320/70	p 189	N86-30251 *	#	E-2650	p 156	N86-10551 *	#	E-2809	p 112	N86-13627 *	#
DOE/NASA-20320/71	p 190	N86-31983 *	#	E-2651	p 137	N86-10463 *	#	E-2812	p 201	N86-29630 *	#
DOE/NASA-50112-61	p 209	N86-21457 *	#	E-2652	p 161	N86-30160 *	#	E-2813	p 65	N86-13370 *	#
DOE/NASA-50112/62-REV	p 210	N86-25303 *	#	E-2654	p 174	N86-14688 *	#	E-2817	p 140	N86-19556 *	#
DOE/NASA-50112/66	p 211	N86-29731 *	#	E-2668	p 57	N86-16258 *	#	E-2820	p 65	N86-17472 *	#
DOE/NASA/0005-3	p 188	N86-28511 *	#	E-2669	p 77	N86-12268 *	#	E-2821	p 208	N86-14106 *	#
DOE/NASA/0032-80/7	p 211	N86-28017 *	#	E-2674	p 101	N86-15394 *	#	E-2825	p 209	N86-21457 *	#
DOE/NASA/0143-1	p 108	N86-27460 *	#	E-2676	p 163	N86-10561 *	#	E-2826	p 11	N86-21517 *	#
DOE/NASA/0153-VOL-2-BK-1	p 183	N86-15722 *	#	E-2679	p 9	N86-10017 *	#	E-2828	p 148	N86-14554 *	#
DOE/NASA/0153-VOL-2-BK-2	p 183	N86-15723 *	#	E-2680	p 206	N86-25284 *	#	E-2829	p 46	N86-16249 *	#
DOE/NASA/0153-VOL-3-BK-1	p 183	N86-15724 *	#	E-2681	p 1	N86-11146 *	#	E-2830	p 121	N86-16487 *	#
DOE/NASA/0153-VOL-3-BK-2	p 183	N86-15725 *	#	E-2683	p 9	N86-14223 *	#	E-2831	p 38	N86-26101 *	#
DOE/NASA/0153-VOL-4-BK-1	p 183	N86-15726 *	#	E-2684	p 27	N86-15313 *	#	E-2832	p 175	N86-18750 *	#
DOE/NASA/0153-VOL-4-BK-2	p 184	N86-15727 *	#	E-2685	p 156	N86-10552 *	#	E-2833	p 140	N86-19555 *	#
DOE/NASA/0153-VOL-4-BK-3	p 184	N86-15728 *	#	E-2686	p 9	N86-10019 *	#	E-2834	p 209	N86-19264 *	#
DOE/NASA/0153-VOL-4-BK-4	p 184	N86-15729 *	#	E-2691	p 11	N86-21505 *	#	E-2835	p 209	N86-19264 *	#
DOE/NASA/0153-VOL-4-BK-5	p 184	N86-15730 *	#	E-2692	p 102	N86-16379 *	#	E-2836	p 113	N86-16457 *	#
DOE/NASA/0167-10	p 211	N86-33211 *	#	E-2696	p 199	N86-14007 *	#	E-2837	p 114	N86-18586 *	#
DOE/NASA/0168-9	p 158	N86-20808 *	#	E-2695	p 68	N86-10290 *	#	E-2839-1	p 27	N86-16218 *	#
DOE/NASA/0255-1	p 185	N86-18773 *	#	E-2696	p 139	N86-15625 *	#	E-2840	p 148	N86-24959 *	#
DOE/NASA/0289-1	p 187	N86-25040 *	#	E-2700	p 56	N86-10280 *	#	E-2844	p 164	N86-18598 *	#
DOE/NASA/0290-02	p 190	N86-31984 *	#	E-2701	p 9	N86-13295 *	#	E-2845	p 37	N86-18329 *	#
DOE/NASA/0290-1	p 183	N86-14727 *	#	E-2702-1	p 206	N86-28775 *	#	E-2846	p 142	N86-23857 *	#
DOE/NASA/0305-1	p 209	N86-17224 *	#	E-2703	p 181	N86-10643 *	#	E-2848	p 88	N86-15380 *	#
DOE/NASA/0310-1	p 187	N86-21979 *	#	E-2704	p 178	N86-28464 *	#	E-2847	p 17	N86-31562 *	#
DOE/NASA/0312-1	p 208	N86-16165 *	#	E-2706	p 184	N86-17839 *	#	E-2848	p 46	N86-17368 *	#
DOE/NASA/0340-1	p 208	N86-16164 *	#	E-2707	p 105	N86-28194 *	#	E-2850	p 37	N86-16233 *	#
DOE/NASA/0341-1	p 185	N86-18774 *	#	E-2709	p 172	N86-10582 *	#	E-2851	p 174	N86-16611 *	#
DOE/NASA/0342-2	p 210	N86-24590 *	#	E-2710	p 86	N86-10311 *	#	E-2852	p 113	N86-16461 *	#
DOE/NASA/0351-1	p 210	N86-25302 *	#	E-2711	p 157	N86-14613 *	#	E-2854	p 10	N86-14224 *	#
DOE/NASA/0352-2	p 105	N86-29042 *	#	E-2713	p 201	N86-25218 *	#	E-2855	p 10	N86-16195 *	#
DOE/NASA/0363-1	p 89	N86-17531 *	#	E-2714	p 101	N86-12311 *	#	E-2856	p 113	N86-17595 *	#
DOE/NASA/0369-3	p 189	N86-29411 *	#	E-2718	p 199	N86-14006 *	#	E-2857	p 212	N86-19274 *	#
DOE/NASA/0457-1	p 209	N86-17226 *	#	E-2722	p 138	N86-13678 *	#	E-2858	p 164	N86-19636 *	#
DOE/NASA/0530-1	p 182	N86-11670 *	#	E-2724	p 86	N86-12292 *	#	E-2860	p 69	N86-17477 *	#
DOE/NASA/0563-1	p 89	N86-21656 *	#	E-2725	p 56	N86-10279 *	#	E-2861	p 46	N86-18343 *	#
DOE/NASA/1005-6	p 182	N86-11668 *	#	E-2726	p 205	N86-11048 *	#	E-2862	p 140	N86-18647 *	#
DOE/NASA/1005-7	p 208	N86-13236 *	#	E-2728	p 138	N86-13679 *	#	E-2863	p 62	N86-28124 *	#
DOE/NASA/1005-8	p 209	N86-19264 *	#	E-2729	p 137	N86-11425 *	#	E-2864	p 164	N86-18599 *	#
DOE/NASA/1005-9	p 210	N86-26261 *	#	E-2730	p 69	N86-12256 *	#	E-2865	p 90	N86-21661 *	#
DOE/NASA/20320-66	p 172	N86-10582 *	#	E-2733	p 57	N86-11224 *	#	E-2866	p 89	N86-16334 *	#
				E-2734	p 201	N86-32247 *	#	E-2870	p 43	N86-18338 *	#
				E-2737	p 111	N86-10380 *	#	E-2871	p 10	N86-19289 *	#
				E-2738	p 111	N86-10381 *	#	E-2872	p 176	N86-25822 *	#
				E-2740	p 199	N86-19125 *	#	E-2873	p 175	N86-16615 *	#
				E-2744	p 57	N86-10281 *	#	E-2876	p 27	N86-16221 *	#
				E-2745	p 48	N86-12246 *	#	E-2877	p 65	N86-18442 *	#
								E-2880	p 113	N86-16458 *	#
								E-2885	p 50	N86-21575 *	#
								E-2886	p 77	N86-19417 *	#
								E-2887	p 123	N86-21757 *	#
								E-2888	p 91	N86-24813 *	#
								E-2889	p 159	N86-24990 *	#

E-2890	p 177	N86-26651 *	E-3075	p 92	N86-28164 *	IAF PAPER 85-289	p 72	A86-15805 *
E-2891	p 104	N86-24838 *	E-3076	p 188	N86-26677 *	IAF-86-37	p 64	N86-32520 *
E-2892	p 89	N86-20541 *	E-3080	p 44	N86-31621 *			
E-2894	p 114	N86-18585 *	E-3081	p 165	N86-28445 *	ITRI-M06136-9	p 89	N86-17531 *
E-2896	p 210	N86-25303 *	E-3082	p 149	N86-27617 *			
E-2897	p 140	N86-19558 *	E-3084	p 71	N86-27426 *	IR-4	p 158	N86-17748 *
E-2898	p 175	N86-19663 *	E-3085	p 63	N86-31650 *			
E-2899	p 159	N86-21856 *	E-3086	p 165	N86-25812 *	JM/85-11	p 27	N86-16220 *
E-2901	p 186	N86-18775 *	E-3089	p 81	N86-25409 *	JM/86-2	p 143	N86-26546 *
E-2905	p 90	N86-21658 *	E-3090	p 71	N86-26376 *	JM/86-6	p 32	N86-30731 *
E-2908	p 187	N86-25039 *	E-3091	p 105	N86-27452 *			
E-2909	p 102	N86-19465 *	E-3092	p 93	N86-31701 *	JN67801	p 42	N86-18334 *
E-2914	p 158	N86-20809 *	E-3093	p 165	N86-27666 *			
E-2915	p 11	N86-21513 *	E-3096	p 166	N86-31912 *	JPL-9950-1037	p 122	N86-20700 *
E-2916	p 149	N86-24964 *	E-3098	p 211	N86-29731 *			
E-2918	p 206	N86-25267 *	E-3100	p 83	N86-31651 *	KU-SM-15	p 195	N86-26067 *
E-2919	p 105	N86-25475 *	E-3101	p 192	N86-26914 *			
E-2921	p 104	N86-24836 *	E-3102	p 189	N86-31979 *	ME84-1	p 108	N86-27460 *
E-2926	p 123	N86-24907 *	E-3106	p 12	N86-27213 *			
E-2928	p 104	N86-25474 *	E-3109	p 161	N86-27661 *	MM-4998-86-13-PT-1	p 179	N86-30227 *
E-2929	p 109	N86-24869 *	E-3112	p 71	N86-31663 *	MM-4998-86-13-PT-2	p 178	N86-28455 *
E-2932	p 160	N86-25793 *	E-3113	p 211	N86-31452 *			
E-2934	p 106	N86-31729 *	E-3114	p 78	N86-31680 *	MSU-ENGR-85-026	p 181	N86-11667 *
E-2936	p 141	N86-23854 *	E-3115	p 124	N86-27578 *			
E-2938	p 61	N86-27418 *	E-3121	p 15	N86-31548 *	MTI-86TR17	p 144	N86-31000 *
E-2942	p 186	N86-21978 *	E-3122	p 93	N86-31700 *			
E-2944	p 11	N86-20357 *	E-3125	p 166	N86-31065 *	MTR-85-556-VOL-2	p 115	N86-24876 *
E-2945	p 63	N86-31649 *	E-3127	p 178	N86-29271 *			
E-2947	p 90	N86-21659 *	E-3130	p 13	N86-31537 *	NAS 1.15:86864-REV	p 104	N86-24839 *
E-2948	p 165	N86-27665 *	E-3131	p 34	N86-31587 *	NAS 1.15:86886	p 69	N86-23661 *
E-2949	p 164	N86-25002 *	E-3135	p 12	N86-28053 *	NAS 1.15:86892	p 148	N86-22915 *
E-2950	p 206	N86-25268 *	E-3137	p 144	N86-28378 *	NAS 1.15:86972-REV	p 181	N86-11666 *
E-2951	p 62	N86-28125 *	E-3137	p 124	N86-31792 *	NAS 1.15:86998	p 60	N86-21578 *
E-2952	p 93	N86-31702 *	E-3138	p 161	N86-30206 *	NAS 1.15:87072	p 111	N86-10379 *
E-2953	p 103	N86-20568 *	E-3140	p 62	N86-28122 *	NAS 1.15:87073	p 13	N86-28055 *
E-2954	p 193	N86-22150 *	E-3141	p 194	N86-28651 *	NAS 1.15:87076	p 137	N86-10463 *
E-2955	p 106	N86-31728 *	E-3148	p 33	N86-31583 *	NAS 1.15:87088	p 163	N86-10561 *
E-2956	p 77	N86-21635 *	E-3154	p 207	N86-30556 *	NAS 1.15:87090	p 206	N86-25284 *
E-2958	p 187	N86-23035 *	E-3155	p 178	N86-28461 *	NAS 1.15:87091	p 9	N86-10017 *
E-2960	p 208	N86-32336 *	E-3156	p 34	N86-31586 *	NAS 1.15:87093	p 9	N86-10018 *
E-2962	p 35	N86-22582 *	E-3157	p 212	N86-30620 *	NAS 1.15:87095	p 37	N86-16232 *
E-2968	p 70	N86-25417 *	E-3158	p 179	N86-30236 *	NAS 1.15:87099	p 199	N86-14007 *
E-2969	p 105	N86-25476 *	E-3162	p 189	N86-30251 *	NAS 1.15:87101	p 68	N86-10290 *
E-2971	p 31	N86-28085 *	E-3163	p 190	N86-31983 *	NAS 1.15:87103	p 56	N86-10280 *
E-2975	p 35	N86-32432 *	E-3166	p 166	N86-31913 *	NAS 1.15:87104	p 9	N86-13295 *
E-2976	p 115	N86-24881 *	E-3167	p 71	N86-29908 *	NAS 1.15:87105	p 100	N86-10341 *
E-2977	p 103	N86-21682 *	E-3170	p 211	N86-29732 *	NAS 1.15:87106	p 181	N86-10643 *
E-2978	p 103	N86-21683 *	E-3171	p 64	N86-32522 *	NAS 1.15:87109	p 172	N86-10582 *
E-2979	p 105	N86-29041 *	E-3174	p 62	N86-31646 *	NAS 1.15:87110	p 86	N86-10311 *
E-2981	p 80	N86-24748 *	E-3177	p 34	N86-31585 *	NAS 1.15:87112	p 201	N86-25218 *
E-2982	p 61	N86-25407 *	E-3178	p 116	N86-32598 *	NAS 1.15:87113	p 101	N86-12311 *
E-2983	p 61	N86-25408 *	E-3182	p 47	N86-31625 *	NAS 1.15:87114	p 156	N86-10551 *
E-2986	p 60	N86-24749 *	E-3194	p 125	N86-32627 *	NAS 1.15:87116	p 199	N86-14006 *
E-2987	p 148	N86-24961 *	E-3201	p 166	N86-32764 *	NAS 1.15:87117	p 86	N86-12292 *
E-2988	p 179	N86-31920 *	E-3203	p 106	N86-32573 *	NAS 1.15:87118	p 56	N86-10279 *
E-2993	p 141	N86-22890 *	E-3204	p 150	N86-31859 *	NAS 1.15:87119	p 205	N86-11048 *
E-2994	p 90	N86-22687 *	E-3212	p 125	N86-31793 *	NAS 1.15:87120	p 138	N86-13679 *
E-2995	p 30	N86-24697 *	E-3222	p 49	N86-31634 *	NAS 1.15:87121	p 137	N86-11425 *
E-2997	p 91	N86-25453 *	E-3227	p 93	N86-32557 *	NAS 1.15:87122	p 69	N86-12256 *
E-2998	p 70	N86-24756 *	E-3237	p 64	N86-32521 *	NAS 1.15:87123	p 57	N86-11224 *
E-2999	p 90	N86-22686 *	E-3241	p 150	N86-32702 *	NAS 1.15:87124	p 111	N86-10380 *
E-3000	p 92	N86-28165 *	E-3244	p 150	N86-32703 *	NAS 1.15:87125	p 111	N86-10381 *
E-3001	p 206	N86-28776 *	E-3245	p 35	N86-32433 *	NAS 1.15:87126	p 182	N86-11668 *
E-3002	p 143	N86-25726 *	E-3249	p 64	N86-32520 *	NAS 1.15:87127	p 157	N86-14613 *
E-3004	p 11	N86-24658 *	E-3828	p 37	N86-16232 *	NAS 1.15:87128	p 1	N86-11146 *
E-3010	p 44	N86-23616 *				NAS 1.15:87129	p 199	N86-19125 *
E-3011	p 104	N86-25473 *	EDR-11984-VOL-1	p 29	N86-21546 *	NAS 1.15:87131	p 57	N86-10281 *
E-3013	p 12	N86-24667 *	EDR-12070	p 158	N86-20808 *	NAS 1.15:87132	p 87	N86-13407 *
E-3014	p 124	N86-30068 *	EDR-12118	p 33	N86-30733 *	NAS 1.15:87133	p 156	N86-10552 *
E-3016	p 33	N86-31582 *				NAS 1.15:87134	p 182	N86-11671 *
E-3020	p 201	N86-25217 *	EE116-81	p 123	N86-25693 *	NAS 1.15:87135	p 205	N86-12134 *
E-3024	p 161	N86-31889 *				NAS 1.15:87136	p 120	N86-12509 *
E-3025	p 149	N86-26596 *	ELR-86-5	p 115	N86-25650 *	NAS 1.15:87137	p 112	N86-12485 *
E-3027	p 13	N86-28063 *				NAS 1.15:87138	p 69	N86-14316 *
E-3028	p 210	N86-26261 *	ELSR-86-8	p 116	N86-30039 *	NAS 1.15:87139	p 48	N86-12246 *
E-3029	p 148	N86-24958 *				NAS 1.15:87140	p 205	N86-12135 *
E-3035	p 91	N86-24817 *	FAA-CT-86-19	p 149	N86-26596 *	NAS 1.15:87141	p 141	N86-21797 *
E-3037	p 190	N86-31980 *				NAS 1.15:87142	p 87	N86-12293 *
E-3041	p 78	N86-25431 *	FCR-6848	p 189	N86-29411 *	NAS 1.15:87143	p 101	N86-12310 *
E-3044	p 212	N86-25321 *	FCR-6868	p 185	N86-18773 *	NAS 1.15:87144	p 9	N86-14219 *
E-3045	p 60	N86-24747 *				NAS 1.15:87145	p 44	N86-11218 *
E-3046	p 123	N86-26520 *	G-21-4314-2	p 29	N86-23598 *	NAS 1.15:87146	p 37	N86-12239 *
E-3047	p 34	N86-31588 *				NAS 1.15:87147	p 141	N86-23854 *
E-3048	p 30	N86-26336 *	GARRETT-21-5418	p 142	N86-24938 *	NAS 1.15:87149	p 192	N86-13899 *
E-3049	p 17	N86-24691 *	GARRETT-21-5869	p 180	N86-26629 *	NAS 1.15:87150	p 87	N86-12294 *
E-3050	p 92	N86-31699 *	GARRETT-31-3725(10)	p 211	N86-33211 *	NAS 1.15:87151	p 138	N86-13677 *
E-3055	p 190	N86-31981 *				NAS 1.15:87152	p 157	N86-11475 *
E-3057	p 190	N86-31982 *	GDC-SP-84-050	p 59	N86-20493 *	NAS 1.15:87153	p 101	N86-13495 *
E-3058	p 149	N86-24967 *				NAS 1.15:87154	p 70	N86-24757 *
E-3059	p 32	N86-28089 *	GTPDL-181	p 31	N86-27285 *	NAS 1.15:87155	p 77	N86-12268 *
E-3060	p 12	N86-26285 *				NAS 1.15:87156	p 208	N86-13236 *
E-3062	p 125	N86-32629 *	HSER-9333	p 13	N86-31536 *	NAS 1.15:87157	p 121	N86-13645 *
E-3064	p 150	N86-31857 *				NAS 1.15:87159	p 9	N86-14223 *
E-3065	p 196	N86-27036 *	IAF PAPER 85-164	p 51	A86-17850 *	NAS 1.15:87160	p 112	N86-14479 *
E-3066	p 177	N86-27680 *	IAF PAPER 85-282	p 126	A86-15800 *	NAS 1.15:87161	p 26	N86-12227 *
E-3072	p 143	N86-26545 *	IAF PAPER 85-288	p 72	A86-15804 *			

NAS 1.15:87162	p 112	N86-14477 *	NAS 1.15:87266	p 70	N86-25417 *	NAS 1.15:88789	p 144	N86-28378
NAS 1.15:87163	p 114	N86-19494 *	NAS 1.15:87267	p 105	N86-25476 *	NAS 1.15:88800	p 161	N86-30206
NAS 1.15:87164	p 164	N86-13749 *	NAS 1.15:87268	p 77	N86-21635 *	NAS 1.15:88801	p 62	N86-28122
NAS 1.15:87165	p 158	N86-19616 *	NAS 1.15:87269	p 206	N86-25267 *	NAS 1.15:88802	p 194	N86-28651
NAS 1.15:87166	p 166	N86-18776 *	NAS 1.15:87270	p 91	N86-24813 *	NAS 1.15:88803	p 78	N86-31680
NAS 1.15:87167	p 27	N86-16219 *	NAS 1.15:87271	p 124	N86-31792 *	NAS 1.15:88804	p 33	N86-31583
NAS 1.15:87168	p 87	N86-13409 *	NAS 1.15:87272	p 31	N86-28085 *	NAS 1.15:88806	p 207	N86-30556
NAS 1.15:87169	p 212	N86-14110 *	NAS 1.15:87273	p 160	N86-25793 *	NAS 1.15:88807	p 178	N86-28461
NAS 1.15:87170	p 193	N86-19008 *	NAS 1.15:87274	p 103	N86-21682 *	NAS 1.15:88808	p 34	N86-31586
NAS 1.15:87171	p 112	N86-13627 *	NAS 1.15:87275	p 103	N86-21683 *	NAS 1.15:88809	p 212	N86-30620
NAS 1.15:87172	p 65	N86-13370 *	NAS 1.15:87276	p 104	N86-25474 *	NAS 1.15:88810	p 189	N86-30251
NAS 1.15:87173	p 87	N86-13408 *	NAS 1.15:87277	p 106	N86-31728 *	NAS 1.15:88811	p 190	N86-31983
NAS 1.15:87174	p 140	N86-19556 *	NAS 1.15:87278	p 60	N86-24748 *	NAS 1.15:88812	p 71	N86-29908
NAS 1.15:87175	p 208	N86-14106 *	NAS 1.15:87279	p 61	N86-25407 *	NAS 1.15:88815	p 211	N86-29732
NAS 1.15:87176	p 138	N86-13678 *	NAS 1.15:87280	p 61	N86-25408 *	NAS 1.15:88818	p 82	N86-31648
NAS 1.15:87177	p 209	N86-21457 *	NAS 1.15:87281	p 60	N86-24749 *	NAS 1.15:88817	p 34	N86-31585
NAS 1.15:87178	p 11	N86-21517 *	NAS 1.15:87282	p 187	N86-25039 *	NAS 1.15:88818	p 116	N86-32598
NAS 1.15:87179	p 207	N86-21427 *	NAS 1.15:87283	p 105	N86-25475 *	NAS 1.15:88820	p 47	N86-31625
NAS 1.15:87180	p 148	N86-14554 *	NAS 1.15:87284	p 115	N86-24881 *	NAS 1.15:88822	p 64	N86-32522
NAS 1.15:87181	p 121	N86-16487 *	NAS 1.15:87285	p 148	N86-24961 *	NAS 1.15:88827	p 166	N86-32764
NAS 1.15:87182	p 175	N86-18750 *	NAS 1.15:87286	p 141	N86-22890 *	NAS 1.15:88828	p 106	N86-32573
NAS 1.15:87183	p 113	N86-16457 *	NAS 1.15:87287	p 90	N86-22687 *	NAS 1.15:88829	p 150	N86-31859
NAS 1.15:87185	p 114	N86-18586 *	NAS 1.15:87288	p 30	N86-24697 *	NAS 1.15:88832	p 125	N86-32627
NAS 1.15:87186	p 164	N86-16598 *	NAS 1.15:87289	p 91	N86-25453 *	NAS 1.15:88833	p 125	N86-31793
NAS 1.15:87187	p 88	N86-15378 *	NAS 1.15:87290	p 70	N86-24756 *	NAS 1.15:88839	p 49	N86-31634
NAS 1.15:87188	p 174	N86-14688 *	NAS 1.15:87291	p 90	N86-22686 *	NAS 1.15:88842	p 93	N86-32557
NAS 1.15:87189	p 57	N86-16258 *	NAS 1.15:87292	p 92	N86-28165 *	NAS 1.15:88847	p 64	N86-32521
NAS 1.15:87190	p 37	N86-18329 *	NAS 1.15:87293	p 35	N86-32432 *	NAS 1.15:88851	p 150	N86-32702
NAS 1.15:87191	p 17	N86-131562 *	NAS 1.15:87294	p 70	N86-24759 *	NAS 1.15:88853	p 150	N86-32703
NAS 1.15:87192	p 46	N86-17368 *	NAS 1.15:87295	p 93	N86-31702 *	NAS 1.15:88856	p 64	N86-32520
NAS 1.15:87193	p 10	N86-16194 *	NAS 1.15:87296	p 11	N86-24658 *	NAS 1.15:88857	p 35	N86-32433
NAS 1.15:87194	p 37	N86-16233 *	NAS 1.15:87297	p 44	N86-23616 *	NAS 1.26:168171	p 177	N86-26652
NAS 1.15:87195	p 102	N86-16379 *	NAS 1.15:87298	p 104	N86-25473 *	NAS 1.26:174645	p 159	N86-23936
NAS 1.15:87196	p 139	N86-18646 *	NAS 1.15:87299	p 12	N86-24667 *	NAS 1.26:174646	p 159	N86-23937
NAS 1.15:87197	p 174	N86-16611 *	NAS 1.15:87300	p 201	N86-25217 *	NAS 1.26:174647	p 159	N86-23938
NAS 1.15:87198	p 113	N86-16461 *	NAS 1.15:87301	p 206	N86-28775 *	NAS 1.26:174652	p 29	N86-23598
NAS 1.15:87199	p 10	N86-14224 *	NAS 1.15:87302	p 33	N86-31582 *	NAS 1.26:174654	p 116	N86-31760
NAS 1.15:87200	p 10	N86-16195 *	NAS 1.15:87303	p 210	N86-26261 *	NAS 1.26:174708	p 30	N86-24693
NAS 1.15:87201	p 113	N86-17595 *	NAS 1.15:87304	p 148	N86-24958 *	NAS 1.26:174709	p 187	N86-25040
NAS 1.15:87202	p 212	N86-19274 *	NAS 1.15:87305	p 179	N86-31920 *	NAS 1.26:174710	p 159	N86-24991
NAS 1.15:87203	p 164	N86-19636 *	NAS 1.15:87306	p 104	N86-24837 *	NAS 1.26:174723	p 187	N86-21979
NAS 1.15:87204	p 69	N86-17477 *	NAS 1.15:87307	p 78	N86-25431 *	NAS 1.26:174734	p 188	N86-27708
NAS 1.15:87205	p 140	N86-18647 *	NAS 1.15:87308	p 212	N86-25321 *	NAS 1.26:174735-VOL-2-BK-1	p 183	N86-15722
NAS 1.15:87206	p 46	N86-18343 *	NAS 1.15:87309	p 60	N86-24747 *	NAS 1.26:174735-VOL-2-BK-2	p 183	N86-15723
NAS 1.15:87207	p 175	N86-17789 *	NAS 1.15:87310	p 123	N86-26520 *	NAS 1.26:174735-VOL-3-BK-1	p 183	N86-15724
NAS 1.15:87208	p 90	N86-21661 *	NAS 1.15:87311	p 34	N86-31588 *	NAS 1.26:174735-VOL-3-BK-2	p 183	N86-15725
NAS 1.15:87209	p 88	N86-15380 *	NAS 1.15:87312	p 30	N86-26336 *	NAS 1.26:174735-VOL-4-BK-1	p 183	N86-15726
NAS 1.15:87210	p 89	N86-16334 *	NAS 1.15:87313	p 92	N86-31699 *	NAS 1.26:174735-VOL-4-BK-2	p 184	N86-15727
NAS 1.15:87211	p 93	N86-18338 *	NAS 1.15:87314	p 190	N86-31981 *	NAS 1.26:174735-VOL-4-BK-3	p 184	N86-15728
NAS 1.15:87212	p 10	N86-19289 *	NAS 1.15:87315	p 190	N86-31982 *	NAS 1.26:174735-VOL-4-BK-4	p 184	N86-15729
NAS 1.15:87213	p 176	N86-25822 *	NAS 1.15:87316	p 206	N86-28776 *	NAS 1.26:174735-VOL-4-BK-5	p 184	N86-15730
NAS 1.15:87214	p 175	N86-16615 *	NAS 1.15:87317	p 149	N86-24967 *	NAS 1.26:174743	p 148	N86-21817
NAS 1.15:87215	p 46	N86-16249 *	NAS 1.15:87318	p 12	N86-26285 *	NAS 1.26:174749	p 211	N86-28017
NAS 1.15:87216	p 27	N86-16221 *	NAS 1.15:87319	p 196	N86-27036 *	NAS 1.26:174758	p 12	N86-27186
NAS 1.15:87217	p 65	N86-18442 *	NAS 1.15:87320	p 177	N86-27680 *	NAS 1.26:174788	p 31	N86-27282
NAS 1.15:87218	p 113	N86-16458 *	NAS 1.15:87321	p 190	N86-31980 *	NAS 1.26:174789	p 13	N86-31536
NAS 1.15:87219	p 65	N86-17472 *	NAS 1.15:87322	p 143	N86-26545 *	NAS 1.26:174792	p 121	N86-14499
NAS 1.15:87220	p 142	N86-24934 *	NAS 1.15:87323	p 143	N86-25726 *	NAS 1.26:174797	p 121	N86-16486
NAS 1.15:87221	p 77	N86-19417 *	NAS 1.15:87324	p 161	N86-31889 *	NAS 1.26:174811	p 139	N86-16518
NAS 1.15:87222	p 164	N86-16599 *	NAS 1.15:87325	p 92	N86-28164 *	NAS 1.26:174813	p 108	N86-27460
NAS 1.15:87223	p 209	N86-19264 *	NAS 1.15:87326	p 188	N86-26677 *	NAS 1.26:174815	p 188	N86-25046
NAS 1.15:87224	p 177	N86-26651 *	NAS 1.15:87327	p 201	N86-29630 *	NAS 1.26:174817	p 200	N86-23371
NAS 1.15:87225	p 114	N86-18585 *	NAS 1.15:87328	p 71	N86-31664 *	NAS 1.26:174818	p 201	N86-23372
NAS 1.15:87226	p 210	N86-25303 *	NAS 1.15:87329	p 44	N86-31665 *	NAS 1.26:174825	p 33	N86-30732
NAS 1.15:87227	p 140	N86-19558 *	NAS 1.15:87330	p 149	N86-27617 *	NAS 1.26:174826	p 207	N86-13219
NAS 1.15:87228	p 123	N86-21757 *	NAS 1.15:87331	p 71	N86-27426 *	NAS 1.26:174827	p 29	N86-21546
NAS 1.15:87229	p 140	N86-19555 *	NAS 1.15:87332	p 63	N86-31650 *	NAS 1.26:174842	p 58	N86-20493
NAS 1.15:87230	p 175	N86-19663 *	NAS 1.15:87333	p 165	N86-25812 *	NAS 1.26:174843	p 60	N86-24746
NAS 1.15:87231	p 159	N86-21856 *	NAS 1.15:87334	p 61	N86-25409 *	NAS 1.26:174869	p 150	N86-31030
NAS 1.15:87232	p 186	N86-18775 *	NAS 1.15:87335	p 71	N86-26376 *	NAS 1.26:174878	p 26	N86-14272
NAS 1.15:87233	p 140	N86-21794 *	NAS 1.15:87336	p 105	N86-27452 *	NAS 1.26:174884	p 142	N86-24938
NAS 1.15:87234	p 90	N86-21658 *	NAS 1.15:87337	p 93	N86-31701 *	NAS 1.26:174889	p 193	N86-27927
NAS 1.15:87235	p 102	N86-19465 *	NAS 1.15:87338	p 124	N86-30068 *	NAS 1.26:174890	p 193	N86-27928
NAS 1.15:87236	p 10	N86-19290 *	NAS 1.15:87339	p 211	N86-29731 *	NAS 1.26:174891	p 142	N86-24931
NAS 1.15:87237	p 158	N86-20809 *	NAS 1.15:87340	p 34	N86-31584 *	NAS 1.26:174892	p 176	N86-21932
NAS 1.15:87238	p 11	N86-21513 *	NAS 1.15:87341	p 63	N86-31651 *	NAS 1.26:174898	p 209	N86-21456
NAS 1.15:87239	p 149	N86-24964 *	NAS 1.15:87342	p 168	N86-31912 *	NAS 1.26:174901	p 57	N86-16259
NAS 1.15:87240	p 103	N86-24835 *	NAS 1.15:87343	p 192	N86-26914 *	NAS 1.26:174904	p 115	N86-24878
NAS 1.15:87241	p 104	N86-24836 *	NAS 1.15:87344	p 150	N86-31857 *	NAS 1.26:174905	p 115	N86-24877
NAS 1.15:87242	p 123	N86-24907 *	NAS 1.15:87345	p 201	N86-32247 *	NAS 1.26:174907	p 208	N86-16185
NAS 1.15:87243	p 109	N86-24869 *	NAS 1.15:87346	p 12	N86-27213 *	NAS 1.26:174911	p 15	N86-30022
NAS 1.15:87244	p 104	N86-24838 *	NAS 1.15:87347	p 161	N86-27661 *	NAS 1.26:174913	p 162	N86-32741
NAS 1.15:87245	p 89	N86-20541 *	NAS 1.15:87348	p 124	N86-27578 *	NAS 1.26:174919	p 15	N86-27268
NAS 1.15:87246	p 106	N86-31729 *	NAS 1.15:87349	p 115	N86-25650 *	NAS 1.26:174923-VOL-1	p 26	N86-13328
NAS 1.15:87247	p 186	N86-21978 *	NAS 1.15:87350	p 63	N86-31652 *	NAS 1.26:174923-VOL-2	p 26	N86-13329
NAS 1.15:87248	p 11	N86-20357 *	NAS 1.15:87351	p 71	N86-31663 *	NAS 1.26:174923-VOL-3	p 26	N86-13330
NAS 1.15:87249	p 63	N86-31649 *	NAS 1.15:87352	p 93	N86-31700 *	NAS 1.26:174924	p 157	N86-11474
NAS 1.15:87250	p 148	N86-24959 *	NAS 1.15:87353	p 166	N86-31065 *	NAS 1.26:174928	p 49	N86-27403
NAS 1.15:87251	p 90	N86-21659 *	NAS 1.15:87354	p 15	N86-31548 *	NAS 1.26:174929	p 49	N86-27404
NAS 1.15:87252	p 206	N86-25268 *	NAS 1.15:87355	p 178	N86-29271 *	NAS 1.26:174930	p 49	N86-27405
NAS 1.15:87253	p 62	N86-28125 *	NAS 1.15:87356	p 189	N86-31979 *	NAS 1.26:174934	p 57	N86-15339
NAS 1.15:87254	p 50	N86-21575 *	NAS 1.15:87357	p 105	N86-29041 *	NAS 1.26:174936	p 124	N86-30073
NAS 1.15:87255	p 103	N86-20568 *	NAS 1.15:87358	p 13	N86-31537 *	NAS 1.26:174943	p 209	N86-17224
NAS 1.15:87256	p 208	N86-32336 *	NAS 1.15:87359	p 34	N86-31587 *	NAS 1.26:174944	p 116	N86-26489
NAS 1.15:87257	p 187	N86-23035 *	NAS 1.15:87360	p 166	N86-31913 *	NAS 1.26:174946	p 174	N86-13755
NAS 1.15:87258	p 35	N86-22582 *	NAS 1.15:87361	p 12	N86-28053 *	NAS 1.26:174948	p 182	N86-12757

NAS 1.26:174951	p 188	N86-25877 *	NAS 1.26:176424	p 37	N86-15323 *	NAS 1.60:2558	p 60	N86-21577 *
NAS 1.26:174952	p 185	N86-25003 *	NAS 1.26:176428	p 27	N86-16220 *	NAS 1.60:2562	p 44	N86-24722 *
NAS 1.26:174961	p 183	N86-14727 *	NAS 1.26:176438	p 121	N86-15544 *	NAS 1.60:2570	p 38	N86-28101 *
NAS 1.26:174964	p 137	N86-10481 *	NAS 1.26:176478	p 139	N86-16519 *	NAS 1.60:2571	p 62	N86-28123 *
NAS 1.26:174970	p 63	N86-31648 *	NAS 1.26:176488	p 46	N86-18341 *	NAS 1.60:2590	p 195	N86-28682 *
NAS 1.26:174971	p 208	N86-16164 *	NAS 1.26:176548	p 102	N86-19484 *	NAS 1.60:2591	p 178	N86-28464 *
NAS 1.26:174978	p 112	N86-18451 *	NAS 1.26:176554	p 186	N86-19742 *	NAS 1.60:2602	p 62	N86-28124 *
NAS 1.26:174979	p 113	N86-18452 *	NAS 1.26:176555	p 114	N86-19493 *	NAS 1.60:2622	p 125	N86-32629 *
NAS 1.26:174980	p 172	N86-10589 *	NAS 1.26:176560	p 192	N86-21092 *	NAS 1.61:1150	p 172	N86-10579 *
NAS 1.26:174985	p 49	N86-27407 *	NAS 1.26:176564	p 77	N86-20517 *	NAS 1.61:1152	p 157	N86-14612 *
NAS 1.26:174986	p 49	N86-27402 *	NAS 1.26:176566	p 122	N86-20700 *	NAS 1.61:1154	p 157	N86-13734 *
NAS 1.26:174988	p 185	N86-18773 *	NAS 1.26:176604	p 140	N86-20722 *	NAS 1.71:LEW-13899-1	p 109	N86-20587 *
NAS 1.26:174990	p 182	N86-32743 *	NAS 1.26:176656	p 107	N86-21704 *	NAS 1.71:LEW-14072-3	p 105	N86-26434 *
NAS 1.26:174991	p 185	N86-18774 *	NAS 1.26:176689	p 114	N86-22782 *	NAS 1.71:LEW-14104-2	p 93	N86-32556 *
NAS 1.26:174994	p 210	N86-25302 *	NAS 1.26:176708	p 114	N86-23781 *	NAS 1.71:LEW-14127-1	p 122	N86-20680 *
NAS 1.26:174995	p 26	N86-12226 *	NAS 1.26:176717	p 205	N86-23468 *	NAS 1.71:LEW-14212-1	p 162	N86-32740 *
NAS 1.26:174996	p 209	N86-17226 *	NAS 1.26:176718	p 187	N86-24007 *	NAS 1.71:LEW-14261-1	p 92	N86-26414 *
NAS 1.26:174998	p 182	N86-12758 *	NAS 1.26:176764	p 142	N86-24933 *			
NAS 1.26:174999	p 174	N86-16610 *	NAS 1.26:176765	p 143	N86-24955 *	NASA-CASE-LEW-13142-2	p 28	N86-20389 *
NAS 1.26:175005	p 28	N86-20393 *	NAS 1.26:176772	p 142	N86-24632 *	NASA-CASE-LEW-13670-1	p 158	N86-19606 *
NAS 1.26:175007	p 189	N86-29411 *	NAS 1.26:176774	p 123	N86-24906 *	NASA-CASE-LEW-13773-2	p 122	N86-20671 *
NAS 1.26:175008	p 203	N86-15113 *	NAS 1.26:176777	p 187	N86-25042 *	NASA-CASE-LEW-13822-1	p 188	N86-25874 *
NAS 1.26:175009	p 174	N86-11526 *	NAS 1.26:176786	p 108	N86-25502 *	NASA-CASE-LEW-13864-1	p 102	N86-19457 *
NAS 1.26:175013	p 88	N86-14355 *	NAS 1.26:176787	p 123	N86-25693 *	NASA-CASE-LEW-13899-1	p 109	N86-20587 *
NAS 1.26:175014	p 88	N86-14354 *	NAS 1.26:176804	p 123	N86-25694 *	NASA-CASE-LEW-13922-1	p 122	N86-20672 *
NAS 1.26:175015	p 178	N86-21952 *	NAS 1.26:176808	p 17	N86-28330 *	NASA-CASE-LEW-13961-2	p 122	N86-21472 *
NAS 1.26:175016	p 115	N86-24875 *	NAS 1.26:176821	p 178	N86-25850 *	NASA-CASE-LEW-14028-1	p 186	N86-18721 *
NAS 1.26:175017	p 115	N86-24876 *	NAS 1.26:176822	p 195	N86-28067 *	NASA-CASE-LEW-14072-1	p 102	N86-19458 *
NAS 1.26:175018	p 158	N86-20808 *	NAS 1.26:176840	p 143	N86-28546 *	NASA-CASE-LEW-14072-2	p 106	N86-32569 *
NAS 1.26:175020	p 30	N86-24695 *	NAS 1.26:176850	p 78	N86-28136 *	NASA-CASE-LEW-14072-3	p 105	N86-26434 *
NAS 1.26:175021	p 175	N86-17788 *	NAS 1.26:176883	p 13	N86-30693 *	NASA-CASE-LEW-14104-2	p 93	N86-32556 *
NAS 1.26:175022	p 59	N86-20497 *	NAS 1.26:176894	p 32	N86-30731 *	NASA-CASE-LEW-14127-1	p 122	N86-20680 *
NAS 1.26:175023	p 14	N86-20379 *	NAS 1.26:176954	p 13	N86-29773 *	NASA-CASE-LEW-14130-1	p 109	N86-32587 *
NAS 1.26:175024	p 14	N86-20380 *	NAS 1.26:176960	p 144	N86-30093 *	NASA-CASE-LEW-14170-1	p 160	N86-25790 *
NAS 1.26:175027	p 89	N86-17531 *	NAS 1.26:176990	p 116	N86-30037 *	NASA-CASE-LEW-14177-1	p 190	N86-32875 *
NAS 1.26:175028	p 27	N86-16218 *	NAS 1.26:177088	p 144	N86-30980 *	NASA-CASE-LEW-14212-1	p 162	N86-32740 *
NAS 1.26:175029	p 158	N86-17748 *	NAS 1.26:177092	p 116	N86-30039 *	NASA-CASE-LEW-14262-1	p 92	N86-26414 *
NAS 1.26:175031	p 139	N86-17865 *	NAS 1.26:177096	p 108	N86-30023 *			
NAS 1.26:175033	p 102	N86-16381 *	NAS 1.26:177132	p 78	N86-28139 *	NASA-CP-2289	p 172	N86-11495 *
NAS 1.26:175035	p 29	N86-20395 *	NAS 1.26:177141	p 32	N86-28946 *	NASA-CP-2383	p 164	N86-22962 *
NAS 1.26:175038	p 28	N86-20390 *	NAS 1.26:177185	p 189	N86-29409 *	NASA-CP-2385	p 68	N86-11260 *
NAS 1.26:175037	p 28	N86-20391 *	NAS 1.26:177194	p 178	N86-28482 *	NASA-CP-2392	p 105	N86-28194 *
NAS 1.26:175038	p 42	N86-18334 *	NAS 1.26:177198	p 206	N86-28750 *	NASA-CP-2404	p 198	N86-12007 *
NAS 1.26:175040	p 28	N86-20392 *	NAS 1.26:177206	p 31	N86-27285 *	NASA-CP-2408	p 184	N86-17839 *
NAS 1.26:175041	p 29	N86-20394 *	NAS 1.26:177223	p 61	N86-27419 *	NASA-CP-2409	p 161	N86-30160 *
NAS 1.26:175043	p 141	N86-23856 *	NAS 1.26:177233	p 178	N86-28455 *			
NAS 1.26:175044	p 142	N86-23857 *	NAS 1.26:177237	p 179	N86-30227 *	NASA-CR-168171	p 177	N86-26652 *
NAS 1.26:175045	p 211	N86-30579 *	NAS 1.26:177260	p 38	N86-27291 *	NASA-CR-174645	p 159	N86-23936 *
NAS 1.26:175047	p 190	N86-31984 *	NAS 1.26:177263	p 48	N86-28358 *	NASA-CR-174646	p 159	N86-23937 *
NAS 1.26:175048	p 91	N86-24818 *	NAS 1.26:177264	p 149	N86-26599 *	NASA-CR-174647	p 159	N86-23938 *
NAS 1.26:175049	p 176	N86-21951 *	NAS 1.26:177279	p 143	N86-27807 *	NASA-CR-174652	p 29	N86-23598 *
NAS 1.26:175050	p 89	N86-20542 *	NAS 1.26:177280	p 193	N86-27930 *	NASA-CR-174654	p 116	N86-31760 *
NAS 1.26:175052	p 91	N86-25454 *	NAS 1.26:177304	p 78	N86-27434 *	NASA-CR-174708	p 30	N86-24693 *
NAS 1.26:175054	p 210	N86-22451 *	NAS 1.26:179451	p 180	N86-26829 *	NASA-CR-174709	p 187	N86-25040 *
NAS 1.26:175057	p 177	N86-27689 *	NAS 1.26:179455	p 160	N86-27643 *	NASA-CR-174710	p 159	N86-24991 *
NAS 1.26:175061	p 70	N86-24780 *	NAS 1.26:179480	p 211	N86-31452 *	NASA-CR-174723	p 187	N86-21979 *
NAS 1.26:175063	p 29	N86-23597 *	NAS 1.26:179471	p 32	N86-28087 *	NASA-CR-174734	p 188	N86-27708 *
NAS 1.26:175064	p 29	N86-21545 *	NAS 1.26:179472	p 108	N86-28261 *	NASA-CR-174735-VOL-2-BK-1	p 183	N86-15722 *
NAS 1.26:175066	p 61	N86-27418 *	NAS 1.26:179473	p 161	N86-28433 *	NASA-CR-174735-VOL-2-BK-2	p 183	N86-15723 *
NAS 1.26:175067	p 30	N86-25357 *	NAS 1.26:179474	p 178	N86-28487 *	NASA-CR-174735-VOL-3-BK-1	p 183	N86-15724 *
NAS 1.26:175072	p 210	N86-24590 *	NAS 1.26:179475	p 105	N86-28902 *	NASA-CR-174735-VOL-3-BK-2	p 183	N86-15725 *
NAS 1.26:175073	p 90	N86-22688 *	NAS 1.26:179478	p 179	N86-30236 *	NASA-CR-174735-VOL-4-BK-1	p 183	N86-15726 *
NAS 1.26:175074	p 89	N86-21658 *	NAS 1.26:179485	p 211	N86-33211 *	NASA-CR-174735-VOL-4-BK-2	p 184	N86-15727 *
NAS 1.26:175076	p 141	N86-22892 *	NAS 1.26:179487	p 62	N86-29901 *	NASA-CR-174735-VOL-4-BK-3	p 184	N86-15728 *
NAS 1.26:175082	p 33	N86-30733 *	NAS 1.26:179662	p 144	N86-31826 *	NASA-CR-174735-VOL-4-BK-4	p 184	N86-15729 *
NAS 1.26:175083	p 144	N86-31000 *	NAS 1.26:179709	p 162	N86-32742 *	NASA-CR-174735-VOL-4-BK-5	p 184	N86-15730 *
NAS 1.26:175084	p 61	N86-26399 *	NAS 1.26:179759	p 118	N86-32600 *	NASA-CR-174743	p 148	N86-21817 *
NAS 1.26:175087	p 103	N86-22713 *	NAS 1.26:2967	p 32	N86-29818 *	NASA-CR-174749	p 211	N86-28017 *
NAS 1.26:175088	p 15	N86-22559 *	NAS 1.26:3936	p 139	N86-15625 *	NASA-CR-174758	p 12	N86-27186 *
NAS 1.26:175089	p 15	N86-22558 *	NAS 1.26:3940	p 11	N86-21505 *	NASA-CR-174768	p 31	N86-27282 *
NAS 1.26:175090	p 188	N86-28511 *	NAS 1.26:3967	p 159	N86-24980 *	NASA-CR-174769	p 13	N86-31536 *
NAS 1.26:175091	p 32	N86-28947 *	NAS 1.26:3976	p 165	N86-27665 *	NASA-CR-174792	p 121	N86-14499 *
NAS 1.26:175092	p 15	N86-23577 *	NAS 1.26:3977	p 184	N86-25002 *	NASA-CR-174797	p 121	N86-16486 *
NAS 1.26:175094	p 212	N86-25310 *	NAS 1.26:3986	p 13	N86-28063 *	NASA-CR-174811	p 139	N86-18518 *
NAS 1.26:175097	p 92	N86-27444 *	NAS 1.26:3994	p 32	N86-28069 *	NASA-CR-174813	p 108	N86-27460 *
NAS 1.26:175098	p 11	N86-23563 *	NAS 1.26:3997	p 31	N86-28068 *	NASA-CR-174815	p 188	N86-25046 *
NAS 1.26:175099	p 149	N86-26596 *	NAS 1.26:4001	p 165	N86-27866 *	NASA-CR-174817	p 200	N86-23371 *
NAS 1.26:175100	p 91	N86-25455 *	NAS 1.26:4002	p 165	N86-28445 *	NASA-CR-174818	p 201	N86-23372 *
NAS 1.26:175105	p 124	N86-28323 *	NAS 1.55:2289	p 172	N86-11495 *	NASA-CR-174825	p 33	N86-30732 *
NAS 1.26:175108	p 203	N86-28729 *	NAS 1.55:2383	p 164	N86-22962 *	NASA-CR-174826	p 207	N86-13219 *
NAS 1.26:175109	p 17	N86-24691 *	NAS 1.55:2385	p 68	N86-11260 *	NASA-CR-174827	p 29	N86-21546 *
NAS 1.26:175111	p 91	N86-24817 *	NAS 1.55:2392	p 105	N86-26194 *	NASA-CR-174842	p 59	N86-20483 *
NAS 1.26:175112	p 31	N86-27283 *	NAS 1.55:2404	p 198	N86-12007 *	NASA-CR-174843	p 60	N86-24746 *
NAS 1.26:175113	p 31	N86-27284 *	NAS 1.55:2406	p 184	N86-17839 *	NASA-CR-174869	p 150	N86-31030 *
NAS 1.26:175115	p 177	N86-25851 *	NAS 1.55:2409	p 161	N86-30180 *	NASA-CR-174878	p 26	N86-14272 *
NAS 1.26:176141	p 111	N86-10377 *	NAS 1.60:2499	p 87	N86-12295 *	NASA-CR-174884	p 142	N86-24938 *
NAS 1.26:176219	p 195	N86-10860 *	NAS 1.60:2513	p 157	N86-12608 *	NASA-CR-174889	p 183	N86-27927 *
NAS 1.26:176220	p 172	N86-10588 *	NAS 1.60:2515	p 69	N86-21614 *	NASA-CR-174890	p 193	N86-27928 *
NAS 1.26:176273	p 43	N86-11212 *	NAS 1.60:2524	p 121	N86-13643 *	NASA-CR-174891	p 142	N86-24931 *
NAS 1.26:176278	p 151	N86-11485 *	NAS 1.60:2529	p 195	N86-28861 *	NASA-CR-174892	p 176	N86-21932 *
NAS 1.26:176300	p 181	N86-11667 *	NAS 1.60:2538	p 160	N86-24992 *	NASA-CR-174898	p 209	N86-21456 *
NAS 1.26:176315	p 182	N86-11670 *	NAS 1.60:2543	p 101	N86-15394 *	NASA-CR-174901	p 57	N86-16259 *
NAS 1.26:176364	p 77	N86-14331 *	NAS 1.60:2544	p 27	N86-15313 *	NASA-CR-174904	p 115	N86-24878 *
NAS 1.26:176373	p 191	N86-14770 *	NAS 1.60:2554	p 123	N86-21755 *	NASA-CR-174905	p 115	N86-24877 *
NAS 1.26:176381	p 204	N86-15122 *	NAS 1.60:2555	p 203	N86-22390 *	NASA-CR-174907	p 208	N86-16165 *
NAS 1.26:176418	p 88	N86-14356 *	NAS 1.60:2557	p 30	N86-24684 *	NASA-CR-174911	p 15	N86-30022 *

NASA-CR-174913	p 162	N86-32741 *	#	NASA-CR-175111	p 91	N86-24817 *	#	NASA-RP-1154	p 157	N86-13734 *	#
NASA-CR-174919	p 15	N86-27268 *	#	NASA-CR-175112	p 31	N86-27283 *	#	NASA-TM-86864-REV	p 104	N86-24839 *	#
NASA-CR-174923-VOL-1	p 26	N86-13328 *	#	NASA-CR-175113	p 31	N86-27284 *	#	NASA-TM-86886	p 89	N86-23661 *	#
NASA-CR-174923-VOL-2	p 26	N86-13329 *	#	NASA-CR-175115	p 177	N86-25851 *	#	NASA-TM-86892	p 148	N86-22915 *	#
NASA-CR-174923-VOL-3	p 26	N86-13330 *	#	NASA-CR-176141	p 111	N86-10377 *	#	NASA-TM-86972-REV	p 181	N86-11666 *	#
NASA-CR-174924	p 157	N86-11474 *	#	NASA-CR-176219	p 195	N86-10860 *	#	NASA-TM-86998	p 60	N86-21578 *	#
NASA-CR-174928	p 49	N86-27403 *	#	NASA-CR-176220	p 172	N86-10588 *	#	NASA-TM-87072	p 111	N86-10379 *	#
NASA-CR-174929	p 49	N86-27404 *	#	NASA-CR-176273	p 43	N86-11212 *	#	NASA-TM-87073	p 13	N86-28055 *	#
NASA-CR-174930	p 49	N86-27405 *	#	NASA-CR-176300	p 181	N86-11667 *	#	NASA-TM-87076	p 137	N86-10463 *	#
NASA-CR-174934	p 57	N86-15339 *	#	NASA-CR-176315	p 182	N86-11670 *	#	NASA-TM-87088	p 163	N86-10561 *	#
NASA-CR-174936	p 124	N86-30073 *	#	NASA-CR-176364	p 77	N86-14331 *	#	NASA-TM-87090	p 206	N86-25284 *	#
NASA-CR-174943	p 209	N86-17224 *	#	NASA-CR-176373	p 191	N86-14770 *	#	NASA-TM-87091	p 9	N86-10017 *	#
NASA-CR-174944	p 116	N86-26489 *	#	NASA-CR-176381	p 204	N86-15122 *	#	NASA-TM-87093	p 9	N86-10019 *	#
NASA-CR-174946	p 174	N86-13755 *	#	NASA-CR-176418	p 88	N86-14356 *	#	NASA-TM-87095	p 37	N86-16232 *	#
NASA-CR-174948	p 182	N86-12757 *	#	NASA-CR-176424	p 37	N86-15323 *	#	NASA-TM-87099	p 199	N86-14007 *	#
NASA-CR-174951	p 188	N86-25877 *	#	NASA-CR-176428	p 27	N86-16220 *	#	NASA-TM-87101	p 68	N86-10290 *	#
NASA-CR-174952	p 165	N86-25003 *	#	NASA-CR-176438	p 121	N86-15544 *	#	NASA-TM-87103	p 58	N86-10280 *	#
NASA-CR-174961	p 183	N86-14727 *	#	NASA-CR-176478	p 139	N86-16519 *	#	NASA-TM-87104	p 9	N86-13295 *	#
NASA-CR-174964	p 137	N86-10461 *	#	NASA-CR-176488	p 46	N86-18341 *	#	NASA-TM-87105	p 100	N86-10341 *	#
NASA-CR-174970	p 63	N86-31648 *	#	NASA-CR-176546	p 102	N86-19464 *	#	NASA-TM-87106	p 181	N86-10643 *	#
NASA-CR-174971	p 208	N86-16164 *	#	NASA-CR-176554	p 186	N86-19742 *	#	NASA-TM-87109	p 172	N86-10582 *	#
NASA-CR-174978	p 112	N86-16451 *	#	NASA-CR-176555	p 114	N86-19493 *	#	NASA-TM-87110	p 86	N86-10311 *	#
NASA-CR-174979	p 113	N86-16452 *	#	NASA-CR-176560	p 192	N86-21092 *	#	NASA-TM-87112	p 201	N86-25218 *	#
NASA-CR-174980	p 172	N86-10589 *	#	NASA-CR-176564	p 77	N86-20517 *	#	NASA-TM-87113	p 101	N86-12311 *	#
NASA-CR-174985	p 49	N86-27407 *	#	NASA-CR-176586	p 122	N86-20700 *	#	NASA-TM-87114	p 156	N86-10551 *	#
NASA-CR-174986	p 49	N86-27402 *	#	NASA-CR-176604	p 140	N86-20722 *	#	NASA-TM-87116	p 199	N86-14006 *	#
NASA-CR-174988	p 185	N86-18773 *	#	NASA-CR-176656	p 107	N86-21704 *	#	NASA-TM-87117	p 86	N86-12292 *	#
NASA-CR-174990	p 162	N86-32743 *	#	NASA-CR-176699	p 114	N86-22782 *	#	NASA-TM-87118	p 56	N86-10279 *	#
NASA-CR-174991	p 185	N86-18774 *	#	NASA-CR-176708	p 114	N86-23781 *	#	NASA-TM-87119	p 205	N86-11048 *	#
NASA-CR-174994	p 210	N86-25302 *	#	NASA-CR-176717	p 205	N86-23468 *	#	NASA-TM-87120	p 138	N86-13679 *	#
NASA-CR-174995	p 26	N86-12226 *	#	NASA-CR-176718	p 187	N86-24007 *	#	NASA-TM-87121	p 137	N86-11425 *	#
NASA-CR-174996	p 209	N86-17226 *	#	NASA-CR-176764	p 142	N86-24933 *	#	NASA-TM-87122	p 89	N86-12256 *	#
NASA-CR-174998	p 182	N86-12758 *	#	NASA-CR-176785	p 143	N86-24955 *	#	NASA-TM-87123	p 57	N86-11224 *	#
NASA-CR-174999	p 174	N86-16610 *	#	NASA-CR-176772	p 142	N86-24932 *	#	NASA-TM-87124	p 111	N86-10380 *	#
NASA-CR-175005	p 28	N86-20393 *	#	NASA-CR-176774	p 123	N86-24906 *	#	NASA-TM-87125	p 111	N86-10381 *	#
NASA-CR-175007	p 189	N86-29411 *	#	NASA-CR-176777	p 187	N86-25042 *	#	NASA-TM-87126	p 182	N86-11668 *	#
NASA-CR-175008	p 203	N86-15113 *	#	NASA-CR-176786	p 108	N86-25502 *	#	NASA-TM-87127	p 157	N86-14613 *	#
NASA-CR-175009	p 174	N86-11526 *	#	NASA-CR-176787	p 123	N86-25693 *	#	NASA-TM-87128	p 1	N86-11146 *	#
NASA-CR-175013	p 88	N86-14355 *	#	NASA-CR-176804	p 123	N86-25694 *	#	NASA-TM-87129	p 199	N86-19125 *	#
NASA-CR-175014	p 88	N86-14354 *	#	NASA-CR-176808	p 17	N86-26330 *	#	NASA-TM-87131	p 57	N86-10281 *	#
NASA-CR-175015	p 176	N86-21952 *	#	NASA-CR-176821	p 176	N86-25850 *	#	NASA-TM-87132	p 87	N86-13407 *	#
NASA-CR-175016	p 115	N86-24875 *	#	NASA-CR-176822	p 195	N86-26067 *	#	NASA-TM-87133	p 156	N86-10552 *	#
NASA-CR-175017	p 115	N86-24876 *	#	NASA-CR-176840	p 143	N86-26546 *	#	NASA-TM-87134	p 182	N86-11671 *	#
NASA-CR-175018	p 158	N86-20808 *	#	NASA-CR-176850	p 78	N86-28136 *	#	NASA-TM-87135	p 205	N86-12134 *	#
NASA-CR-175020	p 30	N86-24695 *	#	NASA-CR-176883	p 13	N86-30693 *	#	NASA-TM-87136	p 120	N86-12509 *	#
NASA-CR-175021	p 175	N86-17788 *	#	NASA-CR-176947	p 32	N86-30731 *	#	NASA-TM-87137	p 112	N86-12485 *	#
NASA-CR-175022	p 59	N86-20497 *	#	NASA-CR-176954	p 13	N86-29773 *	#	NASA-TM-87138	p 69	N86-14316 *	#
NASA-CR-175023	p 14	N86-20379 *	#	NASA-CR-176960	p 144	N86-30093 *	#	NASA-TM-87139	p 48	N86-12246 *	#
NASA-CR-175024	p 14	N86-20380 *	#	NASA-CR-176990	p 116	N86-30037 *	#	NASA-TM-87140	p 205	N86-12135 *	#
NASA-CR-175027	p 89	N86-17531 *	#	NASA-CR-177088	p 144	N86-30960 *	#	NASA-TM-87141	p 141	N86-12797 *	#
NASA-CR-175028	p 27	N86-16218 *	#	NASA-CR-177092	p 116	N86-30039 *	#	NASA-TM-87142	p 87	N86-12293 *	#
NASA-CR-175029	p 158	N86-17748 *	#	NASA-CR-177096	p 108	N86-30023 *	#	NASA-TM-87143	p 101	N86-12310 *	#
NASA-CR-175031	p 139	N86-17665 *	#	NASA-CR-177132	p 78	N86-28139 *	#	NASA-TM-87144	p 9	N86-14219 *	#
NASA-CR-175033	p 102	N86-16381 *	#	NASA-CR-177141	p 32	N86-28946 *	#	NASA-TM-87145	p 44	N86-11218 *	#
NASA-CR-175035	p 29	N86-20395 *	#	NASA-CR-177165	p 189	N86-29409 *	#	NASA-TM-87146	p 37	N86-12239 *	#
NASA-CR-175036	p 28	N86-20390 *	#	NASA-CR-177194	p 178	N86-28462 *	#	NASA-TM-87147	p 141	N86-23854 *	#
NASA-CR-175037	p 28	N86-20391 *	#	NASA-CR-177198	p 206	N86-28759 *	#	NASA-TM-87149	p 192	N86-13899 *	#
NASA-CR-175038	p 42	N86-18334 *	#	NASA-CR-177206	p 31	N86-27285 *	#	NASA-TM-87150	p 87	N86-12294 *	#
NASA-CR-175040	p 28	N86-20392 *	#	NASA-CR-177223	p 61	N86-27419 *	#	NASA-TM-87151	p 138	N86-13677 *	#
NASA-CR-175041	p 29	N86-20394 *	#	NASA-CR-177233	p 178	N86-28455 *	#	NASA-TM-87152	p 157	N86-11475 *	#
NASA-CR-175043	p 141	N86-23856 *	#	NASA-CR-177237	p 179	N86-30227 *	#	NASA-TM-87153	p 101	N86-13495 *	#
NASA-CR-175044	p 142	N86-23857 *	#	NASA-CR-177260	p 38	N86-27291 *	#	NASA-TM-87154	p 70	N86-24757 *	#
NASA-CR-175045	p 211	N86-30579 *	#	NASA-CR-177263	p 48	N86-26358 *	#	NASA-TM-87155	p 77	N86-12268 *	#
NASA-CR-175047	p 190	N86-31984 *	#	NASA-CR-177264	p 149	N86-26599 *	#	NASA-TM-87156	p 208	N86-13236 *	#
NASA-CR-175048	p 91	N86-24818 *	#	NASA-CR-177279	p 143	N86-27607 *	#	NASA-TM-87157	p 121	N86-13645 *	#
NASA-CR-175049	p 176	N86-21951 *	#	NASA-CR-177280	p 193	N86-27930 *	#	NASA-TM-87159	p 9	N86-14223 *	#
NASA-CR-175050	p 89	N86-20542 *	#	NASA-CR-177304	p 78	N86-27434 *	#	NASA-TM-87160	p 112	N86-14479 *	#
NASA-CR-175052	p 91	N86-25454 *	#	NASA-CR-179451	p 160	N86-26629 *	#	NASA-TM-87161	p 26	N86-12227 *	#
NASA-CR-175054	p 210	N86-22451 *	#	NASA-CR-179455	p 160	N86-27643 *	#	NASA-TM-87162	p 112	N86-14477 *	#
NASA-CR-175057	p 177	N86-27689 *	#	NASA-CR-179460	p 211	N86-31452 *	#	NASA-TM-87163	p 114	N86-19494 *	#
NASA-CR-175061	p 70	N86-24760 *	#	NASA-CR-179471	p 32	N86-28087 *	#	NASA-TM-87164	p 164	N86-13749 *	#
NASA-CR-175063	p 29	N86-23597 *	#	NASA-CR-179472	p 108	N86-28261 *	#	NASA-TM-87165	p 158	N86-19616 *	#
NASA-CR-175064	p 29	N86-21545 *	#	NASA-CR-179473	p 161	N86-28433 *	#	NASA-TM-87166	p 186	N86-18776 *	#
NASA-CR-175066	p 61	N86-27418 *	#	NASA-CR-179474	p 178	N86-28467 *	#	NASA-TM-87167	p 27	N86-16219 *	#
NASA-CR-175067	p 30	N86-25357 *	#	NASA-CR-179475	p 105	N86-29042 *	#	NASA-TM-87168	p 87	N86-13409 *	#
NASA-CR-175072	p 210	N86-24590 *	#	NASA-CR-179478	p 179	N86-30236 *	#	NASA-TM-87169	p 212	N86-14110 *	#
NASA-CR-175073	p 90	N86-22688 *	#	NASA-CR-179485	p 211	N86-33211 *	#	NASA-TM-87170	p 193	N86-19008 *	#
NASA-CR-175074	p 89	N86-21656 *	#	NASA-CR-179487	p 62	N86-29901 *	#	NASA-TM-87171	p 112	N86-13627 *	#
NASA-CR-175076	p 141	N86-22892 *	#	NASA-CR-179662	p 144	N86-31826 *	#	NASA-TM-87172	p 65	N86-13370 *	#
NASA-CR-175082	p 33	N86-30733 *	#	NASA-CR-179709	p 162	N86-32742 *	#	NASA-TM-87173	p 87	N86-13408 *	#
NASA-CR-175083	p 144	N86-31000 *	#	NASA-CR-179759	p 116	N86-32600 *	#	NASA-TM-87174	p 140	N86-19556 *	#
NASA-CR-175084	p 61	N86-26369 *	#	NASA-CR-3936	p 139	N86-15625 *	#	NASA-TM-87175	p 208	N86-14106 *	#
NASA-CR-175087	p 103	N86-22713 *	#	NASA-CR-3940	p 11	N86-21505 *	#	NASA-TM-87176	p 138	N86-13678 *	#
NASA-CR-175088	p 15	N86-22559 *	#	NASA-CR-3967	p 159	N86-24990 *	#	NASA-TM-87177	p 209	N86-21457 *	#
NASA-CR-175089	p 15	N86-22558 *	#	NASA-CR-3976	p 165	N86-27665 *	#	NASA-TM-87178	p 11	N86-21517 *	#
NASA-CR-175090	p 188	N86-28511 *	#	NASA-CR-3977	p 164	N86-25002 *	#	NASA-TM-87179	p 207	N86-21427 *	#
NASA-CR-175091	p 32	N86-28947 *	#	NASA-CR-3986	p 13	N86-28063 *	#	NASA-TM-87180	p 148	N86-14554 *	#
NASA-CR-175092	p 15	N86-23577 *	#	NASA-CR-3987	p 32	N86-29818 *	#	NASA-TM-87181	p 121	N86-16487 *	#
NASA-CR-175094	p 212	N86-25310 *	#	NASA-CR-3994	p 32	N86-28089 *	#	NASA-TM-87182	p 175	N86-18750 *	#
NASA-CR-175097	p 92	N86-27444 *	#	NASA-CR-3997	p 31	N86-28086 *	#	NASA-TM-87183	p 113	N86-16457 *	#
NASA-CR-175098	p 11	N86-23563 *	#	NASA-CR-4001	p 165	N86-27668 *	#	NASA-TM-87185	p 114	N86-18586 *	#
NASA-CR-175099	p 149	N86-26596 *	#	NASA-CR-4002	p 165	N86-28445 *	#	NASA-TM-87186	p 164	N86-16598 *	#
NASA-CR-175100	p 91	N86-25455 *	#					NASA-TM-87187	p 88	N86-15378 *	#
NASA-CR-175105	p 124	N86-28323 *	#					NASA-TM-87188	p 174	N86-14688 *	#
NASA-CR-175108	p 203	N86-28729 *	#	NASA-RP-1150	p 172	N86-10579 *	#	NASA-TM-87189	p 57	N86-16258 *	#
NASA-CR-175109</											

NASA-TM-87190	p 37	N86-18329 *	NASA-TM-87293	p 92	N86-28165 *	NASA-TM-88847	p 64	N86-32521 *
NASA-TM-87191	p 17	N86-31562 *	NASA-TM-87294	p 35	N86-32432 *	NASA-TM-88851	p 150	N86-32702 *
NASA-TM-87192	p 48	N86-17368 *	NASA-TM-87295	p 70	N86-24759 *	NASA-TM-88853	p 150	N86-32703 *
NASA-TM-87193	p 10	N86-16194 *	NASA-TM-87297	p 93	N86-31702 *	NASA-TM-88856	p 64	N86-32520 *
NASA-TM-87194	p 37	N86-16233 *	NASA-TM-87298	p 11	N86-24658 *	NASA-TM-88857	p 35	N86-32433 *
NASA-TM-87195	p 102	N86-18379 *	NASA-TM-87299	p 44	N86-23616 *			
NASA-TM-87196	p 139	N86-18646 *	NASA-TM-87300	p 104	N86-25473 *	NASA-TP-2499	p 87	N86-12295 *
NASA-TM-87197	p 174	N86-16611 *	NASA-TM-87301	p 12	N86-24667 *	NASA-TP-2513	p 157	N86-12609 *
NASA-TM-87198	p 113	N86-16461 *	NASA-TM-87302	p 201	N86-25217 *	NASA-TP-2515	p 69	N86-21614 *
NASA-TM-87199	p 10	N86-14224 *	NASA-TM-87303	p 206	N86-28775 *	NASA-TP-2524	p 121	N86-13643 *
NASA-TM-87200	p 10	N86-16195 *	NASA-TM-87304	p 33	N86-31582 *	NASA-TP-2529	p 195	N86-28861 *
NASA-TM-87201	p 113	N86-17595 *	NASA-TM-87305	p 210	N86-28261 *	NASA-TP-2538	p 160	N86-24992 *
NASA-TM-87202	p 212	N86-19274 *	NASA-TM-87306	p 148	N86-24958 *	NASA-TP-2543	p 101	N86-15394 *
NASA-TM-87203	p 184	N86-19636 *	NASA-TM-87307	p 179	N86-31920 *	NASA-TP-2544	p 27	N86-15313 *
NASA-TM-87204	p 69	N86-17477 *	NASA-TM-87308	p 104	N86-24837 *	NASA-TP-2554	p 123	N86-21755 *
NASA-TM-87205	p 140	N86-18647 *	NASA-TM-87312	p 78	N86-25431 *	NASA-TP-2555	p 203	N86-22390 *
NASA-TM-87206	p 48	N86-18343 *	NASA-TM-87313	p 212	N86-25321 *	NASA-TP-2557	p 30	N86-24694 *
NASA-TM-87207	p 175	N86-17789 *	NASA-TM-87314	p 60	N86-24747 *	NASA-TP-2558	p 60	N86-21577 *
NASA-TM-87208	p 90	N86-21681 *	NASA-TM-87315	p 123	N86-26520 *	NASA-TP-2562	p 44	N86-24722 *
NASA-TM-87209	p 88	N86-15380 *	NASA-TM-87316	p 34	N86-31588 *	NASA-TP-2570	p 38	N86-28101 *
NASA-TM-87210	p 89	N86-16334 *	NASA-TM-87317	p 30	N86-26336 *	NASA-TP-2571	p 62	N86-28123 *
NASA-TM-87211	p 43	N86-18338 *	NASA-TM-87318	p 92	N86-31699 *	NASA-TP-2590	p 195	N86-28662 *
NASA-TM-87212	p 10	N86-19289 *	NASA-TM-87319	p 190	N86-31981 *	NASA-TP-2591	p 178	N86-28464 *
NASA-TM-87213	p 176	N86-25822 *	NASA-TM-87320	p 190	N86-31982 *	NASA-TP-2602	p 62	N86-28124 *
NASA-TM-87214	p 175	N86-16615 *	NASA-TM-87321	p 206	N86-28776 *	NASA-TP-2622	p 125	N86-32629 *
NASA-TM-87215	p 46	N86-16249 *	NASA-TM-87322	p 149	N86-24967 *			
NASA-TM-87216	p 27	N86-16221 *	NASA-TM-87323	p 12	N86-26285 *	NASAA-1-5-Z-F	p 116	N86-31760 *
NASA-TM-87217	p 65	N86-18442 *	NASA-TM-87324	p 196	N86-27036 *			
NASA-TM-87218	p 113	N86-16458 *	NASA-TM-87325	p 177	N86-27680 *	NAUFP-202-3	p 207	N86-13219 *
NASA-TM-87219	p 65	N86-17472 *	NASA-TM-87326	p 190	N86-31980 *			
NASA-TM-87220	p 142	N86-24934 *	NASA-TM-87327	p 143	N86-26545 *	P/W/GPD-FR-19134-3	p 62	N86-29901 *
NASA-TM-87221	p 77	N86-19417 *	NASA-TM-87328	p 143	N86-25726 *			
NASA-TM-87222	p 164	N86-16599 *	NASA-TM-87330	p 161	N86-31889 *	PSD-FCR-5715	p 187	N86-25040 *
NASA-TM-87224	p 209	N86-19264 *	NASA-TM-87331	p 92	N86-28164 *			
NASA-TM-87225	p 177	N86-26651 *	NASA-TM-87332	p 188	N86-26677 *	PWA-5774-39	p 31	N86-27284 *
NASA-TM-87226	p 114	N86-18585 *	NASA-TM-87333	p 201	N86-29630 *	PWA-5774-40	p 31	N86-27283 *
NASA-TM-87227	p 210	N86-25303 *	NASA-TM-87334	p 71	N86-31664 *	PWA-5923-14	p 26	N86-14272 *
NASA-TM-87228	p 140	N86-19558 *	NASA-TM-87335	p 44	N86-31621 *	PWA-5966-17	p 157	N86-11474 *
NASA-TM-87229	p 123	N86-21757 *	NASA-TM-87336	p 149	N86-27617 *	PWA-5968-19	p 165	N86-25003 *
NASA-TM-87230	p 140	N86-19555 *	NASA-TM-87337	p 71	N86-27426 *			
NASA-TM-87231	p 175	N86-19683 *	NASA-TM-87338	p 63	N86-31650 *	PWS-5914-39	p 26	N86-12226 *
NASA-TM-87232	p 159	N86-21856 *	NASA-TM-87339	p 165	N86-25812 *			
NASA-TM-87233	p 186	N86-18775 *	NASA-TM-87340	p 61	N86-25409 *	QR-14	p 182	N86-12757 *
NASA-TM-87234	p 140	N86-21794 *	NASA-TM-87341	p 71	N86-26376 *	QR-16	p 182	N86-12758 *
NASA-TM-87235	p 90	N86-21658 *	NASA-TM-87342	p 105	N86-27452 *			
NASA-TM-87236	p 102	N86-19465 *	NASA-TM-87343	p 93	N86-31701 *	RDD:85-4101-12-01:01	p 203	N86-15113 *
NASA-TM-87237	p 10	N86-19290 *	NASA-TM-87344	p 124	N86-30068 *			
NASA-TM-87239	p 158	N86-20809 *	NASA-TM-87345	p 211	N86-29731 *	REPT-06-7963	p 105	N86-29042 *
NASA-TM-87240	p 11	N86-21513 *	NASA-TM-87346	p 34	N86-31584 *	REPT-21-4705	p 141	N86-23856 *
NASA-TM-87241	p 149	N86-24964 *	NASA-TM-87347	p 63	N86-31651 *	REPT-716548-2	p 114	N86-19493 *
NASA-TM-87242	p 103	N86-24835 *	NASA-TM-87348	p 166	N86-31912 *	REPT-86ASE507SA9	p 211	N86-30579 *
NASA-TM-87243	p 104	N86-24836 *	NASA-TM-87349	p 192	N86-26914 *	REPT-94E/2623E	p 139	N86-16519 *
NASA-TM-87246	p 123	N86-24907 *	NASA-TM-87350	p 150	N86-31857 *			
NASA-TM-87247	p 109	N86-24869 *	NASA-TM-87351	p 201	N86-32247 *	RI/RD85-183	p 162	N86-32741 *
NASA-TM-87249	p 104	N86-24838 *	NASA-TM-87352	p 12	N86-27213 *	RI/RD86-116	p 61	N86-26369 *
NASA-TM-87250	p 89	N86-20541 *	NASA-TM-87354	p 161	N86-27661 *	RI/RD86-168	p 160	N86-27643 *
NASA-TM-87251	p 106	N86-31729 *	NASA-TM-87357	p 124	N86-27578 *			
NASA-TM-87253	p 186	N86-21978 *	NASA-TM-88763	p 115	N86-25650 *	R84-926376-15	p 148	N86-21817 *
NASA-TM-87254	p 11	N86-20357 *	NASA-TM-88786	p 63	N86-31652 *	R84-956627-1	p 30	N86-24693 *
NASA-TM-87255	p 63	N86-31649 *	NASA-TM-88787	p 71	N86-31663 *	R84AEB378-VOL-1	p 159	N86-23936 *
NASA-TM-87256	p 148	N86-24959 *	NASA-TM-88788	p 93	N86-31700 *	R84AEB379-VOL-2	p 159	N86-23937 *
NASA-TM-87257	p 90	N86-21659 *	NASA-TM-88790	p 166	N86-31065 *	R84AEB380-VOL-3	p 159	N86-23938 *
NASA-TM-87258	p 206	N86-25268 *	NASA-TM-88791	p 15	N86-31548 *	R84AEB570	p 200	N86-23371 *
NASA-TM-87259	p 62	N86-28125 *	NASA-TM-88792	p 178	N86-29271 *	R84AEB570	p 201	N86-23372 *
NASA-TM-87260	p 50	N86-21575 *	NASA-TM-88793	p 189	N86-31979 *	R85-956896-4	p 11	N86-21505 *
NASA-TM-87261	p 103	N86-20568 *	NASA-TM-88794	p 105	N86-29041 *	R85AEB452	p 142	N86-24931 *
NASA-TM-87262	p 193	N86-22150 *	NASA-TM-88795	p 13	N86-31537 *	R86AEB104	p 162	N86-32743 *
NASA-TM-87263	p 208	N86-32336 *	NASA-TM-88796	p 34	N86-31587 *	R86AEB267	p 203	N86-28729 *
NASA-TM-87264	p 187	N86-23035 *	NASA-TM-88797	p 166	N86-31913 *	R86AEB361	p 32	N86-28087 *
NASA-TM-87265	p 35	N86-22582 *	NASA-TM-88798	p 12	N86-28053 *			
NASA-TM-87266	p 70	N86-25417 *	NASA-TM-88799	p 144	N86-28378 *	SAE PAPER 851573	p 154	A86-40678 *
NASA-TM-87267	p 105	N86-25476 *	NASA-TM-88800	p 161	N86-30206 *	SAE PAPER 851786	p 154	A86-38310 *
NASA-TM-87268	p 77	N86-21635 *	NASA-TM-88801	p 62	N86-28122 *	SAE PAPER 851787	p 154	A86-38311 *
NASA-TM-87269	p 206	N86-25267 *	NASA-TM-88802	p 194	N86-28651 *	SAE PAPER 851788	p 154	A86-38312 *
NASA-TM-87270	p 91	N86-24813 *	NASA-TM-88803	p 78	N86-31680 *	SAE PAPER 851839	p 16	A86-38336 *
NASA-TM-87271	p 124	N86-31792 *	NASA-TM-88804	p 33	N86-31583 *	SAE PAPER 851896	p 146	A86-38359 *
NASA-TM-87272	p 31	N86-28085 *	NASA-TM-88806	p 207	N86-30556 *	SAE PAPER 860444	p 153	A86-37048 *
NASA-TM-87273	p 180	N86-25793 *	NASA-TM-88807	p 178	N86-28461 *	SAE PAPER 860614	p 156	A86-49624 *
NASA-TM-87274	p 103	N86-21682 *	NASA-TM-88808	p 34	N86-31586 *			
NASA-TM-87275	p 103	N86-21683 *	NASA-TM-88809	p 212	N86-30620 *	SAE-860615	p 10	N86-19289 *
NASA-TM-87276	p 104	N86-25474 *	NASA-TM-88810	p 189	N86-30251 *			
NASA-TM-87277	p 106	N86-31728 *	NASA-TM-88811	p 190	N86-31983 *	SAR-4	p 187	N86-24007 *
NASA-TM-87278	p 60	N86-24748 *	NASA-TM-88812	p 71	N86-29908 *			
NASA-TM-87279	p 61	N86-25407 *	NASA-TM-88815	p 211	N86-29732 *	SCT-85-5449	p 33	N86-30732 *
NASA-TM-87280	p 61	N86-25408 *	NASA-TM-88816	p 62	N86-31648 *			
NASA-TM-87281	p 60	N86-24749 *	NASA-TM-88817	p 34	N86-31585 *	SR85-R-5052-16	p 59	N86-20497 *
NASA-TM-87283	p 187	N86-25039 *	NASA-TM-88818	p 116	N86-32598 *			
NASA-TM-87284	p 105	N86-25475 *	NASA-TM-88820	p 47	N86-31825 *	SWRI-7576/30	p 172	N86-10589 *
NASA-TM-87285	p 115	N86-24881 *	NASA-TM-88822	p 64	N86-32522 *			
NASA-TM-87286	p 148	N86-24961 *	NASA-TM-88827	p 166	N86-32764 *	TF/86/1	p 139	N86-16519 *
NASA-TM-87287	p 141	N86-22890 *	NASA-TM-88828	p 106	N86-32573 *			
NASA-TM-87288	p 90	N86-22687 *	NASA-TM-88829	p 150	N86-31859 *	TR-213-1	p 121	N86-16486 *
NASA-TM-87289	p 30	N86-24697 *	NASA-TM-88832	p 125	N86-32627 *	TR-2273-VOL-1	p 193	N86-27927 *
NASA-TM-87290	p 91	N86-25453 *	NASA-TM-88833	p 125	N86-31793 *	TR-2273-VOL-2	p 193	N86-27928 *
NASA-TM-87291	p 70	N86-24756 *	NASA-TM-88839	p 49	N86-31634 *	TR-2390	p 116	N86-26489 *
NASA-TM-87292	p 90	N86-22686 *	NASA-TM-88842	p 93	N86-32557 *	TR-715723-1	p 116	N86-32600 *

TR-716548-1	p 43	N86-11212 * #	US-PATENT-4,560,577	p 102	N86-19458 * #
TR-716548-3	p 46	N86-18341 * #	US-PATENT-4,560,742	p 102	N86-19457 * #
TR-716548-4	p 114	N86-23781 * #	US-PATENT-4,564,787	p 122	N86-21742 * #
TR-85-C-21	p 10	N86-19290 * #	US-PATENT-4,580-791	p 180	N86-25790 * #
TRC-SEAL-4-86	p 162	N86-32742 * #	US-PATENT-4,584,249	p 188	N86-25874 * #
UC-MIE-051586-19	p 161	N86-28433 * #	US-PATENT-4,604,181	p 108	N86-32569 * #
UULU-ENG-86-0503	p 78	N86-28139 * #	US-PATENT-4,607,193	p 109	N86-32587 * #
UULU-ENG-86-2221	p 206	N86-28759 * #	US-PATENT-4,608,452	p 190	N86-32675 * #
UULU-ENG-86-2547	p 115	N86-25650 * #	USAAVSCOM-TR-85-C-12	p 9	N86-10017 * #
UULU-ENG-86-2554	p 116	N86-30039 * #	USAAVSCOM-TR-85-C-15	p 137	N86-10463 * #
US-CLASS-80-39.07	p 28	N86-20389 * #	USAAVSCOM-TR-85-C-17	p 157	N86-14613 * #
US-PATENT-APPL-SN-413101	p 28	N86-20389 * #	USAAVSCOM-TR-85-C-18	p 101	N86-12311 * #
US-PATENT-APPL-SN-434087	p 102	N86-19457 * #	USAAVSCOM-TR-85-C-19	p 137	N86-11425 * #
US-PATENT-APPL-SN-537614	p 122	N86-20672 * #	USAAVSCOM-TR-85-C-20	p 140	N86-19556 * #
US-PATENT-APPL-SN-603374	p 158	N86-19606 * #	USAAVSCOM-TR-85-C-21	p 10	N86-19290 * #
US-PATENT-APPL-SN-625077	p 188	N86-25874 * #	USAAVSCOM-TR-85-C-8	p 13	N86-28055 * #
US-PATENT-APPL-SN-638541	p 122	N86-20671 * #	USAAVSCOM-TR-85-F-1	p 159	N86-24991 * #
US-PATENT-APPL-SN-642310	p 186	N86-19721 * #	USAAVSCOM-TR-86-C-14	p 91	N86-25454 * #
US-PATENT-APPL-SN-649330	p 102	N86-19458 * #	USAAVSCOM-TR-86-C-16	p 150	N86-31857 * #
US-PATENT-APPL-SN-659475	p 109	N86-32587 * #	USAAVSCOM-TR-86-C-18	p 91	N86-25455 * #
US-PATENT-APPL-SN-669140	p 190	N86-32875 * #	USAAVSCOM-TR-86-C-1	p 141	N86-21797 * #
US-PATENT-APPL-SN-672224	p 160	N86-25790 * #	USAAVSCOM-TR-86-C-22	p 105	N86-29041 * #
US-PATENT-APPL-SN-714051	p 122	N86-21742 * #	USAAVSCOM-TR-86-C-23	p 34	N86-31587 * #
US-PATENT-APPL-SN-748536	p 122	N86-20680 * #	USAAVSCOM-TR-86-C-2	p 160	N86-25793 * #
US-PATENT-APPL-SN-761235	p 106	N86-32569 * #	USAAVSCOM-TR-86-C-3	p 140	N86-18647 * #
US-PATENT-APPL-SN-775968	p 109	N86-20587 * #	USAAVSCOM-TR-86-C-4	p 91	N86-24818 * #
US-PATENT-APPL-SN-823713	p 93	N86-32556 * #	USAAVSCOM-TR-86-C-7	p 92	N86-28164 * #
US-PATENT-APPL-SN-832296	p 92	N86-26414 * #	UTSI/85-08	p 139	N86-16518 * #
US-PATENT-APPL-SN-834977	p 105	N86-26434 * #	WAESD-TR-85-0030	p 190	N86-31984 * #
US-PATENT-APPL-SN-875798	p 162	N86-32740 * #	WDL-TR-10138	p 118	N86-31780 * #
US-PATENT-CLASS-136-261	p 190	N86-32875 * #	WDL-TR-10631-VOL-1	p 49	N86-27403 * #
US-PATENT-CLASS-148-1.5	p 190	N86-32875 * #	WDL-TR-10632-VOL-2	p 49	N86-27404 * #
US-PATENT-CLASS-204-192-C	p 102	N86-19458 * #	WDL-TR-10633-VOL-3	p 49	N86-27405 * #
US-PATENT-CLASS-204-192-D	p 102	N86-19458 * #	WGR-86-4-VOL-1	p 114	N86-22782 * #
US-PATENT-CLASS-204-192-R	p 102	N86-19458 * #	WRDC-85-9F4-DIDIS-R1	p 124	N86-30073 * #
US-PATENT-CLASS-204-192C	p 106	N86-32569 * #	WS/CSCI-85-1-6B	p 77	N86-14331 * #
US-PATENT-CLASS-204-192C	p 109	N86-32587 * #			
US-PATENT-CLASS-204-192D	p 106	N86-32569 * #			
US-PATENT-CLASS-204-192D	p 109	N86-32587 * #			
US-PATENT-CLASS-204-298	p 106	N86-32569 * #			
US-PATENT-CLASS-204-298	p 109	N86-32587 * #			
US-PATENT-CLASS-204/298	p 102	N86-19458 * #			
US-PATENT-CLASS-227-27	p 160	N86-25790 * #			
US-PATENT-CLASS-227-28	p 160	N86-25790 * #			
US-PATENT-CLASS-244-134-D	p 122	N86-20671 * #			
US-PATENT-CLASS-29-572	p 190	N86-32875 * #			
US-PATENT-CLASS-29-576B	p 190	N86-32875 * #			
US-PATENT-CLASS-307-264	p 122	N86-20672 * #			
US-PATENT-CLASS-307-270	p 122	N86-20672 * #			
US-PATENT-CLASS-307-566	p 122	N86-20672 * #			
US-PATENT-CLASS-307-570	p 122	N86-20672 * #			
US-PATENT-CLASS-307-572	p 122	N86-20672 * #			
US-PATENT-CLASS-310-324	p 122	N86-20671 * #			
US-PATENT-CLASS-313-106	p 109	N86-32587 * #			
US-PATENT-CLASS-313-107	p 109	N86-32587 * #			
US-PATENT-CLASS-315-3.5	p 122	N86-21742 * #			
US-PATENT-CLASS-315-3.6	p 122	N86-21742 * #			
US-PATENT-CLASS-315-39.3	p 122	N86-21742 * #			
US-PATENT-CLASS-315-5.38	p 109	N86-32587 * #			
US-PATENT-CLASS-330-43	p 122	N86-21742 * #			
US-PATENT-CLASS-357-30	p 190	N86-32875 * #			
US-PATENT-CLASS-357-91	p 190	N86-32875 * #			
US-PATENT-CLASS-384-103	p 158	N86-19606 * #			
US-PATENT-CLASS-384-106	p 158	N86-19606 * #			
US-PATENT-CLASS-39-25.35	p 122	N86-20671 * #			
US-PATENT-CLASS-42-101	p 188	N86-25874 * #			
US-PATENT-CLASS-427-248.1	p 102	N86-19458 * #			
US-PATENT-CLASS-427-38	p 102	N86-19458 * #			
US-PATENT-CLASS-427-39	p 109	N86-32587 * #			
US-PATENT-CLASS-428-446	p 102	N86-19458 * #			
US-PATENT-CLASS-428-473.5	p 102	N86-19458 * #			
US-PATENT-CLASS-428-702	p 102	N86-19458 * #			
US-PATENT-CLASS-429-109	p 186	N86-19721 * #			
US-PATENT-CLASS-429-15	p 186	N86-19721 * #			
US-PATENT-CLASS-429-19	p 186	N86-19721 * #			
US-PATENT-CLASS-429-27	p 188	N86-25874 * #			
US-PATENT-CLASS-429-51	p 186	N86-19721 * #			
US-PATENT-CLASS-429-57	p 188	N86-25874 * #			
US-PATENT-CLASS-528-229	p 102	N86-19457 * #			
US-PATENT-CLASS-528-322	p 102	N86-19457 * #			
US-PATENT-CLASS-528-342	p 102	N86-19457 * #			
US-PATENT-CLASS-528345	p 102	N86-19457 * #			
US-PATENT-CLASS-60-39.02	p 28	N86-20389 * #			
US-PATENT-CLASS-60-736	p 28	N86-20389 * #			
US-PATENT-4,543,302	p 186	N86-19721 * #			
US-PATENT-4,545,553	p 122	N86-20671 * #			
US-PATENT-4,547,686	p 122	N86-20672 * #			
US-PATENT-4,550,561	p 28	N86-20389 * #			
US-PATENT-4,552,466	p 158	N86-19606 * #			

ORIGINAL PAGE IS
OF POOR QUALITY

1. Report No. NASA TM-89887		2. Government Accession No.		3. Recipient's Catalog No.	
4. Title and Subtitle Bibliography of Lewis Research Center Technical Publications Announced in 1986				5. Report Date May 1987	
				6. Performing Organization Code None	
7. Author(s)				8. Performing Organization Report No. E-3574	
				10. Work Unit No.	
9. Performing Organization Name and Address National Aeronautics and Space Administration Lewis Research Center Cleveland, Ohio 44135				11. Contract or Grant No.	
				13. Type of Report and Period Covered Technical Memorandum	
12. Sponsoring Agency Name and Address National Aeronautics and Space Administration Washington, D.C. 20546				14. Sponsoring Agency Code	
15. Supplementary Notes Compiled by Technical Information Services Division, Lewis Research Center.					
16. Abstract This compilation of abstracts describes and indexes the technical reporting that resulted from the scientific and engineering work performed and managed by the Lewis Research Center in 1986. All the publications were announced in the 1986 issues of STAR (Scientific and Technical Aerospace Reports) and/or IAA (International Aerospace Abstracts). Included are research reports, journal articles, conference presentations, patents and patent applications, and theses.					
17. Key Words (Suggested by Author(s)) Bibliographies Abstracts Documentation Indexes (Documentation)			18. Distribution Statement Unclassified - unlimited STAR Category 82		
19. Security Classif. (of this report) Unclassified	20. Security Classif. (of this page) Unclassified		21. No. of pages 348	22. Price* A15	

National Aeronautics and
Space Administration

Lewis Research Center
Cleveland, Ohio 44135

Official Business
Penalty for Private Use \$300

SECOND CLASS MAIL

ADDRESS CORRECTION REQUESTED



Postage and
National Aero
Space Admin
NASA-451

NASA
